TN
1
A5
Vol. 192
NIC

TRANSACTIONS

of the

American Institute of Mining and Metallurgical Engineers

(Incorporated)

American Institute of Mining, Metallurgical, and Petroleum Engineers,

VOLUME 192

PETROLEUM DEVELOPMENT AND TECHNOLOGY

1951

PETROLEUM BRANCH

PAPERS AND DISCUSSIONS PRESENTED BEFORE THE BRANCH AT MEETINGS HELD AT NEW ORLEANS, OCTOBER 4-6, 1950; LOS ANGELES, OCTOBER 12-13, 1950; ST. LOUIS, FEBRUARY 19-22, 1951, AND OKLAHOMA CITY, OCTOBER 3-5, 1951.

PUBLISHED BY THE INSTITUTE
AT THE OFFICE OF THE PETROLEUM BRANCH
408 TRINITY UNIVERSAL BUILDING
DALLAS, TEXAS

Headquarters of the Institute are at 29 West 39th Street, New York, N. Y.

COPYRIGHT, 1951, BY THE
AMERICAN INSTITUTE OF MINING AND METALLURGICAL ENGINEERS
(INCORPORATED)

PRINTED IN THE UNITED STATES OF AMERICA

STORM PRINTING COMPANY, DALLAS, TEXAS

FOREWORD

ONE of the outstanding achievements of 1951 was that the Institute lived within its income for the first time since 1941. This improved financial situation resulted not only from increased income from advertising and new member dues, but also from expense reduction. A study of New York Office business procedures was made by an outside consulting firm, and a number of improvements have already been made, with others still under consideration.

Another outstanding event in this Institute year, and of particular interest to the Petroleum Branch, was the election of Everette Lee DeGolyer as one of the twenty Honorary Members of AIME.

To make our activities conform more closely with the professional activities of Petroleum Branch members, we modified the Technology Committee by providing a vice chairman for each of the divisions of Production, Drilling and Natural Gas. The work of this committee contributed materially to the successful Fall Meetings in Oklahoma City and Los Angeles.

Under the sponsorship of the Henry L. Doherty Memorial Fund, the Petroleum Branch published for the Institute the unique volume, *Petroleum Conservation*, edited by Stuart E. Buckley. In recognition of this and his many other contributions to AIME literature, as well as his effective participation in Branch activities, Mr. Buckley was awarded the sixth Certificate of Service of the Petroleum Branch.

The Branch moved its headquarters office to more suitable quarters; adopted the custom of nominating officers for an additional year ahead; and recommended further organizational modifications to provide latitude for local Petroleum, Metals, or Mining groups, while strengthening the over-all bonds of Institute membership.

This *Transactions* volume contains 45 Technical Papers and 7 Technical Notes in 381 pages. It is the largest volume published since the Branch initiated its publications program in Dallas three years ago.

R. W. FRENCH, *Chairman*
Petroleum Branch, 1951

CLEVELAND, OHIO
January 1, 1952

AIME OFFICERS AND DIRECTORS

For the Year Ending February, 1952

PRESIDENT

Willis McGerald Peirce, New York, New York

PAST PRESIDENTS

D. H. McLaughlin, San Francisco, California
L. E. Young, Pittsburgh, Pennsylvania

VICE-PRESIDENTS

Philip Kraft, New York, New York
J. L. Gillson, Wilmington, Delaware
M. L. Haider, Toronto, Ontario, Canada
A. B. Kinzel, New York, New York
R. W. Thomas, Ray, Arizona

VICE-PRESIDENT AND TREASURER

Andrew Fletcher, New York, New York

DIRECTORS

W. J. Coulter, Denver, Colorado
E. V. Daveler, New York, New York
H. Decker, Houston, Texas
P. E. Fitzgerald, Tulsa, Oklahoma
F. B. Foley, Bayonne, New Jersey
J. L. Head, New York, New York
H. W. Johnson, Chicago, Illinois
C. E. Lawall, Huntington, West Virginia
F. W. Libbey, Portland, Oregon
E. C. Meagher, New York, New York
C. V. Millikan, Tulsa, Oklahoma
T. G. Moore, New York, New York
G. F. Moulton, New York, New York
J. F. Myers, Copperhill, Tennessee
L. F. Reinartz, Middletown, Ohio
A. C. Rubel, Los Angeles, California
G. P. Swift, Watertown, Massachusetts
H. I. Young, St. Louis, Missouri

DIVISION CHAIRMEN—DIRECTORS EX OFFICIIS

R. M. Brick *(Institute of Metals)*, Philadelphia, Pennsylvania
Allison Butts *(Mineral Industry Education)*, Bethlehem, Pennsylvania
Raymond E. Byler *(Minerals Beneficiation)*, San Francisco, California
A. B. Cummins *(Industrial Minerals)*, Manville, New Jersey
R. W. French, Jr. *(Petroleum)*, Cleveland, Ohio
E. D. Gardner *(Mining, Geology and Geophysics)*, Washington, D. C.
Carroll A. Garner *(Coal)*, Hazleton, Pennsylvania
T. L. Joseph *(Iron and Steel)*, Minneapolis, Minnesota
Richard J. Lund *(Mineral Economics)*, Columbus, Ohio
Oliver C. Ralston *(Extractive Metallurgy)*, Washington, D. C.

SECRETARY

Edward H. Robie

ASSISTANT SECRETARIES

Joe B. Alford
John V. Beall
Roy E. O'Brien
E. O. Kirkendall
E. J. Kennedy, Jr.

ASSISTANT TO THE SECRETARY

H. Newell Appleton

PUBLICATIONS MANAGER

Thomas E. Lloyd

ASSISTANT TREASURER

H. A. Maloney

CONTROLLER

George I. Brigden

CONTENTS

Foreword, *by* R. W. French iii

AIME Officers and Directors iv

Petroleum Branch Officers vii

Petroleum Branch Past Chairmen viii

The Anthony F. Lucas Fund and Medal ix

Petroleum Branch Certificate of Service x

Errata xi

PAPERS

DRILLING FLUIDS AND CEMENT

Carrying Capacity of Drilling Muds. By C. E. Williams, Jr., and G. H. Bruce 111

Plastic Flow Properties of Drilling Fluids—Measurement and Application. By J. C. Melrose and W. B. Lilienthal 159

A Modified Low-Strength Cement. By B. E. Morgan and G. K. Dumbauld 165

An Analysis and the Control of Lost Circulation. By George C. Howard and P. P. Scott, Jr. 171

EQUIPMENT

A Gravel Pack Completion for Exclusion of Gas and Water. By Thomas S. West 183

Surface Indicating Pressure, Temperature and Flow Equipment. By M. B. Riordan 257

FLUID INJECTION

The Shuler Jones Sand Pool; Nine Years of Unitized Pressure-Maintenance Operations. By Jack Tarner, W. R. Evans, and H. H. Kaveler 121

Effect of Free Gas Saturation on Oil Recovery by Water Flooding. By C. R. Holmgren and R. A. Morse 135

Primary High Pressure Water Flooding in the Pettit Lime Haynesville Field. By D. W. Akins, Jr. . . 239

Report on Mamou Field Pressure Maintenance Project. By William O. Crego and James M. Henagan . . 263

Results of Gas Injection in the Cedar Lake Field. By R. M. Leibrock, R. G. Hiltz, and J. E. Huzarevich . 357

LOGGING

An Investigation of the Electrokinetic Component of the Self Potential Curve. By M. R. J. Wyllie . . . 1

The Quantitative Application of Radioactivity Logs. By Robert E. Bush and E. S. Mardock 191

The Laterolog: A New Resistivity Logging Method with Electrodes Using an Automatic Focusing System. By H. G. Doll 305

The Guard Electrode Logging System. By John E. Owen and Walton J. Greer 347

MEASUREMENTS OF PHYSICAL PROPERTIES

Laboratory Measurements of Relative Permeability. By J. S. Osoba, J. G. Richardson, J. K. Kerver, J. A. Hafford, and P. M. Blair 47

Capillary Pressure Investigations. By Harry W. Brown 67

Relative Permeability to Liquid in Liquid-Gas Systems. By L. A. Rapoport and W. J. Leas 83

Experimental Investigation of Factors Affecting Laboratory Relative Permeability Measurements. By T. M. Geffen, W. W. Owens, D. R. Parrish, and R. A. Morse 99

Use of Centrifuge for Determining Connate Water, Residual Oil, and Capillary Pressure Curves of Small Core Samples. By R. L. Slobod, Adele Chambers, and W. L. Prehn, Jr. 127

Further Developments in the Laboratory Determination of Relative Permeability. By B. H. Caudle, R. L. Slobod, and E. R. Brownscombe 145

Relative Permeability Studies. By Irving Fatt and Herman Dykstra 249

Interstitial Water Determination by an Evaporation Method. By E. S. Messer 269

NATURAL GAS

Low Temperature Dehydration of Natural Gas. By Louis R. Records and Dwight H. Seely, Jr. 61
Transient Flow in Gas Transmission Lines. By R. H. Olds and B. H. Sage 217
Measuring the Water Vapor Content of Gases Dehydrated by Triethylene Glycol. By Irwin Politziner, F. M. Townsend, and L. S. Reid 301
The Calculation of Pressure Drop in the Flow of Natural Gas Through Pipe. By Fred H. Poettmann . . 317

RESERVOIR ENGINEERING

Pressure Behavior in the Woodbine Sand. By John S. Bell and J. M. Shepherd. 19
A Study of the Dornick Hills—Springer Sand Reservoir, Velma Pool, Oklahoma. By W. B. Davis . . . 29
Special Considerations in Predicting Reservoir Performance of Highly Volatile Type Oil Reservoirs. By Alton B. Cook, G. B. Spencer, and F. P. Bobrowski 37
Interfacial Tensions at Reservoir Pressures and Temperatures; Apparatus and the Water-Methane System. By E. W. Hough, M. J. Rzasa, and B. B. Wood 57
Variable Characteristics of the Oil in the Tensleep Sandstone Reservoir, Elk Basin Field, Wyoming and Montana. By Ralph H. Espach and Joseph Fry 75
Vaporization Characteristics of Carbon Dioxide in a Natural Gas-Crude Oil System. By Fred H. Poettmann 141
The Southwest Antioch Gibson Sand Unit. By T. E. Ockershauser 199
Steady Flow of Two-Phase Single-Component Fluids Through Porous Media. By Frank G. Miller . . . 205
Phase Equilibria in Hydrocarbon-Water Systems, III—The Solubility of Methane in Water at Pressures to 10,000 PSIA. By O. L. Culberson and J. J. McKetta, Jr. 223
The Phase Behavior of a Natural Hydrocarbon System. By Charles F. Weinaug and Howard B. Bradley 233
Fluid Saturation in Porous Media by X-Ray Technique. By A. D. K. Laird and John A. Putnam . . . 275
An Experimental and Theoretical Investigation of Gravity Drainage Performance. By P. L. Terwilliger, L. E. Wilsey, Howard N. Hall, P. M. Bridges, and R. A. Morse 285
Phase Equilibria in Hydrocarbon-Water Systems, IV—Vapor-Liquid Equilibrium Constants in the Methane-Water and Ethane-Water Systems. By O. L. Culberson and J. J. McKetta, Jr. 297
The Effect of Withdrawal Rate on the Uniformity of Edgewater Intrusion. By M. Muskat 327
A Reservoir Analyzer Study of the Woodbine Basin. By R. C. Rumble, H. H. Spain, and H. E. Stamm, III 331
Porosity-Measurement Comparisons by Five Laboratories. By B. J. Dotson, R. L. Slobod, P. N. McCreery, and James W. Spurlock 341

MISCELLANEOUS

Mineralogical Studies of California Oilbearing Formations, I—Identification of Clays. By P. G. Nahin, W. C. Merrill, A. Grenall, and R. S. Crog 151
Relaxation Methods Applied to Oilfield Research. By Herman Dykstra and R. L. Parsons 227

SEPARATE DISCUSSIONS 367

TECHNICAL NOTES

A New Technique for the Measurement of the Formation Factors and Resistivity Indices of Porous Media. By F. Morgan, M. R. J. Wyllie, and P. F. Fulton 371
Fluid Distributions Characterizing Gas-Liquid Flow. By Walter Rose 372
The Calculation of Water Resistivities from Chemical Analysis. By H. F. Dunlap and R. R. Hawthorne 373
Theoretical Note on Linear Absorption Methods of Determination of Fluid Saturation in Porous Media. By Leonard B. Lipson 375
The Interpretation of Chemical Water Analysis by Means of Patterns. By Henry A. Stiff, Jr. 376
A High Temperature Gauge Glass for the Visual Observation of Critical Phenomena. By John R. Spencer 379
A Note on the Interrelationship Between Wetting and Non-Wetting Phase Relative Permeability. By M. R. J. Wyllie 381

INDEX 383

ERRATA

Volume 192, 1951

Technical Note 66, "FLUID DISTRIBUTIONS CHARACTERIZING GAS-LIQUID FLOW," by Walter Rose.

P. 373—Col. 2. Sentence beginning on line 8 should read, "This is because of the hyperbolic type variation between saturation and capillary pressure, which results in large changes in saturation with capillary pressure when the capillary pressure approximates the displacement pressure and small changes when maximum values of capillary pressure obtain."

T. P. 3020, "LABORATORY MEASUREMENTS OF RELATIVE PERMEABILITY," by Osoba, et al.

P. 47—Col. 1. Sentence beginning on next to last line should read, "Knowledge of this characteristic is extremely important in the prediction of the behavior of oil and gas reservoirs and of the ultimate recovery to be expected under various operating conditions.'

PETROLEUM BRANCH OFFICERS AND COMMITTEE CHAIRMEN

For the Year Ending February, 1952

CHAIRMAN

R. W. French
Sohio Petroleum Company
Cleveland, Ohio

VICE-CHAIRMEN

Paul R. Turnbull
La Gloria Corporation
Corpus Christi, Texas

Lincoln F. Elkins
Sohio Petroleum Company
Oklahoma City, Oklahoma

EXECUTIVE COMMITTEE

Paul R. Turnbull
R. W. French
Lincoln F. Elkins

John S. Bell
Humble Oil & Refining Company
Los Angeles, California

Harold Decker
Houston Oil Company of Texas
Houston, Texas

R. C. Earlougher
Earlougher Engineering Company
Tulsa, Oklahoma

Thomas C. Frick
Atlantic Refining Company
Corpus Christi, Texas

John R. McMillan
Fullerton Oil Company
Pasadena, California

Dean H. Sheldon
Consulting Engineer
South Pasadena, California

John E. Sherborne
Union Oil Company of California
Brea, California

R. E. Heithecker, *Treasurer*
Seaboard Oil Company
Dallas, Texas

MEMBERSHIP COMMITTEE

Jack H. Beesley, *Chairman*
Baroid Sales Division
Tulsa, Oklahoma

PRODUCTION REVIEW COMMITTEE

E. W. Berlin, *Chairman*
Socony-Vacuum Company
New York, New York

Vice Chairmen

R. B. Gilmore, *Domestic*
DeGolyer & MacNaughton
Dallas, Texas

A. H. Chapman, *Foreign*
Arabian American Oil Company
New York, New York

PUBLICATIONS COMMITTEE

J. M. Bugbee, *Chairman*
Shell Oil Company
Houston, Texas

John P. Hammond, *Vice-Chairman*
Amerada Petroleum Corporation
Tulsa, Oklahoma

TECHNOLOGY COMMITTEE

Earl M. Kipp, *Chairman*
The California Company
New Orleans, Louisiana

Vice Chairmen

Jack H. Abernathy, *Drilling*
Big Chief Drilling Company
Oklahoma City, Oklahoma

Henry L. Waszkowski, *Production*
Magnolia Petroleum Company
Healdton, Oklahoma

E. G. Trostel, *Natural Gas*
DeGolyer & MacNaughton
Dallas, Texas

Wayne E. Glenn, *for California*
Continental Oil Company
Los Angeles, California

ECONOMICS COMMITTEE

Fred E. Simmons, *Chairman*
Consulting Engineer
New Orleans, Louisiana

STAFF OF THE PETROLEUM BRANCH IN DALLAS

Executive Secretary
Joe B. Alford

Editor, *Journal of Petroleum Technology*
Jess E. Adkins

PETROLEUM BRANCH, AIME

Established as a Division March 24, 1922
Established as a Branch in 1948

PAST CHAIRMEN

Ralph Arnold, 1922
E. DeGolyer, 1923, 1924
F. Julius Fohs, 1925, 1926
John M. Lovejoy, 1927
A. W. Ambrose, 1928
Joseph B. Umpleby, 1929
C. V. Millikan, 1930
C. E. Beecher, 1931
Earl Oliver, 1932
W. E. Wrather, 1933
H. D. Wilde, Jr., 1934
Harry H. Power, 1935
Hallan N. Marsh, 1936
M. Albertson, 1937
George B. Corless, 1938
W. H. Geis, 1939
T. V. Moore, 1940
Eugene A. Stephenson, 1941
Harry P. Stoltz, 1942
C. A. Warner, 1943
W. S. Morris, 1944
M. L. Haider, 1945
H. F. Beardmore, 1946
Howard C. Pyle, 1947
Irwin W. Alcorn, 1948
Lloyd E. Elkins, 1949
John E. Sherborne, 1950
R. W. French, 1951

THE ANTHONY F. LUCAS FUND AND MEDAL

In 1936 the Institute established the Anthony F. Lucas Gold Medal, to be awarded from time to time "for distinguished achievement in improving the technique and practice of finding and producing petroleum." These awards are sponsored by the Petroleum Branch.

Captain Lucas was a pioneer in the oil industry, one of the early wildcatters and a leading mining and petroleum engineer. He was famous as the discoverer of Spindletop. He became a member of the Institute in 1895 and in 1913 was the first Chairman of the Petroleum and Gas Committee of the Institute, the forerunner of the present Petroleum Branch. He also headed the Committee in 1914, 1917, and 1918.

Medals Awarded

J. Edgar Pew, February 1937
Henry L. Doherty, February 1938
E. DeGolyer, February 1940
Conrad (posthumously) and Marcel Schlumberger, February 1941
John Robert Suman, February 1943
Charles Van Ormer Millikan, February, 1944
James Ogier Lewis, 1946
William Noble Lacey, 1947
Wallace Everette Pratt, 1948
William Embry Wrather, 1950

Committee on Awards

Howard C. Pyle, *Chairman*

Until Feb. 1952	*Until Feb. 1953*	*Until Feb. 1954*	*Until Feb. 1955*
A. R. Denison	J. E. Brantly	Lloyd E. Elkins	Raymond F. Baker
M. Gordon Gulley	Fred M. Nelson	W. H. Geis	M. L. Haider
Howard C. Pyle	Wallace E. Pratt	John H. Murrell	John E. Sherborne

Members Ex Officiis

J. J. Forbes	C. L. Moody	W. M. Peirce	Frank M. Porter
Director, B. of M.	President AAPG	President AIME	President API

PETROLEUM BRANCH CERTIFICATE OF SERVICE

Established in 1948, the Petroleum Branch CERTIFICATE OF SERVICE is awarded to recognize and show appreciation for exceptional services of Members to the Branch.

CERTIFICATES AWARDED

EUGENE A. STEPHENSON, 1948

FRED B. PLUMMER, 1948
(posthumously)

EARL OLIVER, 1948

E. JULIUS FOHS, 1949

JOSEPH B. UMPLEBY, 1949

STUART E. BUCKLEY
(Certificate to be presented in 1952)

T.P. 2940

AN INVESTIGATION OF THE ELECTROKINETIC COMPONENT OF THE SELF POTENTIAL CURVE

M. R. J. WYLLIE, GULF RESEARCH AND DEVELOPMENT CO., PITTSBURGH, PENN., MEMBER AIME

ABSTRACT

Eight laboratory-prepared aqueous base drilling muds representing common mud types, and 15 aqueous base drilling muds sampled in the field, have been used in an experimental investigation of the relationship between the streaming potential developed across a mud filter cake and the differential pressure causing filtrate flow.

It has been established that the relationship is of the form, $E_S = kP^y$, where E_S is the streaming potential, P the differential pressure and k and y are constants for any particular mud system at constant temperature. Beyond a certain minimum thickness this relationship is independent of filter cake thickness. Experiment has shown that both k and y are temperature dependent parameters and that in certain mud systems there is a critical value of P above which the simple relationship $E_S = kP^y$ ceases to hold. The constant k tends to be a function of the mud resistivity at 77°F, but the exponent y has not been found to be related to any commonly measured mud property.

Certain field experiments are described which serve to demonstrate that the total SP (self potential) developed opposite a formation may be quantitatively accounted for as the algebraic sum of an electrochemical potential and an electrokinetic potential. A chart to permit the simple use of mean solution activities in the interpretation of electrochemical SP data is given and its use described.

Various field methods for computing the electrokinetic SP component of the total SP are considered and rejected as being unduly complicated and inaccurate. It is shown that the employment of low resistivity drilling muds is essential if optimum accuracy is desired in the use of the S.P. curve for the purpose of computing connate water salinities by the electrochemical SP method. The use of such low resistivity drilling muds is accordingly recommended.

INTRODUCTION

In a previous paper[1] a quantitative analysis of the electrochemical component of the SP (self potential) curve was made and it was shown that the electrochemical* emf, E, could be expressed as $E = 2\bar{t}RT/F \ln a_c/a_m$, where $\bar{t}$ is the transference number of the chloride ion, R is the gas constant, T the absolute temperature of the formation water and mud, a_c the mean activity of the connate water (assumed to be sodium chloride) and a_m the mean activity of the mud (as sodium chloride). The essential accuracy of this expression was confirmed by an investigation[2] of the SP kicks opposite sands of known water salinity. The logs examined had been routine runs in oil wells in a number of Mid-Continent states. Further confirmation of the original analysis of the electrochemical SP is implicit in the paper by Tixier[3] wherein a relationship between the SP and the ratio of connate water and mud resistivities, based only on field data, is given. Allowing for the fact that mud and connate water resistivities were used instead of activities, and that electrokinetic effects were ignored, the constant reported by Tixier is essentially $2\bar{t}RT/F$.

The error involved in the universal substitution of resistivities for activities will receive further reference below. Possible reasons for the fact that the electrochemical properties of shales do not appear to be significantly dependent upon either the nature or the quantity of cation exchange materials, such as clays, they contain has been considered at some length by Wyllie and Patnode.[4] In the same paper, the probable effects of shale thickness and compaction on electrochemical efficiency, and hence the inherent difficulty of obtaining reliable laboratory-scale data, were also pointed out. However, it is

---

[1] References given at end of paper.

Manuscript received in the office of the Petroleum Branch Aug. 9, 1950. Paper presented at the 1950 Petroleum Branch Fall Meeting in New Orleans Oct. 4-6.

*It seems desirable to make specific reference to the effect of pressures and temperatures on electrochemical reactions since the effect of pressure, particularly, seems to be either ignored or confused.[6] The effect of pressure is only marked in those electrochemical reactions involving gases e.g. H_2 gas electrode. Otherwise, the effects are dependent upon volume changes which are negligibly small at the pressures involved in drilling. The effect of pressure on resistivities depends upon concentration of the solute, but generally does not exceed ±5 per cent.[7] The effect of pressure on activities is discussed by Robinson and Harned[8] and is shown to be very small e.g. for $NaCl$ the activity coefficient is only 5 per cent greater at 15,000 psi than at atmospheric pressure. Similarly, Robinson and Harned show that the effect of temperature on activity can be neglected from the logging standpoint.

clear both from a theoretical consideration of the energies involved and from the detailed analysis of the potential and current distributions in a borehole made by Doll[5] that log-recorded electrochemical potentials should be, at best, only asymptotic to the theoretical values.

Thus, from the thermodynamical standpoint, the energy available for release and manifestation as an electromotive force is dependent upon the difference in chemical potential between the mud fluid and connate water. Irrespective of the mechanism whereby the electrochemical potential is set up, this chemical potential difference defines the maximum emf of the cell, and this emf will in turn be measurable at its maximum value only under conditions of no current flow and thus no internal ohmic potential drops in the electrochemical cell.

Such a measurement may be achieved in the laboratory by balancing the cell emf against an equal and opposite emf by the use of a potentiometer. In the field, however, the normal method of logging the SP is contingent upon current flowing in the borehole, and the fact that this must always preclude precise agreement between the measured SP and the actual emf of the electrochemical cell has been fully discussed by Doll.[5] However, under conditions of adequate bed thickness and low bed resistivities, the difference between the measured and theoretical emf's is neglibly small. The recently described Selective SP logging technique[15] may also serve to facilitate quantitative SP calculations by rendering formation geometry less important as a factor affecting the magnitude of the recorded SP. The presence of shale in the formation, which may be considered as an extreme example of the thin bed difficulty, also serves to lower the measured SP below the true value of the emf causing current flow. Thus, it may be said, that while there is a number of reasons to explain log-recorded SP values which are less than the theoretical electrochemical emf's, any errors which are markedly in the opposite sense and which exceed any reasonable errors resulting from errors in the determination of the appropriate mud and connate water activities must betoken the existence of an additional potential. Such marked positive errors* have been observed in tests of the efficacy of the SP method of determining connate water resistivity, particularly striking examples of this effect being noted[2] in the case of the McClosky producing zone in Illinois where the SP was some 40 mv larger than anticipated. The possibility that electrokinetic or streaming potentials were sometimes of greater importance than had been first believed was therefore considered, and experiments to investigate the phenomenon were undertaken.

NATURE AND LOCATION OF ELECTROKINETIC POTENTIALS

Electrokinetic effects of all types result when there is relative movement between a solid and a liquid. The effects are generally ascribed to the fact that there is a potential difference at the solid/liquid interface at which movement occurs, this potential being known as the zeta potential. If this zeta potential results from the presence of electrically-charged layers opposite in sign at the surface of separation of the solid and the liquid, then the application of a pressure which causes movement of the liquid past the solid must result also in the movement of a charge past the solid surface. Such a charge movement represents the flow of current and a potential is immediately set up of a magnitude which follows Ohm's Law. Numerically this streaming potential, as it is called, may be calculated if both the rate and magnitude of the charge moved and the overall resistance of the system are calculable. Since the phenomenon is ultimately dependent upon the magnitude of the zeta potential, a quantity which cannot be theoretically calculated, it has been usual to measure streaming potentials in systems of sufficient simplicity to enable all variables other than the zeta potential to be independently measured, and thus to compute the zeta potential itself. For simple systems and particularly those for which the hydraulic and electrical paths are identical, it has been established that the streaming potential is directly proportional to the pressure causing flow. For any particular zeta potential the streaming potential is also directly proportional to the resistivity of the liquid being flowed (neglecting surface conductance effects and assuming that the solid material past which the liquid flows is a non-conductor). However, since the zeta potential is itself a complex function of the solute concentration and hence the resistivity of the liquid flowing, no extrapolation of the streaming potentials determined for solutions of one resistivity can be made even to solutions of identical chemical nature but of different resistivity.

The fact that the movement of an electrolyte through a solid such as a capillary tube or a more complex system such as an aggregate of sand grains or a fritted diaphragm gave rise to a potential had been noted by C. and M. Schlumberger and E. G. Leonardon,[9] and in their pioneer work on electric logging they first ascribed the SP solely to such electrokinetic effects. In a later paper[10] the same workers modified their original view and the SP was attributed to a combination of electrokinetic and electrochemical effects. Thus, it would appear that at a very early date the principle components of the SP curve had been correctly elucidated. Published investigations of streaming potential phenomena involved in electrical logging are meager but are most extensive for the electrokinetic phenomena obtaining in the logging of cable-tool drilled wells. Since the seat of the major electrokinetic effects appear to be entirely different in rotary-drilled and cable-tool drilled wells, it will suffice to say here that Gillingham[11] in an investigation of the effect of varying the borehole fluid pressure in cable tool wells in Pennsylvania and New York State, found that the ordinary negative SP became more negative when the borehole pressure was increased. More recent analogous experiments by Pirson[12] in the Bradford field gave similar results except that both increased and decreased SP kicks were observed to result from increasing the differential pressure between the borehole fluid and the formations. These latter results point to the existence of positive and negative zeta potentials and not to a consistent negative zeta potential (i.e., solid surface negatively charged with respect to water) as found by Gillingham.

The fact that a deliberate increase in borehole mud pressure in the logging of a conventional rotary-drilled well tends to increase the magnitude of the usual negative SP kick is well-known and has been remarked upon in the literature.[6,13] The location of the streaming potential in a rotary-drilled well in which the formations have been mudded-off with an appreciable thickness of filter cake is not, however, the same as that in a cable-tool drilled well where the formation faces are unprotected by a relatively impervious mud cake. In the latter case, the pressure differential between the hydrostatic pressure of the mud in the hole and the formation pressure results directly in movement of borehole fluid into the formation.

In addition, although not invariably true, the resistivity of the water used in cable-tool well experiments is much higher than the resistivity of high-resistivity rotary drilling muds. The consequence is that the streaming potential is set-up principally by the flow of the high resistivity borehole fluid through the pores of the formation rock matrix and the magnitude of this potential is a function of the zeta potential between the moving borehole fluid and the rock surface. Thus, the streaming potential may here be said to be somewhat dependent upon the nature of the formation solids. In addition, the high resistivity of the flowing borehole fluid contributes to a large streaming potential since, as noted above, by Ohm's Law the streaming potential, for any value of the zeta potential, is directly proportional to the resistivity of the fluid flowing.

---

*Positive in terms of numerical value. Note that the sign of the SP is generally negative.

In a rotary-drilled well mudded-off by a mud filter cake, very different conditions obtain. Here the permeability of the filter cake may be only 10^{-3} md, whereas the permeability of the formation, if of commercial interest, is unlikely to be less than 10 md. In consequence, by far the greatest pressure drop between the hydrostatic pressure of the borehole mud column and the formation pressure occurs across the filter cake, less than 1 per cent of the drop occurring between the formation face of the filter cake and the formation itself. The consequence of this pressure distribution is that the major portion of any streaming potentials occurring in a rotary-drilled well, since they are a function of pressure distribution, must occur across the mud filter cake, any streaming potential component occurring in the formation rock matrix itself being negligible by comparison. A similar conclusion appears to have been reached by Mounce and Rust,[6] by Doll[13] and, originally, by Bayle[14] in 1935. Thus, in rotary-drilled wells, the streaming potential will be predominantly a function of the properties of the drilling mud and its filter cake and not of the formations.

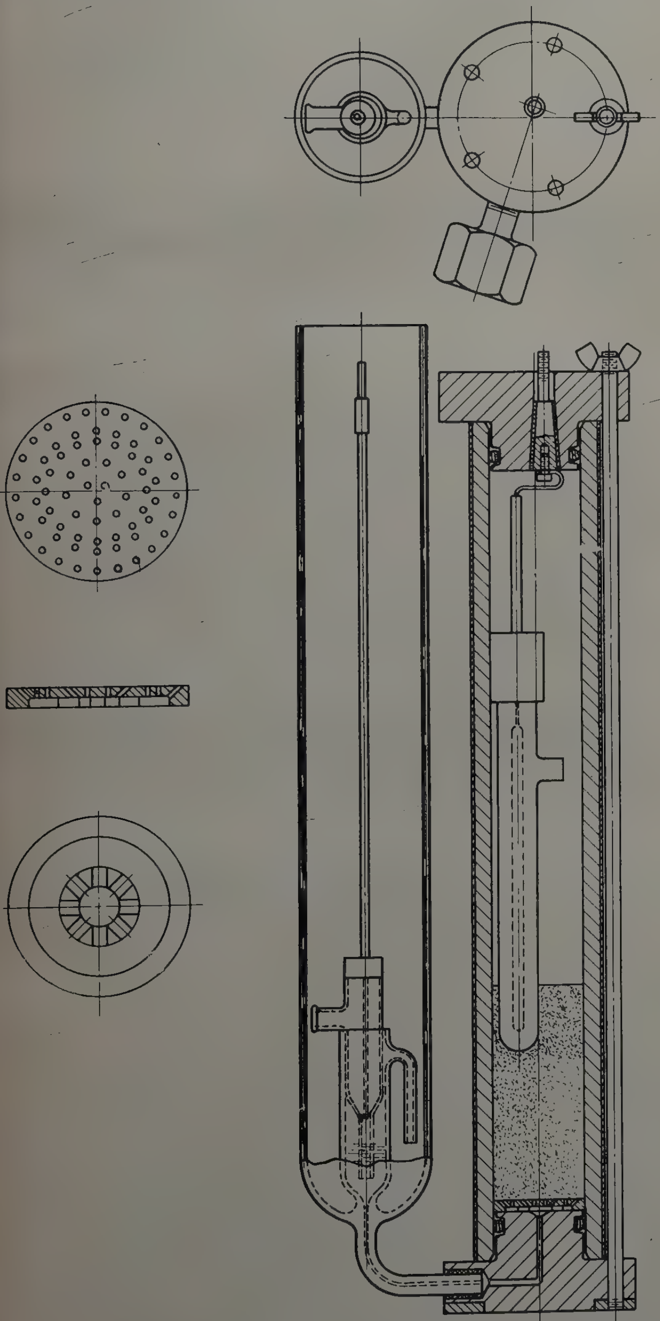

FIG. 1 — CROSS-SECTION OF STREAMING POTENTIAL CELL SHOWING ARRANGEMENT OF CALOMEL ELECTRODES.

The only previous experimental measurement of the streaming potential resulting from the flow of a mud filtrate through its own filter cake appears to have been carried out by Mounce and Rust[6] who observed, for what was described as a typical drilling mud, a 20 mv streaming potential for a 200 psi differential pressure between the mud and its filtrate.

EXPERIMENTAL

Apparatus

The final apparatus developed is shown in its high-temperature form in Fig. 1. Basically the apparatus consists of a 10½-in. long Nylon cylinder of a 3/16-in. wall thickness and a 1-in. internal diameter. To overcome high-temperature creep this cylinder is a tight fit in a 1/16-in. thick cylindrical steel jacket. The lower end of the cylinder is closed by a flanged Lucite plug, pressure tightness being ensured by the use of a neoprene "O"-ring. The Lucite plug is drilled with 1/16-in. diameter holes in the vertical and horizontal directions as shown in Fig. 1 to permit flow of mud filtrate through the Lucite plug and external glass capillary tube into the jacketed external glass-filtrate reservoir. The glass-capillary tube is retained in the plug by the aid of a tygon gasket. Within the cylinder and resting on the Lucite plug is an asbestos-base Bakelite filter disc. The construction of this disc is shown in a detail in Fig. 1.

The top of the cylinder is closed by a flanged stainless steel plug, pressure tightness again being achieved by the use of a neoprene "O"-ring. Through the top of the stainless steel plug passes a conical stainless steel pin insulated from the plug by means of a Nylon sleeve. To the lower end of this pin is soldered a connection to a 5-in. Beckman calomel electrode incorporating an asbestos-wick slow potassium chloride leak. The tip of the electrode is arranged to be about 2-in. from the filter disc when the apparatus is assembled. The terminal connection at the outer end of the Nylon insulated pin is connected to the potential measuring equipment. In addition to the electrode connection, the stainless steel plug may be connected through standard pipe fittings to a source of high-pressure gas.

In routine operation the lower Lucite plug is inserted in the cylinder and a disc of Whatman No. 42 filter paper is placed over the filter disc. About 3 to 4 in. of mud is then poured into the cylinder and the upper plug with attached electrode is inserted into the top of the cylinder. The protective rubber stopper over the side arm of the calomel electrode may conveniently be perforated with a small hole and left in place. The flanges of the upper and lower plugs are then pulled together by the tightening action of five wingnuts threaded on stainless steel rods.

A 2-in. Beckman calomel electrode with asbestos leak is lowered into the jacketed filtrate reservoir and the capillary tube with its tygon gasket pressed into the Lucite plug. This electrode is also connected to the potential measuring apparatus, consisting of a Leeds and Northrup Type *K* potentiometer and Leeds and Northrup thermionic amplifier No. 7673. The accuracy of this equipment is about ±0.1 mv.

Pressure is then applied by means of nitrogen gas to the space above the mud in the cylinder, provision being made in the gas line both for the regulation and for the measurement, by means of a calibrated 6-in. diameter 0 - 500 psig, of the pressure applied.

In high-temperature experiments the mud was warmed to approximately the correct temperature before insertion into the cylinder and the entire apparatus was lowered into a water bath thermostatically maintained within ±0.2°C of the required temperature.

For room-temperature experiments it was found to be more convenient to replace the steel-jacketed Nylon cylinder with a transparent Lucite cylinder of ¼-in. wall thickness. The outer jacket of the external glass filtrate reservoir was also dispensed with in these experiments.

While the general construction of the equipment and the reasons for the design adopted is straightforward, certain features deserve amplification. The final choice of calomel electrodes was only made after extensive tests of silver/silver chloride, lead/lead chloride and inert platinum electrodes had been made. The silver/silver chloride and lead/lead chloride electrodes, although workable in some cases, were found to be undesirably unstable. This is almost certainly a consequence of the heterogeneous nature of drilling muds and the resultant presence in solution of anions in addition to the chloride ion to which alone these electrodes are reversible. The fact that many muds are active oxidation-reduction systems made the use of inert electrodes impossible, the varying redox potentials in the mud and filtrate being superimposed on the streaming potential and leading to a prohibitive instability of the electrode zero.

The insertion of a calomel electrode with a slow-leak type saturated potassium chloride junction within the high-pressure cylinder has a number of advantages. No complex liquid connection leading from cylinder pressures of up to 500 psig to atmospheric is required and for obvious reasons the pressure causing potassium chloride leak into the mud remains merely the hydrostatic head of the potassium chloride solution within the electrode itself. This leak is almost negligible and contamination effects on the mud during the course of an experiment were not measurable. If the potential of the calomel electrode were a sensitive function of pressure, changes of potential caused by pressure would, of course, be algebraically added to the measured streaming potentials. However, the pressure dependence of the potential of a saturated potassium chloride calomel electrode is of the order of microvolts per atmosphere and can be neglected.

The use of the asbestos-base Bakelite filter disc to support the filtering medium employed was to avoid the presence of any metal in the system. As will be shown below, the geometry of the filtering medium does not appear to have any significant effect on the results obtained. The volume of the filtrate path from filter cake to external calomel electrode was kept to a minimum in order to complete the electrical circuit before a large volume of filter cake built-up. This design necessitated the use of a glass-capillary tube which might be considered objectionable as a possible source of streaming potential in series with any streaming effects across the mud filter cake itself. In practice, however, the rate of flow through this capillary tube is so slow, and the resistivity of the filtrates relatively so low, that no detectable streaming potentials exist.

Muds

It may justly be claimed that no two drilling muds are ever identical, and although this does not mean that modern muds cannot be roughly grouped according to their principal components and chemical additives, it does necessarily render rather difficult the choice of suitable muds for any limited series of experiments intended to obtain results of general applicability. With this in mind the following arbitrary selection was made. Eight muds were made for the writer by the mud section of Gulf Research and Development Co.'s Materials and Production Chemistry Division. These muds, although relatively artificial, covered a wide range of types and their preparation is given in detail in the Appendix. In addition, a number of other muds were obtained during routine field drilling operations. These latter muds were sampled at the flow nipple while the mud was being circulated prior to electric logging. The samples were hermetically sealed in cans or bottles and dispatched to the laboratory. In one instance, five mud samples were obtained at depths of 1,300 ft, 2,375 ft, 4,295 ft, 5,600 ft and 5,812 ft in the same well in order that an estimate of the changes occurring during drilling with the same basic type of mud could be studied. In all 15 different field muds from various geographical areas in the United States and abroad were available and were tested. The range covered by the laboratory and field samples included, in addition to more standard types, a silicate mud and two oil-emulsion muds. Details of the conventional mud properties of all the samples studied, including resistivities, are given in Tables I and II, as well as their common, if somewhat uninformative, field descriptions.

Table I

					GEL STRENGTH		CAKE PROPERTIES		RESISTIVITIES				
No.	Type of Mud	Weight lb/gal	pH	Viscosity cp.	Initial gms.	10-min. gms.	30-min. ml.	Cake ins.	64°F ohm-m.	Test Temp. ohm-m.	Slope	Intercept mv	Es for 500 psi
1	3% Starch in high pH mud	8.64	10.7	95.9	4	60	4.0	1/32	6.6	5.8	0.63	0.45	22.5
2	Fresh water clay	9.76	8.3	17.0	0	28	12.4	1/32	7.0	5.9	0.57	0.93	31.0
3	Oil emulsion	10.11	9.1	61.0	0	1	5.6	2/32	3.3	2.9	0.88*	0.125	20.5
4	Oil emulsion + 2% NaCl	10.0	8.3	101.0	81	81	11.1	2/32	0.6	0.52	0.78	0.05	6.5
5	Red lime mud	14.6	12.0	52.5	0	48	28.4	5/32	0.32	0.27	0.83	0.046	8.0
6	Saturated salt water mud	13.75	6.4	50.9	5	36	3.4	1/32	0.08	0.07	0.66	0.017	1.05
7	6% bentonite in distilled water	8.7	8.6	42.7	1	36	13.1	2/32	6.6	5.3	0.70**	0.80	28.0
8	6% Zeogel in 30% NaCl solution	10.1	7.1	10.0	0	0	60.0	5/32	0.06	0.05	0.74	0.01	1.0

*to 140 psi
**to 100 psi

Table II

					GEL STRENGTH		CAKE PROPERTIES		RESISTIVITIES				
No.	Type of Mud	Weight lb/gal	pH	Viscosity cp.	Initial gms.	10-min. gms.	30-min. ml.	Cake ins.	64°F ohm-m.	Test Temp. ohm-m.	Slope	Intercept mv	Es for 500 psi
9	Caustic quebracho, New Mexico	9.9	8.3	18.6	0	16	19.0	4/32	0.58	0.52	0.81	0.105	16.0
10	Caustic quebracho driscose, Oklahoma — 1,300 ft	9.7	11.0	57.2	8	20	5.6	2/32	1.12	0.93	0.78	0.19	23.5
11	Caustic quebracho driscose, Oklahoma — 2,375 ft	9.9	11.3	21.5	0	3	6.2	2/32	1.11	0.92	0.89	0.09	23.0
12	Caustic quebracho driscose, Oklahoma — 4,295 ft	9.7	10.2	9.4	0	1	6.9	2/32	1.31	1.15	0.74	0.21	21.0
13	Caustic quebracho driscose, Oklahoma — 5,600 ft	10.2	10.4	43.5	3	10	4.5	1/32	1.41	1.25	0.82	0.105	27.0
14	Caustic quebracho driscose, Oklahoma — 5,812 ft	10.2	9.2	25.1	0	3	5.2	2/32	1.28	1.12	0.90	0.09	24.0
15	Natural, Venezuela	10.1	9.0	42.7	0	1	9.0	3/32	2.3	2.1	0.84	0.20	44.0
16	Natural, Venezuela	10.2	9.2	45.0	0	2	8.0	2/32	8.0	7.0	0.83	0.28	60.0
17	Chemical, Mississippi	10.1	8.0	69.3	..	..	14.0	3/32	3.7	2.74	0.71	0.36	30.5
18	Lime-caustic-quebracho-impermex, Mississippi	10.85	12.6	15.8	0	5	8.6	1/32	1.55	1.31	0.80	0.24	33.0
19	Lime-caustic-quebracho-impermex, Mississippi	10.95	12.5	17.5	0	0	9.0	1/32	1.4	1.18	0.80	0.21	30.0
20	Water-base gel, Mississippi	9.5	7.8	..	..	..	17.6	3/32	2.7	2.23	0.71*	0.33	22.5
21	Chemical, starch base, Mississippi	11.1	9.4	37.1	0	34	12.5	4/32	1.3	1.07	0.90	0.16	38.5
22	Silicate, Texas	14.9	10.0	>120	5	75	30.4	8/32	0.33	0.28	0.59	0.029	1.15
23	Salty, Denmark	10.0	7.7	13.1	0	1	34.2	4/32	0.06	0.058	..	..	Negligible

*to 200 psi

Tests

All muds were first tested at room temperature, the potential difference between the two calomel electrodes being recorded for increasing gauge pressures over a range from 0 - 500 psi. In nearly all cases, readings were also taken with decreasing pressures. In most experiments, little difficulty was found in returning to the original calomel electrode potential difference on releasing the pressure to atmospheric, but it may be said that unless the original potential is attained within the reproducibility of the potassium chloride junction potentials, the results of the run must be disregarded. In certain instances, alterations of as much as 20 mv were observed in the electrode zero, this potential being destroyed by washing the end of the internal calomel electrode with distilled water. It was apparent that this phenomenon only occurs when a particle of clay lodges firmly across the tiny entrance to the potassium chloride leak in the electrode tip. The clay particle then separates a saturated potassium chloride solution from mud filtrate with the consequence that an electrochemical cell is set-up which, although inefficient, is still capable of setting up a very appreciable emf when separating solutions of widely differing activities.

In high temperature experiments, it must be noted that in addition to the mud, both the internal and external calomel electrodes must also attain temperature equilibrium. If this is not achieved, a drift of the electrode zero will occur owing to changes occurring in the *KCL* concentrations within the electrodes.

Plots of total filtrate versus pressure for given times of filtration were obtained by using substantially the same apparatus as in Fig. 1. The capillary tube with filtrate reservoir was, however, replaced with a short narrow capillary tube bent downward so as to deliver into a 5 cc. graduate vessel.

In experiments involving the building-up of the filter cake on a sandstone basis the filter disc was removed from the cylinder and replaced with 5 mm thick discs of a consolidated Pennsylvania sandstone having a permeability of *c* 300 md and porosity of *c* 0.20. These sandstone discs proved to be force fits in the Lucite cylinder when cut with a 1-in. diamond drill and no circumferential sealing proved to be necessary.

The range of pressure differentials which it was found convenient to cover extended from 0 to 500 psi. This pressure range is equivalent to hole depths down to 7,500 ft in rotary-drilled wells assuming normal bottom-hole pressures and mud weights up to about 75 lb per cu ft. In modern deep drilling, particularly if heavy muds are carried and bottom-hole pressures are abnormally low, differential pressures exceeding 2,000 psi occur. However, it was felt that 500 psi covered directly a reasonably extensive range of drilling conditions and that any conclusions based on observations over this pressure range would in all probability be applicable also under conditions of higher pressure differentials. The results obtained have not led to any serious modification of this supposition.

RESULTS

Preliminary experiments were designed to investigate the streaming potential effects occurring when mud filtrate flowed through the low-pressure side of the apparatus at velocities appropriate to actual filtration conditions. With this object filtrates were obtained from muds numbered 2, 6 and 17 in Tables I and II: these filtrates thus cover a wide range of resistivities. The apparatus was assembled with a Whatman No. 42 filter paper in place and with filtrate half filling the cylinder and entirely filling the channels in the lower Lucite plug and capillary leading to the external filtrate reservoir. The filtrate was then permitted to flow under gravity head and the potential between the calomel electrodes determined both in the absence of flow and while flow occurred. Although the rates of flow under these conditions were found to be far greater than that obtaining during any filtration experiment, no measurable streaming potentials could be detected.

An investigation was then made of the effect of employing the convenient filter disc and filter paper as filter bed as opposed to the more realistic consolidated sandstone. Experi-

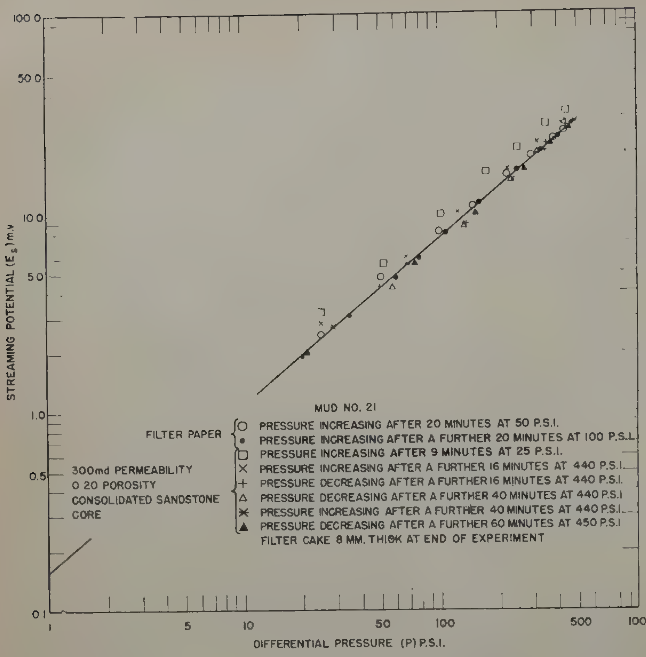

FIG. 2 — EFFECT OF FILTRATION TIME AND NATURE OF FILTER BED MATERIAL ON STREAMING POTENTIAL/DIFFERENTIAL PRESSURE RELATIONSHIP.

ments have been reported[16] which show that the effect of the filter bed material on the rate of filtration of a number of drilling muds, while small, is not entirely negligible.

Fig. 2 shows the results obtained when mud No. 21 was filtered first with the filter disc and Whatman's No. 42 filter paper and then with a 5 mm thickness of consolidated Pennsylvanian sandstone as the filter bed. The results have been plotted in detail on a log-log scale since this type of plot has invariably been found to give remarkably good straight line correlations between pressure differentials inducing flow and the streaming potentials set up. Fig. 2 graphically illustrates a number of points which have been found to be characteristic of most of the muds investigated. The initial plot of streaming potential against pressure differential obtained when sufficient filtrate has been evolved to complete the electrical circuit between the internal and external calomel electrodes is generally a good straight line on a log-log plot but is displaced relative to the points obtained at later stages in the filtration process. While not marked in Fig. 2, these first points may also yield a line having an appreciably different slope from those obtained in later plots. As the filtration process is prolonged and the filter cake thickens, the reproducibility of the plot improves and a stage is rapidly reached when continued filtration makes no appreciable difference to the plot obtained. Fig. 2 is also characteristic of those muds which appear to be entirely reversible, i.e., essentially the same plot is obtained whether the recording is done with increasing or decreasing pressure differentials. Certain muds, however, as will be shown below, are less satisfactory in this respect. In all the muds tested the zeta potential was found to be negative, i.e., the filtrate was positive with respect to the mud.

Fig. 2 shows that after a small thickness of filter cake has been built-up, there is little significant difference between the results obtained on a filter bed of filter paper and one of sandstone. This was confirmed by additional experiments and in consequence the data recorded in this paper are for filter cakes built-up on the filter disc and Whatman's No. 42 filter paper as a filter bed. It may be noted that in Fig. 2 the thickness of the filter cake on the sandstone at the end of the experiment was found to be 8 mm. The fact that beyond a small limiting thickness of filter cake the streaming potential proved to be independent of cake thickness is of interest both theoretically and from a practical standpoint. In this work, experiments on any one mud were continued until reproducible plots were obtained which were independent of continued filtration. The slopes of the best lines drawn through the points plotted for increasing pressure differentials were measured as well as the intercept defining the streaming potential at 1 psi differential pressure (0.16 mv in Fig. 2). These data are recorded in Tables I and II.

Fig. 3 shows an example where the plot of streaming potential versus pressure differential is markedly different when the pressure is decreased from that obtaining when the pressure is increased. This phenomenon is almost certainly a function of the recovery time of a compressible filter cake when the pressure is released. This may be qualitatively shown by prolonging the period of waiting at any pressure as the pressure is diminished before a potential measurement is made. A slow change of potential in the direction of coincidence with the value obtained on an increasing pressure plot is noted. It was not, however, considered generally necessary to await the attainment of equilibrium in this manner since satisfactory plots could be readily obtained by increasing the pressures. It may be noted that Fig. 3 is evidence that at zero pressure the filter cake returns fairly rapidly to a condition characteristic of this pressure since increasing the differential pressures in the final run reproduced the original slope and position of the linear plot. After the necessary pressure reduction from 480 psi to zero had been made, there was a pause of only two minutes before the pressure was incrementally increased to make this run.

With one exception, all the muds tested attained equilibrium at a particular differential pressure at room temperature as the differential pressures were increased within a time less than that necessary to balance the potentiometer and make a reading. The exception was the laboratory prepared fresh water clay mud (No. 2). When testing this mud, a slow drift

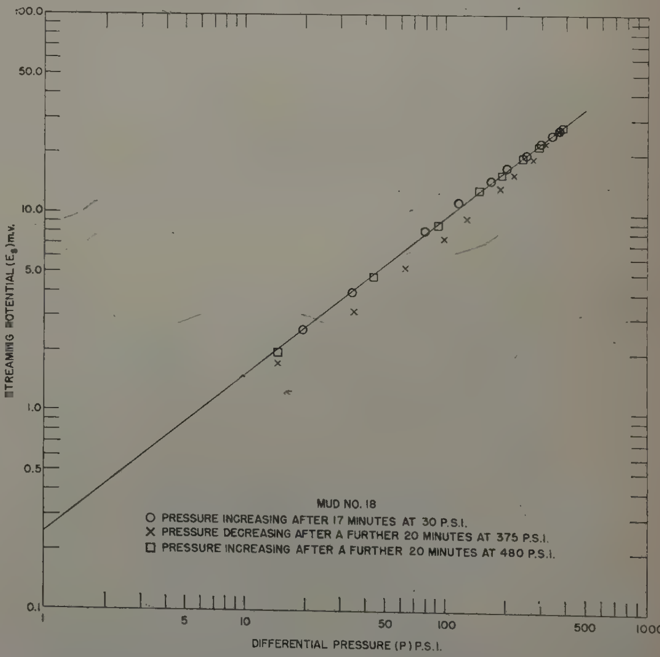

FIG. 3 — EXAMPLE OF A MUD SHOWING SLOW EQUILIBRIUM ATTAINMENT AS DIFFERENTIAL FILTRATION PRESSURE DECREASES.

occurring over a period of about 30 seconds was noted before an equilibrium steady potential could be measured. The particular reasons for the exceptional behavior of this mud are not clear.

Several muds gave at room temperature, a linear plot on log-log scales up to a certain pressure differential and beyond this pressure differential the slope of the line changed rather abruptly. Examples of this effect, which was quite reproducible, are shown in Figs. 4 and 5. Plotted also on these figures are the squares of the total filter loss in ccs occurring in constant time at various constant applied pressure differentials. For comparison, Fig. 6 gives the same type plots for a mud which showed a linear log-log relationship between streaming potential and pressure differential. It will be observed that breaks in the straight-line log-log plots of streaming potential are also accompanied by breaks in the filtrate loss plots, although the pressures at which the breaks occur in Fig. 4 do not appear to be identical. In this example, separate runs of the filter loss occurring in two different times were made. Fig. 4 is particularly interesting, inasmuch as the filtrate loss in a given time does not increase with increasing pressure of filtration, whereas the streaming potential shows a marked increase as the pressure increases over the same range. Further experiments have confirmed the fact that a break in the slope of the log-log plot of streaming potential versus pressure differential also involves a break in the log-log plot of filtrate volume per unit time against constant filtration pressure.

Fig. 7 is a composite plot of the best correlations found between streaming potential and pressure differential at room temperature for all the muds tested and serves to show the very considerable influence of the nature of the mud on the magnitudes of the streaming potentials induced by the same range of pressure differentials.

Fig. 8 is a plot of the intercept of the extrapolated straight lines with the ordinate at 1 psi, against mud resistivity. Although the scatter of points is fairly considerable, it will be observed that there is a clear correlation between the value of this intercept and the resistivity of the mud at the temperature of testing. This temperature was approximately 77°F in all cases.

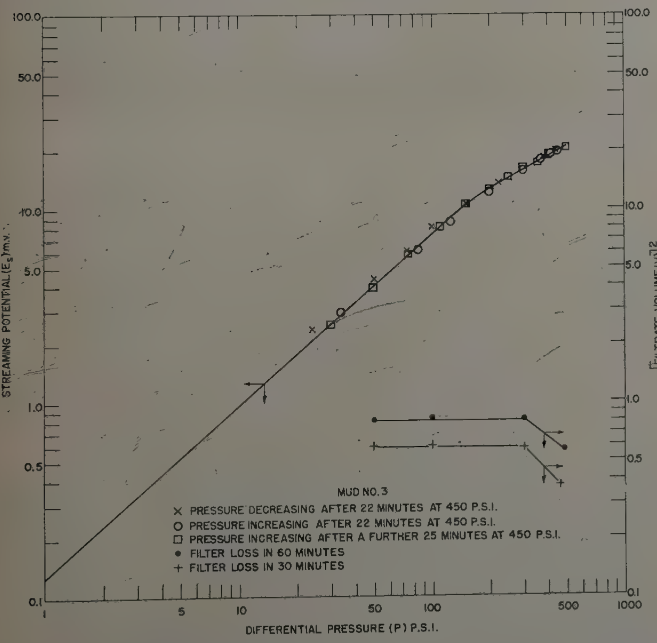

FIG. 4 — EXAMPLES OF MUD SHOWING BREAKS IN STREAMING POTENTIAL/DIFFERENTIAL PRESSURE AND (FILTRATE VOLUME)^2/DIFFERENTIAL PRESSURE LINEAR PLOTS.

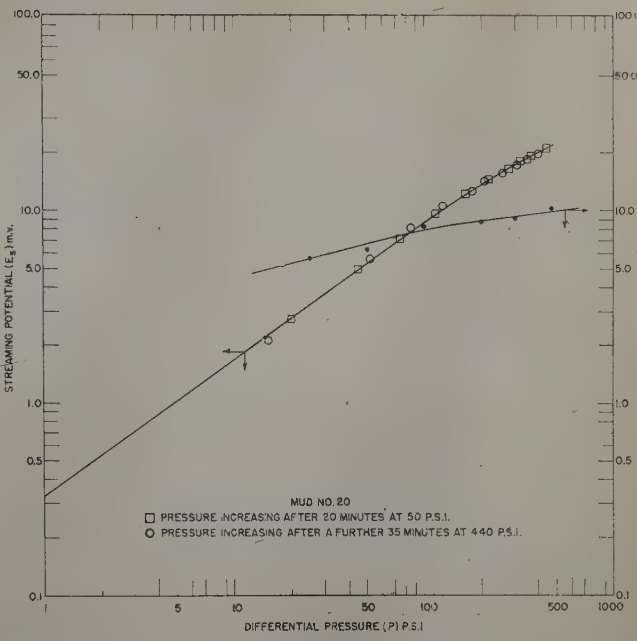

FIG. 5 — EXAMPLE OF MUD SHOWING BREAKS IN STREAMING POTENTIAL/DIFFERENTIAL PRESSURE AND (FILTRATE VOLUME)^2/DIFFERENTIAL PRESSURE LINEAR PLOTS.

Streaming potential measurements at temperatures above atmospheric were made on six of the available muds. The results obtained are shown in Figs. 9, 10, 11, 12 and 13. The securing of data at elevated temperatures proved to be somewhat more difficult and tedious than had been the case in the room temperature work. In almost all tests, the attainment of an equilibrium streaming potential at a particular pressure differential was found to be markedly slower than at room temperature. This slowness seemed to become more evident as the temperature of measurement increased and in this respect the behavior of all muds resembled the previously noted behavior at room temperature of mud No. 4. In spite of this difficulty, reproducibility was satisfactory and the variation in the slopes of the linear plots and particularly the breaks in these slopes (noted in Fig. 10) are believed to be genuine.

FIELD TEST

A field test suitable for establishing that the total SP opposite any formation is satisfactorily accounted for by the algebraic sum of electrochemical and electrokinetic potential effects must be performed under rather carefully controlled conditions if it is to be deemed reliable. In particular, it is necessary to measure with care the salinity of the connate water in the formation of interest, to determine accurately both the formation bottom-hole pressure and the actual hydrostatic head of mud in the hole, and to ensure that the formation thickness, resistivity, freedom from shale interbedding and lack of filtrate invasion all fulfill the requirements[5] for maximum SP development.

These conditions were satisfactorily achieved in a Mid-Continent well where the probable existence of two thick and clean water sands had been established from observations in adjacent wells. In the test well these two sands were diamond cored and the cores examined for presence of shale interbedding or interstitial clays. Although some minor shale streaks were present, both cores were substantially clean, somewhat friable sands, with formation factors of about 12 over thicknesses of 50 ft or more in each case. The SP kicks opposite these sands were also of the flat-topped kind.[2]

At the cessation of diamond coring in each sand, a packer was run on tubing in the rathole and the formation water produced by swabbing the well until the fluid produced gave constant readings of density and resistivity. It is believed that excellent samples of the formation waters were obtained by this technique.

The bottom-hole pressures and temperatures and the hydrostatic head of mud opposite the center of each tested formation were also determined, and a sample of the mud in the hole was in each case secured just prior to the running of the electric logs. The muds secured were Nos. 10 and 11 in Table II. The essential data are given in Table III.

Fig. 14 shows a convenient method of plotting *NaCl* activity, resistivity and salinity data on the same curve so as to facilitate computation of the required activities from the usual salinity and resistivity data. The necessary mean activity coefficients were taken from Latimer,[17] while the resistivity-salinity data are from the International Critical Tables, interpolations being made where necessary. To plot this curve, the mean activity for any concentration of *NaCl* is determined from Latimer's activity coefficient data. These activities are plotted against the resistivity of the corresponding sodium chloride solution at a temperature of 64°F, to give the dashed line shown. Since activity is substantially independent of temperature,[8] it follows that by moving across the chart from the dashed line parallel to the abscissa, the concentration of *NaCl* corresponding to the *NaCl* activity indicated on the upper scale is obtained when the solid 64°F line is intersected. The resistivity of a solution of this activity at any other temperature is then found in the usual manner by moving downwards parallel to the resistiviy axis to intersect the line of appropriate temperature. To find activity from a resistivity measurement (assuming the solution to be *NaCl*) this procedure is reversed. Thus, from the data in Table III, the activity of a 32,232 mg./L. solution is approximately 0.36. While that of a 156,350 mg./L. solution is approximately 1.65.

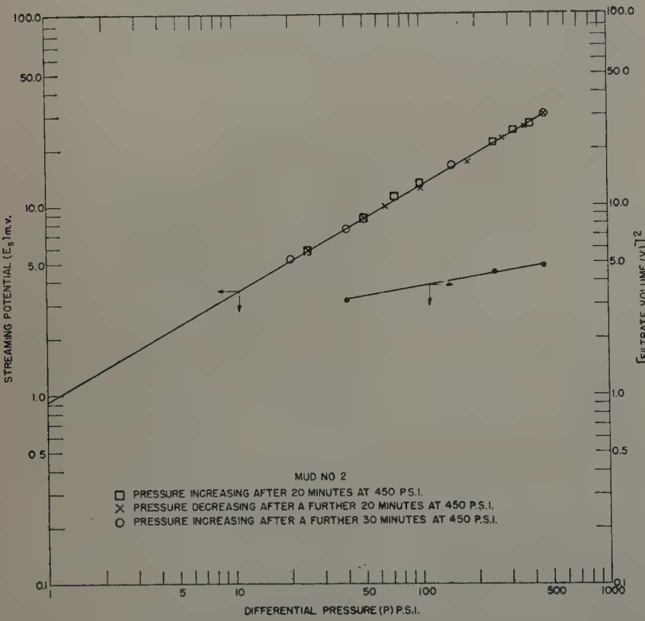

FIG. 6 — EXAMPLE OF LINEAR STREAMING POTENTIAL/DIFFERENTIAL PRESSURE AND (FILTRATE VOLUME)^2/DIFFERENTIAL PRESSURE PLOTS.

Similarly, a mud resistivity of 1.12 at 64°F corresponds to a salinity of 5,800 mg./L. and an activity of approximately 0.08. A resistivity of 1.11 at 64°F gives the same value within the accuracy of the chart. Thus, for the 1,300 ft sand,

$$\frac{\text{Activity of connate water}}{\text{Activity of mud}} = \frac{0.36}{0.08} = 4.5$$

Table III

	1300-ft Sand	2375-ft Sand
Water Analysis (mg./L.)		
Na	11,691	48,982
Ca	446	8,310
Mg	210	2,254
SO_4	1,140	nil
Cl	18,364	96,780
HCO_3	381	24
	32,232	156,350
Bottom-hole pressure	452 psi	963 psi
Mud pressure	660 psi	1247 psi
Differential pressure	208 psi	284 psi
Formation temperature	87°F	98°F
SP	53.5-55.0 mv*	109-111 mv*

*Data from the several SP logs run

From Fig. 15 which is a more accurate* version of Fig. 1, Reference 1, this corresponds, at 87°F, to an electrochemical SP of approximately 47 mv. Thus, the discrepancy between the measured SP and the calculated SP is between 6.5 and 8.0 mv. Fig. 13 gives the laboratory streaming potential curve at 90°F for a sample of the mud in the hole at the time the electric log was run. For a pressure differential of 208 psi, the streaming potential is about 11 mv, and the sign of this potential is such that it would increase the numerical (negative) value of the total SP.

For the 2,375 ft sand, the activity ratio is, similarly, 1.65/0.08 = 20.7. At 98°F, this corresponds to an electrochemical emf of about 96 mv. Hence, the discrepancy between the electrochemical and the total SP measured is here from 13 to 15 mv. From Fig. 13, for a pressure differential of 284 psi the laboratory determined streaming potential at 97°F is about 14 mv. For both sands the difference between the computed and measured streaming potentials is well within the experimental errors involved.

It is of interest in the case of the 2,375 ft sand to note the errors involved if, assuming no knowledge of streaming potentials, calculations of salinity are made on the basis of an SP kick of 110 mv. The activity ratio of 98°F is then 32 and hence the connate water activity is (32) (0.08) or 2.56. From Fig. 14 the salinity is thus about 210,000 mg./L. or 0.06 ohm-meters at 64°F. If the ratio is assumed to be a resistivity ratio, the connate water resistivity would be given by 1.11/32 or 0.035 ohm-meters at 64°F. This represents a highly supersaturated sodium chloride solution, although the error between this resistivity and the true resistivity corresponding to 156,350 mg./L. — 0.066 ohm-meters at 64°F — could be tolerated in approximate log interpretations. Alternatively, of course, by arbitrarily assuming a higher value for the electrochemical constant $2\bar{t}RT/F$ the correct answer could be obtained. There is, however, no theoretical rationale for such a procedure.

One further test made in the above-mentioned Mid-Continent

---

*This curve has been recalculated from the equation $E = 2\bar{t}\,RT/F \ln a_c/a_m$. The symbols were defined in the Introduction. Since $\bar{t}$ is not a true constant but is a function of temperature and concentration this should be taken into account in plotting Fig. 15. The temperature effect is easily incorporated, but for general applicability some mean value of concentration must be chosen. For this purpose, the values for *2N NaCl* were selected. Fortunately, the variation of $\bar{t}$ with concentration is not large.

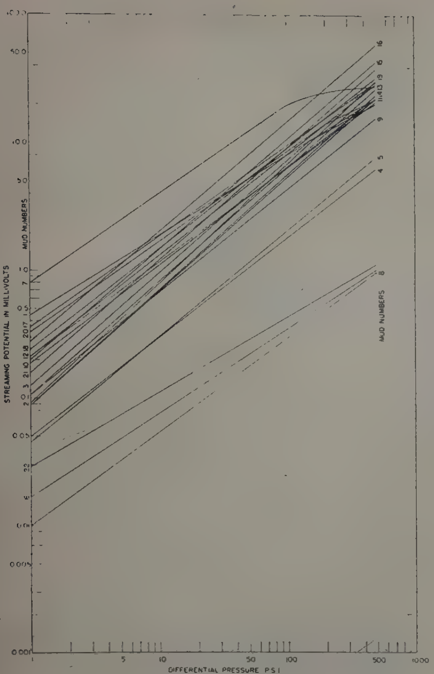

FIG. 7 — RELATIONSHIP BETWEEN STREAMING POTENTIAL AND DIFFERENTIAL PRESSURE FOR ALL MUDS TESTED. MUD NOS. REFER TO TABLES I AND II.

well deserves record, although for a number of practical reasons high experimental precision could not be achieved. At a depth of 4,100 ft in this well, the hydrostatic pressure on the borehole mud column was increased by the expedient of fitting a Schlumberger stuffing box to the well head, speeding up the mud pumps and controlling the pressure developed by judicious bleeding of the mud line. Pressures so developed were read-off on the ordinary mud-pressure gauge and at the same time a SP log was run. The increased mud pressure could not be kept constant but during the running of the SP log appeared to fluctuate only between 200 and 240 psi. Assuming a mean increase of pressure of about 220 psi, it is interesting to compare the increase in SP which would be expected to result from this pressure increase with the increase in SP actually occurring. Such a comparison can only be made on the basis of the very approximate assumption that the mud filter cakes plastering-off the formations are very similar in streaming potential characteristics to those plotted in Fig. 13. Table IV gives the increased SP values for a number of formations in the depth range 765 ft to 3,670 ft.

It will be observed that the increase in SP resulting from the measured mud pressure is not constant nor is there any marked depth trend. The increases noted are at least similar to those which would result from increasing the pressure of Mud No. 10 from 208 to 428 psi and Mud No. 11 from 284 to 504 psi.

DISCUSSION OF RESULTS

In a discussion of the results obtained in this work, it appears desirable first to summarize those conclusions which stem directly from the observations made. A second step is to examine the results and conclusions in the light of such basic theoretical considerations as appear to be applicable, and thus to assess not only the rationality of conclusions which are necessarily based on relatively few experimental data but also to confirm, if possible, their range of applicability. A third step is to examine the practical utility of the conclusions reached.

Firstly, the data in Tables I and II show that neither the normal 30-minute water loss of the standard cake test nor the conventional gel strength or viscosity tests offer any guide to the streaming potential characteristics of a drilling mud. Of all the commonly made mud tests only the mud resistivity at room temperature (*c* 77°F) offers any reliable indication of streaming potential characteristics. The data supporting this contention have been plotted in Figs. 7 and 8.

It would appear that the following relationship between the streaming potential and the pressure differential inducing flow across a filter cake is applicable to drilling muds.

$$E_S = kP^y \quad \ldots\ldots\ldots\ldots \quad (1)$$

Where, E_S = streaming potential, P = pressure differential and k = constant, y = constant.

Fig. 8 indicates that k is considerably dependent upon mud resistivity, thus exerting a major influence on the total value of E_S for any value of P. However, Fig. 8 shows also that no accurate estimate of k is possible purely from a knowledge of mud resistivity, while Fig. 7 shows graphically the controlling effect of the magnitude of the exponent y and also the fact that

Table IV
Increase in SP resulting from *c* 200 psi increase in borehole mud pressure

Depth (ft)	Increase in SP (mv)	Approx. Increase (From Fig. 13)
765	10.0	
967	8.4	
1142	5.7	
1235	7.0	
1272	5.6	
1335	7.4	9.0
1525	7.0	
1640	5.7	
1816	6.4	
1850	7.1	
2245	8.6	
2330	7.4	
2420	8.8	9.5
2503	9.4	
2642	5.7	
2700	0.7	
3068	8.9	
3422	5.1	
3435	0.5	
3582	6.3	

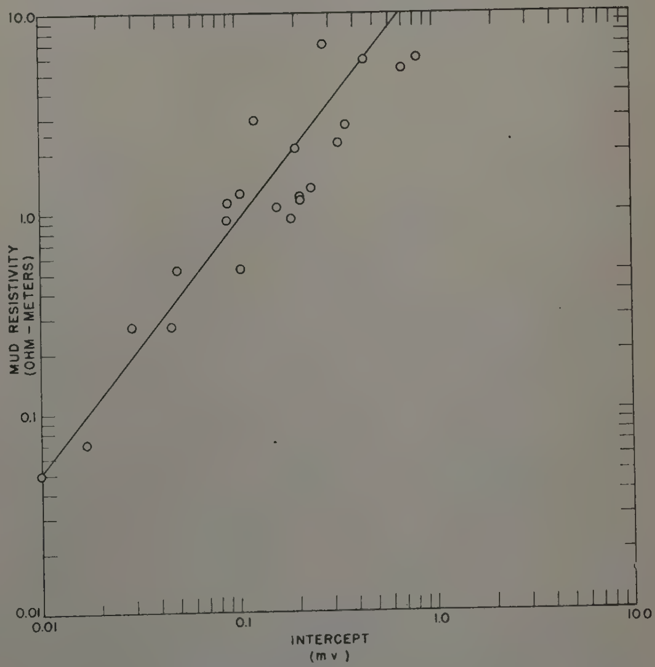

FIG. 8 — RELATIONSHIP BETWEEN MUD RESISTIVITY AT 77°F AND CONSTANT k IN RELATIONSHIP, $E_s = kP^y$.

y need not necessarily be a constant for all values of P. No conventional mud test data appear to give any indication of the value of the exponent y. However, it has been indicated above that a change in the value of y appears to be accompanied by a corresponding alteration in the slope of the log-log plot of the square of the quantity of filtrate produced in a given time versus the differential pressure of filtration. Nevertheless, the slope of this line, as may be seen from Figs. 4, 5 and 6, is not equal to y.

The experimental determination of streaming potential as a function of pressure differential for a particular mud at different mud temperatures indicates that the streaming potential at any given pressure differential is affected by temperature. Although the changes induced by temperature are relatively small in the case of the muds tested in this work, in all cases changes in both k and y were observed. The direction of these changes, i.e., whether an increase or decrease in magnitude, does not appear to be subject to forecast and, in addition, Fig. 10 shows that a mud in which the pressure exponent is constant up to a particular pressure differential at room temperature may not retain this constancy up to the same pressure differential when the mud temperature is increased. Thus, the streaming potential/pressure differential relationship of a mud obtained at one temperature cannot be used to forecast accurately the relationship between these variables at some other temperature. This inability to forecast mud properties at one temperature on the basis of observations made at some other temperature was also the experience of Byck[18] when investigating mud filtrate losses as a function of mud temperature.

Four basic experimental observations need theoretical substantiation and explanation before their universal applicability can be fully assessed. These are: (a) the dependence of k on mud resistivity, (b) the independence of filter cake thickness on streaming potential once a minimum cake thickness has been built up, (c) the relationship between filter loss and the exponent y, (d) the relatively small but unpredictable variation of streaming potential characteristics with mud temperature.

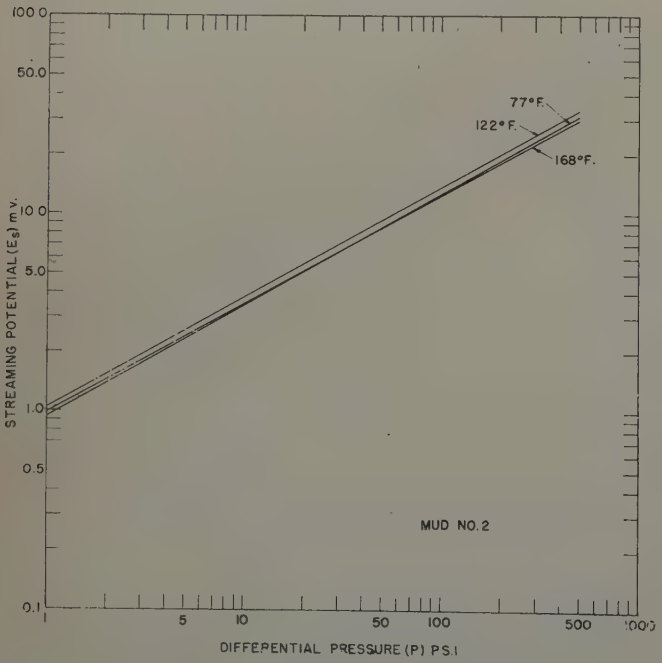

FIG. 9 — INFLUENCE OF TEMPERATURE ON STREAMING POTENTIAL/DIFFERENTIAL PRESSURE RELATIONSHIP, MUD. NO. 2.

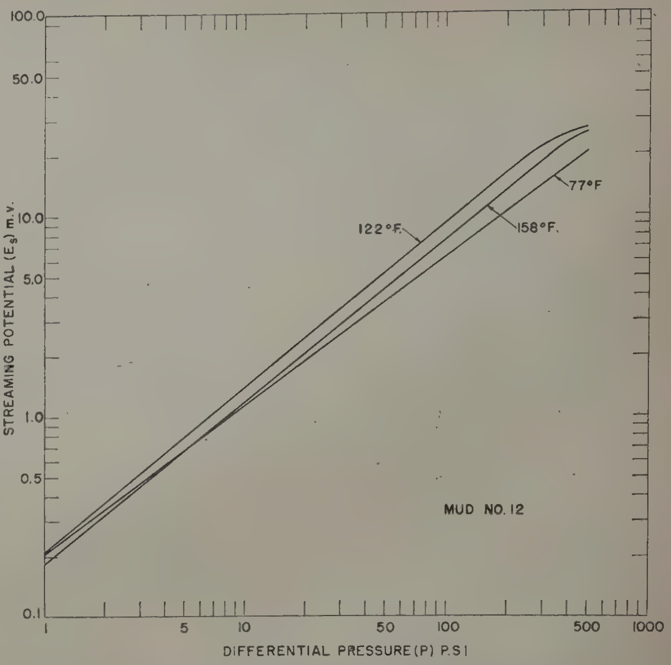

FIG. 10 — INFLUENCE OF TEMPERATURE ON STREAMING POTENTIAL/DIFFERENTIAL PRESSURE RELATIONSHIP, MUD NO. 12.

From D'Arcy's Law the following equation may be derived for flow through a non-compressible filter cake supported on a filter bed:

$$dV/d\theta = \frac{PA}{Z(rL + R)}$$

Where,

$dV/d\theta =$ rate of flow of filtrate in unit volume/unit time

$P =$ pressure differential causing flow

$A =$ area of filter cake and filter bed

$Z =$ viscosity of filtrate

$r =$ specific resistance to flow of filter cake

$L =$ thickness of filter cake

$R =$ initial resistance of unit area of filter bed

But, $L = vV/A$

Where, $v =$ volume of filter cake deposited by unit volume of filtrate

Thus,
$$dV/d\theta = \frac{PA^2}{Z(rvV + RA)} \quad \ldots\ldots \quad (2)$$

For compressible filter cakes the specific resistance to flow, r, is not independent of the differential pressure causing filtration but is itself a function of the applied differential pressure. For convenience and following the suggestion of Lewis and his co-workers[19] this may be written in the form, $r = r'P^s$, where r' and s are constants characteristic of a particular filter cake. It is, however, well to note that as pointed out by Carman[20] the Lewis equation implies that the resistance, r, is zero at the face of the cake where the pressure differential P is zero. This in turn implies that there is no sharp boundary between the filter cake and mud during filtration. This is readily observed to be quite untrue and a clear line of demarcation between cake and mud was always noted in this work. However, equations of the form, $r = r''(1 + k''P)^s$, where k'' is also a constant, which express this latter fact, are of the same form as the Lewis relationship and do not materially affect conclusions based on the simpler Lewis expression. Hence, $r = r'P^s$ will be here used. Similarly, R is not independent of pressure but may be written $R = R'P^m$, where m is a positive fraction. Hence, for compressible filter cakes,

$$dV/d\theta = \frac{PA^2}{Z(r'P^s vV + R'P^m A)} \quad . \; . \; . \; . \; . \quad (3)$$

In the case of drilling muds where the entire accent has been put on a high value of the specific resistance, r, the passage of a relatively small quantity of filtrate V serves to make $r'P^s vV \gg R'P^m A$.

Thus, when a relatively small thickness of mud filter cake has been built up, Equation (3) may be simplified to,

$$dV/d\theta = \frac{PA^2}{Zr'P^s vV}$$

$$= \frac{P^{1-s}A^2}{Zr'vV} \quad . \; . \; . \; . \; . \; . \; . \; . \; . \; . \; . \quad (4)$$

Integration of Equation (4) at constant pressure gives:

$$\frac{Zr'v}{A^2} \cdot \frac{V^2}{\theta} = 2P^{1-s} \quad . \; . \; . \; . \; . \; . \; . \; . \; . \; . \quad (5)$$

Hence, if the time, θ, is held constant, since $Zr'v$ and A^2 are constant for any particular mud and filtration system at constant temperature it follows that:

$$\text{Constant} \cdot V^2 = P^{1-s} \quad . \; . \; . \; . \; . \; . \; . \; . \; . \quad (6)$$

or that the slope of the plot of V^2 versus P on a log-log scale will be $(1-s)$. This is the reason for the plotting of V^2 versus P in Figs. 4, 5 and 6. A break in the normal straight line plot indicates that flow resistance is not increasing as a constant power function of the applied pressure differential.

The foregoing is a simplified picture of a complex and not fully understood process. It may be noted that the resistance to flow is not a constant across a filter cake subjected to a given pressure differential, but varies with variations in porosity across the filter cake (the porosity being least at the low-pressure face, highest at the high-pressure face). This problem has been considered at length by Carman in his excellent critical review of fundamental filtration processes[20] and it is unnecessary here to repeat his proof that, in spite of the non-homogeneous nature of compressible filter cakes, their resistance is solely a function of the total pressure differential across them.

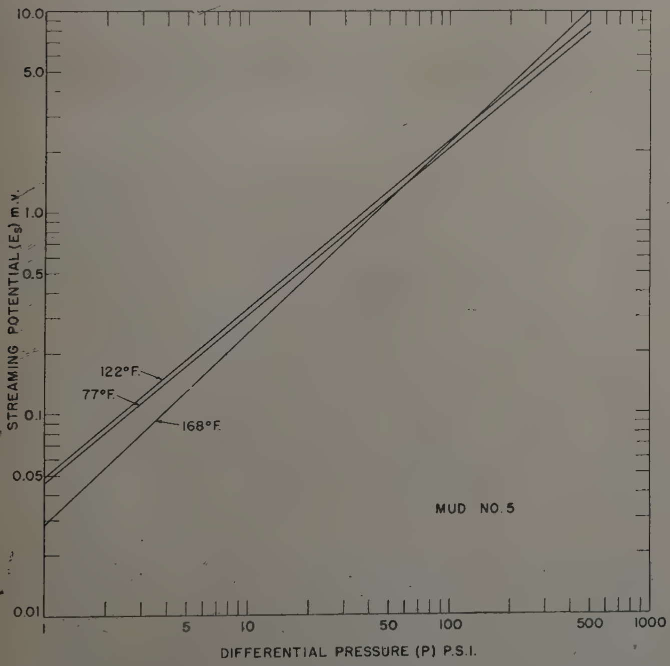

FIG. 11 — INFLUENCE OF TEMPERATURE ON STREAMING POTENTIAL/DIFFERENTIAL PRESSURE RELATIONSHIP, MUD. NO. 5.

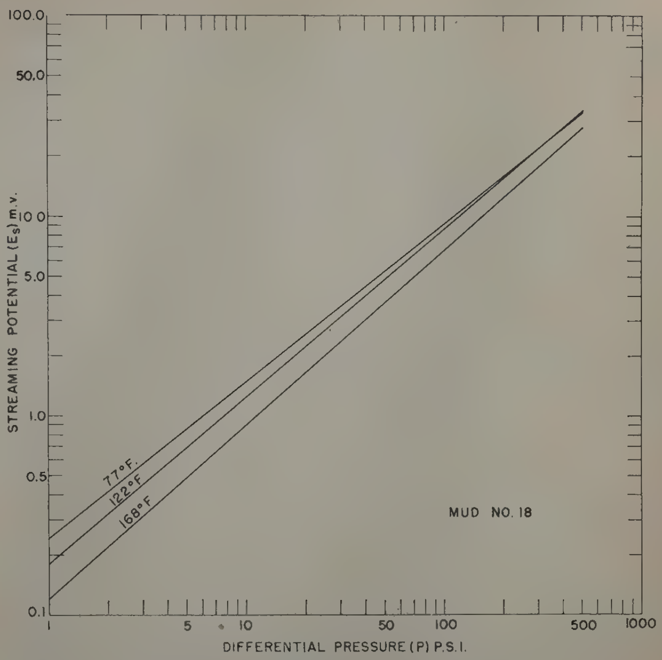

FIG. 12 — INFLUENCE OF TEMPERATURE ON STREAMING POTENTIAL/DIFFERENTIAL PRESSURE RELATIONSHIP, MUD NO. 18.

The theoretical computation of the streaming potential across compressible filter cakes is not a matter which appears to have received any prior treatment in the literature. One important aspect of the problem as it pertains to mud filter cakes has, however, been noted by Bikerman[21] who pointed out that if the matrix of a granular bed were itself a conductor any streaming potential equation must be modified to incorporate this fact. Thus, in a non-compressible granular bed in the region of laminar flow, the velocity of flow is directly proportional to the pressure differential inducing flow (Darcy's Law). If the normal assumption is made that the magnitude of charge flowing is directly proportional to the rate of fluid flow, it follows that the rate of electrical charge flow (current) is also directly proportional to the pressure differential. The streaming potential is the product of this current and an electrical resistance and the normal streaming potential equation expresses the resistance in terms of a geometrical shape factor and the resistivity of the flowing fluid. This implies that the solid matrix is a non-conductor, i.e., that the electrical and hydraulic paths are identical. This is frequently not the case and is never the case in mud filter cakes as presently constituted, since filter cakes contain electrically conducting hydrated clay. Thus, for a mud filter cake the effective electrical resistance is clearly the total filter cake resistance.

In deriving an equation for the streaming potential across a compressible filter cake, it is necessary first to compute the actual rate of fluid flow past the solid — or non-flowing-surface. It then follows that the actual magnitude of current flow is the product of this fluid flow rate, the average charge moved per unit area of stationary/flowing interface and the specific surface area of this interface per unit of filter cake volume.

The apparent linear flow rate is $1/A \cdot dV/d\theta = u$, but the actual rate of flow within the pores of the filter cake is greater than this value. Thus, considering a small thickness dL of filter cake having a constant porosity, ϕ, the actual rate of fluid flow u_e is given by:

$$u_e = u/\phi \cdot T^{1/2} \quad . \; . \; . \; . \; . \; . \; . \; . \; . \; . \quad (7)$$

Where, $T^{1/2} = (\text{tortuosity})^{1/2} = dL_e/dL$

and, $dL_e =$ the actual average length of flow path through the thickness dL.

If S is the specific surface area per unit of filter cake volume of the interface between the moving filtrate and stationary components of the filter cake, and c is the average charge moved per unit surface area, the current, I, is given by:

$$\begin{aligned} \mathrm{I} &= S \cdot c \cdot u_e \cdot A \\ &= S \cdot c \cdot u/\phi \cdot T^{1/2} \cdot A \\ &= S \cdot c \cdot T^{1/2}/\phi \cdot dV/d\theta \\ &= P^{1-s}A^2ScT^{1/2}/Zr'vV\phi \qquad (8) \end{aligned}$$

by substituting the value of $dV/d\theta$ from Equation (4).

If ρ_{fc} is the resistivity of the filter cake, the resistance of the cake, R, is given by:

$$R = \rho_{fc} \cdot dL/A \qquad (9)$$

And, $$E_s = IR \qquad (10)$$

Thus, $$E_s = \frac{P^{1-s}\,A}{Zr'vV} \cdot S \cdot c \cdot T^{1/2}/\phi \cdot \rho_{fc} \cdot dL$$

However, $dL = vdV/A$ and thus, dL may be eliminated

Whence, $$E_s = \frac{P^{1-s} \cdot S \cdot c}{Zr'} \cdot T^{1/2}/\phi \cdot \rho_{fc} \qquad (11)$$

Thus, the streaming potential is independent of cake thickness.

Equation (11) may be written in the form:

$$E_s = \frac{c}{Zr'}\,S \cdot \frac{T^{1/2}}{\phi} \cdot \rho_{fc} \cdot P^{1-s} \qquad (12)$$

In Equation (12) for any given mud at a specific temperature (c/Zr') is a constant. From Equation (6) the exponent $(1-s)$ may be obtained bv plotting V^2 against P, and it is found that $(1-s) < y$ in the experimentally-determined relationship,

$$E_s = kP^y$$

Thus, it would seem that the group $(S \cdot T^{1/2}/\phi \cdot \rho_{fc})$ is a function of pressure alone such that:

$$S \cdot T^{1/2}/\phi \cdot \rho_{fc} = \text{Constant } P^{y-(1-s)} \qquad (13)$$

The probability of Equation (13) being true may be examined and for this purpose it is desirable to apply to mud filter cakes concepts to account for the permeability phenomena of clays introduced by Kozeny,[22] Zunker[23] and particularly Carman.[24]

Fundamentally, these workers believe that the Kozeny equation for fluid flow through porous media is the basic flow equation for these systems and that any deviations from the Kozeny equation must be subject to rational interpretation in terms of peculiarities in the porous medium giving rise to the anomalies. For clays, they showed that if it is postulated that the true porosity applicable to fluid flow is ϕ' and ϕ' is less than the apparent porosity, ϕ, the Kozeny equation applies to flow through clay beds. In other words, it is postulated that there are immovable water sheaths attached to the clay laminae, and thus, ϕ based on total water content is too large. Data to support this contention have been adduced[24] and it has been shown that in any clay system ϕ' is related to ϕ in the following manner, x being a constant:

$$\phi' = \phi - x(1-\phi) \qquad (14)$$

It may be noted that this concept of fixed water sheaths is not at variance with normal theories of the structure of thixotropic mud systems. The concept also explains the fact that clays may have zero permeability but a high water content, i.e., when ϕ' is zero, ϕ is not zero.

A further consequence of the Kozeny-Zunker-Carman theory which results from the peculiar distribution of surface in plate-like clay lamellae, is that, to a close approximation, the specific surface area per unit of bulk volume, S, is related to the specific surface area of the unhydrated (dry) clay, S_o, by the relationship:

$$S = S_o(1-\phi) \qquad (15)$$

and not by the relationship, $S = S_o(1-\phi')$

Equation (13) may then be modified in terms of these concepts to read:

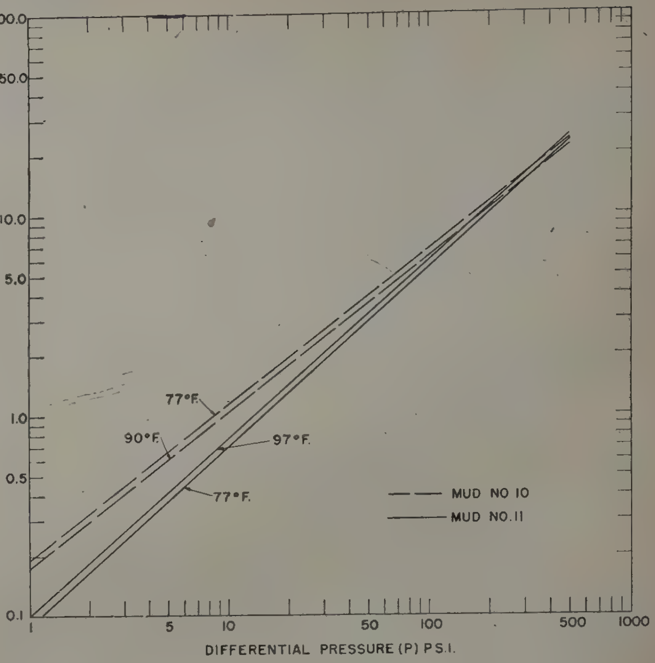

FIG. 13 — INFLUENCE OF TEMPERATURE ON STREAMING POTENTIAL/DIFFERENTIAL PRESSURE RELATIONSHIPS, MUDS NO. 10 AND 11.

$$S_o(1-\phi)\,\frac{T^{1/2}}{\phi'}\,\rho_{fc} = \text{Constant } P^{y-(1-s)} \qquad (16)$$

Note that ϕ' replaces ϕ since this porosity term was originally introduced to account for the void volume available to fluid flow.

In Equation (16), S_o is now a constant in a given system and $(1-\phi)$ may be replaced, from Equation (14), by the expression:

$$(1-\phi')/(1-x)$$

Here $(1-x)$ is also a constant for a given mud system.

Thus, Equation (16) may be written as:

$$\begin{aligned} \frac{S_o(1-\phi')}{(1-x)} \cdot \frac{T^{1/2}}{\phi'} \cdot \rho_{fc} &= \text{Constant} \cdot (1-\phi')\,\frac{T^{1/2}}{\phi'}\,\rho_{fc} \\ &= \text{Constant } P^{y-(1-s)} \qquad (17) \end{aligned}$$

Equation (17) may be further simplified if $T^{1/2}/\phi'$ is written as F, the formation factor of a system of unconsolidated hydrated clay sheaths. This follows from the derivation of Wyllie and Rose.[25] The work of Fricke[26] shows further that in a particular unconsolidated system of particles the formation factor, F, is essentially a function only of the porosity. Hence, to establish the validity of Equation (17) only the resistivity of the filter cake, ρ_{fc}, remains to be shown to be a function of cake porosity and thus of differential pressure, since there are many experimental data[24] to show the effect of P on ϕ'. The value of ρ_{fc} is partly dependent upon F and hence the resistivity of the flowing fluid network. It is, however, also dependent upon the average resistivity of the hydrated solid particles in the filter cake. This latter resistivity is likely to be relatively independent of pressure-produced porosity changes, but F has already been shown to be a function of effective porosity. Hence, a dependence of ρ_{fc} on the value of P only is probable.

The above equations were derived on the basis of a filter cake of uniform porosity characteristics in order to simplify the relationships. For a real filter cake, the porosity varies with thickness. However, this porosity variation is itself a consequence of the variation in differential pressure across the filter cake. Thus, the expression $(1-\phi')F\rho_{fc}$ is a function of the single variable P at any point in the cake. Hence, the function must integrate to give a function only of total differential pressure across the filter cake.

In Table V are given some figures to illustrate the difference between the exponents y and $(1-s)$.

It will be seen that this difference varies considerably, the difference being particularly large for the oil-emulsion mud No. 3. This result may be a consequence of the considerable oil content of the filter cake, since this oil must markedly increase the filter-cake resistivity and thus the streaming potential at a given pressure differential. If this is the explanation, it would appear at least theoretically possible to make a mud having an exponent y which exceeds unity.

Table V

Mud No.	Exponent y	Exponent $(1-s)$	Difference
2	0.57	0.18	0.39
21	0.90	0.37	0.53
20	0.71	0.25 (20-200 psi)	0.46
3	0.88	0 (to 140 psi)	0.88
5	0.83	0.35	0.48
6	0.66	0.38	0.28

It has been shown above that the streaming potential across compressible filter cakes, like the streaming potential across non-compressible porous media, should not be dependent upon thickness. In the early stages of filtration the resistance, R, of the filter bed is not negligible, and hence the streaming potential characteristics of this medium may significantly affect the total recorded streaming potential. This seems to be the principal cause for the experimentally observed discrepancy between early streaming potentials for a given pressure differential and later constant values.

Equation (12) shows that the resistivity of the mud filter cake, ρ_{fc}, appears in the expression for streaming potential and it has been noted that this quantity appears to be a function of pressure differential. If ρ_{fc} is written as $\rho_{fc} = \rho_m(n + mP^z)$, where ρ_m is the mud resistivity and n, m and z are constants, the dependence of the constant k in the expression $E_s = kP^y$ on mud resistivity becomes explicable. The value of the constant n will be affected, particularly, by the quantity of non-conducting solids such as oil or weighting material in the filter cake and by the porosity of the filter cake under zero pressure differential.

The effect of temperature on streaming potential may only be very qualitatively evaluated. It may be noted that resistivity appears in the numerator of Equation (12) and filtrate viscosity in the denominator. Since the variation of aqueous conductivity with temperature is closely similar to the temperature variation of aqueous viscosity, the effect of temperature will be to reduce these two quantities approximately in proportion and a rough cancellation appears probable. The influence of temperature on the magnitude of c is obscure. The relationship

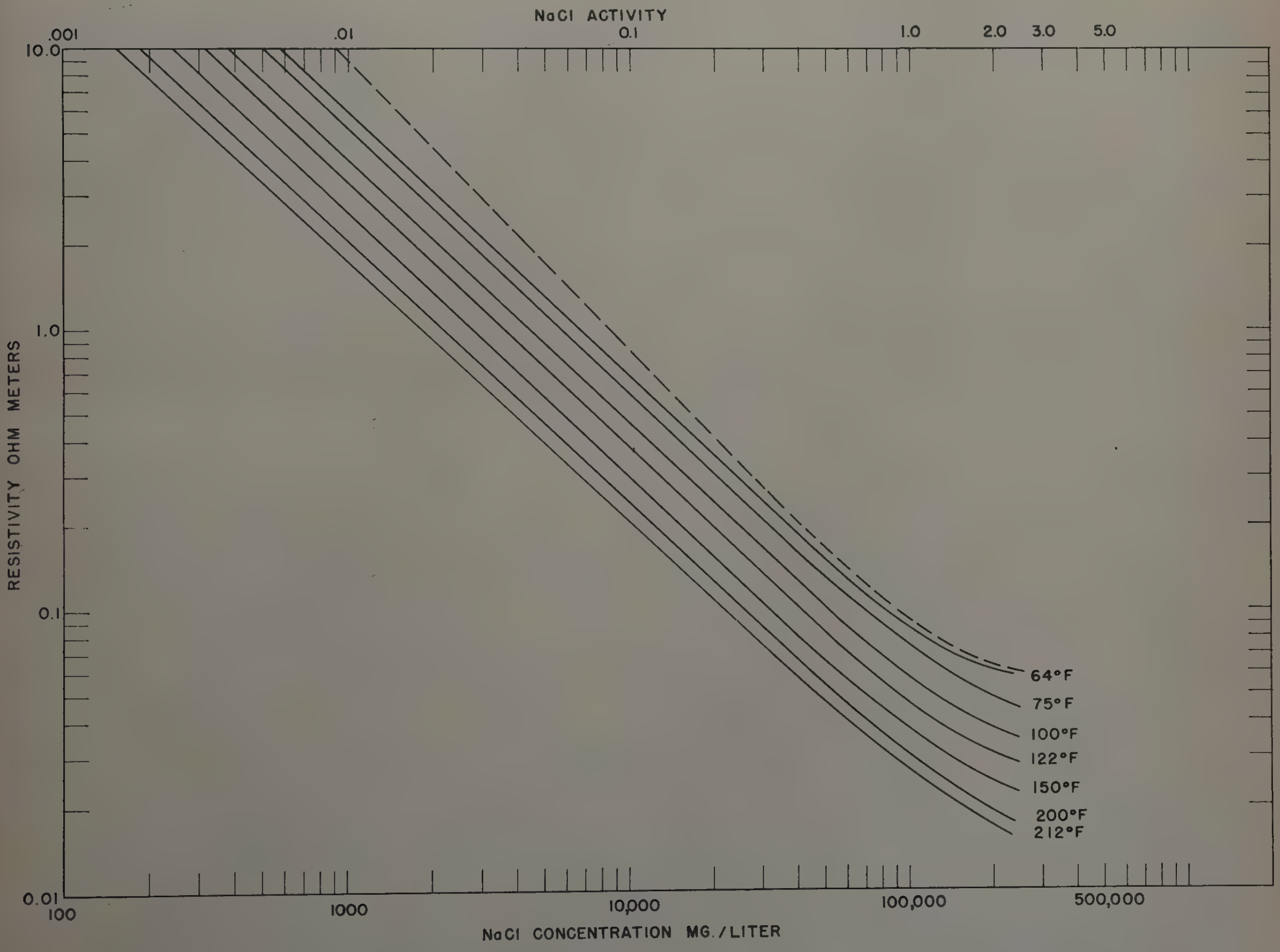

FIG. 14 — CHART FOR INTERCONVERSION OF THE RESISTIVITY, SALINITY AND ACTIVITY OF SODIUM CHLORIDE SOLUTIONS.

between zeta potential and c can only be found if a specific hypothesis as to the distribution of electricity in the double layer at the moving fluid/stationary-surface interface is made. For an idealized plane parallel double layer, if r is the thickness of the double layer, the zeta potential is equal to $4\pi cr/D$, where D is the dielectric constant of the fluid. If an expression of this type applies to the complex filter-cake system and the zeta potential and r remain constant, c will be proportional to D and will decrease about 0.5 per cent °C rise in temperature. However, the zeta potential itself tends to control the stability of a colloidal system and prevent coagulation. The results of Byck[18] on filtrate losses of muds at elevated temperatures tend to show that some flocculation of the filter cake occurs, presumably accompanied by a change in zeta potential as well as r', the specific filter cake resistance. Thus, it would appear that temperature may either increase or decrease the streaming potential for a given pressure differential as a consequence of the complex interplay of a number of imponderables. At any temperature, however, the value of the zeta potential and hence, c, may be expected to be somewhat dependent on the filtrate salinity and thus also on mud resistivity. This dependence probably also contributes to the relationship observed between the streaming potential constant, k, and mud resistivity.

The practical consequences of the streaming potential effect in well logging appear, from the data given, to be of more importance than has generally been believed. It is apparent that when using muds having a resistivity between 1 and 2 ohm-meters at 64°F, streaming potentials of 20 to 30 mv are quite feasible, at depths from 5,000 - 10,000 ft, assuming normal mud weights and bottom-hole pressures. With heavy fresh muds, deep drilling, and particularly, abnormally low bottom-hole pressures, it seems quite possible to have streaming potentials of 50 mv or more constituting perhaps half the total SP and leading to prohibitively serious errors in the calculation of connate water salinities by the electrochemical SP method. These are extreme conditions and it must be recollected that there is evidence from the 0 - 500 psi range of pressure - differential experiments that the exponent y in the relationship $E_s = kP^y$ may not remain constant at the high-pressure differentials envisaged. However, tests have been reported[16] to show that the log-log plot of mud filtrate versus pressure differential may remain a straight line to pressure differentials as high as 3,000 psi; it is thus entirely possible that in many instances the log-log plot of streaming potential versus pressure differential maintains a similar linearity to the highest pressures obtaining even in deep rotary wells.

The experimental determination of the streaming-potential component of the SP curve so as to derive the electrochemical component by difference between the total SP and the electrokinetic SP is not promising. Laboratory experiments on mud samples would represent a prodigous effort on any routine basis, while the method of applying additional borehole mud column pressures and noting the increased SP developed is theoretically feasible but practically profoundly difficult. Thus, theoretically, if $E_s = kP^y$ is assumed, the application of two

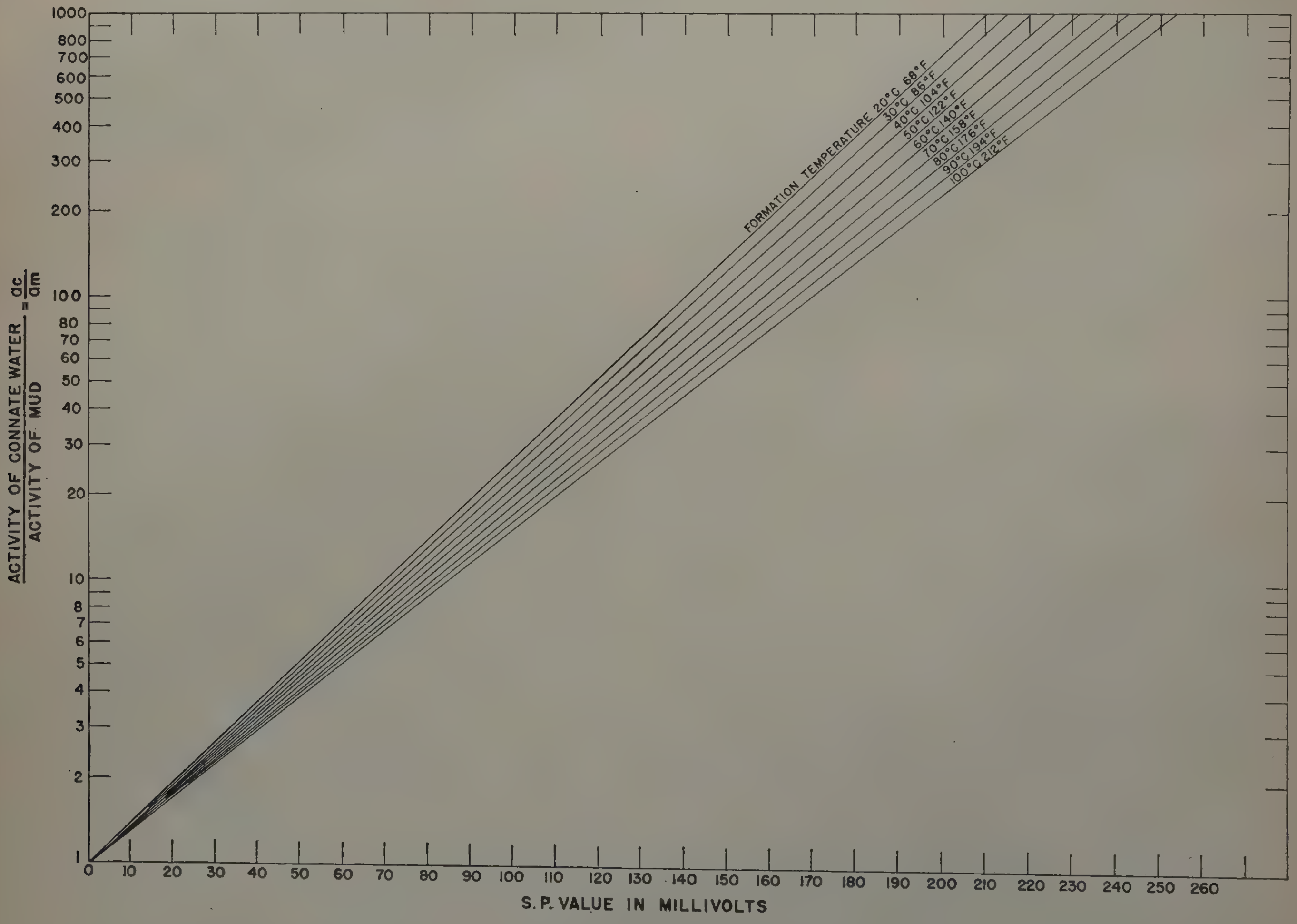

FIG. 15 — RELATIONSHIP BETWEEN CONNATE WATER ACTIVITY RATIO AND CHEMICAL SP FOR VARIOUS FORMATION TEMPERATURES (BASED ON SODIUM CHLORIDE SOLUTIONS).

different hydrostatic pressures (either increased or decreased) to the borehole mud column and the running of three SP curves should enable the constants k and y and thus E_s to be determined if the requisite bottomhole pressure is known. Difficulties result from the small changes in SP induced by the pressure changes imposed on the mud column and the inaccuracies attendant upon picking the necessary shale base lines in each case (see Table IV). The stability of contact potential of the logging electrode becomes a source of serious error when differences of the order of 5 mv are to be measured. More serious even than these technical objections is the necessity of knowing the bottom-hole pressures of the formations of interest. These cannot be reliably assumed and if they are to be measured the formation can in most instances be tested directly, thus destroying the need for any electric-log calculation.

It is probably true that in many wells a small streaming potential component is a blessing in disguise, since the tendency is always for the electrochemical component to be reduced by filtrate invasion, shale interbedding, high formation resistivities and other factors. Thus, the assumption that the measured SP is the electrochemical SP becomes of sufficient accuracy for practical purposes by a compensation of negative and positive (numerical) errors. Nevertheless, although the writer has found this to be true in a very large number of cases, it is clearly undesirable to place undue reliance on an uncontrolled fortuitous compensation of errors of this nature.

The practical solution to the problem of streaming potentials and also to the more accurate calculation of connate water resistivities generally, appears to be the deliberate employment of muds of lower resistivity than has been customary in the past. It has been shown that a lower mud resistivity decreases the streaming potential constant, k, and thus the value of E_s for any value of P. Lower values of y are also desirable but means to achieve this end require further investigation.

The electrochemical emf, $E = 2\bar{t}\,\dfrac{RT}{F}\,ln\ a_c/a_m$

$$= k\ ln\ r$$

where at any temperature and for a particular mud and connate water, k and r are constants.

Thus, $$dE = k\ dr/r$$

$$\underset{\cdot}{\dot{\approx}}\ \triangle E$$

Therefore, $$\triangle E/E\ \underset{\cdot}{\dot{\approx}}\ dr/r \cdot ln\ r$$

or, $$\text{error in } r\ \underset{\cdot}{\dot{\approx}}\ \triangle r/r = \triangle E/E \cdot ln\ r$$

Thus, for any error in the measurement of E, the error in r will be a minimum for small values of r. This conclusion agrees also with the statement of Doll[13] who recommends a small value of r for similar reasons.

Since a decreased mud resistivity implies a higher value of a_m and thus, for any value of a_c, a smaller value of $a_c/a_m = r$ as well as a lower streaming potential, the advantages of low mud resistivities are apparent.

A numerical example based on streaming potentials measured in this work brings out this advantage plainly. Assume a connate water salinity of 100,000 mg./L., formation temperature 86°F and pressure differential of 1,000 psi:

Mud No.	Electrochemical emf (mv)	Streaming Potential mv	Total emf mv	Apparent Salinity from Total emf (mg./L.)
2	−143	−46	−189	Saturated
5	− 45.5	−14.5	− 60	160,000
6	+ 10	− 1.6	+ 8.4	104,000

Additional advantages of more saline muds lie also in the increased accuracy with which estimates of true formation resistivity may be made. A suggestion has been made by Doll[27] that a mud be used which has a resistivity about five times that of the connate water in formations of interest. This suggestion is essentially a compromise and is intended to give not only rather accurate SP logs for the computation of connate water salinities, but sufficient SP development to delineate adequately permeable beds for purposes of correlation.

In addition a mud resistivity similar to that of the connate water resistivity simplifies the interpretation of apparent resistivity logs in terms of true resistivity by keeping to a minimum the adverse effects on such interpretations of the filtrate invaded zone surrounding the borehole. Doll's compromise proposal is reasonable, but the present work indicates the importance of keeping the mud resistivity low in an absolute sense to avoid excessive streaming potentials in wells where mud weights are high and formation pressures low. Thus it may be desirable in wells having low connate water salinities and high pressure differentials to use a mud of lower resistivity and higher activity than the connate water (by a factor again of about 5) and to accept a reversal of the SP curve, i.e., positive SP kicks opposite permeable formations. Such a result is common practice when high activity silicate muds are used at the present time.

ACKNOWLEDGMENTS

The writer is indebted to A. J. Teplitz and F. J. Lydick and their assistants for help in the choice, preparation and routine testing of the laboratory muds used in this investigation. His thanks are due to Paul D. Foote, executive vice-president, Gulf Research and Development Co., for permission to publish this paper.

REFERENCES

1. Wyllie, M. R. J.: *Trans.* AIME (1949), **186,** 17.
2. Wyllie, M. R. J.: *Bull.* AAPG, (1949), **33,** 1892.
3. Tixier, M. P.: *Oil and Gas Jour.,* (1949), **48,** 143.
4. Wyllie, M. R. J., and Patnode, H. W.: *Jour. Phys. and Coll. Chem.,* (1950), **54,** 204.
5. Doll, H. G.: *Trans.* AIME, (1948), **179,** 146.
6. Mounce, W. D., and Rust, W. M.: *Trans.* AIME, (1945), **164,** 288.
7. Adams, L. H., and Hall, R. E.: *Jour. Phys. Chem.,* (1931), **35,** 2145.
8. Robinson, R. A., and Harned, H. S.: *Chem. Reviews,* (1941), **28,** 419.
9. Schlumberger, C. and M., and Leonardon, E. G.: *Trans.* AIME, (1934), **110,** 237.
10. Schlumberger, C. and M., and Leonardon, E. G.: *Trans.* AIME, (1934), **110,** 273.
11. Gillingham, W. J.: *Mineral Industries Expt. Stn. Bull.,* (1937), **21,** Pennsylvania State College.
12. Pirson, S. J.: *Mineral Industries Expt. Stn. Bull.,* (1948), **52,** Pennsylvania State College.
13. Doll, H. G.: *Trans.* AIME, (1950), **189,** 205.
14. Thomas, H. C. H.: *Jour. Inst. Pet. Tech.,* (1935), **21,** 774. Discussion by P. Bayle.
15. Doll, H. G.: *Trans.* AIME, (1950), **189,** 129.
16. Drilling Mud. (Anonymous). (1938), **6,** No. 1.
17. Latimer, W. M.: *Oxidation Potentials.* (1938). p. 325, Prentice-Hall, New York.
18. Byck, H. T.: *Petr. Tech.,* AIME, T.P. 1116, Nov., (1939).
19. Walker, W. H., Lewis, W. K., McAdams, W. H., and Gilliland, E. R.: *Principles of Chemical Engineering,* p. 345 et seq., (1937), McGraw-Hill, New York.

20. Carman, P. C.: *Trans.* Inst. of Chem. Engrs., (1939), **17,** 168.
21. Bikerman, J. J.: *Surface Chemistry*, p. 382 et seq., (1947), Academic Press, Inc., New York.
22. Kozeny, J.: *Kultur techniker,* (1932), **35,** 478.
23. Zunker, F.: *Z. PflErnähr. Dung,* (1932), **A25,** 1.
24. Carman, P. C.: *Jour. of Agri. Sci.,* (1939), **29,** 262.
25. Wyllie, M. R. J., and Rose, W. D.: *Trans.* AIME, (1950), **189,** 105.
26. Fricke, H.: *Phys. Rev.,* (1924), **24,** 575.
27. Doll, H. G.: Private Communication.

APPENDIX

Mud No. 1

Fibergel 22:	10.89	gms.
Tap water containing 6 per cent Zeogel	350.0	ccs.
pH adjusted with *NaOH*		

Mud No. 2

Magcogel	17.5	gms.
Baroid "O"	63.0	gms.
Hi-yield clay	6.15	gms.
Tap water	350.0	ccs.

Mud No. 3

Aquagel	21.0	gms.
Mid-Continent crude	140.0	ccs.
Sodium tallate soap	14.0	gms.
Sodium tripolyphosphate	1.4	gms.
Magcobar	157.5	gms.
Hi-yield clay	14.0	gms.
Tap water	350.0	ccs.

Mud No. 4

Mud No. 3	350.0	ccs.
Sodium chloride	7.0	gms.
Water	70.0	ccs.

Mud No. 5

Magcogel	15.75	gms.
Sodium hydroxide	3.4	gms.
Quebracho	3.4	gms.
Lime	3.93	gms.
Hi-yield clay	47.2	gms.
Tap water	350.0	ccs.

Mud No. 6

Zeogel	8.75	gms.
Magcobar	223.0	gms.
Impermex	8.0	gms.
Tap water + 30 per cent sodium chloride	350.0	ccs.

Mud No. 7

Aquagel	21.0	gms.
Distilled water	350.0	ccs.

Mud No. 8

Zeogel	21.0	gms.
Tap water + 30 per cent sodium chloride	350.0	ccs.

DISCUSSION

By H. G. Doll, Schlumberger Well Surveying Corp., Ridgefield, Conn., Member AIME

The question of the streaming potentials occurring with the filtration of drilling mud into permeable beds has been the subject of the attention of various experimenters for years. However as far as I know no systematic and detailed study of the problem had been made theoretically and in the laboratory before Wyllie's work, which is reported in his excellent paper on "An Investigation of the Electrokinetic Component of the Self Potential Curve."

Being given the efforts made toward deriving more and more quantitative data on reservoir characteristics from electrical logs, the publication of the results of this work by Wyllie is quite timely. His paper provides numerous valuable indications which should make possible a more accurate interpretation of the SP logs.

One of the conclusions made by Wyllie is that the electrokinetic component of the SP log should be made as little as possible, and that the use of low resistivity mud should be recommended to this end. This opinion meets the conclusion I arrived at through different considerations.

I would only make the following remark:

As proposed by the author, when connate water is fresh, the resistivity of the mud can be adjusted below the resistivity of the connate water without being decreased too much, however. The deflections of the SP curve in this case, although reversed, are still large enough to be measured with sufficient accuracy. But, in the case of connate water of high salinity, the use of very low resistivity mud may reduce the spontaneous electromotive forces and, therefore, the amplitude of the deflections on the SP curve, to a very small value. As, on the other hand, these deflections are extremely smooth when mud resistivity is very low, the SP curve may be finally reduced to an almost flat line. I do not think therefore that mud resistivity can be decreased beyond certain limits, without running the risk of ruining the SP log, even for only qualitative purposes.

DISCUSSION

By Hubert Guyod, Consultant, Houston, Tex., Member AIME

In substance Wyllie's paper states that there is an appreciable streaming potential component on the potential graph of electric logs. As evidence, Wyllie points out:

1. That the magnitude of electrochemical potentials is not

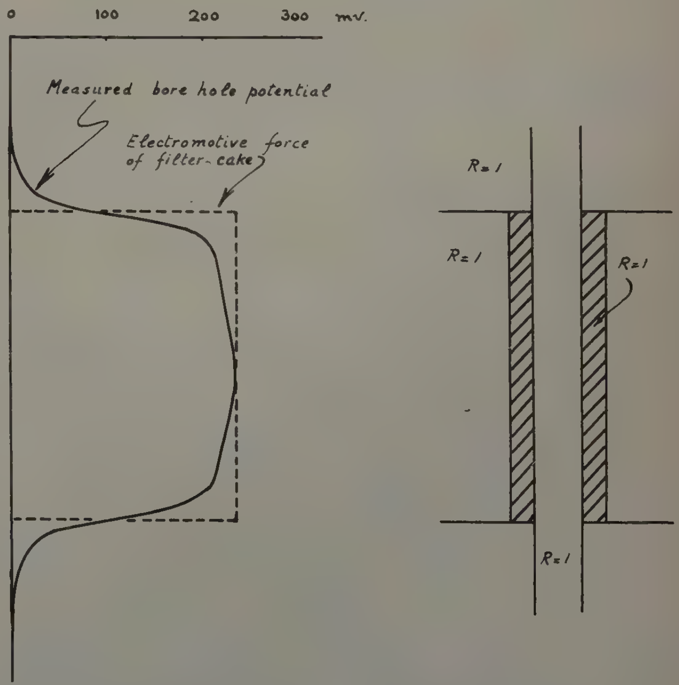

SIMULATED STREAMING POTENTIAL, MODEL EXPERIMENT. HOLE DIAMETER, 1; BED THICKNESS, 8.25; FILTER-CAKE THICKNESS, 0.5; ALL RESISTIVITIES, 1; ELECTROMOTIVE FORCE BETWEEN FACES OF FILTER-CAKE, 237 MV.

large enough to explain fully the total potential.

2. That therefore there are substantial streaming potentials.

I do not agree to the foregoing for the following reasons:

1. At the present time we do not know enough about the agencies which produce electrochemical potentials in bore holes to be certain that the fundamental equation

$$V_T = K \log R_c/R_m$$

applies reasonably well to every sand or sandstone.

2. Even if we would be certain that this equation applied, the fact that the observed potential V_o is sometimes greater than V_T should not be construed as meaning that the difference $V_o - V_T$ is due primarily to streaming potentials. As a matter of fact, there are many other possible causes of potential in the ground although it must be admitted that in rotary holes the electrochemical potential is the dominating factor.

3. The fact that, during the field experiments reported by Wyllie, an increase in pressure increased the observed potential does not mean that the potential increase was due to streaming potentials. In fact, an increase in pressure may cause — and probably will cause — an increase in the electromotive force of the electrochemical potentials. While we perhaps know very little regarding this effect it may account for some, if not all, of the phenomenon observed. Another effect of pressure is to increase not only the negative potential opposite sands but also to increase it opposite shales, although to a less degree. This cannot be explained by streaming potentials. Finally, when an extra pressure is applied on the mud column, and then released, the potential does not return immediately to its original value. There is a marked hysteresis effect: it takes from 15 to 60 seconds for the potential to return to its original value. This hysteresis is difficult to explain when streaming potentials are postulated, while it may be less difficult to account for it if it is assumed that another cause of potential is involved, for instance an increase in the electromotive force of the electrochemical potentials.

4. If and when there is a streaming potential component on the potential graph obtained on a thick sand, the top of the potential kick cannot possibly be flat; the reason therefor, is explained in an article which I wrote in the November 27, 1944, issue of *Oil Weekly*. Fig. 15-10 of this article illustrates the current distribution and the potential graph which would obtain in a bore hole if there are streaming potentials. I am also attaching an experimental potential graph obtained with a model in which I simulated streaming potentials. This graph shows that the potential curve is not flat-topped. While this curve is quantitatively different from Fig. 15-10 it shows definitely two slanted sections *AB* and *CD*. Inasmuch as Wyllie points out that the potential graphs used in his experiments exhibited a flat top, it seems that, if I am right, there could be only negligible streaming potentials.

To summarize, while Wyllie's paper is an important contribution to a better understanding of the potential graph, I do not believe that his experiments are comprehensive enough to permit formulating an opinion on the presence or absence of streaming potentials in bore holes.

AUTHOR'S REPLY TO MR. GUYOD

It would seem that Guyod is completely unable to agree with my conclusions and he outlines rather fully his reasons for disagreement. While it would be foolish to be unduly dogmatic, I nevertheless believe that my conclusions are substantially valid. I will therefore endeavor to deal seriatim with Guyod's objections.

I do not believe it true to say that our knowledge of borehole electrochemical potentials is incomplete in the sense indicated by Guyod. It is true that the detailed mechanism whereby the potential is set up is a complex subject which is bound-up with the whole theory of membrane electrodes. The theory of such electrodes has been discussed at length by many workers since it is not a subject unique in the oil industry: a number of references from the voluminous literature are given in Reference 4 above. It will suffice to say that from the thermodynamical standpoint (which, of course, does not involve reaction mechanisms) the equation for the electrochemical potential across a shale membrane is given by,

$$E = RT/F \ln \frac{a'_{\mathrm{Na}}}{a''_{\mathrm{Na}}} \quad . \quad . \quad . \quad . \quad . \quad . \quad (1)$$

where a'_{Na} and a''_{Na} are single sodium ion activities. When the shale membrane is included in a circuit which also involves a junction potential, the equation becomes that for a cell with transference and,

$$E = 2\bar{t}\ RT/F \ln \frac{a'_{\mathrm{NaCl}}}{a''_{\mathrm{NaCl}}} \quad . \quad . \quad . \quad . \quad (2)$$

where a'_{NaCl} and a''_{NaCl} are now the mean ionic activities of sodium chloride solutions and these mean activities are unequivocably determinable from isopiestic or other independent chemical experiments. May I note once again that it is activities that are involved, not resistivities. The use of resistivities instead of activities is a crude approximation only justifiable in very dilute solutions and certainly not permissible in the great majority of electric log calculations.

Equation (2) is a fundamental equation which indicates the maximum emf that can be obtained from a given set of chemical conditions. Equation (2) can be in error for at least two obvious reasons; because muds and connate waters are not pure sodium chloride solutions and because cation exchange between shales and muds is possible. I have recently dealt with these subjects in some detail[1] and there is no need to repeat my argument. In essence it is indicated that if log potentials are observed which are *much greater* than those given by Equation (2), then some source of potential in addition to the electrochemical potential must be operative down the borehole. Certain such cases have been reported (Reference 2 above) and many others observed by us.

I emphasize that potentials much greater than are given by Equation (2) have been observed; potentials less than are given by Equation (2) are frequently seen since such complications as high formation resistivities, deep mud filtrate invasion, dirty formations or even electrochemically inefficient shale formations (apparently rare) will all serve to give a potential lower than that required by Equation (2).

The fundamental question then is: what is this additional source of potential? It may be noted that this additional potential appears to be such as to increase a negative SP kick, although the purist would be justified in saying that this need not be invariably true since an additional potential which served to decrease the conventional negative SP kick could not readily be distinguished from those other factors, outlined above, which also serve to reduce the electrochemical SP.

Guyod indicates that there are many other possible causes of potential, although he does not list them. With such a statement I am by no means in entire agreement. Certain electrochemical cells, such as those operative in the vicinity of chemically reacting ore bodies, do not appear to be operative in most sedimentary rocks. Again, the general constancy of shale base lines indicates that such potentials, if genuine would have to be quite remarkably uniform. A Dorn potential (Reference 1 above) is conceivable, but such a potential should tend only to modify slightly any slope of the shale base line resulting from thermal effects, e.g., a temperature difference, $\triangle T$, across a permeable bed should shift the base line by an amount equal to $2t \dfrac{R\triangle T}{F} \ln \dfrac{a'_{\mathrm{NaCl}}}{a''_{\mathrm{NaCl}}}$.

Guyod apparently does not gainsay the fact that an increase in the hydrostatic pressure of a mud column will alter the SP kick observed; in general, a negative SP kick is thereby increased. Guyod ascribes these SP changes to pressure induced changes in electrochemical emf, not to a change in streaming potential, in spite of the fact that both in magnitude and direction laboratory experiments confirm the streaming potential hypothesis.

The effect of pressure changes on Equation (2) resides in the effect that the pressure changes may have on the activities of the connate water and mud, designated a'_{NaCl} and a''_{NaCl} respectively. Such pressure induced changes are negligible as I pointed out in a footnote on the first page of the paper, and thus no measurable change in electrochemical potential is to be anticipated. I cannot, therefore, agree with Guyod when he ascribes potential changes to the effect of pressure on electrochemical emf. (It is not irrelevant to note that the glass electrode will record substantially the same *pH* irrespective of its ambient pressure.) Guyod makes the point that not only is the negative potential increased opposite sands but also, to a lesser degree, opposite shales. I am not altogether clear as to the meaning of this statement since the absolute potential of the shale base line on the log is arbitrary and controlled by the potential difference between the borehole and mud-pit electrodes and any bucking potential between them. What is generally important is the potential difference between contiguous sands and shales and this difference is not affected by variations in the absolute potential of the shale base line. I assume that Guyod means that in the absence of any alteration in bucking potential between the two SP electrodes or movement of the mud-pit electrode, the application of pressure alters the recorded position of the shale base line. This does not seem unreasonable to me if it is recollected that the potential between the two SP electrodes — one down the borehole and one in the mud-pit — can only remain constant if the environmental potential of each electrode (chiefly the contact potential, lead/mud) remains constant.

If one electrode is distorted slightly by pressure, particularly if this pressure is rather suddenly applied, its contact potential may alter owing to slight cracking of the surface film built up by reaction with the mud fluid. Thus, a pressure change, by altering the contact potential of the borehole electrode, could alter the absolute potential of the shale base line but not the potential difference between shale and sand. It is this potential difference which is measured before and after the application of pressure and it is changes in this potential difference which I ascribe to a streaming potential. In support of the above hypothesis I note that when we have used reversible SP logging electrodes of the lead/lead chloride type, little, if any, displacement of the recorded shale base line results from pressure changes.

With regard to the hysteresis effect that Guyod cites, it is, I confess a phenomenon which we have not observed. However, I would not deny its existence since the precise recording of the effect clearly requires deliberate and careful coordination between the operators of the mud pumps and casing-head stuffing box and those recording the log; such exact coordination was never attempted by us and hence we have no data on any hysteresis effects occurring during our experiments. However, hysteresis involving times approximating the 15 to 60 seconds quoted by Guyod was noted in laboratory streaming potential experiments.

Such hysteresis was observed with Mud No. 4 at room temperature and with most muds at elevated temperatures. This effect has been noted in the paper. In general the hysteresis took a form opposite to that observed by Guyod; this is evidenced by Fig. 3 which shows that removal of pressure from 500 psi to 100 psi gave a streaming potential some 2.5 mv lower than the equilibrium streaming potential. Thus, after partial removal of pressure the observed potential slowly increased to its equilibrium value. However, similar potential decreases have been observed, although more rarely. Fig. 4 shows such a case, the potential following a pressure decrease being slightly higher than the equilibrium potential. In general, it may be said that the hysteresis effects observed by Guyod are not incompatible with a streaming potential hypothesis. Certainly no known electrochemical hysteresis effects of the type he observed are known to exist.

I fear that I cannot subscribe to Guyod's views pertaining to the effect of a streaming potential component on the shape of a SP curve. The streaming potential across the filter cake is essentially equivalent to a separation of positive and negative charges and may be compared to an additional junction potential. Since the pressure difference between the hydrostatic head of mud and the bottom-hole pressure is substantially constant even for a thick bed, and since I have shown that the actual filter cake thickness does not affect the streaming potential, the streaming potential is substantially constant over the entire area of a mud cake sheathing off a permeable bed. It is true that current flows across the filter cake to maintain this streaming potential, but the pattern of this current does not in any way resemble that drawn in Fig. 15-10 of the paper quoted by Guyod, the lines of current substantially flowing only across the filter cake itself and not taking the circuitous paths through sand and shale shown in that figure. This is partly because in practical instances the filter cake is extremely thin and therefore its resistance is very small in comparison with any alternative conducting paths through sand and shale beds. In Guyod's model experiment the filter cake thickness is 0.5 for a hole diameter of 1.0; i.e., equivalent to 2½ in. in a 10-in. hole if the more reasonable assumption is made that the filter cake is built up in the borehole and not in the formation. Alternatively in Guyod's experiment the filter cake thickness is 1/16.5 as thick as the bed, leading to a 3-ft thickness of cake in a 50-ft bed. I believe that if Guyod postulates a 1-in. filter cake thickness and a 50-ft. bed, he will find that any "pointedness" of the SP curve will be completely undetectable.

It is also relevant to note that the distribution of resistivity shown in Guyod's figure is improbable. The formation factor of filter cakes is approximately two, whereas the minimum for a formation is five. If there is a filter cake then, ipso facto, there must have been filtrate, and the resistivity behind the filter cake will tend to be (5/2) greater than the filter cake resistivity. In general, as also pointed out elsewhere,[2] the streaming potential component may be regarded as a potential algebraically added to the electrochemical potential which, by causing circulatory electrical current to flow at sand-shale boundaries, gives rise to the SP curve by ohmic effects.

I would like to emphasize that although I clearly disagree with Guyod it is most refreshing to have this fundamental disagreement brought out into the open. Too frequently papers which have controversial conclusions are never adequately queried or even mentioned in subsequent publications on the same subject, thus leading to intolerable confusion in the literature.

REFERENCES

1. Wyllie, M. R. J.: Master Section 2, Drilling and Production, Proceedings of the Third World Petroleum Congress, The Hague, 1951. (Advance copies available from the author).
2. Review of Schlumberger Well Logging and Auxiliary Methods, Schlumberger Document No. 2, (1949), pp. 34-35. ★

T.P. 3000

PRESSURE BEHAVIOR IN THE WOODBINE SAND

JOHN S. BELL AND **J. M. SHEPHERD,** HUMBLE OIL AND REFINING CO., MEMBERS AIME

ABSTRACT

A pressure difference of 280 psi measured initially on opposite sides of the major fault in the Hawkins Field led to pressure determinations in the Woodbine sand throughout the East Texas basin. Considering the large area, there is unusually good correlation between pressure losses and points of major withdrawals, these losses indicating that the basin pressure has been materially reduced by withdrawals, primarily from the East Texas Field and secondarily from the old fault-line fields of Limestone and Navarro counties, with the pressure loss varying inversely with the log of the distance from these two main areas of basin withdrawals to the measurement points. Apparently faults located throughout the basin serve as local blocks to continuous pressure gradients.

INTRODUCTION

The pressure anomalies found in the Hawkins Field, Wood County, Texas,[1] shortly after discovery have led to an area-wide investigation of the pressure distribution within the Woodbine sand of the East Texas basin. These pressures were obtained by drill-stem tests made for that sole purpose while drilling wildcat wells to deeper horizons. The Woodbine sand of Gulf Cretaceous Age is or has been productive of oil and gas in 42 different fields, with the 28 oil fields currently active having produced 118,000,000 bbl of oil during 1949. With one exception, producing energy for all Woodbine reservoirs has been from water drive provided predominantly by expansion of the tremendous volume of water contained in the Woodbine sand. This producing mechanism was recognized at an early date and was described mathematically by

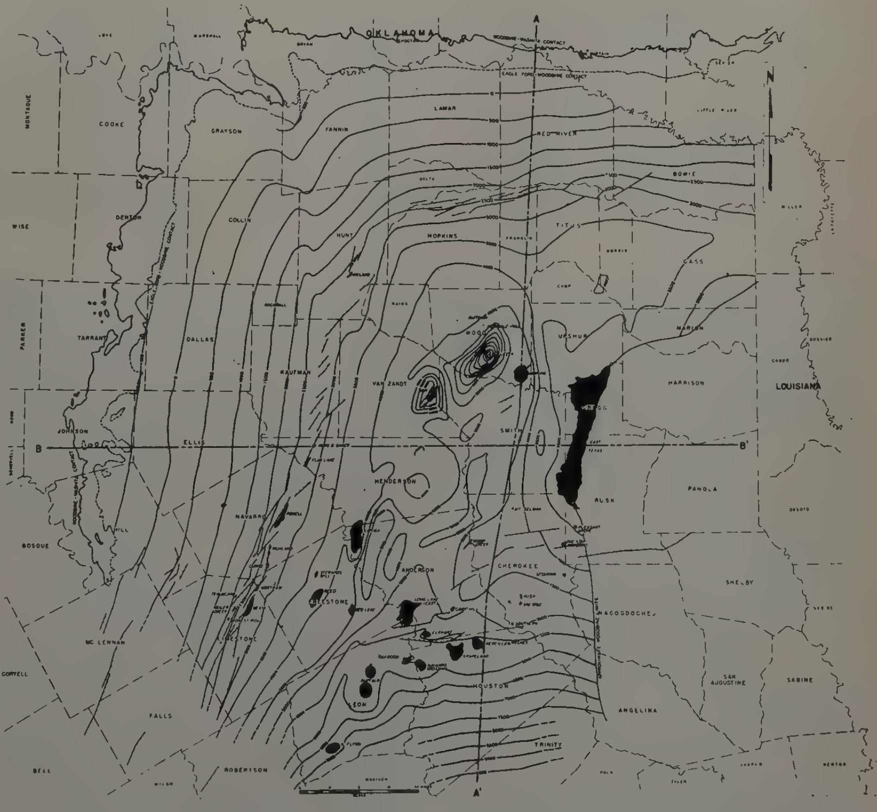

FIG. 1 — STRUCTURE MAP, EAST TEXAS BASIN, CONTOURED ON TOP WOODBINE — 500 FT INTERVAL.

---

[1]References given at end of paper.

Manuscript received in the office of the Petroleum Branch Sept. 15, 1950. Paper presented at the 1950 Fall Meeting of the Petroleum Branch in New Orleans Oct. 4-6.

Muskat[2] and by Schilthuis and Hurst[3] in 1934, and these principles were applied to the East Texas Field performance by Buckley[4] in 1938.

Factual data on the pressure behavior in the Woodbine sand, especially in areas non-productive of oil, have been generally lacking, making estimates of pressures at various points within the basin dependent upon mathematical analyses involving numerous assumptions. Such factual data have been gathered and are now presented as possible aid to the industry in further analysis of the producing mechanism in the Woodbine sand.

DISCUSSION

Geology

The Woodbine formation of Gulf Cretaceous Age has been described by R. T. Hill[5] and others as being comprised of thick blanket sands with interbedded shales. Within the East Texas basin, oil and gas, accompanied by water, have been produced from this formation in at least 42 fields, including the huge East Texas Field. These fields resulting from traps caused by faults, domes, and stratigraphic pinchouts are, with one possible exception, afforded a common aquifer by the continuity of the Woodbine formation which, within the recognized bounds of the East Texas basin, covers some 48 counties embracing 31,500 square miles.

A map has been prepared of the East Texas basin area on which are shown Woodbine producing fields in bold relief, major faults in the area as mapped by the Texas Bureau of Economic Geology, and the Woodbine outcrop. Fig. 1 is a copy of this map, on which are shown top-of-Woodbine contours and cross-sectional lines A-A′ and B-B′. The Woodbine formation within this large regional trough outcrops to the north and west and is pinched out against the Sabine uplift to the east. Southward the formation plunges with regional dip, becoming much less permeable, and is believed to pinch out. Figs. 2 and 3, depicting generalized east-west and north-south cross sections of the East Texas basin, further illustrate these structural features.

Producing Mechanism of the Woodbine Sand

Table I lists the Woodbine fields which have produced oil and gas in the East Texas basin. It will be noted that although Woodbine production is obtained from some 15 counties in the basin, there have been two main areas of production, the first being the Mexia-Talco fault-line fields in Limestone and Navarro counties and the second, the East Texas Field embracing parts of Cherokee, Gregg, Rusk, Upshur, and Smith counties. The fault-line production began in 1920 with oil discovered in the Mexia Field, Limestone County. It was not until several years after discovery of the East Texas Field that it was realized that a common aquifer existed between the fault-line fields and

Table I — Production Data Woodbine Fields[a]

			Oil Production Thousands of Bbl	
Field	County	Year of Discovery	1949	Cum. 1-1-50
(Active 1-1-50)				
East Texas	Cherokee, Gregg, Rusk, Smith, Upshur	1930	93,527	2,669,230
Hawkins	Wood	1940	11,454	107,842
Van	Van Zandt	1929	8,275	203,274
Cayuga	Anderson, Freestone, Henderson	1934	1,944[b]	43,625[b]
Long Lake	Anderson, Leon, Freestone	1933	1,256[b]	26,313[b]
Mexia	Limestone	1920	379	101,632
Powell	Navarro	1923	359	114,745
East Long Lake	Anderson	1941	229[b]	1,995[b]
Wieland	Hunt	1942	121	941
William Wise	Cherokee	1946	90	353
Wortham	Freestone	1924	81	23,564
Navarro Crossing	Houston	1938	89[b]	1,395[b]
Lone Star	Cherokee	1938	74	703
Pleasant Grove	Rusk	1941	53	591
Boggy Creek	Anderson, Cherokee	1925	44	4,427
Quitman	Wood	1948	35	44
Currie	Navarro	1921	18	7,121
Bazette	Navarro	1939	16	338
Merigale Paul	Wood	1946	12	69
Richland	Navarro	1924	9	6,737
Flag Lake	Henderson	1937	6	658
Tehuacana	Limestone	1940	5	74
Normangee Flynn	Leon	1946	3	12
Cedar Creek	Limestone	1927	3	336
Weches	Houston	1948	3	92
Honest Ridge	Limestone	1946	2	9
Southern Pine	Cherokee	1948	1	4
Grapeland	Houston	1936	218[c]	9,791[c]
Elkhart	Anderson	1938	25[c]	35[c]
Oakwood	Leon	1939	16[c]	76[b]
Buffalo	Leon	1934	24[b]	90[b]
Percilla	Houston	1937	20[c]	145[b]
Reed	Freestone	1947	7[c]	18[b]
Red Lake	Freestone	1934	2[c]	4[c]
Steward's Mill	Freestone	1943	7[c]	16[c]
(Inactive 1-1-50)				
Nigger Creek	Limestone	1926	0	2,999
Rusk	Cherokee	1934	0	261
Rowe & Baker	Henderson	1939	0	82
Manziel	Wood	1946	0	6
Camp Hill	Anderson	1935	x	x
Groesbeck	Limestone	1924	x	x
Sessions	Cherokee	1948	0	0
Total			118,020	3,309,788

[a] Data from "Development and Production in East and East Central Texas in 1949," *Statistics of Oil and Gas Development and Production for 1949.*
[b] Includes oil and condensate.
[c] Condensate production.
[x] Information not available.

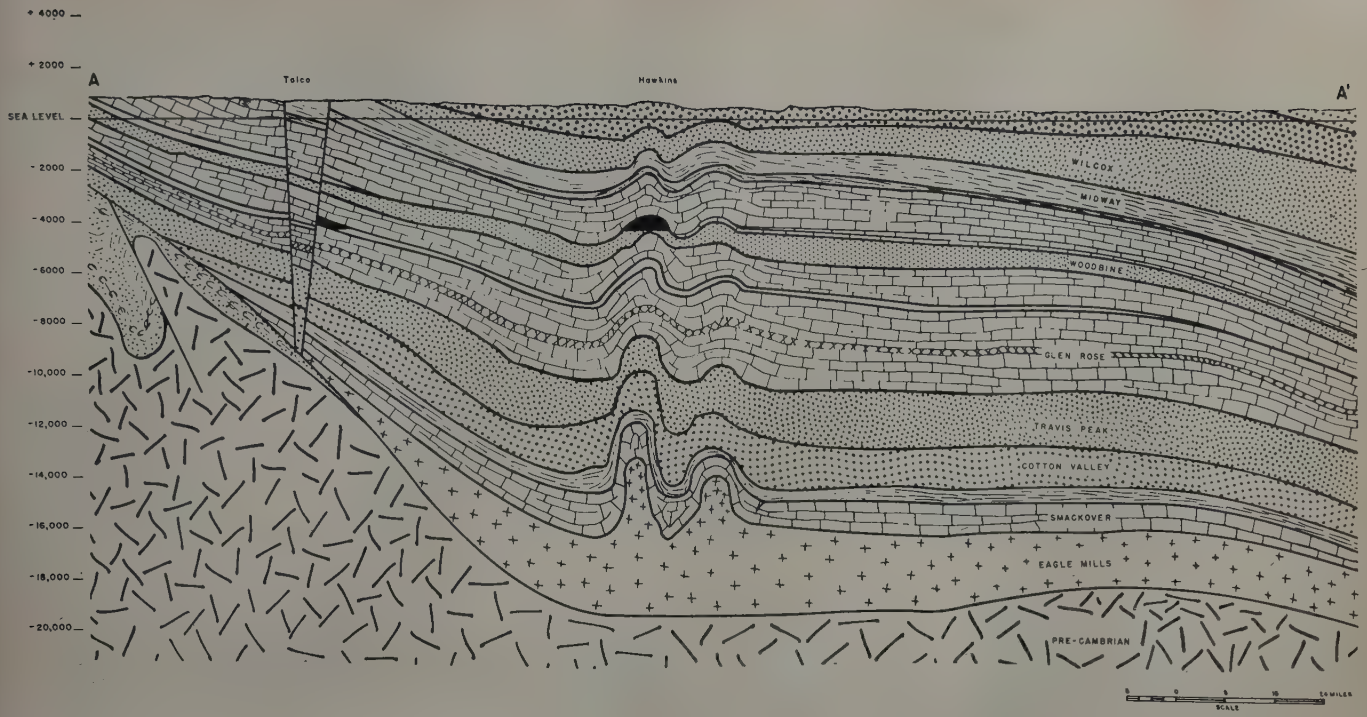

FIG. 2 — CROSS SECTION, EAST TEXAS BASIN — NORTH-SOUTH SECTION A-A′.

the East Texas and Van fields and that the production from a given field in the Woodbine reservoir could influence pressures elsewhere in the basin. In 1934, Muskat in an issue of *Physics*[2] and Schilthuis and Hurst in an AIME paper[3] described the producing mechanism in the East Texas Field, showing the pressure-production performance there to be governed primarily by the expansibility of the large volume of water contained within the Woodbine formation throughout the basin. Again in 1938, Buckley in an API paper[4] reviewed the East Texas Field producing mechanism and presented calculations demonstrating that the rate of availability of water by expansion was limited and that sound production practices in the nature of controlled net water production would be required in the East Texas Field to prevent loss in ultimate oil recovery.

Despite such early recognition that the Woodbine formation provides a common aquifer for its many water-drive fields and that the pressure in this aquifer would decline with production, factual data on the pressure behavior, particularly in areas non-produc-

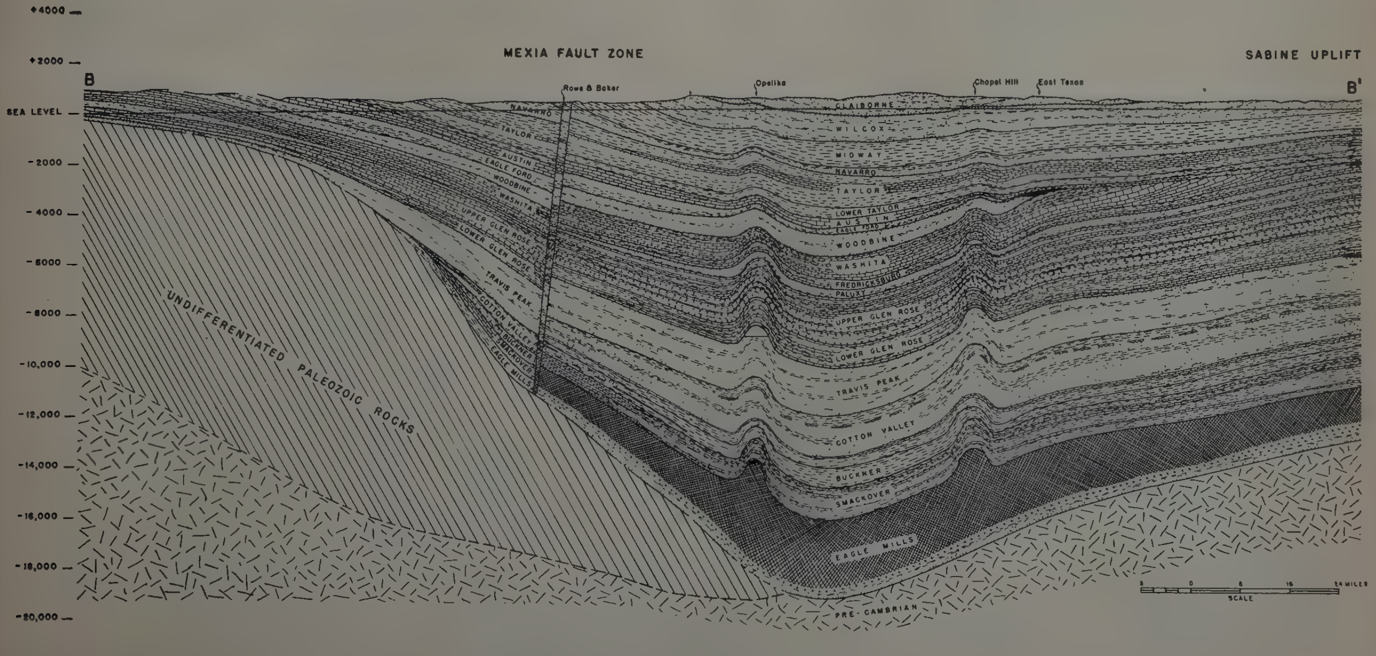

FIG. 3 — CROSS SECTION, EAST TEXAS BASIN — EAST-WEST SECTION B-B′.

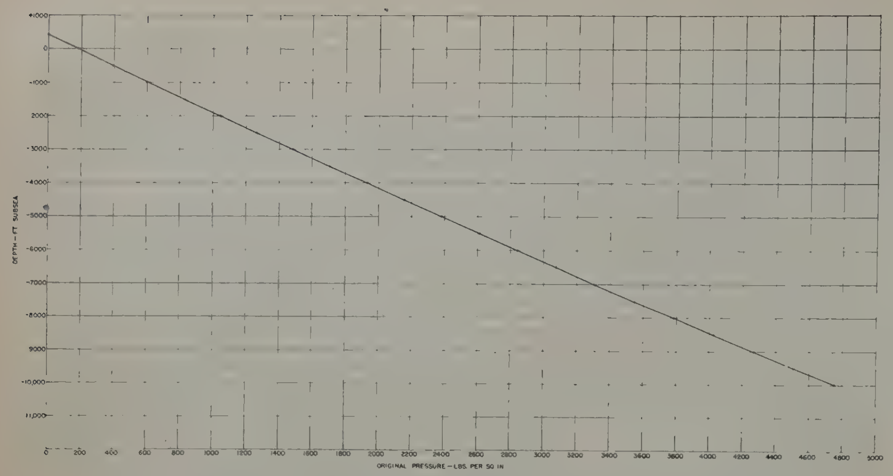

FIG. 4 — ORIGINAL PRESSURE VS. SUBSEA DEPTH, WOODBINE SANDS.

tive of oil, have been generally lacking. Consequently, estimates of pressure at points removed from producing fields have been largely dependent on mathematical calculations which necessarily required numerous assumptions.

Pressure Anomalies in the Hawkins Field

Shortly after discovery of production from the Woodbine sand in the Hawkins Field[1] in December, 1940, it was determined that a major northeast-southwest fault divided the field into two parts. Detailed pressure surveys within the field showed the original pressure in the eastern part of the Hawkins structure to be 1,710 psi corrected to a subsea depth of 4,075 ft; while in the western part of the field, an original pressure of 1,990 lb corrected to the same subsea depth was observed. In attempting to explain this phenomenon, three possibilities were considered: first, that the pressure in East Hawkins was the normal pressure, the West Hawkins pressure being abnormal due to compaction or extraneous force brought on by the extreme faulting; second, that the 1,990 lb in West Hawkins reflected the relative pressure in the water surrounding the field and that East Hawkins was in effect a closed reservoir, the oil being separated from water by some impermeable barrier, and that some pressure had dissipated upward from East Hawkins through fault planes; or, third, that West Hawkins was a closed reservoir, the oil and water being separated by an impermeable barrier, and that the pressure in East Hawkins had equalized or was equalizing with the pressure in the water surrounding the structure.

By visual observation and laboratory examination of cores and by production tests, it was found that the gas-oil and water-oil contacts in East Hawkins were both considerably lower than in West Hawkins, where a heavy asphalt deposit averaging some 40 ft in thickness was found at the base of the producible oil column. Comparisons with pressure information from other Woodbine-producing fields also revealed that the pressure in West Hawkins approached what would have been considered a normal original pressure for its depth. The third assumption was accordingly considered correct, the conclusion being that the initial pressure in East Hawkins was some 280 lb below normal because of East Texas Field withdrawals made during the 10-year period prior to Hawkins discovery.

The interesting pressure relation of East and West Hawkins and the East Texas Field prompted an area-wide study to determine the effect the withdrawals from the East Texas Field had had upon the general pressure in the Woodbine sands. Since 1942, Humble Oil and Refining Co. in its wildcat program within the area has measured the pressure in clean porous water-bearing sands of the Woodbine formation in 57 wells located in 18 counties. The pressures used in this paper were measured during drill-stem tests in which the tool was kept open long enough to assure stabilized static conditions, and pressures were checked in most tests by comparing pressures measured down the drill pipe with pressures obtained by a gauge below the testing tool.

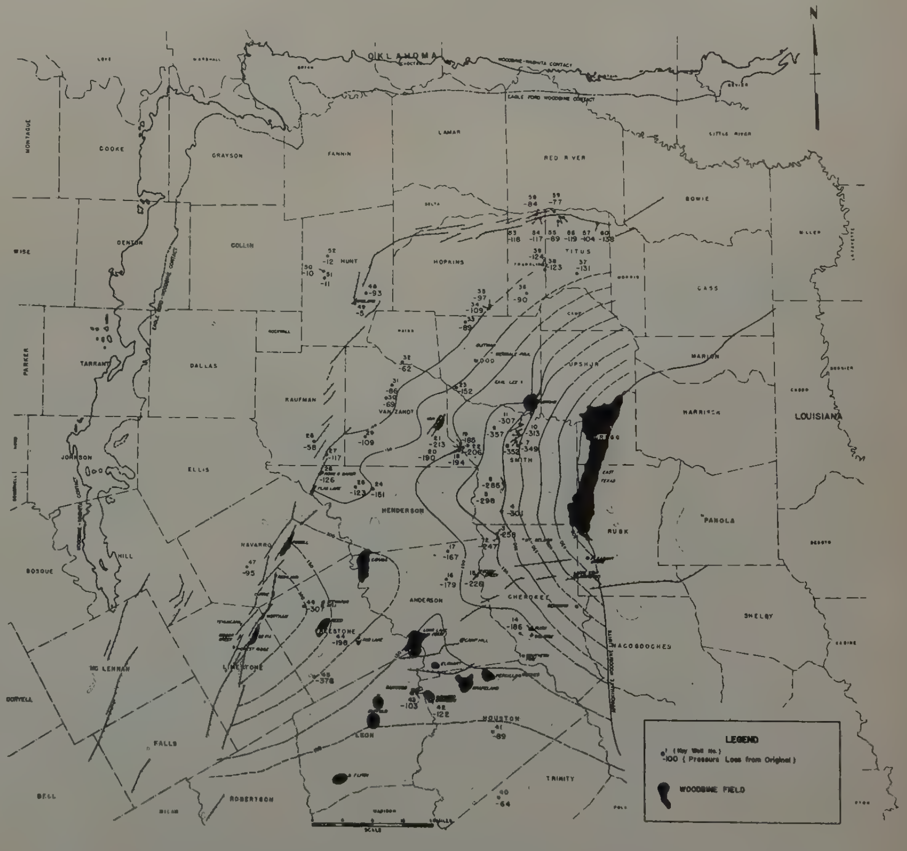

FIG. 5 — PRESSURE LOSS MAP, WOODBINE FORMATION. CONTOUR INTERVAL — 50 PSI.

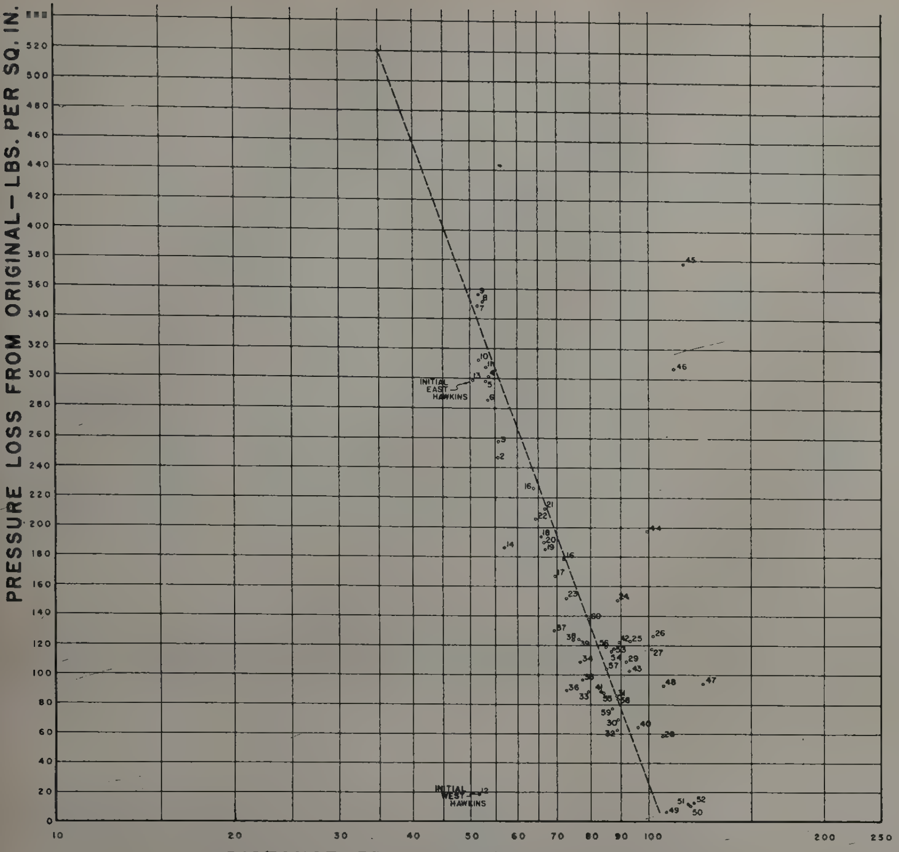

FIG. 6 — PRESSURE LOSSES, ALL WELLS, TOTAL INFLUENCE FOCAL POINT — EAST TEXAS FIELD.

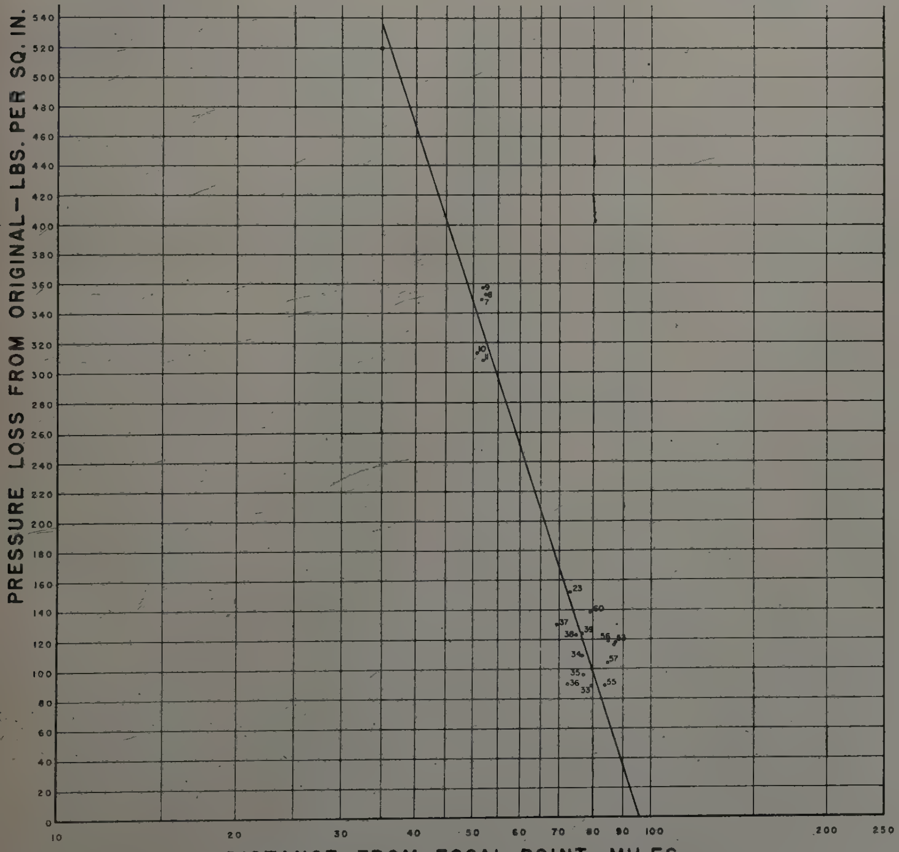

FIG. 7 — PRESSURE LOSSES, WELLS INFLUENCED ONLY BY EAST TEXAS FIELD FOCAL POINT, EAST TEXAS FIELD.

Estimated Original Woodbine Sand Pressures

In order to evaluate the pressures obtained in terms of loss from the estimated original pressures rather than making it necessary to correct all pressures to a given datum, the curve shown by Fig. 4, "Original Pressure versus Subsea Depth, Woodbine Sand," was constructed. This relationship was derived from the integration of a curve representing measured density values versus subsea depths where densities had been corrected for varying water compressibility and formation temperature. The average elevation of the outcrop of the Woodbine formation was determined to be 423 ft by extrapolating to zero pressure a curve of original observed pressure versus subsea depth for Van, East Texas, West Hawkins, Navarro Crossing, Well No. 50 (Lessa Norman 1, Hunt County), and Well No. 41 (C. W. LeGory 1, Houston County).

Distribution of Pressure Loss

Table II shows the calculated original pressures, the measured pressures, and the indicated pressure loss on each of these tests, as well as the date, location, depth of test, and distance from Points *X* and *Y*, which were used in establishing pressure loss—log distance relationships. Fig. 5 is the base map of the East Texas area, on which are shown locations of the test wells, indicated pressure drops from estimated original pressures, and contours of pressure losses. These contours, developed in the conventional manner of straight-line interpolation between actual measurement points, demonstrate that East Texas Field withdrawals have been the major cause of pressure losses in the basin, although fault-line field withdrawals have contributed significantly to such losses. Several unusual configurations which may be noted on the map encouraged a further effort to interpret the data. Considering radial flow principles, it was concluded that these pressure losses should vary with the log of their distance from a point representing a hypothetical focal point of withdrawals from each of the two major areas. This led to the construction of Fig. 6, which is a plot of the pressure loss versus log distance from a point labeled *X*, representing East Texas Field withdrawals, located at the intersection in Panola County of a 20.4-mile arc drawn from the southwest corner and a 12.3-mile arc drawn from the northwest corner of that county. All pressure losses are included on this plot, which indicates a general straight-line trend. This trend is interpreted to indicate further that the East Texas Field withdrawals have been the dominant influence on the pressure behavior within the basin. For illustrative purposes, the original pressures in East and West Hawkins have been corrected to 4,470 ft subsea, and estimated pressure losses have been plotted on the curve. This shows further that of the two pressures, the one measured in West Hawkins was the one abnormal at the time.

In addition to the abnormal West Hawkins pressure, it is noted that some other points fail to correspond satisfactorily with the trend. Considering this probably due to the influence of fault-line production, an effort was made to isolate those points of pressure measurement which were influenced predominantly by only East Texas Field withdrawals. Fig. 7 is a plot comparable to Fig. 6 except that measurements apparently influenced by fault-line production or those shown to be influenced by local fault conditions have been removed. On Fig. 7, indications are that East Texas Field withdrawals have affected pressures for a distance of 65 miles from the field or nearly 100 miles from the imaginary focal point, *X*.

A plot, Fig. 8, was made of pressure loss versus log distance of only those points whose pressure loss resulted solely from fault-line field production, with the hypothetical focal point labeled *Y* located in Limestone County at the intersection of a 5.9-mile arc drawn from the northeast corner and a 32.4-mile arc drawn from the southeast corner of that county. Fig. 8 suggests that the maximum distance of influence of fault-line field production has been approximately 80 miles from Point *Y*. Having separated the indicated pressure loss influence of fault-line field production from that of East Texas Field production, as represented by Fig. 7 and 8, Fig. 9 was then constructed, which corrected points jointly influenced by withdrawals from both areas, showing only the indicated influence of East Texas withdrawals. The accuracy of the corrections made for fault-line field production influence is indicated by the fact that the average curve on Fig. 9, the plot of distance from Point *X* versus pressure losses corrected for fault-line field production interference, corresponds to the average curve on Fig. 7, the plot of distance from Point *X* versus pressure losses not influenced by fault-line field production.

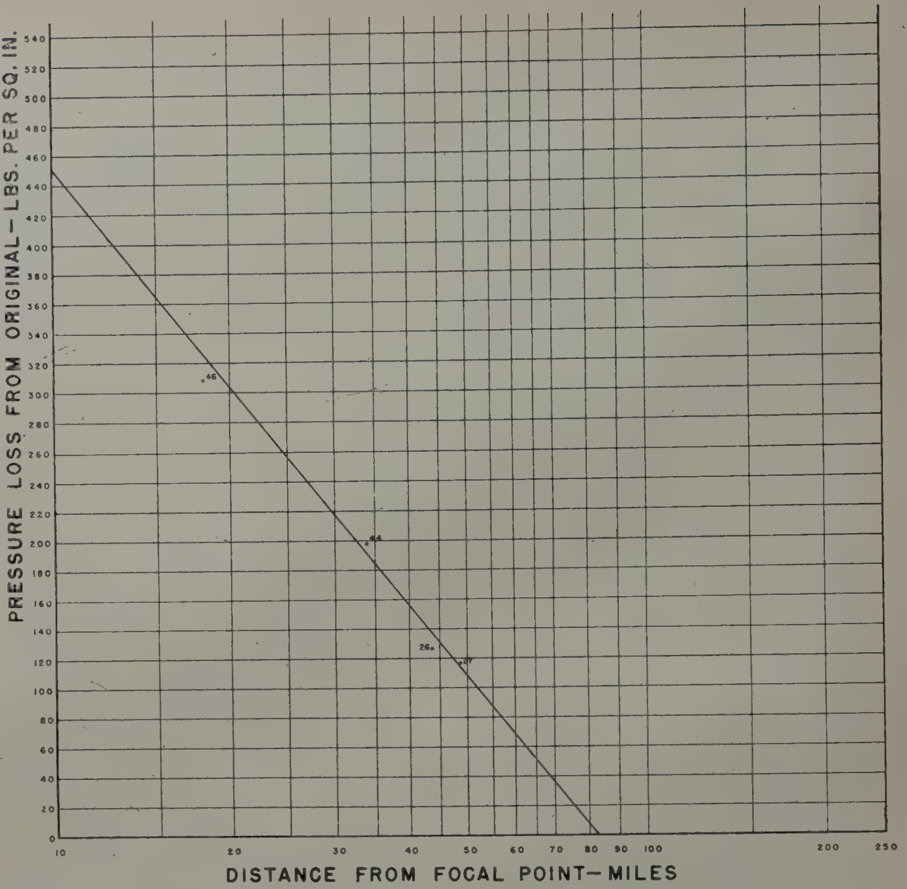

FIG. 8 — PRESSURE LOSSES, WELLS INFLUENCED ONLY BY FAULT-LINE FIELDS FOCAL POINT, FAULT-LINE FIELDS.

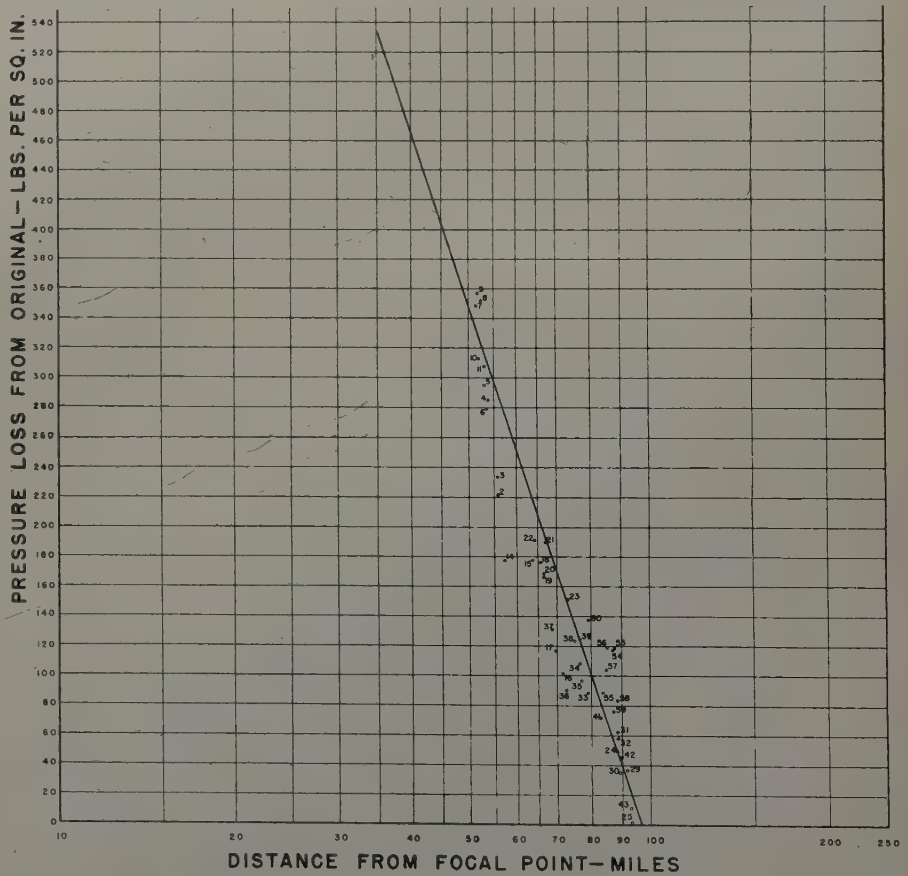

FIG. 9 — PRESSURE LOSSES, ALL WELLS, CORRECTED TO EAST TEXAS FIELD INFLUENCE ONLY FOCAL POINT, EAST TEXAS FIELD.

Fig. 10 is the same map as Fig. 5 except that Points *X* and *Y* are located and arcs have been drawn from these points representing the limit of influence of withdrawals from the East Texas Field and fault-line fields. The area which is affected by withdrawals from both of these sources is cross-hatched. The unusual contour configurations noted, particularly in Van Zandt, Henderson, and Anderson counties, are in this cross-hatched zone. The contour drawn into the Hawkins Field is a result of drainage restrictions caused by the major fault in that field. A few pressure losses indicated on the map vary considerably from those which would be expected; however, some of these variations may be explained by the time over which the pressures were measured, and unknown structural and stratigraphic conditions. Elsewhere it is considered that there is unusually good agreement with the contours and the indicated pattern developed from the pressure loss — log distance relations. Considering the large area involved, there are remarkably few measurements which fail to conform to the expected pattern.

Pressure Behavior Across Faults

In the process of analyzing pressure trends and differences, it has been noticed that pressures on opposite sides of faults quite often show anomalies which indicate a barrier or restriction to drainage across the faults. Specific illustrations of this fact are:

1. in the area of the fault-line fields where the pressure loss in Well No. 47 (B. L. Davis 1, Navarro County) west of the fault line is 95 lb, as compared to a pressure loss east of the fault of 307 lb in Well No. 46 (B. C. Whatley 1, Freestone County);
2. in southeast Kaufman County where Well No. 28 (Lon Hale 1) west of the fault line has a pressure loss of 58 lb as compared to a pressure loss of 117 lb east of the fault line in Well No. 27 (E. N. Rylie 1); and
3. in the area of the Talco Field where the indicated pressure loss of approximately 118 lb basinward from the fault compares with an average loss of 80 lb on the outward side of the fault.

In addition to the unusual configura-

Table II — Pressure in the Woodbine Sand — East Texas Geosyncline

						Depth Section Tested-Ft				Depth of Pressure Measurement-Ft		Pressure at Measurement Depth-psi			Distance From Focal Points, Miles	
						Subsurface		Subsea								
Key No.	Well Name	Field or Area	County	Date of Test	Elevation	From	To	From	To	Sub-surface	Sub-sea	On Test Date	Orig.	Indicated Loss	X	Y
1	1100# Contour	East Texas		1- 1-44	—	—	—	—	—	—	3,324	1,108	1,628	520	35.0	105.9
2	S. T. Stanley 1	Larissa	Cherokee	8-20-44	414	5,389	5,471	4,975	5,057	5,466	5,052	2,158	2,405	247	55.5	73.2
3	W. H. Stephens B-1	Larissa	Cherokee	7-12-44	479	5,760	5,780	5,281	5,301	5,761	5,282	2,252	2,510	258	55.7	73.2
4	Kate E. Sackett 1	Bullard	Smith	5-20 and 21-48	553	5,561	5,630	5,008	5,077	5,622	5,069	2,112	2,413	301	53.6	76.5
5	E. M. Sherlock 1	Tyler	Smith	2- 1-49	570	5,673	5,695	5,103	5,125	5,686	5,116	2,137	2,435	298	53.0	80.3
6	F. Watson 1	Tyler	Smith	8- 4-49	573	5,708	5,746	5,135	5,173	5,742	5,169	2,175	2,460	285	53.4	79.8
7	B. S. Shamburger 1	Sand Flat	Smith	3-24-44	532	5,557	5,645	5,025	5,113	5,641	5,109	2,084	2,433	349	51.2	88.5
8	Roosth & Genecov 1	Sand Flat	Smith	8-31-45	443	5,122	5,163	4,679	4,720	5,159	4,716	1,902	2,254	352	52.1	88.2
9	P. K. Birdwell C-1	Sand Flat	Smith	12- 7-48	437	5,197	5,220	4,760	4,783	5,215	4,778	1,925	2,282	357	51.7	90.0
10	H. E. Kidd 1	Sand Flat	Smith	9-19-47	482	5,627	5,670	5,145	5,188	5,659	5,177	2,150	2,463	313	51.9	90.3
11	E. W. Wintters 1	Red Springs	Smith	6- 5-48	536	5,500	5,571	4,964	5,035	5,562	5,026	2,089	2,396	307	53.0	91.5
12		East Hawkins	Wood	12-40 (Discovery Date)				—	—	—	4,470	1,844	2,142	298	51.3	98.4
13		West Hawkins	Wood	12-40 (Discovery Date)				—	—		4,470	2,124	2,142	18	52.8	97.2
14	New Birmingham Dev. Co. 1	Fastrill	Cherokee	4- 4-45	441	5,490	5,500	5,049	5,059	5,485	5,044	2,216	2,402	186	57.0	79.2
15	W. T. Todd 1	Boggy Creek	Anderson	9-29-45	300	4,645	4,750	4,345	4,450	4,745	4,445	1,906	2,132	226	63.6	65.6
16	R. G. Freeman 1	Brushy Creek	Anderson	11-16-45	562	5,290	5,350	4,728	4,788	5,346	4,784	2,106	2,285	179	71.9	57.2
17	T. O. Milner 1	Fosterville	Anderson	8- 7-48	508	5,646	5,711	5,138	5,203	5,707	5,199	2,305	2,472	167	69.5	59.3
18	T. J. Pool 1	Mt. Sylvan	Smith	11- 9-45	454	5,644	5,675	5,190	5,221	5,671	5,217	2,286	2,480	194	65.7	75.3
19	H. R. Dowell 2	Mt. Sylvan	Smith	7- 6-46	434	5,599	5,620	5,165	5,186	5,616	5,182	2,280	2,465	185	66.5	75.0
20	Frank Woods 1	Mt. Sylvan	Smith	2-22-47	416	5,534	5,585	5,118	5,169	5,580	5,164	2,267	2,457	190	66.3	74.1
21	Perk Beasley 1-S	Mt. Sylvan	Smith	5-12-48	442	5,343	5,442	4,901	5,000	5,884	5,442	2,372	2,585	213	66.9	74.0
22	M. L. Gary 1	Boynton	Smith	4-28-47	448	5,505	5,560	5,057	5,112	5,555	5,107	2,226	2,432	206	64.2	76.7
23	H. Watts 1	Nolan Edwards	Wood	12- 9-49	388	5,779	5,794	5,391	5,406	5,791	5,403	2,415	2,567	152	72.6	84.6
24	W. J. Benge 1	Stockard	Henderson	12-11-46	455	4,691	4,710	4,236	4,255	4,705	4,250	1,893	2,044	151	88.1	51.0
25	A. G. Jones 1	Eustace	Henderson	1- 8-45	377	4,327	4,372	3,950	3,995	4,363	3,986	1,803	1,926	123	93.0	46.2
26	J. Burford 1	Mabank	Henderson	7-24-50	362	3,949	3,983	3,587	3,621	3,973	3,611	1,630	1,756	126	102.2	43.7
27	E. N. Rylie 1	Ham Gossett	Kaufman	11-30-48	375	3,806	3,826	3,431	3,451	3,821	3,446	1,568	1,685	117	101.4	48.6
28	Lon Hale 1	Kemp	Kaufman	7-30-46	409	3,455	3,470	3,046	3,061	3,465	3,056	1,450	1,508	58	105.6	50.1
29	E. E. Lutz 1	West Jackson	Van Zandt	11-15-45	477	4,570	4,595	4,093	4,118	4,591	4,114	1,873	1,982	109	91.7	58.7
30	B. W. Bruce, Jr. 1	Myrtle Springs	Van Zandt	8-10-44	510	4,622	4,700	4,112	4,190	4,696	4,186	1,946	2,015	69	89.0	70.1
31	Joe Surratt 1	Edgewood	Van Zandt	4-26-44	440	4,579	4,605	4,139	4,165	4,605	4,165	1,919	2,005	86	88.6	73.8
32	D. B. Mainard 1	Emory	Rains	12-22-43	375	4,590	4,621	4,215	4,246	4,575	4,200	1,958	2,020	62	88.5	80.6
33	Rio Oil Corporation 1	Yantis	Wood	5-12-47	398	4,806	4,861	4,408	4,463	4,853	4,455	2,047	2,136	89	79.1	99.5
34	P. T. King 1-S	Pickton	Hopkins	2-13-47	470	4,900	5,200	4,430	4,730	5,200	4,730	2,151	2,260	109	76.7	106.2
35	C. D. Nichols 1	Pickton	Hopkins	7- 1-44	472	4,912	4,930	4,440	4,458	4,926	4,454	2,039	2,136	97	77.0	106.8
36	Solon King 1	Scroggins	Franklin	11-23-43	370	4,550	4,600	4,180	4,230	4,513	4,143	1,906	1,996	90	72.3	116.1
37	C. C. Searcy 1	Mt. Pleasant	Titus	6- 9-44	398	4,367	4,441	3,969	4,043	4,250	3,852	1,733	1,864	131	69.3	129.3
38	J. F. Hague 1	Winfield	Franklin	4-26-44	422	4,160	4,170	3,738	3,748	4,164	3,742	1,693	1,816	123	74.7	124.2
39	Angelina Jaggears 1	Winfield	Franklin	10-18-46	433	4,159	4,210	3,726	3,777	4,205	3,772	1,703	1,827	124	76.2	95.0
40	Thompson Bros. Min. Corp. 1	Glendale	Trinity	8-2 to 5-48	184	9,525	9,555	9,351	9,371	9,555	9,371	4,380	4,444	64	96.2	85.8
41	C. W. LeGory 1	Crockett	Houston	8-25-46	385	7,518	7,536	7,133	7,151	7,531	7,146	3,291	3,380	89	83.0	75.9
42	C. C. Hill 2	Navarro Crossing	Houston	1- 9-46	272	6,052	6,099	5,780	5,827	6,092	5,820	2,636	2,758	122	89.6	57.6
43	Leone Plantation 1	Oakwood	Leon	7-18-45	264	5,900	5,917	5,636	5,653	5,895	5,631	2,567	2,670	103	92.4	53.3
44	G. J. Weaver 1	Red Lake	Freestone	6- 4-46	405	4,808	4,838	4,403	4,433	4,808	4,403	1,915	2,113	198	99.3	33.9
45	R. P. McWatters 1	Teague	Freestone	8-26-47	489	4,763	4,775	4,274	4,286	4,770	4,281	1,680	2,058	378	114.9	18.0
46	B. C. Whatley 1	Kirvin	Freestone	2-11 & 12-48	406	3,780	3,830	3,374	3,424	3,830	3,424	1,367	1,674	307	111.0	19.0
47	B. L. Davis 1	Corbet	Navarro	6-8 and 9-48	351	2,237	2,253	1,886	1,902	2,246	1,895	905	1,000	95	123.9	12.0
48	R. P. Barnett 1	South Dixon	Hunt	5-24-49	464	3,508	3,550	3,044	3,086	3,545	3,081	1,431	1,524	93	105.9	92.3
49	Aetna Life Ins. Co. 1	Wieland	Hunt	7-19-42	497	2,823	2,832	2,326	2,335	2,815	2,318	1,183	1,188	5	107.1	88.5
50	Lessa Norman 1	Greenville	Hunt	2- 2-44	559	2,460	2,500	1,901	1,941	2,466	1,907	995	1,005	10	118.7	93.9
51	J. A. Rutherford 1	Greenville	Hunt	11-22-43	540	2,550	2,590	2,010	2,050	2,547	2,007	1,038	1,049	11	117.5	92.1
52	E. M. Anderson 1	Kingston	Hunt	4- 1-44	599	2,130	2,150	1,531	1,551	2,148	1,549	841	853	12	119.9	98.1
53	P. J. Dawson 2-S	Talco	Franklin	4-28-48	374	3,224	3,381	2,850	3,007	3,381	3,007	1,370	1,488	118	87.3	133.2
54	Lena Wims 1-S	Talco	Franklin	11- 9-46	356	3,613	3,702	3,257	3,346	3,700	3,344	1,522	1,639	117	86.8	133.8
55	Hoffman Fee 1-S	Talco	Titus	8- 3-42	311	3,356	3,500	3,045	3,189	3,366	3,055	1,419	1,508	89	83.8	136.2
56	A. W. Batson 1-S	Talco	Titus	12- 2-47	361	3,199	3,397	2,838	3,036	3,397	3,036	1,379	1,498	119	84.7	137.4
57	E. L. Riddle 4-S	Talco	Titus	5-13-44	330	3,212	3,262	2,882	2,932	3,262	2,932	1,349	1,453	104	84.4	147.0
58	T. C. Geron 1	Sulphur River	Franklin	9-20-45	321	3,630	3,713	3,309	3,392	3,708	3,387	1,574	1,658	84	88.5	134.1
59	Guaranty Bond 1	Sulphur River	Titus	9-19-46	313	3,716	3,767	3,403	3,454	3,762	3,449	1,608	1,685	77	86.9	137.7
60	P. H. Pewitt 1	Pewitt Ranch	Titus	11-23-49	278	3,631	3,649	3,353	3,371	3,644	3,366	1,512	1,650	138	79.4	143.1

tions of the contours caused by additive influence of East Texas Field and fault-line field withdrawals, it is noted in a few areas, particularly about the Hawkins Field in Wood County, that local faults within the basin have caused some irregularity in the expected contour behavior. The anomalies in expected pressure behavior resulting from these faults merely serve to point out that the pressure drop is a function of the difficulty and distance of water travel which is greater because of interference in fault areas.

Fig. 11 is a map of the Hawkins Field on which are shown the major fault dividing the field into West and East Hawkins, and pressures taken below the asphalt barrier at various points in West Hawkins, corrected to March 1, 1946. Table III gives data pertinent to those pressure measurements showing the corrections made to 4,470 ft subsea and the extrapolations made to bring the observed pressures to a common date. It will be noted from the figure that across the northern sector of the West Hawkins reservoir there is a pressure difference of approximately 50 lb running northwesterly, from the Esparcia Survey to the Crane Survey. To the south a pressure difference running southeasterly in the amount of approximately 60 psi is indicated from the Esparcia Survey to the Brewer Survey. These gradients over distances less than four miles appear considerable; however, examination of Fig. 9, the plot of distance from Point *X* versus pressure loss for all wells corrected to East Texas Field influence only, indicates that at this distance from the East Texas Field a gradient of approximately 10 lb per mile is normal. Hence, the pressure differentials measured across the West Hawkins Reservoir are normal. However, illustrative of the effect of fault influence on pressure behavior is a comparison of the 1,859-lb H. E. Watson Survey pressure measured in the West Hawkins water zone and a 1,739-lb average water-zone pressure shown for East Hawkins. The 120-lb differential measured within less than a mile distance on opposite sides of this major fault would normally be expected over a distance of 13 miles.

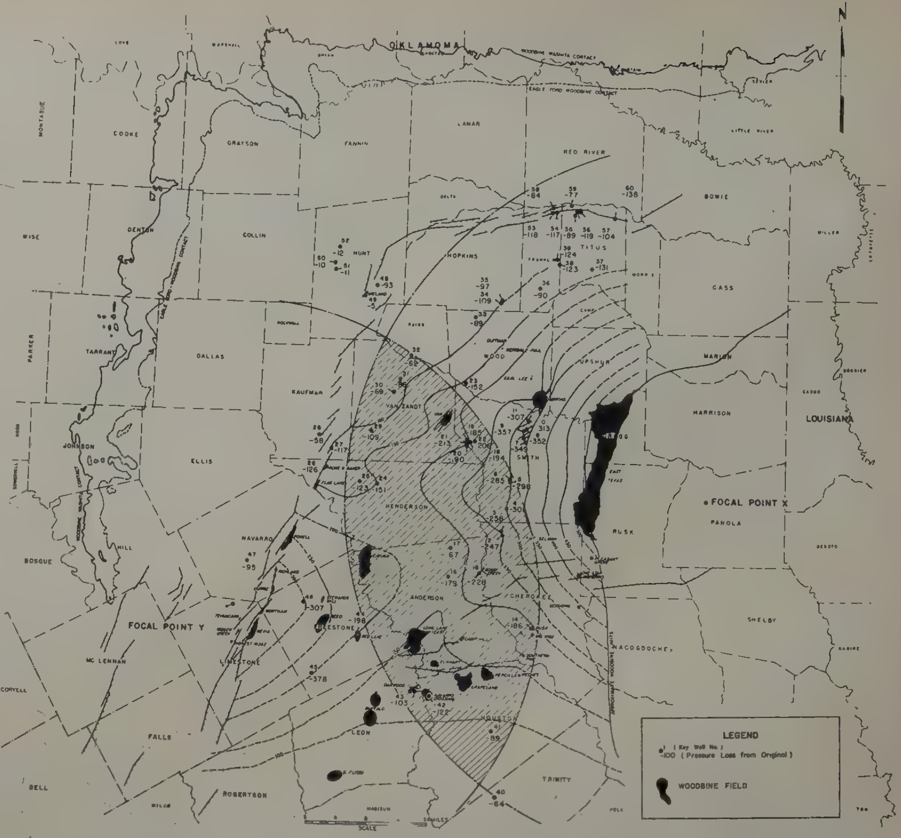

FIG. 10 — PRESSURE LOSS MAP, WOODBINE FORMATION. CONTOUR INTERVAL — 50 PSI SHOWING SPHERES OF INFLUENCE BY MAJOR PRODUCTION AREAS.

Table III — Woodbine Sand Pressures in and Near Hawkins Field

Lease and Well No.	Elev. Ft	Date of Test	Depth Section Tested-Ft Subsurface From	Depth Section Tested-Ft Subsurface To	Depth Section Tested-Ft Subsea From	Depth Section Tested-Ft Subsea To	Depth Pressure Measurement Ft Sub-surface	Depth Pressure Measurement Ft Subsea	Measured Pressure psi	Pressure Corrected 4,470-ft Subsea psi On Test Date	Pressure Corrected 4,470-ft Subsea psi Extrap-olated To 3-1-46
L. A. Bryan B-15	449	8-16-46	4,974	5,000	4,525	4,551	4,969	4,520	1,913	1,890	1,893
A. Crisman 2	410	4-26-46	4,986	5,007	4,576	4,597	5,002	4,592	1,961	1,905	1,906
Lillian Eagle 1	392	3- 6-47	5,080	5,112	4,688	4,720	5,105	4,713	2,020	1,909	1,916
E. M. Faulk 8	434	5- 6-46	4,925	4,953	4,491	4,519	4,948	4,514	1,911	1,891	1,892
E. M. Faulk B-4	471	1- 5-46	4,990	5,018	4,519	4,547	5,013	4,542	1,893	1,860	1,859
M. Greines, Jr. 2	471	3-31-47	5,058	5,077	4,587	4,606	5,070	4,599	1,925	1,866	1,873
B. Hargett 4	385	11-28-45	4,893	4,911	4,508	4,526	4,906	4,521	1,864	1,841	1,839
Jackson-Chism B-1	398	3-22-46	4,936	4,955	4,538	4,557	4,950	4,552	1,907	1,870	1,870
P. H. McKnight 1	358	7- 7-46	5,000	5,052	4,642	4,694	5,047	4,689	1,970	1,870	1,872
W. T. Minshew 3	398	3-13-46	4,908	4,919	4,510	4,521	4,916	4,518	1,874	1,852	1,852
Oscar Mitchell 1	408	1- 3-47	4,855	4,915	4,447	4,507	4,910	4,502	1,850	1,835	1,841
Joe Palmer B-2	408	3-23-46	4,919	4,949	4,511	4,541	4,944	4,536	1,879	1,849	1,849
G. R. Philips 1	427	7- 7-47	5,041	5,054	4,614	4,627	5,049	4,622	1,960	1,891	1,898
F. B. Ponder C-3	423	11- 1-45	4,932	4,939	4,509	4,516	4,945	4,522	1,912	1,888	1,886
J. H. Ponder 6	383	3-26-46	4,910	4,933	4,527	4,550	4,928	4,545	1,887	1,853	1,853
R. Price 4	367	12- 1-45	4,880	4,898	4,513	4,531	4,893	4,526	1,860	1,834	1,832
I. Rutherford 6	372	1- 4-46	4,880	4,890	4,508	4,518	4,887	4,515	1,881	1,860	1,859
W. J. Shamburger 2	431	4-19-46	4,928	4,954	4,497	4,523	4,949	4,518	1,900	1,878	1,878
W. S. Shamburger B-4	447	2- 8-46	5,020	5,076	4,573	4,629	5,071	4,624	1,966	1,896	1,895
T. C. Snow 5	422	12- 2-45	4,921	4,944	4,499	4,522	4,939	4,517	1,881	1,860	1,858
T. C. Snow 6	466	7-18-46	4,962	4,981	4,496	4,515	4,976	4,510	1,879	1,861	1,863

CONCLUSIONS

1. Fluid withdrawals from the Woodbine formation in the East Texas basin, particularly from the East Texas Field and from the fault-line fields, have caused pressure loss in practically all of the East Texas basin contained within the Mexia-Talco fault line.

2. The distribution of this pressure loss is in general relation to the log distance from the two main areas of basin withdrawal.

3. Some of the observed irregularities in anticipated pressure patterns are the result of fault interference.

4. The anticipated initial pressure of any new Woodbine field or any long-range forecast of the pressure behavior in any Woodbine field must consider the over-all pressure pattern in the basin.

5. The apparent reasonableness of this qualitative study indicates that regional pressure investigations as well as local field measurements have practical application.

ACKNOWLEDGMENTS

The authors wish to thank Humble Oil and Refining Co. for making the data included in this report possible by allowing the extensive drill-stem testing program and for permission to publish this information. The authors also express their gratitude for and acknowledge the assistance given by the following Humble personnel: Stuart E. Buckley and the Production Research Division, for their encouragement and aid; members of the Exploration Department and Petroleum Engineering Division, and all the associated groups in the East Texas Division of the Production Department.

REFERENCES

1. Wendlandt, E. A., Shelby, T. H., Jr., and Bell, John S.: *Bulletin of the American Association of Petroleum Geologists*, (1946), **30**, No. 11.
2. Muskat, Morris: *Physics*, (1934), **5**, 71.
3. Schilthuis, Ralph J., and Hurst, William: *Trans.* AIME, (1935), **114**, 164.
4. Buckley, Stuart E.: "The Pressure-Production Relationship in the East Texas Field." *API Drilling and Production Practice*, (1938).
5. Hill, R. T.: *U. S. Geol. Survey Annual Report*, (1901), **21**, Pt. 7, p. 292.

DISCUSSION

By William Hurst, Consultant, Houston, Tex., Member AIME

This is a timely presentation of the excellent paper on "Pressure Behavior in the Woodbine Sand," by John S. Bell and J. M. Shepherd. This reviewer has often wondered when such a paper would be forthcoming as he has never accepted that the infinite effect of radial water encroachment into the East Texas Field would continue indefinitely without encountering the interference of withdrawals from the Woodbine basin by existing fields such as Van, Hawkins, and the Mexia-Talco Fault-Line fields.

In order that there may be no illusion as to the validity for treating the Woodbine formation as an infinite aquifer, as interpreted by the original investigators, it suffices only to inform the reader that no matter what form of water-drive is encountered in a reservoir, that will eventually be affected by interference, the formation will essentially behave as an infinite aquifer until such condition is met. That this has been sustained as late as 1944, or 14 years after the inception of East Texas, is verified by this reviewer's study of the field. Beyond this date he has no further knowledge of the status of the field. Nevertheless, from an examination of Figs. 5 and 10 of this paper, the small pressure loss of from 150 to 200 psi, represented by the region of interference in Henderson and Anderson counties, as compared with the significant loss of 500 psi in the vicinity of the East Texas Field, may even to this time justify the analysis for infinite water-drive into East Texas.

If and when geology and geophysics adequately define the limits of an aquifer, the reservoir engineer can incorporate such limitations in the analytical treatment of the formation. Until such evidence is forthcoming the factual field data will have to provide the information, which is the direction that this problem has taken. There are no unforeseeable difficulties contained in the present interference pattern of the Woodbine formation that cannot be treated analytically. This has been amply provided for in the literature, thanks to the contribution of people engaged in the oil industry. Particularly is this point stressed, because the conformity of the pressure pattern due to the voidage of the aquifer by the existing fields and the depletion of the Woodbine as a whole, is most realistically sustained by mathematical deduction for the mechanics of fluid flow.

In this respect, the specialist has reached that phase of translating engineering into dollars and cents for management. It is fitting to remind you that this progress is not of recent date, but took place in East Texas approximately 20 years ago. The material benefits to the community, the accrued and continued income received by the major, independent, and royalty owner over the years, testify to the vision and fortitude of these early investigators in simulating the performance for the res-

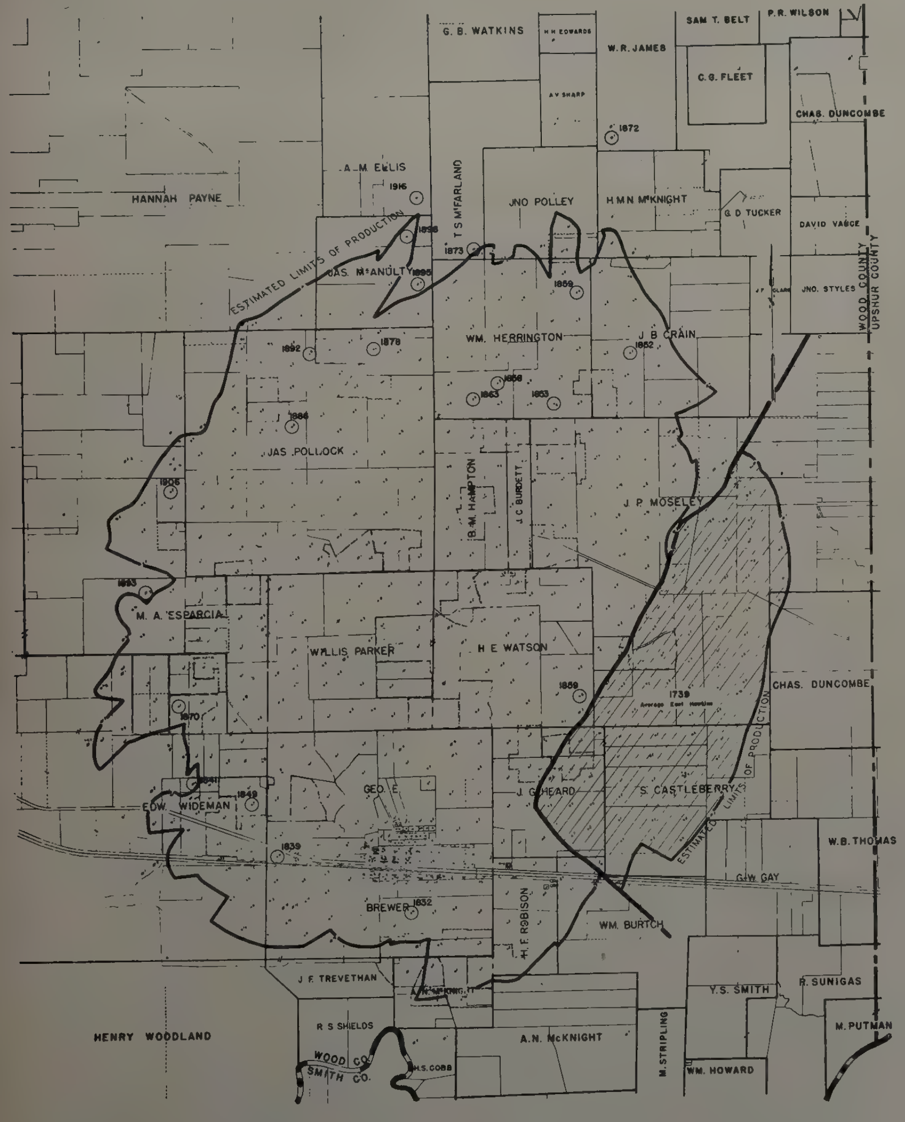

FIG. 11 — WATER ZONE PRESSURE MAP, HAWKINS FIELD, DATUM 4,470 FT SUBSEA. EFFECTIVE DATE, MAR. 1, 1946.

ervoir that today sustains pressure maintenance in the East Texas Field that will assure the continuation of revenue into the future.

To conclude this review, it is recognized that the transient state of pressure change should also have an effect in the interpretation of the interference pattern shown in Fig. 10. Since the compilation of pressures, Table II, is representative from 1942 to the present, the question asked the authors is, has it been possible to make this distinction in the analysis with the data on hand?

DISCUSSION

By M. Muskat, Gulf Oil Corp., Member AIME

The authors are to be congratulated on this excellent paper and their making the results of their study available to the industry. Drill stem testing in wildcat wells for the sole purpose of determining pressures in a locally unproductive formation reflects a most progressive long-range research policy.

The water expansibility theory, as first applied to the East Texas Field, has been accepted as the basis for explaining the water drive performance of many of our major reservoirs. It has served to predict the pressure history of the East Texas Field with remarkable precision over a period of 20 years. Yet, this theory has other important implications with respect to the pressure reaction in the Woodbine aquifer itself, the confirmation of which would be an important factor in the overall evaluation of the water drive oil producing mechanism. The present paper provides just the type of data required for this supplementary analysis.

As noted in the paper, the reported pressure data show the long range pressure reactions to be expected in continuous and permeable fluid bearing porous media. Their correlation with the fluid withdrawals from other fields, as well as East Texas, in the Woodbine sand should settle once and for all the arguments about physically limited drainage radii in permeable continuous reservoirs. The apparent pressure anomalies found across faults also give a gratifying confirmation of the implications of fluid flow concepts generally accepted in explaining oil reservoir performance. The observed large scale shielding effects of impermeable fault barriers is a simple corollary of the compressible liquid flow mechanism, which is even more clearly demonstrated here than in pressure patterns about faults within producing fields.

Recognition and acceptance of the possibility of regional pressure interference in continuous aquifers will facilitate the interpretation and understanding of initial pressure conditions in newly-discovered fields. As also observed elsewhere, this fact will serve to resolve anomalies in pressure histories of fields assumed to react only to their own withdrawals. It may provide explanations in some cases of apparent tilting of water tables. Other applications will undoubtedly develop from a study of the data.

No doubt the authors or their associates will make a quantitative analysis of the pressure observations by the electrical analyzer or similar techniques. It should be especially instructive to determine the quantitative correlations of the data with the theoretical predictions; and it will be interesting to see the implications of such an analysis with respect to the macroscopic expansion capacity of the Woodbine aquifer as well as its gross effective permeability.

★ ★ ★

A STUDY OF THE DORNICK HILLS-SPRINGER SAND RESERVOIR, VELMA POOL, OKLAHOMA

W. B. DAVIS, GULF OIL CORP., TULSA, OKLA., MEMBER AIME

ABSTRACT

This paper presents a summary of the results of a study of the Dornick Hills-Springer sand reservoir of the Velma Pool, Stephens County, Oklahoma. The data are of interest because this type of reservoir is unusual in the mid-continent area.

The reservoir is characterized by very steep dips and a relatively thick producing section. Its up-dip productive limit is defined by truncation of the productive sands, and the down-dip limit is defined by deterioration of sand quality rather than by the presence of an oil-water contact. The crude oil is of 29° API gravity, is relatively viscous and was saturated with dissolved gas at the original reservoir pressure.

Consideration of the physical characteristics of the reservoir indicates that natural water encroachment will be negligible, and that the producing mechanism will be a dissolved gas drive augmented by gravity drainage. Performance to date tends to confirm this.

INTRODUCTION

It is the purpose of this paper to present some of the features of the Dornick Hills - Springer sand reservoir which are unusual in mid-continent operations. The study was undertaken in an attempt to define the producing mechanism or mechanisms that will control reservoir performance, as an aid in determining well completion and production practices.

GEOLOGY

The reservoir under consideration is a series of sand bodies of Pennsylvanian age found in the Lower Dornick Hills and/or Springer formations. For the purpose of this paper, the sand series is referred to as the Dornick Hills-Springer sand.

This sand series lies on the northeast flank of the Velma anticline, and dips very sharply to the northeast in TWP 1S-5W, the average dip being about 45°. However, as shown in Fig. 1, the trend of the pool swings eastward in TWP 1S-4W with a coincident decrease in dip angle. In this portion of the pool the average dip is about 25°. Faults in Sections 30-1S-4W and 32-1S-4W are shown in Fig. 1. These faults show only minor displacements for the horizon contoured in Fig. 1, but they do show a pronounced displacement of the immediately overlying beds. Similar faults are thought to exist in TWP 1S-5W; however, since the detailed geological studies necessary to properly define these faults were not available to the author, no attempt to show them in Fig. 1 has been made.

The up-dip productive limit throughout the pool is determined by the truncation of the Lower Dornick Hills-Springer sand. The down-dip productive limit does not appear to be defined by edge water, but by a gradual reduction in permeability of the sands. No dry hole has produced a significant volume of water from this sand section. There was a small gas cap in TWP 1S-5W.

Most of the wells in TWP 1S-5W encountered an oil sand 70 ft to 150 ft thick, a shale 20 ft to 80 ft thick, and another oil sand 50 ft to 130 ft thick. A few scattered wells in this area encountered other sand bodies below these

---

[1]References given at end of paper.

Manuscript received at office of the Petroleum Branch September 29, 1950. Paper presented at the New Orleans meeting of the Petroleum Branch AIME, October 4-6, 1950.

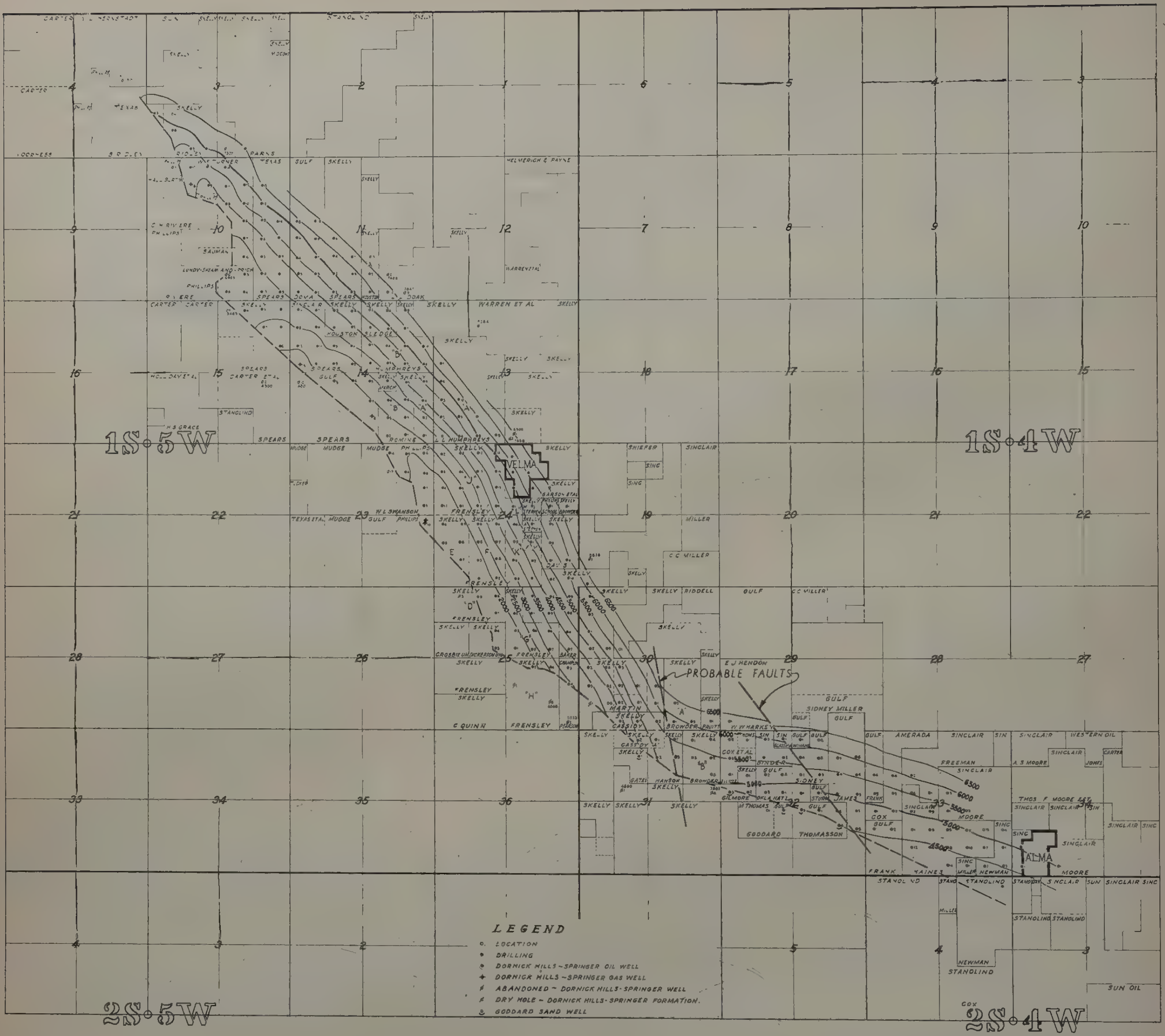
1S-5W
1S-4W
2S-5W
2S-4W
VELMA
PROBABLE FAULTS
LEGEND
○ LOCATION
● DRILLING
DORNICK HILLS-SPRINGER OIL WELL
✦ DORNICK HILLS-SPRINGER GAS WELL
ABANDONED - DORNICK HILLS-SPRINGER WELL
DRY HOLE - DORNICK HILLS-SPRINGER FORMATION.
GODDARD SAND WELL

FIG. 1 — STRUCTURAL CONTOUR MAP OF TOP OF 1ST DORNICK HILLS-SPRINGER SAND. CONTOUR INTERVAL — 500 FT.

two varying from 10 ft to 495 ft thick. These lower sands do not always produce. Most of the wells east of the fault in Section 30-1S-4W penetrated only the first sand. A thin sand found below the first sand, usually referred to as the Goddard sand, produces in several wells near the up-dip productive limit of the first sand in TWP 1S-4W. Goddard sand wells are indicated in Fig. 1. Fig. 2 is a cross section based on electric log data showing sand conditions typical of the main body of the pool.

HISTORY OF DEVELOPMENT

Prior to the last quarter of 1944, most of the oil production in the Velma Pool was from various sand stringers in the Redbeds, Hoxbar, and Deese formations. In November, 1944, Skelly completed Frensley "F" No. 1 in Section 24-1S-5W in the Dornick Hills-Springer sand section. The well initially pumped about 15 bbl of oil per hour and no water. Only one additional well was completed in 1945. About 30 wells were completed in 1946, and development averaged about 70 wells per year during 1947, 1948 and 1949. As of June 30, 1950, 274 oil wells and six gas wells had been completed. The pool is well defined and almost fully developed except for the southeast end. This development is shown graphically in Fig. 3.

Fig. 3 also depicts a history of the top allowables and total oil producing rate for the reservoir considered. In April, 1949, the Oklahoma Corporation Commission issued an order placing a limiting gas-oil ratio of 2,000 cu ft per bbl on all Pennsylvanian production in the Velma Pool. The order also fixed gas well allowables at a volume that would void as much reservoir space as an oil well producing at the limiting ratio. The June, 1950, gas well allowable averages about 200 Mcf/day/well. As a result of the February, 1950, gas-oil ratio survey, two oil wells were penalized for excessive ratios. In several cases, wells penalized for excessive gas-oil ratio have been worked over and the ratio reduced by cementing off per-

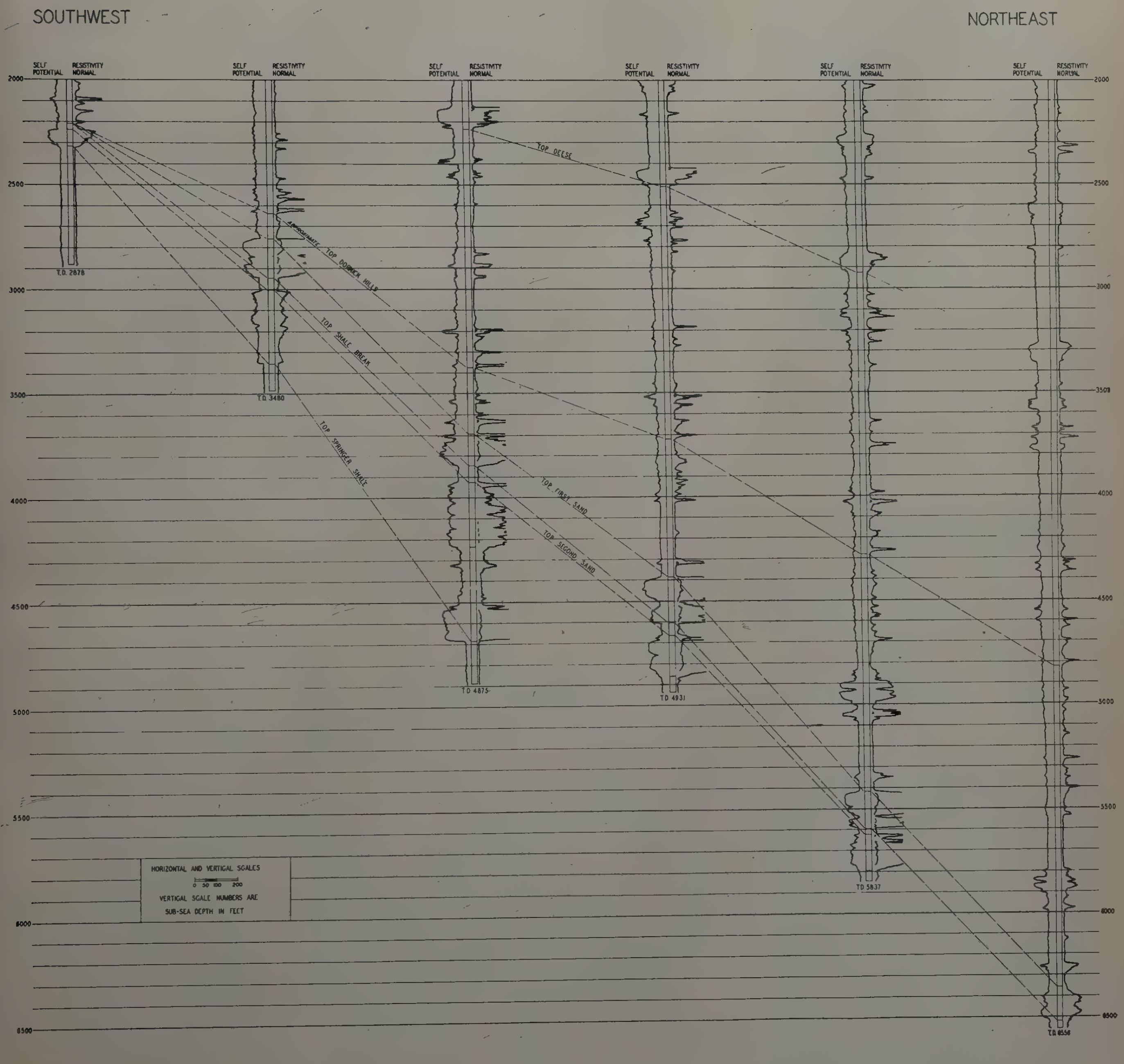

FIG. 2 — NORTHEAST - SOUTHWEST CROSS SECTION OF THE DORNICK HILLS - SPRINGER SAND, VELMA POOL.

forations or cementing a liner and perforating the lower portion of the section previously exposed.

In earlier wells, the usual completion practice was to drill a rotary hole through the pay section, run an electric log, set 7-in. OD casing through the producing section, and perforate opposite those intervals indicated to be sand on the electric log. More recent completion practice in TWP 1S-5W has been to set casing on the top of the second sand and perforate the first sand, or to set casing on the top of the first sand and use an uncemented slotted liner. In TWP 1S-4W, casing is usually set on the top of the one oil sand; however, some operators have used perforated completions in structurally high wells to facilitate the gas-oil ratio control which will be needed should gravity segregation occur to an appreciable extent.

Some wells flowed initially, but most of them pumped from 200 to 500 B/D of 28° API gravity oil. In very few cases did the reported initial production represent the capacity of the well. Producing BHP tests indicated that many wells were capable of producing 1,000-3,000 B/D if pumped down. The February, 1950, survey indicated that 29 wells were incapable of producing the February allowable of 80 B/D.

ROCK AND FLUID CHARACTERISTICS

The original reservoir pressure was 1670 psig at a datum of –4500 ft subsea. Since the average surface elevation is about 1100 ft, the original reservoir pressure was about 700 psi under the hydrostatic gradient. The average vertical gradient in the oil reservoir is 0.36 psi/ft.

Fig. 4 shows typical results of the analysis of a bottom-hole sample. Other than the relatively high viscosity, the sample characteristics are not unusual for a 29° API gravity oil. Since there was a small primary gas cap, the oil should have been saturated at the gas-oil contact (about –2400 ft subsea). Results of bottom-hole sample analyses taken at various structural elevations indicate that the oil at a given depth level in the reservoir was originally saturated at the BHP of that depth. Thus, for a given gravity of oil, the solution gas tends to increase at structurally lower positions.

Table I

Well	Subsea Top 1st Sand	Gross Ft of Section	Net Ft Oil Pay	Avg. Perm. Md	Avg. Poros. %	Est. Connate Water %
A	–3722	335	238	300	21	17
B	–4022	315	194	190	19	---
C	–4871	334	212	70	16	----
D	–5398	292	172	40	14	24
E	–5892	302	65	31	12	24

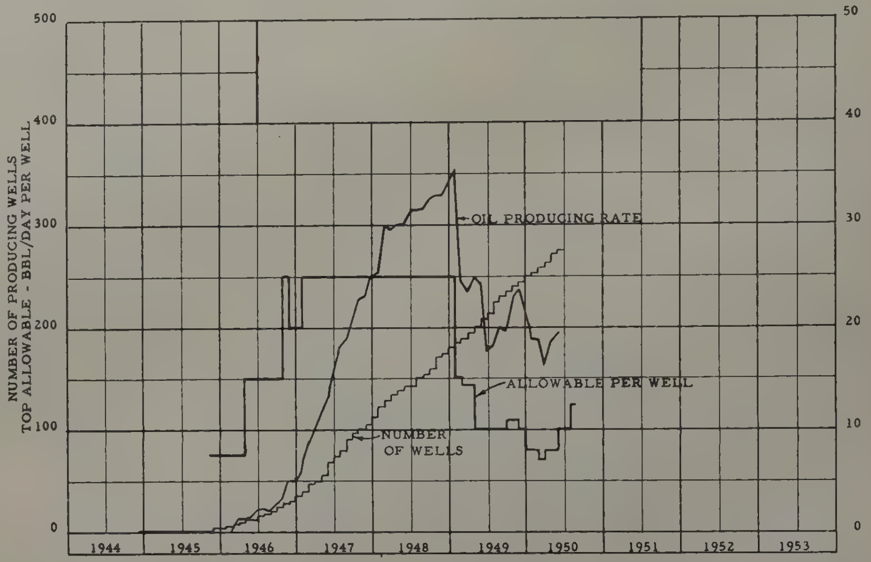

FIG. 3 — DEVELOPMENT AND PRODUCING RATES DORNICK HILLS - SPRINGER SAND RESERVIOR, VELMA POOL, STEPHENS COUNTY, OKLAHOMA.

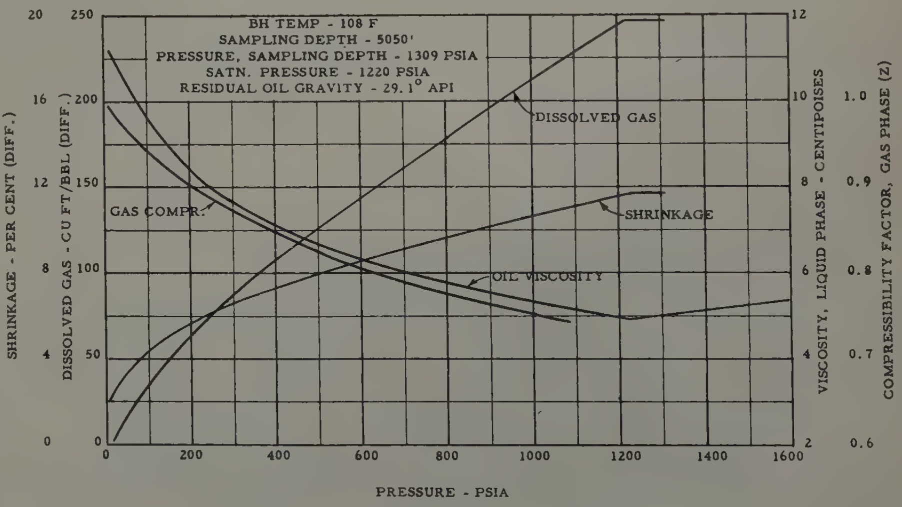

FIG. 4 — TYPICAL BOTTOM-HOLE SAMPLE ANALYSIS DORNICK HILLS - SPRINGER SAND.

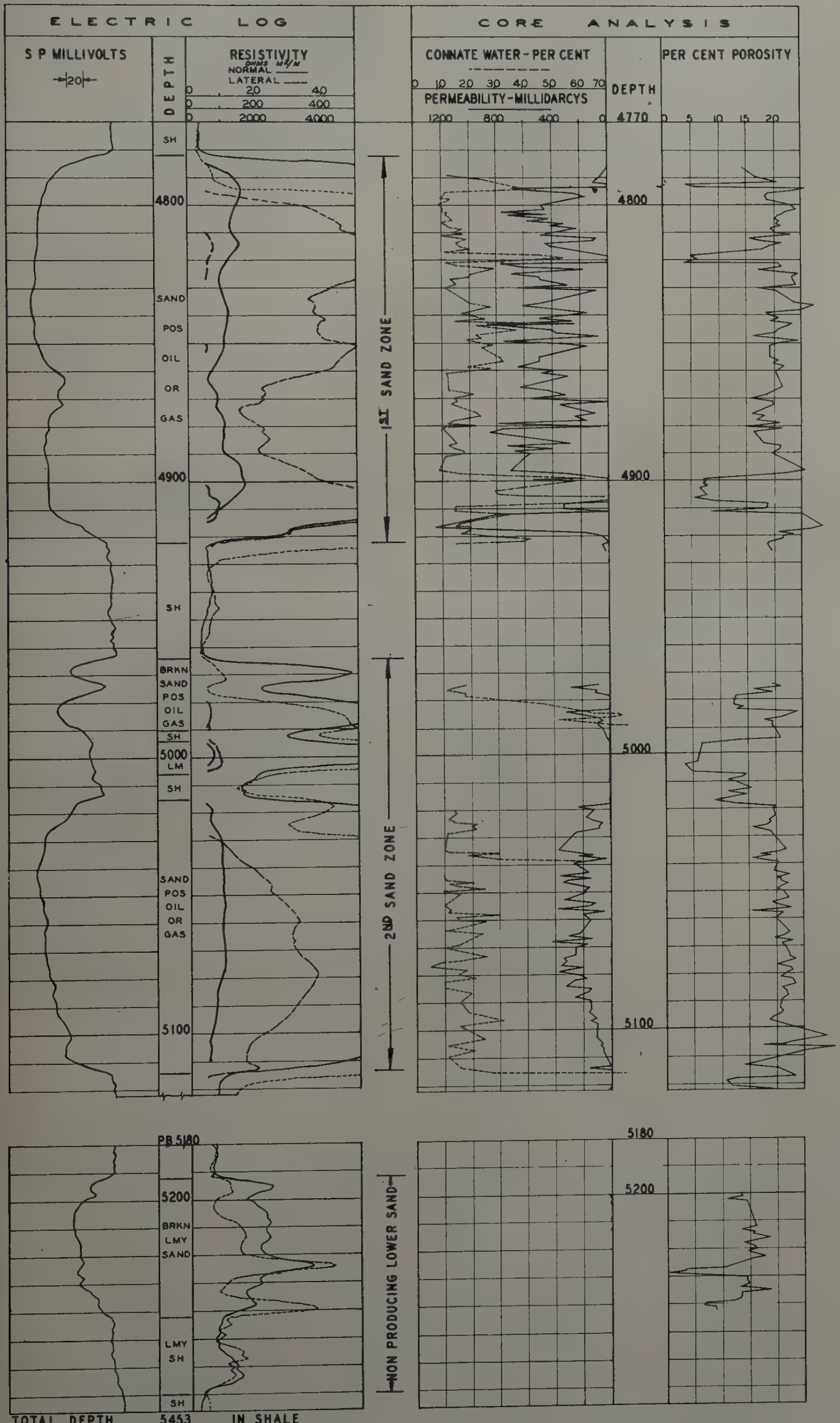

FIG. 5 — GRAPHIC WELL LOG OF TYPICAL WELL IN TWP 1S-5W.

The stock tank oil gravity is fairly constant from the top of the productive closure down to about –5500 ft subsea, and averages about 28° API. In the south end of the pool, the stock tank oil gravity appears to vary approximately with structural position, decreasing down-dip. Fig. 6 is a portion of the structural contour map, on which have been superposed contours depicting the variation of stock tank oil gravity. It is likely that solution gas decreases with decreasing stock tank oil gravity. The fact that most of the wells producing lower gravity oil initially had lower gas-oil ratios tends to confirm this hypothesis.

The Dornick Hills-Springer sand is generally a fine-grained sand containing varying amounts of argillaceous material. In some places it has good permeability parallel to the bedding planes, but because of numerous paper-thin shale partings, permeability normal to the bedding planes is poor. In other places it is very clean sand. The average porosity and average permeability of the section have been found to be relatively uniform at wells of the same structural position but in different areas; however, the porosity and permeability of the sand appear to vary with structural position. This variation is illustrated in Table I by the core data on several wells in the same area. Similar variations in sand character occur in other parts of the reservoir.

The permeability of the sand penetrated by a given well is relatively uniform, and when core analysis results of several wells were arranged in order of increasing permeability, the data for each well were found to have approximately an exponential distribution[1] with *r*, the ratio of maximum to minimum permeability, varying from 15 to 35. The permeability to oil with connate water in place averaged about 50 per cent of the dry core air permeability on 70 samples tested.

Connate water saturations have been measured by the restored state method, by retorting samples of cores taken using oil base mud, and by the use of electric logs. The use of electric logs to calculate connate water has not been entirely satisfactory because the resistivity of the formation water must be known and no well has produced enough water to make it certain that a sample taken was uncontaminated Dornick Hills-Springer sand water. Restored state method results and oil base core results agree very well, usually within 1 per cent saturation; however, electric log calculations usually give values lower than those obtained by the other two methods. The average connate water saturation for the reservoir is estimated at 20 per cent of the pore volume.

Fig. 5 is a graphic well log showing the electric log and core data of a typical well in the main body of the pool. This well had both the first and second sands well developed. It also penetrated a poorly developed, nonproductive third sand. Because of the 45° dip, the actual thickness of these sands measured normal to the bedding planes is only about 70 per cent of that shown on the electric log. For the same reason, the average area drained by a well on 10-acre spacing is about 14 acres. Thus, the electric log thickness multiplied by the spacing may be used to calculate sand volumes.

Results of the analysis of about 3500 ft of core indicate that the average porosity of the oil sand is 18 per cent, the average permeability is 150 md, and the average connate water saturation is 20 per cent. Using these figures and an average formation volume factor of 1.19, the average original stock tank oil in place may be calculated to be 940 bbl per acre ft. In TWP 1S-5W, the first sand averages 108 ft of net pay, and the second sand 91 ft of net pay.* Thus, the original stock tank oil in place averages 187,000 bbl per acre, exclusive of any productive lower sands. In TWP 1S-4W, the first sand averages 113 ft of net pay, making 106,000 bbl per acre average original stock tank oil in place. The presently developed portion of the reservoir is estimated to have originally contained 430 million bbl of stock tank oil in the first and second sands.

RESERVOIR PERFORMANCE

Since this reservoir is, for practical considerations, a closed stratigraphic trap, there is no reason to expect an effective water drive. Past performance has shown no evidence of a significant volume of water influx. A few wells have made very small volumes of water, and in no case has the water producing rate increased.

With a gas saturated crude and such steep dips, it would be anticipated that the effective producing mechanisms would be a dissolved gas drive and gravity drainage. The performance to date tends to support this hypothesis.

Fig. 7 shows some performance data for the reservoir. The BHP curve is labeled "approximate," because it was necessary to correct some pressure measurements 2000 ft below TD and to correct others 2000 ft up into the casing in order to base them all on a common datum. The reservoir has produced about 29,000,000 bbl as of June 1, 1950, an average of 59,000 bbl/psi drop.

The only points shown on the GOR curve are the initial average solution GOR and the August, 1949, and February, 1950, surveys. The latter two points are numerical averages of the ratios of all wells in this reservoir. The accuracy of these numerical averages was checked for a few leases by comparing the numerical average of the survey ratios with weighted average ratios (all gas metered). Generally, they differed by less than 15 per cent. The decrease

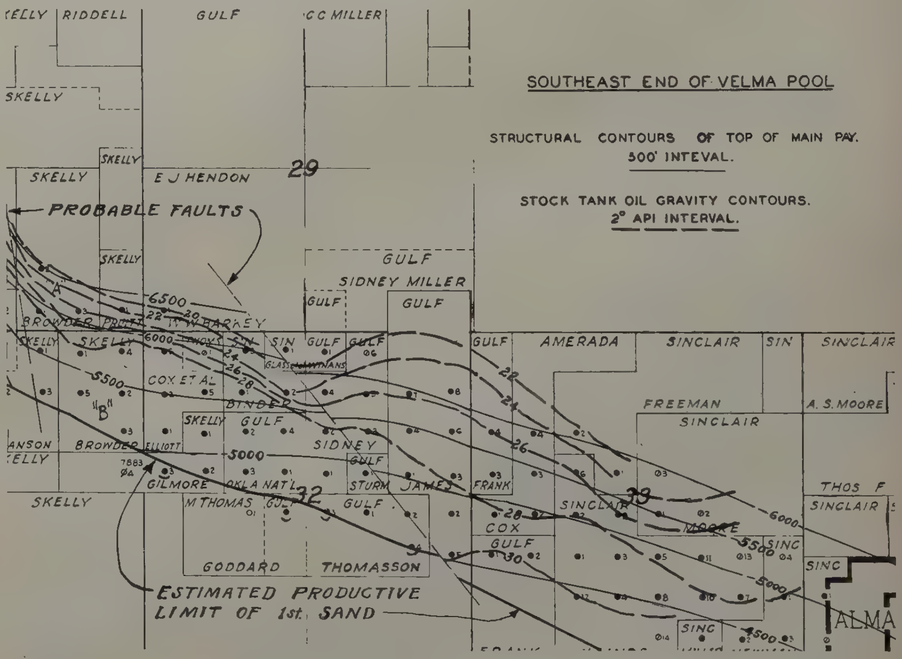

FIG. 6 — SOUTHEAST END OF VELMA POOL.

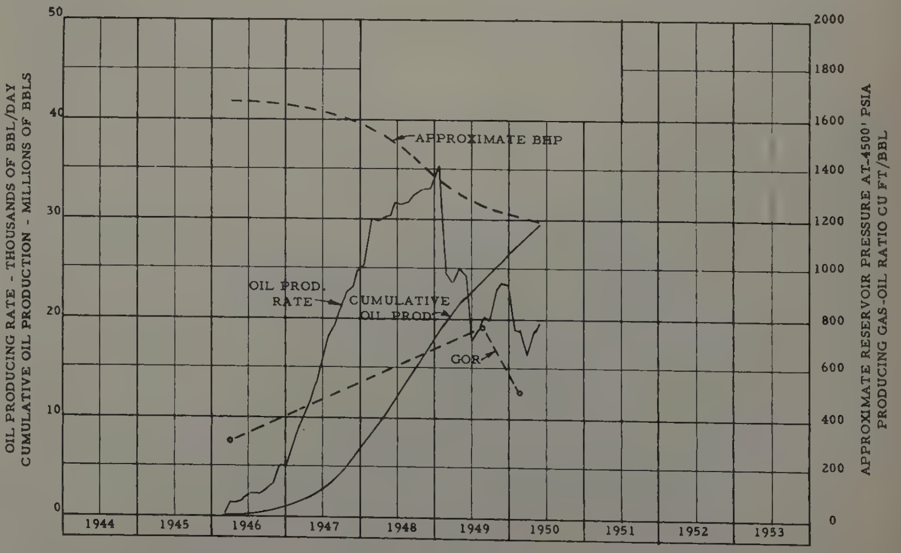

FIG. 7 — DORNICK HILLS - SPRINGER SAND, VELMA POOL PERFORMANCE DATA.

---

*These figures are measured vertically rather than normal to the bedding planes, since oil in place per acre is usually based on surface acres.

in GOR from August, 1949, to February, 1950, is accounted for partially by the fact that some very high GOR wells were successfully worked over, and partially by a general decrease in ratios. Such an occurrence is not common to solution gas drive performance, and is thought to be indicative of gravity drainage effects.

Because there is considerable doubt as to whether the bottom-hole pressure data are representative of reservoir conditions, no attempt has been made to calculate oil initially in place by the use of material balance equations. For the same reason, no attempt has been made to verify or deny by material balance methods the hypothesis that there has been no water influx.

It is apparent that average reservoir performance data are not conclusive as to producing mechanism. In an attempt to find some more definitive data, the performance of several individual wells was examined. Fig. 8 is typical of the performance data of the older wells in the pool. The dissolved gas drive performance was calculated by the method introduced by Muskat,[2] using bottom-hole sample data similar to those shown in Fig. 4. The slope and position of the straight line portion of the K_g/K_o curve used was an average of the field data for some sands of similar texture, and the equilibrium gas saturation was estimated at 9 per cent of the pore volume from some performance data of several early wells in the Dornick Hills-Springer sand that were produced at high enough rates that gravity drainage effects were thought to be small. The basic differential equation describing the pressure history was integrated by the Runge-Kutta method.[3] Because the sand in this area is laminated with paper-thin shale partings, the calculated performance curves were corrected for permeability stratification by the method described by Keller, Tracy and Roe.[4] This method assumes no vertical permeability, and consequently results in some large pressure differentials across shale partings, but it is believed to constitute some improvement over the assumption of an isotropic reservoir. It is apparent that the well performance was following the calculated solution gas drive performance fairly well until cumulative oil recovery reached 5½ per cent of the pore volume. Then the allowable was curtailed sharply, and instead of continuing to rise, the GOR decreased, and at the time of the latest test data shown, the GOR was considerably less than the ratio calculated assuming solution gas drive. This phenomenon also was observed in other wells, and it is believed indicative of some resaturation of the sand around this well by gravity drainage.

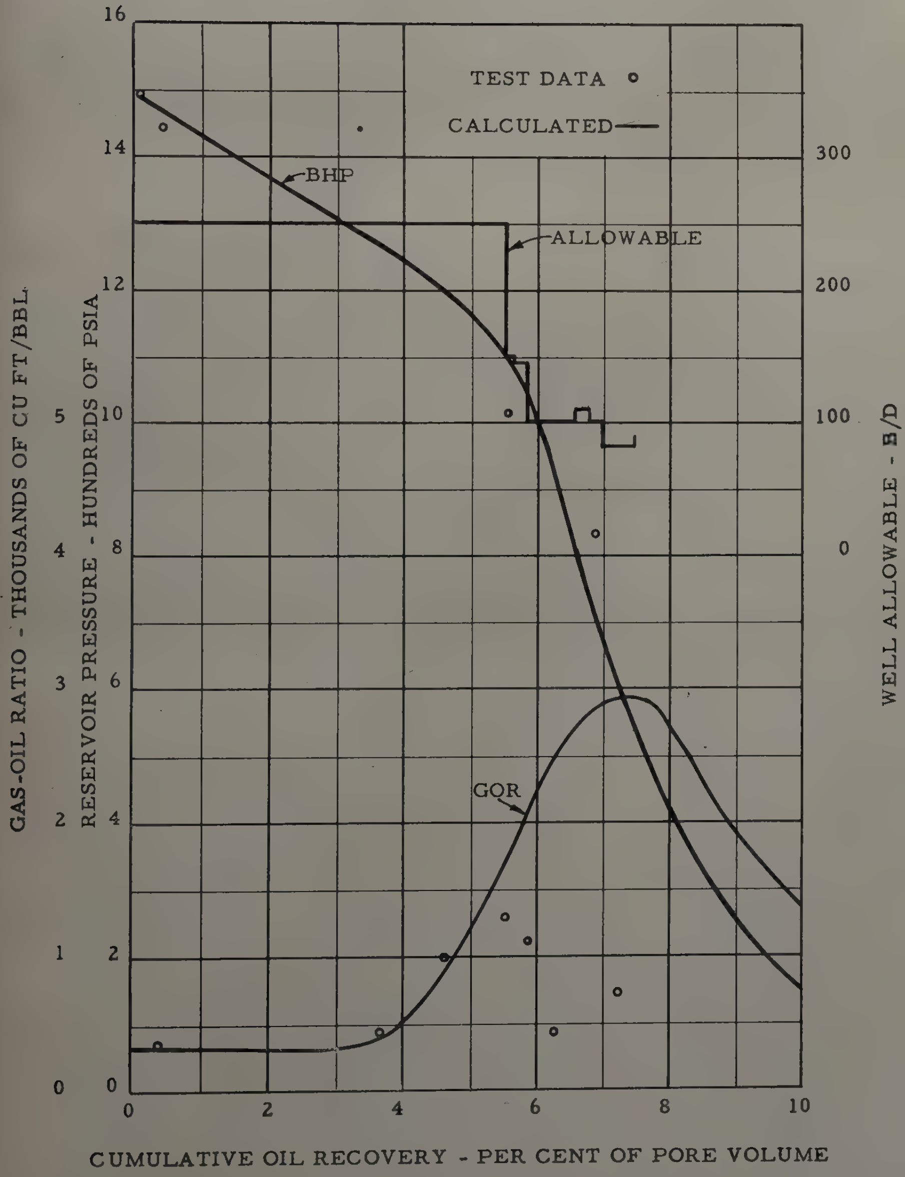

FIG. 8 — DORNICK HILLS - SPRINGER SAND, VELMA POOL. COMPARISON OF ACTUAL PERFORMANCE OF A WELL WITH CALCULATED DISSOLVED GAS DRIVE PERFORMANCE.

It appears solution gas drive has been the principal producing mechanism in this reservoir in the past; however, there is some evidence of the effects of gravity. Probably gravity drainage will play an increasingly important role in the operation of this reservoir as it is further depleted. It does not appear likely that all the gravity drainage oil will be recovered at the structurally low wells as has been the case in some gravity drainage reservoirs, because the decreasing permeability down-dip will cause the oil to drain downward at successively decreasing rates, and this should tend to partially resaturate the sand around wells of intermediate structural positions, causing them to recover some additional oil. In those areas where the sand is laminated by paper-thin shale partings, the rate of gravity drainage will be restricted because the oil will be denied a vertical path and forced to follow the dip angle. If there is an appreciable tendency for the shale partings to divide the sand into closed lenses, considerable oil may be trapped, and the gravity drainage recovery seriously reduced.

The estimated ultimate oil recovery by solution gas drive alone would be 18 per cent of the original stock tank oil in place. The additional oil to be expected because of the effects of gravity cannot be predicted very accurately. Some experiments have indicated that sand samples with permeabilities of 300-1000 md will drain down to as low as 10 per cent residual oil saturation; however, it is unlikely that less permeable samples would reach such a low saturation. If the oil at saturations below 30 per cent is considered immobile, and it is assumed that the gas drive recovery plus an additional 50 per cent of the mobile oil can be recovered, the ultimate recovery will amount to about 37 per cent of the original stock tank oil in place. Probably much of the gravity drainage oil will be produced at relatively low rates over a long life.

ACKNOWLEDGMENTS

The author wishes to acknowledge the assistance of the members of the Production Engineering Section, Tulsa Division, Gulf Oil Corp., in making this study, particularly A. C. Godbold for his advice, and Marion Smith and George Girouard for assembling and interpreting data. The section entitled "Geology" was prepared under the guidance of the Geological Department, Tulsa Division, Gulf Oil Corp., and the geological data shown are the results of studies by members of that department. The author wishes to thank the management of the Gulf Oil Corp. for permission to publish this paper.

REFERENCES

1. Muskat, M.: *Trans.* AIME, (1949), **179**, 313.
2. Muskat, M.: "The Production Histories of Oil Producing Gas Drive Reservoirs," *Jour. of Applied Physics*, March, 1945.
3. Sherwood and Reed: *Applied Mathematics in Chemical Engineering*, McGraw-Hill, (1939), 122.
4. Keller, Tracy, Roe: "Effect of Permeability on Recovery Efficiency by Gas Displacement," presented at Tulsa API Meeting, March, 1949. ★

SPECIAL CONSIDERATIONS IN PREDICTING RESERVOIR PERFORMANCE OF HIGHLY VOLATILE TYPE OIL RESERVOIRS

ALTON B. COOK, MEMBER AIME, **G. B. SPENCER** AND **F. P. BOBROWSKI,** BUREAU OF MINES, UNITED STATES DEPARTMENT OF INTERIOR, BARTLESVILLE, OKLA.

INTRODUCTION

In estimating production gas/oil ratios and oil recoveries from reservoirs containing highly volatile oils it is highly important to include condensate that may be recovered from the gas produced from the reservoir. The volume of the hydrocarbon liquid condensed from the production of the solution gas that has been liberated in some reservoirs may equal or even exceed the volume of recoverable stock-tank oil as estimated by present methods. The usual procedure[1,2,3] in estimating future reservoir performance includes use of relative permeability data of the reservoir rock to gas and oil and includes material-balance calculations utilizing data on the volume of the reservoir fluids, oil and gas production and reservoir pressure decline, and data on the physical properties of the initial reservoir fluids. The inaccuracy in the procedure results from the false assumption that all of the free or liberated gas that enters the well bore of reservoirs containing highly volatile oils remains in the gaseous phase as it is produced.

This paper presents a method for estimating future reservoir performance and oil recoveries based on special laboratory analyses of reservoir-oil samples and recognition of the additional volume of hydrocarbon liquid that will be recovered at various stages of depletion from a solution-gas-drive reservoir. The method also includes calculations of the volume and composition of the hydrocarbon liquids that can be recovered by processing the produced gas in a natural-gasoline plant. The development of the method resulted from a study of laboratory analyses of reservoir samples and of field data obtained from two reservoirs containing oil of the highly volatile type.

Relatively high pressures and temperatures prevail in oil reservoirs discovered at the greater depths of present-day drilling. The contained fluids may have high saturation pressures and large volumes of gas in solution. The oils and gases under these conditions may be almost identical in compositions and densities.[4,5] Also, engineers have noted that, for a number of oil reservoirs and especially the deeper reservoirs, the API gravity of the stock-tank oil increases as the production gas/oil ratios increase. They attributed this increase in API gravity of the stock-tank oil to the formation of condensate as the liberated gas in the reservoir is being produced.

SOURCE OF DATA FOR CALCULATIONS

Subsurface oil samples and well-test data were obtained from the E. Constantin-Lambert Well No. 1 in the Elk City Field, Okla., to demonstrate the need for and a method of calculating future reservoir performance when consideration is given to the recoverable hydrocarbon liquid from the production of solution gas that has been or will be liberated in a reservoir. The Lambert well is located in C, SW¼, SW¼, Sec. 18, T-10-N, R-20-W, Washita County, Okla. At the time of completion it was on the east edge of the development and was producing from conglomerate through 30 perforations in the 5½-in. casing at a depth of 9,859 to 9,864 ft. The well was completed on July 9, 1949, and subsurface oil samples were obtained July 29 and August 1, 1949. Production gas/oil ratio data were obtained during the operation in series of two separators at high and low-pressures of 314 and 44 psia, respectively, and at an average temperature of approximately 60°F. The flowing bottom-hole pressure at the time of sampling was 3,934 psia. The static bottom-hole pressure was not obtained at the time of sampling, as the well could not be shut in long enough for testing because gas produced from the well was used for fuel at an offset drilling well. However, the initial reservoir pressure was calculated to be 4,364 psia from knowledge of pressure gradients in other wells in the field and the depth of the casing perforations in the Lambert No. 1 well.

---

[1] References given at end of paper.

Manuscript received in the office of the Petroleum Branch August 29, 1950. Paper given at the Petroleum Branch Fall Meeting in New Orleans Oct. 4-6, 1950, and at Los Angeles Oct. 12, 13, 1950.

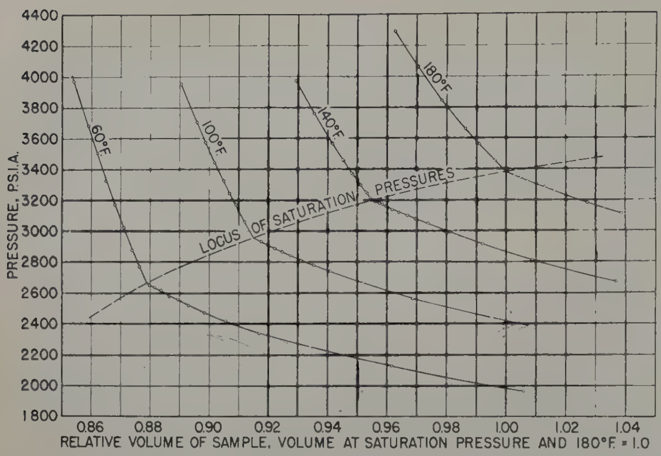

FIG. 1 — PRESSURE-VOLUME-TEMPERATURE RELATIONSHIPS OF SUBSURFACE OIL SAMPLE FROM CONSTANTIN-LAMBERT WELL NO. 1, ELK CITY FIELD, WASHITA COUNTY, OKLA.

The saturation pressure of the duplicate subsurface oil samples was found to be 3,383 psia. The solution gas/oil ratio as determined in the laboratory by the flash-gas liberation method, conducted to simulate producing conditions, was 2,172 cu ft of gas per barrel of stock-tank oil at the separator operating pressure of 314 psia. As this compares favorably with the measured production gas/oil ratio of 2,140 cu ft of gas per barrel of stock-tank oil and as the saturation pressures of the two subsurface oil samples were identical, the subsurface oil samples were considered representative of the initial reservoir oil.* Laboratory data on the samples are shown in Table I and Figs. 1, 2, 3, and 4.

Fig. 1 shows pressure-volume relationships of the reservoir oil at four temperatures — 60°, 100°, 140°, and 180°F. It is of interest to note that the degree of expansion with pressure reduction of the reservoir oil sample at 180°F (reservoir temperature) is almost as great while in the liquid phase as it is after the pressure has been reduced below saturation pressure. The expansion of the liquid phase in a reservoir containing an undersaturated highly volatile oil may account for a large part of the ultimate recovery. Fig. 2 and Table I shows data obtained by the differential gas-liberation procedure. Almost 3,400 cu ft of gas was liberated per barrel of residual oil at 60°F, which caused a reduction in the liquid volume from 3.041 to 1.0. The first gas liberated from the reservoir was almost as dense as air, indicating that the gas was rich in condensable hydrocarbons. The flash gas-liberation experiment (Table I and Fig. 3) conducted to simulate producing conditions when two separators were operated in series, shows that 2,594 cu ft of gas was liberated per barrel of stock-tank oil and that the production of 2.508 bbl of initial reservoir oil was necessary to yield 1 bbl of stock-tank oil. Pressure-viscosity data of the reservoir oil at 180°F are presented in Fig. 4. The viscosity of the Elk City Field reservoir oil was only 0.135 centipoise at the saturation pressure and reservoir temperature; the viscosity is less than that of water, which under the same conditions is 0.35 centipoise.

For the purposes of this study idealized reservoir conditions were assumed because certain necessary data on the Elk City Reservoir were not available. Reservoir conditions were as follows:

1. An initial pressure and temperature of 4,364 psia and 180°F, respectively, existing in the reservoir penetrated by the Constantin-Lambert Well No. 1 in the Elk City, Okla., Field.
2. Initial reservoir oil having the physical properties of the subsurface oil samples obtained from the lambert Well (Table I and Figs. 1, 2, 3, and 4).
3. Relative permeability (K_g/K_o) of reservoir rock as reported by Muskat and Taylor[6] (Fig. 5).
4. Viscosity of reservoir gas as determined by the procedure developed by Bicker and Katz[7] [Fig. 6 for relative viscosity of oil to gas (U_o/U_g)].
5. Solution-gas-drive reservoir.
6. For reservoirs containing volumes of oil and water as follows:

Table I — Differential and Flash Gas-Liberation Data on a Subsurface Oil Sample from Constantin-Lambert Well No. 1, Elk City Field, Washita County, Okla.

Pres., psia	Temp., °F	Relative oil volume, residual oil volume at 60°F = 1.0	Density[1] of liberated gas, gm./ml. (gas at 60°F and 14.4 psia)	Oil density, gm./ml.	Gas in solution, cu ft per bbl of residual oil at 60°F (gas at 60°F and 14.4 psia)
		Differential gas liberation			
4,365[2]	180	3.041		0.491	3,393
3,383[3]	180	3.166		.472	3,393
3,300	180	2.997	[4] 0.001178	.481	3,144
3,183	180	2.792	.001142	.493	2,826
2,918	180	2.515	.001080	.512	2,360
2,673	180	2.330	.001038	.527	2,038
2,208	180	2.074	.000997	.554	1,593
1,378	180	1.781	.000968	.591	1,034
683	180	1.586	.000974	.623	659
192	180	1.427	.001126	.652	376
14.4	180	1.076	.001998	.741	0
14.4	60	1.000		.7970	0
		Flash gas liberation (two separators)			
4,365[2]	180	[5] 2.508		[5] 0.491	2,594
3,383[3]	180	2.612		[5] .472	2,594
3,300	180	[5] 2.472		[5] .481	[5] 2,383
3,183	180	[5] 2.304		[5] .493	[5] 2,113
2,918	180	[5] 2.075		[5] .512	[5] 1,717
2,673	180	[5] 1.922		[5] .527	[5] 1,444
2,208	180	[5] 1.711		[5] .554	[5] 1,070
314.4[6]	60	1.237	[4] .000886	.719	422
44.4[6]	60	1.076	.001396	.755	114
14.4	60	1.000	.001998	.7726	0
		Flash gas liberation (one separator)			
4,365[2]	180	[5] 2.624		[5] 0.491	2,812
3,383[3]	180	2,732		[5] .472	2,812
3,300	180	[5] 2.586		[5] .481	[5] 2,597
3,183	180	[5] 2.409		[5] .493	[5] 2,323
2,918	180	[3] 2.170		[5] .512	[5] 1,921
2,673	180	[5] 2.010		[5] .527	[5] 1,643
2,208	180	[5] 1.790		[5] .554	[5] 1,263
64.4[6]	60	1.044	[4] .001015	.760	69
14.4	60	1.000	.001580	.7737	0

[1] Gas density x 834.4 = specific gravity (air = 1.0).
[2] Initial reservoir pressure.
[3] Saturation pressure.
[4] Gas densities, representative of the gas liberated between two pressures, are shown opposite the lowest pressure at which gas was liberated.
[5] Calculated by using "differential gas-liberation data."
[6] Gas-Oil separator pressure.

---

*These samples should not be considered average for the Elk City, Okla., Field as considerable variations are reported in gas/oil ratios and API gravities of produced oil for the initial tests on wells in the field.

(a) 1,428,600 bbl of pore space containing 1,000,000 bbl of initial reservoir oil and 428,600 bbl of interstitial water (30 per cent).

(b) 1,190,500 bbl of pore space containing 1,000,000 bbl of initial reservoir oil and 190,500 bbl of interstitial water (16 per cent).

(c) 1,000,000 bbl of pore space containing 700,000 bbl of initial reservoir oil and 300,000 bbl of interstitial water (30 per cent).

(d) 1,000,000 bbl of pore space containing 840,000 bbl of initial reservoir oil and 160,000 bbl of interstitial water (16 per cent).

Although the physical properties of the reservoir oil from the Elk City Field are unusual as compared to most reservoir oils, other reservoirs containing oils of the highly volatile type are known; an exceptionally volatile reservoir oil has been described by Sloan.[5] In an effort to show comparisons between the ultimate recovery estimated for the Elk City Reservoir and that for other fields of this type, parallel calculations were made, using the information reported by Sloan.

The initial reservoir pressure and temperature in the unidentified field was 5,252 psia and 212°F, respectively; the reservoir contained an undersaturated oil with a saturation pressure of 4,648 psia. The production separator-gas/stock-tank-oil ratio was 3,390 cu ft per bbl and the formation volume factor was 3.12 when the single-phase reservoir liquid passed through a separator operating at a pressure of 490 psia.

The parallel calculations were made, using the reservoir pressure and temperature and the properties of the reservoir oil reported by Sloan. Recoveries were estimated only for the reservoirs containing 30 per cent interstitial water.

DEVELOPMENT OF A METHOD FOR ESTIMATING RESERVOIR PERFORMANCE

Estimating Reservoir Performance

To calculate the volume of condensate that will be collected in stock tanks or the LPG (liquefied petroleum gas) products that can be extracted by a natural gasoline plant from the production of the solution gas that has been or will be liberated in a reservoir, the following information must be known for all reservoir pressures: (a) The composition of both the oil and gas flowing in the reservoir; (b) the flowing gas/oil ratios in the reservoir (the volumes of gas and oil for each selected pressure decrement); and (c) the volume of condensate for each standard-unit volume of reservoir gas. The authors have developed a technique for obtaining the desired laboratory data and a method of calculating the compositions of reservoir oil and gas for pressures below saturation pressure. Several writers[1,2,3] have contributed to a method for calculating volumes of reservoir gas and oil that will be produced with reductions in reservoir pressure when the volume of the reservoir and certain physical properties of the reservoir rock and fluids are known. Also, Katz and Hachmuth[8] have published equilibrium constants, and Katz[9] has devised a method for calculating gas/oil ratios when the composition of the reservoir fluid is known. Although the method of calculating gas/oil ratios and the equilibrium constants were developed for use in calculating recoveries from the production of liquid-phase hydrocarbons, they also can be used to predict production gas/condensate ratios when the composition of the gas entering the producing wells is known.

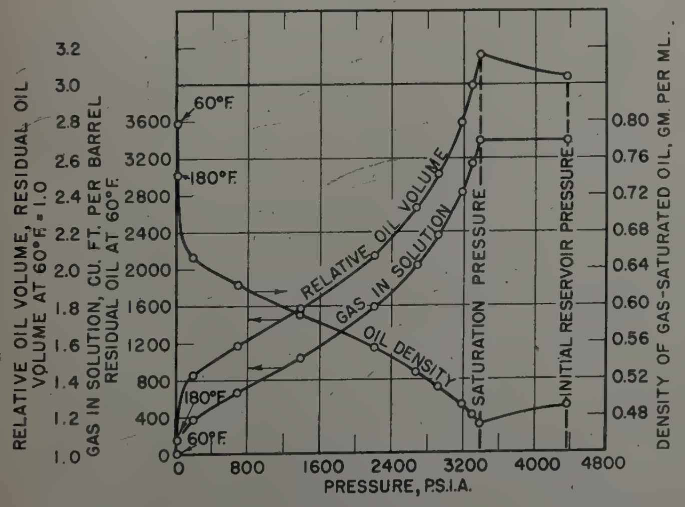

FIG. 2 — DIFFERENTIAL GAS-LIBERATION DATA AT 180°F, SUBSURFACE OIL SAMPLE, CONSTANTIN-LAMBERT WELL NO. 1, ELK CITY FIELD, WASHITA COUNTY, OKLA.

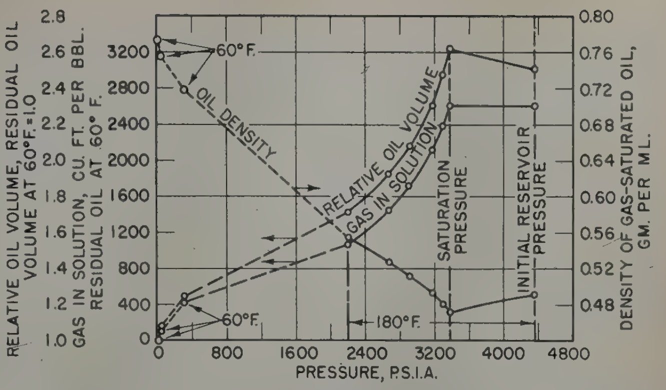

FIG. 3 — FLASH GAS-LIBERATION DATA (TWO SEPARATORS), SUBSURFACE OIL SAMPLE, CONSTANTIN-LAMBERT WELL NO. 1, ELK CITY FIELD, WASHITA COUNTY, OKLA.

With the above information available a new procedure for estimating hydrocarbon-liquid recoveries was developed. It is divided into four major steps as follows:

1. The volumes of oil and liberated gas flowing in the reservoir were calculated for each of 12 assumed reservoir-pressure decrements.
2. The composition of a unit volume of the flowing oil and of the liberated gas in the reservoir were calculated for each of the pressure decrements used in step 1 above.
3. The liquid volume of the various recovered hydrocarbons was calculated from the data obtained under steps 1 and 2; all of the produced fluids were assumed to be processed by a gasoline plant that had an assumed processing efficiency.
4. The volume of recoverable condensate was calculated from equilibrium constants. (The gas liberated in the reservoir and the reservoir oil were assumed to have been produced separately through separators operating at the same pressures as are used in the field.) The volume of recoverable hydrocarbon liquid was the sum of the volume of stock-tank oil (estimated from the volume of reservoir oil entering the producing wells) and the volume of condensate (estimated recovery from the gas entering the producing wells).

The calculation procedures are outlined in more detail in the appendix.

Composition of Reservoir Gas

The gas-liberation process in a reservoir initially containing oil having a high saturation pressure with relatively large quantities of dissolved gas is neither essentially that of the "differential" or "flash" type.* This conclusion was substantiated by material-balance calculations based upon data obtained on the reservoir and subsurface samples of the Elk City Field. The results, illustrated in Fig. 7, show that from the saturation pressure of 3,383 to 2,800 psia almost all of the gas liberated in the reservoir was retained in the reservoir. From 2,800 to 2,000 psia the rate of gas liberation in the reservoir approximates the rate of gas production from the reservoir. From 2,000 psia to abandonment pressure the rate of gas production from the reservoir exceeds the rate of gas liberation in the reservoir, with the result that gas previously liberated is being produced. Thus, during the early pressure depletion of the reservoir the gas-liberation process is essentially the flash type. In the intermediate stage of pressure depletion the gas-liberation process approaches the differential type as the rate of gas liberation approximates the rate of gas production, but differs from this type because of the close association of the oil in the reservoir with large quantities of gas previously released. In the final stage of pressure depletion the rate of gas production exceeds the rate of gas liberation in the reservoir, indicating that the gas-liberation process does not simulate either the differential or the flash type.

Because of the complicated nature of the gas-liberation process and the phase changes that take place in the liberated gas as the pressure is depleted in reservoirs containing highly volatile oils, duplication of this process in the laboratory would be extremely difficult. This, however, is unnecessary as the volume of recoverable hydrocarbon liquid can be determined from data on the composition and volume of each fluid (the reservoir oil and the reservoir gas) entering the well-bores of the producing wells for each pressure decrement. The composition of the liberated gas in a reservoir apparently depends upon the reservoir pressure, within the pressure range in which retrograde condensation occurs, and not the process by which the gas is liberated, as indicated both from theoretical considerations and experimental data obtained on samples of oil and gas from the Elk City Field. Reservoir conditions are simulated in Fig. 8 to illustrate the effect of pressure reduction on the composition of liberated gas in oil reservoirs. If the system undergoes a pressure decrement a minute quantity of gas will be liberated from the oil and collected at *A* and a small quantity of liquid will be condensed from the gas and collected at *B*. If the decrease in pressure is small the compositions of the oil and gas are not affected materially, and thus the oil and gas remain in equilibrium. Also, the liberated gas is in equilibrium with the oil. Therefore, the liberated gas has essentially the same composition as the gas-cap gas, because both gases are in equilibrium with the same oil. Likewise the condensate trapped at *B* is essentially identical to the oil because both the oil and condensate are in equilibrium with the same gas. (The condensate formed in a gas cap directly overlying oil actually may not be identical to the oil, as the oil may contain solid particles in suspension.) With further reduction of pressure on the system, the first liberated gas collected at *A* will undergo the same changes owing to retrograde condensation as the gas-cap gas, and the first condensate collected at *B* will undergo the same gas-liberation conditions as the oil. Thus, it seems logical to assume that, within the pressure range in which retrograde condensation occurs, the gaseous phase of the gas-cap gas will be identical in composition to the gas being liberated.

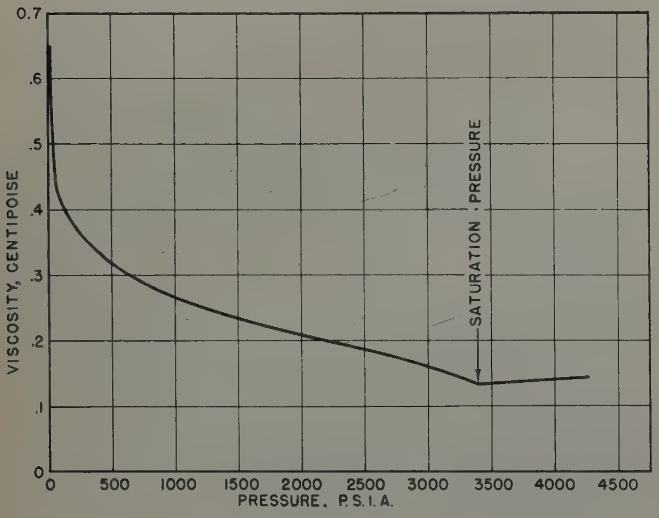

FIG. 4 — PRESSURE-VISCOSITIES AT 180°F, SUBSURFACE OIL SAMPLE, CONSTANTIN-LAMBERT WELL NO. 1, ELK CITY FIELD, WASHITA COUNTY, OKLA.

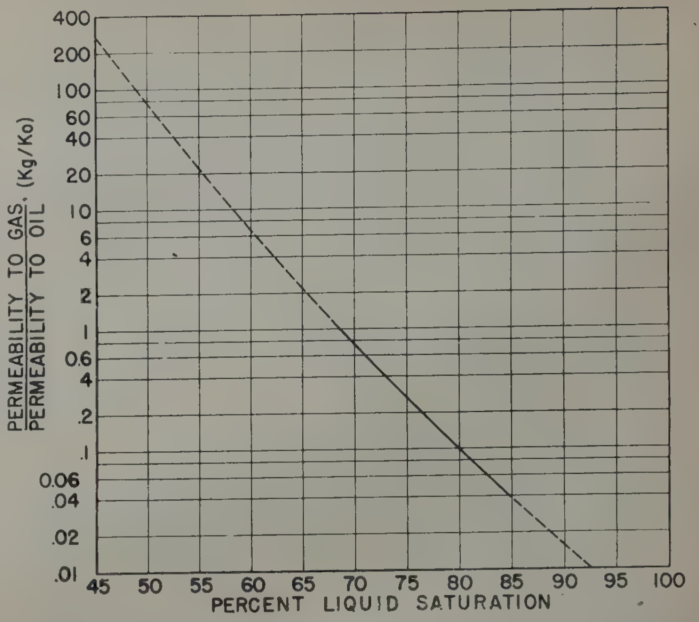

FIG. 5 — PERMEABILITY-SATURATION CURVE USED IN CALCULATIONS OF RESERVOIR PERFORMANCE.

Experimental work conducted on the Elk City Field sample to substantiate the foregoing theory consisted of determining the specific gravity of gases, at standard conditions, liberated under the following conditions in a P-V cell:

1. Gas was liberated differentially at 180°F from a sample of reservoir oil in 18 pressure steps from saturation to atmospheric pressure.
2. Three samples of reservoir oil were flashed separately at 180°F from saturation pressure to 2,500, 2,000, and 1,500 psia, respectively, and the gases were displaced from the P-V cell at constant pressure.
3. Gas was flashed in a P-V cell from a sample of reservoir

---

*In the differential-gas liberation procedure the gas is removed, as it is liberated, from contact with the oil. In the flash-gas liberation procedure the gas remains in contact with the oil throughout the liberation process.

oil at 180°F from saturation pressure to 3,100 psia. The liberated gas was transferred by mercury displacement at a constant pressure from the P-V cell to another P-V cell. The gas was then liberated from the second P-V cell at 180°F in nine pressure steps.

A graph of specific-gravity data obtained by the three procedures described above is shown in Fig. 9. A study of these data shows the specific gravities of the liberated gases to be identical, within the limits of experimental error, for all pressures within the pressure range in which retrograde condensation occurs. The authors concluded that the composition of the gas in the reservoir depends only upon the reservoir pressure throughout the pressure range in which retrograde condensation occurs, as has been shown by theory and laboratory data. Accordingly, gas samples can be obtained, within the pressure range in which retrograde condensation occurs, by either the differential or flash gas-liberation procedure that will be representative of the liberated gas in the reservoir.

The composition of the reservoir gas* from the Elk City Field was obtained by fractional distillation of gas samples liberated by flashing the reservoir oil at reservoir temperature in seven pressure steps from saturation pressure to atmospheric pressure. The gas liberated in each flash step was released through the throttling valve while a constant pressure was maintained in the P-V cell. The gas released from the P-V cell passed through capillary steel tubing to low-temperature fractional gas-analysis equipment, where its composition was determined. Condensation within the capillary tubing was prevented by maintaining the absolute pressure at less than 200 mm of mercury and the temperature of the tubing at slightly above reservoir temperature. After all the gas had been liberated and analyzed, the residual oil was transferred from the P-V cell to the fractional analysis equipment, where it was analyzed. The composition of the liberated gases are shown in Fig. 10. The composition of the residual oil is given in Table II.

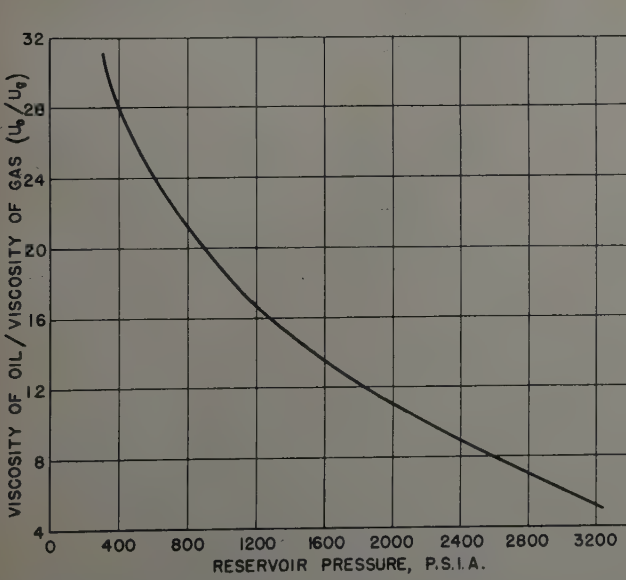

FIG. 6 — OIL AND GAS VISCOSITY RELATIONSHIPS USED IN CALCULATING RESERVOIR PERFORMANCE.

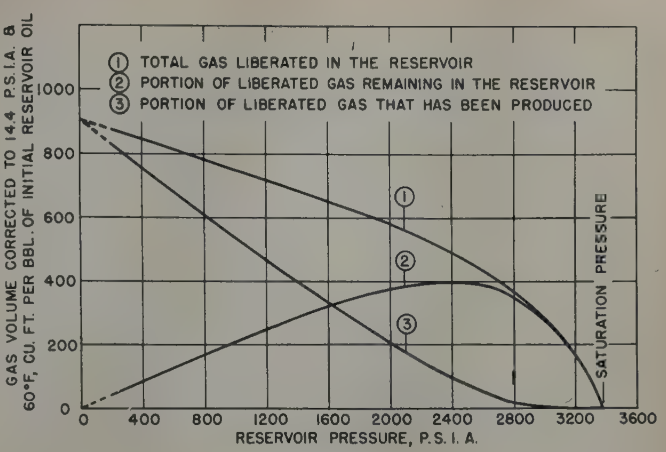

FIG. 7 — DISTRIBUTION OF GAS LIBERATED IN THE RESERVOIR PER BARREL OF INITIAL RESERVOIR OIL (ELK CITY FIELD).

CALCULATED RESERVOIR PERFORMANCE

Calculations were made for several hypothetical reservoirs for a number of declining pressure steps to abandonment pressure. The Elk City Field data and data on a field reported by Sloan[5] were used to determine (a) the production gas/oil ratio and the volume of oil produced, assuming that all of the hydrocarbons entering the producing wells in the gaseous phase passed through the gas-oil separator as gas, (b) the production gas/oil ratio and the volume of produced stock-tank hydrocarbon liquid when consideration was given to the volume of condensate resulting from the production of gas that had been liberated in the reservoirs and would be collected in the stock tanks along with the oil, and (c) the volumes of gas and hydrocarbon liquids recoverable when all produced gas was processed by a natural-gasoline plant (the gasoline plant was assumed to recover all hydrocarbons except the methane, ethane, 50 per cent of the propane, 10 per cent of the butanes, and 5 per cent of the pentanes).

The foregoing calculations were made using the Elk City Field data for four solution-gas-drive reservoirs previously described. Similar calculations limited to reservoirs described above, were made using data reported by Sloan.

Two interstitial water contents were chosen to show the extent to which these variations would affect the reservoir performance when using the Elk City Field data. An interstital water content of 30 per cent was chosen as being typical of many reservoirs. A water content of 16 per cent was obtained from core-analyses data[10] from the North Lindsay Field, Okla., a deep-seated reservoir containing a highly volatile oil.[4]

The results of the calculations to determine reservoir performance are summarized in Table III and illustrated graphically in Figs. 11, 12, 13, and 14. These data indicate that a large part of the recoverable hydrocarbon liquid from deep-seated reservoirs containing highly volatile oil, produced by the solution-gas-drive mechanism, is obtained from the production of the solution gas liberated in the reservoir. They also indicate that a greater ultimate oil recovery will be obtained from a reservoir containing a highly volatile oil if it contains nearly an average quantity of interstitial water instead of a relatively small quantity.

Data presented in Table III (columns 4 and 5) show that ultimate recovery based upon the production of the liquid-phase reservoir fluid alone can be considerably in error. In reservoirs containing oil of the Elk City type the error is 22 to 35 per cent; in reservoirs containing oil of the type described by Sloan the error is approximately 350 per cent. The additional recovery is hydrocarbon liquid condensed during the production of solution gas that was liberated in the reservoir. The recovery can be increased even further by processing the produced gas in a gasoline plant, as is shown in columns 5 and 6. The additional recovery by processing the gas is 50,000 to 60,000 bbl of LPG products for each million bbl of reservoir oil of the Elk City Field type and about 70,000 bbl from the type described by Sloan.

---

*The gas obtained from the flash gas liberations is not representative of the reservoir gas in the pressure range below that in which retrograde condensation occurs (below 1400 psia for the Elk City Field gas). This discrepancy is believed to be of little consequence in estimating reservoir performance because the difference between the gas obtained in the laboratory with that in the reservoir is not appreciable until the pressure decreases below 800 to 600 psia, at which time most of the recoverable reservoir fluids have been produced.

Table III also shows the effect of variations in interstitial water on the calculated hydrocarbon-liquid recoveries. Calculations were made by using the Elk City Field data for interstitial water contents of 30 and 16 per cent. Values shown in lines 3, 4, 7 and 8 are based upon 1,000,000 bbl of pore space. Although the reservoir with an interstitial water content of 30 per cent contains less oil than a similar reservoir with a content of 16 per cent, the estimated ultimate stock-tank hydrocarbon-liquid recovery is greater. A graphical comparison of the recovery from two reservoirs, each containing 1,000,000 bbl of oil initially but one having 30 per cent interstitial water and the other 16 per cent, is shown in Fig. 14.

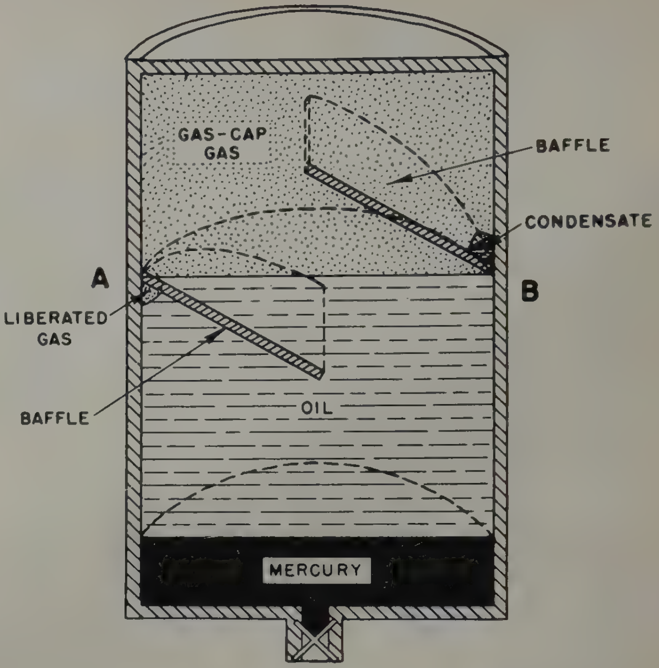

FIG. 8 — ILLUSTRATION OF OIL AND GAS IN EQUILIBRIUM.

EFFECT OF OIL VOLATILITY ON RESERVOIR PERFORMANCE

Data developed in this paper on two highly volatile reservoir oils show that only a small part of the stock-tank oil initially in place will be produced by the solution-gas-drive mechanism. Some pertinent observations are set forth to show reasons for the low recovery.

The changes in oil and gas saturations that take place in a solution-gas-drive reservoir are illustrated in Fig. 15 on the basis of data on the reservoir oil from the Elk City Field. The components (70 per cent oil and 30 per cent interstitial water) of one volume of reservoir pore space initially in the reservoir at saturation pressure would expand with declining pressures according to curve *A*. If gas were liberated from one unit volume of the initial fluid without producing any liquid the decrease in liquid volume resulting from liberation of solution gas would be represented by curve *B* (calculated from shrinkage data obtained through a differential gas-liberation analysis). Curve *C* shows the liquid saturation as calculated by using K_g/K_o relationships and material-balance equations. Curve *D* indicates a constant interstitial water content of 30 per cent. The relative oil saturation is indicated by the horizontal distance between curves *D* and *C*. The volume of reservoir oil produced is indicated by the horizontal distance between curves *C* and *B*. As the pressure is reduced below saturation pressure and until the production gas/oil ratio exceeds the solution gas/oil ratio, the volume expansion of the reservoir oil and that of the liberated gas equals the volume of reservoir oil produced; during the pressure reduction the gas saturation is equal to this expansion plus the shrinkage of the reservoir oil. A large expansion as compared to the shrinkage is therefore an advantage.

Table II — Fractional Analyses of Oil and Gas Samples from Constantin-Lambert Well No. 1, Elk City Field, Washita County, Okla.

Component	High-pressure separator (314 psia and 60°F)		Low-pressure separator (44 psia and 60°F)		Initial reservoir oil[1]	Residual oil from diff. lib.
	Gas	Oil	Gas	Oil		
	Mole Fraction					
Carbon dioxide	0.0017	0.0003	0.0026		0.0014	
Nitrogen	.0335	.0002	.0087		.0200	
Methane	.7391	.0547	.3572	0.0005	.5372	
Ethane	.1150	.0686	.2238	.0226	.0994	
Propane	.0735	.1424	.2488	.1090	.0863	
Isobutane	.0067	.0388	.0392	.0437	.0129	0.0065
Normal butane	.0173	.1055	.0744	.1135	.0392	.0320
Isopentane	.0029	.0443	.0175	.0521	.0148	.0253
Normal pentane	.0030	.0552	.0144	.0686	.0179	.0424
Hexanes	.0020	.0851	.0119	.0985	.0200	.0501
Heptanes plus	.0053	.4049	.0015	.4915	.1509	.8437
Total	1.0000	1.0000	1.0000	1.0000	1.0000	1.0000
Specific gravity of C_7+ residue	[2]	0.810	[2]	0.811	0.809	0.815
Molecular weight of C_7+ residue	[2]	180	[2]	182	178	179

[1] Calculated from data on the volume and composition of the residual oil and the liberated gas.

[2] Insufficient residue for determination of this value.

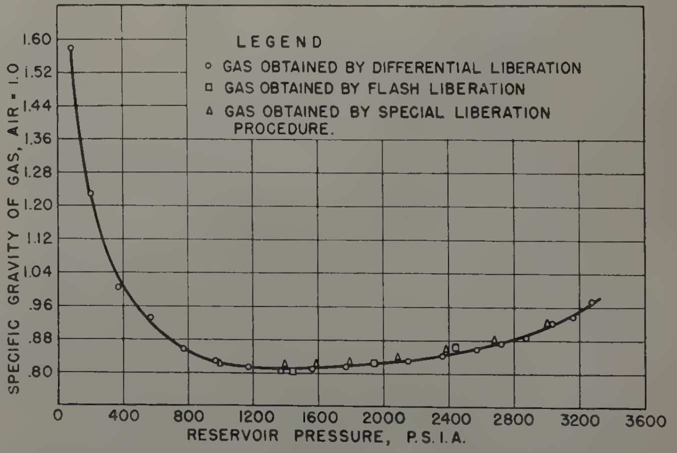

FIG. 9 — SPECIFIC GRAVITY OF LIBERATED GAS (ELK CITY FIELD, OKLA. SAMPLES).

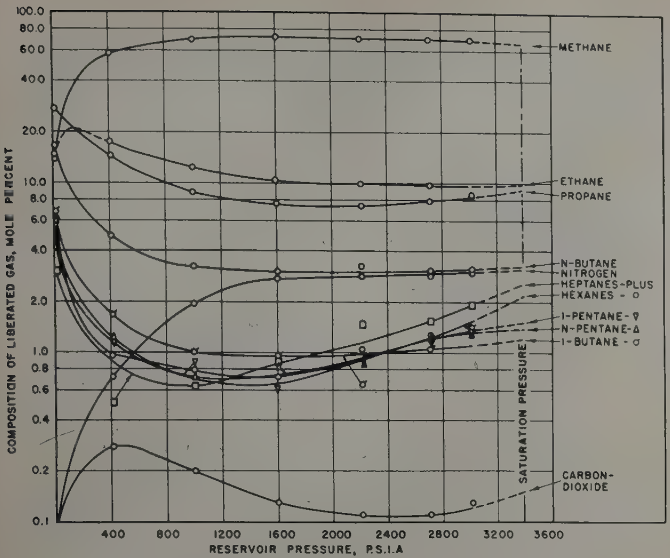

FIG. 10 — VARIATION IN COMPOSITION OF LIBERATED GAS WITH REDUCTION IN PRESSURE (ELK CITY FIELD, OKLA., SAMPLE).

type of oil. The data used to construct these curves were obtained on reservoir samples from the Elk City Field, a field reported by Sloan,[5] the West Edmond, Okla., Field,[11] and the Elk Hills, Calif., Field.[12] (The curves are lettered to correspond with those in Fig. 15). In comparing curves *B* it is apparent that the more-volatile oils undergo a greater shrinkage for a given pressure decrement than the less-volatile type. Curves *A* show that the more-volatile oils expand at a slower rate than the less-volatile oils when the pressure is first reduced below saturation pressure. Thus, for a small reduction in pressure below saturation pressure, there is little expansion of the more volatile oil to expel the reservoir oil to the producing wells whereas the gas saturation due to shrinkage of the oil increases rapidly. As a result, only a small volume of oil will be produced before the production gas/oil ratio exceeds the solution gas/oil ratio. As the pressure is reduced further on this type of oil, additional shrinkage takes place, and the gas saturation in the reservoir increases until almost all of the produced fluid is reservoir gas.

As the expansion exceeds the shrinkage for a small pressure drop below saturation pressure in the less-volatile type of reservoir oil, these properties are the reverse of those of the more-volatile oil. For example, for a pressure drop in the Elk Hills (Calif.) Reservoir that will cause an expansion of 8 per cent, the shrinkage of the oil is only 2 per cent. A gas saturation in the reservoir of 10 per cent (8 per cent expansion and 2 per cent shrinkage) is considered to be approximately the minimum at which gas will flow.[13] Thus, as the expansion equals the production, approximately 8 per cent of the reservoir oil would be produced before the production gas/oil ratio exceeds the solution gas/oil ratio. In contrast, the curves from data reported by Sloan show that only 0.15 per cent of the oil will be produced when the gas saturation of the reservoir equals 10 per cent. The low-recovery efficiency from a highly volatile oil reservoir results from the extremely high rate of oil shrinkage and the low rate of expansion of the oil and liberated gas when pressure are decreased below saturation pressure.

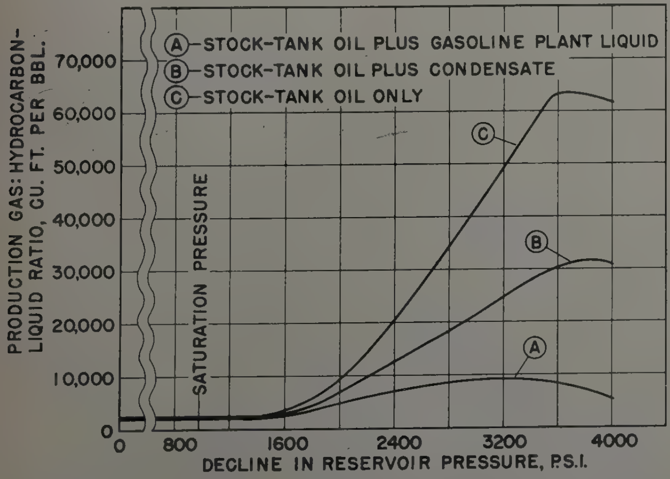

FIG. 11 — GAS/HYDROCARBON-LIQUID RATIOS AS OBTAINED FROM THREE DIFFERENT METHODS OF CALCULATIONS (ELK CITY FIELD DATA BASED UPON 30 PER CENT WATER SATURATION).

SUMMARY

Methods of calculating the volume and composition of hydrocarbon liquid condensed from the produced solution gas that has been liberated in a reservoir are presented in this report. Laboratory data on reservoir-oil samples from the Elk City Field and a highly volatile reservoir oil reported by Sloan[5] were used to show that a large part of the recoverable hydrocarbon liquid from a highly volatile oil reservoir, produced by the solution-gas-drive mechanism, is obtained from the gas-phase fluid entering the producing wells. The calculations show that 18 to 26 per cent of the ultimate stock-tank liquid recovered from the hypothetical reservoirs containing oil of the Elk City Field type will be condensate and approximately 78 per cent of the stock-tank liquid recovered from a reservoir containing oil of the type reported by Sloan will be

Table III — Ultimate Recovery of Highly Volatile Oils Under Various Reservoir Conditions

	1	2	3	4	5	6
				Calculated ultimate hydrocarbon-liquid recovery, bbl[1]		
Line No.	Volume of oil in reservoir initially, bbl	Abandonment pressure, psia	Interstitial water content, pct of reservoir pore space	Stock-tank oil only	Stock-tank oil plus condensate	Stock-tank oil plus gasoline plant liquid
			Elk City Field Sample Data			
1	1,000,000	500	30	83,000	101,000	149,000
2	1,000,000	500	16	58,000	77,000	127,000
3	700,000	500	30	58,200	71,000	105,000
4	840,000	500	16	49,000	65,000	106,000
5	1,000,000	200	30	85,000	105,000	167,000
6	1,000,000	200	16	58,000	79,000	142,000
7	700,000	200	30	60,000	74,000	117,000
8	840,000	200	16	49,000	67,000	120,000
			Sample Data Reported by Sloan			
9	1,000,000	500	30	17,000	75,000	142,000
10	700,000	500	30	12,000	53,000	99,000
11	1,000,000	200	30	17,000	76,000	151,000
12	700,000	200	30	12,000	53,000	106,000

[1] These values include the production from initial reservoir pressure to saturation pressure. The expansion of 1 million bbl of initial reservoir oil to saturation pressure would yield 15,600 bbl of stock-tank oil for the Elk City Field sample data and 11,000 bbl for the sample data reported by Sloan.

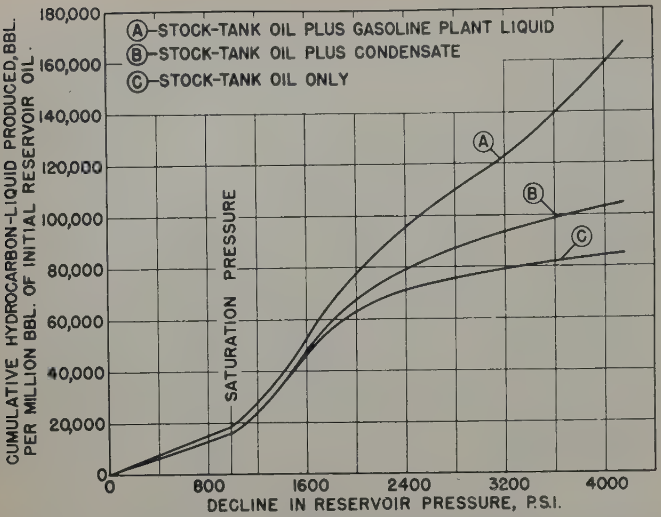

FIG. 12 — VARIATIONS IN HYDROCARBON-LIQUID RECOVERIES OBTAINED BY USING THREE DIFFERENT METHODS OF CALCULATIONS (ELK CITY FIELD DATA BASED UPON 30 PER CENT WATER SATURATION).

Fig. 16 illustrates why recovery of highly volatile oil from a reservoir will be less, even though more energy per unit volume of initial oil is available, than for the less-volatile condensate. Processing the produced gas in a gasoline plant would increase the hydrocarbon-liquid recoveries, in the form of LPG products, by approximately 50 to 100 per cent (50,000 to 70,000 bbl per 1,000,000 bbl of highly volatile oil initially in the reservoir).

Theoretical considerations and experimental results are presented to show that the gas phase in the reservoir can be duplicated in the laboratory, for the declining pressure range in which retrograde condensation occurs, by either the differential or flash gas-liberation procedure. In determining the compositions of the fluids flowing in the Elk City Field reservoir low-temperature fractional analyses of the gas obtained by the flash gas-liberation procedure were used.

APPENDIX

OUTLINE FOR CALCULATING FUTURE RESERVOIR PERFORMANCE

With the detailed information on the reservoir and reservoir fluid available, the recovery of hydrocarbon fluids for a number of reservoir-pressure decrements can be estimated by the procedure outlined in detail below. The volumes of gas and oil flowing in the reservoir are calculated by using material-balance equations.[1,2,3] The composition of the fluids — oil and gas — flowing in the reservoir are calculated from data on the compositions of the residual oil and liberated gas and gas solubility obtained in the laboratory. From knowledge of the volumes and compositions of the fluids flowing in the reservoir the total volumes of the stock-tank oil and the LPG products that can be extracted in a gasoline plant are determined. Equilibrium constants [8,9] and knowledge of the composition of the reservoir gas are used in calculating the volume of stock-tank condensate that will be recovered from the production of the solution gas that has been liberated in the reservoir.

A. Gas/Oil Ratios for the Fluids Flowing in the Reservoir.
  (1) Plot "K_g/K_o versus liquid saturation," Fig. 5.
  (2) Calculate viscosity of gas for reservoir temperature and several pressures. Obtain viscosity of oil for the same pressures. Calculate and plot U_o/U_g, Fig. 6.
  (3) Use flash-gas liberation data (Fig. 3) in material-balance equations and calculate oil and gas production.
  (4) Summarize oil and gas production.

B. Gasoline-Plant Calculations.
  (1) Liquid composition (volume fraction) of reservoir oil (residual oil plus gas in solution equals reservoir oil — use differential gas-liberation data, (Fig. 2).
    (a) Convert mole composition of residual oil to liquid composition (volume fraction).
    (b) Plot mole composition of reservoir gas versus liberation pressure, Fig. 10.
    (c) Obtain gas in solution values for each step shown in differential gas-liberation data in cu ft of gas/per cu ft of residual oil.
    (d) From the figure showing mole composition of reservoir gas (B-1-b) determine average mole composition of liberated gas for each step shown in differential gas-liberation data.
    (e) Convert the volume of "gas in solution" for each step into the equivalent liquid volume at 60°F in cu ft (using handbook for conversion factors).
    (f) Add the equivalent liquid volume of gas in solution (B-1-e) to 1 cu ft of residual oil volume (B-1-a). (The summation of the components of the residual oil and gas in solution gives the volume of the reservoir oil at 60°F per cu ft of residual oil at 60°F.)
    (g) Find the equivalent liquid composition (volume fraction) at 60°F of 1 cu ft of the reservoir oil (at reservoir temperature and pressure) by dividing the values in (B-1-f) by the "relative oil volume factor" at the companion reservoir pressure from the differential gas-liberation data.
    (h) Plot the volume fraction of each hydrocarbon in the reservoir oil versus pressure (B-1-g).
  (2) Liquid volumes of the produced hydrocarbons (reservoir oil plus reservoir gas equals flowing fluid).
    (a) Obtain liquid composition (volume fraction) of

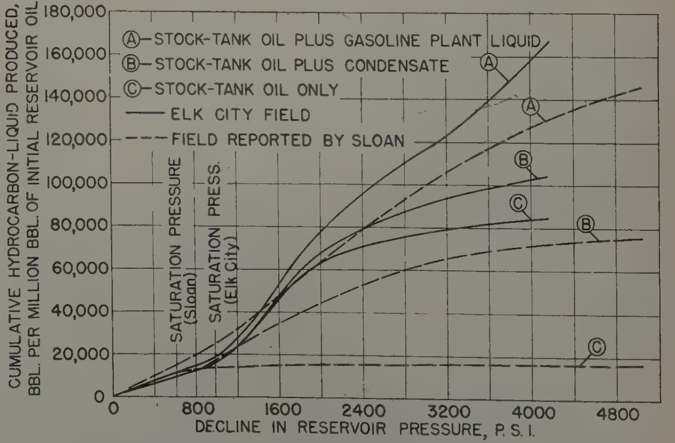

FIG. 13 — COMPARISONS OF CALCULATED HYDROCARBON-LIQUID RECOVERIES FROM DATA ON ELK CITY FIELD SAMPLES AND ON SAMPLES REPORTED BY SLOAN (USING 30 PER CENT INTERSTITIAL WATER ASSUMED).

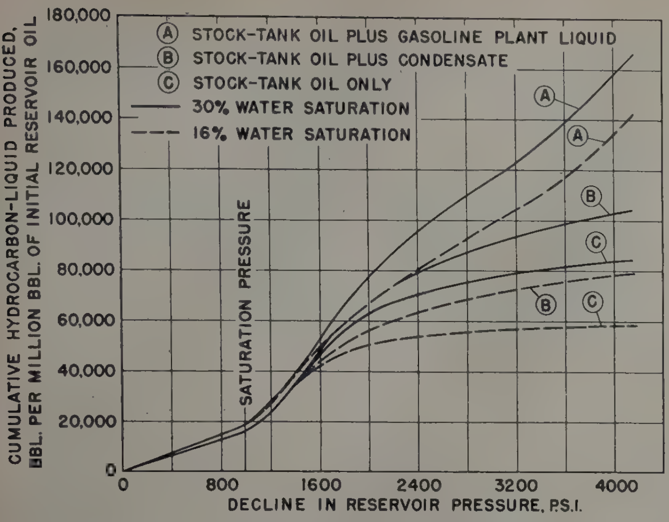

FIG. 14 — EFFECT OF INTERSTITIAL WATER CONTENT ON CALCULATED HYDROCARBON-LIQUID RECOVERIES (ELK CITY FIELD DATA).

1 cu ft of oil in reservoir for the average pressure used in each step of the material-balance calculations in "*A*" from (B-1-h.)

(b) Obtain volume of reservoir oil produced during each step from the material-balance calculations (A-4).

(c) Determine liquid volumes of the hydrocarbons in the reservoir oil produced — liquid compositions (B-2-a) times volume of reservoir oil produced (B-2-b).

(d) Calculate the equivalent liquid volume in cubic feet for each hydrocarbon component of 1 Mcf of reservoir gas from equivalent liquid volume of liberated gas (B-1-e). Plot volume versus pressure.

(e) Obtain volume of produced reservoir gas from material-balance calculations (A-4).

(f) Obtain liquid volume of each hydrocarbon component for the produced reservoir gas — (B-2-d) times Mcf of gas as obtained from (B-2-e).

(g) Obtain total liquid volume of each hydrocarbon-liquid component produced during each step — components in the produced reservoir oil (B-2-c) plus components in the produced reservoir gas (B-2-f).

(3) Mole composition of flowing fluid.

(a) Obtain data from (B-2-g) — liquid volume of components produced during period.

(b) Obtain equivalent liquid volumes of C_1 to C_6 from handbook. Obtain equivalent liquid volume of C_7+ from molecular weight of C_7+ from oil and molecular weight of C_7+ from gas condensate.

(c) Convert from liquid composition (volume fraction) to mole composition.

(4) Total gas/hydrocarbon liquid ratio from gasoline plant.

(a) Start with (B-2-g) — liquid volume of components produced during period.

(b) Calculate the volume of gasoline-plant liquid and gas for each period.

(c) Determine average gas/hydrocarbon liquid ratio for each period.

C. Corrected Gas/Oil Ratio and Stock-Tank Liquid Volumes when Considering the Condensate from the Production of the Gas that was Liberated in the Reservoir.

(1) Determine the volume of condensate obtainable from the produced gas that has been liberated in the reservoir and the produced gas/hydrocarbon liquid ratio.

(a) Refer to curves showing mole composition of reservoir gas versus reservoir pressure (B-1-b).

(b) Use "*K*" constants and calculate total gas/hydrocarbon liquid ratios for several reservoir pressures; construct curve. Also, calculate composition of the liquid and the gas phases.

(c) Using (C-1-b), determine gas/hydrocarbon liquid ratios for pressures that are average for the various periods used in material-balance calculations.

(d) Divide reservoir gas production (A-4) for period by (C-1-c) to obtain condensate produced during period.

(2) Determine the volume of stock-tank hydrocarbon liquid produced and the corrected gas/hydrocarbon liquid ratio for each material-balance step.

(a) Determine the total stock-tank hydrocarbon liquid produced by adding the volume of condensate (C-1-d) to the volume of oil (A-4).

(b) Calculate the equivalent gas-vapor volume for 1 cu ft of condensate (use composition of stock-tank hydrocarbon liquid as obtained by "*K*" constants calculated on the reservoir gas (C-1-b) at an intermediate pressure, 2,400 psia).

(c) Multiply (C-2-b) by condensate produced durin period (C-1-d).

(d) Subtract (C-2-c) from gas produced (A-4) to obtain the corrected volume of gas produced.

(e) Calculate corrected gas/oil ratio and cumulative stock-tank liquid produced from (C-2-a) and (C-2-d).

D. Additional Calculations.

(1) Liberated gas in the reservoir

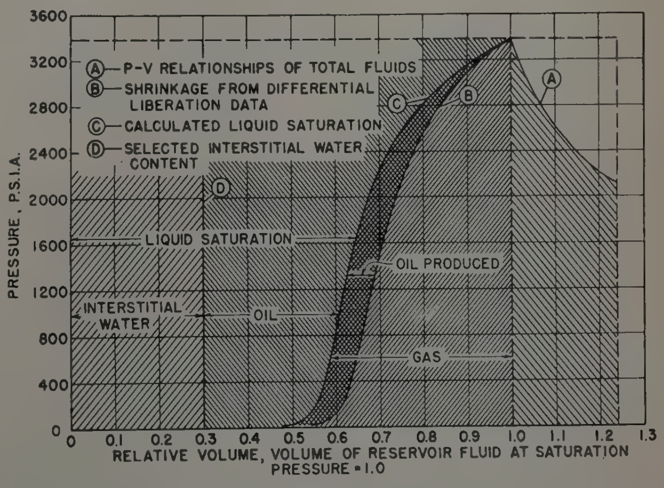

FIG. 15 — RESERVOIR PERFORMANCE INDICATED BY DATA FROM THE ELK CITY FIELD SAMPLES.

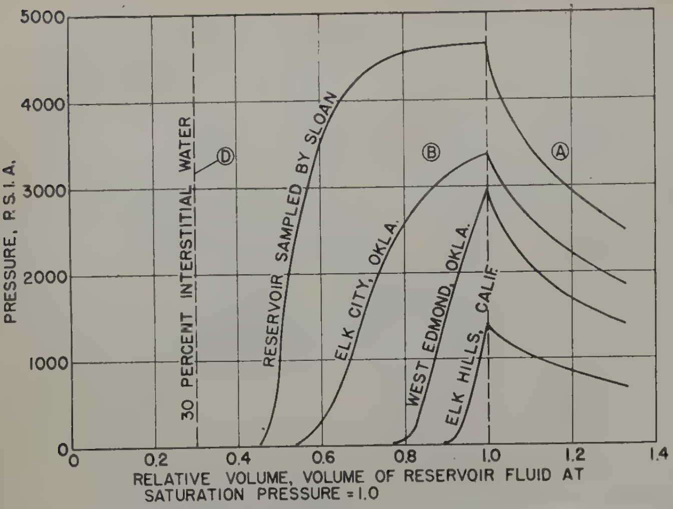

FIG. 16 — COMPARISON OF PHYSICAL PROPERTIES OF RESERVOIR FLUIDS FROM FOUR FIELDS.

   (a) Obtain liquid saturation in reservoir from (A-3).
   (b) Obtain gas saturation in reservoir, 1 minus the liquid saturation (D-1-a).
   (c) Number of cubic feet of gas in reservoir at reservoir pressure and temperature equals the volume of reservoir in barrels times gas saturation (D-1-b) times 5.6146.
   (d) Correct the volume of gas in the reservoir (D-1-c) to standard conditions.
   (e) Total gas liberated in reservoir at a designated pressure equals the volume of gas in the reservoir corrected to standard conditions (D-1-d) plus the total liberated gas produced (A-4) to the same pressure.

(2) Liquid volume of each hydrocarbon component of produced fluid.
   (a) Using data on the liquid volume of each component produced (B-2-g), the liquid-volume-fraction composition of initial reservoir oil (B-1-f), and volume of initial reservoir oil, calculate percentage production of each component.

ACKNOWLEDGMENTS

This study was conducted by the Bureau of Mines Petroleum Experiment Station, Bartlesville, Okla., in cooperation with the State of Oklahoma.

The authors gratefully acknowledge the cooperation of the Constantin Oil Co. for making a well available for testing and subsurface oil sampling. Thanks are extended to John J. Arps, British-American Oil Producing Co., Maurice Dean, Phillips Petroleum Co., Connie L. Wilson, Cities Service Oil Co., and G. B. Shea, R. V. Higgins, E. M. Tignor, and R. Vincent Smith, Bureau of Mines, for criticisms and suggestions that were helpful in the preparation of the final report.

The authors express their appreciation for assistance that has been rendered by R. A. Cattell, Chief, Petroleum and Natural Gas Branch, H. C. Fowler in charge of the Petroleum Experiment Station, and C. J. Wilhelm in direct charge of work reported in this paper.

REFERENCES

1. Babson, E. C.: *Trans.* AIME, (1944) **155,** 120.
2. Tarner, Jack: *The Oil Weekly,* (June 12, 1944) **114,** 32-34.
3. Patton, E. Charles, Jr., *Trans.* AIME, (1947) **170,** 112-155.
4. Cook, Alton B., Spencer, G. B., Bobrowski, F. P., and Dewees, E. J.: *The Petroleum Engineer,* (Sept., 1948) **19,** 158-168.
5. Sloan, J. Paul: The Liquefield Gas Reservoir — A Laboratory Study: Presented at the Fall Meeting of the Petroleum Division, AIME, Dallas, Tex., Oct. 4, 5, and 6, 1948.
6. Muskat, M., and Taylor, M. O.: *Trans.* AIME, (1946) **165,** 81.
7. Bicher, Leo B., Jr., and Katz, Donald L.: *Trans.* AIME (1944) **155,** 246-252.
8. Katz, D. L., and Hachmuth, K. H.: *Industrial and Engineering Chemistry,* (1937) **29,** 1072-1077.
9. Katz, Donald L.: *Trans.* AIME, (1938) **127,** 159-177.
10. Barnes, Kenneth B.: *The Oil and Gas Journal,* (Dec. 8, 1945) **44,** 78.
11. Cook, Alton B., Dewees, E. J., and Harris, H. M.: *The Petroleum Engineer,* (May, 1945) **16,** 85-92. (Tables 3 and 4).
12. Cook, Alton B., and Shea, G. B.: Special Studies of Reservoir Oils in Naval Petroleum Reserve No. 1, Elk Hills Field, Calif.: *Bureau of Mines Rept. of Investigations 4054,* 1947, pp. 47 and 49.
13. Muskat, Morris: *Physical Principles of Oil Production:* 1st edition, McCraw-Hill Company, Inc., New York, p. 275.

★ ★ ★

LABORATORY MEASUREMENTS OF RELATIVE PERMEABILITY

J. S. OSOBA, J. G. RICHARDSON, JUNIOR MEMBER AIME, **J. K. KERVER,** JUNIOR MEMBER AIME, **J. A. HAFFORD** AND **P. M. BLAIR,** JUNIOR MEMBER AIME, HUMBLE OIL AND REFINING CO., HOUSTON, TEX.

ABSTRACT

This paper presents the results of laboratory measurements of relative permeabilities to oil and gas on small core samples of reservoir rock by five methods, and describes the influences of such factors as boundary effect, hysteresis, and rate upon these measurements. The five methods used were the "Penn State," the "single core dynamic," the "gas drive," the "stationary liquid," and the "Hassler" techniques.

In those methods in which the results are subject to error because of the boundary effect, the error may be minimized by the use of high rates of flow. In order to avoid complexities introduced by hysteresis, it is necessary to approach each saturation unidirectionally. Observed deviations of relative permeabilities with rate can be explained as a manifestation of the boundary effect, and disappear as the boundary effect vanishes.

The results indicate that all five methods yield essentially the same relative permeabilities to gas. Of the four methods applicable to the determination of relative permeability to oil, three, the Penn State, single core dynamic, and gas drive, gave relative permeabilities to oil which were in close agreement. The Hassler method gave relative permeabilities to oil which were consistently lower than the results obtained by the other methods.

INTRODUCTION

The relationship between the effective permeability of a reservoir rock to each of the fluids flowing through it and the corresponding fluid saturation is an important characteristic of the reservoir rock. Knowledge of this characteristic is extremely important in the prediction of the behavior of oil and gas reservoirs and of the ultimate recovery to be expected under various operating conditions. These effective permeabilities are usually expressed as the "relative permeability" to a fluid phase, defined as the ratio of the effective permeability to the permeability of the rock to a single phase at 100 per cent saturation.

Relative permeability-saturation relations are not the same for all kinds of reservoir rock, but may vary from formation to formation, and within the different portions of a heterogeneous formation. In studying the performance of a specific reservoir, it is necessary, then, that the relative permeability characteristics of the individual portions of the reservoir be measured. These measurements may be made in the laboratory on small core samples from the reservoir.

Various techniques have been proposed for the measurement in the laboratory of relative permeability-saturation relations. In varying degree, difficulties attend the use of all of the methods which have been proposed. It is the purpose of this paper to discuss the factors which influence the measurement of relative permeability, the difficulties encountered in several methods, and to present comparative results obtained by the use of various techniques.

FACTORS WHICH INFLUENCE THE MEASUREMENT OF RELATIVE PERMEABILITY

It is necessary that the relative permeability data measured in the laboratory yield the same relative permeability-saturation relationships that would govern the flow of fluids through the sample if it were to occupy its original position in the reservoir. Since the core sample upon which the laboratory measurements are made is not surrounded by similar core material as it was in the reservoir, an error in measuring the relative permeabilities may arise from the "boundary effect" which results from a discontinuity in capillary properties of the system at the effluent end of the core. Again, the rates of

---

[1] References given at end of paper.

Manuscript received in the office of the Petroleum Branch September 3, 1950. Paper presented at the Annual Fall Meeting of the Petroleum Branch in New Orleans, La., Oct. 4-6, 1950.

fluid flow used in the laboratory measurement of relative permeability may be higher than those which occur in the reservoir; this seeming lack of reproducibility of reservoir conditions has, in the past, caused some uncertainty as to the validity of applications of the laboratory results. Still another influence on the laboratory measurement of relative permeability is that of hysteresis.

These various factors are discussed in the following sections.

BOUNDARY EFFECT

Nature of the Boundary Effect

In the determination of relative permeability in the laboratory by the passage of two immiscible fluids through a core sample, there exists a discontinuity in capillary properties at the outflow end of the core. This discontinuity occurs where the fluids pass abruptly from the rock, a region of finite capillary pressure, into an open receiving vessel, where capillary pressure vanishes. Because of the capillary forces existing within the core, the rock tends to retain the wetting phase at the outflow end. This results in an accumulation of the wetting phase, so that the saturation of that phase at the outflow boundary is maintained at a higher level than throughout the remainder of the core.

Various investigators[1,2,3] have observed and discussed this "boundary effect" in connection with their studies of relative permeability and capillary behavior. Leverett[2] observed in his experimental flow of oil and water through sands that there was a saturation gradient from a relatively high water saturation at the boundary to a lower one at a relatively large distance from the boundary.

Influence of the Boundary Effect on Relative Permeability Measurements

Where a saturation gradient, such as that due to the boundary effect, exists in a core sample, the actual pressure drop across the core which is effective in causing flow of the wetting phase is less than that causing flow of the non-wetting phase by an amount equal to the difference in capillary pressure at the two ends of the core. If this fact be disregarded, and the pressure drop in the wetting phase be assumed to be that in the non-wetting phase, it is evident that the relative permeability to the wetting phase computed by use of this assumption is too low.

Another possible disturbing influence of the boundary effect on the measurement of relative permeability results from the existence of a saturation gradient. Where such a gradient exists, the relative permeabilities to both phases flowing vary throughout the core with changes in the saturation. If these variations be disregarded, and reliance be placed on the gross measurements made on a core in which there is a saturation gradient, the relative permeabilities to both phases at the average saturation are too low. Any error from this source is superimposed upon that resulting from the use of a spurious pressure drop in the wetting phase.

Means of Avoiding or Minimizing the Boundary Effect

Of the various ways in which the boundary effect may be avoided or minimized in the measurement of relative permeability, the most obvious is that of performing all measurements on a section of the core sample far enough removed from the outflow end to insure that the saturation gradient in the test section is insignificant. In practice, this may be done by use of a single core only with difficulty. A procedure equivalent in principle consists in placing beyond the test core a core sample of similar material. The boundary effect is then transferred to and confined within the latter core. In this procedure the two must be in capillary contact.

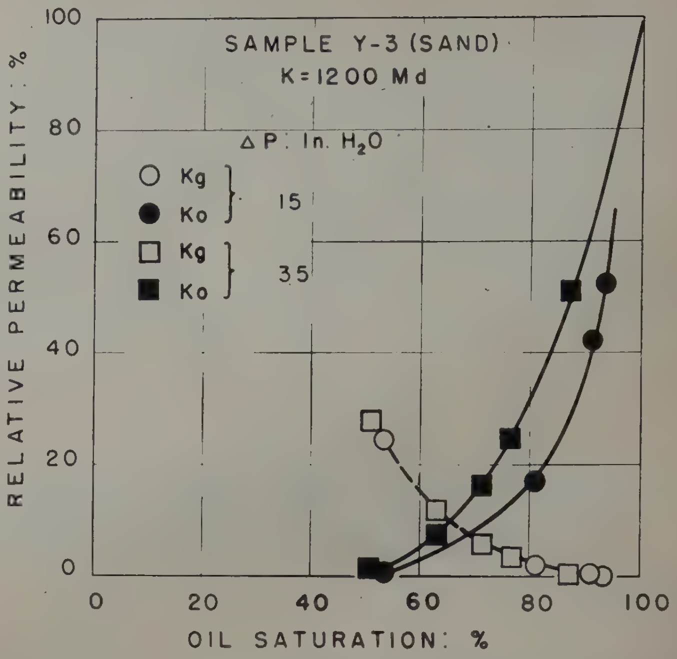

FIG. 1 — EFFECT OF PRESSURE GRADIENT ON RELATIVE PERMEABILITY (LACK OF CAPILLARY CONTACT BETWEEN CORES). PENN STATE.

The boundary effect may also be minimized by the use of high rates of flow. It may be shown by theoretical considerations based on d'Arcy's law, relative permeability-saturation relations, and capillary pressure-saturation relations that the saturation distribution along the core varies for different rates of flow. At low rates of flow the saturation gradient extends over a considerable distance from the outflow end, and at increased rates of flow the gradient extends over shorter distances. It may be concluded that at high rates of flow the error introduced by the boundary effect may be made so small that it will not appreciably affect the measurements of relative permeability.

Another method of avoiding the influence of the boundary effect on the measurement of relative permeability consists in holding the wetting phase stationary by capillary forces and flowing only the non-wetting phase.

Still another method of avoiding the boundary effect consists in maintaining a uniform saturation distribution throughout the core by controlling the capillary pressure at both ends of the core sample. This is accomplished by placing at both ends of the core discs of a material which is permeable only to the wetting phase. In this procedure both phases may be made to flow, with independent control of pressure gradient maintained in each phase.

RATE EFFECT

Some concern has been expressed in the past by various investigators over the apparent dependence of relative permeability on rate of flow used in the laboratory measurements. Since some measurements are made at high rates of flow and others at low rates, the question arises as to whether the relative permeabilities to oil and gas are rate-sensitive in the absence of boundary effect, or whether the observed deviations in measurements in the laboratory with variations in rate of flow through the core sample are solely manifestation of the boundary effect and disappear as the boundary effect is eliminated. It is believed that the latter is correct and that there is no influence on the laboratory measurement of relative permeability exerted by the rate of flow as such in the absence of boundary effect.

HYSTERESIS EFFECT

Relative permeability-saturation relations are not unique functions of saturation for a given core, but are subject to hysteresis; that is, the relative permeability to a fluid at a given saturation depends on whether that saturation is obtained by approaching it from a higher or lower value. Since hysteresis does exist, care must be exercised that the relative permeabilities measured in the laboratory are obtained under conditions wherein each saturation is approached in the desired manner.

The type relative permeability curve that is representative of flow characteristics through the formation in the reservoir depends on the mechanism by which the reservoir is depleted. If the reservoir is depleted by decreasing the oil saturation and increasing the gas saturation, as in a dissolved-gas drive or expanding gas-cap drive, the drainage relative permeability curves should be used. If, however, the reservoir is depleted by decreasing the oil saturation and increasing the water (or wetting phase) saturation, as in a water-drive mechanism, the imbibition relative permeability curves apply.

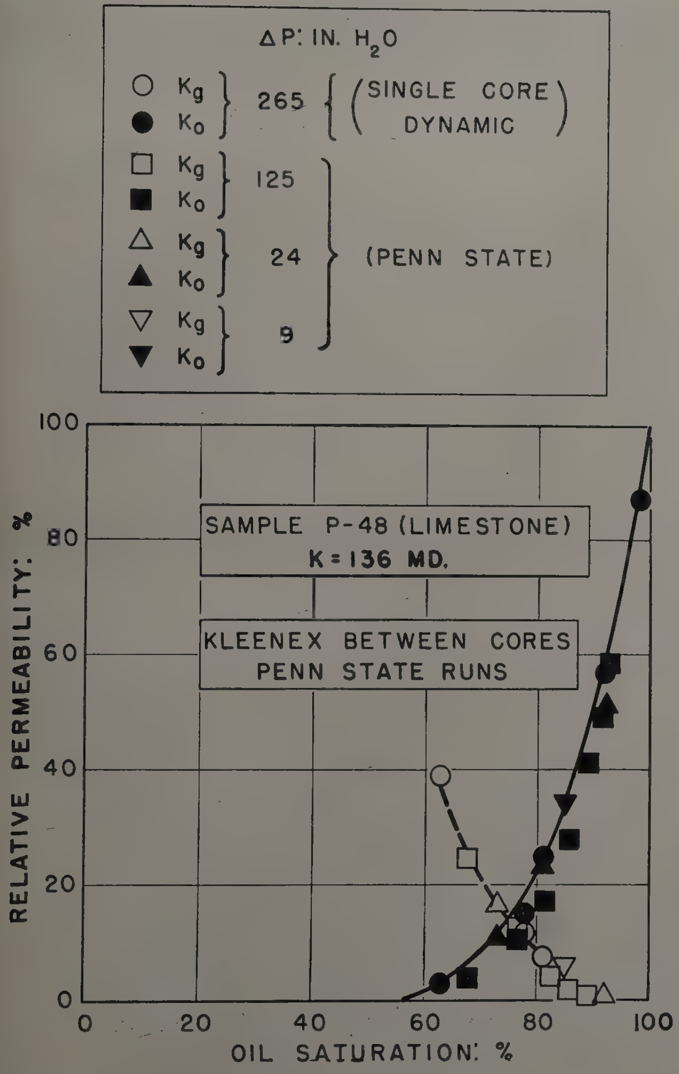

FIG. 2 — EFFECT OF PRESSURE GRADIENT ON RELATIVE PERMEABILITY (CAPILLARY CONTACT BETWEEN CORES). PENN STATE.

PROCEDURES AND RESULTS OF RELATIVE PERMEABILITY MEASUREMENTS

Five procedures for the measurement of relative permeability have been investigated in the work described in following sections. In these techniques the influence of the boundary effect has been avoided or minimized in various ways. Throughout all these investigations, a two-phase system, oil and gas, was used.

Core Samples Used

The core samples used were all from the producing intervals of various reservoirs. Both sandstone and limestone samples were employed. Common to all methods was the preparation of the core samples. These samples, short cylinders ⅞-in. in diameter, were cut from well cores parallel to the bedding planes. After extraction with carbon tetrachloride, they were mounted in Lucite cylinders with an outside diameter of 1½ in. The end of the samples and of the surrounding plastic were faced, and a small concentric groove was cut in one end at the junction of the rock and Lucite. Access to this groove, a piezometer ring, was provided by a small hole drilled into it through the Lucite.

Penn State Method

The Penn State[4] method, so-called because it was devised at Pennsylvania State College, attempts to avoid the influence of the boundary effect by use of a test core sample between two samples of similar material, the three being in capillary contact. In theory, the boundary effect may thus be confined to the downstream sample, with no saturation gradient existing in the sample under test. The purpose of the upstream core is to act as a mixing section for the two fluid phases.

Relative permeabilities were measured by the Penn State method by use of kerosene and helium as the two fluid phases. The cores were first saturated with the oil, and then oil was allowed to flow through them at a rate that gave a predetermined pressure drop. The gas was then allowed to flow at a very low rate. After the system had reached equilibrium, the test core was removed quickly, and the oil saturation was determined by weighing. The core sections were then reassembled, and flow of both phases was resumed at the

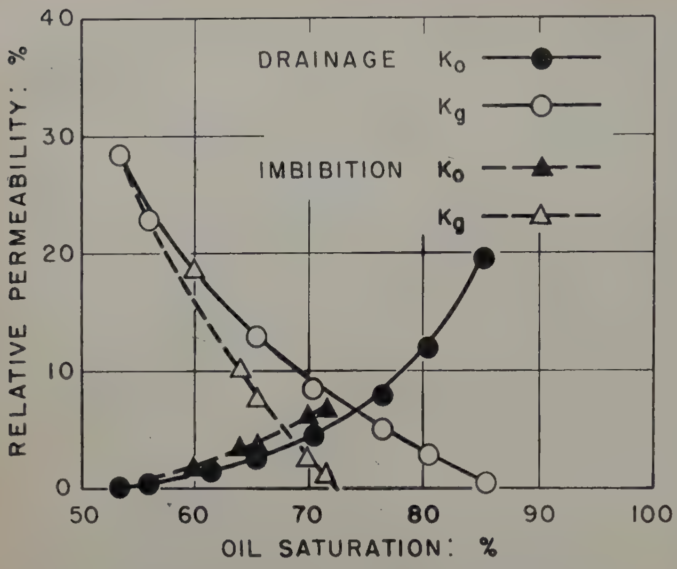

FIG. 3 — HYSTERESIS — RELATIVE PERMEABILITY. PENN STATE.

rates which had existed previously. The rate of flow of the oil phase was then decreased slightly, and the rate of flow of the gas was increased simultaneously to maintain the pressure drop across the core at its previous value. After equilibrium had again been attained, the test section was removed and the saturation was determined. This stepwise procedure was repeated until a complete relative permeability curve had been obtained at incremental changes in the fluid saturation.

Much difficulty was encountered initially in relative permeability measurements by the Penn State apparatus when the flow rate was varied over wide limits. In early experiments, the kerosene was presaturated with gas at the pressure at which the kerosene was introduced into the apparatus. With saturated kerosene as the wetting phase, it was observed that the measured relative permeabilities to both oil and gas were erratic. When experiments were conducted with kerosene from which most of the dissolved gases had been removed, the erratic deviations disappeared. A degassed oil phase was accordingly used in all subsequent work.

Another difficulty observed with the Penn State technique was that due to a boundary effect. Although, in theory, the Penn State technique should give results that are free from boundary effect errors, it was observed that the saturation gradient was not always eliminated from the test sample because capillary contact did not always exist between the test sample and the end sample, or "boundary effect absorber." This was particularly true in the case of samples that were loosely consolidated. The lack of capillary contact between cores caused the relative permeability-saturation relationships to appear to be a function of the applied pressure gradient or flow rate. This variation with pressure gradient was more pronounced in the oil curve than in the gas curve, since the measured pressure drop across the test section was not the actual pressure drop effective in causing flow of the oil.

Fig. 1 shows the increase with pressure gradient of relative permeabilities measured with poor capillary contact between the core samples. Although in this illustration there is shown practically no variation in the relative permeability to gas with increase in pressure gradient, similar tests on other cores did indicate a small variation. Deviations of the type illustrated by Fig. 1 may be expected to result from boundary effect errors if good capillary contact does not exist between the tested core and the boundary absorption core.

Fig. 2 illustrates results of determinations in which good capillary contact between cores appeared to be achieved. The cores used in these determinations were limestone, so that the faces remained flat and true under repeated tests. Layers of Kleenex were placed upon the cores to insure capillary contact. The relative permeabilities were in this case independent of pressure gradient over a wide range, even though the pressure drop across the core was varied from 9 to 125 in. of water. One point obtained with a pressure drop across the core of only 9 in. of water agreed quite well with measurements obtained under conditions of much higher pressure drop. This point also agreed with measurements obtained by another method, the single core dynamic method, at a pressure drop of 265 in. of water.

The effects of hysteresis in measurements made by the Penn State method are illustrated in Fig. 3. In this figure the solid curves, which are drainage curves, were obtained by starting with the sample at 100 per cent oil saturation and progressively decreasing the saturation to a value of 53 per cent. The dashed curves, which are imbibition curves, were obtained by then increasing the oil saturation. If, instead of starting the imbibition curve at a saturation of 53 per cent, the imbibition run were started at an oil saturation of zero, the relative permeability to gas would have been lower than that shown by the curve in Fig. 3, and would have reached zero at a lower oil saturation. The relative permeability to oil would have been increased correspondingly.

Single Core Dynamic Method

In this method the boundary effect is minimized by the use of a rate of fluid flow which is high enough to make insignificant the effects of the saturation gradient in the short test core.

The equipment used in this method was similar to that employed in the Penn State technique, except that a single core, mounted in Lucite, was used. The oil and gas phases were

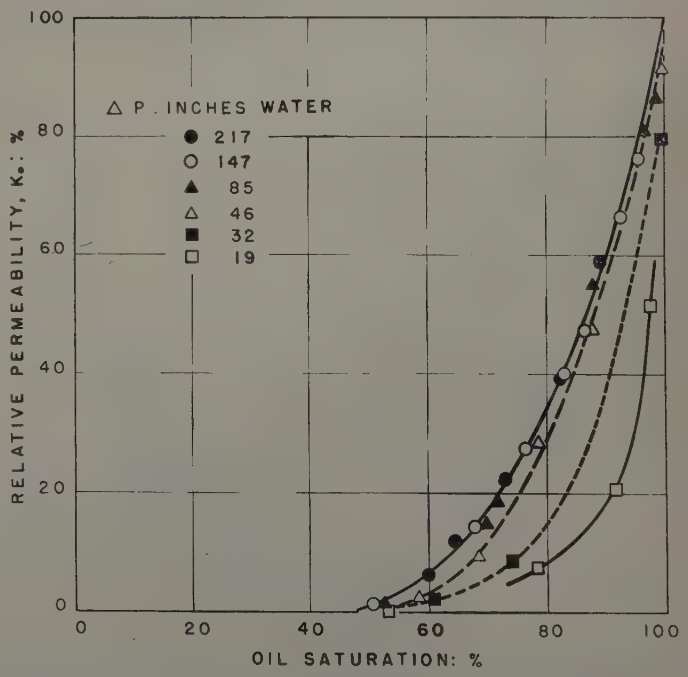

FIG. 4 — RATE EFFECT — RELATIVE PERMEABILITY. SINGLE CORE DYNAMIC.

introduced directly into the core from a feed head. No boundary effect absorber was used.

In making determinations by this method, the core sample was initially saturated completely with the oil phase. A rate of flow of the oil was then established which would correspond to a predetermined pressure drop across the core. Helium was then admitted to the core at a low rate. After equilibrium had been established, the oil saturation was determined by weighing. Successively higher gas flow rates, and correspondingly lower oil rates were employed in succeeding steps to determine complete relative permeability-saturation relations.

It was found that at low rates of fluid flow the measured relative permeability to oil varied with the flow rate. When a sufficiently high rate of flow was attained, however, this variation disappeared, and the relative permeability became independent of flow rate. This effect is illustrated in Fig. 4, which portrays results obtained on a sand core of high permeability. The core sample was approximately an inch long. Kerosene was used as the liquid phase.

In Fig. 4, it may be observed that the measured relative permeability to oil increased with increasing pressure drop until the pressure drop attained a value of about 85 in. of water. Thereafter, further increases in pressure gradient, or flow rate, caused no change in the relative permeability. The gas curve, not shown in this illustration, was the same for all pressure differences except for the lowest value of 19 in. of water, which gave slightly depressed values of the relative permeability to gas.

In order to investigate the effect of change of rate of flow on measurements made by this technique, without introducing possible complications due to change in pressure drop, a series of measurements was made with oils of various viscosities, flowing under an essentially constant pressure gradient. In these runs the viscosities of the oils ranged from 1.8 to 25 centipoises.

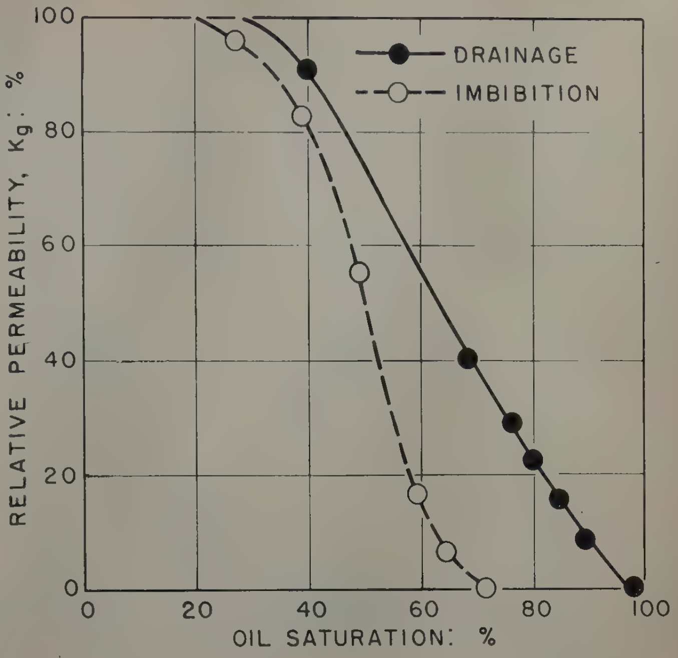

FIG. 6 — HYSTERESIS — RELATIVE PERMEABILITY. STATIONARY-LIQUID.

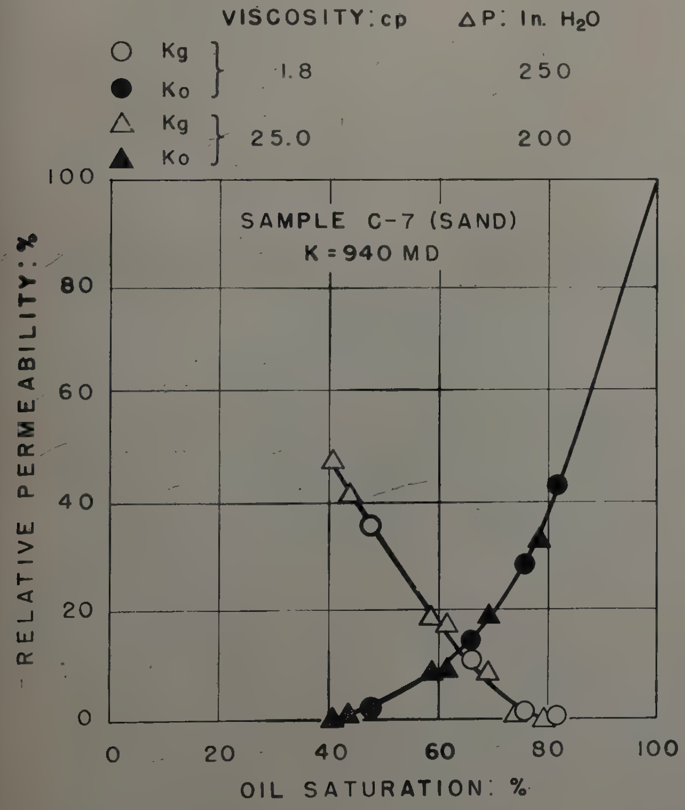

FIG. 5 — EFFECT OF OIL VISCOSITY ON RELATIVE PERMEABILITY. SINGLE CORE DYNAMIC.

Results typical of these determinations are shown in Fig. 5. In the case illustrated, the pressure drop was maintained high enough to render insignificant the error due to the boundary effect. It is apparent from Fig. 5 that a fourteenfold difference in rate of flow had no effect on the relative permeability-saturation relations.

The results illustrated in Figs. 4 and 5 show that relative permeability is not a function of rate of flow in the absence of boundary effects.

Stationary Liquid Method

In the stationary liquid method,[5] the boundary effect is avoided by holding the wetting phase stationary within the core by capillary forces. Only the non-wetting phase is permitted to flow. This is accomplished by the use of a very low pressure gradient across the core. The method is applicable only to the determination of relative permeability to the non-wetting phase.

In the use of this method, relative permeability-saturation curves for gas were obtained by starting with the core completely saturated with oil. The oil saturation was then reduced by blotting the core with Kleenex. When the oil saturation was reduced to less than that corresponding to the equilibrium gas saturation, gas was passed upward through the core under a pressure drop of 1 in. of water. The relative permeability to gas at that point was measured, and the oil saturation was determined by weighing. This process was repeated until the complete relation of the gas relative permeability to saturation was obtained.

It was thought possible that blotting the ends of the sample with Kleenex and determining the relative permeability im-

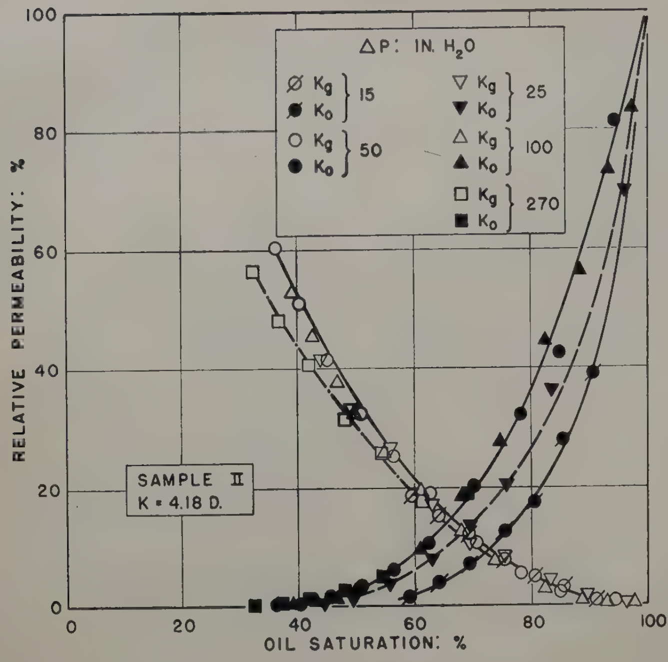

FIG. 7 — RELATIVE PERMEABILITY — GAS DRIVE.

mediately might not give the oil within the core sufficient time to arrange itself into its true drainage distribution. An experiment was accordingly conducted in which the sample was blotted with Kleenex and was then allowed to stand 24 hours before the relative permeability to gas was determined. The relative permeability curves were identical in the two cases.

Other experiments were conducted to determine whether or not the manner in which the oil saturation of the core was reduced affected the relative permeability-to-gas curves. To check this, in addition to blotting the core with Kleenex, the oil saturation in the sample was reduced by two other means. One method was to desaturate the sample by displacing the oil with gas in a porous diaphragm cell. Another method used to desaturate the core was to place the sample in the Penn State apparatus and to continue flow until equilibrium was reached. The sample was then removed from the Penn State apparatus and the relative permeability to gas was measured in the stationary liquid apparatus. The relative permeabilities to gas in all three cases gave identical curves. On the basis of these findings, it was considered satisfactory to determine the gas permeability immediately after desaturation by blotting with Kleenex.

Although the manner in which the core was desaturated apparently had no effect on the determination of gas permeability, it was found that a core which had been desaturated and then allowed to imbibe oil exhibited a marked hysteresis effect. This effect is shown in Fig. 6. In obtaining the results illustrated in Fig. 6, the drainage curve was determined by the ordinary stationary liquid technique. The oil saturation was then reduced to zero by drying, and the core was then allowed to imbibe oil in incremental steps. The relative permeability to gas was determined at each step. The hysteresis effect shown in Fig. 6 is apparently the same as that which has been observed in determinations made by the Penn State method.

A limited number of gas relative permeability-saturation relationships were determined with the sample containing, in addition to the oil, a low brine saturation corresponding to connate water. The investigation showed that the presence of the brine had no effect on the relative permeability to gas.

For a number of cores the oil saturation was reduced until the relative permeability to gas was either 100 per cent or very close to it. Capillary pressure curves were determined for some of these cores, so that the "irreducible minimum" saturations were known. In all such cases the relative permeability to gas reached 100 per cent at oil saturations greater than the irreducible minimum saturations.

Gas Drive Method

In this method the influence of the boundary effect is minimized by the use of a high rate of flow. The method differs from the stationary liquid method in that both phases flow simultaneously; it differs from the single core dynamic method in that only gas is admitted to the core. The flow of both phases results from the displacement of portions of the oil by the flowing gas: hence, the name, "gas drive." This method was first suggested by Hassler[6] in 1936.

In making measurements by the use of this method, the core was first saturated with a high viscosity (19 centipoises) oil. An oil with a relatively high viscosity was chosen so that it would be forced out of the core slowly, thereby increasing the accuracy with which relative permeability could be measured.

Gas at a predetermined pressure was forced through the core for 5 seconds, and the volume of gas flowing during this

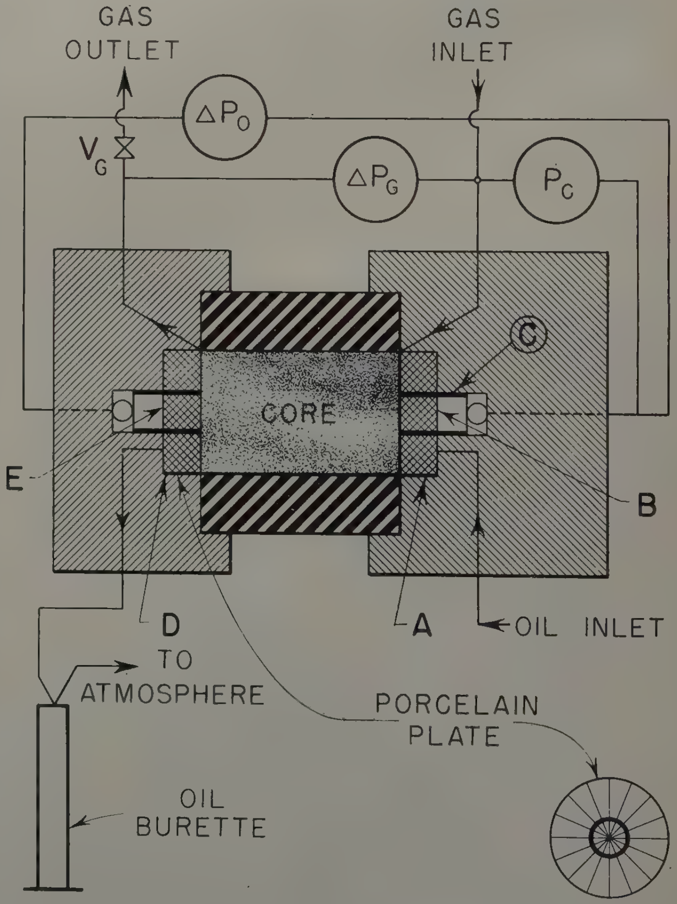

FIG. 8 — RELATIVE PERMEABILITY APPARATUS (HASSLER'S PRINCIPLE).

period was measured. The oil saturation in the core was then determined by weighing. The core was again subjected to gas flow for another short interval of time, and the reduced saturation was determined. The procedure was repeated until completed relative permeability-saturation relations were obtained.

The manner in which the relative permeability varied with the pressure across the sample was similar to that observed in the single core dynamic method. This is illustrated by Fig. 7, which shows typical results obtained by the gas drive method under different pressure gradients. It may be observed that the relative permeability to oil increased with incerasing pressure drop until a pressure drop of about 50 in. of water was attained. Thereafter increase of pressure gradient had no further effect on the relative permeability to oil.

No significant change of relative permeability to gas appeared to result from increasing pressure gradient until a pressure drop of 270 in. of water was used. At this high pressure gradient the relative permeability to gas was decreased. This deviation was probably due to inertial effects encountered at high rates of gas flow.

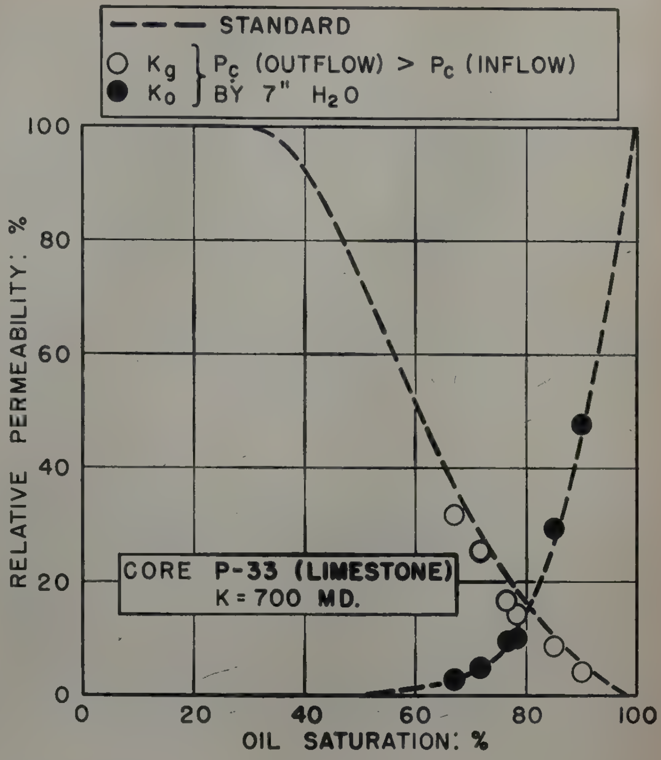

FIG. 10 — EFFECT OF CAPILLARY PRESSURE GRADIENT, HASSLER TECHNIQUE.

Hassler Method

The boundary effect is avoided in the Hassler method[7] by controlling and making equal the capillary pressure at both ends of the core. This is accomplished by placing the core between two discs permeable only to the wetting phase. This permits a uniform saturation to be maintained throughout the length of the core, even at low rates of flow.

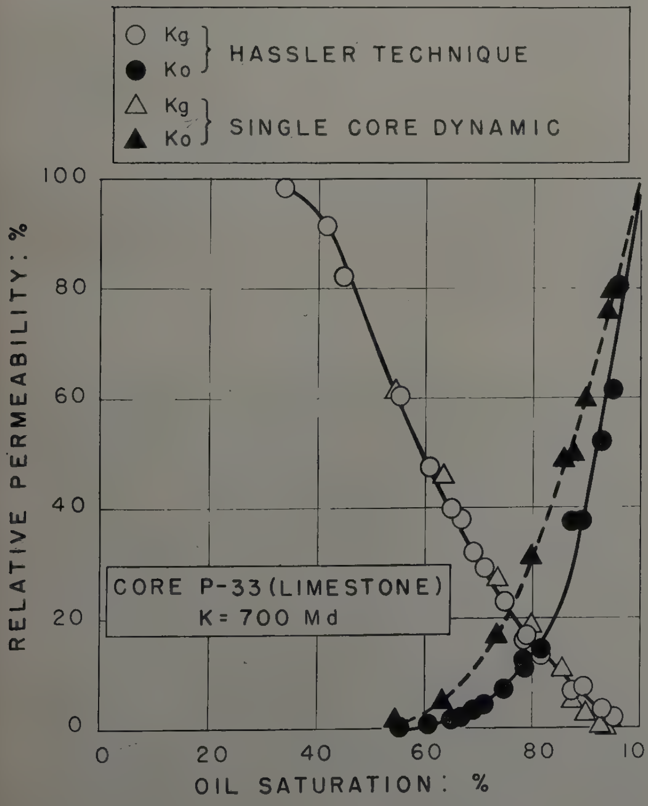

FIG. 9 — RELATIVE PERMEABILITY, HASSLER TECHNIQUE.

The apparatus for measurements made by the Hassler method is shown in Fig. 8. The semi-permeable discs at each end of the core allow oil, but not gas, to pass. They also permit the pressure drop in the oil phase to be measured independently of that in the gas phase.

In the measurement of relative permeability, the sample to be tested was saturated with oil, and then was placed in the apparatus with a few layers of Kleenex at both ends to insure good contact between the core and semi-permeable discs. Oil entered the core through disc *A*. Disc *A* was isolated from the small disc *B* by the metal sleeve *C*. The pressure in the oil at the inflow end was measured through the disc *B*. Gas entered the core through radial grooves in the face of disc *A*. The difference between the pressure in the oil and in the gas at the inflow end is the capillary pressure and was measured by the gauge P_c.

The oil and gas passed through the sample at rates such that the pressure drop in the two phases across the core was the same. This was accomplished by adjusting valve V_g, which controlled the rate of flow of gas through the sample, so that the pressure drop in the gas phase was equal to the pressure drop in the oil phase. This was done so that the capillary pressure at the outflow end would be equal to the capillary pressure at the inflow end. The gas left the core through radial grooves in disc *D*, and the pressure of the oil at the outflow end was measured through disc *E*. After equilibrium was reached, the sample was removed and the saturation of the sample was determined by weighing.

Typical results obtained by the Hassler method are shown in Fig. 9. In this illustration are also shown curves obtained on the same limestone core by the single core dynamic method.

It is evident from these data that the Hassler results on permeability to oil were lower than those obtained by the other method. The gas curves were in good agreement .

Ordinarily, a depression of the oil relative permeability curve would suggest the presence of a saturation gradient. To investigate experimentally the apparent depression of the oil curve shown in Fig. 9, an experiment was performed in which a saturation gradient was deliberately imposed across the core. To this end, the capillary pressure at the outflow end was made about 7 in. of water higher than the capillary pressure at the inflow end. The results that were obtained are shown in Fig. 10, compared with the results obtained when no saturation gradient was presumed to exist. The oil curves of Figs. 9 and 10 were nearly identical. The gas curve obtained by imposition of the saturation gradient was depressed only slightly.

Relative permeability measurements made with a higher capillary pressure at the inflow end than at the outflow end again gave an oil relative permeability curve that was the same as the curve of Fig. 9, and a gas relative permeability curve that was depressed slightly. The foregoing experiments failed to provide an explanation of the apparent depression of the oil curve of Fig. 9.

By use of the same core employed in the above determinations, an investigation was conducted to determine the characteristics of relative permeability curves obtained with oil and gas flowing in opposite directions within the same core. The procedure for this run was the same as for an ordinary run, except that the gas inlet and outlet were interchanged. The pressure drop in each of the phases was adjusted to about 2 in. water to keep the saturation gradient within the core to a minimum. The results of this experiment are shown in Fig. 11, and are seen to agree with the relative permeability curves obtained in the usual manner. The accuracy of the measurements in this investigation were not as great as in a normal run because of the lower pressure drops that were used for the two phases. The results indicated that the relative permeability curves were the same whether the two phases flowed concurrently or in opposition.

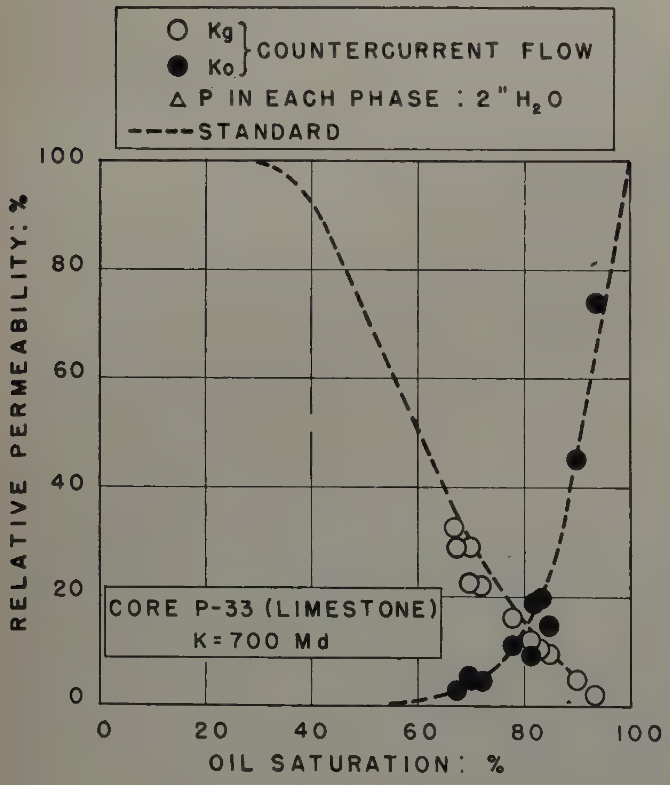

FIG. 11 — EFFECT OF COUNTERCURRENT FLOW, HASSLER TECHNIQUE.

COMPARISON OF RESULTS

The Penn State, the single core dynamic, the gas drive, and the Hassler techniques gave the same curves for relative permeability to gas, as shown in Figs. 12 and 13. The stationary liquid method in some cases gave curves for relative permeability to gas which were in good agreement with those obtained by the other methods. In general, however, the relative permeability to gas determined by the stationary liquid technique was lower than that by the other methods in the region of the equilibrium gas saturation. This resulted in an equilibrium gas saturation which was greater than the value obtained by the other methods.

Measurements of the relative permeability to oil made by the single core dynamic, the Penn State, and the gas drive methods gave the same results except in the regions of high oil saturation, where the values obtained by the gas drive technique were sometimes high. The relative permeability to oil measured by the Hassler method gave results which were lower than those obtained by the other three methods. Comparisons of the results of the different methods may be seen in Figs. 9, 12, and 13.

The Hassler technique is the slowest of all the methods for measuring relative permeability, requiring about one week per sample. The gas drive technique is the fastest, requiring only about an hour for running the complete relative permeability curves. One or two cores can be analyzed a day by means of the single core dynamic or the Penn State techniques. About four cores can be analyzed a day by the stationary liquid technique.

CONCLUSIONS

1. In those methods of determination of relative permeability in which the results are subject to error because of the boundary effect, the error may be minimized by the use of high rates of flow.

2. No variation of relative permeability with variation of rate in the absence of boundary effects has been found. Deviations of relative permeability with rate have been observed only where boundary effects are known to exist, and disappear as the boundary effect vanishes.

3. Hysteresis exists in the measurement of relative permeability. Since relative permeability is not a unique function of saturation because of hysteresis, care must be exercised that relative permeabilities measured in the laboratory are obtained under conditions wherein each saturation is approached in the desired manner.

4. The results of measurements by the Penn State, single core dynamic, stationary liquid, gas drive, and Hassler methods indicate that all yield essentially the same values of relative permeability to gas except in the region of the equilibrium

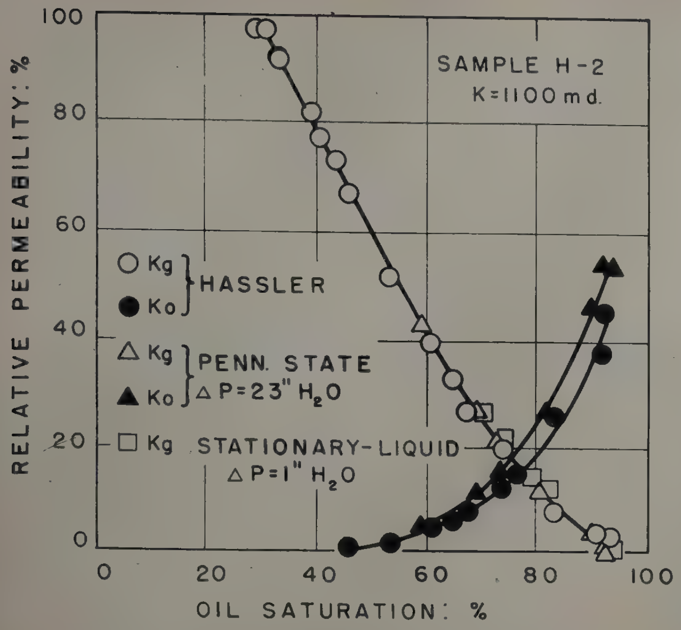

FIG. 12 — RELATIVE PERMEABILITY — THREE METHODS.

gas saturation, where the values given by the stationary liquid method are generally lower.

5. Of the methods applicable to the determination of relative permeability to oil, three, the Penn State, single core dynamic, and gas drive, give relative permeabilities which are in close agreement. The Hassler method to date has given relative permeabilities to oil which have been consistently lower than results obtained by the other methods. The reason for this difference has not been explained.

REFERENCES

1. Leverett, M. C., and Lewis, W. B.: *Trans.* AIME, (1941) 142, 107.
2. Leverett, M. C.: *Trans.* AIME, (1941) 142, 152.
3. Hassler, G. L., Brunner, E., and Deahl, T. J.: *Trans.* AIME, (1944) 155, 155.
4. Morse, R. A., Terwilliger, P. L., and Yuster, S. T.: *The Oil and Gas Journal,* (Aug. 23, 1947) 109.
5. Leas, W. J., Jenks, L. H., and Russell, Charles D.: *Trans.* AIME, (1950) 189, 65.
6. Hassler, G. L., Rice, R. R., and Leeman, E. H.: *Trans.* AIME, (1936-37) 118, 123, 114.
7. Hassler, G. L.: U. S. Patent No. 2,345,935, April, 1944.

DISCUSSION

By V. A. Josendal and B. B. Sandiford, Union Oil Co. of California, Wilmington, Calif.

The authors are to be commended for attacking the problem of laboratory measurements of relative permeability on so broad a front. It is remarkable that essentially the same curves can be obtained by so many different methods.

However, even though the authors have obtained similar relative permeability curves by five different methods, it is possible that some of their measurements may include reproducible errors. In particular their method of obtaining saturations may be faulty. It has been found in Union Oil Co. laboratories in work with the Penn State method that saturations could not be obtained accurately by weighing in either the two-phase liquid system or in particular in the gas-liquid system. If gas is present, reduction of the pressure to atmospheric before weighing causes the gas to expand and an unknown amount of fluid is forced out of the core. Another possible source of error arises from water absorption by the Lucite.

The different relative permeability to oil values obtained by the Hassler method as compared to the other three applicable methods is disturbing. Only one curve can apply in the reservoir for a given set of conditions. However, it is not certain from the data presented whether the observed difference is caused by errors in technique or actually represents different flow and fluid displacement mechanisms.

This difference could be checked by using more accurate techniques in comparing the Hassler method with one of the other three. The Penn State method might well be chosen for this comparison as it appears to be the only one of the three in which uniform saturation conditions can be established. An attempt should be made to minimize nonuniformity of saturation and all possible errors in saturation measurement and pressure measurement. In the Hassler method the pressure taps should be placed on the side of the core so

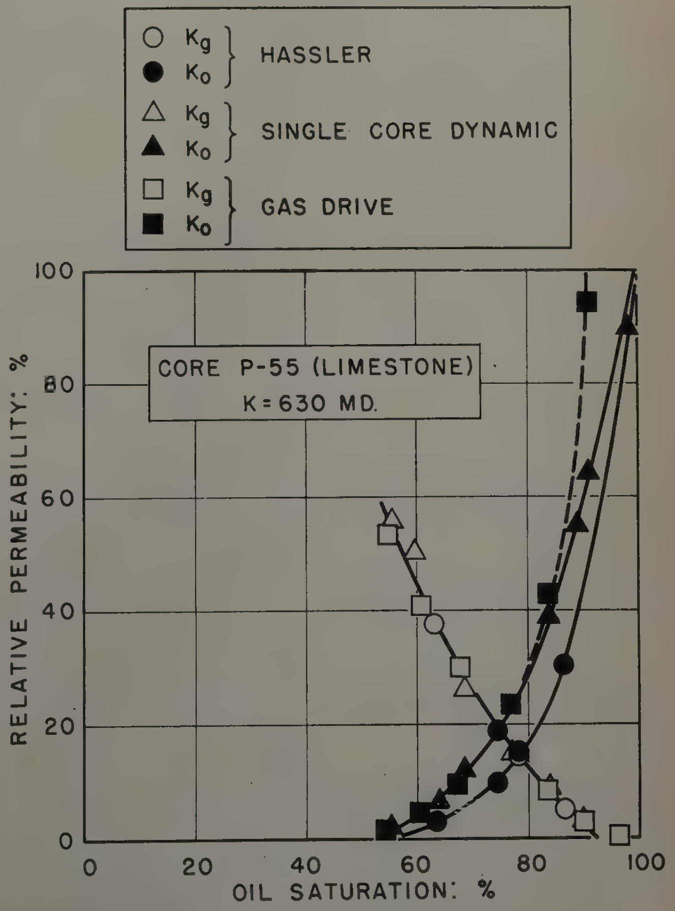

FIG. 13 — RELATIVE PERMEABILITY — THREE METHODS.

that each tap measures the true pressure over the cross section of the core, unappreciably affected by any non-parallel flow. The Penn State method could be modified so that a single long core is used, obviating the need for reliance on capillary contact between sections. In each method effort should be made to replace weighing by some improved technique for saturations.

AUTHOR'S REPLY TO V. A. JOSENDAL AND B. B. SANDIFORD

The authors believe that the measurement of saturation by weighing is sufficiently accurate for use in relative permeability determinations at the pressures used. Theoretical calculations using the gas-oil ratio, viscosity, and saturation show that the quantity of oil that may be forced from a core by the expansion of gas is very small. Furthermore, specific experiments were conducted in which a partially saturated core was placed in a chamber under gas pressure and the pressure instantaneously reduced to atmospheric. No oil was forced out of the core due to the expansion of gas within the pore space.

A special plastic having negligible water absorption is substituted for the Lucite mounting material in the experimental techniques in which water is one of the liquids present.

The authors recognize that the relative permeability to oil obtained by the Hassler technique is lower than those obtained by the other methods. These differences have been consistently present in a large number of very accurate comparisons, of which only a few of the representative curves are shown in the paper. No definite conclusions have been reached as to the possibility of different flow or fluid displacement mechanisms.

This paper does not attempt to recommend a specific method for general use, but rather to point out the progress made and the correlations obtained in the various laboratory methods of relative permeability measurement.

★ ★ ★

INTERFACIAL TENSIONS AT RESERVOIR PRESSURES AND TEMPERATURES; APPARATUS AND THE WATER-METHANE SYSTEM

E. W. HOUGH, M. J. RZASA AND **B. B. WOOD,** STANOLIND OIL AND GAS CO., TULSA, OKLA., MEMBERS AIME

ABSTRACT

An apparatus for the determination of fluid-fluid interfacial tension by the pendant drop method has been constructed. The apparatus is refined beyond those previously described in that the samples are introduced into an evacuated windowed cell without contacting air or mercury.

Interfacial tension data are reported for the water-methane system between 74 and 280°F and 15 and 15,000 psi.

The variation of wettability of the stainless-steel dropper tip with pressure and temperature was observed incidentally to the measurements.

INTRODUCTION

The most refined previous apparatus for the determination of fluid-fluid interfacial tension at reservoir conditions was built by Hauser and Michaels.[1] These authors used the pendant drop method, previously investigated by Andreas, Hauser, and Tucker.[2] Recently, Fordham[3] has made the pendant drop method an absolute one by numerical integration of the differential equation of drop shape. It is necessary to know the difference in density of the two fluids and the acceleration due to gravity in order to evaluate the interfacial tension from measurements of drop dimensions. Contact angle is not involved in the measurements by this method.

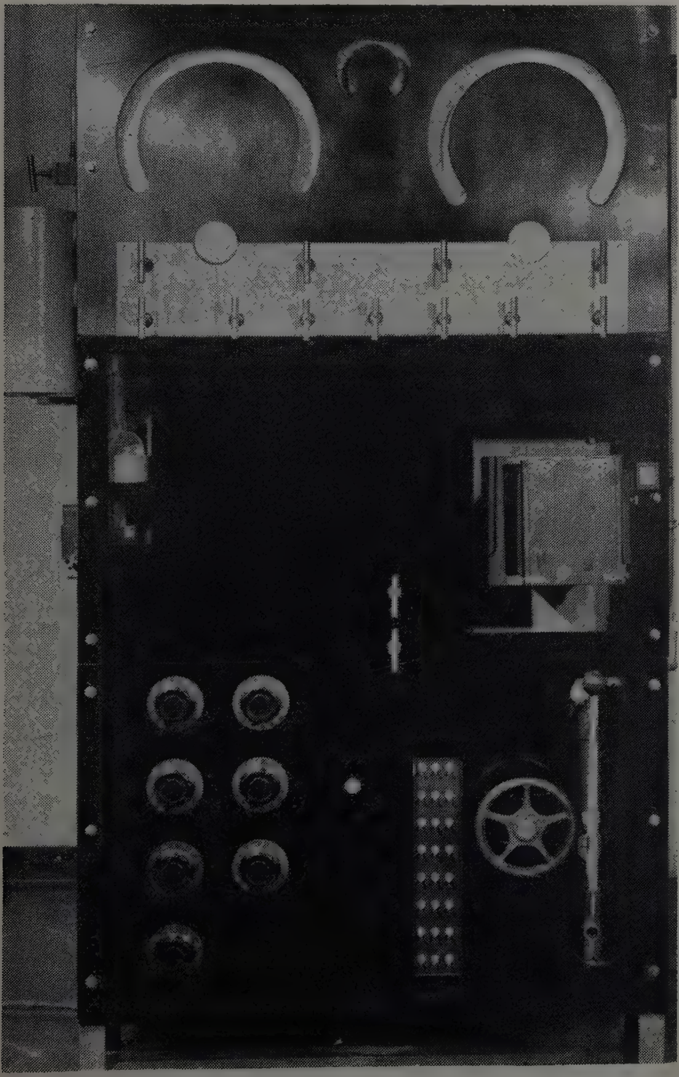

FIG. 1 — FRONT VIEW OF APPARATUS.

Some precise tests of the method have been made at atmospheric pressure and 77°F by Douglas,[4] who found agreement with established values to within about 0.1 per cent for water and air, cyclohexane and air, benzene and air, and benzene and water. No values of interfacial tension from the recent pendant drop apparatus[1] have been published by Hauser and Michaels. However, values for the water-benzene and water-decane systems are given in Michaels' thesis[5] for pressures from 15 to 10,000 psi and temperatures from 73 to 268°F. Some determinations on gas-oil and gas-water systems in the range of 15 to 4,000 psi and 78 to 178°F have been made by Hocott,[6] by the drop-volume method. The capillary rise method has been used to investigate the interfacial tension in gas-oil systems at 88°F to several thousand psi by Swartz.[7] Other determinations in gas-oil systems at pressures under 1,000 psia have been made by Jones,[8] and Beecher and Parkhurst.[9] The scarcity of data for pressures above 5,000 psi is apparent.

APPARATUS

An assembly drawing of the working section of the interfacial tension apparatus is given in Fig. 2. The pendant drop (A) is housed in a pressure chamber having glass windows (B). An agitator (C) is provided. The metal parts of the apparatus coming into contact with the sample are made of AISI Type 316 steel. Drain grooves are provided around the windows so that the sample in contact with the O-rings is not returned to the working section when the pressure is reduced.

A schematic arrangement of the apparatus is given in Fig. 3. The working section containing the pendant drop (A) is filled by samples from bombs (B) with the aid of the vacuum system (C). The O-ring sealed pistons (D) used to separate the sample from the hydraulic fluid are shown together with the pressure production and measurement system (E).

A front view of the apparatus is shown in Fig. 1. Most of the hydraulic system is at the top of the panel. The pump and displacement piston are at the lower right. The Variacs for the air bath heaters, the camera, and the vacuum gauge are also visible on the panel. The working section together with a window closure and a drop-forming tip closure are shown in Fig. 9. The carbon arc light source with filter is visible in the upper part of the picture. Two sides of the air bath with the impeller and a part of the convection shield can also be seen. The assembled air bath is shown in Fig. 10.

---

[1] References given at end of paper

Manuscript received in the office of the Petroleum Branch September 14, 1950. Paper presented at the Petroleum Branch Fall Meeting in New Orleans, La., Oct. 4-6, 1950.

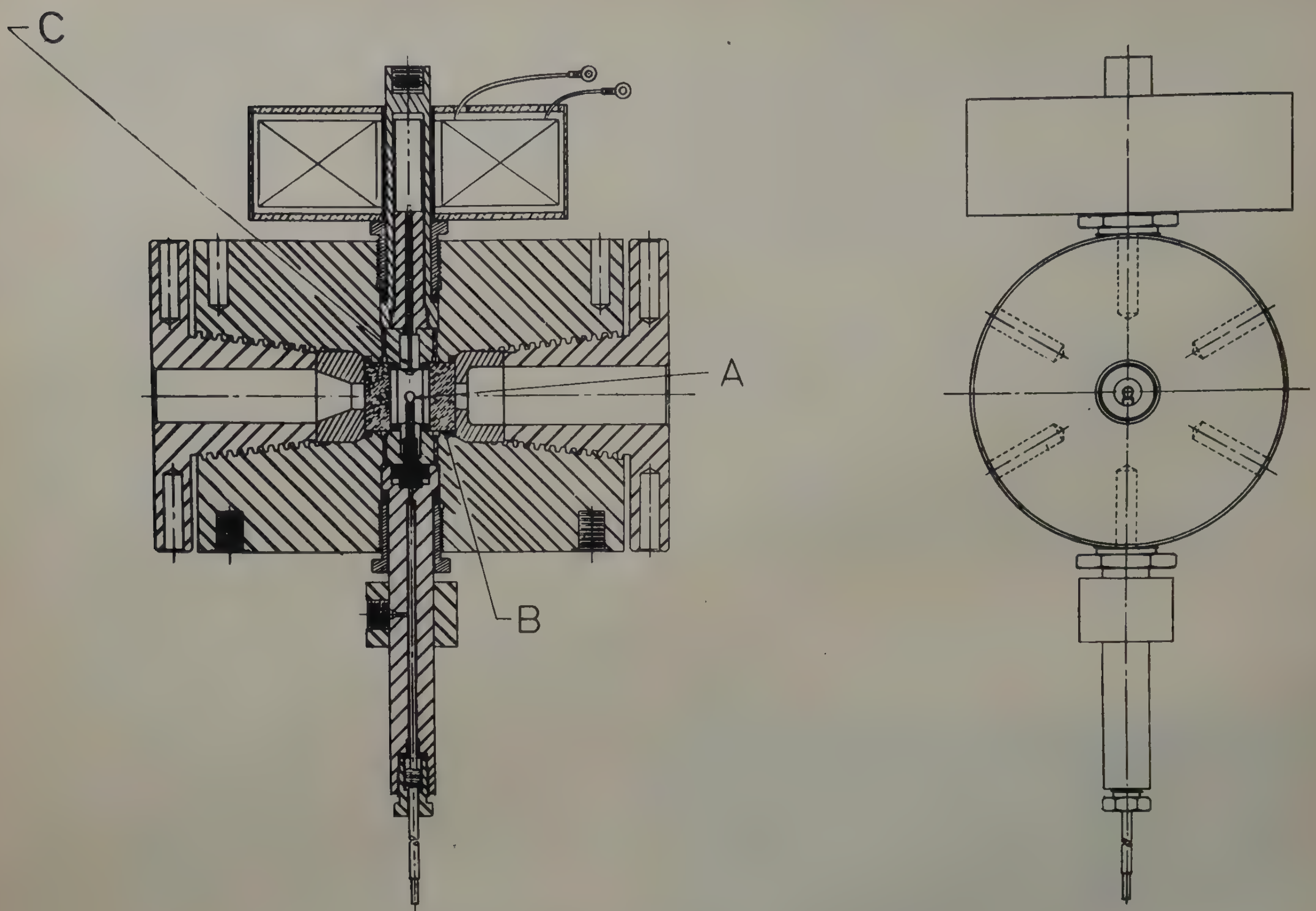

FIG. 2 — WORKING SECTION OF INTERFACIAL TENSION APPARATUS.

A part of the camera is visible in the foreground. The parts for a cylinder containing an O-ring sealed piston are on top of the air bath. The valves for the sample-introduction system are at the top of the picture.

MATERIALS

Distilled water having a resistivity of about 0.3 x 10^6 ohm cm was used. Pure grade methane obtained from the Phillips Petroleum Co. was used without further purification. This material contains 0.995 mole fraction methane. Cleaning solution was employed in the final cleaning of all parts of the apparatus which would, at any time, come into contact with the samples.

EXPERIMENTAL RESULTS

Water-Methane Interfacial Tensions

The results of the interfacial tension measurements for the water-methane system are given in Figs. 4 and 5 and in Table I. These results were obtained for 15-second-old drops, having diameters of about 0.08 in., formed on a tip having a diameter of 0.0472 in. For pressures below about 5,000 psia, or temperatures below about 160°F, the reproducibility of a given measurement is less than 1 dyne/cm. Under these conditions, the effects of pressure hysteresis, which are shown but not explained in Fig. 4 and Fig. 5, were as much as several times this value. The reproducibility at the highest temperature (280°F) and pressure (15,000 psia) encountered is estimated to be 2 dynes/cm., and the effect of pressure hysteresis is probably several times this value. No attempt has been made to explain the general shape of the isotherms or isobars because of the scarcity of thermodynamic data for the water-methane system.

The variation of interfacial tension with drop age at the lowest and highest pressures on the 100° and 280°F isotherms is portrayed in Fig. 6. In general, a maximum value is present for times under about two minutes. Density data for water and methane were taken from the literature.[10,11,12]

Wettability Changes

An interesting variation of the wettability of stainless steel samples with pressure and temperature was noticed incidentally to the determinations of interfacial tension. For example at 215.4°F and 1,005 psi, one AISI Type 316 steel dropper tip was wetted preferentially by the water in the drop as can be seen from Fig. 7A. When the pressure was increased to

Table I — Smoothed Values of Interfacial Tension in the Water-Methane System

Temp (°F)	74	100	160	220	280
Press (psia)	Interfacial Tension (dynes/cm)				
15	75.5	70	63.5	57.3*	52.8*
1,000	67	60	55.5	50.7	46.3
5,000	53.0	23	24.7	24.5	21.3
10,000	48.6	22	26	28	25.5
15,000	46.5	26	30	31	30.5

*Extrapolated value.

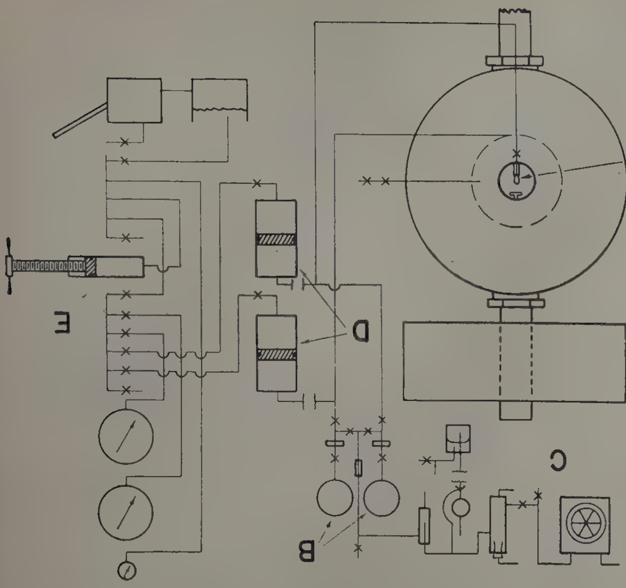

FIG. 3 — SCHEMATIC ARRANGEMENT OF APPARATUS.

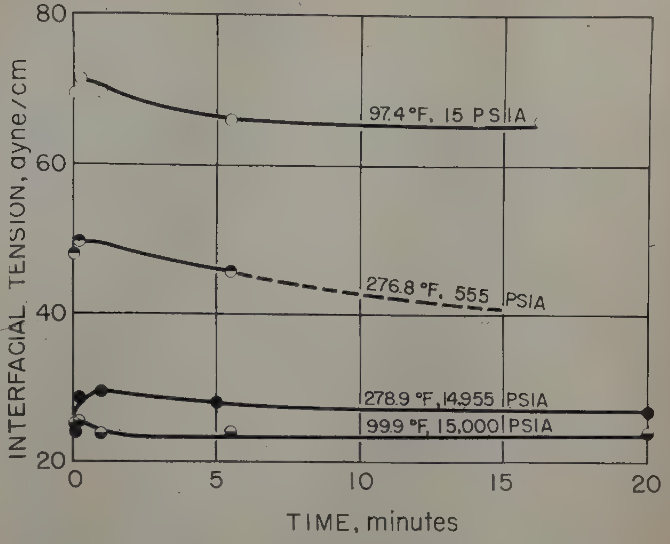

FIG. 6 — VARIATION OF INTERFACIAL TENSION WITH DROP AGE.

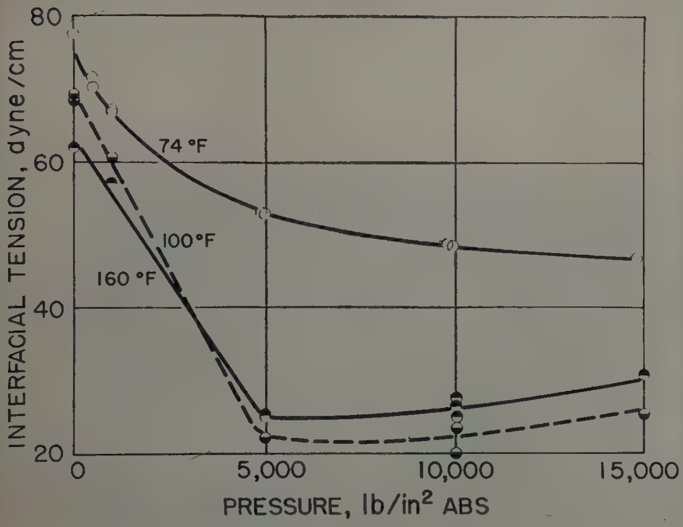

FIG. 4 — INTERFACIAL TENSION IN THE WATER-METHANE SYSTEM.

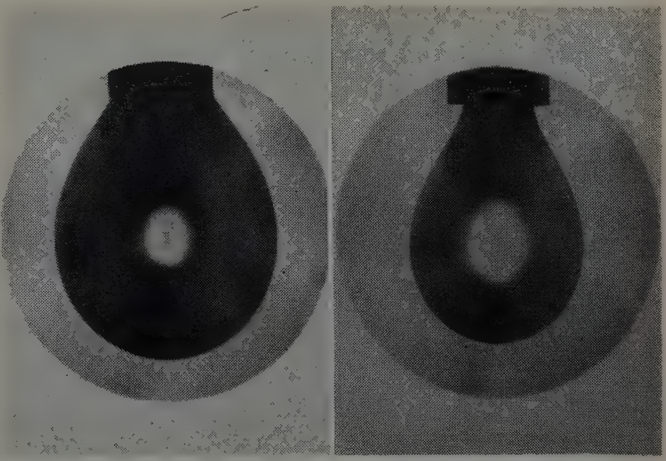

FIG. 7 — CHANGE IN WETTABILITY OF A SAMPLE OF AISI TYPE 316 STEEL.

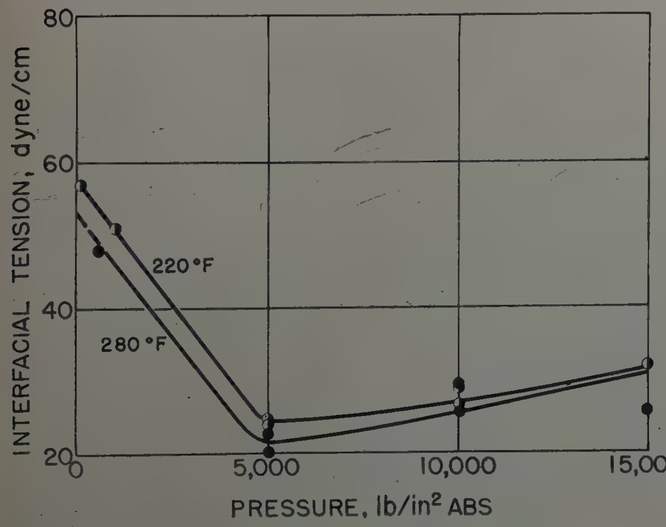

FIG. 5 — INTERFACIAL TENSION IN THE WATER-METHANE SYSTEM.

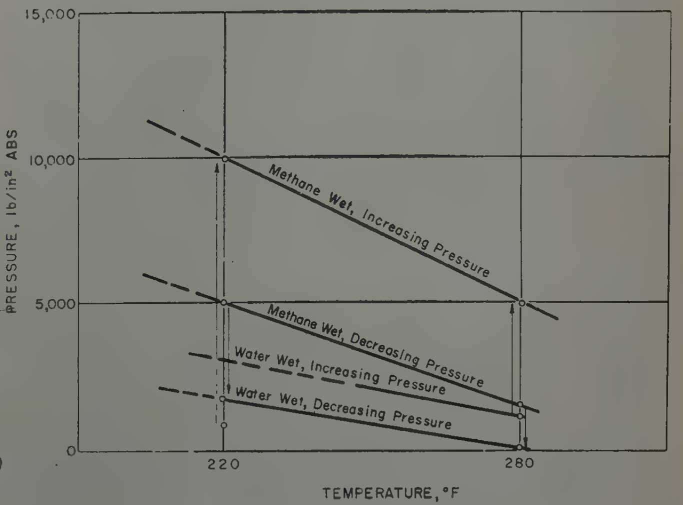

FIG. 8 — WETTABILITY OF A SAMPLE OF AISI TYPE 316 STEEL IN WATER-METHANE SYSTEM.

5,005 psi, and the temperature held nearly constant, this tip was wetted preferentially by methane as can be seen from Fig. 7B. For pressures between 1,005 psi and 5,005 psi, the wettability of the tip was uncertain. When a drop was placed on the tip between these pressures, it might wet part of the tip, or all of it or none of it. The pressures for the variation of wettability appear to be higher for a second sample of the same type of steel. For the second sample, boundaries of 2,000 psi for water-wet behavior and 10,000 psi for methane-wet behavior were established at 220°F, for increasing pressure.

Furthermore, hysteresis appears to be present. For the second sample, for decreasing pressure, the limits were about 5,000 and 2,000 psi, for methane-wet and water-wet behaviors, respectively. The behavior of the second sample is depicted in Fig. 8 at two temperatures. The authors suggest that the behavior of reservoir rock under these conditions might be worthy of investigation.

CONCLUSIONS

An apparatus has been built for the determination of interfacial tensions at reservoir pressures and temperatures and used for the methane-water system. The data show changes in interfacial tension in the 15 to 15,000 psi pressure range from 70 to 22 dynes/cm at 100°F and from 53 to 21 dynes/cm at 280°F. Data on the variation of wettability of stainless steel samples in water and methane have been obtained as a function of pressure and temperature. One sample was water-wet at 2,000 psi and methane-wet when the pressure was increased to 10,000 psi at 220°F. These limits were about 1,000 psi and 5,000 psi at 280°F.

ACKNOWLEDGMENT

The authors wish to express their appreciation to the Stanolind Oil and Gas Co. for permission to prepare and publish this paper.

REFERENCES

1. Hauser, E. A., and Michaels, A. S., *Jour Phys. and Coll. Chem.*, (1948) **52,** 1157-1165.
2. Andreas, J. M., Hauser, E. A., and Tucker, W. B., *Jour. Phys. Chem.*, (1938) **42,** 1001-1019.
3. Fordham, S., *Proc. Roy. Soc.*, (1948) **A194,** 1-16.
4. Douglas, H. W., *Jour. of Sci. Inst.*, (1950) **27,** 67-69.
5. Michaels, A. S., "The Measurement of Interfacial Tension at Elevated Pressure and Temperature," Ph.D. Thesis, Mass. Inst. of Tech., May, 1948.
6. Hocott, C. R., *Trans.* AIME, (1939) **132,** 184-190.
7. Swartz, C. A., *Physics*, (1931) **1,** 245-253.
8. Jones, D. T., *Trans.* AIME, (1936) **118,** 81-88.
9. Beecher, C. E., and Parkhurst, I. P., *Petroleum Development and Technology in 1926,* The Maple Press Co., York, Pa., (1927) 51-69.
10. Olds, R. H., Reamer, H. H., Sage, B. H., and Lacey, W. N., *Ind. Eng. Chem.*, (1943) **35,** 922-924.
11. Kvalnes, H. M., and Gaddy, V. L., *Jour. Amer. Chem. Soc.*, (1931) **53,** 394-399.
12. Dorsey, N. E., *Properties of Ordinary Water Substance,* Reinhold Pub. Corp., NYC (1940) 207-225.

★ ★ ★

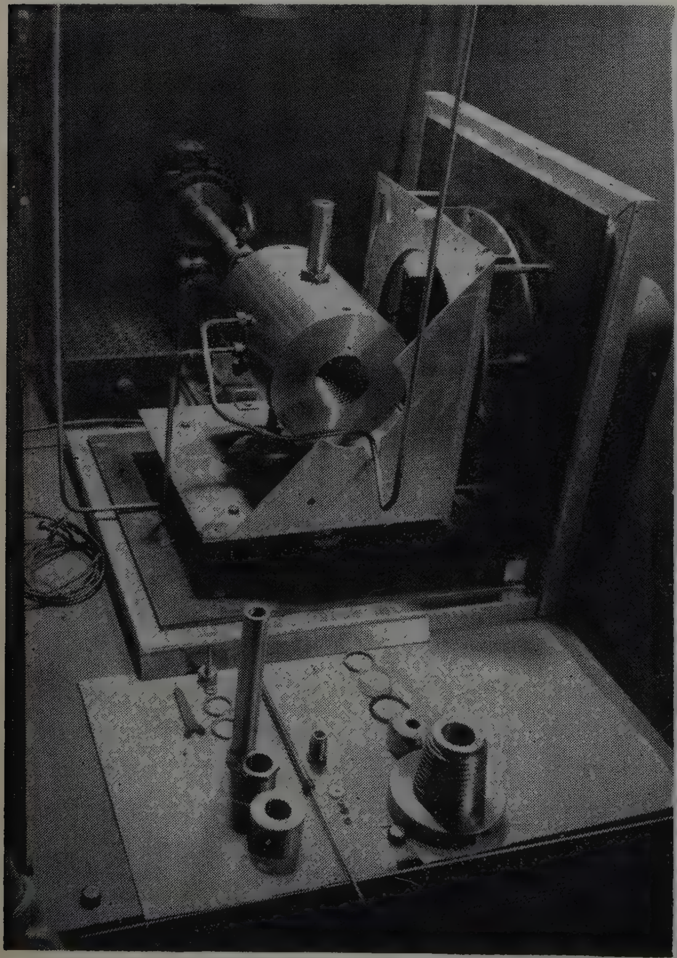

FIG. 9 — WORKING SECTION.

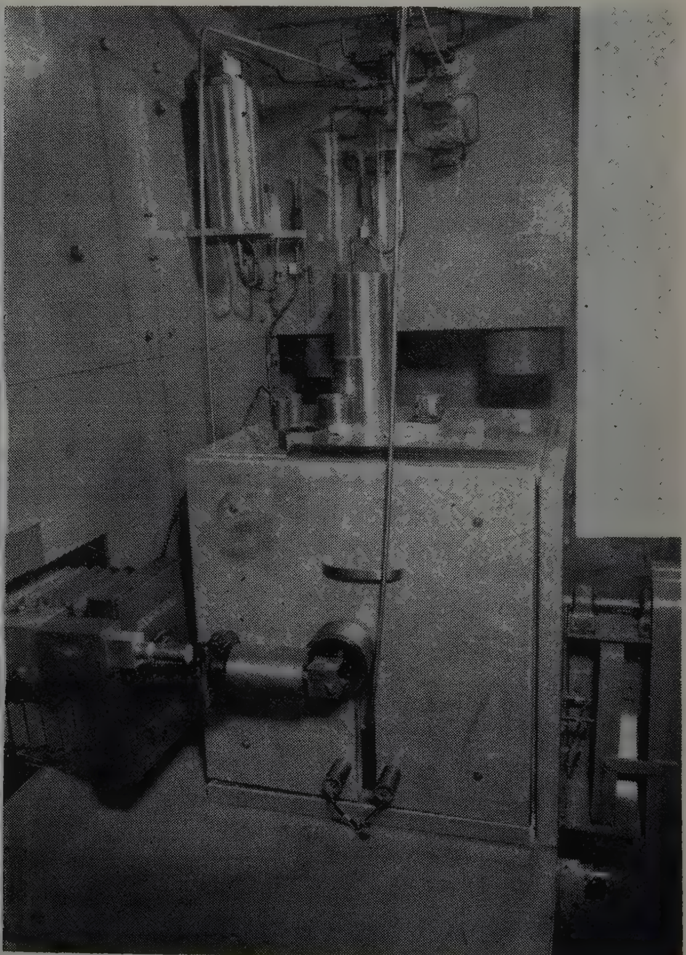

FIG. 10 — AIR BATH.

T.P. 3022

LOW TEMPERATURE DEHYDRATION OF NATURAL GAS

LOUIS R. RECORDS AND **DWIGHT H. SEELY, JR.,** JUNIOR MEMBER AIME, SOHIO PETROLEUM CO.,
OKLAHOMA CITY, OKLA.

ABSTRACT

A process for low-temperature dehydration of natural gas utilizing Joule-Thomson effect in expansion through a throttling orifice has been tested in a full-scale field installation. The results of these tests are presented in the form of performance curves from which the process may be easily evaluated.

The effect of separation temperature on condensate recovery from the process is also shown.

INTRODUCTION

The transportation of natural gas from producing well to the consumer has always encountered the problem of hydrate prevention. This problem has become increasingly important in the past ten years due to the rapid increase in produced gas volumes, production pressures, transportation pressures and distance from producing wells to consumer.

Natural gas, as normally produced from gas or gas-condensate wells, is saturated with water vapor at well-head conditions of temperature and pressure. The solution of the hydrate problem requires but one basic process — dehydration of the gas to a water content which will result in a water dew-point below the minimum temperature to be encountered from the producing well to the point of consumption.

Much of the recent development of gas and gas-condensate reserves in the Gulf Coast Area has been in locations which are accessible only by water. High well-head pressures, pipeline construction and maintenance costs and the desirability of final central gas-condensate separation facilities have stimulated the development of dehydration equipment which can be installed at each well and which will permit hydrate-free transportation of both gas and condensate in the same line to central facilities.

There are four types of natural gas dehydration processes now used:

1. Adsorptive processes.
2. Absorptive processes.
3. Chemical reaction processes.
4. Refrigeration processes.

The first three of these processes are indirect in that they require use of adsorbents, absorbents or reactive chemicals. These materials require regeneration and part of the total gas stream is consumed in the regenerative process. Indirect processes have a wide range of flexibility as defined by allowable operating pressure and temperature, but most are not easily adapted to automatic operation.

The refrigeration process described in this paper was designed for installation at the producing well-head. It requires no regenerative cycle and with normal well-head temperatures no external source of heat. The flexibility of this process is limited only by the pressure drop which may be allowed between well-head and transportation line.

THEORY

There are three basic physical concepts involved in the low temperature dehydration process. These are:

1. Formation of hydrocarbon hydrates.
2. Joule-Thompson effect resulting from the expansion of gaseous mixtures through a throttling orifice.
3. The equilibrium composition characteristics of water vapor and gaseous hydrocarbon mixtures.

The chemical composition and physical structure of hydrates have been described by several investigators.[3,4,8,10] Specific conditions of temperature, pressure and composition as well as the requirements for turbulence and presence of free water necessary for hydrate formation have been described by Katz.[6] Natural gas hydrates, as they are found in plugged gas pipe lines, have the appearance of packed snow. The mass of these hydrates has low continuous porosity and permeability.

Joule-Thomson effect, or the reduction in temperature which occurs when natural gas is throttled through a restrictive orifice, is the basic phenomenon which permits efficient use of refrigeration for the purpose of dehydrating natural gas. Joule-Thomson coefficients for gaseous mixtures of methane with ethane and with butane have been reported by Budenholzer, Sage and Lacey.[2] Brown[1] predicted temperature drops for pressure drops from enthalpy-entropy calculations. Aside from this work there were no fundamental data found which would be applicable to natural gas mixtures of varying spe-

---

[1] References given at end of paper.

Manuscript received in the office of the Petroleum Branch August 9, 1950. Paper presented at the Annual Fall Meeting of the Petroleum Branch in New Orleans, La., Oct. 4-6, 1950.

cific gravity. It was by assumption that the expansion of gas in equipment to be used in this process would be isenthalpic that the successful operation on the process was calculated.

The water vapor content of natural gas at saturation has been determined by several investigators.[5,7,9,11] All of these investigators show that the concentration of water in the vapor phase is reduced as a direct function of temperature and as an inverse function of pressure.

The low temperature dehydration process effects a degree of dehydration by:

1. Reducing the temperature of a water-saturated gaseous mixture by expansion through a restrictive orifice.
2. Reducing the equilibrium water content of the gaseous mixture as a direct function of temperature.
3. Forming and separating hydrate particles from the gaseous mixture by gravity difference.

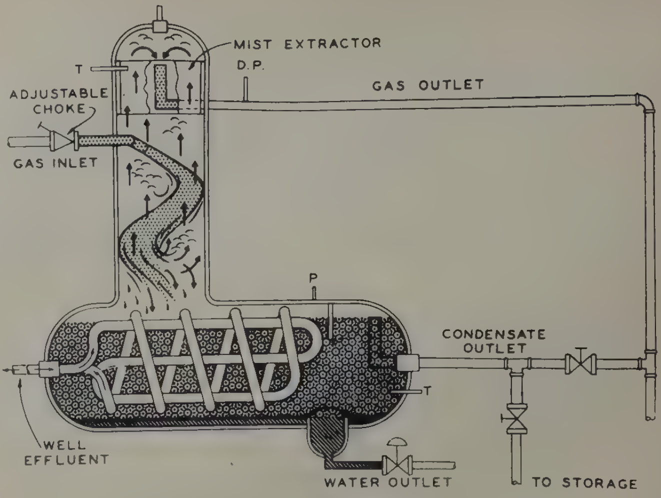

FIG. 1 — HYDRATE SEPARATOR.

TEST EQUIPMENT

The only equipment used in this test which was not of standard oil field type was the hydrate separator. This separator, shown in Fig. 1, was constructed with a vertical section 16 in. in diameter and 60 in. high, and a horizontal section 24 in. in diameter and 60 in. long. Gas entered this vessel after passing through an adjustable choke where the pressure was reduced throughout the test range. The temperature drop accompanying this pressure drop resulted in the condensation of a portion of the hydrocarbons and water vapor present and in the formation of hydrocarbon hydrates. The tangential flow of the entering mixture aided the separation of the hydrocarbon gases from the liquid hydrocarbons and hydrate particles.

The hydrocarbon gases passed upward through a mist extractor and into the gas outlet line. The liquid hydrocarbons and hydrate particles fell to the horizontal section where sufficient heat was added from the well effluent stream passing through a tube bundle to melt the hydrate particles. The condensed hydrocarbons and water from the hydrates were separated by gravity difference and withdrawn through separate outlets. The hydrocarbon liquids were either recombined with the dehydrated gas or run to storage and the water was removed to disposal.

Provision was made for temperature, pressure and dew-point measurement as shown in Fig. 2. Temperatures were measured by ASTM grade bulb-type thermometers, pressures were measured by bourdon-type gauges and dew-points by the Bureau of Mines Dew-Point Tester.

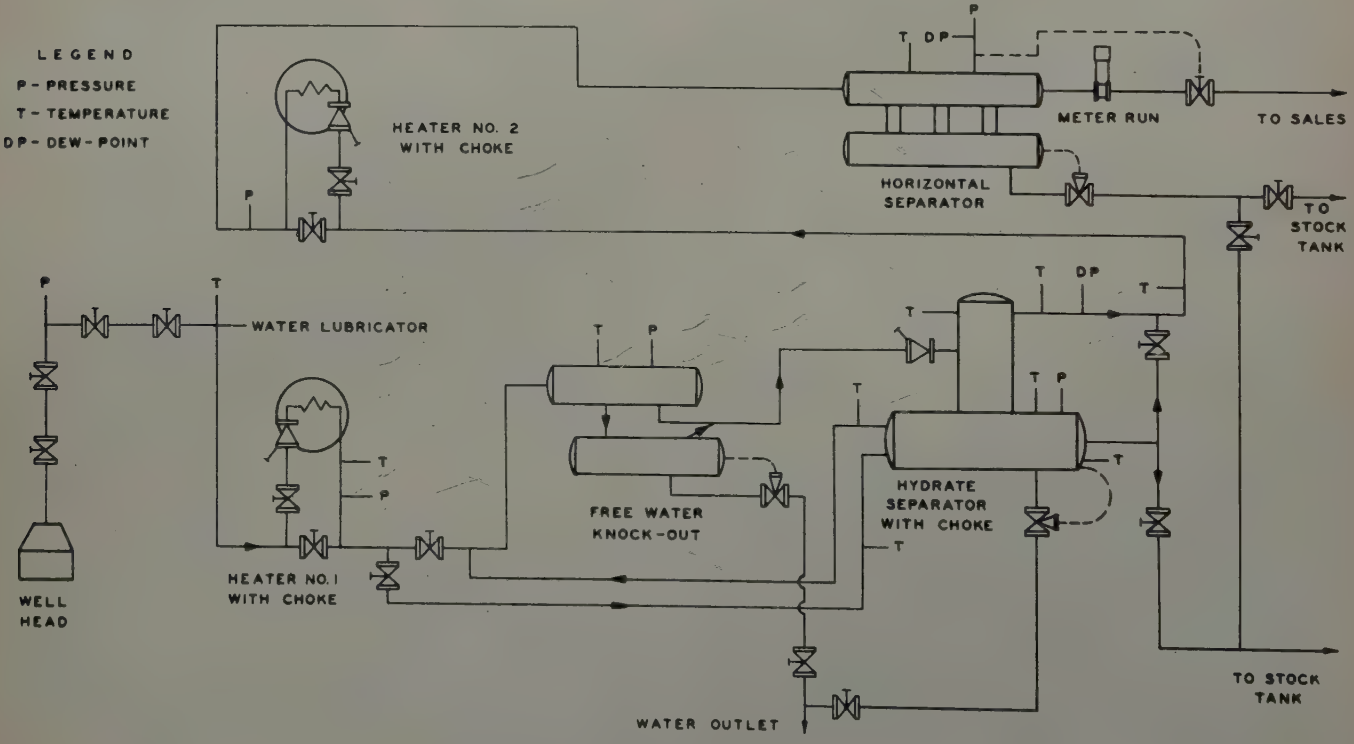

FIG. 2 — FLOW DIAGRAM — LOW TEMPERATURE DEHYDRATION UNIT.

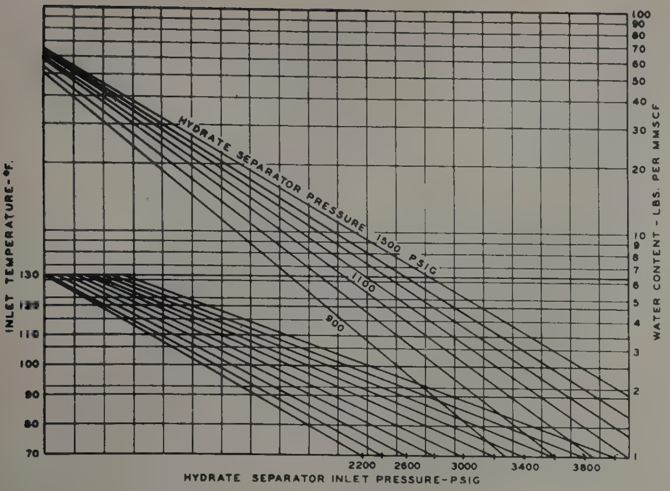

FIG. 3 — LOW TEMPERATURE DEHYDRATOR PERFORMANCE CURVES (BASED ON 0.64 SP GR GAS).

A schematic diagram of all equipment used in the test is shown in Fig. 2. This equipment was installed in such a manner that conditions of water content of the well effluent, producing well-head temperature and pressure, hydrate separator pressure, transportation line pressure drop and temperature could be simulated throughout a reasonable operating range.

The choke installed in Heater No. 1 was used to control the flowing well-head pressure. Heater No. 1 was used to control flowing temperature. The free water knock-out was used to remove excessive volumes of free water from the system.

The function of the hydrate separator has been described above.

Heater No. 2 and the choke at this heater were used to control simulated conditions of transportation line temperature and pressure drop.

The horizontal separator was used to separate the condensed hydrocarbons and gas which were recombined after discharge from the hydrate separator.

Hydrocarbon liquids were measured in a calibrated 25-bbl tank which had inlet connections at both top and bottom. The bottom inlet was flush with the inside of the tank shell. The top inlet was through a short nipple and 90° ell so that the condensate was diverted down and fell on the surface of the stock-tank liquid.

TEST PROCEDURE

Prior to each test run the well was opened to flow at a rate of approximately 10 MMcf/D to remove any volume of fluid which might have collected in the well bore. After the well had flowed for sufficient time to unload the fluid head, flow was reduced to the test rate of 1½ MMcf/D.

If the flowing temperature for a particular test was to be greater than that encountered from normal operation of the well, the well effluent was produced through Heater No. 1. To eliminate the possibility of undersaturation of the well effluent when heat input at Heater No. 1 was high, duplicate runs were made while injecting fresh water into the producing line. The water was injected at a constant rate and in sufficient volume to insure water-saturated vapor and liquid phases at the highest temperature in the system. None of these duplicate runs indicated discrepancy from previous data.

If the test pressure for a particular test was to be lower than that obtainable from normal well production, the choke upstream from Heater No. 1 was adjusted to provide the desired test pressure throughout the remainder of the system.

Flow rate was controlled by combined regulation of the choke at Heater No. 1, the choke at the hydrate separator and the choke at Heater No. 2.

The discharge pressure from the hydrate separator was controlled by dual regulation of the choke at the hydrate separator and at Heater No. 2.

Transportation line pressure drop and temperature were controlled by regulation of the line choke and Heater No. 2.

The pressure at the horizontal separator was controlled by sales line pressure and regulated by a pressure regulator on the discharge line from this separator.

With all conditions of pressures and temperatures regulated as described above, the system was allowed to operate for a period of six to eight hours, during which time temperatures, pressures, dew-point determination and volumes of gas and liquids removed from the system were recorded.

The variable conditions simulated throughout these tests were as follows:

Condition	Minimum	Maximum
Producing well-head pressure	2,200 to	3,750 psig
Flowing well-head temperature	70° to	130°F
Hydrate separator discharge pressure	900 to	1,500 psig
Transportation line pressure drop	0 to	600 psig
Transportation line temperature	40° to	90°F

Dew-point temperatures were converted to water content values from the data of McCarthy, Boyd, and Reid.[7]

RESULTS

The results obtained from these tests are shown in Figs. 3 to 9.

The many independent variables in this process preclude a precise presentation of all results in the form of direct data plots. The transposition and interpolation of observed data required for the construction of the performance curves involves a maximum deviation from observed data of less than 3 per cent with average deviation less than one-half of 1 per cent.

Fig. 3 summarizes the performance of this process throughout the test range. From Fig. 3 the water content of the gas from the hydrate separator can be determined for any condi-

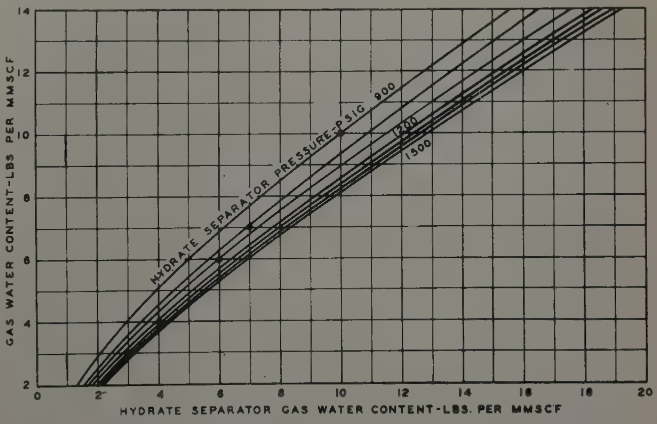

FIG. 4 — WATER CONTENT CHANGE OF DEHYDRATED GAS AFTER RECOMBINING WITH CONDENSATE.

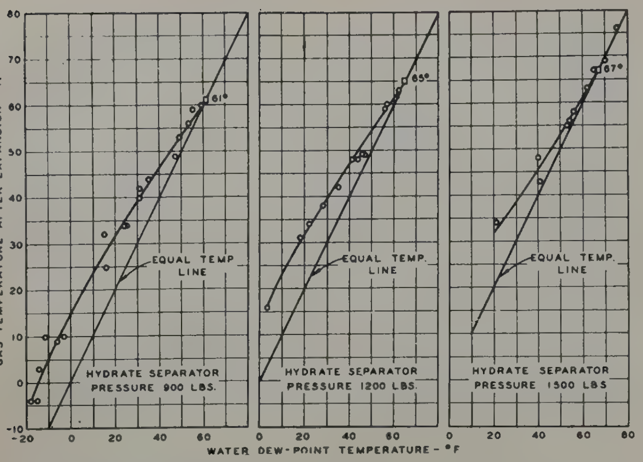

FIG. 5 — WATER DEW-POINT TEMPERATURE VERSUS HYDRATE SEPARATOR TEMPERATURE.

tions of inlet pressure and temperature and hydrate pressure. Use of these curves is described in a later section of this paper.

The change in water content of the dehydrated gas from the hydrate separator after recombination with condensate from this vessel is shown in Fig. 4. These curves are used in conjunction with Fig. 3 when the gas and condensate streams from the hydrate separator are to be recombined and again separated in a conventional gas-condensate separator. These curves show the magnitude of the partial resaturation of the under-saturated gas which exchanges water with a condensate upon recombination. This resaturation is not usually significant at conditions where the water content of the dehydrated gas is low and becomes progressively smaller as the water content increases until reversal takes place and the gas is further dehydrated. The points of reversal are shown for the various pressures by points on each pressure line in Fig. 4. Since resaturation is essentially a function of water solubility in the liquid phase and water vapor equilibrium in the vapor phase, it is significant that final separation pressure and temperature did not appreciably effect water content change.

A plot of the minimum gas temperature (temperature after expansion) versus water dew-point temperatures of the gas from the hydrate separator is shown in Fig. 5. From these curves it is evident that the dehydrating capacity of this process is not limited to the saturated water content at the lowest temperature in the system. Below the hydrate expectancy temperature (shown by the square points on Fig. 5) it was observed that the water dew-point temperature was lower than the lowest temperature observed in the system. It is probable that the lowest temperature in the system was at the vena contracta near the inlet nozzle, however, since the maximum temperature difference between the point of measurement in the hydrate separator and a point approximately 8 ft from this vessel in the gas outlet line was 2°F, it can be assumed that the lowest temperature in the system was not more than two or three degrees lower than that observed in the hydrate separator. Since the phenomenon of temperature/dew-point difference was observed only at temperatures below the hydrate expectancy temperature, or where hydrates were present, it is evidenced that natural gas hydrates have an adsorptive and/or absorptive capacity to remove water from the vapor phase.

Fig. 6 is a plot showing the temperature drop due to pressure drop observed in the hydrate separator. This plot is read by entering with initial pressure-temperature conditions and following the curved guide lines to final conditions of pressure and temperature. These curves show that the temperature drop per pound pressure drop is dependent on initial pressure and temperature.

While the primary purpose of these tests was to determine the dehydration capacity of the low temperature process, the condensate recovery data show that additional stock tank liquids can be recovered with low temperature gas-condensate separation.

The heat added to the condensed liquids in the hydrate separator and the cold area at the gas inlet resulted in a vaporization and refluxing action in this vessel. By this action light hydrocarbons were removed from the condensate and the remaining liquid was stabilized.

Fig. 7 is a plot of stock tank liquid recovered at various separation temperatures. These curves show the retrograde loss when pressures are increased from 900 to 1,500 lb, and the increase in stock tank liquid as separation temperatures are reduced.

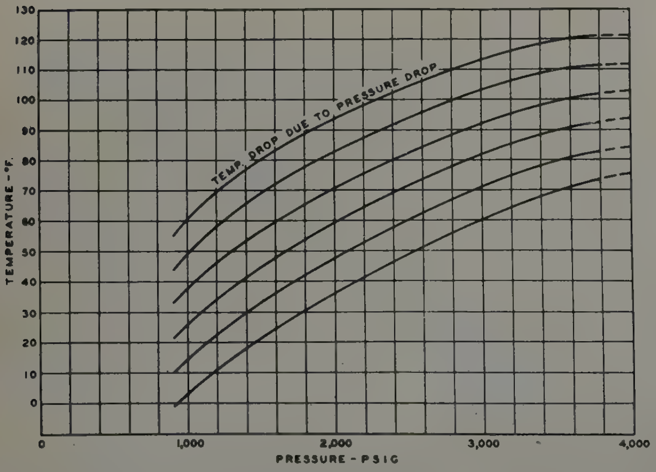

FIG. 6—NATURAL GAS EXPANSION—TEMPERATURE REDUCTION CURVE (BASED ON 0.64 SP GR GAS).

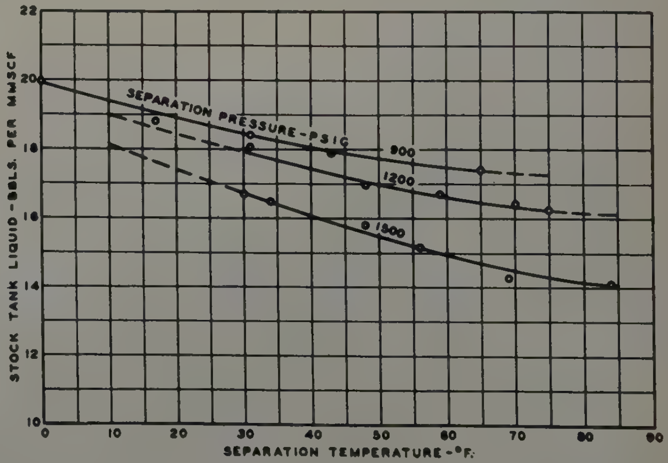

FIG. 7 — STOCK TANK RECOVERY (CONDENSATE INLET AT BOTTOM OF STOCK TANK).

Table I — Analysis of Well Effluent

Component	Mol %
CO_2	0.20
CH_4	92.80
C_2H_6	3.47
C_3H_8	1.16
IC_4H_{10}	0.39
NC_4H_{10}	0.35
IC_5H_{12}	0.14
NC_5H_{12}	0.11
C_6+	1.38
	100.00

Fig. 8 is a cross-plot of Fig. 7 showing stock tank liquid recovery versus separation pressure with parameters of temperature.

In Fig. 9 the effect of stock tank inlet location on stock tank recovery is shown. The fact that recoveries were lower when condensate was produced into the bottom inlet was due to the stripping action of the hydrocarbons vaporized by the pressure reduction between the separator and the stock tank. This action could be reduced by "staging" or incremental pressure reduction between separator and stock tank, with the vapors evolved at each stage removed before final entry into the stock tank.

CONCLUSIONS

Before drawing conclusions from the results presented above, it should be emphasized that one factor, the composition of the well effluent, was constant throughout these tests. An analysis of the hydrocarbons produced at the well-head is shown in Table I.

Based on relative thermodynamic property changes with change in natural gas gravity, the effect on dehydration results of composition difference, as normally experienced in natural gas and gas-condensate reservoirs, should not be great.

Specific conclusions drawn from the results of these tests are:

1. That natural gas can be dehydrated effectively at low temperatures resulting from expansion of the gas through a throttling orifice.
2. That the low temperature dehydration process is direct, continuous and limited only by available pressure drop through the process.
3. That water content change of dehydrated gas at pressures between 900 and 1,500 psig, when combined with water saturated condensate at the same pressure, primarily is a function of initial water content of the dehydrated gas and the pressure at which combination occurs.
4. That volumes of stock tank liquids recovered from low temperature and high pressure separation of gas and condensate are increased if these liquids enter near the top of the storage tank rather than at the bottom.

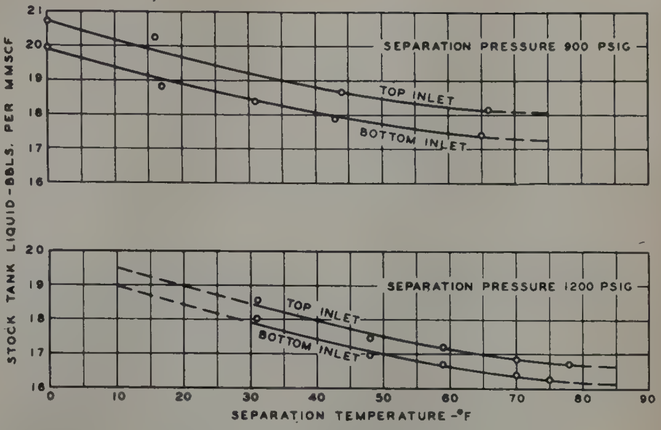

FIG. 9 — EFFECT OF STOCK TANK INLET LOCATION.

Additional Development of the Low Temperature Process

Since the tests described in this paper were completed, two significant changes have been made in the low temperature process. The first of these is the addition of a heat exchanger so that the cold gas from the hydrate separator is used to cool the well effluent before it enters the free water knock-out. This heat exchange extends the operating range of this process by controlling the inlet temperature variable.

The second change in the process has been in the flow of the well effluent into the hydrate separator. By separating gas

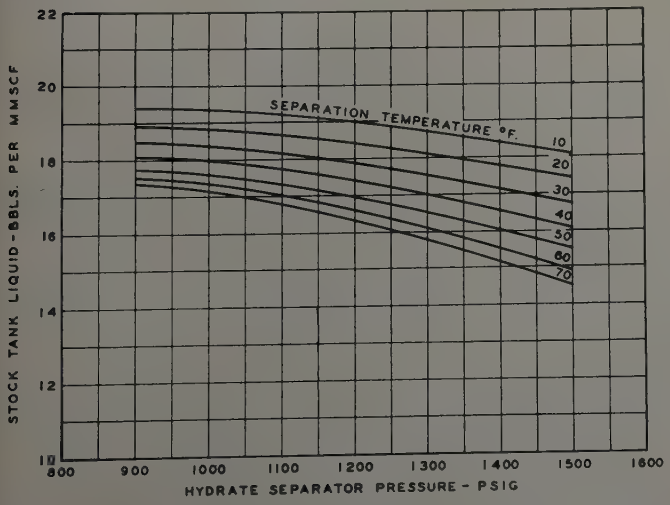

FIG. 8 — STOCK TANK RECOVERY (CONDENSATE INLET AT BOTTOM OF STOCK TANK).

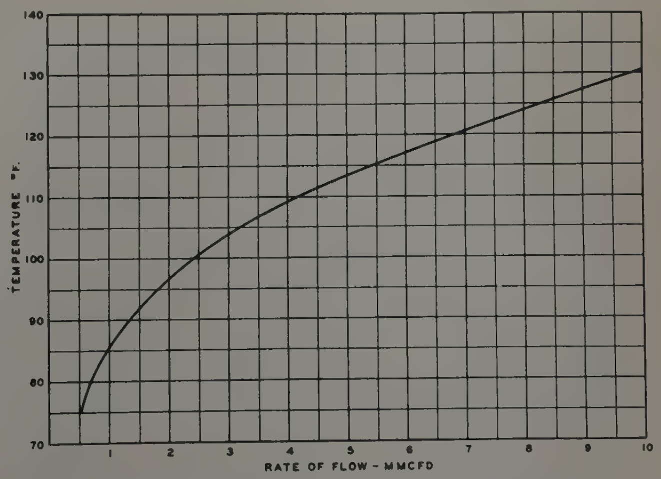

FIG. 10 — APPROXIMATE FLOWING WELLHEAD TEMPERATURES FOR GAS WELLS OF SOUTH LOUISIANA AREA.

from the liquid and expanding each through separate hydrate separator inlets, lower gas temperatures and consequently lower water content in the dehydrated gas is possible.

Use of Performance Curves

Fig. 3 is used to evaluate the performance of the low temperature process as follows:

Enter at the available hydrate separator inlet pressure (available wellhead pressure) on the bottom scale (range: 2,200 to 4,000 psig). Read along the diagonal guide lines to the point of intersection with inlet temperature line (horizontal lines range: 70 to 130°F). From this intersection read vertically to the intersection of the diagonal hydrate separator pressure lines (normally gas delivery line pressure). This last intersection is the water content to be expected and is read from the right-hand logarithmic scale. If the water content determined for a particular installation is above maximum specification, the feasibility of heat exchange between cold dehydrated gas and inlet stream can be investigated by fixing maximum allowable water content and available inlet pressure, then determining the temperature to which the inlet must be reduced.

If the dehydrated gas stream is to be recombined with condensate from the hydrate separator, final water content can be determined by Fig. 3 and Fig. 4. Water content of the gas from the hydrate separator is determined from Fig. 3, and this value is corrected directly by entering Fig. 4 with the hydrate separator gas water content and reading the corrected water content corresponding to the correct hydrate separator pressure.

In the preliminary stages of this work, it was noted that very little flowing well-head temperature data were available. A survey of 35 wells from 12 fields in the Gulf Coast Area was made; Fig. 10 is an average plot of the flowing temperatures measured. This curve is at best an approximation and should be used with the realization that wide deviations are probable, depending on many factors including producing depth, pressure, gas-oil ratio and volume of free water produced.

ACKNOWLEDGMENT

The authors express appreciation for the assistance of C. M. Netherland and J. E. Owens of the Sohio Petroleum Co., who performed the field tests, correlated data and contributed to the opinions presented herein.

REFERENCES

1. Brown, G. G.: *Trans.* AIME, (1945) **160,** 65.
2. Budenholzer, Sage and Lacey: *Ind. Eng. Chem.,* (1939) **31,** 1228, (1940) **32,** 384.
3. Deaton and Frost: *Monograph 8,* U. S. Bureau of Mines, (1946).
4. Hammerschmidt, E. G.: *Ind. Eng. Chem.,* (1934) **26,** 851-855.
5. Hammerschmidt, E. G.: *Chem. Eng. Progress,* (1947) **43,** 361.
6. Katz, D. L.: *Trans.* AIME, (1944) **155.**
7. McCarthy, Boyd and Reid: *Trans.* AIME, (1950) **2,** 241-242.
8. Miller and Strong: *Am. Gas Assoc. Monthly,* (1946) **2,** 63-67.
9. Olds, Sage and Lacey: *Ind. Eng. Chem.,* (1942) **34,** 1223.
10. Roberts, Brownscombe and Howe: *O. and G. J.,* (1940) **39,** 37-40.
11. Skinner: *M. Ch. E. Thesis,* University of Oklahoma, (1948).
12. Wade: *Pet. Engineer,* (1943) **14,** 102.

★ ★ ★

CAPILLARY PRESSURE INVESTIGATIONS

HARRY W. BROWN, HUMBLE OIL AND REFINING CO., HOUSTON, TEX., JUNIOR MEMBER AIME

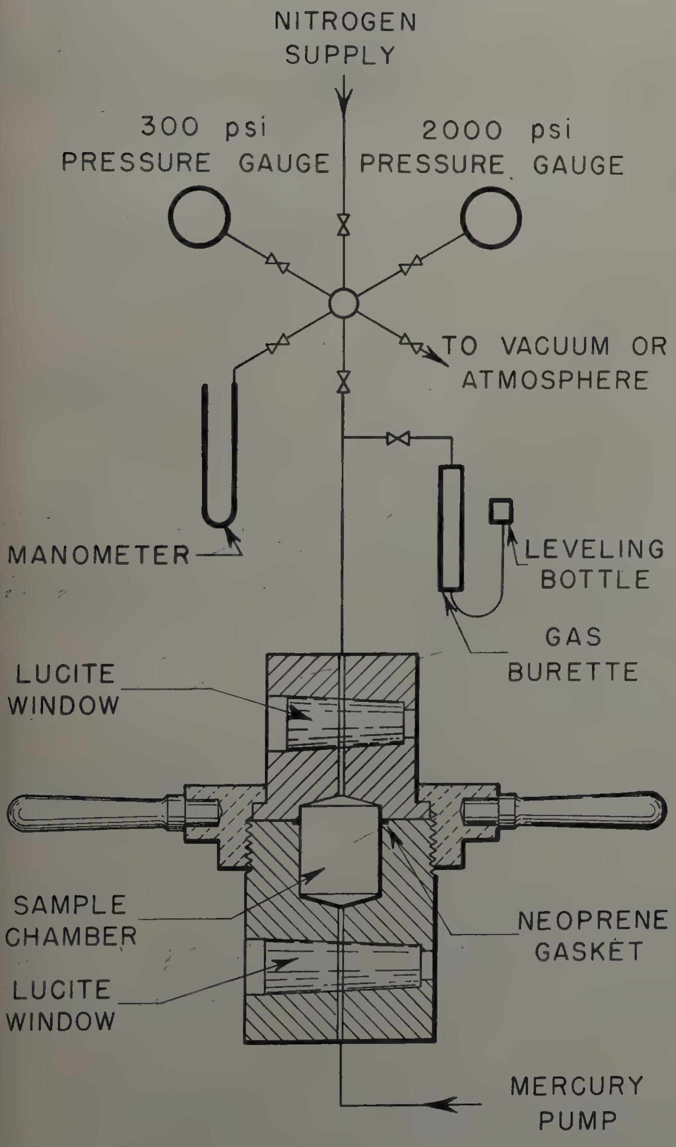

FIG. 1 — CAPILLARY PRESSURE APPARATUS, MERCURY-INJECTION METHOD.

ABSTRACT

This paper presents results of static capillary pressure measurements made both by the restored-state and by the mercury-injection methods, and of dynamic capillary pressure measurements made by the Hassler technique.

The results indicate a variation from sample to sample of the factor used to convert capillary pressure obtained by mercury injection to those applicable to a water-gas system. Static capillary pressures measured by the restored-state method were found to be in close agreement with dynamic capillary pressures, indicating that data obtained from static measurements may be utilized with confidence in the solution of dynamic problems of fluid flow.

Experimental data are presented on the use of "*J*-curves" for the correlation of capillary pressure-saturation relations for a number of cores from a particular geologic formation. It is shown that the correlation was improved in some cases by restricting it to certain lithologic classifications.

INTRODUCTION

The Meaning and Importance of Capillary Pressure

The coexistence of two or more immiscible fluids within the voids of a porous medium, such as reservoir rock, gives rise to capillary forces. Because of the interfacial tension existing at the boundary between two immiscible fluids in a pore space, the interface is curved, and there is a pressure difference across the interface. This pressure difference is termed the capillary pressure.

The magnitude of the capillary pressure between two immiscible fluids which together fill a porous medium depends upon several factors: the textural properties of the medium, the wettability of the medium, the interfacial tension between the fluids, the respective saturations of the fluids, and the manner in which these saturations are attained. For a given pair of immiscible fluids in a particular sample of reservoir rock, the capillary pressure is a unique function of the fluid saturation, provided that the saturation of the fluid which wets the rock has previously been decreased unidirectionally from an initially complete saturation. Similarly, for a given pair of fluids at a particular saturation which has been achieved by a

---

[1] References given at end of paper.

Manuscript received in the office of the Petroleum Branch Aug. 25, 1950. Paper presented at the Petroleum Branch Fall Meeting in New Orleans, La., Oct. 4-6, 1950.

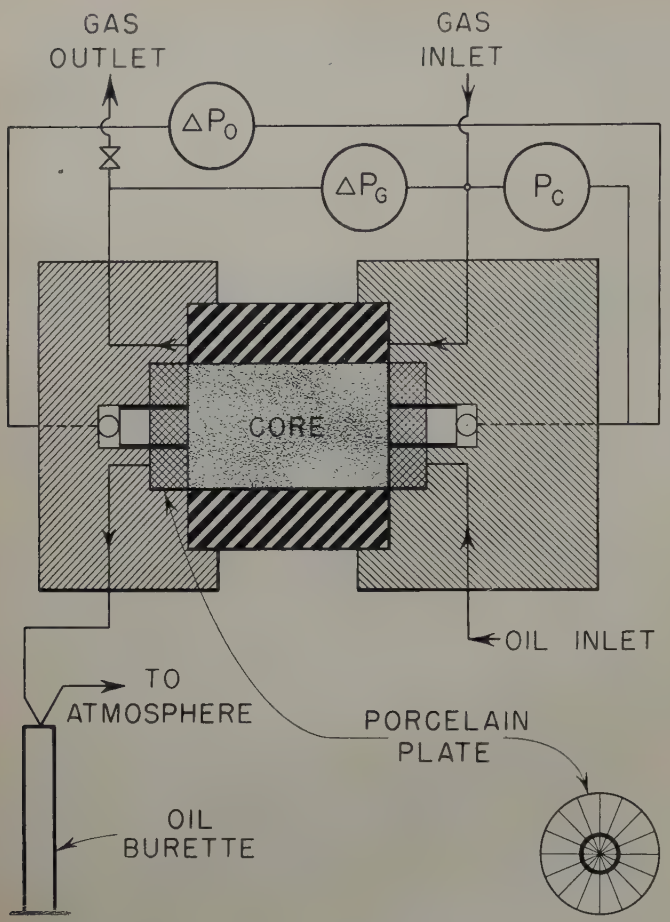

FIG. 2 — DYNAMIC CAPILLARY PRESSURE APPARATUS (HASSLER'S PRINCIPLE).

previous decrease of saturation of the wetting fluid, the capillary pressure depends upon the textural properties and wettability of the reservoir rock.

Although the absolute magnitude of the capillary pressures in most petroleum reservoirs is usually not large, the effects of these capillary pressures are extremely important. Together with gravity they control the original distribution of the fluid saturations within the reservoir, particularly the distribution of connate water. By virtue of their effect on the shapes of the fluid interfaces within the pore spaces, they control in large measure the relative freedom of movement of fluids present in the reservoir, and are important factors in influencing the behavior and distribution of fluids in the production processes.

Previous Investigations on Capillary Pressure

Methods of measuring capillary pressures of fluids in small core samples, and of determining the relation between these capillary pressures and fluid saturations have been given by Leverett[1] and by Bruce and Welge.[2] These authors have proposed the use of the "restored-state" technique, in which the core sample, saturated with a wetting fluid, is placed on a porous diaphragm permeable to the wetting phase. By the application of a known pressure to the non-wetting phase which is confined above the diaphragm, a portion of the wetting phase is expelled from the core sample. By the use of successively higher pressure increments in this procedure a relation between the capillary pressure and fluid saturations may be obtained.

Another technique for determination of capillary pressure has been proposed by Purcell.[3] In this technique, mercury, the non-wetting phase, is injected under pressure into an evacuated core sample. The mercury vapor, together with any residual gas present, corresponds to the wetting phase. The mercury-injection method has the advantage of rapidity of operation, since equilibrium is attained in a short time after the application of each pressure increment. In contrast, equilibrium at each step is attained in the restored-state technique only after a matter of days.

Both the restored-state and mercury-injection techniques are static methods. Dynamic capillary pressures may be determined by a modification of the technique developed by Hassler[4] for measuring relative permeability. In this method both phases are permitted to flow through the core sample, with control being exerted over the pressure difference existing between them. At equilibrium the two phases continue to flow, but their respective saturations do not change.

Leverett[1,5] and Rose and Bruce[6] have pointed out the heterogeneity of reservoir rock and the dependence of capillary pressure on textural properties of the rock. These authors have also proposed a method of correlating the relationship of capillary pressure to saturation with textural properties of rock, in order to extend the applicability of capillary pressure measurements. This method of correlation involves the use of the "*J*-curve," which is discussed in later sections.

PROBLEMS INVESTIGATED IN THIS WORK

Of the numerous problems existing in the measurement and application of capillary pressures, three were investigated during the course of this work.

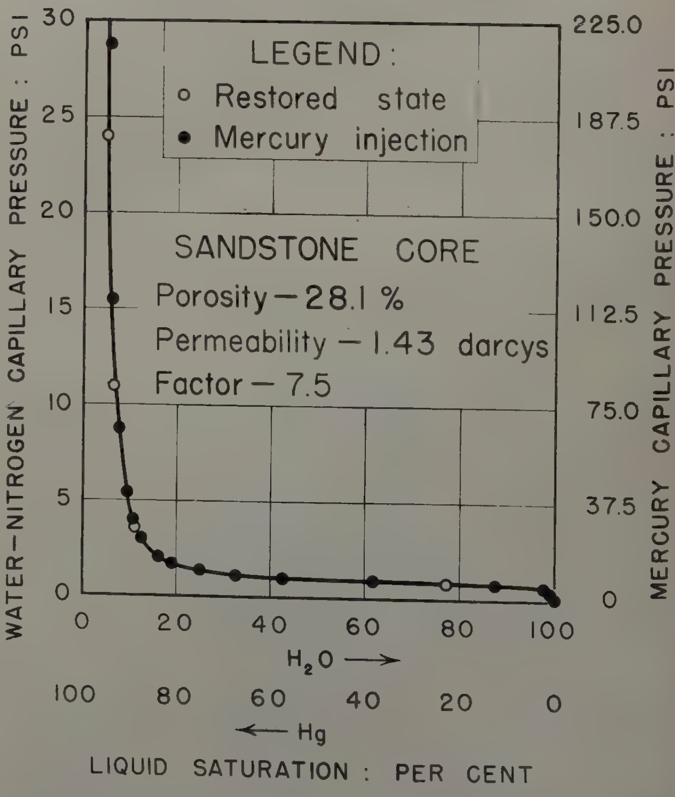

FIG. 3 — CAPILLARY PRESSURES BY RESTORED-STATE AND MERCURY-INJECTION METHODS.

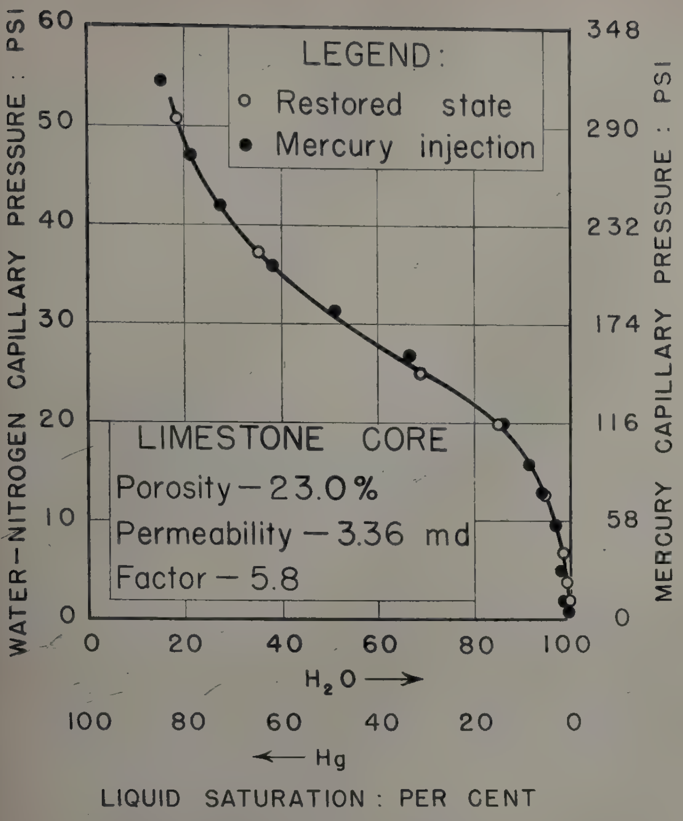

FIG. 4 — CAPILLARY PRESSURES BY RESTORED-STATE AND MERCURY-INJECTION METHODS.

Correlation of Results of Restored-State and Mercury-Injection Methods

Although the restored-state technique is probably the most commonly used method and is generally considered to be the most reliable, the mercury-injection technique has the practical advantage of being much more rapid. Since fluids similar to those encountered in the reservoirs may be used in the restored-state determination, the results are usually more directly applicable to reservoir problems; the results of the mercury-injection method, on the other hand, must be converted by means of a conversion factor to yield those capillary pressures which would be obtained with reservoir fluids. To convert capillary pressures obtained by the mercury-injection method to those obtained by the restored-state technique using water and gas, Purcell[3] has suggested a constant conversion factor which is independent of the character of the reservoir rock.

In view of the complicated character of the material comprising most reservoir rock, and in view of the limited amount of work which has been reported on capillary pressure measurements by the mercury-injection technique, it was deemed advisable to investigate the two methods on a comparative basis. In particular, it was thought pertinent to examine the constancy of the conversion factor for cores from various types of formations.

Comparison of Static and Dynamic Capillary Pressures

Most of the determinations of capillary pressure-saturation relations have been made under static conditions. Although it has been presumed that capillary pressures have an important effect on oil recovery by causing fluid movements to take place when a reservoir is flushed by gas or water, it has not been known whether, when the fluids are in motion, the capillary pressures are the same as when the fluids are at rest. Several papers[1,6,7,8] presented in recent years have proposed methods of applying static capillary pressure data to the solution of dynamic problems of flow. Because of the fundamental nature of the differences between the static and dynamic systems, the validity of such application is subject to some question.

In investigating the various problems connected with capillary pressure determinations, it was particularly desired to compare capillary pressures measured under conditions of static equilibrium with those measured under conditions of dynamic equilibrium during flow.

Correlation of Capillary Properties of Rock with Rock Texture

The method of correlating capillary pressure-saturation relations with permeability, porosity, and wettability of the rock which has been proposed by Leverett[1,5] and by Rose and Bruce[6] requires the use of a dimensionless "capillary pressure-function" group. A plot of this dimensionless group against wetting phase saturation gives the curve generally known as the capillary pressure-function curve or "*J*-curve." It has been suggested that this curve is unique for core samples from a particular geologic formation. If this be true, it is apparent that the *J*-curve, once derived for a particular formation, is of signal importance either in permitting the computation of capillary pressure-saturation relations from known values of permeability and porosity, or in permitting the calculation of the permeability from known values of capillary pressure and porosity. Adequate information on the subject has been lacking, however, and the need for additional data prompted an attempt to confirm the correlation.

EXPERIMENTAL PROCEDURE

Static Capillary Pressure Measurements

Static capillary pressure-liquid saturation relations for core samples were obtained by use of both the restored-state technique and the mercury-injection method. The core samples

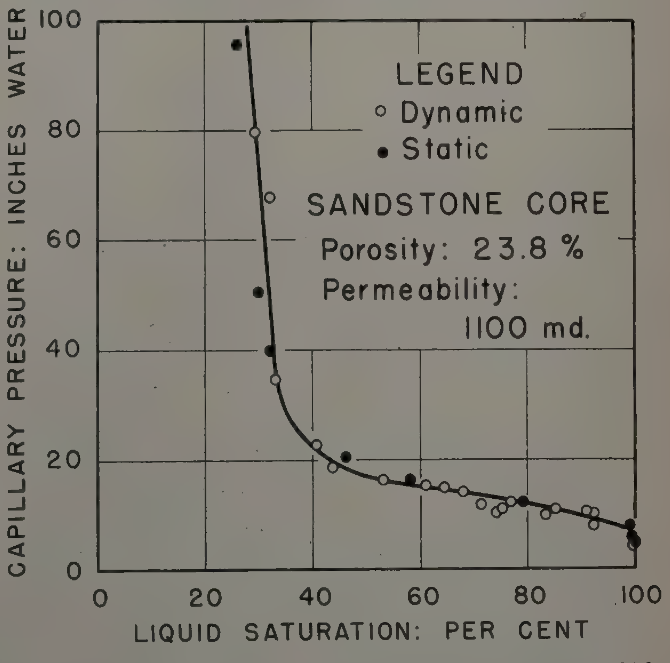

FIG. 5 — CAPILLARY PRESSURES BY STATIC AND DYNAMIC METHODS.

used in these measurements consisted of both limestone and sandstone samples from producing zones.

Restored-State Technique

The displacement cell employed in measurements made by the restored-state technique was of the conventional type, the essential feature of which is the porous porcelain diaphragm. This diaphragm is so chosen that when it is saturated with the fluid to be displaced from the core, it is permeable only to that fluid. When capillary contact is established between the diaphragm and the saturated core, the application of a suitably chosen constant pressure differential across the diaphragm will cause fluid to be displaced from the core, through the diaphragm, to the extent that sufficient fluid remains to satisfy capillary forces. The pressure differential applied across the porous diaphragm is the capillary pressure, because, by definition, capillary pressure is the difference between the pressures of the wetting and non-wetting phases. The quantity of fluid remaining in the core is determined by weighing.

All of the restored-state results presented in this paper were obtained under conditions of decreasing wetting phase saturation.

Mercury-Injection Method

The apparatus used to determine capillary pressure curves by the mercury-injection method was patterned after that described by Purcell[3] and is shown in Fig. 1. The essential components of the apparatus were a mercury displacement pump, a gas burette, a sample holder (shown in detail), and a manifold system wherein the gas pressure could be varied from a high vacuum to the pressure in a commercial nitrogen cylinder.

The gas burette was an addition to the original apparatus, and was added so that the porosity, as well as the capillary pressure curve, could be determined with the same apparatus. Prior to this modification only one of the two quantities needed to determine porosity could be measured with the mercury apparatus, *i.e.*, bulk volume. This made it necessary to determine the solid volume in a separate apparatus. The addition of the gas burette, connected to the chamber of the mercury apparatus, made it possible to determine the solid volume of the sample by the conventional gas-expansion technique. A steel blank of known volume was used to calibrate the system, thus simplifying the calculation of the solid volume of the core sample. This change obviously increases the utility of the apparatus, and should make possible the design of a more compact and portable unit for field use.

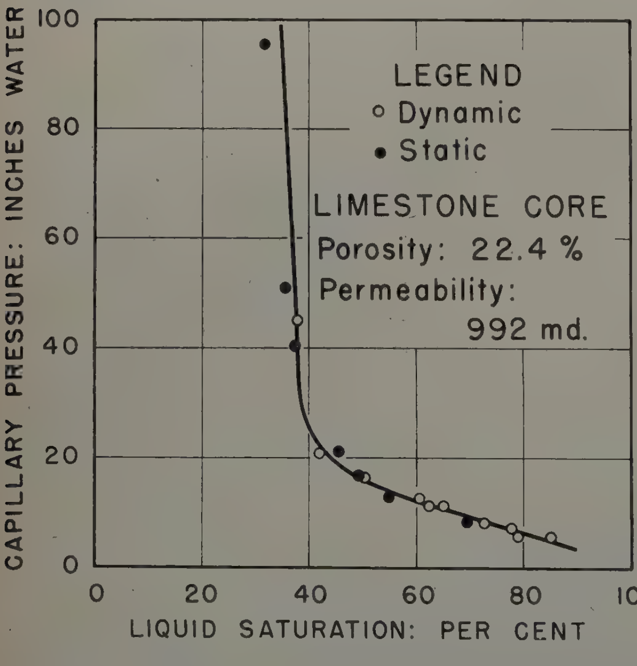

FIG. 6 — CAPILLARY PRESSURES BY STATIC AND DYNAMIC METHODS.

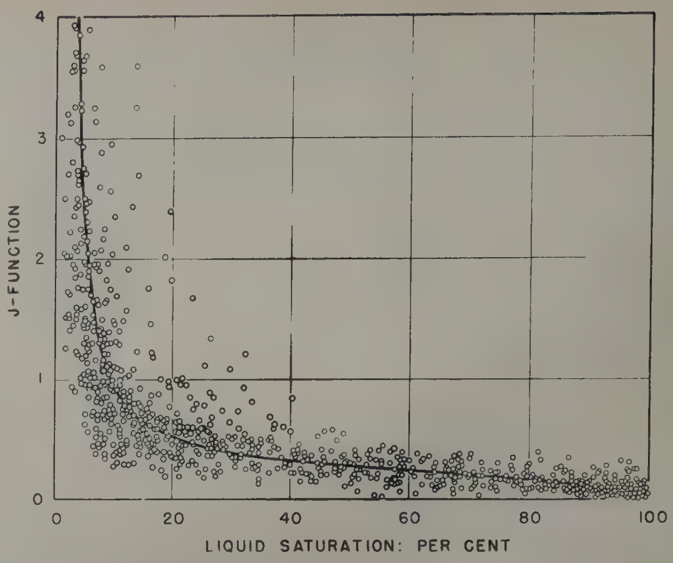

FIG. 7 — J-CURVE FOR ALL CORES, EDWARDS FORMATION, JOURDANTON FIELD.

In operation, the core sample was enclosed in the pressure-tight chamber, the system was pressurized to a predetermined pressure, and the solid volume of the sample was determined by the conventional gas-expansion technique. Next, the system was evacuated, and the volume between two reference marks on the Lucite windows above and below the chamber was determined by introducing mercury into the system with a mercury pump. This volume was subtracted from the known volume of the sample chamber to obtain the bulk volume of the sample. The vacuum pump was then isolated from the system and gas was admitted in increments, thereby increasing the pressure on the mercury surrounding the sample. The penetration of mercury into the pores of the core was indicated by a recession of the mercury-gas interface from the reference mark on the upper Lucite window, and the amount of penetration was determined by advancing the piston of the mercury pump until the mercury meniscus was again at the reference mark. The procedure of alternately building up the pressure and advancing the pump piston was continued until the desired maximum pressure was reached.

DYNAMIC CAPILLARY PRESSURE MEASUREMENTS

During the course of research in fluid mechanics conducted to determine relative permeabilities of reservoir rock to oil and gas, an apparatus designed in principle after that developed by Hassler[4] was constructed which makes it possible to fix directly the capillary pressure between gas and oil, and to maintain that pressure at a fixed and known level while the fluids are flowing.

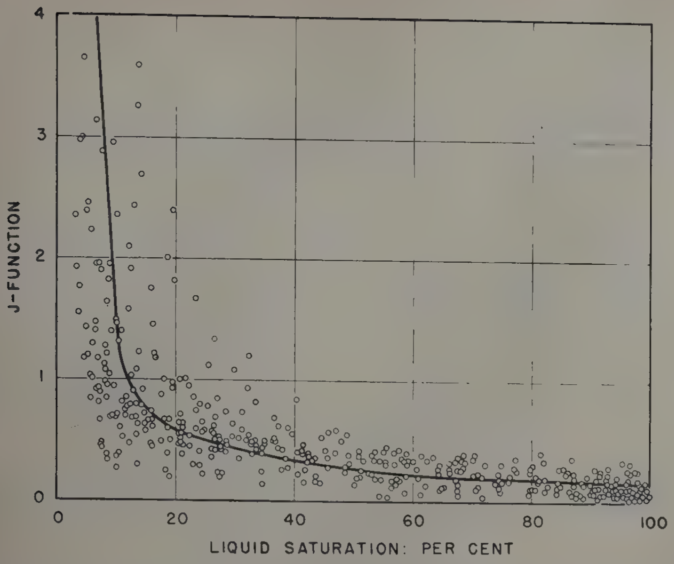

FIG. 8 — J-CURVE FOR LIMESTONE CORES, EDWARDS FORMATION, JOURDANTON FIELD.

The essential features of the Hassler-type apparatus, used to measure dynamic capillary pressures, are shown in Fig. 2. Each of the two end plates consists of a central disc diaphragm and an outer ring diaphragm. The two diaphragms, of porous porcelain, are isolated from each other by means of a metal cylinder. The face of each end plate is grooved to facilitate the passage of gas. The oil is flowed through the outer rings, and the center discs are utilized for measuring the pressure in the oil phase.

In operation, gas and oil were admitted to the core at two different pressures, this pressure difference being the capillary pressure. Since it was possible to measure the pressure drop in the oil phase from one core face to the other by the use of the center section of the porous plate, the gas pressure drop was adjusted at the outlet end until its pressure drop just equaled the pressure drop in the oil phase. When this condition had been attained, equal capillary pressures existed at each end of the core and the saturation was essentially the same throughout the core, if the sample was homogeneous. Any saturation variations due to expansion of the gas were very small because of the low pressure differences employed. While approaching this state of equilibrium, the pressure drop in the gas phase was maintained at a higher value than that in the oil phase. In consequence, prior to equilibrium the saturation at the inlet end was lower than that at the outlet end because of the decreasing capillary pressure gradient in the direction of flow. The liquid in each portion of the core was, therefore, being displaced to a region of higher saturation. The capillary pressure data obtained under these conditions should correspond, as nearly as is physically possible, to the drainage curve arrived at by static methods.

After attaining equilibrium in the manner described above, the core sample was removed and the saturation was determined by weighing.

Determination of Lithologic Properties of Core Samples

A petrographic study was conducted to determine the lithologic character of the core samples which were used in correlating capillary pressure curves. These samples were all from the Edwards formation (Cretaceous Age) of the Jourdanton Field in southwest Texas.

These samples were all carbonate rock, but some were classified as limestone and the others as dolomite or dolomitic limestone.

These samples were predominantly of the intercrystalline porosity type, though some samples had solution-enlarged pores as well.

The samples were divided by visual methods into the following textural groups, classified according to grain size:

1. Micrograpular — characterized by not being visibly crystalline in reflected light under 20-power magnification, but individual grains being barely discernible in thin section with 50-power magnification.
2. Fine-grained — visibly crystalline under 20-power magnification, but individual grains not recognizable. Average grain size about 0.02 mm.
3. Coarse-grained — individual grains easily recognizable under 20-power magnification. Dimensions of individual grains exceed 0.04 mm.

RESULTS

Comparison of the Restored-State and Mercury-Injection Methods

Capillary pressure-liquid saturation curves obtained by both the displacement cell and the mercury-injection apparatus were found to be nearly identical when plotted with appropriate scale relationships between the water-gas capillary pressure and the mercury capillary pressure. This identity of results indicates that the capillary pressure-saturation curves obtained by the two methods are geometrically similar, one curve being obtainable from the other for any given core by multiplication of the capillary pressure by a constant. In Figs. 3 and 4 are presented capillary pressure curves obtained by the two methods of capillary pressure measurement for sandstone and limestone cores, respectively.

The results of these studies confirm in general the results published by Purcell,[3] with the exception that Purcell's use of a constant conversion factor for all cores is questionable in the light of the data shown in Figs. 3 and 4. The constant

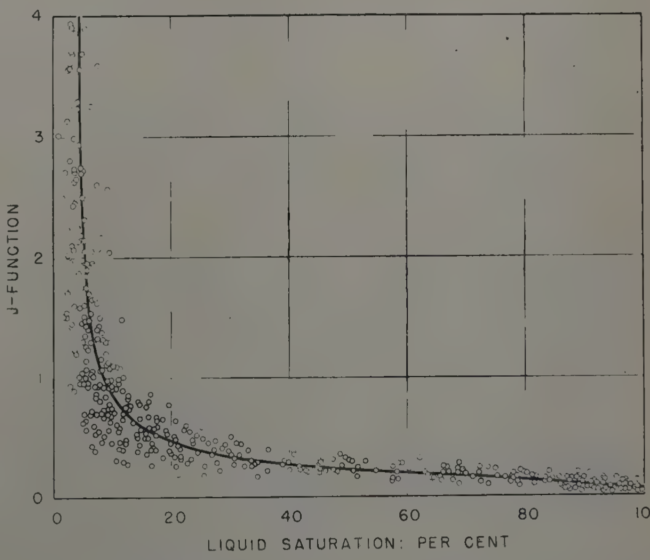

FIG. 9 — J-CURVE FOR DOLOMITE CORES, EDWARDS FORMATION, JOURDANTON FIELD.

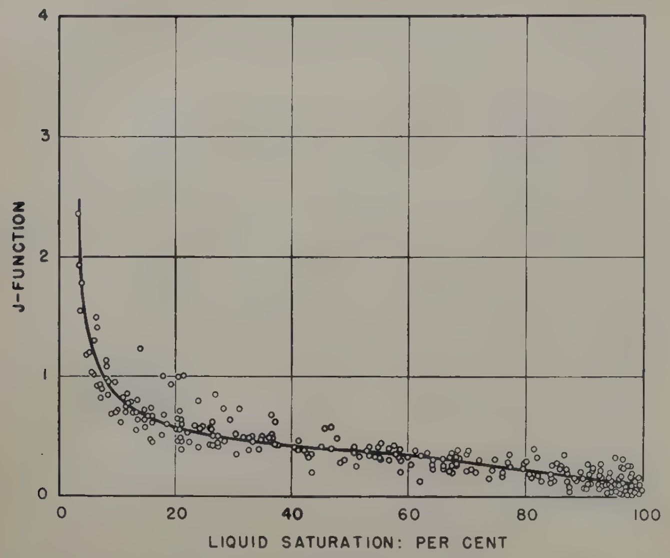

FIG. 10 — J-CURVE FOR MICROGRANULAR LIMESTONE CORES, EDWARDS FORMATION, JOURDANTON FIELD.

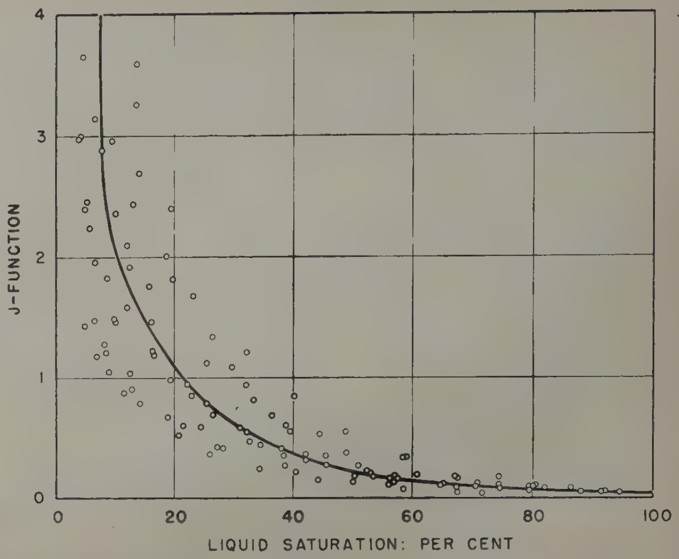

FIG. 11 — J-CURVE FOR COARSE-GRAINED LIMESTONE CORES, EDWARDS FORMATION, JOURDANTON FIELD.

conversion factor used by Purcell was arrived at by assuming the following values:

Surface tension of water: 70 dynes per cm

Surface tension of mercury: 480 dynes per cm

Contact angle of water against the solid: 0°

Contact angle of mercury against the solid: 140°

The conversion factor is then,

$$\frac{\text{(Mercury Capillary Pressure)}}{\text{(Water-Air Capillary Pressure)}} = \frac{-(480)\ (\cos 140^\circ)}{(70)\ (\cos 0^\circ)} = 5.25$$

Purcell, in presenting his results, used as a first approximation for the conversion factor a value of 5.0, and found fair agreement between the results of the two methods.

In contrast, it was found in this study that the agreement could be made almost exact if a different factor, ranging from 5.4 to 8.3, were used for each core sample. The fact that the lowest factor encountered experimentally was 5.4 suggests that the theoretical value of 5.25 may be a limiting value. This supposition is substantiated by the known sensitivity of water surface tension to contamination, making it quite possible that the figure of 70 dynes per cm is a maximum. Therefore, the use of a higher constant factor than that used by Purcell seems justified, and is supported by experimental experience. Data obtained to date indicate that the value of such a factor should be set tentatively as 6.4 for limestone and 7.2 for sandstone. It is expected that future experience will dictate revisions, but for the present these proposed values will, in general, give better correlations.

As stated, it was found that agreement between the two methods for measuring static capillary pressure could be made almost exact, provided the appropriate conversion factors were employed. The determination of one capillary pressure point by the restored-state technique permits the calculation of this factor for a core, if the point is properly located. Fig. 3 may be used to exemplify what is meant by proper location of the point. It may be observed in this figure that the wetting phase saturation is most sensitive to changes in capillary pressure along the horizontal portion of the curve. It is here that the correlating factor must cause the two curves practically to coincide, if large errors in saturation are to be avoided. The known point, therefore, must be in this region. The determination by this procedure of the correct correlating factor makes it possible to obtain a complete curve in detail by the rapid mercury-injection method, and then to convert the mercury curve to a restored-state curve.

Comparison of Dynamic and Static Capillary Pressure Measurements

Comparisons are presented in Figs. 5 and 6 between static and dynamic capillary pressure data for a sandstone and a limestone sample. The two methods show almost exact agreement for each core, and confirm the validity of the assumption that static capillary pressure data apply to flowing systems as well as to static systems, and hence can be utilized in the solutions of dynamic problems of fluid flow. It must be remembered, however, that in each of the two methods only two phases, oil and gas, were present. Neither the two-phase system of oil and water nor the three-phase system of water-oil-gas was investigated.

Correlation of Capillary Properties of Rock with Rock Texture

Leverett's[1,5] capillary pressure function relationship, proposed by Rose and Bruce[6] for correlating capillary pressure curves for samples from the same formation, is

$$J(S_w) = (P_c/\gamma \cos \theta)\,(K/\phi)^{0.5}$$

where

P_c = capillary pressure

K = permeability

ϕ = porosity

γ = interfacial tension between the two fluids, and

θ = the contact angle between the interface separating the two fluids and the surface of the rock.

The group $(P_c/\gamma \cos \theta)\,(K/\phi)^{0.5}$ is dimensionless, and, as shown, is designated as $J(S_w)$, the S_w referring to the saturation of the wetting fluid. A plot of $J(S_w)$ versus wetting phase saturation results in the capillary-pressure-function curve. This curve is more familiarly known as the *J*-curve.

The *J*-curve was employed to correlate capillary pressure liquid saturation data obtained from core samples of the Edwards formation in the Jourdanton Field. The capillary pressure-liquid saturation data were obtained by the restored-state method on cores from various depths in seven wells of this field. The porosities of these cores varied from 9.5 to 28.2 per cent, and the permeabilities varied from 0.346 to 186 md.

On plotting the capillary-pressure function, $J(S_w)$, against wetting phase saturation it was found that all the data points fell roughly along the same trend. The result, presented in Fig. 7, gives support to the proposal of Rose and Bruce.[6] It was felt, however, that some refinement of the curve would be desirable.

Subsequent studies of the data showed that the curve might be better for cores in the same lithologic classification. Consequently, the cores were divided into groups and plotted as separate *J*-curves according to whether they were limestone, Fig. 8, or dolomite, Fig. 9.

The only improvement noted by this division was for the dolomite samples. As shown by a comparison of Fig. 9 with Fig. 7, the scattering of points was reduced materially, giving much less spread of the data points.

To investigate quantitatively this improvement, the permeabilities of 40 dolomite samples were calculated using the *J*-curve for all cores, Fig. 7, and the *J*-curve for dolomites only, Fig. 9. These calculated permeabilities are compared with the measured permeabilities in Table I. The per cent error, or deviation from the measured value, was determined for each core. The average error for all samples was found to be 71.5 per cent when using the *J*-curve for all cores, Fig. 7. The use of the dolomite *J*-curve, Fig. 9, reduced the average deviation to 48.0 per cent. The variations in porosity and permeability for this group of cores covered such a wide range, threefold for porosity and 500-fold for permeability, that these average per cent errors should be fairly representative for any similar

Table I — Comparison Between Measured and Calculated Permeabilities for Dolomite Cores Using *J*-Curves Indicated

				J-Curve for All Edwards Samples		*J*-Curve for Dolomite Only	
	Core Sample No.	Porosity (fraction)	Measured Permeability K_m (md.)	Calculated Permeability K_c (md.)	Deviation %	Calculated Permeability K_c (md.)	Deviation %
Well No. 1	58	.279	186.0	205.0	10.2	144.0	22.6
	65	.225	70.3	155.0	121.0	108.0	53.6
	66	.254	137.0	189.0	38.0	141.0	2.9
	69	.246	154.0	324.0	110.3	274.0	77.9
Well No. 2	1	.117	1.03	1.78	72.8	1.26	22.3
	4	.104	0.346	2.42	599.0	1.68	386.0
	5	.206	20.6	27.4	33.0	20.8	1.0
	6	.159	2.51	4.14	65.0	3.30	31.4
	7	.143	1.97	4.46	126.4	3.19	61.9
	8	.127	7.17	11.1	54.7	7.92	9.5
	10	.201	34.0	42.0	23.6	30.0	11.8
	11	.237	45.0	72.9	62.0	52.1	15.8
	14	.134	1.99	2.11	6.0	1.50	24.6
	18	.113	4.55	7.56	66.1	5.4	18.7
	30	.125	2.29	5.19	126.7	3.7	61.5
	32	.234	160.0	111.0	30.6	78.9	50.7
	33	.200	113.0	112.0	0.9	79.7	29.4
Well No. 3	10	.214	15.9	10.0	37.1	7.18	54.7
	12	.133	2.85	6.85	140.3	4.82	69.1
	16	.236	30.6	17.4	43.1	13.3	56.5
	18	.171	10.7	25.4	137.0	18.9	76.6
	19	.187	53.5	77.5	44.8	57.4	7.3
Well No. 4	1	.220	8.9	11.9	33.7	8.5	4.5
	3	.154	4.07	3.86	5.2	2.94	27.8
	4	.170	2.79	2.25	19.4	1.61	42.3
	7	.253	14.3	15.7	9.8	10.7	25.2
	16	.202	93.0	116.0	24.7	81.9	11.9
	24	.276	28.5	144.0	405.0	106.0	272.0
Well No. 5	3	.131	2.62	7.79	200.0	5.58	115.0
	4	.117	5.07	3.80	25.0	2.71	46.5
	5	.122	1.26	0.785	37.7	0.561	55.5
	6	.155	6.13	6.09	0.7	4.35	29.0
	7	.204	40.8	27.1	33.6	21.8	46.5
	8	.249	67.5	81.2	20.3	62.1	8.0
	9	.212	34.5	39.7	15.1	34.6	0.3
	11	.237	52.5	50.5	3.8	41.5	21.0
	12	.228	53.0	82.5	12.0	60.6	18.1
	14	.235	43.8	50.0	14.2	38.3	12.4
	17	.250	39.5	31.5	20.2	23.8	39.7
	18	.223	74.0	97.7	32.0	73.9	0.1
			Average Deviation, %		71.5		48.0

$$\%\ \text{Deviation} = \left(\frac{K_c - K_m}{K_m}\right) 100$$

group of cores from this formation. In this case, therefore, the breakdown of Edwards core samples into two groups, limestone and dolomite, improved the correlation for the dolomite group.

The limestone samples of Fig. 8, were subdivided into two groups according to their texture. One group was the microgranular type, and the other was coarse-grained. As shown in Figs. 10 and 11, respectively, this breakdown into lithologic groups according to texture appears to improve the correlation for both groups.

The dolomites were divided into fine and fine-to-coarse grained dolomites as one group, and coarse-grained dolomites as the other. The improvement in the individual *J*-curves over the *J*-curve for all dolomites was negligible.

The two remaining groups, fine-grained and fine-to-coarse grained limestone were neglected, since the number of cores available was not judged sufficient.

It is apparent from these data that the *J*-curve may have utility in correlating capillary pressure data obtained on samples from a single formation, but that the results derived from its use may be of limited precision. It is also apparent that the correlation may be improved by restricting it to specific lithologic types of samples.

CONCLUSIONS

1. A comparison of the mercury-injection method with the restored-state method of measuring capillary pressure showed that the two yielded nearly identical results if the proper conversion factor were chosen for each core sample, but that the conversion factor was not constant for all samples. This factor was found to average 6.4 for limestone samples and 7.2 for sandstone samples.
2. Static and dynamic methods of obtaining drainage capillary pressure curves gave nearly identical results. This identity confirms the validity of the use of static capillary pressure data in dynamic problems of fluid flow.
3. Data on a number of samples of Edwards limestone support the use of the *J*-curve in correlating capillary pressure data obtained on core samples from a single formation. The correlation may be improved by restricting its use to specific lithologic types from the same formation.

ACKNOWLEDGMENT

The author wishes to express his appreciation for the assistance and cooperation of the persons who contributed to this paper: J. O. Barry, formerly of the Exploration Department, Humble Oil and Refining Co., for the petrographic studies and J. K. Kerver and W. O. Winsauer in securing much of the laboratory data.

REFERENCES

1. Leverett, M. C.: *Trans.* AIME, (1941) **142,** 152-169.
2. Bruce, W. A., and Welge, H. J.: "Restored-State Method for Determination of Oil in Place and Connate Water," API Division of Production, Amarillo, Tex., May 22-23, 1947.
3. Purcell, W. R.: *Trans.* AIME, (1949) **186,** 39-48.
4. Hassler, G. L.: *Method and Apparatus for Permeability Measurement,* U.S. Patent No. 2,345,935, April 4, 1944.
5. Leverett, M. C., Lewis, W. B., and True, M. E.: *Trans.* AIME, (1942) **146,** 175-193.
6. Rose, W., and Bruce, W. A.: *Trans.* AIME, (1949) **186,** 127-142.
7. Rose, W.: *Trans.* AIME, (1949) **186,** 111-126.
8. Gates, J. I.,, and Lietz, W. T.: "Relative Permeability of California Cores by the Capillary Pressure Method," API Paper No. 801-26F presented before Spring Meeting of Pacific Coast District, May 11-12, 1950.

★ ★ ★

DISCUSSION

By W. R. Purcell, Shell Oil Co., Houston, Tex., Junior Member, AIME

Of the various interesting experimental results reported in Brown's paper, those concerning the conversion of water/nitrogen capillary pressures appear to warrant additional comment. Brown suggests that his observed conversion factors, ranging from 5.4 to 8.3, are higher than the factor of 5.25, previously proposed by the writer, because of a reduction by contamination of the surface tension of water to a value below the 70 dynes per cm which was used in calculating the factor 5.25. One would suspect, however, that the mercury would be as susceptible to contamination as the water, if not more so, and it seems difficult, therefore, to resolve all of the differences merely on the basis of surface tension lowering alone. It should be pointed out that the factor 5.25 as originally proposed was calculated on the assumption that the pores of a rock sample behave as a group of circular capillary tubes. It would seem reasonable therefore, to conclude that the departure of the observed conversion factors from the idealized theoretical value of 5.25 reflects to a large degree the effect of departure of pore geometry from the hypothetical cylindrical tube. It is my opinion that, in the consideration of capillary pressure phenomena, the effect of pore geometry is equally as great as that of surface and interfacial forces,[1] and it is this effect of pore geometry which has been neglected by Brown, and previously by the writer, in considering conversion factors for changing capillary pressures as determined by one system to equivalent values for another system.

REFERENCES

1. Purcell, W. R.: *Trans.* AIME, (1950) **189,** 369.

DISCUSSION

By W. A. Bruce, Carter Oil Co., Tulsa, Okla., Member AIME

It is of interest to me to note that Brown suggests refinement of the *J*-function technique to the extent of subdivision of porous material from a formation into two or more distinct groups. This seems to be a desirable practice if the rock is divisible into distinctly different classifications such as dolomite or calcite as in Figs. 8 and 9 above. However, petrographic classification is not necessarily the key to the *J*-function, probably because a number of petrographic factors such as grain size and standard deviation are already properly accounted for macroscopically by the permeability and porosity values that go to make up the *J*-function. ★ ★ ★

T.P. 3018

VARIABLE CHARACTERISTICS OF THE OIL IN THE TENSLEEP SANDSTONE RESERVOIR, ELK BASIN FIELD, WYOMING AND MONTANA

RALPH H. ESPACH, MEMBER AIME, AND **JOSEPH FRY,** U. S. BUREAU OF MINES, LARAMIE, WYO.

ABSTRACT

In the spring of 1943, when it was evident that the Tensleep sandstone in the Elk Basin Field, Wyoming and Montana, held a large reserve of petroleum, Bureau of Mines engineers obtained samples of oil from the bottom of nine wells and analyzed them for such physical characteristics as the volumes of gas in solution, saturation pressures or bubble points, shrinkage in volume caused by the release of gas from solution, expansion of the oil with decrease in pressure, and other related properties. The composition of the gas in solution in the oil was studied. The pressures and temperatures existing in the reservoir and the productivity characteristics of the oil wells were determined.

The data obtained indicate that the oil in the Tensleep Reservoir of the Elk Basin Field has unusually varying physical characteristics, such as a saturation pressure of 1,250 psia and 490 cu ft of gas in solution in a barrel of oil at the crest of the structure and a saturation pressure of 530 psia and 134 cu ft of gas in solution in a barrel of oil low on the flanks. The hydrogen sulfide content of the gas in solution in the oil varies from 18 per cent for oil on the crest to 5 per cent for oil low on the flanks of the structure. Of even greater significance is the fact that these and other variable characteristics of the reservoir oil are related to the position of the oil in the structure. Many geologists and petroleum engineers have considered that all the oil in a petroleum reservoir has rather uniform physical characteristics and that equilibrium conditions prevailed in all underground accumulations of oil and gas; that such is not always so is borne out by the results of the study by the writers.

INTRODUCTION

The Rocky Mountain region is one in which may be found striking examples of the unusual in oil and gas accumulations, as is evident from the following: The high helium content (7.6 per cent) of the gas in the Ouray-Leadville limestone sequence in the Rattlesnake Field, New Mexico, and gases of similar helium content in other fields; 50° to 55° API gravity distillate in solution in carbon dioxide gas and recoverable through retrograde condensation, in the North McCallum Field, Colorado; the occurrence of gas, oil, or both in closely related structures contrary to the usual concepts of gravimetric segregation; the accumulation of gas and/or oil in structures closely related to other structures that apparently are more favorable but do not contain oil or gas accumulations; the high hydrogen sulfide content (as high as 42 per cent) of the gas associated with oil in some fields in the Big Horn Basin, Wyoming; and the wide range of fluid characteristics found in the Elk Basin reservoir.

Elk Basin, an interesting old oil field that has been producing oil from the Frontier formation since 1915, is situated in a highly eroded basin resulting from the erosion of the crest of an anticline and some of the underlying softer shales. The field came back into national prominence during 1943 when it became known that it was the largest single reserve of new oil discovered in the United States that year. The Tensleep sandstone was found to contain oil in November, 1942, when a well drilled to a depth of 4,538 ft (44 ft into the Tensleep sandstone) flowed oil at the rate of 2,500 B/D. By the end of 1949, 137 oil-producing wells and five dry holes had been drilled, and approximately 32 million bbl of oil had been produced. Approximately 6,000 acres may be considered productive of oil in the Tensleep Reservoir, and estimates of the oil that will be produced average 200 million bbl.

The Tensleep Reservoir has further interest because it has greater closure than any oil field in the Rocky Mountain region; the closure of the Elk Basin anticline is variously estimated at 5,000 to 10,000 ft, of which the top 2,000 ft of the structure contained oil.

SUBSURFACE OIL SAMPLING

Fig. 1 is a structural map of the Elk Basin Tensleep Reservoir, on which the nine wells used in this study and the numbers corresponding to the well designations hereafter referred to are shown. Wells 1, 2, 3, 4, and 8 were tested and sampled during October and November, 1943, and Wells 5, 6, 7, and 9 during June and July, 1944.

An electromagnetic type sampler developed by the Bureau of Mines and described by Grandone and Cook[1] was used in obtaining the subsurface oil samples.

As the wells were tubed nearly to bottom, the sampler was run as far as possible in the tubing but never below the top perforations.

The following procedure was used in testing and sampling the wells: A well was shut in for at least three days, after

---

[1] References given at end of paper.

Manuscript received in the office of the Petroleum Branch Aug. 31, 1950. Paper presented at the Petroleum Branch Fall Meeting in New Orleans, La., Oct. 4-6, 1950.

which shut-in subsurface pressures and temperatures were measured. Generally, the well then was allowed to flow at a 10 to 20-bbl-per-hour rate for approximately one day, when a flowing temperature and pressure traverse was run. One day later, at the same production rate, a subsurface sample was obtained and transferred to a storage container. A second subsurface sample of oil then was procured; and, if in transferring, the pressure and volume data duplicated those of the first sample, both were considered satisfactory for analyses. After the sampling was completed the flow rate of the well was increased to two higher rates and subsurface pressure traverses were obtained at each rate. A 12-hour subsurface pressure build-up was obtained when the well was shut in following the highest rate of flow. A pressure gauge recorded the tubing and casing pressures at the wellhead during the tests. The oil produced by the well during the tests was gauged in lease tanks at regular intervals and the separator gas was measured with a recording orifice meter. The essential data pertaining to the wells are given in Table 1.

Wells 7 and 9 were not producing when sampled. Well 7 had flowed most of the indicated production; but the flow gradually lessened, and the well finally stopped flowing. It was sampled several days later. Well 9 was swabbed unsuccessfully to cause it to flow; it had been standing for about 30 days before sampling, and as tubing had not been run to bottom, it was necessary to sample the oil at a relatively high point in the well.

It will be noted that Wells 2 and 3 have essentially the same structural position, and for the purposes of this study it might seem that one well would suffice. Well 3, however, produced from the upper 44 ft of the Tensleep formation, and Well 2 was completed so that only the zone between 66 and 192 ft below the top of the Tensleep formation produced oil through the tubing. Sampling both wells provided an excellent opportunity to study the possibility of the existence of more than one reservoir in the Tensleep formation, a postulate that had merit because of the rather extensive dolomitic zones extending throughout the sandstone body at depths greater than 70 to 80 ft in the formation. The almost identical results obtained in the analyses of the oil samples from both wells indicated that the oils were the same and that the Tensleep formation contained only one reservoir.

RESERVOIR-OIL CHARACTERISTICS

The subsurface oil samples were analyzed by the differential gas-liberation method outlined by Grandone and Cook.[1] The laboratory analyses of the oil samples were made at the Petroleum Experiment Station (now Petroleum and Oil-Shale Experiment Station), Bureau of Mines, Laramie, Wyo., during several months following sampling of the wells. The general results are given in Table II. Individual gas-liberation data for the nine samples are not presented, but Figs. 2, 3, and 4 show how the data changes for the oil at wells 1, 6, and 8.

In these figures, the graphs of "expansion of sample" are self-explanatory. The values for the gas in the "gas in solution" graphs are figured at conditions of 60°F and 14.4 psia pressure. The "relative oil-volume" graphs show the volume relationship between the oil in the reservoir under reservoir conditions and the residual oil at 60°F. The "density of sample" graphs indicate the change in density as changes in pressure and release of solution gas occur. The "specific gravity of gas in solution" graphs show the gravity of the gas that is in solution in the oil at the different pressures and in volume as shown by the "gas in solution" graphs. The values for the specific gravity of the gas in solution were obtained by using a 220-ml gas-density balloon, weighing samples of gas liberated between pressure points and calculating the composite to any pressure by using the volumes and weights of the several increments of liberated gas.

The "hydrogen sulfide content of gas in solution" graphs show the percentage of hydrogen sulfide in the gas that is in solution in the oil at the different pressures and in volume as shown by the "gas in solution" graphs. The percentages of H_2S were obtained by running both Tutwiler and Orsat analyses of the increments of liberated gas during analyses of samples from wells 5, 6, 7, and 9 and Orsat analyses for acid gases of the increments of liberated gas during analyses of samples from Wells 1, 2, 3, 4, and 8. Where Orsat values alone were determined, 5 to 6½ per cent was subtracted from them as a correction for the carbon dioxide content of the gas. The "hydrogen sulfide content of gas in solution" graphs represent values obtained from: The determined percentages of hydrogen sulfide in the several increments of gas liberated between any two pressures; the volumes of the several increments; and the calculated composites of these to various pressures.

Of interest in connection with the "gas in solution" graphs are the data on the H_2S contents of the several increments of

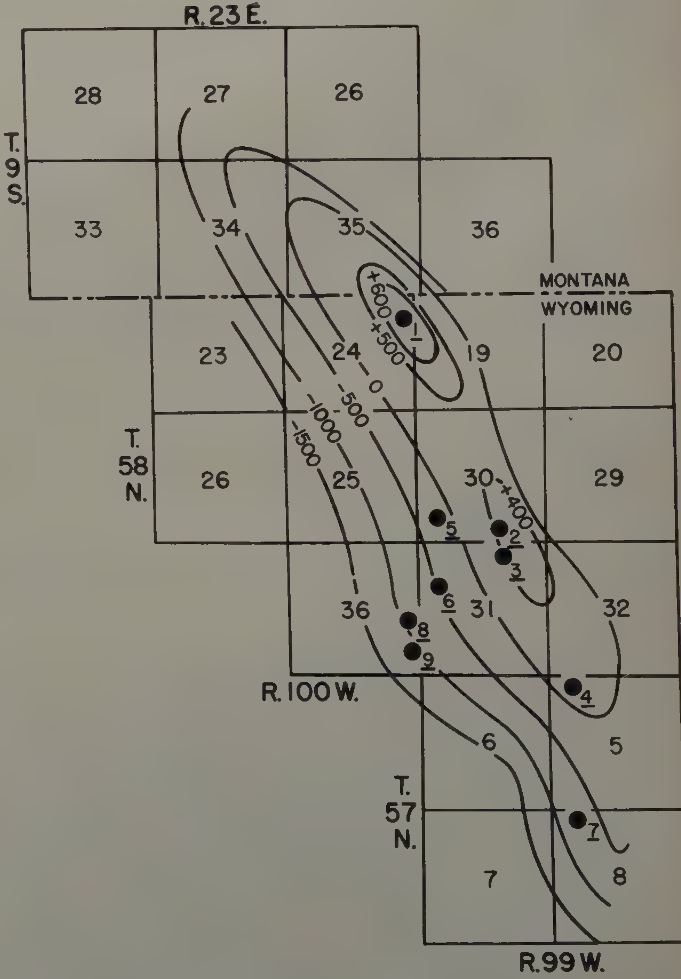

FIG. 1 — ELK BASIN, TENSLEEP RESERVOIR MAP.

Table I — Data Relative to Wells Sampled, Tensleep Reservoir, Elk Basin Field

Well No.	Date of well completion	Date of sampling	Oil produced to sampling date, bbl	Gravity of produced oil, °API	Top of Tensleep formation: Elevation, ft	Top of Tensleep formation: Original pressure, psia[1]	Top of Tensleep formation: Temperature, °F[2]	Sampling point: Elevation, ft	Sampling point: Pressure, psia	Flow rate while sampling B/D
1	9- 9-43	11- 4-43	20,000	31.8	+655	1853	112	+488	1564	922
2	3- 9-43	10-23-43	114,000	31.4	+471	1917	115	+283	1734	454
3	4-18-43	10-15-43	130,000	31.1	+422	1934	116	+413	1644	536
4	7- 6-43	10- 4-43	34,800	31.0	+ 89	2049	121	– 30	1905	420
5	4-28-44	6-11-44	6,200	30.6	–117	2120	125	–265	1570	486
6	5- 2-44	6-21-44	9,200	30.0	–397	2218	129	–557	1720	240
7	4- 4-44	6-15-44	13,800	29.1	–683	2319	134	–773	1882	shut-in
8	8- 7-43	10- 9-43	52,700	28.4	–887	2392	137	–1044	2023	440
9		5-31-44	200[3]	27.1	–1107	2472	141	–643	1770	shut-in

[1] Calculated from estimated original reservoir pressure of 2,080 psia at sea-level datum and density of subsurface samples.
[2] From temperature gradient chart for the Elk Basin structure.
[3] Production by swabbing in an attempt to cause the well to flow. Well was pumped after sampling.

gas liberated during the differential gas liberation of a subsurface sample of oil. Such data from the sample of oil from Well 1 are given in Table III. The great change in H_2S content of the gas as it is released from solution when the pressure is lowered is significant. It reflects the solubility of H_2S in crude oil. The "hydrogen sulfide content of gas in solution" graphs indicate that at Elk Basin the H_2S content of the gas from the oil in the reservoir would increase as reservoir pressures decreased in accordance with the graphs provided the gas/oil ratio during production would not exceed that in solution in the oil. However, gas/oil ratios will increase in solution-gas-drive reservoirs as the pressure declines. The percentage of hydrogen sulfide in the gas evolving from solution also will increase as reservoir pressure declines; this relationship is shown in Table III for an oil sample from Well 1: The relationship is similar for oil samples from other wells. These two factors will cause a decrease in the percentage of hydrogen sulfide in the produced gas as reservoir pressures decline, for the volume of gas produced in excess of the volume of gas in solution in the oil will have a smaller percentage content of hydrogen sulfide and will act as a diluent for the solution gas. Later in the life of the reservoir when declining gas/oil ratios become effective, an increase in the H_2S content of the produced gas can be expected.

Owing to the method by which the data were obtained, those data relating to the specific gravity of the increments of gas liberated from the subsurface oil samples and the hydrogen sulfide content of the gas samples are the least accurate of all results reported. In fact, the data show changes in one or two instances that are inconsistent with the data from other samples.

The writers are indebted to two of the operators for information on the viscosity of the reservoir oil from Well 2. Oil from Well 2 is representative of the oil in the upper 500 or more feet of closure. The viscosity in centipoises of the oil at a temperature of 123°F and at several gauge pressures and the estimated viscosities of the oil near the edge of the reservoir are given in Table IV.

DISCUSSION

A review of the data given in Table II and shown in Figs. 2, 3, and 4, reveals a very interesting conclusion that should be considered in all studies of petroleum reservoirs; namely, that the oil in a reservoir may have rather widely varying physical characteristics.

In general, many engineers and geologists have reasoned that, considering the length of time involved in the formation of an oil field, equilibrium must have been attained between

Table II — General Results of Analyses of Subsurface Oil Samples, Tensleep Reservoir, Elk Basin Field

Well No.	Gravity, °API: At original reservoir pressure	Gravity, °API: Residual oil, after liberation of gas	Gas-liberation temperature, °F	Saturation pressure, psia	Gas in solution cu ft/bbl residual oil[1]	Relative oil volume[2]	Expansibility factor[3]	Specific gravity of gas in solution	Hydrogen sulfide content of gas in solution, per cent
1	45.4	30.7	121	1250	490	1.223	82×10^{-7}	0.989	18.2
2	44.9	30.2	121	1255	478	1.220	82×10^{-7}	.996	15.8
3	45.4	30.6	121	1250	469	1.221	79×10^{-7}	1.001	16.6
4	44.3	30.6	123	1235	459	1.212	77×10^{-7}	1.011	16.5
5	44.6	30.2	129	1177	437	1.210	[4]84×10^{-7}	1.028	15.2
6	42.3	29.5	133	990	350	1.178	70×10^{-7}	1.048	13.4
7	39.2	29.1	134	772	225	1.122	68×10^{-7}	1.021	6.4
8	37.3	27.7	140	695	205	1.116	64×10^{-7}	1.026	10.1
9	34.9	27.0	141	530	134	1.086	63×10^{-7}	1.041	4.9

[1] Based upon differential gas-liberation method. Base, 14.4 psia and 60°F.
[2] Ratio of reservoir-oil volume (at original reservoir conditions at top of Tensleep formation) to residual-oil volume at 60°F.
[3] Volumes per volume per psi pressure change, reservoir oil at pressures above saturation pressure.
[4] This figure probably is in error. Corresponding data from other samples indicate that it should have been approximately 75×10^{-7}.

the fluids in a reservoir and if any of the oil was saturated with gas under existing pressures and temperatures, then all of it was saturated or very nearly so, or, conversely, if some of the oil was undersaturated, then all of it would be undersaturated to about the same degree. Some recorded observations in other fields seem to indicate that equilibrium conditions may not exist in all fields, but incontrovertible proof of that has been lacking. Estabrook and Rader[2] noted the presence of a "zone of dead oil" in the Second Wall Creek sand in the Salt Creek Field and reported that "the distribution of dissolved gas in the oil seems to have been fairly uniform over the field except toward the edges."

Study of the magnitude of change of properties of the subsurface oil samples from Elk Basin definitely indicates that the fluids in a reservoir are not necessarily in equilibrium. It is concluded that either extremely long periods of time are necessary to effect equilibrium or that accumulation can be quite young, or is still taking place in some petroleum reservoirs.

Table III — Hydrogen Sulfide Content of Liberated Gas, Differential Gas Liberation, Oil Sample from Well 1

Pressure range in which gas increment liberated, psia	Hydrogen sulfide content of gas increment, per cent
1250 to 835	7.6
835 to 725	5.1
725 to 625	5.9
625 to 535	6.8
535 to 450	6.1
450 to 365	10.2
365 to 300	13.0
300 to 225	16.0
225 to 165	19.4
165 to 120	26.7
120 to 85	28.6
85 to 60	35.0
60 to 45	38.0
45 to 11	36.1

RELATIONSHIP OF OIL CHARACTERISTICS TO RESERVOIR STRUCTURE

The relationship of the characteristics of the oil to the location of the oil in the Elk Basin, Tensleep Reservoir, is shown in Fig. 5. In Fig. 5 values of the saturation pressure, gas in solution, relative oil volume, density of the reservoir oil, specific gravity of the gas in solution, and hydrogen sulfide content of the gas in solution for the nine subsurface oil samples are plotted as ordinates against the common abscissa of sea-level elevations of the top of the Tensleep formation over the structure. The nine wells shown in Fig. 1 are identified by number along the abscissa of Fig. 5 at positions corresponding to the elevation of the top of the Tensleep in each well. Although the wells are plotted according to formation "tops" the oil from each of these wells came from some greater depth, depending on the penetration (160 to 200 ft) of the formation in each well.

The composite sample data for the oil from each of the wells sampled, as derived from the individual analyses, are shown in Fig. 5 to have a very definite relationship to the structure of the reservoir from which the oil came. To the writers' knowledge, this is the first time that results of detailed reservoir oil sampling have been published showing such a relationship to exist.

A study of Fig. 5 would indicate that possibly the subsurface sample of oil from Well 7 was not truly representative of the reservoir oil at Well 7 and that the sample had been conditioned somewhat. This was referred to in the section on subsurface oil sampling. The data for the specific gravity of the gas in solution show the least consistent relationship of all the data. Attention has been called earlier in this report to the manner in which these data were acquired.

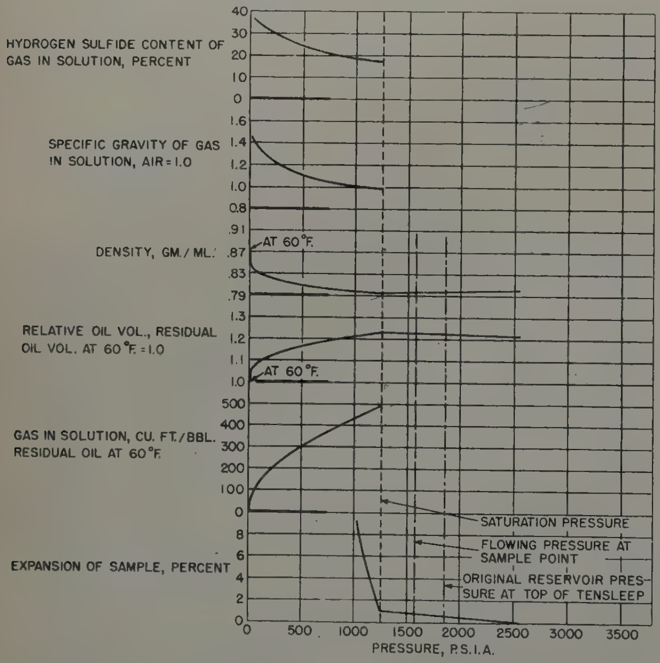

FIG. 2 — RESULTS OF DIFFERENTIAL GAS-LIBERATION ANALYSIS AT 121°F, SUBSURFACE OIL SAMPLE FROM WELL 1, ELK BASIN FIELD.

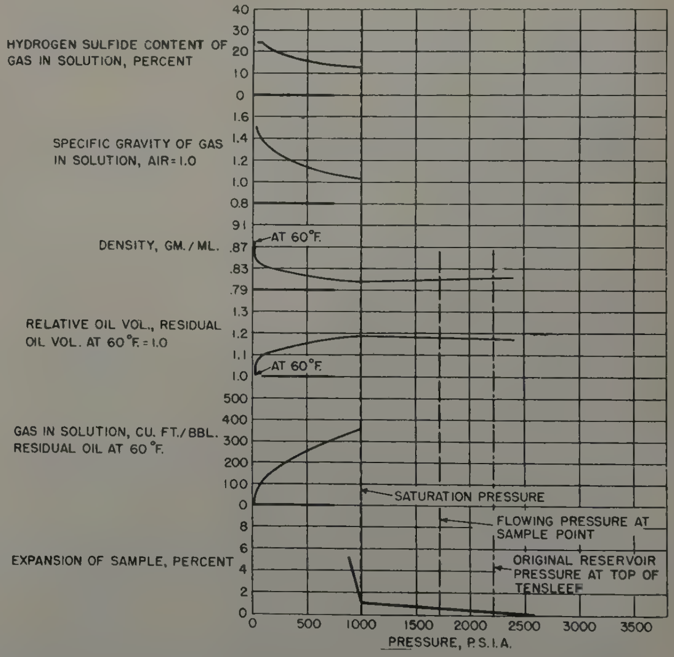

FIG. 3 — RESULTS OF DIFFERENTIAL GAS-LIBERATION ANALYSIS AT 133°F, SUBSURFACE OIL SAMPLE FROM WELL 6, ELK BASIN FIELD.

Table IV — Viscosity of Reservoir Oil

Pressure, psi	Oil from Well 2, centipoises	Oil from edge wells, centipoises (estimated)
2500	1.59	4.6
2000	1.50	—
1500	1.42	4.3
1150	1.35	—
1000	1.40	—
800	1.50	4.1
600	1.65	4.0
400	1.82	4.1
200	2.05	4.7
0	4.50	8.0

The physical characteristics of the oil throughout the crestal 500 to 600 ft of the reservoir are very much alike — all oil samples from the crestal part of the reservoir showed a saturation pressure of 1,235 to 1,250 psia and contained 460 to 490 cu ft of gas in solution based on 1 bbl of residual oil. As a consequence of this gas in solution, 1.22 bbl of oil in the reservoir are required to produce 1 bbl of residual, or approximately stock-tank, oil. At a depth of about 100 ft above sea level, a decided change begins to occur in the character of the reservoir oil—the saturation pressure becomes lower and the volume of gas in solution decreases. The other characteristics begin to change also. These changes continue with depth until the oil from a well in which the top of the producing formation is at an elevation of 1,107 ft below sea level, contains only 134 cu ft of gas in solution per barrel of oil (on a residual oil basis) and its saturation pressure is only 530 psia. Edge water is present in the reservoir at an elevation of about 1,500 ft below sea level. The writers have no information on the characteristics of the oil coming from wells in which the top of the Tensleep sandstone is below a depth of 1,107 ft below sea level. Characteristics may be inferred from extension of the several curves to elevations of 1,200 or 1,500 ft below sea level.

The hydrogen sulfide content of the gas in solution in the oil as compared to the volume of gas in solution in the different oil samples is a rather interesting relationship; the gas in solution in the oil on top of the structure contains 18 per cent hydrogen sulfide, that in solution in the oil on the edge of the structure contains 5 per cent, and the variation is almost directly proportional to the volume of gas in the different samples. This suggests a plausible hypothesis for the movement and characteristics of the fluids in the reservoir which is consistent with the supposition that equilibrium has not yet been attained in the whole mass of reservoir oil and which has been included in another article[3] concerning the Elk Basin Field.

ACKNOWLEDGMENTS

The work covered in this report was conducted under a cooperative agreement between the Bureau of Mines, United States Department of the Interior, and the University of Wyoming.

The writers and those engaged in the work appreciate the assistance of the operators in the Elk Basin Field, who gave the engineers of the Bureau of Mines access to their properties, supplied the wells for testing and sampling purposes, and furnished most of the information pertaining to the Tensleep reservoir itself.

The report was prepared under the general supervision of R. A. Cattell, Chief, Petroleum and Natural Gas Branch, Bureau of Mines, Washington, D. C., and H. P. Rue, Chief, Fuels Technology Division, Region IV, Petroleum and Oil-Shale Experiment Station, Bureau of Mines, Laramie, Wyo. The constructive criticisms of the manuscript by C. B. Carpenter

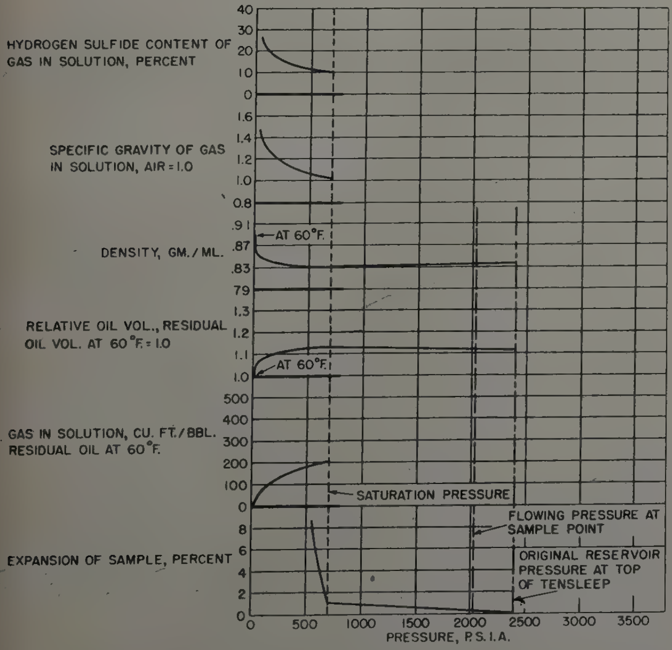

FIG. 4 — RESULTS OF DIFFERENTIAL GAS-LIBERATION ANALYSIS AT 140°F, SUBSURFACE OIL SAMPLE FROM WELL 8, ELK BASIN FIELD.

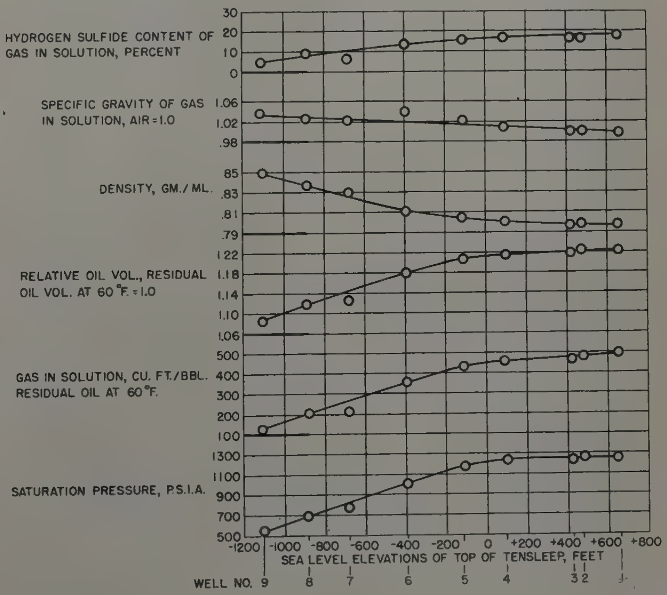

FIG. 5 — RELATIONSHIP OF THE CHARACTERISTICS OF THE OIL AT ORIGINAL CONDITIONS TO THE LOCATION OF THE OIL IN THE TENSLEEP RESERVOIR, ELK BASIN FIELD.

(deceased), A. B. Cook, H. C. Miller, and E. M. Tignor, engineers of the Bureau of Mines, are gratefully acknowledged. The work of three engineers, formerly at the Laramie Experiment Station — H. Karl Schmidt and Warren J. Mason on the first group of oil samples and Raymond A. Morgan on the second group of samples — in addition to that of the writers, resulted in acquiring the data presented in this report. O. C. Heustis prepared the illustrations.

REFERENCES

1. Grandone, Peter, and Cook, Alton B.: *Collecting and Examining Subsurface Samples of Petroleum,* U. S. Bureau of Mines Technical Paper 629, (1941), 12-19, 59-64.
2. Estabrook, E. L., and Rader, C. M.: *Trans.* AIME, (1925), 216.
3. Espach, Ralph H., and Fry, J.: U. S. Bureau of Mines Report of Investigations 4768, (1950).

DISCUSSION

By Henry J. Welge, Carter Oil Co., Tulsa, Okla.,
Member AIME

For some time geologists and engineers have tacitly assumed that the elapsed time during which petroleum reservoirs have been relatively undisturbed is sufficiently large so that their fluids are in complete equilibrium with one another. Hence the authors are to be commended for directing attention to the possibility of the occurrence of non-equilibrium conditions in certain petroleum reservoirs. Work recently performed at The Carter Oil Co. Research Laboratory substantiates this point. In the interest of adding to the picture, a portion of the work done recently is herewith presented.

In order to test the possibility of an incomplete approach toward equilibrium by diffusion of gas downstructure in the Elk Basin Pool, calculations have been made of the minimum time required for the attainment of the present gas distribution at the downstructure wells (6, 7, 8, and 9 on Fig. 1) by diffusion. The calculations presume a constant dissolved gas content of 467 cu ft per bbl at all times at levels higher than the present sea level contour (Fig. 1). They also assume that no, or relatively little, gas was in solution elsewhere in the reservoir at the time of trap formation. In other words, the picture assumed is that of gas (or gas-rich oil) present initially in the upper part of the reservoir, overlying relatively "dead" oil. It is well known that rather long intervals of time are required for a solute to diffuse through a liquid if long distances have to be traversed. The calculations were made in order to see how long a time interval is required in the instance of the Elk Basin Pool, and to compare it with the geologic time available.

The relation governing unsteady state diffusion is mathematically identical with that treating heat diffusion. For conductors of certain shapes, the solutions have been given graphically.[1,2]

The special case of a constant high concentration of gas at the head of a petroleum column, maintained by the presence of a gas cap diffusing downward into the oil, is analogous to heat flow through a slab of uniform cross-sectional area, from a constant temperature source at one face toward an opposite insulated face.

The solution for the slab shape assumes a uniform cross-sectional area normal to the direction of diffusion. This condition would prevail approximately on the elongated southwest and northeast flanks of the pool, as indicated in Fig. 1 of the paper under discussion. With the aid of this graphical solution, it is possible to compute the time required for the present gas distribution to be attained. The value used in this calculation for the diffusion constant, D, is 0.43 sq ft per year, and it compares favorably with values given in the literature.[3] The lengths used for the diffusion paths toward the downstructure wells have been estimated with the aid of the field map, Fig. 1.

The computations are summarized in the table below.

1. Well No.	6	7	8	9
2. Gas-oil ratio, cu ft/bbl = G	350	225	205	134
3. Gas concentration ratio, $Y = (467\text{-}G)/467$	0.25	0.518	0.56	0.713
4. Horizontal distance (Fig. 1) from oil-water contact to well, ft = a	3440	3020	1780	1200
5. Horizontal distance from oil-water contact to sea level contour = b	4970	7040	4970	4970
6. Position ratio $n = a/b$	0.692	0.430	0.359	0.242
7. Angle of dip (Fig. 1), degrees	20	12	20	20
8. Inclined distance from sea level contour to oil-water contact, ft = R	5280	7190	5280	5280
9. R^2, ft^2, x 10^{-6}	27.9	51.9	27.9	27.9
10. X (from Y and $n^{1,2}$)	0.33	0.30	0.32	0.22
11. Diffusional time = $X\ R^2/D$ years x 10^{-6}	21.4	36.2	20.8	14.3

It will be noted from the last line in the table that the times required for diffusion are long, of the order of 15-40 million years, and are not incompatible with the hypothesis that gas diffused downstructure from the crestal region of high gas concentration throughout the geologic time elapsed since trap formation, without reaching complete equilibrium in the time available.

Several other possible explanations for the observed variation in composition of the petroleum in the Elk Basin Field have also been considered. In all cases they can explain only relatively small variations in composition. For example, Sage and Lacey[4] have computed for a similar reservoir the variation expected because of gravitational segregation. They found that, over as much as 2,000 ft of closure, the expected variation for methane was only about 1/20 of the average amount of methane in solution. This explanation obviously would not account for the differences observed at Elk Basin.

Considering, finally, the possibility of segregation due to temperature difference between the top and bottom of the oil column, Sage and Lacey[5] have found that the change in solubility of natural gas expected with a temperature change of from 120°F to 140°F was also about 1/20 of the total gas solubility.

Apparently considerations other than the assumption of incomplete attainment of equilibrium lead to the conclusion that comparatively little variation in petroleum composition should be observed in a reservoir at equilibrium, even though its closure extends over several thousand feet. This conclusion is demonstrated by the existence of a number of oil reservoirs having a large closure, but whose petroleum is of substantially uniform composition. Therefore, when a considerable variation in composition is encountered, as at Elk Basin, a satisfactory explanation may be incomplete diffusional approach toward equilibrium.

REFERENCES

1. Gurney and Lurie: *Ind. Eng. Chem.*, (1923) **15**, 1173.
2. McAdam: *Heat Transmission*, p. 30ff, New York, (1933), McGraw-Hill.
3. Arnold: *J. Am. Chem. Soc.*, (1930) **52**, 3943ff.
4. Sage and Lacey: *Trans.* AIME (1939) **132**, 120.
5. Sage and Lacey: *Ind. Eng. Chem.*, (1936) **28**, 249.

DISCUSSION

By Michael J. Rzasa, Stanolind Oil and Gas Co., Tulsa, Okla., Member AIME

Espach and Fry are to be commended on publishing material which shows the change in physical characteristics of crude oil in a unit reservoir with elevation. However, there are several statements and conclusions in their paper which are worthy of attention.

In Table III, the authors have shown the hydrogen sulfide content of liberated gas from oil samples from Well No. 1. These data show that during the first pressure increment of 1,250 to 835 psia, the hydrogen sulfide content of the gas decreased from 7.6 to 5.1 per cent. Inspection of equilibrium vaporization constants for hydrogen sulfide would indicate that these results are to be expected in the particular pressure range under consideration. As further expected, the hydrogen sulfide content of further gas increments increases with pressure reduction. I am not sure what the authors mean by stating that the hydrogen sulfide content of the gas from the oil in the upper part of the reservoir would increase with pressure decrease, provided the gas-oil ratio during production did not exceed that in solution in the oil, and that increasing gas-oil ratios would result in decreasing the hydrogen sulfide content of the produced gas, because any volume of gas in excess of that in solution in the oil will contain smaller percentages of hydrogen sulfide than the solution gas. The amount of hydrogen sulfide which will come out of solution with pressure decrease is determined not only by the absolute amount of oil which releases this gas, but also by the vaporization characteristics of hydrogen sulfide. Since all the other components in the released gas will increase in absolute amount as the producing gas-oil ratio increases, it would seem to me that the hydrogen sulfide content would not necessarily decrease, but would appear in approximately the same proportion as given in Table III.

One point of great significance is the statement of the authors that their work proves that equilibrium in the Elk Basin Sand has not been attained. This conclusion is based on the fact that the physical characteristics of the oil from the deeper wells differ considerably from those upstructure. The change in elevation between Well No. 1 and Well No. 9 is approximately 1,750 ft. The very fact that there is this change in physical characteristics of the oil with change in elevation shows that the conclusion reached by the authors is incorrect. Thermodynamic equilibrium demands that this change in properties occur with change in elevation.

In ordinary engineering work it is customary to assume that pressure, temperature, and the composition of a phase are the independent variables sufficient to define the state of the system. This conclusion ignores gravitational and other types of energy associated with the system and it assumes that the pressure is uniform on the system. Stated in other words, when gravity is taken into account, the phase rule is no longer $f = c + 2 - p$, but becomes $f = c + 3 - p$.

Under equilibrium conditions, the chemical potential or molal free energy of all components must be equal to zero. It can be shown from thermodynamics that relationship exists between the change in composition of a fluid and change in elevation under isothermal conditions. Previous publication of calculations on a Dominguez Field crude oil show that for a change in elevation of 2,000 ft, the bubble point of the oil at 160°F changes approximately 885 psi. Furthermore, the isothermal effects indicating change in composition with elevation would be expected to be enhanced by a gradual increase in temperature as depth is increased.

With deeper depth, the crude oil will contain higher proportions of the heavier components and consequently a lower bubble point. With greater proportion of heavier components in a crude oil, the gas in solution and the relative oil volume will also decrease as depth from some datum is increased. Obviously, with increase in pressure the density of the oil will increase and the specific gravity of the gas in solution will also increase. These qualitative conclusions are borne out by the data published by Espach and Fry, and further substantiate the statement that thermodynamic equilibrium does exist at Elk Basin.

It would be of significance and value if the chemical composition of the crude oil at various elevations in Elk Basin were published as a part of this paper in order that such thermodynamic calculations can be made.

AUTHOR'S REPLY TO MR. RZASA

M. J. Rzasa's comment that change in composition of reservoir oil with elevation is to be expected at conditions of thermodynamic equilibrium is correct. This does not, however, make incorrect the conclusions reached by the authors. The magnitude of change reported in the Elk Basin study between the properties of the reservoir oil from Wells 1 and 9, with some 1,750 ft difference in elevation, is many times too great to be consistent with changes expected at conditions of thermodynamic equilibrium. Although changes in liquid composition of the reservoir oil were not available to be compared with the change of composition as defined by thermodynamic equilibrium, it is apparent upon examination of Sage and Lacey's[1] sample calculations, showing such small changes in composition, that equilibrium is not the explanation for the changes in properties of the original oil in the Tensleep Reservoir of the Elk Basin Field. This is substantiated further by a study of the properties versus structure of the original reservoir oil in the Weber Reservoir of the Rangely Field, Colo.[2] The Weber sandstone at Rangely and the Tensleep sandstone at Elk Basin are geologically equivalent formations. Labora-

Table V — Composition as a Function of Depth, Based on Subsurface Oil Samples from the Weber Sandstone Reservoir, Rangely Oil Field, Colo.

	Depth, ft[1]	Butanes and lighter, mol per cent liquid	Pentanes and heavier, mol per cent liquid
	0	44.29	55.71
	840	30.57	69.43
Change:	840	–13.72	+13.72

[1] Measured from gas-oil interface.

tory analyses of reservoir oil sampled at Rangely provided nearly identical change in oil properties, solution gas/oil ratio, saturation pressure, etc., per foot change of reservoir elevation with the change reported for the Elk Basin study. Considerably more data on composition of the reservoir oil were obtained for the Rangely samples, so that the change in composition of the reservoir oil samples might be compared with calculated change at conditions of thermodynamic equilibrium in the reservoir.

The change in mol per cent liquid composition of the butanes and lighter fraction of the reservoir oil calculated by use of equations defining thermodynamic equilibrium is shown in Table VI. This change will account for only one fourteenth of the actual change found by sampling, as shown in Table V. For the single component methane in the liquid phase, the calculated change was only one thirtieth of the actual change found by sampling. It is difficult to reconcile the magnitude of change of reservoir oil properties with elevation found at both Rangely and Elk Basin with conditions of the thermodynamic equilibrium. It is thought that the small changes in composition of the reservoir oil defined by thermodynamic equilibrium fix the limit toward which the Elk Basin Reservoir oil was approaching, but had certainly not reached at the time of discovery.

Table VI—Composition as a Function of Depth, Based on Calculated Effect of Gravitational Concentration of Components for the Weber Sandstone Reservoir Oil, Rangely Oil Field, Colo.

	Depth, ft[1]	Butanes and lighter, mol per cent liquid	Pentanes and heavier mol per cent liquid
	0	44.29	55.71
	840	43.35	56.65
Change:	840	− 0.94	+ 0.94

[1] Measured from gas-oil interface.

We believe that the change of 885 psi in bubble point as calculated by Rzasa from Dominguez crude oil data and due to 2,000 ft change in elevation at thermodynamic equilibrium is in error and that these data indicate a change of about 70 lb.

A few comments will be made to clarify the percentage hydrogen sulfide content of gas produced from wells as reservoir pressure declines. In Fig. 6 the upper curve is the percentage hydrogen sulfide content of the solution gas versus pressure as taken from Fig. 2 of the subject paper. A reservoir oil sample taken when the reservoir pressure is at any value between 1,880 psia (original pressure) and 1,250 psia (saturation pressure), when differentially liberated to atmospheric pressure, will yield solution gas of quantity equal to the solution gas/oil ratio at 1,250 psia pressure. This gas will contain 18.2 per cent hydrogen sulfide. A reservoir oil sample taken at any lower pressure, for instance, 600 psia will yield solution gas of quantity equal to the solution gas/oil ratio at 600 psia, and this gas will contain 23.7 per cent hydrogen sulfide. If the produced gas/oil ratio were only the solution gas/oil ratio, the percentage hydrogen sulfide would follow the upper curve of Fig. 6 as the reservoir pressure declines.

The lower curve of Fig. 6 is the hydrogen sulfide content of liberated gas. It is the information of Table III of the subject paper plotted versus mid-point pressures. This curve provides the percentage hydrogen sulfide content of a differential quantity of gas liberated from the reservoir oil sample for a small pressure decline. For example, as the pressure declines from 725 psia to 625 psia, gas will be liberated in a quantity equal to the difference in the solution gas/oil ratios at the two pressures and of approximately 5.9 per cent hydrogen sulfide content. This gas will be liberated in the reservoir.

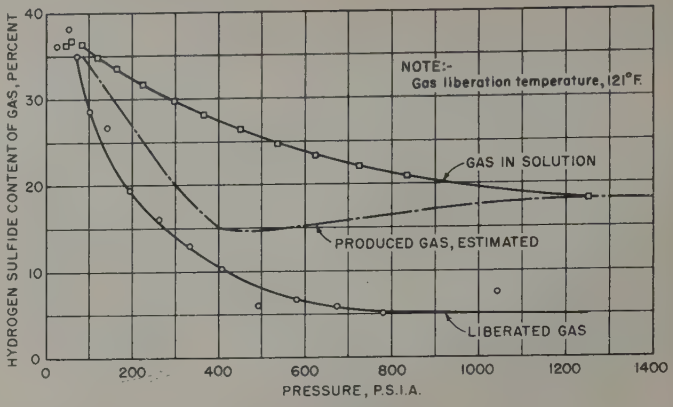

FIG. 6 — ESTIMATE OF PERCENTAGE HYDROGEN SULFIDE CONTENT OF PRODUCED GAS FROM WELL 1, ELK BASIN FIELD.

If some of this free gas is produced from the reservoir in addition to the reservoir oil, the produced gas at the wellhead will be a mixture of solution gas from the reservoir oil and free gas from the reservoir. It is obvious that the percentage hydrogen sulfide in the produced gas will be reduced from the values of the upper curve of Fig. 6 by the free gas produced from the reservoir. A qualitative estimate of the variance of percentage hydrogen sulfide content of the produced gas with reservoir pressure is made in Fig. 6. The values trend away from the upper solution gas curve as free gas produced from the reservoir accounts for increasing percentages of the produced gas/oil ratios. This will occur as reservoir pressures are reduced from saturation pressure and will continue until the produced gas/oil ratios reach a maximum value. As the pressure is further reduced and the produced gas/oil ratios decline, the values will trend toward the upper "solution gas" curve. It is true that for the period of production characterized by extremely high produced gas/oil ratios the values will be nearly equal to the lower or "liberated gas" curve or the values of Table III of the subject paper. For the initial portion of the pressure decline the values will be more nearly equal the values of per cent hydrogen sulfide of the "solution gas" curve.

REFERENCES

1. Sage, B. H., and Lacey, W. N.: *Trans.* AIME, (1939), 132, 120.
2. Cupps, C. Q., Lipstate, P. H., Jr., and Fry, J.: U. S. Bureau of Mines Report of Investigations 4761, (1950). ★ ★

T.P. 3021

RELATIVE PERMEABILITY TO LIQUID IN LIQUID-GAS SYSTEMS

L. A. RAPOPORT AND **W. J. LEAS,** MEMBER AIME, THE CARTER OIL CO., TULSA, OKLA.

ABSTRACT

As a preliminary, consideration is given to the conventional definition of relative permeability and to the conditions governing the simultaneous flow of oil and gas through porous media.

For the conditions of flow prevailing throughout most of a gas drive reservoir, the oil and gas can reasonably be supposed to be in capillary equilibrium with each other. Under these conditions, and these conditions only, the relative permeability to liquid can be expressed as a function of saturation. The relative permeability to liquid in that case is dependent upon the distribution of fluids which itself is shown to be related to the capillary pressure, and, in turn, to the saturation. As a consequence, relative permeability to liquid can be expressed in terms of the volume and surface area of a network of liquid channels bounded by the rock and the gas phase. While the volume of this network can be evaluated accurately, the surface area cannot. However, for any such volume, maximum and minimum values of the corresponding surface area can be calculated from capillary pressure data. It is then possible to establish for any saturation the limits within which the value of the relative permeability to liquid must lie.

As a consequence of the theoretical development, the validity of an experimental method for measuring relative permeability to liquid which utilizes a stationary gas phase is demonstrated. In this method capillary barriers are cemented to the ends of the core sample to permit the maintenance of capillary equilibrium between the two phases. At the same time, this procedure eliminates undesirable secondary phenomena such as end effects, fissure effects, etc., the presence of which adversely affect the results of other laboratory methods.

The results obtained by theoretical calculations, and experimentally, are discussed. In view of the overall precision that can presently be obtained in reservoir calculations, the agreement between the calculated and measured relative permeability to liquid data can be considered satisfactory.

In conclusion, for reasons of economy and simplicity, the procedure of calculating limiting relative permeability to liquid curves from capillary pressure data is indicated for general engineering purposes. It is shown that the above procedure can easily be extended to the cases where connate water is present. Its use for reservoir studies is particularly recommended in conjunction with the method for measuring relative permeability to gas[1] which simultaneously yields the capillary pressure data necessary for the calculations.

THEORETICAL

Definition of Relative Permeabilities — Basic Equations for Heterogeneous Flow

The equations by which the relative permeability concept is defined and upon which the formulation of all of the gas-oil flow problems rests at the present time are expressed as:

$$V_L = \frac{k_L}{\mu_L} \text{ Grad } P_L = \frac{k\,K_L}{\mu_L} \text{ Grad } P_L \quad . \quad . \quad . \quad . \quad (1a)$$

$$V_G = \frac{k_G}{\mu_G} \text{ Grad } P_G = \frac{k\,K_G}{\mu_G} \text{ Grad } P_G \quad . \quad . \quad . \quad . \quad (1b)$$

where $_L$ and $_G$ refer to liquid and gas; V is the volumetric rate of flow per unit gross area, μ the viscosity, Grad P the potential gradient, and k the specific permeability of the porous medium.* (For horizontal flow, Grad P becomes the pressure gradient; otherwise, gravity must be included.) According to these expressions, each of the constituent phases is considered similar to a homogeneous system where the volumetric rate of flow is proportional to the pressure gradient, and for each of which the constants of proportionality, k_L and k_G, are termed effective permeabilities, by analogy to the specific permeability as defined by Darcy's law in its original form. In order to obtain a convenient basis of comparison, the effective permeabilities are referred to the specific permeability, k, of the considered porous medium, with the help of the relations:

$$\begin{aligned} k_L &= K_L\ k \\ k_G &= K_G\ k \quad . \quad . \quad . \quad . \quad . \quad . \quad . \quad . \quad . \quad . \quad (2) \end{aligned}$$

K_L and K_G are defined as the relative permeabilities to the liquid and to the gas phase respectively, and frequently expressed in per cent of specific permeability. It may be seen that Equations (1), which appear to be a direct generalization of Darcy's law, correspond to the assignment at any given time of a set of "local" permeabilities to each point of the porous medium, and represent in a differential form the two fluid flow system as a simple superposition of the individual single flow systems.

The above interpretation implies that the effective or relative permeabilities are independent of pressure or rate of flow,

---

[1] References given at end of paper.

Manuscript received at the office of the Petroleum Branch Aug. 23, 1950. Paper presented at the Petroleum Branch Fall Meeting in New Orleans, La., Oct. 4-6, 1950.

*Nomenclature at the end of the paper.

an assumption which appears to be substantiated by most of the experimental results. It seems reasonable, therefore, to consider at first the relative permeability concept on the basis of the conventional assumption (suggested by experimental observations), that relative permeabilities are functions of saturation only. The theoretical and experimental methods presented in this paper are confined to liquid-gas systems, for which it can be shown that each phase taken separately satisfies the conditions under which Darcy's law applies.

ANALYTICAL EXPRESSION FOR SPECIFIC PERMEABILITIES

Until recently the specific permeability, *k*, such as defined by Darcy's original relation

$$V = \frac{1}{\mu} k \text{ Grad } P \qquad . \ . \ . \ . \ . \ . \ . \ . \ . \ (3)$$

had to be considered as a purely empirical characteristic. A theoretical expression for Darcy's law and an analytical interpretation of the specific permeability were established by J. Kozeny in 1926.[2] His theory is essentially based upon a statistically homogeneous and isotropic distribution of the pore voids. It excludes any other simplifying assumption such as representing the porous medium by bundles of capillary tubes or by layers of spheres, etc., and leads to the final equation

$$V = \frac{1}{\mu} \cdot \frac{f^3}{t\,A^2} \cdot \text{Grad } P \qquad . \ . \ . \ . \ . \ . \ . \ (4)$$

where *A* is the interstitial surface area per unit of bulk volume, *f* the porosity, and *t* a textural constant. By identification of Equations (3) and (4), it is possible to express the total permeability as

$$k = \frac{1}{t} \; \frac{f^3}{A^2} \qquad . \ . \ . \ . \ . \ . \ . \ . \ . \ . \ . \ . \ (5)$$

According to theoretical,[3] as well as numerous direct experimental results,[4,5,6,7] it appears possible to assign to the textural constant, *t*, the average value of 5, so that Equation (5) can be rewritten as

$$k = \frac{1}{5} \; \frac{f^3}{A^2} \qquad . \ . \ . \ . \ . \ . \ . \ . \ . \ . \ (6)$$

Up to the present time, direct experimental checks of the Kozeny equation had been carried out only for unconsolidated granular beds. However, with help of the thermodynamical approach presented in Appendix A, a more complete verification of the theory has been made. (See Appendix B.) It was found that on the average the values of permeability computed according to Equation (6) were within ±12 per cent of the corresponding experimental measurements. These results were established over the widest possible range of homogeneous core material, with permeabilities varying from 15 md to 17,000 md and porosities varying from 9.3 to 35 per cent. Its consistency can, therefore, be considered as a good confirmation of Kozeny's theory, as well as of the constant value to be assigned to the textural constant.

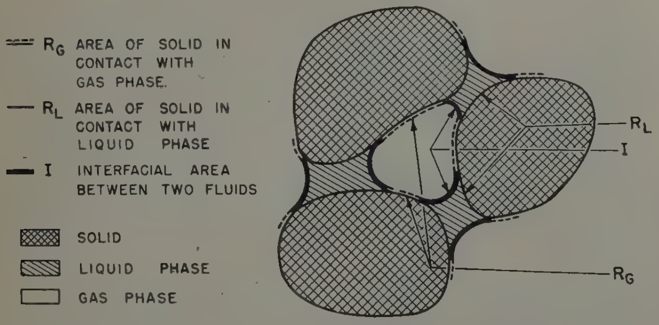
R_G AREA OF SOLID IN CONTACT WITH GAS PHASE.
R_L AREA OF SOLID IN CONTACT WITH LIQUID PHASE
I INTERFACIAL AREA BETWEEN TWO FLUIDS
SOLID
LIQUID PHASE
GAS PHASE
R_L
I
R_G

FIG. 1 — HYPOTHETICAL REPRESENTATION OF FLUID DISTRIBUTION IN RESERVOIR.

The important physical concept to be derived from Kozeny's theory is that the porous medium must essentially be considered as a "flow matrix" of irregular shape. All these irregularities do, however, statistically average so that the permeability is determined only by the inside area and volume as indicated by Equation (5). It is then possible to define the following conditions for the general application of Darcy's law, and for its extension to multiphase systems:

(a) Continuity of the pressure gradient, which requires the continuity of the flowing phase throughout the system.

(b) Microscopically steady flow pattern, *i.e.*, laminar flow — as opposed to turbulent or oscillatory regimes.

(c) Existence of a flow matrix defined by its inside surface area and volume per unit of bulk volume.

CORRELATION OF THE RELATIVE PERMEABILITY FUNCTIONS AND FLUID DISTRIBUTIONS

Fluid Distribution at Static Equilibrium

Since the specific permeability depends exclusively upon the structural properties of the porous medium, the study of relative permeabilities must include consideration of the spatial distribution of each of the phases.

When two fluids in a given proportion, or under given externally imposed conditions occupy a porous medium, their distribution at static equilibrium is determined by surface energy relations. These surface energy relations are best visualized with the help of the phenomena pertaining to interfacial tension and contact angle. The contact angle determines the curvature of the interface between two immiscible fluids which, under the influence of the interfacial tension gives rise to the capillary pressure. Under static conditions, stable equilibrium is attained when the external forces such as gravity, or artificially imposed pressure, upon one of the phases are balanced by those of capillary pressure. For a given capillary pressure (*i.e.*, to that which is required to balance the external forces) there is a corresponding curvature, the same for all the existing interfaces. Considering then the geometry of the porous medium, it is seen that for a given curvature, there must correspond a certain position of the interfaces, *i.e.*, a definite microscopic fluid distribution and a definite saturation. As a consequence, it can be anticipated that inside the porous medium each constituent phase has a definite geometrical form determined by the saturations.*

In order to obtain quantitative results based on the above descriptive picture, the thermodynamic aspects of the capillary equilibria must be considered. Stable equilibrium at a given saturation corresponds to the minimum level of free energy — in this case free surface energy — that can be reached. The first condition for stable equilibrium is that each of the constituent phases be continuous. Furthermore, in a two fluid system, the "wetting" fluid is the one which has the smaller tension of adhesion against the rock. Consequently, at stable equilibrium the wetting fluid has to be distributed in such a way as to cover always the greatest possible surface of solid. On the other hand, the non-wetting fluid will be distributed in such a manner as to cover the smallest possible surface of the solid, and, at the same time, to expose the smallest possible interfacial area to the wetting fluid. It may then be seen that for a gas-liquid system the liquid having a tendency to preserve the greatest contact area with the solid will always fill the smaller pore openings, whereas the gas remains in the larger ones.

---

*Such a relationship can exist only under conditions of stable equilibrium, since hysteresis phenomena exclude the possibility of defining capillary pressure in an unequivocal manner.

Fig. 1 illustrates in a schematic way the areas referred to above for which the following relationships can be established:

$A_L = R_L + I =$ Total surface area of the liquid (wetting fluid) system.

$A_G = R_G + I =$ Total surface area of the gas (non-wetting fluid) system.

$A = R_G + R_L =$ Total surface area of the solid system, *i.e.*, total grain surface. . . . . . . (7)

where R_L represents the contact area between the solid and the liquid, R_G the contact area between the solid and the gas, and I the interfacial area between the two phases.

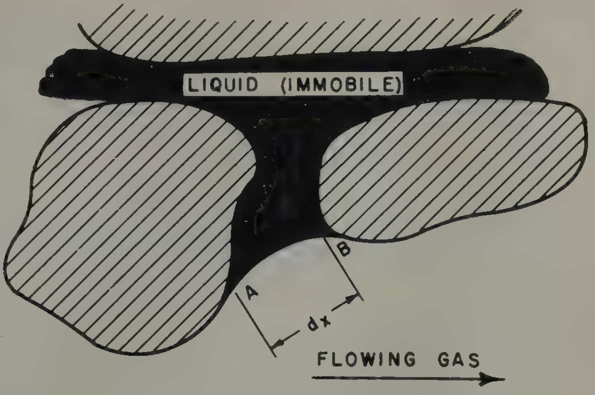

CAPILLARY PRESSURE AT A = P_C

CAPILLARY PRESSURE AT B = $P_C - \frac{\delta P_G}{\delta x} dx = P_C - dP_C$

FIG. 2 — EFFECT OF FLOW ON THE EQUILIBRIUM OF AN INTERFACE.

Extension of Static Fluid Distribution to Flow Conditions; Definition of Parallel Flow

At static equilibrium, the distribution of two fluids in a porous medium depends essentially on the position of the interfaces, and as long as the pressure drop across a given interface remains constant, neither its shape nor its position will be changed. If, starting from a given static capillary equilibrium, flow is produced, a pressure gradient giving rise to this flow is established in each phase. For each interface this "flowing" pressure gradient may be considered as a local disturbance that is superimposed on a previously existing static equilibrium of capillary forces. Hence, the pressure drop across each interface, instead of being constant, over the entire interface varies from one point to another (see Fig. 2). Each interface will, therefore, have a tendency to modify its position in such a way as to equilibrate the resultant effect of the previously existing static pressure and the superimposed pressure variation corresponding to the flowing pressure gradients. Under conditions of steady state flow, it may be visualized that each interface will establish itself in a position of "dynamic equilibrium." Theoretically, this position is different from that of static equilibrium; however, for the purpose of analysis it is admissible to treat that type of flow for which the "disturbing" action of the flowing pressure gradient is negligible. Such an approach is justified whenever the flowing pressure gradient is sufficiently small in comparison to the capillary pressure, which is actually the case under most of the practical field conditions.

The flowing pressure gradients that usually prevail over the greatest part of natural reservoirs have a maximum of some pounds per foot, for instance 10 psi/ft. The dimensions of the interfaces can be considered as being of the same order of magnitude as those of the pore openings, *i.e.*, 1/10 mm as a maximum (in homogeneous media). That means that the change in capillary pressure, dP_c, resulting from the flowing pressure gradient over the dimensions of a given interface will in the average not exceed 1/300 psi. The capillary pressure itself, however, that establishes across the interface, is usually of the order of one psi and certainly no less than 0.3 psi. Consequently, the ratio dP_c/P_c which indicates the relative importance of the local disturbance, can always be expected to be smaller than 0.01 and may, therefore, be neglected as far as the micromechanism of flow is concerned.

For reasons of simplicity, one of the fluids had been assumed to remain stationary. In most cases, however, both fluids are flowing in the same direction, so that the actual dynamic disturbance is due to the difference of the flowing pressure gradients and might be still smaller than indicated above.

The above example shows that when the flowing pressure gradients are an order of magnitude smaller than the capillary pressure, and when the flow originates from a condition of stable (static) capillary equilibrium, the distribution of the flowing fluids remains stable and the same as at static capillary equilibrium. The movement of the phases can then be visualized as if they were flowing in an independent manner through two interwoven but distinct networks of channels. These networks, bounded partly by rock and partly by the other fluid, can be considered as extending "in parellel" throughout the system. Such a situation will be referred to as "parallel flow." It is a generalization of the concept of laminar flow in hydraulics, which defines a steady state streamline pattern.

In the reservoir (and in many laboratory experiments), the liquid saturation generally decreases in the direction of flow; furthermore, there is usually an overall (slow) decrease of saturation with time. However, once it has been recognized that the perturbation due to flow is small enough so as not to modify locally the nature of the capillary equilibrium phenomena, one can consider this perturbation as a differential element causing the saturation and fluid distribution to vary as continuous functions of space and time. It is then always possible to divide the total space into sufficiently small portions for each of which rigorously parallel flow can be admitted, if sufficiently small time intervals are considered. It is concluded that any heterogeneous flow system can be treated as a succession in time and space of "elementary" parallel flows, if throughout the system the saturation varies in a continuous manner (with time and space) and capillary equilibrium is preserved.

ANALYTICAL EXPRESSION FOR RELATIVE PERMEABILITY TO LIQUID

Referring to the conditions of applicability of Darcy's law, it is readily seen that in the case of parallel flow, such as described above, Darcy's law can be extended to each of the constituent phases; hence, Equation (5) can be applied to the liquid phase in the following manner:

(a) The replacement of the absolute porosity, f, by Sf — the

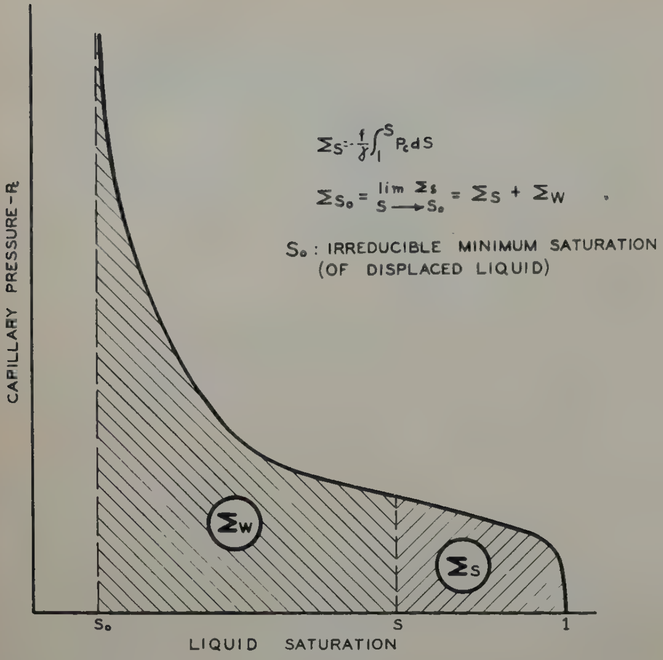

FIG. 3 — EXAMPLE OF CAPILLARY PRESSURE CURVE.

liquid filled pore volume per unit of bulk volume, *i.e.*, by the "effective porosity" with respect to the liquid.

(b) The substitution of the inside pore area, or total grain surface, A by A_L, which represents the total boundary area of the liquid phase "flow matrix."

By substitution of the above terms into Equation (5), the effective permeability to the liquid phase is obtained

$$k_L = \frac{S^3 f^3}{t\ A_L^2} \quad . . . . \quad (8)$$

and division of Equation (8) by Equation (5) gives the expression for relative permeability to liquid

$$K_L = \frac{S^3}{\left(\frac{A_L}{A}\right)^2} \quad . . . . \quad (9)$$

In order to obtain a more usable expression for the relative permeability to liquid, the following considerations must be taken into account. It is generally recognized that toward the end of a capillary displacement process an irreducible minimum saturation, S_o, is reached,[8] and no more liquid can be forced out, except by diffusion (the effects of which will be considered as negiligible in the present treatment). At this saturation the effective permeability to liquid becomes zero. Therefore, it seems logical to treat in first approximation the irreducible liquid as an essentially stationary element which reduces the porosity of the porous medium as well as the volume of flowing liquid. Once this liquid is considered as part of the solid framework, it is necessary to use an "effective" area, A_E, representing the surface that separates the flowing fluid from the immobile flow matrix composed of solid and stationary fluid, instead of the specific solid surface, A; furthermore, instead of using the total liquid saturation, S, a "reduced saturation," S', has to be introduced.

$$S' = \frac{S - S_o}{1 - S_o} \quad . . . . \quad (10)$$

On substitution into Equation (9) the following expression for the relative permeability to liquid is then obtained:

$$K_L = \frac{S'^3}{\left(\frac{A_L}{A_E}\right)^2} = \left(\frac{S - S_o}{1 - S_o}\right)^3 \left(\frac{A_E}{A_L}\right)^2 \quad . . . \quad (11)$$

It will be noted that the derivation of Equation (11) implies the two following assumptions:

(a) The molecular layers at the interfaces between solid/liquid and gas/liquid are stationary. If they were not, the basic Kozeny treatment should be slightly modified so as to take into account a certain "slippage" of the fluid on part of its boundaries.

(b) The textural constant of the wetting fluid "matrix" is the same as that of the total pore space. Such an approximation seems to be justified since in general the possible variations of the textural constant have been recognized to be comparatively small.

EVALUATION OF LIMITING RELATIVE PERMEABILITY TO LIQUID FUNCTIONS FROM CAPILLARY PRESSURE DATA

The calculation of K_L, the relative permeability to liquid, requires a knowledge of the surface areas, A_L and A_E. With the help of a thermodynamic approach indicated in Appendix A, the following expressions can be derived from a liquid/gas capillary pressure curve:

$$A_G = \Sigma_S = -\frac{f}{\gamma} \int_1^S P_c dS \quad . . . . \quad (12)$$

$$A_E = \Sigma_{S_o} = -\frac{f}{\gamma} \int_1^{S_o} P_c dS \quad . . . . \quad (13)$$

$$A_L = \Sigma_w + 2I = -\frac{f}{\gamma} \int_S^{S_o} P_c dS + 2I \quad . \quad (14)$$

in which the integrals indicate the areas under the P_c vs. S curves measured between the indicated limits (see Fig. 3). It is seen that a system of three equations is obtained for the four unknowns A_G, A_E, A_L, and I. Consequently, while the values for A_G and A_E are directly indicated, separate solutions cannot be defined for A_L or I.

In order to evaluate A_L, it is necessary to introduce an additional assumption concerning the distribution of the fluids. Such an assumption, expressed in terms of R_G, R_L, and I, will then represent one more independent equation, which together with the above relations will furnish a system from which all the unknowns can be solved. It might be recalled that on the basis of thermodynamic considerations only a more or less complex "trend" could be indicated for the liquid distribution, namely maximum contact area with the solid compatible with a minimum amount of interfacial area. In order to express such a trend in a more exact manner, it would be necessary to consider in detail the geometry of the porous medium, which depends on very many parameters such as grain size distribution, sphericity or shape factor of the grains, packing, consolidation, etc. Obviously, at the present time, it is impossible to treat such a geometrical complex in a general and precise way. Therefore, no exact additional relation can be established that would lead to unique solutions for A_L and I. The only logical approach that can be attempted consists of establishing the most general limiting conditions of fluid distribution that could be expected to apply to any, or at least to most, of the possible geometrical systems. According to such a principle, separate calculations for the minimum and for the maximum values of K_L will be shown.

Evaluation of Limiting K_L Minimum Function

In accordance with the previously established relations, Equations (7), (12), and (14), the following system of equations can be considered:

$$\Sigma_w = A_L - 2I \quad \ldots \quad (15)$$

$$\Sigma_S = R_G + I \quad \ldots \quad (16)$$

where Σ_S and Σ_w have a well defined value at any saturation and can, therefore, be considered as "constants" in regard to the unknowns A_L, I, and R_G. It is readily seen that according to Equation (15) for any set of Σ_S and Σ_w, *i.e.*, for any saturation, a maximum value will be obtained for A_L if I is maximum and that according to Equation (16) the maximum for I obtains if R_G is assumed to be zero. Consequently, the maximum value that A_L may take at any saturation is

$$A_L\ (\text{Max.}) = \Sigma_w + 2\ \Sigma_S = \Sigma_{S_o} + \Sigma_S \quad \ldots \quad (17)$$

According to Equation (11) it is clear that at any saturation the smallest possible value will be obtained for the relative permeability to liquid, K_L, if a maximum area, A_L, is considered, so that

$$K_L(\text{Min}) = S'^3 \left[\frac{A_E}{A_L(\text{Max})}\right]^2 = S'^3 \left[\frac{\Sigma_{S_o}}{\Sigma_{S_o} + \Sigma_S}\right]^2 . \quad (18)$$

Physically the derivation of K_L(Min) means that the distribution of the fluids is such as not to permit the existence of any contact between the gas phase and the solid surface. The gas can then be visualized as flowing inside a network of channels completely surrounded by liquid, as schematically represented in Fig. 4, and it might be noticed that such an assumption concerns only the disposition of the fluids, and does not correspond to any hypothesis about the geometry of the porous medium itself.

Evaluation of Limiting K_L Maximum Function

Referring to the system of Equations (15) and (16), it is seen that the theoretical absolute minimum value for A_L would obtain under the assumption $I = 0$, *i.e.*, $A_L = \Sigma_w$. Such a situation would correspond to $R_G = A_G$, *i.e.*, to the assumption of having the gas phase — and equally the liquid phase — bounded exclusively by solid surfaces. In that case, the porous medium should be visualized as formed by non-interconnected capillaries. It is clear that such an assumption is by far too limiting and leads actually to K_L values which are too high. Thus, instead of considering — even for the purpose of limiting conditions — a porous medium as equivalent to a bundle of capillary tubes, it is reasonable to represent it as an isotropic random packing of grains. Under this more general assumption, interfaces must exist between the gas and liquid, and none of the three surface areas, I, R_G, R_L is zero. The lowest possible value of the ratio I/R_G can then be evaluated. The use of this value in Equation (16) leads to a minimum value of I, of A_L, and consequently, to a maximum of K_L.*

With the help of general capillary pressure relationships, it is possible to show that

$$\frac{I}{R_G} > \frac{Sf}{1-f}\left(\frac{P_m}{P_c}\right)^2 \quad \ldots \quad (19)$$

where P_c represents the capillary pressure at any saturation, S, and P_m the mean value of P_c corresponding to the saturation range S to S_o. The above inequality leads to the following minimum value of A_L:

$$A_L(\text{Min}) = \left[\Sigma_w + \frac{2\ \Sigma_S}{1 + \frac{1-f}{Sf}\left(\frac{P_c}{P_m}\right)^2}\right] . \quad (20)$$

and the final expression for the limiting maximum relative permeability to liquid is then obtained as

$$K_L(\text{Max}) = S'^3 \frac{\Sigma_S{}^2}{\left[\Sigma_w + \frac{2\ \Sigma_S}{1 + \frac{1-f}{Sf}\left(\frac{P_c}{P_m}\right)^2}\right]^2} . \quad \ldots \quad (21)$$

EXPERIMENTAL

Principle of the Method

The experimental method has been conceived so as to measure the relative permeability to the liquid phase under the conditions of parallel flow defined previously. According to

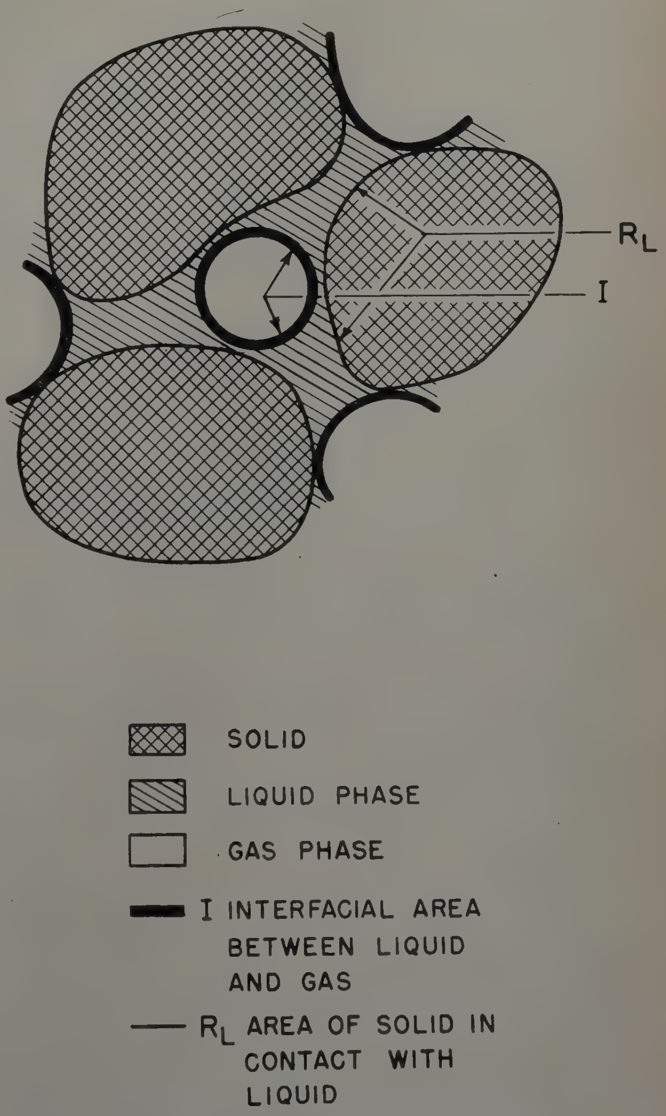
R_L
I
▩ SOLID
▨ LIQUID PHASE
☐ GAS PHASE
I INTERFACIAL AREA BETWEEN LIQUID AND GAS
R_L AREA OF SOLID IN CONTACT WITH LIQUID

FIG. 4 — SCHEMATIC REPRESENTATION OF COMPLETE GAS CHANNELING.

---

*The detailed treatment for the derivation of K_L maximum is indicated in Appendix C.

these conditions, capillary equilibrium must be maintained between the two phases throughout the entire core specimen. The main difficulty in obtaining such an equilibrium results mostly from different sorts of "end-effects," the influence of which extends back into the core. In the experimental method presented, the capillary pressure between gas and liquid is established by means of semi-permeable barriers, and controlled by the pressure imposed upon the gas. The elimination of secondary phenomena as outlined above is obtained by cementing the capillary barriers, permeable to liquid only, to each end of the core sample. The experimental procedure can then be outlined as follows:

(1) The ensemble of core and end plates is fully saturated with liquid.

(2) Through a central orifice in one of the end plates, gas is forced into the core and liquid is displaced through both the end plates until the system comes to equilibrium, *i.e.*, reaches a saturation which corresponds to the capillary pressure that has been imposed upon the gas.

(3) The liquid is then allowed to flow through the system, whereas the gas remains immobile, held back by the semi-permeable barriers. The flowing pressure gradient in the liquid is kept constant and sufficiently low so as not to disturb the capillary equilibrium and the previously established saturation.

(4) When perfectly steady state conditions are reached, the exact values of the pressure drop in the liquid over the length of the core sample and the rate of flow are determined. The effective and, consequently, the relative permeabilities are then obtained and plotted against the corresponding saturation.

Description of Experimental Apparatus and Procedure

The relative permeability to liquid cell is shown in Fig. 5. In general construction it resembles the relative permeability to gas cell[1] and many of the parts are interchangeable. Not shown in the diagram are the "O" ring seal between tube T3 and the porous plate, and the grooves in the face of the metal plates B1 and B2 for the distribution of liquid to the porous plates. These grooves ensure that the liquid phase is free to move unidirectionally through the core, thereby eliminating any divergent or convergent flow except in the immediate vicinity of the gas inlet tube T3. The ratio of the area of the end of this tube to the cross sectional area of the core is 1/64 so that any resulting perturbations in the flow pattern are negligible. Gas is admitted to the core through the tube T3, which is connected to a gas pressure source and to a manometer with which the pressure of the gas phase is measured. Liquid enters the cell through tube T1 and leaves through tube T2. These tubes are connected through a commutating valve to the flowmeter.

The flowmeter consists of two precision-bore calibrated glass tubes which are side by side in the same horizontal plane. The right end of one tube and the left end of the other are connected to a commutating valve. Liquid fills only a portion of each tube and the application of gas pressure to the gas-liquid interface in one of the tubes causes the liquid in that tube to flow through the core into the other tube. When the first tube is nearly empty of liquid, the gas pressure to that tube is released, the commutating valve is turned, and the gas pressure is applied to the second tube, which is now nearly full of liquid. It, in turn, is emptied and the liquid reappears in the first tube. This cycle can be repeated indefinitely and though sizable volumes of liquid can be passed through the core, only a few milliliters of liquid are required. The fact that the liquid-gas interfaces in the tubes are in the same horizontal plane eliminates any gravitational gradient in the liquid phase, and only the differential gas pressure acting on the interfaces needs to be measured to determine the pressure gradient causing flow in the liquid phase.

The commutating valve permits the reversal of fluid flow in the flowmeter tubes while maintaining at all times the same direction of flow within the core. A bleeder valve in one of the flowmeter lines permits the adjustment of the volume of liquid within the system. Since the two flowmeter tubes are parallel and of the same internal diameter, the two interfaces move at the same rate and in the same direction when liquid is flowing through the core under steady state conditions. By measuring the velocity of the interfaces and the differential gas pressure acting upon them, the effective permeability of the core under test can be calculated.

The flowmeter also indicates the amount of liquid expelled from the core. At the start of the relative permeability measurement the liquid saturation of the core is unity and the differential linear separation of the interfaces is noted. As long as the liquid saturation of the core remains fixed, the separation of the interfaces remains constant. When the gas pressure applied through the gas inlet tube T3 exceeds the threshold pressure of the core, liquid is expelled from the core and appears in the flowmeter tubes as a change in the separation of the interfaces. This permits the calculation of the liquid saturation of the core at any time. A scheme similar to this has recently been described.[9]

Several factors must be considered in the selection of the plates which function as semi-permeable barriers. Firstly, the

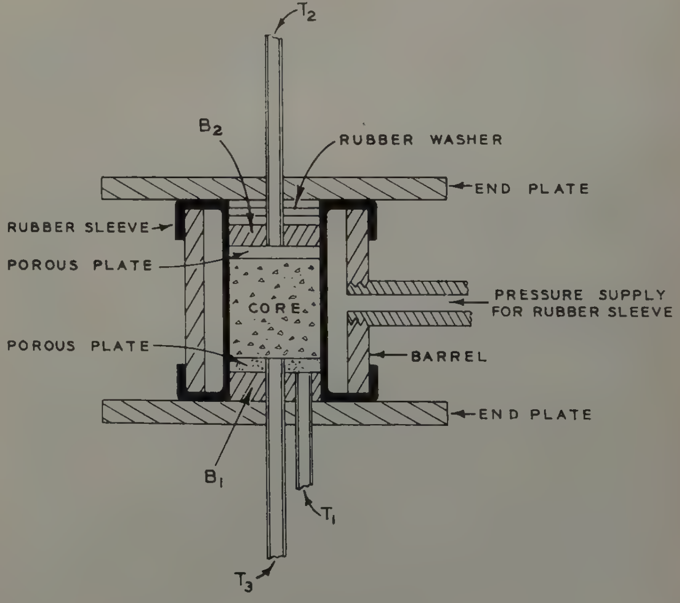

T_1 & T_2 = FLOW TUBES FOR LIQUID PHASE
B & B_1 = BACKING PLATES
T_3 = TUBE FOR GAS PHASE

FIG. 5 — RELATIVE PERMEABILITY CELL.

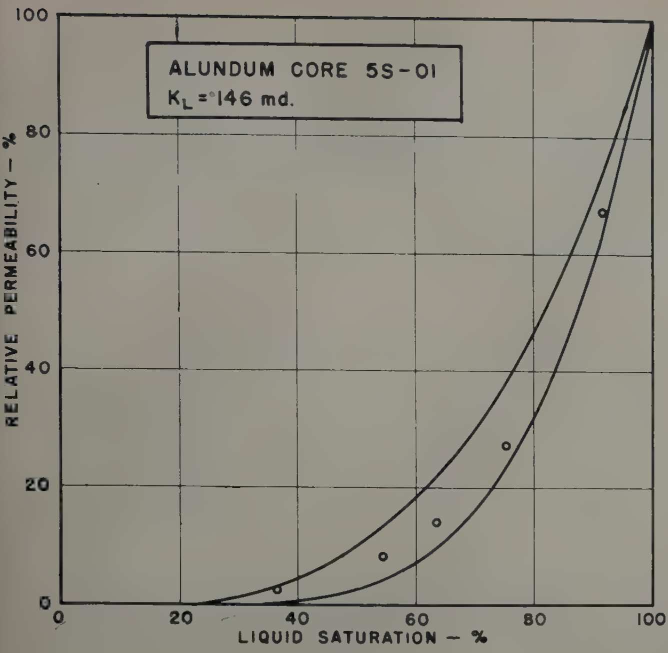

FIG. 6

pore size of the plates must be such that they remain fully saturated with liquid at all gas pressures to which they are exposed. Secondly, they must have as high a transmission coefficient to liquid as is possible (in conformity with the first requirement) so that changes in the relative permeability of the core will not be unduly suppressed. This can, in part, be accomplished by using thin plates, yet they must remain thick enough to withstand breakage. The elimination of undesirable "fissure effects" is accomplished by cementing the plates to the core.

After the core to be tested has been cut to shape and extracted, its pore volume and permeability (to n-decane) are measured. It is dried and the porous end plates are cemented in the following manner. The core and plates are fully saturated with water. A plaster of Paris slurry is spread over one side of the outlet plate, which is pressed against the end of the core to expel the excess plaster of Paris.* The core with outlet plate is dried and its permeability to n-decane is measured. It is redried and the inlet plate is cemented in the same manner as was the outlet plate. The ensemble is then put into the cell where its liquid permeability is determined at a liquid saturation of unity.

Air, under pressure, is then admitted to tube T3 and a portion of the liquid in the core is expelled into the flowmeter. When equilibrium is reached, the differential separation of the interfaces in the flowmeter tubes becomes zero and the permeability of the ensemble at a liquid saturation less than unity is measured. The air pressure in T3 is again increased and the cycle is repeated until the permeability of the ensemble falls to a value too low to be measured. From these measurements the effective permeability of the core and end plates is obtained, and the relative permeability can then be determined for each corresponding liquid saturation.

RESULTS AND DISCUSSION

Results

The results obtained with n-decane and air using three alundum cores and three natural cores are shown in Figs. 6 to 11. The solid curves are the limiting K_L values calculated from displacement data obtained on these cores using a single-core displacement cell[10] with decane displaced by air. The limiting curves for the three alundum cores are much the same. This is to be expected since their capillary pressure curves were similar. With the exception of two points on Core 59A-15, the data fall within the limiting values. The agreement between the calculated and experimental data for the alundum cores is good for each core.

In considering the three natural cores, it is seen that the limiting K_L values vary widely both as to position and spread. Here again their position is determined by the shape of the capillary pressure curve. Generally, it has been observed that a capillary pressure curve of near zero slope which undergoes a sharp transition to a vertical slope at the minimum saturation results in a large spread between the calculated K_L limits, whereas capillary pressure curves which have an appreciable slope even at high liquid saturations usually result in a very narrow spread of the limiting K_L values. Considering the narrow spread, the agreement is good for the Bohanon core. Three runs were made on the Elk Basin core and the results cluster about the lower limiting curve. No single run has points which lie either entirely above or below the lower curve. The Bartlesville core has narrow limits and the experimental data which seem to be slightly S-shaped fall partly outside the limits. On the whole, the agreement obtained with the alundum cores is better than that obtained with the natural cores. Although the exact reasons for this are not known, it is possible that the higher degree of homogeneity of the alundum cores is a contributing factor.

Although K_L results obtained by the Botset[11] and "Penn State"[12] methods might be regarded as questionable,[13] their rather extensive use warrants their mention. The results ob-

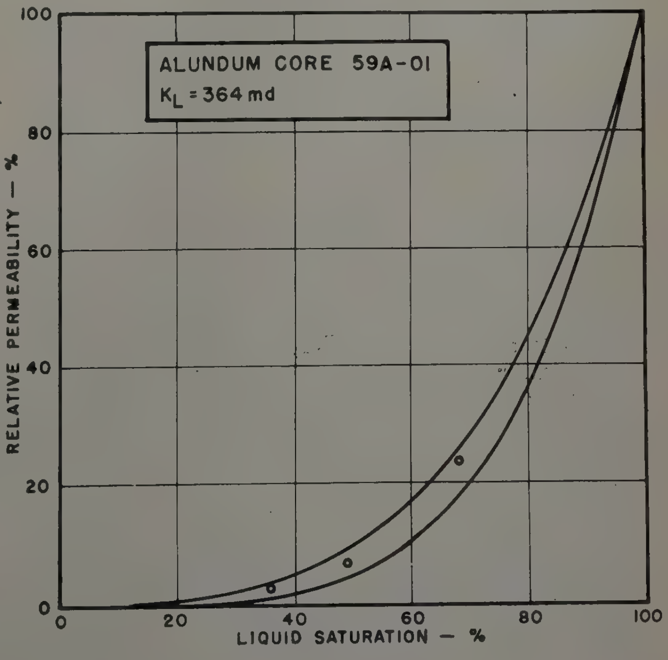

FIG. 7

---

*This procedure of saturating the core prior to affixing the plates minimizes the possibility of plugging the core through movement of the plaster slurry into the core if it were applied to a dry core. The liquid permeability of a core whose porous plates were attached in this manner was found to be unchanged after their removal.

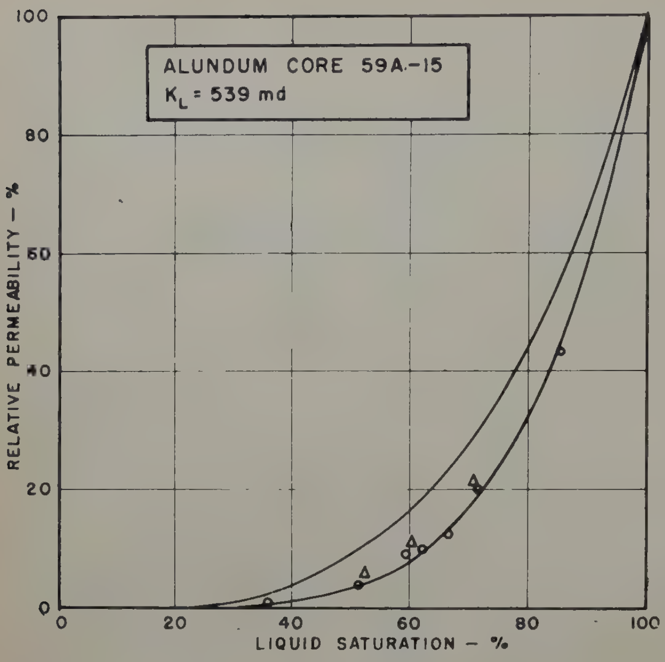

FIG. 8

tained by these methods on an unconsolidated sand and on a synthetic sandstone are shown in Figs. 12 and 13. The experimental points show greater scattering, which might be expected since no difference in pressure exists between the phases, so that appreciable "end effects" can be anticipated. The majority of the points, however, lie within the calculated limits.

DISCUSSION OF THE RESULTS

Validity of the Parallel Flow Concept

The theoretical and experimental methods presented in this paper for the determination of relative permeability to liquid are confined to the strict consideration of parallel flow mechanisms, *i.e.*, to the case where the flowing fluids remain in capillary equilibrium with each other. In most practical instances, it is recognized that parallel flow may be "perturbed" by secondary phenomena, mainly the release of gas bubbles. Such bubbles do not correspond to capillary equilibrium, and furthermore, cannot be subject to laminar flow. It can be anticipated, however, that in any point of the reservoir the existence of separate gas bubbles corresponds to a relatively short transient stage. Due to rapid diffusion effects and possible mechanical transportation, the separate bubbles have the tendency to reach stable capillary equilibrium and to merge into a continuous gas body. Recent experiments performed in this laboratory have indicated that (under atmospheric conditions) the time required in order to reach phase continuity — and consequently capillary equilibrium — is of the order of 24 hours.

It is clear that the formation of a continuous gas phase becomes possible only after a certain minimum amount of bubbles, corresponding to the "equilibrium gas saturation" has been released from solution. The phenomenon of equilibrium gas saturation must be considered as a determining factor for the flowing behavior of the gas phase, and it is for that reason that a theoretical derivation of the relative permeability to gas function has not yet been presented. For the liquid phase, the continuity of which can always be expected to be uninterrupted, it is however, a reasonable approximation to derive the relative permeability function under the assumption that capillary equilibrium exists throughout the entire range of saturation. Accordingly, for most practical purposes the use of the parallel flow concept and the application of the presented methods appears to be justified in the case of any liquid-gas flow system.

Discussion of the Experimental Method

In the presented experimental technique, undesirable features of other methods have been overcome. The use of cemented porous end plates permits the maintenance of a pressure difference between the gas phase and the liquid phase, and eliminates end effects and fissure effects. These latter correspond to a progressive invasion by the gas phase of the microscopically large voids which exist between the core and porous plates (or two adjacent core sections) as shown by direct-X-ray measurements.[14] Furthermore, there is no distortion of the flow pattern from linear flow since at the ends of the core there are no pressure taps or sizable areas for gas flow. The determination of the pressure gradient is subject to unequivocal measurement and is effective over the complete length of the core.

In the tests run by this method, the pressure gradients did not exceed a few centimeters of water. Under such conditions the use of an immobile gas phase is justified insofar as the theoretical discussions have shown that the relative permeability to liquid so obtained can be expected to be the same as though both phases were flowing.

It is recognized that due to the immobility of the gas, a saturation distribution exists throughout the core. The procedure of plotting directly the measured relative permeability of the core against its average saturation might, therefore, be subject to a systematic error. However, the small pressure

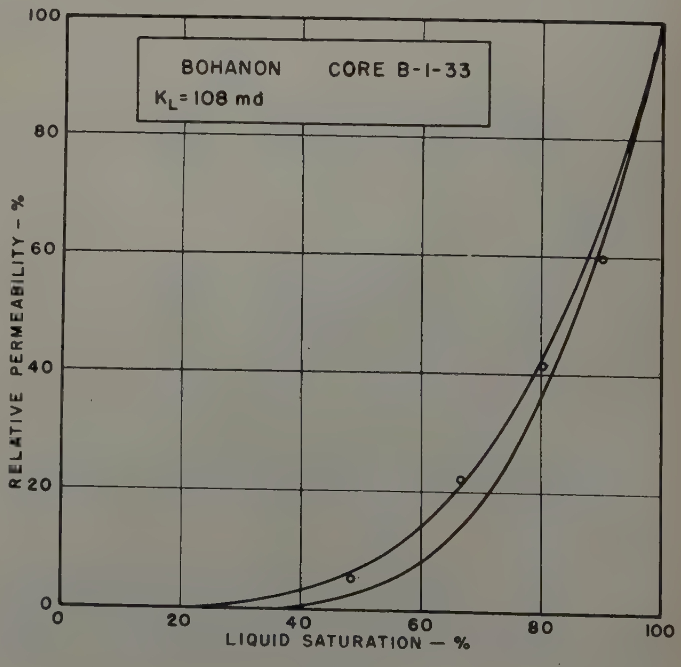

FIG. 9

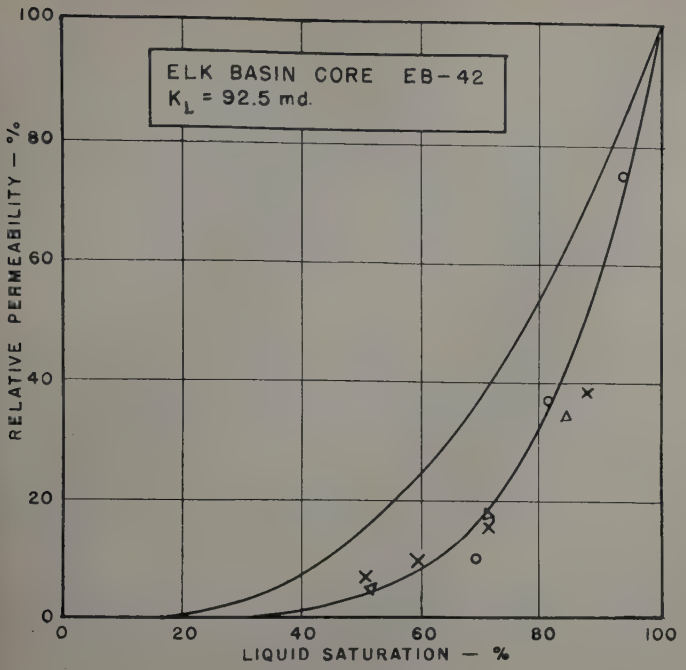

FIG. 10

gradients and rates of flow used in the present experiments preclude a large correction. To verify this, the points *x* in Fig. 10 were obtained using a pressure gradient which was twice that used for the other points. These points therefore correspond to a steeper saturation distribution. Since, however, the agreement between all the runs is very close, it appears that at the rates of flow used, the effect of any saturation distribution is very small.

Under identical experimental conditions, two separate runs were made using cores 59A-15, Fig. 8, and EB-42, Fig. 10. The results of the first run are indicated by circles and the second by triangles. All points lie within a narrow band no wider than would be expected on the basis of normal experimental deviations, so that the reproducibility of the method can be considered as satisfactory.

Validity of the Calculated Data

Since the limiting K_L functions are expressed essentially by the cube of the "reduced" saturation, $S' = S - S_o/1 - S_o$, they are very sensitive to the variations of the parameter, S_o, in the regions of low saturations, *i.e.*, when S approaches S_o. The determination of the proper irreducible minimum saturation, S_o, to be used in the calculations is comparatively delicate in view of diffusion effects, which can be quite important in liquid/gas systems. Both calculated limiting K_L curves might, therefore, be subject to a systematic error, namely too high, in the regions of low saturation, since the diffusion effects cause an apparent decrease of S_o. This effect is apparent in Figs. 8 and 10, and has been observed in several other instances.

The limiting K_L curves presented in this report were calculated from decane/air P_c curves. Although this is justified for the purpose of checking the calculated results against the direct K_L measurements (which were obtained on decane-air systems), the procedure should be slightly modified for practical application. It is necessary to take into account the possibility of swelling clay minerals frequently contained in natural cores. Strictly speaking, the calculations should, therefore, be based upon P_c curves obtained by the displacement of decane (or any other suitable hydrocarbon) by air in the presence of connate brine. However, it can be anticipated that sufficiently reliable results will be obtained by simply using the brine/air displacement curves that are usually available. Justification for such a procedure is indicated by recent experimental determinations of relative permeability to gas, which yielded practically identical results with and without having a "connate" liquid phase present.[1]

The fact that instead of calculating a unique K_L function, only limiting curves are determined, might be examined in the light of the overall degree of precision that can be obtained by the present techniques. In many cases it can be observed that the spread between the experimental data is of the same order of magnitude as that of the theoretical curves. Furthermore, in view of the sampling problems associated with petroleum reservoirs, the present need is actually for approximate data on a large number of reservoir cores rather than precise data on only a few. In many practical instances, the use of the theoretical limiting K_L curves might, therefore, be desirable. Engineering calculations can be carried out either by using separately the upper or the lower curve, or by constructing the average curve and determining (by comparison to the limiting curves) the maximum error introduced.

CONCLUSIONS

From the foregoing work the following conclusions are drawn:

(1) By means of a theoretical analysis of fluid micro-behavior, it has been shown that the relative permeabilities needed

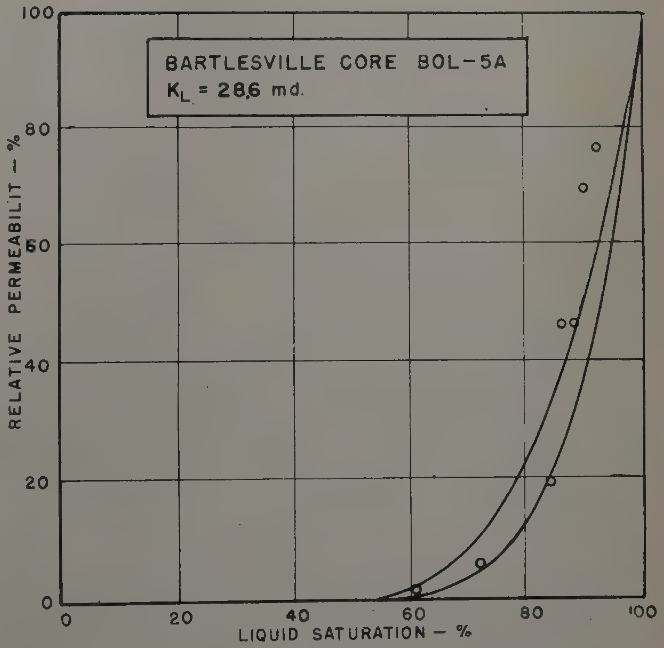

FIG. 11

for studies of liquid-gas reservoirs are directly related to the distribution of fluids and must primarily be functions of saturation.

(2) A procedure for calculating limiting K_L curves from capillary pressure data has been established. The possibility of applying the calculated curves to the case where connate water is present has been indicated.

(3) An experimental method based upon the use of cemented capillary barriers and upon the principle of an immobile gas phase has been developed for measuring the relative permeability to liquid. It has been shown that in the above method the undesirable phenomena such as end effects, fissure effects, etc., common to other types of procedures, have been eliminated.

(4) The general validity and the comparative simplicity of the experimental method have been demonstrated. It has been found that good agreement exists between the experimental and calculated data.

(5) For reasons of economy and simplicity, the calculation of limiting K_L curves seems indicated for routine engineering purposes. It is particularly recommended for use in conjunction with a method developed previously for determining relative permeability to gas,[1] which yields K_G and P_c data simultaneously.

ACKNOWLEDGMENT

The authors wish to thank the Carter Oil Co. for permission to publish this paper. They are particularly indebted to W. A. Bruce and Charles D. Russell for their valuable suggestions and helpful assistance during the course of this research and in the preparation of this report, and to Miss J. J. Hume for much of the experimental data and calculations.

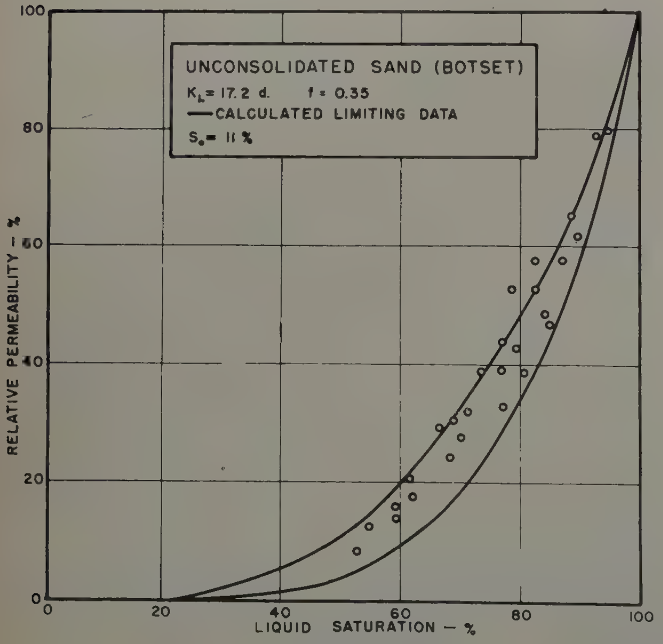

FIG. 12

NOMENCLATURE

(Symbols by Order of Appearance)

Usual Subscripts: L refers to liquid
G refers to gas
I refers to interfaces
S refers to saturation

V — Volumetric Rate of Flow per Unit Cross Sectional Area
k — Specific or Effective Permeabilities
K — Relative Permeability
P — Pressures
μ — Viscosity
f — Porosity
t — Textural constant
A — Total Boundary Areas (in cm^2 per cm^3 of bulk volume)
I — Interfacial Surface Area Between Liquid and Gas (in cm^2 per cm^3 of bulk volume)
R_L — Contact Area Between Liquid and Solid (in cm^2 per cm^3 of bulk volume)
R_G — Contact Area Between Gas and Solid (in cm^2 per cm^3 of bulk volume)
P_c — Capillary Pressure
S — Liquid Saturation
S_o — Irreducible Minimum Liquid Saturation as Obtained from Capillary Pressure Curve
S' — Reduced Liquid Saturation
Σ — Areas Under the Capillary Pressure Curve Times the Quantity – (f/γ)
γ — Interfacial Tension Between Liquid and Gas
F — Free Surface Energy
θ — Contact Angle of Liquid Against Solid in presence of Gas

REFERENCES

1. Leas, Jenks and Russell: *Trans.* AIME, (1950) **189**, 65.
2. Kozeny, J.: *Ueber Kapillare Leitung des Wassers im Boden*, Berichte der Wiener Akademie, (1927) **136A**, 271-306.
3. Fowler, J. L., and Hertel, K. L.: "Flow of Gas Through Porous Media," *Jour. of Applied Physics*, (1940) **11**, 496-502.
4. Schriever, Wm.: *Trans.* AIME, (1930) 329-336.
5. Traxler and Baum: *Physics*, (1936) **7**, 9-14.
6. Carman, P. C.: *Trans.* Inst. Chem. Engr., (1937) **15**, 150-166.
7. Coulson: University of London Ph.D. Thesis, "The Streamline Flow of Liquids Through Beds Composed of Spherical Particles," (1935).
8. Levertt, M. C.: *Trans.* AIME, (1941) **142**, 152.
9. Brownscombe, Slobod and Caudle: "Laboratory Determination of Relative Permeability," *Oil and Gas Journal*, Feb. 9 and 16, 1950.
10. Rose and Bruce: *Trans.* AIME, (1949) **186**, 127.
11. Wyckoff and Botset: "The Flow of Gas-Liquid Mixtures Through Unconsolidated Sands, *Physics*, (1936) **7**, 325.
12. Morse, Terwilliger and Yuster: "Relative Permeability Measurements on Small Core Samples," Mineral Industries Experiment Station, Technical Paper 124, Pennsylvania State College.
13. Henderson and Meldrum: "Progress Report on Multiphase-Flow Studies," *Producers Monthly*, (March, 1949).

14. Morgan, McDowell and Doty: *Trans.* AIME, (1950) **189**, 183.
15. King, F. H.: "Principles and Conditions of the Movements of Ground Waters," *U. S. Geol. Survey*, (1897, '98), **2**, 192.
16. Darapsky, Zeitschr: *Math. Phys.*, (1912) **60**, 170.
17. Siegel: *Der Chemie Ingenieur*, (Liepzig, 1933) **1**, Part 2.
18. Kozeny, J.: "Die Durchlässigkeit des Bodens," *Kulturtechniker*, (1932) 478.

APPENDIX A
THERMODYNAMICAL ASPECTS OF DISPLACEMENTS IN POROUS MEDIA

The capillary pressure curve obtained by displacing the wetting phase from an initially fully saturated porous medium may be defined as representing an isothermal equilibrium process, or more exactly, a succession of equilibria. The pressure on the non-wetting phase (gas) is increased in a stepwise fashion resulting in the gradual displacement of the wetting phase (liquid). As this equilibrium process takes place, it can be said that (a) the interfacial area between phases is varying in a continuous fashion, probably increasing until the irreducible minimum liquid saturation is reached, and (b) the solid/liquid contact area diminishes and is replaced by a solid/gas, or more exactly by a solid/liquid-film/gas area. For the total system formed by the liquid and the solid, the displacement process represents an isothermal-isobaric transformation. During such a transformation it is known that the external work done against the system (by the non-wetting gas phase) is equal to the increase of free energy of this system. The capillary pressure curve can thus be interpreted as representing the change of free surface energy that takes place in the porous medium during the displacement process.

Referring to the definition of surface areas as given by Equation (7), the change in free surface energy due to an increase of the interfacial area can be stated as:

$$dF_I = \gamma\, dI \quad \text{(A-1)}$$

If during the process of desaturation, solid area previously covered by the liquid phase is covered by gas, the increase of the "solid-gas" contact area is dR_G, and the corresponding change in free surface energy can be stated as

$$dF_s = dR_G\, \gamma \cos\theta \quad \text{(A-2)*}$$

Addition of Equations (A-1) and (A-2) obtains:

$$dF = dF_I + dF_s = \gamma\,(dI + dR_G \cos\theta) \quad \text{(A-3)}$$

where γ represents the interfacial tension between the two fluids, and θ the contact angle. But dF is the total change in free (surface) energy corresponding to a change in saturation dS, and is, consequently, equal to the work Pdv done against the system, or if a core of unit bulk volume is considered:

$$dF = -P_c\cdot f\cdot dS = \gamma\,(dI + dR_G \cos\theta) \quad \text{(A-4)}$$

In the case where the contact angle θ is zero, $\cos\theta = 1$, and

$$P_c\cdot f\cdot dS = -\gamma\,(dI + dR_G) \quad \text{(A-5)}$$

or

$$P_c\, f\cdot dS = -\gamma\cdot dA_G \quad \text{(A-6)}$$

and

$$A_G = -\frac{f}{\gamma}\int_1^S P_c\, dS \quad \text{(A-7)}$$

In explanation of the above equations, if, during the displacement process, equilibrium is not attained, or if an unstable film is left on the rock surface, the work of displacement may have a considerably different value than that indicated in the general Equation (A-4). Equilibrium is obtained, however, if the contact angle θ is zero, which is usually the case in liquid gas systems. The exact value of A_G can be derived only if $\theta = 0$, since up to the present no relationship exists which would permit the separate identification of dI and dR_G.

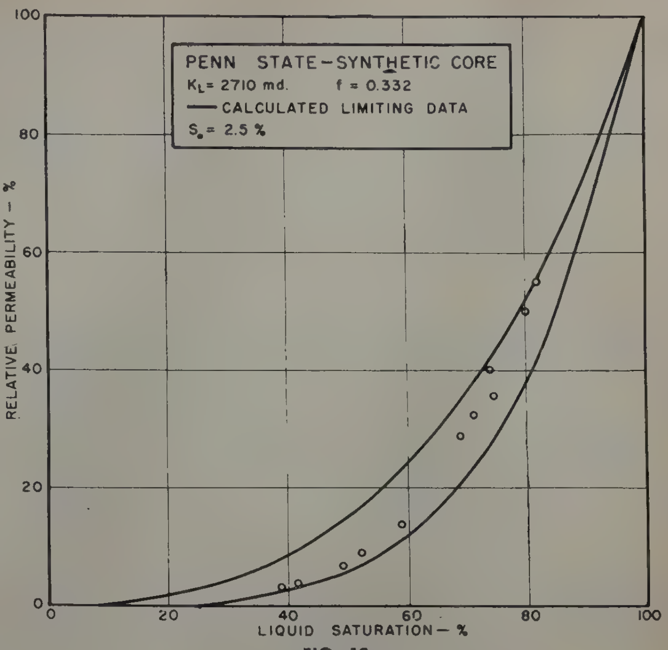

FIG. 13

Under the above circumstances, the areas under the capillary pressure curve can be assigned the following meanings (see Fig. 3):

$\Sigma_S = -\frac{f}{\gamma}\int_1^S P_c\, dS$ represents the interfacial area at the saturation S together with the rock area exposed to the non-wetting phase, less the amount, I_B, of interfaces that existed at the bulk surface of the fully saturated core; I_B is comparatively very small and can be neglected so that

$$\Sigma_S = -\frac{f}{\gamma}\int_1^S P_c\, dS = I + R_G - I_B \simeq I + R_G = A_G\,. \quad \text{(A-8)}$$

The maximum limiting value of the above integral can be represented by

$$\Sigma_{S_o} = -\frac{f}{\gamma}\int_1^{S_o} P_c\, dS = R_{G(\text{LIM})} + I_{(\text{LIM})} \quad \text{(A-9)}$$

In this expression $I_{(\text{LIM})}$ represents the interfacial area between the gas and the "connate" liquid, and consequently $R_{G(\text{LIM})}$ the (maximum) gas/solid contact area that obtains at the irreducible minimum liquid saturation. On the basis of considering the connate liquid as being immobile, it is seen that Σ_{S_o} which corresponds to the envelope of the connate liquid and solid area, represents the surface area A_E of the total effective flow matrix,* so that

$$\Sigma_{S_o} = -\frac{f}{\gamma}\int_1^{S_o} P_c dS = A_E = R_G + R_L \quad \text{(A-10)}$$

---

*This relation implies that the receding liquid leaves a film over the solid surface. It is, however, understood that the liquid particles of this molecular film have no actual bearing upon the distribution and the flow mechanism of the fluids.

*Such an interpretation is equivalent to treating I_{LIM} as part of the total "solid" area, which always remains covered by the liquid phase and is, therefore, automatically included in R_L at any saturation.

Is is then finally seen that

$$\Sigma_W = \Sigma_{S_o} - \Sigma_S = -\frac{f}{\gamma}\int_S^{S_o} P_c dS = A_E - R_G - I \quad . \quad \text{(A-11)}$$

or, combining Equations (A-10) and (A-11)

$$\Sigma_W = R_L - I = A_L - 2I \quad \text{(A-12)}$$

The above derived relations (A-8), (A-10), and (A-12) are used for the derivation of K_L(Max) and K_L(Min),

APPENDIX B
CALCULATION OF SPECIFIC PERMEABILITIES FROM CAPILLARY PRESSURE DATA

According to the derivations presented in the Main Report and in Appendix A, the specific permeability of a porous medium can be expressed as

$$k = \frac{1}{5}\,\frac{(1-S_o)^3\,f^3}{(A_E)^2} \quad \text{(B-1)}$$

or using Equation (A-10)

$$k = \frac{f}{5}\,\gamma^2\left[\int_1^{S_o} P_c\,dS\right]^{-2}(1-S_o)^3 \quad . \quad . \quad . \quad \text{(B-2)}$$

where f, S and S_o are fractional; P_c is expressed in dynes per sq cm, γ in dynes per cm, and k in sq cm.

The above relations imply that not all of the fluid filling a porous body participates in the flow, and that the fraction held immobile is approximately equal to the irreducible minimum saturation as indicated by capillary displacement experiments.* Equation (B-2) may be used to calculate the specific permeability from capillary pressure data.

Table I shows the comparison between calculated and measured dry air permeability for 27 samples which vary widely in permeability, porosity, and textural characteristics. It might be noted that in 21 cases the calculated permeability is smaller than that actually measured. Such a systematic trend may be explained by the fact that the measured dry air permeabilities have not been corrected for gas slippage effects.

It is seen that the average discrepancy between the measured and the calculated results is greater for the natural cores than for the artificial cores. It must, however, be indicated that the degree of precision of the experimental data on most of the natural core samples is not very high. The core material itself seemed to be extremely sensitive to chemical agents so as to be subject to definite changes (in surface and even textural characteristics) with time.

In the light of these remarks the overall agreement between calculated and measured values of permeability can be considered as satisfactory and may be interpreted as a good verification of the presented theoretical approach.

APPENDIX C
DERIVATION OF THE LIMITING K_L MAXIMUM

Under any circumstances, it can be considered that the gas inside the porous medium is flowing through a certain channel system surrounding clusters of rock grains containing liquid in their interstices. The assembly of all these clusters may be treated like an entirely water saturated "reduced" porous medium, the porosity of which would be equal to

$$\frac{Sf}{1-f+Sf}$$

so that under the assumption of isotropic random packing,

$$\frac{a_L}{a_s} = \frac{\text{total cross sectional liquid area}}{\text{total cross sectional solid area}}$$

$$= \frac{Sf}{1-f} = \frac{\text{water volume}}{\text{rock volume}} \quad \text{(C-1)}$$

A schematic illustration is given in Fig. 14, where one pore opening between two rock grains is represented.

The total outside surface area of the "reduced" porous medium is equal to $A_G = I + R_G$. The following interpretation can then always be given to the ratio

$$\frac{I}{R_G}$$

namely,

$$\frac{I}{R_G} = \frac{\text{liquid surface exposed to gas}}{\text{solid surface exposed to gas}} \quad . \quad \text{(C-2)}$$

Under the previous assumption of isotropic packing, the inequality

$$\frac{I}{R_G} > \frac{a_L}{a_s} = \frac{Sf}{1-f} \quad \text{(C-3)}$$

can be established with help of the following reasoning. The liquid is the wetting phase so that it actually "spreads" over the rock, creating a total liquid-gas contact area, I, that is greater than the (average) cross sectional area, a_L of the pore space containing the water. As a consequence, the total solid surface that remains exposed to the gas, R_G, will be smaller than the (average) cross sectional area, a_s, of the solid grains so that one has simultaneously:

$$C.I = i > a_L \quad \text{(C-3}^a\text{)}$$

$$C.R_G = r < a_s \quad \text{(C-3}^b\text{)}$$

where i and r represent the projections of the curved surfaces I and R_G respectively on the considered cross-sectional plane. C is the factor of projection or shape factor of these surfaces, and is assumed to be the same for the rock grains and the interfaces. By combination of (C-3^a) and (C-3^b), inequality (C-3) is obtained. In fact, at low liquid saturations C is smaller for the interfaces than for the rock which still increases the resultant inequality (C-3).

The ratio

$$\frac{i}{a_L}$$

can be approximated in the following way: the surface i can

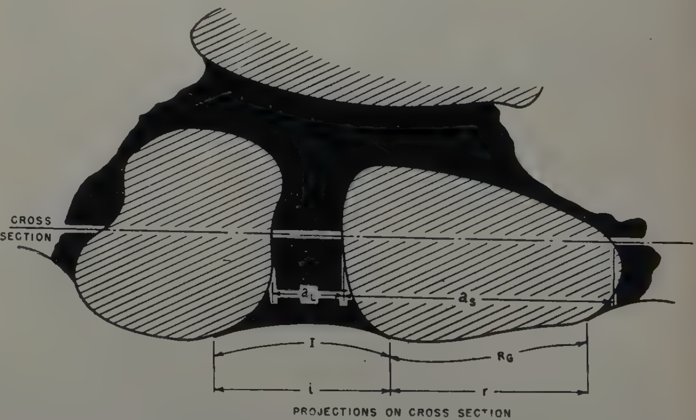

FIG. 14 — SCHEMATIC COMPARISON BETWEEN ROCK SURFACES AND INTERFACES.

---

*It has already been recognized by King,[15] and later by Kozeny,[18] as well as by other workers,[16,17] that in a single phase system some part of the fluid seems to be held back in internal angles and fissures, and in zones of grain contacts where molecular forces of adhesion become prevalent. Therefore, in the original Kozeny equation,[5] the porosity, f, should be assigned a slightly lower value, and the surface area, A, should actually correspond to some "effective flow matrix" and not to the specific solid surface.

be considered as corresponding to a mean hydraulic radius given by

$$h_I = \frac{2\ \gamma}{P_c} \quad \ldots\ldots\ldots \quad (C\text{-}4)$$

whereas the mean hydraulic radius of the pore space, *i.e.*, that corresponding to the cross sectional area, a_L can be shown to be given by

$$h_L = \frac{2\ \gamma}{P_m} \quad \ldots\ldots\ldots \quad (C\text{-}5)$$

where P_m represents the mean capillary pressure over the saturation range S to S_o, *i.e.*,

$$P_m = \frac{1}{S - S_o} \int_S^{S_o} P_c dS \quad \ldots\ldots \quad (C\text{-}6)$$

The ratio of the surfaces i and a_L can then be expressed as

$$\frac{i}{a_L} = \left(\frac{h_I}{h_L}\right)^2 = \left(\frac{P_m}{P_c}\right)^2 \quad \ldots \quad (C\text{-}7)$$

Combining Equation (C-7) with the relations (C-3), (C-3^a), and (C-3^b) gives

$$\frac{I}{R_G} > \frac{Sf}{1-f}\left(\frac{P_m}{P_c}\right)^2 \quad \ldots\ldots \quad (C\text{-}8)$$

from whence

$$I \text{ minimum} = R_G \cdot \frac{Sf}{1-f}\left(\frac{P_m}{P_c}\right)^2 \quad \ldots \quad (C\text{-}9)$$

The combination of (C-9) and the relation

$$A_G = I + R_G = -\frac{f}{\gamma}\int_1^S P_c ds \quad \text{(See Appendix A, Equation A-8)}$$

yields

$$I \text{ Minimum} = A_G \cdot \frac{1}{1 + \frac{1-f}{Sf}\left(\frac{P_c}{P_m}\right)^2} \quad . \quad (C\text{-}10)$$

Substitution of the above expression in the equation

$$A_L = -\frac{f}{\gamma}\int_S^{S_o} P_c dS + 2I \quad \text{(See Appendix A, Equation A-12)}.$$

gives

$$A_L \text{ Minimum} = -\frac{f}{\gamma}\left[\int_S^{S_o} P_c dS + \frac{2\int_1^S P_c dS}{1 + \frac{1-f}{Sf}\left(\frac{P_c}{P_m}\right)^2}\right] \quad \ldots\ldots\ldots \quad (C\text{-}11)$$

In accordance with Equations (11) of the Main Report and (A-10) of Appendix A, the final expression for the maximum of the relative permeability is then given by

$$K_L \text{ Maximum} = \frac{S'^3\left[\int_1^{S_o} P_c dS\right]^2}{\left[\int_S^{S_o} P_c dS + \frac{2\int_1^S P_c dS}{1 + \frac{1-f}{Sf}\left(\frac{P_c}{P_m}\right)^2}\right]^2} \quad (C\text{-}12)$$

or using the symbols of the Main Report and Appendix A

$$K_L \text{ Maximum} = \frac{S'^3\ [\Sigma s_o]^2}{\left[\Sigma_w + \frac{2\ \Sigma_S}{1 + \frac{1-f}{Sf}\left(\frac{P_c}{P_m}\right)^2}\right]^2} \quad . \quad (C\text{-}13)$$

DISCUSSION

By Charles G. Dodd, U. S. Bureau of Mines, Bartlesville, Okla., Member AIME

The authors' work is a most stimulating contribution to the study of the complex problems involved in the flow of fluids through porous media. This reviewer has profited greatly from a study of the paper which undoubtedly represents the end product of much careful analysis. The following comments are presented in an effort to implement rather than detract from the value of the ideas presented.

Among the fundamental assumptions, stated and implied, upon which the paper is based are the following: (1) In single-phase fluid flow through a porous medium the fluid filling all minute crevices, cracks and pores is stagnant and does not participate in flow. (2) The total volume of stagnant liquid may be identified with the irreducible minimum liquid saturation measured by a capillary pressure experiment. (3) If a flowing liquid is under consideration, the volume of each pore which is filled with stagnant liquid is determined by the curvature of the liquid-gas interface, *i.e.*, by the solid geometry and the surface tension of the liquid. (4) There is no slippage at the boundary between flowing liquid and stagnant liquid. (5) In relative permeability to liquid measurements when the gas phase is immobile there is no slippage at the liquid-gas interfaces within the voids of the porous medium. (6) In analyzing the free energy change involved in the displacement of liquid from a porous medium by gas it is assumed that a solid-liquid interface is replaced by a solid surface covered by a liquid film having the surface tension of the bulk liquid or by a surface of equal energy. It would be profitable to discuss these assumptions in turn.

The Kozeny equation[1] has been applied by Carman[2,3,4] and others to determination of the specific surface areas of finely divided materials by measuring the fluid permeabilities of unconsolidated beds. The method has enjoyed wide acceptance in recent years, and the surface areas measured thereby agree well with area measurements made by independent methods, although it is recognized[5] that the internal areas of porous silica gels, etc., are not evaluated by the method. For permeability experiments to measure a solid surface area, the solid surface must offer a frictional resistance to flow, and the flowing fluid must everywhere contact the surface. In recent work at the Bureau of Mines laboratories[6] we have obtained agreement to better than three per cent between the specific surface areas of a sample of 70- to 100-mesh glass beads as calculated from liquid permeability experiments to water and isoöctane, and precise, independent miscroscopic measurements. These glass beads were of the average size of grains in many sandstone reservoir rocks. Packed beds of the beads probably would retain 10 to 15 per cent water at completion of a displacement experiment as an irreducible minimum water saturation, but no correction was made for this in our work such as the authors suggest in their Equation (B-1). On the basis of the above remarks, it is felt that assumptions (1) and (2) do not have general applicability to all porous systems. However, in the case of sandstone reservoir rock material, for example, the presence of cementing material, clay minerals, and very fine silt between coarser sand grains alters the picture. Undoubtedly the fluid in such fine crevices does not participate in flow.

In the case of assumption (3) it is difficult to understand how the curvature of a hypothetical liquid-gas interface can determine the boundary between flowing and stagnant liquid in a continuous liquid phase. It would seem more appropriate to attribute such a phenomenon to attraction of the solid for the stagnant liquid, but no analysis of this situation has been developed. On the other hand the concept serves as a working hypothesis to stimulate further research.

Assumption (4) is a difficult one to accept, but it may sit better on further reflection. Assumption (5), on the other hand, seems to be untenable. It is involved in the authors' definition of A_L which is used throughout their development. This reviewer would suggest that the analysis be reconsidered on the basis of a more plausible definition of A_L, eliminating the gas-liquid interface as one where friction is involved.

In Appendix A the authors, apparently without realizing it, have made assumption (6), which seems a reasonable one to this reviewer if the saturating liquid wets the solid with a zero contact angle. The authors assume the work done in the displacement process is that necessary to form new liquid surface having an area A_G. It should be pointed out that this results in R_G always being zero, a condition the authors use in evaluating their minimum K_L function. However, if R_G is always zero, the ratio I/R_G used in evaluating the maximum K_L function loses its significance.

REFERENCES

1. Kozeny, J.: *Sitzber. Akad. Wiss. Wien, Math.-naturw. Klasse*, (1927) **136**, (Abt. IIa), 271.
2. Carman, P. C.: *Trans.* Inst. Chem. Engrs. (London, 1937), **15**, 150.
3. Carman, P. C.: *J. Soc. Chem. Ind.* (London), (1938), **57**, 225 T.
4. Carman, P. C.: *Ibid.*, (1939), 58, 1.
5. Sullivan, R. R., and Hertel, K. L.: *Advances in Colloid Science*, I, 37-80, Interscience Publishers, Inc., New York, (1942).
6. Dodd, C. G., Davis, J. W., and Pidgeon, F. D.: *J. Phys. and Colloid Chem.*, in press.

AUTHOR'S REPLY TO MR. DODD

Dodd's very clear analysis of the assumptions used in the theoretical developments of this paper contributes toward the recognition of some fundamental aspects of fluid mechanics in porous media and represents a most valuable basis for constructive discussions. The authors want to take this opportunity for indicating that one of their main purposes has been to attempt the definition of a series of "working hypotheses" and to outline thereby a logical basis for further research.

With respect to assumption (5) the authors can hardly follow the views expressed by Dodd. It is not excluded that there may be some slippage at the liquid-gas interfaces. Accordingly, a more elaborate derivation could possibly be worked out, provided there were any tangible indication as to the exact amount of slippage to be accounted for. It can be anticipated that the consideration of slippage on part of the liquid boundaries would lead to a situation that is somewhat different from what is usually admitted, namely applicability of Darcy's law to each of the flowing phases. It is believed that in any event neither the principle of the theoretical treatment nor the nature of the boundaries would be altered. At this time, therefore, it does not appear that the definition of the liquid boundary A_L ought to be modified or even that the assumption of zero slippage at the liquid-gas interfaces is untenable.

It is felt that some confusion might arise in connection with the comments concerning assmption (6). As Dodd points out, there is actually no formation of true molecular contact between the gas and the solid surface since it is implied that the latter remains at all times covered by a liquid film. This film must be visualized merely as an immobile coating layer of infinitesimal thickness. With respect to the spatial distribution of fluids, it is necessary to distinguish between the interfacial area, I, separating the gas from the flowing bulk liquid, and the area of triple contact "gas/liquid - film/solid" which for reasons of simplicity has been termed "solid-gas" contact area, R_G. From the foregoing it is then clear that R_G must always be assigned a definite value and that it becomes zero only in the case of complete gas channeling such as may be seen from Figs. 1 and 4.

DISCUSSION

By M. R. J. Wyllie, Gulf Research and Development Co., Pittsburgh, Pa., Member AIME

The authors are to be congratulated on a most interesting and provocative paper which will, I am sure, give rise to much discussion. For this reason it is my intention to discuss here only those aspects of the authors' work which appear to be fundamentally at variance with certain published works of Rose and myself.[1,2] My hope is either to reconcile the differences or failing that, at least to underline them so that some later worker may be in a better position ultimately to resolve them.

Firstly, I am most happy to see that more work applying the Kozeny equation to consolidated porous media is now in print; nevertheless, I feel that a word of caution is in order since the application of the Kozeny equation to such media has not yet received wide support; indeed, Carman, one of the principal protagonists of the theory, has outlined at length the rather severe theoretical requirements which must be met before its use is justified.[3] Nevertheless, I agree that the validity of this equation when applied to consolidated porous media can only be tested by experiment and the authors data make further such tests possible.

Where I differ from the authors is (a) in the employment of the "effective porosity" concept in the type of porous media used by them and (b) in the magnitude of the Kozeny constant, t, applicable to consolidated porous media.

With regard to (a) I believe that this concept, as suggested by Kozeny,[4] Zunker[5] and Carman[6] for clays, is valid; I have found it useful myself[7] for the theoretical treatment of fluid flow through mud filter cakes. Nevertheless, clays are unique in that they undoubtedly absorb strongly an appreciable water film. Thus, the concept of the effective flow porosity of a clay particle system being less than the porosity determined solely by the amount of "interstitial" water present in the system is not unreasonable; indeed some such postulate is essential if the well-known fact is to be rationalized that the permeability of a clay particle system may be essentially zero when its porosity is appreciable. A similar concept may apply to all porous systems, as pointed out by the authors; here the discussion by Carman[8] quoting the results of King,[9] Erikson[10] and Darapsky,[11] all of whom tended to a view similar to that held by the authors, is relevant. Nevertheless, it is, I believe, important to note that all direct substantiations of the Kozeny equation, including those cited by the authors, involve the use of the total surface areas and total porosities of the systems investigated; *i.e.*, in Equation (5) of the authors, k, f and A were directly measured and thus t found. It is, of course, possible that, by the use of appropriate effective porosities and surface areas, the same constants would have been found by the workers quoted in the authors' references;[4,5,6,7] nevertheless, this was not done and hence it does not appear wholly appropriate for the authors to cite these data as a justification of their choice of a Kozeny constant of 5.

It may be emphasized that, as noted by the authors, the Kozeny constant of 5 is experimentally proved to be only an approximate figure for flow through isotropic unconsolidated porous media. In non-isotropic unconsolidated porous media the constant varies with the direction of flow being, respectively, approximately 3 and 6, for flow parallel to and perpendicular to the long axes of a bed of fibers.[12] It is the view of Sullivan and Hertel[12] and of Rose and myself[2] that the Kozeny constant is a function of what has been called the tortuosity of the porous system through which flow occurs. In the case of the fiber bed quoted above the tortuosities are approximately 1 and 2 respectively and, if a reasonably constant shape factor of about 3 is assumed (Carman[8] adduces evidence for this), the directional Kozeny constants of 3 and 6 are obtained as the product of the tortuosity and shape factor. In consolidated porous media, Rose and I[2] have noted from electrical evidence that tortuosities much higher than those applicable to unconsolidated systems seem applicable, and hence we assume that Kozeny constants much exceeding 5 are applicable to such unconsolidated systems. We have adduced some experimental evidence to support this contentio In addition we have noted[1] that tortuosity appears to vary with saturation in all porous media and give as the relationship between T, the tortuosity at 100 per cent saturation, and T_e, the tortuosity at some saturation, S, of wetting phase, the relationship,

$$T_e/T = S^2I^2$$

where I is the electrical resistivity index pertaining to the saturation, S. It may be noted that a variation of tortuosity with saturation has recently been suggested also by Fatt and Dykstra.[13]

It is important then to point out that Rapoport and Leas use a constant of 5 for consolidated porous media and specifically state that to a good approximation they believe there is no variation of the constant with saturation. Hence their position is quite different from that of Rose and myself and clearly the divergence in outlook can only be settled by reference to the experimental facts. Table I in the authors' paper gives experimental results which the authors cite as a general confirmation of their theoretical reasoning. They note that although the agreement between measured and computed permeabilities is not precise, there are considerable experimental difficulties attached to work of the kind carried out and thus the over-all average agreement of ±12 per cent between computed and measured permeabilities supports the validity of the Kozeny constant of 5 which they employed in all cases. Certainly I do not question the experimental difficulties involved in compiling Table I and the overall agreement noted must, therefore, be considered as rather good support of the

Table I—Comparison Between Calculated and Measured Specific Permeabilities

NATURAL CORES						ARTIFICIAL CORES					
Formation	Designation	$f\%$	K_M in md	K_C in md	$\frac{K_C - K_M}{K_M}$ in %	Core Material	Designation	$f\%$	K_M in md	K_C in md	$\frac{K_C - K_M}{K_M}$ in %
Third Deese Sand	B14	9.3	15.7	30.0	+90.0						
Third Deese Sand	B 3	15.4	17.0	24.5	+44.0						
Bartlesville Sand		21.2	25.0	22.8	– 8.8						
Third Deese Sand	B13	11.3	26.0	39.5	+29.0	Alundum	C1	21.8	30.8	28.8	– 6.5
Third Deese Sand	B10	14.2	117.0	86.5	–26.6	Alundum	C2	24.2	72.2	55.3	–27.0
Third Deese Sand	B25	13.6	127.5	104.0	–18.5						
Third Deese Sand	B 5	16.3	133.0	103.0	–22.5						
Third Deese Sand	B37	15.8	139.0	108.0	–22.0						
Third Deese Sand	B27	14.8	154.0	112.5	–27.0						
Third Deese Sand	B33	16.2	159.0	131.0	–17.5						
Third Deese Sand	B19	12.6	174.5	149.0	–14.5	Alundum	C3	24.5	177.0	144.0	–18.6
Third Deese Sand	B55	15.3	182.5	199.0	+ 9.0						
Third Deese Sand	B41	16.6	213.0	150.0	–29.5						
Third Deese Sand	B 1	17.0	226.0	158.0	–32.0	Alundum	1186/35/2	23.4	220.0	198.5	–10.0
Third Deese Sand	B48	17.3	243.0	192.0	–21.0						
Third Deese Sand	B 8	16.8	301.0	244.0	–18.6						
Third Deese Sand	B 4	17.8	470.0	271.0	–42.5	Alundum	C4	27.4	567.0	566.0	0.0
Nichols Buff Sand		21.5	660.0	590.0	–10.6	Alundum	C5	30.0	1,385.0	982.0	–28.8
Bromide Sand		18.3	2,543.0	2,710.0	+ 6.6	Penn State		33.2	2,710.0	2,700.0	– 0.03
Unconsolidated Sand		35.0	17,200.0	12,000.0	–30.0						

Average Error on Natural Cores: 26.0 Per Cent

Average Error on Artificial Cores: 13.1 Per Cent

Average Error: 22.6 Per Cent

$f\%$ = Porosity

K_M = Measured Permeability in md

K_C = Calculated Permeability in md

$\frac{K_C - K_M}{K_M}$ = Error in Per Cent authors' contentions; alternatively the data may be indicative of the fact that there are at least two plausible methods of skinning this particular cat.

The computed permeabilities in Table I are derived essentially from the relationship:

$$k = \frac{1}{5} \frac{(1-S_o)^3 f^3}{A^2_E} \quad . \; . \; . \; . \; . \; . \; . \; . \quad (1)$$

whereas. Rose and myself have suggested.[2]

$$k = \frac{1}{t} \frac{f^3}{A^2} \quad . \; . \; . \; . \; . \; . \; . \; . \; . \quad (2)$$

with $t > 5$ in all cases. (Actually $t = F^2 f^2 t_s$ where F = formation factor and t_s = shape factor and is approximately = 2.5 – 3.0.)

Now in all cases $(1-S_o)^3 f^3 < f^3$ and it seems probable that $A_E < A$. (It seems pertinent to note that the use by the authors of $-f/\gamma \int_1^{S_o} P_c dS = A_E$ is not wholly in accordance with the recommendations of Leverett in Reference[8] of the authors.) Depending upon the relative values of $(1-S_o)^3 f^3$, A_E^2 and t it would appear that both Equations (1) and (2) above could give approximately correct values of k. At this stage I do not believe it possible to decide which of the two equations is the more fundamental.

REFERENCES

1. Wyllie, M. R. J., and Rose, W. D.: *Trans.* AIME, (1950) **189**, 105.
2. Wyllie, M. R. J., and Rose, W. D.: *Nature* (Lond.) (1950) **165**, 972.
3. Carman, P. C.: *Discussions of the Faraday Soc.*, (1948) No. 3, 72.
4. Kozeny, J.: *Kultur techniker* (1932) **35**, 478.
5. Zunker, F.: *Z. Pfl Ernähr. Düng.*, (1932) **A25**, 1.
6. Carman, P. C.: *J. of Agri. Sci.*, (1939) **29**, 262.
7. Wyllie, M. R. J.: *Trans.* AIME, (1951) **192**, 1.
8. Carman, P. C.: *Trans. Inst. Chem. Eng.*, (Lond.) (1937) **15**, 150.
9. King: *19th Annual Rept.*, U.S.G.S., (1897-8), **2**, 59.
10. Erikson, S.: *J. Gasbeleucht*, (1920) **63**, 615.
11. Darapsky: *Z. Math. Phys.* (1912) **60**, 170.
12. Sullivan, R. R., and Hertel, K. L.: *Advances in Colloid Science*, Interscience Publishers, (1942).
13. Fatt, I., and Dykstra, H.: "Relative Permeability Studies," presented at AIME Fall Meeting, (1950), Los Angeles, Calif.

AUTHOR'S REPLY TO MR. WYLLIE

The authors fully appreciate the importance of Wyllie's comments. They feel, however, that a sufficiently detailed answer would require considerable divergence from the issue at hand. In the near future it is planned that a note containing additional experimental data will be written concerning the significance of the textural constant.

DISCUSSION

By J. S. Osoba, Humble Oil and Refining Co., Houston, Tex.

The authors have presented a useful method of calculating relative permeability to the wetting phase under drainage conditions when the capillary pressure versus saturation relations are known for reservoir rock. The agreement between calculated and experimental relative permeabilities is proof of the validity of the calculated method provided the experimental method is free of errors.

Several methods of measuring relative permeability have been investigated in our labortory. The relative permeability to the wetting phase measured by three of these methods, the Penn State, single core dynamic, and gas drive technique, were nearly identical to the curves calculated from the capillary pressure curves using Rapoport and Leas' equation for K_L(min). One method, the Hassler method, which is most nearly like the method used by Rapoport and Leas, gave a relative permeability to the wetting phase that was lower than the calculated curve, using the equation for K_L(min).

Since there are laboratory methods whereby the relative permeability to the wetting phase can be measured and the results coincide with the calculated relative permeability to the wetting phase, and since these methods are many times faster and less difficult to operate than the method presented in this paper, I do not believe the authors are justified in concluding that their method of calculating relative permeability is superior to experimental methods.

With reference to another point in the paper, in calculating specific permeability by the Kozeny equation [Equation (6)], the result is very sensitive to the value chosen for the irreducible minimum saturation on the capillary pressure curve. This is due to the fact that the irreducible minimum saturation determines the factor A [in Equation (6)], and a small variation in this irreducible minimum causes a large change in A. Since this factor appears in the equation as A^2, the accurate determination of this factor is very important. It would be of some help in evaluating the data presented in Table I if the procedure used to determine the factor A were explained.

AUTHOR'S REPLY TO MR. OSOBA

Osoba's statement concerning the agreement that he found between the calculated curves and direct measurements of liquid relative permeability is most gratifying and provides a further substantiation of the theory advanced by the authors.

It is readily admitted that there is a certain resemblance between the Hassler method and the experimental technique presented in this paper insofar as both require the use of semipermeable capillary barriers. It may, however, be stated that the results obtained by the Hassler method are subject to a systematic error due to the distortion of the flow pattern from linear whereas the procedure used by the authors has been conceived so as to eliminate any such anomalies.

As regards the superiority, from the viewpoints of cost and time, of experimental methods over that of calculating, the latter has been recommended merely in preference to that experimental method which is presented in this paper. The authors certainly do not deny the possibility of more economical methods. They would, on the contrary, advocate the use of more advantageous methods, as soon as their reliability and economy could be sufficiently demonstrated.

★ ★ ★

T.P. 3053

EXPERIMENTAL INVESTIGATION OF FACTORS AFFECTING LABORATORY RELATIVE PERMEABILITY MEASUREMENTS

T. M. GEFFEN, JUNIOR MEMBER AIME, **W. W. OWENS, D. R. PARRISH,** AND **R. A. MORSE,** JUNIOR MEMBER AIME, STANOLIND OIL AND GAS CO., TULSA, OKLA.

ABSTRACT

Laboratory studies of several factors affecting measurements of relative permeability were made using the three-section plastic-covered core technique. Results show that the core assembly, properly constructed, will perform as a single unit, and that the testing technique will, under suitable conditions of pressure gradient, gas expansion, and migration of partial water saturation, permit measurement of flow characteristics not affected by technique. Wettability equilibrium is readily established in cores exhibiting strong wetting preference to water or oil when initially saturated with water. Laboratory tests must be conducted so that saturation changes represent those that occur in the reservoir. Immediate implications of saturation history are (1) that the possibility exists of increasing the displacement efficiency of solution gas drive reservoirs over the natural process, and (2) residual gas saturations following water flooding in gas or gas condensate reservoirs will be 15 to 50 per cent pore space rather than 1 to 11 per cent as generally believed.

INTRODUCTION

Solutions of petroleum reservoir problems pertaining to production performance require the use of true relative permeability characteristics. This relationship of fluid conductivity and saturation has been obtained by reservoir engineers in four ways, namely:

1. From past gross reservoir performance and the extrapolation of this data based on experience,[1,2]
2. By using published fluid flow relationships obtained in laboratory studies on general type porous materials,[3,4,5]
3. By attempting a mathematical derivation of flow behavior,[6] using some experimentally obtained characteristics of reservoir rocks, and
4. By laboratory flow tests using representative rock samples of a reservoir.

The first three methods listed above have shortcomings which make their use limited or questionable. Production characteristics of only certain processes are obtained from field data and these are not available at the beginning of a reservoir's producing life, at which time they are desirable. It is fortuitous if general fluid flow characteristics obtained experimentally have accurate application to specific field problems. Also, it is felt that at this time there is not sufficient knowledge of the flow behavior of oil, water, and gas in porous materials to enable applicable analytical description of this to be made based on other measured rock characteristics.

Measurement of relative permeability in the laboratory offers the only direct method subject to adequate checking for determination of flow characteristics applicable to field problems. Primarily, this paper deals with laboratory experiments to establish the effects of several factors on the measurement of relative permeability and the practical significance of this knowledge.

Laboratory flow tests are essentially model studies; the gross reservoir being represented by a small rock sample. It is necessary to simulate in experiments all the factors of importance which influence flow in the reservoir, as well as to eliminate effects peculiar to the model studied to assure measurement of valid flow behavior.

Factors which affect the measurement and behavior of fluid flow in porous materials have been studied by other investigators.[3,7,8,9,10,11] This analysis is not intended to evaluate fully all factors involved, but to establish first the validity of measurements by the technique used and then study flow behavior under various conditions. The studies reported are as follows:

1. Effects of pressure gradient,
2. Effects of gas expansion in tests conducted at near atmospheric pressure,
3. Effects of migration of a partial water saturation in oil-gas-water systems,
4. Effects of wettability characteristics of the system, and
5. Effects of the fluid saturation history.

The first three are important only in laboratory measure-

---

[1] References given at end of paper.

Manuscript received in the office of the Petroleum Branch Sept. 27, 1950. Paper presented at the Fall Meeting of the Branch in New Orleans, La., Oct. 4-6, 1950.

ments, whereas the last two are significant in general flow characteristics.

Studies reported herein deal only with intergranular sandstone systems.

TESTING EQUIPMENT AND GENERAL PROCEDURE

Steady state flow experiments were conducted using three-section Lucite-covered core plugs similar to those used by Morse, Terwilliger, and Yuster.[12] A few modifications were made on the method cited.

Core Assembly

Fig. 1 shows a schematic diagram of a core assembly. Only one highly permeable porous plug is used instead of two, as was originally suggested; this immediately following a metal plate having a 1/16-in. orifice in its center. A minimum voidage is left in the assembly upstream from the orifice; this was found important in limiting slug-type flow, especially in tests flowing gas at low flow rates and large liquid/gas ratios. The molding process incorporated the use of a Lucite shell machined to fit the required cores instead of powdered plastic. This has been found advantageous in simplifying the molding process and assuring centering of the core plugs in the Lucite sheath. Copper wire, to afford electrical contacts, is pulled through the Lucite cover and tightened around the cores before they are molded. Input power electrodes are the orifice plate at the inlet end and a brass screen wire (40-mesh) placed at the outlet end.

Apparatus and Equipment

Delivery of liquids at constant rate to the core assembly is facilitated by two micropumps, one each for oil and water (Fig. 2). The pumps utilize a piston with a rubber O-ring packing, traveling inside bored cylinders. These are driven by an electric motor through variable speed hydraulic transmissions. Mechanical gear boxes are arranged so that the input speed to the pump can be chosen as equal to or 1/100 of the output speed of the transmission. This arrangement permits pumping liquids from the 1-in. ID cylinders over a rate range of 0.5 to 900 cu cm per hr. Since the pump cylinders are of uniform bore, input flow rates are determined by measuring the speed of the pump drives. Flow of air to the core is maintained by throttling a constant pressure through a needle valve placed in the mixing head of the core assembly. Rates of air flow are measured at the outlet by timing the travel of a detergent film in a graduated burette. Pressure drops are measured with a strain gauge pressure transducer having a very small fluid displacement necessary for its actuation. Test core saturations are determined gravimetrically after removing the test core from the assembly by means of a quick-opening clamp. A four-electrode a-c conductivity circuit is used to determine water saturation distributions, and the attainment of equilibrium during flow.

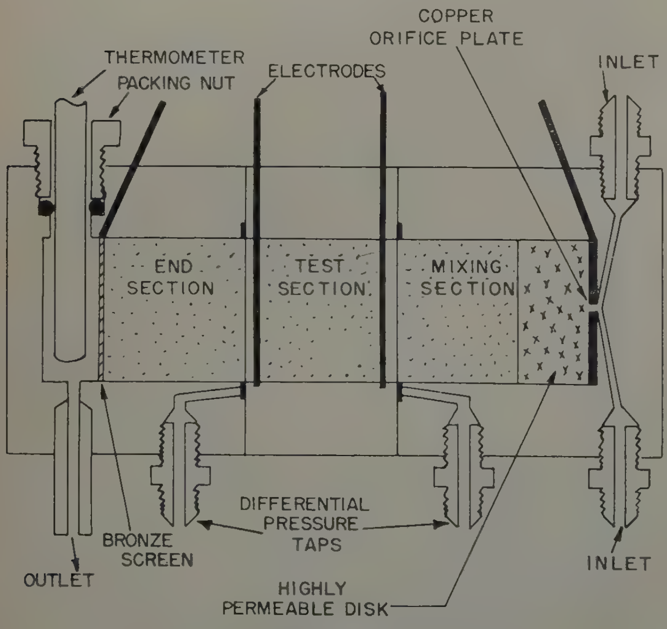

FIG. 1 — THREE-SECTION CORE ASSEMBLY.

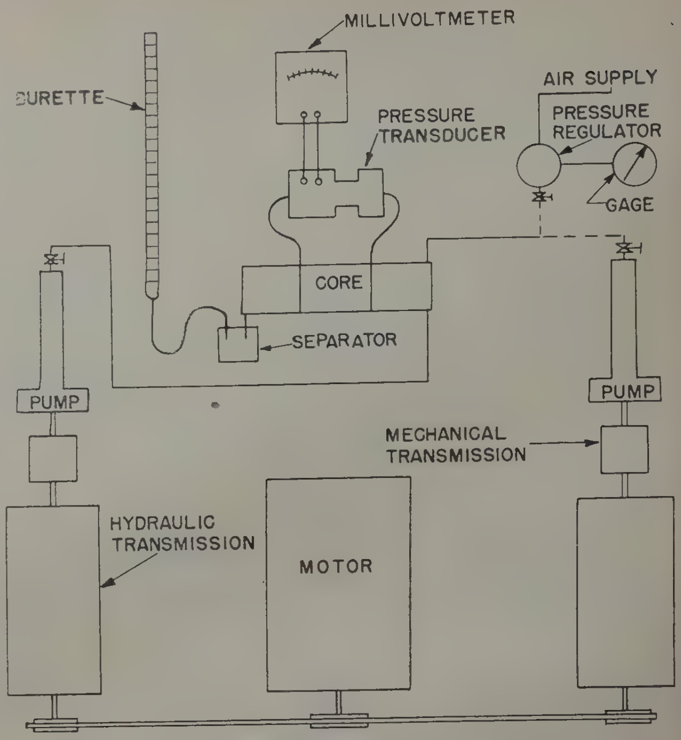

FIG. 2 — FLOW DIAGRAM FOR RELATIVE PERMEABILITY TESTS.

General Testing Procedure

Core assemblies are flushed with several pore volumes of pentane, then air dried before being evacuated and saturated with a liquid, usually a prepared brine. The specific liquid permeability of the test section is measured, after which the core assembly is subjected to the flow of oil, water, or gas, or any combination of these fluids, as the test requires. Test readings are made at equilibrium conditions, determined when differential pressure and electrical resistance readings (when available) become constant with constant fluid injection rates. An extra step is necessary in systems flowing a gas. Electrical measurement of test core resistance is made after flow is stopped and pressure in the core equalized at atmospheric pressure. This electrical conductivity is correlated with saturations determined gravimetrically and is used to evaluate saturations in the core during the flowing phases of the test.

Description of Fluids Used

Pure fluids were used in all studies. The brine used was prepared from distilled water and *NaCl* with 50 ppm formaldehyde added to retard bacterial growth. The oil phase was a close-cut fraction of decane to dodecane. Both brine and oil were prefiltered through fine bacteriological filters to remove suspended solids. Air was used as the gas phase.

RESULTS AND DISCUSSION

Effects of Pressure Gradient on the Measurement of Oil/Water Relative Permeability

A saturation gradient exists in all multiphase flow systems. Leverett[8] has explained this as being due to a capillary discontinuity occurring at the outflow boundary of the porous system and has referred to this phenomenon as "end effect." Physically what occurs is a piling up of the wetting fluid toward the downstream boundary of the system. Analytical expressions can be written to describe the effects on flow measurements of this saturation gradient in a system. The gradient is affected by capillary pressure and relative permeability characteristics, fluid properties and flow rates or pressure differentials. The computations necessary are complex and require a knowledge of the true relative permeability characteristics. Therefore, an experimental evaluation of this factor is the feasible approach. The disturbing effect a saturation gradient has on measurement of relative permeability is two-fold:

1. Relative permeability of flowing fluids is correlated with saturations. Measurements in a finite portion of the flow system containing a saturation gradient result in determination of the average saturation and a summation of the fluid conductivity. Since relative permeability and saturation are not related linearly throughout the entire range of interest, the computed effective fluid permeabilities are not unique with calculated saturations. This influence on the measured flow characteristics is of little consequence when the saturation gradient covers a range in which the relative permeability-saturation curve is nearly linear, or when the existing saturation gradient is small. However, from a practical standpoint, this effect is of special importance in measurements of relative permeability to gas, as the region of economic importance in solution gas drive reservoirs is at gas saturations where the gas relative permeability-saturation curve is not linear. Calculations have shown that gas relative permeabilities measured over a 5 per cent uniform saturation gradient can be in the order of magnitude of 25 per cent lower than the true value associated with the average saturation.
2. A saturation gradient in a flowing system establishes the presence of a capillary pressure gradient. Thus each of the flowing phases will have a different pressure drop over the same increment of flow path. Pressure drop in the wetting phase will be less than that in the non-wetting.

Laboratory measurements of pressure gradient, for the sake of expediency and simplicity, are usually made in the non-wetting phase, as it is at the higher absolute pressure and its measurement requires no unusual auxiliary equipment. It is the general practice to attribute this pressure drop to both flowing phases. This practice then does not yield an absolutely true measurement of wetting phase relative permeability. But a measurement can be made which, for all practical purposes, is the true value — this over a flow path increment in which the saturation gradient is small, and therefore the capillary pressure gradient is percentage-wise extremely small compared to the total pressure drop.

The most disturbing effects of saturation gradients on relative permeability measurements occur in determinations made when measuring overall pressure drops in a bounded system. Three-sectioned core assemblies[11] were conceived to remedy this situation by measuring flow behavior a distance away from the outlet boundary where saturation gradients are greatest. Validity of results obtained by this method depends on the core performing as a single unit and pressure gradients sufficient to confine disturbing influence of end effect to the end core segment.

Oil-brine tests were performed using a three-sectioned Lucite-covered core assembly of acidized Nellie Bly sandstone. Electrical conductivity ring electrodes were installed on all three core sections, separating the assembly into 12 parts, thus permitting determination of saturation profiles during flow. The procedure was initially to saturate the core assembly with brine, then measure the specific permeability of the central or test section. The saturation of each of the core segments was reduced to an "irreducible" brine saturation by using semipermeable water-wet diaphragms. At this saturation, the capillary diaphragms were removed and the relative permeability to oil measured. Oil and brine were then simultaneously injected at oil/water ratios of 100:1; 10:1; 1:1; and 1:10, consecutively. At each flowing ratio, several equilibrium runs, each at different flow rates, were made. Electrical conductivity readings were measured at equilibrium conditions, and after the final run at each ratio, the test section was weighed.

Specific permeability of the test section measured with brine was 482 md and its porosity 25.5 per cent. Table I gives the calculated results of the steady state flow tests. It should be noted that at each flowing fluid ratio, the calculated oil/brine

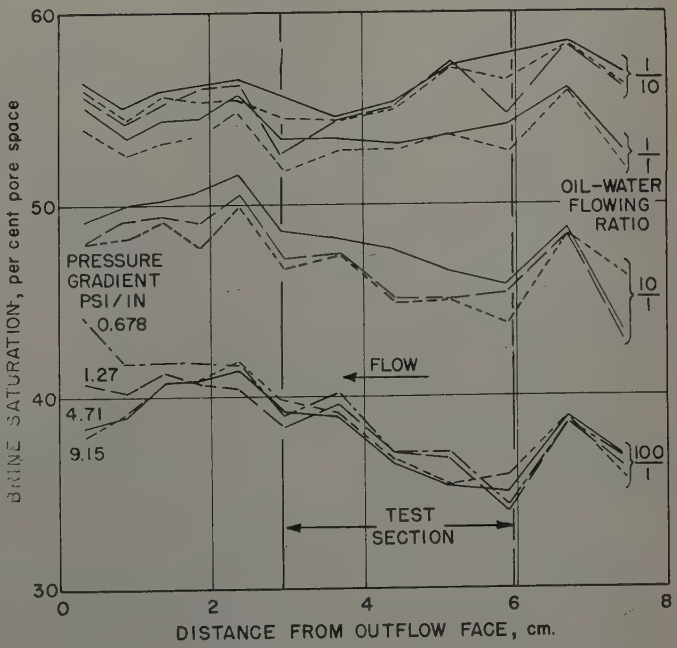

FIG. 3 — SATURATION PROFILES AT VARIOUS OIL/WATER FLOWING RATIOS.

(K_o/K_w) relative permeability ratio varies slightly from run to run. This was due to slight variations in the flowing ratio upon changing flow rates. The important observation is the consistency of the saturation value at each flowing ratio. Saturations in the test core at any ratio agreed within a range of 0.6 per cent to 1.4 per cent pore space, which is within limits of experimental accuracy. Therefore, for the range of pressure gradients used, there was no disturbing "end effect" on the measured values of relative permeability determined on the middle segment of the core assembly. Any important "piling up" of the wetting phase must have been confined to the end core segment. Fig. 3 shows this was the situation. Saturations measured along the three segments of the core are shown for each two-phase flow run. The variation in saturation profiles at any ratio shown are not as disturbing as they first appear, due to the expanded saturation scale. Profiles of the runs for the nominal oil/brine flowing ratio of 100:1 are the only ones which show any trend for an increasing brine saturation toward the outflow end of the system, and the magnitude decreases with increases in pressure gradient. All other runs do have slight variations in brine saturation at the end of the flow system, but do not have the trend which is associated with "end effect." In no case does the saturation gradient caused by "end effect" extend appreciably into the test section.

Relative permeability determinations are not always made under such satisfactory conditions. Other porous systems having basic characteristics different from the core tested can, with the pressure gradients used, have a disturbing "end effect" which extends into the test core section. A method for determining experimentally the range of pressure gradients which will result in true measurements is possible. At low wetting phase saturations, the capillary pressure is at a maximum and so "end effect" is most disturbing to flow measurements. In this saturation range, if increasing the pressure gradient at constant flow ratio results in no change in saturation, then the minimum useful pressure gradient is defined. Subsequent flow runs using pressure gradients above this minimum will result in true relative permeability measurements as tested.

Table I — Effects of Pressure Gradient on Relative Permeability Measurement

Oil/Water Flow Ratio	K_o/K_w	Average Brine Saturation Per Cent	Pressure Gradient psi/in.
Infinite	Infinite	14.2	2.04
100:1	150.6	36.9	4.71
100:1	149.4	37.2	9.16
100:1	149.4	37.3	1.27
100:1	152.3	37.7	0.678
10:1	15.76	47.3	14.34
10:1	15.36	45.9	4.93
10:1	15.04	46.3	0.994
1:1	1.488	53.5	1.24
1:1	1.510	52.9	3.05
1:10	0.1507	56.0	16.47
1:10	0.1507	55.6	8.14
1:10	0.1537	55.1	2.43
0	0	57.7	15.91

Referring again to Fig. 3 and observing the saturations at the planes of contact, it is noted that there is an apparent drop in brine saturation at these positions. It must be recognized that the planes of contact, due to their physical makeup, have a pore geometry somewhat different from the remainder of the porous system and will therefore have a different electrical conductivity-saturation calibration. Saturations shown were based on a calibration derived for the entire test section and so values given at the planes of contact may not be true ones. Even so, the fact that flow characteristics were consistent with changes in pressure gradient definitely establishes that no disturbing flow effects were present.

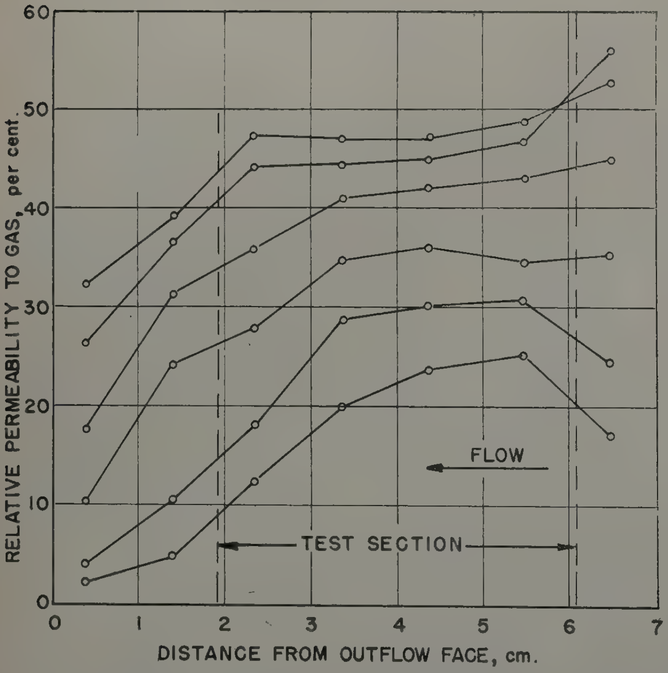

FIG. 4 — GAS RELATIVE PERMEABILITY PROFILES DURING AIR INJECTION INTO A PARTIALLY OIL-SATURATED TENSLEEP CORE.

Effects of Gas Expansion in Tests Conducted at Near Atmospheric Pressure

The expansibility of gas adds another complexity to the measurement of relative permeability in a gas-liquid system to those already covered in the two-liquid system. This effect is especially important in laboratory tests conducted using pressure differentials of the same order of magnitude as the absolute pressures. The volumetric rate of gas flow becomes progressively greater from inlet to outlet due to pressure reduction. Under certain flow conditions, this produces an increasing gas saturation in the direction of flow. As previously discussed, this saturation gradient can influence the accuracy of flow measurements.

Laboratory tests to determine experimentally the effects of gas expansion on relative permeability measurements were made using a three-section core assembly of Tensleep sand. Magnesium rings were spaced along each of the three core segments and after molding, were leached out with acid to make piezometer rings. The core assembly was thus divided into seven segments over which pressure drop could be measured by mercury U-tube Manometers. Fluids used in the tests were oil and air.

In the first test, the core was initially saturated with oil, and air only was injected into the assembly, with each successive equilibrium run having a higher injection pressure. The downstream face of the assembly was maintained at atmospheric pressure; thus, each succeeding run had a higher gas saturation. Results of these tests are shown in Fig. 4 as relative permeability to gas profiles. The general trend of the results indicates the presence of "end effect" which, under the conditions of the test, produced an implied saturation gradient extending into the test section of the core assembly. Under these flow conditions it is apparent that "end effect" is of large magnitude and errors in gas relative permeability measurements would result.

A second series of tests was performed by simultaneously injecting oil and air, with each successive run having a higher air/oil flowing ratio. Results are shown in Fig. 5 as relative permeability to gas profiles. Two things notable about these profiles, in comparison to those of Fig. 4, are (1) that the range of relative permeability in any one test is smaller than in the previous tests, and (2) that the trend of the gas relative permeability in these tests is increasing toward the outflow end of the assembly, which is in the opposite direction to the tests in which gas alone was injected. Obviously, the expansion of the gas under these conditions of flow influences the saturation gradient in a manner opposite to that of "end effect" alone. This effect is most pronounced in the range of low absolute pressures and may be minimized by using differential pressures small compared to the absolute pressure. Fig. 6 shows the results of the second run, in which the fluids were injected simultaneously, as gas to oil relative permeability ratio profiles. It is recognized that the differential pressure measured in the gas phase is not the same as in the oil, as has been assumed in these calculations. However, over the short increments of the core that were used in making measurements this error would be small. The curves of Fig. 6 show the effects of gas expansion downstream in the system.

One significant feature of these data is the consistent correlation of the results over the entire core assembly, which indicates that capillary continuity existed between each core segment at all saturations. Thus, in an air-liquid system, as in a two-liquid system, three-section core assemblies perform as a single continuous core.

Gas expansion may have another detrimental effect on measurements of relative permeability in methods which utilize saturation determinations by gravimetric means. In the particular technique represented herein, it is possible, under certain saturation conditions, when using gas pressures in the order of magnitude of 1 atmosphere gauge, that removal of the test section from the flow system into the atmosphere will cause an expulsion of as much as 10 per cent of the pore space liquid. Thus the saturations based on weights will be nonrepresentative of those existing during the flow portion of the test. A method which permits saturation determinations to be made while gas is flowing is desirable.

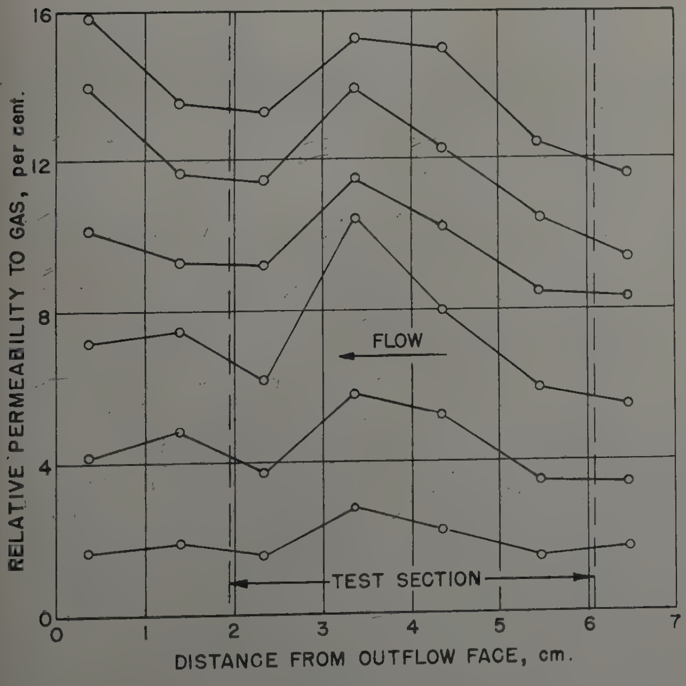

FIG. 5 — GAS RELATIVE PERMEABILITY PROFILES DURING GAS-OIL STEADY STATE FLOW IN TENSLEEP CORE.

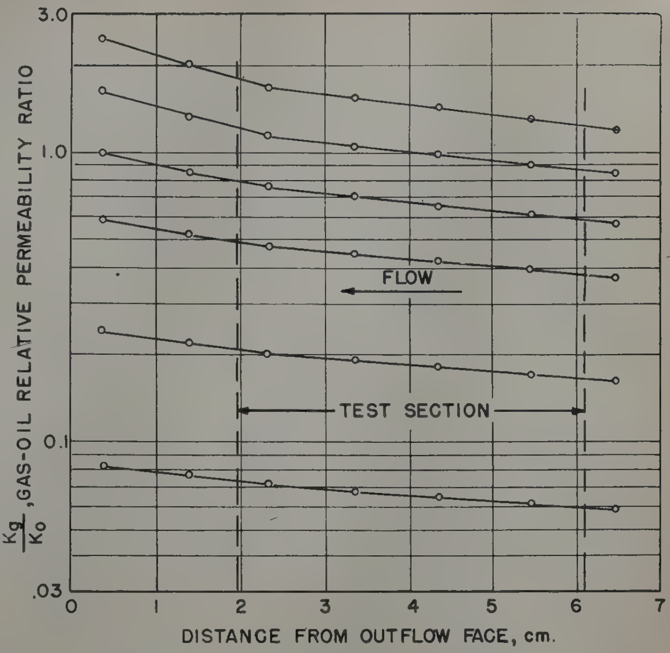

FIG. 6 — RELATIVE PERMEABILITY RATIO PROFILES DURING GAS-OIL STEADY STATE FLOW IN TENSLEEP SANDSTONE.

Effects of Migration of a Partial Water Saturation in Oil-Gas-Water Systems

Relative permeability tests simulating conditions of a gas drive reservoir require the presence of a water saturation to represent reservoir connate water. If core saturations are determined gravimetrically, this water must remain constant. Also, any migration of the water, even though its average saturation does not change, will alter the flow characteristics of the oil and gas. In the laboratory, core water saturations can be reduced by displacement with oil by pumping many pore volumes through (dynamic method)[13] or by use of semipermeable pads (static method).[14,15] In each case the established water saturation will reach an equilibrium with the imposed capillary pressure distribution. Subsequent flow conditions will alter this capillary equilibrium and tend to readjust the water saturation. If the entire core assembly has been previously reduced to an "irreducible minimum" water saturation, its mobility, for all practical purposes, is zero and so no migration can take place.

The dynamic method of reducing water in a core to a low value is associated inherently with a changing saturation gradient due to "end effect." Thus there will be water in the core which is mobile and so migrate with changes in flow conditions. Laboratory tests to show this phenomenon were made on the same sample of Tensleep sand previously described.

Oil was injected into the pre-brine-saturated core assembly and a relative permeability to oil profile obtained (Fig. 7). Flow was then stopped for 16 hours, after which the oil relative permeability profile showed a decided drop in magnitude all along the core assembly. This drop in permeability to oil can only be attributed to the increase in water saturation over that which existed previously. It has been calculated that the volumetric amount of water necessary to show this change in total oil conductivity was 0.1 cu cm. This amount of water was available for redistribution in the core in water previously present as "end effect" and also that which adhered to the outflow face of the core. Continuation of flow for four hours resulted in an oil relative permeability profile which closely approached the initial one. It is evident from these data that the water saturation was mobile and that its movement within the core would have a detrimental effect on gas-oil flow measurements.

A solution to this problem is to evaluate individually each of the existing fluid saturations, but this approach requires complex equipment and so a simpler method is more acceptable. The use of a capillary pressure type water desaturation method can establish in the entire core assembly an "irreducible minimum" saturation and thus prevent water migration.

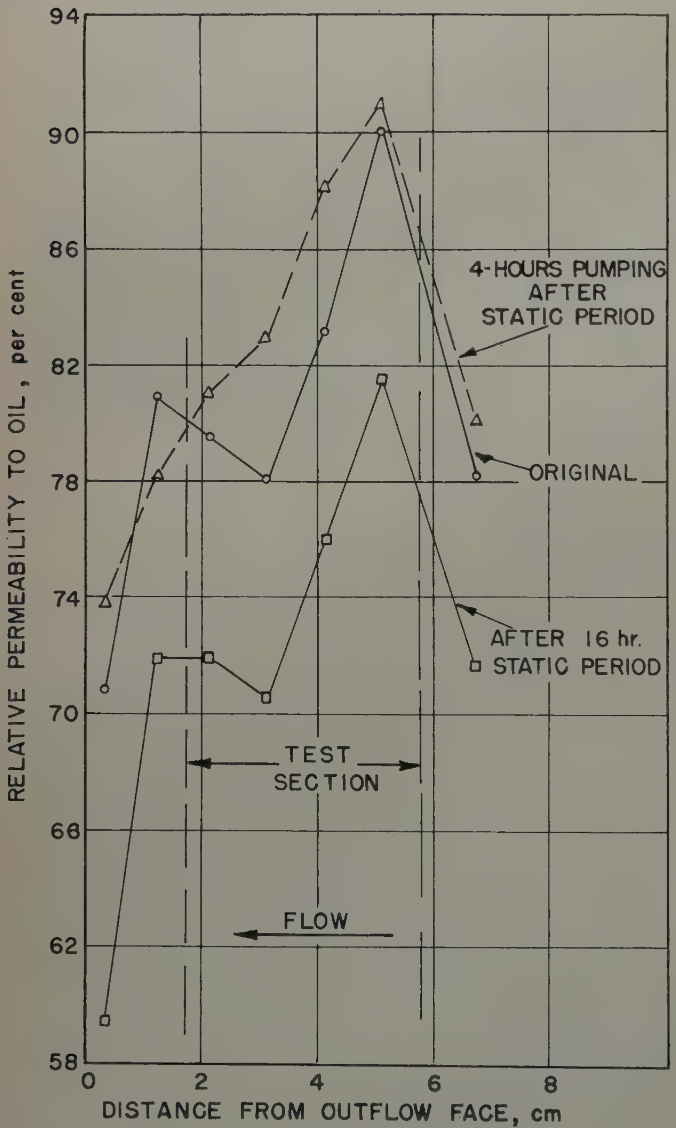

FIG. 7 — EFFECTS OF WATER MIGRATION ON OIL RELATIVE PERMEABILITY.

Validity of Testing Technique

Tests described have demonstrated that three-sectioned core assemblies perform as a continuous unit and with certain precautions measurements of relative permeability can be made which are independent of the testing technique.

Effects of Wettability Characteristics on Oil/Water Relative Permeability

The effects of wettability characteristics on fluid flow in porous materials and the performance of reservoirs has been postulated by Ryder,[16] and others.[11,17] Therefore, it is not deemed necessary to dwell at length on the theoretical aspects involved. Suffice it to say here that the relative positions of the fluids in individual pore spaces are controlled primarily by the wettability characteristics of the system. The wetting fluid will be adjacent to the solid surfaces of the pores. This and other complexities due to the differences in microscopic distribution of the fluids in oil and water wet sands result in marked differences in their flow behavior. Certain qualitative features of the relative permeability curve are used as criteria in establishing the predominant-wettability characteristic of a porous system. It is recognized that the practical problem concerns only systems containing oil and water — gas is assumed always to be a non-wetting phase. The features mentioned are:

1. In a two-liquid system, the non-wetting phase relative permeability curve approaches 100 per cent at low wetting phase saturation.
2. Wetting phase relative permeability reaches a maximum of 5 to 50 per cent at residual non-wetting phase saturation conditions.

An investigation of the effects of wettability characteristics on flow behavior was conducted using core samples of the Nellie Bly sandstone as the porous material. General characteristics of this sand have been described by Holmgren.[18] Oil-water steady state flow tests were made both before and after treating the sample with Dri-film 9977 to render the surfaces preferentially oil wet. Three sets of flow tests were performed.

1. Core surface as before Dri-film treatment and brine used as initial saturating fluid.
2. After treatment to render surface preferentially oil wet and initially saturated with brine.
3. Surface treated to be oil wet and initially saturated with oil.

Results of these tests are shown graphically in Fig. 8. Test 1 data indicate that the core was predominantly water wet, based on the qualitative features suggested previously. Typical oil wet flow behavior is suggested by results of Test 3. These two tests were performed similarly, having the preferential wetting liquid in contact with the pore walls before the introduction of the second phase. A more apparent comparison of these data can be made in the correlation of Fig. 9. Log relative permeability ratio K_w/K_o and K_o/K_w are related to saturation, S_w and S_o. The two sets each compared log K_o/K_w versus S_w show wide disagreement. But comparing them on a similar basis, namely, log relative permeability ratio of non-wetting phase to wetting phase versus the wetting phase

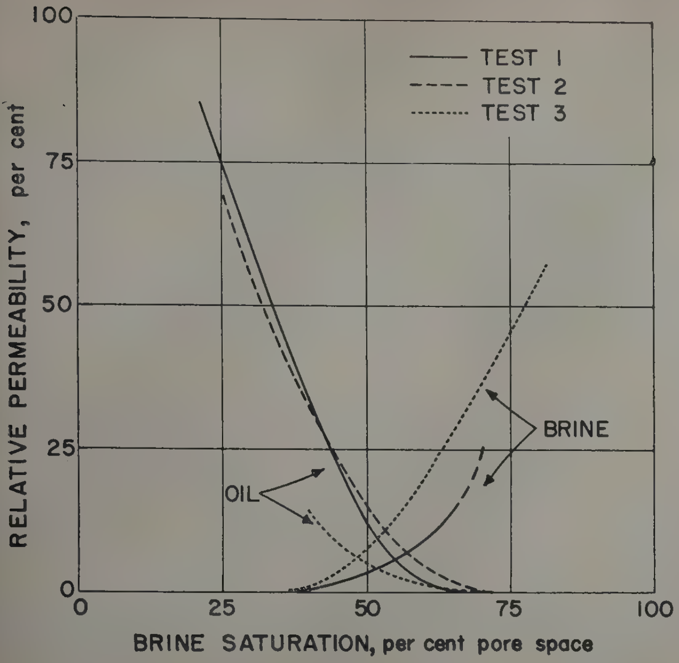

FIG. 8 — EFFECT OF WETTABILITY ON FLOW BEHAVIOR, NELLIE BLY SANDSTONE.

saturation, the peformance curves become alike. It is possible that the relationships so shown would be identical (saturation disagreement now 3 to 5 per cent pore space), if allowances were made for the unaccounted water absorbed by Lucite in Test 3 and the differences in chemically retained water (water of hydration of iron oxides) in the two tests. This test core was not equipped with electrical conductivity rings, so all saturations were obtained gravimetrically, which inherently limits accuracy of saturation determinations by approximately 2 per cent pore space. Therefore, it is reasonable to conclude that the fluids in Test 3 exchanged positions and flow behavior from conditions in Test 1.

Test 2, as shown in Fig. 8, conformed closely to results of Test 1. The initial saturating phase in both cases was brine, but the core in Test 2 was treated to be oil wet. Apparently, the affinity for oil was not too strong under conditions of Test 2 and in the short-duration laboratory test, the fluids were not able to arrange themselves in a microscopic distribution in equilibrium with the wettability characteristics of the system.

Other tests using samples of the Third Bradford sand were run using brine as the initial saturating phase. Results were in agreement with those of Henderson and Yuster,[10] giving qualitative flow characteristics indicative of a preferentially oil-wet sand. Obviously, in short-duration laboratory flow tests on preferentially oil-wet sands when the cores are initially saturated with brine, the degree of oil wettability will determine whether or not the true equilibrium flow behavior will be measured. For practical purposes, only systems exhibiting intermediate oil preferential wettability will be troublesome if brine is used as the initial fluid to contact the pore walls. A porous material in this range of wettability preference should possibly be initially saturated with oil in the laboratory or permitted sufficient time to reach wettability equilibrium to yield true flow behavior.

No attempt is made herein to formulate a method to establish the existing wettability characteristics of a petroleum reservoir. It must be recognized that the possibility exists that core samples of reservoirs received for testing in the laboratory may be altered by various means from their original condition.

Effects of Saturation History

There are two saturation histories that occur naturally in the production of petroleum: displacement of a wetting phase by a non-wetting and vice versa, *e.g.*, oil displacement by a gas or by brine. For reasons of simplicity, the discussion which follows will consider gas as always being a non-wetting phase and brine a wetting phase. Oil will be considered a wetting phase with respect to gas and a non-wetting phase relative to brine. It is generally assumed that these conditions exist in the majority of sandstone petroleum producing reservoirs. The two types of flow mechanisms are each associated with separate types of relative permeability characteristics. The differences can be attributed to the manner in which the fluids are distributed among the various pore sizes. The statistical saturation distribution, unique to each saturation history, is explained by visualizing the movement of fluids in porous materials.

A naturally occurring porous material is composed of a multitude of pore units of various sizes and shapes combined in a random order. Consider the case of the pores completely filled with brine and a non-wetting fluid, gas, advancing into it. Each pore unit, composed of a body and several comparatively small openings leading into it, will perform individually. Gas will enter those pore constructions with which it comes in

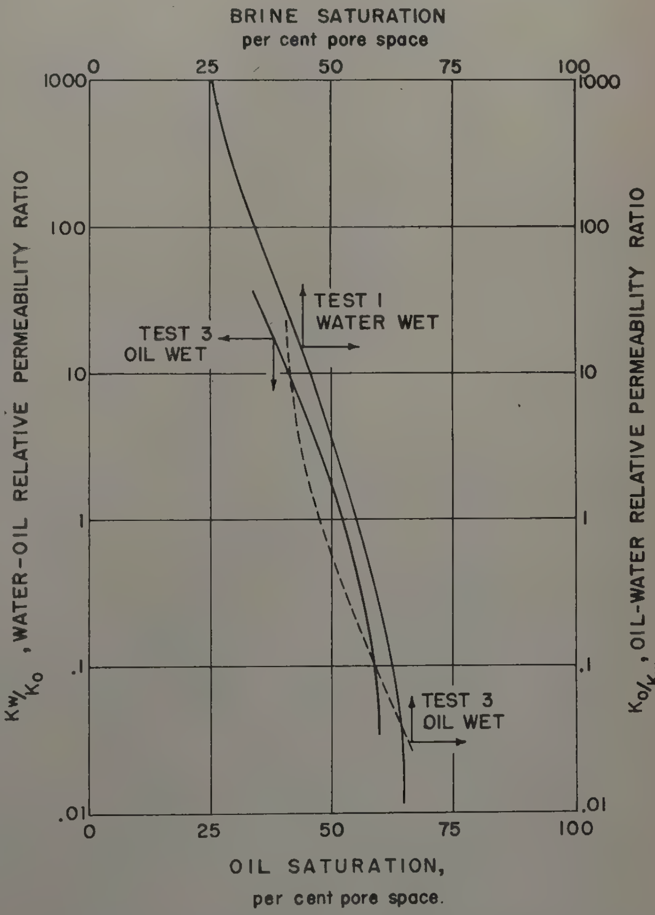

FIG. 9 — COMPARISON OF FLOW BEHAVIOR IN WATER-WET AND OIL-WET SYSTEMS.

contact whose displacement pressure it exceeds. When an entrance constriction has been displaced, the pore body, by virtue of its larger radius, will also be displaced. Flow of gas through a pore unit will take place when two or more of its constricted portions are displaced by gas. Not all of the brine in the re-entrant angle portion of pores is displaced by the initial advance of gas into a pore. Gas can exist continuously through the length of a porous material as a high gas saturation in only 1 to 2 per cent of the pore units. Under these conditions of saturation, the gas flows as a continuous phase through a winding path which connects pore units containing at least two constrictions whose displacement pressure has been exceeded. The minimum saturation associated with independent flow of gas is termed the "critical gas saturation." Any pore unit having only one constriction displaced will not contribute to the gas conductivity.

Pore units may exist in the system which contain constrictions of such radius that, by equilibrium capillary pressure considerations, they should be displaced, but are not. This is due to the complexity of the pore size distribution which prevents a direct path of travel of the displacing gas to all pore units. These two conditions exist over a major portion of the gas saturation range and are the factors which complicate any attempts to describe flow behavior analytically. Simply, it may be stated that not all pores in a system over the entire saturation range perform according to the equilibrium capillary pressure saturation relationship attributed to the gross system, and that gas exists in some pore bodies connected to the continuous stream of gas by only one constriction and so do not add to the gas conductivity. The nature of the gas relative permeability curve can be explained by the above discussion. As gas saturation increases, so does the rate of increase in its permeability, due to the addition of more conductive pore bodies, which contained gas at lower saturation, but did not contribute to gas flow. Using the same type of analysis, and recognizing that the pore bodies are relatively more conductive than their constrictions, brine flow behavior can be explained.

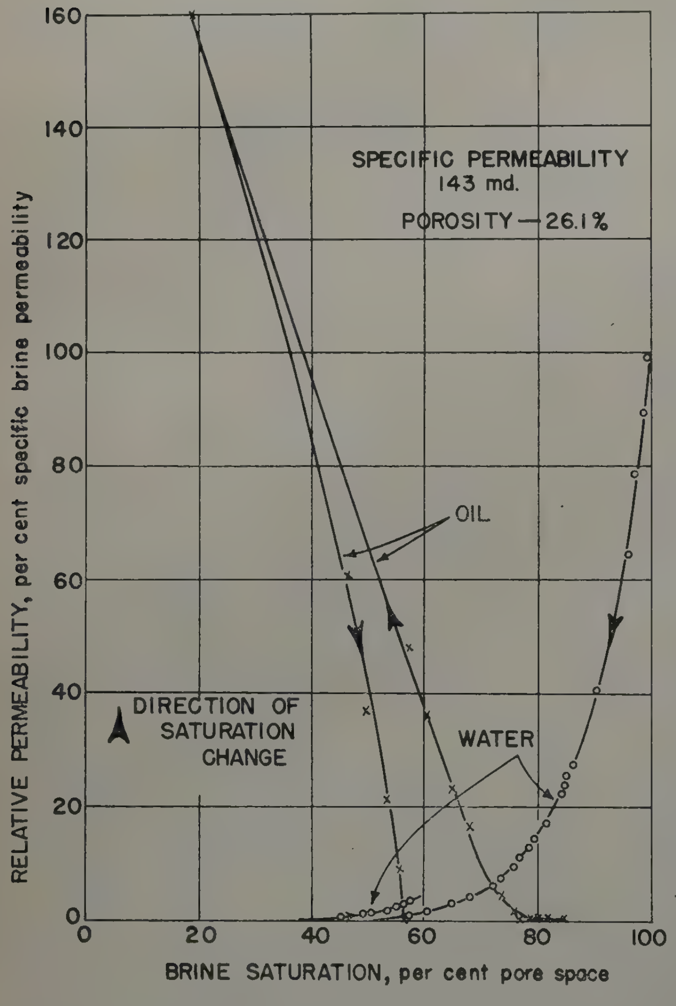

FIG. 10 — OIL-WATER FLOW CHARACTERISTICS, NELLIE BLY SANDSTONE.

The flow mechanism described represents the natural flow process of a gas drive. Gas displacement of oil, even in the presence of connate water will, in general, be the same as the described gas displacement of water. In heterogeneous porous systems, this flow process is characterized by a low "critical gas saturation" which has a detrimental effect on the efficiency of oil displacement. Field data indicate that values for this gas saturation are in the range of less than 1 to 5 per cent pore space. Laboratory values have been reported much higher than this, but it is thought that these were influenced by technique and should be the same order of magnitude as field data.

Statistical saturation distribution of fluids in the system in a water flood mechanism is different from that described. Initially the brine is located as a film over the pore walls, in the re-entrant angle portion of the pore unit constrictions, as well as completely filling some of the minute pores. Oil fills the remaining pore space. Each capillary opening, by virtue of its size and saturation, will tend to imbibe any available water and so displace any oil it contains. The oil saturation will be reduced by changes in the oil-water interface curvature in the continuous oil phase. As the curvature becomes less, some pore constrictions, due to their size, will become completely filled with water. Once the curvature has been reduced to a value permitting all of the constrictions of a pore unit to be filled with water, the pore body oil will be isolated from the continuous oil phase and so trapped and unrecoverable by practical displacement forces. This accounts for the high "residual oil saturation" associated with water flooding. Oil remaining in the pore bodies will be in a thermodynamically unstable state and will tend to diffuse through the water and out of the system, but this mechanism is not of practical importance in oil recovery. Numerous laboratory tests on cores of various types of synthetic and naturally occurring porous materials have indicated that trapped oil saturations range from 15 to 50 per cent pore space. As in the gas drive mechanism, the shape of the oil/water relative permeability relationships can be explained by using the above concepts.

The mechanisms of displacement described above, although referred to specific fluid systems, hold for any single wettability system. Thus displacement of gas by water and displacement of water by oil will have similar relative permeability characteristics to displacement of oil by water and displacement of water by gas, respectively. Experimental data have been published by Leverett[3] to show that water and oil flow behavior are not affected by a 1600 to 1 change in their viscosity ratio. This is the same order of magnitude of comparative viscosity ratios of a water-gas and a water-oil system. Also, interfacial tension over a wide range has been shown not to affect flow behavior. Therefore, it is reasonable to expect that a system in which wettability does not change the nonwetting phase (oil or gas) and the wetting phase (brine or oil) will have flow characteristics independent of the nature of the fluids, and in any two immiscible fluids system, both typical gas drive and water flood mechanisms are possible. Relative permeability is then not a single-valued function of saturation, but must be associated with a specific saturation history.

Core samples of the naturally occurring Nellie Bly sandstone and a synthetic porous material of LA type alundum were used in the experimental investigation of saturation history effects. Each core assembly was equipped with electrical conductivity rings on all three sections. Two fluid systems, air-brine and oil-brine, were investigated in each porous material. A test entailed initially saturating the core assembly with brine, then injecting simultaneously air or oil with brine, with each succeeding equilibrium run having a lower brine saturation. After attaining a low brine saturation, the fluids were injected, with successive runs having a higher brine saturation until brine alone was injected.

Effects of saturation history on oil-brine relative permeability characteristics of the Nellie Bly sample tested are shown in Fig. 10. The wide deviation of flow behavior under conditions of the saturation history imposed is readily apparent. One data point, at 18.5 per cent brine saturation, shows an oil relative permeability in excess of 100 per cent. This can be explained as all effective permeabilities were compared to the specific permeability to brine of the 143 md. This value is only half the specific permeability to air, which is greatly in excess of the expected variation due to gas slippage alone. Therefore, it is reasonable to assume that this core sample contained substantial amounts of hydratable materials. It is thought that the arrangement of hydrated particles in pore spaces is different in the presence of oil and water than when in water alone, and causes this phenomenon. Many other cores containing hydratable materials tested in this laboratory have shown this same behavior.

Additional tests on the Nellie Bly oil-brine system were made by establishing a partial oil saturation, then flooding the core with brine. The oil saturation before each successive brine flood was increased over the previous one. In several of these tests, an intermediate run was made by flowing both fluids. Fig. 11 is a plot of these data as oil/brine relative permeability ratio on a log scale versus the brine saturation. The original flow characteristics obtained by an increasing oil saturation history are reproduced within 2.5 per cent in values of saturation. This is a tolerable agreement, considering that some of the previously hydrated materials could have been removed during flow, and the limits of experimental accuracy associated with this type of testing. The point of interest is that each maximum oil saturation results in a different flow behavior upon increasing the brine saturation. Further experiments have shown, once an oil saturation has been established and the flow behavior determined in an oil desaturation direction, that this flow behavior is reversible and reproducible, provided the previous maximum oil saturation is not exceeded.

Similarly tests in the air-brine system were made and these results are compared with some of the data of the oil-brine tests in Fig. 12. Quantitatively, the flow characteristics of the two systems are not in agreement. But qualitatively, the ef-

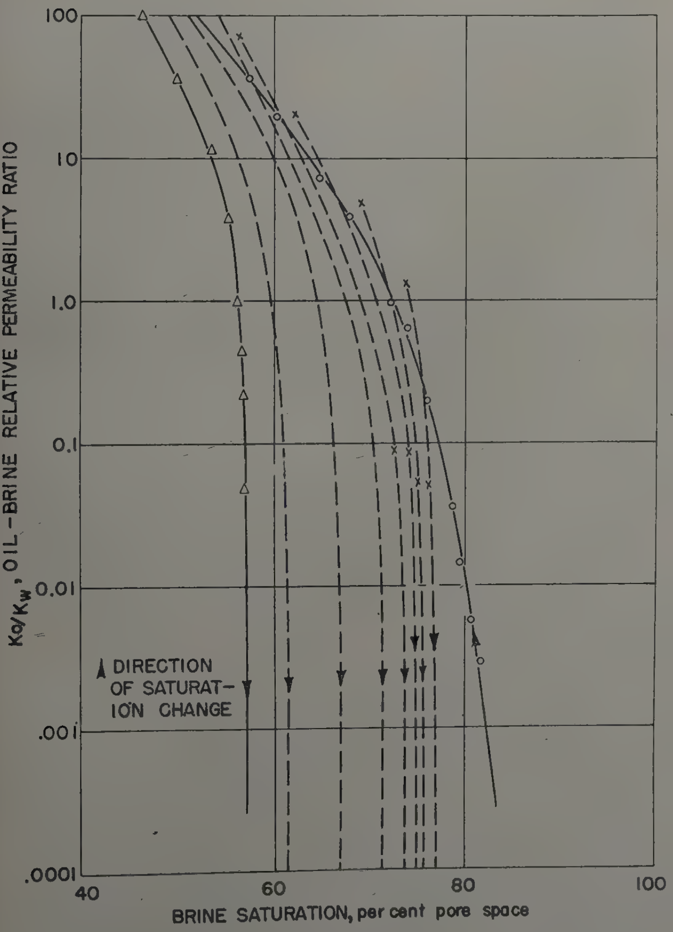

FIG. 11 — EFFECT OF SATURATION HISTORY ON OIL-FLOW BEHAVIOR, NELLIE BLY SANDSTONE.

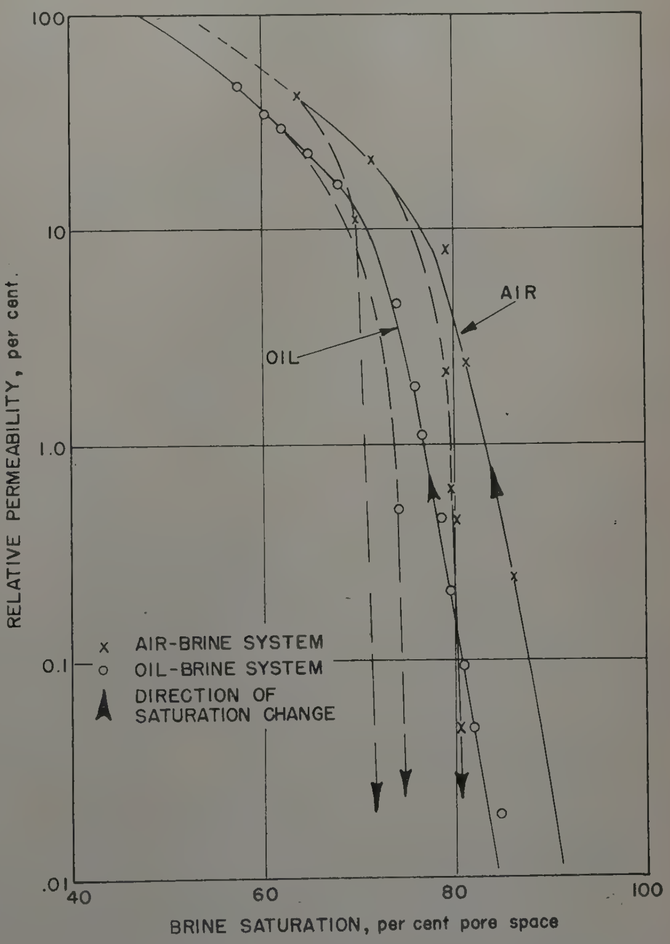

FIG. 12 — COMPARISON OF OIL AND AIR FLOW BEHAVIOR IN TWO-PHASE SYSTEMS, NELLIE BLY SANDSTONE.

fects of saturation history are the same. Differences in the wettability characteristics of the two systems is thought to be a contributing factor to the lack of quantitative agreement.

A saturation of practical significance is that at which the nonwetting (oil or gas) phase will not flow as an independent phase. In a gas drive mechanism, this is usually referred to as the "critical saturation." In Fig. 13, the saturation profile of the core assembly under various flow conditions is shown. The two uppermost profiles are for the initial flow tests of the oil-brine and air-brine systems. Both show that the non-wetting phase flowed through the core at low saturations. Several core segments have saturations to oil or gas of less than 1 per cent. These profiles do not represent the minimum oil or gas saturations that could exist; they were the first measured. It is evident that the "critical saturation" to gas or oil is approximately 1 per cent.

In a water drive flow mechanism, the displaced phase becomes discontinuous and will not flow at a saturation referred to as the "residual." Fig. 13 shows saturation profiles for both the oil-brine and the air-brine systems at these conditions. In each case, after an oil or air saturation has been established, the core was subjected to a water flood. The lower profile is for the oil-brine system, showing a residual oil saturation in the test section of 44 per cent pore space. The oil saturation of the entire core assembly is generally uniform, varying a maximum of only 3.5 per cent. Saturation profiles for gas-brine tests also shown in Fig. 13 do not show the same uniformity but show a residual gas saturation of up to 32 per cent of the pore space. Data for the lower gas profile were taken one-half hour after brine breakthrough. The existing gradient is attributed to three factors:

1. An increasing gas saturation downstream was originally established due to expansion effect of gas. (This factor has been previously explained.)
2. Differential compression of the trapped gas by the flowing brine.
3. Gas saturation removed by solution in the brine. (A large number of pore volumes of brine had been flowed through the system.)

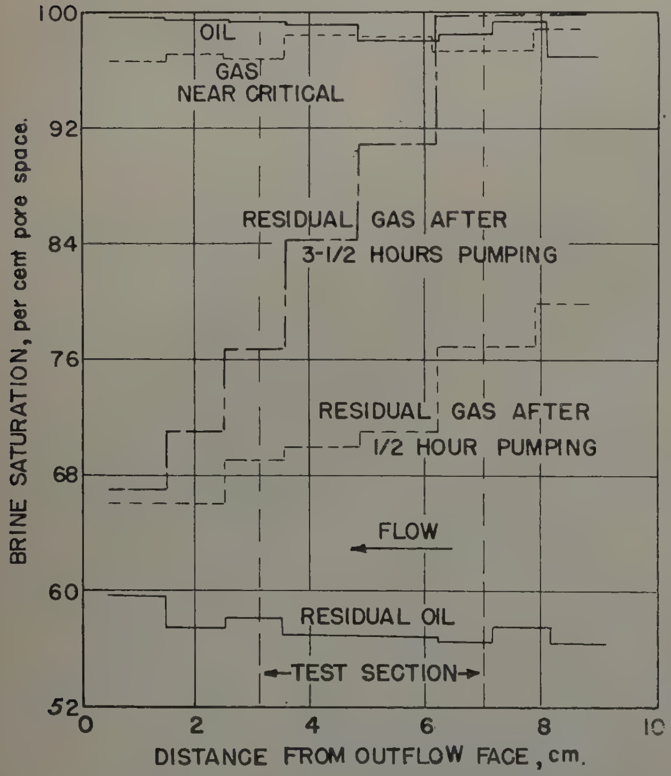

FIG. 13 — SATURATION PROFILES, NELLIE BLY SANDSTONE.

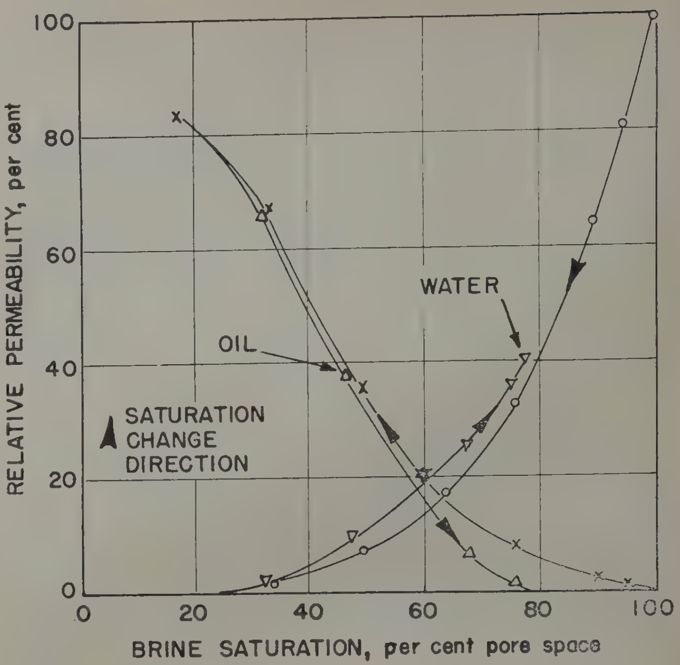

FIG. 14 — OIL-WATER FLOW CHARACTERISTICS, LA TYPE ALUNDUM, SPECIFIC PERMEABILITY 640 MD, POROSITY 24.6 PER CENT.

The last factor is more evident in the remaining profile, which was taken three hours after the first. Portions of the upstream end of the core assembly show 100 per cent brine saturation and the rest of the core segments a differential increase in brine saturation. The last core segment, which is least susceptible to a reduction in gas saturation by solution and compression, shows very little change. By this analysis, it is concluded that a gas saturation of at least 32 per cent was trapped in these tests and so was unrecoverable by water displacement mechanism.

Residual values for oil and gas are not the same in these tests for two reasons:

1. Maximum oil saturation attained before water displacement was 81.3 per cent compared to 42 per cent for air. It was shown previously (Fig. 11) that the residual saturation is a function of the maximum attained non-wetting phase saturation.
2. Questionable wettability characteristics of this core sample add to the probability that the oil and gas residual saturations would not be identical.

Oil/brine relative permeability tests for the alundum core are shown in Fig. 14. As for the Nellie Bly, each saturation history results in a separate flow behavior. In the increasing oil saturation tests, oil permeability was measured at an oil saturation of 5 per cent. This is not the lowest oil saturation at which oil would flow, so the "critical oil saturation" is lower than this — probably less than 1 per cent pore space. A residual oil saturation of 24 per cent pore space was measured.

It is significant to note that even in this type porous material, which has a narrow range of pore sizes compared to natural sands, there is an appreciable residual oil saturation.

Flow characteristics of air and brine are compared to those of oil and brine in Fig. 15 as non-wetting to wetting phase relative permeability ratio on a log scale versus brine saturation. The close agreement of these is apparent. As did the oil, air indicated a "critical saturation" of approximately 1 per cent and a residual saturation of 24 per cent. The physical nature of the solid surfaces of this core make it preferentially water wet in the presence of either oil or air with brine and so wettability is not a factor in its flow behavior of the two-fluid systems studied.

Practical Significance of Saturation History

The wide variation of flow behavior in a two-phase system makes it imperative that laboratory tests be conducted with a saturation history simulating that of the reservoir being represented. In addition, the ideas presented have important economic implications in the production of oil and gas.

The natural method of displacement of oil by gas is recognized to be inefficient. It has been shown that a statistical saturation distribution of gas different from that which occurs under natural operations is possible and that this produces, by virtue of the higher gas saturation which does not flow as a free phase, a higher oil displacement efficiency. Thus it is a distinct possibility that gas drive reservoirs can be produced in a manner which will approach 15 to 50 per cent gas saturation as a "critical saturation."

An immediately important implication of indicated high residual gas saturations following water displacement of gas is in the evaluation of recoveries to be expected from gas and gas condensate reservoirs under water drive, either natural or induced. Evaluating the gas recovery from this type of field using relative permeability characteristics representative of a progressively increasing gas saturation history could result in a very serious error. Residual gas saturations by tests simulating the reservoir saturation changes (decreasing gas saturation) are indicated in the range of 15 to 50 per cent, rather than the 1 to 11 per cent usually assumed.

Confirmation of the validity of residual gas saturation as obtained from relative permeability tests has been made using a one-ft long core. Brine was injected upward into the core at calculated rates of rise of one and 40 in. per day and in each case the "residual gas saturation" agreed within experimental accuracy with results on a small core plug relative permeability test conducted with the proper saturation history.

CONCLUSIONS

1. Three-section, plastic-covered core plug assemblies, properly constructed, will perform during fluid flow as one continuous core.

2. Pressure gradients can be selected which will confine the disturbing boundary effects to the end core section and thus permit measurement of true relative perme acteristics of the middle core segment.

3. Gas-oil flow tests in cores containing a partia uration, representing connate water, must have the assembly reduced to an "irreducible minimum" wa tion. This will prevent migration of water and enable saturations to be determined gravimetrically.

4. The practice of initially saturating test cores with brine will result in two-phase flow behavior which will be in equilibrium with its existing wettability characteristics, except in cases of a limited degree of oil wettability. In this later instance, the procedure required for representative data has not been established.

5. Relative permeability is not a single-valued function of saturation. The saturation history involved affects the statistical saturation distribution of the fluids in the pore space. Laboratory tests to represent flow in a reservoir must have a similar saturation history.

6. Relative permeability characteristics of a system, in which wettability does not change, are not influenced by the physical properties of the fluids involved. That is, a gas-

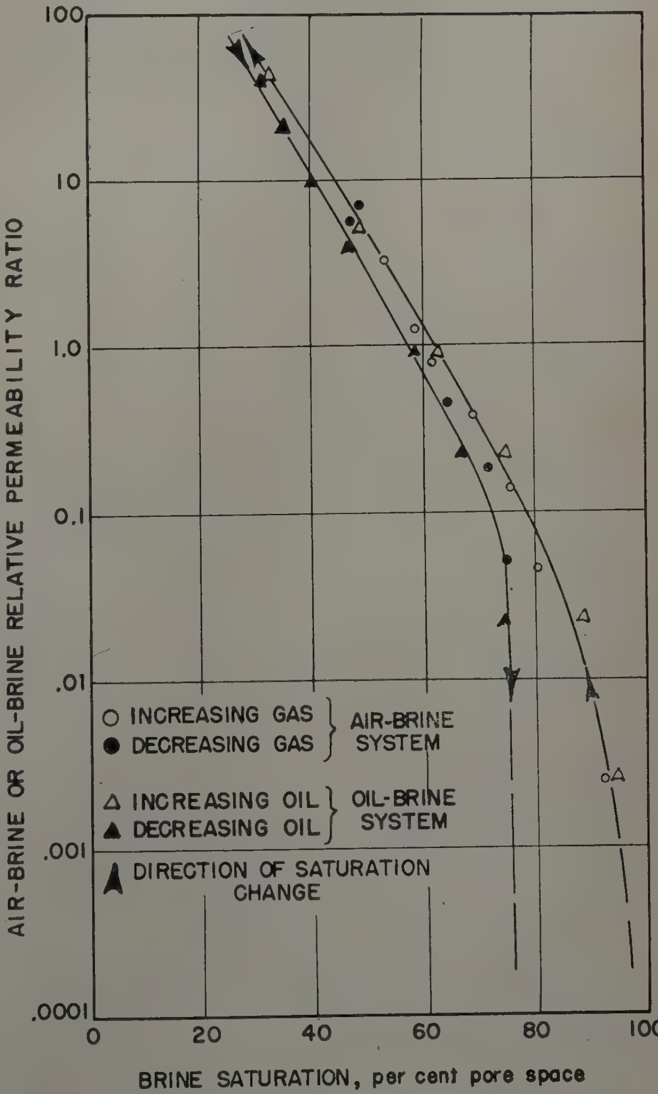

FIG. 15 — COMPARISON OF OIL AND GAS FLOW BEHAVIOR IN ALUNDUM CORE.

fe water and oil-water flow system perform identically provided saturation histories are the same.

7. The numerous relative permeability saturation relationships possible in porous systems containing gas imply that oil displacement by gas can be made more efficient than the natural process. A method is not offered, only the possiblity suggested.

8. A substantial amount of gas will remain in the pore space of a water invaded gas or gas condensate reservoir. It is estimated that the range of the trapped gas saturation will be 15 to 50 per cent pore space and not the "critical gas saturation" usually taken as 1 to 11 per cent pore space.

ACKNOWLEDGMENTS

The authors wish to express their appreciation to the Stanolind Oil and Gas Co. for permission to present this paper. The assistance of Lawton Ragsdale in the collection of much of the data is herewith gratefully acknowledged.

REFERENCES

1. Elkins, L. E.: *API Drill. and Prod. Prac.*, (1946) 160.
2. Gooch, F. W., and Watson, M. S., Jr.: *World Oil*, (1950) **130**, No. 1, 135.
3. Leverett, M. C.: *Trans.* AIME, (1939) **132**, 149.
4. Botset, H. G.: *Trans.* AIME, (1940) **136**, 91.
5. Leverett, M. C., and Lewis, W. B.: *Trans.* AIME, (1941) **142**, 107.
6. Rose, Walter: *Trans.* AIME, (1949) **186**, 111.
7. Wyckoff, R. D., and Botset, H. G.: *Physics*, (1936) **7**, 325.
8. Leverett, M. C.: *Trans.* AIME, (1941) **142**, 152.
9. Henderson, J. H., and Meldrum, A. H.: *Prod. Monthly*, (Mar. 1949) 12.
10. Henderson, J. H., and Yuster, S. T.: *Prod. Monthly*, (Jan. 1948) 13.
11. Muskat, M.: *Physical Principles of Oil Production*, McGraw-Hill Co., (1949) 271-304.
12. Morse, R. A., Terwilliger, P. L., and Yuster, S. T.: *Oil and Gas Jour.*, (Aug. 23, 1947) 109.
13. Slobod, R. L.: *Trans. AIME*, (1950) **189**, 359.
14. McCullough, J. J., Albaugh, F. W., and Jones, P. H.: *Drill. and Prod. Prac.*, (1944) 180.
15. Bruce, W. A., and Welge, H. J.: *Oil and Gas Jour.*, (July 26, 1947) **46**, No. 12, 223.
16. Ryder, H. M.: *World Oil*, (June 1948) **128**, No. 2, 142-158.
17. Pirson, S. J.: *Elements of Oil Reservoir Engineering*, McGraw-Hill Book Co., (1950).
18. Holmgren, C. R.: *Trans.* AIME (1949) **179**, 103. ★ ★ ★

T.P. 3026

CARRYING CAPACITY OF DRILLING MUDS

C. E. WILLIAMS, JR., ASSOCIATE MEMBER AIME, AND **G. H. BRUCE,** HUMBLE OIL AND REFINING CO.,
HOUSTON, TEX.

ABSTRACT

The trend toward deeper drilling, together with the attendant increase in power requirements for circulation of the drilling fluid, has emphasized the need for a critical examination of the factors affecting the removal of bit cuttings from the hole by the drilling fluid. The ability of drilling fluids to lift cuttings is called their carrying capacity.

A series of laboratory and field experiments has been conducted to determine the minimum annular velocity necessary to remove cuttings, and to investigate the effects of properties of drilling fluids on their carrying capacities.

Consideration of the results of these experiments led to the following conclusions:

1. Turbulent flow in the well annulus is most desirable from the standpoint of cutting removal.
2. Low viscosity and low gel are advantageous in removing cuttings.
3. Increase in mud weight is effective in increasing carrying capacity.
4. The carrying capacity is higher when the pipe is rotated than when it is not.
5. If turbulent flow can be maintained, an annular velocity slightly higher than the slip velocity of the largest cuttings to be transported should keep the bore hole clean. This implies velocities of 100 to 125 ft per minute rather than the presently used 175 to 225 ft per minute.

INTRODUCTION

Power Savings by Reduction of Annular Velocities

A large portion of the power expended in drilling operations is consumed in circulating the drilling fluid. An important factor in establishing the rate of mud circulation is the minimum velocity in the annulus necessary to remove bit cuttings. Empirically, it has been found that average annular mud velocities of about 200 ft per minute will remove cuttings. It was not definitely known, however, whether annular velocities of about 200 ft per minute were just above the minimum necessary to remove cuttings, or whether such velocities could be materially reduced without sacrifice of the ability of the mud to remove cuttings. It is apparent that if annular velocities could be reduced without impairment of cutting removal, a considerable saving in power requirements would result.

Need for Research on Carrying Capacity

The ability of a drilling fluid to transport cuttings is called its carrying capacity. Although it has been recognized that the carrying capacity of a mud is affected by mud properties such as viscosity and density[1,2,3,4] there have been various views in the industry as to the effects of these mud properties on carrying capacity.

The economic importance of the problem of carrying capacity and the scarcity of information on the subject indicated that research on the problem was needed.

THE FACTORS AFFECTING CARRYING CAPACITY

Qualitative Determination of Factors

The mechanism of cutting transport is closely related to that involved in the separation of material by settling processes. A considerable amount of research has been done on settling problems, and discussions of sedimentation theory can be found in standard texts.[5,6] Consideration of the information available from these sources, together with consideration of the mechanism of cutting transport, leads to the conclusion that the factors affecting carrying capacity are the dimensions of the system, the physical properties of the cuttings, and the physical properties of the drilling fluid.

System Dimensions and Their Effect

The dimensions of the fluid circulating system of importance to carrying capacity are the bore hole size, drill pipe size, pump capacity, and pump speed. These dimensions determine the annular velocity of the drilling fluid.

Physical Properties and Their Effects

The physical properties involved in the interaction between mud and cuttings are the density and shape of the cuttings and the density, viscosity and gel strength of the drilling fluid. The effect of the density factor on carrying capacity is fairly obvious; high density difference between cuttings and fluid results in a low buoyant force and therefore decreases carrying capacity. The effect of cutting shape is less obvious. Although

---

[1] References given at end of paper.

Manuscript received in the office of the Petroleum Branch, Aug. 27, 1950. Paper presented at the Fall Meeting of the Branch in New Orleans, La., Oct. 4-6, 1950.

the velocity of fall through quiescent Newtonian fluids for particles of regular shapes may be calculated from well-known equations,[5] little information is available in regard to irregular shapes falling in moving fluids of non-Newtonian character such as drilling fluids.

The non-Newtonian characteristics[7-12] of most drilling fluids severely restrict the prediction of the effect of viscosity, as it is ordinarily measured, upon the carrying capacity of the fluid. If the reasoning of hydrodynamics were applicable, it would be expected that higher viscosities would result in lower fall velocities and therefore in higher carrying capacity.

The effect of gel strength on carrying capacity has received little attention in the literature.

Experimental Determination of Factors

In the conduct of experiments designed to yield information on carrying capacity, an attempt was made to determine the minimum annular velocity sufficient to remove cuttings, to obtain correlation between measurable mud properties and carrying capacity, and to test the validity of various equations applying to the slippage of solid particles in fluids. The experiments were carried out in two distinct phases; a field phase and a laboratory phase.

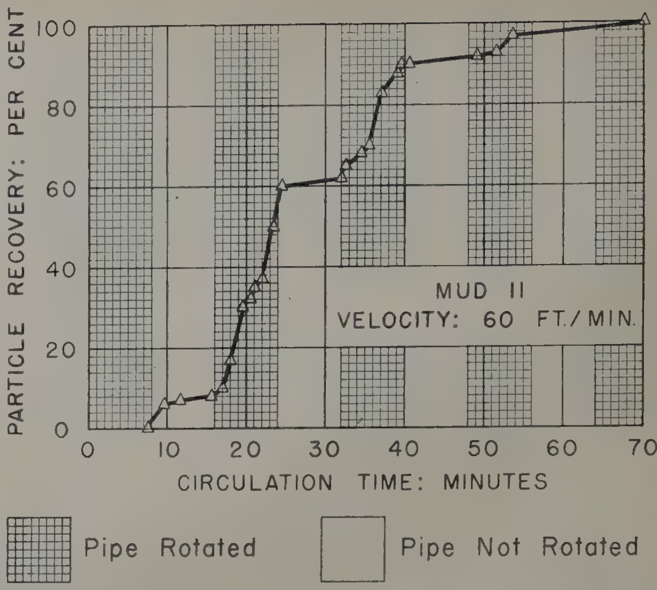

FIG. 1 — EFFECT OF DRILL PIPE ROTATION ON PARTICLE RETURN.

FIELD PHASE OF EXPERIMENTS

Equipment and Materials

The field phase of the experiments was carried out in a 500-ft experimental well at Pierce Junction, Tex. The well was cased to bottom with 7-in. casing and was plugged at the bottom. The initial layout did not include provisions for rotating the drill pipe, nor was an effort made to center the pipe in the casing. Initially 2½-in. line pipe was used to simulate the drill pipe. Centering guides were later installed on the line pipe to prevent channeling of the mud. Subsequently, the line pipe was removed and a 2⅞-in. drill pipe was suspended from a rotary table, thus permitting pipe rotation.

Provisions were made for inserting simulated cuttings into the drill pipe and for recovering the cuttings at the surface. Particles used to simulate cuttings were glass spheres, ceramic chips and aluminum discs. Glass spheres and ceramic chips were unsatisfactory because of their frangibility, so that most of the work was done using three sizes of aluminum discs which were hammered slightly to give them a shape similar to that of actual cuttings. These three sizes of discs will be referred to as small, medium, and large particles. The type of particles used and their characteristics are given in Table I.

Twenty-three fluids were tested as transport media. The fluid densities ranged from 8.33 lbs per gal (water) to 14.8 lbs per gal; viscosities ranged from 1 to 200 centipoise; and initial gels ranged from 0 to 90 grams Stormer. The properties of a number of the fluids are listed in Table II.

Procedure

The general procedure followed at Pierce Junction was to insert a given number of simulated cuttings into the drill pipe and to pump them slowly to the bottom. When the cuttings reached bottom, the desired circulation rate was established,

Table I—Properties of Particles Used as Simulated Cuttings (Field Experiments)

Type of Particle	Material	Diameter in.	Thickness in.	Density lb/cu ft	Thickness / Diameter	Remarks
Sphere	Glass	1.00	—	159	—	
Sphere	Glass	0.73	—	159	—	
Sphere	Glass	0.70	—	159	—	
Sphere	Glass	0.57	—	159	—	
Sphere	Glass	0.24	—	159	—	
Sphere	Glass	0.20	—	159	—	
Disc*[1]	Aluminum	0.750	0.250	168	0.333	All discs hammered to roughen their surfaces and to give them a shape similar to bit cuttings.
Disc*[2]	Aluminum	0.750	0.125	168	0.167	
Disc	Aluminum	0.625	0.125	168	0.200	
Disc	Aluminum	0.625	0.063	168	0.100	
Disc	Aluminum	0.625	0.031	168	0.050	
Disc*[3]	Aluminum	0.500	0.125	168	0.250	
Ceramic Chips	Broken Pottery	—	—	150-160	—	Various shapes and thickness; ground to bits by drill pipe.

*These three sizes of discs were used to obtain most of the data.

[1] Large disc or large particle.

[2] Medium disc or medium particle.

[3] Small disc or small particle.

Table II — Properties of Muds Used in Field Experiments

Mud No.	Viscosity		Initial Gel Strength gms - Stormer	Mud Weight lb/gal	Remarks
	Marsh Funnel Sec	Stormer cps at 600 rpm			
7	41	23	3	10.4	
8	63	56	35	10.4	
9	72	65	40	10.4	Same as mud No. 8. Aged for 1 day.
10	107	97	90	12.3	
11	67	88	6	12.5	Phosphate treated.
12	99	144	6	14.8	Phosphate treated.
13	255	$>$200 (570 gms)	12	14.8	Very thick. Phosphate treated.
14	49	34	2	12.3	Phosphate treated.
15	70	83	3	12.2	Phosphate treated.
16	111	138	10	12.3	Phosphate treated.
17	31	4	2–	9.4	Field mud from Bassett-Blakely C-3, Danbury Field, Jan. 3, 1949.
18	37	23	36	9.6	El Paso clay added to mud No. 17. 15 lb clay per bbl of mud No. 17.
19	34	10	2–	9.6	Mud No. 18 after caustic-quebracho treatment with 50-50 caustic-quebracho solution.
21	28	1	0	8.33	Water.
22	44	30	2–	12.4	Field mud from Liverpool Gas Unit No. 1, Danbury Field, Jan. 21, 1949.
23	35	11	0	12.4 to 11.6	Mud No. 22 diluted with water, then weighted with Baroid.
24	41	13.5	0	9.4	Molasses.

and the number of cuttings recovered and their time of return were recorded. Each different fluid was subjected to the same procedure. When runs were made with the drill pipe rotating, a fixed rotary speed of 110 rpm was established along with a fixed circulation velocity. The circulation velocity reported is the average across the annular cross section, obtained by dividing the volumetric displacement of the pump by the cross sectional area of the annulus.

RESULTS

Treatment of Data

The data obtained at Pierce Junction were plotted as particle recovery versus circulation time. The particle recovery was expressed as the percentage of particles recovered at the surface, based on the number added. The slopes of the recovery-time curves are an indication of the fluid's ability to lift cuttings; steep slopes, *i.e.*, high percentage/time ratios, indicate high lifting ability, whereas gradual slopes indicate low lifting ability.

Effects of Drill Pipe Rotation

In the initial tests at Pierce Junction, before provisions were made for centering or rotating the pipe, very low percentages of small spheres and flat particles were returned to the surface. Because particles which were lost in the hole could be removed by circulating water or by thinning the circulating fluid, this effect was attributed to channeling of the fluid and subsequent trapping of the particles in the stagnant, gelled sections. When the drill pipe was centered by use of centering guides and the tests were repeated, the recovery of particles was increased. When the drill pipe was rotated, a further increase was obtained.

Although drill pipe rotation is normal in a drilling well, its importance to the removal of cuttings must be emphasized. The curve of percentage recovery versus circulation time given in Fig. 1 is an excellent illustration of the effect of drill pipe rotation. During periods of no rotation, almost no particles appeared at the surface. During rotation, the particles were rapidly removed from the hole. This effect was most pronounced in muds of high viscosity and high gel strength. Variation of the rotating speed from about 35 to 150 rpm produced no appreciable change in particle recovery. Curves shown in Figs. 2, 3 and 4 were obtained with the drill pipe rotating at 110 rpm. Apparently the normal rotating speeds of drilling wells are sufficient to take advantage of this effect.

Effect of Density

Increasing the density of a fluid while maintaining its other properties as constant as possible resulted in an increase in its carrying capacity. This is illustrated in Fig. 2.

Effects of Viscosity and Gel

In carrying out the experiments at Pierce Junction, numerous attempts were made to correlate gel strength and viscosity with the carrying capacity of the mud. These endeavors failed to reveal any definite correlation between viscosities and gel strengths as measured by the Stormer or Marsh funnel viscosimeters and the ability of the fluid to lift cuttings from the hole. However, some general relations were observed.

Before the effects of viscosity and gel are discussed, it should be emphasized that viscosity and gel strength as determined by the instruments used to test drilling fluids are not easily separated. A high gel-strength mud will, in general, be quite viscous, but the reverse is not necessarily true. A high viscosity mud will have high gel strength if its viscosity is due to highly dispersed clays, but it will have little or no gel strength if the viscosity is caused by a high content of relatively inert solids. For these reasons, the muds here discussed will generally be referred to as high-viscosity, high-gel muds

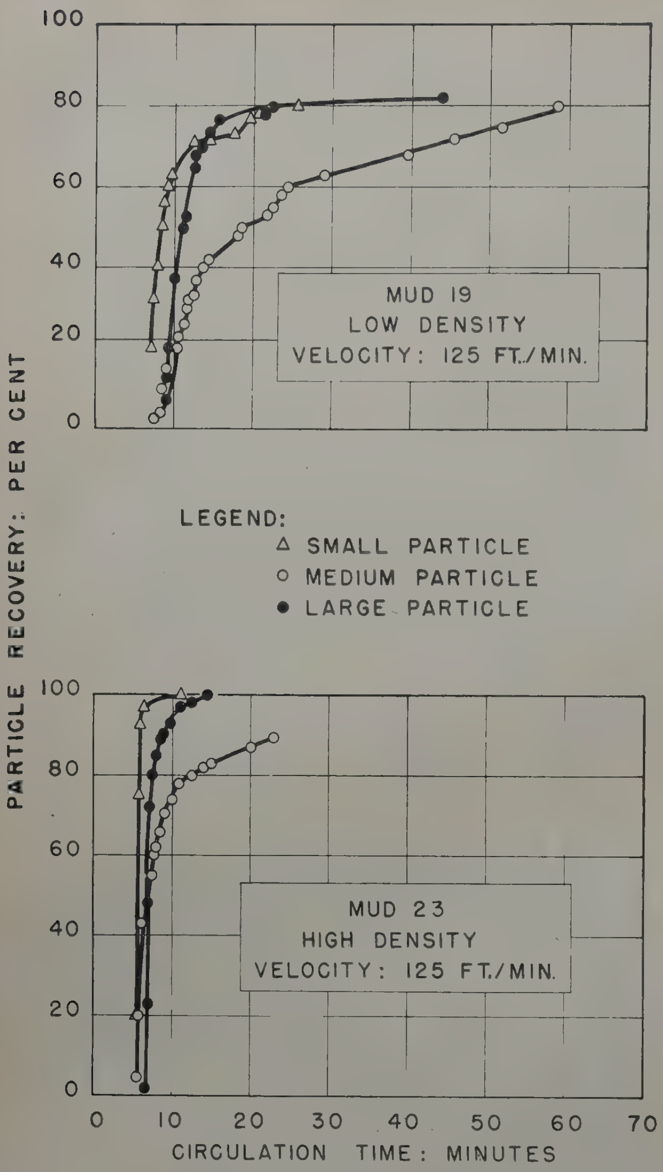

FIG. 2 — EFFECT OF MUD DENSITY ON PARTICLE RETURN.

and low-viscosity, low-gel muds. For the purposes of this discussion, high gel is considered to be anything over six grams initial gel strength on the Stormer viscosimeter, and high viscosity as anything over 15 centipoise at 600 rpm Stormer. These values, however, cannot be considered as representing any exact physical properties of the fluids.

Generally, it was found that low-viscosity, low-gel fluids were superior to high-viscosity, high-gel fluids in removing cuttings. This point is well illustrated by the data presented in Figs. 3 and 4. The curves show that not only did the low-viscosity, low-gel fluids bring the cuttings to the surface more rapidly than did the high-viscosity, high-gel fluids, but they also brought up larger percentages of the particles at lower rates of circulation. An exception to this may be noted in Fig. 3, where the high-viscosity, high-gel mud returned a larger percentage of the large particles. However, this mud did not effectively remove the smaller particles. The higher carrying capacity of the low-viscosity, low-gel muds is particularly noticeable for the medium particles, which closely resemble bit cuttings in their behavior.

The low-viscosity, low-gel fluids closely resemble Newtonian fluids in their behavior, and the behavior of solid particles in them can be calculated with some degree of accuracy using ordinary slip velocity equations.[5] The rate at which a cutting is removed from the hole is, of course, the difference between the annular velocity of the fluid and the slip velocity of the particle.

The slip velocity equations cannot be used with any expectation of good results if the fluid is highly viscous and has high gel strength. This fact is illustrated in the bottom grid of Fig. 3. The large particles appeared at the surface first, whereas slip velocity calculations indicate that they should appear last as they did when a low-viscosity, no-gel fluid such as water was used. This so-called reverse order effect could not be explained on the basis of data obtained at Pierce Junction.

Another phenomenon of interest which was difficult to explain on the basis of slip velocity equations was encountered when high-viscosity, high-gel muds were circulated in the hole. The first particles returned to the surface at velocities higher than the average velocity of the mud. This effect was assumed to be due to the distribution of point velocities existing in the annulus,[13] an assumption which was later vertified in the laboratory phase of the experiments.

Possibility of Reducing Annular Velocity

Figs. 2, 3 and 4 show that mud velocities much lower than 200 ft per minute were sufficient to remove cuttings from the bore hole at Pierce Junction. When water was circulated at 124 ft per minute, the slowest particles came up with a net velocity of about 10 ft per minute.

These data indicate that it may be possible to effect an appreciable reduction in the annular velocities now used in the field and still maintain efficient cutting removal.

LABORATORY PHASE OF EXPERIMENTS

Since certain effects obtained at Pierce Junction could not be explained on the basis of theoretical considerations, an investigation of some of the fundamental forces acting on the particles in transport was initiated. Such information as the effects of velocity distribution on particle transport, whether particles were transported in a preferred portion of the annulus, the particle attitude during transport, the effect of drill pipe rotation on particle transport, the velocity distribution in non-Newtonian fluids, and numerous other facts were needed to complete the project.

Equipment and Materials

To obtain the information outlined above, a laboratory model of a well annulus was constructed. A photograph of this equipment is shown in Fig. 5. As indicated in the photograph, the annulus consisted of a transparent outer column and center pipe. The transparent column was 5 ft long and had an inside diameter of 4 in. The center pipe ran completely through the column and had an outside diameter of 1 in.

The equipment was designed so that drill pipe rotation could be simulated, so that viscosity velocity distributions and type of flow could be observed, and so that visual observation of particles in transport could be made.

Fluids used in this apparatus included water, glycerine and an ultrabentonite suspension. The ultrabentonite suspension was a translucent fluid possessing thixotropy and gel strength similar to those characteristics shown by most drilling fluids.

Particles used to simulate cuttings in the laboratory apparatus included glass spheres, aluminum spheres, aluminum discs, and some actual rock bit cuttings. The properties of the particles are given in Table III. The aluminum discs included the same three sizes as those used in the Pierce Junction phase of the experiments. These discs were not hammered, since tests showed no essential difference between the performance of these discs and the particles used at Pierce Junction.

Procedure

The general procedure followed was to establish a flow rate sufficient to lift the particle to be studied, insert the particle into the column and make visual or photographic observation of the particle as it was transported up the annulus. Fluid velocity distributions were obtained by injecting dye through ten radially spaced needles in the base of the column and measuring the traverse time of the dye over a specified distance through the column. Motion picture records were made of the performance and attitude of the various particles in transport in the annulus.

RESULTS

Validity of Slip Velocity Equations as Applied to Particle Transport in an Annulus

Initial investigation of slip velocity data on glass spheres, aluminum spheres, and aluminum discs indicated that considerable deviation existed between slip velocities as measured in quiescent fluids and those measured by suspending a given particle in the annulus and adjusting flow velocities. It was found that when the fluid in the column was flowing in turbulent flow an empirical equation could be used to predict the slip velocity of a particle being transported. This equation (applicable only to turbulent flow) makes corrections for the finite dimensions of the annulus and thus actually corrects for velocity distributions in turbulent flow. It is as follows:

$$V_s = \frac{V_c}{1 + d/D}$$

where:

V_s = slip velocity

d = diameter of particle

D = equivalent diameter of annulus (four times hydraulic radius)

$$V_c = 1.35 \sqrt{\frac{t}{d}} \sqrt{\frac{gd(\rho_p - \rho_f)}{\rho_f}} \text{ for flatwise fall of a disc}$$

$$V_c = 18 \sqrt{\frac{t}{d}} \sqrt{\frac{gd(\rho_p - \rho_f)}{\rho_f}} \text{ for edgewise fall of a disc}$$

$$V_c = 1.74 \sqrt{\frac{gd(\rho_p - \rho_f)}{\rho_f}} \text{ for spheres}$$

g = gravitational constant

ρ_f = density of fluid

ρ_p = density of particle

A comparison of the velocities calculated from this equation with those observed in the column is shown in Table III.

An attempt to obtain the same type of correction for particles transported in a fluid in viscous flow (glycerine) did not yield satisfactory results for flat particles, primarily because the viscous velocity distribution exerted a turning torque on such particles. The torque effect exerted by the fluid caused them to be turned on edge as they approached the walls, so that their slip velocities continuously changed until they reached the walls.

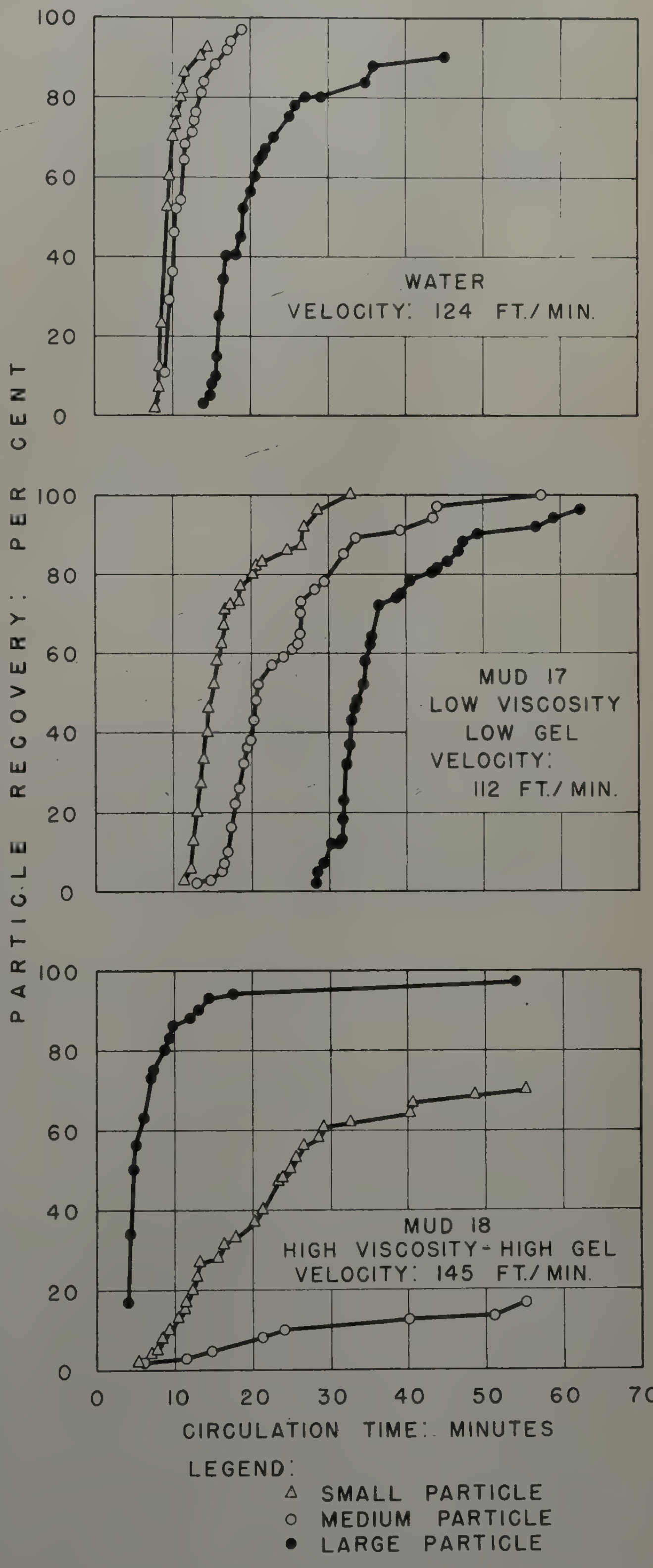

FIG. 3 — EFFECT OF FLUID PROPERTIES ON PARTICLE RETURN.

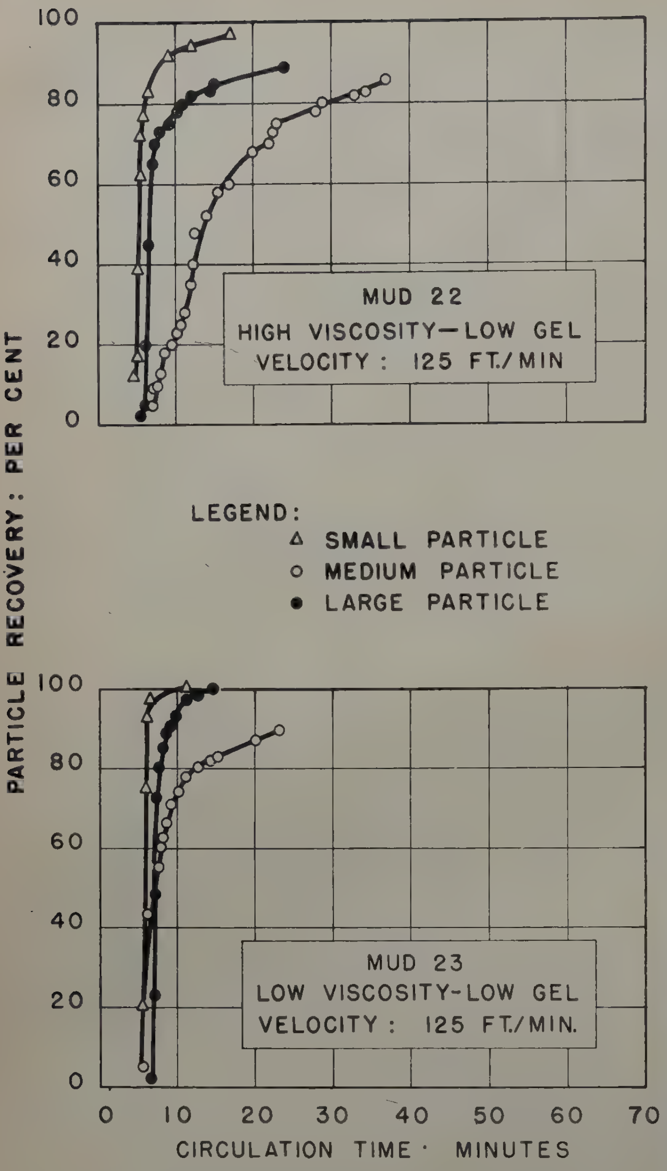

FIG. 4 — EFFECT OF MUD TREATMENT ON PARTICLE RETURN.

Velocity Distributions in Viscous and Turbulent Flow and Their Effects on Carrying Capacity

It has long been known that two distinct types of flow are encountered in the movement of fluids. Because of the nature of the flows, they have been classified as viscous[13] and turbulent[14] respectively. In turbulent flow the fluid elements move in countless eddies, swirls and so-called "turbs." In viscous flow, the fluid elements follow the streamlines.

The distribution of point velocities across the annulus in the two types of flow is distinctly different. This difference is illustrated in Fig. 6. The point velocities in turbulent flow represent a statistical vector average of all the velocities of the fluid elements. The fluid element velocity vectors are in one direction only when the fluid is in viscous flow; therefore the point velocities are the unidirectional velocities of the elements making up the streamline at that point.

The behavior of particles (aluminum discs) in the two types of flow is not the same. Under conditions of turbulent flow, when water was used as the transporting fluid, the discs were transported in the order small, medium, large, without any tendency to be turned on edge or forced against the walls. While rising, all of the discs exhibited a rocking or oscillatory motion characteristic of a leaf falling in air. Fig. 7 represents the discs rising in a turbulent distribution with the center pipe stationary.

Under conditions of viscous flow, when glycerine was used as the transporting fluid, the behavior of the discs depended on their dimensions. The large disc moved up the annulus with no apparent tendency to be either turned on edge or moved to either wall. The medium disc was turned on edge against either the center pipe or the outer wall, where it fell for a considerable distance on edge before rising again. The small disc was turned on edge against either the outer wall or the center pipe, where it fell on edge only a very short distance, then rose again. In some instances the medium and small discs were plastered against the walls and could not be removed without increasing the fluid velocity considerably. Figs. 8, 9 and 10 illustrate the behavior of the three discs transported by glycerine in viscous flow with the center pipe stationary.

Particles are transported most efficiently and carrying capacity is the highest when the largest area of the particle is perpendicular to the direction of transport. This is the normal position of fall. A disc falling in viscous slip falls about 1.5 times faster on edge than it does in the normal position; in turbulent slip the factor is 13. It is to be noted that it is possible for a particle to fall in turbulent slip while the fluid is in viscous flow. For these reasons it is advantageous to keep

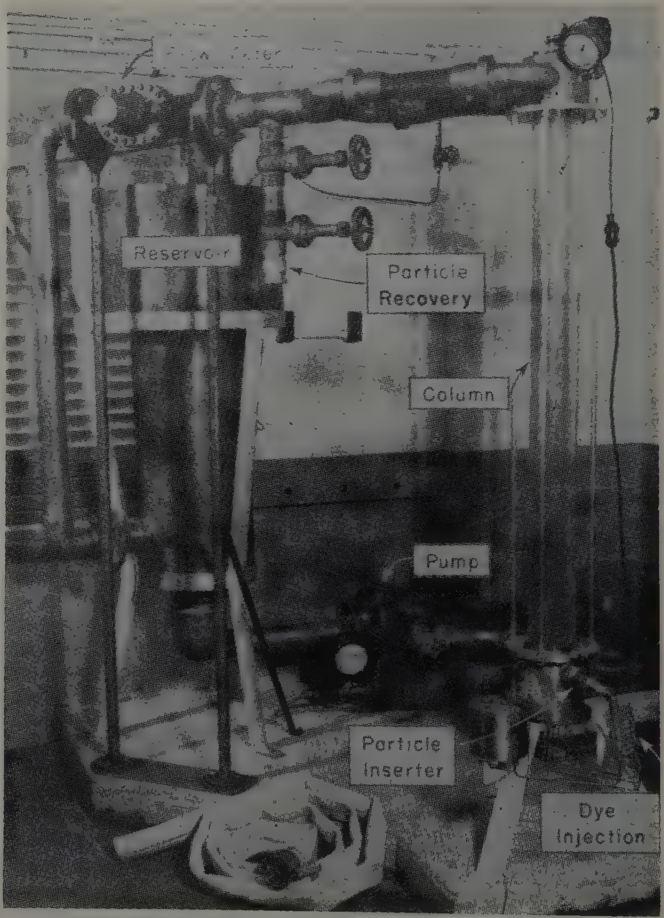

FIG. 5 — ANNULAR MUD FLOW EQUIPMENT.

the particles away from the walls and flat in the stream. This can be done by maintaining turbulent flow conditions in the annulus.

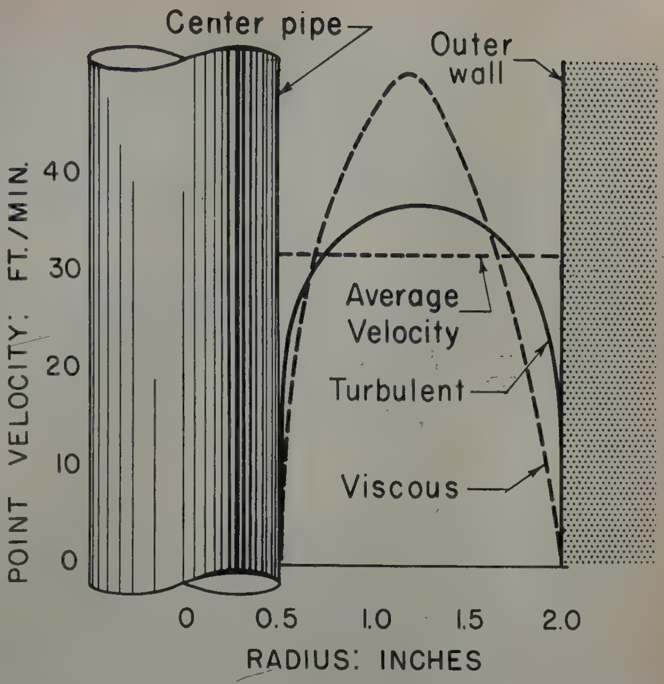

FIG. 6 — COMPARISON OF VISCOUS AND TURBULENT VELOCITY DISTRIBUTIONS (CENTER PIPE STATIONARY).

The Torque Effect and Its Relation to Carrying Capacity

The so-called torque effect has been mentioned previously as the cause of the discs turning on edge when transported by fluids in viscous flow. Consideration of some fundamental hydraulic concepts provides a good explanation of the cause of the turning torque exerted on the particle by the fluid.

Streamline or viscous flow may be considered to be the movement of the fluid in a group of concentric cylinders of infinitesimal thickness; the cylinders in turn are made up of individual streamlines. These streamlines may be thought of as individual fluid jets. The force exerted on a plate perpendicular to a jet of fluid is given by $F \propto WV/g$, in which F is the force on the plate, W the weight of fluid striking the plate in unit time, V the velocity of the fluid, and g the gravitational constant. An increase in velocity increases the force.

Reference to the viscous velocity distribution shown in Fig. 11 shows that the velocity increases from zero at the walls to a maximum near the center of the stream. Since the force exerted by the fluid on the particle is directly proportional to the velocity of the fluid, the force also increases from zero at the walls to a maximum near the center. As previously mentioned, the natural attitude for flat particles falling in static bodies of fluid is horizontal, *i.e.,* their largest dimension is perpendicular to the direction of fall. This same attitude would be adopted in a rising fluid if it were not for the velocity distribution introduced by the finite dimensions of the system. A particle in the natural flat position is projected across regions of different velocities. As shown in Fig. 11, F_4 is greater than F_2 because V_4 is greater than V_2. A torque about the center of gravity of the particle is produced by the action of these unequal forces. This torque tends to turn the particle toward the outside of the stream.

As the particle becomes inclined, force component F_H becomes effective. The combination of torque and force components pushes the particle against the wall on edge. After reaching a position on edge against the wall, the particle begins to slide down the wall. If the velocity gradient at the wall is sufficiently large, the particle will be dislodged and returned to the stream, where the cycle will be repeated. An illustration of this cycle is given in Fig. 9. If the particle is thin and the forces holding it against the wall are sufficiently large, the particle will continue to slide down the wall on edge, or it will stick against the wall.

Examination of the turbulent velocity distribution in Fig. 6 shows that the torque effect will be much smaller in turbulent flow than in a viscous distribution. Over a large part of the

Table III — Properties and Slip Velocities of Particles Used in Laboratory Experiments

Particle Type	Material	Density lb/cu ft	Diameter in.	Thickness in.	d/D	V_c ft/min	V_o ft/min	V_s ft/min
Sphere	Glass	162.6	0.940	—	0.313	210	148.5	160
Sphere	Aluminum	173.7	0.753	—	0.251	198.5	160.5	158.7
Sphere	Glass	150.4	0.687	—	0.229	168.5	139.0	137.0
Sphere	Ni-Steel	553.0	0.187	—	0.0624	208.0	179.0	195.7
Sphere	Brass	532.0	0.312	—	0.104	262.0	225.0	237.0
Sphere	Steel	473.0	0.281	—	0.0937	233.0	201.0	213.0
Sphere	Aluminum	170.5	0.187	—	0.0624	97.7	90.3	91.8
Disc	Aluminum	167.8	0.625	0.126	0.209	61.2	47.6	50.7
Sphere	Aluminum	176.0	0.875	—	0.292	216.3	170.0	167.3
Sphere	Steel	485.0	0.156	—	0.052	176.0	164.0	167.0
Sphere	Glass	154.0	0.173	—	0.0577	86.4	78.0	81.5
Disc	Aluminum	167.0	0.630	0.067	0.210	44.9	40.5	37.1
Disc*	Aluminum	168.0	0.750	0.250	0.250	86.5	71.0	69.2
Disc*	Aluminum	168.0	0.750	0.125	0.250	61.5	45.0	49.1
Disc*	Aluminum	168.0	0.500	0.125	0.167	61.0	43.0	52.3

*These three discs used to obtain most of the results reported herein.
d = particle diameter.
D = equivalent diameter of annulus.
V_c = calculated slip velocity from conventional equation for turbulent slip.
V_o = observed slip velocity in laboratory model under turbulent flow and turbulent slip conditions.
$V_s = \dfrac{V_c}{1 + d/D}$ = slip velocity calculated by equation correcting for velocity distribution and "wall effects."

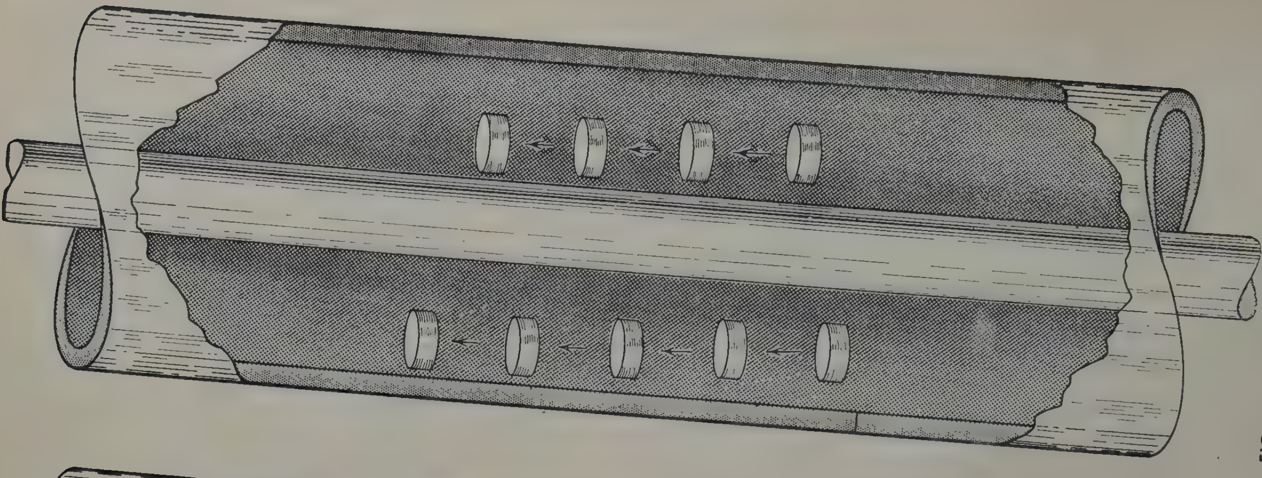

FIG. 10 — LARGE DISCS TRANSPORTED IN VISCOUS FLOW (CENTER PIPE STATIONARY).

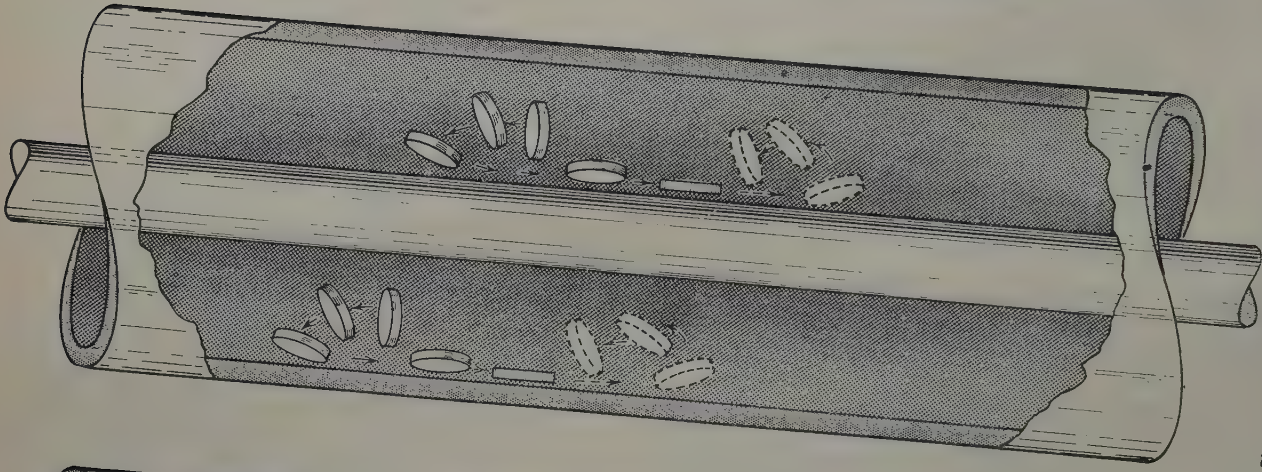

FIG. 9 — MEDIUM DISCS TRANSPORTED IN VISCOUS FLOW (CENTER PIPE STATIONARY).

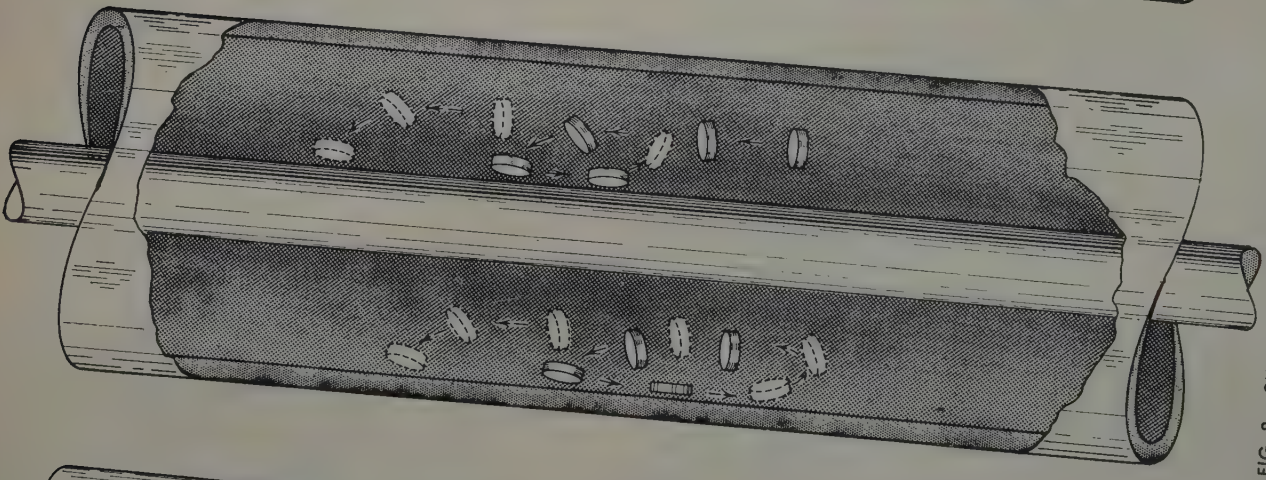

FIG. 8 — SMALL DISCS TRANSPORTED IN VISCOUS FLOW (CENTER PIPE STATIONARY).

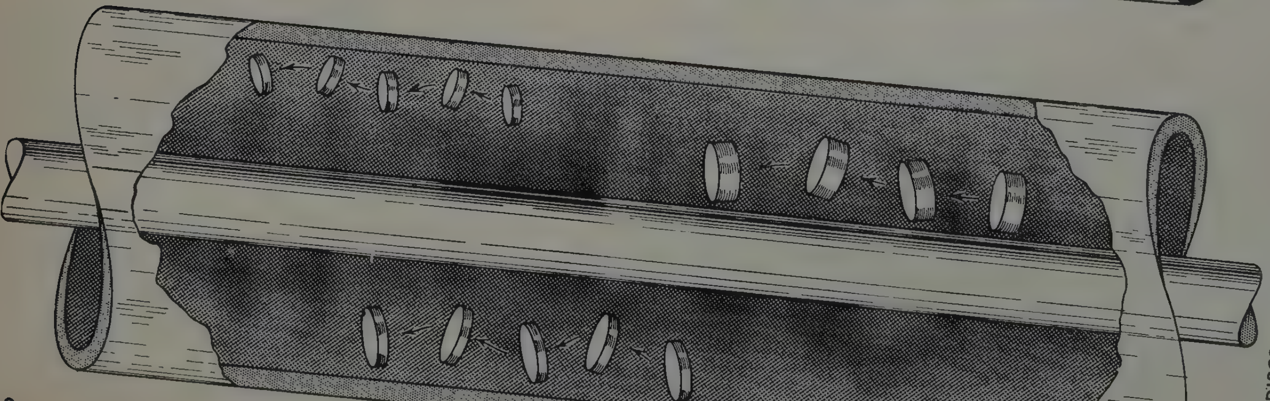

FIG. 7 — DISCS TRANSPORTED IN TURBULENT FLOW (CENTER PIPE STATIONARY).

annulus, the differences in velocity in turbulent flow are relatively small. This causes a corresponding decrease in the inequality of the forces causing the torque. Furthermore, the eddies and swirls existing in the stream tend to keep the particles from sticking to the walls.

Since the torque effect decreases carrying capacity, its minimization is desirable. This can be effected by maintaining turbulent flow in the annulus.

Particle Thickness to Diameter Ratio and Its Effect on Carrying Capacity

The fact that the behavior of discs transported by a fluid in viscous flow depended on the dimensions of the discs prompted an investigation of the effect of the dimensions on their behavior. It was found that the behavior of the discs could be predicted fairly well if their thickness to diameter ratios were known.

An investigation was made of aluminum discs ¾ in. and ½ in. in diameter and of various thicknesses to determine the critical value of thickness to diameter ratio below which the torque effect in a viscous distribution would turn the discs on edge. It was found that discs usually turned on edge if their thickness to diameter ratio was less than 0.3. It was also found for the range of sizes investigated that discs with thickness to diameter ratios greater than about 0.8 remained continuously on edge while being transported. This latter point is understandable if it be recalled that when a plane is passed through the center of a disc parallel to the disc axis and the thickness to diameter ratio is greater than 0.78, the area of the plane intercepted by the disc is greater than the area of one circular face. As previously mentioned, particles fall so that the greatest area is normal to the direction of fall. The results of the investigation indicated that discs with thickness to diameter ratios ranging from 0.3 to about 0.8 usually are transported in a horizontal attitude.

Particles with thickness to diameter ratios less than 0.3 are difficult to remove from the hole. When such particles are encountered, the carrying capacity of the drilling fluid with respect to them decreases unless the fluid is maintained in turbulent flow.

The Effect of Center Pipe Rotation on Carrying Capacity

Center pipe rotation increased carrying capacity in viscous flow by preventing the small and medium particles from slipping down the wall of the center pipe. The centrifugal forces set up by rotation threw the discs into regions of high velocity existing in the center portion of the annulus where they were readily transported. Fig. 12 illustrates the effect of center pipe rotation upon transport of the medium particle. The effect of rotation was not nearly so pronounced for fluids in turbulent flow as it was for those in viscous flow.

Transport of Rock Bit Cuttings

Observations of rock bit cuttings transported by fluids in both viscous and turbulent flow showed that the same principles that applied to the discs also applied to the cuttings. Most cuttings were easily turned on edge and forced to the walls when the flow of fluid was viscous. The cuttings were readily transported when the flow of the fluid was turbulent.

Although no attempt was made to determine exact values of thickness to diameter ratios for the cuttings, estimates of this ratio indicated that very few of the cuttings had ratios of the thickness to diameter greater than the critical value of 0.3. This is thought to be typical of most rock bit cuttings.

CORRELATION BETWEEN FIELD AND LABORATORY RESULTS

In the light of the information obtained in the laboratory, the results obtained at Pierce Junction can be more easily understood.

Transport of Medium Discs and Reverse Order Effects

The difficulty encountered at Pierce Junction in removing the medium particles from the hole was caused by their low thickness to diameter ratio (0.167), which allowed them to be turned on edge by the torque effect. Once on edge they slid down the hole so that they had to be transported over the same distance for a number of times. That this effect was most noticeable in highly viscous muds was to be expected in view of the more effective turning moment exerted by such muds. This also accounts for the so-called reverse order effect. Since the medium particles had to be transported over a greater distance than either the large or small particles, it was to be expected that they would reach the surface at a later time. The thickness to diameter ratio of the small particles was 0.250; of the large particle 0.333. Because of the magnitude of these ratios, the turning moment exerted on these particles by the viscous muds was smaller than that exerted on the medium particles. Because of this, the large particles were often more easily removed from the hole than were the medium particles.

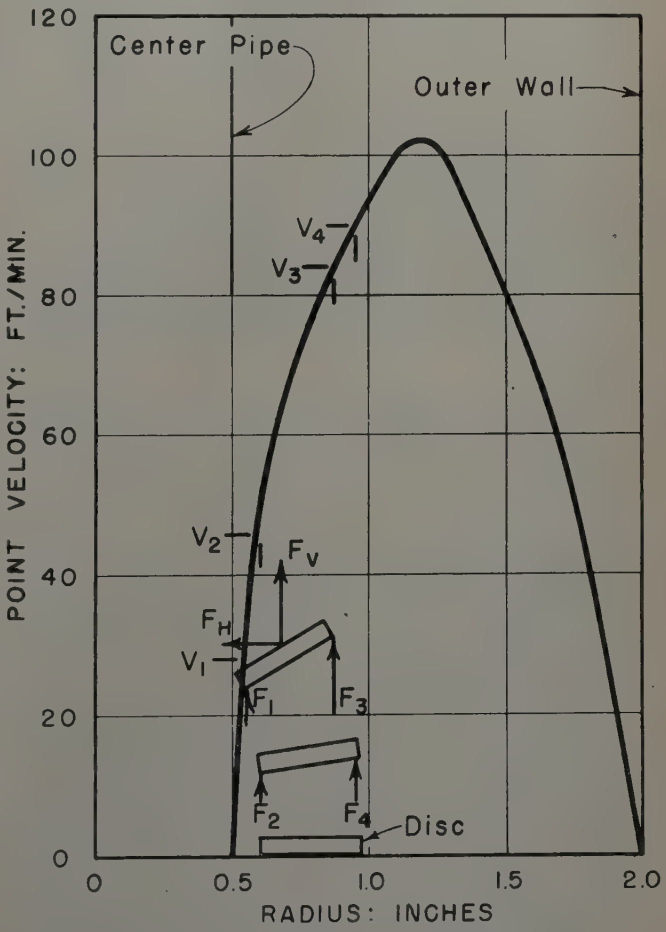

FIG. 11 — TORQUE EFFECT ON PARTICLES (VISCOUS FLOW).

Effectiveness of Drill Pipe Rotation

The effectiveness of drill pipe rotation in increasing carrying capacity is caused in part by the fact that it aids in creating turbulence, and in part by the fact that it helps prevent the existence of stagnant, gelled pockets between the drill pipe and the wall of the bore hole. The centrifugal forces set up by the pipe also help to increase carrying capacity because they tend to project the particles away from the pipe into regions of higher velocity, where they are more easily transported.

CONCLUSIONS

The conclusions reached from consideration of the information obtained in the laboratory and at Pierce Junction may be summarized as follows:

1. Turbulent flow in the well annulus is most desirable from the standpoint of removing cuttings.
2. Low viscosity and low gel strength are advantageous in removing cuttings.
3. Increase in mud weight is effective in increasing carrying capacity.
4. Rotation of the drill pipe increases carrying capacity.
5. If turbulent flow can be maintained, an annular velocity slightly greater than the slip velocity of the largest cuttings to be transported should keep the bore hole clean. This implies velocities of 100 to 125 ft per minute rather than the presently used 175 to 225 ft per minute.

REFERENCES

1. Beck, R. W., Nuss, W. F., and Dunn, T. H.: "The Flow Properties of Drilling Muds," Paper No. 901-23-H presented at Spring Meeting of Southwestern District, API Division of Production, Fort Worth, Tex., March 27-29, 1947.
2. Hall, H. N., Thompson, Howard, and Nuss, Frank: *Trans.* AIME, (1950) **189**, 35-46.
3. MacDonald, G. C.: "Transporting Rotary Bit Cuttings," *World Oil*, (April, 1949) **128**, No. 13, 114-118.
4. Piggott, R. J. S.: "Mud Flow in Drilling," *Drilling and Production Practice 1941*, API, (1942) New York.
5. Walker, W. H., Lewis, W. K., McAdams, W. H., and Gilliland, E. R.: *Principles of Chemical Engineering*, 3rd Edition, McGraw-Hill Book Co., Inc., New York and London, (1937).
6. Lewis, W. K., Squires, L., and Broughton, G.: *Industrial Chemistry of Colloidal and Amorphous Materials*, The MacMillan Co., New York, (1944).
7. Lawrence, A. S. C.: "Anomalous Flow of Colloidal Solutions," *Proceedings of the Royal Society of London*, (Jan., 1935) **148A**, 59-87.
8. Hatschek, Emil: *The Viscosity of Fluids*, D. Van Nostrand Co., New York, (1928).
9. Ambrose, H. A., and Loomis, A. G.: "Fluidities of Thixotropic Gels: Bentonite Suspensions," *Physics (Journal of Applied Physics)*, (1933) **4**, 265-273.
10. Hershey, M. D.: "The Theory of Lubrication," *Journal of the Franklin Institute*, (June, 1935) 677-702.
11. Hershey, M. D.: "The Theory of Lubrication," *Journal of the Franklin Institute*, (Aug., 1935) 187-214.
12. Reiner, Marcus: *Ten Lectures on Theoretical Rheology*, Rubin Mass, Jerusalem, (1943).
13. Lamb, Horace: *Hydrodynamics*, Dover Publications, New York, (1945).
14. Bakhemeteff, Boris A.: *The Mechanics of Turbulent Flow*, Princeton University Press, Princeton, New Jersey, (1936).

★ ★ ★

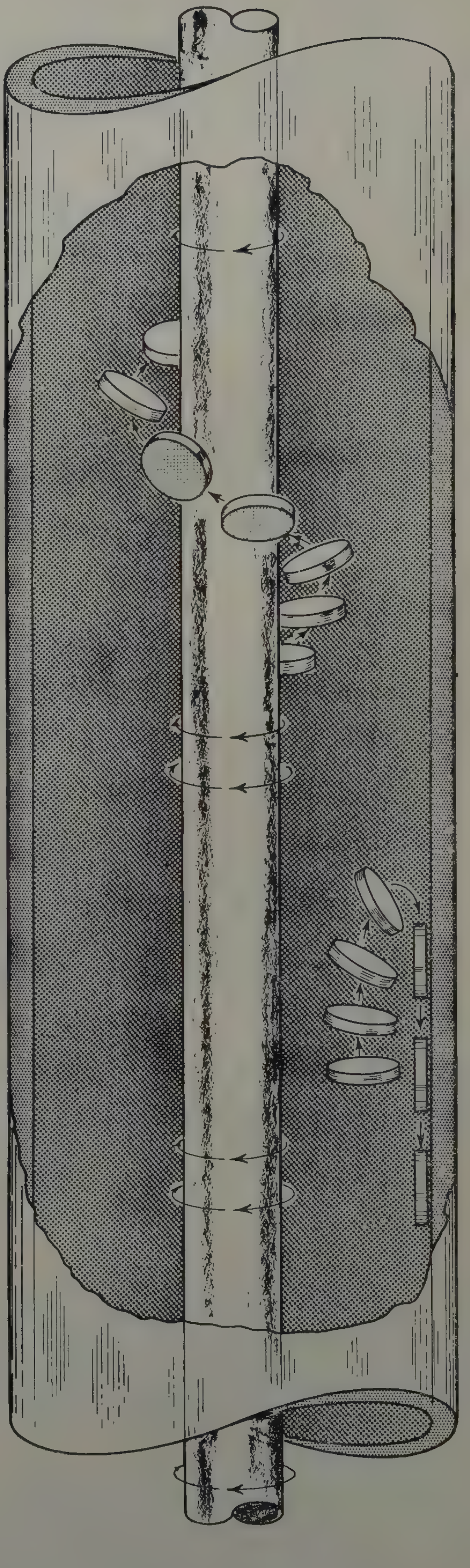

FIG. 12 — MEDIUM DISCS TRANSPORTED IN VISCOUS FLOW (CENTER PIPE ROTATED).

T.P. 3054

THE SHULER JONES SAND POOL; NINE YEARS OF UNITIZED PRESSURE-MAINTENANCE OPERATIONS

JACK TARNER, W. R. EVANS AND **H. H. KAVELER,** MEMBERS AIME, PHILLIPS PETROLEUM CO.,
BARTLESVILLE, OKLA.

ABSTRACT

The geological features, development history and engineering detail of the Shuler Field and the results of approximately two years of unitized operation of the Shuler Jones Sand Pool, were discussed in a prior publication.[1] The purpose of this paper is to present the results of pressure maintenance in the Shuler Jones Sand Pool after nine years of unit operation.

GENERAL INFORMATION

The Shuler Jones Sand Pool is located in and about Section 18, Township 18 South, Range 17 West, Union County, Ark. The pool was discovered in September, 1937, unitized in February, 1941, and subjected to gas injection operations in July, 1941. Water was first returned to the reservoir in July, 1944.

The reservoir is an anticlinal trap covering about 4,000 acres. The 154,000 acre-ft of sandstone initially consisted of approximately 150,000 acre-ft of productive oil zone and 4,000 acre-ft of gas-cap. The average depth of production is 7,400 ft. Maximum closure of the reservoir is 135 ft and the oil column lies between a gas-oil contact at –7,270 ft and a water-oil contact at –7,370 to –7,380 ft. The field is approximately four miles long, east and west, and one and one-half miles wide.

The sand grains are angular and vary from fine to medium size. The porosity of the sandstone averages 20.2 per cent. The specific permeability averages 400 md. Some zones have as high as 30 per cent porosity and specific permeability of 4,000 md. The reservoir rock is not uniform in character but consists of sandstone zones interspersed with shale. The variation in rock characteristics is evident in the electric log and core analyses presented in the original publication. Asphalt present in the pore space of the sandstone limited the reservoir to the southeast and apparently blocked any encroachment of water from that direction.

The initial reservoir pressure at a subsea depth of 7,300 ft was 3,520 psi. The reservoir temperature was 198°F. Initially, the solution gas volume was 765 cu ft per bbl and the reservoir volume factor was 1.45. The gas solubility and formation-volume-factors of the reservoir liquid are related with reservoir pressures above 300 psi as follows:

Solution gas, cu ft per cu ft,

$$S = 0.0334\,P + 18.65$$

Formation volume factor of reservoir oil,

$$FVF = 8.0 \times 10^{-5}\,P + 1.168$$

Gas volume factor, standard cu ft of gas equivalent to one cu ft of gas at reservoir conditions of temperature and pressure,

$$F = .062\,P - 4$$

Pressure (P) measured in psia.

The equation for the gas volume factor presented above is based on a direct measurement of a sample of the gas and is a correction of that used in the original paper.

The gravity of the oil produced is from 32 to 34° API.

CALCULATION OF INITIAL OIL IN PLACE

The Jones Sand production history is interesting because it lends itself to analysis by material balance. Production statistics from discovery of the Jones Sand through 1949 and material balance calculations of the initial stock tank oil in place are shown in Table I.

The usual procedure in testing the application of material balance calculations is to compute the apparent initial volume of oil in place, using production and pressure information obtained at different time periods. If the apparent oil in place volumes computed increase with successive time periods, water encroachment is indicated and approximations must be made to correct for its influence. The first requirement in utilizing such calculations is reliable reservoir pressure, accumulated gas, oil and water production, and PVT data. Calculations of apparent oil in place in the Jones Pool, based on field data

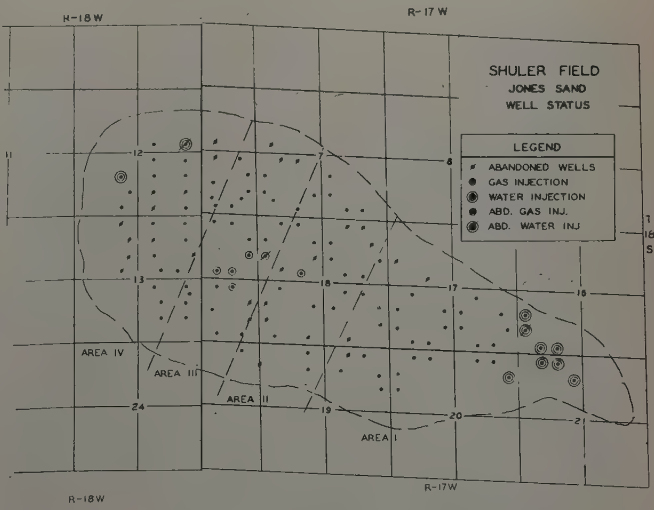

FIG. 1 — WELL STATUS, SHULER FIELD, JONES SAND.

---

[1] References given at end of paper.

Manuscript received in the office of the Petroleum Branch, Sept. 13, 1950. Paper presented at the Branch Fall Meeting in New Orleans, La., Oct. 4-6, 1950.

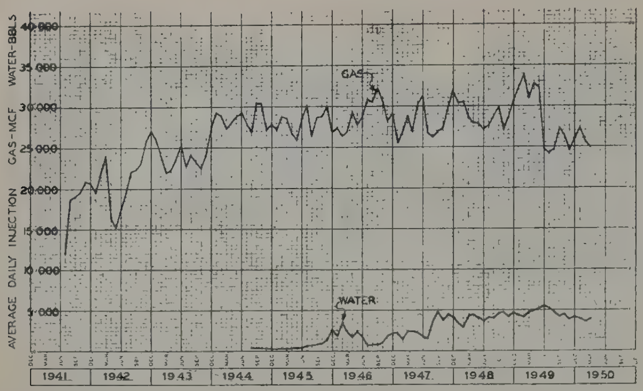

FIG. 2—DAILY VOLUMES OF GAS AND WATER INJECTED, SHULER UNIT.

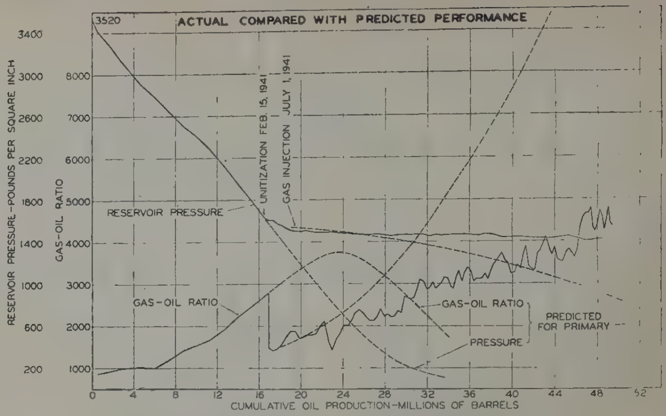

FIG. 3 — PERFORMANCE OF SHULER JONES SAND POOL.

prior to unitization, gave values of from 100 to 109 million bbl. The results were well within the uncertainty of production records and no water-drive was indicated. Calculations of apparent oil in place after unitization gave steadily increasing values because of the greater accuracy of factual data and water influx was indicated. The calculated values of oil in place became consistent if the term in the material balance equation correcting for water encroachment was based on the premise that the water influx at any time was proportional to the reservoir pressure decline from initial. The water encroachment factor was found to be 80 bbl of water per month per lb of reservoir pressure decline from initial. By July, 1950, the indicated rate of water encroachment was 5,500 B/D. The encroachment factor, when applied to the apparent oil in place calculations, resulted in a determination of 100 million bbl of initial stock-tank oil in place.

The increase above the 100 million bbl, calculated from the production data during the latter part of 1948 and the first part of 1949, is caused probably by the determined average pressure being higher than true reservoir pressure. In the latter part of 1948 the pressures in the East part of the pool, the area with the major water injection, increased rapidly and caused a less accurate determination of true reservoir pressure than is possible when a more or less uniform pressure occurs throughout the entire reservoir.

GAS INJECTION

A casinghead-gas gasoline plant and compressor station was completed and gas was returned to the gas cap of the reservoir in July, 1941, five months after unitization of the Jones Reservoir. Five wells are used for injection purposes at the present time (Fig. 1). Gas injection volumes have varied from 25 to 35 million ft per day (Fig. 2). The well-head injection pressures are approximately 150 lb below the reservoir pressure. Early experience dictated the necessity of scrubbing all injection gas at the discharge of the compressors and eliminating all air from the gathering system, if low injection pressures were to be maintained. Scale deposit on the sand face of the injection wells is removed by acid treatment.

Part of the time during the past nine years gas injection volumes have exceeded produced volumes because "make-up" gas from the Cotton Valley Sands and Smackover Limestone was returned to the Jones Reservoir. The injection of Smackover Lime gas was discontinued because sour gas caused mechanical trouble in the compressors and scale deposits on the sand face of the injection wells. The supply of Cotton Valley gas has declined to an insignificant volume and the injected gas now consists mainly of gas produced from the Jones Sand.

The accumulated volume of injected gas amounted to 89 per cent of the gas volume produced from the Jones Sand as of July, 1950. The injected gas volume of 83 billion cu ft exceeds slightly the estimated volume of 80 billion cu ft of solution and free gas that was initially in place in the reservoir. The accumulated injected volume would, at reservoir pressure conditions existing in July, 1950, occupy a space of 175 million bbl, which compares with a total initial volume of reservoir space of 240 million bbl. Measured in other terms, the injected gas volume would occupy a reservoir space three times the volume of the available 60 million bbl of free gas space which existed in July of 1950. These relationships are a measure of the gas handled during a period in the life of the Jones Sand Pool when 50 per cent of the initial oil in place was recovered and produced gas/oil ratios did not exceed 4,500 cu ft per bbl.

WATER INJECTION

In July, 1944, salt water produced in the northwest part of the field was returned to the reservoir through wells in that area (Fig. 1). Fresh-water injection was started in May, 1945, into one well located on the eastern edge of the field and continuous fresh-water injection was started in November, 1945. The combined fresh and salt water injection rate has ranged from 4,000 to 5,000 B/D from the last half of 1947 through the first half of 1950 (Fig. 2). The water-injection program has resulted in daily production rates of as high as 600 B/D from some wells originally shut down because of excessive gas/oil ratios.

Pressure maintenance has been primarily the result of gas-injection as the volume of injected water on a daily average has been equal to no more than 10 per cent of the reservoir volume of the daily injected gas.

RESULTS AS COMPARED WITH PREDICTIONS OF UNITIZED OPERATIONS

The Shuler Jones Sand Unit was justified on a prediction of future behavior as are all projects of that general nature. The prediction[1] led to the conclusion that the producing gas-oil ratio under gas injection would be approximately 20,000

Table I — Production Statistics — Jones Sand Pool, Shuler Field, Arkansas

End of Month	Reservoir Pressure, psia	Average Gas/Oil Ratio Cu Ft Per Bbl: Producing for Period	Net for Period	Accum. Net	Accum. Water Prod. (1,000 Bbl)	Accum. Water Injected (1,000 Bbl)	Accum. Net Water Produced (1,000 Bbl)	Accum. Oil Produced (1,000 Bbl)	Apparent Initial Oil in Place (Million Bbl)	Accum. Water Encroached (Million Bbl)	Initial Oil-in-Place (Million Bbl)
Sept., 1937	3,548										
July, 1938	3,153	990	990	917				2,818	107.2	0.1	104
Jan., 1939	2,813	1,000	1,000	974				6.030	109	0.4	104.5
July, 1939	2,533	1,420	1,420	1,054				8,751	106.2	0.9	100.8
Jan., 1940	2,318	1,660	1,660	1,170				11,259	107.1	1.4	100.8
July, 1940	1,978	2,220	2,220	1,331				13,998	103.8	2.1	97.9
Jan. 1941	1,658	2,710	2,710	1,509				16,552	100.4	2.9	95
July, 1941	1,542	1,834	955	1,512	5		5	19,006	107.9	3.9	101.7
Jan., 1942	1,524	1,769	278	1,366	36		36	21,474	108.6	4.8	101.1
July, 1942	1,510	1,780	141	1,256	94		94	23,722	106.4	5.8	97.5
Jan., 1943	1,497	2,306	68	1,159	175		175	25,927	110.2	6.8	100
July, 1943	1,490	2,238	97	1,082	306		306	27,922	111.8	7.8	100.2
Jan., 1944	1,496	3,179	143	1,015	487		487	29,810	114.2	8.8	101
July, 1944	1,496	3,079	256	964	717	11	706	31,617	117.5	9.8	102.8
Jan., 1945	1,489	3,029	–60	912	911	76	835	33,350	117.1	10.8	101.1
July, 1945	1,498	3,312	–36	868	1,110	147	963	34,987	119.4	11.8	101.7
March, 1946	1,488	3,127	55	821	1,364	576	788	37,161	120.1	13.2	100.7
Aug., 1946	1,494	3,554	92	793	1,495	800	695	38,538	121.9	14.0	101.1
March, 1947	1,471	3,468	229	763	1,784	1,163	621	40,432	121.5	15.2	99.6
Sept., 1947	1,461	3,312	244	746	2,038	1,669	369	42,064	122.6	16.0	99.6
March, 1948	1,454	3,666	397	759	2,321	2,367	–46	43,698	125.7	17.2	101.8
Sept., 1948	1,474	3,812	427	746	2,795	3,116	–320	45,319	132.7	18.2	106.3
March, 1949	1,429	4,648	755	737	3,121	3,925	–804	46,898	129.7	19.3	103.5
Sept., 1949	1,437	4,723	585	731	3,421	4,820	–1,399	48,197	132.8	20.3	104.8
March, 1950	1,432	4,393	638	726	3,649	5,398	–1,749	49,412	134.2	21.3	105

cu ft per bbl when 54 million bbl of oil were recovered and when, on the basis of 90 per cent return of the produced gas, the reservoir pressure would decline to approximately 600 psi. In retrospect, these estimates were substantially on the side of underestimating the performance of the pool. At the present time over 50 million bbl have been recovered (approximately 50 per cent of the oil in place) and the average gas/oil ratio is less than 4,500 cu ft per bbl. The reservoir pressure is 1,400 psi (Fig. 3).

A reasonable expectation of primary recovery without unitization would have been 34 million bbl, hence, 16 million bbl, or 47 per cent more oil has been recovered. The pool, 13 years after discovery, has produced one-half its initial oil content and is producing at an annual oil allowable rate equal to 2.5 per cent of the volume of oil that was initially in place (Fig. 4). Approximately 60 per cent of the current production is obtained by natural flow.

Predictions of recoverable oil under gas-injection or waterflooding operations are sometimes tempered to the extreme because of some notion about the erratic nature of the permeability of the producing formation, the presence of shale inclusions or some other condition of the reservoir rock. The result is a predicted recovery usually lower than ultimately realized. Predicted reserve estimates based on past performance trends under competitive operation, projected into future performance under unit operations, may not adequately treat the effect of selective production on oil recovery. In Shuler, the effect of selective production on oil recovery has been much more effective than was attributed to that feature at the time the original estimates were made.

UNIT OPERATIONS WITHOUT GAS INJECTION

The Shuler Unit could have operated as a unit for selective production of oil and with all produced water returned to the reservoir. Such a program has been advocated for some fields on the theory that injected gas will by-pass oil and not be of material benefit to the unit program. If such a program had been employed in Shuler, material balance calculations indicate that the pressure would have declined as shown by Curve *C* of Fig. 6 and ultimate oil recoveries would have varied from 37 to 45 million bbl. Much of the oil production would have

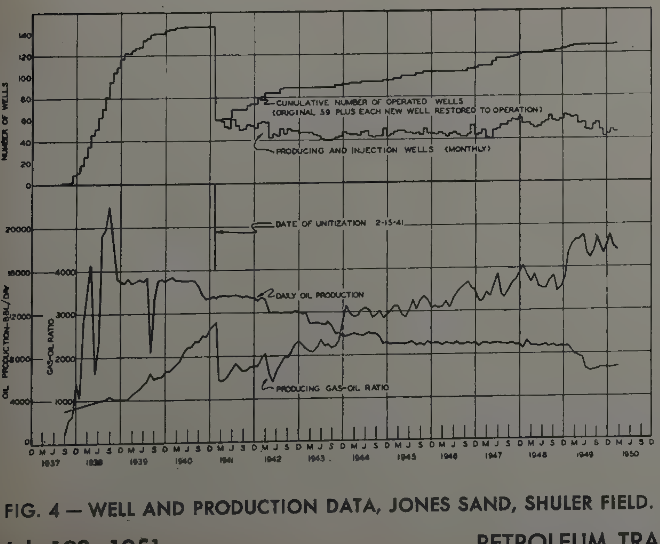

FIG. 4 — WELL AND PRODUCTION DATA, JONES SAND, SHULER FIELD.

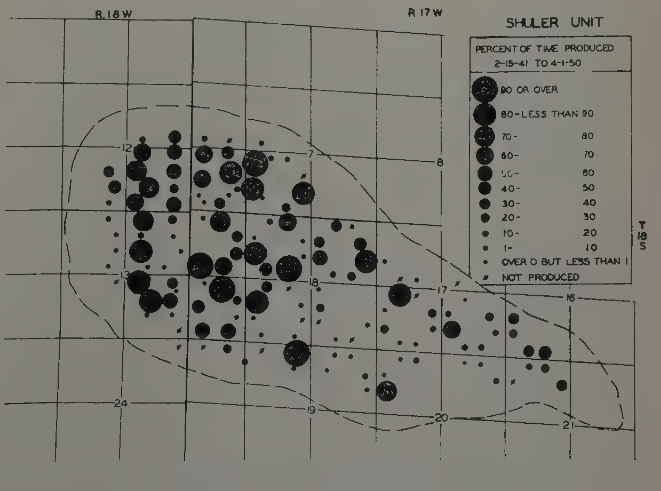

FIG. 5 — PER CENT OF TIME PRODUCED, SHULER UNIT.

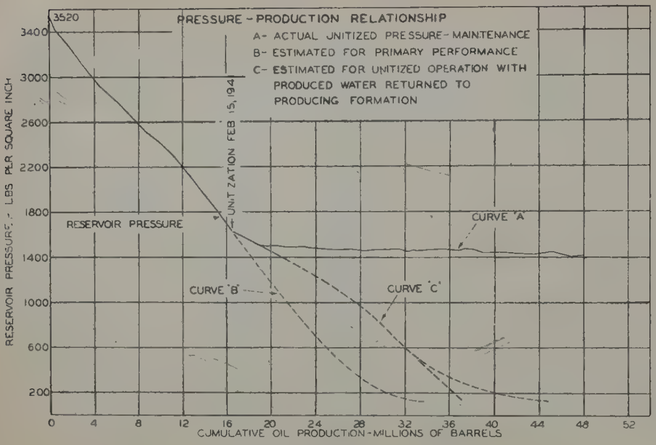

FIG. 6 — PRESSURE-PRODUCTION RELATIONSHIP, SHULER JONES SAND POOL.

required artificial lift equipment. The program would have shown an advantage over primary production history, Curve *B*, but would not have enabled the high rates of recovery nor the ultimate recovery experienced with the present plan.

FEATURES OF THE UNIT OPERATIONS

The Shuler Jones Sand Pool had 149 wells which could be operated to obtain the allowed oil production. Only 40 to 60 wells have been operated at any time and 126 of the 149 have been used at some time or other during the past nine years either for production or injection purposes (Fig. 4). The unit has operated only five wells more than 90 per cent of the time and 34 wells more than 50 per cent. Sixty-three wells have been operated less than 10 per cent of the time and 27 wells have not been operated for even one per cent of the unit life. A graphic picture of the per cent days each well has been operated since formation of the unit is presented in Fig. 5.

The Jones Sand Pool can be divided into four areas of equal reservoir volumes for discussion of the areas of oil withdrawals. Such a division is shown in Fig. 1, and the oil produced from each of those divisions is given in Table II. Area I, which covers the entire east part of the pool, produced 160 bbl per acre-ft to the date of unitization as compared with 129, 86, and 72 for Areas II, III, and IV, respectively.

The east part of the pool (Area 1) has less sand thickness than the west part and because of the greater oil withdrawals, a low pressure was created in that part prior to the unitization (Fig. 7). In February, 1941, when the field was unitized, that gradient from west to east was 545 lb. Shutting in the high ratio and low pressure wells resulted in reducing that gradient to 102 psi by July, 1941. Thereafter gas injection operations and selective production of oil created an almost uniform pressure condition throughout the entire reservoir. Commencing in August, 1947, the intensified water injections created a high pressure condition in the east part of the field, and today a gradient of over 1,500 psi exists in an east to west direction. The pressure at the eastern edge is almost at initial pressure.

Gas injection in the western part of the field, Areas III and IV, has permitted greater withdrawals from those areas and as of March 1, 1950, Area I has produced 303 bbl per acre-ft as compared with 286, 315, and 406 respectively, for Areas II, III, and IV. Area IV has produced better than 60 per cent of its initial oil in place and in July, 1950, was producing 27 per cent of the pool production.

CONCLUSION

The Shuler Jones Sand Pool is an example of what may be accomplished in the way of increased oil production when accepted engineering principles for the production of oil are applied through unit operations. The Jones Sand Pool initially contained 100 million bbl of oil and has produced one-half of that volume, or about 50 million bbl, in 13 years of producing life, nine of which were under unit operations. Primary production from the field would have been 34 million bbl, hence unit operations had in nine years made possible an increased recovery of oil amounting to 50 per cent more than would normally have been produced.

ACKNOWLEDGMENT

The authors thank Melvin T. Zoldoske for calculations and assembling data presented, and the Shuler Jones Sand Unit Operators Committee for permission to publish this paper.

REFERENCES

1. Kaveler, H. H.: *Trans.* AIME, (1944) **155**, 58-87.

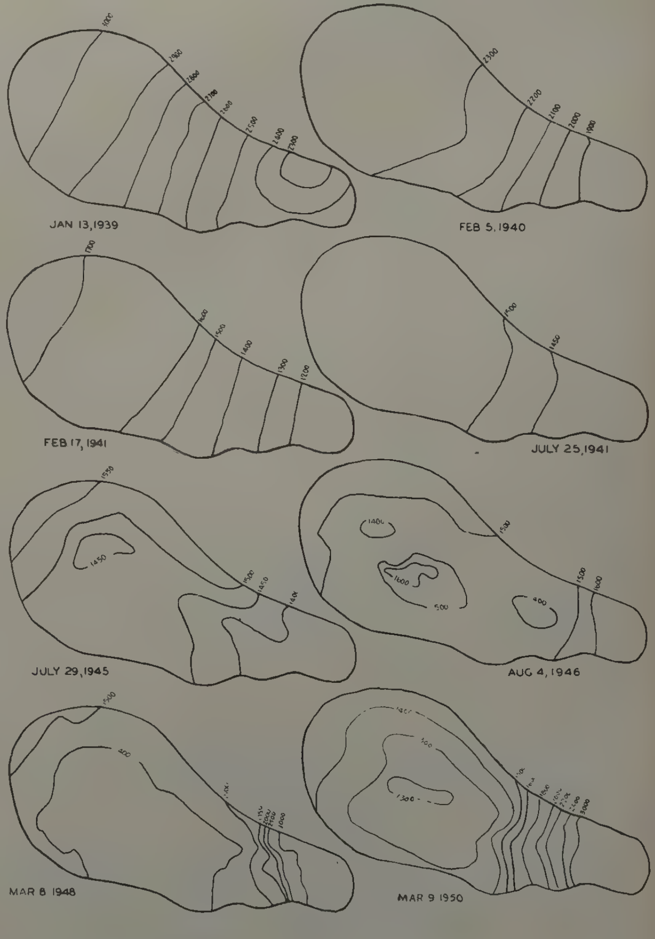

FIG. 7 — PRESSURE MAP, SHULER FIELD, JONES SAND.

Table II — Oil Production Areas of Equal Saturated Sand Volume — Jones Sand Pool

	AREA I			AREA II			AREA III			AREA IV		
Period	For Period	Total	Per Acre Ft	For Period	Total	Per Acre Ft	For Period	Total	Per Acre Ft	For Period	Total	Per Acre Ft
9-17-37 to 2-14-41	5,979,831	5,979,831	160	4,833,578	4,833,578	129	3,228,778	3,228,778	86	2,711,925	2,711,925	72
2-14-41 to 1- 1-42	352,717	6,332,548	169	1,045,093	5,878,671	157	1,107,810	4,336,588	116	1,825,782	4,537,707	121
1- 1-42 to 1- 1-43	529,835	6,862,383	183	1,083,713	6,962,384	186	1,151,494	5,488,082	146	1,723,488	6,261,195	167
1- 1-43 to 1- 1-44	579,882	7,442,265	199	962,126	7,924,510	211	985,278	6,473,360	173	1,404,311	7,665,506	204
1- 1-44 to 2- 1-45	640.228	8,082,493	216	648,330	8,572,840	229	1,054,344	7,527,704	201	1,502,228	9,167,734	245
2- 1-45 to 3- 1-46	370,337	8,452,830	225	624,409	9,197,249	245	894,262	8,412,966	224	1,656,114	10,823,848	289
3- 1-46 to 4- 1-47	399,873	8,852,703	236	391,094	9,588,343	256	1,220,594	9,642,560	257	1,525,072	12,348,920	329
4- 1-47 to 3- 1-48	788,008	9,640,711	257	192,399	9,780,742	261	690,855	10,333,405	276	1,307,839	13,656,759	364
3- 1-48 to 3- 1-49	917,052	10,557,763	282	464,482	10,245,224	273	752,041	11,085,456	296	1,103,450	14,760,209	394
3- 1-49 to 9- 1-49	397,671	10,955,434	292	236,223	10,481,447	280	426,878	11,512,334	307	286,082	15,046,291	401
9-1 -49 to 2-28-50	416,018	11,371,452	303	267,915	10,749,362	286	311,642	11,823,976	315	211,160	15,257,451	406

Pool Total — 150,000 productive acre ft
Each Area — 37,500 productive acre ft

DISCUSSION

By Lincoln F. Elkins, Sohio Petroleum Co., Oklahoma City, Okla., Member AIME

The paper, "Engineering Features of Shuler Field and Unit Operations,"[1] presented eight years ago and its sequel, the present paper on "Nine Years of Unitized Pressure Maintenace Operation in the Shuler Jones Sand Pool" combine to make a very important contribution to petroleum engineering literature. Comparison of actual production performance with early engineering forecasts helps to evaluate and improve engineering methods. The authors and the unit operators should be highly commended for publishing this comparison.

The main thesis of the paper is the efficient operation and high recovery that has been attained through gas injection and unit operation. This operation which has resulted in recovery of 50 per cent of oil in place initially warrants considerable study by all so that essential features of the operation can be copied to improve oil recovery efficiency in other fields where applicable.

The relation between oil recovery and gas injection volume for nine gas injection projects were presented in a previous paper[2] and are repeated here in Fig. 1. To this has been added the performance data of the Shuler Jones Sand Pool calculated in the same manner, assuming that recovery is due to displacement by injected gas and expansion of gas released from solution in oil prior to the period of gas injection. Essentially this is a plot of percentage oil recovery versus cumulative hydrocarbon withdrawal (formation volume of oil and gas measured at formation pressure at the time of production) with hydrocarbon-filled reservoir volume as a base. Displacement efficiency during recovery of the first 10 to 15 million bbl of oil at Shuler was in line with that obtained in the other fields. At higher recoveries, displacement efficiency was apparently much better than that experienced in other fields. Only 1/10 to 1/25 as much cumulative gas volume was required to recover 50 per cent of oil in place initially. Casual examination shows the main difference is that gas injection at Shuler was at elevated pressures while gas injection in these other projects with 50 per cent recovery was at low pressure. However, gas injection pressures were quite high in some of the projects reported and early trends indicate general conformance with the behavior of the low pressure gas drive projects. Therefore, it is important to study the behavior of the Shuler Jones Sand Pool in detail before attributing this high recovery efficiency to maintenance of pressure at a high level. Pressure maintenance has contributed largely to flowing substantially all the production with attendant economy of operation.

Net voidage of some 5,700 B/D of oil and gas, with no decline in pressure, during the period of January, 1943, to August, 1946, indicates water influx of that magnitude. The authors' more detailed material balance calculations show the pressure-production performance to be duplicated by assumption of 100 million bbl of oil in place initially and water influx which totals about 29 million bbl as of March, 1950. This is an important difference in interpretation of performance from that given in the earlier paper,[1] in which oil in place initially was calculated by material balance methods to be 116.5 million bbl and water encroachment was considered to be negligible. Since July, 1941, when gas injection was started, about 30 million bbl of oil have been produced which, with gas in solution, would occupy about 39 million bbl space. During this period water encroachment was about 23 million bbl and water injection was 5.4 million bbl, making a total of 28.4 million bbl of water added to the oil reservoir. Only 3.6 million bbl of water were produced. Water influx and injection thus ranged from 64 per cent net to 73 per cent gross part of the formation volume of oil produced. With water displacement being such high percentage of oil production volume, the recovery efficiency and low gas/oil ratio performance can hardly be considered due largely to gas injection and pressure maintenance. Selective production made possible through unit operation has certainly permitted maximum displacement efficiency to be obtained from the combined water drive and gas injection.

With 25 per cent residual oil phase saturation in the water-invaded portion of the reservoir, some 50,000 acre-ft would be required to contain the 31 million bbl net water influx and injection. If in addition 10 per cent free gas saturation remains in the area, some 67,000 acre-ft would be required. The paper includes no detail of areal water invasion, but it may be reasonable to assume the watered-out area is nearly limited by a line enclosing the wells produced a large percentage of the time, as illustrated in Fig. 5. The oil area outside this line is approximately 2,100 acres and the reservoir volume associated therewith is about 40,000 acre-ft as determined from the isopach map in the previous paper on Shuler.[1] If oil displacement efficiency of the invading water has been sufficient to confine all the water in this area, oil recovery therefrom must have been 20 to 25 million bbl or more with production of only 3.6 million bbl of water. This would be unusual in itself to achieve better than 60 per cent oil recovery with such low overall percentage water production. If water has invaded a considerable part of the undeveloped area of the field it would be difficult to determine what portion of the oil recovery has been due to displacement by gas and what part has been due to displacement by water. In my opinion, it may reasonably be questioned that the oil reservoir volume outside the limits of drilling is not considerably greater than that used in the previous and present papers on Shuler. Only three dry holes were drilled. Material balance calculations of oil in place initially may not be reliable enough

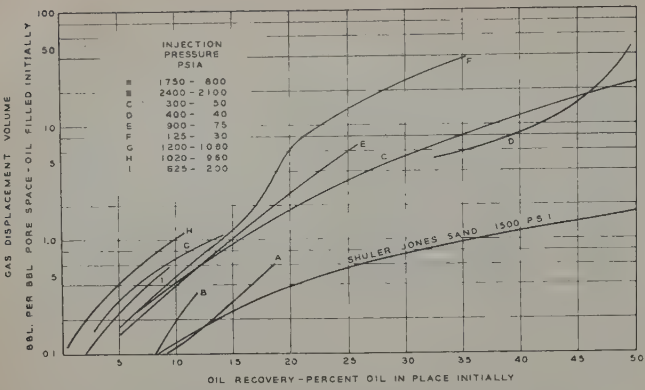

FIG. 1 — GAS INJECTION REQUIREMENTS FOR OIL RECOVERY SANDSTONE RESERVOIRS.

to determine accurately the extent of oil reservoir beyond present wells. This calculation is controlled largely by oil and gas production prior to unitization during which gas production was estimated from periodic well tests. The much more accurate measurement of gas production and gas injection during unit operation does not help greatly in calculation of oil content because the change in formation pressure during this period was so limited. Incidentally, average connate water saturation would have to be approximately 39 per cent for the unusually complete core analysis and electric log data of this pool to conform with the 100 million bbl oil content estimated in this paper. This seems high for a sand having as many high permeability zones as does the Jones sand.

The authors report results of calculations of the pressure-production relationship for primary operation and unit operations without gas injection for comparison with the actual experience of the unitized pressure-maintenance program. In the oral presentation it was explained that the relation for unit operation without gas injection was calculated with the assumption that gas-oil ratios would be the same as actually experienced with gas injection. While this assumption might reasonably well define much of the relation between cumulative production and reservoir pressure, it should not necessarily determine the ultimate recovery if effects of displacement of oil by water have approached that indicated by the analysis presented in this discussion. A similar question applies to the calculation of performance and ultimate recovery by primary operation. Therefore the quantitative conclusion of the paper should be re-evaluated in view of the water drive performance that is evident.

REFERENCES

1. Kaveler, H. H.: *Trans.* AIME, (1944) 155, 58-87.
2. Elkins, Lincoln F., and Cooke, John T.: *Trans.* AIME, (1949) 186, 180-188.

AUTHOR'S REPLY TO MR. ELKINS

The authors first wish to correct and apologize for the error which occurred in Table I of the original paper, in the next to the last column which is entitled "Accumulated Water Encroached." The values which appeared in that column in the original paper were for a term in the material balance equation. The corrected values are presented in the table which is printed with the present draft of the paper. The accumulated water encroached to March, 1950, is calculated to be 21.3 million bbl rather than 29.1 million bbl.

The comments of Elkins and others concerning the effect of water encroachment and the effect of gas injection into the Jones Sand, should lead everyone to the realization of the difficulty of making reservoir engineering predictions of future operations of an oil field. In very few fields has as much fundamental data concerning the fluid characteristics of the oil and gas, or the rock characteristics of the producing zone been made available as has been collected for the Shuler Jones Sand reservoir. In spite of the wealth of material available and 13 years of production history, there remains a difference of opinion between engineers on the relative part that gas and water have played in causing the recovery of additional oil.

Elkins calls attention to the fact that the Shuler Jones Sand relationship of "gas displacement volume to oil recovery," when plotted on his Fig. 1, indicates a better performance than experienced in other gas injection projects. Individual fields are not identified in his figure so it is not possible to analyze those features which may be different from the Shuler Field. One difference may be that Shuler Field with its many wells permitted a greater degree of selective production.

The authors of the present paper readily admit that the encroached water has aided in maintaining a higher degree of oil saturation in the portion of the reservoir swept by the injected gas. It could not do otherwise. Both encroached water and injected water were material to the degree of success of the gas injection program and in maintaining a low gas/oil ratio throughout the producing life. What is generally overlooked by those who advocate that water encroachment has been the prime factor is that water itself, without the aid of the injected gas, would not have made possible as successful a pressure maintenance operation in the Shuler Field. The authors must agree with Lincoln Elkins when he calls attention to the fact that the relationship presented in Fig. 6 of the paper which shows the cumulative oil production versus reservoir pressure for the pool, had it been operated without gas injection but with all water returned to the reservoir, does not necessarily determine the ultimate recovery that would have been realized by such an operation. Elkins' statement is correct, but the fact remains that without gas injection the pressure in the reservoir after the recovery of 32 million bbl of oil would have been less than 600 psi. Continued water flooding would have recovered more oil but it would have been at the expense of very high lifting cost and the higher lifting costs would have resulted in abandonment of the field at a lesser ultimate oil recovery than will be possible under present operations with low lifting cost.

Elkins calls attention to the fact that additional oil may lie outside the boundary of the pool as delineated in the present paper. There is always the possibility of additional oil lying outside the boundary of any field but in this particular case, it is not probable. Attention is also called to the fact that 39 per cent water saturation is high for sand having permeability of the Jones Sand. The authors admit that the 39 per cent calculation is high and have attributed the error to the measurement of porosity. In 1937 and 1938 when these cores were analyzed, the analysis method did not take into consideration the asphaltic content in the pore space of the sand. The porosity reported in the paper is a total porosity and not an effective porosity. Because effective porosity is less than total porosity, water saturation would be less than 39 per cent if the reservoir were to contain the 100 million bbl of oil in place.

★ ★ ★

USE OF CENTRIFUGE FOR DETERMINING CONNATE WATER, RESIDUAL OIL, AND CAPILLARY PRESSURE CURVES OF SMALL CORE SAMPLES

R. L. SLOBOD, ADELE CHAMBERS, MEMBERS AIME, AND **W. L. PREHN, JR.**, ATLANTIC REFINING CO., DALLAS, TEX.

ABSTRACT

The centrifuge has been found to be an extremely useful tool for determining capillary pressure curves and for establishing connate water and residual oil in small core plugs. The use of the centrifuge for determining the properties of small core plugs has been discussed in the literature,[1,2] but practically no experimental evidence has been presented justifying the use of this method in preference to other methods (mainly disc method) now in use. Data have been accumulated and are now presented demonstrating the advantages of the centrifugal method, some of which are: (1) rapid establishment of equilibrium, (2) excellent precision yielding very reproducible results, (3) availability of high pressure differences between phases, (4) simple operational procedure, and (5) ability to establish connate water, residual oil, or to obtain complete capillary pressure curve in one day or less. A commercially available centrifuge capable of speeds up to 3,800 rpm, and a high speed attachment providing a maximum rate of rotation of 18,000 rpm were used in this work in conjunction with core holding tubes designed specifically for this application.

In view of the outstanding advantages associated with the use of the centrifuge the conclusion has been drawn that this method should be used in place of the more tedious, slower, and less reliable disc method for determining capillary pressure curves and for establishing connate water and residual oil in small core plugs.

INTRODUCTION

The need for accurate values of connate water, residual oil, and capillary pressure curves in reservoir engineering has been recognized for many years, and the extent of the effort devoted toward solving these problems is reflected in the large number of papers[3-11] which have appeared in the literature during the past decade. Most of the methods discussed in the recent literature employ a porous disc as a semi-permeable membrane to separate two immiscible phases and make possible the application of an explicit difference in pressure between two phases in the core. Thus, in the determination of the capillary pressure curve the wetting phase (water) is displaced by the non-wetting phase (air or oil).

Several investigators[1,2] have used centrifugal forces to develop pressure differences between phases. As a result of the first work[1] in this field the conclusion was reached that "the more rapid centrifugal method for measuring irreducible saturation may have equal value, (compared to use of discs) but more work is required to establish this point." This work was followed in 1945 by a more detailed study[2] in which the concepts of this experimental work were more clearly enunciated. A method for calculating saturation for any given speed of rotation based on the observed volume of water displaced was developed and a wider application of the method was suggested.

The absence of any subsequent pertinent literature on this subject is interpreted as indicating that no additional work has been completed to substantiate or deny the earlier claims and suggestions of promise contained in the original papers on this subject. One purpose of this report is to provide evidence designed to establish the practical value of centrifugal methods in determining core properties such as connate water and capillary pressure curves. It is also our purpose to suggest a broadening of the scope of this tool to include determinations of residual oil by gas or water drives.

THEORY AND PRACTICE IN USE OF CENTRIFUGE

Hassler and Brunner[2] have clearly presented the basic concepts involved in the use of the centrifuge by relating the performance of a small core in a field of high acceleration to the

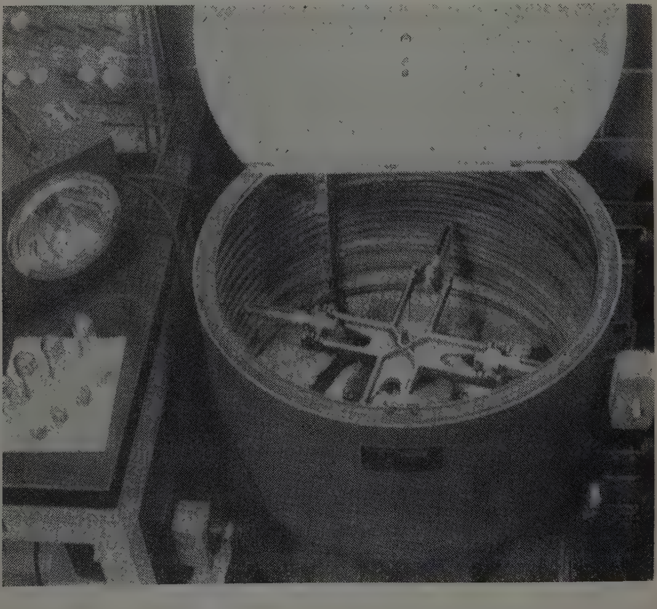

FIG. 1 — CENTRIFUGE SHOWING COIL, STROBOSCOPE, AND TWO TYPES OF CORE HOLDERS.

---

[1] References at end of paper.

Manuscript received in the office of the Petroleum Branch August 16, 1950. Paper presented at the Petroleum Branch Fall Meeting in New Orleans Oct. 4-6, 1950.

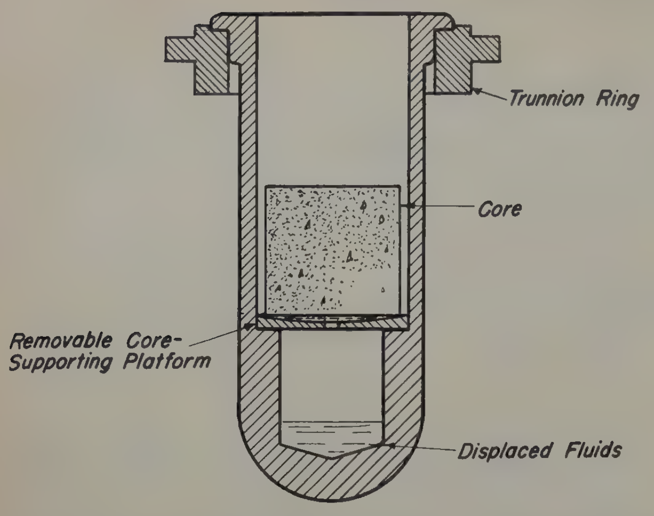

FIG. 2 — CORE HOLDER WITH BOTTOM WELL FOR DISPLACED FLUIDS FOR USE IN NORMAL SPEED CENTRIFUGE.

known action of gravity drainage in a vertical column of uniform composition. If long uniform cores were available from all reservoirs, and allowing sufficient time for equilibrium, connate water values and the capillary pressure curve itself could be obtained by analyzing sections of a core at various heights above the free water level. The pressure difference between the phases in this case can be calculated by the basic equation, $\triangle P = (\rho_1 - \rho_2) gh$, where $\triangle P$ is the pressure difference between the phase 1 and 2, at height h above the reference level, ρ_1 and ρ_2 the densities of the two fluids present in the porous medium and g, the acceleration due to gravity.

In the centrifuge, however, only a short core is used, but large pressure differences between the phases are developed in spite of a small value of h because of the extremely high acceleration which is developed at high rotational speeds. The relationship (developed below*) expressing the pressure difference between the phases in psi at any height h in the core rotating at speed n (rpm) with a radius of rotation r is $\triangle P = 1.578 \text{ x } 10^{-7} (\rho_1 - \rho_2) n^2 rh$ (ρ in g/cm^3, r and h in cm).

If a core containing water is rotated at an appropriate speed in a tube containing oil or air around the core, the water can be displaced down to the connate water value while air or oil replaces the displaced phase. If a capillary pressure curve is desired, intermediate speeds of rotation are used, the speed and volume of displaced water being measured for each equilibrium state. Similarly, if a residual oil value is desired, the core containing connate water and oil is placed in a tube surrounded by air or water and rotated in the centrifuge. When air is the displacing phase, the displaced oil accumulates in a small chamber at the bottom of the tube. When water is the displacing phase, the displaced oil accumulates on top of the water layer. Other determinations, such as evaluation of critical gas saturation, may also be possible by proper utilization of the centrifuge.

Apparatus

A standard International Size 2 Centrifuge modified with a cooling coil and compressor was used in this work, operating at various speeds up to 3,800 rpm (Fig. 1). The refrigerated model PR-1 Centrifuge might be preferable since slightly higher speeds are possible with this model. The centrifuge was mounted on a portable vibrationless stand made by International. For extremely high speeds (18,000 rpm with resulting acceleration of 25,000 gravities at tip of centrifuge tube) a multispeed attachment with four place conical head was used. This attachment is belt driven and rotates 4.6 times the speed of the central driving shaft. For speed control a large Variac was found to be superior to the variable resistance generally supplied with the centrifuge. The tachometer supplied with the centrifuge and a calibrated stroboscope (Type 631-B Strobotac — General Radio) were used to measure rotation speeds.

A number of special tubes for supporting the core specimen were designed with strength consistent with the large forces developed at the high speeds of rotation. The simplest holder used in these studies consists of a straight cylindrical tube with a bed of sand to support the core. This system with water surrounding the core is ideally suited for establishing residual oil by water drive in a core saturated with oil and connate water. Such a tube can be used in both the conventional trunnion rings for normal centrifugal speed, or in the special high speed attachment. Merely to establish connate water saturation in a core, or to establish residual oil by air drive, the holder shown in Fig. 2 is used in the normal speed centrifuge. These tubes contain a well at the bottom where displaced liquid is collected and kept out of contact with the core. The special holder shown in Fig. 3 is used in establishing connate water in core samples that require the higher pressure differences between the phases attained by the higher rate of rotation in the high speed attachment. The special design is required because of the angle at which the tube is held in the high speed head. Finally, the holder shown in Fig. 4 is used for obtaining the capillary pressure curve for the system air displacing water, the displaced water being measured in the pipette contained in the lower end of the tube.

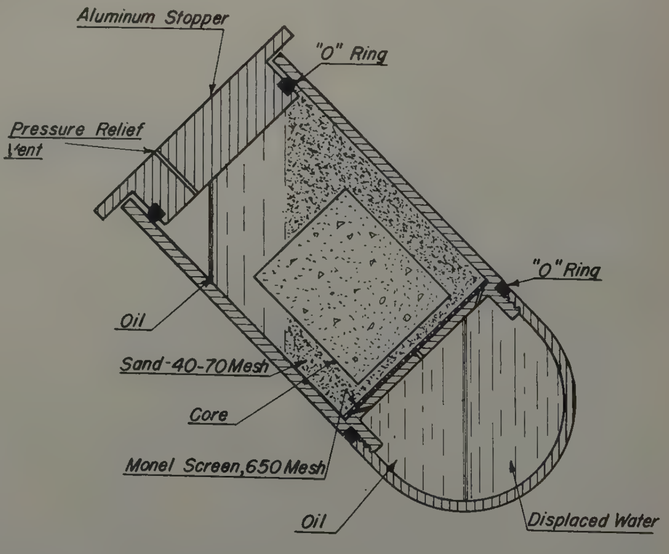

FIG. 3 — CORE HOLDER WITH BOTTOM WELL FOR DISPLACED FLUIDS FOR USE IN HIGH SPEED CENTRIFUGE.

---

*The basic equation for acceleration in the centrifuge is $a = \frac{v^2}{r}$. If n is in rpm, then $v = \frac{2\pi rn}{60}$, and $a = \frac{4\pi^2 rn^2}{3600}$. Dividing this equation by g to get g', the ratio between the acceleration in the centrifuge and that of gravity gives $g' = 0.0000111\ n^2 r$. By combining this equation with the equation for $\triangle P = (\rho_1 - \rho_2) gh$ and converting the units from g/cm^2 to psi by multiplying by 0.01422 we get $\triangle P = 1.578 \text{ x } 10^{-7} (\rho_1 - \rho_2) n^2 rh$. The only instance in which the value of $\triangle P$ need be known accurately is in the determination of the capillary pressure curve. In these cases a 0.8 ratio between the radii from the center of the system to the top of the core and to the base of the core was always exceeded, as specified by Hassler. In other cases, this equation gives an approximate answer which is accurate enough for most purposes.

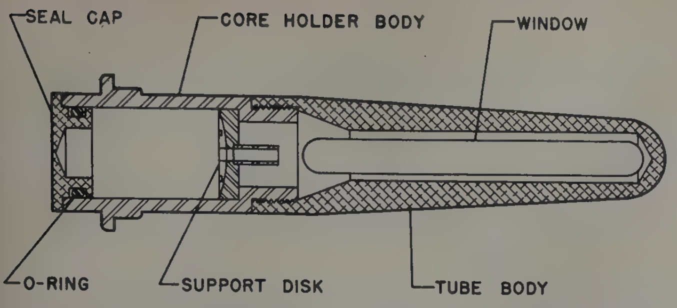

FIG. 4 — CORE HOLDER FOR USE IN OBTAINING CAPILLARY PRESSURE CURVES.

Since the circuit driving the stroboscope did not operate below 600 flashes per min, at rotational speeds below 600 rpm a special contractor using a cam driven directly by the shaft of the centrifuge was used to operate a microswitch. The opening and closing of this switch was used to initiate the flashing of the light source.

Procedure

A core plug, approximately 1 in. long and ¾ in. in diameter is used in all of the studies discussed. The core sample is always cleaned and then saturated with a sodium chloride brine (approximately 5 per cent). From the dry weight and the saturated weight the porosity is determined. The saturated core is then subjected to one or more of the operations described below. Whenever possible, a material balance approach is used to evaluate each process, but in all cases where accurate values are required, the final saturation of the core plug is determined directly, either by weighing, which is accurate when one of the two phases present is air, or by direct analysis using vacuum distillation to remove the saturants and a liquid nitrogen trap to collect and measure the liquid saturants from the core. Final dry weight is used to check on loss of solid from the core. The temperature of the centrifuge is maintained at approximately 75°F to eliminate significant errors from evaporation.

The method used to establish connate water saturation in the cores depends upon the required pressure difference between the phases for the particular core and on the choice of air or water as the displacing phase. For the tightest cores, the maximum pressure difference between phases should be used. To accomplish this the high speed head and the tube shown in Fig. 3 to contain the core are used. The use of air as the displacing phase will provide the maximum $\triangle P$ between phases, but some difficulty in reproducibility has been experienced in this system. In most studies using the high speed head oil has been used as the displacing phase with excellent results. Generally, the water saturated core is placed in a bed of 40-70 mesh sand (to prevent splitting of core from high local pressure) which is confined with a fine monel screen and supported by the shelf shown in Fig. 3. The displacing oil phase is added, and the unit closed with a cap containing an O-ring seal and a small vent hole. The pairs of tubes are balanced to within 0.1g, inserted into the high speed head, and then rotated at 18,000 rpm ($\triangle P$ between phases at midpoint of core is approximately 105 psi) until equilibrium is attained. The time required for most cores is of the order of one hour, although very tight cores may require several hours to approach equilibrium even closely. For looser cores which do not require excessively high pressure differences, the simpler tube shown in Fig. 2 can be used in the normal speed head centrifuging 4 or even 8 cores simultaneously using standard equipment to hold the core tubes. In this normal speed operation the core is placed on a monel platform which is supported on a shoulder cut into the wall of the monel tube. The storage space below the supporting plate has sufficient volume to hold all of the displaced water without allowing the collected water to contact the bottom of the core. At a speed of 3,800 rpm a $\triangle P$ between phases of 14 psi is developed at the center of the core for the oil-water system and 50 psi for the air-water system. Generally, one hour is sufficient time for the system to come to equilibrium. In some cases it is desirable to mount the core in capillary contact with a disc ⅛ in. to ¼ in. thick. In this way, the end effect is transferred to the disc and a slightly greater net $\triangle P$ between the phases operates to drive the core down to connate water more effectively. No trouble with capillary contact is experienced here because of the extremely large force acting to push the core into contact with the disc. Kleenex is also used here to improve the quality of contact.

To determine residual oil by air drive, the core plug containing connate water and oil is placed in the tube shown in Fig. 2. With air as the only other component present in the tube, the system is rotated at 3,800 rpm for approximately one hour. The displaced oil is collected in the bottom of the tube. The residual oil may be calculated from the weight of the core knowing the connate water value. Generally, a direct determination using the vacuum distillation technique is used to measure directly the residual oil.

Residual oil by water drive is determined by placing the core containing connate water and oil in a bed of coarse sand in the tube shown in Fig. 3. The core is then covered with water, the tube closed, and then centrifuged for one hour in the high speed attachment at 18,000 rpm.

The capillary pressure curve for the system air displacing water is obtained using the special core holder shown in Fig. 4. The fully water saturated core is placed in the holder, and the unit then placed in the centrifuge. The system is rotated at a number of different speeds selected to cover the range of pressure differences between phases required for the particular core. At each speed setting, the rate of rotation is maintained constant until no additional water is observed to collect in the pipette. In accordance with Hassler's recommendation, the speed of the centrifuge should not be allowed to decrease at any time during the run. Pipettes are read to the nearest 0.01 cu cm while rotating by use of light flashes from a stroboscope. Generally, 30 to 45 minutes is sufficient time to establish equilibrium at each point. A complete curve with 6 or 8 points may be obtained in one working day. In actual practice eight cores are run simultaneously. Subtracting the volume of displaced water from the original water content gives the average saturation, $\bar{s}$, in the core. The correct value of saturation to use in plotting the capillary pressure curve is determined by using the method suggested by Hassler[2] in

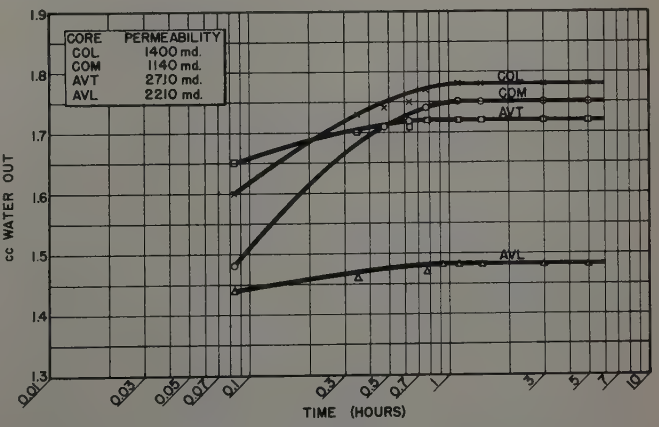

FIG. 5 — INTERSTITIAL WATER SATURATION IN CORE CENTRIFUGED AT 2,300 RPM USING WATER-AIR SYSTEM.

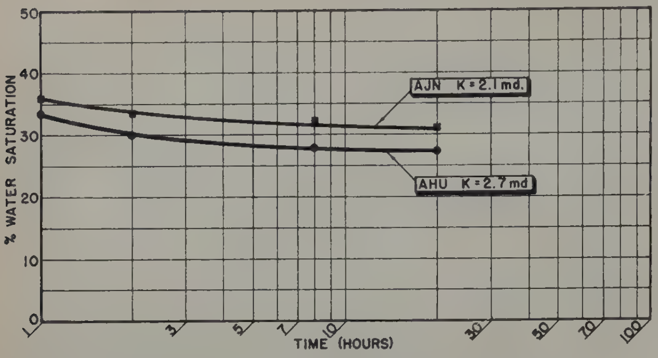

FIG. 6 — STUDY OF TIME REQUIRED FOR RELATIVELY TIGHT CORES TO COME TO EQUILIBRIUM IN HIGH SPEED WATER-OIL SYSTEM.

which the slope of the curve for $Z\bar{s}$ plotted against Z gives the value of saturation consistent with Z, where Z is the pressure difference between the phases at the top of the core (maximum $\triangle P$ in core). The value for Z is calculated assuming a constant value for acceleration from top to bottom of core calculated on the basis of the radius of rotation measured from the center of the centrifuge to the center of the core.

RESULTS

Establishment of Connate Water: Air-Water and Oil-Water Systems

The time required for loose cores to come to equilibrium using air to displace water at 2,300 rpm (maximum $\triangle P$ between phases = 35 psi) was found to be approximately one hour. The rate of approach to equilibrium is shown in Fig. 5. In the four cores studied with permeabilities ranging from 1,140 md to 2,710 md, no change in fluid saturation was observed after one hour of centrifuging. These data were obtained in the equipment used to obtain capillary pressure curves, the volume of expelled water being measured directly. Other data, not presented, indicate that most cores of 200 md permeability or higher will attain or closely approach equilibrium in less than two hours for the system air-water at speeds of 3,800 rpm. Studies using the high speed (18,000 rpm) apparatus to displace water by air have been discontinued. Results obtained were generally low and somewhat variable. Evaporation losses and trouble from other causes such as cavitation may be the explanation. This system does provide the maximum $\triangle P$ between phases and may be useful for extremely tight cores when all of the extraneous variables are properly controlled.

The time required for establishing equilibrium when displacing water by oil in the high speed centrifuge (18,000 rpm) is shown by the data in Table I. These six cores represent five different fields. The more permeable cores (several hundred md) apparently attain equilibrium in one or two hours. Cores of intermediate permeability (15 to 100 md) apparently are close to equilibrium after two hours of centrifuging, but the amount of data is insufficient to make a sweeping generalization for this case. Extremely tight cores (2 md), however, definitely are not at equilibrium after two hours of centrifuging. The above results on two tight cores are shown in Fig. 6. From these curves it is evident that the cores are close to equilibrium at 20 hours, and it is probable that a tenfold increase in centrifuging time would produce no more than one or two per cent decrease in water saturation. These data also indicate that the more practical time of eight hours gives a reasonably close approach to the correct connate water value.

Table I — Water Content as a Function of Centrifuging Time — Water - Oil System at 18,000 rpm

		Time in Centrifuge-Hours				
Core	K(md)	0.25	1.0	2.0	8.0	20.0
AJN	2.1	39.4	36.2	33.5	32.2	31.0
AHU	2.7	—	33.5	30.1	27.8	27.3
APT	16	—	35.4	34.3	—	—
BVR	67	—	27.4	26.5	—	—
EU	458	—	26.4	26.4	—	—
AVX	885	—	13.0	—	12.0	—

The reproducibility in connate water values obtainable using the centrifuge are shown in Table II. The reproducibility in most cases is within a few tenths of one per cent of the pore space. This result is superior to any previous results observed in this laboratory using the disc method or a flowing oil phase

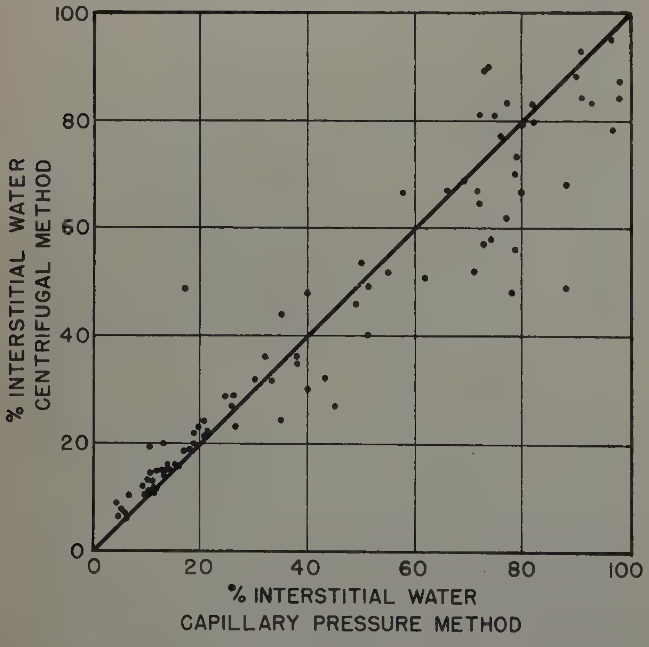

FIG. 7—CORRELATION PLOT OF INTERSTITIAL WATER BY CENTRIFUGAL METHOD WITH INTERSTITIAL WATER BY CAPILLARY PRESSURE METHOD.

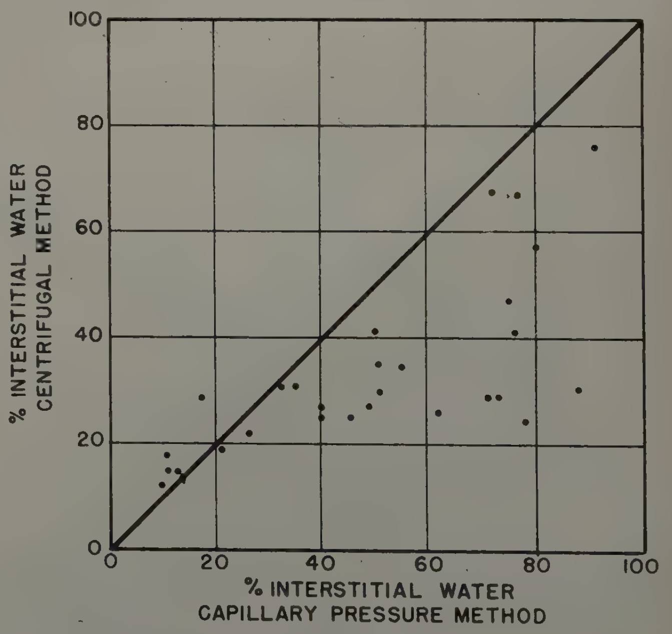

FIG. 8 — CORRELATION — INTERSTITIAL WATER BY CENTRIFUGE VS. CAPILLARY PRESSURE METHOD FOR TIGHT CORES.

(dynamic method) to displace the water. The reproducibility has been so good that small changes in the core which developed with use, such as changes in the wetting characteristics leading to changes in the connate water value, can be detected. The checking values cited in Table II were generally obtained on successive days. When results obtained over an interval of several months with other operations performed on the core were compared, differences of the order of several per cent of the pore space were observed (Table III). These differences are obviously significant in view of reproducibility to within several tenths of one per cent for unchanged cores.

To obtain reliable connate water data the pressure difference between the phases developed in the centrifuge must be sufficient to displace the water from the pore spaces. Consequently, either the system which develops the maximum $\triangle P$ between phases must be used in all cases (not always desirable since this involves the use of the high speed head which holds only four cores at one time and requires more careful watching of the equipment) or the system used must be selected on the basis of known core properties (permeability unless capillary size distribution is known). The various systems used, listed in order of decreasing effectiveness in displacing water from the core are shown in Table IV. End butts act to transfer the zone of minimum $\triangle P$ between phases from the lower end of the core to the porous medium used for the end butt. Consequently, the zone of high water saturation, generally called the end effect, is largely removed from the core and put into the end butt. In addition, the height of the liquid column is increased by the thickness of the butt leading to a slightly higher value for $\triangle P$ between the phases throughout the core.

The $\triangle P$ between phases is 0 psi at the bottom of the core, where 100 per cent water saturation is assumed to exist, and it increases to a maximum at the top. The value of $\triangle P$ at the top of a 1 in. core for typical systems is shown in Table IV. The maximum $\triangle P$ is approximately 750 psi for the high speed air-water systems.

Table II — Reproducibility of Connate Water Values: Air - Water and Oil - Water Systems

		Connate Water Values by Analysis			
		Low Speed: Air-Water		High Speed: Oil-Water	
Core	K(md)	Test 1	Test 2	Test 1	Test 2
CPC	3100	9.0	9.1	—	—
COS	2500	11.2	11.3	—	—
COT	2100	10.5	10.6	—	—
CPA	1700	13.1	13.8	—	—
COF	1350	—	—	16.8	16.8
AVX	885	14.4	14.1	13.9	14.6
COP	460	22.3	22.5	—	—
EU	458	—	—	27.3	26.4
1188	453	—	—	8.5	8.4
BVR	67	—	—	26.5	27.4
APT	16	—	—	35.4	35.4
AHU	2.7	—	—	33.7	33.7
AJN	2.1	—	—	36.8	36.2

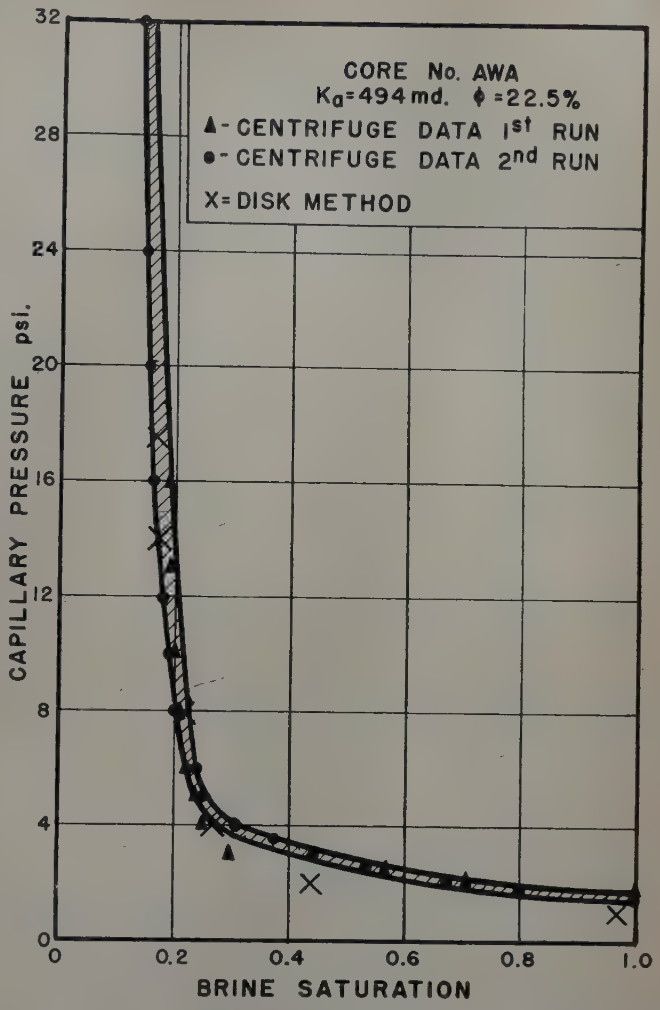

FIG. 9 — CAPILLARY PRESSURE CURVE SHOWING REPRODUCIBILITY.

Results of connate water determinations on a number of cores using the six different systems are shown in Table V. These data show that for many of the more permeable cores the normal speed air-water system or the air-water system with end butt is as effective in desaturating the core as the high speed water-oil system (cores COY, COX, AVX, and 1189). The tighter cores (BVR, ATF, and AUE) show the real need for the extremely high pressure differences between the phases produced in the high speed head. At this stage it is not clear whether the results obtained using the high speed head for the air-water system are reliable. Cavitation,[1] possible evaporation losses, and other experimental difficulties may account for the generally lower results obtained in this system.

In order to evaluate further the reliability of the centrifuge method for establishing connate water in core plugs approximately 100 cores, on which capillary pressure studies using the disc method had been made, were selected. An interstitial* water determination with the normal speed air-water system was made on each of these cores. The results are shown in Fig. 7.

The data in Fig. 7 demonstrate a good correlation between the centrifugal method and the capillary pressure system. The

Table III — Change in Connate Water Value Showing Change in Core

		Connate Water Value for Oil-Water System: Using High Speed Head		
Core	K(md)	Orig. Value	Later Value	Difference
COF	1350	14.5%	16.8%	2.3
EU	458	31.1	27.3	3.8
BVR	67	25.0	26.5	1.5
APT	16	30.8	35.4	4.6
AHU	2.7	29.1	33.7	4.6
AJN	2.1	32.2	36.8	4.6

---

*Interstitial water denotes water saturation for some stated experimental condition. At a sufficiently high pressure difference between the phases, the interstitial water saturation will become equal to the connate (irreducible) water saturation.

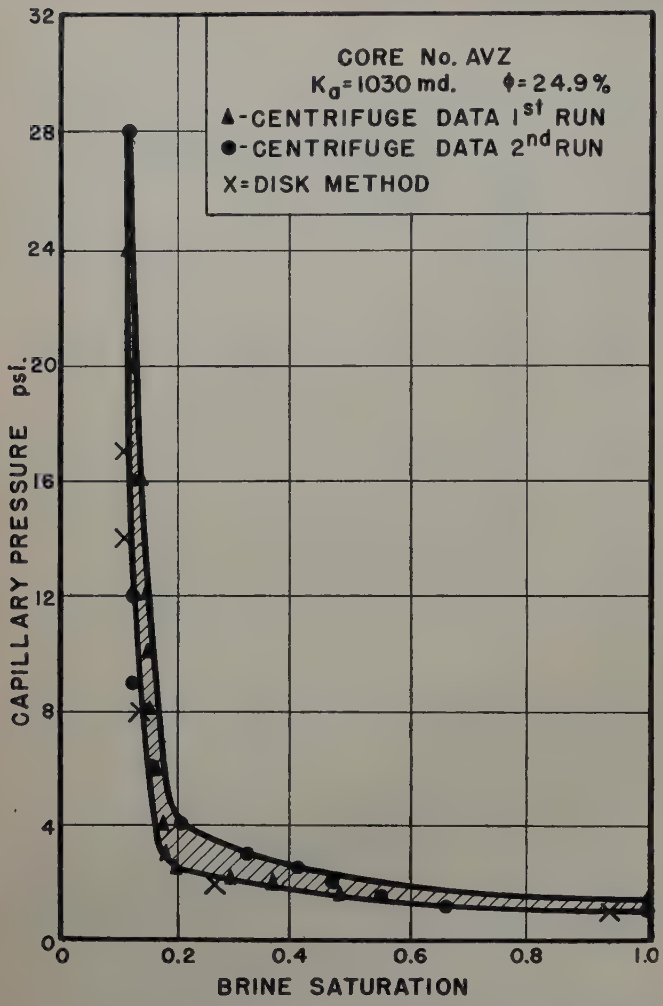

FIG. 10 — CAPILLARY PRESSURE CURVE SHOWING REPRODUCIBILITY.

cores in this study were divided into two groups. The cores of group I (shown in Table VI) had capillary pressure curves which were vertical in the higher pressure region (10 to 16 psi between phases for oil-water and up to 50 psi for air-water) indicating that the saturations at the completion of the capillary pressure runs were at the connate water value. The connate water values on these cores obtained using the air-water system in the centrifuge are in fairly close agreement with the capillary pressure values. In most cases the centrifugal method gave a slightly higher water saturation. In cases such as this, true connate water was apparently attained in the capillary pressure method, and the centrifuge value is slightly in error because of the end effect previously discussed. If greater precision is desired, this end effect can be eliminated by the use of butts.

In Table VII are listed the second group of cores which had connate water value greater than 30 per cent or which did not have vertical capillary pressure curves at the highest displacing pressures (16 psi) used. Lower values of interstitial water saturation were observed on the majority of these cores by centrifuging in the low speed air-water system as compared to the capillary pressure method. Inadequate pressure, poor capillary contact, or failure to wait the extremely long time necessary to establish true equilibrium in the capillary pressure system could explain these results. A number of these cores were run in the high speed centrifuge (oil-water system) in order to obtain a better value for connate water. These results are given in Table VII and are shown in Fig. 8. Almost all of the values are seen to lie well below the regression line, indicating that the pressures used in the capillary pressure work were clearly inadequate.

Capillary Pressure Curves: Air-Water System

Capillary pressure curves have been obtained on more than 30 cores by use of the centrifugal method described under "Procedure." At least two determinations have been made on more than 16 different cores. Very good agreement between check runs was generally observed. Typical results on three cores are shown in Figs. 9 to 11. Points on the capillary pressure curve obtained in another laboratory by use of the disc method are represented by x's in these plots to show the general agreement in value between the two methods. The reproducibility observed may be summarized quantitatively by stating that for all of the duplicate runs made the average spread in saturation at 24 psi pressure difference between the phases was 2.7 per cent, and the average pressure spread at

Table IV — Pressure Difference Between Phases at Top of Core 1-in. Long

System		$\triangle P$ Max.
High Speed Centrifuge:	Air-Water	750 psi
(18,000 rpm)	Oil-Water	210 psi
Normal Speed Centrifuge (3,800 rpm):		
	Air-Water with ¼-in. end butt	125 psi
	Air-Water	100 psi
	Oil-Water with ¼-in. end butt	35 psi
	Oil-Water	28 psi

Constants:

Average Radius of Rotation for 1-in Core — Normal Speed 16.5 cm

Average Radius of Rotation for 1-in Core — High Speed 4.25 cm

Effective height of 1-in. core when supported at slope in high speed head = 3.26 cm

Density of 50,000 ppm Chloride Brine = 1.053

Density of Oil = 0.758

Equation used: $\triangle P = 1.578 \times 10^{-7} (\rho_1 - \rho_2) n^2 r h$;
$\triangle P$ = psi; $\rho = g/cc$; n = rpm;
r = cm; h = cm

Table V — Water Saturation Values Obtained to Demonstrate Relative Effectiveness of Various Centrifuge Methods

		Normal Speed				High Speed	
		Oil-Water System		Air-Water System			
Core	K(md)	No End Butt	End Butt	No End Butt	End Butt	Oil-Water	Air-Water
AVT	2710	—	7.7	6.7	5.7	—	—
AVL	2210	10.7	—	7.7	6.6	—	—
COY	1800	—	—	12.1	—	12.3	—
COX	1600	—	—	14.5	—	14.8	—
COF	1350	—	—	20.0	—	14.5	—
AVX	885	—	—	14.4	—	13.9	—
COG	570	—	22.3	20.6	17.8	18.0	—
1189	470	18.1	—	9.8	—	10.8	—
COP	460	—	—	22.3	20.5	19.5	18.3
EU	458	—	—	36.2	—	31.1	21.5
1188	453	—	—	8.9	—	8.5	5.4
AEP	316	25.3	—	20.0	18.2	—	—
AEQ	203	—	24.7	22.8	19.9	—	—
AWB	138	—	—	26.8	—	22.0	—
BVO	84	—	30.7	27.2	26.4	25.2	—
BVR	67	40.1	—	29.4	27.2	26.5	—
ATF	5.4	—	—	49.1	—	29.0	24.4
AUE	4.3	—	—	54.5	—	33.0	—

95 per cent saturation was only 0.4 psi. These results were obtained in cores from five different fields with permeabilities ranging from 3.5 to 1,030 md. From the excellent reproducibility observed in this study, the conclusion has been drawn that the centrifuge method is sufficiently reliable to replace the disc method which is much less reliable and which is at best only of comparable precision.

Residual Oil: Water Drive and Oil Drive

A small amount of data has been obtained showing that reproducible residual oil values can be obtained either by driving the core with water or with air. Some of the values for water drive are shown in Table VIII. In some cores the agreement is excellent (within several tenths of 1 per cent of the pore space). In others the variation is greater than 1 per cent of the pore space. Unfortunately, as a result of the materials and methods used in this laboratory, the wetting characteristics of cores apparently change with use, resulting in changes in the observed value for residual oil. This difficulty is expected to be overcome by modifications in procedure and materials used so that results reproducible to a fraction of 1 per cent of the pore space can be attained.

Table VI — Comparison of Interstitial Water Values Obtained by Centrifugal Method (Low Speed Water-Air System) and by Capillary Pressure Method

Core	K (md)	Cap. Pres.*	Centrifuge
CPC	3100	4.5	9.0
AVT	2710	5.2	6.7
COS	2500	10.6	11.2
CPD	2400	6.8	10.6
AVN	2318	5.8	6.0
AVS	2230	5.7	7.2
AVL	2210	5.3	7.7
COT	2100	9.6	10.5
COY	1800	9.6	12.1
CPA	1700	10.3	13.1
COX	1600	10.7	14.5
COR	1540	14.8	16.0
COL	1400	13.8	14.7
COF	1350	13.0	20.0
COZ	1300	11.0	13.3
COM	1140	14.0	16.1
AVZ	1030	11.2	11.6
COH	975	17.0	18.9
AVV	954	11.0	11.1
AVW	926	10.9	11.4
AVX	885	13.5	14.1
COI	680	20.6	24.7
COO	680	18.0	19.1
AVY	679	13.2	15.2
COG	570	11.0	20.6
COJ	525	19.7	23.0
CON	500	19.1	19.8
AWA	494	16.3	16.6
1189	470	9.8	9.8
COP	460	21.2	22.3
1188	453	9.0	8.9
AES	351	20.9	21.5
AEP	316	19.0	20.0
COQ	315	25.1	28.9
APL	237	13.8	15.1
APK	227	12.6	15.3
AWC	204	26.4	23.0
AEQ	203	20.9	22.8
AWB	138	26.0	26.8
APH	89	18.7	21.8
ATF	5.4	17.4	49.1

*All Cores Apparently at Connate Water from Capillary Pressure Curve.

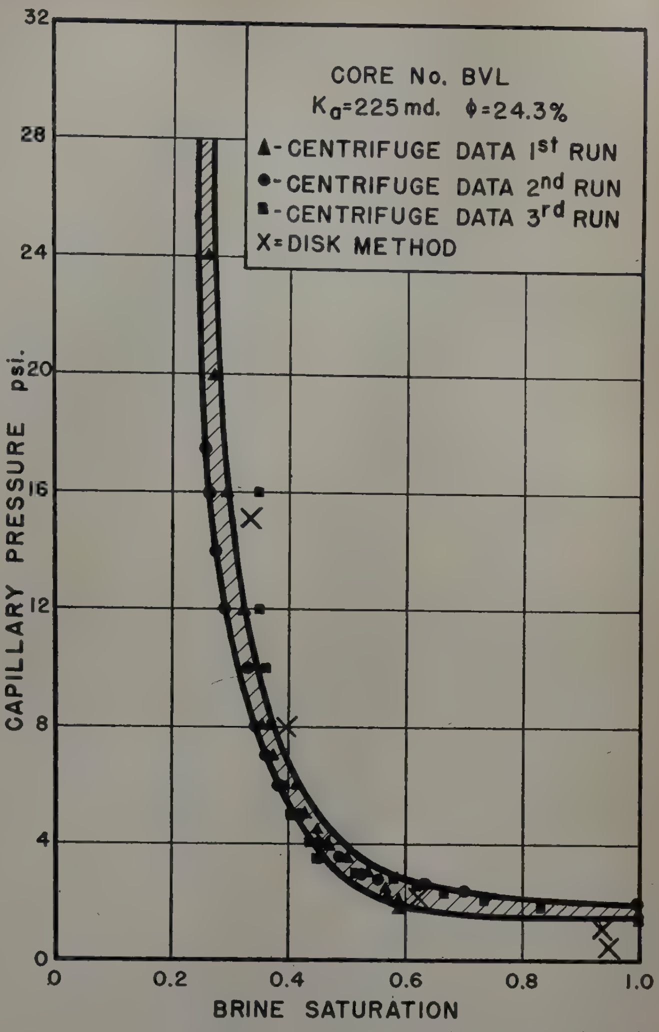

FIG. 11 — CAPILLARY PRESSURE CURVE SHOWING REPRODUCIBILITY.

As a result of considerable experience with the centrifuge in establishing connate water and residual oil in core samples for use in subsequent experimental work, particularly in the laboratory determination of relative permeability, the versatility, reliability, and convenience of this method have been amply demonstrated. Moreover, this tool can be used to facilitate relative permeability determinations by rapidly establishing residual oil saturation after the point has been reached where the oil saturation changes slowly with time in the relative permeability apparatus. After residual oil is established, the relative permeability of air (or water) may be determined in the relative permeability equipment. The use of the centrifuge as outlined above, in which cores are provided with desired saturants present, has proved to be extremely valuable, and in future applications this use may possibly exceed in importance the determination of core properties merely for their own sake.

Other applications such as the determination of critical gas saturation and studies at simulated reservoir conditions possibly may be carried out in the centrifuge.

CONCLUSIONS

1. In the evaluation of the property of core plugs the centrifuge can be used to establish connate water saturation,

residual oil by air or water drive, and can be used to obtain capillary pressure curves.

2. The use of the centrifuge for connate water, residual oil, and capillary pressure studies has many advantages, particularly with respect to the disc method now in common use. These are:
   a. Little development cost is involved as most of the parts are commercially available.

Table VII — Comparison of Interstitial Water Saturations Attained by Centrifugal Methods with Those Obtained by Capillary Pressure Methods

Cores with vertical capillary pressure curves and with residual (water) values above 30%:

Core	K(md)	Cap. Pres.	Low Speed Water-Air	High Speed Water-Oil
EU	458	32.1	36.2	31.1
COV	360	26.1	28.6	—
XY	345	37.8	36.1	—
BVL	225	34.8	23.6	—
COK	140	30.2	32.0	—
BVO	84	44.5	27.2	25.2
BVN	84	43.3	31.9	—
BVR	67	40.0	29.4	25.0
API	46	32.8	31.6	—
APQ	38	37.8	34.5	—
BVM	27	51.0	40.0	35.4
APU	22	54.5	52.3	34.1
APT	16	35.3	43.5	30.8
AHF	3.1	40.3	48.0	27.3
AHU	2.7	71.1	52.0	29.1
AHG	2.2	61.5	50.5	25.6
YZ	0.6	50.0	53.5	41.3
Cores of which the capillary pressure curve was not vertical:				
CBW	12.4	92.6	82.9	—
ZH	4.4	73.6	58.0	—
BAG	3.8	78.5	56.4	—
CGI	3.6	81.7	79.8	—
AHA	3.5	88.3	49.0	29.8
AAC	2.7	65.8	67.3	—
CGP	2.7	72.2	81.2	67.5
ANG	2.7	48.6	46.1	27.4
CGV	2.4	78.4	48.0	33.6
CHH	2.3	97.5	87.4	—
ANB	2.2	50.8	48.6	29.6
AOR	2.1	80.0	79.6	57.1
AXV	2.1	72.8	57.0	29.1
CGN	2.0	76.5	83.2	67.1
CGK	1.9	98.0	83.6	—
ATX	1.8	82.1	83.3	—
CHD	1.4	72.4	67.8	—
AHB	1.3	57.5	66.5	40.0
AYB	1.0	75.4	80.5	47.0
BAF	1.0	78.5	73.0	—
BLW	1.0	69.0	69.5	—
CGH	0.9	89.9	88.3	—
AZU	0.8	79.6	66.6	—
CGJ	0.7	73.2	88.9	—
AKO	0.6	97.0	77.8	—
AZW	0.5	88.1	67.5	—
AZX	0.5	71.4	64.7	—
CGG	0.4	91.1	83.5	—
CGL	0.3	95.5	94.5	—
CHG	0.3	91.0	93.4	76.3
AZI	0.2	75.7	77.3	41.0
AZM	0.2	78.9	70.4	—
AZN	0.2	76.5	62.1	—

Table VIII — Reproducibility in Residual Oil Determinations Using Water to Displace Oil from Cores Containing Connate Water

		Residual Oil Values — % of Pore Volume				
Core	K(md)	Run 1	Run 2	Run 3	Run 4	Avg.
COP	460	21.3	21.3	—	—	21.3
1447	283	14.4	10.2	11.4	10.2	10.8
AWB	138	21.7	19.6	—	—	20.7
API	16	34.3	34.3	—	—	34.3
1443	7.5	29.2	31.8	30.6	28.8	30.1
1437	4.8	24.0	24.0	26.4	23.6	24.6
1439	0.86	30.8	28.7	30.1	32.2	30.4

   b. The initial cost is low.
   c. Apparatus is a simple, compact system requiring little manipulation, which makes it nearly foolproof and results in very little lost data.
   d. System reaches equilibrium rapidly, making results available more quickly. The time loss usually experienced as a natural result of equipment failure and experimental difficulties in long drawn out experiments is not present. More accurate data are also obtained because equilibrium is really attained instead of just approached.
   e. Results are more accurate because sources of error such as poor capillary contact and failure to attain equilibrium are absent and because higher pressure differences between phases necessary for many cores are available.
   f. Results are reproducible with greater precision than in other known methods.
   g. The theoretical basis of the work appears to be sound since the principle of drainage which is involved in the centrifuge is closely related to that in the reservoir.

3. The centrifuge is particularly applicable to establishing connate water in cores either for determining that value or for experimental work in which cores containing connate water are needed.

ACKNOWLEDGMENT

The authors wish to acknowledge with gratitude the cooperation of Dean W. Lee Hart and the personnel of Southwestern Medical College of the University of Texas in making available their equipment for preliminary investigation.

REFERENCES

1. McCullough, J. J., Albaugh, F. W., and Jones, P. H.: *API Drill. and Prod. Prac.*, (1944), 180-188.
2. Hassler, G. L., and Brunner, E.: *Trans.* AIME, (1945), **160**, 114-123.
3. Amyx, J. W., and Yuster, S. T.: *Producers Monthly*, (Dec. 1946), **11**, No. 2, 10-13.
4. Bruce, W. A., and Welge, H. J.: *Oil and Gas Jour.*, (July, 1947), **156**, No. 21, 223-238.
5. Calhoun, J. C., Jr., Lewis, Maurice, Jr., and Newman, R. C.: *Trans.* AIME, (1949), **186**, 189-196.
6. Hassler, G. L., Brunner, E., and Deahl, T. J.: *Trans.* AIME, (1944), 155-174.
7. Leverett, M. C.: *Trans.* AIME, (1941), **142**, 152-169.
8. Rose, Walter, and Bruce, W. A.: *Trans.* AIME, (1949), **186**, 127-142.
9. Stahl, C. D., and Nielsen, R. F.: *Producers Monthly*, (Jan., 1950), **14**, No. 3, 19-22.
10. Thornton, O. F., and Marshall, D. L.: *Trans.* AIME, (1947), **170**, 69-80.
11. Yuster, S. T., and Stahl, C. D.: *Producers Monthly*, (Dec., 1948), **13**, No. 2, 24-29.

★ ★ ★

EFFECT OF FREE GAS SATURATION ON OIL RECOVERY BY WATER FLOODING

C. R. HOLMGREN AND **R. A. MORSE,** JUNIOR MEMBERS AIME, STANOLIND OIL AND GAS CO., TULSA, OKLA.

ABSTRACT

The production of oil by water flooding can be substantially increased by the maintenance of free gas saturation in the reservoir during the flooding operation. This effect is accomplished by the alteration of oil relative permeability characteristics and the occupation by gas of pore space that would otherwise be filled with residual oil. The amount of reduction in residual oil can be calculated from appropriate water-oil relative permeability characteristics.

This paper presents experimental data in support of the foregoing conclusions and an example of the calculations. The microscopic pore saturation concepts of the mechanism are discussed. A method of practical application to field floods is presented together with discussion of certain limitations.

INTRODUCTION

The presence of free gas has been reported by a number of investigators to significantly affect the oil recovery which can be obtained from sandstone flow systems by water flooding.[1,2,3,4,5] The effect of gas, noted in every instance, has been to cause lower residual oil saturations than could be obtained by water flooding the same systems in the absence of free gas. The degree of improvement in recovery has been observed to vary widely, depending on the systems used and the conditions of the tests. The increased oil recovery obtained because of the presence of gas during a water flood has been variously attributed to changes in physical characteristics of the oil, selective plugging action of the gas, inclusion of oil mist in the free gas phase, and the additional sweeping or driving action of the free gas.

All but the first of these suggestions imply changes in the displacement mechanism. The change in viscosity and interfacial tension of the oil phase, within the pressure range used for all the experimental work, is certainly not sufficient to account for the differences in residual oil saturation noted unless there is a drastic change in the displacement process.[1]

One other effect which logically seems capable of causing differences in residual oil saturation of the magnitude noted in the experimental work is that of simple replacement. In a water-wet system containing oil, water, and gas, it is to be expected that the gas will exist inside the oil. This is the position of minimum free surface energy, since the gas-oil interfacial tension will be less than the gas-water interfacial tension. There is no apparent reason to expect that the existence of free gas within the oil phase should alter the saturation at which the non-wetting phase (now oil and gas) should become discontinuous and hence trapped so as to be unrecoverable by direct displacement by water. If this is the situation, then trapping of a certain percentage of gas saturation during water flood should result, at infinite water-oil ratio, in a like reduction of oil saturation below that attainable by flooding in the absence of free gas. It is visualized that the gas will exist as bubbles inside the discontinuous residual oil as illustrated in Fig. 1, with the size of the oil bubbles being substantially unchanged due to the presence of the gas. As a practical matter, it can be anticipated that the presence of a free gas saturation inside the oil phase will reduce the relative permeability to oil which will exist at any particular water saturation. This reduction will be caused by two factors — the addition of the gas-oil interface, and the reduction of area available for oil flow in the pores containing gas. This reduction in oil permeability at any particular water saturation will result in water breakthrough at a lower water satu-

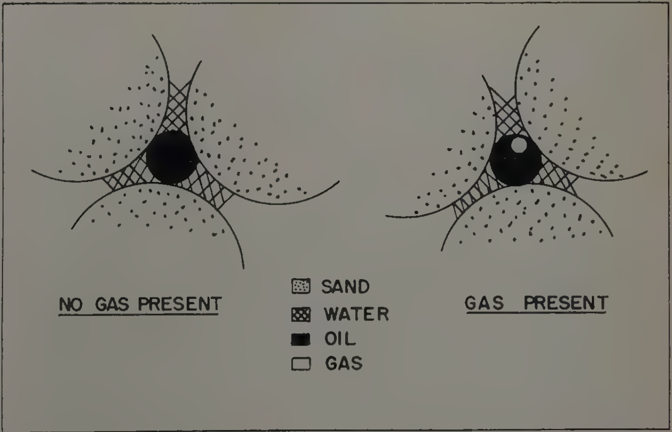

FIG. 1 — CONCEPT OF OIL AND GAS LOCATIONS IN PORE SPACE AT RESIDUAL OIL SATURATION.

---

[1] References given at end of paper.

Manuscript received in the office of the Petroleum Branch Sept. 15, 1950. Paper presented at the Petroleum Branch Fall Meeting in New Orleans, La., Oct. 4-6, 1950.

ration and higher water-oil ratios for a given water saturation following breakthrough, than would be obtained if gas were not present.

It has been impossible to quantitatively evaluate, from the available experimental work, the effects of free gas on water flooding because of one complicating factor common to all experimental work; that of unmeasured variations of gas saturation at the water flood front. Water flooding of a linear system, partially saturated with oil and gas, results in the formation of an increasingly wide oil bank ahead of the injected water. The moving oil bank will displace gas ahead of it, reducing the gas saturation to some residual value immediately behind the front of the oil bank. The movement of the oil bank will cause the pressure on the residual gas to be increased above the value at which it was trapped. The amount that the pressure on the gas will be increased, before the water flooding front reaches it, will depend on the width of the oil bank, the oil permeability, and the flow rate. As the pressure increases, the gas will be reduced in volume due to compression and solution. If the pressure is increased enough between the time the gas is trapped and the arrival of the water flood front, all of the gas may be put into solution in the oil, causing the system to revert to one of two liquid phases. The gas saturation existing at the water flood front may have any value between zero and the maximum residual gas trapped at the front of the advancing oil bank. If improved water flooding oil recovery is dependent on the existence of a free gas phase, the mere existence of an initial gas saturation before flooding begins would not necessarily insure that lower oil saturations could be obtained than could be obtained by flooding a completely liquid saturated system.

One way to avoid the complication of varying gas saturation during the water flooding process would be to conduct the flood at a pressure differential which is very small compared to the absolute pressure of the system. In this way the residual gas saturation at the water flood front can be kept substantially the same as that in the entire oil bank. The amount of this residual gas saturation should then be merely a function of the relative permeability characteristics of the sand and the saturation conditions prior to the flood.[6] Experimental work reported in this paper was conducted under these conditions with the specific objective of isolating the effects of a static free gas phase on water flooding recovery as differentiated from any alteration in the displacement mechanism occasioned by the presence of mobile gas.

APPARATUS AND MATERIALS

The core in this investigation was five in. in diameter and five ft long. It was quarried from an outcrop near Sand Springs, Okla., and ground to a cylindrical shape. This sandstone, which is known as the Nellie Bly, is well consolidated and has an average porosity of about 27.4 per cent. The average specific permeability to water of this core was 612 md.

Piezometer rings made of brass cups and tubing were placed on the core at intervals. End plates, thermocouples, and an additional conductivity ring were attached and the assembly sealed with a viscous rubber compound which set up into a hard impervious coating. This core assembly was mounted in a heavy steel housing. Outlets from the piezometer rings were electrically insulated through the housing so that piezometer rings served as conductivity electrodes as well as pressure measurement taps.

Fig. 2 is a schematic diagram of the apparatus, which consists of the core assembly, liquid-gas separators, recording flowmeters, filters, and sight gauges. Means were provided to record differential pressures across any desired interval or intervals along the core. Electrical conductivity, from which brine saturation could be obtained, could also be measured across any desired interval. The entire apparaus was designed to operate at pressures up to 1,000 psi and temperatures to 150°F.

The oil used in these experiments was a close-cut naphtha having a density of .767 gm/cc and a viscosity of 0.990 cp at 80°F. In the experiments the oil was saturated with methane at pressures varying from 388 to 517 psi, and under these conditions, the approximate viscosity range was from .75 to .85 cp.

The water was a prepared brine having approximately 33,000 ppm *NaCl*. Sodium nitrate was added to inhibit corrosion and the *pH* value was adjusted to about 7.7. The gas used was commercial grade (96 per cent) methane.

PROCEDURE

The core was initially saturated 100 per cent with brine, the reference electrical conductivity was obtained, and the brine saturation reduced to a value in the range of 26.4 to 30 per cent by flooding with oil. The oil circulated to reduce the water saturation was saturated with methane. When the water saturation had been reduced to a sufficiently low value, with the remaining pore volume being saturated with live oil, the core was further prepared for the flood tests by one of the three following methods:

1. A gas drive was conducted at constant pressure until the gas saturation was increased to a sufficiently high value that subsequent oil flooding would obtain the desired residual gas saturation. Fig. 3 is a plot of the relationship between the maximum gas saturation obtained by the gas drive versus the residual gas saturation retained in the core following oil flooding. Once the desired maximum gas saturation was obtained, gas-saturated oil was injected into the core under low pressure differentials in order to displace excess free gas. Circulation of the oil was maintained until no further gas was produced from the core. Once the residual gas saturation became stabilized, the core was ready for water flooding.[6]

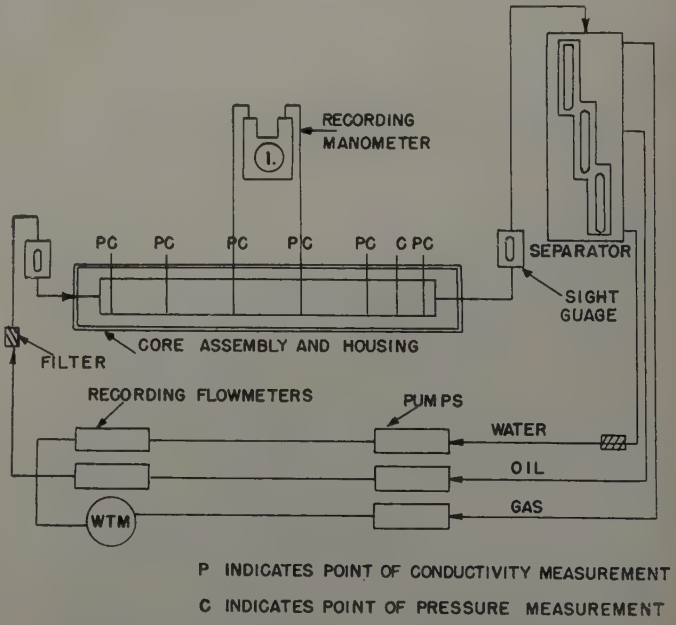
RECORDING MANOMETER
1.
PC
PC
PC
PC
PC
C PC
SEPARATOR
SIGHT GUAGE
CORE ASSEMBLY AND HOUSING
FILTER
RECORDING FLOWMETERS
PUMPS
WATER
OIL
GAS
WTM
P INDICATES POINT OF CONDUCTIVITY MEASUREMENT
C INDICATES POINT OF PRESSURE MEASUREMENT

FIG. 2 — SCHEMATIC SKETCH OF EXPERIMENTAL EQUIPMENT.

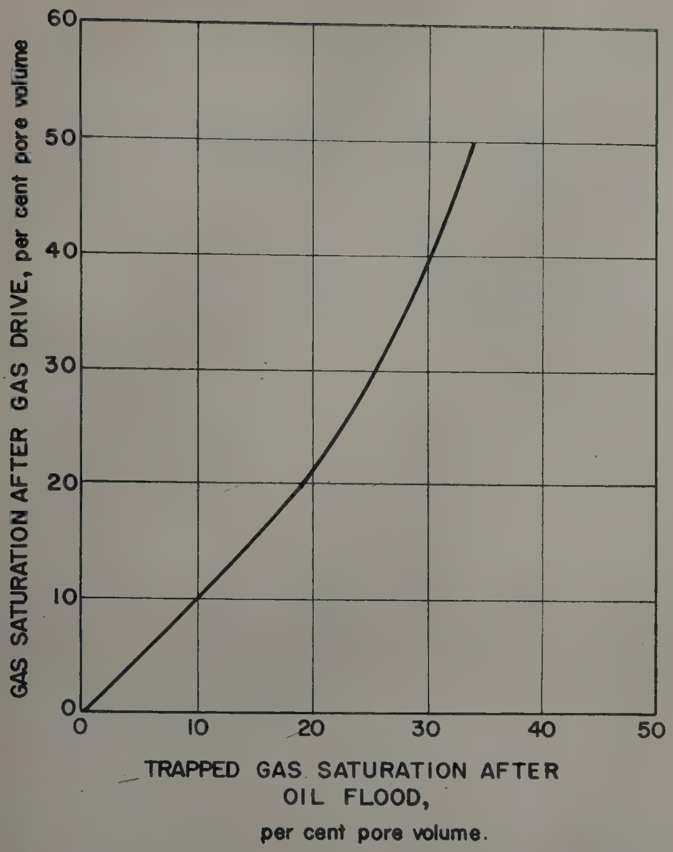

FIG. 3 — RELATIONSHIP BETWEEN MAXIMUM GAS SATURATION OBTAINED BY GAS DRIVE AND TRAPPED GAS SATURATION AFTER OIL FLOOD.

2. A procedure identical with (1) above was used to establish a certain gas saturation which was followed by pressure reduction in the system to allow expansion of the trapped gas saturation. The amount of pressure reduction was small enough that no free gas was produced due to expansion of the trapped gas. Oil was circulated at the lower pressure to remove any super-saturated liquid and to insure that the gas saturation had not been increased to the point where it would be produced upon water flooding.
3. Previous to one flood the system was subjected to an internal gas drive down to a pressure of 300 psia from an original saturation pressure of 500 psia.

The fluids were contained in a closed system after the establishment of 100 per cent liquid saturation so that any variation in either oil or water content was reflected in a change in level in the production separator. This separator was calibrated so that production could be measured to an accuracy of 0.1 per cent of the pore volume. The average gas saturation prior to water flooding was determined by means of a material balance in the liquid system. Once the core had been prepared as outlined above, the water flood was conducted by injection of water at rates low enough that the maximum pressure gradient in the flow system was less than 2.7 psi/ft. Flooding was continued until the water-oil ratio was above 100.

It was originally planned to obtain free gas saturations below the equilibrium value, which was expected to be of the order of magnitude of seven to eight per cent, by a slight reduction of pressure on the system saturated with water and gas-saturated oil. It was believed, on the basis of experimental work reported by other investigators, that such a process would result in the most uniform possible distribution of free gas. However, initial attempts to obtain gas saturation by this means resulted in failure. Equilibrium vaporization data indicated that only slight pressure reductions would be necessary to form gas saturation of less than ten per cent. Such pressure reductions on the system resulted in almost no oil production and hence no free gas formation. It was found that the pressure could be reduced in excess of 50 lb below the equilibrium bubble point prior to any significant production. Reduction of the pressure to the point where oil production started resulted in gas saturations which were not reproducible from one run to the next. Supersaturation of the oil below the bubble point pressure, as indicated here, is not a peculiar characteristic of this rock-fluid system. It has been observed in every system where investigation of the phenomenon has been made, and is presently a subject of investigation in this laboratory. The technique was then revised to obtain a stable free gas saturation by means of gas drive followed by oil flooding at constant pressure, as described above.

After the water flood, the final gas saturation was determined as a check on original material balance calculations. This was done by circulating dead oil, furnished from a container external to the regular flow system through the core and into the separator. The difference between the amount of liquid produced into the separator and the amount of dead oil injected into the system, at the time when the core reached 100 per cent liquid saturation, represented the amount of gas in the system at the start of the dead oil flood, since the dead oil absorbed and replaced the free gas in the pore space. At the finish of a flood, the dead oil was flushed from the core by gas-saturated oil, and the water saturation reduced by further oil circulation, making the core ready for another experimental cycle.

RESULTS

Tables I and II summarize the pertinent data on saturation conditions prior to water flooding, at water breakthrough, water-oil ratio of approximately 100, and final conditions. Portion of this data are shown graphically in Fig. 4.

The flood in Run 1 shown in Table I was conducted with the core initially 100 per cent saturated with water and live oil to establish a standard of comparison for the later tests in which free gas was to be present prior to flooding. The data from this run check very closely with the performance of a number of other floods in which the oil was not saturated with gas.

Table I

Summary of Data for Floods in Which Static Gas Saturation Was Obtained by Oil Flood Only

Run Number	1	2	3	4	5	6
Original Water Sat., % Pore Vol	30.0	28.3	28.4	27.7	27.2	27.0
Original Oil Sat., % Pore Vol	70.0	63.0	62.7	70.0	47.5	56.0
Original Gas Sat., % Pore Vol	0	8.7	8.9	2.3	25.3	17.0
Average Outlet Pressure, psia	517	465	465	388	505	490
Oil Prod. to Breakthrough, % Pore Vol	33.0	31.2	33.0	36.8	26.0	30.2
Total Oil Produced, % Pore Vol	36.0	33.1	36.0	37.9	30.7	32.7
Water Sat. at Breakthrough, % Pore Vol.	63.0	59.5	61.4	64.5	53.2	57.2
Residual Oil Sat. (at 100-1 water-oil ratio) % Pore Vol	34.0	29.9	26.7	32.1	18.8	23.5
Water Saturation, % Pore Vol. (at 100-1 water-oil ratio)	66.0	62.1	64.1	66.4	56.7	59.1
Final Water Saturation, % Pore Vol	66.0	62.1	64.1	66.4	58.7	60.1
Final Gas Sat., % Pore Vol. (by difference)	0	8.0	9.2	1.5	24.5	16.6
Final Gas Sat., % Pore Vol. (by dead oil replacement)	..	..	9.2	2.1	24.6	17.2
Reduction in Resid. Oil from Run 1 % Pore Volume	...	4.1	7.3	1.9	17.2	10.7
Average Flow Rate, cc/min	1.62	1.40	1.47	1.25	1.50	1.52
Total Water Throughput, Pore Vols	.613	.592	.626	.669	4.381	1.240

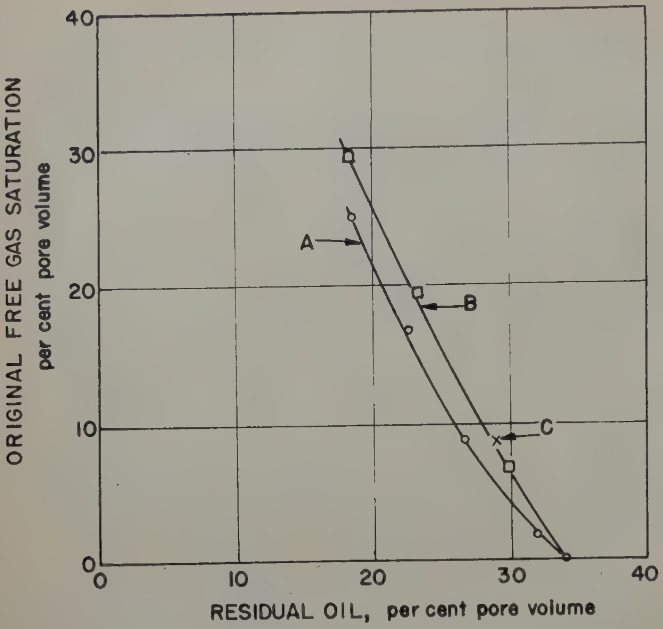

FIG. 4 — RELATION BETWEEN FREE GAS SATURATION AND RESIDUAL OIL SATURATION AT 100:1 WATER-OIL RATIO. CURVE A — GAS TRAPPED BY OIL FLOOD ONLY; CURVE B—GAS TRAPPED BY OIL FLOOD AND EXPANDED BY PRESSURE REDUCTION; POINT C — GAS ESTABLISHED BY INTERNAL DRIVE.

The initial gas saturation for the series of tests summarized in Table I was established by gas driving followed by oil flooding with no change in pressure. It is believed that this method yields the most uniformly distributed gas saturation possible. It will be noted from these tests that at low gas saturations, the reduction in oil saturation below that of the reference run is only slightly less than the free gas saturation. Each succeeding increment of initial free gas saturation results in a smaller decrease in oil saturation, at reasonable water-oil ratios, until, at the highest gas saturation used (25.3 per cent), the total reduction was 15.2 per cent of the pore volume. This trend has been anticipated and is caused by the decreasing relative permeability to oil occasioned by increasing gas saturation.

An attempt was made, in Run 5, to check the postulation that the total saturation of the non-wetting phase or phases (oil or oil plus gas) ultimately attainable at infinite water-oil ratios should be independent of the amount of free gas. This water flood was conducted for a period of ten days with a resultant oil production increase of two per cent above that at a water-oil ratio of 100. The rate of oil production was so low that several weeks of additional flooding time would have been necessary to reach the same water saturation as that obtained on the reference flood. Because of the excessively long time involved, the flood was discontinued without establishing the relationship between gas saturation and residual non-wetting phase saturation at zero permeability to oil. This point has little significance from the standpoint of application to field flooding, but should be established to clarify present concepts on the microscopic aspect of fluid displacement.

It was recognized that the relationship between residual oil and original gas saturation was not unique but would depend on the distribution of the saturation.[6] For example, the effect on oil recovery of an average gas saturation of 20 per cent resulting from 33 per cent saturation in only 60 per cent of the pore openings would be expected to differ from that of the same average gas saturation distributed uniformly in every pore. It is tentatively believed that the extremes possible in gas saturation distribution are those obtained by

(1) flooding at constant pressure from an initial maximum gas saturation, or

(2) displacement of liquid by increasing gas saturation.

Accordingly, the initial gas saturations for the runs summarized in Table II were established by trapping a certain amount of residual gas by oil flooding and expanding that gas by pressure reduction.

The data from this series of tests, shown as Curve *B* in Fig. 4, clearly demonstrate that a given gas saturation established by the gas expansion technique resulted in somewhat less increased oil recovery than the same saturation established by the flooding at constant pressure technique. However, by either method, the residual oil saturation could be very substantially reduced from the case in which no free gas was present.

In one test, Run 10, the initial gas saturation was established by internal gas drive (Point *C*, Fig. 4).

INTERPRETATION OF RESULTS

If the effect of static free gas saturation during water flooding is merely replacement of residual oil combined with reduction of oil permeability, it should be possible to calculate these effects by means of the frontal drive method of Buckley and Leverett.[7] The only complication is that the necessary water-oil relative permeability relationship must be measured with the proper static gas saturation. In order to determine the applicability of such a procedure, relative permeabilities were measured at 25 per cent gas saturation in the system upon which the above discussed floods were conducted. The preliminary treatment of the core to establish the gas saturation was the same as that used for the first series of tests — gas drive followed by oil flood at constant pressure. After the gas saturation was established, oil and water were injected simultaneously into the core at fixed ratios until saturation equilibrium was established at each flowing ratio. Equilibrium was determined by stabilization of electrical conductivity and pressure differentials. The saturations and pressure drops for the relative permeability calculations were measured in the center foot of the five-ft core to eliminate disturbing end effects. Flow rates were low enough so that the over-all pressure differentials were less than ten psi. The relative permeability data at 25 per cent gas saturation are shown in Fig. 5 together with the relative permeability characteristics on the

Table II

Summary of Data for Floods in Which Static Gas Saturation Was Obtained by Oil Flood Followed by Pressure Reduction or by Internal Gas Drive

Run Number	7	8	9	10
Original Water Saturation, % Pore Vol	26.8	29.0	27.2	26.4
Original Oil Saturation, % Pore Vol	43.5	51.3	65.8	64.9
Original Gas Saturation, % Pore Vol. (Before Expansion)	26.1	14.4	5.3	0.
Original Gas Saturation, % Pore Vol. (After Expansion)	29.7	19.7	7.0	8.7
Final Water Saturation, % Pore Volume	54.5	60.2	63.0	64.1
Final Oil Saturation, % Pore Volume	16.7	22.4	29.8	28.8
Residual Oil, % Pore Volume (at 100 to 1 water-oil ratio)	18.2	23.1	29.8	29.0
Residual Oil, % Pore Volume* (at 100 to 1 water-oil ratio) (Before Expansion)	18.0	23.3	29.0	34.0
Final Gas Saturation, % Pore Volume (by dead oil replacement)	29.2	17.7	7.4	8.9

*This is the residual oil that previous data indicate would have been attained had the system been flooded under conditions before gas expansion.

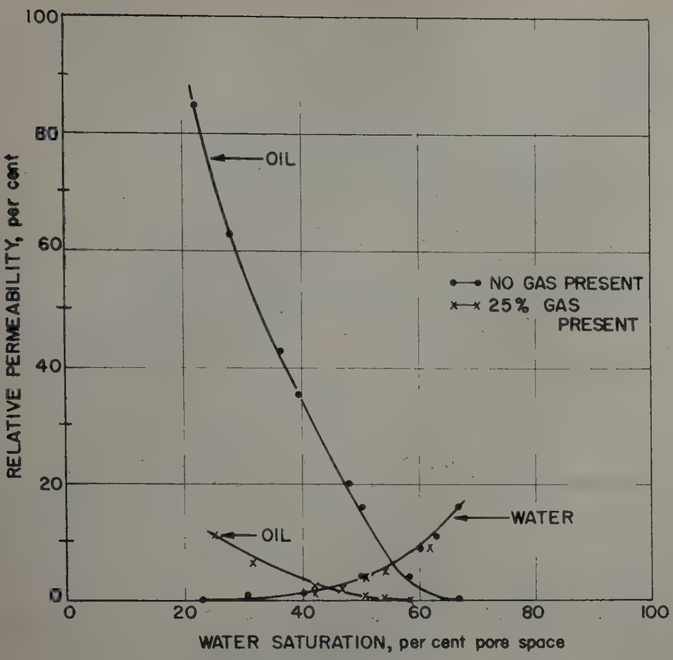

FIG. 5 — RELATIVE PERMEABILITY TO OIL AND WATER FOR TWO SYSTEMS IN NELLIE BLY SANDSTONE.

same system containing only oil and water. At any particular water saturation, oil relative permeability is drastically reduced when free gas is present, but water permeability is identical for the two conditions. A very important factor is that permeability to oil persists to much lower oil saturations with free gas present.

Fig. 6 is a plot of the construction necessary to compute the average water saturation at water breakthrough by the Buckley and Leverett frontal drive method with simplifications added by Pirson.[8] The calculations in this figure are for the reference run when no gas saturation was in the system. The computed average water saturation at water breakthrough is 65 per cent compared to the experimental value of 63.0 per cent. This difference can be attributed largely to dispersion of the flood front caused by capillary forces neglected in the simplified calculation. Fig. 7 shows the results of the same type computation for the system containing 25 per cent free gas saturation. The calculated average water saturation at breakthrough is 54.5 per cent; the experimentally obtained value, 53.2 per cent.

If the replacement of residual oil by gas had been in a 1:1 ratio, the reduction in residual oil would be equal to the gas saturation, or 25 per cent. Since a 1:1 ratio is not achieved, the reduction in residual oil at water breakthrough should equal the gas saturation less the difference in water saturations at breakthrough. From the computation of Figs. 5 and 6, this would be .25 − (.65 − .545) = .145 or 14.5 per cent. The difference obtained experimentally was 15.5 per cent. The close check between the experimental results and those calculated from appropriate relative permeability data leads to the conclusions that:

(1) The effects of free gas in water flooding are the alteration of oil relative permeability characteristics and the occupation of space which would otherwise be filled with residual oil.

(2) The reduction in residual oil which can be expected by the maintenance of free gas saturation during water flooding in a particular reservoir rock can be calculated from appropriate water-oil relative permeability characteristics.

The degree of improvement in oil recovery by water flooding which can be accomplished by maintenance of free gas saturation during the flood can be expected to vary widely between different reservoir materials. It would be gross speculation to attempt estimation of the benefits to be derived from a particular reservoir without measurements on cores from that reservoir.

PRACTICAL APPLICATION

It is obvious from the foregoing that maintenance of a maximum free gas saturation during water flooding can very substantially reduce residual oil saturation and hence increase oil recovery, providing it is feasible for application to a particular reservoir. Improved recovery of the magnitude indicated by the experimental work reported herein, could result in doubling the water flooding recovery from some semi-depleted fields. Of comparable importance in the water flooding of depleted reservoirs are the smaller volume of water required for fill-up, the earlier start of water flood production, and a more uniform oil producing rate.

One readily apparent means of accomplishing the maintenance of such a gas saturation is by gas injection to build up the reservoir pressure to such a level that the pressure differential across the oil bank will be a small fraction of the absolute pressure and thereby reduce compression of the gas present. A means of eliminating a large part of the loss of free gas due to solution in the oil is the injection of a gas of low solubility, such as nitrogen.

A very significant feature in the application of free gas saturation maintenance during water flooding is the reduction

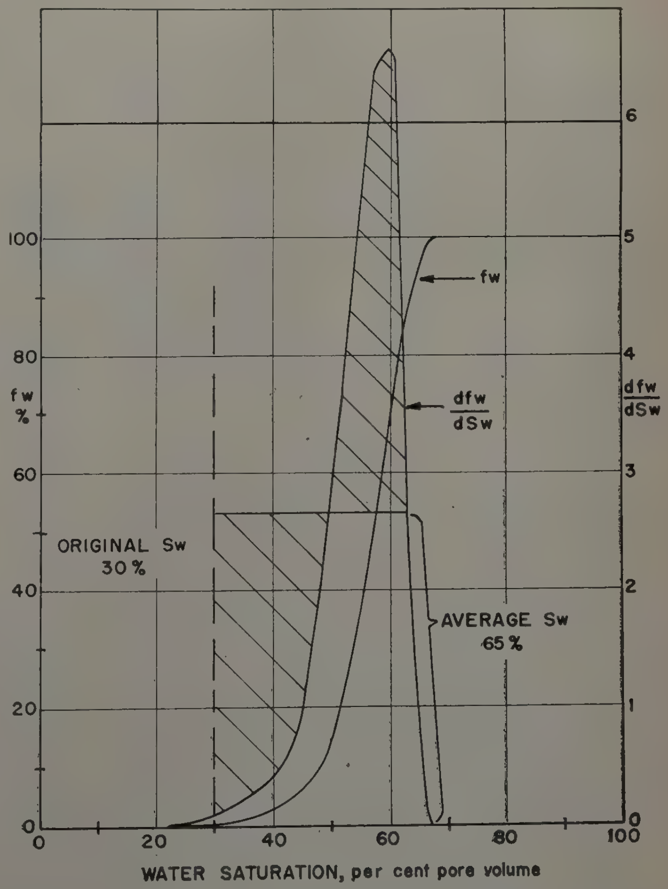

FIG. 6 — COMPUTATION BY FRONTAL DRIVE METHOD OF BREAKTHROUGH WATER SATURATION WITH NO GAS PRESENT.

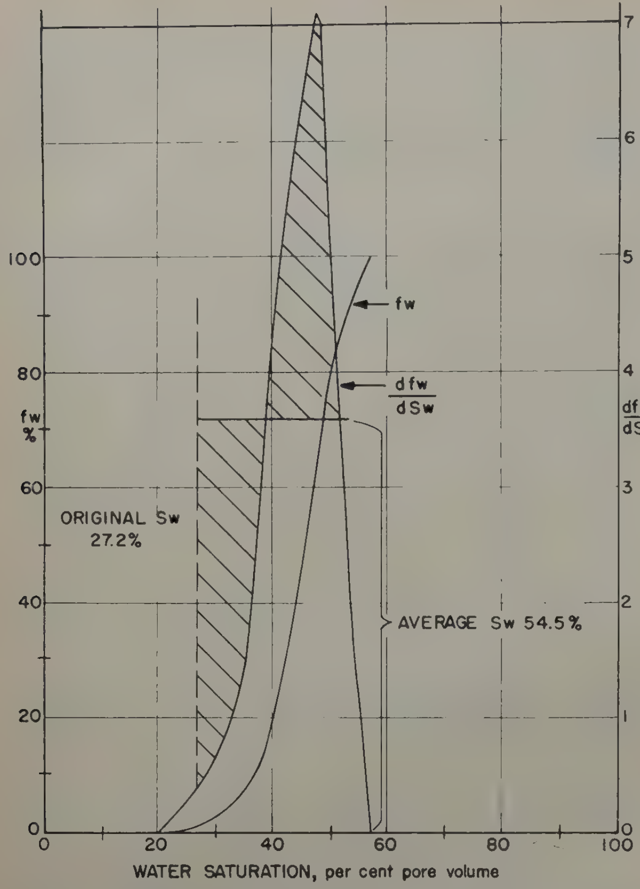

FIG. 7 — COMPUTATION BY FRONTAL DRIVE METHOD OF BREAKTHROUGH WATER SATURATION WITH 25 PER CENT GAS SATURATION PRESENT.

in capacity of producing wells. High gas saturation in the reservoir can reduce oil permeability to the order of magnitude of 1/10 the specific permeability as indicated by the relative permeability curves of Fig. 5. This permeability reduction will cause a reduction of the same magnitude in the productivity indices of the wells. Whether operations can be conducted at such reduced producing capacities may be of controlling importance in determining application to some fields.

Whether it will be economically feasible to reduce pressure in primary water drive fields to cause internal evolution of free gas ahead of the water flood front will be determined by a number of factors, such as

(1) The shrinkage of oil, resulting from pressure reduction necessary to obtain the gas saturation, compared to the expected decrease in ultimate oil saturation.

(2) Marked decreases in productivity indices of producing wells and hence an increased tendency for water coning.

(3) Variation in oil properties with structure. Some high relief reservoirs have much lower bubble point oil at the water-oil contact than further up structure. Under such conditions it would be almost impossible to obtain free gas at the water-oil contact without depletion by internal gas drive of the upstructure part of the field.

ACKNOWLEDGMENT

The writers thank the management of Stanolind Oil and Gas Co. for permission to publish this paper, and acknowledge the assistance of Herman Teel, who aided in the collection of experimental data.

REFERENCES

1. Schiffman, Louis, and Breston, J. N.: "The Effect of Gas on Recovery When Water Flooding Long Cores," *Producers Monthly* (January, 1950), **14,** No. 3.
2. Pfister, R. J.: "More Oil from Spent Water Drives by Intermittent Air or Gas Injection," *Producers Monthly* (September, 1947), **11,** No. 11.
3. Holmgren, C. R.: *Trans.* AIME (1949), **179,** 103.
4. Krutter, Harry, and Day, Robert J.: *J. of Pet. Tech.*, (Nov., 1943).
5. Dykstra, Herman, and Parsons, R. L.: "The Prediction of Oil Recovery by Water Flood." Paper presented at Spring Meeting of API, May, 1948.
6. Geffen, T. M., Owens, W. W., Parrish, D. R., and Morse, R. A.: *Trans.* AIME, (1951), **192,** 99, J. of Pet. Tech., (April, 1951).
7. Buckley, S. E., and Leverett, M. C.: *Trans.* AIME, (1942), **146,** 107.
8. Pirson, S. J.: *The Elements of Oil Reservoir Engineering*, McGraw-Hill Book Co., N. Y. C., (1950).

★ ★ ★

T.P. 3058

VAPORIZATION CHARACTERISTICS OF CARBON DIOXIDE IN A NATURAL GAS-CRUDE OIL SYSTEM

FRED H. POETTMANN, JUNIOR MEMBER AIME, PHILLIPS PETROLEUM CO., BARTLESVILLE, OKLA.

ABSTRACT

The vaporization characteristics of carbon dioxide in a League City natural gas - Billings crude oil system were studied at three temperatures, 38°, 120°, and 202°F and for pressures ranging from 600 to 8,500 psi. Variation of carbon dioxide concentration up to 12 mole per cent in the composite showed no effect on the equilibrium vaporization ratios (*K* values) of the hydrocarbon constituents or on the *K* value of carbon dioxide itself. It was shown that carbon dioxide is more soluble in crudes than in distillates which is contrary to the behavior of methane.

A working chart of carbon dioxide *K* values is presented.

INTRODUCTION

The study of the equilibrium vaporization ratios of mixtures of paraffin hydrocarbons has been rather thorough.[2,6,7,8,9] In the past few years considerable attention has been paid to the vaporization characteristics of the so-called noncondensable gases such as nitrogen, carbon dioxide, and hydrogen sulfide in mixtures of hydrocarbons, since they usually occur to some extent in most crude oils and natural gases.[1,3,4,5] Knowledge of this behavior is useful to both the production and refining phases of the petroleum industry.

This paper reports the equilibrium vaporization ratios (*K*'s) of carbon dioxide in a mixture of League City natural gas and Billings crude oil, and compares them to those obtained in a natural gas-distillate system.[5] The equilibrium vaporization ratios for the hydrocarbon components in this system had previously been studied by Roland.[7] In addition to the determination of the *K* values for carbon dioxide, the *K* values for methane and ethane were also determined in order to observe what effect, if any, the presence of carbon dioxide had on these *K* values. The concentration of carbon dioxide was also varied in order to observe the effect of this variable on the carbon dioxide *K* values.

EXPERIMENTAL PROCEDURE

The apparatus used in this study consisted of a stainless steel equilibrium cell of about 2 liters capacity. The cell was mounted on trunions permitting rocking in a thermostatically controlled oil bath. Two high pressure valves fitted with steel tubing were mounted on the top of the cell, one was used for sampling the equilibrium gas phase and the other for sampling the equilibrium liquid phase by means of an induction tube within the cell. Stainless steel tubing from the bottom of the cell led to a mercury reservoir and manifold which was connected to a free-piston type pressure gauge manufactured by the American Instrument Co. and to a volumetric pump. The temperature of the oil bath was measured by means of a calibrated mercury-in-glass thermometer. The recorded temperatures are believed to be accurate to ±0.5°F. The pressures are correct to ±2 psi.

The crude oil used in this study was stock tank oil obtained from the Wilcox formation in the Billings Field, Noble County, Okla. The natural gas was obtained from the League City Field, Galveston County, Tex. The oil was treated with anhydrous calcium sulfate in order to remove the last traces of water. To insure a supply of constant composition gas at room temperature the cylinders of League City gas were cooled to about 30°F, inverted, and the condensed liquid was allowed to drain from the cylinders. The analysis of the gas and crude are tabulated in Table I. The carbon dioxide came from Pure Carbonic, Inc., and was stated to have a purity of 99.5 per cent or better.

The procedure used to obtain samples of the equilibrium liquid and vapor was similar to that employed by others making use of the rocking type equilibrium cell.[6,7,8]

The equilibrium cell was evacuated and calculated quantities of carbon dioxide, natural gas, and crude oil were charged to the cell to the desired pressure. In charging the equilibrium cell an attempt was made to maintain the ratio of the natural gas to crude oil as close as possible to that employed by Roland.[7] After the cell was charged, samples of

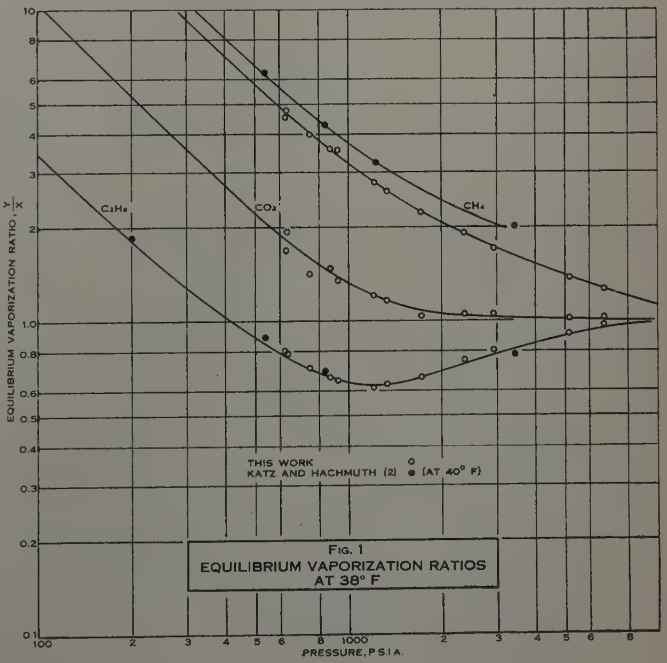

Fig. 1
EQUILIBRIUM VAPORIZATION RATIOS
AT 38° F

---

[1] References given at end of paper.

Manuscript received in the office of the Petroleum Branch Aug. 9, 1950.

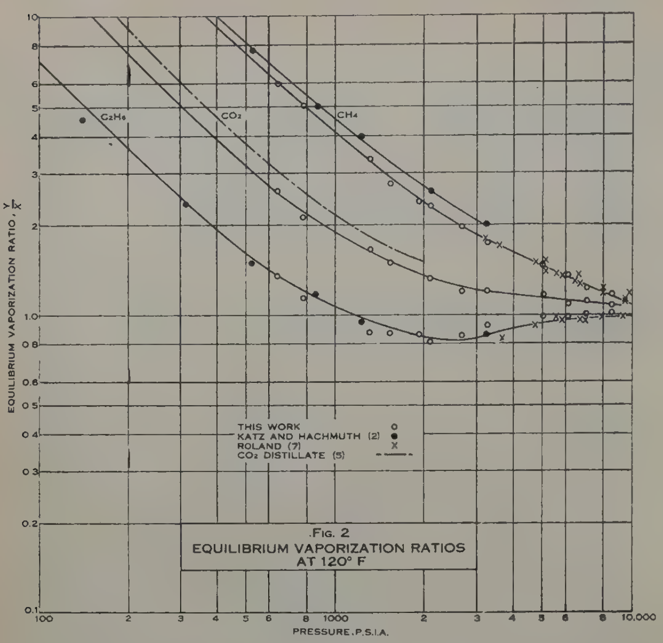

Fig. 2
EQUILIBRIUM VAPORIZATION RATIOS AT 120° F

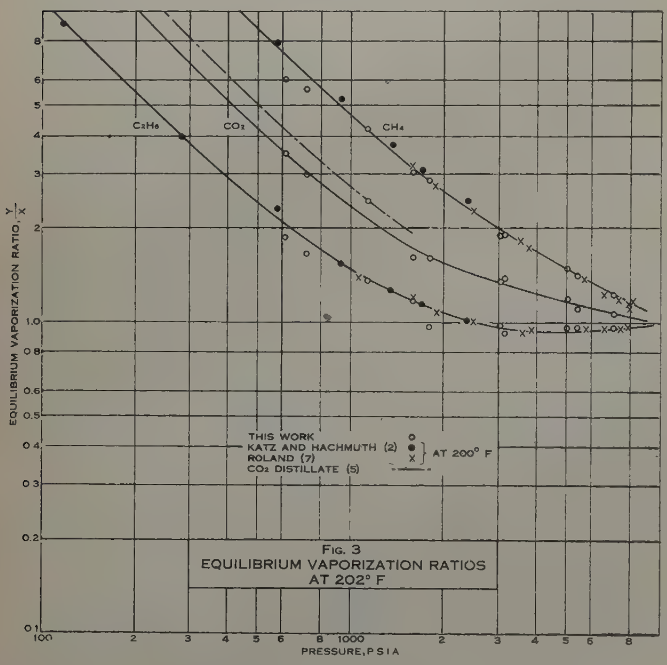

Fig. 3
EQUILIBRIUM VAPORIZATION RATIOS AT 202° F

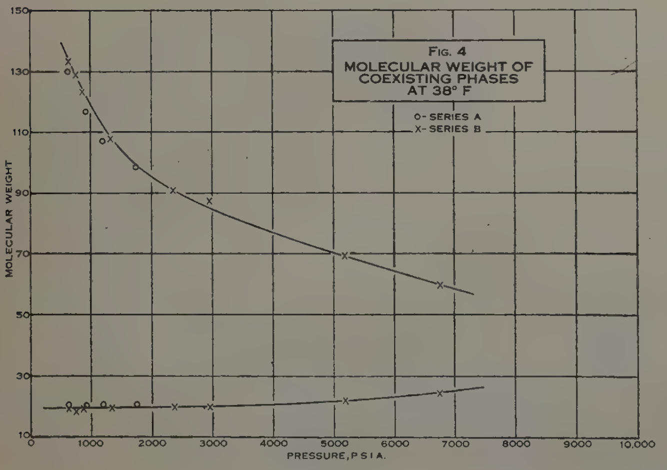

Fig. 4
MOLECULAR WEIGHT OF COEXISTING PHASES AT 38° F

equilibrium liquid and vapor were removed until one of the phases was depleted. By sampling the proper quantities of vapor and liquid the over-all composition of the fluid in the cell was maintained relatively constant.

After the pressure in the cell was adjusted to the desired value by adding or removing mercury in the cell, the cell was rocked to insure equilibrium between the phases. The samples of vapor and liquid were then obtained by constant pressure displacement with mercury. The phase being sampled was flashed into a trap and the gas leaving the trap was caught in previously evacuated glass bulbs of known capacity. In using this procedure it was assumed that all of the methane, carbon dioxide, and ethane went into the gas phase and none remained behind in the liquid phase remaining in the trap. The trap liquid was weighed and its molecular weight and gravity determined. The total moles of gas trapped in the glass bulb were calculated. The carbon dioxide content of the gas was determined by means of the infrared spectrometer and the methane and ethane content was determined by means of the mass spectrometer.

Two series of samples were taken, series *A* composite charge contained about 11.50 mole per cent carbon dioxide and series *B* about 6.25 per cent carbon dioxide.

EXPERIMENTAL RESULTS

Table II shows a summary of the experimental results obtained in this investigation. A total of 34 pairs of equilibrium vapor and liquid samples were taken. The *K* values were investigated at three temperatures, 38°, 120°, and 202°F. Pressures ranged from 600 to 8,500 psi.

The composite analyses shown on Table II were determined by means of a material balance and the analyses of the phases sampled.

The *K* values obtained are plotted in Figs. 1, 2, and 3, as the logarithm of *K* versus the logarithm of pressure for each temperature investigated.

In making the composite calculations, the molecular weights of the coexisting equilibrium vapor and liquid phases were also determined and are shown plotted on Figs. 4, 5, and 6 for the three temperatures investigated.

Table III summarizes the data on the molecular weights and specific gravities of the trap liquids. These data are plotted in Fig. 7.

DISCUSSION OF RESULTS

In addition to the data obtained in this study, the data of Roland[7] and Katz and Hackmuth[2] are also plotted on Figs. 1, 2, and 3. The data of Roland[7] for the Billings crude oil-League City gas system for methane and ethane agree very well with those determined in this study indicating that the

Table I — Analysis of Oil and Gas

	Billings Crude	League City Gas
Carbon Dioxide	....	1.20
Methane	....	90.89
Ethane	1.41	4.40
Propane	1.44	1.91
Butanes	2.19	0.93
Pentanes	3.68	0.34
Hexanes	5.48	0.15
Heptanes Plus	85.80	0.18
Sp Gr	0.8353 60/60 F	
Mole Wt	205	

Table II — Summary of Experimental Results

	Equilibrium		Composite				Vapor Phase				Liquid Phase				Equilibrium Ratio		
Charge No.	Pressure PSIA	Temp °F	CO_2	CH_4	C_2H_6	C_3^+	CO_2	CH_4	C_2H_6	Mol Wt	CO_2	CH_4	C_2H_6	Mol Wt	CO_2	CH_4	C_2H_6
			Mole Per Cent				Mole Per Cent				Mole Per Cent						
A	1742	38.0	11.00	72.39	3.68	12.93	10.00	81.20	3.20	20.63	9.53	36.12	4.79	98.37	1.049	2.248	0.668
A	1204	37.0	11.22	72.63	3.67	12.48	11.30	80.70	3.10	20.61	9.36	28.82	5.05	107.00	1.207	2.800	0.614
A	920	38.5	11.49	74.55	3.74	10.22	11.50	85.10	3.40	20.60	8.48	23.86	5.22	117.06	1.356	3.566	0.651
A	636	38.0	11.75	75.96	3.77	8.52	13.00	82.80	3.70	20.62	6.66	17.38	4.70	130.15	1.952	4.764	0.787
B	6762	36.0	6.04	79.71	3.89	10.36	6.04	83.65	4.09	24.60	5.85	66.49	4.23	60.43	1.031	1.258	0.966
B	5192	39.0	6.05	79.93	3.88	10.14	6.01	85.54	4.04	22.67	5.89	61.99	4.43	69.44	1.020	1.379	0.911
B	2959	38.0	6.08	80.61	3.84	9.47	5.80	88.00	3.90	19.92	5.48	51.06	4.83	87.20	1.058	1.723	0.807
B	2371	38.0	6.09	80.71	3.85	9.35	6.10	90.30	3.60	19.74	5.76	47.01	4.77	90.83	1.059	1.921	0.754
B	1336	38.0	6.12	80.30	3.80	9.78	6.30	90.00	3.60	19.33	5.39	34.40	5.65	109.00	1.169	2.616	0.637
B	872	39.0	6.17	80.47	3.70	9.66	6.40	88.80	3.40	19.48	4.33	24.72	5.11	123.55	1.478	3.592	0.665
B	749	38.0	6.17	80.11	3.73	9.99	6.00	89.40	3.50	18.65	4.26	22.09	4.91	128.84	1.408	4.047	0.713
B	631	38.0	6.27	80.54	3.73	9.46	6.40	88.10	3.70	19.20	3.76	19.46	4.63	133.27	1.702	4.527	0.799
A	8554	120.0	11.12	72.86	3.66	12.36	11.82	75.95	3.27	33.62	10.96	64.86	3.16	58.94	1.078	1.171	1.034
A	7052	120.0	11.12	72.95	3.67	12.26	11.82	78.08	3.68	28.07	10.63	63.51	3.65	64.27	1.112	1.229	1.008
A	5064	120.0	11.11	72.95	3.67	12.27	12.49	79.49	3.83	24.44	10.71	54.30	3.87	73.44	1.166	1.464	0.990
A	3241	120.0	11.11	73.28	3.68	11.93	11.65	81.47	3.58	22.35	9.65	46.39	3.86	87.36	1.208	1.756	0.927
A	2112	120.0	10.99	72.61	3.67	12.73	11.39	81.44	3.50	21.34	8.62	35.01	4.31	104.55	1.322	2.326	0.812
A	1319	120.0	11.37	73.32	3.75	11.56	12.00	83.20	3.70	20.74	7.35	24.98	4.22	107.52	1.633	3.330	0.877
A	786	120.0	11.64	75.32	3.74	9.30	12.20	82.80	3.70	21.73	5.70	16.31	3.22	141.56	2.140	5.077	1.149
B	6130	120.0	6.05	80.20	3.87	9.88	5.87	84.74	4.11	24.00	5.40	62.69	4.18	71.94	1.087	1.351	0.983
B	2691	120.0	6.09	80.86	3.84	9.21	6.20	90.00	3.80	20.17	5.21	45.31	4.44	97.96	1.190	1.986	0.856
B	1937	120.0	6.08	80.29	3.82	9.81	....	88.60	3.80	19.79	....	36.83	4.41	110.40	.....	2.406	0.862
B	1541	120.0	6.13	80.96	3.76	9.15	6.50	88.10	3.80	19.74	4.36	31.93	4.36	120.33	1.491	2.759	0.872
B	642	120.0	6.36	81.99	3.69	7.96	6.60	89.40	3.80	19.70	2.53	15.04	2.81	156.98	2.609	5.944	1.352
A	7155	202.0	11.09	72.98	3.68	12.25	11.62	78.66	3.71	30.25	10.86	63.71	3.86	63.52	1.070	1.235	0.961
A	5047	201.5	11.06	72.82	3.68	12.44	11.64	81.48	3.72	24.91	9.73	54.77	3.86	77.21	1.197	1.488	0.964
A	3160	202.0	11.06	72.65	3.68	12.61	12.54	82.08	3.68	22.34	9.04	42.54	3.99	100.10	1.386	1.929	0.922
A	1820	202.5	11.27	72.28	3.77	12.68	12.10	82.60	3.90	21.80	7.50	28.81	3.77	108.87	1.613	2.868	0.967
A	1138	202.5	11.59	74.69	3.74	9.98	12.60	82.10	3.90	21.66	5.12	19.39	2.87	144.95	2.460	4.234	1.359
A	722	203.0	11.85	78.07	3.73	6.35	12.30	81.10	3.80	22.02	4.11	14.42	2.26	163.29	2.990	5.620	1.680
B	5439	202.0	6.08	80.61	3.84	9.47	6.09	84.68	3.73	23.65	5.49	59.60	3.86	79.12	1.109	1.421	0.966
B	3056	202.0	6.10	80.88	3.83	9.19	6.40	87.90	3.90	20.60	4.73	46.13	3.96	104.15	1.353	1.905	0.985
B	1607	202.0	6.10	80.70	3.74	9.46	6.00	88.20	4.00	20.33	3.67	29.21	3.38	133.97	1.635	3.020	1.183
B	616	202.0	6.56	84.89	3.73	4.82	7.00	86.80	3.80	20.31	2.00	14.60	2.02	166.84	3.500	6.034	1.881

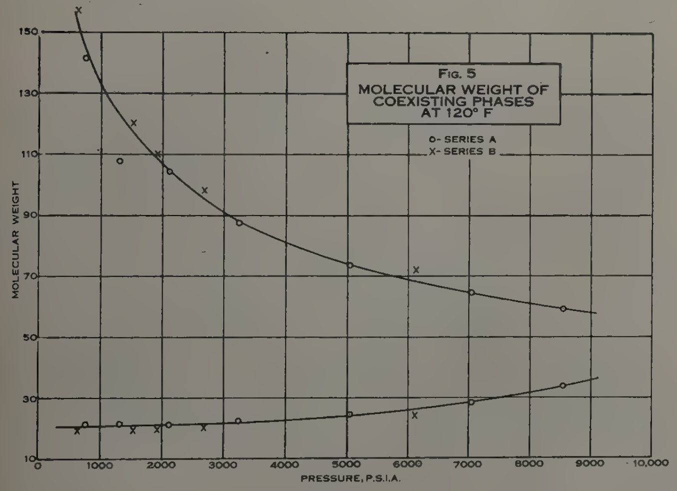
FIG. 5 MOLECULAR WEIGHT OF COEXISTING PHASES AT 120° F

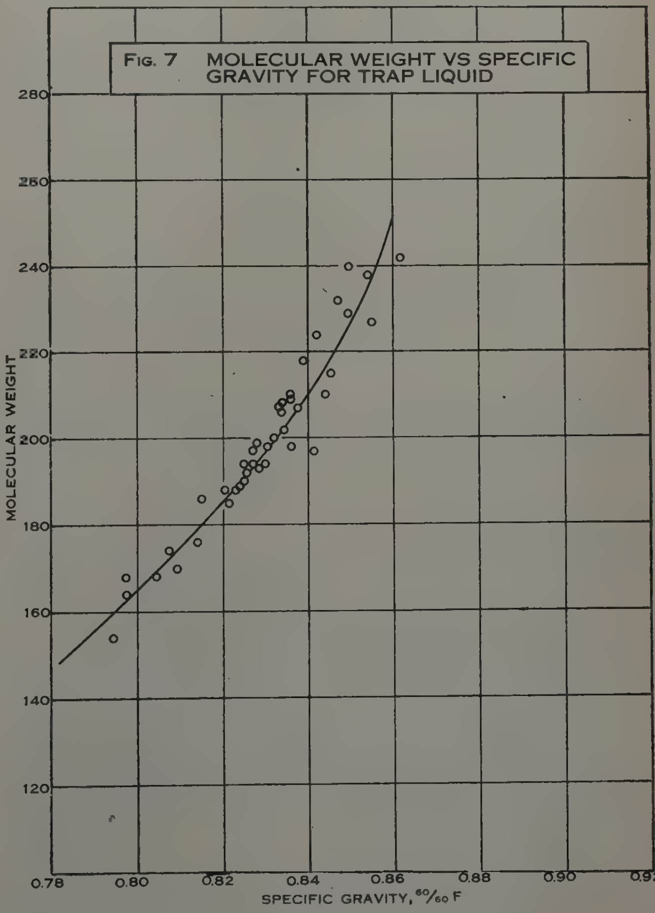
FIG. 7 MOLECULAR WEIGHT VS SPECIFIC GRAVITY FOR TRAP LIQUID

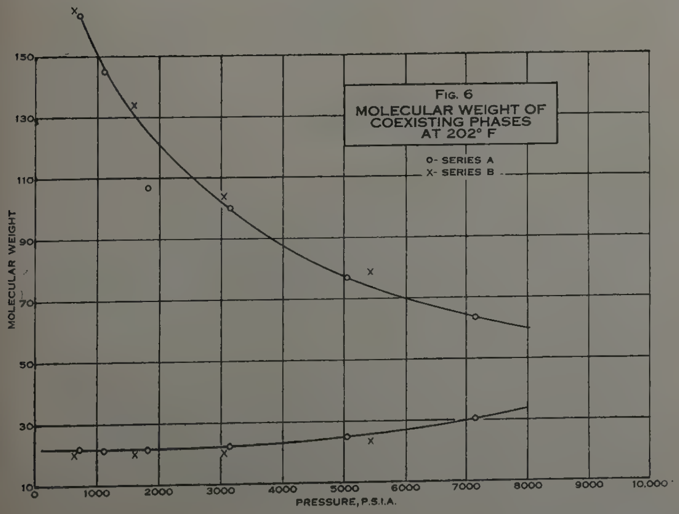
FIG. 6 MOLECULAR WEIGHT OF COEXISTING PHASES AT 202° F

presence of carbon dioxide up to 12 mole per cent in the composite composition has no effect on the *K* values of the hydrocarbon constituents. The data of Katz and Hackmuth[2] for methane and ethane are also plotted for comparison.

Two ranges of carbon dioxide concentration were studied to determine the effect of composition on the equilibrium vaporization ratio of carbon dioxide itself. Over the range of concentrations studied, 6 and 12 per cent, there appears to be no variation in the *K* values for carbon dioxide. This was also the case for carbon dioxide in a natural gas - distillate system.[5] As was anticipated from a previous study,[5] at pressures below the region of the convergence pressure of the system carbon dioxide is more soluble in a crude oil system (smaller *K* values) than in a distillate as is shown by the dot-dashed lines on Fig. 2 and 3. This is contrary to the behavior of methane which is less soluble (larger *K* values) in crudes than in distillates.

In order to obtain a working chart of carbon dioxide *K*'s, the curves on Figs. 1, 2 and 3 were cross plotted as the logarithm of *K* versus temperature for lines of constant pressure, (Fig. 8). At pressures below 600 psi, the chart is based on extrapolated data.

By calculating the mole fraction of vapor in the equilibrium cell at various pressures, Roland[7] showed that the temperatures of 120°F and 200°F were above the critical temperature of the mixture in the cell. Similar calculations made in this study agree with those of Roland. In addition, 38°F also is above the critical temperature of the mixture studied.

The curves of Figs. 4, 5 and 6 showing the molecular weight of the coexisting vapor and liquid phases at various pressures for the three temperatures studied appear to have a convergence pressure corresponding to the convergence pressure of the equilibrium vaporization ratios at their respective temperatures. The molecular weight corresponding to this convergence pressure might possibly provide a means of characterizing the mixtures in any correlation involving the convergence pressure.

SUMMARY

Equilibrium vaporization ratios have been determined for carbon dioxide in a natural gas-crude oil system for temperatures of 38°, 120° and 202°F and for pressures ranging from 600 to 8,500 psi. No significant variation was shown in the equilibrium vaporizations ratios of the hydrocarbons or the carbon dioxide itself for carbon dioxide concentrations up to 12 mole per cent in the composites. As was anticipated from a previous study, carbon dioxide is more soluble in a crude than in a distillate.

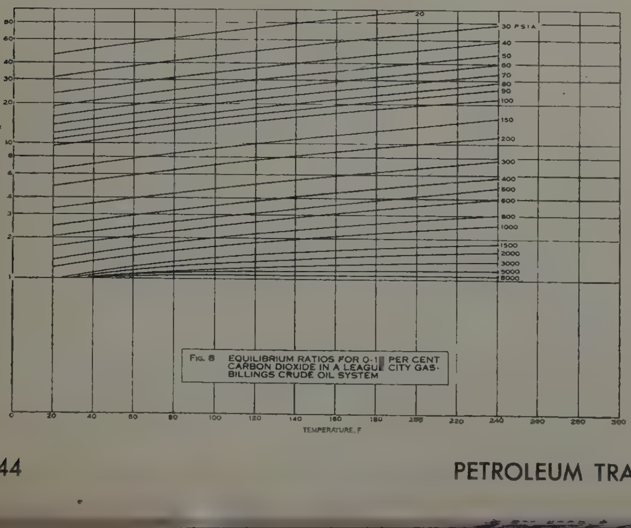

FIG. 8 EQUILIBRIUM RATIOS FOR 0-1[illegible] PER CENT CARBON DIOXIDE IN A LEAGU[illegible] CITY GAS-BILLINGS CRUDE OIL SYSTEM

Table III — Molecular Weights and Specific Gravity for Trap Liquids

Specific Gravity 60/60 F	Molecular Weight
0.8616	242
0.8267	194
0.8541	238
0.8141	176
0.8455	215
0.7976	164
0.8360	198
0.8552	227
0.8147	186
0.8440	210
0.7946	154
0.8361	209
0.8300	194
0.8271	197
0.8253	190
0.8343	206
0.8286	193
0.8228	188
0.8321	200
0.8256	192
0.8203	188
0.8361	210
0.8469	232
0.8095	170
0.8420	224
0.7976	168
0.8497	229
0.8075	174
0.8327	207
0.8496	240
0.8044	168
0.8304	198
0.8342	202
0.8392	218
0.8412	197
0.8252	194
0.8302	198
0.8342	208
0.8242	189
0.8233	189
0.8216	185
0.8282	199
0.8376	207

These ratios, along with those determined for carbon dioxide in a distillate[5] and various binary mixtures of hydrocarbons[3,4] should provide a fairly complete picture of the vaporization characteristics of carbon dioxide in hydrocarbon mixtures.

ACKNOWLEDGMENT

The author wishes to express his appreciation to the management of Phillips Petroleum Co. for permission to publish this report; to Vernon Thornton and H. W. Rollman for their aid in the analysis of the gas samples and to Andrew F. Bertuzzi and other members of the Production Research Section of the Research Department for their aid during some of the sampling operations.

REFERENCES

1. Brown, G. M., and Stutzman, L. F.: *Chem. Eng. Prog.*, (1949), **45**, 142.
2. Katz, D. L., and Hachmuth, K. H.: *Ind. Eng. Chem.*, (1937), **29**, 1072.
3. Olds, R. H., Reamer, H. H., Sage, B. H., and Lacey, N. N.: *Ind. Eng. Chem.*, (1949), **41**, 475.
4. Poettmann, F. H., and Katz, D. L.: *Ind. Eng. Chem.*, (1945). **37**, 847.
5. Poettman, F. H., and Katz, D. L.: *Ind. Eng. Chem.*, (1946), **38**, 530.
6. Roland, C. H., Smith, D. E., and Kaveler, H. H.: *Oil and Gas J.*, (1941), **39**, (46), 128.
7. Roland, C. H.: *Ind. Eng. Chem.*, (1945), **37**, 930.
8. Standing, M. B., and Katz, D. L.: *Trans.* AIME, (1944), **155**, 232.
9. Webber, C. E.: *Trans.* AIME, (1941) 141, 192.

★ ★ ★

T.P. 3056

FURTHER DEVELOPMENTS IN THE LABORATORY DETERMINATION OF RELATIVE PERMEABILITY

B. H. CAUDLE, R. L. SLOBOD, AND **E. R. BROWNSCOMBE,** MEMBERS AIME, ATLANTIC REFINING CO., DALLAS, TEX.

ABSTRACT

An earlier publication has discussed three methods for obtaining relative permeability data on small core samples and the apparatus and technique for the capillary pressure displacement method. This paper describes the apparatus and technique for the solution gas and the dynamic displacement methods and presents a routine procedure for obtaining oil-gas and water-oil relative permeability data.

Theoretical and experimental considerations are presented to show that the end effect commonly associated with the dynamic flow mechanism is extremely small where constant rates are employed in the flowing phase. An effect of flow rate on relative permeabilities obtained by the dynamic system is found only when gas is one of the flowing phases and this effect is ascribed to a form of channeling in the capillary system.

The apparatus and procedures used to obtain relative permeability data with three phases flowing are described and some preliminary results of the use of this method are shown.

INTRODUCTION

In a previous publication from this laboratory there appeared a brief discussion of the concepts behind three basic methods for obtaining relative permeability data.[1] These three methods were called the capillary pressure displacement method, the solution gas displacement method, and the dynamic displacement method — the names being suggestive of the type of process used for obtaining the desired saturation prior to making the permeability measurements. In the same publication, the apparatus and technique for the capillary pressure displacement method were described and some typical results obtained by this method were presented. This paper will present:

1. The routine procedure used to obtain complete relative permeability data on small core samples with two phases flowing;
2. The experimental techniques for the solution gas and dynamic displacement methods for obtaining relative permeability data;
3. The results of some studies on the mechanism of fluid flow through consolidated porous media; and,
4. The preliminary results on the determination of relative permeability for a system in which three phases are flowing.

TECHNIQUE AND APPARATUS FOR THE DETERMINATION OF RELATIVE PERMEABILITY WITH TWO PHASES FLOWING

In order to obtain relative permeability data on a small core sample which will describe the various phases of reservoir depletion, it is necessary that the methods used duplicate, as closely as possible, the various mechanisms involved in reservoir depletion. It is important that, in any type of relative permeability determination, the core be originally at virgin reservoir conditions with respect to the fluids within the pore spaces, (for example, oil used to displace water from core until connate water saturation established), and that the subsequent saturation changes in the core be analagous to the reservoir depletion mechanism for which the data are to be used.

PROCEDURE OF DETERMINING RELATIVE PERMEABILITY DATA WITH TWO PHASES FLOWING

A standardized procedure has been set up for obtaining relative permeability data and other information on small core samples. This procedure essentially consists of 11 steps as shown below:

1. Determination of the capillary pressure curve.[2] This information is used to help select samples for relative permeability determinations and to characterize, in general, the pore size distribution of the sample.
2. Determination of the specific permeabilities to air, oil. and water. These values are those on which the relative permeability calculations are based.
3. Reduction of the core to connate water by an oil drive using the high speed centrifuge.
4. Determination of the critical gas saturation value and the associated relative permeability to oil by the solution gas drive method.
5. Determination of the relative permeabilities to oil and gas in the region where both phases are flowing by the capillary pressure method.
6. Reduction of the sample to residual oil in the centrifuge by an air drive, and the determination of the relative permeability to gas at this point.

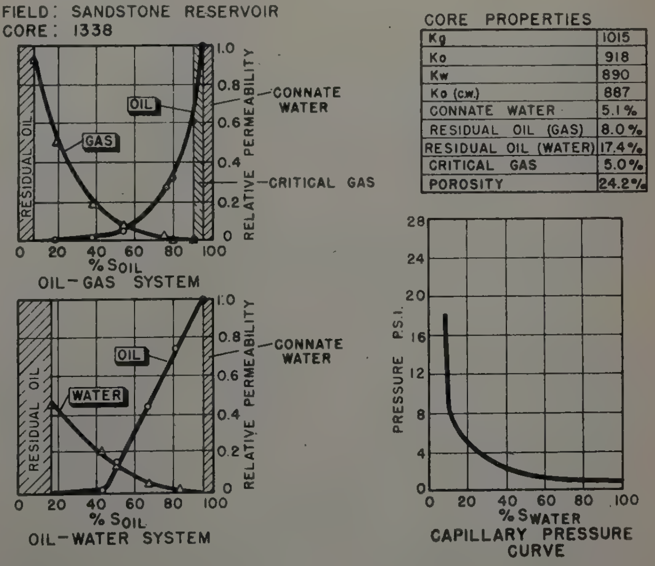

CORE PROPERTIES

Kg	1015
Ko	918
Kw	890
Ko (cw.)	887
CONNATE WATER	5.1%
RESIDUAL OIL (GAS)	8.0%
RESIDUAL OIL (WATER)	17.4%
CRITICAL GAS	5.0%
POROSITY	24.2%

FIG. 1 — RELATIVE PERMEABILITY AND CAPILLARY PRESSURE DATA.

---

[1] References given at end of paper.

Manuscript received in the office of the Petroleum Branch August 10, 1950. Paper presented at the Petroleum Branch Fall Meeting in New Orleans, La., Oct. 4-6, 1950.

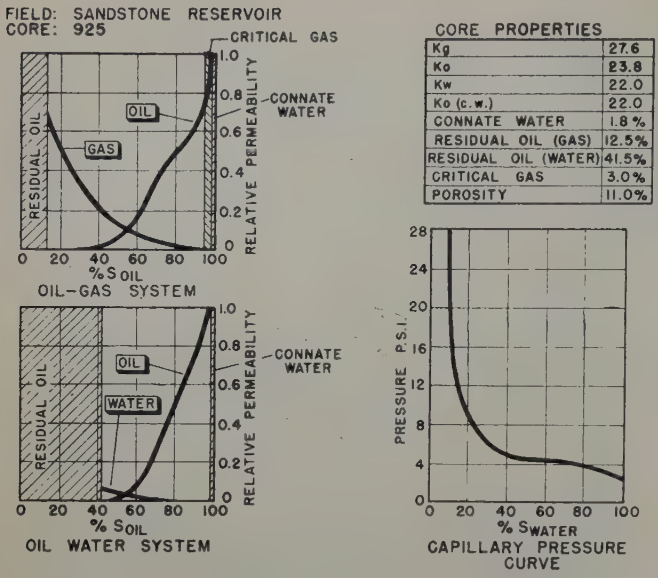

CORE PROPERTIES

Kg	27.6
Ko	23.8
Kw	22.0
Ko (c.w.)	22.0
CONNATE WATER	1.8 %
RESIDUAL OIL (GAS)	12.5%
RESIDUAL OIL (WATER)	41.5%
CRITICAL GAS	3.0%
POROSITY	11.0%

FIG. 2 — RELATIVE PERMEABILITY AND CAPILLARY PRESSURE DATA.

7. Analysis of the remaining fluid content of the sample to check the saturation determinations in Steps 4 through 6. This completes the study of the gas-oil flow system.
8. Reduction of the sample to connate water by an oil drive in the centrifuge — the same as in Step 3.
9. Determination of the relative permeability to oil and water by the dynamic method.
10. Reduction of the sample to residual oil by a water drive using the high speed centrifuge and the determination of the relative permeability to water at that saturation value.
11. Analysis of the fluid content of the sample to check saturation values obtained during the relative permeability determinations.

Some representative data obtained by the use of this procedure are shown in Figs. 1 through 4. The specific permeabilities to air, oil, and water, and the effective permeability to oil at connate water are shown for each sample represented. For reasons which were explained in a previous publication,[1] the base value used to calculate relative permeabilities is the specific permeability to water (of the appropriate salinity). Each of these sets of relative permeability data are close to the average data obtained for the fields represented, but do not necessarily hold for other reservoir materials even though the basic core properties (such as specific permeability, connate water, etc.) may be similar. A striking example of the individuality of relative permeability data is furnished by the data presented in Fig. 2. All of the samples from this field which have been studied exhibit the extremely high residual oil values with displacement by water and the low permeability to water at this point. Relative permeability data on other reservoirs of similar permeability have exhibited no such marked difference between the residual oil values for water and gas. This example also stresses the need for relative permeability data obtained on samples of the reservoir being studied since such peculiarities may occur in any system and cannot be predicted with present knowledge.

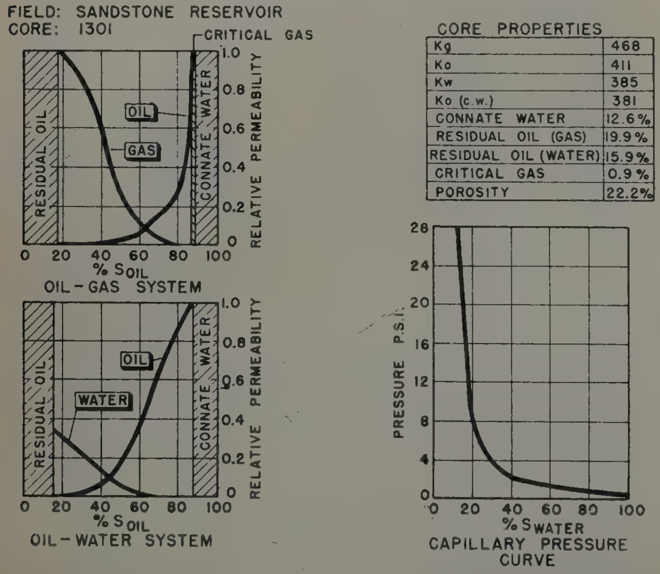

CORE PROPERTIES

Kg	468
Ko	411
Kw	385
Ko (c.w.)	381
CONNATE WATER	12.6%
RESIDUAL OIL (GAS)	19.9%
RESIDUAL OIL (WATER)	15.9%
CRITICAL GAS	0.9%
POROSITY	22.2%

FIG. 3 — RELATIVE PERMEABILITY AND CAPILLARY PRESSURE DATA.

DESCRIPTION OF THE SOLUTION GAS DRIVE RELATIVE PERMEABILITY METHOD

The solution gas drive method, which is used to obtain the critical gas saturation value and the relative permeability to oil at that point, consists of allowing gas to evolve from solution by reducing the pressure on a core containing live oil and connate water. This evolution of gas creates a gas saturation within the sample which is a few per cent higher than the critical gas saturation value. This small amount of excess gas is then flushed from the pore space by a flow of dead oil at very low pressures and flow rates. This reduces the gas content to the critical gas saturation value. Normally two to three pore volumes of dead oil flushed through the core are sufficient to displace this excess gas. When the critical gas saturation value has been reached, this same flow of dead oil through the sample is used to measure the permeability to oil associated with this saturation. A schematic diagram of the apparatus used for these studies is shown in Fig. 5. The core sample, containing oil and connate water, is held in a Hassler-type core holder during both the measurements of permeability and the replacement of the original oil in place with live fluid. An initial effective permeability to oil at the connate water saturation is measured at atmospheric conditions by a flow of oil from the constant rate pump. The associated pressure drop along the core is measured by a Nullmatic Differential Pressure Transmitter (T in Fig. 5) having a measured differential pressure range of 5 to 50 in. of water.* Following this measurement the oil flow is stopped

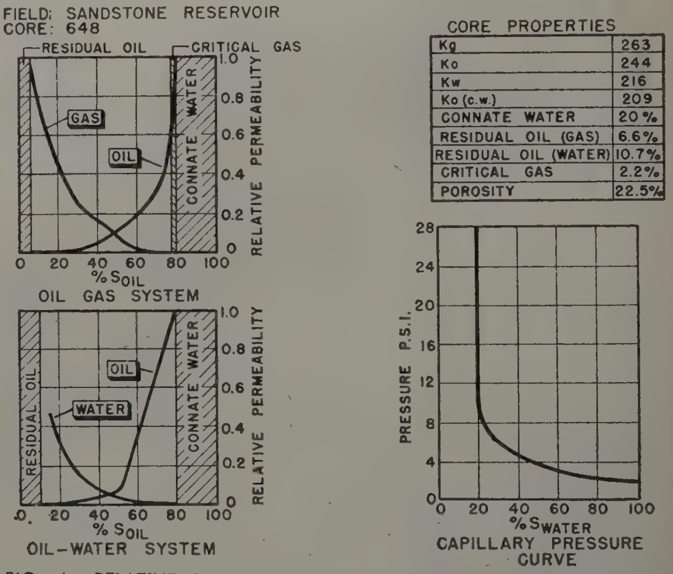

CORE PROPERTIES

Kg	263
Ko	244
Kw	216
Ko (c.w.)	209
CONNATE WATER	20 %
RESIDUAL OIL (GAS)	6.6%
RESIDUAL OIL (WATER)	10.7%
CRITICAL GAS	2.2%
POROSITY	22.5%

FIG. 4 — RELATIVE PERMEABILITY AND CAPILLARY PRESSURE DATA.

---

*Manufactured by the Moore Products Co., Philadelphia, Pa.

and the dead fluid in the sample is replaced by oil containing air in solution at approximately 30 psig pressure. The live oil reservoir serves for both mixing and storing the live fluid. In replacing the dead oil in the core sample with live fluid, the entire system (exclusive of the constant rate pump) is placed under pressure equal to the bubble point of the live oil by means of the pressure regulator NR-1 and the additional pressure necessary to induce flow of the live fluid through the sample is imposed upon the live oil reservoir with the air loaded regulator NR - 2. It has been found that a flow of 10 to 15 pore volumes through the core sample insures displacement of the dead oil originally in place. The portion of the flow system containing the sample is then reduced to atmospheric pressure to allow the gas to be evolved from solution. Several hours standing at atmospheric pressure is usually necessary for complete evolution of gas in consolidated sand samples, due to the resistance of the capillary system to bubble formation when relatively low pressure changes are involved. It has also been found that the evolution of gas in a small core plug (seven-eighths in. in diameter by one in. long) will only increase the gas saturation of that sample to three to four per cent of the pore space above the critical gas saturation value, even though there be several pore volumes of gas liberated in the pore space of the sample. This same phenomenon was found by other investigators in this field.[3] The flowable gas in the core sample is flushed from the pore space with a small (two or three pore volumes) flow of oil at a low rate from the constant rate pump. The displacement of this excess gas is followed by observation of the output end of the core and by the changing permeability to oil, which becomes constant when the critical gas saturation value is reached. The amount of gas then present is determined by comparing the weight of the sample submerged in oil with a similar weight obtained when the core contained no gas. Critical gas saturation values for the sandstone reservoir samples studied average two to three per cent of the pore space.

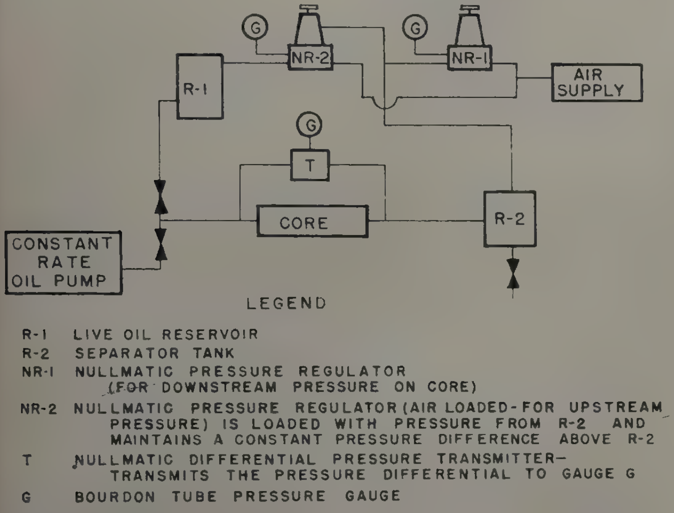
G
NR-2
G
NR-1
R-1
AIR SUPPLY
G
T
CORE
R-2
CONSTANT RATE OIL PUMP
LEGEND
R-1 LIVE OIL RESERVOIR
R-2 SEPARATOR TANK
NR-1 NULLMATIC PRESSURE REGULATOR (FOR DOWNSTREAM PRESSURE ON CORE)
NR-2 NULLMATIC PRESSURE REGULATOR (AIR LOADED-FOR UPSTREAM PRESSURE) IS LOADED WITH PRESSURE FROM R-2 AND MAINTAINS A CONSTANT PRESSURE DIFFERENCE ABOVE R-2
T NULLMATIC DIFFERENTIAL PRESSURE TRANSMITTER—TRANSMITS THE PRESSURE DIFFERENTIAL TO GAUGE G
G BOURDON TUBE PRESSURE GAUGE

FIG. 5 — SCHEMATIC DIAGRAM OF THE SOLUTION GAS RELATIVE PERMEABILITY EQUIPMENT.

DESCRIPTION OF THE DYNAMIC RELATIVE PERMEABILITY METHOD FOR A WATER-OIL FLOW SYSTEM

The dynamic displacement method is patterned after that described by Yuster, *et al.*,[4] and, essentially, differs only in the use of a Hassler-type core holder and constant rate positive displacement pumps to preset the desired flow rates. A schematic diagram of the equipment used is shown in Fig. 6. The core sample is placed in the center section of the three-piece holder in such a manner that the ends extend beyond the pressure taps in the piezometer rings. The core is immediately preceded and followed by butt pieces of the same or similar material to distribute the flow across the face of the sample and eliminate any saturation gradient which might be caused by a boundary effect. These sections are also preceded by a premixing butt of loose porous material and an orifice plug made of plastic. This arrangement allows the pressure measurements to be made on the sample with no intervening core faces which might introduce errors into the measurements. The procedure used with this equipment in order to determine the relative permeabilities to oil and water is as follows. The core sample, saturated with oil and connate water, is placed in the apparatus and the effective permeability to oil at this condition is measured. A small flow of water is then introduced simultaneously with the oil to increase the water saturation in the core. The approach to equilibrium in this two phase flow system is followed by observing the changing pressure drop which stabilizes when the liquid saturations have become constant. This pressure and the preset flow rates allow the calculation of effective and relative permeabilities and the corresponding saturation is obtained by removing and weighing the core sample on an analytical balance. The sample is then replaced in the apparatus and further points on the relative permeability curves are obtained in the same manner using increasingly higher ratios of water to oil flow rates. The final point in this determination, with the sample reduced

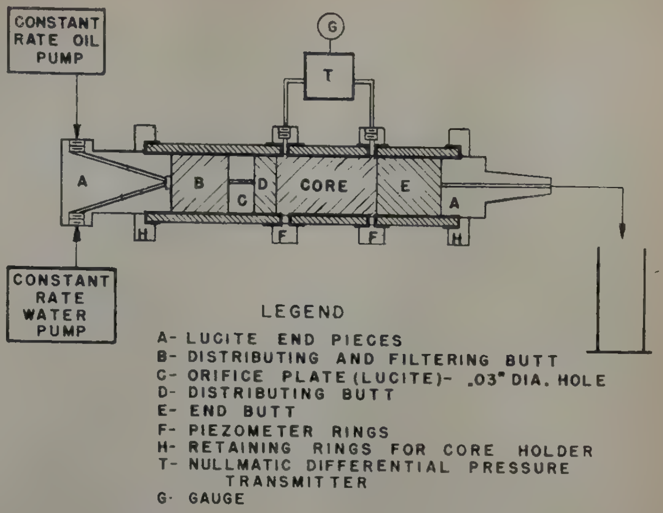
CONSTANT RATE OIL PUMP
G
T
A
B
C
D
CORE
E
A
H
F
F
H
CONSTANT RATE WATER PUMP
LEGEND
A- LUCITE END PIECES
B- DISTRIBUTING AND FILTERING BUTT
C- ORIFICE PLATE (LUCITE)- .03" DIA. HOLE
D- DISTRIBUTING BUTT
E- END BUTT
F- PIEZOMETER RINGS
H- RETAINING RINGS FOR CORE HOLDER
T- NULLMATIC DIFFERENTIAL PRESSURE TRANSMITTER
G- GAUGE

FIG. 6 — SCHEMATIC DIAGRAM OF THE DYNAMIC RELATIVE PERMEABILITY EQUIPMENT.

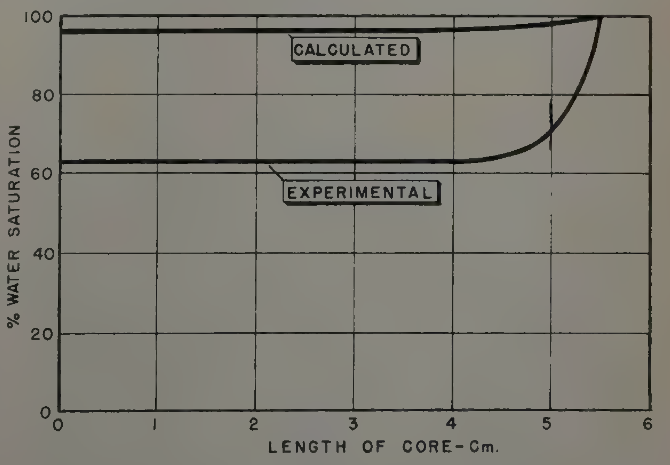

FIG. 7 — CALCULATED AND EXPERIMENTAL END EFFECT IN AN OIL-WATER FLOW SYSTEM.

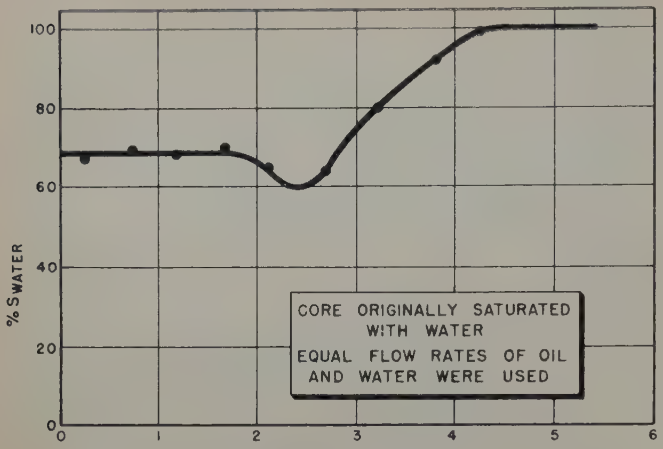

FIG. 8 — INTERFACE MOVEMENT THROUGH A CORE SAMPLE.

to residual oil by a water drive, may be obtained with this apparatus, but it has been found faster and more accurate to use the high speed centrifuge to obtain the saturation condition and then merely measure the effective permeability to water at this point. From these data, relative permeability curves such as those shown in Figs. 1 through 4 may be obtained.

STATISTICAL METHOD FOR AVERAGING RELATIVE PERMEABILITY DATA FOR A NUMBER OF SMALL CORE SAMPLES

It is recognized that when relative permeability determinations have been made on several samples from a petroleum reservoir, some method is needed for averaging these data to obtain a set of relative permeability curves which may be used in reservoir engineering calculations. The method to be described in this paper consists of a statistical averaging of relative permeability data from individual samples which have been placed on a directly comparable basis. With this method the relative permeability and the permeability ratio curves are plotted as a function of that portion of the total porosity in which simultaneous two-phase flow may take place (*i.e.*, that portion of the total porosity in which neither the k_g/k_o nor the k_w/k_o ratios are infinite). This eliminates the differences in these curves due to individual values of the connate water, residual oil, and critical gas saturations. In averaging these curves the greatest reliance is placed upon the experimentally determined permeability ratio curves since they, as a group, show less individual peculiarities than do the relative permeability curves. An essential aid is the use of a semi-logarithmic plot of the data instead of the conventional Cartesian coordinate presentation. Average saturation values are determined arithmetically at equal values of relative permeabilities and permeability ratios. The average curves are replotted on the basis of total porosity using average values for connate water, residual oil and critical gas saturations. This averaging method does not take into account such inhomogeneities in the reservoir as permeability streaks, channeling, etc.

MISCELLANEOUS STUDIES IN TWO AND THREE-PHASE FLOW SYSTEMS USING THE DYNAMIC DISPLACEMENT METHOD

In addition to the routine relative permeability work described, investigations are being carried out leading towards the understanding of the mechanisms of multiphase fluid flow in porous media and towards the development of other types of relative permeability determinations. The results of some of these investigations are discussed below.

Saturation Gradient Due to Boundary Effect In a Two-Phase Flow System

In order to study the possible effect of flow rate on relative permeability data obtained by the water-oil dynamic flow mechanism theoretically as well as experimentally, it was felt that the so-called end effect (a saturation gradient along the length of the core due to the absence of any pressure difference between the phases at the output face of the porous media being studied) would be the major cause of such a rate effect. A mathematical consideration of this problem utilizing Darcy's Law, relative permeability curves, and a capillary pressure curve resulted in the development of an expression describing the end effect in a water-oil flow system as shown below:

$$\frac{dp}{dl} = \frac{Q\mu}{kA} \quad \ldots\ldots\ldots\ldots \quad (1)$$

where:

k = permeability (cm^2)
Q = flow rate (cm^3/sec)
l = length (cm)
μ = viscosity (centipoise)
p = pressure (dynes)
A = cross sectional area (cm^2)

Darcy's Law holds for each phase in the flowing system. Subtracting the equation as applied to water from the equation applied to oil:

$$\frac{dp_o}{dl} - \frac{dp_w}{dl} = \frac{Q_o\mu_o}{Ak_o} - \frac{Q_w\mu_w}{Ak_w} \quad \ldots \quad (2)$$

or letting $dp_o - dp_w = d(\triangle P)$ where $\triangle P$ is the pressure difference acting between the phases, transposing and integrating:

$$l = \int_{S_w = X}^{S_w = 1.0} \frac{A\ d(\triangle P)}{\frac{Q_o\mu_o}{k_o} - \frac{Q_w\mu_w}{k_w}} \quad \ldots\ldots\ldots \quad (3)$$

where X is the lowest water saturation obtainable under the imposed flow conditions and would, therefore, be the equilibrium saturation value in any portion of the porous media where the end effect was non-existent. In Equation (3), l is

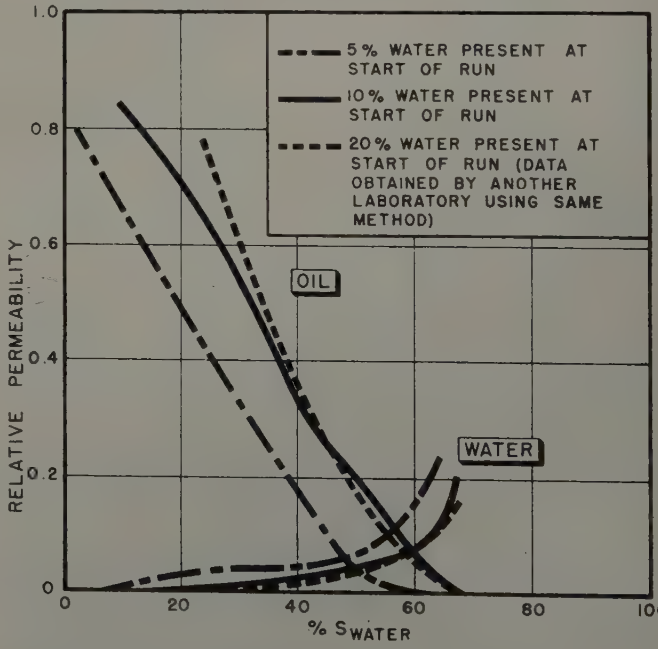

FIG. 9 — EFFECT OF VARYING THE ORIGINAL WATER SATURATION ON DYNAMIC RELATIVE PERMEABILITY.

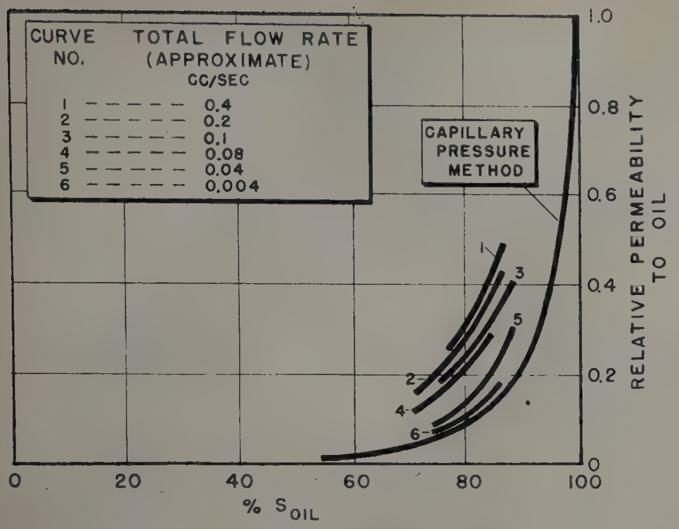

FIG. 10 — EFFECT OF FLOW RATE IN THE GAS-LIQUID DYNAMIC FLOW SYSTEM.

the distance from the output end of the core where a water saturation between X and 1.0 may exist. The relationship of S_w and $\triangle P$ is given by the capillary pressure curve; k_o and k_w may be given as functions of $\triangle P$ by combining the capillary pressure curve with the relative permeability curve.

By solving Equation (3) graphically for a system in which oil and water would flow in equal rates through a synthetic core material of fused alundum, a plot was obtained of the saturation distribution to be expected with this system. It may be seen from Equation (3) that the largest end effect is to be expected at low flow rates and where the wetting phase is displaced by a non-wetting phase since the $\triangle P$ for any given saturation would be larger where that saturation was approached by a drainage rather than by an imbibition mechanism. The calculations were made for these conditions and the saturation gradient calculated is shown in Fig. 7. To check these calculations experimentally, an alundum rod two cm in diameter and 5.5 cm long was cut into eleven 0.5 cm sections and was substituted for the core and end butts in the dynamic apparatus with Kleenex layers being placed between the sections to insure capillary contact. The conditions used in the calculations were followed with the flow rate being 0.00005 cu cm per second for each phase. When an equilibrium condition had been reached in the flow experiment, the segments were immediately separated and analyses of the fluid content of each were made. The saturation gradient thus obtained is shown in Fig. 7 along with that calculated from relative permeability data by the method described. A very striking discrepancy can be seen between these two curves in that the end effect which, according to the calculations, should have extended well through the entire length of the sample, was actually confined to the last cm of its length.

It was thought that this discrepancy might be due to the inapplicability of the drainage (capillary pressure) curve to the desaturating mechanism used since it had previously been found that high pressures were associated with non-wetting phase fronts moving through a core. To determine the mechanism of the movement of such an interface, a segmented alundum rod was again used in a dynamic flow system with oil and water flowing at equal rates into the water saturated sample. The rod was taken apart for analysis when the oil interface had progressed only three-fourths of the length of the sample. Analysis of the fluid content of the segments proved the saturation distribution to be as shown in Fig. 8. These results were reproduced using a different segmented sample (of larger diameter) and using gas as the non-wetting phase. These experiments led to the hypothesis that even at very low flow rates there is a large enough pressure gradient associated with a non-wetting phase interface movement to reduce the wetting phase saturation immediately behind this interface to a value lower than the equilibrium saturation value eventually established. This indicates that the equilibrium saturation in a two-phase flow system is approached by an imbibition rather than by a drainage mechanism in a constant rate dynamic flow system even though the wetting phase is being displaced by a non-wetting phase.

In order to check into this possibility more fully, the capillary pressure vs. saturation curve which would be necessary to calculate the experimentally determined saturation gradient was constructed from the experimental data. This curve was found to have the shape and general appearance of an imbibition rather than of a drainage-type curve and appeared quite similar to the imbibition curves described in the literature.[5]

Since, in the routine determination of relative permeability to oil and water by the dynamic method, an imbibition mechanism is used explicitly (that is, oil is displaced by water), the end effect encountered is also small. From the low flow rates mentioned above to flow rates three orders of magnitude higher there has been found no effect of rate on relative permeability data obtained with a two liquid flow system by the dynamic method.

The Effect of Initial Interstitial Water Saturation On Dynamic Relative Permeability Determinations

It has been found, however, that in the routine determinations of relative permeabilities to oil and to water by the dynamic method, the amount of water present as interstitial water at the start of the determination will materially affect the relative permeability data obtained. Fig. 9 shows this effect on a sandstone sample for which 10 per cent is the irreducible water saturation as determined by the high speed centrifuge method. It may be seen that not only the starting points, but also the actual configurations of the relative permeability curves vary with the amount of interstitutial water originally present. The magnitude of this effect for original water saturations varying from 5 to 15 per cent is shown by the curves in Fig. 9. It is felt that, except for special studies, the amount of water present at the start of a relative permeability determination should be the irreducible water saturation of the sample.

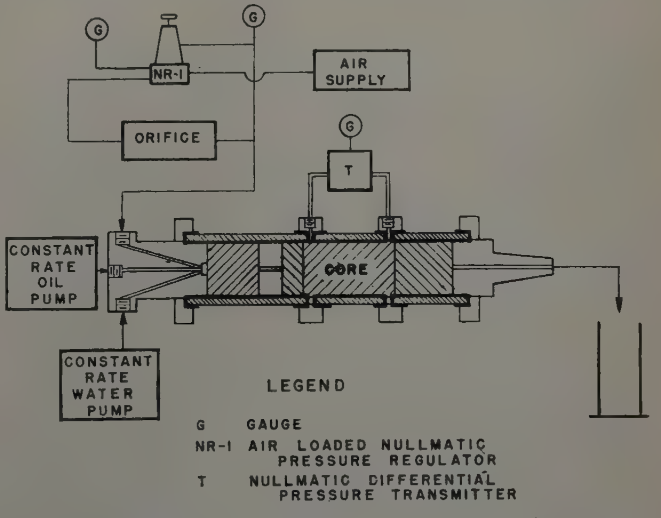
G
G
NR-1
AIR SUPPLY
ORIFICE
G
T
CONSTANT RATE OIL PUMP
CORE
CONSTANT RATE WATER PUMP
LEGEND
G GAUGE
NR-1 AIR LOADED NULLMATIC PRESSURE REGULATOR
T NULLMATIC DIFFERENTIAL PRESSURE TRANSMITTER

FIG. 11 — SCHEMATIC DIAGRAM OF THE THREE-PHASE DYNAMIC FLOW EQUIPMENT.

The Dynamic Flow System Using Gas and Liquid As the Flowing Phases

In a two-phase dynamic system where gas is one of the flowing phases, there is a definite effect of flow rate on the resulting relative permeability data. This effect is in the direction of decreasing the permeability to both phases with decreasing total flow rates. This effect is demonstrated by the experimental results shown in Fig. 10. The relative permeability to gas behaves in a similar manner, but is not presented in order to avoid confusion in the figure. Also shown is the relative permeability to oil curve for this sample obtained by the capillary pressure method. It may be seen that at the lower rate shown the relative permeability to oil is close to, and within experimental error of, that curve obtained by the capillary pressure method. Determinations at each of these flow rates were made with the segmented alundum rod and the results indicated that no end effect was present in any of these determinations to account for this effect of rate. It seems likely that the increase in effective permeability to each phase with increasing flow rates is due to a form of channeling caused by the high velocities of the gas flowing through the capillary system. A high velocity gas flow through a capillary system can sweep the oil phase from restrictions in its path which would normally be closed to the flow of gas and at the same time carry a portion of the oil phase through the core as droplets in the gas phase, and thus increase the permeability to each phase. Such a phenomenon in a gas-oil flow system has been observed in microscopic studies of an unconsolidated porous system. In a previous publication,[1] the opinion was expressed that relative permeability data obtained by the capillary pressure and the dynamic methods would differ due to the different displacement mechanisms involved. On the basis of recent work, such as that described above, it is now felt that the two methods will give similar results for gas-oil flow systems. However, the flow rates necessary to eliminate the effect of rate for a gas-oil system in the dynamic method are so low that the use of this method as a routine tool for obtaining relative permeabilities to gas and oil is impractical because of the length of time required to reach an equilibrium value. This conclusion is based primarily on data obtained in experiments in which only oil and gas were present. A small amount of experimental data suggests that it may be modified if connate water is present during the determination.

RELATIVE PERMEABILITY DETERMINATIONS WITH THREE PHASES FLOWING SIMULTANEOUSLY

Using the gas-liquid two-phase study as a guide for the flow rates necessary in the gas phase, some preliminary work has been done in setting up and studying a system in which three phases flow simultaneously. A dynamic method was chosen because of several experimental difficulties which may be foreseen in the use of the capillary pressure method for this work. The only modification necessary was the addition to the regular two liquid dynamic apparatus of a metering device to produce a constant flow rate of gas through the sample under study. A schematic diagram of the apparatus in use is shown in Fig. 11. The gas metering device shown in the upper left hand corner consists of an air loaded pressure regulator and a very tight core plug which is used as an orifice. The spring load of the regulator (NR - 1) is set to the pressure which will give the desired flow rate through the core plug (orifice), and this pressure differential is held, regardless of the buildup of back pressure in the fluid flow system, by the air loading feature of the regulator. The core sample under study is handled as in the two liquid dynamic system except that it has been necessary to analyze the fluid content of the core by vacuum distillation after the determination of each point in order to obtain a saturation value. Since the flow rates must be low in order to avoid an effect of rate due to the presence of gas, from two to five days have been necessary to reach an equilibrium value on each point determined.

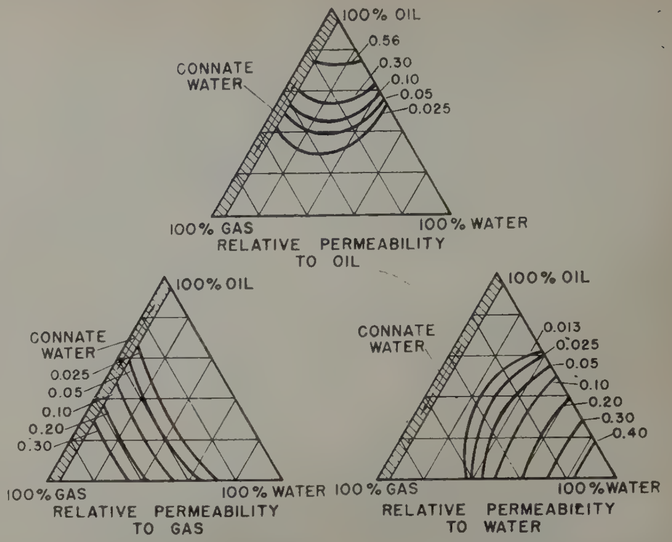

FIG. 12 — RELATIVE PERMEABILITY OF A THREE FLOWING PHASE SYSTEM.

As yet, not enough three-phase data have been gathered on a single sample to permit a complete description of the resulting relative permeability characteristics. However, Fig. 12 shows the results obtained to date upon a consolidated sandstone sample. The isoperms for gas and oil agree in general configuration with those presented in the literature.[6] However, where these earlier investigators found the relative permeability to water to be dependent only upon the water saturation, it has been found in this case that the water permeabilities as well as the gas and oil permeabilities are dependent upon the saturations of all three phases. These data, as presented in Fig. 12, are obtained when the sample under study originally contains oil and connate water and the oil content is decreased by simultaneously increasing the water and gas saturations. A form of hysteresis has been observed when the oil saturation in the core is increased after originally being reduced to connate water and residual oil with a gas drive. The relative permeabilities to all three phases are decreased in this case below those observed when the core originally contains oil and connate water. Obtaining a complete relative permeability history with three phases flowing on a single core sample by this method will necessarily require a long period of time, but it is felt that such data will be extremely useful in calculating field performance for reservoirs being produced by simultaneous water and gas drives, by water drive on a partially gas depleted field, etc.

REFERENCES

1. Brownscombe, E. R., Slobod, R. L., and Caudle, B. H.: *Oil and Gas J.*, (1950), **48**, No. 40, 68.
2. Slobod, R. L., Chambers, Adele, and Prehn, W. L., Jr., *Trans.* AIME, (1951), **192**, 127. *J. of Pet. Tech.*, III. No. 3, 127.
3. Muskat, M., and Botset, H.: *Trans.* AIME, (1939), **132**, 172.
4. Morse, Terwilliger and Yuster: *Producers Monthly*, (1947), **11**, No. 10, 19.
5. Welge, H. J.: *Trans.* AIME, (1949), **179**, 133.
6. Leverett, M. C., and Lewis, W. B.: *Trans.* AIME, (1941), **142**, 107.

★ ★ ★

T.P. 3059

MINERALOGICAL STUDIES OF CALIFORNIA OIL-BEARING FORMATIONS

I—IDENTIFICATION OF CLAYS

P. G. NAHIN, W. C. MERRILL, A. GRENALL AND **R. S. CROG,** MEMBER AIME, UNION OIL CO. OF CALIFORNIA, WILMINGTON, CALIF.

ABSTRACT

A progress report of an experimental investigation into the role of clay in reservoir performance is presented. The paper gives some of the reasons for considering clay as a significant component and outlines the objectives of a broad field of study which it is intended to pursue. Descriptions of the analytical methods used are given; these include X-ray diffraction, electron miscroscopy, thin section petrography, infrared spectroscopy, and cation exchange analysis. A suite of the more important clay minerals has been assembled and characterized by these methods for use as standards in core analysis. From the data obtained it appears that although no one method of analysis is diagnostic for all of the clay minerals the infrared technique shows considerable promise in this direction. For the present, one or more supplementary methods should be used to confirm the clay mineral identifications.

The methods of analysis are applied to field cores taken from representative and widely differing strata especially as regards their susceptibility to damage by fresh water. Wells completed in the Stevens and Gatchell Zones in San Joaquin Valley are particularly clear-cut examples of this behavior with Stevens Zone wells being more adversely affected by fresh water. Cores from these zones have been studied and are discussed. It appears that differences in this behavior can be ascribed to differences in the nature of the contained clays. The value of the infrared spectra of the clay fractions in establishing the identity of the predominant clay minerals is given particular emphasis.

INTRODUCTION

It is a challenge to the technical resources of the petroleum industry that when the economic limit of production is reached, from 40 to 70 per cent of the oil in California reservoirs remains unproduced even by use of the best presently known methods of recovery. The magnitude of this abandoned volume of oil can be appreciated when it is considered that to 1950 in excess of 8 billion bbl[1] has been produced from California reservoirs with estimated economically recoverable reserves in known fields and pools totaling nearly 4 billion bbl.[24] If for every barrel of oil produced there is at least another barrel still in place, it is evident that the revenue obtained from the recovery of only a few per cent of this volume would repay the cost of the required research manyfold.

From well completion experience, production behavior, and a growing body of laboratory data it now appears certain that the mineral composition of a producing stratum has an important bearing on the productivity and ultimate yield. In addition to the organic component and water, the cores consist of gravel, sand, silt, and clay* in diverse variety of (a) composition and (b) texture. It is the composite effect of these two factors which is probably responsible in large measure for the way in which the oil flows to the well. The role of the clay and fine-size accessory minerals is not clear but there is a growing opinion, based on their physical and chemical properties, that it is a significant one. Of particular importance are the prime facts:

1. The silt and clay fractions of the reservoir matrix possess the highest surface area per gram, and

2. The silt and especially the clay fractions are the most chemically reactive of the inorganic constituents present.

Only within the last few years has the knowledge of clay mineralogy and the techniques of identifying the clay minerals reached such a stage as to enable reliable inquiry into the composition of argillaceous sediments.[2,8,10,11,12,16,26] It is the purpose of this and succeeding papers to add to the fund of information on the role which these materials play in the production of petroleum from California formations by correlating their presence and associated properties with observed reservoir behavior. In the present paper attention is directed to their possible influence on damage by fresh water.

OBJECTIVES

The attack on this problem divides naturally into two broad phases:

1. Determination of the nature of the clays and their relationships to the other mineral components, and

2. Determination of the physico-chemical relationships between the clays and the interstitial fluids.

In the work described in this paper the emphasis has been on Phase 1, which stems logically from the necessity of identifying and understanding the materials to be dealt with in Phase 2.

Based on the authors' present opinion that not all of the minerals which occur in oil-bearing formation are of equal importance in their effects on the flow and recovery of oil, it was decided to focus attention first upon the clay minerals content and then, later perhaps, work into the field of the normally larger size non-clay minerals and fractions. The

---

[1] References given at end of paper.

Manuscript received in the office of the Petroleum Branch September 28, 1950. Paper presented at the Petroleum Branch Fall Meeting in Los Angeles, Calif., Oct. 12-13, 1950.

*The grade scale used is that of the U. S. Bureau of Soils.[22]

Table I — Descriptions of Reference Clays and Associated Minerals

Designation and Source Locality	X-Ray Diffraction, Phases[d] and Three Most Intense Reflections, Å	Resume of Petrographic Analysis	Description of Electron Micrograph	Infrared Absorptions, μ[a]	Cation Exchange Capacity[b]
"Wyoming" Bentonite Sodium Montmorillonite (Belle Fourche, S. Dak.)	Montmorillonite, Quartz (minor) 11.0 4.46 1.49	platy to fibrous crystals, scattered grains of quartz and feldspar partly altered to montmorillonite	platy to amorphous, tenuous background		74
"Wyoming" Bentonite, Coarse Colloid, 40D2[c] (Belle Fourche, S. Dak.)	Montmorillonite 12.5 4.46 1.49		aggregates of plates, less amorphous than unfractionated clay, fine particle background	2.8 6.1 6.6 6.9 9.6 11.0 12.6	86
Nontronite (Lost Valley Damsite Tamarack, Idaho)	Nontronite 14.9 4.54 1.53	resembles montmorillonite even to aggregate index although about 5% of pellets are of index higher than balsam; most of sample may not be the usual nontronite	more fine particles and diffuse background than montmorillonite		
Nontronite (Garfield, Washington)	Nontronite 14.9 4.54 1.53		generally subhedral to anhedral but with occasional laminar stacking and lath-like development	g	90
Hectorite (Hector, San Bernardino County, California)	Hectorite 11.8 4.53 3.15	similar to Na- and Ca- montmorillonite	faintly striated glassy anhedral laths	2.8 6.1 7.0 9.9	154[23]
Illite (Native "Grundite") (Goose Lake, Grundy County, Illinois)	Illite Quartz (minor) 10.2 4.48 2.58	superficially resembles montmorillonite, but aggregate index above balsam; minor amounts quartz, feldspar, apatite (?)	like montmorillonite but of more sharply crystalline laminarity	2.7 6.1 7.0 9.7 12.6 12.9	16
Illite (from Fithian Shale) (Fithian, Vermilion County Illinois)	Illite Quartz (trace) 10.2 4.48 2.58	relatively large (0.2-0.3 mm.) transparent crystals, positive elongation, aggregate index above balsam, nearly uniform extinction under crossed nicols	more homogeneous than "Grundite", gives appearance of a "euhedral montmorillonite"		35[14]
Muscovite (Spruce Pine (?), North Carolina)	Muscovite (major) Kaolin(?) (minor) 9.93 4.43 3.32	0.01 mm. grains, oriented cleavage faces, index, birefringence, elongation, extinction standard for muscovite	crystalline, micaceous, irregular aggregates tending toward conchoidal fracture, of particle size several orders larger than montmorillonite or illite	2.7 3.1 6.12 6.66 7.4 9.7 10.9	<1
Muscovite (Unknown)	Muscovite (major) 10.0 4.46 3.33		small rounded "pebbles" type particles very different from North Carolina muscovite		<1
Kaolin ("Hydrite Clay") (Georgia, U.S.A.)	Kaolin, Quartz (minor) 7.2 4.45 3.59	grains and tiny flakes (1-2μ), too small to resolve optical characteristics, indices appear higher than balsam, birefringence low	characteristic euhedral hexagonal and psuedohexagonal platelets	2.7 8.9 9.6 9.90 10.7 11.0 12.6 13.2	3
Anauxite (Tesla, California)	Kaolin, Quartz (minor) 7.2 3.58 1.48	majority grains and pellets <0.15 mm. diam.; smaller grains colorless, clear in transmitted light; aggregate index above balsam; birefringence in low grays, platy to fibrous crystals, pos. elongation	larger aggregates irregular but smallest flakelets show typical euhedral hexagonality	2.7 8.9 9.6 9.9 10.7 11.0 12.6 13.3	~3
Halloysite ("White Clay") (Eureka, Utah)	Major (?)[e], Illite (minor), Quartz (trace) 4.39 2.56 1.47	sample may be impure; 60-75% is colorless, amorphous, index above balsam (halloysite?), 15-20% of grains similar to Ca-montmorillonite; other grains suggest allophane, kaolinite	acicular, tubular, cylindrical, bilaminar, rather uniform size distribution when dispersed	8.9 9.6 11.0	6 10[15]
Halloysite (Lawrence County, Indiana)	Major (?)[e] Kaolin (trace) Quartz (trace) 4.83 4.39 2.45	aggregate index above balsam, medium to weak birefringence, may not be same form of halloysite as Eureka clay	similar to Eureka, Utah, halloysite		6 10[15]
Allophane (Lawrence County, Indiana)	? 5.72 3.49 2.94	clear, colorless practically isotropic (amorphous), clastic grains, tendency toward conchoidal fracture; index below balsam, optically resembles volcanic ash; few grains montmorillonite, kaolinite (?)	subhedral to anhedral, some tendency toward 120° angularity	g	
Talc (Johnson, Vermont)	Talc (major) (?) (minor) 9.42 3.13 4.53	platy to linear cross-sections, high index, high birefringence, parallel extinction, pos. elong., neg. uniaxial interference, talc confirmed	massive flat plates of irregular shape with sharp edges and points	g	~0
Pyrophyllite (Staley, North Carolina)	Pyrophyllite (major)[f] Quartz (major) 9.3 4.44 3.07	same general optical character as talc but with interference figure of large axial angle of ca. 60° (talc angle very small, muscovite ca. 40°)	platy, laminar, crystalline, with some very thin individual lamellae	8.9 9.4 10.6	~0
Feldspar ("Bainbridge") (Unknown)	Feldspar (major)[f] Quartz (major) 4.03 3.19 3.67	pure potash feldspar, absence of microcline twinning, neg relief; grain size 0.03-0.10 mm.; approx. 2% quartz (pos. relief)	angular, irregular, coarsely crystalline, some platy elongation	g	~0

---

[a] These are absorptions which after further study may prove to be of diagnostic significance.

[b] Approximate, in milliequivalents per 100 grams.

[c] Fraction sedimented in a Sharples Supercentrifuge bowl of 4.45 cm ID and 19.76 cm in length at 40,000 rpm using Drag No. 2 (flow rate of 725 ml per minute).

[d] Based on comparison with the ASTM Alphabetical Index of X-ray Diffraction Patterns (Covering Original Set of Cards), June, 1945, and (Covering the First Supplementary Set of Cards), August, 1945; Philadelphia.

[e] X-ray diffraction pattern is not in complete agreement with the data of ASTM Index for materials designated as halloysite. However, the halloysite of this investigation gives the same electron micrograph as do the halloysites taken from a number of widely scattered localities and illustrated in a recent API Project No. 49 report.[9]

[f] Both components estimated to be present in nearly equal amounts.

[g] Insufficient observation.

particular problem set was the identification and quantitative determination of the clays extracted from a carefully selected group of Union Oil Co. cores taken from seven wells in four California fields.

In order to obtain reliable identifications of the clay minerals it was necessary to assemble a suite of clay reference standards with which to compare the clay fractions separated from the cores. For this purpose 22 reference clays and associated minerals, a representative group of which is described in Table 1, were collected and characterized by the analytical techniques described below. Unfortunately, and solely because of unavailability of the necessary equipment, the differential thermal analysis method was not used. It should be mentioned that this reconnaissance survey was begun before the appearance of the excellent reports published by API Project 49 and others[17,20,21] on clay mineral standards.

ANALYTICAL METHODS

X-Ray Diffraction

The X-ray equipment consisted of a standard General Electric XRD unit fitted with Debye-Scherrer cameras. Copper radiation was employed.

The samples were prepared by crushing the material to pass a 100-mesh screen and then pressing the powder into a metal wedge supplied with the G.E. oscillating type holder. Developing and fixing procedures were standardized to permit film intercomparison.

Electron Microscopy

The micrographs were taken at 7,200 diameters with an RCA type EMU 50 kv electron miscroscope and subsequently enlarged to X45,000. The best resolutions obtained varied from 20 to 70 Å.[19] The scale on all figures is 1μ. Specimens were prepared and transferred to the instrument according to conventional procedures.[27]

In order to ensure selection of most representative fields the following specifications were adhered to: 10 different fields on two plates of five frames each were taken. A minimum of six photographically acceptable frames, two or more of which satisfied the requirement of being most representative was used for each sample. Pairs of plates were taken until these standards were met. Two plates were usually sufficient. To be acceptable a frame had to show adequate dispersion, contrast, focus, and be either generally representative of the specimen or reveal in detail some especially interesting feature.

Thin-Section Petrography

The clay reference samples were examined in the form of standard "grain" slides and in some cases as a single "smear."

The core chips were impregnated with shellac, ground with kerosene as lubricant and mounted on glass with Lakeside 70 cement. The finished sections were covered with Canada balsam and examined in the petrographic microscope.

Cation Exchange

Two methods for determining base exchange capacity (BEC) were used. Both were taken from the literature and then modified to suit the amounts of materials available.

Saturation with Ammonium Ion

As finally adopted the method for samples of one gram or more was a combination of the University of Wisconsin[3] and University of Illinois procedures.[4] Twenty-five ml of $1N$ ammonium acetate was added to the dried one-gram sample and shaken at intervals for one hour. The clay was centrifuged, washed once with $1N$ ammonium acetate and four times with neutral ethyl alcohol. The washings were poured through paper filter supported by a stainless steel wire funnel. Finally the clay was transferred to the filter and washed with 150 ml of ethyl alcohol to remove the last traces of NH_4^+ and the analysis completed by semi-micro Kjeldahl.

Colorimetric Manganese

Where the total amount of separated clay fraction was less than one gram and was required for several other types of analyses it was necessary to use a semi-micro method of BEC analysis. Starting with the procedure of Bower and Truog,[3] saturation replacement of the cation exchange ions with Mn^{++} and the colorimetric determination of the latter as MnO_4^-, the following modified procedure was developed:

Thirty ml of $1N\ MnCl_2$ was added to the ground dried sample and shaken until the clay was dispersed. The mixture was allowed to stand for 16 hours to effect the exchange. Using centrifugation-decantation the sample was washed with two additional 30 ml portions of $1N\ MnCl_2$ and finally with 30 ml portions of neutral ethyl alcohol until chloride-free. The sample was transferred quantitatively to a 400 ml beaker and 20 ml of concentrated sulfuric acid was added. Wet oxidation of all residual organic matter with about 5 ml of hydrogen peroxide was effected on a hot plate until the supernatant liquid was clear. The sample was diluted to 150 ml, filtered and washed with 100 ml of water. Two-tenths gram of para sodium periodate was added to oxidize the Mn^{++} to MnO_4^-. The volume of the sample was reduced to 175 ml at just below the boiling point, transferred to a 250 ml volumetric flask and diluted to the mark. The optical density was determined at $\lambda = 526\ m\mu$ with a Model DU Beckman spectrophotometer. The BEC was calculated from graphs made with standard solutions.

The amounts of manganese present in the reference clays as determined by emission spectra were negligible, *e.g.*, $\ll 0.001$ per cent in montmorillonite and <0.01 per cent in illite. No spectra were taken of the core clays.

With the approximately 0.1-gram samples the precision is about ±5 per cent in the montmorillonite range of BEC values and ±10 per cent for the very low values in the kaolin range.

Infrared Spectroscopy

It has been shown[5,6] that uncalcined montmorillonites exhibit characteristic absorptions in the infrared at 2.75μ and 2.92μ, attributed, respectively, to vibrations of unbonded or free hydroxyl (lattice or structural OH) and to hydrogen bonded (surface and interlayer hydration water) hydroxyl, $O{:}H{:}O$. This interesting observation suggested that infrared analysis might be used to differentiate the various clay reference minerals on the basis of these or some other characteristic absorptions. Moreover, the results of a number of clay analyses indicated the entire near infrared spectrum from 2 to 15μ to be of diagnostic interest.

Because experience showed that in some cases the larger particles gave less definitive spectra the clay was first fractionated by means of a Sharples Type 1A supercentrifuge to yield a colloid fraction of average particle size $0.1 - 0.06\mu$ in radius.[7] The fine fraction was then suspended in three different concentrations, *viz.*, 0.1, 0.05, 0.01 gram of clay in 10 ml of $0.001N$ aqueous ammonia. It was necessary to use these three concentrations in order to cover the wide range of absorptions encountered in the 2 to 15μ region. The suspensions were deposited by means of a dropper on a single crystal silver chloride (Harshaw Chemical Co.) cell window to cover completely the area traversed by the beam. The cell window and suspension were then placed in a vacuum oven, dried at 50°C, removed and scanned in a research model of the Beckman IR-2 infrared spectrophotometer.

The per cent transmission versus wavelength graphs were plotted for each of the sample thicknesses in its particular spectral region and then joined in a continuous spectrum by moving the ordinates up or down as required for continuity. This results in a spectral curve which is qualitative in the sense that it shows the location of characteristic absorptions, gives the general spectral pattern, but does not enable accurate comparison of the relative magnitudes of the peaks obtained at different sample thicknesses.

It is, of course, realized that this is not orthodox infrared technique but for the purpose of a preliminary qualitative comparison of the different clay minerals it has proved adequate in demonstrating gross spectral differences. Thus, all of the major peaks are reproducible, although because of errors in the manual conversion of the original energy transmitted versus wavelength graphs to per cent transmission vs. wavelength plots some differences occur in regard to the minor peaks.

RESULTS AND DISCUSSION OF THE ANALYTICAL METHODS

X-Ray Data

On the basis of patterns obtained in this work it appears that:

1. The three strongest lines generally used to characterize montmorillonite and illite in massive form may not be completely diagnostic when applied to materials undergoing diagenetic alteration.
2. It is generally difficult to distinguish montmorillonite, nontronite and hectorite from one another without employing more refined techniques.
3. Kaolinite and anauxite cannot be distinguished with certainty.
4. The sodium, calcium, and cadmium exchange salts of a given montmorillonite yield essentially the same diffraction patterns. This might be expected on the basis that the replacement of one set of external exchange ions by another can occur without perceptible alteration of the arrangement of the lattice ions.
5. The three important sodic, potash, and calcic feldspars are not readily distinguished from one another by X-rays alone.

Electron Micrographs

Examination of the electron micrographs showed the rather wide diversity of structural habits which these minerals possess. Some of these habits are so distinctive that they are diagnostic by themselves, such as in the cases of kaolinite and halloysite. However, in general, the electron micrographs were not diagnostic and must be interpreted with caution. Thus, two different samples of muscovite strikingly dissimilar electronmicrographically gave identical X-ray diffraction patterns.

Petrographic Data

The data from the petrographic optical analyses as given in Table 1 are mainly of value as confirmatory evidence for identity as revealed by the other methods used. In the case of the feldspars, however, it is particularly clear-cut even to the extent of distinguishing between microline and orthoclase which are identical chemically but have different optical properties.

Cation Exchange Data

The cation exchange capacities supplement the other data of Table I in the sense that there are indicated no inconsistencies with the exchange capacities normally obtained for these materials. Thus, should the X-ray and electron micrograph data raise some question as to whether the Garfield, Washington, clay mineral is nontronite or illite, the cation exchange capacity of 90 milliequivalents per 100 grams would be good evidence against the latter. This follows from the well-known fact that the montmorillonites have cation exchange capacities in the range 60-120, the illites in the range 15-40 milliequivalents per 100 grams.

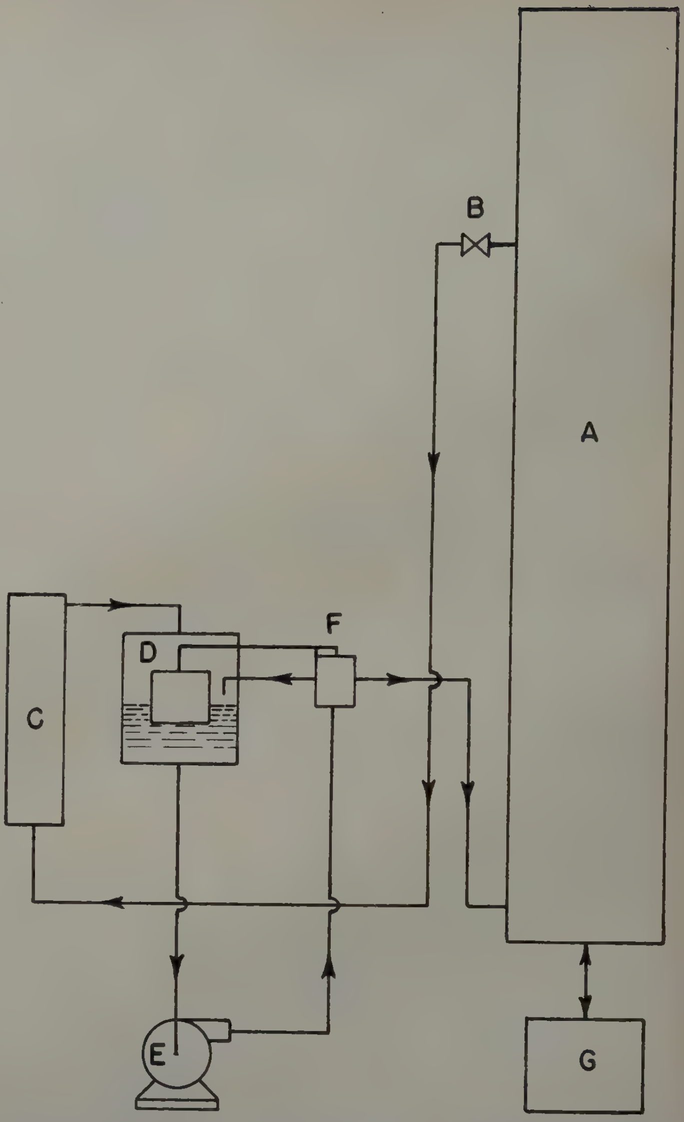

FIG. 1 — SCHEMATIC FLOW DIAGRAM OF CLAY SEPARATOR. A — ELUTRIATOR, B — "O"-RING SHUT-OFF VALVE, C — SUPERCENTRIFUGE BOWL, D — FLOAT ASSEMBLY, E — PUMP, F — "O"-RING FLOW REGULATOR, G — VIBRATOR-DRIVE MOTOR.

Chemical Data

Although no assemblage of chemical data is reported here chemical analysis has been useful in the characterizations of some of the reference minerals. Both emission spectrographic and standard chemical tests were employed. Examples of cases in which chemical data may be confirmatory are in the determination of K_20 content in illite and of high iron in nontronite. An example in which chemical analysis may be the deciding factor is the differentiation of anauxite from kaolinite on the basis of a silica:alumina ratio of 3:1 for the former and 2:1 for the latter.

Infrared Data

The most interesting aspect of the spectra is that in overall configuration as well as in regard to specific absorptions they are all apparently significantly different from one another. This observation raises a question of the highest importance for those concerned with the accurate identification of the clay and related minerals: can the infrared absorption spectra of these inorganic materials serve to differentiate readily and accurately the various minerals of very similar lattice structure which now require the use of more than one of the previously mentioned methods of analysis? It would appear from the data obtained that the answer may be in the affirmative. The results should be considered, however, as only preliminary in nature. Further work is necessary to isolate the effects on the spectra of such factors as degree of uniformity of particle size, nature of the exchange ions, the role of various impurities, role of isomorphous replacement within the lattice, etc.

ANALYTICAL SUMMATION

From the foregoing, it appears that although no one method of analysis is diagnostic for all of the clay minerals the infrared technique shows considerable promise in this direction. For the present, however, one or more supplementary methods should be used to confirm the clay mineral identifications.

ANALYSES OF NATURAL CORES

Core Samples

The core samples from the Dominguez, Paloma, Rosecrans, and Northeast Coalinga Fields, all of which were taken with oil base drilling fluid, are listed and described in Table II. They were of the conventional type 2½ in. in diameter and cut away to approximately 2 in. diameter before disaggregation in order to remove possible drilling mud infiltration. The cleaned cores were reduced (but not pulverized) to grain size, leached in toluene, then dioxane and dried.

Fractionation Equipment and Procedure

The separation and fractionation procedure employed, aside from the type of equipment, was essentially that developed by Bray, Grim and Kerr[7] except that the separation process was made continuous. This change in operating procedure from batchwise to continuous separation of the clay from the non-clay components proved advantageous in that the yield of clay was greater and the time required to achieve maximum separation was materially shortened.

The isolation of the clay fractions involved two major steps.

1. Separation of the total clay component, and
2. Size-fractionation of the total clay component.

The arrangement of apparatus used to accomplish these steps is illustrated in Fig. 1. In Step 1 two kilograms of leached and disaggregated core was charged to a mechanically vibrated Lucite elutriator *A* containing three gallons of dilute aqueous ammonia, the vibrator-drive motor *G* was started, the Sharples Type 1A air-driven supercentrifuge was set at 40,000 rpm with Drag No. 3 (largest nozzle size: 1,200 ml per minute flow rate), valve *B* was opened and pump *E* was started. The float assembly *D* and constant flow rate regulator *F* ensured constancy of particle size range and enabled uninterrupted operation of the elutriator through the by-pass arrangement provided by *F*. After eight hours of continuous cycling the centrifuge bowl *C* was emptied of its clay content. The operation was continued for a period of several days until after the last eight-hour period the bowl was empty.

Step 2 was carried out by suspending the total clay component in three gallons of dilute ammonium hydroxide solution and passing it through the supercentrifuge at different flow rates and speeds of rotation. This step, of necessity, was not continuous and involved the use of only the centrifuge part of the separator assembly. To assure no loss of fine fraction the effluent from each run was re-used as suspension medium for the succeeding run. The conditions for the individual separations are described in the footnotes to Table IV.

RESULTS OF CORE ANALYSES AND DISCUSSION

The various fine fractions obtained from the cores were subjected to examination by X-ray diffraction, electron microscopy, infrared spectroscopy and in some cases, when the amount of material available permitted, to chemical and cation exchange analysis. The petrographic thin section analyses were performed on the unseparated cores (Table II). In general, the silt fraction varied from 2 to 10 per cent and the total colloid fraction from 0.1 to 2 per cent by weight of the air-dried cores.

Table II — Descriptions of Cores

Field	Zone	Age	Relative Sensitivity to Fresh Water	Carbonate Content, %	Resume of Petrographic Analysis (Compositional)
Dominguez	3	Pliocene	—	2.62	Ca. 60% feldspars, chiefly orthoclase, 25-30% quartz 10-15% muscovite, altered biotite and accessories; feldspar alterations very fine-grained may be mainly sericitic with lesser kaolin.
Dominguez	3	Pliocene	—	2.71	Similar to preceding; relatively large concentration of "heavy minerals" as hornblende, pyroxene, epidote, apatite, etc.
Paloma	Stevens	Upper Miocene	+	0.74	Mainly quartz, feldspars of sericitic alteration; fine-grained dust may be kaolinitic; biotite, chlorite.
Dominguez	Lower 7	Miocene	+	2.04	Ca. 30% quartz, 60% sericitically altered orthoclase, microcline, sodic plagioclase feldspars, kaolin (?); remainder is muscovite, biotite, apatite, zircon, etc.
Dominguez	Upper 8	Miocene	+	2.17	Mainly altered (to kaolin?) orthoclase or untwinned albite feldspars; remainder is quartz, chlorite, and sericitic muscovite.
Dominguez	8	Miocene	+		
Rosecrans	Odea	Miocene	+	0.29	Chiefly ca. equal amounts quartz and all types of fresh to highly altered feldspars yielding small crystals of indices both above and below balsam; identification indeterminate, may be montmorillonite, illite, sericite (fine-grained muscovite); ca. 5% biotite, and alterations tending to chlorite and iron oxides.
Rosecrans	Odea	Miocene	+	0.48	Similar to preceding.
N.E. Coalinga	Gatchell	Eocene	—	Nil	Ca. 60% quartz, 35% chiefly orthoclase and minor microcline and plagioclase feldspars; ca. 5% kaolinite or anauxite in aggregate grains of same dimensions as other clastic grains; traces chlorite, muscovite.
N.E. Coalinga	Gatchell	Eocene	—	Nil	Similar to preceding except that component believed to be kaolin is spread in patches of tiny micron-sized grains (pellets disaggregated in mounting?)

Table III — Preliminary Identification of Clays in Cores by X-ray Diffraction

Core		Size Fraction		
Field	Zone	40D2[c]	40D1[d]	E40D1[e]
Paloma	Stevens	"mont."[a,f] (ms)[h] quartz (s) feldspar (ms)	"mont." (s) quartz (m) feldspar (w)	"mont." (s) barite (ms)
Rosecrans	Odea	"mont." (vf) kaolin (s) (oriented)	"mont." (w) kaolin (ms) (oriented)	"mont." (m) kaolin (m) (oriented)
Dominguez	Third	"mont." (m) kaolin (w) quartz (f)	"mont." (w)	"mont." (m)
N.E. Coalinga	Gatchell	kaolin[g] (vvs)	kaolin (s) (oriented) "mont." (vvf)	b

[a] The quotation marks indicate merely that the observed lines are associated with the montmorillonite group of clay minerals and that identification of the particular member or members is uncertain.
[b] Insufficient sample for analysis.
[c, d, e] See corresponding footnotes to Table IV.
[f] Relative Order of "Montmorillonite" Content
40D2: Paloma > Dominguez > Rosecrans > N.E. Coalinga
40D1: Paloma > Dominguez = Rosecrans > N.E. Coalinga
E40D1: Paloma > Rosecrans > Dominguez.
[g] Visual comparison of the patterns for this core and kaolinite shows that they are exactly alike. Comparison with the anauxite pattern shows that some of the relative intensities of the lines differ but essentially the patterns are identical. It appears unlikely that, with our present technique, distinction between kaolinite and anauxite can be made with any degree of certainty.
[h] s = strong, m = medium, w = weak, f = faint, v = very.

In the interest of brevity only portions of the data obtained in the different examinations of the several cores are presented and discussed, since the primary purpose at this time is to indicate the efficacy of the combined usage of these methods. Toward this end, therefore, the main emphasis will be placed on the degree of correlation observed in the cases of the very differently water sensitive Paloma and Northeast Coalinga cores.[25]

A composite of the X-ray results in the preliminary identification of the clay minerals present in the colloid fractions of cores from each of the four fields studied is given in Table III. Table IV presents the cation exchange capacities of the sand, silt, and clay fractions for all of the cores. In the case of the Paloma and Northeast Coalinga cores direct comparisons of the X-ray diffraction patterns, electron micrographs, and infrared absorption spectra are given in Figs. 2, 3, and 4, respectively. The correlations of the fine fractions identifications for these cores obtained by the six different methods of analysis are given in Table V.

Examination of these data indicate the following:

1. The cation exchange capacities are generally proportional to the particle size. The exceptions may be caused by incomplete fractionation, error in the exchange capacity determination, or they may be real. The recent work of Johnson[18] which demonstrates that the lateral surface and exchange capacities for both montmorillonite and kaolin are inversely related makes the latter not likely. This conclusion is supported by the results of Grim and Bray[13] in their study of the base exchange capacity as a function of particle size for a wide range of clays. A plausible source of relatively high exchange capacity in the largest fractions may lie in the inability to separate from the unaltered feldspar component the diagenetically developed clay particles in which resides the exchange capacity. Further petrographic and supplementary work is necessary to clear up this point.

2. The exchange capacity data are inconclusive as regards correlation with susceptibility to fresh water damage. Thus, the Dominguez cores of both relatively high and low water sensitivity all have relatively higher exchange capacity clays than the more sensitive Paloma cores. This inconclusiveness, to some extent, may stem from the fact that the samples are not clays exclusively but contain minerals of low or zero base exchange capacity, as indicated by the X-ray results of Table III.

3. The X-ray data of Table III, with the possible exception of the Rosecrans core, indicate a possible connection between the amount of bentonitic clay present and water sensitivity. Perhaps a more important factor than the amount of potentially swellable clay present is the manner in which such a clay component is interlaminated with the non-swelling minerals in the reservoir matrix.[11]

4. The degree of certainty with which the clay minerals fractions of the Paloma and Northeast Coalinga cores can be identified (Table V) appears to be dependent on the extent of correlation among the different tests employed. Thus, for the Stevens Zone fractions the X-ray patterns show the presence of montmorillonite group mineral, the electron micrographs are also vague as to the precise nature of the "montmorillonite" mineral(s), the petrographic description of the unfractionated core appears to gain in diagnostic significance in connection with the next three methods.

The chemical analysis of nearly four per cent K_2O is consistent with the presence of either illite and a lesser amount of potash feldspar or montmorillonite and a larger amount of the feldspar component in admixture with quartz; similarly the presence of montmorillonite, unaltered feldspar and quartz or a relatively large amount of illite with respect to quartz and/or feldspar can explain the 37.7 milliequivalents per 100 grams of cation exchange capacity resident in the coarse colloid and increasing toward the fine colloid fraction; finally, the infrared spectrum (Fig. 4) seems to be diagnostic for illite in giving a pattern very nearly the same as the pattern for the Grundy County, Illinois, illite of known structure and properties.

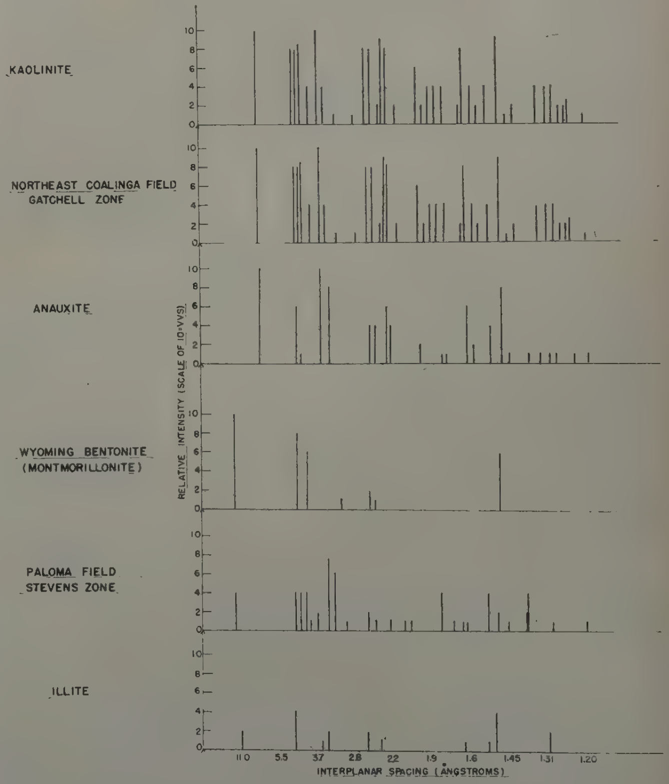

FIG. 2 — COMPARISON OF X-RAY DIFFRACTION PATTERNS OF CORE CLAYS AND CLAY MINERAL STANDARDS.

In the case of the Gatchell Sand the problem of identification is simpler beginning with any one of the six methods; the task in each case is to determine whether the kaolin is predominantly nearer in composition to kaolinite or anauxite (the other kaolin minerals dickite and nacrite have not yet been considered.) The X-ray patterns clearly identify the material as kaolin; the electron micrograph of the 9D3 silt fraction definitely indicates kaolinite but the micrograph of the 40D2 coarse colloid fraction is less diagnostic in that the very small particle size makes more difficult the differentiation between kaolinite and anauxite; chemical analysis based on the silica: alumina ratio of 2.7 indicates that the silt fraction in overall composition may approach anauxite with its theoretical silica: alumina mole ratio of 3; the cation exchange analysis correlates well with the known values for kaolin minerals and, finally, as in the case of the Stevens Zone fractions the infrared spectrum of the coarse colloid fraction indicates that the main component present, at least in this fraction, may be anauxite and not kaolinite (Fig. 4).

CONCLUSIONS

From the data and discussion, it is concluded that, for the particular cases of the Stevens Zone and Gatchell Sand cores, the clay minerals identifications are in harmony with the observed sensitivity of these strata to fresh water; *viz.*, the predominance of illite and/or "montmorillonite" in the Stevens Zone core is consistent with susceptibility to damage by fresh water; likewise, the predominance of kaolin as kaolinite, anauxite or both is in accord with the relative immunity of the Gatchell Sand to such damage.

ACKNOWLEDGMENT

The authors wish to thank the many members of the Research Department of the Union Oil Co. of California whose combined efforts aided in obtaining these results.

It is a pleasure, too, to record the contribution of Professor Ian Campbell of California Institute of Technology who performed the petrographic analyses and otherwise gave freely of his expert opinion. Finally, the authors wish to thank the Management of Union Oil Co. of California for permission to publish this paper.

Table IV — Cation Exchange Capacities[a] of Sand, Silt, and Clay Fractions of Selected California Cores

Core		Size Fraction					
Field	Zone	140-270 Mesh	<270 Mesh	Silt (9D3)[b]	Coarse Colloid (40D2)[c]	Fine Colloid (40D1)[d]	Superfine Colloid (E40D1)[e]
Dominguez	3	6.6	8.1	23.1	58.9	115	
Dominguez	3	6.8	10.0		53.5	106	
Paloma	Stevens	2.9	3.6	16.4	37.7	68.5	
Dominguez	Lower 7	3.7	6.7	26.6	95.0	53.9	43.0
Dominguez	Upper 8	9.1	17.2	24.2	65.3	102	
Dominguez[f]	8				97.1	50.9	
Dominguez[g]	8				73.5	105	103
Dominguez[h]	8	9.8	7.2	45.3	52.3	82.0	113
Rosecrans	Odea	9.4	8.0	21.2	56.7	96.5	
Rosecrans	Odea	9.9	15.3	29.5	40.2	(114)[i]	(65)[i]
N.E. Coalinga	Gatchell	5.1	3.4	2.4	16.6		38.5
N.E. Coalinga	Gatchell	3.0	5.0	2.2	12.1		

[a] The cation exchange capacity is expressed as milliequivalents per 100 grams.

[b] Fraction sedimented in bowl of 4.45 cm ID and 19.76 cm in length at 9,000 rpm using Drag No. 3 (flow rate of approximately 1,200 ml per minute).

[c] Same as (b), with Drag No. 2 but at 40,000 rpm and flow rate of 725 ml per minute.

[d] Same as (c), with Drag No. 1 but at flow rate of 138 ml per minute.

[e] Fraction recovered from effluent of 40D1.

[f] Core dispersed in distilled water without prior chemical treatment.

[g] Same core as (f) treated with 1N acetic acid and 1N ammonium acetate prior to dispersion in dilute aqueous ammonia.

[h] Same core as (f) dispersed in dilute aqueous ammonia without prior chemical treatment.

[i] Result is in doubt because sample could not be ground satisfactorily.

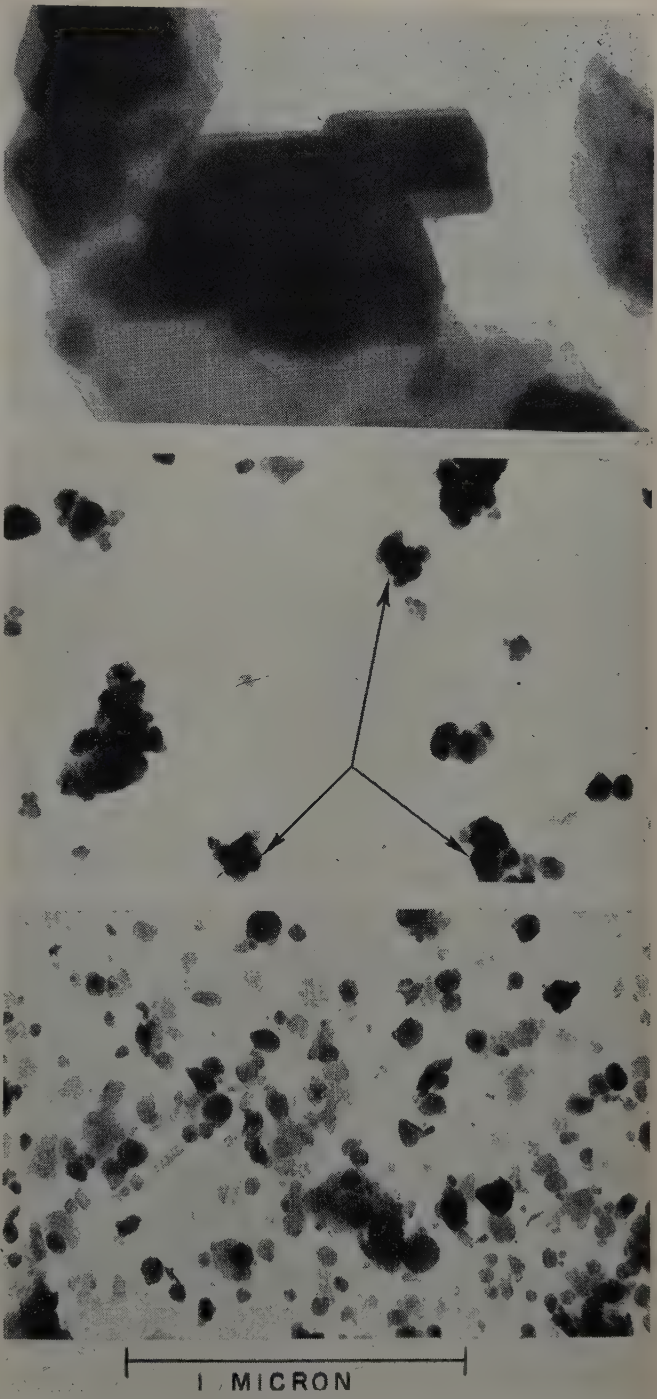

FIG. 3 — ELECTRON MICROGRAPHS OF CORE CLAYS. MAGNIFICATION X45,000. TOP — NORTHEAST COALINGA FIELD, GATCHELL ZONE, SILT FRACTION. CENTER — NORTHEAST COALINGA FIELD, GATCHELL ZONE, COARSE COLLOID FRACTION. BOTTOM — PALOMA FIELD, STEVENS ZONE, SUPERFINE COLLOID FRACTION.

REFERENCES

1. API and American Gas Association: "Reports on Proved Reserves of Crude Oil, Natural Gas Liquids, and Natural Gas," (December 31, 1949), 4.
2. Bates, T. F., Gruver, R. M., and Yuster, S. T.: *Producers Monthly*, (1946), 10, No. 10, 16-19.
3. Bower, C. A., and Truog, E.: *Ind. Eng. Chem.* Anal. Ed., (1940), 12, 411-413.
4. Bray, R. H.: "Base Exchange Procedures," Department of Agronomy, Agriculture Experiment Station, University of

Illinois, College of Agriculture, Urbana, Ill., (January, 1942).

5. Buswell, A. M., Krebs, K., and Rodebush, W. M.: *J. Am. Chem. Soc.*, (1937), **59,** 2603.
6. Buswell, A. M., and Dudenbostel, B. F.: *J. Am. Chem. Soc.*, (1941), **63,** 2554-58.
7. Bray, R. H., Grim, R. E., and Kerr, P. F.: *Bull. Geol. Soc. Amer.*, (1935), **46,** 1909-26.
8. Case, L. G.: *Bull.* AAPG, (1933), **17,** 66-79.
9. Davis, D. W., Rochow, T. G., Rowe, F. G., Fuller, M. L., Kerr, P. F., and Hamilton, P. K.: Preliminary Report No. 6, API Project 49, Columbia University, New York (1949).
10. Grim, R. E.: *Recent Marine Sediments,* (AAPG Symposium, 1939), 466-95.
11. Grim, R. E.: *Bull.* AAPG, (1947), **31,** 1491-99.
12. Grim, R. E., Dietz, R. S., and Bradley, W. F.: *Geol. Soc. Am. Bull.*, (1949), **60,** 1785-1808.
13. Grim, R. E., and Bray, R. H.: *J. Am. Ceram. Soc.*, (1936), **19,** 307-15.
14. Grim, R. E., Bray, R. H., and Bradley, W. F.: *Am. Mineral,* (1937), **22,** 813-29.
15. Grim, R. E.: *J. Geol.*, (1942), **50,** 225-75.
16. Hughes, R. V.: *Producers Monthly,* (1947), **11,** No. 4, 13-16; No. 5, 12-14; No. 6, 10-17.
17. Hunt, J. M., Wisherd, M. P., and Bonham, L. C.: *Anal.* Chem., (1950), **22,** 1478-98.
18. Johnson, A. L.: *J. Am. Ceram. Soc.*, (1949), **32,** 210-14.
19. Kinsinger, W. G., Hillier, J., Picard, R. G., and Zieler, H. W.: *J. Applied Physics,* (1946), **17,** 989.
20. Kerr, P. F., and collaborators: Series of six Preliminary Reports on API Project 49, Clay Mineral Standards, Columbia University, New York (1949 and 1950).
21. Keller, W. D., and Pickett, E. E.: *Am. J. Sci.*, (1950), **248,** 264-73.
22. Pettijohn, F. J.: *Sedimentary Rocks,* Harper and Brothers, New York, (1949), 16.
23. Ross, C. S., and Hendricks, S. B.: U. S. Geol. Prof. Paper 205-B, (1945), 23-79.
24. Report of California Conservation Committee of California Oil Producers (1949).
25. Sherborne, J. E., and Fischer, P. W.: *World Oil,* (1949), **129,** No. 7, 112-26.
26. Taylor, E. M.: *Jour. Inst. Petr. Tech.*, (1930), **16,** 681-85.

Table V—Correlation of Fine Fractions Identifications for Cores from Stevens Zone and Gatchell Sand

Method	Stevens Zone	Gatchell Sand
X-Ray Diffraction	40D2[c]: "montmorillonite" (ms) E40D1[c]: "montmorillonite" (s)	40D2: kaolin (vvs) 40D1: kaolin (s)
Electron Microscope	40D2: "montmorillonite" (illite?) E40D1: "montmorillonite" (illite?)	9D3[b]: kaolinite 40D2: kaolinite, anauxite
Petrographic	(on unfractionated core) mainly feldspars of sericitic alteration; to (illite?)	(on unfractionated core): kaolinite or anauxite
Chemical Analysis	40D2: 3.9% K_20[a] (from illite and/or potash feldspar?)	9D3: $SiO_2/Al_2O^3=2.7$ (anauxite?)
Cation Exchange	40D2: 37.7 m.e./100 gm. 40D1: 68.5 m.e./100 gm. Montmorillonite	9D3: 2.4 m.e./100 gm. (kaolin) 40D2: 16.6 m.e./100 gm. (kaolin)
Infrared	40D2: mainly illite	40D2: mainly anauxite

[a] By emission spectrographic densitometric comparison with the North Carolina muscovite and the two illites from Goose Lake and Fithian, Ill., described in Table I.

(b), (c) See Corresponding footnotes to Table IV.

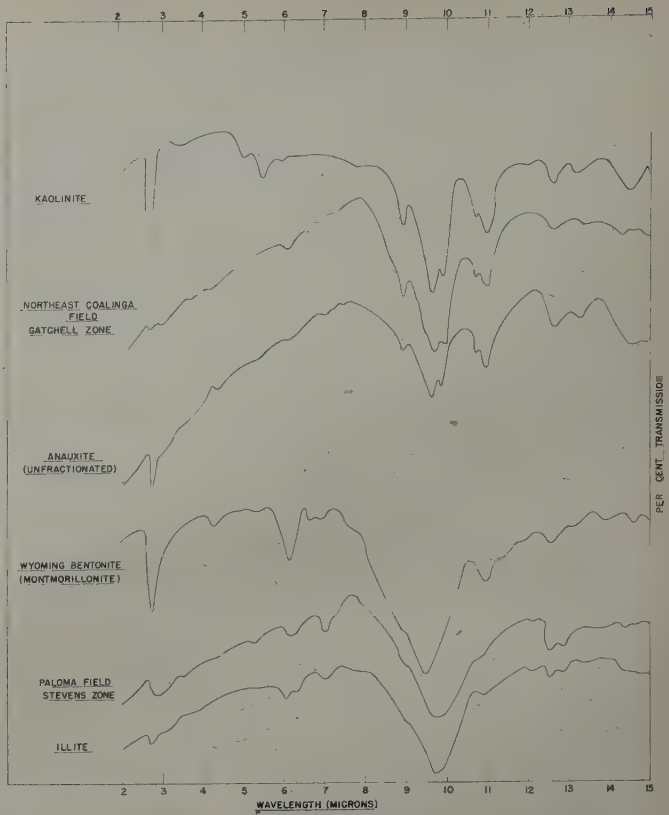

FIG. 4 — COMPARISON OF INFRARED SPECTRA OF CORE CLAYS AND CLAY MINERAL STANDARDS.

27. Zworykin, V. K., Morton, G. A., Ramberg, E. G., Hillier, J., and Vance, A. W.: *Electron Optics and the Electron Microscope,* New York, John Wiley and Sons, (1945), 281-337.

DISCUSSION

By W. T. Cardwell, Jr., Member AIME, California Research Corp., La Habra, Calif.

Among papers pertaining to this subject, the present paper is outstanding for its large amount of firsthand experimental information and its small amount of unsupported speculation.

It is especially noticeable that the authors have refrained from statements regarding the mechanism of formation damage by fresh water. They are evidently dissatisfied with the mere recitation that clays swell up and block pores. They state that "perhaps a more important factor than the amount of potentially swellable clay present is the manner in which such a clay component is interlaminated with the non-swelling minerals in the reservoir matrix."

I believe that the authors would agree that none of the analytical methods they have used tells whether a clay is a highly swelling clay. The identification of a clay as a member of the montmorillonite group is necessary, but not sufficient, because there are poorly swelling montmorillonites.

I should like to ask if the authors considered the performance of swelling tests on the fine fractions from the Stevens and Gatchell zones.

AUTHORS' REPLY TO MR. CARDWELL

The authors did consider the importance of determining the swelling characteristics of the fine fractions and believe that such data, were it available, would aid in study of the mechanism of formation damage by fresh water. Admittedly this study of swelling is one of many possible directions in which to continue the program as outlined in our paper. ★ ★

PLASTIC FLOW PROPERTIES OF DRILLING FLUIDS— MEASUREMENT AND APPLICATION

J. C. MELROSE AND **W. B. LILIENTHAL,** MAGNOLIA PETROLEUM CO., DALLAS, TEX.

ABSTRACT

The application of Bingham's law to the behavior of drilling fluids in a rotational viscometer permits the expression of viscometric data in terms of plastic viscosity and yield value, the flow properties of a plastic fluid. A commercially available rotational viscometer is described, and when modified to a multispeed type viscometer, is shown to provide a simple and convenient instrument for the measurement of these properties both in the laboratory and in the field. The data obtained are shown to be useful in defining and understanding mud control problems relating to chemical treatment and to the hydrodynamic behavior of muds.

INTRODUCTION

The highly complex drilling fluids which are required for deep drilling often give rise to new and unusual mud control problems. Rapid and economic solutions to these problems may require, on the one hand, better understanding of the changes which contaminants and chemical treating agents produce in the colloidal and inert solids of the mud, or, on the other hand, closer control of the hydrodynamic behavior of the mud. The latter objective obviously can be achieved only if a correct rheological analysis of the flow behavior of drilling muds is available and if this is accompanied by the appropriate rheological measurements. The purpose of this paper is to describe such measurements in the field, and to show how the resulting data can be of value in solving difficult mud control problems.

It is now generally recognized that Bingham's law of plastic flow can be utilized in describing the hydrodynamic behavior of drilling fluids in the non-turbulent flow range. Beck, Nuss, and Dunn[1] have recently applied this law to the flow of mud in small pipes, and Rogers[2] has reviewed the rather extensive literature on this subject. So far, however, the use of Bingham's law has been restricted to the analysis of mud flow in pipes or capillary tubes, and it has not been directly applied to the flow in rotational viscometers. In the work to be reported, the Reiner-Riwlin[3] equation for the flow of a plastic fluid in a rotational viscometer has been utilized to permit the expression of multispeed viscometric data in terms of plastic viscosity and yield value, the two absolute flow properties of a plastic fluid.

With regard to the application of these measurements, the calculation of the relationship between pumping rate and pressure drop, both in the drill pipe and annular space, has long been a subject of interest. Beck, Nuss, and Dunn,[1] following Caldwell and Babbitt,[4] base their calculations for non-turbulent flow on Buckingham's integration of Bingham's law for pipe flow and measurements of the plastic viscosity (rigidity in their terminology) and yield value. In the case of turbulent flow, Fanning's equation is employed, and the pressure drop is relatively insensitive to the flow properties of the mud. Since flow in the drill pipe is likely to be turbulent at usual circulation rates, the plastic flow properties will chiefly influence the pressure drop in the annular space. As pointed out by Beck,[1] the control of this component of the total pressure drop may be of special importance where lost circulation problems are encountered. Other hydrodynamic problems to which it should be possible to apply measurements of the plastic flow properties include predictions of the velocity distribution in non-turbulent flow and the critical velocity for transition to turbulence.

Plastic viscosity and yield value, as absolute flow properties, will reflect the colloidal or surface-active behavior of the solids present in drilling fluids. Measurements of these properties should therefore find application in developing a better understanding of such behavior and in characterizing the type and condition of these solids. Garrison and ten Brink[5] have utilized multispeed viscometric data in this manner, although their measurements were not expressed in terms of the absolute flow properties.

In connection with the application of these measurements, it should be recognized that the presently used one-point viscosity measurements are relative in nature. The API Stormer 600-rpm measurement, for example, is a function of both plastic viscosity and yield value, as well as mud weight, and will often be misleading when its application to mud control problems is attempted.

NOMENCLATURE, UNITS, AND DEFINITIONS

In Fig. 1 an idealized plot is given of the flow variables involved in any viscometric measurement. It is seen that the flow behavior of plastic fluids is characterized by two constants — plastic viscosity, μ_p, and yield value, ϕ. Other workers have used the term rigidity for plastic viscosity or the term mobility for its reciprocal. The term plastic viscosity, however, emphasizes the close relation this property bears to the viscosity of a true fluid and is expressed in the familiar viscosity units of centipoises. The yield value is expressed in lbs/100 sq ft, the units adopted for gel strength measurements with the API shearometer.

Definitions of these properties based on rheological or macroscopic flow considerations follow from Fig. 1. The plastic viscosity of a substance obeying Bingham's equation is defined

---

[1] References given at end of paper.

Manuscript received in the office of the Petroleum Branch Aug. 12, 1950. Paper presented at the Petroleum Branch Fall Meeting in New Orleans, La., Oct. 4-6, 1950.

as the constant ratio of a given change in the shearing stress to the corresponding change in the rate of shear when the body is undergoing permanent deformation or flow. This same definition applies also to the viscosity of a true or Newtonian fluid. The yield value of a plastic substance may be defined as the difference between the shearing stress and the product of the plastic viscosity and rate of shear. If Bingham's law is obeyed at very low rates of shear, the yield value is also the shearing stress which must be exceeded for permanent deformation or flow to take place.

PLASTIC FLOW, PLUG FLOW AND THIXOTROPY

Several aspects of the plastic flow of drilling fluids deserve comment before proceeding to a description of the instrument used in the present work. First, at some low rotor speed (usually below 100 rpm in any practical viscometer), a curvature toward the origin will occur in the linear relationship between rotor speed and stator torque (see Fig. 1). This curvature, often referred to as the plug flow region, has been shown by Reiner and Riwlin,[3] in the case of a fluid obeying Bingham's equation, to begin when the yield value exceeds the shearing stress at the wall of the outer cylinder of a rotational viscometer. Thus, the phenomenon of plug flow is characteristic of and not a deviation from the behavior of a "Bingham body." It should be stated, however, that deviations from Bingham's law are to be expected in this low shear rate range in the case of systems, such as most drilling muds, which show highly time-dependent gel strength properties.

The existence of such time effects, generally referred to as thixotropy, introduces the second complication encountered in observations of the laminar flow behavior of drilling muds. Several workers[6] have proposed the use of "hysteresis loop" and "thixotropic level" concepts to characterize systems showing such effects. It has been observed by the authors, however, particularly in the case of highly chemically treated field muds, that equilibrium torque readings with a rotational viscometer may be reached in a matter of a few minutes, provided that each such reading is preceded by an equilibrium at a higher rotor speed. (At a constant rotor speed the torque will then increase toward the equilibrium value; the opposite occurs if the reading is preceded by an equilibrium at a lower speed, and somewhat longer times are involved). These observations indicate that the mud flow in field systems, in situations where a simple laminar type of flow is expected to prevail, may be very nearly at a steady state, as defined by equilibrium torque readings.

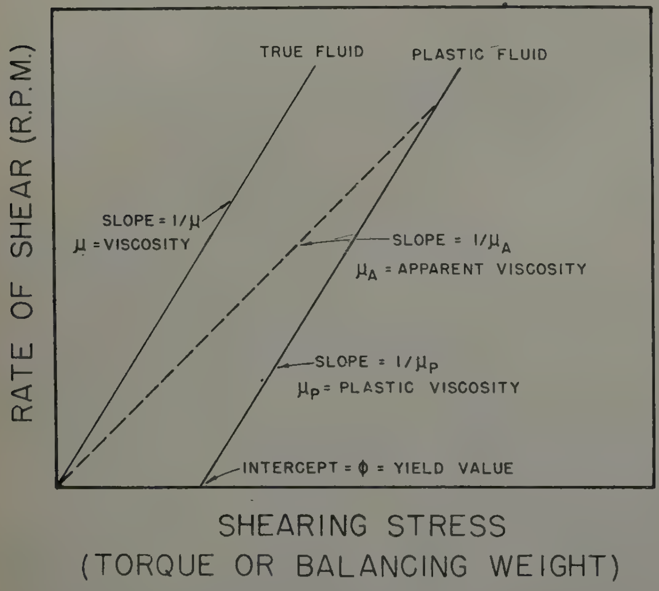

FIG. 1 — FLOW DIAGRAM FOR PLASTIC FLUIDS.

If characterization of the "thixotropic property" of the mud is desired, it is felt that this may be furnished by measurements of the increase in gel strength with increasing periods of rest time. Some of the complications which arise in obtaining such measurements have been discussed by Cardwell.[7] Slippage, probably caused by syneresis, may also be a serious problem when rest times of the order of 30 minutes or longer are involved. The authors believe that the usual techniques for avoiding these difficulties cannot be easily applied to instruments suitable for field measurement of the plastic flow properties defined above and that gel strength data can best be obtained with an instrument designed specifically for such measurements. Mud problems which require this type of rheological analysis include the prediction of bottom hole pressure surges developed by up and down swabbing and when breaking circulation, as well as the prediction of the ability of the mud to suspend cuttings on shutdown.

INSTRUMENT DEVELOPMENT

In plotting data obtained with a rotational viscometer according to the scheme of Fig. 1, *i.e.*, viscometer rotor speed (rate of shear) versus the torque on the stator (shearing stress), a straight line will result for a plastic and thixotropic fluid if two requirements are met: first, that the viscometer be run long enough at each speed to reach an equilibrium torque reading; and second, that the design of the viscometer rotor and stator be such that a strictly linear calibration relationship results, *i.e.*, kinetic energy and end effects are absent. (These effects also introduce a density dependence, as in the Stormer viscometer).

In addition to giving a straight-line plot of the observed data, a suitable viscometer should possess sufficient compactness, ruggedness, and simplicity of operation for use in the field as well as in the laboratory. Precision and reproducibility should be of the order of ±2 per cent.

A survey of rotational viscometers which were available commercially revealed that none of them completely filled the requirements set forth above. Experimentation with the Stormer viscometer, the rotational viscometer most commonly used in oil field work, indicated that it was unsatisfactory for adaptation to such purposes. One commercially available viscometer, the Fann V-G Meter,* met all of the desired requirements with the exception of the multispeed feature, so it was decided to alter this instrument accordingly. This viscometer, employing a motor-driven outer cylinder turning around a stator that could be balanced to a null point by means of suspended weights, had a number of very desirable features: compactness, a rugged bearing system, a 6-volt d.c. motor for use with an automobile storage battery, and a suitable rotor and stator design.

The multispeed control feature was obtained by substitution of a variable speed type CRX governor unit, made by the Lee Engineering and Manufacturing Co., Milwaukee, Wis., for the constant-speed governor supplied with the motor. It was necessary to lengthen the motor housing by about two inches in order to install a manually set cam-driven push-rod control for the governor. By adjustment of this mechanism, rotational speeds of approximately 600, 500, 400, 300, and 200 rpm could be set, maintained, and duplicated.

---

*Manufactured by the Geophysical Machine Works, Houston, Tex.

Fig. 2 is a photograph of the instrument with the rotor partially immersed in a water-jacketed sample container. The disassembled stator and rotor are shown at the side of the instrument. A high speed switch on the left side of the gear housing operates a governor release mechanism, making available a top, uncontrolled speed of about 1,100 rpm. In order to obtain equilibrium torque readings, the mud sample is first sheared at this speed for about a minute, after which torque readings can be made at successively lower speeds. Usually, when making such a "down curve," the equilibrium torque will be reached in about the length of time required for adjusting the balancing weight.

CALIBRATION AND REPRODUCIBILITY

The calibration of a multispeed rotational viscometer for use with plastic fluids can best be accomplished with a series of true fluids of known viscosities. The test fluids used in calibrating the viscometer described above were glycerol-water solutions, the viscosities of which had been determined with Fenske-Ostwald capillary viscometers. A linear calibration relationship was found, indicating that kinetic energy and end effects were negligible as desired. This relationship is described by the equation:

$$\mu = \frac{AG}{Z} \qquad (1)$$

where

μ = viscosity, centipoises
G = balancing weight (torque), gms
Z = rotor speed, rpm
A = calibration constant

The constant A determined from the calibration data may be compared with a theoretical value calculated from the dimensions of the viscometer by means of the Couette-Margules equation.

In the case of plastic flow the above variables are related by the equation:

$$\mu_p = \frac{AG - B\phi}{Z} \qquad (2)$$

Since calibration fluids for plastic flow do not exist, the constant B must be determined from the little-known equation of Reiner and Riwlins[3] for the flow of a plastic fluid in a rotational viscometer, which gives

$$B = \frac{(100)\ (30/\pi)\ ln\ (r_c/r_b)}{(0.20886)} \qquad (3)$$

where

r_c = radius of outer cylinder, cm
r_b = radius of inner cylinder, cm
$30/\pi$ = factor for converting from rad/sec to rpm
100 = factor for converting from poises to cp
0.20886 = factor for converting from dynes/cm^2 to lbs/100 sq ft

Equation (2) may conveniently be applied to the calculation of plastic viscosity and yield value from experimental data on drilling fluids if the data are plotted as in Fig. 1. Denoting the intercept on the balancing weight (torque) axis, where $Z = 0$, as G_o, and the weight reading at the highest speed available as G_{max}, Equation (2) may be solved as follows:

$$\mu_p = k_1(G_{max} - G_o) \qquad (4)$$

$$\phi = k_2\ G_o \qquad (5)$$

where

$k_1 = A/Z_{max}$
$k_2 = A/B$

The accuracy of the calibration constant A determin described was ±1 per cent. In the case of routine meaments of mud, employing a procedure suitable for use in the field, there are two main factors other than the previous history of the sample which affect the reproducibility of results with a given instrument. The first is the technique of the operator, and the second is the judgment employed in drawing a straight line through the data on the rpm versus balancing weight plot. With reference to the first factor influencing reproducibility, tests were made on a series of 26 widely different laboratory-prepared muds, data on each mud being obtained independently by two or three operators. Results from these tests gave an average deviation from the mean of the two or three observations of about ±3 per cent for both plastic viscosity and yield value. Deviations resulting from different individuals plotting the data amounted to approximately 2 per cent for the plastic viscosity and 5 per cent for the yield value.

Deviations from linearity in the rpm versus balancing weight plot, *i.e.*, from ideal plastic flow at the rates of shear used, have been within the indicated accuracy of the method except in cases where solids are settling rapidly in the sample. However, in this event, valid viscosity measurements are impossible to make with any type of rotational viscometer.

EXPERIMENTAL RESULTS

In order to show how measurements of the plastic flow properties of muds, as obtained with the multispeed viscometer, may be utilized, the results of several laboratory investigations will be presented. The first investigation was carried out for the purpose of establishing relationships between the multispeed viscometric measurements and those now in com-

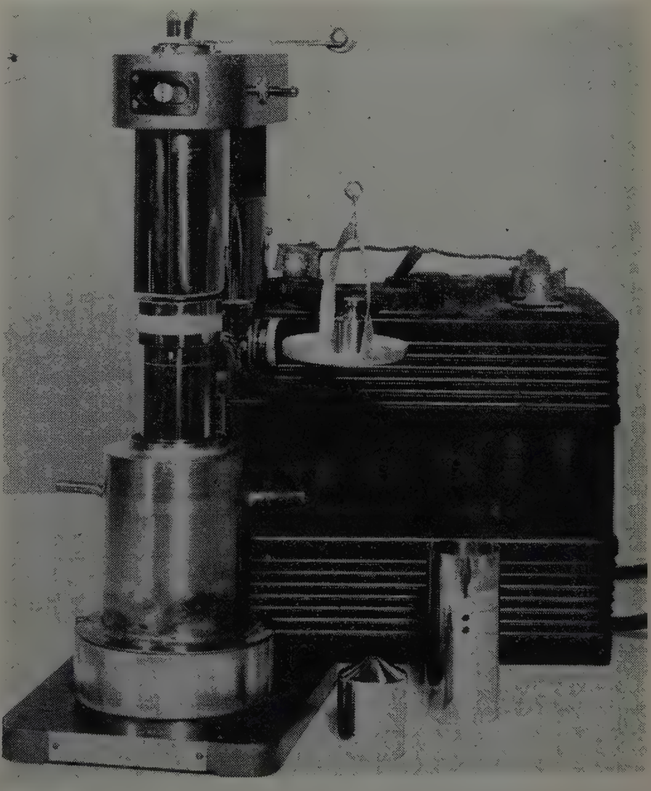

FIG. 2 — MULTISPEED VISCOMETER, FIELD MODEL.

mon usage, while the second was concerned with the response of the plastic flow properties to chemical treatment.

Relationships with Stormer Viscosity And Gel Measurements

Twenty-six muds prepared in the laboratory, and representing a variety of mud systems, were used in the first investigation. During the preparation and testing of each mud, special efforts were made to insure identical handling and measuring procedures, in order to minimize any variations which might be due to such factors; each measurement was checked by two or three operators. The correlations which were found between the various viscometric measurements are shown in Figs. 3, 4, and 5.

In the case of the correlation of the Stormer viscosity with the plastic flow properties (Fig. 3) and the Stormer-multispeed viscometer initial gel correlation (Fig. 4), straight-line relationships were found. As indicated in Figs. 3 and 4, these relationships are not greatly dependent on the mud system, except for the case of the salt-contaminated mud. The correlations of the initial and ten-minute gels and the initial shear strength with the yield value, on the other hand, resulted in power functions, which were affected by the type of mud system. The actual data are not shown in Fig. 5, since the average deviation from the plotted lines was of the order of 25 per cent.

Chemical Treatment Studies

In the investigation of the effect of chemical treatment on the plastic flow properties, a bentonite-kaolinite base mud containing about 30 weight per cent solids was prepared and treated with various quantities of quebracho, Calgon, and sodium acid pyrophosphate. Fig. 6 shows the effect of added quebracho on plastic viscosity, yield value, and Stormer viscosity. Similar curves were obtained for the phosphate treatments. It is seen that "viscosity reduction" by chemical treatment is accomplished entirely by a reduction in the yield value, while the plastic viscosity actually increases somewhat.

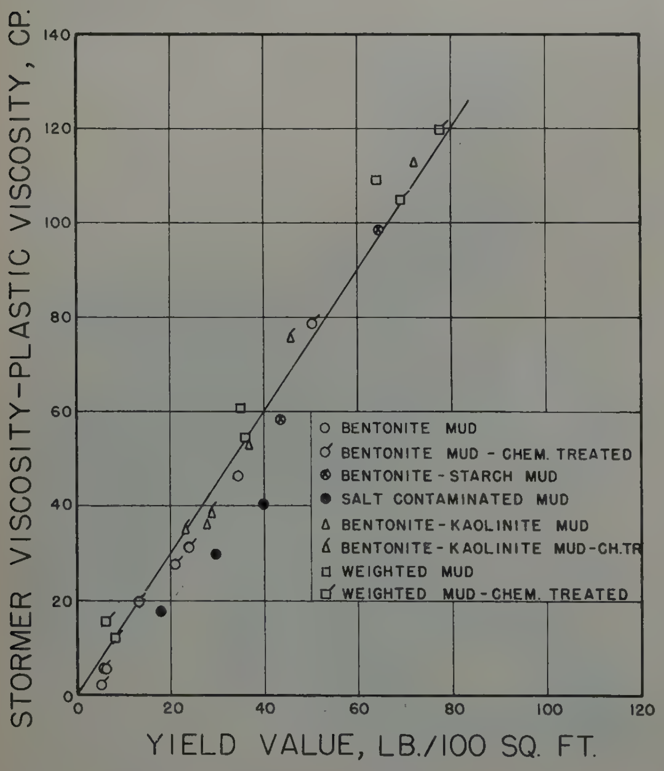

FIG. 3 — CORRELATION OF STORMER VISCOSITY WITH PLASTIC FLOW PROPERTIES.

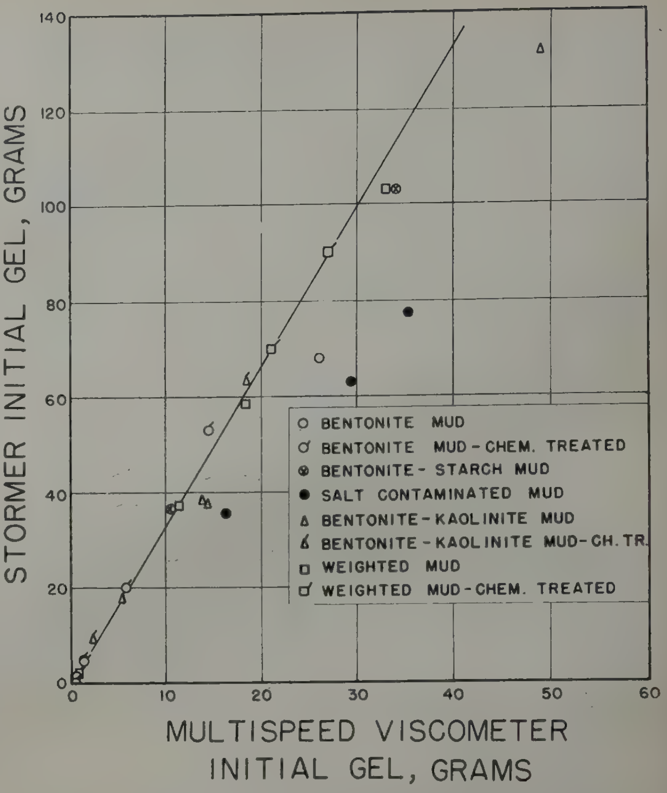

FIG. 4 — CORRELATION OF INITIAL GELS.

Since the plastic viscosity of a mud is not reduced by chemical treatment, the higher the plastic viscosity/yield value ratio, the less is the susceptibility of the mud to chemical treatment. This concept is illustrated in Fig. 7, in which plastic viscosity is plotted against the yield value for a large number of muds which are available in the laboratory. The compositions of these muds fall into four groups, which may be described as follows:

(1) high-solids muds including bentonite-kaolinite systems, native clays, and salt-water clays

(2) bentonite-water muds

(3) high-solids muds containing three per cent bentonite and varying percentages of Gulf Coast shale

(4) alkaline-tannate-lime muds, representing samples over the entire mud weight range from 9.0 lb/gal (67.2 lb/cu ft) laboratory-prepared muds to 18 lb/gal (134.4 lb/cu ft) field muds. While some were starch muds, all had been treated with caustic soda, quebracho, and lime.

From Fig. 7 it may be seen that these groups give a family of curves corresponding to different susceptibilities to chemical treatment, as defined above.

DISCUSSION AND INTERPRETATION OF RESULTS

Correlation with Stormer Measurements

It is well known that any single point viscosity measurement on a plastic fluid, such as the Stormer 600-rpm reading, is actually an apparent viscosity, *i.e.*, a value equivalent to the viscosity of a true or non-plastic fluid giving the same observed stress reading as the plastic fluid at the particular rate of shear chosen (see Fig. 1). Thus, Equations (1) and (2) may be combined to define such an apparent viscosity, μ_a, in terms of the plastic flow properties:

$$\mu_a = \mu_p + (B/Z)\,\phi \qquad (6)$$

This equation also shows that the apparent viscosity varies linearly with the reciprocal of the rotor speed, Z, as is illustrated by the data of Garrison and ten Brink[5] and Bednarski.[8] Where the apparent viscosity versus reciprocal rpm plots given by these workers are linear, it is indicated that the muds investigated obeyed the law of plastic flow.

The correlation of the Stormer viscosity, μ_s, with the plastic flow properties is shown in Fig. 3 to be of the form predicted by Equation (6) when μ_s is substituted for the apparent viscosity. The deviations of the data from a single relationship are smaller than would be expected from a consideration of the peculiarities of the Stormer design, such as a considerable density dependence due to kinetic energy and end effects and the opportunity for the existence of a non-flowing plug inside the rotor.

In the case of the Stormer-multispeed viscometer initial gel correlation (Fig. 4), a correlation of the expected form was also found. The proportionality factor was close to that calculated from the respective viscometer dimensions. The correlations of Figs. 3 and 4 may be used where approximate conversions from multispeed viscometer data to Stormer data are required.

The reason for the power functions obtained for the correlations of Fig. 5 is not known. When the Stormer initial gel strength values are converted to the units of lbs/100 sq ft, the data of Fig. 5 show that the initial gel strength and initial shearometer reading are both less than the yield value, all three measurements being expressed in the same units. This confirms previous reports[7] that at very low rates of shear Bingham's law is no longer followed. It is felt, however, that this fact does not constitute a limitation of the usefulness of measurements of the plastic flow properties with regard to those applications which were mentioned above, since the yield value measured by the present method, together with the plastic viscosity, determines the relationship between the rate of shear and shearing stress throughout most of the range of laminar flow.

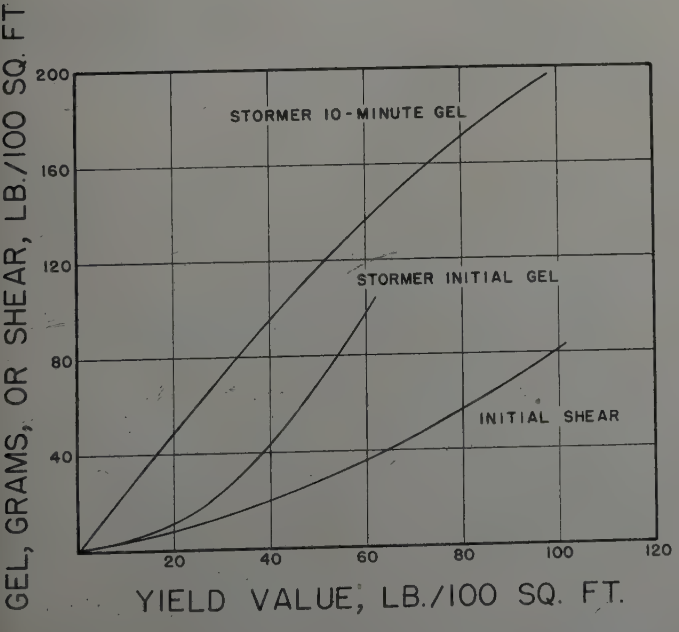

FIG. 5 — CORRELATION OF INITIAL AND 10-MINUTE GELS WITH YIELD VALUE.

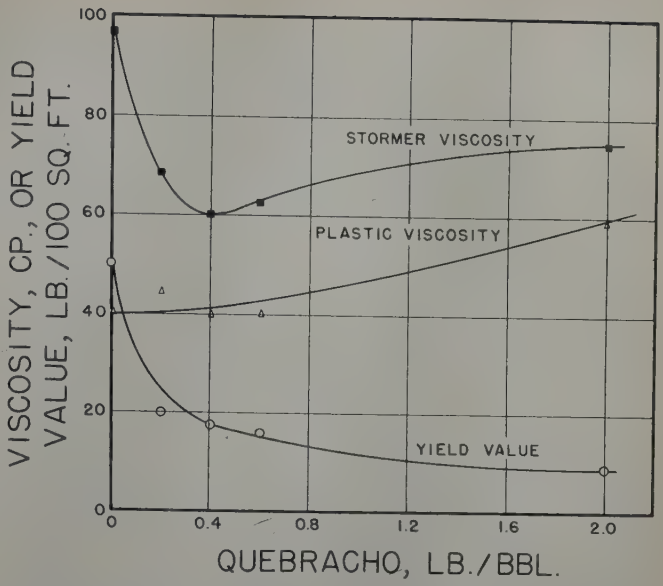

FIG. 6 — EFFECT OF QUEBRACHO TREATMENT ON BENTONITE-KAOLINITE MUD.

Application to Chemical Treatment

In developing explanations for the changes in plastic viscosity and yield value with addition of deflocculating agents, it is helpful to give a partial and limited interpretation of these two viscometric properties in terms of the colloidal or sub-microscopic structure of drilling muds. From the purely rheological definitions of these properties given above, it may be seen that in the case of a plastic fluid such as a drilling mud the frictional resistance to flow, measured by the shearing stress or viscometer torque reading, is composed of two parts (see Fig. 1). The first is proportional to the rate of shear and thus is largely the resistance to flow due to the mechanical friction of the particles.

Since the plastic viscosity is a measure of this proportionality, this property will be a function of solids concentration and shape, as predicted by an extension of Einstein's equation for the hydro-dynamic interaction effects of dispersed solids on the viscosity of a suspension.[9] If the particles carry an electric charge, the plastic viscosity might also be expected to increase with decreasing particle size, as described by Smoluchowski's modification of Einstein's equation. Since the action of deflocculating agents or "viscosity reducing" chemicals should not produce more symmetrical or larger particles, but rather the opposite, it would be expected that reduction of the plastic viscosity by such treatment would be difficult if not impossible. The observed increase in plastic viscosity (Fig. 6), on the other hand, can be explained as the result of dispersion of clay aggregates in the mud.

The second type of resistance to flow is independent of the shear rate and is due to the "gel forces" acting between the particles of the suspension. It is believed that both attractive and repulsive forces are operative, the latter originating primarily from the electrical charge carried by the particles. This component of the total resistance to flow is measured by the yield value, which may then be expected to be a function of the concentration of the mud solids and those factors, such as surface charge and potential, which affect the interparticle forces. Since deflocculating agents are thought to adsorb on the solid particles, thus altering the chemical nature of their surfaces and affecting the interparticle forces, the "viscosity reduction" due to such chemical agents should be almost entirely the result of a decrease in the yield value, as is observed.

Application to Pressure Drop Calculations

One of the primary aims of chemical treatment of muds is, of course, to control the hydrodynamic behavior upon which several of the most important functions of muds are based. In this connection the plastic flow properties measured as described above may be used to predict pressure drops in certain cases of laminar flow. It should be noted that the Buckingham equation for pipe flow cannot be used to describe flow in an annulus, even if the equivalent diameter (four times the hydraulic radius) is substituted for the pipe diameter.[10] Drill pipe rotation will obviously cause further complications in the case of flow in a well annulus.

Another factor which is often overlooked is that if the temperature of the mud sample at the time of measurement is considerably different from average well conditions, corrections for the effect of temperature on the plastic flow properties should be made. In the case of water-base muds, the magnitude of the correction for the plastic viscosity may be estimated from the effect of temperature on the viscosity of water. Such a consideration indicates that for a difference of 80°F between the average well temperature and the temperature at which the mud is measured, the corrected plastic viscosity will be of the order of half the measured value. Since the slope of the apparent viscosity versus reciprocal rpm plot for a drilling mud is proportional to its yield value [see Equation (6)], the data presented by Bednarski[8] show that the effect of temperature on the yield value varies widely among different muds and in some cases the yield value at 160°F may be twice that at 80°F.

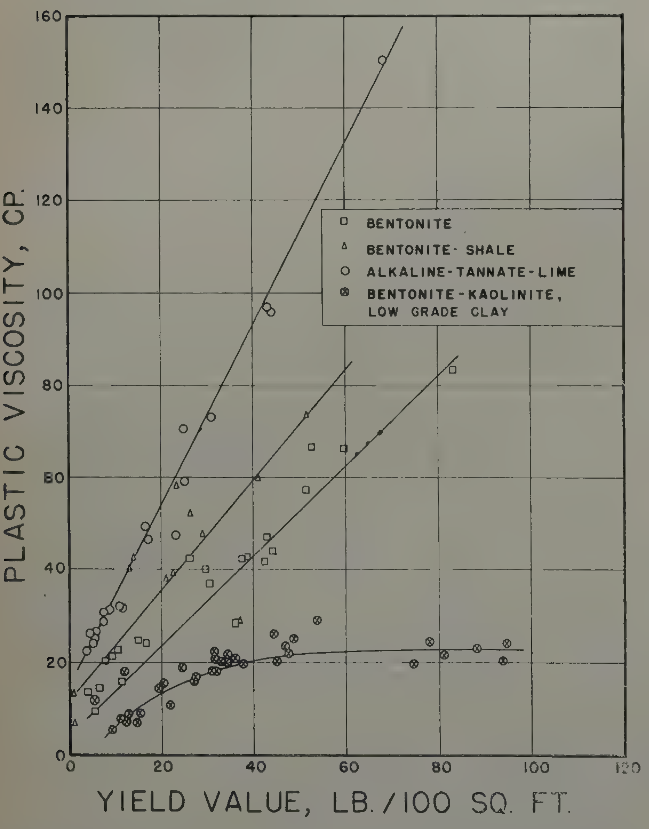

FIG. 7 — PLASTIC VISCOSITY-YIELD VALUE CORRELATION FOR VARIOUS MUD SYSTEMS.

These estimates of the effect of temperature have been applied to a pipe flow pressure-drop calculation for a mud of 20 cp plastic viscosity and 10 lbs/100 sq ft yield value, as measured at 80°F. The result was a pressure drop 60 per cent higher than that calculated from the measured properties.

CONCLUSIONS

1. A commercially available rotational viscometer modified to permit multispeed operation, has a straight-line calibration and is sufficiently rugged for field as well as laboratory use.

2. The behavior of water-base drilling fluids in this viscometer with few exceptions is described by the law of plastic flow, provided that equilibrium torque readings are obtained. The steady-state laminar flow behavior of muds is therefore characterized by the variables, plastic viscosity and yield value.

3. The measurements with the multispeed viscometer are approximately related to Stormer viscometer measurements by the following equations:

$$\mu_S = \mu_p + 1.5\ \phi$$
$$G_S = 3.3\ G_F$$

where

μ_S = Stormer 600 rpm viscosity, cp
μ_p = plastic viscosity, cp
ϕ = yield value, lbs/100 sq ft
G_S = Stormer initial gel, gms
G_F = multispeed viscometer initial gel, gms

4. The plastic flow properties may be interpreted in terms of the concentration and surface properties of the solids present in the mud. Such considerations can be used to explain the action of chemicals in "viscosity reduction" and suggest that the susceptibility of a mud to chemical treatment can be predicted from plastic viscosity and yield value data.

5. The pressure drop of a mud in laminar flow, *e.g.*, in a well annular space, will depend on the plastic flow properties. In order to make pressure drop calculations, knowledge of the effect of temperature on the plastic flow properties is required, since the yield value at average well temperatures may be considerably greater than that measured at the surface.

ACKNOWLEDGMENT

The authors wish to express their appreciations to the Magnolia Petroleum Co. for permission to publish this paper. Acknowledgment is also made for the cooperation of J. G. Savins and G. A. Spencer, who did much of the experimental work.

REFERENCES

1. Beck, R. W., Nuss, W. F., and Dunn, T. H.: API *Drill. and Prod. Prac. 1947,* (1948), 9-22.
2. Rogers, W. F.: *Composition and Properties of Oil Well Drilling Fluids,* (1948), 213-232.
3. Reiner, M., and Riwlin, R.: *Kolloid Z.,* (1927), **43,** 1-5; Reiner, M.: *Deformation and Flow,* (1949), 43-46.
4. Caldwell, D. H., and Babbitt, H. E.: *Ind. Eng. Chem.,* (1941), **33,** 249-256.
5. Garrison, A. D., and ten Brink, K. C.: *Trans. AIME,* (1940), **136,** 175-194.
6. Green, H.: *Industrial Rheology and Rheological Structures,* (1949), 45-72.
7. Cardwell, W. T., Jr.: API *Drill. and Prod. Prac. 1941,* (1942), 104-112.
8. Bednarski, V. N.: *Pet. Eng.,* (1948), **20,** 192-204.
9. Eirich, F., and Riseman, J.: *J. Polymer Sci.,* (1949), **4,** 417-434.
10. van Olphen, H.: *J. Inst. Petr.,* (1950), **36,** 223-234. ★ ★ ★

T.P. 3062

A MODIFIED LOW-STRENGTH CEMENT

B. E. MORGAN, JUNIOR MEMBER AIME, AND **G. K. DUMBAULD,** MEMBER AIME, HUMBLE OIL AND REFINING CO., HOUSTON, TEX.

ABSTRACT

The need for a low-strength cementing composition for use in well cementing is reviewed and results are presented of laboratory and experimental field tests of a modified cement having a controlled ultimate tensile strength of approximately 200 psi. The modified cementing composition may be prepared from either high early strength or normal portland cements by the addition of bentonite clay and a suitable agent for dispersing and controlling the set of the slurry. Substitution of the modified cement for conventional slow-set cements may give better completion results in many wells because the modified cementing composition has lower set strength, lower slurry density, and greater slurry stability than conventional cement slurries. The lower ultimate strength allows greater penetration with less shattering of the set cement when perforating casing and cement. The lower slurry density allows the placement of longer columns of cement slurry, and the greater slurry stability reduces the possibility of having an uncemented section caused by the settling of cement particles before the cement sets.

INTRODUCTION

High strength has always been one of the accepted criteria of a good cement. During the early use of portland cement in well cementing, emphasis was placed upon securing cements with higher strengths. In 1931, Barkis[1] reported that, "Normal oil well cements have been improved to develop greater strengths and uniformity of product, which has aided in producing successful jobs in cementing the deeper strings."

As long as most wells were completed by the open-hole method, the use of cements having high strengths seemed desirable, and there was no objection raised against high-strength cementing compositions. For a number of years, however, the industry has been completing a large number of wells by setting and cementing casing through productive horizons and then obtaining production by gun-perforating the section of casing opposite the desired interval. Although this method has been generally successful, difficulties have been experienced in some cases in completing or recompleting wells because of apparent lack of adequate penetration by the bullets through the casing and surrounding sheath of cement and into producing formation. In addition to the penetration trouble, there have been indications that fracturing and shattering of the set cement by perforating might be a contributing factor in causing the failure of some jobs to exclude water or gas from oil producing zones. The possibility that cements having high set strengths were contributing to the difficulty in obtaining satisfactory perforating results has received attention during recent years. Gun perforating tests conducted in 1944 showed that the depth of bullet penetration into set cement varied with the hardness of the cement, the greater the strength of the cement the less being the penetration. In 1946, Farris[2] pointed out that high strength cements were not needed in well cementing, and in 1947, data published by Oliphant and Farris[3] showed that set cement was perforated without shattering at approximately 150 psi tensile strength, whereas at approximately 300 psi tensile strength severe cracking and shattering occurred. Oliphant and Farris suggested that wells be perforated at the proper time interval after placement of the cement so that the set cement would have the desired strength.

Several difficulties may be encountered in trying to perforate a cement job at the correct time to catch the tensile strength near 150 psi. The rate of strength development of different cements varies considerably. This fact is illustrated by results of tensile strength measurements presented in Fig. 1. These data show that at 175°F the tensile strengths of three conventional slow-set cements varied from 75 to 235 psi at the end of 12 hours. After 24 hours, the tensile strengths varied from 200 to 455 psi. The rate of strength development is affected, also, by the temperature of the formation, and this adds to the uncertainty of perforating at the correct time, since accurate well cementing temperatures may not be known in many cases. Furthermore, in the recompletion of wells it is sometimes necessary to perforate cement which has set for a long period and has developed maximum or final strength.

In view of the apparent need for a cementing composition having a controlled ultimate strength, an investigation was

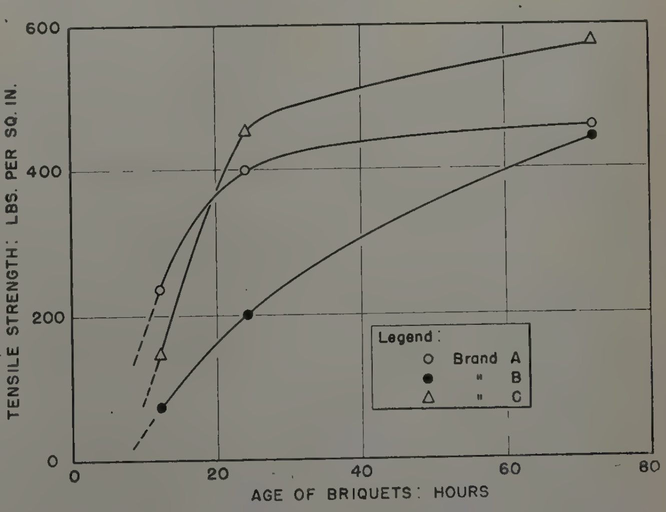

FIG. 1 — STRENGTH DEVELOPMENT OF THREE CONVENTIONAL SLOW-SET CEMENTS CURED UNDER WATER AT 175°F.

---

[1] References given at end of paper.

Manuscript received in the office of the Petroleum Branch Aug. 17, 1950. Paper presented at the Petroleum Branch Fall Meeting in New Orleans, La., Oct. 4-6, 1950.

Table I — Physical Properties of Modified Low-Strength Cements

	Modified High Early Strength[1]	Modified Normal Portland[2]
Water to cement ratio, gal per sack:	10	9
Pumpability Time, hrs: Halliburton Consistometer at atmos. pres.:		
Temp. of Test: 150°F	4½	—
Temp. of Test: 175°F	4¼	4¼
Temp. of Test: 200°F	3¼	—
Well Simulation Tests:[3]		
Schedule 5 (8,000 ft)	2⅔	3
Schedule 6 (10,000 ft)	2	2¾
Schedule 7 (12,000 ft)	1½	2¼
Schedule 8 (14,000 ft)	1⅓	1-11/12
Schedule 9 (16,000 ft)	1⅙	1⅔
Schedule 10 (18,000 ft)	1⅙	1⅓
Tensile Strength, psi:		
Cured under water at 150°F		
Age of Briquets: 12 hrs	65	—
Age of Briquets: 1 day	125	—
Age of Briquets: 3 days	190	—
Cured under water at 175°F		
Age of Briquets: 12 hrs	135	—
Age of Briquets: 1 day	175	154
Age of Briquets: 3 days	185	—
Age of Briquets: 7 days	198	198
Cured under water at 200°F		
Age of Briquets: 12 hrs	155	—
Age of Briquets: 1 day	160	—
Age of Briquets: 3 days	210	—
Wet Permeability, md:		
Cured under water at 175°F		
Age of Test Specimen: 1 day	0.05	0.11
Age of Test Specimen: 7 days	0.004	0.005

[1] A high early strength cement with 15 lb. of bentonite and 0.5 lb. of calcium lignosulfonate added per sack of cement.

[2] A normal portland cement with 15 lb. of bentonite and 0.5 lb. of calcium lignosulfonate added per sack of cement.

[3] According to API Code 32.

initiated several years ago in an attempt to develop such a composition.

LABORATORY INVESTIGATION OF MODIFIED CEMENT

Composition

The set strength of cement is reduced by an increase in the water-to-cement ratio of the slurry; however, the cement particles in high water-to-cement ratio slurries settle out, allowing a water-cement separation to occur.[4,5] This sedimentation of high water-to-cement slurries may be avoided by the addition of bentonite clay.[6] Hence, it appeared that a stable cementing composition with a controlled ultimate set strength might be produced by using the correct amount of mix water to prepare a slurry of portland cement and bentonite clay. However, laboratory tests revealed that the addition of a small amount of a dispersing agent was needed to disperse the mixture of cement, clay, and water, and to allow adjustment of the set time.

It was found by laboratory tests that a cementing composition with an ultimate tensile strength of approximately 200 psi could be prepared by adding 12 - 15 lb bentonite clay and approximately 0.5 lb calcium lignosulfonate per sack of high early strength cement, and using enough mix water to make a slurry with a water-to-cement ratio of about 10 gal per sack. Additional tests also showed that a satisfactory modified cementing composition could be prepared from normal portland cement by the addition of the same quantities of bentonite clay and calcium lignosulfonate, but with the addition of enough mix water to make a slurry with a water-to-cement ratio of about 9 gal per sack.

Pumpability, Strength and Permeability

A satisfactory well cementing composition must retain its fluidity long enough to be pumped into place, then it must develop sufficient strength and impermeability to form an effective seal within a reasonable length of time. These properties may be evaluated in the laboratory by pumpability, tensile strength, and permeability tests. The results of such tests of modified low-strength cements are presented in Table I. For comparison, similar laboratory data for three conventional slow-set cements are presented in Table II. The pumpability times of the modified cement slurries were found to be about the same as the pumpability times of the conventional slow-set cement slurries, and the permeability of the set modified cements, although greater than the permeability of the conventional cements, was considered to be sufficiently low to make a good seal. The 7-day tensile strengths of the modified cements were approximately 200 psi, whereas the 7-day tensile strengths of the conventional cements varied from 398 to 667 psi. The modified cement developed most of its strength within the first 24 hours.

These data indicated, therefore, that for the cementing of many wells either high early strength or normal portland cement containing bentonite clay and calcium lignosulfonate could be substituted for existing slow-set cements.

Perforating Properties

Since the modified low strength cement was developed in an attempt to obtain better perforating results through cemented casing, the depth of penetration into conventional and modified cements by both bullet and jet perforators was determined in aboveground setups prepared by placing the test cement slurries in the annulus formed by positioning casing inside a 55-gal barrel. In order to make the test more severe, two strings of pipe were used in two of the setups prepared with modified cement. In these two assemblies, the entire volume of the 55-gal barrel, excluding the inside of the smaller pipe, was filled with modified cement slurry. After the cement slurries had set long enough to develop most of their strength, the casing was perforated and the penetration and fracturing of the set cements were observed. The results of these perforating tests, presented graphically in Fig. 2, are summarized below. The results shown in the following table represent the average penetration of all perforations which lodged within the set cement. Perforations which passed completely through the test setups were not considered in compiling the data in this table.

Comparative Penetration into Conventional and Modified Cements

Type of Perforator	Pipe Used in Tests	Total Penetration, in. Conventional Cement	Total Penetration, in. Modified Cement
Bullet Gun No. 1	5½" - 15# J-55 Csg.	11/16	4-1/16
Bullet Gun No. 2	5½" - 17# N-80 Csg.	2-1/4	——
Bullet Gun No. 2	5½" - 17# N-80 Csg. inside of 9⅝-32.3# H-40 Csg.	——	5-7/16
Jet Gun	5½" - 17# N-80 Csg.	6-3/4	——
Jet Gun	5½" - 17# N-80 Csg. inside of 9⅝-32.3# H-40 Csg.	——	10-1/2

These tests showed that penetration by either bullet or jet was better through casing cemented with modified cement than it was through casing cemented with conventional cements. Also, very little or no fracturing of the set modified cement was caused by perforating, whereas quite severe fracturing of the conventional cements was evident in some of the surface tests. These results indicated that substitution of modified cement for conventional cements offered a method of obtaining better production in areas where difficulty is experienced in obtaining satisfactory penetration of the casing and the surrounding sheath of set cement. It also appeared that the modified cement might form a more effective seal than conventional cements, since perforation of the set modified cement did not cause fracturing.

Although better penetration by perforation was the primary objective in the development of the modified cement, there are two properties of the modified cement slurry which are not found in existing conventional cement slurries and which may be advantageous in the cementing of wells. One is greater slurry stability and the other is lower slurry density.

Slurry Stability

The modified cement slurry remains in suspension until it sets, whereas slurries of conventional slow-set cements settle out before they set, allowing a water-cement separation to occur. This property is illustrated by the data presented in Fig. 3, which show that slurries of the modified cement set to a volume approximately equal to the original slurry volume. On the other hand, a layer of clear water collected above conventional slow-set cement slurries before they set. It is possible that in some cases a considerable portion of the vertical distance behind the casing in a well may be void of set cement when a conventional slow-set cement is used. When casing is cemented with a cement slurry which settles out before it sets, any irregularity in the diameter of the hole may allow bridging of the cement particles and cause an uncemented section to occur immediately below the bridge point. If this occurs, the cement job may fail to seal off the formations at a critical interval. This possible cause of cementing failure may be avoided by use of the modified cement.

Slurry Density

The modified cement containing 12-15 lb of bentonite and 0.5 lb calcium lignosulfonate per sack of cement produces a slurry with a density of approximately 13½ lb per gal at a water-to-cement ratio of about 10 gal per sack, whereas conventional slow-set cements produce neat slurries with a density of approximately 16 lb per gal at a water-to-cement ratio of about 5 gal per sack. The lower density of the modified cement slurry allows the placement of long columns of cement slurry in areas where formations will not support long columns of heavier conventional cement slurries. This property is particularly valuable in those cases in which there is danger of losing circulation in the interval to be cemented.

FIELD USE

In order to explore the utility of the modified cement and the problems connected with its use, arrangements were made for field use of the modified cement on an experimental basis. Thirty-five field jobs had been completed at the time of the writing of this paper. Twenty-one of these jobs were performed to cement the production string of casing for original completions. The other fourteen jobs were performed in working over old wells, five of which were liner jobs and nine of which were squeeze jobs. A brief discussion of each type job is presented below.

Cementing of Production String

Of the 21 jobs in which the modified cement was used to cement casing for the original completion, 18 jobs were performed in an attempt to evaluate the possible advantage of a low density slurry in the placement of a long column of cement slurry in areas where weak formations fail to support a long column of conventional cement slurry. Sixteen of these jobs were performed in wells located in Coke and Runnels counties, Tex. One well was located in Marion County, Miss., and one was in Jefferson Davis County, Miss. On several jobs performed in these areas with the use of conventional cement, returns were lost during the placement of the cement slurry. When this happened, it was necessary to perforate the casing and perform a second cement job in order to obtain adequate fill-up around the casing. Often several cement jobs were necessary before the weak formation was sealed and the desired fill-up was obtained. This procedure is time-consuming and expensive. It was thought that the lower density of the modified cement slurry would allow the placement of sufficient slurry to seal off all the troublesome zones by the primary cement job. Temperature surveys after cementing with modified cement showed that adequate fill-up had been obtained in 17 of the 18 wells. In the case of the one

Table II — Physical Properties of Conventional Slow-Set Cements

	Brand A	Brand B	Brand C
Water-to-cement ratio, gal per sack:	4½	4½	4½
Pump Time, hrs., Halliburton Consistometer at atmos. pres.:[1]			
Temp. of Test: 140°F	7	5-1/12	8½
Temp. of Test: 160° F	7⅙	4⅓	7⅓
Temp. of Test: 180°F	9⅗	4	6⅙
Temp. of Test: 200°F	4¼	2¾	4
Well Simulation Tests:[1,2]			
Schedule 5 (8,000 ft)	4-5/12	4	5
Schedule 6 (10,000 ft)	3½	2-5/12	4
Schedule 7 (12,000 ft)	2-5/12	1-11/12	2⅙
Schedule 8 (14,000 ft)	1⅙	1½	1½
Schedule 9 (16,000 ft)	1-1/10	1⅛	1⅓
Schedule 10 (18,000 ft)	1	1-1/12	1⅙
Tensile Strength, psi:[1,2]			
Cured under water at 140°F			
Age of Briquets: 1 day	352	203	368
Age of Briquets: 2 days	453	300	492
Age of Briquets: 7 days	535	455	617
Cured under water at 160°F			
Age of Briquets: 1 day	358	233	357
Age of Briquets: 2 days	478	308	508
Age of Briquets: 7 days	500	398	603
Cured under water at 180°F			
Age of Briquets: 1 day	377	302	457
Age of Briquets: 2 days	490	403	610
Age of Briquets: 7 days	507	593	667
Wet Permeability, md:			
Cured under water at 175°F			
Age of Test Specimen: 1 day	0.002	0.026	0.009
Age of Test Specimen: 7 days	<0.001	<0.001	<0.001

[1] Data obtained and furnished by Petroleum Engineering Division Service Laboratory, Humble Oil and Refining Co.

[2] According to API Code 32.

well in which fill-up was not satisfactory, full returns were obtained throughout the cementing operations, but the top of the cement was not as high as desired. It appeared that in this case an insufficient volume of cement slurry was used.

The cementing of Sallie Odom D-1, Runnels County, Tex., was typical of the 17 jobs which were completed successfully:

> After 9⅝-in. surface casing was set at 363 ft, 7⅞-in. hole was drilled to 5,294 ft and 5½-in. casing was cemented at 5,291 ft with 650 sacks of modified cement. A temperature survey after cementing located the top of the cement at 1,120 ft, which indicated that the cement job was satisfactory, since no troublesome zones were believed to exist above that point. The well was completed satisfactorily by the open-hole method.

Three of the 21 primary cement jobs were done in an effort to evaluate the possible advantage of a low-strength set cement in obtaining better perforating results through the production string of casing and the surrounding sheath of cement. Production after perforating the casing indicated that a good primary cement job had been obtained in all three jobs. Interesting results obtained on Seeligson C-126, Kleberg County, Tex., are described below.

> After 9⅝-in. surface casing was set at 2,002 ft, 8⅝-in. hole was drilled to the total depth of 7,200 ft and 5½-in. casing was cemented with 660 sacks of modified cement. Rotowall type scratchers were attached to the casing from 7,090 to 7,100 ft and from 7,105 to 7,125 ft. Clear salt water was produced through 24 bullet perforations from 7,112 to 7,116 ft. Ninety sacks of conventional cement slurry were squeezed through these perforations. The surface breakdown pressure was 4,300 psi and the squeeze pressure was approximately 5,000 psi. Afterwards, the well produced clean oil with a low gas/oil ratio through perforations from 7,093 to 7,101 ft. The behavior of the squeeze job indicated that a good seal between the casing and the formation had been obtained with the primary cement job. Also, the production of clean oil through perforations just 11 ft above previous perforations through which clear salt water was produced indicated that the seal was not destroyed by perforation.

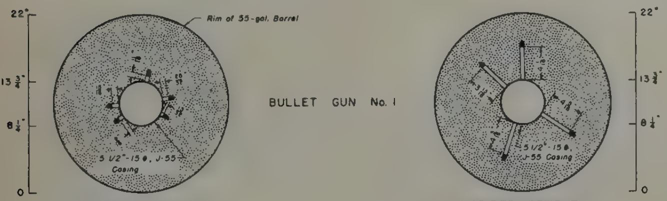

CONVENTIONAL CEMENT
Tensile strength 416 lbs. per sq in

MODIFIED CEMENT
Tensile strength 211 lbs per sq in

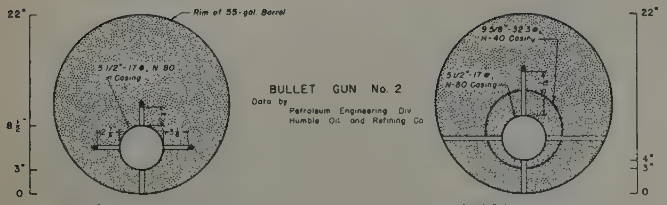

CONVENTIONAL CEMENT
Tensile strength 659 lbs per sq. in

MODIFIED CEMENT
Tensile strength 204 lbs per sq in

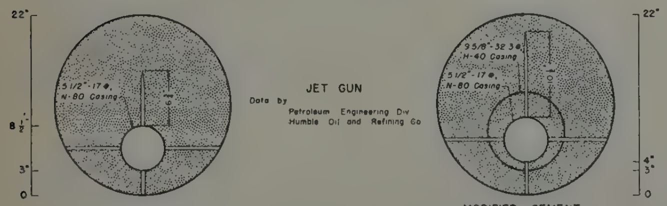

CONVENTIONAL CEMENT
Tensile strength 659 lbs per sq. in.

MODIFIED CEMENT
Tensile strength 204 lbs per sq in

FIG. 2 — COMPARATIVE PENETRATION INTO CONVENTIONAL SLOW-SET AND MODIFIED LOW-STRENGTH CEMENTS.

Cementing of Liner

Modified cement was used to cement liners in working over five wells which had been completed originally by the open-hole method. After several years of production, the gas/oil ratio of these wells became excessively high and it was thought that this condition might be corrected by setting liner in the open hole and obtaining production through perforations in the liner. All these jobs were done on wells in the Means Field, Andrews County, Tex. A typical job on J. S. Means 20 is described below.

> This well was completed originally by setting 5½-in. casing at 4,183 ft with 7¾-in. open hole to 4,532 ft, and acidizing the open hole. Since the open hole was drilled originally to a diameter of 7¾ in. and probably contained enlarged sections, it was thought that the well could be recompleted more readily by perforating through the liner and set cement if modified cement were used instead of conventional cement. The workover job was done, therefore, by setting 4-in. liner in the open hole with the modified cement, jet-perforating the liner, and acidizing the formation through the perforations. After the workover job was completed, the well was able to make its unpenalized allowable with a gas/oil ratio below 1,500 cu ft per bbl. The results indicated that the liner was cemented successfully with the modified cement and that satisfactory oil production was established through perforations in a fairly thick sheath of cement.

Squeeze Cementing

One of the nine squeeze cement jobs was done in order to obtain a set cement which could be readily perforated even though a thick sheath of set cement surrounded the casing. Since this well, J. H. P. Davis 23, Fort Bend County, Tex., had produced a large amount of sand, it was probable that the section surrounding the perforated casing was enlarged. After the squeeze job, satisfactory production was obtained by gun-perforation of the original producing interval against which the modified cement slurry had been squeezed.

The other eight squeeze jobs were done in an attempt to shut off either water or gas production in wells which were producing through perforated casing. In each case cement slurry was squeezed through the existing perforations and the casing was reperforated. Most of these jobs were done in attempts to shut off water production, and the casing was reperforated in either the same interval or slightly higher in the same producing zone. A typical job of this type, performed on the Kenedy Jr. B-6, Kenedy County, Tex., is described below.

> This well was producing oil and a small amount of salt water through perforations from 6,922 to 6,926 ft when the water production increased from 2 per cent to 80 per cent within an interval of one month. Ninety sacks of modified

cement slurry was squeezed through these perforations with a final surface squeeze pressure of 3,300 psi. After the casing was jet-perforated from 6,915 to 6,925 ft, the well flowed approximately 65 per cent oil, 35 per cent salt water. The results on this workover job were inconclusive, since it was impossible to determine whether the squeeze job failed to seal off the water or whether the interval perforated contained water.

Although the use of modified cement seemed advantageous in squeeze cementing a well which contained an enlarged section in the producing interval, no definite advantage was evident in ordinary squeeze cement jobs performed to shut off either gas or water production.

In all the field jobs performed to date, no difficulty in the placement of the modified cement slurry and no failure attributable to the cement itself has occurred except on one squeeze job. During this squeeze job, it was impossible to pump the excess cement slurry out by reverse circulation. Regular circulation (long way) was established, but the retrievable tool became lodged in the casing during its removal. Inadequate mixing of the dry cement, clay, and lignosulfonate may have caused the cement slurry to set faster than expected, but other factors may have been responsible for the difficulty. The exact cause of the trouble was not identifiable.

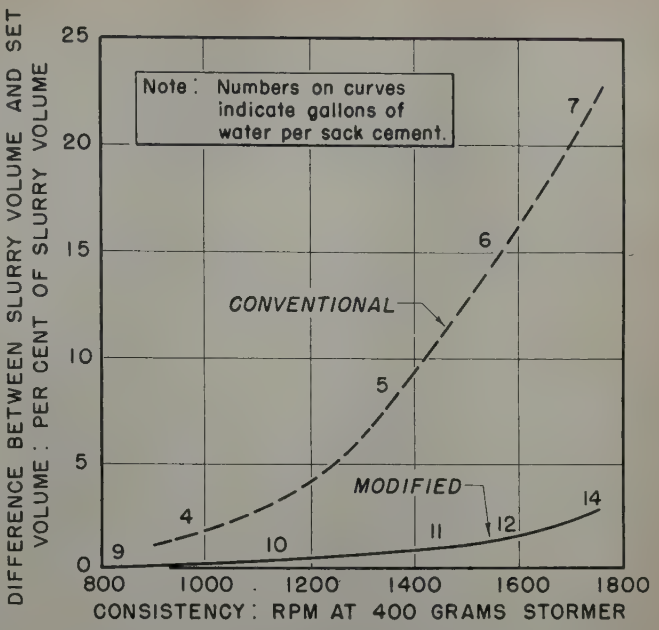

FIG. 3 — TREND OF SEDIMENTATION OF MODIFIED LOW-STRENGTH AND CONVENTIONAL SLOW-SET CEMENT SLURRIES.

MIXING, COMPOSITION AND COST OF MODIFIED CEMENT

The mixing of the three dry constituents — normal portland cement, bentonite clay, and calcium lignosulfonate — was done at bulk-cement plants. For the field jobs performed to date, the clay and lignosulfonate were added separately as the cement was transferred from railroad cars to bulk-cement trucks. In most cases, the mixing has been fairly satisfactory but it has required close supervision. Better mechanical facilities for the dry mixing are needed in order to assure proper mixing of the dry constituents without excessive supervision.

The modified cement tends to lump and to form a very thick slurry which appears to be poorly mixed; however, the agitation which occurs as the slurry passes through the pumps is sufficient to deliver a well-mixed slurry into the borehole. Slurry samples obtained from the line between the discharge of the pumps and the wellhead are smooth and lump-free even though the slurry in the sump tub is very lumpy. A smooth slurry relatively free of lumps in the sump tub is desirable, however, because it facilitates the weighing of the slurry and the judging of the slurry consistency and density by visual observation. On several field jobs, a small mechanical mixer in conjunction with the usual jet mixer has given smooth, lump-free slurries in the sump tub. Also, certain improvements to jet mixers have resulted in more satisfactory mixing of the modified cement slurry.

Observations of the first few field jobs indicated that slurries prepared in the field were thicker than slurries prepared in the laboratory. This was probably due to the difference in slurry mixing. In order to find the optimum bentonite clay concentration for field use, the clay content was varied from 9 to 14 lb per sack of cement on several succeeding field jobs. These results indicated that the modified cement slurry possessed the desirable consistency when the clay content was about 12 lb per sack of cement; therefore, most of the field jobs have been performed with 12 lb of clay per sack of cement. Variations in the lignosulfonate content have ranged from 0.3 to 0.6 lb per sack of cement; however, the lignosulfonate content has been near 0.5 lb per sack of cement for most of the field jobs. On several field jobs, chopped cellophane was added to help combat any tendency to lose slurry to weak formations. The water-to-cement ratios of the slurries have varied from about 9 to 12 gal per sack with slurry densities from approximately 13.7 to 12.7 lb per gal, respectively.

The cost of materials to prepare a given volume of modified cement slurry is at present about 15 to 20 per cent less than the cost of materials to prepare the same volume of conventional slow-set cement slurry. With cement at $1.10 per sack, bentonite clay at $1.75 per 100 lb, and calcium lignosulfonate at $12.00 per 100 lb, materials for preparing one cu ft of modified cement slurry with a water-to-cement ratio of 10 gal per sack cost $0.75. In comparison, 1 cu ft of regular neat cement slurry with a water-to-cement ratio of 5 gal per sack costs $0.96. This comparison does not include the cost of mixing the bentonite clay and calcium lignosulfonate with the cement.

CONCLUSIONS

1. The results of laboratory-scale tests show that a modified low-strength composition having pumpability and permeability properties satisfactory for well cementing may be prepared by the addition of clay and a dispersing agent to normal portland cement. The slurry has lower density and better stability than conventional cement slurries. The set modified cement is more readily penetrated by bullets or jets than is conventional cement.

2. The results of field tests indicate that the low density of the modified cement slurry is advantageous in the cementing of casing through zones in which there is danger of losing circulation with higher density slurries of conventional cement. This property of the modified cement slurry has apparently eliminated in some cases the time and expense of the stage cementing which would have been necessary with the use of conventional slurries.

3. The results of field tests indicate that the greater ease of penetration of the modified cement may be helpful in assur-

ing the perforation of fairly thick cement sheaths, and in preventing loss of seal due to shattering of the cement.

4. The results of field tests indicate that the modified cement has no particular advantage over conventional cement in squeeze cementing operations, unless the cement is to be squeezed into an enlarged hole section and subsequently perforated.

5. The relatively low cost of materials for the modified cement offers an economic advantage over the cost of conventional cement.

ACKNOWLEDGMENT

The authors wish to express their appreciation to R. A. Salathiel for his thoughts and efforts during the early development of this work, to G. E. Cannon for his help in arranging the field jobs and to Humble Oil and Refining Co.'s division and district personnel who conducted the field jobs. Appreciation is also extended to the management of Humble for permission to publish this paper.

REFERENCES

1. Barkis, Bruce: "Cements and Cementing Practices," API, *Production Division Proceedings*, (1931) **157.**
2. Farris, R. F.: *Trans.* AIME, (1946), **165.** 175-188.
3. Oliphant, S. C., and Farris, R. F.: *Trans.* AIME, (1947), **170**, 225-242.
4. Craft, B. C., Johnson, T. J., and Kirkpatrick, H. L.: *Trans.* AIME, (1935), **114**, 62-68.
5. Coleman, J. R., and Corrigan, G. L.: *Trans.* AIME, (1941), **142**, 205-215.
6. Willson, Cedric: "Gel Cements and Their Application in Oil-Well Cementing Operations," API *Drill. and Prod. Prac.*, (1941), 293-299.

DISCUSSION

By W. C. Goins, Jr., Gulf Oil Corp., Houston, Tex.

The authors of the paper are certainly to be complimented on their interesting and well prepared paper, and on their valuable contribution to the technique of oil well cementing. I feel that due to the economies and low slurry densities afforded by the modified cements that we shall eventually see a rather extensive use of these materials. This should be particularly true in those areas where trouble is experienced in obtaining a satisfactory "fill-up" during casing cementing.

I have been associated with some recent laboratory experimental work with modified cements of the same and similar compositions as that of the authors. I would like to state that the results of this work verifies the authors' contentions that cements of this composition satisfy requirements as to strength, pumpability, and stirring time. I think it should be emphasized that although the modified cements as described are prepared from standard portland cement, they exhibit stirring times which make them comparable to slow-set cements. This is due not only to the increased water-cement ratio used, but also to the strong retarding action of the calcium lignosulfonate.

Recently laboratory tests were made of modified cement slurries prepared from two different brands of portland cements. Stirring of the slurries was continued while the temperature and pressures were increased at a rate designed to simulate the conditions of cementing in average Gulf Coast wells. The stirring time to 100 poises viscosity was then taken as the pumpable time of the slurries. These tests were made in a Stanolind Super-Pressure Thickening Time Tester in accordance with the methods of simulating casing setting operations as set forth in the API *Code for Testing Cements Used in Wells.* They showed that at a depth of 10,000 ft cements of a composition near that described had a pumpable time of from one to one and one-half hours in excess of that required to mix and displace 300 sacks of cement to that depth during casing setting. Increasing the calcium lignosulfonate to 0.6 per cent gave slurries which were pumpable for as long as any of four slow set cements in 10,000 and 14,000 ft simulated casing cementing tests where the slow set cements were prepared as normal 40 per cent slurries. I think this indicates that the use of the modified cements need not be confined to those shallow depths at which portland cements are normally employed.

One question which undoubtedly would be raised elsewhere, if not here, is whether the slow set cements could be used to prepare modified cements, in which case it might be assumed that the calcium lignosulfonate could be omitted. Our own experience, though somewhat limited in scope, indicates that it would be somewhat questionable. With one slow-set cement made up as a modified product, the use of 10 per cent bentonite seemed to completely destroy the slow-setting properties. With two other slow-set cements pumpability tests of modified slurries indicated that they might be used, but with another the slurry pumped for an excessively long period of over 8 hours in simulated deep well tests. These tests were made in a super-pressure consistometer, as described before, and without any added calcium lignosulfonate.

Since these tests indicated erratic performance of the slow-set cements when made into slurries of the modified type, and since all of the portland cements tested gave consistent results, it was felt that regular portland cement should be used. Also, the cost of the lignosulfonate, plus the cost of mixing it into the dry cement, is less than the difference in price between portland and slow-set cements. I should like to ask the authors whether slow-set cements should be used for the purpose of making modified cements of the type they have described.

AUTHORS' REPLY TO MR. GOINS

We wish to thank Goins for his pertinent remarks and for emphasizing that modified cements prepared with normal portland cements, bentonite clay, and calcium lignosulfonate possess suitable pumpability properties for use in deep wells.

In answer to the question about the use of conventional slow-set cements to prepare modified cements of the type described in the paper, our experience has been about the same as the experience which you reported. Early in our investigation, we found that the pumpability time of slow-set cements containing large percentages of bentonite clay varied considerably from brand to brand. We did very little work, therefore, in an effort to produce a high bentonite content cement slurry using slow-set cements. Instead, most of our work was done with high early strength and normal portland cements. We found that the pumpability time of slurries prepared with high early strength or normal portland cement, bentonite, and calcium lignosulfonate varied little from brand to brand. We found, furthermore, that the pumpability time could be extended by increasing the concentration of calcium lignosulfonate, thereby affording a means of controlling the pumpability time of the slurries.

In summary, it appears that some brands of slow-set cements may be suitable for producing high bentonite content cement slurries, while other brands may not be suitable for this purpose.

★ ★ ★

T.P. 3096

AN ANALYSIS AND THE CONTROL OF LOST CIRCULATION

GEORGE C. HOWARD, MEMBER AIME, AND **P. P. SCOTT, JR.,** STANOLIND OIL AND GAS CO., TULSA, OKLA.

ABSTRACT

During the drilling of wells, fractures which are created or widened by drilling fluid pressure are suspected of being a frequent cause of lost circulation. A study of the variables which are believed by the authors to be related to fracturing led to the premise that the presence of an effective lost circulation material in a drilling mud stream would serve to plug small fractures at the moment they are encountered or created and thereby eliminate a possible cause of lost circulation by preventing fluid pressure from widening and extending the fractures.

A large number of lost circulation materials were classified and tested in simulated fractures and in shallow wells. Granular type materials with a gradation of particle sizes were found to be the most effective for plugging. Within the limits of pumpability, the concentration in mud of each lost circulation material tested was found to be a controlling factor in determining the maximum size fracture which could be sealed. A new type centrifugal sorter was given preliminary tests and found to be capable of concentrating cuttings for rejection and reclaiming lost circulation materials.

INTRODUCTION

The control and prevention of lost circulation of drilling fluids is a problem frequently encountered during the drilling of oil and gas wells.

Lost circulation or lost returns may be defined as the loss to formation voids of the drilling fluids or cement slurries used in the process of rotary drilling and well completion. The loss may vary from a gradual lowering of mud level in the pits to a complete loss of returns. Not to be confused with lost circulation is the continuous reduction in mud volume caused by the loss of the fluid phase of muds as filtrate and the solid phase as filter cake during the continuous filtration process which occurs on permeable formation surfaces.

The loss of drilling fluids and their costly constituents is only one of the detrimental effects experienced when circulation is lost. The loss of drilling time, plugging of potentially productive formations, stuck drill pipe, blow-outs, excessive inflow of water, and excessive caving of formations are other effects which contribute to make the control and prevention

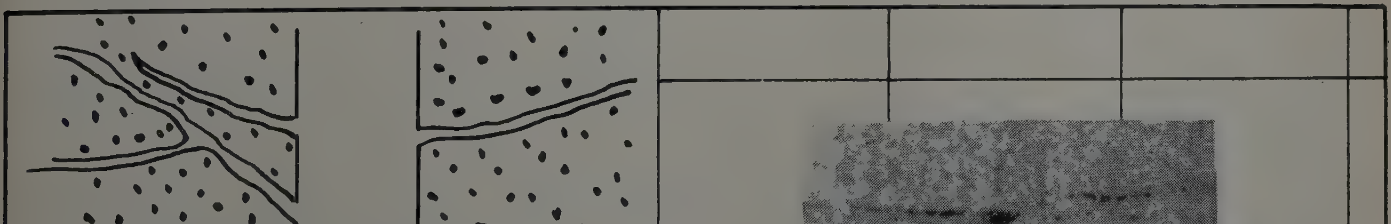

FIG. 1 — NATURAL OR INTRINSIC FRACTURES.

---

[1] References given at end of paper.

Manuscript received in the office of the Petroleum Branch Feb. 19, 1951. Paper presented at the Annual Meeting of the AIME in St. Louis, Mo., Feb. 19-21, 1951.

Table I — Identifying Features

Natural Fractures	Induced Fractures	Cavernous	Unconsolidated Formations
1. May occur in any type rock. 2. Loss is evidenced by gradual lowering of mud in pits. If drilling is continued and more fractures are exposed, complete loss of returns may be experienced.	1. May occur in any type rock, but would be expected in formations with characteristically weak planes such as shale. 2. Loss is usually sudden and accompanied by complete loss of returns. Conditions are conducive to the forming of induced fractures when mud weight exceeds 10.5 lb/gal. 3. Loss may follow any sudden surge in pressure. 4. When loss of circulation occurs and adjacent wells have not experienced lost circulation, induced fractures should be suspected.	1. Normally confined to limestone. 2. Loss of returns may be sudden and complete. 3. Bit may drop from a few inches to several feet just preceding loss. 4. Drilling may be "rough" before loss.	1. Gradual lowering of mud level in pits. 2. Loss may become complete if drilling is continued. 3. Since it is known that the rock permeability must exceed 100 darcys before mud can penetrate and that oil or gas sand permeability seldom exceeds 3.5 darcys, it is improbable that loose sands are ever the cause of mud loss to an oil or gas sand unless the loss can be attributed to the ease with which this type of formation fractures.

of loss of circulation one of the most challenging problems of the industry. Not uncommon is abandonment of wells due to failure to regain circulation.

The magnitude of the problem prompted the initiation of an investigation of the various aspects of lost circulation. The objectives of this paper are to present the results of this investigation to date and to stimulate interest and discussion.

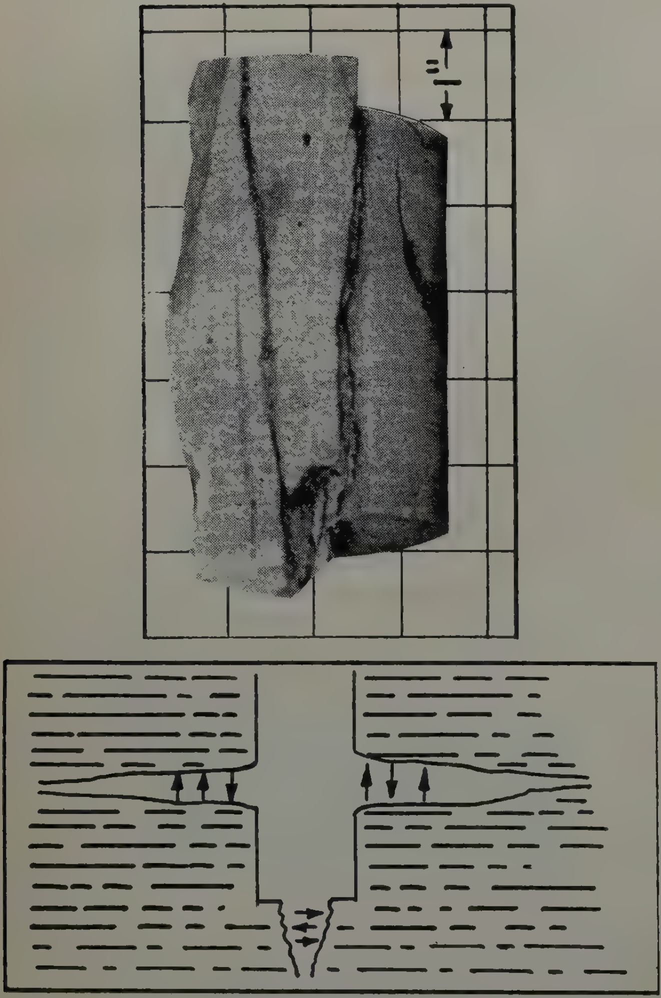

FIG. 2 — INDUCED OR CREATED FRACTURES.

FACTORS AFFECTING LOST CIRCULATION

A. TYPES OF FORMATIONS CAUSING LOST CIRCULATION

Classification

Study of literature disclosed that the types of formations or subsurface conditions which are the cause of, or are susceptible to, lost circulation have been classified numerous times by various authorities, and that there is an agreement among most authorities that the subsurface conditions fall in four categories.[1,9,18,24]

1. Natural or Intrinsic Fractures (Fig. 1).
2. Induced or Created Fractures (Fig. 2).
3. Cavernous Formations (crevices and channels) (Fig. 3).
4. Unconsolidated or Highly Permeable Formations (loose gravels) (Fig. 4).

Coring of wells has shown that induced fractures may be horizontal, vertical, or at various angles to a bore.

Induced or created fractures are distinguished from natural fractures primarily by the fact that the loss of mud to induced fractures requires the imposition of pressure of sufficient magnitude to break or split, or to part formations, while the loss of mud to natural fractures requires only sufficient pressure to exceed that of the fluid within the formation. The latter condition presupposes that in their undisturbed state some natural fractures may be wide enough to permit mud entry without compacting superimposed, underlying, or adjacent formations, and certainly the size fractures observed in many cores indicate that this is possible. In this paper, the terms natural and intrinsic fractures refer only to those fractures conforming to the conditions above. The term "fractures" used alone refers to both natural or intrinsic and induced or created fractures.

Cavernous formations differ from fractures in that caverns are probably a result of solution phenomena. Loss of mud to caverns occurs when the mud pressure exceeds the formation pressure of the caverns.

The loss of mud to loose gravel requires that the intergranular passages be of sufficient size to permit whole mud entry and, as in the case of natural fractures and caverns, the mud pressure logically must exceed the formation pressure.

Recognition

Positive identification of the type of formation causing lost circulation always is an important factor in determining a means of regaining circulation. To assist in identifying the type of formation, field observations made during and just

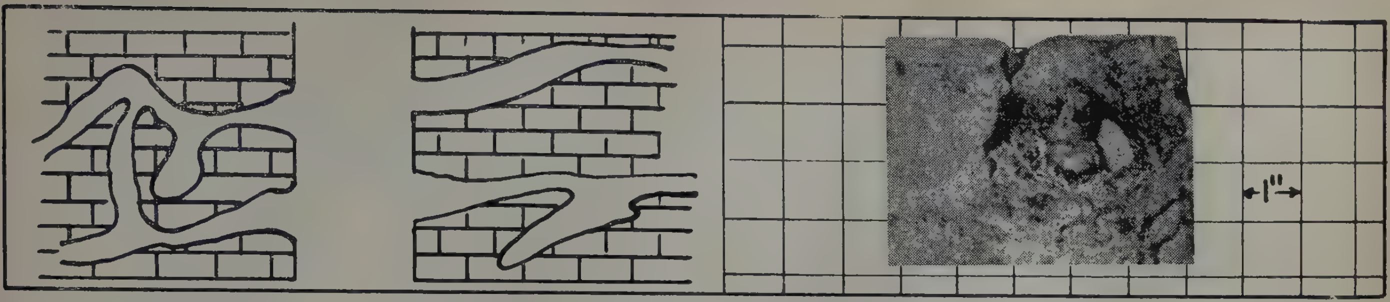

FIG. 3 — CAVERNOUS FORMATIONS.

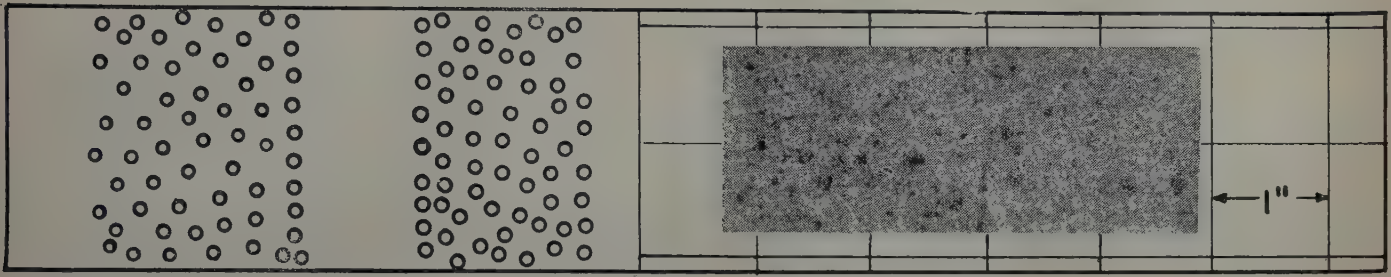

FIG. 4 — UNCONSOLIDATED OR HIGHLY PERMEABLE FORMATIONS (LOOSE GRAVELS.)

prior to the occurrence of lost circulation that are believed indicative of the type of lost circulation being encountered, together with a few other distinctive characteristics, are compiled in Table I.

Probably the most difficult type of lost circulation to control or prevent is that occurring in formations containing caverns; however, the fact that this type of lost circulation is not common in all producing areas tends to subordinate it in the opinion of the authors to the problem of controlling circulation lost to induced fractures. Such fractures are believed to be created most frequently while drilling into the abnormally high pressure formations which are encountered in a geographical belt along the coast of the Gulf of Mexico, and in sections of East and West Texas, and North Louisiana, although induced or created fracturing may possibly occur in many normal pressure areas. When penetrating these formations the use of heavy drilling muds is necessary. As a result, in many instances, the sum of the pressure of the high hydrostatic head required to control the abnormal formation pressure, plus the pressure required to circulate, may approach that pressure which will part, split, or breakdown formations and result in loss of drilling fluids. Under these circumstances, it is quite evident that any slight increase in pressure by any one of several means to be discussed later may be sufficient to destroy the close balance of pressure between formation and drilling fluid and result in the creation or widening of a fracture.

B. HOLE CONDITIONS

To define more clearly the problem of loss of mud to induced fractures, it was necessary to determine the well conditions which might contribute to or cause loss of circulation to this type fracture.

The requirements for forming fractures are pressure and surfaces upon which the pressure may act so that the resultant forces are of sufficient magnitude and are exerted in such a manner so as to tend to part or split formations.

A study of possible well bore anomalies indicates that the following conditions may exist and any one of these conditions might lead to formation fracturing and loss of mud.

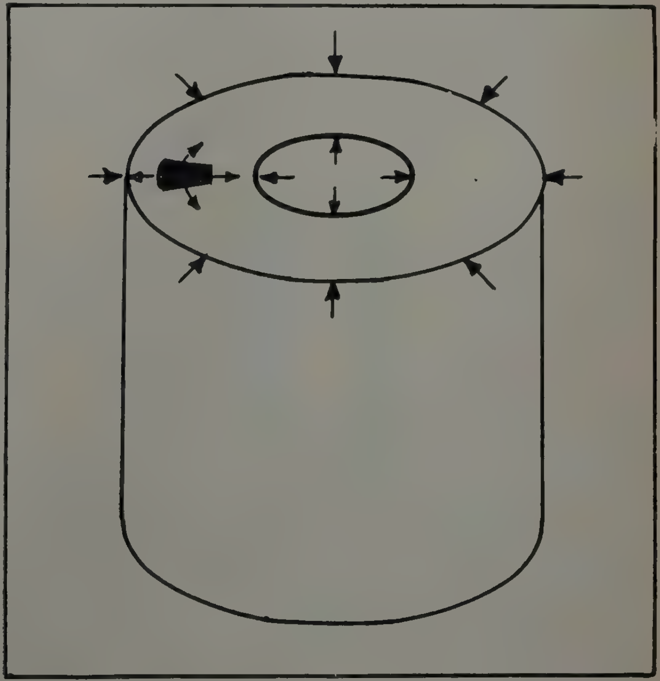

FIG. 5 — HOMOGENEOUS, IMPERMEABLE WALLS FOR FRACTURING ACCORDING TO THICK WALL CYLINDER THEORY.

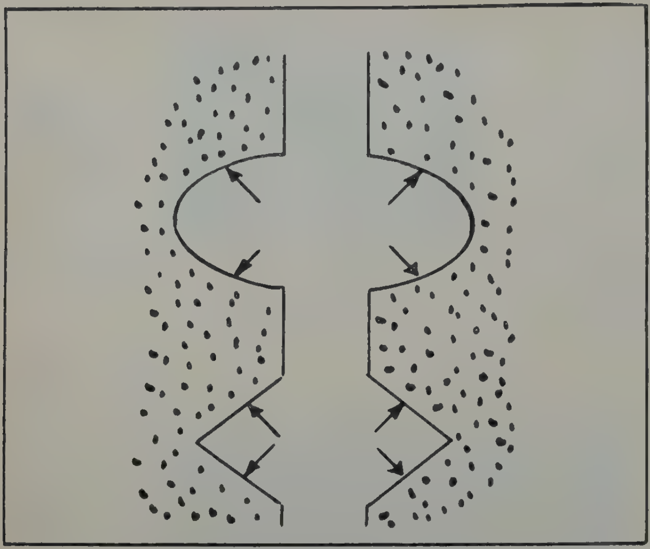

FIG. 6 — WELL IRREGULARITIES SUCH AS NOTCHES AND ELLIPTICAL ENLARGEMENTS CAUSING FRACTURING.

Homogeneous, Impermeable Walls

These conditions (Fig. 5) permit the application of the thick wall cylinder theory wherein vertical fractures occur when the internal (fluid) pressure exceeds the tensile strength of the rock, plus the unknown external pressure acting to prevent the rock from breaking in tension.

Well Irregularities

Irregularities which may cause fracturing are notches and elliptically shaped enlargements (Fig. 6).

Pressure may tend to part formations at the enlargements. At the most, the pressure must exceed the sum of the rock strength, plus the effective overburden pressure. Effective overburden pressure is defined as the pressure required to inject a fluid into a formation after it has been fractured.

Intrinsic Fractures

Drilling fluids may enter intrinsic fractures (Fig. 7), permitting pressure to act in directions perpendicular to fracture planes. The fractures widen to allow further fluid entry. The pressure need only to exceed the effective overburden pressure, plus the pressure required to extend the fractures.

Permeable Zones

Drilling fluids may enter permeable zones (Fig. 8), causing pressure to be exerted in the porous media. Formations are fractured permitting further fluid entry. At the most, pressure must exceed the sum of effective overburden pressure plus the pressure required to overcome the strength of the rock in the permeable zone along the weakest plane.

Closed Hydraulic System

With a well closed-in (Fig. 9), any surface pressure not only increases bottom hole pressure but may also place a portion of a formation in tension by exerting an upward force on the pipe equal to the surface pressure times the inside cross-sectional area of the pipe. This condition is probably significant in shallow wells only.

It is possible that any or all of these conditions may be present in a single well; thus when pressure reaches a critical magnitude, it may be expected that induced fracturing and loss of circulation will occur first in the weakest zone.

C. DRILLING FLUID PRESSURE

Pressure to Fracture

A review of the records of squeeze cementing, acidizing, and hydraulic fracturing operations in 276 wells in the Mid-Continent and Gulf Coast areas shows that bottom hole pressure gradients in wells that were intentionally fractured in the process of treatment varied 0.65 psi to 1.14 psi per ft of depth. Values as low as 0.55 to 0.60 psi per ft of depth have been reported from other sources. These pressure gradients are obtainable with muds weighing from 10.5 lb/gal to 22 lb/gal. A plot of the pressure required to fracture the formations appears in Fig. 10. The significance of the depicted data is that it may be possible to fracture formations with the hydrostatic pressure created with muds weighing less than those frequently employed in current drilling operations. After the occurrence of fracturing, the pressure required to displace fluids into formations is substantially lower than that required for fracturing. See Fig. 11.

The data in Figs. 10 and 11 emphasize the importance of maintaining the lowest possible pressure against formations to

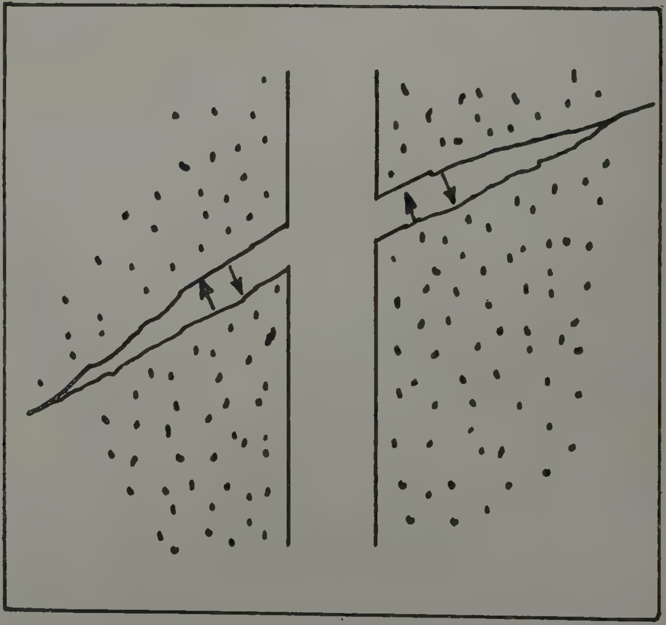

FIG. 7 — INTRINSIC FRACTURES AS THE CAUSE OF ADDITIONAL FRACTURING.

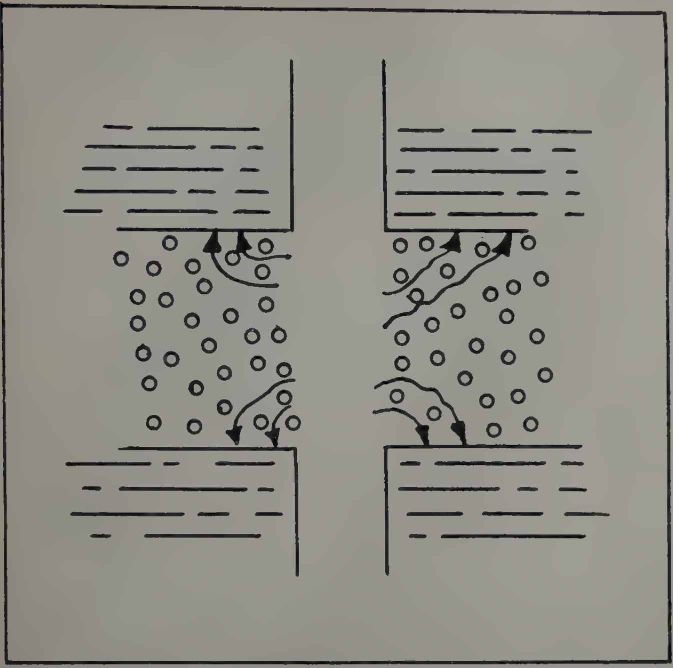

FIG. 8 — PERMEABLE ZONES AS THE CAUSE OF FRACTURING.

prevent lost circulation and are intended to serve as a guide in predicting what pressure may be regarded as in the critical zone.

Causes of Excessive Pressure

It has already been shown that the hydrostatic head of a column of mud may be sufficient to fracture a formation even before imposing the additional pressure required for circulation of the mud. With the hydrostatic pressure near a critical point and reduction of mud weight limited by the pressure necessary to control formation fluid pressure, the variables which affect the circulating pressure become an important consideration.

Changes in certain mud properties may directly or indirectly affect the circulating pressure. The most important are:

1. Drilling Mud Weight.

In addition to a reduction in hydrostatic head, it has been demonstrated by other investigators that as mud weight decreases, the pumping pressure for a constant circulating rate decreases proportionately.[6]

2. Flow Properties.

Experimentation has shown that drilling muds behave as plastic fluids[30,40,41] and, therefore, while in laminar flow, any reduction of yield value and rigidity permits an appreciable reduction in pump pressure while maintaining a constant rate of flow. The effect of varying the flow properties is shown in Fig. 12. If the yield value t_y and rigidity n, as defined by curve A are reduced to t_{y1} and n_1, as defined by curve B, it may be noted along the ordinate that the pressure drop required for a constant velocity in the region of laminar flow is much lower for curve B than curve A. In the region of turbulent flow the change in pressure from curves A to B for a constant velocity is less pronounced.

3. Filtrate Rate.

A high filtrate rate mud may indirectly increase pressure against formations by creating a thick filter cake which restricts mud flow up the annulus or may cause bridging.

Other causes for increases in pressure are:

1. Inertia of Mud Column.

When circulation is stopped for a period of time, any sudden application of pressure to start circulation may impose an unnecessarily high pressure peak on a formation due to the gel strength and inertia of the column of mud.[2]

2. High Circulating Rate.

The use of high circulating rates to remove cuttings in many instances imposes excessive pressure on formations. The same efficiency of cutting removal may be achieved without danger of causing lost circulation by altering the mud properties.

3. Hole Enlargements.

Hole enlargements may reduce mud velocity so as to allow cuttings to accumulate and then bridge at the point where the annulus is nearer normal causing pressure surges.

4. Surging of Pumps.

The results of an investigation conducted on a drilling rig in West Texas indicated that a variation in bottom hole annular pressure greater than 250 psi may be expected due to pump surges. Such a surge in a well 5,000 ft deep would be equivalent to increasing the mud weight over 1 lb/gal.

5. Swelling of Casing Protectors.

Swelling of casing protectors may cause restrictions in the annulus which necessitate increases in pump pressure to maintain a desired circulating rate.

6. Lowering of Drill Pipe.

One of the frequent causes of increased pressure is rapid lowering of the drill pipe. The bit forces fluid ahead at a greater rate than the fluid can flow back through the fluid ports. This failure of the fluid ports to accommodate the displaced mud may result in a pressure peak on the exposed formations.

PREVENTION OF LOST CIRCULATION TO FRACTURES

Precautionary measures to eliminate high pressure and pressure surges evidently many times fail to prevent the creation of fractures and loss of mud. The difference in the pres-

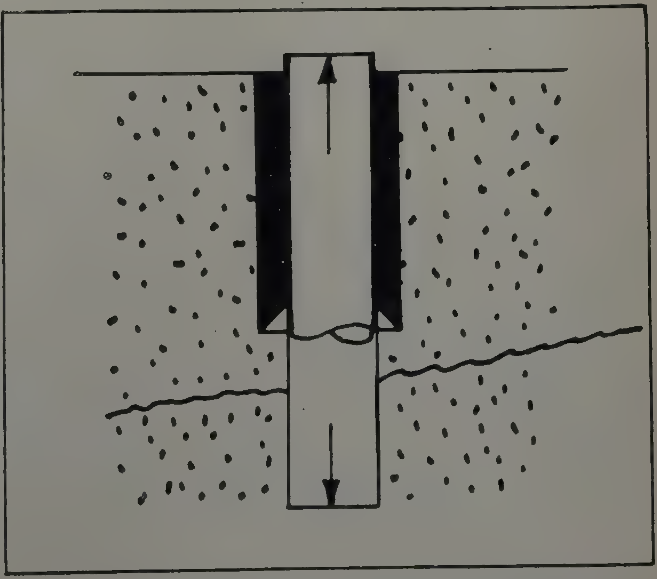

FIG. 9 — CLOSED HYDRAULIC SYSTEM CAUSING FRACTURING.

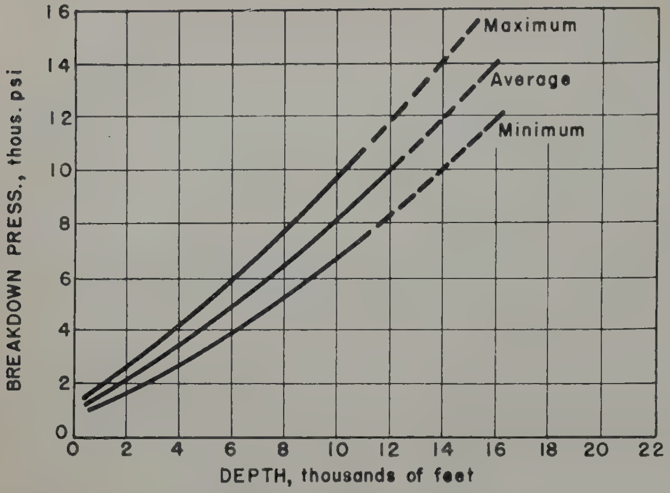

FIG. 10 — FORMATION BREAKDOWN PRESSURES OBSERVED DURING TREATMENT OF 276 WELLS IN THE MID-CONTINENT AND GULF COAST AREAS.

sure capable of fracturing formations and that required to control formation pressure is often so slight that loss of circulation is unavoidable. Study of possible means of preventing fracturing under this condition suggests that the presence of a suitable material in the mud at the instant fractures occur or are encountered should serve to plug the fractures immediately and thereby prevent the fluids from entering and widening the fractures. Such a preventative measure would achieve its effectiveness by sealing the fractures in their incipient state rather than after they have been widened and extended by inflow of mud. Practical application of this theory would now suggest the use in the mud stream of the maximum effective concentration of the most effective lost circulation material for plugging fractures.

A series of tests were initiated to determine the most effective materials for plugging fractures and to determine the maximum effective concentration of these materials.

Comparison of Materials

With a variety of lost circulation materials available, tests and organized study were facilitated by first classifying the materials with respect to their physical properties. It was found that almost all lost circulation materials fall into one of the four following classifications:

1. Fibrous — additives which have relatively little degree of rigidity and are pictured as tending to mat or entangle on the surface of or within a formation capable of taking mud.
2. Granular — additives which have rigidity and thus are able to bridge and wedge either at the face of or within formations capable of taking mud.
3. Lamellated — additives with the appearance of thin layers, scales, flakes, or sheets which may or may not have any degree of rigidity. The action of such an additive is to mat as shingles over a formation face or bridge in restrictions in a fracture.
4. Dehydratable — materials which are capable of being deprived of their carrier or extraneous fluids and thus formed into a semisolid plug through which drilling fluid particles cannot penetrate.

To compare selected materials representative of all four types, tests were made of the ability of the materials to seal simulated fractures and loose sands and gravels.

Fractures were simulated by placing cement on both sides of a metal shim, 18 in. long, centered inside of a pipe, 5½ in. in diameter, which was lined with sheet rubber, ½ in. thick. Removal of the shim after the final set of the cement created a smooth fracture 4 in. wide, 18 in. long, and with a clearance equal to the thickness of the shim (see Fig. 13). Pressure taps were placed at intervals along the pipe. The test fractures described were so designed to permit expansion or enlargement should pressure be imposed on the fracture planes. In this manner bottom hole lost circulation conditions

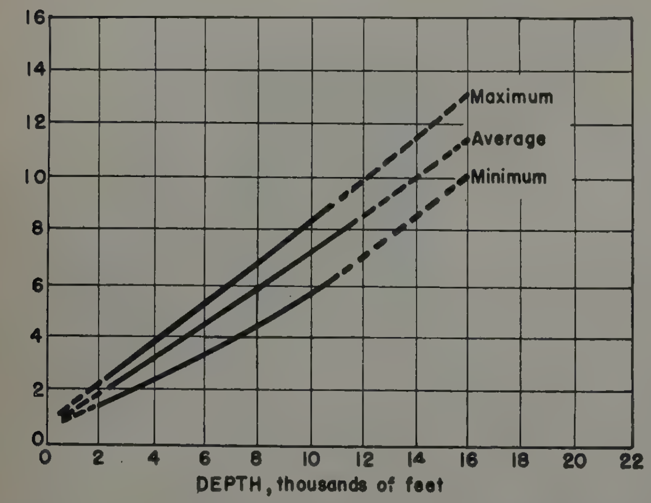

FIG. 11 — PRESSURES TO INJECT FLUIDS INTO FRACTURES AS OBSERVED DURING THE TREATMENT OF 276 WELLS IN THE MID-CONTINENT AND GULF COAST AREAS

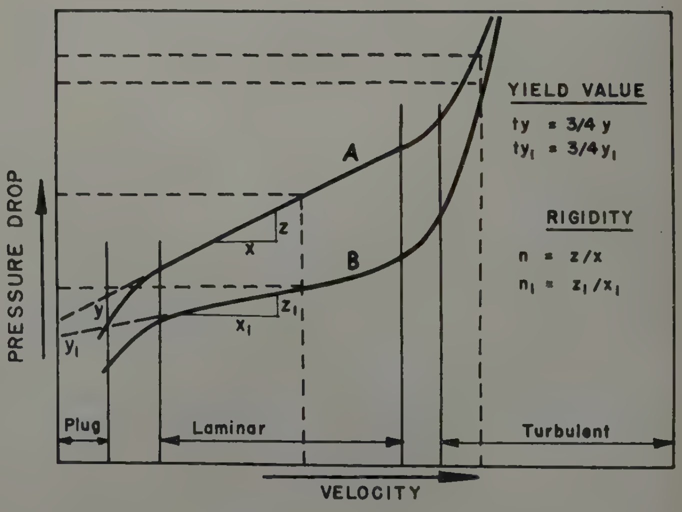

FIG. 12 — EFFECT OF CHANGING MUD FLOW PROPERTIES.

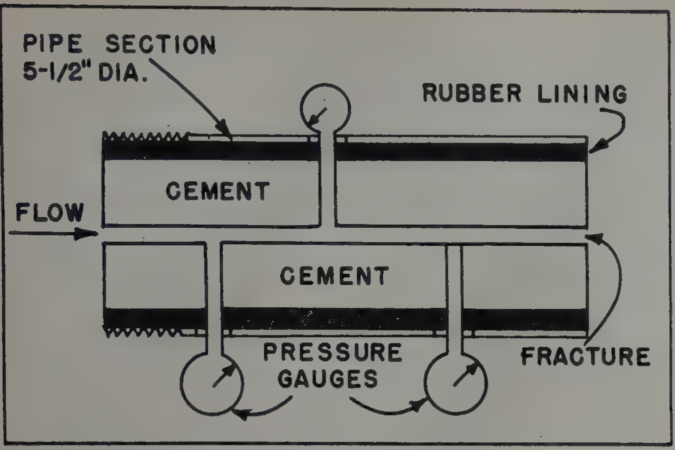

FIG. 13 — SIMULATED TEST FRACTURE.

were partially simulated. The pipe sections containing the simulated fractures with clearances of from .017 to more than 0.2 in. were hung in a vertical position from a manifold connected to a piston type pump. This range of fracture clearances was selected because it compared to that observed in cores removed from wells following loss of circulation and cement squeeze operations. The testing procedure consisted of pumping drilling mud containing controlled concentrations of lost circulation materials through the fractures until a seal was effected which would withstand 1,000 psi pressure differential. With each size fracture the concentration of material was increased in small increments until a seal was achieved or until the poor pumpability of a high concentration precluded further tests. The volume of mud which passed through a fracture before obtaining a seal was measured and recorded. If 40 gal were pumped through a fracture and failed to seal, the particular concentration was judged incapable of sealing the size fracture being tested. The results of representative tests are shown in graphical form in Fig. 14. The importance of the use of the maximum effective concentration of material is clearly demonstrated in this figure. For example, as in the case of the fibrous material, a concentration of 12 lb/bbl is indicated to be capable of sealing a fracture with a clearance of 0.11 in.; whereas a concentration of 4 lb/bbl was found capable of sealing a fracture with a clearance of only .07 in. Within the limits of pumpability any concentration in excess of 12 lb/bbl would not seal any fracture larger than .11 in.; therefore 12 lb/bbl becomes the maximum effective concentration of the particular fibrous material.

Fig. 15 presents a summary of the evaluation tests by listing the additives in the order of effectiveness which in the tests was determined by the size fracture which was sealed. This compilation indicates that the most effective materials for plugging fractures and withstanding high pressure differentials are the granular type.

Material Plugging Characteristics

In agreement with previous work with granular materials, it was found that the effectiveness of all granular materials is dependent upon a proper gradation of particle sizes to give the bridged mass of particles a sufficiently low permeability to prohibit the passage of fluids and thereby be an effective seal.

Inspection of the seal effected by fibrous, granular, and lamellated materials revealed that the seal occurred at the entrance of the fractures, thus fluid pressure was prevented from being exerted within and widening the fractures, as was evidenced by the zero readings on pressure gauges connected to the fracture while the pressure at fracture face read 1,000 psi. This manner of sealing may offer an effective solution to the problem of prevention of mud loss to fractures.

The results of tests conducted in a number of laboratory shallow wells indicate that dehydratable materials such as cement or high fluid loss mud have been successful in regaining circulation in formations previously fractured. These results were substantiated by a test in the High Island Field at a depth of 1,538 ft where a formation was intentionally fractured just below the surface casing. The use of a set-killed high-water-loss cement forced into the fracture permitted an increase in circulation pressure to a value above that originally required to breakdown the formation. This action is similar to that which is experienced when obtaining high final pressures during cement squeeze operations. The effectiveness of a dehydratable material may depend upon the presence of a permeable zone and it is improbable that shale sections could afford in the walls of all fractures the permeability necessary to allow dehydration. However, this does not preclude the possibility of the material dehydrating through its own mass within the fracture itself, once a bridge is formed in a restriction, so as to form a plug capable of preventing the flow of whole mud and loss of circulation.

All of the materials, except the dehydratable type, were tested through loose gravel and sand and found capable of effecting a seal. Due to the similar sealing characteristics of all the materials in sands and gravels, no comparison was made in this respect.

With granular materials indicated to be most suitable for preventing fracturing, additional tests were initiated to substantiate the merits of these materials. The first series of tests consisted of squeezing a low-water-loss cement containing a granular lost circulation material into a well in a simulated homogeneous formation to determine the ability of the material to prevent enlargements of fractures. An example of the

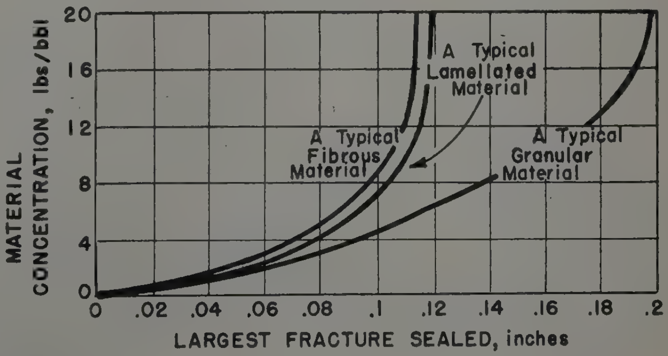

FIG. 14 — EFFECT OF CONCENTRATION OF LOST CIRCULATION MATERIALS WHEN SEALING FRACTURES.

results obtained in these tests is shown in Fig. 16, which shows a horizontal cross-section of the well after the cement slurry had set under pressure. The formation was fractured, but extension of the fractures appeared to have been prohibited by the bridging of the granular material at the initial stages of the fractures.

The second series of tests was conducted in shallow wells drilled in the laboratory yard. The ability of granular lost circulation material to prevent the occurrence of lost circulation was illustrated in a test in two ft of open hole in a well 15 ft deep. The formation was fractured at a pressure of 1,100 psi and mud containing a granular material pumped into the hole. The material sealed the fracture and permitted the imposition of 3,000 psi pressure. The well was pumped dry, and by employing a system of mirrors, the open hole section was photographed. A picture typical of those obtained appears in Fig. 17, where granular materials bridged and matted at the entrance of two fractures may be seen. This test indicated that the presence of a surface sealing lost circulation material in the mud permitted the application of pressure well above that normally required to fracture the formation and apparently prevented the fluid pressure from acting within the fracture already created.

Disposing of Cuttings and Reclaiming Lost Circulation Materials

To use lost circulation materials while penetrating zones susceptible to lost circulation would require that the materials be added to the mud stream frequently to compensate for losses on the shale shaker or that the shale shaker be removed and the accumulation of cuttings be disregarded until the concentration became high. In the latter case, the cuttings could be removed by jetting them off the bottom of the mud pits or by replacing the shale shaker. Both methods result in a loss of lost circulation materials. To reduce this loss, several measures were considered, including the use of ore shaking table which utilizes the difference in particle density and size and the use of a centrifugal sorter.

The use of a new type centrifugal sorter was favored over the other means because of its ability to handle many different lost circulation materials regardless of their physical properties.

The centrifugal sorter, a cross-section of which is shown in Fig. 18, operates by a power impeller forcing the mud containing cuttings and lost circulation materials into a rotating, perforated, separating impeller within a shell or chamber. As the mud enters the individual perforations of the separating

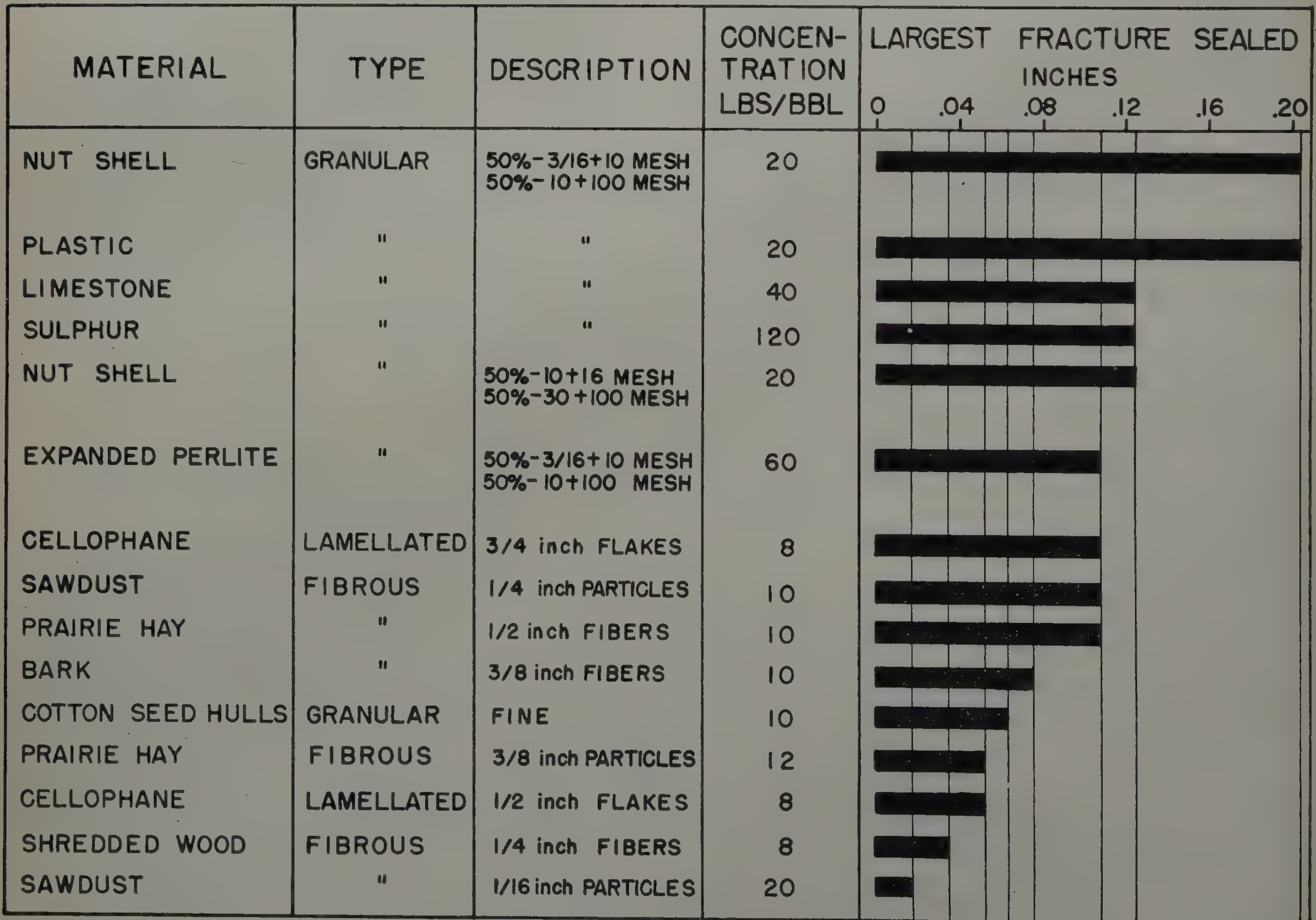

MATERIAL	TYPE	DESCRIPTION	CONCENTRATION LBS/BBL
NUT SHELL	GRANULAR	50%-3/16+10 MESH 50%-10+100 MESH	20
PLASTIC	"	"	20
LIMESTONE	"	"	40
SULPHUR	"	"	120
NUT SHELL	"	50%-10+16 MESH 50%-30+100 MESH	20
EXPANDED PERLITE	"	50%-3/16+10 MESH 50%-10+100 MESH	60
CELLOPHANE	LAMELLATED	3/4 inch FLAKES	8
SAWDUST	FIBROUS	1/4 inch PARTICLES	10
PRAIRIE HAY	"	1/2 inch FIBERS	10
BARK	"	3/8 inch FIBERS	10
COTTON SEED HULLS	GRANULAR	FINE	10
PRAIRIE HAY	FIBROUS	3/8 inch PARTICLES	12
CELLOPHANE	LAMELLATED	1/2 inch FLAKES	8
SHREDDED WOOD	FIBROUS	1/4 inch FIBERS	8
SAWDUST	"	1/16 inch PARTICLES	20

FIG. 15 — SUMMARY OF MATERIAL EVALUATION TESTS.

impeller, centrifugal force tends to throw the high density cuttings back into the chamber, while part of the low density materials are allowed to pass through with the mud. Cuttings are carried out the reject line while an almost unchanged concentration of lost circulation material is carried out the discharge line.

For testing purposes, the sorter was assembled with both reject and discharge lines emptying into the suction tub.

The lost circulation materials tested consisted of ground nut shells, ⅛ in. sawdust, ground plastic, ⅜ in. and ¾ in. cellophane flakes, and ½ in. prairie hay. Mud properties, sorter RPM, and discharge rates were varied and the efficiency of separation observed. To determine additive and cutting concentrations, samples were taken at the discharge and reject outlets. The samples of cuttings and materials were screened, washed, separated in a mixture of bromoform and alcohol, dried, and weighed. Results of tests are shown in Table II.

Analysis of the compiled data shows that the suction concentration of 100-mesh and larger cuttings was reduced from 100 lb/bbl to less than 2 lb/bbl, while a nearly constant concentration of lost circulation material was maintained from suction to discharge. It was noted during tests that the weight of mud containing barite was not altered when passing through the sorter and mud filtrate rate and viscosity were not affected.

The use of the sorter in the field to serve as a means for concentrating cuttings to be rejected and for reclaiming lost circulation materials might introduce technical difficulties which were not apparent in the laboratory. The effectiveness under actual operating conditions remains to be determined by field tests.

CONCLUSIONS

From the test data compiled to date and from the results of the study of the factors believed by the authors to affect lost circulation, it may be concluded that by incorporating the maximum effective concentration of a proper gradation of granular material in a mud stream when zones susceptible to lost circulation are penetrated, it should be possible in many instances to reduce to a minimum the loss of circulation to fractures by the effective plugging action of granular materials at the moment such fractures are created or encountered. More specifically, the study has shown as follows:

1. Induced fractures may be a frequent cause of lost circulation.
2. The pressure normally employed while drilling may in many instances be sufficient to cause fracturing of rock formations.
3. Granular lost circulation materials in a proper gradation of particle sizes were found by laboratory tests to be the most effective type material for controlling mud loss to fractures.
4. Limited test data indicate that dehydratable materials are effective for regaining circulation.
5. Tests in shallow and simulated wells indicate that the maximum effective concentration of a proper gradation of

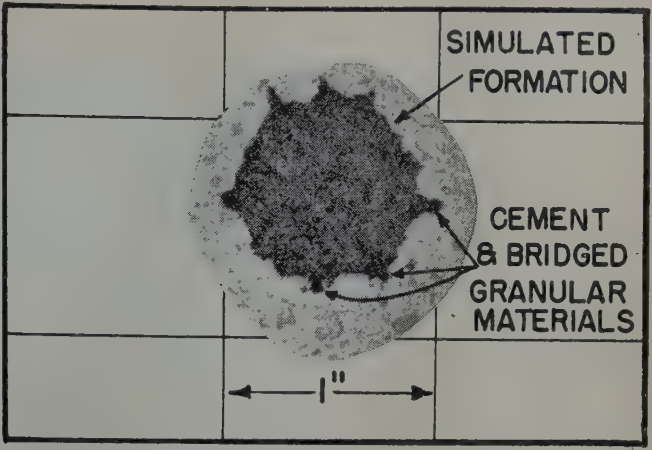

FIG. 16 — EFFECT OF GRANULAR MATERIALS IN CEMENT.

Table II — Results of Tests with Centrifugal Sorter Used for Separating Bit Cuttings and Lost Circulation Materials

LOST CIRCULATION MATERIAL			SUCTION PIT ANALYSIS				REJECTED MUD ANALYSIS								DISCHARGE MUD ANALYSIS								
			Mud Properties			Cuttings Conc.	Lost Circ. Material	Cuttings			Mud				Lost Circ. Material	Cuttings			Mud				
								Concentration in lb./bbl. Retained on U. S. Standard Sieve								Concentration in lb./bbl. Retained on U. S. Standard Sieve							
Test No.	Conc. lbs./bbl.	Type	Wt. lbs./gal.	Vis cp	Fluid Loss cc/7½ Min.	lbs./bbl. (Approximate)	Concentration lbs./bbl.	No. 40	No. 100	No. 200	Vol. gpm	Wt. lb./gal.	Vis cp	Fluid Loss cc/7½ Min.	Concentration lbs./bbl.	No. 40	No. 100	No. 200	Vol gpm	Wt. lbs./gal.	Vis cp	Fluid Loss cc/7½ Min.	RPM
1	23	Walnut Shell Gnd -10+16 Mesh	9.5	48	14	None	25.8	—	—	—	200	—	—	—	20.6	—	—	—	300	9.5	48	14	1000
2	20	Walnut Shell Gnd -3/16"+10 Mesh	9.6	48	14	None	24.6	—	—	—	200	—	—	—	21.0	—	—	—	300	9.6	48	14	1000
3	18	Walnut Shell Gnd -10+16 Mesh	11.4	60	12	10	17.0	12.2	1.1	3.1	300	11.4	—	—	19.0	0.2	0.6	3.1	300	11.4	60	12	1000
4	9	Pine Sawdust 1/8"	9.5	57	—	10	8.9	—	15.5	3.3	300	—	—	—	8.8	—	0.3	2.2	300	9.5	57	—	1200
5	8	Pine Sawdust 1/8"	9.5	135	—	10	8.9	—	12.8	3.5	300	—	—	—	8.7	—	0.6	2.6	300	9.5	130	—	1200
6	12	Ground Plastic -10+200 Mesh	9.5	60	—	10	11.9	14.7	1.4	2.2	300	—	—	—	10.2	0.8	0.4	2.2	300	9.5	58	—	1100
7	20	Prairie Hay 1/2"	9.5	35	—	5	25.0	—	6.8	1.0	300	—	—	—	15.0	—	(Trace)	1.0	300	9.5	36	—	1100
8	8	Cellophane 3/8"	9.5	45	—	5	9.3	6.2	0.2	1.1	300	—	—	—	6.3	(Trace)	(Trace)	1.0	300	9.5	45	—	1100
9	8	Cellophane 3/8"	9.5	50	—	2	11.0	—	20.0	—	14	—	—	—	7.8	—	1.0	—	500+	9.5	50	—	1200
10	10	Walnut Shell Gnd -10+16 Mesh	9.5	30	—	2	9.7	4.2	1.0	—	60	—	—	—	8.5	0.6	0.8	—	425+	9.5	30	—	1100
11	6	Walnut Shell Gnd -10+16 Mesh	9.5	56	—	70	6.0 Nuts	119.0	—	—	300	—	—	—	6.0 Nuts	19	—	—	300	9.5	56	—	1000
	4	Pine Sawdust					4.8 Saw								3.3 Saw								
12	5	Walnut Shell Gnd -10+16 Mesh	9.5	56	—	75	5.9 Nuts	140.0	2.2	—	300	—	—	—	3.7 Nuts	0.4	1.5	—	300	9.5	56	—	1400
	3	Pine Sawdust 1/8"					3.0 Saw								3.0 Saw								
13	10	Walnut Shell Gnd -10+16 Mesh	9.5	56	—		11.0 Nuts	184.0	4.0	—	300	—	—	—	9.0 Nuts	1.0	1.8	—	300	9.5	54	—	1400
	8	Pine Sawdust 1/8"				100	8.4 Saw								7.5 Saw								
	8	Cellophane 3/4"					8.5 Cello.								7.3 Cello.								

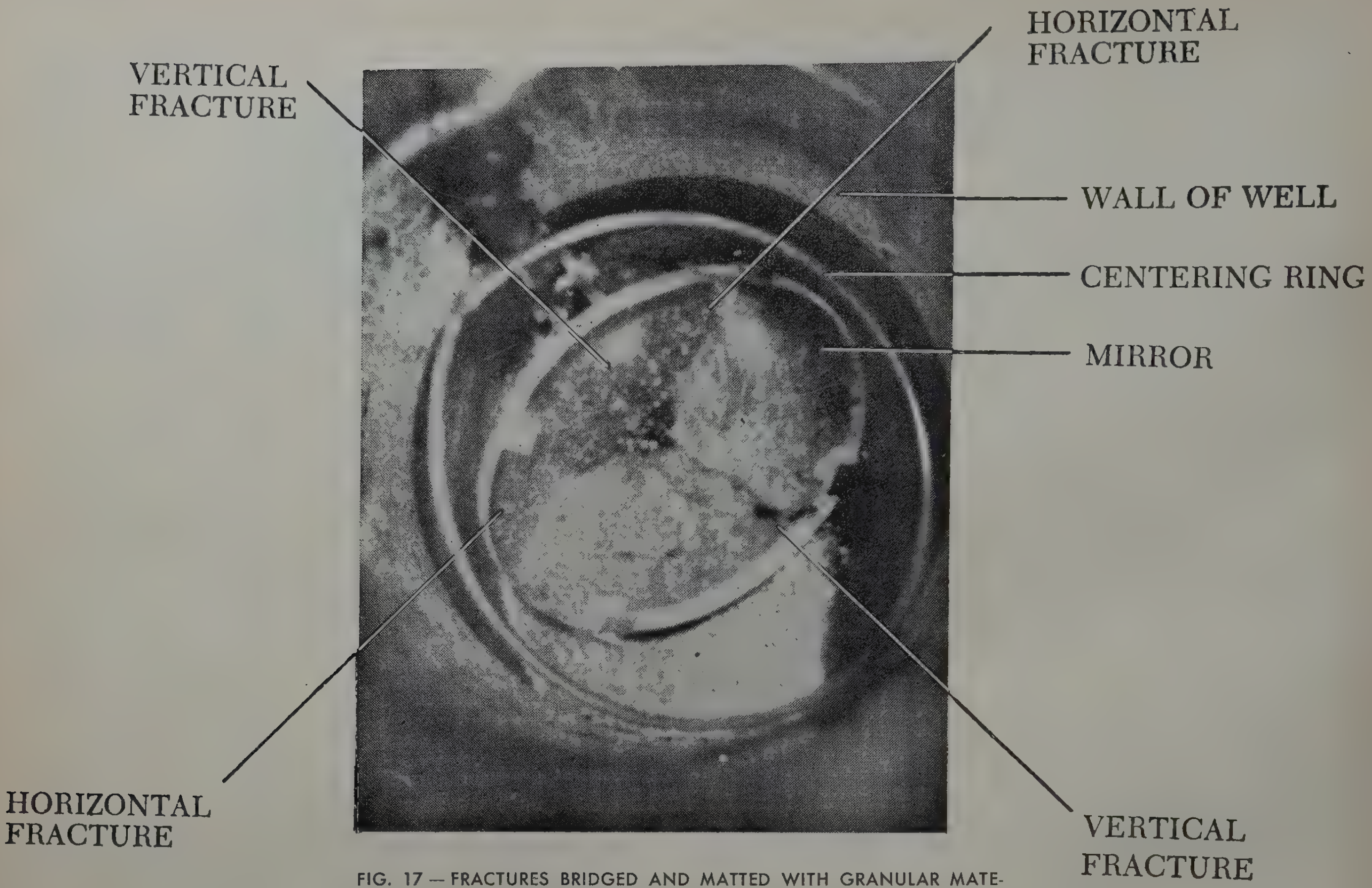

FIG. 17 — FRACTURES BRIDGED AND MATTED WITH GRANULAR MATERIAL AS PHOTOGRAPHED IN SHALLOW TEST WELL.

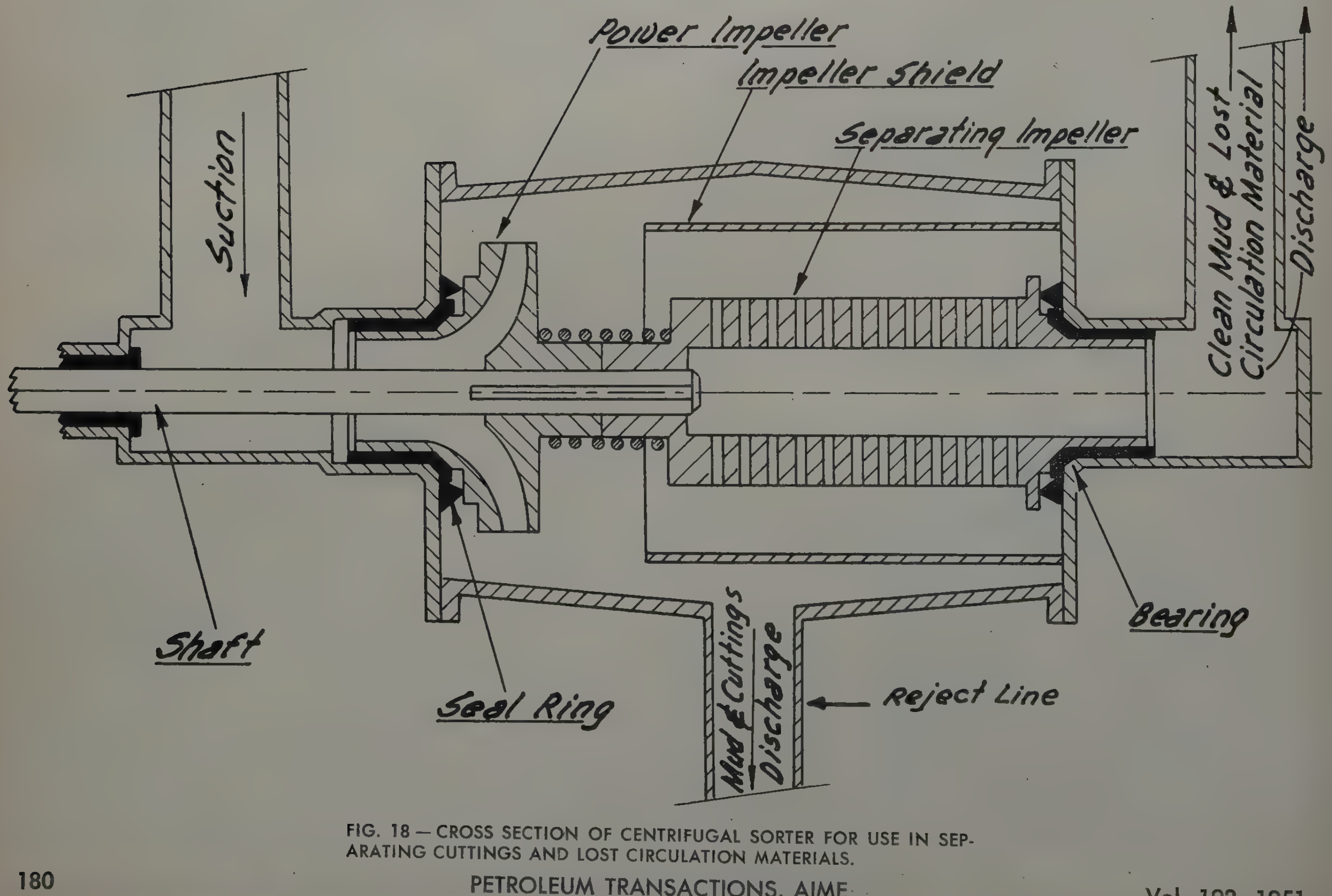

FIG. 18 — CROSS SECTION OF CENTRIFUGAL SORTER FOR USE IN SEPARATING CUTTINGS AND LOST CIRCULATION MATERIALS.

granular material in drilling fluids permits the imposition of higher pressure than normally is required to fracture formations.

6. In laboratory tests a new type centrifugal sorter was found suitable for concentrating cuttings to be rejected and reclaiming lost circulation materials.
7. The concentration in mud of a lost circulation material is a critical factor affecting the ability of the material to seal fractures.

The problem of lost circulation is of sufficient importance to justify considerable work in the future. While it is the hope of the authors that the methods of prevention and control of lost circulation advanced in this paper will aid materially in the solution of the problem, it is fully recognized that additional effort must be directed towards a more positive method.

ACKNOWLEDGMENT

The authors wish to express their appreciation to the management of the Stanolind Oil and Gas Co. for permission to prepare and publish this paper.

REFERENCES

1. Silent, R. A.: API *Drill. and Prod. Prac.*, (1936), 60-67.
2. Chaney, P. E.: *Oil and Gas Jour.*, (April 21, 1949), 210-215.
3. Byck, H. T.: API *Drill. and Prod. Prac.*, (1940), 40-44.
4. Short, E. H., Jr.: *Oil and Gas Jour.*, (January 6, 1944), 56-59.
5. Stearns, G. M.: *Oil and Gas Jour.*, (May 25, 1944), 119.
6. Cannon, G. C., and Sullins, R. S.: API *Drill. and Prod. Prac.*, (1946), 29-33.
7. Hertel, F. W., and Edson, E. W.: *Trans.* AIME, (1930), **86**, 387-388.
8. Anon.: *Oil and Gas Jour.*, (Sept. 22, 1949), 266-268.
9. Morris, J. I.: *World Oil*, (April, 1949), 105-112.
10. Townsend, A. A.: *World Oil*, (April, 1949), 124-127.
11. Sawdon, W. A.: *Petr. Engr.*, (April, 1935), 29-31.
12. Scamman, C. W.: *Petr. Engr.*, (June, 1949), B13-B18.
13. Bryson, F. E.: *World Oil*, (June, 1948), 100-102.
14. Chaney, P. E.: API *Drill. and Prod. Prac.*, (1942), 31-46.
15. Lindsay, C. A.: *Oil and Gas Jour.*, (Dec. 14, 1946), 92-105.
16. Stormont, D. H.: *Oil and Gas Jour.*, (Sept. 1, 1949), 51-65.
17. Parsons, C. P., and McQuiston, H. L.: *Oil and Gas Jour.*, (April 18, 1935), 50-86.
18. Louden, E. W.: *World Oil*, (Sept., 1948), 85-94.
19. Sawdon, W. A.: *Petr. Engr.* (Feb., 1936), 27-30.
20. Leach, G. L.: *Petr. Engr.*, (Dec., 1940), 94-100.
21. Barberii, E. E.: *Oil and Gas Jour.*, (July 28, 1949), 280-284.
22. Howard, G. C., and Fast, C. R.: *Trans.* AIME, (1950), **189**, 53.
23. Torrey, P. D.: API *Drill. and Prod. Prac.*, (1939), 211-213.
24. Rogers, W. F.: *Composition and Properties of Oil Well Drilling Fluids*, Gulf Pub. Co., (1948).
25. Sidwell, C. V.: *World Oil*, (Nov., 1949), 123-130.
26. Core, C.: *Oil Weekly*, (Sept. 13, 1943), 25-28.
27. Stone, J. B.: *Oil and Gas Jour.*, (Aug. 8, 1940), 44-45.
28. Gates, G. L.: "Correlation of Certain Properties of Oil Well Drilling Mud Fluids with Particle Size Distribution, U. S. Bureau of Mines, RI 3645, (1942).
29. Cannon, G. E.: API *Drill. and Prod. Prac.*, (1934), 42-47.
30. Anon.: *Petr. Engr.*, (Oct., 1931), 17.
31. Williams, N.: *Oil and Gas Jour.*, (March 15, 1934), 13-18.
32. Anon.: "Plastics Used in Experiment by Sun Oil Co.," Stanolind News Letter, Anse La Butte Area, (Jan. 31, 1948).
33. Anon.: "Drilling and Completion, First State Bank of Stratford 'A' No. 1, Sherman County, Tex.," Stanolind Central Division Engineering Memorandum, Hugoton Field, Kans., (Sept. 13, 1948).
34. Personal communications with cement manufacturers.
35. Anon.: "Experimental Use of Air-Cut Mud for Prevention of Lost Circulation," Stanolind News Letter, Rocky Mountain Division, (Dec. 11, 1945.)
36. Muskat, M.: *Flow of Fluids Through Homogeneous Media*, McGraw-Hill Co., (1937).
37. Coberly, C. J.: API *Drill. and Prod. Prac.*, (1937).
38. Vogler, A. F.: "Jelflake Aids in Deep Well Drilling," *Drilling*, (Oct. 25, 1946).
39. Caldwell, D. H., and Babbitt, H. E.: *Ind. Eng. Chem.*, (1941), **33**, 249-256.
40. Pigott, R. J. S.: API *Drill. and Prod. Prac.*, (1941), 91-103.
41. Beck, R. W., Nuss, W. F., and Dunn, T. H.: API *Drill. and Prod. Prac.*, (1947), 9-22.

★ ★ ★

DISCUSSION

By George E. Cannon, Member AIME, Humble Oil and Refining Co., Houston, Tex.

Howard and Scott have done an excellent job in the evaluation of lost returns materials and their analysis of the problem is both concise and complete; however, there are two statements in the analysis which we believe should be clarified. These statements are in the Drilling Fluid Pressure section under Causes of Excessive Pressure, and are as follows:

1. Drilling Mud Weight. The statement that drilling mud weight has an effect on mud pressure is true; however, the majority of pressure increase or decrease due to increased or lowered mud weight occurs inside the drill pipe. Because of this, circulating pressure in the annular space is not appreciably affected by mud weight as implied by the statement; therefore, mud weight would have a greater tendency to cause fractures through exerting a hydrostatic head than through increased frictional resistances.

2. Flow Properties. This statement is also true in that flow properties of a drilling fluid affect the pressure required to move the fluid at a constant velocity in laminar flow; however, cases are rare in which flow of fluid in the annulus is laminar. Such a small velocity is required to achieve turbulent flow in the annular space that laminar flow seldom exists.

DISCUSSION

By Preston E. Chaney, Sun Oil Co., Beaumont, Tex.

In evaluating fibrous or granular materials for controlling lost circulation, it is essential that we understand the mechanism responsible for lost circulation. In those cases where circulation is lost to gravel beds, cavernous or highly fractured formations, the use of granular materials is quite logical and has a reasonable chance of success.

However, in the case of abnormal pressure wells, in which the hydrostatic pressure of the mud column approximates the overburden pressure the use of such materials is not so clearly indicated. By methods such as spinner surveys, and temperature surveys using chilled or heated muds it has been established that circulation is lost to non-porous shale beds at least as often as to sands under abnormal pressure conditions.

In such cases, circulation is lost by tensile failure of the formation produced by internal pressure in excess of the compressive load of the overburden. Since this involves the same factors as the failure of a pressure vessel, the laws governing the design of thick walled pressure vessels should apply. Elastic theory teaches that a pressure vessel, even though the wall thickness be infinite as compared to the diameter of the bore, cannot withstand an internal pressure in excess of the ultimate tensile strength of the material from which it is constructed. This conclusion is certainly not obvious, but may be visualized as follows: Internal pressure is first applied to the fibers nearest the bore of the pressure vessel. This load can be shared by more distant fibers only by elongation of these internal fibers. The diameter, and therefore, the circumference of the bore must increase in order to permit transfer of the load to these more distant fibers. If the internal pressure be in excess of the ultimate strength of the material, the internal fibers are stressed to failure before the most distant fibers accept any appreciable portion of the stress.

Our problem thus resolves to the question of the best method of operating a pressure vessel stressed to its ultimate strength. It is not sufficient to plaster the cracks produced by failure of the walls of the bore hole because this merely transfers the problem to fibers more distant from the well bore, but no more capable of withstanding the load than those which failed originally.

We must either increase the tensile strength of the walls of the bore hole, or decrease the pressure applied to the formation. At present we have no means for appreciably increasing the tensile strength of the formation. Therefore we must concentrate on reducing the applied pressure to the minimum consistent with safe drilling practice. The minimum mud weight is dictated by the requirement that the hydrostatic pressure of the mud column be slightly in excess of the formation fluid pressures encountered. This is the absolute minimum pressure that must be applied to the walls of the bore hole.

However, in addition to this pressure, there are numerous surge or peak pressures resulting from balling of the bit or drill collars, rapid lowering of the drill pipe, or sudden starting of the pumps when starting circulation. The magnitude of these surge pressures is demonstrated by Goins,[1] and is quite large in terms of equivalent mud weight increase. These surge pressures are at least partially within our control and we should make every effort to eliminate them.

An additional pressure loading on the well bore is the pressure differential in the annulus required to circulate the mud. This pressure is dependent upon the rate of circulation and the viscosity of the mud, both of which are subject to control within limits. It seems desirable to reduce circulation rate to the minimum consistent with cutting removal, even though this requires a considerable reduction in drilling rate. Also, it seems essential to maintain the mud viscosity at a minimum. It is in this connection that I question the advisability of adding granular materials to prevent or combat lost circulation under abnormal pressure conditions. If such materials be added to a concentration sufficient to reduce the pumpability of the mud, it seems they might aggravate rather than correct the trouble.

REFERENCES

1. Goins, W. C., Jr., Weichert, J. P., Burba, J. L., Jr., Dawson, D. D., Jr., and Teplitz, A. J.: *Oil and Gas Jour.*, (April 12, 1951), 86.

AUTHORS' REPLY TO MR. CHANEY

Chaney's criticism is well founded — *if* the thick wall cylinder theory applies directly to porous rock formations, failure would be expected at or in the range of the tensile strength of the surrounding rock. The formation breakdown pressure would, therefore, be equal to rock strength (approximately the tensile strength if the thick wall cylinder theory applies), plus the confining effect of the overburden. Applying this rule to the 15 ft shallow well test, cited as an example in the reference paper, the formation breakdown would be expected to occur at approximately 540 psi, or 525 psi (tensile strength) plus 15 psi (overburden). In this shallow test the initial breakdown with mud occurred at 1,100 psi. The difference in the 540 psi calculated and the 1,100 psi actually observed in this test is partly accountable to surges in pressure during breakdown operations and is partly believed to be due to variations in tensile strength of the sandstone, as compared to the tensile strength of a tested sample. The 3,000 psi pressure imposed and held for better than 30 minutes in this previously fractured shallow well, after the introduction of granular lost circulation recovery material, indicated that pressures greatly in excess of the tensile strength of the surrounding rock, plus the overburden pressure, can be imposed by incorporating a proper gradation in size of a granular material in the drilling mud.

★ ★ ★

T.P. 3060

A GRAVEL PACK COMPLETION FOR EXCLUSION OF GAS AND WATER

THOMAS S. WEST, MEMBER AIME, BLANCO OIL CO. AND AL BUCHANAN PRODUCTION CO., SAN ANTONIO, TEX.

ABSTRACT

A gravel pack completion is described which, in addition to sand screening, permits the exclusion of water and gas from the oil production.

A gravel pack composed of alternate layers of different particle sizes is employed which has horizontal but not overall vertical permeability to drilling mud. A packer is run on the tubing and set in the screen member, around which the gravel layers are placed. The hydrostatic pressure of a mud column prevents the entry of fluid above (or below) the level of the packer. The producing level may be changed by raising or lowering the tubing.

Vertical coning is controlled by replacing the mud column with oil and continually injecting oil into the sand section above (or below) the packer.

Three well histories with this completion are described in detail. Statistics on the first 100 completions of this general type are given.

INTRODUCTION

Gravel pack type completions have heretofore been almost exclusively for the purpose of preventing sand production. This paper describes and presents well data on a gravel pack procedure which is primarily a selective completion method. Although complete sand screening is achieved, the exclusion of gas and water is the primary objective. The application of this procedure is therefore not limited to unconsolidated sands. Application to hard sand or limestone reservoirs is equally feasible.

GRAVEL PACK PROCEDURE

Figs. 1 and 2 illustrate the gravel pack procedure employed. The gravel is placed by means of the frangible disc type dump bailer shown by Fig. 1.[1] This bailer has its lower end closed by a plate glass or steel rimmed cement disc. This disc breaks when the bailer passes over the liner allowing the gravel to be deposited around the liner. The liner employed is usually 2⅜ in. to 2⅞ in. OD and 1.995 in. or 2.07 in. ID (ID of 2-in. tubing or 2-in. line pipe). Two types of slotted sections have been employed. One type employs horizontal hacksaw cut or milled slots of about 1/32 in. width opposite the producing section. The other type employs the same type of horizontal slot, but slots are placed in groups of six at intervals of about 8 in. A cage composed of half round vertical bars, spaced apart, is then welded to the pipe over the slotted sections. This liner has the bottom end closed, usually by bull plugging. The upper end is closed, while placing the gravel, by a cap which is held in place by means of a shear pin. This cap has a mandrel attached to it which extends downward inside of the liner to within a few inches of its lower end. The top of the liner cap is formed to fit a releasing type wire line core barrel overshot. The liner is lowered to bottom on the wire line by means of this overshot and released. The length of the liner is usually sufficient to extend to about 20 ft above the highest level to which gravel is to be placed, the upper end of the liner always being in the casing. The dimensions of the liner and bailer are such with respect to the casing size that the bailer will always pass over the liner. After releasing the liner the bailer is run to bottom. Passage of the empty

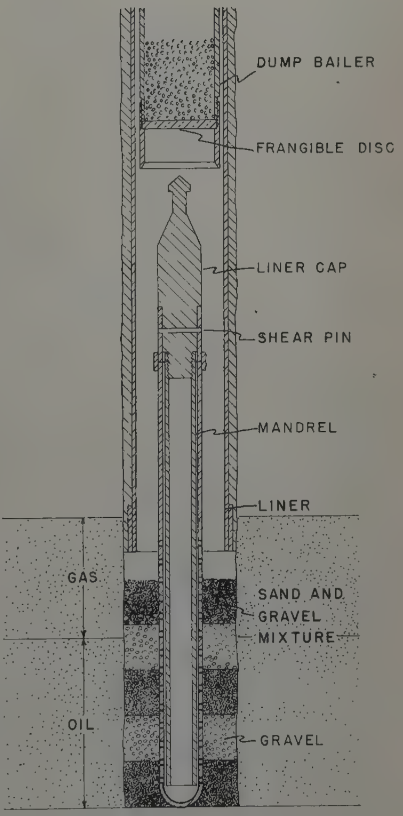

FIG. 1 — GRAVEL PACK PROCEDURE EMPLOYED.

---

[1] References given at end of paper.

Manuscript received in the office of the Petroleum Branch, Sept. 3, 1950. Paper presented at the Fall Meeting of the Branch in New Orleans, La., Oct. 4-6, 1950.

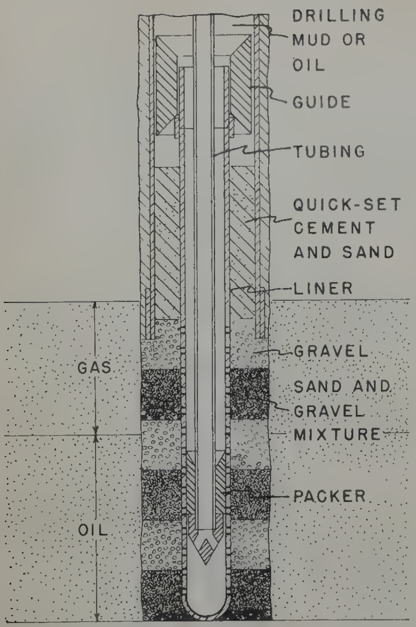

FIG. 2 — GRAVEL PACK PROCEDURE EMPLOYED.

bailer over the liner in this way serves to centralize the liner, this being the only procedure for this purpose which has proved necessary in practice.

Two types of layers are then dumped around the liner. One layer is composed of gravel of the grain size required to screen the sand. This size is determined from screen analysis of the producing sand; the gravel grain size being not larger than six times the sand grain size at the 10 per cent point on a sieve analysis curve of the sand using U. S. standard sieve series. This, of course, refers to the coarsest 10 per cent of the sand. The resulting grain size is usually about 1/16 in. The other layer is composed of this gravel with sufficient sand mixed with it to fill the gravel pore spaces. In order to prevent the sand and gravel from separating while this mixture is being dumped it is also necessary to use a binder. A binder is available for this purpose which will not only hold the sand and gravel together while being deposited but which will later flow out under about 50 psi pressure differential leaving an intimately mixed permeable sand and gravel layer. A layer is thus provided which will not flow through liner slots required for the gravel size necessary to screen the sand but which has pore space size approximating that of the producing sand. For example, drilling mud will not flow through these layers. Also exceedingly fine-grained sand may be successfully screened. The thickness of these layers is usually from 6 in. to 12 in. The thickness of the layer deposited can be determined to within about 2 in. by observing "pick up" of the dump bailer.

Alternate horizontal layers of the above two types are placed around the liner opposite the producing section and usually to about four or five ft above the bottom of the casing and at least this distance above the highest liner slot. A mixture of quick-set cement and sand is then dumped around the liner and directly on top of the gravel. The volume of cement is such that the upper four or five feet of the liner, including the cap, is above the cement. Cement is dumped with the same bailer employed for dumping gravel. After the cement has set (usually about two hours after dumping) the cement fill up is checked by running the dump bailer empty. If cementing is satisfactory the liner cap is engaged by means of the wire line overshot employed in running it. The shear pin holding the cap to the liner is sheared by an upward pull on the wire line and the cap and attached mandrel retrieved. The design of the liner cap is such as to permit recovery with a conventional 2 in. overshot should the core barrel type fail.

An inwardly beveled guide is run next by means of the wire line to facilitate the entry of a packer into the liner. This guide is run on a special tool which releases only when the guide passes over the liner. The guide rests on a collar provided for this purpose near the top of the liner. The length of the guide is such as to permit its positive recovery by means of a wire line type spear.

A cup type packer assembly is then run on flush joint heavy walled $1\frac{3}{4}$-in. OD tubing attached to the lower end of the tubing string. The heavy walled tubing section is usually of about the same length as the liner. Fig. 8 shows the type of packer assembly employed for shutting off the upper portion of the sand section such as required for excluding gas. For obtaining a shut-off both above and below the producing section, two groups of packers are mounted on a mandrel having two vertical fluid passages formed by a vertical partition. One of these passages is a by-pass extending from above the upper to below the lower packer. This passage permits the entry of mud or oil into the gravel layers below the lower pack section from the annular space between the casing and tubing. The other vertical passage permits fluid flow from the space between the packer sections to the tubing. Two methods of obtaining a shut-off of a desired portion of the producing section may be employed with these types of completion.

Water or Gas Shut-Off by Mud Column Pressure

One of the above methods is that of employing the hydrostatic head of a fluid which will not flow into the producing sand or through the mixed sand and gravel layers, but which will flow into the gravel layers. For example, if a gas shut-off is desired for the conditions shown by Fig. 2 the annular space between the casing and tubing may be filled with drilling mud. This mud will flow into the gravel layers at all levels above the packer assembly but will not flow into the producing sand or through the mixed sand and gravel layers because of the formation of an impermeable filter cake. If the hydrostatic head of the mud column exceeds the bottom hole pressure in the gas sand the entry of the gas into the well space is positively prevented. Fluid production enters the tubing below the packer through both the gravel and mixed sand and gravel layers since the latter are also permeable. A completion results which not only provides a positive shut-off in the hole space but which also permits the changing of the producing level by simply raising or lowering the tubing. The optimum producing level may thus be found after completion rendering unnecessary accurate information as to the location of the gas-oil or oil-water contacts or a preliminary guess as to what extent coning may occur. Furthermore, dependence is not made upon these contacts remaining at the same level. Precise depth measurements are also not necessary although always desirable.

By using the double packer assembly a shut-off is obtained both above and below the zone being produced. As previously described, a by-pass is provided into this case which allows mud from the casing-tubing annulus to invade the gravel layers below the packer assembly as well as above it.

Water or Gas Shut-Off By Oil Injection

The second method for obtaining a shut-off with the alternate layer type completion is that of supplying a fluid to the casing and tubing annulus which will flow into the section of the producing sand in which a shut-off is desired. For example, for the conditions shown by Fig. 2, oil may be continually pumped down between the casing and tubing. If the face of the gas sand and adjacent gravel pack has been cleaned by back-flowing, oil flow into the gas sand results. An oil-saturated zone in the gas section is thus created adjacent to the well and in the area in which vertical coning principally occurs. Any tendency to cone results in a downward flow of oil from the previously gas-saturated section. By continually supplying oil to the casing-tubing annulus vertical coning results in the production of this oil rather than gas. As the packer assembly is raised higher a greater percentage of the oil produced is from the casing and tubing annulus, but even if the packer is above the gas-oil contact, gas will not be produced. This type of completion provides both a positive shut-off in the hole space and also a method for controlling vertical coning.

The oil injection type of completion is also applicable to preventing the upward coning of water. However, since the viscosity contrast between oil and water is less than that between oil and gas, the number of cubic feet of circulating oil per cubic foot of water coning is greater than for an equal volume of gas coning. Also the fact that gas is compressible still further reduces the volume of gas coning as measured on the surface under standard conditions in proportion to that required for the same volume of oil coning. This latter fact also indicates the use of this method for control of coning to be more favorable for application to deep wells than shallow ones. At least the volume of oil which must be supplied to the casing-tubing annulus to control a given volume of gas coning decreases with depth.

Optimum Gravel Size

One question which arises when considering the use of relatively fine gravels or sand and gravel mixtures is whether the fluid productivity is substantially reduced. Fig. 3 shows data which was published by Hill.[2] This curve shows the experimentally determined relation between permeability of the gravel pack and the ratio of the gravel size to the sand grain size at the 10 per cent point on a sieve analysis curve. The gravel permeability values were obtained in a test cell after fluid flow through sand into the gravel until apparently stable conditions as to sand invasion resulted. The permeability of the sand invaded gravel pack was then measured. It will be noted that maximum permeability of the sand invaded gravel pack occurs when the grain size of the gravel is about six times the grain size of the sand at the 10 per cent point on the sieve analysis curve. Tests which we have conducted indicated this also to be the largest gravel/sand grain size ratio for which no sand production can be induced regardless of rate of fluid flow. The grain size ratio for no sand production would obviously also correspond rather closely to the grain size ratio for which no sand invasion occurs. Any sand particle capable of entering the gravel pack should ultimately be produced with a sufficient rate of fluid flow since the passage between the gravel grains are about the same throughout. Thus for gravel/sand grain size ratio greater than six, sand invasion occurs. The pore spaces of the gravel are filled with sand, reducing the permeability. For gravel/sand grain size ratio less than six no sand invasion occurs, the permeability decreasing simply because the smaller gravel grains result in smaller pore spaces.

Our results also indicate that grain size ratio greater than six represents an unstable condition. In this range sand production is related to the rate of fluid production. Sudden increases in rate of fluid production may result in sand production. This may produce a cavity behind the gravel pack into which shale or shaly sand may cave ultimately resulting in the plugging of the gravel pack. This sequence of events has been frequently observed when relatively large gravel such as pea gravel is employed.

The dotted or upper curve in Fig. 3 shows the ratio of fluid productivity with the gravel in place to that of the open hole. This curve has been calculated for corresponding permeability values shown by the lower curve for a gravel pack filling the annular space between a $2\frac{3}{8}$-in. OD liner and a 6-in. open hole. Calculation of fluid productivity was made by use of Muskat's formula for calculating the influence of discontinuous radial variations in permeability.[3] It will be noted that maximum reduction of fluid productivity because of the gravel pack is only about three per cent for the experimentally determined values for permeability of sand invaded gravel. Also that fluid production is reduced only 15 per cent if the space between the liner and open hole is filled with sand or a sand and gravel mixture having the same permeability as the producing sand. The relations between permeability and gravel/sand grain size ratio shown by Fig. 3 are strictly true only for the sand

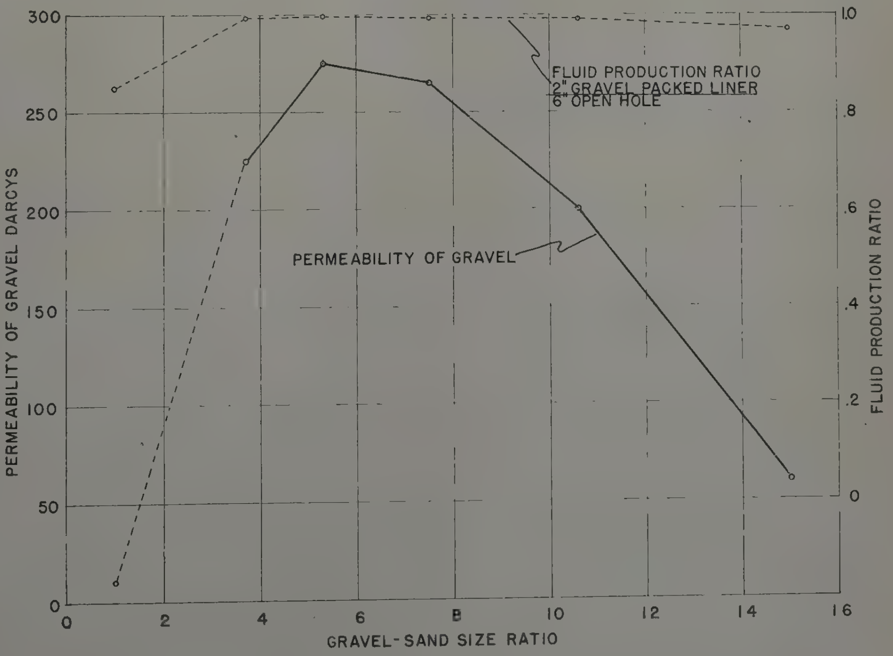

FIG. 3 — RELATION BETWEEN PERMEABILITY OF PACK AND RATIO OF GRAIN SIZE TO SAND.

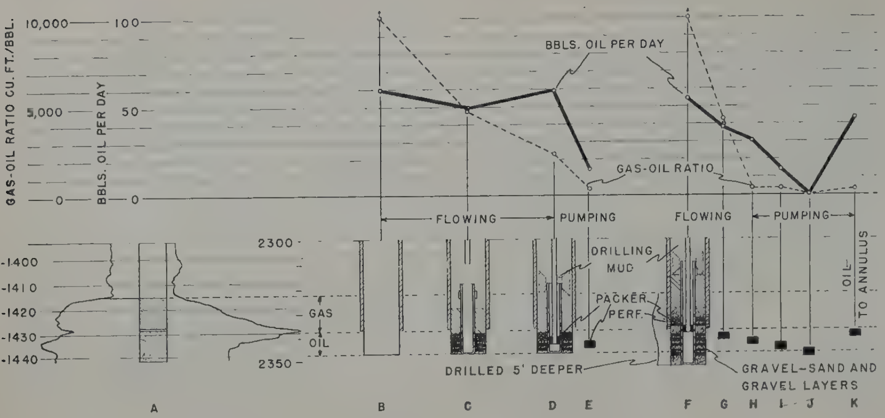

FIG. 4 — RESULTS OF ALTERNATE LAYER TYPE COMPLETION TO WELL IN QUIEN SABE FIELD, WEBB COUNTY, TEXAS.

sample employed in Hill's experiment. However, these values approximate values obtained with usual oil producing sands.

Clean-Out Procedure Prior to Gravel Packing

The use of gravel having gravel/sand ratio less than six has usually been impractical in the past because of the difficulty of maintaining a clean sand face while placing the gravel. If drilling mud is or has been present opposite the sand section, the resulting filter cake will not flow through the finer gravels or gravel-sand mixtures. If no filter cake is present and the hole filled with water, oil or similar liquid, any flow of liquid into the sand will usually result in the formation of a thick filter cake of relatively large particle size material due to the filtering out of sediment or scale on the face of the sand. Such filter cake may have a greater tendency to plug the gravel than would drilling mud.

Attempts to apply fine gravels to old unconsolidated sand wells have usually resulted in plugging of the gravel pack with commonly used procedures for cleaning out before gravel packing. Such wells frequently have large cavities in the sand section. These cavities are usually filled, or partially filled, with sand and/or shale cavings. Such cavities ordinarily cannot be completely cleaned out with a bailer or sand pump or by fluid circulation although it may be possible to reach the original bottom of the hole. This condition usually results in a layer of sand and shale or silt between the gravel and the sand face resulting in initial plugging or reduced fluid production.

Fluid flow from the sand has been most commonly employed for cleaning the sand face prior to gravel packing in low pressure sands. After drilling out the casing shoe and open hole section the tubing is run and swabbed until fluid flow from the sand results. If gas flow develops, gas is bled through a small choke until the well heads up with fluid and dies. The tubing is then pulled and sand or cavings in the open hole section cleaned out with a sand pump or bailer. This procedure requires the sand to be consolidated to such an extent that caving does not occur with the pressure due to the fluid column in the hole equal to the bottom hole pressure of the sand.

Soluble Mud

For cases in which the walls will not stand up as required above, a mud has been developed which forms a water soluble filter cake. A dump bailer is employed for spotting about 100 ft of this mud on bottom. By spudding the bailer with the fluid column in the hole equal to the bottom hole pressure of the sand, any fine material on the sand face is forced off by momentary fluid flow due to swabbing action of the bailer and held in suspension in the mud column. Fluid flow into the hole while soluble mud is being dumped may also be induced by bailing from the top of the fluid column. Such fluid flow may be employed for moving cavings into the hole resulting in their suspension in the soluble mud. By alternately bailing out the resulting mud and sand mixture and dumping clean mud, cavings may be effectively cleaned out of large cavities. A special bailer has been developed which accomplishes these two results simultaneously, mud being discharged at bottom at the same time an equal amount of fluid is pulled into the bailer about 100 ft above bottom. When clean mud returns are secured from the latter level the hole may be loaded with oil or water to support the walls against caving during the gravel pack operation. A hydrostatic head due to fluid column in the hole exceeding that in the sand results in the formation of a relatively thin (1/16 in. or less) filter cake on the sand face which may be dissolved after gravel packing by washing with water or which will be ultimately dissolved by connate water from the adjacent formations even if washing is not employed.

Several high pressure wells have been gravel packed by filling the hole with saturated brine. Such brine solutions may be prepared which have weights as high as 10 lb per gal.

Another method employed on high pressure wells has been that of spotting 200 ft to 300 ft of soluble mud on bottom back of tubing having a production packer on its lower end. This packer is then set and tubing swabbed. When sufficient flow has occurred to clean the sand face the packer is released. This results in a flow of soluble mud past the sand face and into the tubing. Any sand or cavings present are carried into the tubing and at the same time a soluble filter cake is formed on the sand face. By providing a valve on the bottom of the tubing which closes when it is picked up, most of the sand and cavings resulting from swabbing are brought out in the tubing.

TYPICAL FIELD RESULTS

Case 1

Fig. 4 shows the results of an alternate layer type completion to a well in the Quien Sabe Field in Webb County, Tex. Production is from the Lopez sand of the Mirando series at a depth of about 2,300 ft. The depths shown are subsea values. About 15 ft to 18 ft of gas saturation is present in the upper portion of the sand section with about 6 ft to 9 ft of oil saturation in the lower part of the sand. The sand is clean, uniform and medium grained but contained one hard non-permeable sand streak, the casing having been set on this. This point was believed, on the basis of drill stem test data on the offset well, to be five ft below the gas-oil contact. Subsequent development indicates that casing was set approximately at the gas-oil contact.

When swabbed in prior to gravel packing this well made a large volume gas with a spray of oil.

The completion shown by Fig. 4-C was then tried. The lower portion of the sand section was packed with alternate layers to within about three ft of the bottom of the casing. A non-permeable mixture of gravel, sand, silt, aquagel and grease was placed in this space. The liner was then cemented in the usual manner. A 24-hour production test yielded 48 B/D flowing through ¼-in. choke with gas/oil ratio of 4,700 cu ft per bbl.

A packer of the type previously shown was next run to the indicated level, Fig. 4-D. The results of tests with the packer set at various levels are shown. With the bottom of the packer six ft below the bottom of the casing (Fig. 4-D), production was 58 B/D flowing with a gas/oil ratio of about 2,300 cu ft per bbl. With the bottom of the packer eight ft below the bottom of the casing (Fig. 4-E), production was 15 B/D pumping with gas/oil ratio of 250 cu ft per bbl.

Since it was believed that the entire sand section had not been penetrated, the gravel pack was removed and the well drilled five ft deeper with a spudder. The bottom five ft of the casing was then perforated to provide a greater zone for oil injection into the gas sand. This section was again gravel packed using alternate layers of sand and gravel about one ft thick, these layers also covering the perforated section. Production tests were then run with the packer at various levels with the annular space between the casing and tubing filled with drilling mud. Results of these tests are shown graphically (Fig. 4-F to 4-J). The production varied from a spray of oil with a large volume of gas for a packer position above the gas-oil contact to a complete gas shut-off with oil production by pumping for the two lower packer positions. No fluid production resulted when the packer was positioned below the permeable section of the sand. Also of interest is the similarity of fluid production for a given level of the packer to that obtained for the same packer level on the previous alternate layer completion.

The mud column was then circulated out with water and after thorough washing this was followed by oil which had been filtered through a sand filter. The packer was set 4 ft below the casing (Fig. 4-K) and oil pumped down the annular space between casing and tubing through a sand filter with a walking beam type pump. The gas/oil ratio was immediately reduced to 250 while oil production was 42 B/D. It will be noted that gas/oil ratio was 4,200 at this packer level with mud in the annulus (Fig. 4-G). This well has produced with low gas/oil ratio for slightly more than two years with packers at this level. Less than 1 bbl of oil per day has been supplied to the casing on the average.

Tests previously conducted using a sand and gravel filled test cell indicated that 16 bbl of oil per day would have been required if the condition and laws of flow of the coning path had approximated that of the test cell. Using a cell containing a 6 in. sand column, a rate of flow of 1 bbl of oil per day resulted with an upstream pressure of 550 psia and atmospheric downstream pressure. For the same conditions the rate of gas flow as measured at 14.7 psia and 60°F was 6,000 cu ft per day. This suggested an oil/coning gas ratio of 1 bbl of oil for each 6,000 cu ft of coning gas for a bottom hole pressure of 550 psia. The oil/gas ratio would, of course, decrease as bottom hole pressure increases since the reservoir volume occupied by a given volume of gas will decrease as the bottom hole pressure increases.

It was discovered that the gas section ultimately quit taking oil under hydrostatic head of the oil column even though filtered oil was being pumped down along supposedly clean casing and tubing surfaces. The gas/oil ratio also started rising at this time. The packers were raised out of the liner and flow secured from the entire sand section. Packers were then lowered to the previous level. The sand again took oil, and gas/oil ratio was again reduced to 250 cu ft per bbl.

Equipment

To prevent gas lock, 1-in. tubing is used for sucker rods, the oil coming up through the 1-in. and the gas rising in the annular space between the 1-in. and 2-in. tubing. A 4-in. OD chamber is provided around the seating nipple to permit the gas to by-pass the seating nipple and pump. A hollow polish rod was employed which has a slot for the oil to pass into a space between two packing glands which connects with lead lines. This construction avoids the use of hose connection as commonly used in this type of pumping.

Case 2

Fig. 5 shows results of an alternate layer completion on the north offset to the well just described. In this case the casing was purposely set about six ft above the gas-oil contact. Sixteen ft of

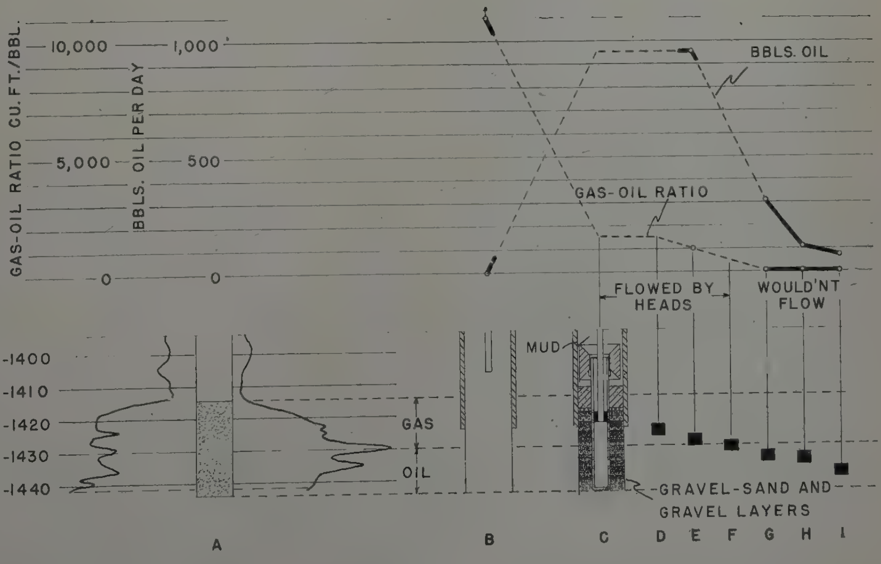

FIG. 5 — RESULTS OF ALTERNATE LAYER COMPLETION OF NORTH OFFSET.

the gas sand and 14 ft of oil sand were penetrated in this well.

The procedure originally planned for thoroughly cleaning the sand face was to allow the well to flow on a small choke until it headed up with oil and died. Sand was then to be cleaned out with a sand pump and the section gravel packed. The open hole section was underreamed to about eight in. with a cable tool underreamer to remove any cement sheath which might have been present on the sand face. However, when swabbed, gas flow without any trace of oil developed. Although the well was flowed for four days on a ¼-in. choke, no trace of oil was secured.

A temporary gravel pack was placed with coarse gravel filling the lower eight ft and alternate sand and gravel layers about this level. By setting packer just below the gas-oil contact, oil production resulted. The packer was then raised and the well flowed into the pit for 14 hours as a means of cleaning it. Oil production was about 550 bbl during this period, this being at the rate of approximately 950 B/D. The gas/oil ratio was not determined but was estimated as less than 2,000 cu ft per bbl. This low ratio partly resulted from the high rate of oil production.

The temporary gravel pack was then removed and that shown placed. The tests shown are by swabbing down for each packer position and then measuring the rate of fill up in the tubing by running the swab. The rate of fill up for a pressure differential of 400 psi was then calculated for each packer position. The gas/oil ratio was estimated by measuring the gas flow from the tubing during fill up.

One surprising result was that the gas volume was very greatly reduced by the gravel pack even without the use of the packer. This could be explained if it is assumed that most of the gas volume came down outside the casing due to faulty cementing. The path for flow would substantially be closed after gravel packing if sand production from the gas zone occurred filling this space with sand. Sand in the gas section below the casing was low in permeability and might not have been capable of producing a large gas volume.

Fig. 5, C to I, is a graphical representation of oil production and gas/oil ratio for various levels of the packer. Oil production for the three lowest packer positions ranging upward from the lowest level, was 75, 195, and 312 B/D respectively. The gas volume was negligible for these packer levels. Accurate measurement of fluid production by measuring rate of fill up in tubing was impossible for higher packer levels both because of high rate of fill up and the production of gas. The maximum rate of production was assumed to be that obtained on the previously mentioned test with a temporary gravel pack in place, that is, 950 B/D.

The above tests were made with the tubing-casing annulus filled with drilling mud. This mud was replaced with oil after about a year without backflowing to remove the mud filter cake from the gas section. About 20 gal of oil per day is required to keep the casing-tubing annulus filled.

The well has thus far produced approximately three years with this completion without appreciable change in gas/oil ratio or oil production. The packer has been positioned four ft above bottom during this time.

Case 3

Fig. 6 shows data on an alternate layer completion in the Oakville Field of Live Oak County, Tex. This well is near two wells which were abandoned about seven years ago after failure to shut-off gas and water by squeeze cementing after five squeeze jobs on each. One of these wells was 150 ft from the well on which data is shown and the other 330 ft from it.

Production is from the Pettus sand at a depth of 2,710 ft. The upper 28 ft of the sand section is gas saturated and the lower 10 ft penetrated oil saturated. Casing was set at the gas-oil contact. Bottom hole pressure is about 1,250 psi. To control pressure the hole was loaded with saturated brine while cleaning out and gravel packing, this well having been completed without the use of soluble mud. Tubing swab was run until the oil and gas flow occurred. Gas was then bled off through a small choke until sufficient oil flowed in to kill the well. Cavings were then cleaned out with a sand pump and alternate layer gravel pack placed. This completion is illustrated by Fig. 6-D. Brine was then replaced by drilling mud. The packer assembly was positioned so as to have its bottom point eight ft below the gas-oil contact (Fig. 6-E). Initial production was 50 B/D on 7/32 in. choke with a gas/oil ratio of 1,000 cu ft per bbl. Gas/oil ratio gradually rose. At the end of 10 days gas/oil ratio was near 2,000:1. Choke size was reduced to ⅛ in. Oil production was about 20 B/D on this choke. The gas/oil ratio continued to rise until at the end of 1½ months the ratio was near 10,000 cu ft per bbl.

After a shut-in period while waiting on equipment, the drilling mud in the annular space between casing and tub-

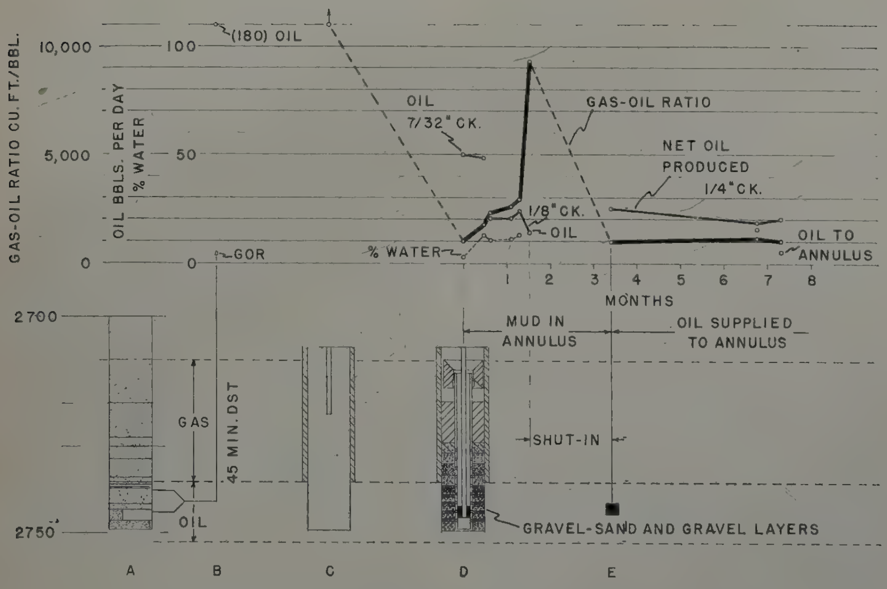

FIG. 6 — DATA ON ALTERNATE LAYER COMPLETION, OAKVILLE FIELD, LIVE OAK COUNTY, TEX.

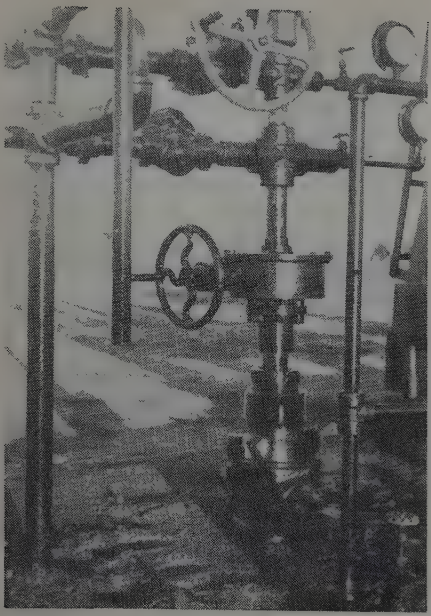

FIG. 7 — SURFACE PORTION OF BACKFLOW ARRANGEMENT.

ing was replaced with oil. Oil was supplied by a walking beam pump and pumped to the casing through a sand filter.

Oil injection into the gas section resulted in an immediate reduction in gas/oil ratio to approximately 1,000 cu ft per bbl. This value remained approximately constant for the six-month period during which it was closely observed. The last point on the gas/oil ratio and oil production curve is a 15-day average. During this time the oil supplied to the casing annulus has also been measured. Average value for the latter is five bbl per day.

Oil is continuously injected down the annular space between the tubing and casing. However a pressure relief valve is provided which results in oil flowing back to the stock tank if the casing fills. Oil supply to the casing is regulated by throttling of the intake line to the minimum amount necessary to control gas/oil ratio. Continuous flooding of the gas sand with oil does not occur because the sand face periodically plugs with scale and similar material. When oil flow into the sand stops, the oil which has been injected into the gas sand is produced and gas/oil ratio starts rising at which time the gas section is backflowed. Although oil is continuously supplied to the casing, flow into the sand is intermittent, the gas section thus being periodically cleared of oil.

BACK FLOW EQUIPMENT

Fig. 7 shows the surface portion of the backflow arrangement. A port is provided immediaely above the packer assembly which may be opened by rotation of the tubing allowing flow into the tubing from the annulus and from the sand section above the packer. This type packer assembly including the backflow port is shown in Fig. 8. The hand wheel (Fig. 7) rotates the tubing by means of a worm gear. The only change in connections required is that of disconnecting the flow lines. This type of backflow has the advantage that any material which has settled out of the fluid column in the annulus is also recovered as well as that filtered out on the sand face.

PUMPING EQUIPMENT

Pumping equipment was installed because the earlier well, 150 ft from this location, had a somewhat lower productivity index and would not produce the allowable by natural flow, Oil is supplied to the casing by the walking beam pump through a sand filter. A line from the pump suction leads to the stock tank into which the well produces through a gun barrel. Thus the stock tank gauge shows the net oil produced. To prevent gas locking, 1-in. tubing is used for sucker rods, the oil coming up through the 1-in. while the gas rises in the annular space between the 1-in. and 2-in. tubing. A 4-in. OD chamber is provided around the seating nipple and pump to permit the to by-pass this point. A hollow polish rod having a slot for oil to pass into a space between two packing glands which connects with the lead lines is employed.

After producing two years, the above well developed excessive water production as a result of edge water encroachment. It has now been recompleted at a higher level as a gas well.

SUMMARY OF FIELD USE

One hundred wells have been completed with the described type of gravel pack procedure to date. Sixty-five of these are in the Quien Sabe and North Albercas Fields of Webb County, Tex. One or more completions have also been made in Jim Hogg, Zapata, Duval, McMullen, Live Oak, Victoria, Fort Bend and Brazoria counties. Alternate layers have been used in 18 of the above, the gravel pack in the remainder being composed of uniform gravel.

Double packers were run in three of the alternate layer completions. A water shut-off was obtained in two of these; water production was reduced by about 50 per cent in the other. In the latter case only four ft of sand was present above the water level. A complete fluid shut-off could be obtained in this case, however, when packer was raised above the top of the sand section.

Single packers were run for shutting-off gas in case of 12 alternate layer completions. All of these were initially tested with the annular space between the casing and tubing filled with drilling mud or with at least the bottom of the fluid column composed of drilling mud. In all cases an initial gas shut-off was secured. This includes two recent cases in which the lower two ft of a

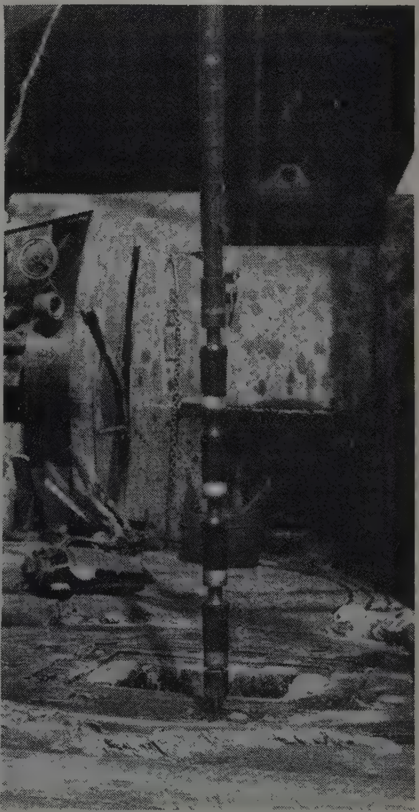

FIG. 8 — PACKER ASSEMBLY FOR SHUTTING OFF UPPER PORTION OF SAND SECTION.

35 ft sand section was oil saturated while the upper 33 ft was gas saturated. In two completions high gas/oil ratio later developed evidently as a result of vertical coning. In these cases gas was successfully controlled by continuous injection of oil into the gas sand.

Failure resulted in six of the above 100 cases because initial plugging of the gravel pack. Most of these cases occurred during the early use of this procedure and before the development of soluble mud. Three of these cases were on old wells having large cavities All obviously resulted from inadequate clean out procedure, the plugging appearing to be due to a layer of cavings or filtered out material between the gravel and sand face.

Five cementing failures also occurred in the above 100 cases. This, of course, refers to failure of the cement around the liner which holds the gravel pack in place. All except two of these wells were successfully recompleted. No attempt at recompletion was made in these two cases. Cementing failure appeared to be principally due to dilution of cement while dumping. A cementing technique has since been developed which would have avoided most failures.

CONCLUSIONS

In conclusion, the advantages to be gained by this completion procedure may be summarized as follows:

1. A positive method for shutting off gas and water is provided.
2. The producing level may be easily changed at any time. The optimum producing level may be determined after completion. This makes the following unnecessary:
    a. Exact information as to the location of the gas-oil or oil-water contact.
    b. A preliminary guess as to the extent of vertical coning.
    c. Dependence upon the gas-oil or oil-water contact remaining at the same level.
    d. Precise depth measurement.
3. Complete sand screening is achieved, and
4. A method for controlling vertical coning is provided.

REFERENCES

1. West, T. S.: *Trans.* AIME, **170**, 250.
2. Hill, K. E.: API *Drill. and Prod. Prac.*, (1941), 134.
3. Muskat, M.: *Flow of Homogeneous Fluids*, McGraw-Hill Book Co., New York, (1937), 403-409.

DISCUSSION

By Bruce Barkis, B&W, Inc., Houston, Tex., Member AIME

Gravel packing for the control of sand entry in unconsolidated sand fields has been an accepted practice for some years. Current usage of fine gravels in the size range reported by West, clean placement fluids of the heavy brine type, and improved tools for gravel placement are responsible for the higher percentage of successful jobs of this type.

West's report of the usage of alternate layers of fine gravel and sand, aided by mud or oil seals, to control gas and oil entry in the open hole and lower pressure in completions of South Texas indicates that gas/oil ratio control can be accomplished in a fairly thin vertical section by materials providing a fairly low differential pressure.

A large percentage (90-95 per cent) of the wells which are gravel packed on the Upper Texas and Louisiana Gulf Coast are old producers. Almost every one of these wells has been completed through gun perforations in 5-20 ft sand sections. Assuming an average 10 ft perforated section with 6½-in. hole per ft, results in only about 12 sq in. of drainage opening. The difficulty of cleaning the surface of such small sand exposure, and of keeping it clean during the placement of the gravel, coupled with the additional complication of high fluid entrance, because of the small drainage area, suggests that large increases in sand exposure, by jet shooting or cutting, milled out sections or other form of window completion, would provide the amount of sand surface necessary for satisfactory gravel formation contact.

Sand production, in an oil well, and the velocity of the entering fluid are closely related. Further assuming a fluid production of 60 B/D, from the above section, or an average of one B/D ½-in. hole results in an entrance velocity of 7.2×10^3 ft/sec and according to Gumpertz, sand production at such velocity can easily be expected. This data further suggests that increased sand exposure is very desirable.

★ ★ ★

THE QUANTITATIVE APPLICATION OF RADIOACTIVITY LOGS

ROBERT E. BUSH, LANE-WELLS CO., HOUSTON, TEX., AND **E. S. MARDOCK,** MEMBER AIME, WELL SURVEYS, INC., TULSA, OKLA.

ABSTRACT

The object of this paper is to report recent developments in the quantitative interpretation of radioactivity logs. The use of reference lines is described in the application of the new zero radioactivity reference line for the determination of neutron derived porosities is discussed. Illustrated examples are shown of logs from the reef limestone of the North Snyder Field and from the Lansing-Kansas City limestone of central Kansas.

A method of using an interrelation factor calculated from the neutron and gamma ray curves, called the neutron productivity number, for the estimation of productivity from sandstone formations is discussed. When used in a relative manner the neutron productivity number has aided in predicting whether a given zone will produce gas or liquid or whether it is too shaly to produce. Examples of logs from wells in the Freites District, Venezuela, and in East Texas are shown to illustrate the application of the neutron productivity number.

INTRODUCTION

The petroleum industry was introduced to some of the preliminary results of investigations into the quantitative interpretation of radioactivity logs in October, 1949.[9] It was stated at that time that the methods presented were entirely relative because they involved the use of reference points obtained from the radioactivity log, *i.e.*, shale reference lines, dense zone reference lines, or a combination of both shale and dense zone reference lines. These relative methods offered many advantages to the industry in interpreting radioactivity logs in terms of porosity with particular application to limestone and dolomite reservoirs. However, these relative methods did not offer the wide range of applicability desired because the establishment of reliable reference points from shale in some areas were difficult. It was recognized that a more reliable means of establishing reference lines was vitally needed. Such a method is now available through the introduction of an instrumental zero device. It is the purpose of this paper to discuss the application of this new zero reference to the quantitative interpretation of radioactivity logs.

Previously all applications of quantitative interpretations of radioactivity logs have been made in limestone reservoirs with little or no emphasis placed on sandstone reservoirs. A brief resumé of investigations into the quantitative interpretation of radioactivity logs in sandstone reservoirs is presented here. This discussion deals primarily with the interrelation of the gamma ray and neutron curves and the response of the latter to the density of the fluids filling the pore space in relatively homogeneous sandstones of uniform porosity. The authors believe that the methods presented herein are only applicable locally to specific fields and reservoirs, and that they probably do not offer a wide range of applicability.

However, the authors believe that the wider use of the new instrumental zero references in sand areas will reveal more information about the specific response of the gamma ray and neutron curves to changes in lithology and saturation.

Two applications of quantitative interpretation using the new instrumental zero references are presented. Examples are given which show the comparison of logs and porosity in the limestones and dolomites of West Texas and Kansas. Logs of wells in Venezuela and East Texas are compared with the drill stem test data, production data, etc., to illustrate the interrelation of the gamma ray and neutron curves and the use of methods involving these interrelations to determine certain saturation variables.

THE QUANTITATIVE APPLICATION OF RADIOACTIVITY LOGS TO LIMESTONE AND DOLOMITE RESERVOIRS

The theoretical basis for the gamma ray and neutron curves has been discussed elsewhere.[9] The method of recording the logs and apparatus involved has also been thoroughly covered and will not be discussed here.[1,2,3,4,9]

It has been shown that the neutron curve responds exponentially to liquid filled porosity over the 1½ to 35 per cent

---

[1]References given at end of paper.

Manuscript received in the office of the Petroleum Branch Sept. 8, 1950. Paper presented at the Fall Meeting of the Petroleum Branch in New Orleans, La., Oct. 4-6, 1950.

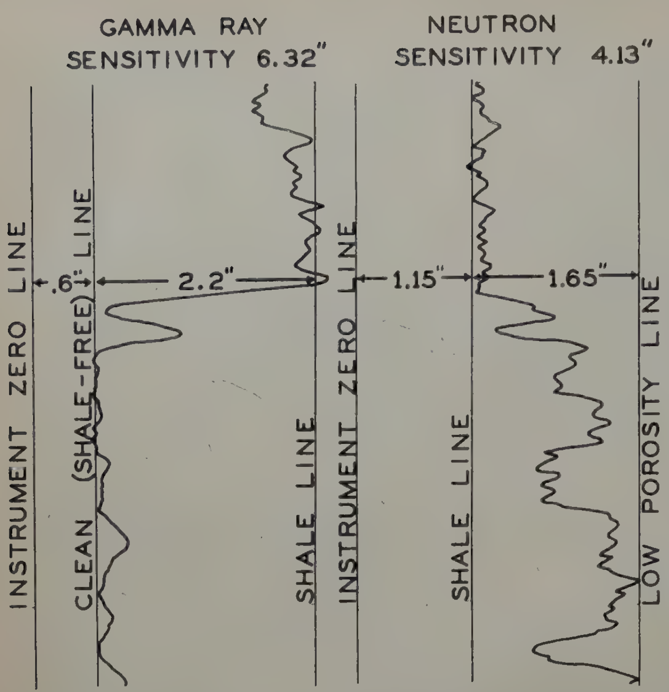

FIG. 1 — RELATIONSHIP BETWEEN RELATIVE REFERENCE LINES AND THE ZERO RADIOACTIVITY REFERENCE LINES FOR 7" CASED HOLE.

range in limestones and dolomites.[9] It is assumed therefore that the relationship between the neutron curve deflections and porosity for a given zone, can be determined graphically by using this relationship to weight the average line drawn through a plot of the scattered values of the neutron curve deflections and the corresponding porosities.

Introduction of Instrumental Zero Reference Lines

Previous work has made use of relative methods in which reference lines were established from the shale line of the neutron curve. However, shale lines were not always easily established and it was therefore quite apparent that some method of obtaining a better zero reference was needed. A zero locating device has now been added to the existing logging equipment. It is now possible to determine the position of zero radioactivity on the log at any time during the logging operation. Fig. 1 shows the relationship between the instrument zero and the shale reference lines for the gamma ray and neutron curves in a typical limestone area. To acquire more adequate control of the sensitivity, a sensitivity selector is now available which permits accurate measurements of the sensitivity and the setting of any desired sensitivity. The addition of this equipment makes it possible to standardize sensitivities for given logging conditions; *i.e.*, under given casing and core hole sizes.

To illustrate the application of quantitative methods to limestone reservoirs, a well in the reef limestone of the North Snyder Field, Scurry County, Tex., was chosen because core data were available within the same well for both cased hole and open hole conditions. Fig. 2 shows the correlation of the radioactivity log and the core porosity log of a standard Oil Co. of Texas well in the North Snyder Field.

Preparation of the Radioactivity Log For Quantitative Interpretation

To prepare the radioactivity log for quantitative interpretation the location of the absolute zero reference line is determined at one or more points within the zone of interest and throughout the remainder of the log on both the gamma ray and neutron curves. The porosity determined by core analysis is then plotted on the same vertical scale as the radioactivity log and correlated core by core with the neutron curve. Where physical bore hole conditions such as casing or bit size are changed within a well it is necessary to prepare a separate quantitative interpretation chart for each section of the well. A data sheet showing the depth, the gamma ray curve deflection from zero, the neutron curve deflection from zero, and the porosity of the corresponding core sample is then prepared, throughout the cored section, until all of the data necessary to prepare the neutron derived porosity curve are recorded.

Neutron Derived Porosity Curve

By assuming that the neutron curve responds in an exponential manner to liquid filled porosity, the establishment of the neutron derived porosity curve is facilitated if the data are plotted on semi-log graph paper with the neutron curve deflection as the abscissa (linear scale) and the per cent core porosity as the ordinate (log scale). The neutron derived porosity curve is determined by drawing the straight line that best fits the scattered points. When the neutron curve deflections are plotted in units of distance of pen travel (inches) it is necessary to adjust for changes of sensitivity when applying the data of one log to that of another log. The relationship of the sensitivity to the deflection is linear and therefore the neutron derived porosity curve may be adjusted to another sensitivity by multiplying it by the ratio of the new to the old sensitivity.

However, if the neutron curve deflection is divided by its sensitivity, an invariant quantity is obtained which is applicable to any log. This quantity has been called a standard unit, and the neutron derived porosity curve may be plotted in either standard units or inches of deflection as desired. Figs. 2 and 3 show an example of the use of standard units, while an example of a neutron derived porosity curve plotted in inches of deflection is shown by Figs. 5 and 6. The value in standard units for any neutron curve deflection may be found by dividing the curve deflection (in inches) at the given point by the sensitivity of the curve.

The neutron derived porosity curve shown in Fig. 3 represents data obtained from that portion of the cored section which had been cased with 7-in. pipe (Fig. 2). This curve may be applied to any other well in the area in which 7-in. casing is set and on which an absolute zero reference line was obtained.

This curve (Fig. 3), with its relatively small scattering, is typical of the reef limestones in this region and has been found to be applicable over wide areas of West Texas.

The same procedure was followed for the 6¼ in. open hole condition. The gamma ray and neutron curve deflections from zero were determined opposite each of the corresponding core porosities, and each deflection divided by its respective log sensitivity, thus converting to standard units. The neutron standard units opposite clean limestone (as shown by the gamma ray curve) were then plotted as the asbscissa (linear scale) versus the per cent porosity as the ordinate (log scale) on semi-log graph paper and the average neutron derived porosity curve established by drawing a straight line through these points. Fig. 4 shows the neutron derived porosity curve for 6¼ in. open hole. This curve may also be applied to any well in this area with 6¼ in. open hole on which a radioactivity reference line was obtained.

Comparison of Lansing - Kansas City Logs and Porosities

Fig. 5 compares the logs and core porosity data for a well producing from the Lansing - Kansas City section, Stafford County, Kans.

In addition, this example illustrates the application of a method of averaging the core porosities in order that the lengths of the core samples will agree more closely with the length of the sample affecting the neutron curve. The length of the neutron curve sample is approximately two ft while the core porosities were obtained from permeability plugs which were selected as representative of one-ft intervals of the core. This difference in length will result in a greater degree of scattering of the points used in determining the neutron derived porosity curve. The neutron curve subsurface instrument is not influenced to the same degree by each longitudinal unit of the interval sampled, as the middle portion of the sample (of approximately one ft of its total length) exerts the greatest influence while in the remainder of the sample (over the six in. at the ends) the influence of the sample on the neutron curve decreases to zero. The determination of the weighting factors would be too complicated to perform for a practical example and therefore a rough approximation was resorted too. This has been done by avering the porosities for three one-ft intervals of core so that the middle foot of core is weighted at full value while the foot below and the foot above is weighted by one-half; that is, the porosity of the middle portion is taken at full value, one-half the value of the porosities of the adjacent intervals is added and their sum is divided by two. The result is shown in Fig. 5 in the column labeled "Per Cent Weighted Porosity." It will be noted that much better agreement exists between these values and the neutron curve than exists between the unweighted porosity values and the curve.

The neutron derived porosity curve for the Lansing - Kansas City well is shown in Fig. 6. Here the neutron curve deflections are plotted in inches.

To apply this neutron derived porosity curve to logs of other wells having the same physical bore hole conditions it is necessary to apply a correction if the log was run on a different sensitivity. This correction may best be made by selecting two points on the base neutron derived porosity curve, on even porosity lines, *i.e.,* two per cent porosity and 20 per cent porosity. The neutron curve deflection in inches is determined for each of these points and each is multiplied by the ratio of the sensitivity of the new log to that of the old log, in order to obtain the correct deflection to be plotted along the corresponding porosity line. These points are then connected by a straight line, giving the corrected neutron derived porosity curve, which may then be applied to the neutron curve being considered.

Application to Logs for Which No Instrumental Zero Is Available

The neutron derived porosity curve established from a given log may be applied to another log having only a shale reference line, by determining the location of the shale reference line in relation to the absolute zero reference line on the base log, and measuring this distance in inches, which figure is divided by the sensitivity of the base log to obtain the distance from shale to zero in terms of standard units. The location of zero may be placed on the new log by multiplying the sensitivity of the log by the number of standard units obtained and positioning the zero this distance to the left of the shale reference line (Fig. 1). The neutron derived porosity curve determined from the base log may then be applied as if the absolute zero were known. The accuracy of this method of

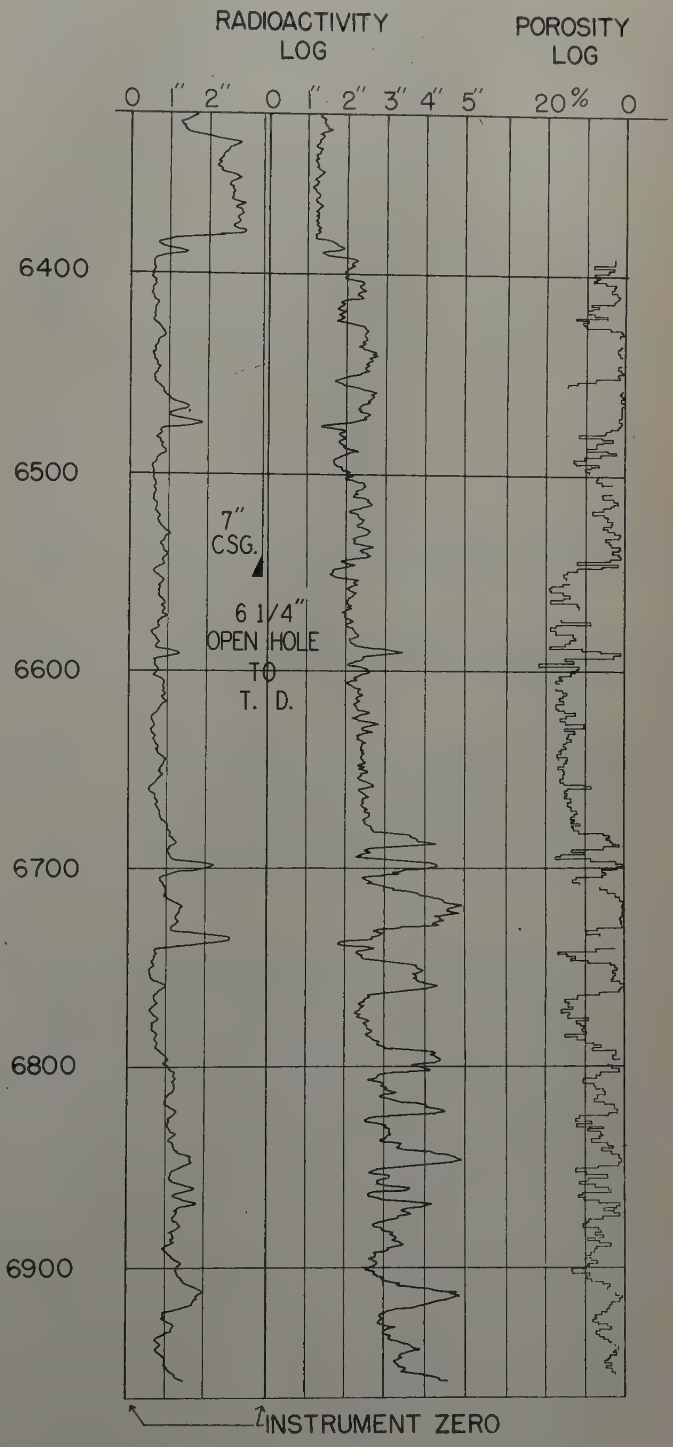

FIG. 2—COMPARISON OF THE RADIOACTIVITY LOG AND CORE POROSITIES IN KELLY-SNYDER FIELD, TEXAS.

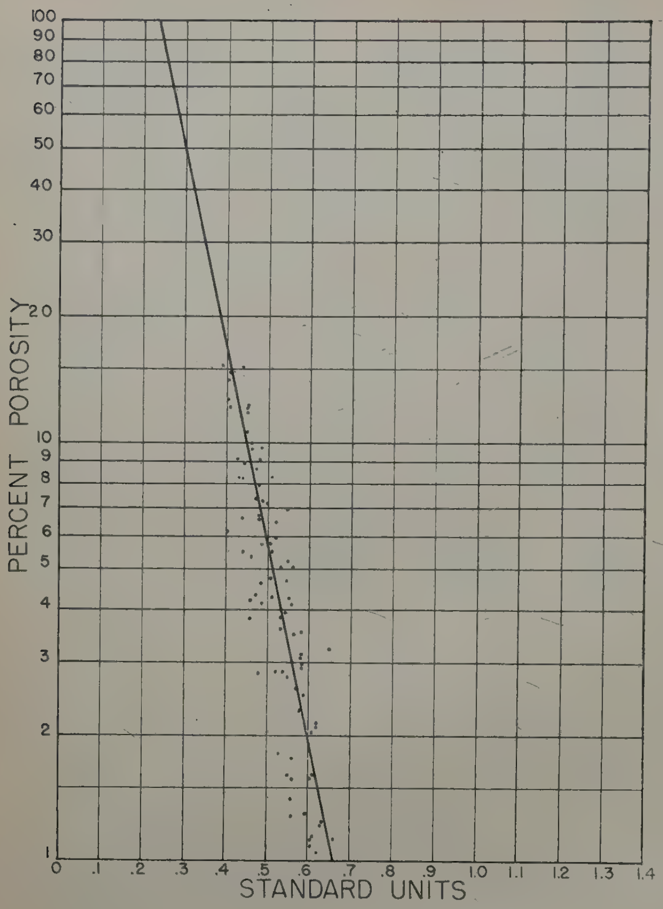

FIG. 3 — NEUTRON DERIVED POROSITY CURVE FOR 7" CASED HOLE, KELLY-SNYDER FIELD.

establishing absolute zero is dependent upon the constancy with which the average shale line is established from well to well and the accuracy of the response of the neutron curve.

APPLICATION OF QUANTITATIVE METHODS OF INTERPRETATION TO SAND FORMATIONS

It has been known for some time that the gamma ray curve can be used to estimate the relative shale content of the sand and for this purpose a linear relationship may be assumed to exist between the deflection of the gamma ray curve and the shale content of the sand. The gamma ray curve is affected solely by the gamma radiation emitted by naturally occurring radioactive elements distributed among certain of the rocks composing the earth's crust. In some rocks the radioactive elements are present in a very constant concentration. The radioactive content of shale, for example, is often sufficiently constant in a given production zone that the percentage of shale at a given depth may be estimated by comparing the gamma ray curve deflection at the given depth with the gamma ray curve deflection at a point opposite pure shale. The neutron curve, on the other hand, responds to lithology in a much more complicated manner. This curve reflects lithologic conditions in terms of the effect produced on the neutrons emitted from the source by the hydrogen content of the rock, the cross sections for the scattering and capturing of neutrons of the elements composing the rock, and the atomic density of these elements in the rock.

In clean (silt and shale-free) limestone or dolomite formations the effects of the hydrogen content and that of the cross section for neutron capture act in combination to shift the neutron curve to the left. The scattering cross section and density effects also act in combination and shift the curve to the right.[9] In the simple case where the neutron curve deflections opposite mixtures of dolomite or limestone and liquid hydrocarbons or water were studied, it was found that a simple exponential relation exists.[9] However, this simple relationship will not apply to most sandstones because of their more heterogeneous chemical composition and the resulting more complex effect on the neutron curve. All of the requirements for calculating a neutron derived porosity for sandstones from the neutron curve are not known, but in addition to the three factors previously enumerated there may be factors which depend on the chemical composition of the matrix and cementing material. Because these factors are still unknown, the neutron curve has not, as yet, been used to determine porosity in sandstones.

However, it has been found that in certain cases the neutron and gamma ray curves can be used in combination to assist in estimating the productivity of a sand section; *i.e.*, whether the section is too shaly to produce or whether it will produce gas or liquid. This use depends upon the reliability of the

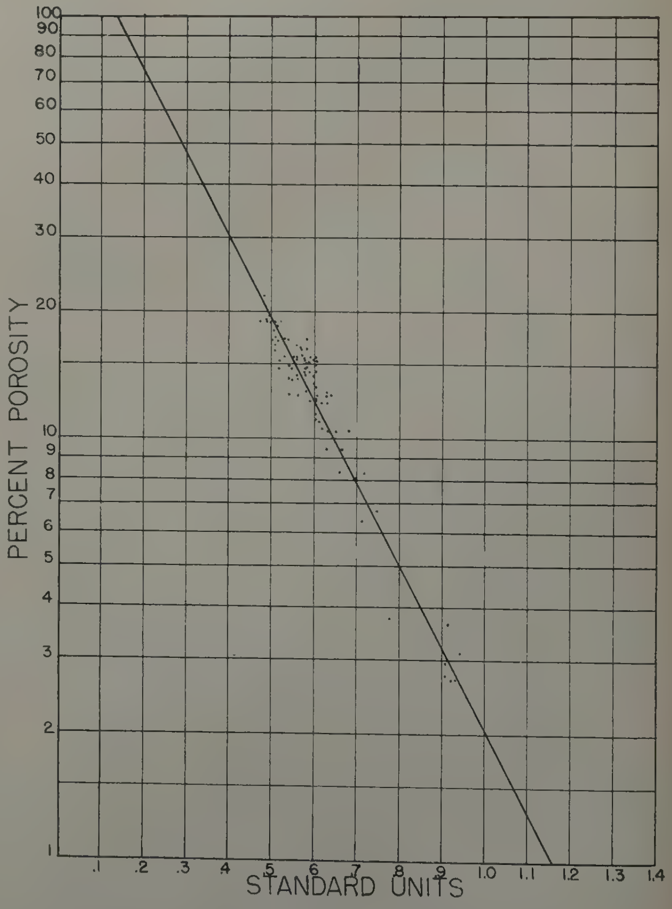

FIG. 4 — NEUTRON DERIVED POROSITY CURVE FOR 6¼" OPEN HOLE, KELLY-SNYDER FIELD.

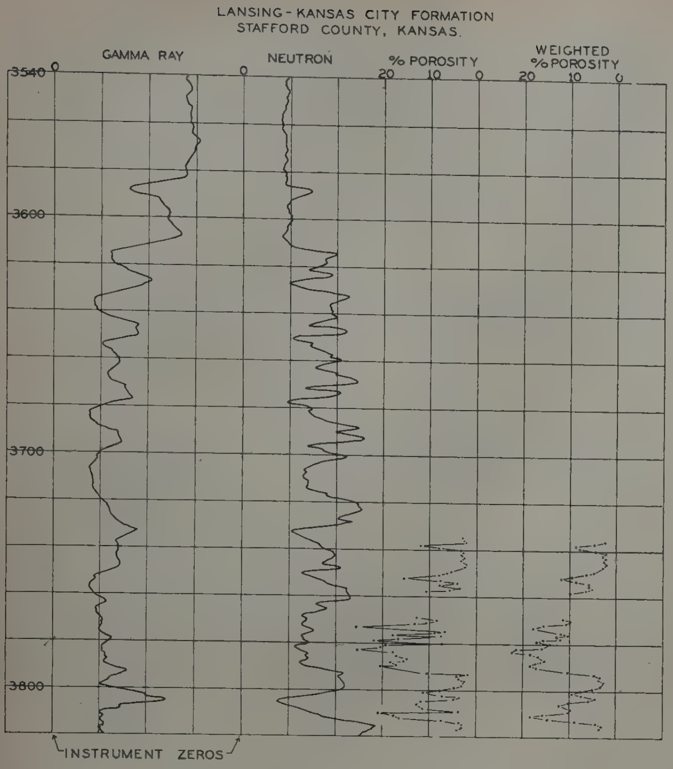

FIG. 5 — COMPARISON OF THE RADIOACTIVITY LOG AND CORE POROSITIES IN STAFFORD COUNTY, KANSAS.

gamma ray curve for estimating the amount of shale present and the application of this curve in a compensatory manner to the neutron curve. Shale contains large proportions of chemically bound water and hydrocarbons; and therefore the neutron curve is affected by shale in a similar manner to that produced by its constituent substances when in the free liquid state. The gamma ray curve may be used to calculate a factor which has a compensatory effect for shale on the neutron curve deflections, and with its aid it is sometimes possible to estimate the productivity of shaly sands from the neutron curve. This factor has been called the gamma ray shale factor.

Calculation of the Gamma Ray Shale Factor (G_s)

The gamma ray shale factor is an empirically derived function of the per cent total gamma ray curve deflection. The total gamma ray curve deflection is the distance between the deflection values for clean, silt-free, shale-free sandstones and the deflection values for the pure shale. The per cent total gamma ray curve deflection is obtained by dividing observed gamma ray curve deflection at a given depth by the total gamma ray curve deflection and multiplying by 100. G_s is expressed as a logarithmic function of the total gamma ray curve deflection (D_g) as follows:

$$G_s = 1 + \log\left[1 + \log\left(D_g + 1\right)\right] \quad . \quad . \quad . \quad . \quad (1)$$

G_s varies from 1 to 1.477 as D_g varies from 0 to 100. A plot of the values of G_s versus the values of $(D_g + 1)$ are shown in Fig. 7.

Application of Gamma Ray Shale Factor To Sand Formations

A relative method using an interrelation factor calculated from the per cent total neutron curve deflections and the gamma ray shale number has been developed, making it possible to predict the productivity of a zone within certain limitations. This interrelation factor has been called the neutron productivity number (N_p). Using a method based on the use of the neutron productivity number, it has been possible to determine the type of production to be obtained from the zone in question in many instances.

The neutron productivity number (N_p) is determined in the following manner:

$$N_p = G_s\left(D_n + 1\right) \quad . \quad . \quad . \quad . \quad . \quad . \quad . \quad . \quad . \quad . \quad (2)$$

where:

D_n is the per cent total deflection for the neutron curve and G_s is the gamma ray shale factor, or:

$$N_p = \left(D_n + 1\right)\left[1 + \log\left[1 + \log\left(D_g + 1\right)\right]\right] \quad . \quad . \quad (3)$$

The neutron productivity number should be used only in a relative manner by comparing the productivity numbers calculated from the curves of a well whose productivity is to be estimated, with the values of productivity numbers for wells producing from the same section. To establish neutron productivity numbers for producing sections of a field, drill stem tests and production tests diagnostic for individual sections

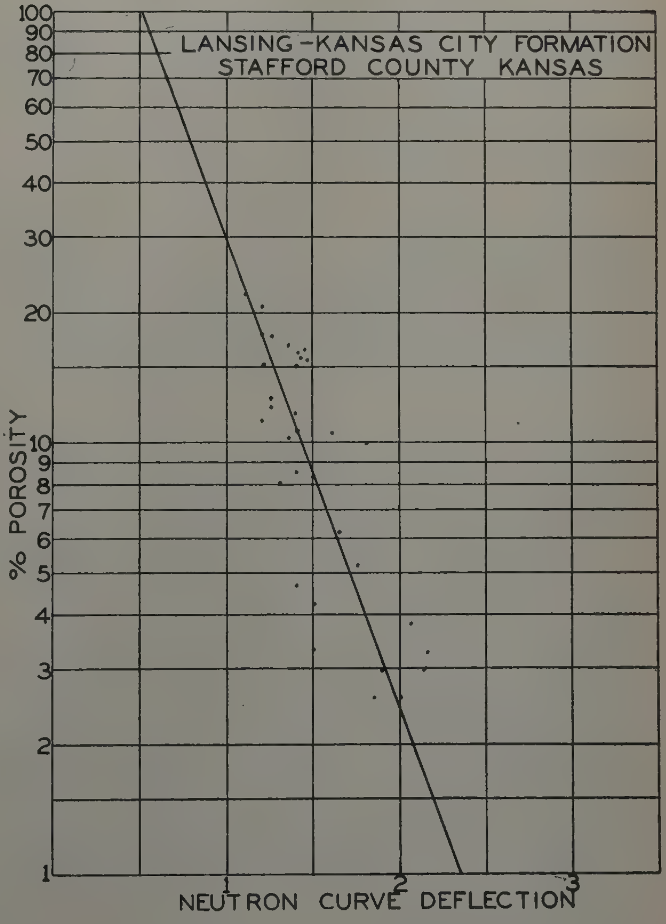

FIG. 6 — NEUTRON DERIVED POROSITY CURVE FOR 4½" CASED HOLE, STAFFORD COUNTY, KANSAS.

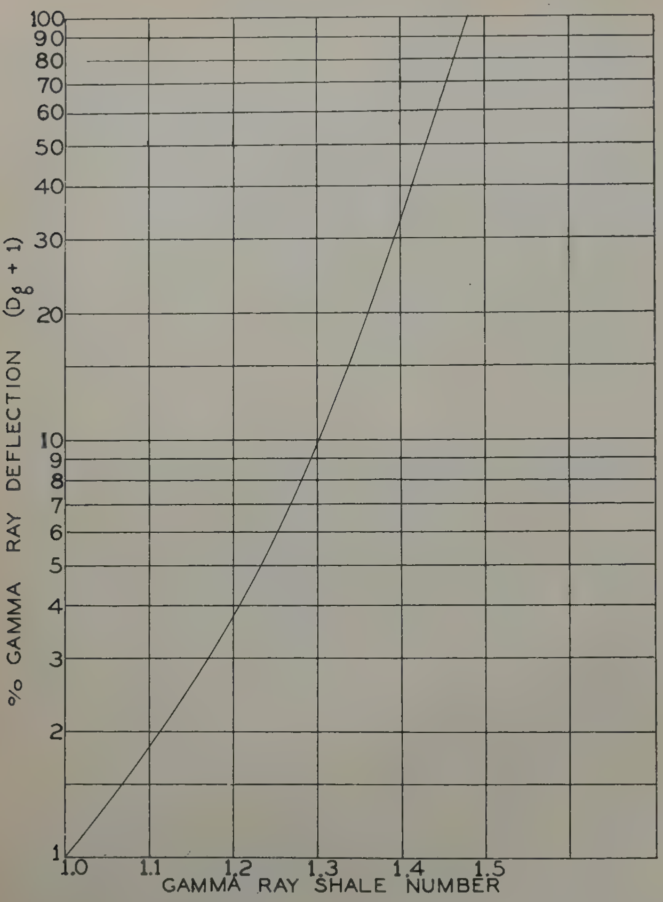

FIG. 7 — RELATIONSHIP BETWEEN GAMMA RAY SHALE NUMBER AND GAMMA RAY CURVE DEFLECTION.

must be compared with the productivity numbers calculated from the logs. The neutron productivity numbers calculated from the log of a well whose productivity is unknown, but which penetrates the same sections can be compared to the neutron productivity numbers for the known wells and an estimate made of the probable production to be expected.

Calculation of the Neutron Productivity Number

The variables D_g and D_n are determined from their respective curves as follows. First, average shale lines are determined for each curve, which are labeled "100" and "0" on the gamma ray curve and the neutron curve, respectively. A typical clean section is then selected on the gamma ray curve and a line is drawn through these deflections parallel to the shale line previously drawn. This line is labeled "0" and the deflection between the line marked "0" and "100" is known as the "total gamma ray curve deflection," (D_{gt}). A line is drawn through the deflections of the neutron curve opposite a clean zone known to be producing liquid hydrocarbon or water, and it also is drawn parallel to the shale line. This line is labeled "100" and the distance between this line and the shale line of the neutron curve is called the "total neutron curve deflection," (D_{nt}).

The per cent total curve deflections D_g and D_n, are obtained by dividing the curve deflections opposite a particular depth and zone, measured from the appropriate zero line, by the total deflection in inches of that curve, (the distance between the zero and the maximum lines). This is illustrated in Fig. 8.

The second step in calculating N_p is to determine the values of D_g and D_n by measuring the deflection of the particular zone desired and comparing this value with the total deflection for the gamma ray and neutron curves, respectively. Thus,

$$D_g = \frac{D_{go}}{D_{gt}} \quad . \; . \; . \; . \; . \; . \; . \; . \; . \; . \; . \quad (4)$$

where:

D_{go} is the distance measured from the zero line for the gamma ray curve deflection, and D_{gt} is the distance for total deflection of the curve. Similarly for the neutron curve:

$$D_n = \frac{D_{no}}{D_{nt}} \quad . \; . \; . \; . \; . \; . \; . \; . \; . \; . \; . \quad (5)$$

The logarithms of the values for D_g are then determined from any table of logarithms and the values substituted in Equation (3).

N_p may be calculated more easily, however, by using the nomograph shown in Fig. 9, for here it is only necessary to lay a straight edge across the nomograph, aligning the values of $(D_n + 1)$ and $(D_g + 1)$ on their respective indices and the value for N_p will be found on the N_p index at its point of intersection with the straight edge.

Response of the Neutron Productivity Number

N_p is an index which may indicate the per cent of shale, liquid or gas. The limits described in the following illustration must not be taken as generally applicable, because it was found that these limits apply only in partcular areas. It is necessary that values of N_p be determined and compared with drill stem tests, production tests or perforating data in the particular area or field being considered before the range of values may be known. From such data the following table was compiled:

Values of N_p	Condition
1 to 75	Shale
75 to 168	Liquid Filled Porosity
168 to 500	Gas Filled Porosity

Specific Applications of the Neutron Productivity Number

To illustrate the application of the neutron productivity number in sand areas, wells in the Freites District, Venezuela and the Buffalo Field of East Texas were selected. These wells are thought to have penetrated a relatively uniform porosity throughout the sand bodies.

The first example, shown in Fig. 8, is of a well in the Freites District, Venezuela. The interval 7,295 - 2,323 ft was perforated and on test flowed at the rate of 534 B/D. The maximum value reached by N_p in this interval on the log was approximately 150. The interval 7,445 - 7,455 ft was not tested but is believed by the operator to contain gas. The N_p value of nearly 300 calculated from the log confirms this opinion. The interval 7,480 - 7,660 ft was not tested but is believed by the operator to contain fluid. The value of 120 for N_p tends to confirm this opinion.

The values of N_p were calculated from the log by establishing the reference lines in the manner described previously, and applying D_g and D_n to the nomograph.

Also shown in Fig. 8 is the radioactivity log of the Lone Star Producing Co. Mary Jones No. 4, Buffalo Field. The main Woodbine sand from 5,695 ft to 5,724 ft apparently is a uniformly clean (silt and shale-free) sand. This zone was tested through perforations in the 5½-in. casing from 5,704.5 ft to 5,712.5 ft and produced gas with very little oil. These perforations were squeezed and the casing reperforated from 5,706 ft to 5,714 ft. A completion test of these perforations yielded 81.81 B/D of oil with little gas.

The values for D_g and D_n throughout the entire section were determined, and N_p was calculated from the nomograph (Fig. 9). The gas-oil contact is placed at 5,704 ft with a value of 160 N_p (table above) representing the approximate separation value.

The Lone Star Producing Co. W. D. Recknor No. 1, Buffalo Field, is another example of the application of the table. In this well the 5½-in. casing was perforated from 5,741 ft to 5,745 ft resulting in the production of oil with a low gas/oil ratio. It will be noted that the N_p value at the depth 5,742 ft is 92 and at 5,740 ft the N_p value is 260, placing the gas-oil contact between 5,740 ft and 5,742 ft. Although the section at 5,742 ft is indicated by the gamma ray curve as shaly, the value of 92 after application of the N_p curve would indicate that it should be productive of liquid. The low values of N_p in the interval from 5,728 to 5,736 ft are probably due to the invasion of large quantities of drilling fluid. The sands indicated from 5,754 ft to 5,758 ft are known to be water bearing and were used as the 100 per cent line on the neutron curve. The values of N_p were computed by the use of the nomograph as previously described, Fig. 9. Had the N_p curve not been computed for this log, it would have been difficult to place the gas-oil contact within a two-ft zone due to the influence of shale at exactly the point of contact.

The values established for this field are usable over a limited area and should be improved with each subsequent well that is drilled and tested. The method described here is particularly applicable to the shaly sands in which the influence of shale reduces the intensity of the neutron curve and prevents the visual identification from the neutron curve of gas-liquid interfaces which is possible in clean sands.

SUMMARY AND CONCLUSIONS

The use of a device for determining the position of zero radioactivity and a sensitivity selector switch of greater versatility has been discussed and their application to actual logs of the limestones of West Texas and Kansas has been shown by illustration. Using the new instrumental zero reference line, the application of quantitative methods to the radioactivity logs will provide a means of estimating porosity. This is done by comparing the intensity of the neutron curve deflections with the porosities from the core samples and plotting this relationship to establish a neutron derived porosity curve. This curve may then be applied to unknown wells of similar bore hole conditions on which radioactivity logs have been obtained. The data shown in this paper are applicable to wells having 7-in. cased holes or 6¼-in. open holes in the reef limestone of West Texas and to 4½-in. cased holes in the Lansing - Kansas City zone in Kansas.

A relative method of utilizing an interrelation factor calculated from the gamma ray and neutron curves called the neutron productivity number has been discussed. The neutron productivity number calculated for given depth intervals within the zone of interest will aid the interpretation of radioactivity logs in determining gas-liquid contacts in shaly sands and sandy shales. The use of the neutron productivity number is recognized as a relative method of comparison and is limited in applicability to those areas and reservoirs in which the neutron curve is definitive of gas in the reservoir. Greater

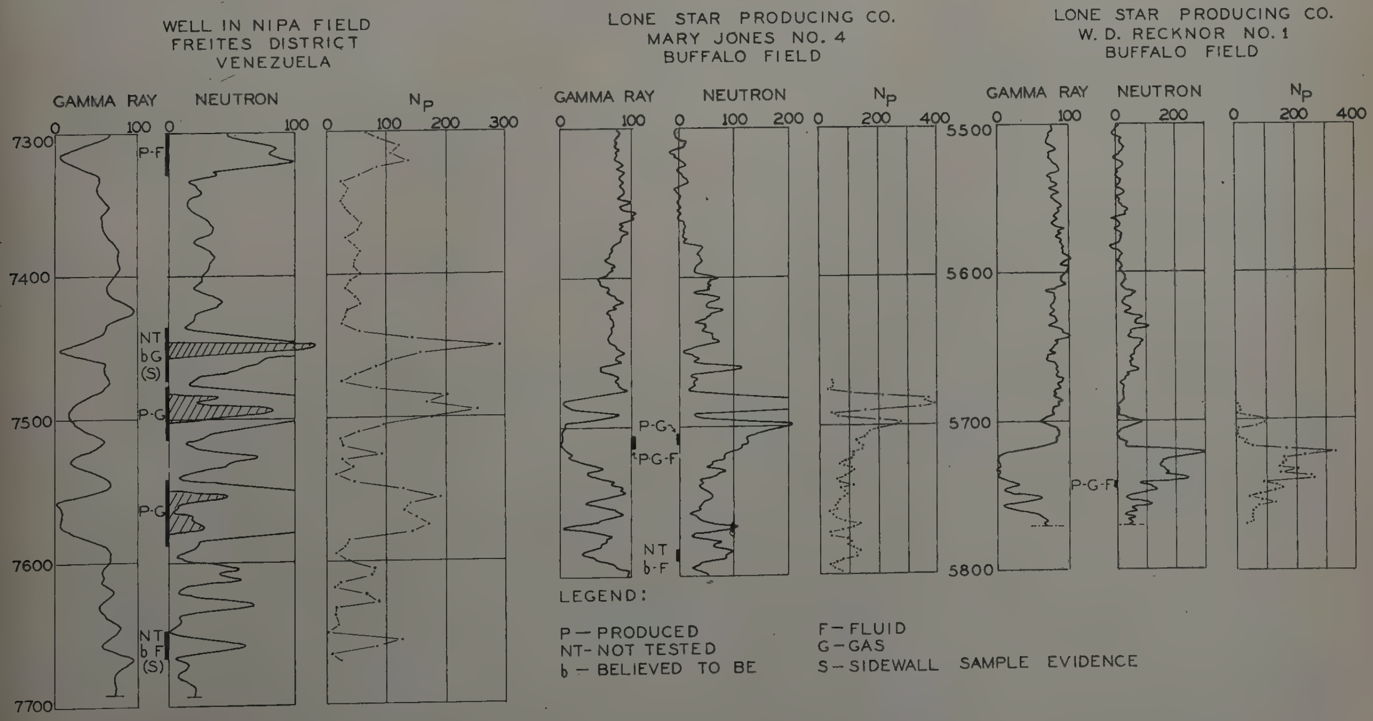

FIG. 8 — APPLICATION OF NEUTRON PRODUCTIVITY NUMBER.

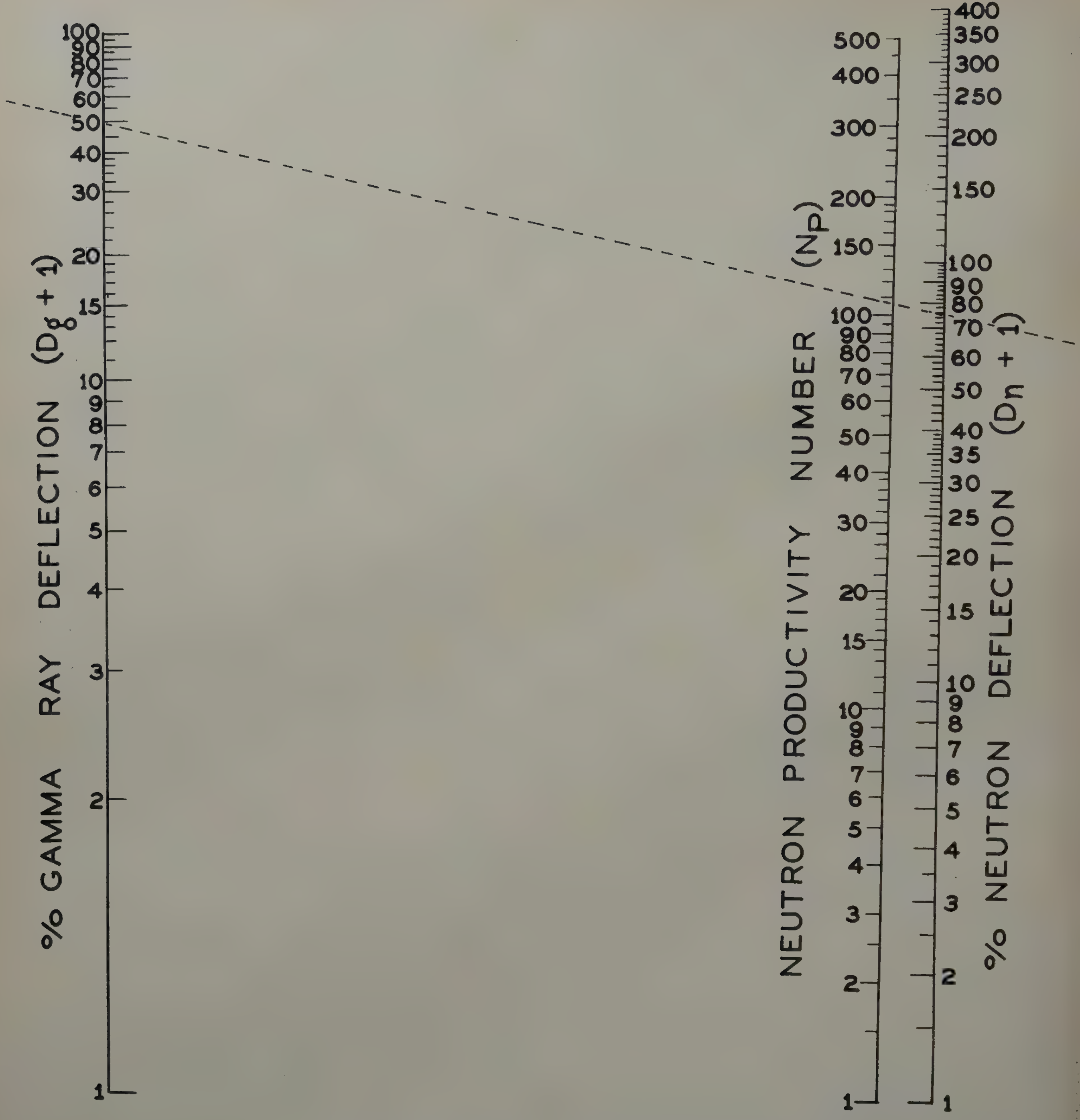

FIG. 9—NOMOGRAPH FOR COMPUTING THE NEUTRON PRODUCTIVITY NUMBER

versatility and a wider range of applicability may be provided by the use of new radiation zero devices and it is hoped their use will result in an extension of quantitative methods for sand areas.

ACKNOWLEDGMENT

The authors wish to thank the Lane-Wells Co. and Well Surveys, Inc., for permission to publish this paper. They also wish to express their appreciation to the oil companies whose cooperation and assistance made this paper possible. The authors wish to acknowledge the assistance of the members of the staffs of the Lane-Wells Co. and Well Surveys, Inc., who have aided in the preparation of the manuscript.

REFERENCES

1. Green, W. G., and Fearon, R. E.: *Geophysics*, (July, 1940), 5, 272.
2. Pontecorvo, B.: *Oil and Gas Jour.*, (Sept. 11, 1941), 32.
3. Russell, W. L.: AAPG Bul. (Sept., 1941), **25**, No. 9.
4. Jackson, W., and Campbell, J. L. P.: *Trans.* AIME, **165**, 241.
5. Campbell, J. L. P., and Winter, A. B.: *Oil Weekly*, (Jan. 6, 1946).
6. Mercier, V. J.: *Oil Weekly*, (Oct. 14 and 21, 1946).
7. Fearon, R. E.: *Nucleonics*, (June, 1949), **4**, No. 6, 30-92.
8. *Ibid.* (April, 1949), **4**, No. 4, 67-75.
9. Bush, R. E., and Mardock, E. S.: *Trans.* AIME, (1950), **189**, 19.

* * *

T.P. 3057

THE SOUTHWEST ANTIOCH GIBSON SAND UNIT

T. E. OCKERSHAUSER, THE GLOBE OIL AND REFINING CO., OKLAHOMA CITY, OKLA., MEMBER AIME

INTRODUCTION

The Southwest Antioch Oil Field located in T2&3N - R2&3W, Garvin County, Okla., was discovered in February, 1946, by The Globe Oil & Refining Co. and The Vickers Petroleum Co. at their Melinda Gibson No. 1. Oil production was encountered at a depth of 6,525 ft in 14 ft of lower Pennsylvanian sandstone.

The producing sand, locally called the "Gibson" or "Third Deese," is a sand bar deposit strung along the west flank of the Pauls Valley uplift in a northwest-southeast direction. The oil reservoir is defined to the east by the edge of sand deposition along the uplift and to the west by the gradation of sand into shale. Within the Antioch Unit, the sand dips from 150 to 400 ft per mile southwesterly and has a pay thickness varying from 10 to 55 ft and averaging 28 ft.

Several areas of Gibson production have been developed, including the Katie pool on the south, the Elmore Area of the Southwest Antioch Gibson Sand pool, the Southwest Antioch Gibson Sand pool proper, the Southwest Maysville pool and the New Hope pool on the north. Production extends over a belt 22 miles long by about two miles wide and is continuous except into the Katie and New Hope pools. It appears that drilling will soon prove these intervening areas productive. To March 1, 1950, approximately 18,000 acres have been developed with 450 Gibson wells. It is likely this count will ultimately reach 32,000 acres with 800 wells.

RESERVOIR

The natural production of oil from the Gibson reservoir is primarily due to solution gas expansion though gravity also plays a part. There is no indication of water drive or evidence that an initial gas cap existed.

Gibson oil has a stock tank gravity of 43° API and was saturated at the original reservoir pressure of 2,925 psi. It contained 1,340 cu ft of gas per bbl in solution and had a high shrinkage of 70 per cent. Connate water amounts to 15 per cent. Reservoir temperature is 130°F.

Porosity averages 15.5 per cent and permeability ranges from less than one md to over 1,000. Based on measurement of 400 core plugs from 15 wells, 78 per cent of the permeabilities fell within the 10 to 1,000 md bracket and averaged 167.

Primary oil recovery is estimated at 140 bbl per acre-ft or 22 million bbl for the present 137-tract unit. Due to unitization

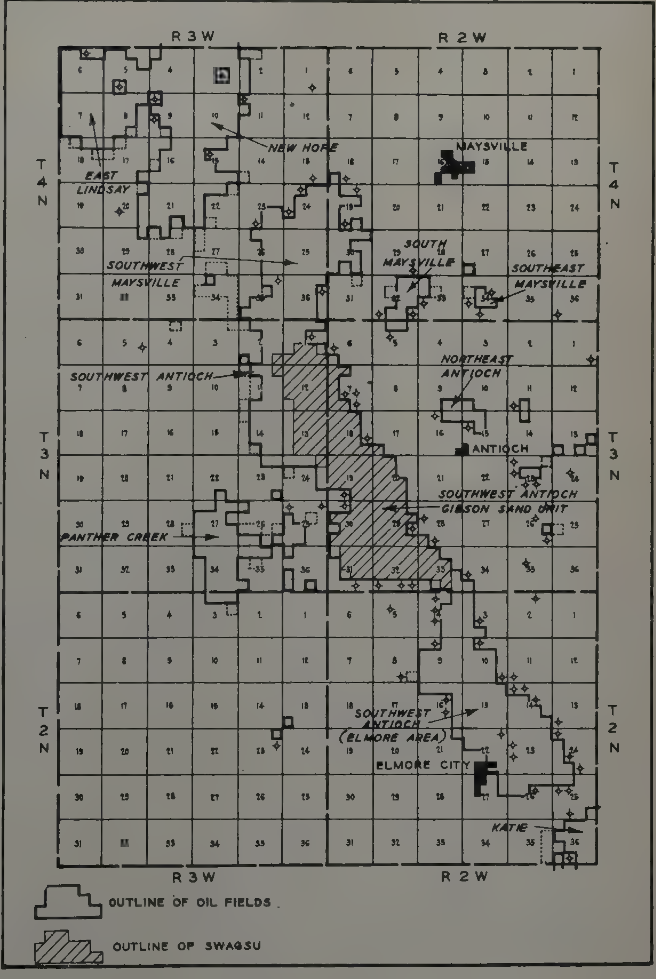

FIG. 1 — MAP SHOWING OIL FIELDS IN VICINITY OF THE SOUTHWEST ANTIOCH GIBSON SAND UNIT.

Mauscript received in the office of the Petroleum Branch, Aug. 30, 1950. Paper presented at the Petroleum Branch Fall Meeting in New Orleans, La., Oct.4-6,1950.

and gas injection, it is expected that recovery will be increased to 260 bbl per acre-ft or to a total of 41 million bbl — about doubled.

UNITIZATION

It appeared to oil operators early in the development of the Southwest Antioch pool, that oil recovery could substantially be increased under a program of unit operation and gas injection. This belief was verified by a study completed in February, 1947. It was realized that to put such a program into effect, the full cooperation of royalty owners was necessary and desirable. To this end a meeting of royalty owners was called and operators helped organize the Southwest Antioch Royalty Owners Association.

This association played an important part in creating and perfecting the unit. Their technical experts actively participated in operator's meetings and had access to all information. To keep its membership advised, there were several meetings of the association in the towns of Antioch and Maysville. Operator representatives attended a number of these gatherings to discuss unitization.

On Jan. 6, 1948, the Oklahoma Corporation Commission heard and approved the petition creating the Southwest Antioch Gibson Sand Unit without objection from royalty owners or oil operators. Operation of the 67 wells comprising the original unit was assumed by The Globe Oil & Refining Co. as Unit Operator on April 1, 1948.

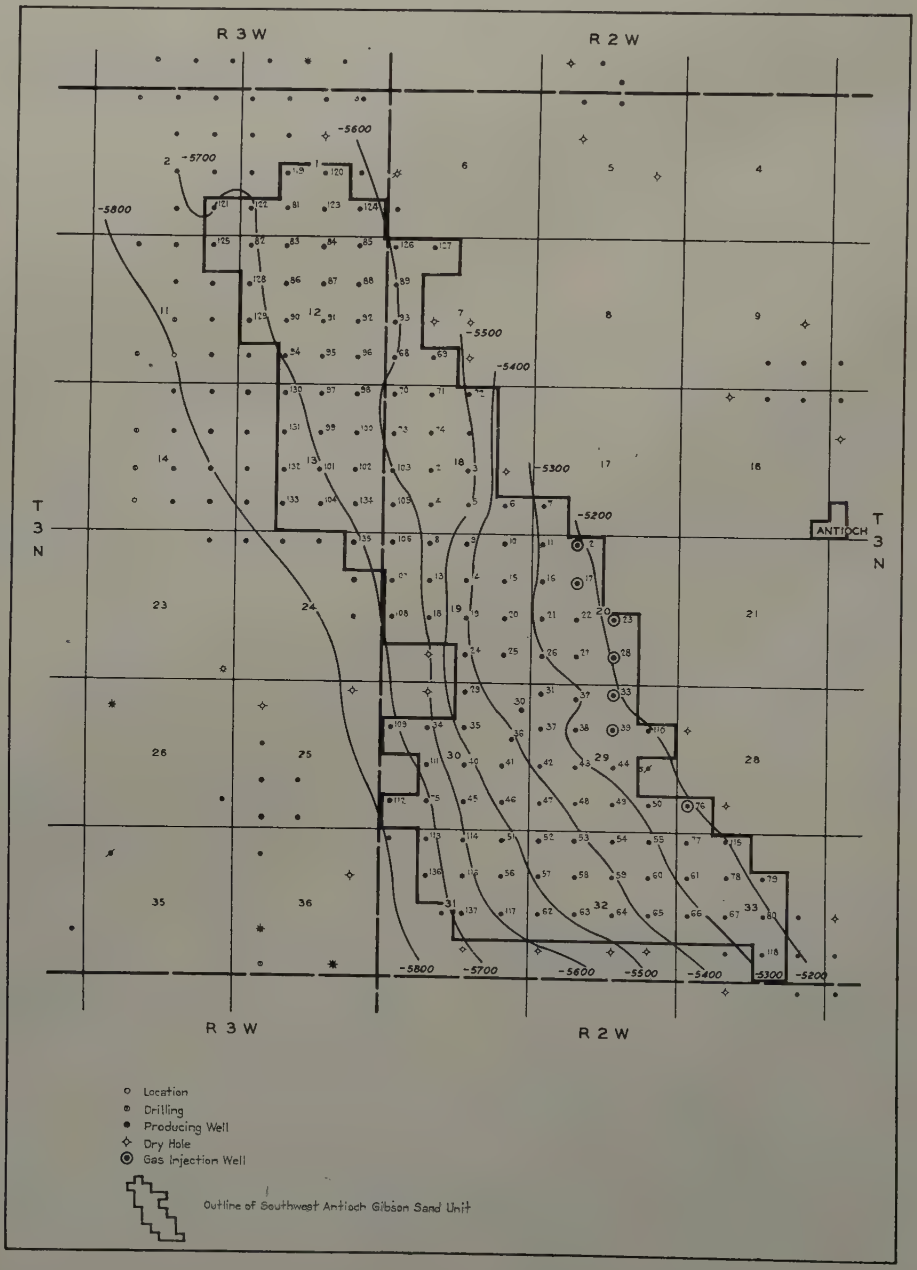

FIG. 2 — STRUCTURE MAP, GIBSON SAND, SWAGSU.

The Antioch Unit has been enlarged three times without incident and has grown in size from 67 to 137 wells. A fourth enlargement is now being considered which will increase this number to approximately 180 wells.

Under the "Plan of Unitization" adopted by the Southwest Antioch Unit, only producing 40-acre tracts are taken in. The original participation formula based half of tract interest on net pay and half on ability to produce up to 150 B/D of oil with a maximum of 375,000 cu ft of gas. The formula has since been modified to include a reservoir pressure factor.

Operation

Operating provisions of the "Plan of Unitization" stipulate:

"The oil produced from the Unit Area shall be produced from those wells in the Unit Area from which the same can be obtained with the smallest loss or dissipation of reservoir energy reasonably possible under practical operating conditions as they may exist from time to time;" and

"Gas wells and wells which produce oil with gas/oil ratios found to be excessive in relation to the gas/oil ratios of other wells producing oil from the Unit Area shall be shut in or the production therefrom restricted in such manner as to make the most effective utilization of the gas energy of the reservoir reasonably possible under practical operating conditions as they may exist from time to time."

Production operations from the beginning have been conducted in accordance with these principles. During the first

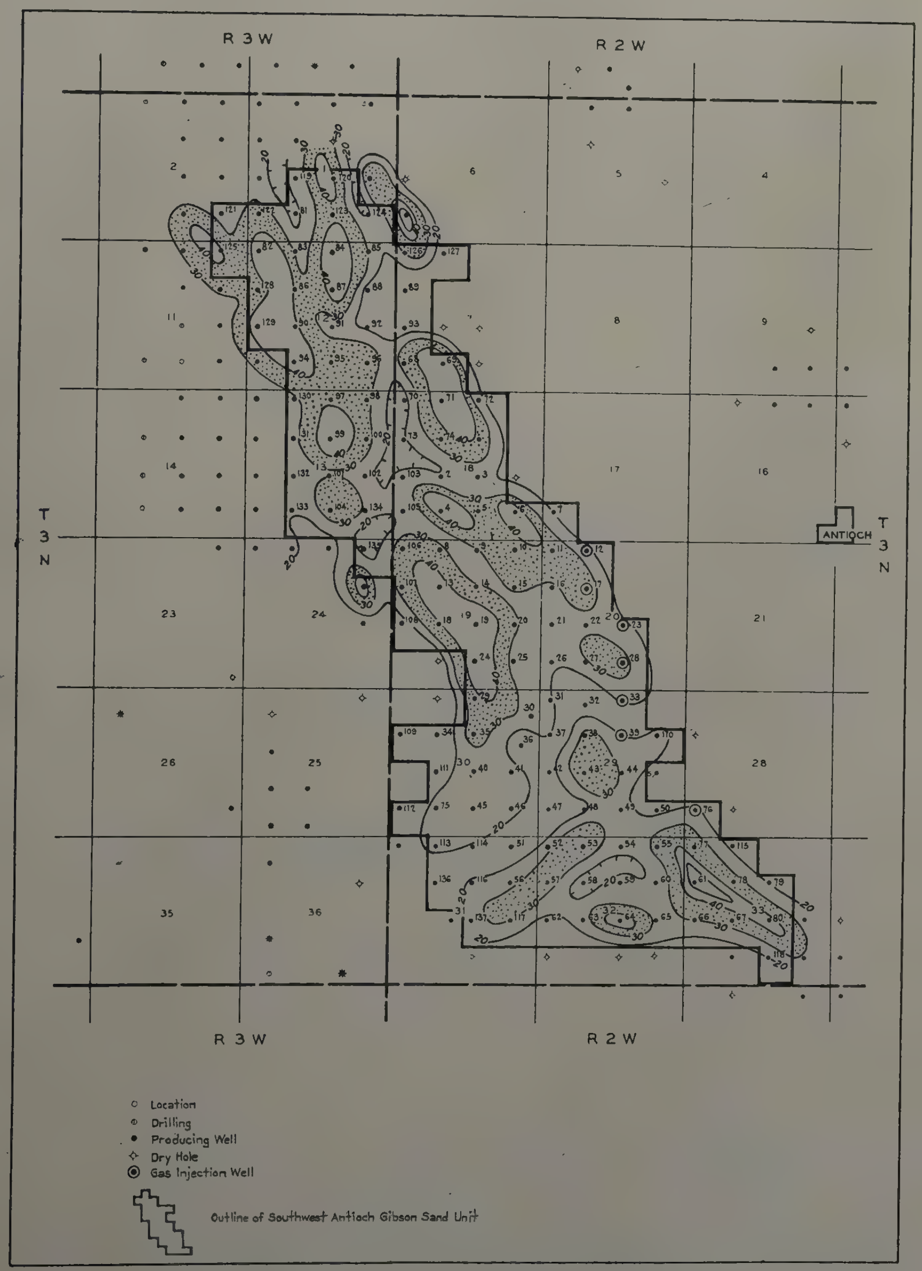

FIG. 3 — THICKNESS MAP, GIBSON SAND, SWAGSU.

month of operation, as a result of selective oil production, average gas/oil ratio for the Unit Area was lowered from 3,000 to 2,200 cu ft per bbl or about a third more oil was produced for the same volume of gas.

In order to determine the amount of oil to be produced from each well and determine the distribution of gas to input wells, gas/oil ratios are taken monthly and reservoir pressures are measured three to four times a year.

Injection

Gas from the Unit is processed and compressed for injection by the plant of the Warren Petroleum Corp., *et al.* Injection of 9 MMcf/D of gas started during August, 1948, with one 600-HP compressor. A second 600-HP machine, which was placed in operation during October, 1948, boosted input to 15.5 MMcf/D. Present capacity of 25 MMcf/D was reached in June, 1949, with the addition of a third 800-HP compressor.

Gas is being returned to the Gibson sand through seven injection wells situated at high structural positions near the sand edge on the east side of the pool. Injectivity rates at individual wells range from 2 MMcf/D to in excess of 5.5 MMcf/D at 2,400 psi pressure. During 21 months operation, a total of over 10 billion cu ft of gas has been put back into the reservoir.

The effects of gas injection were first noticed during the second month of injection when a material lessening in the rate of bottom hole pressure decline occurred near input wells; some wells even showed small pressure increases. At one pro-

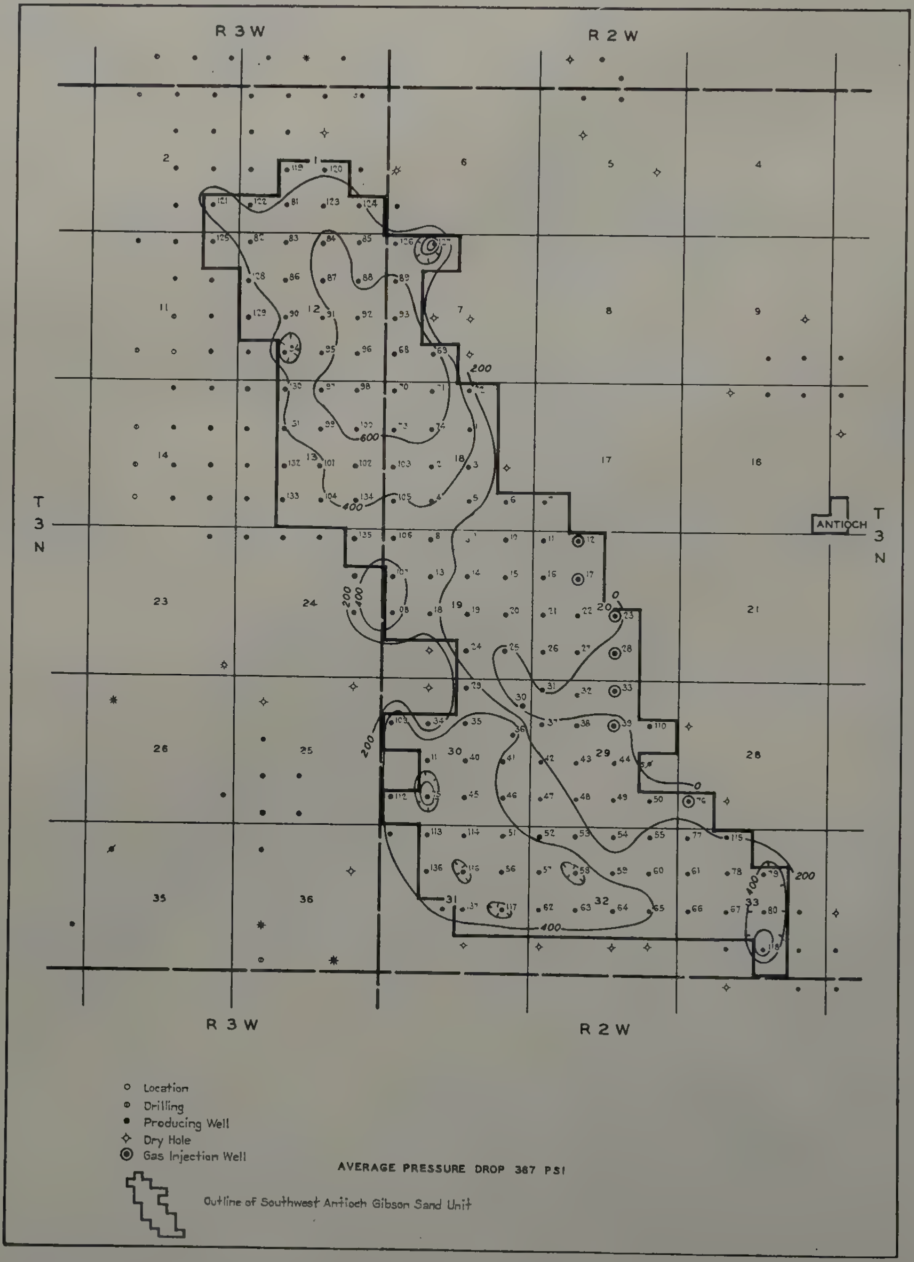

FIG. 4 — BHP CHANGE MAP, SEPTEMBER, 1948, THROUGH FEBRUARY, 1950, SWAGSU.

ducer, during the third month of injection, oil rate tripled and gas/oil ratio fell to one-third. During the fourth month at another well, oil gravity increased from 40° to 60° API. This change in liquid character was caused by injection of gas at a diagonally offsetting well which formerly produced high gravity oil.

The advance of the gas front away from injection wells has been fairly uniform, conforming closely with structure. There has been no tendency for gas to channel or break through. From a comparison of pressure drops at individual wells with the average drop for the Unit since the beginning of injection, it appears gas has influenced 45 wells, an area of about 2,000 acres, and has been felt as far away as 6,500 ft from input wells.

PERFORMANCE

The 137 wells comprising the present Unit have produced a total of 10.8 million bbl of oil to March, 1950. Of this amount 9 million bbl or about 85 per cent has come from the 80 wells in the first enlarged Unit. Inasmuch as a longer history is available on these wells and they have recovered the major portion of the oil, their behavior is a reliable indication of reservoir performance.

At the time of unitization, April 1, 1948, gas/oil ratio was 2,900 cu ft per bbl and was increasing rapidly. Had conventional operation continued, gas/oil ratio by now would be in excess of 10,000. Actually it is 4,800. It appears that a minimum of twice as much oil is now being recovered per cu ft

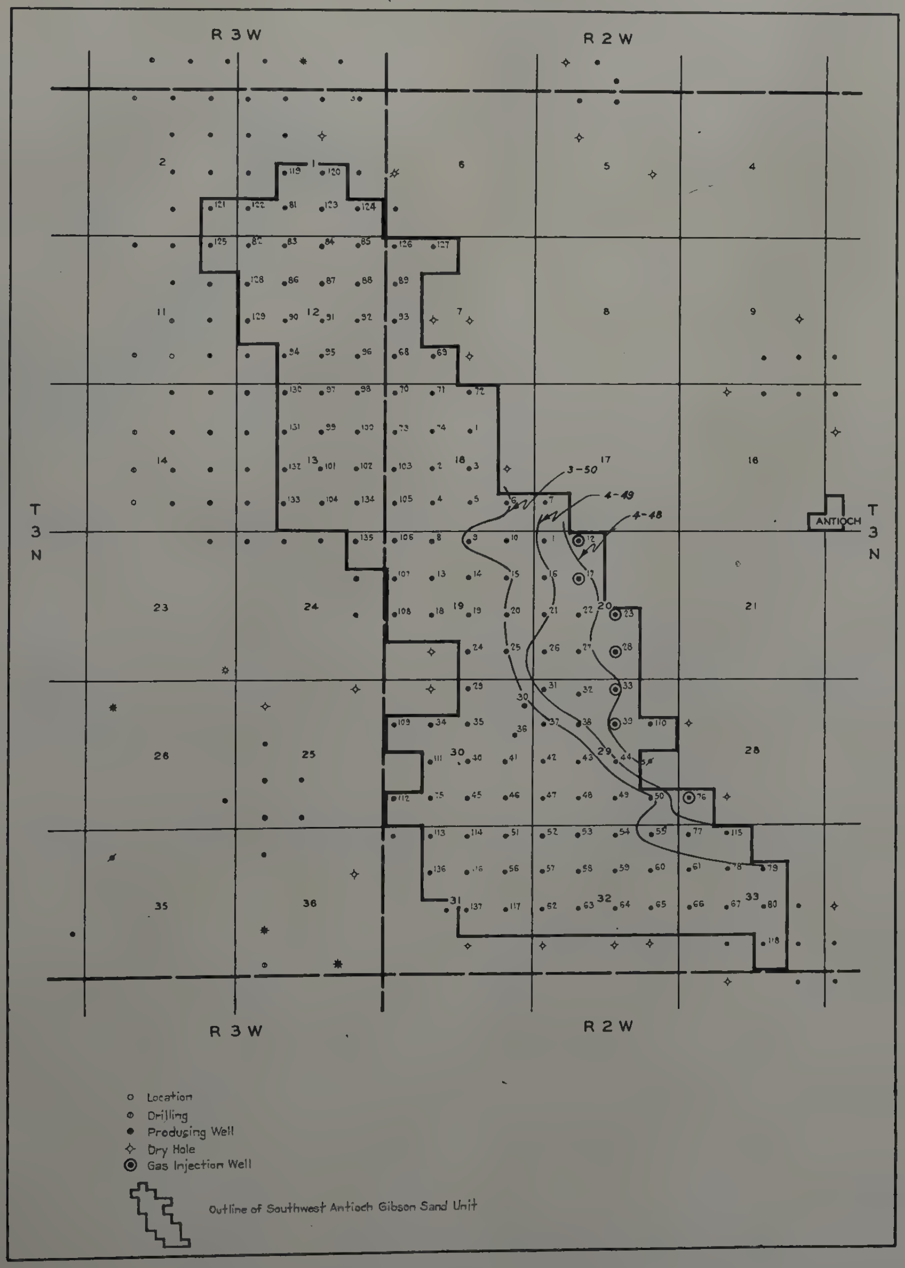

FIG. 5 — TIME-POSITION 10,000 GOR CONTOUR, VICINITY GAS INJECTION, SWAGSU.

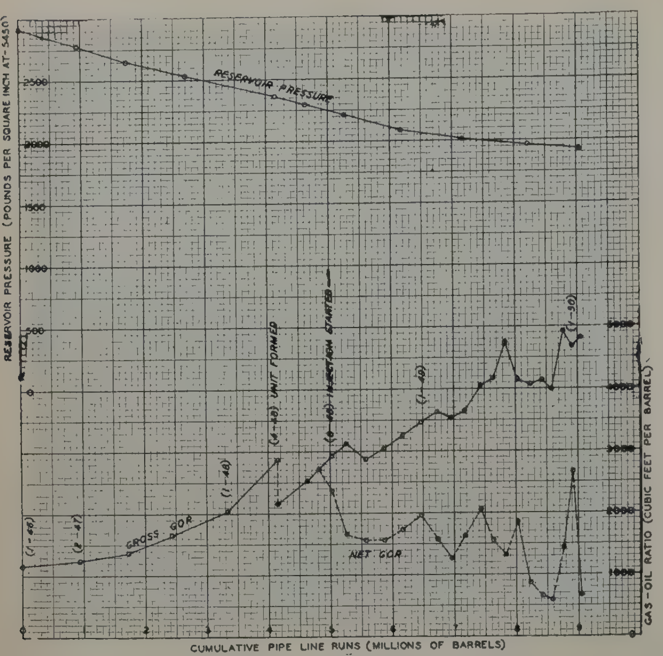

FIG. 6 — RESERVOIR PERFORMANCE, 80 TRACT UNIT, SWAGSU.

of gas than would have been recovered had conventional operation continued.

A total of 5.2 million bbl of oil and 18.1 billion cu ft of gas have been produced under Unit operation and 9.2 billion cu ft of gas have been returned to the reservoir. Net gas/oil ratio has averaged 1,725 cu ft per bbl. This compares to an average ratio of 1,645 cu ft per bbl before unitization, during which period 3.9 million bbl of oil and 6.4 billion cu ft of gas were produced. Considering only the interval of gas injection, 4.2 million bbl of oil have been recovered at a net ratio of 1,565 cu ft per bbl.

The effect of gas injection is readily apparent from an examination of reservoir pressure decline which shows a decided reduction in rate during December, 1948, five months after gas injection started. Prior to this time 7,370 bbl of oil were produced per pound pressure drop. Since this date, each pound drop in pressure has accounted for the recovery of 17,790 bbl or approximately 140 per cent more oil.

The public, much to the harm of unitization, frequently is of the impression that reduced production rate inevitably accompanies unit operation. Comparison with the production rate of competitively operated wells in the Elmore Area of the pool, shows that such a belief is unjustified, at least in the case of the Antioch Unit.

Both groups of wells produce from the same source of supply, wells are very nearly the same age, and the reservoir is approximately in the same state of depletion. The Unit has produced the top allowable rate set by the Corporation Commission; whereas, the average well in the Elmore Area has produced substantially under the maximum allowable. Over a period of 17 months since gas injection started, Unit wells produced an average of 93.5 B/D of oil per well compared to 73.8 B/D for wells in the Elmore area. The difference of 19.7 B/D amounts to the production of 7,200 bbl of additional oil in a year's time from each well in the Unit. To royalty owners this means an increase in annual income of $2,400.00 per well.

★ ★ ★

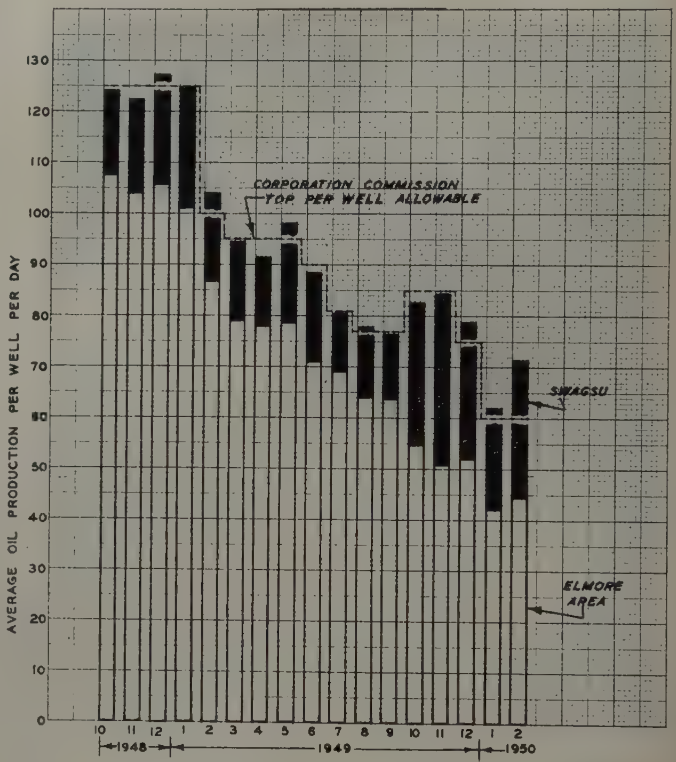

FIG. 7 — COMPARATIVE APPROACH OF SWAGSU AND ELMORE AREA PRODUCTION TO MAXIMUM ALLOWED BY THE CORPORATION COMMISSION.

T.P. 3079

STEADY FLOW OF TWO-PHASE SINGLE-COMPONENT FLUIDS THROUGH POROUS MEDIA

FRANK G. MILLER,* U. S. BUREAU OF MINES, SAN FRANCISCO, CALIF., MEMBER AIME

ABSTRACT

This report presents developments of fundamental equations for describing the flow and thermodynamic behavior of two-phase single-component fluids moving under steady conditions through porous media. Many of the theoretical considerations upon which these equations are premised have received little or no attention in oil-reservoir fluid-flow research. The significance of the underlying flow theory in oil-producing operations is indicated.

In particular, the theoretical analysis pertains to the steady, adiabatic, macroscopically linear, two-phase flow of a single-component fluid through a horizontal column of porous medium. It is considered that the test fluid enters the upstream end of the column while entirely in the liquid state, moves downstream an appreciable distance, begins to vaporize, and then moves through the remainder of the column as a gas-liquid mixture. The problem posed is to find the total weight rate of flow and the pressure distribution along the column for a given inlet pressure and temperature, a given exit pressure or temperature and given characteristics of the test fluid and porous medium.

In developing the theory, gas-liquid interfacial phenomena are treated, phase equilibrium is assumed and previous theoretical work of other investigators of the problem is modified.

Laboratory experiments performed with specially designed apparatus, in which propane is used as the test fluid, substantiate the theory. The apparatus, materials and experimental procedure are described. Comparative experimental and theoretical results are presented and discussed.

It is believed that the research findings contributed in this paper should not only lead to a better understanding of oil-reservoir behavior, but also should be suggestive in regard to future research in this field of study.

INTRODUCTION

In recent years much time and effort has been consumed in both theoretical and experimental studies of the static and dynamic behavior of oil-reservoir fluids in porous rocks. Although lack of sufficient basic oil-field data, principally concerning the properties and characteristics of reservoir rocks and fluids, largely precludes quantitative application of research results to oil-field problems, qualitative application has become common practice. In effect, oil-reservoir engineering research is serving as a firm foundation for oil-field development and production practices leading to increased economic recoveries of petroleum. This province of research, however, still poses many perplexing problems.

The thermodynamic behavior of two-phase fluids moving through porous media constitutes one facet of reservoir-fluid-flow research that has not received the attention it deserves. This report embodies a theoretical discussion of this subject and a description of a series of related laboratory experiments. The significance of the problem to oil field operations is indicated but in particular the report centers around a theory and method for analyzing the steady, macroscopically linear, two-phase flow of a fluid (a single molecular species) through a horizontal column of porous medium.

For simplicity in showing how the thermodynamic behavior of two-phase fluids moving through porous media affects oil-reservoir performance problems, attention is focused temporarily on a particular well producing petroleum from an idealized water-free solution-gas drive reservoir, the reservoir rock being a horizontal, thin, fairly homogeneous sandstone of large areal extent confined between two impermeable strata.

The flowing hydrocarbon fluid is considered to exist entirely as a liquid at points in the reservoir remote from the well; however, the decline in fluid pressure in the direction of the well causes vaporization of the hydrocarbon to begin at a radial distance r from the well. Upstream from r the fluid moves entirely as a liquid and downstream from r it moves either entirely as a gas or as a gas-liquid mixture depending on the properties of the hydrocarbon and on the thermodynamic process it follows during flow.

The distance r would be variable under transient flow conditions, but for purposes of analysis the flow is considered to be steady at the particular instant of observation during the flowing life of the well of interest. If the flow were isothermal and the hydrocarbon a pure substance, the fluid would be entirely gaseous downstream from r. Thus, this isothermal flow process for a pure substance would require that the heat of vaporization be supplied at r, over zero length of porous medium, at the precise rate necessary to maintain the constant temperature. This means that the solid matrix of the porous medium (reservoir rock) and the surroundings (impermeable strata confining the reservoir rock) would have to serve as infinite heat sources. Heat-transfer requirements would be somewhat less severe for the isothermal flow of a multicomponent hydrocarbon as bubble and dew points at the same temperature correspond to different pressures. In this instance isothermal conditions would be sustained without complete vaporization of the fluid over zero length of porous medium.

Nevertheless, as the flow is in the direction of decreasing

Manuscript received in the office of the Petroleum Branch Sept. 30, 1950. Paper presented at the West Coast Fall Meeting of the Petroleum Branch, AIME, in Los Angeles, Calif., Oct. 12-13, 1950.

*This paper is a report of part of the research performed by the author in fulfilling the requirements for a PhD degree in mechanical engineering at the University of California.

pressure, isothermal flow of either a single-component or multicomponent hydrocarbon represents a maximum limiting condition as no other thermodynamic, decreasing-pressure, vaporization process would require as great a rate of heat transfer to the fluid. In contrast, a minimum limiting condition is represented by a thermally-isolated flow system, defined as one in which no heat is transferred to the flowing fluid from the solid matrix of the porous medium or from the impermeable strata confining the system.

As pointed out by O'Brien and Putnam[1] the flow conditions in an oil reservoir apparently are intermediate between the foregoing maximum and minimum limiting conditions. Those authors indicate that a petroleum-bearing stratum could be represented by a fluid-filled porous medium, confined above and below by constant-temperature impermeable beds from which heat is transferred along various paths, solid and fluid, through the porous media. Flow problems relating to this system, however, depend on complete knowledge of the heat-transfer characteristics of the system and such information is not presently available. In this connection O'Brien and Putnam indicate further that isothermal and adiabatic flow may be very nearly the same for the flow of a crude oil and natural gas mixture in an oil reservoir. They cite an example pertaining to the adiabatic flow of such a mixture and show that the fluid temperature drops only a few degrees for a drop in pressure from 3,000 to 400 psia.

The laboratory study described in this report is based on the foregoing considerations. In an effort to start with the simplest appropriate two-phase flow system it was deemed advisable to investigate the two-phase flow behavior of a single-component fluid. This restriction rules out isothermal flow as a single component will not flow isothermally in two phases. Accordingly, adiabatic conditions were adopted.

In studying the adiabatic system it was found necessary to modify and extend the O'Brien-Putnam flow theory. The modified theory, concerning fundamental relations between rates of flow and pressure differentials, is substantiated by the experiments.

SCOPE OF PROBLEM

The investigation described in this paper is intended to contribute to the solution of the general problem of determining the flow behavior of oil-reservoir fluids in subsurface porous rocks. It is well known that this general problem represents a large field of widely diversified research in the petroleum producing industry. The scope of the present work is confined to the development and test of equations that describe the flow and thermodynamic characteristics of a single-component two-phase fluid moving through a porous medium under conditions of adiabatic flow.

The fluid-transmitting capacity and the geometry of the porous medium have no direct bearing on the principles of the analysis. For convenience, therefore, the test flow system was made by packing a suitable conduit with a clean, previously sized unconsolidated sand. As the bulk cross-sectional area of the resultant sand column was sensibly constant, the flow was macroscopically linear. Propane was selected as the test fluid. Adequate thermodynamic and viscosity data[2,3] are available for this substance. Moreover, a hydrocarbon fluid was selected in preference to other fluids because of the interest of the oil-producing industry in the behavior of hydrocarbons. To simplify the analysis the flow was specified as steady.

In conformance with the preceding discussion the flow system was designed to prevent transfer of heat between the flowing fluid and its surroundings (the sand grains and the walls of the flow conduit). Furthermore, in the experiments, the propane entered the column of sand as a liquid, began to vaporize an appreciable distance from the inlet and discharged from the column as a gas-liquid mixture.

To avoid the introduction of unnecessary complications regarding the meaning of pressures measured in the two-phase flow portion of the system, the column of sand was installed in a horizontal position.

Five flow experiments were performed. Total (gas plus liquid) weight rates of flow were measured and pressure and temperature distribution data were collected.

The ensuing theory, substantiated by the propane-flow experiments conducted with the described flow system, discloses that gas and liquid weight rates of flow as a function of distance along the sand column, and pressure and temperature distributions, may be calculated if the inlet pressure and temperature and the outlet pressure or temperature are given. In addition, pressure and temperature distributions and gas and liquid weight-rate-of-flow distributions, may be calculated if the constant total weight rate of flow and the inlet pressure and temperature, are given.

In developing the theory, capillary phenomena are treated. Based on the work of Aboul-Seoud,[4] it is assumed that phase equilibrium is attained at all cross-sections of the column of sand perpendicular to the direction of flow.

THEORY

Nomenclature

The symbols used in mathematical analyses in this report are as follows:

x = distance along column of porous medium
x_o = value of x at which vaporization begins
L = subscript denoting liquid
G = subscript denoting gas
W = weight rate of flow (with no subscript, W = total weight rate $= W_G + W_L$)
H = enthalpy per unit weight of fluid
U = kinetic energy per unit weight of fluid
P = fluid pressure
P_1 = fluid pressure at upstream end of column of porous medium
P_E = fluid pressure at downstream end of column of porous medium
P_G' = equilibrium, plane-surface, vapor pressure
T = absolute temperature
f = weight of gas per unit weight of gas-liquid mixture passing a transverse section of column in unit time

$\bar{f}$ = weight of gas per unit weight of gas-liquid mixture instantaneously at a transverse section of column
Q = volumetric rate of flow (with no subscript, Q = total volumetric rate $= Q_G + Q_L$)
$\bar{v}$ = specific volume
A = bulk cross-sectional area of column of porous medium
ε = fractional porosity
ρ = wetting-phase content (fraction of pore space occupied by liquid)
t = time variable
u = average miscroscopic velocity
k = homogeneous-fluid permeability
k_L = permeability to liquid (with gas present)
k_G = permeability to gas (with liquid present)
μ = absolute viscosity
$F_L(\rho) = k_L/k$
$F_G(\rho) = k_G/k$

---

[1] References given at end of paper.

$F(P)$ = pressure function = $\left[\dfrac{k_L/k}{\mu_L \bar{v}_L} + \dfrac{k_G/k}{\mu_G \bar{v}_G}\right]$

P_c = capillary pressure

R = universal gas constant

M = molecular weight of gas

Development of Flow Equations

For steady two-phase (gas-liquid mixture) flow, continuity principles immediately lead to

$$\frac{dW_G}{dx} + \frac{dW_L}{dx} = 0 \quad . . . . . . (1)$$

or

$$W_G + W_L = W = \text{constant} \quad . . . . . . (2)$$

The general energy equation, which is premised on conditions of steady flow, provides means for determining the thermodynamic process undergone by the flowing fluid. Regarding that equation, it is evident that the described flow system involves no "shaft work" and that the horizontal position of the column implies no changes in potential energy. Therefore,

$$dH + dU = 0 \quad . . . . (3)$$

Equation (3) is not limited to single-phase flow; it applies equally well to two-phase flow. In either instance, however, H and U are to be based on a unit weight of fluid flowing.

If it is assumed that Darcy's law is valid for the system under discussion, viscous forces would predominate and the heat energy generated by friction would be very large compared to kinetic energy changes. Thus, for any two transverse sections in the system, a finite distance apart,

$$\triangle H = 0 \quad . . . . (4)$$

hence,

$$H = \text{constant} \quad . . . . (5)$$

which means that the fluid follows an isenthalpic process. As a consequence the fluid will flow in two phases (gas and liquid) if the (H, T) or (H, P) conditions along the column fall within the two-phase region on an ordinary thermodynamic chart for the test fluid (Fig. 1).

Based on Equations (2) and (5) the enthalpy of the fluid passing any transverse section in the column in unit time is given by

$$W_L H_L + W_G H_G = WH = \text{constant} \quad . . . . (6)$$

Suppose that the fluid enters the column (at $x = 0$) entirely as a liquid but that the flowing-fluid pressure has become reduced to its saturation intensity at x_0. For an isenthalpic process the fluid must exist downstream from x_0 as a gas-liquid mixture. Under these conditions the flowing fluid would follow a path as represented by path ABC in Fig. 1.

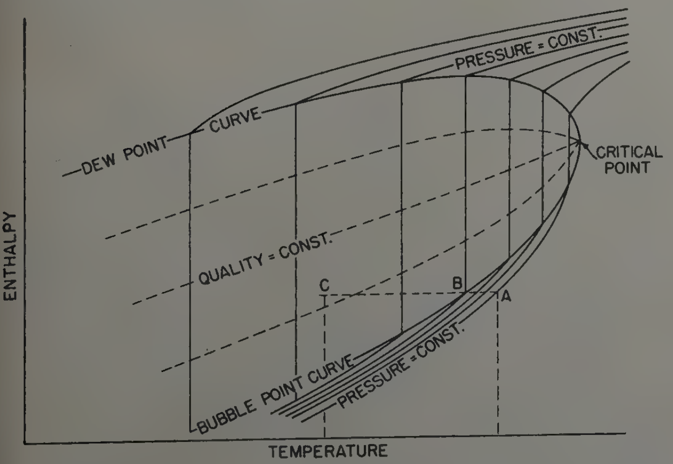

FIG. 1 — SCHEMATIC ENTHALPY-TEMPERATURE CHART FOR PROPANE (AFTER O'BRIEN AND PUTNAM).

In unit time a weight W of liquid enters the column, and during the same unit of time a weight W_L of liquid and W_G of gas departs from any arbitrarily selected transverse section at x. Thus, for the length of column bounded by zero and x, the fraction (f) that vaporizes, of an original unit weight of entering liquid, may be expressed by

$$f = \frac{W_G}{W} \quad . . . . (7)$$

Substituting in Equation (2),

$$1 - f = \frac{W_L}{W} \quad . . . . (8)$$

hence,

$$\frac{1-f}{f} = \frac{W_L}{W_G} \quad . . . . (9)$$

Equation (6) becomes

$$(1-f) H_L + f H_G = H \quad . . . . (10)$$

or

$$f = \frac{H - H_L}{H_G - H_L} \quad . . . . (11)$$

In the thermodynamics of single-component static systems, the righthand member of Equation (11) is a well-known expression for "quality," the weight of gas present in a unit weight of a gas-liquid mixture. For a static system H would be the enthalpy per unit weight of mixture present, and H_G and H_L the respective enthalpies per unit weight of gas and liquid present. For the foregoing dynamic system (see Equation 6), it has been shown that an isenthalpic process is one which requires the enthalpy of the fluid passing any transverse section in unit time to be the same for all transverse sections of the column. Consequently, for a dynamic system enthalpies are to be expressed on a per-unit-weight-of-fluid-flowing basis. As charts like Fig. 1 are prepared from data collected with static systems, it is desirable to show how they may be applied to dynamic systems of the kind under discussion.

In this respect, suppose that it is possible to separate and collect the gas and liquid discharged in unit time from the transverse section at x. If the collected gas is kept entirely in the gaseous state at the pressure and temperature at x, it will be saturated and occupy a volume Q_G, numerically equal to the volumetric rate of gas flow at x. Likewise, if the collected liquid is kept entirely in the liquid state at the pressure and temperature at x, it will be saturated and occupy a volume Q_L, numerically equal to the volumetric rate of liquid flow at x. Furthermore, if these collected and separated fluids are recombined to the total volume $(Q_G + Q_L)$ without change in their common pressure or temperature, the weights of gas and liquid in the resultant mixture will be equivalent numerically, to the respective weight rates of flow of the two phases at x, namely W_G and W_L. The quality of the resultant mixture, therefore, will be W_G/W.

Accordingly, the quality of the mixture *passing* x in unit time is W_G/W, which is f (Equation 7). Hence, the lines of constant quality on Fig. 1 are lines along which the fraction vaporized (f) is constant.

Again considering the foregoing hypothetically collected and recombined fluid, produced from transverse section x in unit time, the specific volumes of the collected gas and liquid, respectively $\bar{v}_G$ and $\bar{v}_L$, are equal to Q_G/W_G and Q_L/W_L; thus, the specific volume of the resultant mixture as a whole is given by

$$\bar{v} = \frac{Q_L + Q_G}{W_L + W_G} = \frac{Q}{W} \quad . . . . (12)$$

It follows that $\bar{v}$ is the specific volume of the mixture passing x in unit time.

It is to be emphasized that the weight fraction of gas in the *mixture instantaneously at x* is quite different than the weight fraction of gas in the *mixture passing x in unit time.*

In this respect the weight of gas instantaneously in an elemental length δx of the column, upstream but adjacent to x, is $(1/\bar{\gamma}_G) \quad [A \cdot \delta x \cdot \mathcal{E} \cdot (1-\rho)]$ and the weight of liquid is $(1/\bar{\gamma}_L) \ (A \cdot \delta x \cdot \mathcal{E} \cdot \rho)$ so that the weight fraction $\bar{f}$, of gas in the element is

$$\bar{f} = \frac{1}{1 + \left(\frac{\rho}{1-\rho}\right)\frac{\bar{\gamma}_G}{\bar{\gamma}_L}} \quad . \quad . \quad . \quad . \quad . \quad . \quad . \quad (13)$$

To find a corresponding expression for the weight fraction of gas in the mixture passing x in unit time, attention is focused on average microscopic velocities of the two phases. In this connection, the liquid is assumed to be the wetting phase and the gas the nonwetting phase. Part of the gas may be stationary in the form of discrete bubbles enlodged in pores surrounded by liquid. Part of the liquid may be stationary owing to the blocking of its passage through gas-locked pore channels. Neglecting pressure differentials, at x, across curved gas-liquid interfaces, the enthalpies of the flowing gas and stationary gas are the same because they are subjected to the same pressure and temperature. Similar reasoning applies to the liquid.

Let the average particle of liquid at the upstream end of the foregoing elemental length of column reach station x in time δt, and the average particle of gas reach station x in time $\delta t'$. Then, as δx may be made arbitrarily small, the average microscopic velocity of the liquid in the macroscopic direction of flow, at x, is $(\delta x/\delta t) = u_L$; likewise, the corresponding microscopic velocity of the gas is $(\delta x/\delta t') = u_G$.

Based on continuity principles

$$W_G = \frac{A \cdot \mathcal{E} \cdot (1-\rho)u_G}{\bar{\gamma}_G} \quad . \quad . \quad . \quad . \quad . \quad . \quad . \quad (14)$$

$$W_L = \frac{A \cdot \mathcal{E} \cdot \rho u_L}{\bar{\gamma}_L} \quad . \quad . \quad . \quad . \quad . \quad . \quad . \quad . \quad . \quad (15)$$

hence,

$$f = \frac{W_G}{W_G + W_L} = \frac{1}{1 + \frac{\bar{\gamma}_G}{\bar{\gamma}_L}\left(\frac{\rho}{1-\rho}\right)\frac{u_L}{u_G}} \quad . \quad . \quad . \quad (16)$$

Comparison of Equations (13) and (16) indicates that $\bar{f}$ and f are equal only if u_L and u_G are equal. The relationship between these microscopic velocities can be investigated by application of Darcy's law to the two phases independently* and by recourse to Equations (14) and (15):

$$W_L = \frac{A \cdot \mathcal{E} \cdot \rho \cdot u_L}{\bar{\gamma}_L} = -\frac{Ak_L}{\mu_L \bar{\gamma}_L} \cdot \frac{dP}{dx} \quad . \quad . \quad . \quad . \quad (17)$$

$$W_G = \frac{A \cdot \mathcal{E} \cdot (1-\rho)u_G}{\bar{\gamma}_G} = -\frac{Ak_G}{\mu_G \bar{\gamma}_G} \cdot \frac{dP}{dx} \quad . \quad . \quad . \quad (18)$$

from which

$$\frac{u_L}{u_G} = \frac{k_L}{k_G}\frac{\mu_G}{\mu_L}\left(\frac{1-\rho}{\rho}\right) \quad . \quad . \quad . \quad . \quad . \quad . \quad . \quad . \quad . \quad (19)$$

$$= \frac{F_L(\rho)}{\rho} \cdot \frac{(1-\rho)}{F_G(\rho)} \cdot \frac{\mu_G}{\mu_L} \quad . \quad . \quad . \quad . \quad . \quad . \quad . \quad (20)$$

Knowledge of fluid viscosities and of the characteristics of relative permeability curves (for example, see References 5, 6 and 7), shows conclusively that it would be wholly fortuitous for the righthand member of Equation (20) to equal unity; hence, u_L and u_G cannot be assumed equal. Consequently, it would be invalid to assume equality of f and $\bar{f}$ as was done by O'Brien and Putnam (X in their nomenclature is the same as $\bar{f}$ in this report).

Applying Darcy's law, Equation (2) becomes

$$W = -Ak\left[\frac{k_L/k}{\mu_L\bar{\gamma}_L} + \frac{k_G/k}{\mu_G\bar{\gamma}_G}\right] \cdot \frac{dP}{dx} \quad . \quad . \quad . \quad (21)$$

Integrating over a length of column between the inlet end of the column and an arbitrarily selected transverse section at x:

$$Wx = Ak \int_{P}^{P_1} F(P)dP \quad . \quad . \quad . \quad . \quad . \quad . \quad . \quad (22)$$

in which $F(P)$, the pressure function, is equivalent to the term in brackets in Equation (21), and P_1 the fluid pressure at the inlet.

Equation (22) may be used to determine the theoretical discharge rate, W, from the system. In this instance let x be the total length of the flow column, causing P to be the outlet pressure. If small increments of pressure are taken along path ABC in Fig. 1, then Equation (11) may be used to determine the distribution of f along the column. O'Brien and Putnam advanced this method of calculation, but in using f as though it were the same as $\bar{f}$ they applied Equation (13) — setting f equal to the righthand member of that equation — thereby calculating ρ erroneously. They then used the incorrect values of ρ in conjunction with relative-permeability curves to obtain k_L/k and k_G/k. Thus, their theory requires modification.

In this respect, it is only necessary to use Equation (9) for determinations of distributions of k_L/k and k_G/k. From Equations (17) and (18):

$$\frac{W_L}{W_G} = \frac{k_L}{k_G} \cdot \frac{\mu_G}{\mu_L} \cdot \frac{\bar{\gamma}_G}{\bar{\gamma}_L} \quad . \quad . \quad . \quad . \quad . \quad . \quad . \quad . \quad . \quad . \quad (23)$$

Substituting for (W_L/W_G) in Equation (9) and rearranging terms,

$$\frac{k_L}{k_G} = \frac{\mu_L\bar{\gamma}_L}{\mu_G\bar{\gamma}_G}\left(\frac{1-f}{f}\right) \quad . \quad . \quad . \quad . \quad . \quad . \quad . \quad . \quad . \quad (24)$$

Equation (24) can be used to determine the k_L/k_G — ratio of relative permeabilities — distribution along the column. Relative-permeability data show k_L/k, k_G/k and k_G/k_L as functions of ρ; hence, with the k_L/k_G distribution known, it is possible to plot $F(P)$ against P. The area under the resulting curve, between the limits of P_1 and P represents the value of the integral in Equation (22). It follows that W may be calculated.

With the theoretical total weight rate of discharge established, Equation (22) may be applied further to determine the theoretical pressure distribution. To accomplish this calculation, successive values of P (less than the inlet pressure and greater than the outlet pressure) are selected. In each instance the integral of Equation (22) is evaluated graphically and corresponding values of x determined.

Gas-Liquid Interfacial Curvature

Charts like Fig. 1 are based not only on equilibrium thermodynamics, but are constructed from data collected with instruments that cause gas-liquid interfaces to be, sensibly, plane surfaces. In the foregoing analysis, therefore, it is assumed that equilibrium thermo-dynamics applies and that the curved surfaces of gas-liquid phase separation in the porous medium may be treated, thermodynamically, as plane surfaces.

According to the kinetic theory there is a continuous exchange of molecules between the phases of a single-component gas-liquid mixture, phase equilibria being attained when the rate of vaporization and rate of condensation are equal. Aboul-Seoud[4] has made a theoretical proof, substantiated by experiment, indicating that phase equilibrium is attained almost instantaneously in a single-component two-phase flow system of the kind under discussion.

---

*Wyckoff and Botset[5] were the first investigators to apply Darcy's law in two-phase flow.

It is desirable, however, to indicate the effects of gas-liquid interfacial curvature and disclose a means for determining whether capillary pressures are negligible. By definition

$$P_c = P_G - P_L \quad . . . . (25)$$

hence, the gradient of the capillary pressure in a direction x is given by

$$\frac{dP_c}{dx} = \frac{dP_G}{dx} - \frac{dP_L}{dx} \quad . . . . (26)$$

It is pointed out that Equations (25) and (26) have been derived for static systems only. As a first approximation, therefore, suppose that Equation (26) applies to the gas-liquid mixture instantaneously at an arbitrarily selected transverse section in the two-phase flow portion of the test column of porous medium. Then, the pressure gradients in Equations (17) and (18) would differ by (dP_c/dx).

Considering that the liquid and gas respectively are the wetting and nonwetting phases, the Kelvin-Helmholtz equation,[8,9] pertaining to static equilibrium at curved surfaces of gas-liquid phase separation, may be written

$$P_c = P_G - P_G' + \frac{RT}{M\bar{\gamma}_L} \ln \frac{P_G'}{P_G} \quad . . . . . . (27)$$

Assuming that this equation applies at any arbitrarily selected transverse section in the two-phase flow portion of the column of porous medium, and substituting for P_c from Equation (25), results in

$$P_L = P_G' - \frac{RT}{M\bar{\gamma}_L} \ln \frac{P_G'}{P_G} \quad . . . . (28)$$

As the liquid is the wetting phase $P_G' > P_G$; hence, $P_L < P_G'$. Therefore, if liquid pressures and temperatures are measured along the column of porous medium in the direction of flow and in the two-phase flow portion of the system, gas-liquid interfacial curvature would be manifest by liquid temperatures greater than the normal (plane-surface) saturation temperatures corresponding to the measured pressures.

The same line of reasoning indicates that gas-liquid interfacial curvature is unimportant, thermodynamically, if the corresponding values of the liquid pressures and temperatures are plotted on a pressure-temperature diagram and found to coincide, within the limits of experimental accuracy, with the normal (plane-surface) equilibrium vapor-pressure curve. Under these conditions, $P_L = P_G'$, and from Equation (28) it follows that $P_G' = P_G$; thus $P_c = 0$ and $(dP_c/dx) = 0$.

Equation (22) was developed without consideration of a capillary-pressure gradient distribution (Equation 26) along the two-phase fluid portion of the flow column. Experimental verification of the flow theory — applying Equation (22) — will depend, therefore, on whether capillary pressure gradients are negligible.

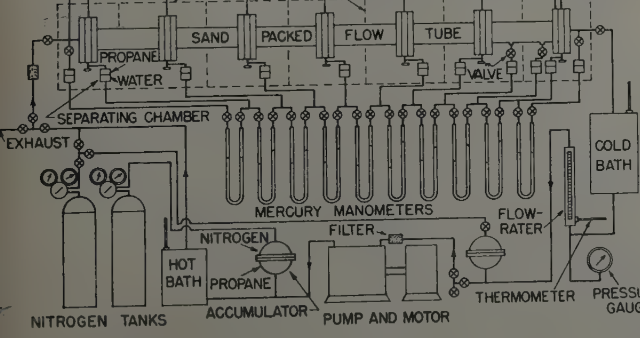

FIG. 2 — SCHEMATIC DIAGRAM OF APPARATUS USED IN PROPANE-FLOW EXPERIMENTS.

In conformance with Muskat's[10] reasoning pertaining to the characteristics of "capillary pressure-desaturation" curves, the existence of the "equilibrium gas saturation" will preclude any discontinuity in capillary pressure at the transverse section in the flow column where vaporization begins. Recognizing, moreover, that vaporization is a continuous process throughout the two-phase fluid portion of the system, there would be no discontinuous accumulation of the wetting phase at the outlet end of the column. Consequently, if, also, there are no stratification discontinuities in the porous medium comprising the column, there will be no discontinuities in the distribution of capillary pressure along the column. Thus, negligible capillary pressure may be taken as tantamount to negligible capillary-pressure gradients.

For a single-component liquid in the vicinity of the saturated liquid line (path AB, Fig. 1), $(\partial T/\partial P)_H$ usually is quite small. For this reason the isenthalpic process followed by the flowing liquid in the all-liquid flow portion of the system will very nearly coincide with an isothermal process. If, therefore, a normal vapor-pressure chart is plotted and pressure and temperature distribution data, collected from the experimental flow system, are superimposed upon the chart, the all-liquid flow portion of the system should be indicated by a series of points forming a straight line parallel to the pressure axis, the pressures corresponding to these points being greater than the saturation pressure corresponding to their common temperature. Points based on data collected in the two-phase fluid portion of the system will fall, within the limits of experimental accuracy, on the vapor-pressure curve, if capillary pressures are negligible. This procedure for plotting data was followed with respect to the ensuing propane-flow experiments. The results indicate isothermal flow in the all-liquid flow portion of the column of sand and that capillary pressures are small.

It is of further significance to note that the foregoing straight line through pressure-temperature points representing all-liquid flow, may be extrapolated to the vapor-pressure curve to find the pressure and temperature at which vaporization begins. These data together with the experimentally-determined pressure and temperature distribution curves will serve to indicate the transverse section at which vaporization begins.

EXPERIMENTAL EQUIPMENT AND TECHNIQUE

Apparatus

The apparatus used in making the experimental study of the adiabatic, two-phase, steady flow of propane through a horizontal column of sand is illustrated schematically in Fig. 2. The flow tube was about five ft long and was constructed from six lengths of nominal two-in. diameter "extra-strong" steel pipe, connected together in a line by forged-steel flanges.

The flange-type units at the extreme ends of the sand-packed conduit were made by drilling, tapping and otherwise preparing blind flanges to provide the confined column of sand with an entry and exit for the test fluid. Blind flanges also were used to construct the flange-type units to which manometer lines and thermocouple lead wires are connected (Fig. 2). Each of these special units was equipped with a built-in ring-type piezometer, similar to the kind made by Wyckoff and Botset,[5] and was machined to accommodate a fluid-tight, electrically insulated coupling device, which permitted insertion of the thermocouple junctions (copper-constantan) in the system and in the sand, without the necessity for conventional thermocouple wells.

The flow tube composed of the pipe sections and flange units was covered with a layer of heat-insulating material (magnesite) about one-half in. thick (this coating is not shown in the sketch). Furthermore, the tube as a whole was enveloped, as shown, by a circular, compartmented sheet-metal air duct. Hot and cold air lines leading to each compartment provided the means for fixing the temperature distribution in the air along the outside of the flow tube to correspond to the temperature distribution of the flowing propane inside the tube. In this respect, the thermocouple circuit (not detailed in the sketch) that was used, was arranged so that temperature differences between the outside and inside of the flow tube could be detected.

The separating chambers were made from nominal 1½-in. diameter steel pipe and were about two in. long. They were an integral part of the manometer lead lines and were mounted on the sand-packed flow tube, inside the sheet-metal duct. During a two-phase flow experiment and while pressures were being measured, the propane in each chamber along the two-phase flow portion of the column of sand existed as a saturated liquid in connection with and at the temperature of the fluid inside the main conduit. Liquid water separated the propane in the chambers from the mercury in the manometers.

The pressure gauge at the inlet end of the system was an accurately-calibrated test gauge having a maximum capacity of 300 psi and a least count of one psi.

Each of the manometers was a glass *U*-tube assembly long enough to indicate a maximum deflection of 48 in. in the mercury levels in the two limbs and strong enough to withstand a total fluid pressure of at least 265 psia. All the manometer lead lines were copper tubing, equipped with brass needle valves and Imperial fittings.

The first manometer on the left (Fig. 2) indicated the pressure drop across the inlet to the flow system. The entering liquid first passed through a Tyler 200-mesh copper retaining screen, against which the sand was packed, and then diverged to fill the sand column. Similarly, the last manometer on the right indicated the pressure drop across the outlet, which also was provided with a retaining screen, and which caused convergence of the flow lines. The intermediate manometers, as shown, indicated pressure differences across various longitudinal sections of the column of sand.

The gas-liquid mixture discharging from the flow tube was conducted through a refrigeration unit to condense it. This unit was a thermostatically controlled water bath through which the discharge line passed in the form of a coil of copper tubing. The propane that departed from the cold bath was entirely liquid and remained in this state until it returned to the column of sand. The total weight rate of flow was determined by metering the condensed propane with a rotameter (commercially known as a Flowrater). This instrument was calibrated with liquid propane as the test fluid, over a range of pressures and temperatures. Accordingly, the pressure and temperature at the meter, as well as the meter reading, were recorded during each flow experiment.

The propane that departed from the Flowrater was passed through a porous-meter filter and then through a two-cylinder, variable-speed, diaphragm-type, reciprocating pump, to increase its pressure. The pistons of the pump displaced lubricating oil, which, in turn, caused a reciprocating motion of a flexible, corrosion-resistant, metal diaphragm, separating the propane from the lubricating oil.

The propane discharged by the pump was conducted through the hot bath (thermostatically controlled) to raise its temperature and was then conducted through another porous-metal filter before re-entering the column of sand.

Each of the two accumulators shown (Fig. 2) was made from two hollow hemispheres of steel, bolted together with a flange joint. The two halves of each accumulator were separated at the flange joint by a flexible, fluid-tight diaphragm, the upper half of the unit having been filled with nitrogen gas in connection with a tank of nitrogen and the lower half having been filled with propane in connection with the propane-flow line. The pressure regulator and two pressure gauges at each tank of nitrogen were used to measure the pressure in the nitrogen tank and to control and measure the pressure of the nitrogen in the accumulator. The accumulator at the right (Fig. 2) was used primarily to dampen pulsations in the propane-flow line and thereby facilitate reading of the Flowrater, and the accumulator on the left was used to increase and decrease the quantity of propane in the propane-flow circuit.

Materials

The propane used in the two-phase flow experiments contained 99+ mol per cent propane. The purity was tested by collecting vapor-pressure data at a few temperatures within the range of interest. The results were compared to the published data of Sage, Schaafsma, and Lacey[2] and the agreement was good.

A steam-cleaned Monterey beach sand was selected as the raw material for preparation of the synthetic sand used in the propane-flow experiments. Visual inspection of this beach sand disclosed that it was composed predominantly of quartz grains, with a moderate proportion of feldspars and a very small percentage of ferromagnesian minerals. It contained a trace of calcareous material (apparently fragments of sea shells), but no organic matter was evident.

This raw stock was used as the source from which a supply of each of seven size fractions of sand grains was obtained. The four coarsest size fractions desired, nominally 14-28, 28-35, 35-48, and 48-65 Tyler mesh, were separated from the Monterey beach sand directly and in sufficient quantity with the appropriate nest of sieves and a sieve shaker. It was necessary, however, to grind the raw material in a ball mill before the three finer fractions, nominally 65-100, 100-200 and 200-325 Tyler mesh, could be recovered in sufficient quantity with the sieves and shaker.

The four coarsest fractions were "de-dusted" by washing them thoroughly with tap water. Following this operation, they were treated with concentrated hydrochloric acid to remove acid-soluble material and washed on a filter with tap water until the filtrate would fail to change the color of blue litmus paper. Finally, they were dried by placing them in an oven at 350°C for 72 hours.

The fineness of much of the material from the mill caused agglomerates to form on the screens during the sieving operations with the three finest fractions. These operations, therefore, were followed with a more refined secondary process of size fractionation. In this respect, each of the three products obtained from the sieving operations was rendered "clean cut" by further separation of water, applying Stokes' law[11] of settling velocities.

The products of the wet-separation process were treated with concentrated hydrochloric acid and then washed thoroughly on a filter with tap water until the filtrate would fail to change the color of blue litmus paper (as was done with the coarse fractions). The acid-free grains were washed with isopropyl alcohol to remove water and then with petroleum ether to remove alcohol. After the petroleum ether evaporated from the grains, they were dried in the same manner as the coarse fractions — by placing them in an oven at 350°C for 72 hours.

The finest of the seven end-product sand fractions, which passed through a 200 Tyler mesh sieve (opening = 74 microns) and was retained on a 325 Tyler mesh sieve (opening = 44 microns), was subjected to a Klein hydrometer analysis[12] and found to contain particles as small as 24 microns in Stokes' diameter.

The sand used in the propane-flow experiments was made by blending the seven foregoing clean-cut fractions. In terms of a Tyler sieve analysis, the end-product blend contained, respectively, 11.0, 8.7, 11.0, 11.0, 12.1, 22.0, and 24.2 per cent of 14-28, 28-35, 35-48, 48-65, 65-100, 100-200, and 200-325 mesh grains.

A testing machine (for determining the tensile and compressive strengths of engineering materials) was used in the sand-packing operations, the flow tube being in a vertical position in the machine with the packing being done against the upstream end. The sand was introduced in 250-gram increments, each having the foregoing end-product grain size distribution. After each increment was put in the tube the sand was compressed under a compaction pressure of 1,000 psi with simultaneous jarring of the tube. In each instance the upper surface of the sand was ruffled slightly, before another increment was introduced, so that stratification discontinuities would be eliminated. The thermocouple junctions were buried in the sand, at selected distances along the tube, during the packing operation. The average porosity of the resultant column of sand was calculated to be 27.3 per cent.

Experimental Procedure

After the tube was packed and assembled, the homogeneous-fluid permeability distribution of the column of sand was determined with dry air, by application of standard test procedure. Over a period of several days this test was repeated twice and the permeability distribution was found to be unchanged, indicating that the column was stable. Moreover, the test was repeated again with all-liquid propane as the fluid medium, between the third and fourth two-phase flow experiments. The results agreed with those obtained in the dry-air flow tests.

Preparatory to two-phase flow experimentation the system (Fig. 2) was twice evacuated and purged with the test grade of propane gas. With the system filled with this propane gas at about 20 psia and room temperature, action was taken to introduce liquid propane. A high-pressure container (conventional "gas bottle") of the test grade of saturated liquid and gaseous propane was inverted, connected to the suction line on the pump, and elevated so that the saturated liquid propane would tend to gravitate into the system. Precautions were taken to remove air from the connecting line and a filter was assembled in this line to preclude entrance of foreign matter into the system. The needle valve (Fig. 2) at the downstream end of the flow tube then was closed and the pump used to transfer propane from the supply tank to the system. This operation was performed at room temperature and as the fluid pressure increased in the system, gaseous propane condensed. The maximum pressure was controlled by shutting off the pump and by appropriately actuating the accumulator diaphragms. This propane-transfer operation was completed when the propane-supply tank was disconnected from the pump and the system filled at room temperature with liquid propane with the accumulator diaphragms about midway between the upper and lower extremities of their vertical paths of travel.

The second operation performed in making the apparatus ready for two-phase flow experimentation, was to circulate the propane in the system, and simultaneously, to establish a predetermined air-temperature distribution in the duct enveloping the flow tube, to adjust the temperatures of the hot and cold baths as required, to withdraw propane from the propane-flow circuit, as necessary, with the accumulators, and to regulate the pump speed. In this operation, establishment of a predetermined pressure and temperature for the liquid propane entering the flow tube and establishment of a predetermined pressure or temperature for the gas-liquid mixture leaving the flow tube, fixed the necessary bath temperatures, the amount of propane to be withdrawn by the accumulator, and the pump speed.

As a first approximation a linear temperature distribution was established in the air duct, in the direction of propane flow. After steady-flow conditions were attained, temperature differences, between the air outside the flow tube and the propane inside, were measured. The air temperatures then were adjusted to match the propane temperatures. When steady-flow conditions again were attained, this temperature measurement and adjustment process was repeated. It was found that the inside and outside fluid-temperature distributions would remain coincident after two or three such adjustments and that little additional regulation of the pump speed and hot and cold bath temperatures, was necessary.

Finally, under conditions of steady flow, with no appreciable transfer of heat across the walls of the flow tube and with liquid propane entering the tube and a gas-liquid mixture of propane discharging from the tube, temperature and pressure distributions in the propane, in the direction of flow, were measured, as well as the total weight rate of flow of the propane. At the conclusion of each of the five experiments the propane in the system was vented to the atmosphere, with nitrogen from one of the tanks of nitrogen (Fig. 2).

EXPERIMENTAL AND THEORETICAL RESULTS

Pressure-Temperature Data and the Vapor-Pressure Chart

Fig. 3 depicts a segment of the normal (plane-surface) vapor-pressure curve for propane, plotted from data published by Sage, Schaafsma, and Lacey.[2] Experimentally obtained pressure and temperature data from the present two-phase propane flow experiments are super-imposed on this chart. Each experimental point shown represents the pressure and temperature measured at some transverse section in the sand-packed flow tube during two-phase flow experimentation.

As described previously, the flow would be essentially isothermal in the all-liquid flow portion of the system. All-liquid flow is reflected on the chart for each of the five experiments, by the points that are above the vapor-pressure curve and form a straight line parallel to the pressure axis.

It has been indicated further that gas-liquid capillary pressures and capillary-pressure gradients would be of negligible magnitude if experimentally measured liquid pressure-temperature data, pertaining to the two-phase flow portion of the tube, fell on the vapor-pressure curve. As the liquid propane was the wetting phase in the experiments, the experimental points on Fig. 3 represent liquid pressure-temperature data. With the exception of one or two points, data pertaining to the two-phase flow portion of the tube fall, within the limits of experimental accuracy, on the vapor-pressure curve. Accordingly, this method of analysis indicates that the magnitudes of capillary pressures and capillary-pressure gradients, are negligible.

Selection of Relative-Permeability Relations

Theoretical calculations of pressure distributions and weight rates of flow, as made with Equation (22), for comparison to experimental results, require that k_L/k and k_G/k be known as functions of pressure. These functions, evidently, may be determined indirectly from the proper independent relationship between k_L/k_G and k_L/k, considering that Equation (24) yields k_L/k_G as a function of pressure. Validity of the theory

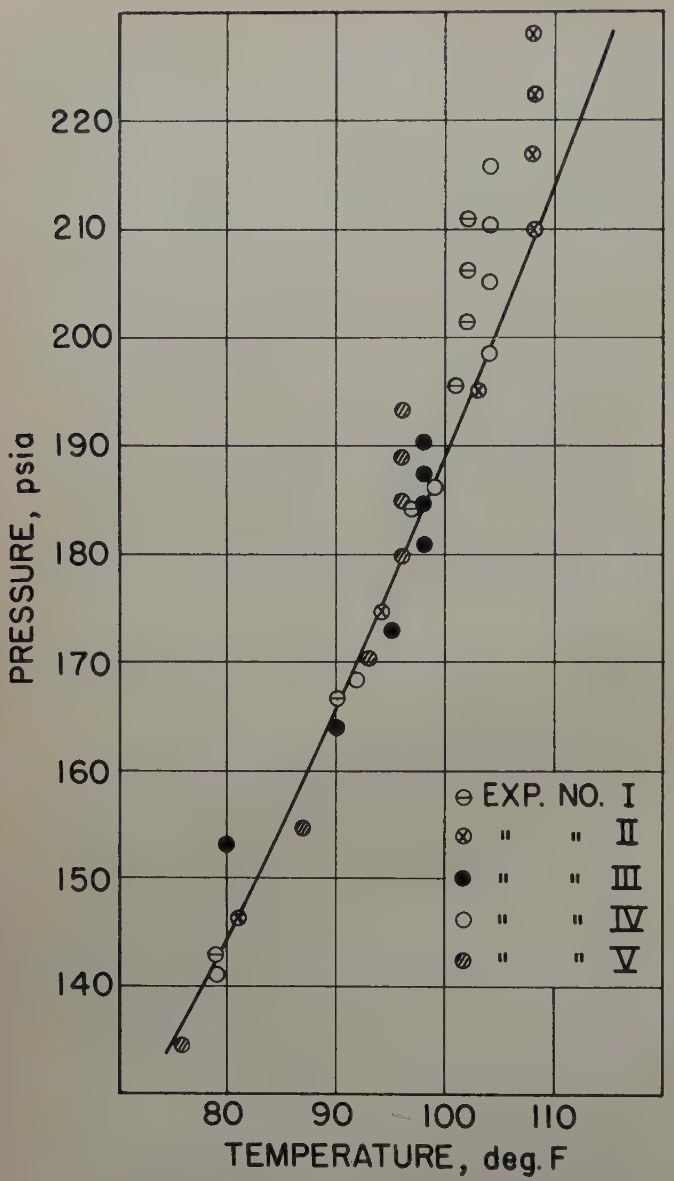

FIG. 3 — VAPOR-PRESSURE CURVE FOR PROPANE WITH SUPERIMPOSED PRESSURE-TEMPERATURE DATA FROM PROPANE-FLOW EXPERIMENTS.

must be assumed, however, if the necessary relationship between k_L/k_G and k_L/k is to be established with the test column of sand and two-phase fluid (propane), under conditions of adiabatic flow. Some other more appropriate course of action, therefore, is required to establish this relationship.

Based on the findings of Wyckoff and Botset,[5] the relative permeabilities of unconsolidated sands to either the wetting or nonwetting fluid depend almost entirely on the wetting-phase content of the sands. In this respect, those investigators experimented with a number of two-phase fluids and unconsolidated sands (ranging in homogeneous-fluid permeability from 17.8 to 262 darcys), and found that the relative permeabilities were practically independent of the test two-phase fluid and were influenced very little by the textural characteristics of the sands. When k_G/k and k_L/k data from all their experiments were plotted, on the same chart, against wetting-phase content, it was found that the plotted points, as a whole, indicated only one wetting-phase and one nonwetting phase relative-permeability curve, the scattering of the points about these curves being moderate and probably within the limits of experimental accuracy.

Consequently, it appears that the Wyckoff-Botset results could be used to plot a relationship between k_L/k_G and k_L/k that would describe reasonably well the relative-permeability characteristics of all unconsolidated sands. One could hardly expect this relationship to be exact, however, in describing the column of sand used in the propane-flow experiments as it had a homogeneous-fluid permeability of the order of one darcy. The foregoing findings, nevertheless, disclose that the relationship in question should represent a curve that lies in the vicinity of the Wyckoff-Botset curve.

Pursuant to this line of reasoning, data from one of the five propane-flow experiments were considered. The inlet temperature and pressure and the outlet pressure measured in this experiment (No. II), were used with the average curve through the Wyckoff-Botset results (Fig. 4) to calculate by Equation (22) the theoretical weight rate of flow and pressure distribution. The calculated results were compared to the experimental results and the curve shifted accordingly. The new curve was applied similarly and the curve-shifting procedure repeated until good agreement of calculated and experimental results was obtained. The final curve, located in this manner, is the propane-flow curve of Fig. 4. It falls well within the limits of experimental accuracy of the Wyckoff-Botset results. This propane-flow curve then was used in conjunction with Equation (22) to calculate total weight rates of flow and pressure distributions pertaining to the other four experiments.

In this conection the greatest experimentally-measured total weight rate of flow was approximately 100 per cent greater than the smallest total weight rate of flow, and the pressure and temperature distributions along the test column of sand varied widely among the five experiments. Thus, agreement of calculated and theoretical results for the four experiments used in testing the theory, would indicate that the propane-flow curve of Fig. 4 is independent of weight rates of flow and fluid properties, and, therefore, dependent only on the porous medium.

Substantiation of Theory

In making theoretical calculations the pressure and temperature of the all-liquid stream entering the column of sand and the pressure of the gas-liquid mixture discharging from the column, were considered as given. The problem was to find the corresponding pressure distribution and total weight rate of fluid flow.

In this respect, Table I presents a comparison of experimentally measured and theoretically calculated pressure distributions and total weight rates of flow. Substantiation of the theory is based on results pertaining to experiments I, III, IV and V, as data collected in experiment II were used as an aid in determining the propane-flow curve of Fig. 4.

Omitting experiment II, therefore, it is found that for experiment I the theoretical total weight rate of flow is 4.8 per cent greater than the corresponding experimental rate, and for experiments III, IV and V, the theoretical rates, respectively, are 5.4, 2.5 and 0.7 per cent less than the experimental rates. Similarly, the maximum difference between theoretical and experimental pressures for experiments I, III, IV and V are, respectively, 0.6, 0.6, 2.1 and 0.8 psi. In these experiments, in the same order, the total experimentally measured pressure differentials between the upstream and downstream ends of the sand column, were 67.9, 37.2, 74.6 and 58.8 psi.

Limitations of the experimental equipment and method of calculation disclose that the foregoing results (Table I) serve as a substantiation of the theory. Regarding the equipment, the test pressure gauge at the upstream end of the column of sand was sensitive to one psi, the calibrations of the Flowrater indicated that that instrument could introduce errors up to about three or four per cent in the total weight rates of flow, and calibrations of the thermocouple circuit indicated that errors of the order of 1°F were likely to occur in temperature measurements. In connection with the method of calculation used, experiment II (Table 1) shows a theoretical weight rate of flow 0.3 per cent greater than the experimental rate and a maximum difference of 1.5 psi between theoretical and experimental pressures, the total drop in pressure in this experiment having been 81.5 psi between the upstream and downstream ends of the column of sand. Thus, as data from experiment II were used in finding the propane-flow curve of Fig. 4, differences between theoretical and experimental results for the other four experiments could be expected to be as great as those cited for experiment II. Homogeneous-fluid permeabilities measured for various increments of length along the sand column, were assumed, in the calculations pertaining to two-phase flow, to apply to the centers of the increments; hence, unknown local variations in homogeneous-fluid permeability would introduce errors. Finally, graphical methods of analysis were necessary in the calculations. It is estimated that these methods could introduce errors of the order of one or two per cent or more. Many of the viscosity data were obtained by extrapolation of curves.

Experimentally determined pressure distributions in the two-phase flow portion of the column of sand, are represented graphically in Fig. 5. This figure shows the ranges of pressure used in the experiments, indicates comparative pressure gradients and delineates the part of the column in which the fluid existed in two phases. The lefthand terminus of each of the curves defines the transverse section at which vaporization started, determined by a method of calculation described subsequently.

Details of an Application of Method Of Theoretical Calculation

The method used in making theoretical calculations is presented by developing theoretical results pertaining to experiment V, which was representative of all the experiments.

The pressure and temperature of the all-liquid propane stream entering the column of sand in this experiment were 193.2 psia and 96°F, respectively. With these data it is found[2] that the enthalpy of the compressed entering liquid is 24.4 Btu per lb of fluid flowing; thus, the constant enthalpy (H) of the process established (see Fig. 1).

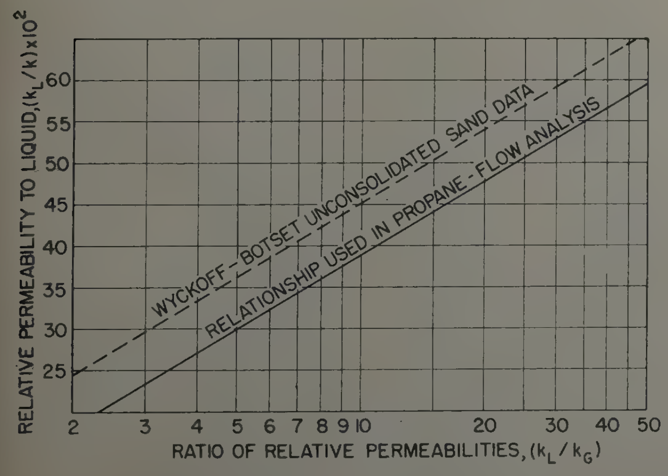

FIG. 4 — RATIO OF RELATIVE PERMEABILITIES AS FUNCTIONS OF RELATIVE PERMEABILITY TO LIQUID.

Table I—Comparison of Theoretical and Experimental Pressure Distributions and Total Weight Rates of Flow

Distance along column of sand, ft	Experiments									
	I		II		III		IV		V	
	Experimental and theoretical pressures, psia									
	Exp.	Theor.	Exp.	Theor.	Expt.	Theor.	Exp.	Theor.	Exp.	Theor.
0.000	210.8	210.8	227.8	227.8	190.3	190.3	215.6	215.6	193.2	193.2
0.833	206.0	205.8	222.1	222.2	187.3	187.6	210.2	210.4	188.9	189.0
1.669	201.4	200.9	216.6	216.7	184.6	185.0	205.0	205.4	184.8	184.9
2.510	195.5	194.9	209.7	209.9	180.7	180 6	198.5	199.1	179.6	179.7
3.351	184.1	184.3	195.1	196.6	173.1	173.2	186.2	186.9	170.2	169.4
4.187	166.5	166 9	174.6	175.7	164.0	164.0	168.4	167.5	154.7	154.2
4.570	156.9	157.0	164.5	163.8	159.8	159.2	158.8	156.7	146.4	145.9
4.778	149.8	150.1	155.7	155.3	156.4	156 2	149.7	149.1	140.4	140.3
5.028	142.9	142.9	146.3	146.3	153.1	153.1	141.0	141.0	134.4	134.4
	Experimental and theoretical total weight rates of flow, lb/hr									
	11.88	12.45	14 35	14.40	7.045	6.664	13.42	13.08	10.36	10.29

For saturated liquid propane an enthalpy of 24.4 Btu per lb corresponds to a pressure of 180.1 psia. At this pressure, therefore, vaporization started in the column (see Fig. 3).

To find the transverse section in the column, at which the pressure was 180.1 psia, it is noted first (Fig. 3) that the flow was essentially isothermal in the part of the column upstream from the place of initial vaporization. Moreover, the measured total weight rate of flow was 10.36 lb per hr, and at distances of 1.669 and 2.510 ft along the column, the measured pressures were 184.8 and 179.6 psia, respectively. In the indicated incremental length of sand column, the bulk cross-sectional area was 0.0237 sq ft and the homogeneous-fluid permeability 1.001×10^{-11} sq ft. Graphing of published data[2,3] discloses that the product of specific volume and absolute viscosity was 62.18×10^{-9} ft · sec for the liquid propane that was flowing between the transverse sections at which the pressures were 184.8 and 180.1 psia, respectively. Hence, application of Darcy's law in the conventional manner to homogeneous-liquid flow, gives 2.440 ft from the upstream end of the sand column as the distance to the transverse section where vaporization started (see Fig. 5).

Figs. 6 and 7 are, respectively, the pressure-function and integrated-pressure-function charts. These charts are necessary in determining the theoretical total weight rate of flow and pressure distribution. Data used in the preparation of these figures are entered in Table II and were developed as discussed below.

In Table II, the pressures at the upstream and downstream ends of the column, 193.2 and 134.4 psia, respectively, were measured; and, the pressure at which vaporization started (180.1 psia) was determined by the foregoing procedure. The pressure range from 180.1 to 134.4 psia was subdivided arbitrarily as shown in Column 1 so that data could be developed for constructing Figs. 6 and 7.

In the all-liquid flow portion of the sand column k_G/k obviously would have been zero and k_L/k unity; hence, for this part of the system $F(P)$ would be the reciprocal of $\mu_L \bar{v}_L$ (see Equations 21 and 22). This reciprocal was calculated to be 16.08×10^6 ft^{-1} · sec^{-1}, and the horizontal segment of the $F(P)$ vs P curve (Fig. 6) thereby became established.

Table II contains two entries of $F(P)$ for the pressure 180.1 psia. At the upstream side of the transverse section at which vaporization started, the fluid in the sand was entirely in the liquid state, and therefore, $F(P)$ for that section would be 16.08×10^6 ft^{-1} · sec^{-1} if it were approached from the upstream side. In accordance with the concept of an "equilibrium gas saturation,"[5] however, the pore space in the sand at the section in question would have contained a fixed quantity of static gas but no moving gas. This means that k_G/k would have been

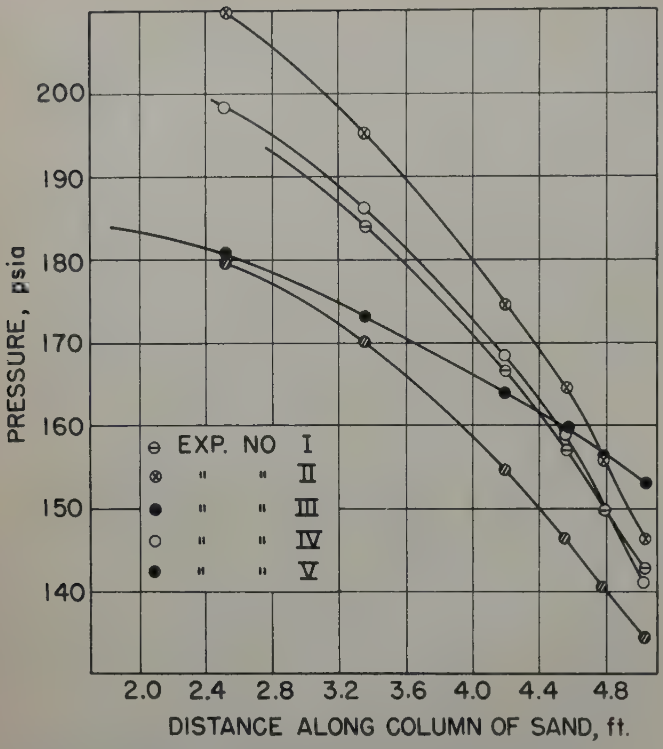

FIG. 5 — EXPERIMENTALLY-DETERMINED PRESSURE DISTRIBUTIONS IN TWO-PHASE FLOW PORTION OF TEST COLUMN OF SAND.

zero and k_L/k less than unity at the section. Hence, if the relative permeability of the liquid at the section is denoted by $(k_L/k)_e$, "the equilibrium permeability," and the section approached from the downstream side $F(P)$ for the section would be $(k_L/k)_e/(\mu_L\bar{v}_L)$.*

For unconsolidated sands, Wyckoff and Botset found that $(k_L/k)_e \doteq 0.79$. This value was used in the present analysis. A considerable error in this value would have no appreciable effect on the theoretically calculated results (Fig. 6).

With respect to the two-phase flow in the column of sand, published data[2,3] on saturated liquid and gaseous propane were used to plot $(\mu_L\bar{v}_L/\mu_G\bar{v}_G)$ and $(H-H_L)/(H_G-H_L)$ as functions of pressure. These plots were the source for data entered in Columns 2 and 3 of Table II. This information and application of Equation (24) led to the calculated values of k_L/k_G shown in Column 3. In turn, the data in Column 3 were used with the propane-flow curve of Fig. 4 to determine the corresponding relative permeabilities (k_L/k and k_G/k). Further use of the foregoing published data to plot $\mu_L\bar{v}_L$ and $\mu_G\bar{v}_G$ as functions of pressure, together with knowledge of k_L/k and k_G/k as functions of pressure, resulted in the entries in Columns 5 and 6. Corresponding entries in these columns were added to give the $F(P)$ entries in Column 7, which were used to construct Fig. 6.

Data for the construction of the integrated-pressure-function chart (Fig. 7) are entered in Column 7 of Table II. These data were obtained by dividing the total area under the curve in Fig. 6 into vertical strips and determining the area of each strip by application of either Simpson's rule or the trapezoidal rule. As the widths of the strips were governed by the pressure entries in Column 1, knowledge of their areas led directly to the entries in Column 7, which were used to construct Fig. 7.

To calculate the theoretical total weight rate of flow, Equation (22) was put in the form

$$W = \left[\sum_{i=1}^{i=8} \frac{A_i k_i}{\Delta x_i}\right] \cdot \int_{P_E}^{P_1} F(P)dP \quad . \quad . \quad . \quad (29)$$

in which subscript i refers to the eight length increments into which the column was divided;* P_I and P_E are the fluid pressures respectively at the upstream and downstream ends of the column.

The integral term in Equation (29) represents the total area under the curve in Fig. 6 and was calculated to be 706.42 x 10^8 lb · ft^{-3} · sec^{-1} (see Table II, Column 8). The term in brackets was calculated to be 2.473 x 10^{13} ft^{-3}. Hence, the theoretical total weight rate of flow was found to be 2.857 x 10^{-3} lb per sec or 10.29 lb per hr as compared to 10.36 lb per hr for the measured rate.

To find the theoretical pressure at the upstream end of the n-th increment ($n = 1, 2, 3, 4, 5, 6, 7$ or 8), the upper limits of the integral and summation in Equation (29) are changed to P_n. Under these conditions, the value of the integral may be calculated, as the theoretical weight rate of flow will be known. The calculated value of the integral, then, is used in conjunction with Fig. 7 to find P_n, the theoretical pressure at the upstream end of the n-th increment. Table I contains results determined in this manner.

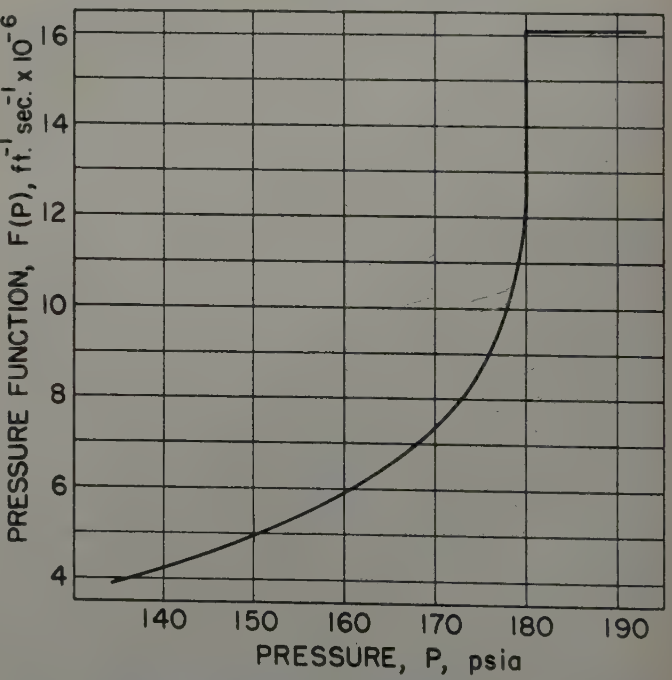

FIG. 6 — GRAPHIC REPRESENTATION OF PRESSURE FUNCTION (BASED ON THEORETICAL CALCULATIONS PERTAINING TO EXPERIMENT V).

---

*It is of interest to find that there would be a discontinuity in the fluid pressure gradient at the transverse section under consideration. Applying Darcy's law, the pressure gradient at the upstream side would be $-(W\mu_L\bar{v}_L/Ak)$ and at the downstream side $-(W\mu_L\bar{v}_L)/[Ak(k_L/k)_e]$; hence the ratio of upstream to downstream gradients would be $(k_L/k)_e$.

*These eight incremental lengths were limited, respectively, to the following ranges of distance ($\triangle x$) along the sand column (measured in ft from the inlet face): 0.000 to 0.833, 0.833 to 1.669, 1.669 to 2.510, 2.510 to 3.351, 3.351 to 4.187, 4.187 to 4.570, 4.570 to 4.778, and 4.778 to 5.028. Starting at the upstream end of the column and proceeding downstream, the homogeneous-fluid permeabilities (k) of these increments were, respectively, 1.191, 1.244, 1.001, 0.8950, 0.8812, 0.9110, 0.7951 and 1.006 sq ft x 10^{-11}. Considered in the same order their average bulk cross-sectional areas (A) were, respectively, 0.02042, 0.02036, 0.02037, 0.02044, 0.02025, 0.02027, 0.02027, and 0.02027 sq ft.

CONCLUSION

The subject matter of this paper concerns the thermodynamic aspects of the steady flow of a single-component gas-liquid mixture, through porous media. The underlying, fundamental two-phase fluid-flow theory pertaining to this subject is developed, and laboratory experiments substantiating the theory are described.

It is pointed out in the paper that the thermodynamic process followed by oil-reservoir fluids while moving through porous underground rock formations is of significance in predictions of oil-reservoir behavior. Moreover, the flow of multi-component hydrocarbon fluids in these rocks is indicated to be intermediate between isothermal and adiabatic, but not susceptible to exact classification owing to a lack of necessary, detailed, heat-transfer data on subsurface rocks and fluid mixtures.

In an effort to perform the described experiments with the simplest appropriate two-phase flow system, it was decided that a single-component fluid should be used. This decision made isothermal flow impossible; hence, on the basis of the foregoing considerations, adiabatic flow was adopted for study.

In this respect, the experiments reported relate specifically to the steady adiabatic flow of propane in two phases through a horizontal column of sand, mounted in a specially designed apparatus. The propane, in all the experiments, entered the column entirely as a liquid, started to vaporize an appreciable distance downstream from the inlet, and then flowed in two phases throughout the remainder of the column.

Regarding the theory, the problem posed was to calculate the total weight rate of flow and the pressure distribution along the column of sand, for a given pressure and temperature of the all-liquid entering stream, a given pressure or temperature of the discharging gas-liquid mixture, and given sand and fluid characteristics. A comparison of theoretical and experimental results has been presented and discussed to show that the theory may be applied to solve this problem.

The theory, as developed herein, is premised on work done by O'Brien and Putnam.[1] The present paper shows, however, that equations developed by those investigators for calculating wetting-phase content and used by them in determining weight rates of flow and pressure distributions were not correct.

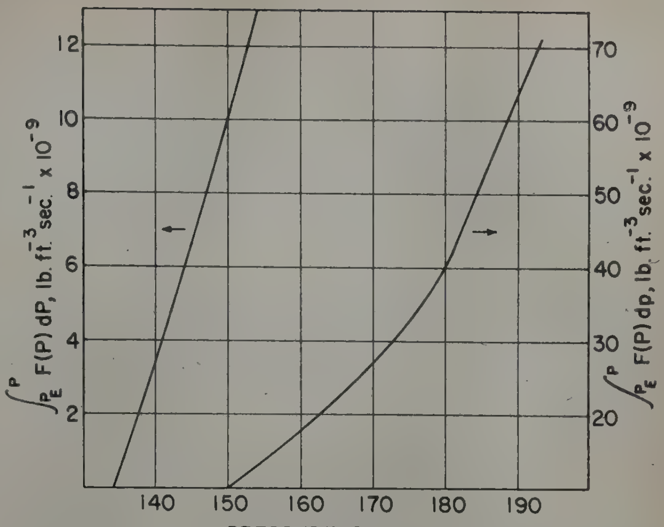

FIG. 7 — GRAPHIC REPRESENTATION OF INTEGRATED PRESSURE FUNCTION (BASED ON THEORETICAL CALCULATIONS PERTAINING TO EXPERIMENT V).

Attention is given in the present paper, moveover, to gas-liquid interfacial phenomena. The analyses made in this connection indicate that capillary pressures and their gradients are of negligible magnitude for single-component two-phase flow systems of the kind investigated.

Furthermore, the agreement among theoretical and experimental results indicates that the assumption of phase equilibrium, made in the development of the theory, is valid for the system studied.

In conclusion, the material offered in this paper should lead to a better understanding of oil-reservoir behavior in that the investigation pertains to the flow of a two-phase hydrocarbon fluid in sand. Substantiation of the theory suggests that it would be desirable to follow the reported work with a similar study of the two-phase flow of a multi-component hydrocarbon gas-liquid mixture through sand.

Table II — Data for Construction of Pressure-Function and Integrated-Pressure-Function Charts (Figs. 6 and 7, Respectively)

(1)	(2)	(3)	(4)	(5)	(6)	(7)	(8)
P psia	$\frac{\mu_L \bar{v}_L}{\mu_G \bar{v}_G}$ dimensionless	$\frac{H - H_L}{H_G - H_L}$ dimensionless	$\frac{k_L}{k_G}$ dimensionless	$\frac{k_L/k}{\mu_L \bar{v}_L}$ ft^{-1} . sec^{-1} x 10^{-6}	$\frac{k_G/k}{\mu_G \bar{v}_G}$ ft^{-1} . sec^{-1} x 10^{-6}	$F(P)$ ft^{-1} . sec^{-1} x 10^{-6}	$\int_{P_E}^{P} F(P)dP$ lb . ft^{-3} . sec^{-1} x 10^{-8}
134.4	0.3622	0.1067	3.032	3.477	0.4154	3.892	0.00
135	0.3631	0.1047	3.105	3.570	0.4174	3.987	3.57
140	0.3704	0.09386	3.576	3.872	0.4011	4.273	33.31
145	0.3779	0.08224	4.217	4.223	0.3784	4.601	65.26
150	0.3850	0.07038	5.086	4.610	0.3489	4.959	99.68
155	0.3916	0.05908	6.238	5.067	0.3181	5.385	136.92
160	0.3978	0.04762	7.956	5.575	0.2788	5.854	177.38
165	0.4037	0.03598	10.82	6.248	0.2331	6.481	221.79
170	0.4091	0.02417	16.52	7.152	0.1771	7.329	271.34
175	0.4137	0.01293	31.58	8.567	0.1122	8.679	328.57
180.1	—	0.00000	∞	12.71*	0.0000	12.71	403.08
180.1	—	”	”	16.08	”	16.08	403.08
193.2	—	”	”	”	”	”	706.42

$^{*}(k_L/k)_e \doteq 0.79$ — from Wyckoff - Botset[5] results.

ACKNOWLEDGMENTS

Credit is due to the Division of Mineral Technology of the College of Engineering of the University of California for providing laboratory facilities for the experimentation.

Appreciation is expressed to the American Petroleum Institute (Project 47-A) for supplying experimental equipment and to R. W. Ravenscroft, project engineer, and his staff, for cooperative assistance rendered in the construction of apparatus and collection of data.

The author offers his special thanks to Prof. J. A. Putnam, director of Project 47-A, for his encouragement, counsel and guidance throughout the course of the investigation. Special thanks are offered also to Hassan Aboul-Seoud with whom the planning and performance of the experiments was a joint undertaking.

For many helpful suggestions and comments, and for reviewing manuscript copies of the report, grateful acknowledgment is made to Dean M. P. O'Brien, College of Engineering, University of California; to Prof. T. Vermeulen, College of Chemistry, University of California; to G. B. Shea, Chief, Fuels Technology Division, Region III, U. S. Bureau of Mines; and to the members of the API Project 47-A Advisory Committee.

REFERENCES

1. O'Brien, M. P., and Putnam, J. A.: "Some Problems of Horizontal Steady Flow in Porous Media," AIME T.P. 1349, *Petr. Tech.*, (July, 1941).
2. Sage, B. H., Schaafsma, J. G., and Lacey, W. N.: *Ind. Eng. Chem.*, (Nov., 1934), **26**, No. 11, 1218-1224.
3. Sage, B. H., and Lacey, W. N.: *Ind. Eng. Chem.*, (July, 1938), **30**, No. 7, 829-834.
4. Aboul-Seoud, Hassan: "Equilibrium Considerations in Two-Phase Flow of Hydrocarbons through Unconsolidated Sands." Unpublished Ph.D. thesis, University of California, Division of Mineral Technology, 1950.
5. Wyckoff, R. D., and Botset, H. G.: *Physics*, (Sept., 1936), **7**, No. 9, 325-345.
6. Botset, H. G.: *Trans.* AIME, (1940), **136**, 91.
7. Martinelli, R. C., Putnam, J. A., and Lockhart, R. W.: *Trans.* AIChE, (Aug. 25, 1946), **42**, No. 4, 681-705.
8. Edlefsen, N. E., and Anderson, A. B. C.: Thermodynamics of Soil Moisture, *Hilgardia* (A Journal of Agricultural Science, published by the California Agricultural Experiment Station), (Feb., 1943), **15**, No. 2, 142-146.
9. Calhoun, John C., Jr., Lewis, Maurice, Jr., and Newman, R. C.: *Trans.* AIME, (1949), **186**, 189.
10. Muskat, M.: *Physical Principles of Oil Production.* McGraw-Hill Book Co., Inc., New York, (1949), 311-321.
11. Lamb, Horace: *Hydrodynamics.* Dover Publications, 6th ed., New York, (1945), 597-599.
12. Klein. Alexander: "An Improved Hydrometer Method for Use in Fineness Determinations." ASTM Symposium on New Methods for Particle Size Determination in the Subsieve Range, Washington Spring Meeting, (Mar. 4, 1941).

DISCUSSION

By E. C. Babson, Union Oil Co. of California, Member AIME

Miller has succeeded in obtaining remarkable agreement between experimental results and analytical theory, indicating that phase equilibrium is attained very rapidly under the conditions of his experiments.

The relative permeability data used in calculating the pressure gradients, however, were not established for the sand column used in the experiments but were obtained by shifting Botset's K_g/K_o curve to reach an overall fit on one of the runs. The relation established in this manner was used in the calculations for all runs.

There is, therefore, a possibility that the agreement between theory and experiment is due to compensating errors. When consideration is given to the excellent agreement at each pressure tap for each run, it must be admitted that this possibility is remote, but it still exists and should be recognized.

AUTHOR'S REPLY TO MR. BABSON

Babson's comment regarding relative-permeability data is well taken. Perhaps this matter should have been discussed in more detail in the paper.

The paper includes a statement to the effect that validity of the theory must be assumed if the relationship between k_L/k_G and k_L/k is to be established with (and for) the test column of sand, under conditions of adiabatic flow with two-phase propane. The Wyckoff-Botset unconsolidated-sand data were utilized in the described manner, therefore, as a recourse.

If this procedure had not been followed, then the collection of independent relative-permeability data for the test sand column would have been necessary. Considering the high sensitivity of calculated weight rates of flow and pressure distributions to such data, it is evident that an independently-determined k_L/k_G vs k_L/k curve would most probably require shifting (within the limits of experimental accuracy) before an acceptable agreement of theory and experiment were obtained. As this shifted curve would have about the same theoretical significance as the propane-flow curve of Fig. 4, it too, would give rise to a remote possibility of an unsound agreement of theory and experiment. Accordingly, one concludes that no important gain would result from the collection of independent relative-permeability data.

★ ★ ★

T.P. 3081

TRANSIENT FLOW IN GAS TRANSMISSION LINES

R. H. OLDS, NAVAL ORDNANCE TEST STATION, INYOKERN, CHINA LAKE, CALIF., AND **B. H. SAGE,** MEMBER AIME,
CALIFORNIA INSTITUTE OF TECHNOLOGY, PASADENA, CALIF.

INTRODUCTION

The transient flow of gases in long pipe lines is a problem of industrial interest. The present discussion deals with the application of the conservation of momentum and material to the transient flow of gas in conduits which are long with respect to their diameter. Solutions of the resulting equations include consideration of variations in friction and specific volume of the fluid as functions of time and position along the conduit. The changes in state along the pipe line are established as a function of time. The methods proposed may be extended to other situations.

The flow of compressible fluids under steady conditions[1] has been considered in detail. Primary emphasis was placed on the development of simple means of taking into account the non-uniform flow[1] realized in long conduits under such conditions. Binder[2] discussed the essential differences between the flow of compressible and noncompressible fluids. Bonilla[3] proposed direct methods of solution for equations describing isothermal flow in long pipes. Similar considerations limited to steady flow have been discussed by Ruth.[4] Palsgrove[5] suggested a graphical means of solving specific problems relating to the flow of gases in conduits of uniform section. Some of the basic concepts of the flow of a compressible viscous fluid in straight tubes have been described by Kuo.[6] Problems of this type require knowledge of the equation of state of the fluid. In many cases it has been convenient to assume that the fluid follows the relationship ascribed to a perfect gas.

The treatment of unsteady flow of compressible fluids is less complete. This state of affairs results from the fact that the differential equations relating pressure and flow rate with time and position for unsteady flow are nonlinear in character.[7] Muskat and Wyckoff[8] presented an excellent treatment of the situation in laminar flow where inertia forces were not of controlling importance. Somewhat earlier Hurst[9] discussed the unsteady flow of fluids in petroleum reservoirs. Hetherington, MacRoberts, and Huntington[10] established experimentally the pressure distribution and accumulative flow rate of natural gas through an unconsolidated sand. Recently Joffe[11,12] considered the specific problem of the flow of natural gas in relatively long pipe lines for unsteady conditions with emphasis upon the economic feasibility of the storage of gas in such a reservoir. These discussions were based upon approximations of the partial differential equations applying to the conditions of flow. The results were descriptive of the physical situation and indicated the effectiveness of large pipe lines as cyclic storage facilities for natural gas. The advent of analog computers[13] has increased materially the practicality of solving nonlinear partial differential expressions. Several iterative numerical and graphical methods[14,15,16] have been developed to solve nonlinear equations. However, it appears that the pair of simultaneous nonlinear partial differential equations involved in problems of this nature are not directly susceptible to solution by presently available analog computer or formal iterative numerical techniques. Nevertheless, graphical analyses afford a means of obtaining data of engineering value without special equipment.

MATHEMATICAL CONSIDERATIONS

Since the length of the conduit is large in comparison to the cross section in the cases to be considered, it is possible to treat the characteristics of the flow as independent of position in the cross section of the conduit. This possibility follows since the energy connected with the velocity profile is small compared to that required to overcome the friction associated with its movement throughout the length of the line. Average values of the pressure, velocity, kinetic energy, momentum, and specific volume may be assigned to the fluid at any particular cross section. From a mathematical viewpoint this may be expressed in the following way for velocity:

$$u = u(\theta X) \quad . \quad . \quad . \quad . \quad . \quad . \quad . \quad . \quad . \quad . \quad (1)$$

The uncertainties introduced by such assumptions usually are negligible when the ratio of length to diameter is greater than the order of 1,000. On this basis a volume element may be considered to occupy the entire cross section of the conduit. Such an element is presented in Fig. 1.

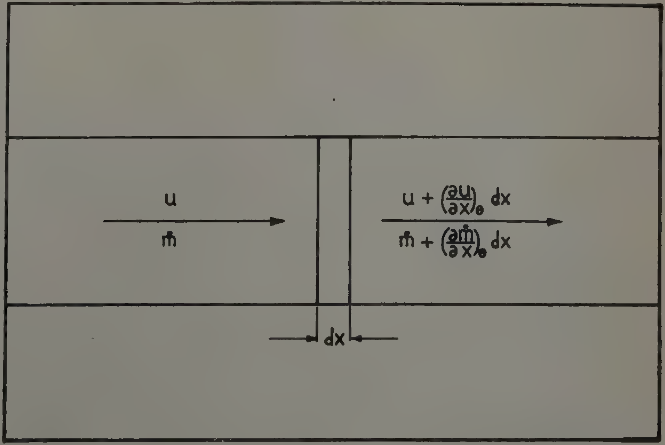
u
ṁ
$u + \left(\frac{\partial u}{\partial x}\right)_\theta dx$
$\dot{m} + \left(\frac{\partial \dot{m}}{\partial x}\right)_\theta dx$
dx

FIG. 1 — VOLUME ELEMENT IN A LONG PIPE LINE.

---

[1] References given at end of paper.

Manuscript received by the Petroleum Branch Oct. 27, 1950.

A material balance applied to the volume element yields the following expression for a conduit of cross-sectional area A:

$$\frac{\partial \sigma}{\partial \theta} + \frac{1}{A}\frac{\partial \dot{m}}{\partial X} = 0 \quad . \ . \ . \ . \ . \ . \ . \ . \ . \quad (2)$$

The foregoing equation represents the fact that the difference in the material entering and leaving a particular part of the pipe line in a given time is equal to the change in the quantity of material within the section of the pipe line under consideration.

A force balance upon the differential element of volume shown in Fig. 1, which is equivalent to assuming conservation of momentum, is given by the following equation:

$$\frac{1}{gA}\frac{\partial \dot{m}}{\partial \theta} + \frac{\partial}{\partial X}\left(P + \frac{\dot{m}^2}{g\sigma A^2}\right) + \frac{\tau\pi d}{A} = 0 \quad . \quad (3)$$

Following conventional practice,[17] the shear per unit length is empirically related to the conditions of flow and the friction factor in the following manner:

$$\frac{\tau\pi d}{A} = \frac{\mathrm{f}}{2\sigma g}\frac{\dot{m}^2}{dA^2} \quad . \ . \ . \ . \ . \ . \ . \ . \ . \quad (4)$$

A combination of Equations (3) and (4) yields the expression:

$$\frac{1}{gA}\frac{\partial \dot{m}}{\partial \theta} + \frac{\partial}{\partial X}\left(P + \frac{\dot{m}^2}{g\sigma A^2}\right) + \frac{f\dot{m}^2}{2\sigma g d A^2} = 0 \quad . \quad (5)$$

For the majority of conditions encountered in the transient flow of natural gas in long pipe lines the inertia effects are small, and it is believed that except in special circumstances where numerous large changes in velocity are encountered the forces associated with the acceleration of the flow can be neglected without introducing appreciable error. In the examples to be considered the neglect of these inertia terms did not introduce errors greater than 0.8 per cent in the reported values of pressure. If the inertia effects are neglected, Equation (5) simplifies to the following form:

$$\frac{\partial P}{\partial X} + \frac{f\dot{m}^2}{2\sigma g d A^2} = 0 \quad . \ . \ . \ . \ . \ . \ . \ . \ . \quad (6)$$

The evaluation of Equations (2) and (6) requires a knowledge of the relationship between pressure and specific weight of the gas. In the present instance it is not necessary to employ a complex equation of state and the following expression appears adequate for the present discussion:

$$\sigma = \frac{P}{bT - P\underline{V}} = \frac{P}{bT - PB} \quad . \ . \ . \ . \ . \ . \ . \quad (7)$$

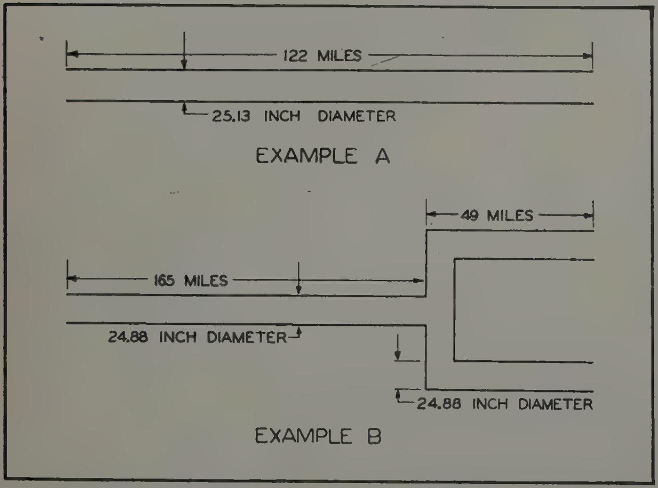

FIG. 2—SCHEMATIC DIAGRAM OF PHYSICAL SITUATION FOR EXAMPLES A AND B.

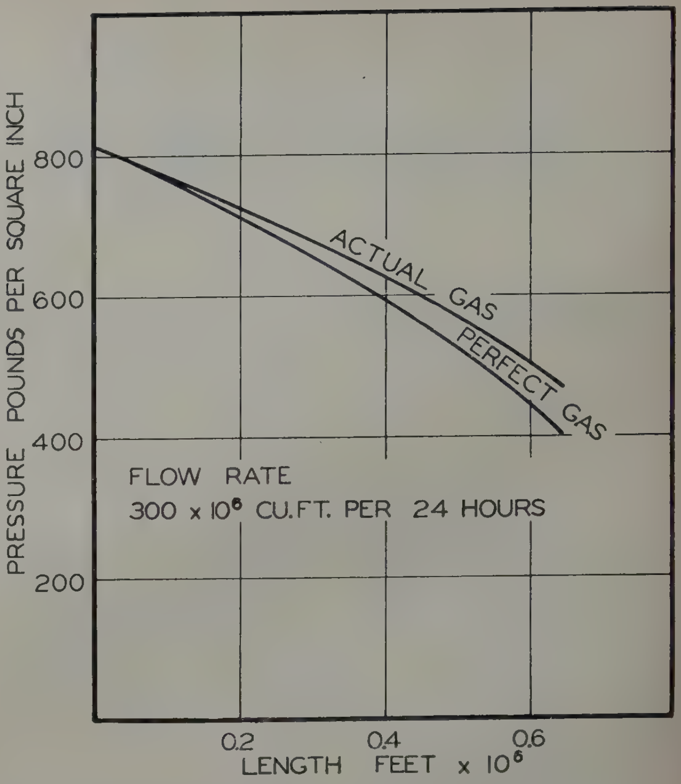

FIG. 3 — PRESSURE AS A FUNCTION OF POSITION UNDER STEADY-STATE CONDITIONS IN EXAMPLE A.

Or, neglecting terms of order $(PB/bT)^2$ this may also be written in the form:

$$\sigma = \frac{1}{bT}\left(P + \frac{B}{bT}P^2\right) \quad . \ . \ . \ . \ . \quad (8)$$

The residual volume $\underline{V}$ has been considered a constant for the range of pressure of interest as is indicated in the third term of Equation (7) and Equation (8).

Table I — Description of the Situation

	Example A	Example B
Length of pipe line,		
miles	122	214*
feet	$0.6442\mathrm{x}10^6$	$1.131\mathrm{x}10^6$
Diameter of conduit, feet	2.094	2.072
Temperature, degrees F	60	60
Upstream pressure, psi	815	..
Flow rate, cu ft/24 hr	$300\mathrm{x}10^6$**	$300\mathrm{x}10^6$
Composition of gas, mole fraction		
methane	0.94	----
ethane	0.04	----
propane and heavier	0.02	---
Average molecular weight	17.28	19.79
Viscosity of gas, lb, sec/sq ft	$0.2799\mathrm{x}10^{-6}$	$0.2108\mathrm{x}10^{-6}$
Residual specific volume, cu ft/lb	0.05471	0.0495
Constants of Equations (9) and (10)		
a	0.019724	..
c	0.07534	0.11754
n	0.1205	0.1454

*The line is 214 miles in length with the final 49 miles made up of a pair of conduits, each of the same cross section as the single conduit making the preceding 165 miles of the system.

**Measured at 60°F, 14.73 psia.

SPECIAL CONDITIONS

The remaining portion of this discussion is concerned with two special problems which differ materially as to the physical situations. The units of measure used in the two examples have been chosen somewhat differently. However, the force-length-time system of dimensions has been employed. The situation associated with each of the pipe lines is presented in a part of Table I, and in Fig. 2 is depicted a diagrammatic sketch of their arrangement.

The friction associated with the flow was established from the correlation of Pigott,[18] which is based in part upon the experimental work of Nikuradse.[19] The friction factor is empirically related to the Reynolds number in the following way:

$$f = cRe^{-n} \quad . \; . \; . \; . \; . \; . \; . \; . \; . \; . \; . \quad (9)$$

It is assumed that viscosity is independent of pressure over the range of conditions encountered. If the diameter of the line is uniform, it follows that the friction factor becomes a single-valued function of the weight rate of flow as is indicated below.

$$f = a\underline{\dot{m}}^{-n} \quad . \; . \; . \; . \; . \; . \; . \; . \; . \; . \; . \quad (10)$$

Further consideration of the problem necessitates treatment of a specific set of boundary conditions and the discussion will be applied to each situation separately.

Example A

The physical situation involved in this problem is set forth in a part of Table I. It is desired to determine the variation of pressure with respect to time at the exit of a pipe line 122 miles in length when flow suddenly is curtailed at the inlet while gas is withdrawn continuously at the outlet at a constant rate of 300 x 10^6 cu ft per day.*

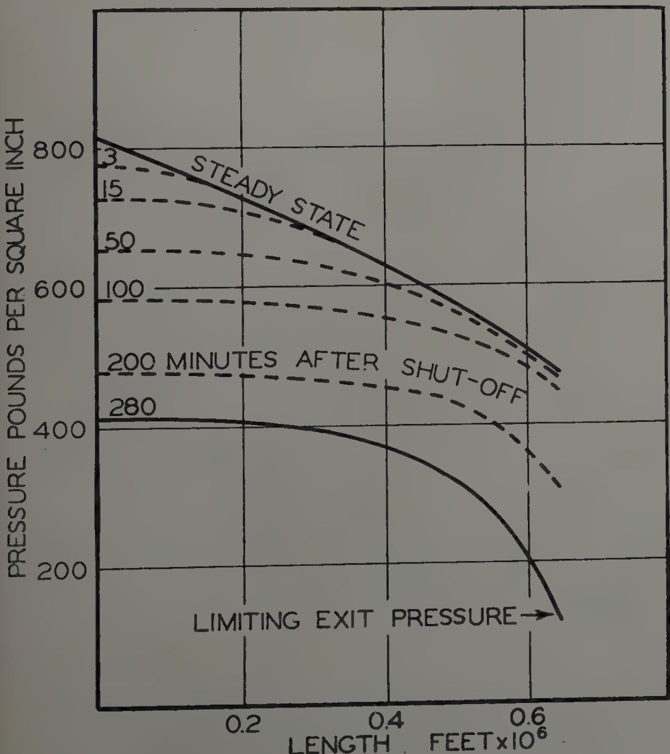

FIG. 4 — PRESSURE DISTRIBUTION FOR UNSTEADY CONDITIONS IN EXAMPLE A.

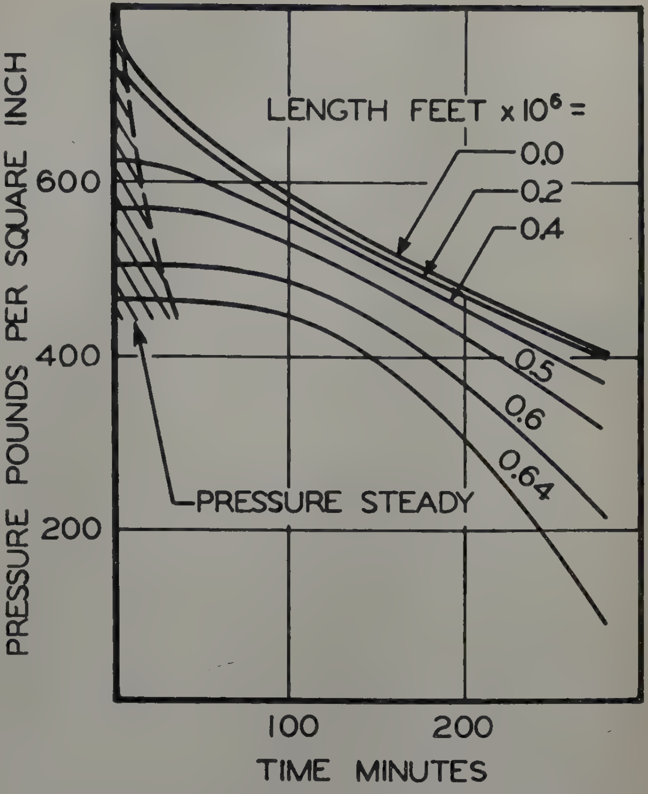

FIG. 5 — VARIATION IN PRESSURE WITH TIME FOR EXAMPLE A.

The viscosity of the gases employed is reported in a part of Table I and is based upon experimental measurements of viscosity of similar gases.[20] In Example A the friction factor is related to the weight rate of flow by the following equation:

$$f = 0.019724\underline{\dot{m}}^{-0.1205} \quad . \; . \; . \; . \; . \; . \; . \quad (11)$$

The associated values of the constants of Equations (9) and (10) are shown in a part of Table I. In this instance the specific volume at 60°F may be expressed in terms of the pressure by the relation:

$$V = \frac{1}{\sigma} = \frac{322.72}{P} - 0.05471 \quad . \; . \; . \; . \; . \quad (12)$$

A combination of Equations (6), (7), and (10) followed by appropriate integration results in the following expression for steady flow:

$$\frac{P_2 - P_1}{B} + \frac{bT}{B^2} \, ln \frac{bT/B - P_2}{bT/B - P_1} = \frac{a\underline{\dot{m}}^{(2-n)}}{2gdA^2} (X_2 - X_1) \; . \quad (13)$$

In the case of a perfect gas where the residual volume, *i.e.*, the assumed constant B is zero, Equation (13) reduces to a simpler form.

$$P_1^2 - P_2^2 = \frac{abT\underline{\dot{m}}^{(2-n)}(X_2 - X_1)}{gdA^2} \quad . \; . \; . \; . \quad (14)$$

The application of the specific volumetric data of Equation (12) in Equation (13) and the substitution of the boundary conditions listed in Table I yield the following expression for the distance along the pipe line under steady conditions of flow as a function of the prevailing pressure:

$$X - X_1 = \frac{-4.2044 \times 10^6}{(0.019724)\underline{\dot{m}}^{1.8795}} \left\{ 815 - P + 13582 \log_{10} \frac{5083.7}{5898.7 - P} \right\} \quad . \; . \; . \; . \; . \; . \; . \; . \; . \; . \; . \; . \quad (15)$$

In Fig. 3 is shown the pressure as a function of position along the pipe line for a flow rate of 300 x 10^6 cu ft per 24 hr.

In the case of unsteady flow both Equations (2) and (6) must be satisfied. Under these circumstances the pressure gradient may be expressed in a slightly different form from that originally employed in Equation (6).

---

*All volumetric measurements relating to the quantity of gas correspond to a temperature of 60°F and a pressure of 14.73 psia. The indicated volumetric rate corresponds to 160.7 lb of gas per second.

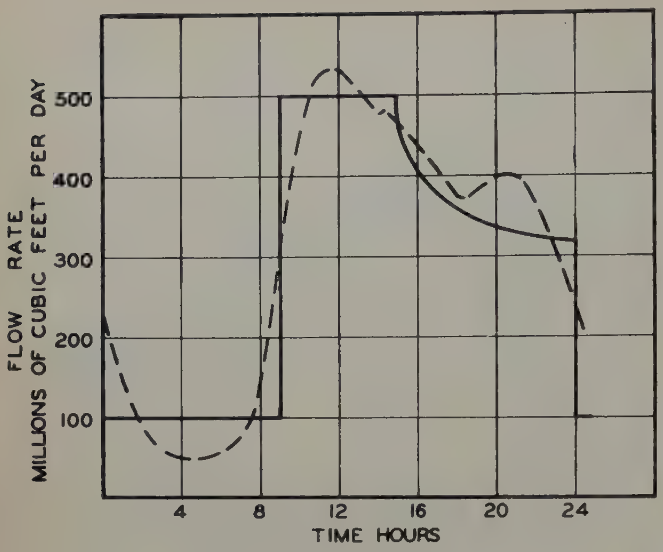

FIG. 6 — VARIATION IN OUTPUT RATE FOR EXAMPLE B.

$$\frac{\partial P}{\partial X} = \frac{bT}{P}\left(\frac{PB}{bT} - 1\right)\frac{a}{2gdA^2}\,\underline{\dot{m}}^{(2-n)} \quad . \quad . \quad . \quad (16)$$

The change in pressure with respect to time may be obtained directly from Equations (2) and (7).

$$\frac{\partial P}{\partial \theta} = -\frac{bT}{A}\left(\frac{PB}{bT} - 1\right)^2 \frac{\partial \underline{\dot{m}}}{\partial X} \quad . \quad . \quad . \quad . \quad . \quad (17)$$

Both Equations (16) and (17) are applicable at all points in the pipe line. An iterative graphical procedure was employed to construct a solution for these equations which satisfied the required boundary conditions. The details of a similar graphical operation are set forth in the latter part of this paper.

The situation at various times after the flow is interrupted is shown in Fig. 4 upon the assumption of perfect gas behavior. It is apparent that during the initial period after shutoff there has been no change in the downstream pressure. Fig. 4 also depicts the pressure distribution after an elapse of 280 min. At this time the exit pressure has decreased to 115 psi, which was considered to be the minimum pressure feasible for the operation of the transmission line. Fig. 5 shows the estimated variation in the pressure with respect to time at various points along the pipe line. Little or no change in pressure at the exit is obtained for a period of about 45 min. Subsequent to that interval, the exit pressure decreases at an increasing rate until the effectiveness of the line as a storage facility is substantially exhausted after about 280 min.

Example B

The physical situation considered in this example is markedly different from that of the preceding one. The gas entered a pipe line 214 miles in length which was made up of 165 miles of single conduit and 49 miles of two parallel conduits of the same cross section as that of the first part of the line. This design was employed to increase the storage capacity of the system under transient conditions. The system was operated at an input rate of 300 x 10^6 cu ft per 24 hr. The output rate of flow varied as indicated in Fig. 6. In the interest of ease of computation the continuous distribution indicated by the dotted curve was simplied to the discontinuous relation shown by the full line. It was desired to determine the pressure distribution in the pipe line during a 24-hr period corresponding to the withdrawal rates indicated in Fig. 6 while the input flow rate remained constant at 300 x 10^6 cu ft per day. The total withdrawal per 24 hr was 300 x 10^6 cu ft.

In this instance the specific weight of the gas at 60°F is related to the pressure in the following way:

$$\sigma = 0.003547\,(P + 0.000176\,P^2) \quad . \quad . \quad . \quad (18)$$

The friction factor was related to the Reynolds number in accordance with Equation (9).

$$f = 0.11754\,\mathrm{Re}^{-0.1454} \quad . \quad . \quad . \quad . \quad . \quad . \quad . \quad . \quad (19)$$

A combination of the foregoing isothermal equation of state and the expression for friction with Equations (2) and (6) leads to the following expressions in which the distance is expressed in miles, the time in hours, and the flow rate in millions of cubic feet per day:*

$$\frac{\partial}{\partial \theta'}\,(P + 0.000176\,P^2) + 33.014\,\frac{\partial \dot{V}'}{\partial X'} = 0 \quad . \quad . \quad (20)$$

$$\frac{\partial}{\partial X'}\,(P^2 + 0.0001173\,P^3) + 0.10788\,\dot{V}'^{1.8546} = 0 \quad . \quad (21)$$

Under steady-state conditions Equation (20) vanishes and Equation (21) may be integrated to yield:

$$\left[P^2 + 0.0001173\,P^3\right]_{P_1}^{P_2} = 0.10788\,\dot{V}'^{1.8546}\,(X_1 - X_2) \quad . \quad (22)$$

In Fig. 7 is presented the pressure distribution in the pipe line for two limiting conditions of steady flow rates. The first is associated with the maximum entrance pressure of 970 psi which yields an exit pressure of 518 psi. The second condition is related to the minimum acceptable exit pressure of 265 psi which necessitates an entrance pressure of 870 psi. These conditions correspond to the limiting range of steady operation which permits the transmission of 300 x 10^6 cu ft of gas per

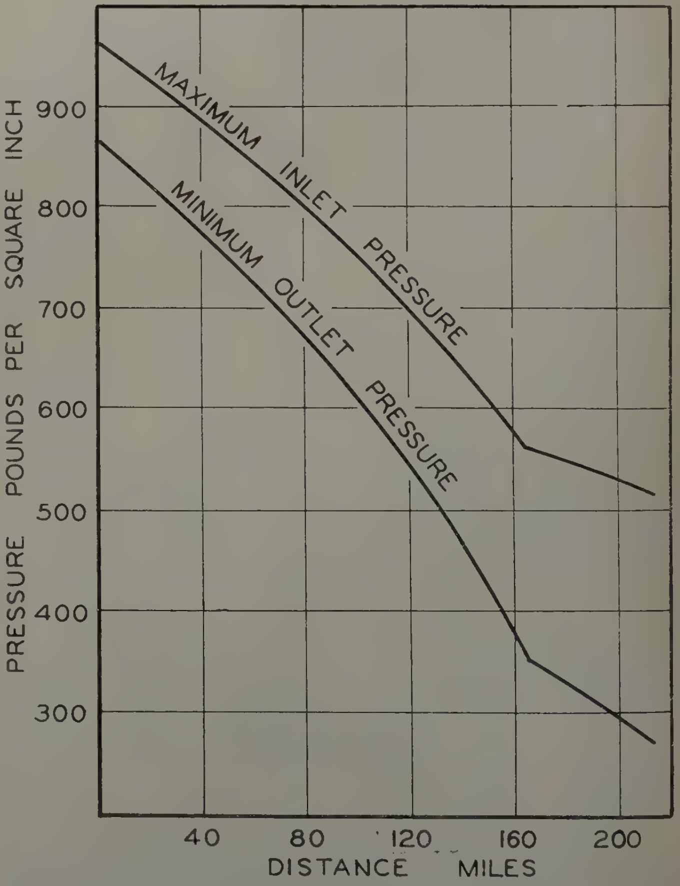

FIG. 7 — PRESSURE DISTRIBUTION FOR STEADY FLOW CONDITIONS IN EXAMPLE B.

---

*Measured at 60°F, 14.73 psia.

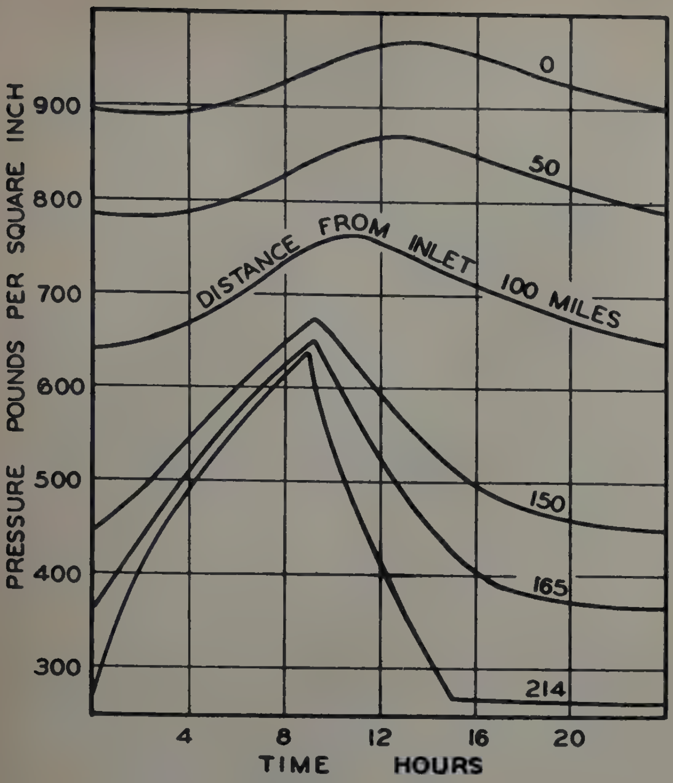

FIG. 8 — PRESSURE VARIATION FOR TRANSIENT CONDITIONS IN EXAMPLE B.

24 hr. It was assumed in the last 49 miles of the conduit that the flow was divided equally between the two conduits.

The discontinuity in the slope of the pressure distribution curves in Fig. 7 corresponds to the point where the flow divides between the two identical conduits. The transition from steady to cyclic exit conditions involved secondary transients which were also completely dissipated by the end of the first cycle.

The distribution of pressure in the pipe line is depicted in Fig. 8 as a function of time and position. At the entrance to the conduit a cyclic variation in pressure from 890 to 970 psi is obtained during a given 24-hr period. At the exit the pressure changes from a minimum value of 270 to a maximum of 640 psi. The discontinuous nature of the slope of this curve results from the assumption shown in Fig. 6 of discontinuous changes in the demand rate of flow. In actual practice the rate of flow would not change discontinuously and the rate of change of pressure with time at the exit would be continuous. The pressure distribution in the pipe line for several different periods in the cycle constitutes Fig. 9.

A GRAPHICAL METHOD OF SOLUTION

The pattern of graphical operations used in constructing solutions for the examples described in this paper was devised only after effort had been expended in attempting to apply other approaches. An explanation of the step-wise solution employed in connection with Equations (20) and (21) follows:

1. Consider the pipe line at some known conditions throughout its length. In the present case initial conditions corresponding to steady-state flow of 300 x 10^6 cu ft per day were chosen.
2. Permit the output flow to vary in accordance with the prescribed cycle and graphically construct a family of curves representing $\dot{V}'$ vs X for various arbitrarily chosen times. This step appears somewhat difficult, but in practice it may be accomplished crudely by using "intuitive guesses" to approximate the behavior of the system.
3. With the aid of Equation (21) compute $P^2 + 0.0001173\,P^3$ for several values of X. This may be accomplished by graphical integration of $\dot{V}'^{1.8540}$ with respect to X.
4. Plot curves representing the quantity $P + 0.000176\,P^2$ for the range in values of X. Graphical integration of these curves with respect to X will determine the total gas content of the pipe line at each of the arbitrarily chosen times adopted in Step 2.
5. Compute from the input and output flow rates the time corresponding to each curve in Steps 2 and 4 by correlating the cumulative difference in these flow rates with the net change in gas content of the pipe line.
6. Cross plot $P + 0.000176\,P^2$ with respect to time and differentiate the resulting curves with respect to time.
7. Compute $\frac{\partial \dot{V}'}{\partial X}$ with the aid of Equation (20) and integrate graphically plots of this quantity with respect to X so as to obtain a new set of relations between flow rate, position, and time.

The process beginning with Step 3 may now be repeated to obtain a second approximation. In this example the convergence was found to be sufficiently rapid so that only three iterations of the above-described steps were required to yield a substantial convergence. In this manner, starting from the assumed initial conditions, computations for the second example in this paper were carried through two complete cycles, corresponding to a period of 48 hr. It was found that the pressure distribution at the end of the first cycle did not differ significantly from that at the end of the second cycle. It was concluded, therefore, that the assumption of an arbitrary initial condition for the pipe line did not materially influence the behavior of the system after the first cycle.

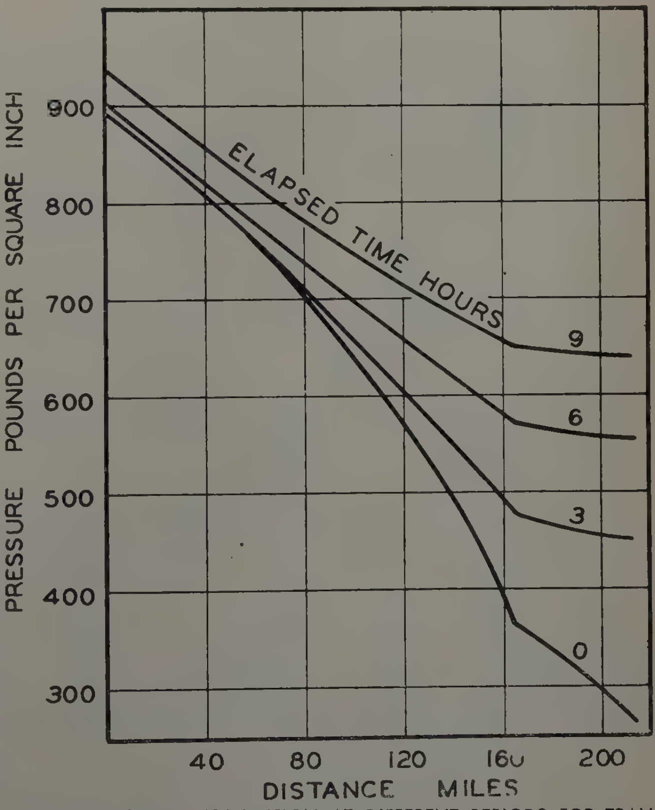

FIG. 9 — PRESSURE DISTRIBUTION AT DIFFERENT PERIODS FOR TRANSIENT CONDITIONS OF FLOW IN EXAMPLE B.

SUMMARY

The foregoing Examples A and B demonstrate the fashion in which the partial differential equations describing the conservation of momentum and material may be applied to the prediction of the pressure distribution in long pipe lines carrying gas under transient conditions. Example A considers a problem wherein the flow at the entrance to the pipe line is interrupted and the second predicts the cyclic pressure distribution to be anticipated in a gas transmission line with a constant input and a cyclic demand rate.

The graphical procedures outlined here for solving these problems may be expected to yield satisfactory results for wide variations in flow conditions, provided situations involving shock waves and supersonic flow do not arise.

ACKNOWLEDGMENT

The authors are grateful to The Stearns-Roger Manufacturing Co., to the Southern Counties Gas Co. of California, and to the Southern California Gas Co. for financial support in the study of Examples A and B, respectively. V. J. Berry assisted in the assembly of the manuscript.

NOMENCLATURE

A — cross-sectional area, sq ft
a — constant defined in Equation (10)
B — constant defined in Equation (7)
b — specific gas constant
c — constant defined in Equation (9)
d — diameter of pipe line, ft
f — friction factor
g — acceleration resulting from gravity, ft per sec per sec
$\dot{\underline{m}}$ — total weight rate of flow, lb per sec
n — exponent of Equation (9)
P — pressure, psi
T — thermodynamic temperature, °R
u — velocity, ft per sec
$\underline{V}$ — residual specific volume, cu ft/lb
$\dot{V}'$ — volumetric flow rate, cu ft x 10^6 per 24 hr
V — specific volume, cu ft/lb
X — distance along pipe line, ft
X' — distance along pipe line, miles
τ — shear at boundary of flowing stream, lb per sq ft
θ — time, sec
θ' — time, hr
σ — specific weight, lb per cu ft
ln — natural logarithm
log — Briggs' logarithm
Re — Reynolds number

REFERENCES

1. Rouse, H.: *Fluid Mechanics for Hydraulic Engineers*, McGraw-Hill, (1938).
2. Binder, R. C.: *Chem. and Met. Eng.*, (1944), **51**, 99.
3. Bonilla, C. F.: *Ind. Eng. Chem.*, (1939), **31**, 618.
4. Ruth, B. F.: *Ind. Eng. Chem.*, (1939), **31**, 985.
5. Palsgrove, G. K.: *Rensselaer Polytechnic Instit. Bull.*, (1932), No. 37.
6. Kuo, Y. H.: *Jour. Math. and Phys.*, (1943), **22**, 13.
7. Fry, T. C.: *Elementary Differential Equations*, D. Van Nostrand, (1929).
8. Muskat, M., and Wyckoff, R. D.: *The Flow of Homogeneous Fluids Through Porous Media*, McGraw-Hill, (1937).
9. Hurst, W.: *Physics*, (1934), **5**, 20.
10. Hetherington, C. R., MacRoberts, D. T., and Huntington, R. L.: *Trans.* AIME, (1942), **146**, 166.
11. Joffe, J.: *Chem. Eng.*, (Nov., 1949), **56**, 112.
12. Joffe, J.: *Chem. Eng.*, (Aug., 1949), **56**, 130.
13. McCann, G. D., Wilts, C. H., and Locanthi, B. N.: *Proc. Inst. Radio Engrs. Trans.*, (1949), **37**, 954.
14. Scarborough, J. B.: *Numerical Mathematical Analysis*, The Johns Hopkins Press, (1930).
15. Southwell, R. V.: *Relaxation Methods in Engineering Science*, Oxford University Press, (1940).
16. Southwell, R. V.: *Relaxation Methods in Theoretical Physics*, Oxford University Press, (1946).
17. Daugherty, R. L.: *Hydraulics*, McGraw-Hill, (1937).
18. Pigott, R. J. S.: *Mech. Eng.*, (1933), **55**, 497.
19. Nikuradse, J.: *VDI*, Forschungsheft 356 (1932).
20. Sage, B. H., and Lacey, W. N.: *Trans.* AIME, (1938), **127**, 118.

★ ★ ★

T.P. 3082

PHASE EQUILIBRIA IN HYDROCARBON-WATER SYSTEMS

III—The Solubility of Methane in Water at Pressures to 10,000 PSIA

O. L. CULBERSON, GULF RESEARCH AND DEVELOPMENT CORP., HARMARVILLE, PA., AND **J. J. McKETTA, JR.,** MEMBER AIME, DEPARTMENT OF CHEMICAL ENGINEERING, THE UNIVERSITY OF TEXAS, AUSTIN, TEX.

ABSTRACT

Experimental and smoothed data are presented for the solubility of methane in water for temperatures of 77, 100, 160, 220, 280, and 340°F at pressures to 10,000 psia.

The minimum solubility phenomenon exists within this temperature range to pressures of 10,000 psia.

INTRODUCTION

The study of hydrocarbon-water systems has been extended to the determination of the solubility of methane in water at pressures to 10,000 psia. The experimental apparatus, and the technique, are the same as that previously reported.[1,2]

In the determination of the solubility of methane in water, only two phases were present at temperatures between 100 and 340°F, these being the vapor phase and the water-rich liquid phase. The determinations involved the agitation of methane and water in an equilibrium cell, withdrawal of a sample from the liquid phase, and the analysis of the sample. The experimental values determined in this manner are presented in Table I and in Fig. 1.

Since experimental and analytical techniques have improved since the initial experiments with this equipment, it was decided to repeat the 77°F isotherm determinations.[2] Fig. 1 shows that the individual results for this isotherm are much

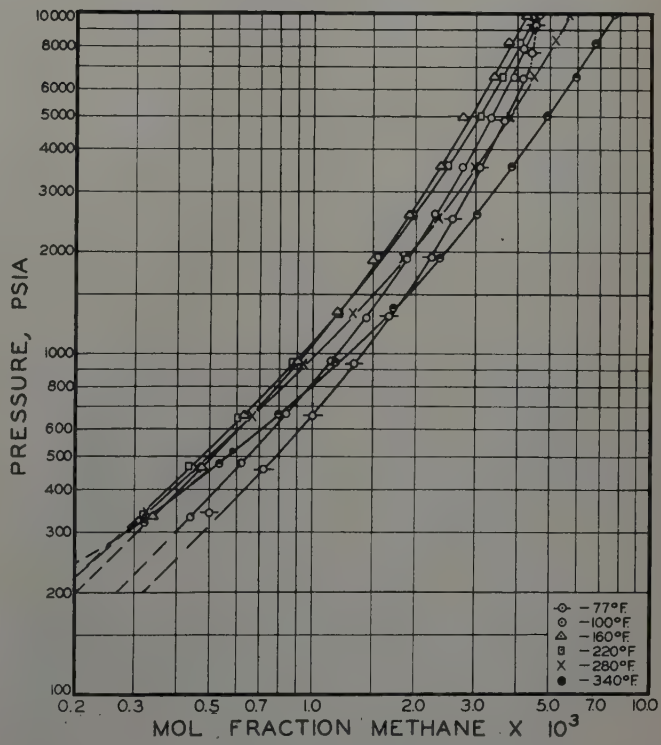

FIG. 1 — SOLUBILITY OF METHANE IN WATER AT CONSTANT TEMPERATURE.

---

[1] References given at end of paper.

Manuscript received in the office of the Petroleum Branch Nov. 16, 1950.

Table I — Experimental Values for the Solubility of Methane in Water
Pressure: Lb/Sq In. Abs (psia) Solubility: Mol Fraction CH_4

77°F		100°F		160°F		220°F		280°F		340°F	
psia	*MF* CH_4	psia	*MF* CH_4	psia	*MF* CH_4	psia	*MF* CH_4	psia	*MF* CH_4	psia	*MF* CH_4
341	0.000497	330	0.000440	331	0.000340	333	0.000323	336	0.000326	323	0.000323
459	0.000717	477	0.000619	467	0.000470	466	0.000432	464	0.000460	475	0.000535
659	0.001000	664	0.000839	659	0.000632	468	0.000472	654	0.000673	662	0.000789
934	0.001317	950	0.001123	943	0.000909	652	0.000611	941	0.000938	949	0.001150
1290	0.001678	1270	0.001440	1320	0.001183	945	0.000886	1310	0.001326	1360	0.001725
1930	0.002235	1900	0.001890	1880	0.001500	1310	0.001188	1900	0.001857	1920	0.002355
2495	0.002585	2575	0.002290	2555	0.001924	1900	0.001560	2480	0.002346	2580	0.003025
3515	0.003110	3535	0.002760	3535	0.002385	2535	0.001980	3555	0.003015	3580	0.003835
4810	0.003660	4910	0.003330	4925	0.002770	3570	0.002510	4975	0.003805	5045	0.004875
6440	0.004170	6525	0.00391	6525	0.00342	4965	0.00314	6525	0.00449	6525	0.00595
7795	(0.004370)	7870	0.00417	8220	0.00375	6525	0.00361	8270	0.00518	8210	0.00680
9300	(0.004450)	9895	0.00465	9865	0.00424	8190	0.00408	9835	0.00574	9995	0.00775
						9875	0.00451				

more nearly consistent than the data previously reported.[2] In Table I the data for the 77°F isotherm are in parentheses for pressures above 6,800 psia. These parenthetical values are non-equilibrium solubilities determined when the liquid phase co-existed with vapor and hydrate phases. The original purpose of this investigation was the study of vapor-liquid equilibrium. For those pressures at which the hydrate formed, samples of the liquid phase nevertheless were taken. However, the attainment of equilibrium in hydrate systems is a slow tedious process,[4] and the parenthetical values are therefore the solubilities measured before the hydrocarbon in the vapor phase had been completely transposed to the hydrate phase.

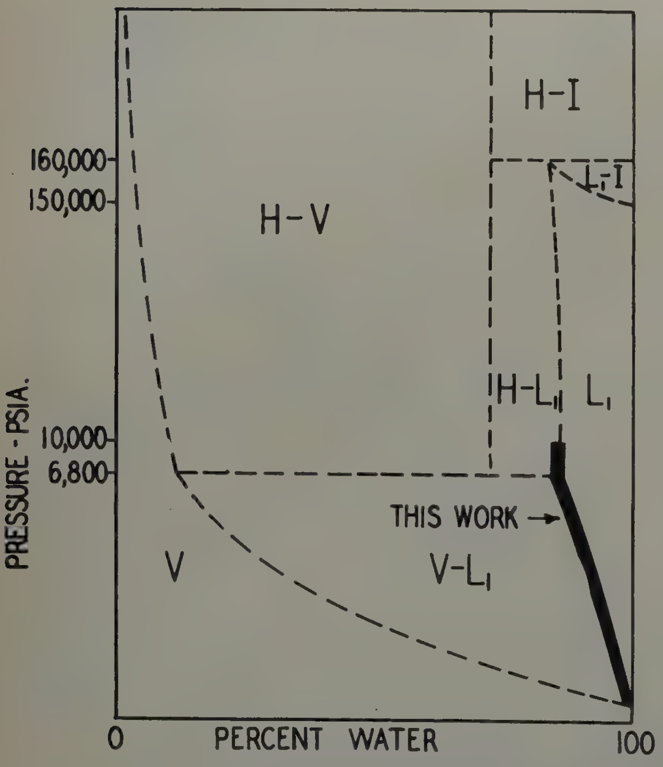

FIG. 2 — SCHEMATIC P-X DIAGRAM OF THE METHANE-WATER SYSTEM AT 77°F.

Kobayashi and Katz[6] reported the co-existence of vapor, hydrate, and liquid at 6,800 psia and 77°F; they also have presented a schematic P-T diagram of the methane-water system. Fig. 2 was prepared from this P-T diagram and shows a schematic P-X diagram of the methane-water system at 77°F. The heavy solid line indicates the location of the present work and illustrates clearly the solid hydrate-liquid water phase equilibria above 6,800 psia at 77°F. Because the equilibrium cell used in this investigation was not equipped with observation ports, the hydrate formation was noted by the anomalous behavior of the cell contents as compared with vapor-liquid equilibria.[4]

The smoothed values for the solubility of methane in water are given in Table II. The solubilities at 200 psia were obtained by interpolation between the authors' data and that of Winkler[7] at one atmosphere.

Fig. 3 is the temperature-solubility diagram for the methane-water system based upon the smoothed values. The exhibition of the minimum solubility phenomenon persists strongly at pressures to 10,000 psia. Comparison with the T-X diagram for the ethane-water system[1] shows that the minimum solubilities occur over about the same range of temperatures for the two systems. This would not necessarily have been expected, since the temperatures are very near to the critical of ethane and considerably removed from that of methane. Evidently the critical properties of the solute do not constitute a good basis for correlating solubility. As was discussed regarding the ethane-water system, for the higher pressures the methane-water system also shows the probability of a maximum solubility following the minimum solubility as the temperature is increased.

Comparison of the methane-water system with the ethane-water[1] and a natural gas-water[3] system is made in Fig. 4. At low pressures, the solubilities of the ethane and the methane are very nearly the same, the solubility of the methane being slightly greater at 500 psia. As the pressure increases, the solubility of the methane increases more than that of the ethane so that at 10,000 psia the solubility of the methane is more than twice that of the ethane. However, at one atmosphere the solubility of the ethane is 30 per cent greater than that of the methane.[7] The natural gas-water system shown contained in part 88.51 per cent methane and 6.02 per cent ethane. Fig. 4 indicates that for the range of pressures shown the hydrocarbons are not additively soluble in the water independent of each other. If they were, the solubility of the natural gas should be the sum of that of the two hydrocarbons plus an allowance for the other hydrocarbons in the gas. Since the solubilities of the heavier hydrocarbons are as yet unknown, it cannot be determined whether or not the solubilities are additive on the basis of the composition of the solute gas. Some work on this basis in which the solubilities of the heavier hydrocarbons were extrapolated from those of the methane and ethane indicated that the solubility of a mixture is not additive on the composition basis. Such solubility extrapolations are hazardous, even within a given system; however, the effect of the solute's being a mixture of gases is noticeable. At the lower pressures, the solubility of the natural gas is greater than that of the pure methane. Since the ethane is, and the other hydrocarbons may be, nearly as soluble as the methane at low pressures, their presence increases the solubility of the natural gas to a value greater than that of the pure methane. At the higher pressures their relatively small solubility in comparison to methane decreases the solubility of the natural gas below that of the methane. The solubility is therefore an additive function; but until more data are available, the exact nature of that function cannot be determined.

It is often convenient in the oil or natural gas industries to have gas-liquid solubility data expressed in cubic feet of gas

Table II — Smoothed Values for the Solubility of Methane in Water in the Vapor-Liquid Region

Pressure psia	Mole Fraction $CH_4 \times 10^3$ 77°F	100°F	160°F	220°F	280°F	340°F
200	0.329	0.273	0.203	0.188	0.165	0.131
400	0.640	0.528	0.407	0.383	0.388	0.428
600	0.925	0.760	0.599	0.572	0.607	0.699
800	1.170	0.986	0.780	0.752	0.811	0.960
1000	1.380	1.199	0.945	0.930	1.016	1.230
1250	1.629	1.425	1.133	1.148	1.272	1.569
1500	1.862	1.620	1.308	1.339	1.521	1.895
2000	2.263	1.953	1.608	1.662	1.980	2.456
2500	2.588	2.247	1.861	1.961	2.359	2.945
3000	2.868	2.503	2.094	2.233	2.678	3.373
3500	3.110	2.738	2.309	2.478	2.984	3.770
4000	3.332	2.962	2.516	2.701	3.279	4.148
5000	3.724	3.360	2.888	3.100	3.815	4.849
6000	4.041	3.701	3.221	3.447	4.272	5.500
7000	4.312*	3.987	3.519	3.757	4.685	6.108
8000	....	4.236	3.782	4.034	5.070	6.687
9000	....	4.461	4.007	4.296	5.441	7.238
10000	....	4.670	4.211	4.538	5.793	7.750
14.7	0.0186**	0.0010**				

*Hydrate-Vapor-Liquid Equilibrium at 6800 psia.
**Winkler[7]

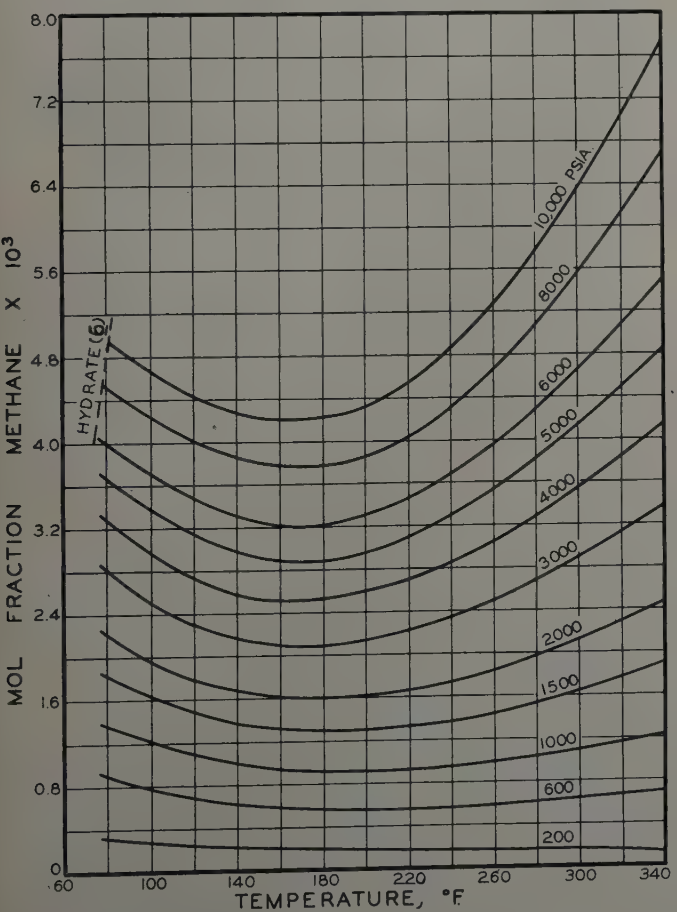

FIG. 3 — SOLUBILITY OF METHANE IN WATER AT CONSTANT PRESSURE.

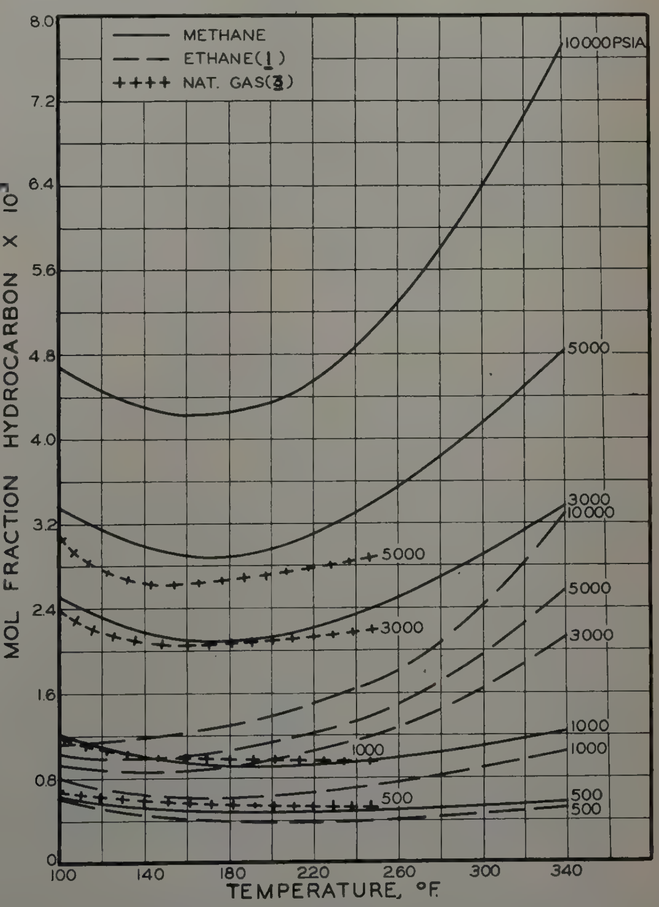

FIG. 4—COMPARISON OF SOLUBILITIES OF HYDROCARBONS IN WATER.

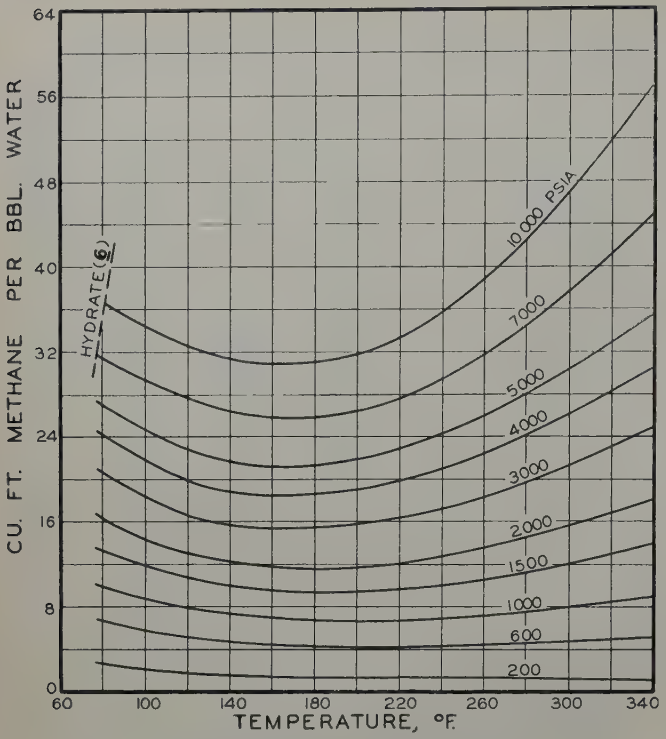

FIG. 5 — VOLUMETRIC SOLUBILITY OF METHANE IN WATER.

per barrel (42 gal) of liquid. This has been done in Fig. 5. The volume of methane is referred to 60°F and 14.7 psia. The curves for the various pressures have the same characteristics as those of Fig. 3, since the data for Fig. 3 were multiplied by 7,370 to obtain the data for Fig. 5. In both Figs. 3 and 5 the hydrate region is indicated on the basis of observations of the authors, but primarily upon the work of Kobayashi and Katz.[6]

MATERIALS

The water used was distilled, and deaerated by boiling before use. The methane used had the following composition as analyzed by the Gulf Oil Corp.: nitrogen, 0.27 per cent; carbon dioxide, 0.21 per cent; methane, 98.72 per cent; ethane, 0.60 per cent; propane, 0.13 per cent; butanes plus, 0.07 per cent.

ACKNOWLEDGMENT

The writers wish to express their appreciation to the Gulf Oil Corp. for extending the Gulf Oil Fellowship to Culberson for this investigation. The Phillips Petroleum Co. generously supplied the pure grade methane used in this work.

REFERENCES

1. Culberson, O. L., and McKetta, J. J.: *Trans.* AIME (1950) **189,** 319.
2. Culberson, O. L., Horn, A. B., and McKetta, J. J.: *Trans.* AIME (1950) **189,** 1
3. Dodson and Standing: API *Drill. and Prod. Prac.* (1944) 173.
4. Frost and Deaton: *Oil and Gas Jour.* (1944) **45,** No. 12, 170-8.
5. Katz, D. L.: Texas A&M *Eng. Exp. Sta. Bulletin 114* (1949) 30.
6. Kobayashi and Katz, D. L.: *Trans.* AIME, T.P. 2579 (March, 1949).
7. Winkler: *Z. physik. Chem.* (1899) **9,** 171.

★ ★ ★

T.P. 3145

RELAXATION METHODS APPLIED TO OIL FIELD RESEARCH

H. DYKSTRA AND **R. L. PARSONS**, MEMBERS AIME, CALIFORNIA RESEARCH CORP., LA HABRA, CALIF.

ABSTRACT

A numerical method for solving partial differential equations in steady state fluid flow is described. This method, known as the "relaxation method," has two advantages over analytical methods: (1) practically any problem can be solved, and (2) a solution can be obtained quickly. A disadvantage is that the solution is not general. The method is applied to core analysis and relative permeability measurement to calculate constriction effects and to calculate the true pressure drop measured by a center tap in a Hassler type relative permeability apparatus. Further applications are suggested.

INTRODUCTION

Many problems in fluid flow cannot be solved analytically because of the nature of the boundary conditions. For many problems, however, an exact answer is not necessary because boundary conditions are not exactly defined or the parameters describing the porous medium are not accurately known. The relaxation method can be used to obtain an approximate answer easily and quickly for the flow of incompressible fluids in porous media. The method can also be used for other types of problems, such as determining the stress in a shaft under load, or the temperature distribution during steady state heat flow. In this discussion only calculations concerned with the flow of fluids in porous media will be considered. The method was introduced by R. V. Southwell in 1935.[1]

THEORY

The treatment given here follows that given by Emmons.[2] Consider a porous medium to be replaced entirely by a net of tubes of equal length and uniform cross-sectional area as shown in part in Fig. 1. Assume that the net of tubes behaves exactly like the porous medium which it replaces; that is, the net can be made fine enough to reproduce exactly the porous medium. Assume also that Darcy's Law can be used to calculate the flow from one point to another point through these tubes. The flow from point 1 to point 0 is

$$Q_{1\text{-}o} = \frac{KA}{\mu a}(P_1 - P_o) \quad \ldots\ldots\ldots \quad (1)$$

where a is the distance between points; K is the "permeability" of a tube; A is the cross-sectional area of a tube; μ is the viscosity of the liquid in the porous medium; and $(P_1 - P_o)$ is the pressure difference between point 1 and point 0. In like manner the flow can be calculated from points 2, 3, and 4 to point 0. The net flow into point 0 is

$$Q_o = \frac{KA}{\mu a}(P_1 + P_2 + P_3 + P_4 - 4P_o) \quad \ldots \quad (2)$$

For an incompressible fluid the net flow into point 0 will be zero or, $Q_o = 0$. This says that at point 0 fluid is neither being accumulated nor depleted. Therefore,

$$P_1 + P_2 + P_3 + P_4 - 4P_o = 0 \quad \ldots\ldots \quad (3)^*$$

If, now, with specified boundary conditions, the pressure is known at a finite number of points in a given region, as at the points shown in Fig. 1, Equation (3) will be satisfied at every point. If, on the other hand, the pressure is not known, the pressure can be guessed at these points. Then, unless the guess is perfect, Equation (3) will not be satisfied at all of the points.

When Equation (3) is not satisfied, let

$$\delta = P_1 + P_2 + P_3 + P_4 - 4P_o \quad \ldots\ldots \quad (4)$$

where δ is an apparent error and is called the residual at point 0. Equation (4) shows how much the pressure guess is in error at point 0 with respect to the surrounding points. A positive residual means that the pressure is too low, and a negative residual means that the pressure is too high.

To bring the residual, δ, to zero in order to satisfy Equation (3), it is necessary to make changes in the pressure guesses. Equation (4) shows that a $+1$ change in P_o will change the residual at point 0 by -4. A $+1$ change in the pressure at any of the four surrounding points will change the residual at point 0 by $+1$. Thus it can be seen that a change at any point will affect the residual at that point and the four surrounding points. By changing the pressure from point to point, all of the residuals can eventually be brought nearly to zero and the problem will be solved. This procedure is the essence of relaxation methods and is used to relax the residuals so that Equation (3) is satisfied at every point.

The procedure can be most easily explained in detail by solving a simple problem. As Southwell says, "To explain every detail of a practical technique is to risk an appearance of complexity and difficulty which may repel the reader. A

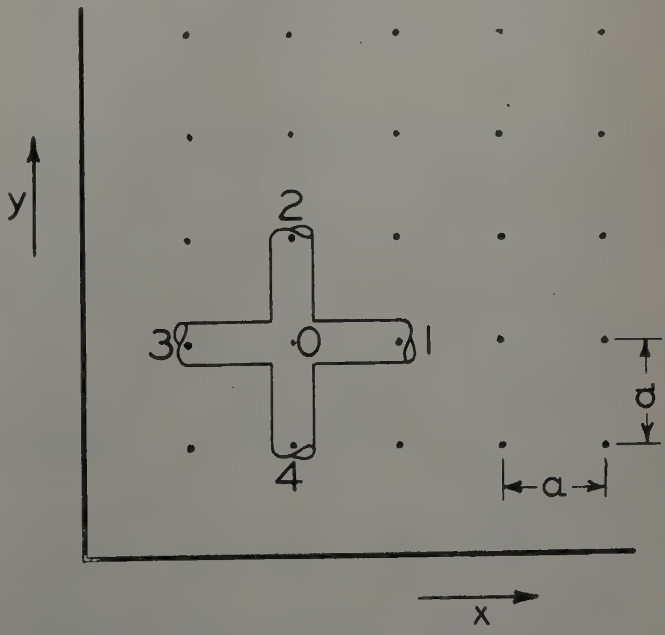

FIG. 1 — REPRESENTATION OF A POROUS MEDIUM BY A NETWORK OF CONDUCTING TUBES.

---

[1] References given at end of paper.

Manuscript received in the office of the Petroleum Branch September 10, 1950. Paper presented at the Petroleum Branch Fall Meeting in Los Angeles, Calif., Oct. 12-13, 1950.

*In the Appendix Equation (3) is shown to be approximately equivalent to Laplace's equation.

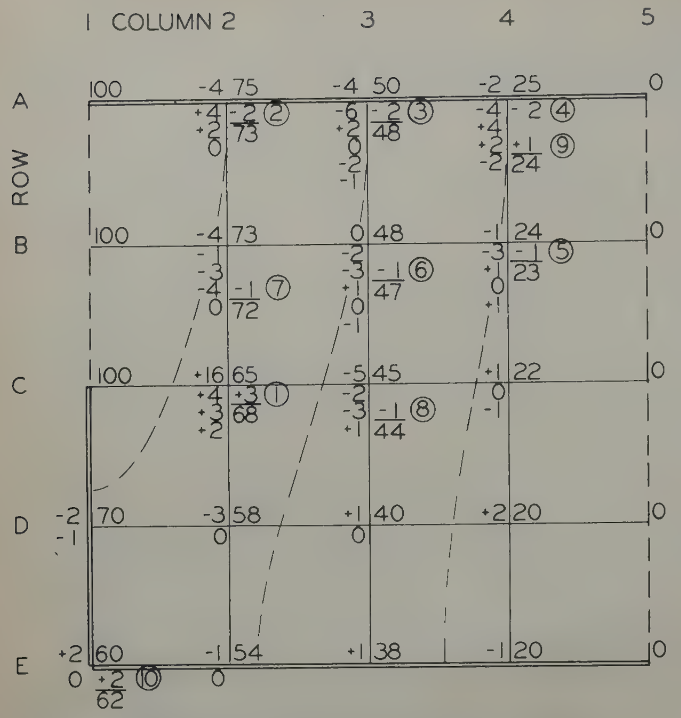

FIG. 2a — APPROXIMATE SOLUTION OF A TWO DIMENSIONAL FLOW PROBLEM WITH THE LEFT FACE PARTLY OBSTRUCTED.

verbal description of the tying of a 'reef knot' would make that simple operation appear quite formidable."

APPLICATIONS

Two-Dimensional Fluid Flow

The first problem that will be solved is a two-dimensional fluid flow problem as shown in Fig. 2a. The upper and lower boundaries are impermeable, and the lower half of the left face of the porous medium is also impermeable. Pressure is applied to the left face, and the flow per unit K/μ and per unit thickness of the porous medium is to be calculated. In order to calculate the flow, it is only necessary to know the average pressure over any plane surface parallel to the right boundary.[3]

The problem is laid out to scale with sufficient room to make the calculations as shown in Fig. 2a. A square grid, known as a relaxation pattern, is laid out on the drawing. A coarse net (few points) is used first. The known pressures, which for this problem are the pressure on the right face, 0, and the pressure on the upper half of the left face, 100, are written in just above and to the right of the point to which they refer. Dimensionless pressures are used. Equipotential lines are sketched in to the best of the calculator's ability. The pressure is then guessed at each point. Fig. 2a shows the equipotential lines and the guesses. Residuals are calculated for each point not on the impermeable boundaries according to Equation (4) and are placed to the left of the pressure guesses. If the pressure is known exactly for a particular point, for example, on the inflow boundary in Fig. 2a, then that point has no residual.

Residuals at the boundaries can be calculated in two ways. Both ways are illustrated in the solution of this problem. For the upper boundary the image of the plane below the upper boundary is mapped onto the plane above the upper boundary. This mapping in no way changes the problem because the upper impermeable boundary which is a streamline remains a streamline when the lower plane is folded 180° onto the upper plane. Equation (4) becomes

$$\delta = P_1 + P_3 + 2P_4 - 4P_0 \quad \text{(4a)*}$$

because $P_2 = P_4$. Equation (4a) is now used to calculate the residuals on the upper boundary. The above method for calculating residuals is preferred because all residuals can then be directly compared.

The second method of calculating residuals is illustrated for the lower boundary and the boundary on the left side where the residuals are obtained by assuming that the tube along the impermeable boundary has one-half the area of the tubes connecting the points inside the boundaries. The flow from point 1 to point 0 on the lower boundary is then

$$Q_{1\text{-}0} = \frac{1}{2}\,\frac{KA}{\mu a}\,(P_1 - P_0) \quad \text{(1a)}$$

and similarly for flow from point 3. Equation (2) for the net flow into point 0 on the lower boundary becomes

$$Q_0 = \frac{KA}{\mu a}\left(\frac{1}{2}P_1 + P_2 + \frac{1}{2}P_3 - 2P_0\right) = 0 \quad \text{(2a)}$$

so that the equation for calculating residuals along the lower boundary is

$$\delta = \frac{1}{2}P_1 + P_2 + \frac{1}{2}P_3 - 2P_0 \quad \text{(4b)}$$

For points along the left boundary the equation is

$$\delta = P_1 + \frac{1}{2}P_2 + \frac{1}{2}P_4 - 2P_0 \quad \text{(4c)}$$

and for the corner point

$$\delta = \frac{1}{2}P_1 + \frac{1}{2}P_2 - P_0 \quad \text{(4d)}$$

Equations (4b), (4c), and (4d) are now used to calculate the residuals at points on the lower boundary and on the left boundary. The problem now has been set up with the pressure estimates and the calculated residuals.

To relax** the residuals, one begins by changing the largest residual first. If a residual is surrounded by residuals of the same sign, the correction is usually made large enough to change the sign of the residual but to leave its magnitude about the same. This is called "over-relaxing." If a residual is surrounded by residuals of opposite sign, the correction is usually less than that required to bring the residual to zero.

In Fig. 2a the largest residual is at point *C-2* (row *C*, column *2*); therefore, this residual was changed first. The order in which the residuals were changed is given by the circled numbers. Because the residual at point *C-2* is surrounded by residuals of opposite sign, a correction of +3 (instead of +4) is placed under the pressure estimate, which adds –12 to the residual at the point (making the residual +4) and adds +3 to each of the surrounding residuals. The new residuals are placed under the old residuals, the addition being made mentally. The second change is made at point *A-2*. Here a correction of –2 is placed under the pressure estimate, which changes the residual by +8 and adds –2 to the residual on the right and to the residual below.

Relaxation thus proceeds from point to point until all of the residuals have been relaxed to a minimum. After relaxation is complete, the corrections are added to the original pressure guess. It will be noted that the original pressure guess is not changed during the relaxation procedure. Only after relaxation is complete are the corrections added to the original guess. The solution is shown in Fig. 2a.

The flow through the section without the impermeable boundary at the left side is

---

*Note that the subscripts refer to the exact arrangement of the points shown in Fig. 1. Point 0 does not refer to a specific point but refers to any point in the relaxation pattern.

**The grid with the original guesses, some or all of which are in error, may be thought of as being under a strain. The process of solution is one of relaxing these strains nearly to zero.

$$Q = \frac{KA\triangle P}{\mu L} = \frac{100KA}{\mu L}$$

The flow through the constricted section is calculated from the average pressure drop between the right hand side and the first line of points. The average pressure along the first line of points is 21.7. The flow through the constricted section then is

$$Q = \frac{21.7\ KA}{\mu \frac{L}{4}} = \frac{86.8\ KA}{\mu L}$$

so that the ratio of constricted flow to unconstricted flow is

$$\frac{Q_c}{Q} = \frac{86.8}{100} = 0.868$$

A more exact answer can be obtained by advancing to a finer mesh and increasing the number of points. An additional calculation was made with points placed in the center of the grid squares of Fig. 2a. The new grid lines connecting the points on the finer net are not parallel, but are at an angle of 45° to the grid lines connecting the points on the coarse net used first. The relaxation procedure, however, is carried out in the same manner. The results of the calculations are shown in Fig. 2b. The average pressure across the same plane as used for calculating the results from Fig. 2a is 21.0. The ratio of constricted flow to unconstricted flow is therefore

$$\frac{Q_c}{Q} = 0.84$$

The exact answer calculated analytically is 0.820.

The time required to obtain the two solutions by one experienced in relaxation methods is approximately as follows:

1. To set up the problem, sketch in the streamlines, and guess the pressures — 15 minutes.
2. To calculate and relax the residuals — 20 minutes.
3. To check for errors and calculate the answer — 10 minutes.
4. To set up the problem on a finer net and to calculate and relax the residuals again — 30 minutes.
5. To check for errors and calculate the answer — 15 minutes.

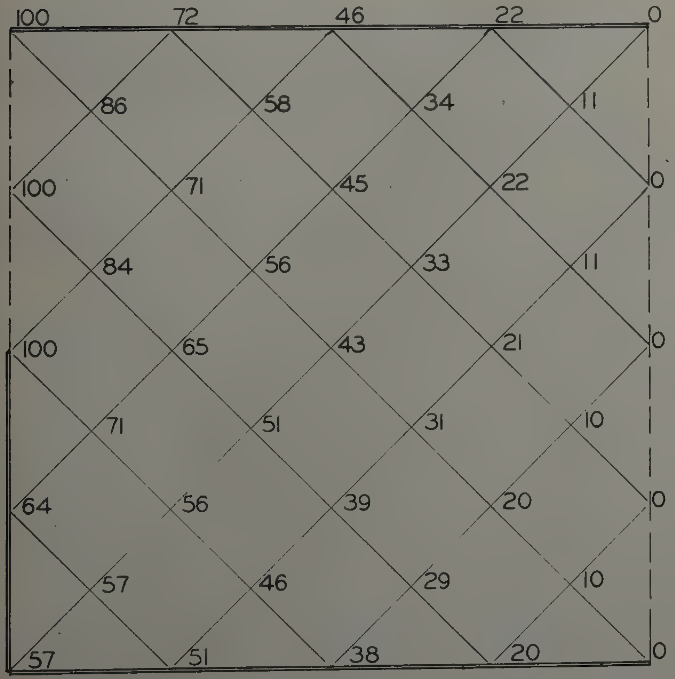

FIG. 2b — ADVANCE TO A FINER NET FOR THE PROBLEM ILLUSTRATED IN FIG. 2a.

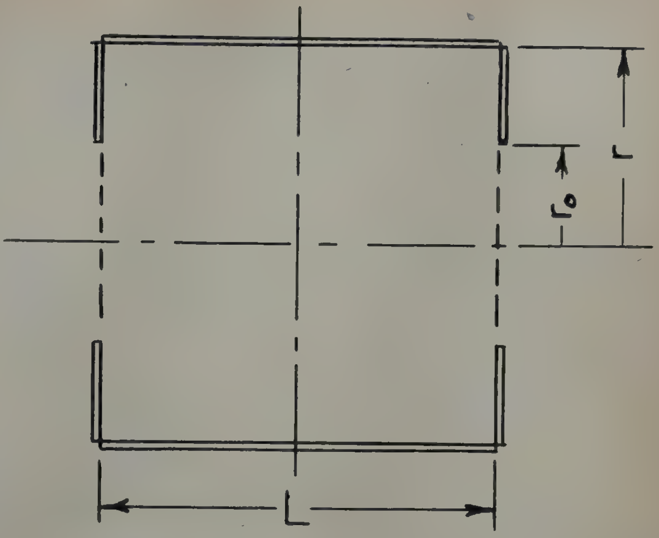

FIG. 3 — EXAMPLE OF THREE DIMENSIONAL FLOW WITH AXIAL SYMMETRY.

The time required to obtain an answer on the coarser mesh was 45 minutes, and on the finer mesh, 45 minutes. The total time required to obtain an answer within three per cent was 90 minutes. The time required to set up the problem and to sketch in the equipotential lines as accurately as possible is usually well spent. A poor guess could easily double the time required to relax the residuals.

Three-Dimensional Flow with Axial Symmetry

An example of three-dimensional flow is shown in Fig. 3, where a cylindrical core has its two faces partially obstructed so that axial symmetry is preserved. This problem may be solved in two dimensions on a plane through the axis of the core, but the relaxation equations will be different than those for the previous example. Only one-quarter of the section through the axis is used because of symmetry.

From the relaxation equation derived in the Appendix, the following equation is obtained for calculating the residuals for this example

$$\delta = P_1 + P_2 + P_3 + P_4 - 4P_o + \frac{1}{2n}(P_2 - P_4) \quad . \quad . \quad (5)$$

where P_o is in the n'th row from the axis of the cylindrical core, as shown in Fig. 4. Equation (5) is the same as Equation (4) with the added terms $\frac{1}{2n}(P_2 - P_4)$. This means that the residuals are calculated in the same manner as for the two-dimensional problem but with the above term added to each residual.

Equation (5) can be rewritten as

$$\delta = P_1 + \left(1 + \frac{1}{2n}\right)P_2 + P_3 + \left(1 - \frac{1}{2n}\right)P_4 - 4P_o \,. \quad (5a)$$

This equation shows that a change in P_2 will affect the residual at point 0 by $\left(1 + \frac{1}{2n}\right)$ times the change in P_2 and a change in P_4 will affect the residual at point 0 by $\left(1 - \frac{1}{2n}\right)$ times the change in P_4. The relaxation equation for points on the center line is

$$\delta = P_1 + 4P_2 + P_3 - 6P_o \quad . \quad . \quad . \quad . \quad . \quad . \quad . \quad (5b)$$

The solution of a problem where $L = 2r$ and $r_o = \frac{3}{4}r$ is given in Fig. 5. The average pressure on the first line of points

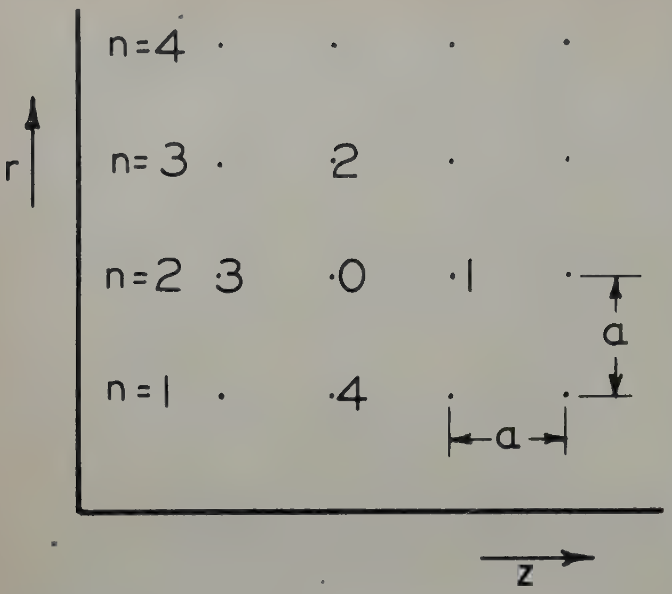

FIG. 4 — REPRESENTATION OF THREE DIMENSIONAL FLOW WITH AXIAL SYMMETRY.

from the right side is 117. For an unconstricted core the pressure would be 125. The ratio of constricted flow to unconstricted flow is therefore

$$\frac{Q_c}{Q} = \frac{117}{125} = 0.935$$

For this problem a more exact answer was obtained by using a finer net. A coarse net was used first. After the pressure was determined for each of the points on the coarse net, interpolation gave the pressures at intermediate points on the finer net. Residuals were calculated for the points on the finer net and were relaxed again to obtain the final solution.

Advancing to a finer net to get a more exact answer does not require a finer net over the whole region.[1] Usually a finer net is placed only in a region of high potential gradient. With additional points placed on only part of the region, a great deal of labor can be saved during the solution of a problem. The answer obtained is just as accurate as an answer obtained by using the finer net over the whole region.

FURTHER APPLICATIONS

Core Analysis

The example worked out in the previous section can be extended to calculate the ratio of constricted flow as a function of the open per cent area of the core face. Two additional calculations were made and the results are shown in Fig. 6. The calculated per cent constricted flow is not exact because a fine enough mesh was not used. However, the results are believed to be within three per cent of the exact ratio.

The curve of Fig. 6 can be used to determine the constriction to flow when a core face is partly covered by a porous plate that is symmetrically placed with respect to the axis. Such a setup is used in some types of relative permeability measurements. Homogeneous permeability is assumed and the diameter of the core is equal to its length. The results can also be applied to determine the effect of partly covering a core face with wax during routine permeability measurements of cores.

Another application of relaxation methods is found in relative permeability work where the pressure in the wetting phase is measured by center taps whose permeability is usually the same as the permeability of the porous end plates. Calculations were made by relaxation methods to obtain the true pressure drop as a function of the ratio of the permeability of the porous end plate to the permeability of the core. The schematic diagram and results of the calculations are shown in Fig. 7.

The problem was solved with the following conditions and assumptions:

1. Core diameter equals core length.
2. A particular end plate configuration is used as shown in Fig. 7.
3. The core has homogeneous permeability.
4. Infinitesimal thickness of paste for capillary contact is used between core and plate.
5. Fluid connection between end plate and center tap is through the core only.

Only if all these assumptions are true can the pressure correction given in Fig. 7 be applied quantitatively for the relative permeability setup used. However, pressure corrections can be calculated for any ratio of core length to core diameter and any end plate configuration. For assumptions different than those given in Items 3, 4, and 5, only qualitative statements can be made. If a core contains bedding planes parallel to the axis of the core, and if permeability perpendicular to the bedding plane is much less than the permeability parallel to the bedding plane, the pressure correction will be greater than that given in Fig. 7. If a finite thickness of paste with a conductivity greater than that of the porous end plate is used for capillary contact, the correction will be less than that given in Fig. 7.

Nonisotropic Permeability

Problems involving nonisotropic permeability can also be handled by relaxation methods. Referring to Equation (1) and Fig. 1, let the permeability in the x-direction be m times the permeability in the y-direction, or

$$K_x = mK_y$$

The net flow into point 0 will be

$$Q_o = \frac{mK_yA}{\mu a}(P_1 - P_o) + \frac{K_yA}{\mu a}(P_2 - P_o) + \frac{mK_yA}{\mu a}(P_3 - P_o) + \frac{K_yA}{\mu a}(P_4 - P_o) \quad . \ . \ . \quad (6)$$

or

$$Q_o = mP_1 + P_2 + mP_3 + P_4 - 2(1 + m)P_o = 0 \quad (7)$$

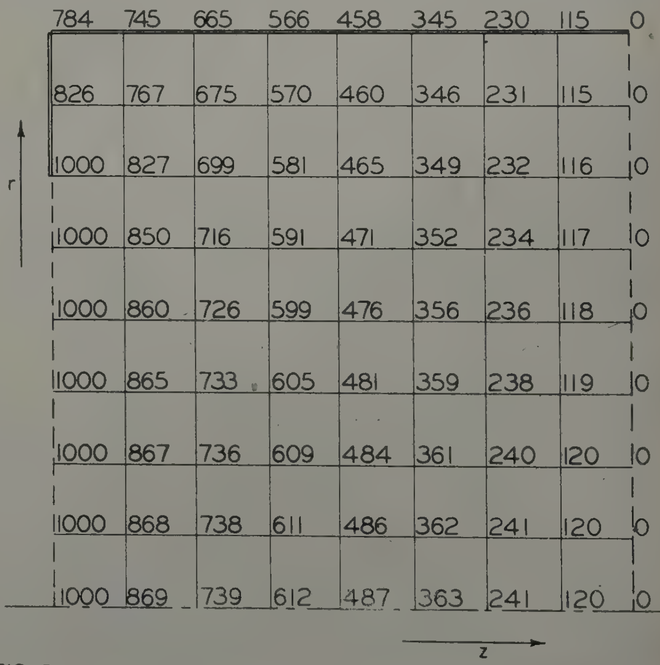

784	745	665	566	458	345	230	115	0
826	767	675	570	460	346	231	115	0
1000	827	699	581	465	349	232	116	0
1000	850	716	591	471	352	234	117	0
1000	860	726	599	476	356	236	118	0
1000	865	733	605	481	359	238	119	0
1000	867	736	609	484	361	240	120	0
1000	868	738	611	486	362	241	120	0
1000	869	739	612	487	363	241	120	0

FIG. 5 — APPROXIMATE SOLUTION TO PROBLEM ILLUSTRATED IN FIG. 3.

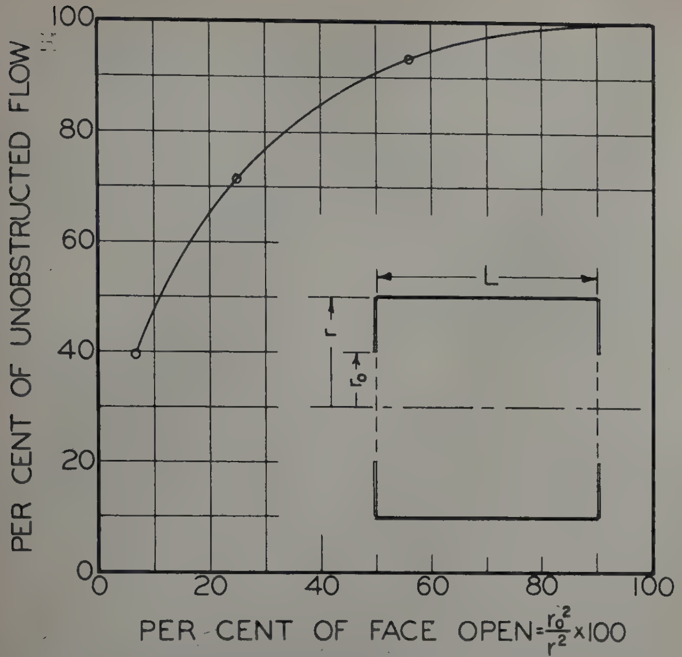

FIG. 6 — PER CENT OF UNOBSTRUCTED FLOW AS FUNCTION OF THE PER CENT OF FACE OPEN FOR CYLINDRICAL CORE WHOSE FACES ARE SYMMETRICALLY OBSTRUCTED.

so that the equation for calculating residuals becomes

$$\delta = mP_1 + P_2 + mP_3 + P_4 - 2(1+m)P_o \quad . \; . \quad (8)$$

Other types of inhomogeneity can also be handled by the proper substitution for K in Equation (1).

SUMMARY

Relaxation methods have many applications in oil field research. They not only can be used to obtain solutions for problems in fluid flow, but can be used to obtain a solution to almost any potential problem, such as the potential distribution between two or more electrodes, or the temperature distribution in steady state heat flow.

In conclusion, the steps required to obtain a solution are briefly summarized as follows:

1. Draw to scale the region for which the pressure distribution is desired. Make the drawing large enough to leave plenty of space for relaxing the residuals.
2. Place a square grid system, or relaxation pattern, on the drawing. Use a coarse net for the first approximation.
3. Place the known pressure points on the drawing.
4. Sketch in equipotential lines as accurately as possible.
5. Guess the pressures at the remaining points.
6. Determine the relaxation equations and calculate the residual at each point.
7. Relax the residuals starting with the largest residual first. In general, when a change of one-half makes the surrounding residuals larger, the residuals have reached a practical minimum.
8. If a residual is surrounded by residuals of the same sign, make the correction large enough to change the sign of the residual but to leave its magnitude about the same. This is known as "over-relaxing" and enables one to arrive at a solution more rapidly.
9. If a more accurate answer is desired, or a region of high potential gradient is to be studied, advance to a finer net. A finer net is sometimes necessary only in the region of high potential gradient.
10. Determine intermediate pressures by interpolation and repeat steps 6 and 7.
11. Check for errors. If any are found, relax the residuals again.

APPENDIX
DERIVATION OF RELAXATION EQUATIONS

During flow of incompressible fluids in porous media, the pressure distribution resulting from applied boundary conditions must satisfy Laplace's equation, which in two dimensions is

$$\frac{\partial^2 P}{\partial x^2} + \frac{\partial^2 P}{\partial y^2} = 0 \quad . \; . \; . \; . \; . \; . \; . \; . \; . \quad (1)$$

Laplace's equation can be replaced by an approximately equivalent equation by letting derivations be represented by finite difference equations.

Referring to Fig. 1 in the text, the first derivative, $\frac{\partial P}{\partial x}$ between points 0 and 1 can be expressed as

$$\left(\frac{\partial P}{\partial x}\right)_{0\text{-}1} \cong \frac{P_1 - P_o}{a} \quad . \; . \; . \; . \; . \; . \; . \; . \quad (2)$$

and between points 3 and 0 as

$$\left(\frac{\partial P}{\partial x}\right)_{3\text{-}0} \cong \frac{P_o - P_3}{a} \quad . \; . \; . \; . \; . \; . \; . \; . \quad (3)$$

where a is the spacing between the points. The second derivative can be expressed as

$$\left(\frac{\partial^2 P}{\partial x^2}\right) \cong \frac{\left(\frac{\partial P}{\partial x}\right)_{0\text{-}1} - \left(\frac{\partial P}{\partial x}\right)_{3\text{-}0}}{a} = \frac{P_1 + P_3 - 2P_o}{a^2} \,. \quad (4)$$

In like manner,

$$\left(\frac{\partial^2 P}{\partial y^2}\right)_o \cong \frac{P_2 + P_4 - 2P_o}{a^2} \quad . \; . \; . \quad (5)$$

Substituting Equations (4) and (5) in Equation (1) gives

$$P_1 + P_2 + P_3 + P_4 - 4P_o = 0 \quad . \; . \; . \; . \; . \; . \quad (6)$$

When Equation (6) [Equation (3) in text] is satisfied by a finite number of points, Laplace's equation will be solved approximately.

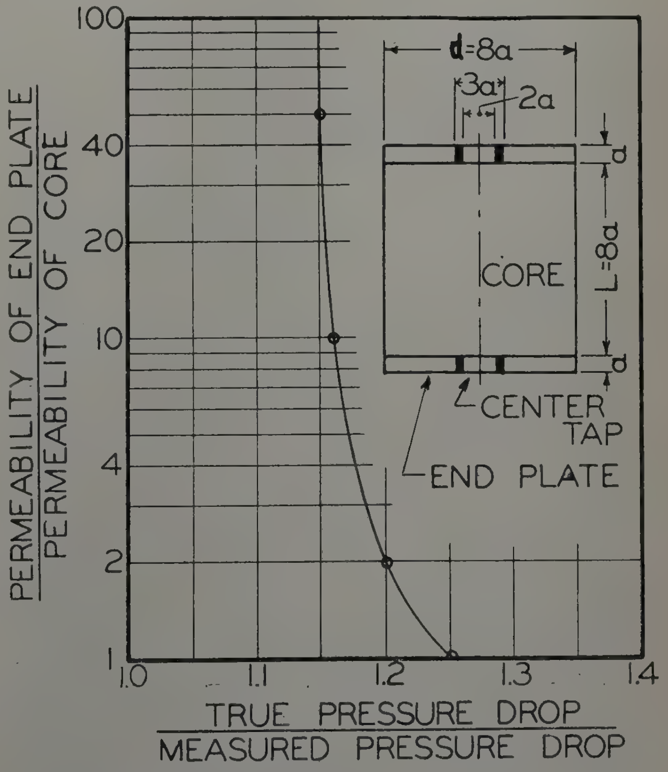

FIG. 7 — TRUE PRESSURE DROP MEASURED BY A POROUS CENTER TAP IN A HASSLER TYPE RELATIVE PERMEABILITY SETUP.

Laplace's equation in cylindrical coordinates is

$$\frac{\partial^2 P}{\partial r^2} + \frac{1}{r}\frac{\partial P}{\partial r} + \frac{\partial^2 P}{\partial z^2} + \frac{\partial^2 P}{\partial \theta^2} = 0 \quad . \quad . \quad . \quad . \quad (7)$$

With axial symmetry, $\frac{\partial^2 P}{\partial \theta^2} = 0$, so that Laplace's equation may be simplied to

$$\frac{\partial^2 P}{\partial r^2} + \frac{1}{r}\frac{\partial P}{\partial r} + \frac{\partial^2 P}{\partial z^2} = 0 \quad . \quad . \quad . \quad . \quad . \quad (8)$$

From Equations (2), (3), and (4), and Fig. 4, the following equations may be derived:

$$\left(\frac{\partial^2 P}{\partial r^2}\right)_o \cong \frac{P_2 + P_4 - 2P_o}{a^2} \quad . \quad . \quad . \quad . \quad (9)$$

$$\frac{1}{r}\left(\frac{\partial P}{\partial r}\right)_o \cong \frac{1}{r_o}\,\frac{P_2 - P_4}{2a} \quad . \quad . \quad . \quad . \quad . \quad . \quad (10)$$

$$\left(\frac{\partial^2 P}{\partial z^2}\right)_o \cong \frac{P_1 + P_3 - 2P_o}{a^2} \quad . \quad . \quad . \quad . \quad . \quad (11)$$

Substituting Equations (9), (10), and (11) in Equation (7),

$$\frac{1}{a^2}(P_1 + P_2 + P_3 + P_4 - 4P_o) + \frac{1}{r_o}\,\frac{1}{2a}(P_2 - P_4) = 0 \quad . \quad (12)$$

Let $r_o = na$, where a is the grid spacing. Then

$$P_1 + P_2 + P_3 + P_4 - 4P_o + \frac{1}{2n}(P_2 - P_4) = 0 \quad . \quad . \quad . \quad (13)$$

For the axis where $r = 0$, $\frac{1}{r}\left(\frac{\partial P}{\partial r}\right) \rightarrow \frac{\partial^2 P}{\partial r^2}$ as $r \rightarrow 0$ so that Equation (8) becomes

$$2\left(\frac{\partial^2 P}{\partial r^2}\right) + \frac{\partial^2 P}{\partial z^2} = 0 \quad . \quad . \quad . \quad . \quad . \quad . \quad (14)$$

Substituting Equations (9) and (11) in Equation (14) and observing that $P_2 = P_4$

$$P_1 - 4P_2 + P_3 - 6P_o = 0 \quad . \quad . \quad . \quad . \quad . \quad . \quad (15)$$

REFERENCES

1. Southwell, R. V.: *Relaxation Methods in Theoretical Physics,* Oxford Press (1946).
2. Emmons, H. W.: *Trans.* ASME (1943) **65,** 607.
3. Muskat, M.: *Flow of Homogeneous Fluids Through Porous Media,"* J. W. Edwards, Inc., Ann Arbor, Mich. (1946) 163.

DISCUSSION

By T. J. Nowak, Union Oil Co. of Calif., Member AIME

The authors made an ingeneous application of the relaxation method of Southwell to the steady state flow of fluids in porous media. As a matter of interest, the relaxation method is a recent development which has already emerged as an essential weapon of research. It is effective on problems which are difficult to solve or cannot be solved by orthodox analysis. Therefore, its introduction to oil field research is a noteworthy contribution. Through its application to Hassler type permeability study its usefulness has been demonstrated by pointing out to us the errors which are introduced by the customary neglect of the distortion produced in the equipotential lines. Review of the paper will be made on the basis of qualitative evaluation of the various mathematical procedures that can be used for solving the problems presented.

There are available, in general, three methods of solving fluid flow problems in porous media: an analytical solution, a solution by electrical analogy, and an approximate numerical solution. The analytical solution involves the orthodox application of pure mathematics based on purely abstract reasoning with no regard to the limits of uncertainties in the physical data. Its aim is to obtain a general and exact solution. Because of the abstract reasoning involved and the complexity of the final solution as well as the excessive time required to make the calculations, the analytical analysis has not been widely applied. As to the electrical analogy approach, it is often used either as an auxiliary tool of the analytical method or for solving problems impossible to solve analytically. However, it requires expensive and complicated equipment which normally rules it out.

It is common to use one of the various approximate numerical and/or graphical solutions. They provide a quick answer within some prescribed degree of accuracy but suffer from the fact that general and exact solution is not obtained. The relaxation method is one of the latest and best of the numerical solutions available.

Emphasis has been placed in the paper on the speed and accuracy of this method. It appears from the approach used in getting at the problems that the significant advantage lies in the revolutionary change of outlook which is introduced towards the problem. For example, in the solution of the three-dimensional flow problem illustrated in Fig. 3, it becomes evident that the attention is fixed not on the wanted equipotential line distribution through the core but on the data of the problem. The computer's task was to assume a pattern on the basis of all the physical intuition he has on the problem and bring unaccounted or residual quantities within specified range of uncertainty, thus accounting for the data.

It is unfortunate that the orthodox analytical approach was not presented to the problem of Fig. 3 as this would clearly show how the abstract mathematical outlook is transformed by the relaxation method into a tangible outlook. However, one can refer to the paper, "Flow Into Slotted Liners and an Application of the Theory to Core Analysis" by C. R. Dodson and W. T. Cardwell, Jr., reported in Vol. 160, AIME *Transactions,* in which an analytical approach was presented to essentially the same problem as in Fig. 3. The exceptions were that a cubical core was used whose face was obstructed by rectangular strips extending symmetrically from the opposite edges of the core's face. The results obtained give the same conclusions which can be drawn from the curve in Fig. 6.

In conclusion, I would like to inquire if the authors have considered solution of nonsteady state flow problems in porous media by the relaxation method and, if so, would they present a list of things to be considered in applying this method to nonsteady state problems?

AUTHORS' REPLY TO MR. NOWAK

We wish to thank Mr. Nowak for his thoughtful comments. His question concerning the application of the relaxation method to nonsteady state flow problems can be answered as follows:

The relaxation method differs from other numerical methods in that it permits the "relaxation" of a "strain" which exists between the correct answer and an assumed answer. It is true that computation with a "strain," a small number, is easier than computation with the variable possessing the strain which is ordinarily a much larger number, and this is one reason for the applicability of the relaxation method; however, the real reason is that relaxing permits the elimination of a difference between the correct answer and an assumed answer. For steady state flow, the correct "answer" is known to be that the sum of all the flow into and out of a point in a grid must be zero. For an assumed answer, the net flow into or out of each point is calculated, usually quite easily, and its difference from zero is the "strain" which must be relaxed. Relaxation is accomplished by changing the pressure at the grid point which affects the "strain" in a known way.

For nonsteady state flow such a procedure is not possible, because we cannot compute the strain. We do not know beforehand the extent to which the flow into a point should be greater than or less than zero; hence we do not know the extent to which an assumed answer differs from the correct answer.

★ ★ ★

THE PHASE BEHAVIOR OF A NATURAL HYDROCARBON SYSTEM

CHARLES F. WEINAUG, CHAIRMAN, DEPARTMENT OF PETROLEUM ENGINEERING, UNIVERSITY OF KANSAS, LAWRENCE, KANS., AND **HOWARD B. BRADLEY,** PHILLIPS PETROLEUM FELLOW, UNIVERSITY OF TEXAS, AUSTIN, TEX., MEMBERS AIME

ABSTRACT

The phase behavior of a naturally occurring hydrocarbon system whose critical temperature is near the reservoir temperature has been described.

The same volume per cent liquid was observed for the first time at three different pressures for isotherms immediately below the critical temperature. The shapes of the isothermal equilibrium constant curves necessary to predict this phenomena are discussed and illustrated.

INTRODUCTION

The phase behavior of a number of hydrocarbon systems has been reported; however, very little data are available on natural occurring hydrocarbon systems whose critical temperature is near the reservoir temperature. This appeared to be the case for the fluid studied here; therefore the pressure-volume-temperature data for this system were determined for presentation.

METHOD

The PVT data were obtained with equipment similar to that described by Weinaug and Katz,[1] consisting principally of a two-section, double-windowed gauge mounted in a constant temperature air bath. The procedure followed was essentially that used by Katz and Kurata[5] except that a cathetometer, reading direct to 0.01 cm, was used to determine the height of each extreme phase limit.

The system studied was formed by recombining vapor and liquid samples from the first stage separator of the well. Portions of these samples were displaced with mercury into the cell which had previously been filled with mercury. A predetermined amount of the liquid sample was introduced, while an excess of vapor was admitted. The resulting mixture was brought to equilibrium at the condition of the separator during sampling. By adding mercury to maintain the pressure, enough vapor was displaced to give a gas/oil ratio within the cell equal to that produced by the separator at the time of sampling. The remaining material was then considered to be equivalent to the reservoir fluid. An analysis of material in the cell, computed from analysis of vapor and liquid samples and the separator gas/oil ratio, is given in Table I.

Table I — Composition of Hydrocarbon System

Component	Mole Per Cent
Carbon Dioxide	0.13
Nitrogen	0.76
Methane	53.91
Ethane	14.20
Propane	9.64
Iso Butane	1.25
Normal Butane	4.29
Iso Pentane	1.12
Normal Pentane	1.87
Hexane	2.72
Heptanes +	10.11
Molecular Weight of Heptanes +	178.50

---

[1] References given at end of paper.

Manuscript received in the office of the Petroleum Branch August 5, 1950. Paper presented at the Fall Meeting of the Petroleum Branch in New Orleans, La., Oct. 4-6, 1950.

Pressure volume determinations were made under isothermal conditions for the recombined sample. The pressure on the reservoir fluid was increased by addition of mercury until a single uniform phase existed within the cell. Temperature of the air bath was adjusted to the desired value and maintained constant for a period of at least three hours before any measurements were made. The bubble or dew point pressure was then found by the removal of small quantities of mercury until the first indication of a second phase appeared. Pressure was recorded and then reduced further by the withdrawal of additional quantities of mercury. Between each removal, vapor and liquid within the cell were brought to equilibrium by rocking the air bath. After establishing equilibrium, the volume of each phase was determined as described above.

EXPERIMENTAL RESULTS

The data obtained for the isotherms have been tabulated in Table II, plotted in Fig. 1, and cross plotted in Fig. 2 to give the familiar pressure-temperature phase diagram. The 196.2, 201.3, 212.4 and 226.4°F isotherms exhibited normal behavior of hydrocarbon systems above their critical temperatures. Nothing unusual was observed in the determination of the 80.5, 101.2 and 121.1°F isotherms. However, the 141.0, 161.0, 170.9, 181.0 and 191.2°F isotherms showed phase behavior which the authors believe has not been reported previously. As the pressure was reduced, a small quantity of vapor formed when the system entered the two-phase region. This quantity of vapor continued to increase rapidly at the expense of the liquid phase with only slight reduction in pressure. Vaporization continued until a maximum volume per cent vapor was reached, and from this point further decrease in pressure produced condensation. The quantity of liquid increased at the expense of the vapor phase; however, larger reductions in pressure were necessary than were required initially to produce a comparable phase change. This last behavior is identical to retrograde condensation and progressed as pressure was

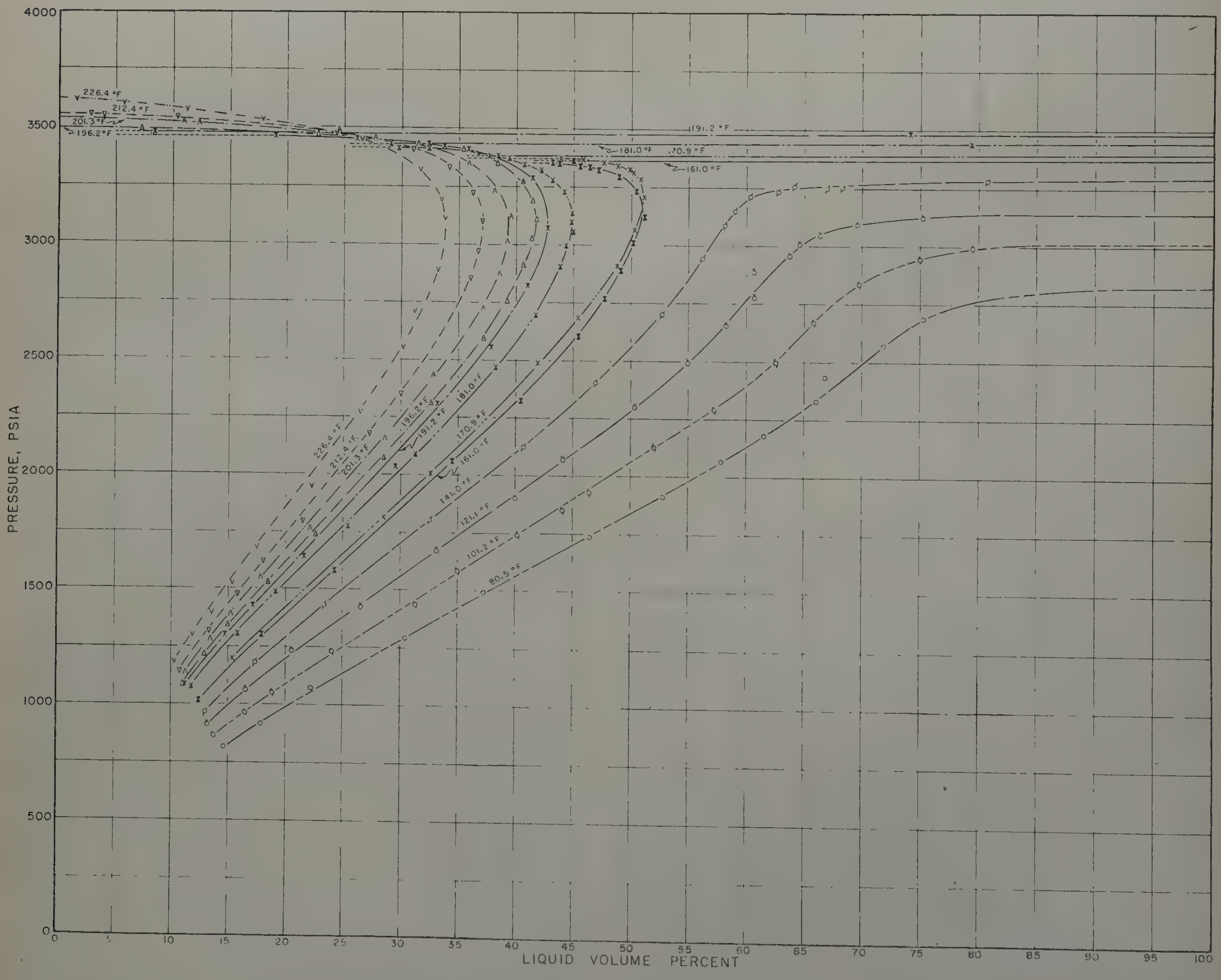

FIG. 1 — PERCENTAGE LIQUID ISOTHERMS.

Table II — Experimental Phase Data

Pressure psia	Vol. of System cc	Vol. of Liquid cc	Volume Per Cent Liquid
	Temperature 80.5°F		
2855			Single Phase
2825			Definite Separation
2690	30.1	22.6	75.2
2570	30.6	22.0	71.7
2435	31.3	21.0	66.9
2330	32.1	21.2	66.0
2180	33.7	20.7	61.5
2070	35.1	20.3	57.8
1915	37.3	19.7	52.8
1735	41.0	19.0	46.4
1495	48.0	17.9	37.2
1290	57.4	17.4	30.4
1070	70.8	15.7	22.2
915	84.3	15.0	17.8
815	98.3	14.3	14.6
	Temperature 121.1°F		
3175			Single Phase
3170			Two Phases
3150			Two Phases
3140			Two Phases
3125	31.0	23.3	75.2
3090	31.2	21.7	69.5
3045	31.5	20.9	66.3
3005	31.7	20.5	64.6
2955	31.9	20.3	63.7
2885	32.3	19.5	60.6
2780	33.0	20.0	60.6
2655	33.8	19.7	58.2
2490	35.1	19.3	54.9
2290	37.3	18.8	50.3
2065	41.0	18.1	44.1
1900	44.0	17.5	39.9
1670	50.4	16.7	33.1
1425	60.2	16.0	26.5
1230	71.2	14.6	20.5
1060	84.1	13.9	16.5
910	100.2	13.3	13.2
	Temperature 161.0°F		
3375			Single Phase
3365			Two Phases
3355	32.8	14.8	45.0
3350	32.8	14.1	43.1
3345	32.8	14.3	43.7
3340	32.8	14.9	45.5
3335	32.8	15.2	46.3
3320	32.9	15.5	47.2
3295	32.9	16.1	49.0
3230	33.2	16.8	50.5
3125	33.8	17.3	51.1
3015	34.4	17.2	50.1
2890	35.4	17.3	49.1
2765	36.5	17.4	47.6
2605	38.0	17.2	45.3
2320	41.5	16.8	40.5
2060	46.4	16.0	34.5
1580	61.2	14.9	24.3
1305	75.2	13.4	17.8
1015	100.0	12.4	12.4
	Temperature 101.2°F		
3040			Single Phase
3015			Two Phases
2995	30.3	24.1	79.3
2945	30.4	22.8	74.9
2835	30.8	21.5	69.6
2670	31.7	20.4	65.8
2500	32.9	20.5	62.5
2290	34.8	19.9	57.1
2130	37.1	19.3	51.9
1930	40.2	18.6	46.3
1855	41.8	18.5	44.0
1740	44.4	17.8	40.1
1585	49.3	17.2	34.9
1435	55.1	17.2	31.2
1230	65.8	15.8	24.0
1050	78.8	14.8	18.8
960	87.1	14.3	16.4
860	99.8	13.7	13.7
	Temperature 141.0°F		
3360			Single Phase
3285	31.9	25.7	80.7
3255	32.0	20.5	64.0
3255	32.1	21.9	68.2
3250	32.0	21.4	66.9
3235	32.0	20.1	62.7
3210	32.1	19.4	60.2
3150	32.4	19.1	58.9
3090	32.7	19.0	58.1
2945	33.5	18.8	56.2
2705	35.2	18.5	52.6
2405	37.9	17.8	46.9
2125	42.6	17.3	40.6
1805	49.8	16.2	32.5
1430	64.1	14.9	23.3
1180	79.7	13.8	17.3
965	100.0	13.0	13.0
	Temperature 170.9°F		
3410			Single Phase
3395			Single Phase
3380	31.1	11.7	37.6
3370	31.1	13.6	43.8
3365	31.1	14.3	45.8
3355	31.1	14.8	47.6
3340	31.2	15.2	48.8
3325	31.2	15.6	49.8
3310	31.3	15.7	50.1
3285	31.4	15.9	50.7
3205	31.9	16.3	51.1
3070	32.6	16.4	50.3
2910	33.8	16.5	48.8
2690	35.7	16.2	45.3
2485	37.6	15.8	41.9
2005	45.8	14.9	32.6
1810	50.7	14.3	28.5
1195	80.0	12.2	15.3

Table II — Continued

Pressure psia	Vol. of System cc	Vol. of Liquid cc	Volume Per Cent Liquid
	Temperature 181.0°F		
3465			Single Phase
3445	33.6	26.7	79.4
3430	33.6	9.7	28.9
3420	33.7	10.0	29.6
3415	33.7	10.9	32.3
3395	33.8	12.0	35.6
3380	33.9	13.0	38.3
3370	34.0	13.4	39.3
3345	34.0	13.9	40.6
3320	34.2	14.4	42.0
3280	34.3	14.8	43.1
3225	34.6	15.3	44.1
3140	35.1	15.7	44.8
3100	35.4	15.9	44.8
3055	35.9	16.1	44.9
2995	36.4	16.1	44.4
2910	37.0	16.2	43.8
2700	39.0	16.2	41.5
2460	41.8	16.0	38.3
2090	48.7	15.3	31.3
1775	57.5	14.5	25.3
1490	69.1	14.3	19.2
1305	80.1	12.6	15.8
1070	99.9	11.7	11.7
	Temperature 196.2°F		
3495			Two Phases
3490	33.5	2.4	7.1
3470	33.5	7.6	22.6
3405	33.9	12.0	35.3
3350	34.2	13.1	38.3
3270	34.6	14.0	40.5
3190	35.0	14.5	41.3
3105	35.6	14.8	41.6
3025	36.3	15.0	41.2
2910	37.4	15.2	40.6
2755	39.0	15.3	39.1
2595	40.8	15.2	37.2
2310	44.8	14.6	32.5
2070	49.9	14.2	28.4
1730	59.9	13.5	22.6
1530	68.4	12.5	18.3
1335	79.4	11.9	15.0
1215	88.0	11.3	12.8
1080	99.9	10.9	10.9
	Temperature 212.4°F		
3560			Single Phase
3555	34.8	0.9	2.7
3550	34.8	1.4	3.9
3540	34.8	3.6	10.3
3480	35.1	9.5	24.3
3410	35.5	11.0	31.0
3335	36.0	12.3	34.1
3225	36.7	13.3	36.2
3105	37.6	13.9	37.0
2970	39.0	14.3	36.7
2855	40.1	14.4	36.0
2355	46.8	14.0	30.0
2180	50.5	13.7	27.2
1800	61.2	13.1	21.4
1625	68.5	12.3	18.0
1480	75.6	11.9	15.8
1315	85.3	11.4	13.3
1140	99.7	10.6	10.7

Pressure psia	Vol. of System cc	Vol. of Liquid cc	Volume Per Cent Liquid
	Temperature 191.2°F		
3495			Single Phase
3485	33.3	24.7	74.1
3475	33.4	2.8	8.3
3465	33.4	6.3	18.9
3450	33.4	8.7	26.1
3435	33.5	10.1	32.3
3425	33.6	11.3	33.7
3405	33.6	12.0	35.7
3370	33.8	13.0	38.4
3290	34.2	14.1	41.3
3075	35.6	15.2	42.8
2995	36.2	15.3	42.3
2825	37.8	15.5	41.0
2695	39.2	15.5	39.6
2555	40.8	15.5	37.9
2305	44.3	14.7	33.1
2030	50.2	14.3	28.5
1640	62.7	13.5	21.5
1425	74.5	12.5	17.2
1300	80.6	11.9	14.7
1070	99.8	11.1	11.1
	Temperature 201.3°F		
3565			Single Phase
3530	34.6	3.7	10.7
3520	34.6	4.2	12.2
3490	34.8	8.5	24.4
3460	34.8	9.6	27.6
3435	35.0	11.0	31.4
3350	35.4	12.7	35.8
3230	36.2	14.0	38.7
3120	37.0	14.6	39.4
3010	38.0	14.9	39.1
2870	39.2	15.1	38.5
2725	40.8	15.1	37.1
2430	44.6	14.6	32.7
2160	50.1	14.2	28.5
1760	61.5	13.6	22.0
1550	70.2	12.5	17.8
1390	79.4	12.2	15.3
1280	86.5	11.6	13.4
1135	99.4	11.0	11.1
	Temperature 226.4°F		
3625			Single Phase
3615	35.5	0.5	1.4
3600	35.5	2.0	5.6
3575	35.6	4.0	11.1
3535	35.8	6.4	17.8
3450	36.3	9.6	26.4
3325	37.1	11.7	31.5
3200	38.0	12.7	33.4
3115	38.7	13.1	33.8
2890	41.0	13.4	33.2
2710	43.1	13.4	31.1
2555	45.2	13.6	30.1
2275	50.0	13.2	26.4
1950	58.6	13.0	22.2
1685	68.0	11.9	17.5
1525	75.6	11.6	15.3
1395	83.2	11.2	13.5
1300	90.0	10.6	11.8
1180	100.2	10.3	10.3

reduced until a maximum volume per cent liquid was reached. Normal vaporization took place with further pressure reduction until the system filled the cell.

DISCUSSION OF RESULTS

The system studied exhibited unusual behavior only in the region below the critical temperature, and therefore the discussion will be limited to these data. The discussion above shows that as pressure on this system is increased, normal condensation takes place until a maximum percentage of liquid is formed. At this point further increase in pressure causes the percentage of liquid to decrease: retrograde phenomenon. The liquid volume continues to decrease until it reaches a minimum value, at which point further pressure increments result in large increases in the percentage of liquid, and the system passes into the single phase region through a bubble point. This new behavior will be referred to as *renascent* vaporization or condensation.

This new phenomenon is probably related to data obtained by Eilerts, Barr, Mullens and Hanna,[2] who noted the existence of two liquid phases in the region of critical temperature. Also it might be a degeneration of that observed by Kay.[3] These data are plotted in Fig. 3.

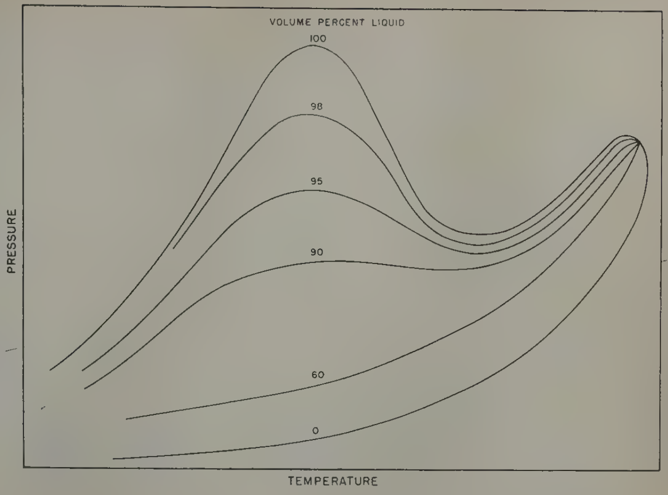

FIG. 3 — PHASE DIAGRAM OF A HYDROGEN AND A PETROLEUM NAPHTHA.

Interesting possibilities develop in the consideration of shapes of equilibrium constant *vs* pressure curves, necessary to predict renascent behavior at constant temperature. As pressure is increased from a low value, equilibrium constants for hydrocarbon systems decrease, as shown in Fig. 4, points *A* to *B* for each curve. This trend continues until a minimum value is reached for each curve except methane, (see points *B*). With rising pressure, all methane curves determined to date show a continuous decrease in the equilibrium constant value. These decreasing constants indicate normal condensation when pressure is raised. After minimum values are reached in the curves for constituents heavier than methane, equilibrium constants increase as pressure is raised. This trend continues to denote normal behavior until rate of change in curves for heavier constituents counteracts the diminishing values for methane. For further additions of pressure the curves then indicate retrograde behavior, which progresses until the system passes into the single phase region. However, in this case the retrograde behavior gives way to rapid condensation when pressure is raised.

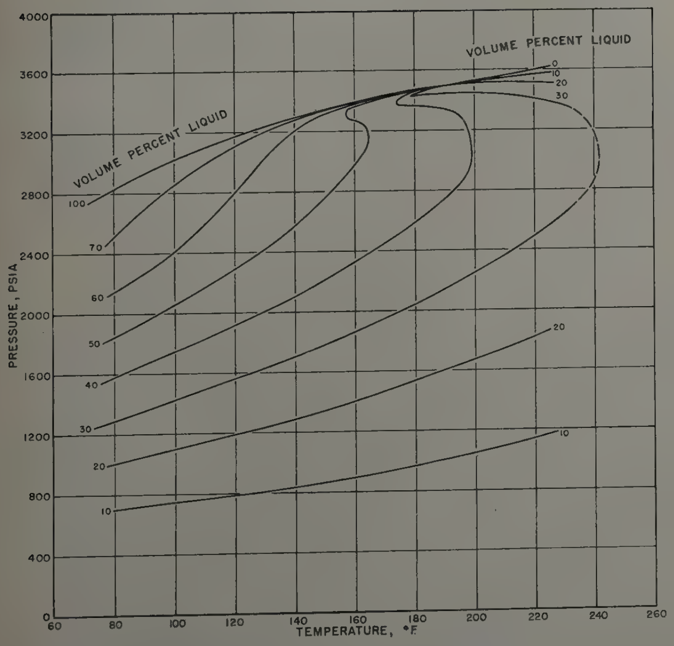

FIG. 2 — PHASE DIAGRAM OF A NATURAL HYDROCARBON SYSTEM.

This new behavior could be predicted by the use of several types of equilibrium constant curves. First, if an inflection occurred in the curves for heavier constituents, such as illustrated by points *C* and the dotted lines in Fig. 4, the rate at which equilibrium values for heavier components increased would subside and allow the decreasing values for methane to become dominant again. Thus, condensation would be indicated for further rises in pressure. It should be noted that these inflections would have a tendency to cause the curves to diverge rather than converge, as denoted by the convergence pressure concept.

Another type of curve which would indicate this behavior is already apparent in the values for methane reported by Standing and Katz.[4] With rising pressures the methane curves tend to level off and values shown become almost constant, (see points *A* to *B*, Fig. 5). This change results in the prediction of retrograde behavior at lower pressures. However, at higher pressures a point of inflection occurs, (point *B*), with a sudden decline in equilibrium values for methane, even though pressures are rising steadily. This rate of decrease could be sufficient to overcome the effect of the increasing equilibrium constants for heavier constituents, and thus renascent vapori-

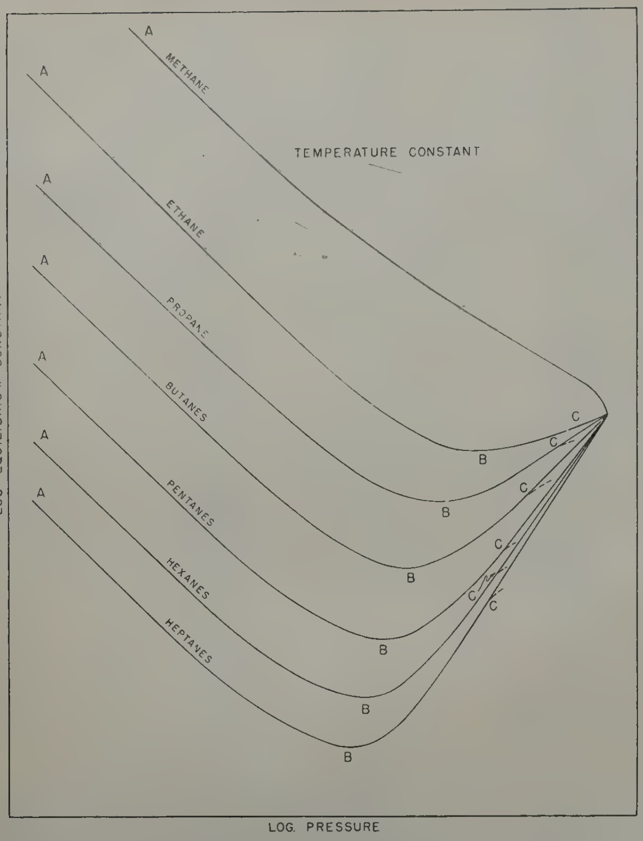

FIG. 4 — CHANGES IN EQUILIBRIUM CONSTANTS WITH PRESSURE.

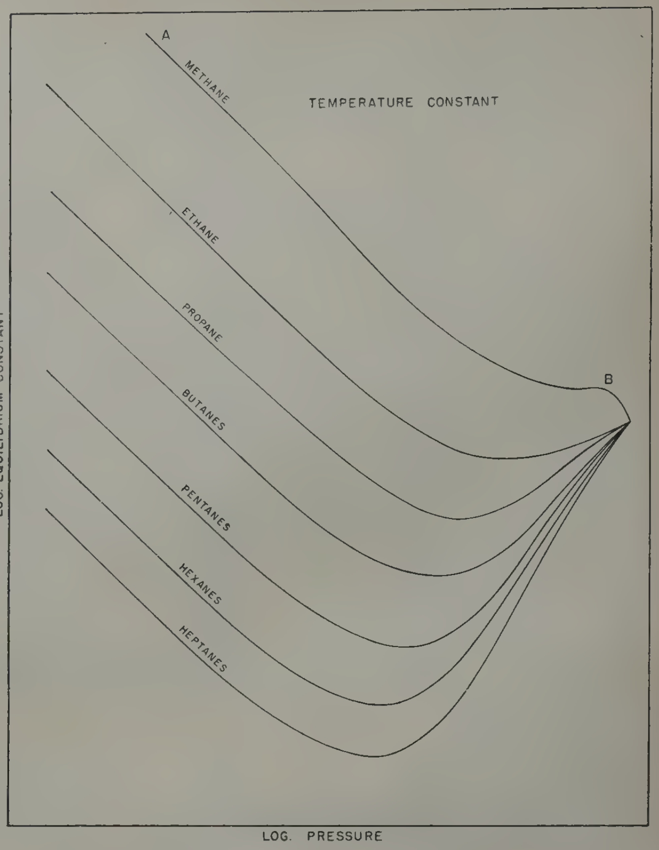

FIG. 5 — CHANGES IN EQUILIBRIUM CONSTANTS WITH PRESSURE.

zations would be indicated. Since methane is present in a much greater quantity than any other constituent, small changes in values for the methane equilibrium constant will produce large changes in the indicated phase behavior.

It is probable that the curves which may be used to predict renascent vaporization or condensation will be some combination of the two types presented above.

ACKNOWLEDGMENT

The authors of this paper wish to acknowledge the cooperation and support of the Department of Petroleum Engineering and the Bureau of Engineering Research of the University of Texas, under whose auspices the work was done.

REFERENCES

1. Weinaug, C. F., and Katz, D .L.: *Ind. Eng. Chem.* (1943) **35**, 239.
2. Eilerts, C. K., Barr, V. L., Mullens, N. B., and Hanna, Betty: *Petroleum Engineer* (1948) **19**, 154.
3. Kay, W. B.: *Chemical Review* (1941) **29**, 501.
4. Standing, M. B., and Katz. D. L.: *Trans.* AIME (1944) **155**, 232.
5. Katz, D. L., and Kurata, F.: *Ind. Eng. Chem.* (1940) **32**, 817.

★ ★ ★

PRIMARY HIGH PRESSURE WATER FLOODING IN THE PETTIT LIME HAYNESVILLE FIELD

D. W. AKINS, JR., OHIO OIL CO., SHREVEPORT, LA., MEMBER AIME

ABSTRACT

The case history of a combination gas and water flood instituted early in the life of a field is described. It was recognized from the beginning that recovery would be low, under normal production methods, from the several separate, thin beds of porous limestone which had such poor native permeability that the wells would not produce without acidizing. It is thought that the combination flood gives excellent recovery efficiencies for this type of reservoir. The chief function of the gas flood now is to maintain bottom hole pressure in that part of the reservoir which will not be affected by the water injection program until later. Present estimates are that ultimate recovery will be approximately double the recovery expected under the original solution gas drive mechanism. Wide (80-acre) spacing has enhanced the economics of the over-all field program by the elimination of more than $5,000,000 worth of unnecessary wells.

INTRODUCTION

The Haynesville Pettit Field was discovered in November, 1941, with the completion of T. L. James Co.'s Callie Akin No. 1, located in the W ½ of the NE ¼ Section 27-23N-8W, Claiborne Parish, La., at an approximate depth of 5,300 ft. The center of the field is about two miles north and a mile west of the town of Haynesville, La. A total of 189 producing wells have been drilled on 14,500 acres. An additional nine dry holes were drilled. The Louisiana-Arkansas state line divides the field so that 34 wells are in Arkansas and 155 are in Louisiana.

Governmental sections are divided equally to contain eight production units making 80-acre spacing where the sections are regular. Along the state line in Louisiana there is an irregular tier of sections, each of which contains approximately 456 acres. When divided equally into eight production units the spacing is 57 acres per well for these three and a fraction productive sections. All Haynesville Pettit wells are identified by their section number followed by their position in the section as determined by numbering the production units counterclockwise beginning in the upper right corner of the section.

All of the producing wells in the field except two are unitized and operated by the Haynesville Operators Committee. These two wells are located in the extreme northern part of the field in Arkansas. Efforts to bring them into the Unit are being continued.

The Pettit operators organized the Haynesville Operators Committee and the field became a unit operation May 1, 1944.

GEOLOGY

The Pettit is Lower Cretaceous in age and is defined as the uppermost porosity in the Sligo formation. The unitized area known as the Haynesville Pettit Field is composed of two separate zones of porosity approximately 40 ft apart and without connection between the two, except in wells. These zones are known as the Upper Pettit and the Lower Pettit. The Upper Pettit is separated into two sections throughout most of its area by a relatively thin but quite impervious shale streak. These are called the "A" and "B" sections of the Upper Pettit.

All of these lenticular zones are composed of coquina limestone and a small percentage of normal oolites. The large

---

Manuscript received in the Petroleum Branch office August 20, 1950. Paper presented at the Petroleum Branch Fall Meeting in New Orleans, La., Oct. 4-6, 1950.

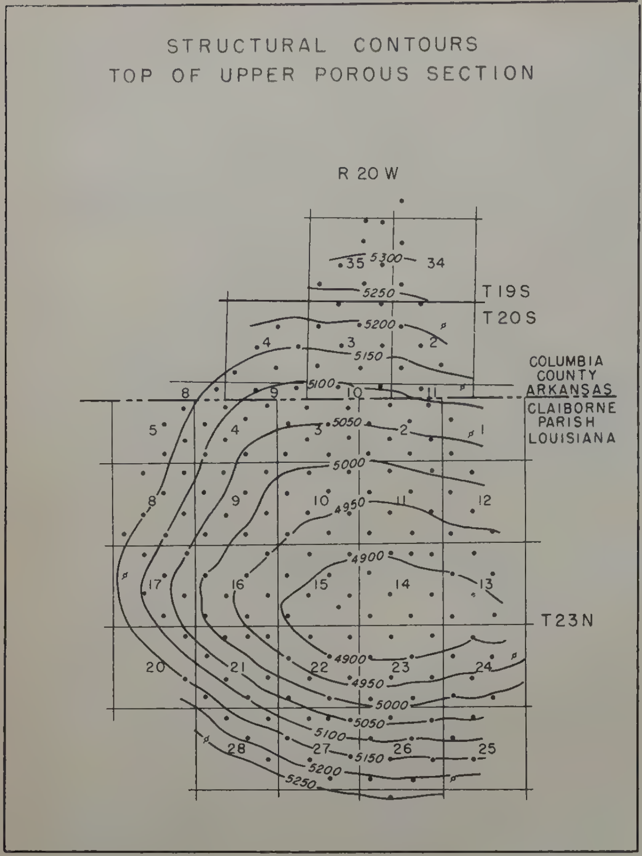

FIG. 1 — STRUCTURE MAP, PETTIT LIME, HAYNESVILLE FIELD.

shell fragments, small fossils and oolites were at one time subjected to partial solution, and then later calcium carbonate in the form of fine crystals was precipitated in such a way as to build up on the particles and to line the interstices so that there resulted a fairly porous rock with relatively low permeability. Porosity averages about 19 per cent. Permeability is rather uniform in the separate zones, averaging about 23 md. The maximum permeability measured was 250 md.

Fig. 1 is a structure map on top of the porosity in the "A" section of the Upper Pettit. The contour interval is 50 ft. The structure has only 20 ft of closure, as that is the relief between the highest well and the 4,900-ft contour which probably could be closed. It can readily be seen that the field is a combination structural and stratigraphic trap. There is a structural range of more than 500 ft between producing wells in a north-south direction and more than 250 ft between wells on top of the structure and those near the limit of production on the west flank. Observe that a dry hole was drilled in Section 24. This dry hole is more than 400 ft higher structurally than productive wells to the north.

Fig. 2 is an isopach map of the Upper Pettit which shows the effective thickness based on Schlumberger electric log readings. Thickness is a factor in participation and the operators agreed arbitrarily that only readings of 14 mv and above on the SP curve with a simultaneous reading of 20 ohms and above on the normal resistivity curve would be considered productive. The isopach is based on this interpretation of the electric logs. The map shows that the thickness varies from zero to 19 ft using these parameters. The cross hatching shows the areal extent of the "B" section and its position relative to the "A" section. In the lower left-hand corner of the figure is a typical Schlumberger log showing the electric characteristics and relative positions of the porous zones. The maximum reading on the self potential side of the log is about 52 mv and the maximum reading on the resistance side is about 40 ohms (off scale) in the Upper Pettit. Corresponding maximum readings in the Lower Pettit are somewhat less.

Fig. 3 shows a typical producing section in the field. Note the shale streak separating the Upper Pettit into the "A" and "B" sections. The impervious barrier which varies from zero to six ft in thickness extends over approximately two-thirds of the field. The shale break is barely perceptible on the log of well 15-1, and the "A" and "B" sections merge in this area.

RECOVERY MECHANISM

When the field was developed it was the practice to set casing through and perforate opposite all productive zones. All wells were acidized, as the formation was too tight to produce without acid.

Production is a very dark paraffin base oil and when produced in lease stock tanks the gravity throughout the field varied from 38° to 40° API. There was no gas cap.

Bottom hole sample analysis indicated that the oil was undersaturated at original reservoir conditions. Solution gas/oil ratio was determined to be 460 cu ft per bbl and saturation pressure at reservoir temperature to be 2,331 psi. Formation volume factor was 1.33 to zero gauge separator pressure.

The original bottom hole pressure was 2,440 psi at 5,000 ft subsea, which is about normal for the depth. There was no "bottom" water in the reservoir. The nine dry holes which almost circle the field found the limits of production to be controlled entirely by the disappearance of porosity and permeability. The connate water increases from about 18 per cent to 35 per cent as the permeability decreases. Average connate water is about 23 per cent of the pore space. The pressure production history and gas/oil ratio history shown in Fig. 4 is typical of a solution gas drive mechanism.

UNITIZATION AND GAS INJECTION

In 1943, when the field had about 90 producing wells, it became apparent that recovery would be quite low unless something could be done to retard the downward trend in bottom hole pressure and the accelerating rise in gas/oil ratio. After about a year of negotiations, principally over participation, the majority of the 22 operators and 1,400 royalty owners signed the Haynesville Unitization and Pressure Maintenance Agreement which became effective May 1, 1944.

As soon as appropriate orders were issued by the Louisiana Conservation Commission and the Arkansas Oil and Gas Commission, construction work was started on a field gathering system and a gasoline absorption-compressor plant. The return of gas started in January, 1945. By then the field gas/oil ratio had increased from the original 460:1 to about 2,230:1, and bottom hole pressure had dropped from the original 2,440 psi to about 1,400 psi.

Gas injection was started in four of the structurally highest wells in the field. A short time later a fifth well was added about a mile west. This well had a much higher effective permeability than the other wells and was later shut in.

Oil production continued to decline in spite of the gas return program, and in November, 1945, dropped to 150,000 bbl per month compared to 340,000 bbl per month at the time of unitization. The operators were very anxious to step up production in order to show a faster return on the money invested.

The amount of gas the plant could handle was the limiting factor on oil production. The higher the field gas/oil ratio the lower the field oil production. After considerable discussion it was decided to add additional compressor capacity to increase the volume of gas to the plant from 15.7 MMcf/D to 22.5 MMcf/D. Installation of two additional 800 hp compressors was completed in January, 1946, making seven 800's or a total of 5,600 hp. Oil production was increased approximately 80,000 bbl per month immediately.

It was apparent, however, that it would still be a very long time before most of the wells would be affected by the gas return program and probably some wells would never be affected within the economic life of the project because of the distances involved, the low permeability of the formation generally, and an impermeable barrier which separates parts of the Upper Pettit in the northern part of the field.

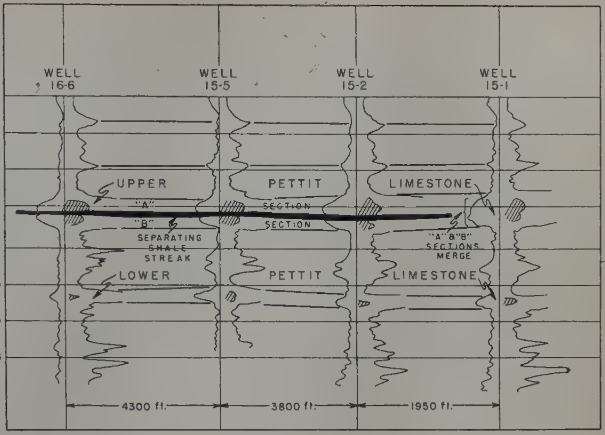

FIG. 3 — TYPICAL PRODUCING SECTION, PETTIT LIME, HAYNESVILLE FIELD.

There was a definite and beneficial change now in the gas/oil ratio and bottom hole pressure trends, and production was up to a satisfactory rate, but reservoir voidage was too high and ultimate recovery estimates, then about 21 per cent, were not satisfactory. Fig. 5, which is a plot of the field reservoir voidage, shows that even with the stepped up gas return program daily voidage was still about 27,000 bbl of reservoir space.

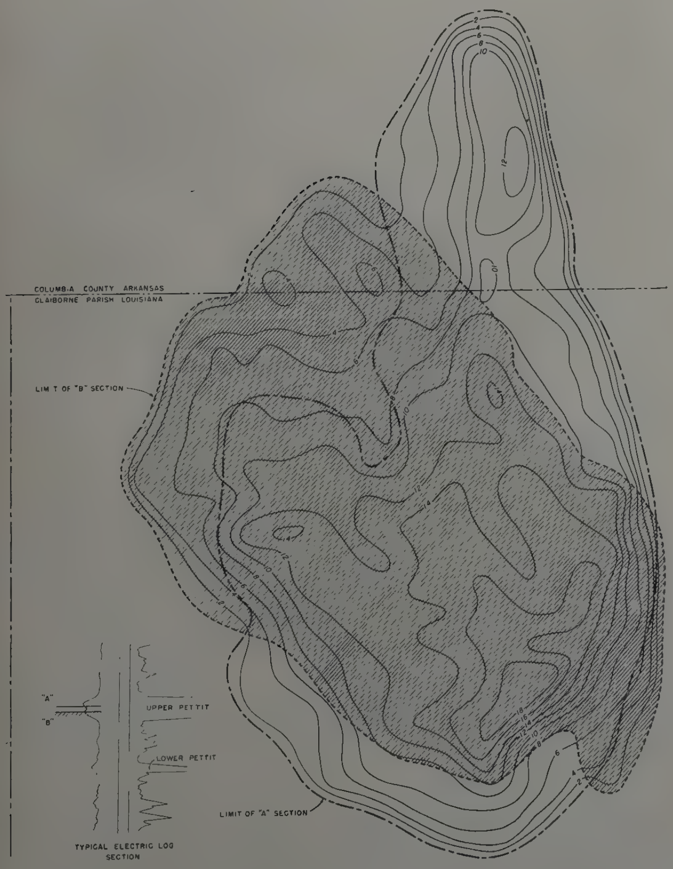

FIG. 2 — ISOPACH MAP, UPPER PETTIT LIME, HAYNESVILLE FIELD.

WATER FLOODING

The idea of an additional program whereby water would be returned to the formation as an adjunct to the gas injection program took a considerable amount of selling. There was no record of a similar case. Already gas was being injected into the rather tight limestone. The distance between wells is great — most of them are more than 1,800 ft apart. There was no source of water available except from fresh water wells which would have to be drilled for that purpose. There was concern about the effect the fresh water might have on the shale known to be present in the reservoir. If only a small amount of swelling should result from the injection of fresh water the 23 md permeability would surely be reduced and might even be lowered to zero. There was some speculation as to whether the reservoir would take water at all. If water could be injected at a reasonable pressure, would the volume be large enough to affect a material portion of the reservoir?

There were a lot of questions that needed to be answered about water flooding a field such as this, and after considerable study and discussion it was decided to try water injection in one well on an experimental basis. The well selected was in the northern part of the field near the state line. This area was too far from the gas injection wells to have been affected

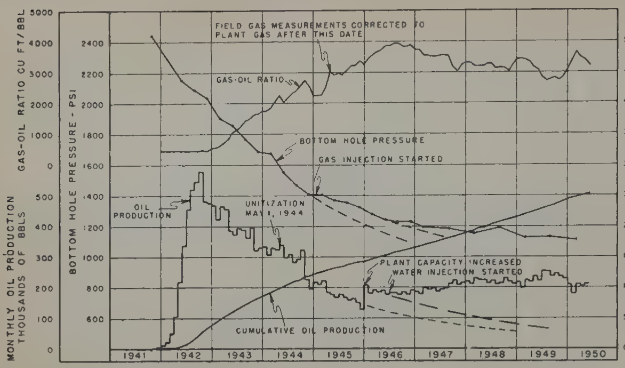

FIG. 4 — PERFORMANCE HISTORY, PETTIT LIME, HAYNESVILLE FIELD.

by that program. The gas/oil ratio of the well (then 6481:1) chosen for the experiment was so high that the well was to be shut in anyway.

Experimental water injection began in well 2-1 in March, 1946. The well took 1,100 bbl of water at 1,200 lb wellhead pressure and after a while it was decided to try injection in another well. Well A-10-1 in the same general area was selected and injection started in June. This well had considerably greater capacity than the first one, and after a while it was decided to expand the program further. Two additional wells were added in July, 1946, making a total of four.

The nearest producing well (A-11-3) to the original injection well (2-1) was shut in immediately after injection was started in order to observe whether changes in bottom hole pressure were taking place in this area. An increase in bottom hole pressure was noted after the injection of 34,000 bbl in 2-1. Well 2-8, another offset to 2-1, showed an increase in bottom hole pressure after injection of 21,000 bbl of water.

The producing characteristics of these wells offsetting water injection wells began to show very great changes. Gas/oil ratios started dropping as the water flood approached and oil production began to increase. An offset (2-3) to the second injection well (A-10-1) showed a drop in gas/oil ratio from 5,609:1 in July to 3,500:1 at the end of November. The productive capacity of this well increased from 42 B/D on tests in July (it could not be produced regularly because of high gas/oil ratio) to 135 B/D in November.

On another well the gas/oil ratio dropped from 6,400:1 in September to about 1,000:1 in December. Another well (2-2), an offset to the original injection well (2-1), was tested periodically from June through December, and it showed similar changes in characteristics while shut in. These tests proved that the gas saturation around the well bore decreased and oil saturation increased whether the well was produced or not. It was necessary to increase the size of the choke several times in order to handle the increased oil production. The gas/oil ratio decreased from nearly 5,000:1 in June to about 1,000:1 in November while shut in except for the tests. Oil production tests showed increases from about 60 B/D in June to about 80 B/D in August, 110 B/D in September and over 200 B/D in November.

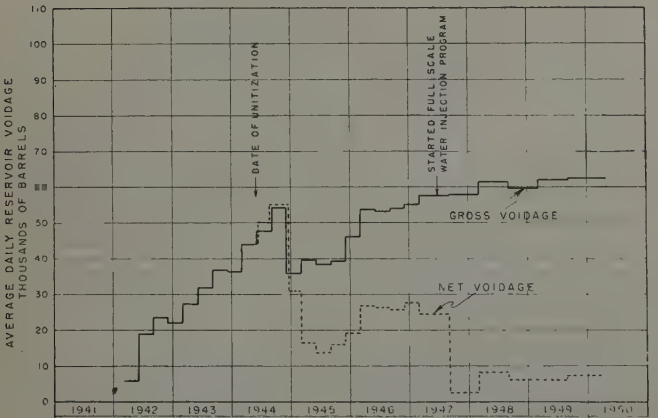

FIG. 5 — FIELD RESERVOIR VOIDAGE, PETTIT LIME, HAYNESVILLE FIELD.

Additional water injection wells were added so as to establish a line drive approximately along the state line. In this way the wells in Arkansas which were too far from the gas injection area to be benefited by the gas return program could derive benefit from the water return program. A line drive in this part of the field would also have the desirable effect of forestalling any accusation that oil was being driven from one state to the other, thereby preventing collection of the severance tax in the state where the oil was originally located.

Without exception, the producing wells just ahead of the water front were materially benefited. Fig. 6 shows the production history of well A-2-5, which is an offset to one of the original water injection wells. Note that the gas/oil ratio was about 6,750:1 the first of October, 1946, before the well began to show the effect of water injection. Eight months later the well was producing at solution ratio and at higher oil rates than at any time in its history prior to that time. It produced at solution ratio for 18 months thereafter until abandoned as a producer. It was later used as a water input well. Observe the plateau in the cumulative oil production curve during 1945 and 1946. The well had to remain shut in six full months during that time because of excessive gas/oil ratio. Then as the gas/oil ratio dropped, production increased to a peak of 7,900 bbl in January, 1948. It is apparent that the increase in cumulative production from 61,000 bbl to 181,000 bbl is due entirely to water flooding.

By September 1, 1947, 17 producing wells had been converted to injection wells and 2,874,997 bbl of water had been injected. Water injection data at six month intervals are shown in the following tabulation.

Date	No. of Inj. Wells	Cumulative Water Inj. (Bbl)
9/1/47	17	2,874,997
3/1/48	21	5,800,069
9/1/48	26	8,545,944
3/1/49	29	11,210,548
9/1/49	30	14,012,575
3/1/50	30	15,834,831

Currently about 19,000 B/D of water are being injected in 30 wells at an average pressure of 2,396 lb. Fig. 7 shows the water injection area superimposed on the isobaric map of March 1, 1950. Cumulative injection as of May 1, 1950, was 17,742,366 bbl, of which 1,907,535 bbl were produced, leaving

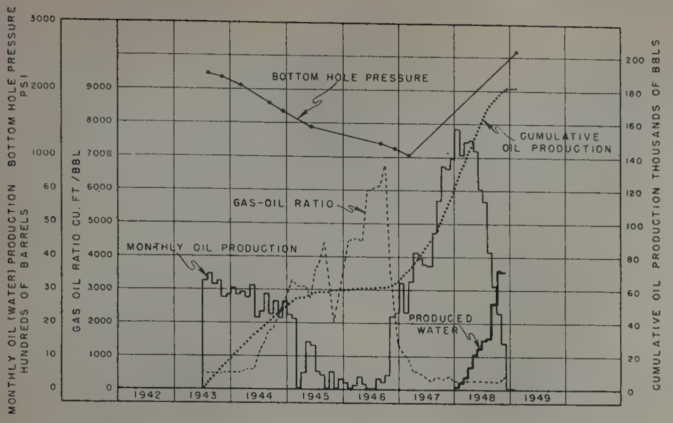

FIG. 6 — PILOT WELL A-2-5 PERFORMANCE CURVE, PETTIT LIME, HAYNESVILLE FIELD.

15,834,831 bbl net injected. Fig. 8 is a plot of the water injection history to June 1, 1950.

It will be necessary to flood the "A" and "B" sections of the Upper Pettit selectively if maximum efficiency is to be achieved. The relative position of these sections is shown on the isopach map of the Upper Pettit in Fig. 2. For the purpose of clarity the "A" and "B" sections are shown separated in Figs. 9 and 10. The estimated position of the water flood front Jan. 1, 1950, is shown on each map. In addition, the area occupied by injected gas is shown in Fig. 9.

Currently all gas injection is in the "A" zone in the central part of the field near the top of the structure. The stippled portion of the map in Fig. 9 is the area estimated to be partially swept by gas on Jan. 1, 1950. The cross-hatched area at the edge of the zone is the estimated extent of the flood front when the economic limit of the water flood operation is reached. Most of the water is being injected into the "B" section. It will simplify the operation if the water flood front in the "B" is kept ahead of the front in the "A." This is difficult because the shale break between the two is rather thin in some areas and entirely missing in other parts of the field. Plugback operations, necessary for separating the sections, are most successful when carried out from the bottom of the hole upward. Then, too, permeability in the "B" is usually higher and more uniform than it is in the "A."

It is predicted that by early 1952 full scale injection into both reservoirs can be started without danger of trapping large quantities of oil behind the flood front. The trap shown, centering in Section 4 (see Fig. 7), appears unavoidable because of rock characteristics. This area will be reduced materially below that shown here, however, before the economic limit of the operation is reached.

Two lenses of the Lower Pettit, which contain about 22 per cent of the estimated reserves, are not shown. Gas is being returned to the south lens through one injection well. After the water flood has advanced sufficiently in the "A" and "B" sections of the Upper Pettit, it is planned to water flood the Lower Pettit also.

RECOVERY AND FLOODING EFFICIENCIES

Calculation of the efficiency of recovery from the Haynesville Pettit Field is complicated by a number of factors, some of which are: (1) production is from multiple zones in various degrees of isolation; (2) the distance between wells in these tight reservoirs is great; (3) the reservoirs, and different parts of the same reservoir, were in various stages of depletion at the time repressuring began; (4) portions of the reservoir were already cycled with gas at the time water flooding began; and (5) portions of the reservoirs are to be flooded with water only.

For the purpose of this discussion four types of efficiencies are recognized. They are defined as follows:

(1) Displacement Efficiency — the ratio of the volume of pore space occupied by the injected fluid to the volume of pore space originally occupied by hydrocarbons in the flooded portions of the reservoir. Ordinarily this ratio is expressed as a per cent.

(2) Pattern Efficiency — the ratio of volume of pore space originally occupied by hydrocarbons in the flooded portion of the reservoir to the volume of pore space originally occupied by hydrocarbons in the entire reservoir.

(3) Flood Efficiency — the product of displacement efficiency and pattern efficiency.

(4) Recovery Efficiency — the ratio of the stock tank oil produced to the stock tank oil originally in place in the reservoir.

The first three of these efficiencies are applicable to the mechanism itself, and the fourth is the resultant of all factors

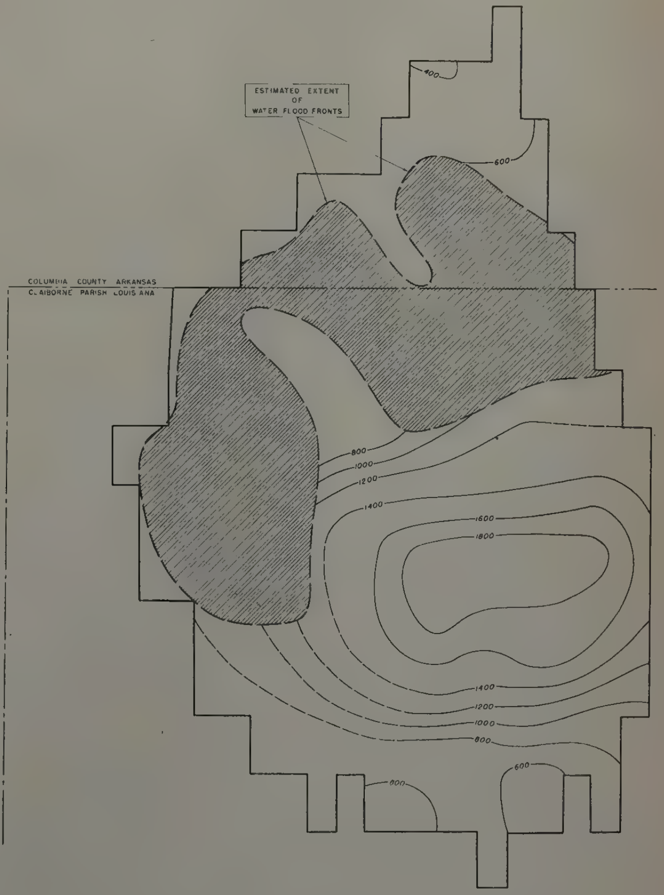

FIG. 7 — ISOBARIC MAP SHOWING AREA OF WATER INJECTION TO MARCH 1, 1951.

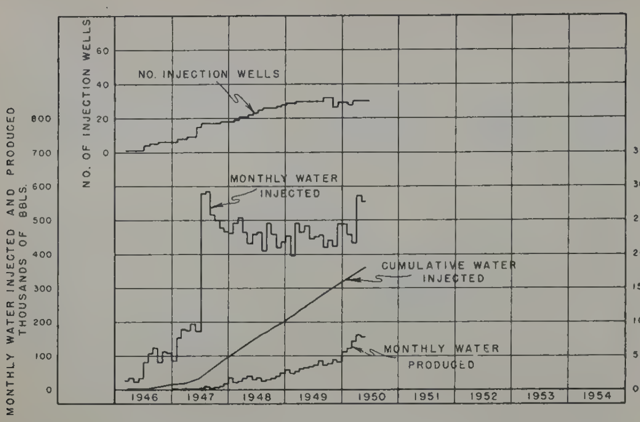

FIG. 8 — WATER INJECTION HISTORY, PETTIT LIME, HAYNESVILLE FIELD.

including the first three efficiencies. The displacement efficiency is more dependent on the permeability profile and the amount of water production that can be handled than any other factors. The pattern efficiency reflects such variables as well spacing and position and type of flooding program.

Unfortunately, only a few wells were cored in this field, and as a result there is a scarcity of data available for predicting efficiencies by profile and frequency distribution methods.

An early electrical model study was made so that displacement efficiency in the area of the two expermiental water injection wells could be calculated. The offset (A-11-3) to the first water injection well (2-1) began producing water nine months (261 days) after initial injection. Breakthrough in the offset (2-3) to the second injection well (A-10-11) occurred after seven months (211 days). Fig. 11 shows the calculated position of the water fronts at the time of breakthrough as determined by the electrical model study. Also shown are the calculated position of the fronts when pressure effects were first noted in each of the offset wells, and when changes in gas/oil ratio were first observed in each of the offset wells. Increases in bottom hole pressures were measured when the flood front had advanced 300-400 ft radially from the injection well. Changes in gas/oil ratios usually occurred when the front had moved about half way between injection and production wells. Displacement efficiencies as determined by the model study were 32.8 per cent around the first injection well at the time of first breakthrough, and 41.3 per cent around the second injection well at the time of the first breakthrough. The average of the two displacement efficiencies is 37 per cent. Additional oil production during the time the wells produce water would, of course, improve the displacement efficiency figure.

As the flood front advances efficiencies are calculated from time to time. The most recent study made, after nearly three years of water injection history and five years of gas injection history, indicates that the following efficiencies will probably be obtained:

Reservoir*	Displ. Eff. %	Ult. Pattern Eff. %	Ult. Flood Eff. %	Recovery Eff. %
Upper Pettit "A"	43	90.0	38.7	35.9
Upper Pettit "B"	42	90.0	37.8	35.0
Lower Pettit (NW)	30	60.0	18.0	15.4
Lower Pettit (SW)	35	73.0	25.0	22.8

*See Appendix Tables I-III for sample calculations.

The displacement efficiency in the tabulation above was calculated by using the volumetric data from isopach maps and the average porosities and connate water together with injected and produced volumes of water to define the displacement. The pattern efficiency is a conservative estimate based on an early model study. The product of these two gives the flood efficiency. By using this flood efficiency and determining the original oil in place, we are able to determine the reservoir pore space occupied by hydrocarbons at the end of flooding. With predictions of bottom hole pressure and gas/oil ratio trends and the use of relative permeability relationships, the gas saturation can be determined. The amount of abandoned oil is then calculated. The recoverable stock tank barrels are calculated and this figure is divided by the original stock tank barrels in place to give the recovery efficiency.

The data for determining these efficiencies are obtained from the maps of Figs. 9 and 10, which show the predicted limits of an extended study of the permeability and production data, with model studies, well spacing and plan of operation considered. No attempt is made to predict the separate effect of either gas or water flooding. The efficiencies tabulated above reflect the overall effect of both cycling programs. The principal cause of the difference in efficiencies, as between reservoirs, is the degree of adaptability of that particular reservoir to flooding within economic limits.

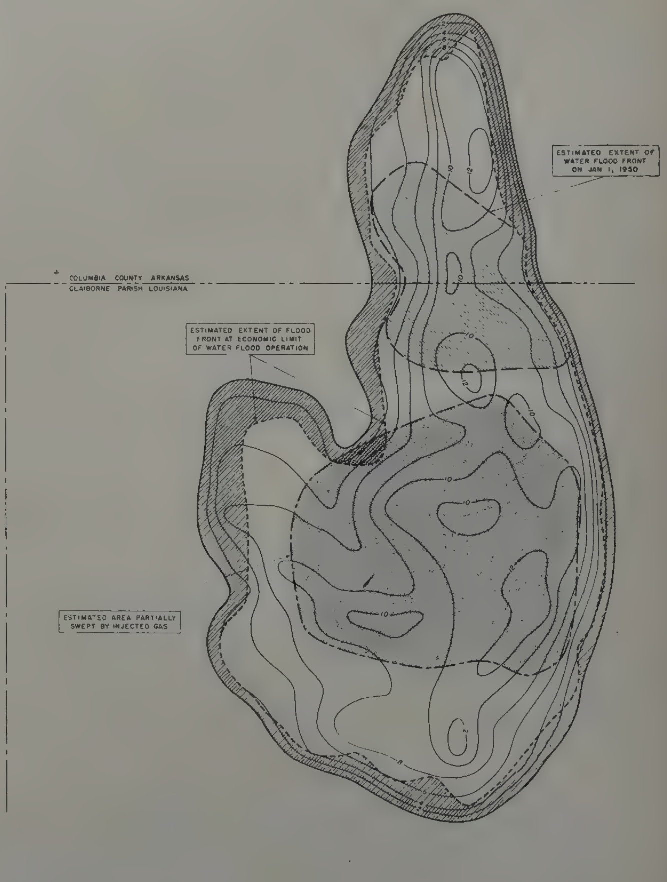
ESTIMATED EXTENT OF WATER FLOOD FRONT ON JAN 1, 1950
COLUMBIA COUNTY ARKANSAS
CLAIBORNE PARISH LOUISIANA
ESTIMATED EXTENT OF FLOOD FRONT AT ECONOMIC LIMIT OF WATER FLOOD OPERATION
ESTIMATED AREA PARTIALLY SWEPT BY INJECTED GAS
10

FIG. 9 — ISOPACHOUS AND INJECTED FLUID LIMITS, UPPER PETTIT "A" ZONE.

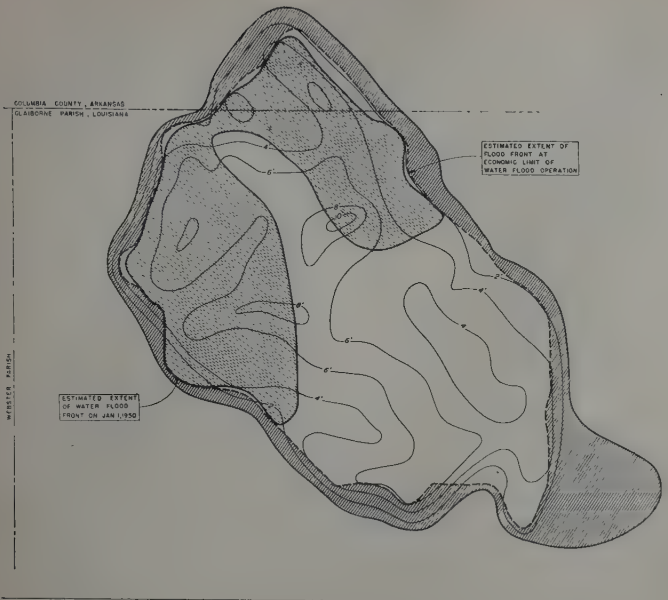
COLUMBIA COUNTY, ARKANSAS
CLAIBORNE PARISH, LOUISIANA
WEBSTER PARISH
ESTIMATED EXTENT OF FLOOD FRONT AT ECONOMIC LIMIT OF WATER FLOOD OPERATION
ESTIMATED EXTENT OF WATER FLOOD FRONT ON JAN 1, 1950
2'
4'
6'
8'
10'

FIG. 10 — ISOPACHOUS AND INJECTED FLUID LIMITS, UPPER PETTIT "B" ZONE.

From gas/oil ratio data an attempt was made to spot check some oil saturations in various portions of the producing "B" zone using the relation:[1]

$$(G/O)_{\text{Produced}} = (K_g/K_o)\,(U_o/U_g)\,(P/P_b)\,(520/T_r)\,(1/Z)\,(V_r/V_s) + (G/O)_{\text{Sol.}}$$

This assumes horizontal flow in an isotropic sand of uniform connate water saturation. Using monthly average gas/oil ratios and the latest isobaric maps and the reservoir fluid properties this equation was solved for K_g/K_o. Using an earlier K_g/K_o *vs* S_o curve of the Pettit reservoir[2] values of S_o were obtained and plotted in per cent of pore space in Fig. 12.

Within the water flood front itself use was made of water/oil ratio values at the time of abandonment to calculate relative permeabilities from the following equation:[3]

$$W/O = (K_w/K_o)\,(U_o/U_w)$$

From these values and relative permeability-saturation plots corrected to 23 per cent connate water,[4] the oil saturations were determined for several wells and plotted as shown in Fig. 12. This, of course, assumes a high rate of unidirectional flow in a 100 per cent liquid saturated medium. Also, gravity and capillary forces are considered negligible.

While the absolute value of these oil saturations is questionable, it is believed that the relative values indicate the effect of the water flood mechanism, as well as the effect of the previous gas injection program.

A profile of fluid saturation in per cent of pore space was taken across the "B" zone reservoir as shown in Fig. 12. The profile shows the approximate saturation distribution in the area in which the best production results are being obtained in front of the flood at the present time, and seems to substantiate the existence of a considerable oil bank in front of the flood. A small amount of data across the east side of the field indicates that the oil saturation is about 60 per cent. Low values of oil saturation and therefore high values of gas saturation in front of the flood bank from the center of Section 10 south and westward can be expected for the reason that gas has been injected in this portion of the reservoir. Records show that gas was injected in Well 15-6 in the early days and that oil saturation to the west was lowered considerably. No gas was ever injected into the "B" zone on the east side. The high gas saturation observed in the southeast portion of the reservoir would indicate leakage from the "A" zone due to poor well completions, or additional drainage area to the east of the isopach limits. The latter is borne out by the recoveries noted in that area and by the fact that a well was just recently completed in the NE ¼ of Section 30 as a Pettit producer.

On the basis of the saturations obtained above some computations were made using all available data to help determine the magnitude of a few important factors, such as bypassing, residual oil, displaced oil and recovery prior to and following flooding. From the approximate amount of oil produced from the watered-out area the recovery efficiency to date has been 32.9 per cent of the original stock tank oil in place. The average residual oil in the watered-out area (Fig. 12) is 34.5 per cent. This value represents the limit beyond which a well cannot be economically operated. It seems somewhat high when compared with sandstones but the type of porosities are entirely different, which probably account for the high value. Subtracting the produced and residual oils from the original in-place estimates gives the amount of oil that has either been bypassed or is in the present flood bank ahead of the water front. This value is 18.6 per cent of the original stock tank oil in place. To estimate the amount of oil in the flood bank, the difference between the average calculated oil saturations ahead of the oil bank and the average calculated oil saturation in the oil bank was obtained. This saturation per cent was applied to the pore space determined to be in the flood bank area. Early experiments showed the width of the flood bank to be about 900 ft in an average section of the reservoir. On this basis, 743,000 bbl of oil have been pushed from the watered area to the present flood bank. Therefore,

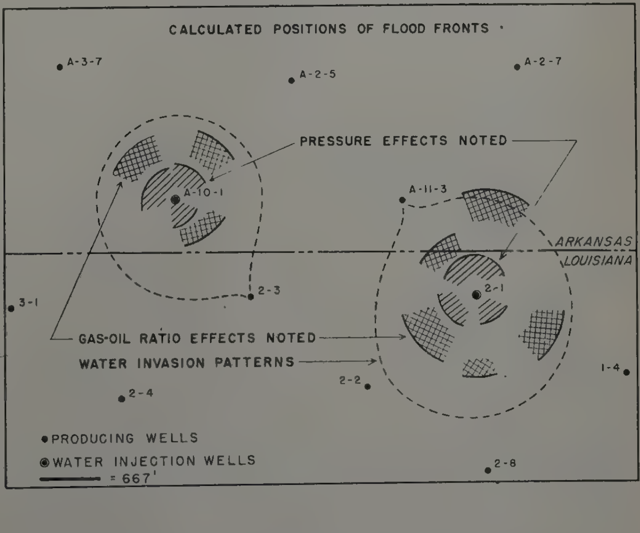

FIG. 11 — STUDY OF WATER INJECTION RESULTS IN EARLY PILOT TEST WELLS, PETTIT LIME, HAYNESVILLE FIELD.

---

[1] References given at end of paper.

at present 14.1 per cent of the producible stock tank oil has been bypassed. However, some wells are still producing with various water cut percentages within the flooded area and this production will lower the bypassed percentage and raise the recovery efficiency.

The amount of displaced oil was determined from the amount of water injected into the reservoir and the amount needed for fill-up of gas saturated space. These determinations indicate that the amount of stock tank oil recovered at the time water flooding began was 15.4 per cent of the original oil in place. Since water flooding began 17.5 per cent of the original oil in place has been produced.

Summary of "B" Zone Efficiencies

	Per cent
1. Displacement efficiency (1/1/50)	42
2. Estimated ultimate pattern efficiency	90
3. Ultimate flood efficiency	37.8
4. Ultimate recovery efficiency	34.7
5. Recovery efficiency to date (1/1/50)	32.9
6. Recovery efficiency prior to water flood	15.4
7. Recovery efficiency since water flood	17.5
8. Average residual oil (% pore space)	34.5
9. Producible stock tank oil bypassed or in flood bank (% original in place)	18.6
10. Producible stock tank oil pushed into flood bank (% original in place)	4.5
11. Producible oil bypassed to date (1/1/50) (% original in place)	14.1

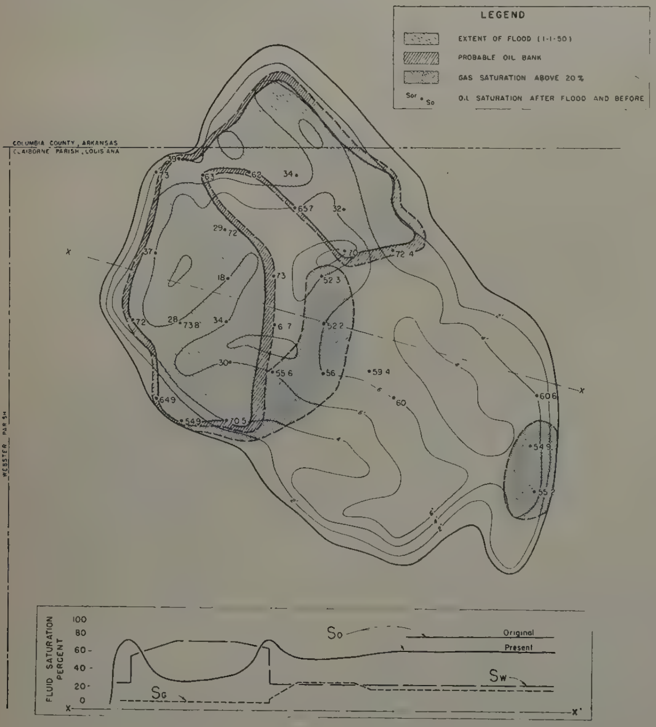
LEGEND
▨ EXTENT OF FLOOD (1-1-50)
▨ PROBABLE OIL BANK
▨ GAS SATURATION ABOVE 20%
Sor • So OIL SATURATION AFTER FLOOD AND BEFORE
COLUMBIA COUNTY, ARKANSAS
CLAIBORNE PARISH, LOUISIANA
WEBSTER PARISH
X
X'
FLUID SATURATION PERCENT
100
80
60
40
20
0
So
Original
Present
Sw
Sg
X
X'

FIG. 12 — MAP AND CROSS-SECTION OF FLUID SATURATION DISTRIBUTION, HAYNESVILLE PETTIT LIME "B" ZONE.

CONCLUSIONS

Economic results can be obtained with a combination gas and water flooding program in low permeability, relatively deep reservoirs, drilled on 80-acre spacing. After observing the Haynesville Pettit Lime combination flood for three years, it is estimated that ultimate recovery will be increased from the 18 per cent expected by natural depletion, to 34 per cent. Several factors have contributed to the success of this operation: (1) the Pettit lime in this area is susceptible to acid treatment; (2) a good supply of pure water (low total solids content) is available from shallow wells; and (3) it was possible to unitize the field early in its life.

Although flooding efficiency is higher with water than with gas, the gas injection program has contributed materially to increased ultimate recovery, primarily by arresting the decline in bottom hole pressure. It is recognized that a large quantity of oil will be left unrecovered in the reservoir. The higher the FVF of this unrecovered oil, the fewer the number of barrels of stock tank oil remaining, and the higher the ultimate recovery. In addition, less operating expense has resulted from the gas injection program because of the extended flowing life of the wells. And finally, the gas return program has made it possible to employ gas lift to handle the larger quantities of oil and water production at considerable savings in lifting expense.

ACKNOWLEDGMENT

The writer wishes to thank The Ohio Oil Co. for permission to prepare and present this paper for publication. Recognition is made of the able assistance of G. A. Clark, reservoir engineer in the Shreveport Division, who was very helpful in the preparation of this report, particularly the section dealing with efficiencies. Appreciation is also expressed for the cooperation of the engineering staff of the Haynesville Operators Committee who supplied most of the data. Liberal use was made of the reports, maps, graphs, etc., that are prepared and distributed by the Unit operators to the member companies from time to time.

REFERENCES

1. Horner, W. L.: *Secondary Recovery of Oil in the United States*, API (1942) 45.
2. Elkins, L. E.: *API Drilling and Production Practice* (1946) 160.
3. Leverett, M. C.: *Trans.* AIME (1939) **132,** 149.
4. Jones, Park J.: *Petroleum Production*, Vol. 1, Chap. 10.
5. Ervin, P. S.: "Results of Experimental Water Flooding in the Haynesville Field, Pettit Zone, A Lime Reservoir Originally Under Dissolved Gas Drive." Presented at the Spring Meeting of the Mid-Continent District API Division of Production, Amarillo, Tex., May 22-23, 1947.

APPENDIX

Calculation of Water Flood Efficiencies

Explanation of Tables I - III inclusive in the appendix is as follows:

1. Surface acres of reservoir is the planimetered area of the reservoir shown in Figs. 9 and 10.
2. Weighted thickness is obtained from the same isopachous maps.
3. Average porosity is based on core analysis data.

4. Average connate water value is from core analysis data.
5. Pore space occupied by hydrocarbons is calculated from the first four factors.
6. Water injected is from the well record files.
7. Water produced is from well record files which are based on tests made at regular weekly intervals.
8. Net injected water is the difference between values for No. 6 and No. 7, corrected to reservoir temperature of 179°F. Factor = 1.03.
9. Surface acres within flood front is from Figs. 9 and 10 showing water flood status.
10. Average thickness is from the same isopach map for the flooded area.
11. Hydrocarbon pore space within water flood limit is based on data from lines 10, 9, 4, and 3, above.
12. Pattern efficiency, at present status, is line 11 divided by line 5.
13. Displacement efficiency is line 8 divided by line 11.
14. Surface acres within ultimate economic flood front limits is from Figs. 9 and 10 showing water flood data.
15. Average thickness of floodable area is from the same isopach map.
16. Hydrocarbon pore space within flood limits is obtained from data given in lines 15, 14, 4, and 3.
17. Ultimate pattern efficiency is line 16 divided by line 5.
18. Overall water flood efficiency is line 13 multiplied by the conservative pattern efficiency of 90 per cent.

Table I — Calculation of Water Flood Efficiencies Upper Pettit Lime

	"A"	"B"
1. Surface acres of reservoir	11,269	10,238
2. Weighted average effective lime thickness, ft	6.803	4.521
3. Average porosity, %	19.2	21.9
4. Average connate water, %	23	23
5. Pore space originally occupied by hydrocarbons, bbl	87,900,000	60,600,000
6. Water injected, 1/1/50, (surface conditions), bbl	5,508,748	10,280,906
7. Water produced, 1/1/50, (surface conditions), bbl	220,442	1,148,342
8. Net injected water (reservoir conditions), bbl	5,446,982	9,406,541
9. Surface acres within water flood limit	1,497	2,970
10. Average thickness of flooded area	7.31	5.70
11. Hydrocarbon pore space within water flood limit, bbl	12,556,209	22,152,195
12. Pattern efficiency at present status, %	14.3	36.6
13. Displacement efficiency, 1/1/50, %	43	42
14. Surface acres within ultimate economic flood front limits	8,928	8,271
15. Avg. thickness of area within ultimate economic water flood limits, ft	7.913	5.136
16. Hydrocarbon pore space within ultimate economic water flood limits, bbl	81,010,000	55,630,000
17. Estimated ultimate economic pattern efficiency, %	92.2*	91.8*
18. Overall water flood efficiency, %	38.7	37.8

*For purposes of conservation an overall pattern efficiency of 90 per cent is used in this report.

Calculation of Recovery Efficiencies

Explanation of data in Table II.

1. Surface acres of reservoir is the planimetered area of the reservoir shown in Figs. 9 or 10, depending on the reservoir concerned.
2. Weighted thickness is obtained from the same isopachous map.
3. Average porosity is based on core analysis data.
4. Average connate water value is from core analysis data.
5. Oil originally in place is from calculations based on data of first four factors.
6. Original reservoir pressure is first recorded data on the "A" and "B" sections.
7. Reservoir temperature is from temperature surveys.
8. Formation volume factor at the original reservoir pressure of 2,440 psig is based on bottom hole sample analysis.
9. Stock tank oil originally in place is line 5 divided by line 8.
10. Displacement efficiency is water flood value from table on water flood efficiency calculations.
11. Pattern efficiency is from the same table.
12. Water flood efficiency is product of lines 10 and 11.
13. Reservoir pore space occupied by water at end of operations is product of lines 5 and 12.
14. Reservoir pore space occupied by oil and gas at end of economic operations is difference between lines 5 and 13.
15. Estimated average BHP during water flood operations is based on data shown in Fig. 4, and projected to correlate with general predicted plan of operations.
16. Equivalent gas saturation is explained under next line.
17. Calculations for gas saturation of the residual oil are based upon data from relative permeability — fluid saturation curves which are based on past performance. Data shown in Fig. 4 indicates that the future gas/oil ratio will be approximately 2,750 cu ft per bbl at 15.025 psia or 2,810 cu ft per bbl at 14.7 psia. During the period of water flooding operations it is anticipated that the BHP will average 1,050 psig; see Fig. 4. At this pressure gas in solution, as shown by a differential vaporization curve, will be about 235 cu ft per bbl. Free gas/oil ratio then would be 2,810 minus 235 or 2,575 cu ft per bbl. At reservoir conditions of 1,050 psig and 179°F, a compressibility factor of 0.93, this volume of gas would be 40.61 cu ft or 7.234 bbl. Formation volume factor, from a differential liberation curve for the oil at 1,050 psig is 1.223. Relative volume of gas to oil then would be 5.91. At a viscosity of .01470 for the gas and 0.945 for the oil, the relative permeability relation would then be 5.91x(.01470 divided by 0.943) or .92. Then the relative permeability-saturation curve shows that the equivalent gas saturation is 13 per cent. By use of the relationship $PV = ZnRT$ the gas saturation at 3,250 psig is 4.055 per cent.
18. Reservoir pore space occupied by gas at end of operations is product of lines 17 and 14.
19. Reservoir pore space occupied by oil at the end of operation is the difference between lines 14 and 18.
20. Oil FVF, at average reservoir pressure (1,050 psig) during flooding, is obtained from differential vaporization curves for Haynesville Pettit Oil.
21. Equivalent stock tank oil to be abandoned in reservoir is line 19 divided by line 20.
22. Total recoverable oil, stock tank conditions, is the difference between line 9 and line 21.
23. Overall recovery efficiency on the basis of stock tank oil is line 22 divided by line 9.

Table II — Calculation of Initial Reserves and Recoverable Reserves, Upper Pettit Lime, "A" Section

1. Surface acres of reservoir	11,269
2. Weighted average effective lime thickness, ft	6.803
3. Average porosity, %	19.2
4. Average connate water, %	23
5. Oil originally in place, reservoir bbl	87,900,000
6. Original reservoir pressure, psig	2,440
7. Reservoir temperature, °F	179
8. Formation volume factor at original conditions	1.331
9. Stock tank oil originally in place, bbl	66,000,000
10. Displacement efficiency, %	43
11. Ultimate economic pattern efficiency, %	90
12. Overall water flood efficiency, %	38.7
13. Reservoir pore space occupied by water at end of operations, bbl	34,000,000
14. Reservoir pore space occupied by oil and gas at end of economic operations, bbl	53,900,000
15. Estimated average BHP during water flood operations, psig	1,050
16. Equivalent gas saturation	13.0
17. Residual gas saturation at 3,250 psig abandon. pressure	4.055
18. Reservoir pore space occupied by gas at end of operation, bbl	2,185,600
19. Reservoir pore space occupied at end of operation, bbl	51,714,000
20. Oil FVF at average reservoir pressure as flooded	1.223
21. Equivalent stock tank oil to be abandoned in reservoir	42,284,500
22. Total recoverable oil, stock tank conditions	23,715,500
23. Overall recovery efficiency (basis stock tank oil), %	35.9

Table III — Analysis of Saturation Distribution Data as Applied to "B" Zone Recovery Efficiency

1. Pore space inside watered area (bbl) ref. Fig. 12	28,800,000
2. Connate water estimate at 23% (bbl)	6,600,000
3. Hydrocarbon pore space within flood area (bbl)	22,200,000
4. Cumulative oil production from flood area (approx.) (bbl)	5,489,000
5. Original stock tank oil in hydrocarbon pore space (bbl)	16,670,000
6. Recovery efficiency to date in flooded area	32.9%
7. Stock tank oil remaining in flooded area as of 1/1/50 (bbl) 5 – 4	11,181,000
8. Average residual S_o from W/O, K_w/K_o computations (in % pore space)	34.5%
9. Residual oil remaining in flooded area (bbl) 8 x 1	9,940,000
10. Stock tank residual oil remaining in flooded area (bbl) 9 ÷ 1.23	8,080,000
11. Producible stock tank oil in flood bank or bypassed (bbl) 7 – 10	3,101,000
12. Stock tank oil in flood bank or bypassed, % of original stock tank oil, 11 ÷ 5	18.6%
13. Average S_o in flood bank from G/O, K_g/K_o relationships (% pore space)	66.7%
14. Average S_o in "B" Reservoir outside flood effect from G/O, K_g/K_o relationships (% pore space)	55.8%
15. Average S_o increase due to flood bank effect (% pore space) 13 – 14	10.9%
16. Average S_o increase due to flood bank effect (% of hydrocarbon pore space) 15 ÷ .77	14.2%
17. Probable pore space affected by present flood bank (bbl)	8,380,000
18. Probable oil in flood bank from within water line area (res. bbl)	914,000
19. Probable oil in flood bank from within water line area (stock tank bbl) 18 ÷ 1.23	743,000
20. Probable stock tank oil bypassed after some movement (bbl) 11 – 19	2,358,000
21. Per cent of original stock oil in place bypassed by present front	14.1%
22. Net water injected in "B" zone (bbl corrected to reservoir conditions)	9,406,500
23. Net water required for fillup of probable gas saturation (17%)	4,900,000
24. Probable oil displaced from watered out area 21 – 22	4,506,500
25. Oil produced due to water displacement, 23 – 18	3,592,500
26. Stock tank oil produced due to water displacement, 24/1.230	2,920,000
27. Stock tank oil produced prior to water flood, 4 – 25	2,569,000
28. Per cent of original stock tank oil recovered when flood began	15.4%
29. Per cent of original stock tank oil recovered to date by water flood	17.5%

T.P. 3078

RELATIVE PERMEABILITY STUDIES

I. FATT AND H. DYKSTRA, CALIFORNIA RESEARCH CORP., LA HABRA, CALIF., MEMBERS AIME

ABSTRACT

Relative wetting phase permeabilities calculated from capillary pressure-saturation data are compared with measured relative permeability data. The equation relating relative permeability to capillary pressure-saturation data is derived by assuming that a porous medium is analogous to a bundle of capillary tubes. The equation includes a term to correct for the difference between fluid path length and length of core. Relative oil permeability data in the water-oil-gas system are presented, and it is shown that if the water is considered part of the rock matrix, the relative oil permeability curve is typical of a wetting phase relative permeability curve. Apparatus for measuring two and three-phase relative permeabilities are described.

INTRODUCTION

The difficulty in measuring relative permeability of cores has made it desirable to have a correlation between relative permeability and some more easily measured property of porous media. Such an easily measured property is the capillary pressure-saturation relation.

In the past there has been a tendency to separate the capillary pressure concept from the very complex pore geometry and to consider that the capillary pressure-saturation curve gives only some characteristic distribution of interfacial curvature between two fluids.[1] Recently, however, it has been realized that if capillary pressure data are to yield information concerning pore size distribution[2] and fluid flow in porous media, the pore must be assumed to have a simple shape such as a cylinder or a sphere.[3]

Childs and George[4] showed that relative water permeability could be calculated from the capillary pressure-water saturation curve by assuming that the pores are cylinders in which the fluid flowing obeys Poiseuille's Law, and that the capillary pressure curve indicated the size and number of pores. Purcell[5] derived an equation relating the permeability of a porous medium to the capillary pressure curve by assuming the porous medium to be analogous to a bundle of capillary tubes. Gates and Lietz[6] calculated relative permeability by an equation derived from Purcell's equation.

In this paper an equation is derived giving the relative water permeability as a function of water saturation by assuming that the core sample can be represented by a bundle of capillary tubes in which the fluid path length is not the same as the bulk length, and in which the fluid path length varies with saturation.

THEORY

For a bundle of N capillary tubes the flow through dN tubes will be

$$dQ = q_{av}\ dN \quad \dots\dots\dots\dots \quad (1)$$

where Q is the total flow rate through all the tubes and q_{av} is the average flow rate through the tubes in the interval dN.

If the interval dN is made small the average flow rate through a tube in the interval dN is given by Poiseuille's Law,

$$q_{av} = \frac{\pi r^4 \triangle P}{8 \mu l} \quad \dots\dots\dots\dots \quad (2)$$

where $\triangle P$ is the pressure drop across the tube of length l and radius r, and μ is the viscosity of the fluid. Substituting for q_{av} in Equation (1),

$$dQ = \frac{\pi r^4 \triangle P}{8 \mu l}\ dN \quad \dots\dots\dots\dots \quad (3)$$

Darcy's Law for linear flow of an incompressible fluid in a porous medium is

$$Q = \frac{KA \triangle P}{\mu L} \quad \dots\dots\dots\dots \quad (4)$$

where K is the permeability and $\triangle P$ is the pressure drop across a bundle of tubes which has replaced the porous medium of length L and cross-sectional area A. Differentiating Darcy's Law with A, $\triangle P$, μ, and L constant,

$$dQ = \frac{A \triangle P}{\mu L}\ dK \quad \dots\dots\dots\dots \quad (5)$$

Equating (3) and (5) gives

$$dK = \frac{\pi r^4 L}{8 A l}\ dN \quad \dots\dots\dots\dots \quad (6)$$

If the pores are assumed to be cylinders

$$dV = \pi r^2 l dN \quad \dots\dots\dots\dots \quad (7)$$

where V is the volume of flowing fluid in the pores. Substituting for dN in Equation (6) gives

$$dK = \frac{r^2 L}{8 A l^2}\ dV \quad \dots\dots\dots\dots \quad (8)$$

By definition the saturation, S, of the core is

$$S = \frac{V}{V_p} = \frac{V}{\phi A L} \quad \dots\dots\dots\dots \quad (9)$$

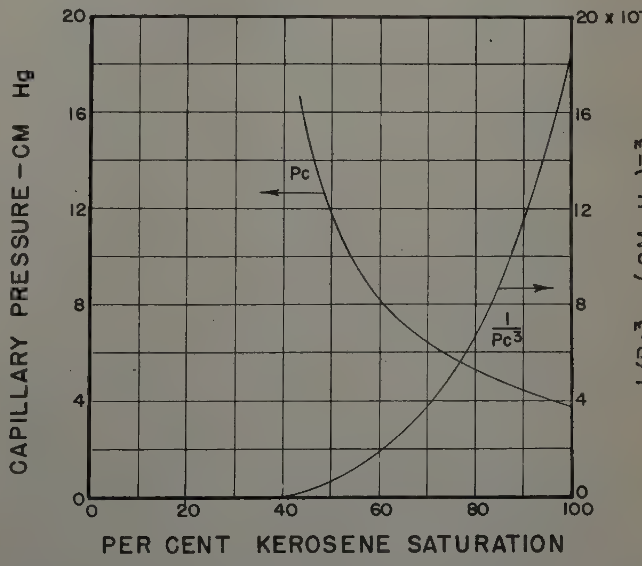

FIG. 1—CAPILLARY PRESSURE CURVE. DATA FROM FIG. 33 OF GATES AND LIETZ.[6]

---

[1] References given at end of paper.

Manuscript received in the office of the Petroleum Branch, AIME, Sept. 14, 1950. Paper presented at the Fall Meeting of the Branch in Los Angeles Oct. 12-13, 1950.

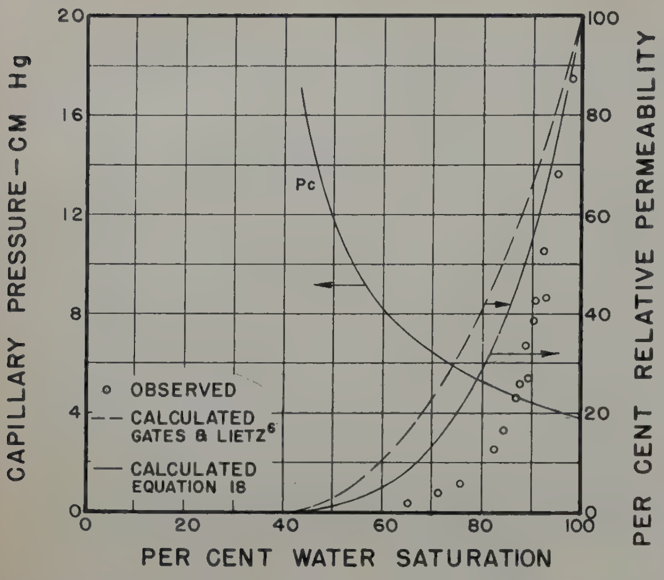

FIG. 2 — RELATIVE PERMEABILITY AND CAPILLARY PRESSURE CURVES. DATA FROM FIGS. 26 AND 33 OF GATES AND LIETZ.[6]

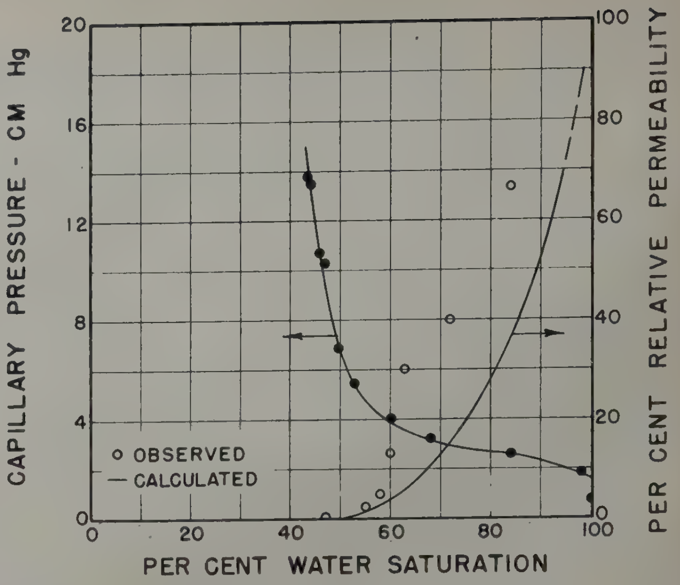

FIG. 3 — RELATIVE WATER PERMEABILITY AND CAPILLARY PRESSURE CURVES IN WATER-OIL SYSTEM. SAND: BASAL TUSCALOOSA, MISS. PERMEABILITY: 125 MD. POROSITY: 15 PER CENT.

where V_p is the total pore volume and ϕ is the porosity. Differentiating Equation (9) and substituting for dV in Equation (8) gives

$$dK = \frac{r^2 \phi L^2}{8l^2} dS \quad \ldots \ldots \ldots \quad (10)$$

Equation (10) contains the pore radius, r, and the fluid path length, l. These terms are not directly measurable and therefore must be related to some other property of the core.

The ratio of the fluid path length, l, to the length of the core, L, has been termed the tortuosity, t, or

$$t = \frac{l}{L} \quad \ldots \ldots \ldots \ldots \quad (11)$$

The tortuosity, t, has not yet been related directly to a measurable core property. A reasonable assumption regarding t can be obtained by considering what happens to the wetting phase in the pore spaces as the core is desaturated. During desaturation the wetting phase retreats into the smaller pores and into the crevices between sand grains. Liquid in such crevices has a small radius of curvature and by the derivation given in this paper is considered to be in small pores. It can be reasoned then that liquid flowing in the crevices and small pores will travel a more tortuous path than liquid flowing through the large pores. As a first approximation t can be assumed to vary inversely as r, or

$$t = \frac{a}{r^b} \quad \ldots \ldots \ldots \ldots \quad (12)$$

where a and b are constants. Substituting Equations (11) and (12) in (10) gives

$$dK = \frac{\phi \, r^{2(1+b)}}{8a^2} dS \quad \ldots \ldots \ldots \quad (13)$$

The pressure, P_c, across a curved interface between two fluids[1] is

$$P_c = \frac{2 \sigma \cos \theta}{r} \quad \ldots \ldots \ldots \ldots \quad (14)$$

where r is the radius of curvature, σ the interfacial tension at the interface, and θ the liquid-solid contact angle. When Equation (14) is applied to porous media the pressure term is known as the capillary pressure, and r is the pore radius at which a non-wetting phase just displaces a wetting phase out of the pore. Equation (14) thus gives r as a function of the capillary pressure. Substituting for r in Equation (13) gives

$$dK = \frac{\phi (2 \sigma \cos \theta)^{2(1+b)}}{8a^2 P_c^{2(1+b)}} dS \quad \ldots \ldots \quad (15)$$

If the constants, a and b, were known, the effective permeability, K_e, at any saturation could be calculated by integrating Equation (15) from zero saturation to the desired saturation, S

$$K_e = \frac{\phi (2 \sigma \cos \theta)^{2(1+b)}}{8a^2} \int_0^S \frac{dS}{P_c^{2(1+b)}} \quad \ldots \quad (16)$$

The relative permeability, K_r, however, can be calculated without knowing the constant, a, if the constant, b, is known

Table I — Calculation of Wetting Phase Relative Permeability From the Equation

$$K_r = \frac{\int_0^S \frac{dS}{P_c^3}}{\int_0^{100} \frac{dS}{P_c^3}}$$

S Per cent	P_c cm Hg	$\frac{1}{P_c^3}$ $(cm\ Hg)^{-3}$	Area from 0 to S in²	K_r Per cent
100	3.8	18.2 x 10^{-3}	4.15	100
95	4.1	14.5	3.13	75
90	4.4	11.7	2.31	56
85	4.8	9.0	1.68	40
80	5.3	6.7	1.19	29
75	5.8	5.1	0.82	20
70	6.4	3.8	0.54	13
65	7.1	2.8	0.34	8.2
60	8.0	2.0	0.20	4.8
55	9.4	1.2	0.10	2.4
50	11.6	0.6	0.04	1.0
45	15.0	0.3 x 10^{-3}	0.01	0.2

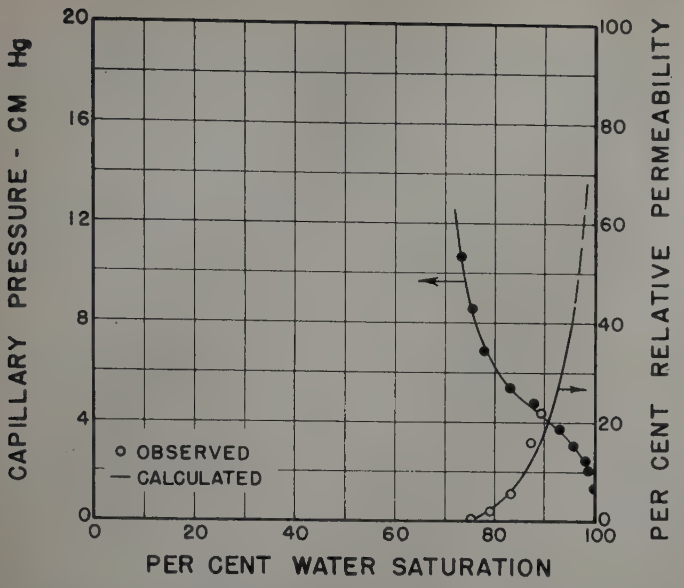

FIG. 4 — RELATIVE WATER PERMEABILITY AND CAPILLARY PRESSURE CURVES IN WATER-OIL SYSTEM. SAND: BASAL TUSCALOOSA, MISS. PERMEABILITY: 100 MD. POROSITY: 26 PER CENT.

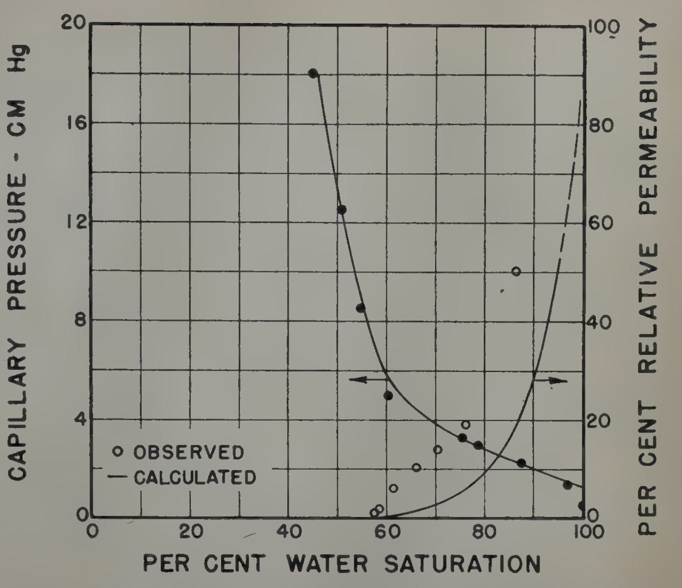

FIG. 5 — RELATIVE WATER PERMEABILITY AND CAPILLARY PRESSURE CURVES IN WATER-OIL SYSTEM. SAND: BASAL TUSCALOOSA, MISS. PERMEABILITY: 129 MD. POROSITY: 22 PER CENT.

or assumed, because by definition $K_r = K_e/K$, thus giving

$$K_r = \frac{\int_0^S \frac{dS}{P^{2(1+b)}}}{\int_0^{100} \frac{dS}{P_c^{\,2(1+b)}}} \quad \ldots \ldots \ldots \quad (17)$$

RESULTS

Comparison of Calculated and Measured Relative Water Permeability Data

Gates and Lietz[6] have calculated relative permeabilities using Equation (17) with b assumed to be zero, that is, the tortuosity independent of the pore radius and thus independent of the saturation. This paper compares measured data with calculated data for $b = \frac{1}{2}$, that is the tortuosity is a function of pore radius and therefore dependent on the saturation. For $b = \frac{1}{2}$ Equation (17) becomes

$$K_r = \frac{\int_0^S \frac{dS}{P_c^{\,3}}}{\int_0^{100} \frac{dS}{P_c^{\,3}}} \quad \ldots \ldots \ldots \quad (18)$$

To calculate relative permeability from Equation (18), $\frac{1}{P_c^{\,3}}$ is plotted against saturation, S and the area under the $\frac{1}{P_c^{\,3}}$ *vs* S curve is obtained by graphical integration or by planimetering. As an example, capillary pressure-saturation data from Gates and Lietz[6] (their Figs. 26 and 33) are used to calculate relative permeability of the wetting phase, which for the example given is kerosene in the kerosene-air system. The capillary pressure, P_c, and $\frac{1}{P_c^{\,3}}$ *vs* the saturations, S are shown in Fig. 1 and Table I. The area under the $\frac{1}{P_c^{\,3}}$ *vs* S curve from zero saturation to saturation, S, was obtained by graphical integration and is shown in column 4 of Table I. The areas given in column 4 are divided by the total area under the $\frac{1}{P_c^{\,3}}$ *vs* S curve to give the per cent relative permeability in column 5. The calculated curve is plotted in Fig. 2. The relative permeability data and the curve calculated by Gates and Lietz[6] are also shown in Fig. 2.

Relative water permeability and capillary pressure data in the water-oil system were obtained in this laboratory on five California cores and four Mississippi cores. Relative water permeabilities were calculated from capillary pressure data by means of Equation (18). The measured data and the calculated curve for each core, shown in Figs. 3 through 11, are in fair agreement.

Comparison of measured and of calculated relative permeability data indicates that the constant, b, may not be the same for all types of sands. For the Basal Tuscaloosa sand b

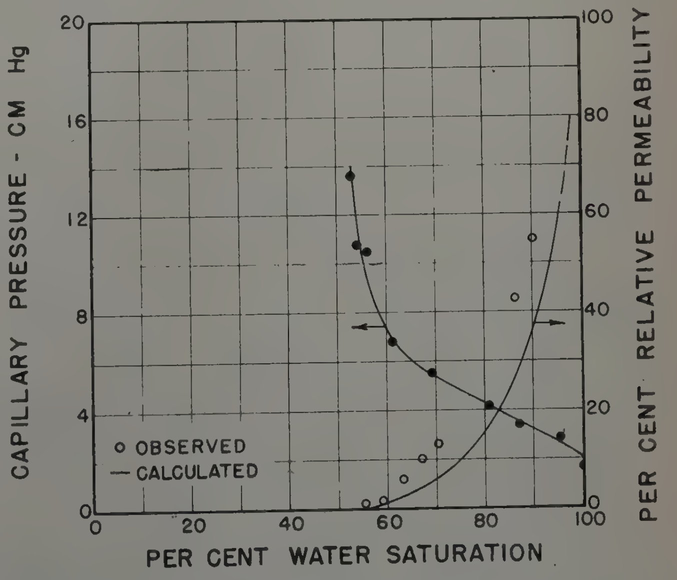

FIG. 6 — RELATIVE WATER PERMEABILITY AND CAPILLARY PRESSURE CURVES IN WATER-OIL SYSTEM. SAND: BASAL TUSCALOOSA, MISS. PERMEABILITY: 58 MD. POROSITY: 18 PER CENT.

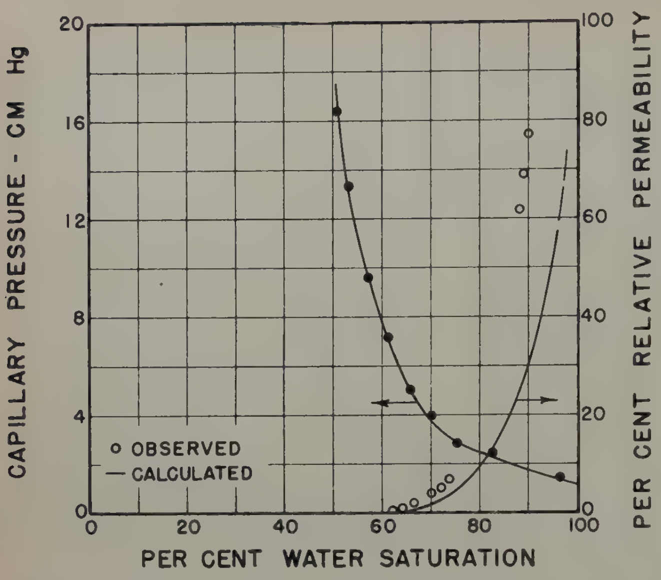

FIG. 7 — RELATIVE WATER PERMEABILITY AND CAPILLARY PRESSURE CURVES IN WATER-OIL SYSTEM. SAND: GATCHELL, NORTHERN SAN JOAQUIN VALLEY, CALIF. PERMEABILITY: 180 MD. POROSITY: 18 PER CENT.

less than ½ will give a better check, whereas for the Gatchell sand $b = \frac{1}{2}$ appears to give the best check. For most of the data presented by Gates and Lietz[6] b greater than ½ will give a better check. As more relative permeability data are obtained, an average b term may be chosen for each type of sand to give the best fit between calculated curves and experimental data.

Relative Oil Permeability Data in Water-Oil-Gas System

Relative oil permeability data in the water-oil-gas system are shown in Figs. 12 and 13 for two Mississippi cores. The data of Figs. 12 and 13 are replotted in Fig. 14 as $\frac{K_o}{K_o \text{ at } S_g=0}$ vs S_g, where K_o is the effective oil permeability at gas saturation, S_g. The above ratio is obtained by dividing the effective oil permeability at each water saturation by the effective oil permeability at the same water saturation and zero gas saturation. The data fall approximately on the same curve. The curve is typical of a wetting phase relative permeability curve. This seems to indicate that in the water-oil-gas system the water can be considered part of the rock matrix with oil as the wetting phase and gas as the nonwetting phase.

Considering interstitial water as part of the rock matrix suggests the possibility of calculating $\frac{K_o}{K_o \text{ at } S_g=0}$ in the water-oil-gas system by using Equation (18) from the oil-gas capillary pressure curve with interstitial water present. The method of calculating $\frac{K_o}{K_o \text{ at } S_g=0}$ is illustrated by using the data from Figs. 14 and 15 of Gates and Lietz.[6] The calculations are carried out as illustrated in the previous example, except that P_c, $\frac{1}{P_c^{\,3}}$, and $\frac{K_o}{K_o \text{ at } S_g=0}$ are plotted against gas saturation. The calculated and experimental results* are given in Figs. 15 and 16. The agreement between the calculated curves and the observed data is good.

Calculation of relative permeabilities from capillary pressure-saturation data greatly simplifies the problem of obtaining relative permeabilities. With some assurance of fair to good agreement between calculated and observed relative permeabilities, much time and expense can be saved by obtaining capillary pressure-saturation data and calculating relative permeabilities by Equation (18).

---

*The relative permeability with interstitial water present as plotted by Gates and Lietz[6] in their Figs. 12 through 15, is the same as $\frac{K_o}{K_o \text{ at } S_g = 0}$ used in this paper. To obtain the relative oil permeability (defined in the API Code 27) as a function of gas saturation it is only necessary to multiply $\frac{K_o}{K_o \text{ at } S_g = 0}$ by the effective oil permeability with interstitial water present and to divide by the permeability of the core.

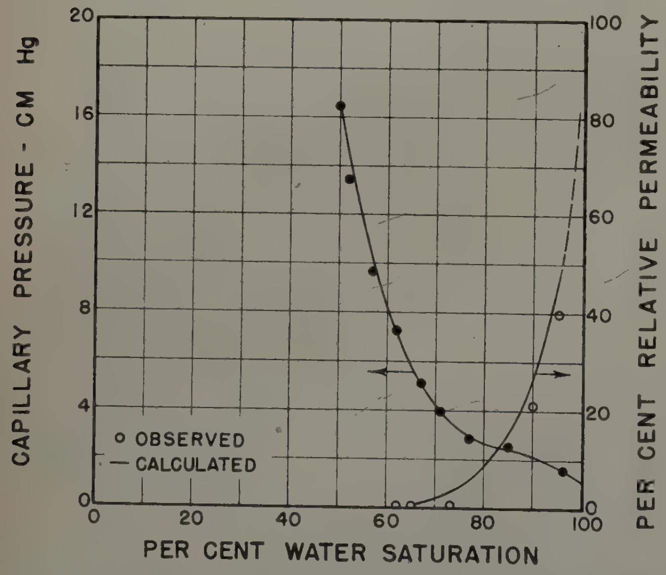

FIG. 8 — RELATIVE WATER PERMEABILITY AND CAPILLARY PRESSURE CURVES IN WATER-OIL SYSTEM. SAND: GATCHELL, NORTHERN SAN JOAQUIN VALLEY, CALIF. PERMEABILITY: 140 MD. POROSITY: 14 PER CENT.

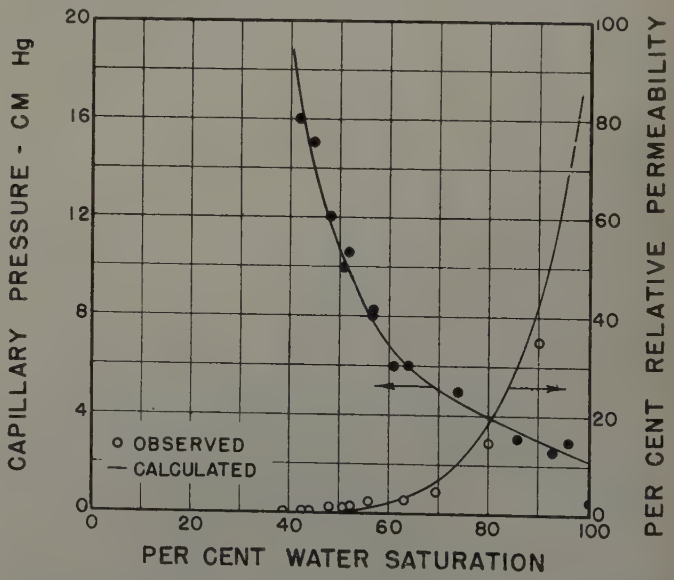

FIG. 9 — RELATIVE WATER PERMEABILITY AND CAPILLARY PRESSURE CURVES IN WATER-OIL SYSTEM. SAND: GATCHELL, NORTHERN SAN JOAQUIN VALLEY, CALIF. PERMEABILITY: 80 MD. POROSITY: 11 PER CENT.

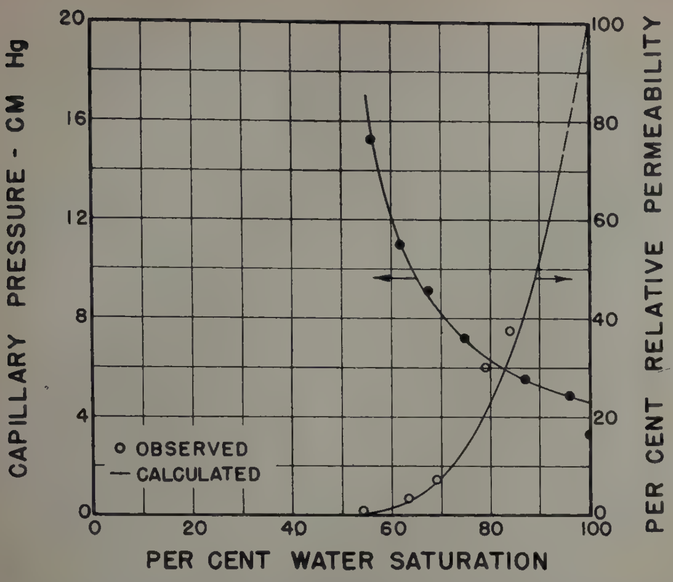

FIG. 10 — RELATIVE WATER PERMEABILITY AND CAPILLARY PRESSURE CURVES IN WATER-OIL SYSTEM. SAND: McADAMS, NORTHERN SAN JOAQUIN VALLEY, CALIF. PERMEABILITY: 13 MD. POROSITY: 10 PER CENT.

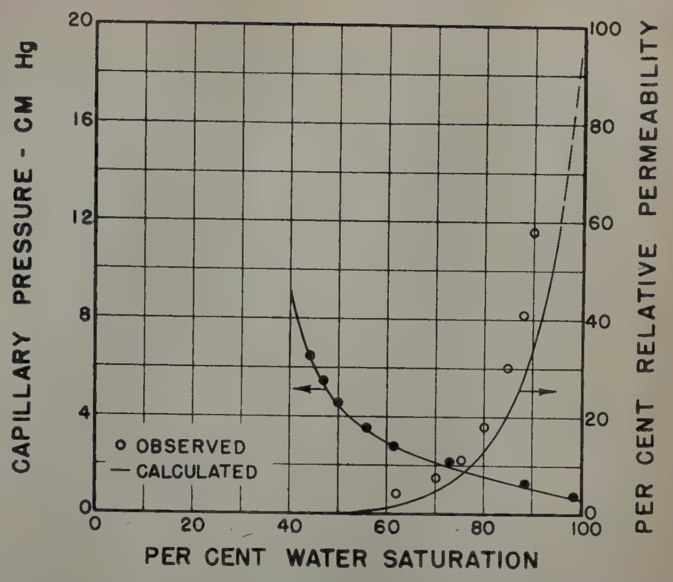

FIG. 11 — RELATIVE WATER PERMEABILITY AND CAPILLARY PRESSURE CURVES IN WATER-OIL SYSTEM. SAND: VAQUEROS, NORTHERN SAN JOAQUIN VALLEY, CALIF. PERMEABILITY: 47 MD. POROSITY: 12 PER CENT.

APPARATUS

Relative Water Permeability Apparatus

The relative water permeability apparatus is shown in Fig. 17 for the water-oil system. The apparatus is all glass except the nickel flow lines between the core and the pipets. Flow rates as low as 10^{-5} cc per sec are measured in 0.1 ml graduated pipets, the flow rate into the core being measured in one pipet and the flow rate out of the core being measured in the other pipet at the same level. When the flow rates are identical, the core is at saturation equilibrium. Bypass stopcocks are used to return the water in the measuring pipets to the zero mark. A fine sintered glass filter is used to filter the water before it passes through the core. The end plugs are Monel metal to which porous plates are cemented with De Khotinsky cement. The porous plate* has a permeability of about 50 md and entry pressure of about three psi in the water-oil system. The porous plate covers the whole face of the core.

Before effective water permeabilities can be measured in the apparatus shown in Fig. 17, the pressure drop across the porous end plates must be known as a function of flow rate. To obtain this calibration, flow rates at different pressure drops are measured with the porous plates in capillary contact. The product of the flow rate, q, and the viscosity, μ, is plotted against the pressure drop, ΔP, and the slope of a straight line thus obtained gives $\left[\frac{\Delta(\Delta P)}{\Delta(q\mu)}\right]_{\text{plates}}$. The plate calibration is independent of capillary pressure.

To measure effective water permeability, a water saturated core is placed between the porous end plates of the core holder and the assembly is immersed in oil. The desired water saturation is obtained by imposing a capillary pressure on the core. The water removed from the core is measured in the volume changer shown in Fig. 17. The saturation at equilibrium is calculated from the volume of water removed and the pore volume. Thus a capillary pressure-water saturacurve is also obtained in the apparatus. At each water saturation, flow rate is measured as a function of the pressure drop across the core and porous end plates. The slope of the line obtained is $\left[\frac{\Delta(\Delta P)}{\Delta(q\mu)}\right]_{\text{total}}$. The effective water permeability is calculated from the equation

$$K_w = \frac{L}{A}\left\{\frac{1}{\left[\frac{\Delta(\Delta P)}{\Delta(q\mu)}\right]_{\text{total}} - \left[\frac{\Delta(\Delta P)}{\Delta(q\mu)}\right]_{\text{plates}}}\right\}$$

Use of the $\left[\frac{\Delta(\Delta P)}{\Delta(q\mu)}\right]$ plot for calculating permeability by

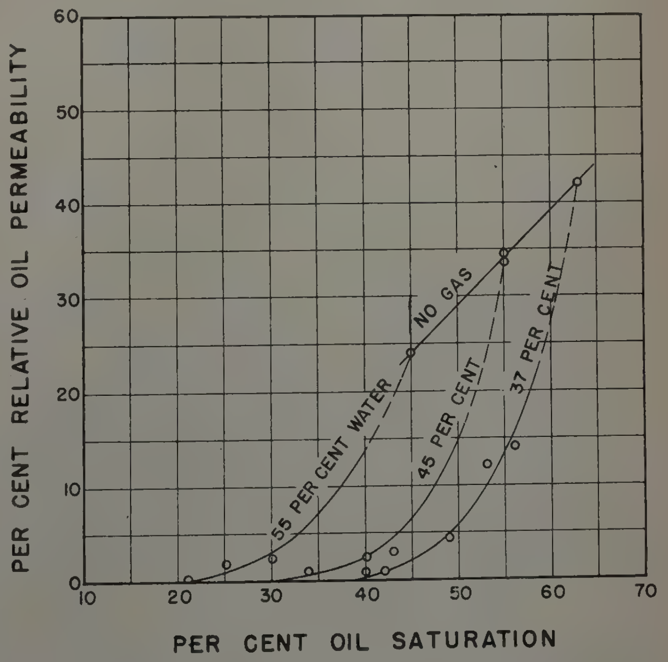

FIG. 12 — RELATIVE OIL PERMEABILITY IN WATER-OIL-GAS SYSTEM. SAND: BASAL TUSCALOOSA, MISS. PERMEABILITY: 124 MD. POROSITY: 26 PER CENT.

---

*Allen filter disk made by Allen Filter Co., Toledo, Ohio.

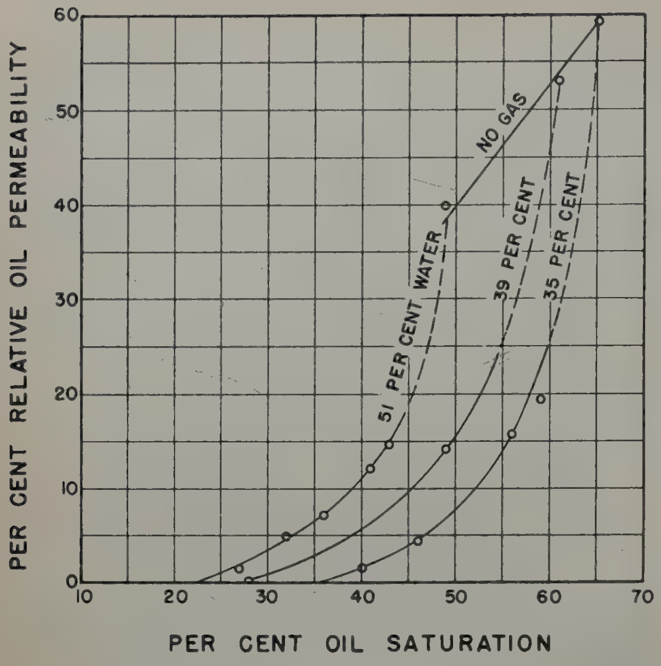

FIG. 13 — RELATIVE OIL PERMEABILITY IN WATER-OIL-GAS SYSTEM. SAND: BASAL TUSCALOOSA, MISS. PERMEABILITY: 100 MD. POROSITY: 26 PER CENT.

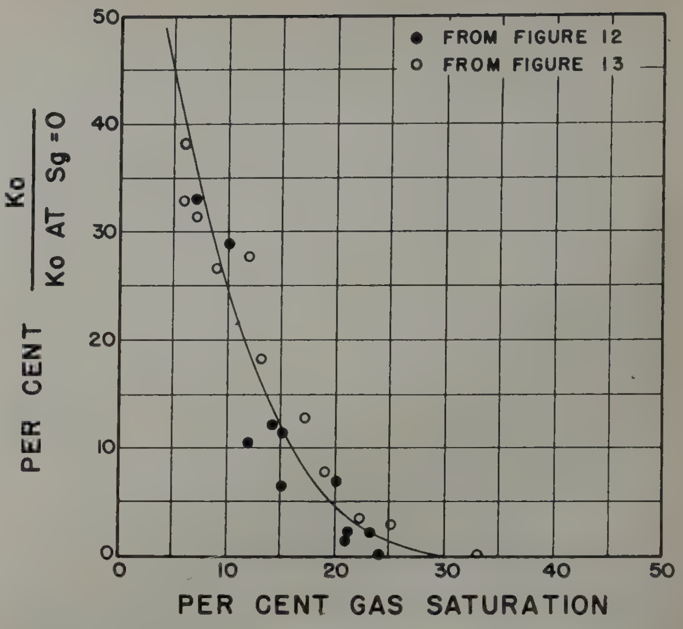

FIG. 14 — $\frac{\text{Effective Oil Permeability}}{\text{Effective Oil Permeability at } S_g=0} = \frac{K_o}{K_o \text{ at } S_g=0}$ IN WATER-OIL-GAS SYSTEM.

Darcy's law gives a more accurate permeability from the data than a permeability obtained by averaging permeabilities calculated from each point. On the $\left[\frac{\Delta(\Delta P)}{\Delta(q\mu)}\right]$ plot an obviously erroneous measurement can be easily seen and omitted from consideration in drawing the best straight line.

The above method of measuring effective water permeability has certain advantages over the method using a static manometer with a pressure tap in the center of the porous end plates. The advantages are: (1) No time is lost while waiting for a static manometer to come to equilibrium with the core; (2) no correction is needed due to constriction of flow caused by a center tap; (3) the pressure drop across the core is obtained by subtracting one direct measurement from another, whereas the static manometer does not measure the true pressure drop across a core.[7]

The magnitude of the $\left[\frac{\Delta(\Delta P)}{\Delta(q\mu)}\right]$ terms involved in calculating effective water permeability are shown in Table II for a 47 md core. Inasmuch as the core and porous plates are in series, the pressure drops are directly proportional to the $\left[\frac{\Delta(\Delta P)}{\Delta(q\mu)}\right]$ terms. Table II shows that the ratio of the pressure drop across the plates to the total pressure drop ranges from 0.23 to 0.02, so that the probable error in the calculated pressure drop across the core is only slightly greater than the probable error in the total pressure drop.

For cores of high permeability the probable error in the pressure drop across the core may be appreciably greater than that for cores of low permeability. However, as the water saturation decreases the effective water permeability decreases

Table II — Calculation of K_{ew} From the ΔP vs $q\mu$ Plot

Core of Fig. 11, $K = 47$ md, $L = 3.08$ cm, $A = 5.05$ cm^2

S_w	$\left[\frac{\Delta(\Delta P)}{\Delta(q\mu)}\right]_{total}$	$\left[\frac{\Delta(\Delta P)}{\Delta(q\mu)}\right]_{plates}$	$\left[\frac{\Delta(\Delta P)}{\Delta(q\mu)}\right]_{core}$	K_{ew}
Per cent	cm-md	cm-md	cm-md	md
90	2.90 x 10^{-2}	0.67 x 10^{-2}	2.23 x 10^{-2}	27.2
88	3.81	0.67	3.14	19.3
85	5.0	0.67	4.3	14.1
80	7.8	0.67	7.1	8.5
76	12.3	0.67	11.6	5.2
70	19.0	0.67	18.3	3.3
62	34.4 x 10^{-2}	0.67 x 10^{-2}	33.7 x 10^{-2}	1.8

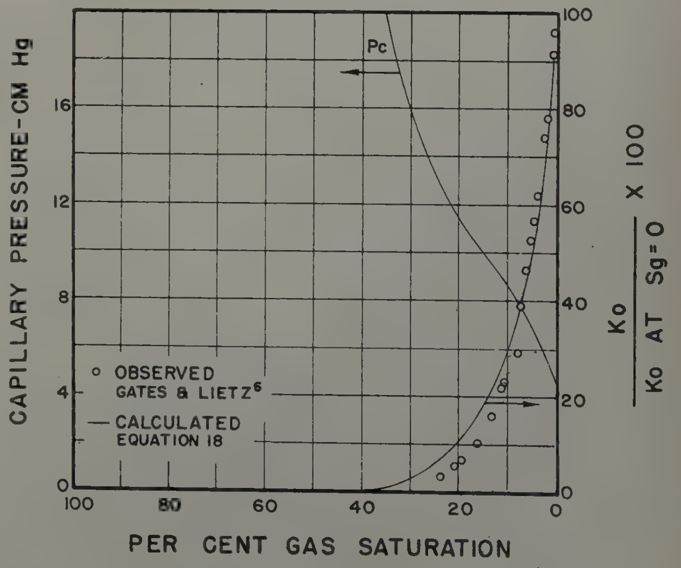

FIG. 15 — $\frac{\text{Effective Oil Permeability}}{\text{Effective Oil Permeability at } S_g=0} = \frac{K_o}{K_o \text{ at } S_g=0}$ IN WATER-OIL-GAS SYSTEM. OBSERVED DATA FROM FIG. 14 OF GATES AND LIETZ.[6] INTERSTITIAL WATER = 46 PER CENT.

more rapidly, so that the probable error in the calculated pressure drop across the core again approaches the probable error in the total pressure drop.

Relative Oil Permeability Apparatus

The apparatus for measuring relative oil permeability in the water-oil-gas system is the same as the relative water permeability apparatus shown in Fig. 17 with the exception of the core holder. Detail of the core holder is shown in Fig. 18. The porous diaphragms are made oil-wet by treating ordinary water-wet porous diaphragms with "Dri-Film."[8]

In the water-oil-gas system, water is present as an immobile phase to correspond to connate water in the reservoir. A relative oil permeability curve may be obtained for several different constant water saturations.

Before effective oil permeabilities can be measured, the pressure drop across the oil-wet porous end plates must be known as a function of flow rate. The porous end plate calibration is determined exactly as is done for the relative water permeability.

The desired water and oil saturations are first obtained in a capillary pressure apparatus. The core is then placed in the core holder of the relative oil permeability apparatus. A capillary pressure is imposed on the oil to give a desired gas saturation. Air enters the core through the hole in the center of the porous end plates. Effective oil permeabilities and oil saturations are measured and calculated as is done for relative water permeability.

REFERENCES

1. Leverett, M. C.: *Trans.* AIME (1941) **142**, 152.
2. Ritter, H. L., and Drake, L. C.: *Ind. Eng. Chem.* Anal. Ed. (1945) **17**, 782.
3. Ritter, H. L., and Erich, L. C.: *Anal. Chem.* (1948) **20**, 665.
4. Childs, E. C., and George, N. C.: *Discussions of the Faraday Society* (1948) **3**, 78.

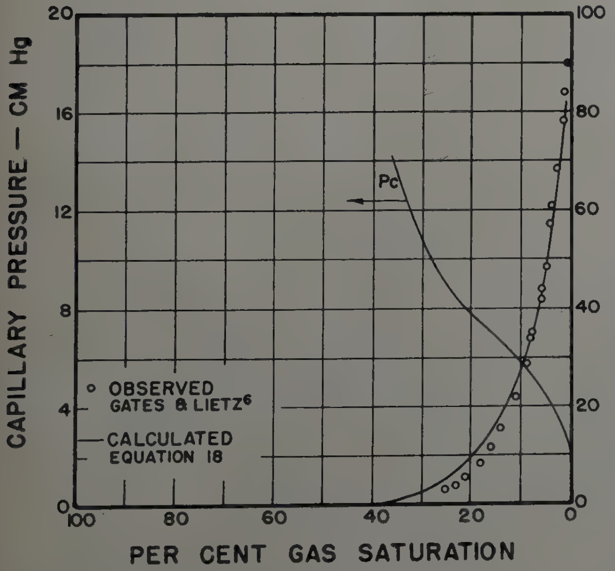

FIG. 16 — $\frac{\text{Effective Oil Permeability}}{\text{Effective Oil Permeability at } S_g = 0} = \frac{K_o}{K_o \text{ at } S_g = 0}$ IN WATER-OIL-GAS SYSTEM. OBSERVED DATA FROM FIG. 15 OF GATES AND LIETZ.[6] INTERSTITIAL WATER = 43 PER CENT.

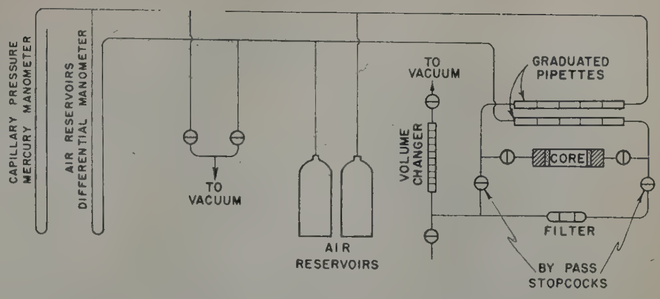

FIG. 17 — RELATIVE WATER PERMEABILITY APPARATUS.

5. Purcell, W. R.: *Trans.* AIME (1949) **186**, 39.
6. Gates, J. I., and Lietz, W. Tempelaar: "Relative Permeabilities of California Cores by the Capillary Pressure Method." Paper presented API Meeting, Los Angeles, Calif., May 12, 1950.
7. Dykstra, H., and Parsons, R. L.: *Trans.* AIME (1951) **192**, 227, (*J. of Pet. Tech.*, Aug., 1951).
8. Norton, F. J.: "Organo-Silicon Films," *General Electric Review* (August, 1944).

DISCUSSION

By John I. Gates, Shell Oil Co., Los Angeles, Calif., Member AIME

This paper is another valuable addition to our growing knowledge concerning relative permeability, and we are indebted to the authors for its presentation.

To me the paper makes three important contributions.

First, it presents a simplified apparatus for measuring relative wetting phase permeabilities by the capillary pressure method. Those of us who have used this method know that the accurate measurement of the pressure drop across the core is the most difficult part of the operation. The authors have eliminated this measurement by determining the pressure drops across the diaphragms at various flow rates. This pressure drop is then subtracted from the total pressure drop across the system (which is easily measured) to obtain the pressure drop across the core. The advantages of this technique are enumerated in the paper.

There are, however, some difficulties which should be pointed out. The end diaphragms should have permeabilities of the same order of magnitude as the core so that the pressure drop across the diaphragms will be a fraction of the total pressure drop. The entrance pressure of the diaphragms must also be high enough to allow desaturation of the core to the desired degree without penetration of fluid. Diaphragms meeting these requirements are not easy to find. Care must be taken to see that there is nothing in the flowing liquid which will tend to plug the diaphragms; otherwise, the permeabilities of the diaphragms will change during the test and therefore the pressure drops for given flow rates will increase.

Finally, some consideration must be given to the pressure drop across the capillary contact material. In our laboratory we have used finely ground diatomaceous earth for contact material and have found that the combined permeability of the diaphragm and contact material decreased as higher pressures were applied to the gas phase. Possibly the authors have some technique for eliminating this difficulty which they would be willing to explain.

The second important contribution in the paper is the modification of the formula for calculating relative wetting phase permeabilities from capillary pressure curves. In our formula, the relative permeability curve of a system of capillary tubes

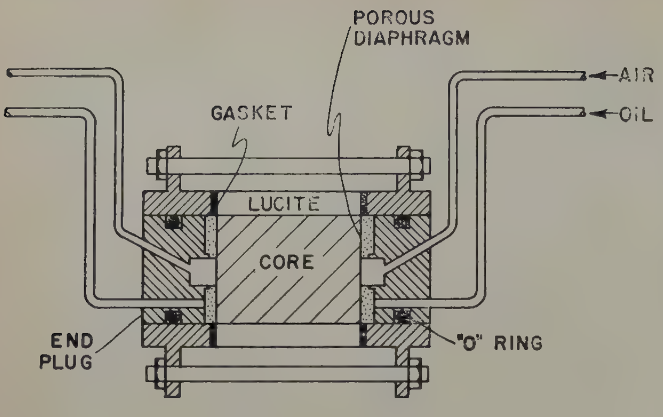

FIG. 18 — CORE HOLDER.

having the same capillary pressure curve as the core was calculated. When these calculated curves were compared to the measured curves, it was found that they deviated more and more as the core was desaturated. The calculated relative permeability values were made to approach the measured values by multiplying by an average tortuosity coefficient which decreased with decreasing saturation. The authors have assumed that the tortuosity is related to pore radius and have developed a revised formula for calculating relative permeabilities from capillary pressure curves. It is interesting to note that their formula is similar to ours and differs only in the power to which the capillary pressure is raised. The assumption that the tortuosity is related to the pore size has received some verification in our laboratory. We have noted that the change of the coefficient of tortuosity with saturation is related to the change of the pore size with saturation. The use of the revised formula would therefore appear justified. Numerous tests must be made, however, before it will be known whether the constant b is determined by a particular field or zone or whether it is related to some measurable property of the core.

The third contribution of the paper is the confirmation that the oil acts as the wetting phase in the core even though interstitial water is present. The work in our laboratory has also confirmed this conclusion. This is an important point since, as the authors point out, we can then calculate relative oil permeabilities from oil capillary pressure curves when interstitial water is present. It also has other valuable implications. The interstitial water can then be considered part of the rock matrix for some problems. The manner in which the oil is displaced by other flowing fluids is influenced by the way in which the oil wets the core. Probably many other implications will be become apparent as we study the problem.

These contributions are definite advances in the study of relative permeability relations.

DISCUSSION

By J. W. Wilson, Union Oil Co. of Calif.

The authors have made an interesting modification in the equation used by Purcell and by Gates and Lietz in an effort to eliminate the correction factor called "lithology factor" by Purcell for homogeneous flow, and "coefficient of tortuosity" by Gates and Lietz for multiphase flow. Since the new "constant" seems to vary less than the old "constants," progress has been made.

There is one disturbing feature of the "bundle of capillaries concept." It is assumed that all capillaries above a certain size contain only the non-wetting phase (oil, let us say), while all smaller capillaries contain only water. For this idealized system we could calculate relative permeability curves from the capillary pressure relation somewhat similar in appearance to those obtained in practice. They would possess the feature, however, that at every saturation, the sum of the oil and water relative permeabilities would equal 1. In actual experience, this is far from true. It is possible to account for the deficiency by a "tortuosity factor," and admittedly it is logical to expect each phase to interfere with the freedom of flow of the other in an interconnected system. To use only the pore radius as the measure of this factor does not seem quite adequate, however, especially if one considers the problem of applying the concept to the calculation of the nonwetting phase permeability. Here we would need a "tortuosity factor" of infinity when the oil is in the largest pores (up to the equilibrium oil saturation), with a *decreasing* factor as the oil is introduced to smaller and smaller pores.

With respect to the experimental technique, I would like to ask if it is not likely that the effective permeability to the wetting phase of the end plates decreases at increasing capillary pressure. Such variation would introduce an error into the method of calculating pressure drop used by the authors. The fact that a plate 1/16-in. thick will have a lower breakthrough pressure than one ⅛-in. thick indicates that there is probably penetration of a plate by the non-wetting phase over much of its surface at capillary pressures approaching the breakthrough pressure, and, of course, there would be virtually complete displacement of the non-wetting phase from any regions between the plate and core not in good contact. In our laboratory we use side taps to measure pressure drop, and have often observed appreciable decreases in effective permeability in the end plates at the lower wetting phase saturations.

AUTHORS' REPLY TO MESSRS. GATES AND WILSON

Wilson's comments imply that, if the bundle of capillary tubes analogy were an accurate picture of a porous medium, our method of calculating relative wetting phase permeability should also be applicable to the calculation of the nonwetting phase relative permeability. If one carries out the calculation for, say, the relative oil permeability in the water-oil system, the calculated curve does not have the form of the measured relative oil permeability curve. Upon closer examination, however, one notes that, if the calculated curve is shifted to the left, it takes on the appearance of part of the nonwetting phase curve.

The simple bundle of tubes analogy predicts symmetry between the wetting and nonwetting phase relative permeability. Although few data are available, laboratory results indicate a tendency toward symmetry for the nonwetting and wetting phase relative permeability curves. Cores for which the relative water permeability curve is far to the right on the usual plot also yield relative oil or gas permeability curves which are to the right of the center of the plot.

We realize that the bundle of capillary tubes concept is too simple. The results of its use to date, however, have given us encouragement.

To answer the question about the change in combined permeability of the porous diaphragms and contact material we can say that we have found no change in combined permeability up to one psi capillary pressure. The maximum capillary pressure that we have used is three psi at which pressure the decrease in combined permeability may be as much as 10 per cent. However, by referring to Fig. 11 and Table II of the paper, one can see that at capillary pressures greater than one psi the pressure drop across the diaphragms and contact material is less than two per cent of the total pressure drop. Consequently a decrease of 10 per cent in the combined permeability of diaphragms and contact material causes a negligible change in overall pressure drop.

★ ★ ★

SURFACE INDICATING PRESSURE, TEMPERATURE AND FLOW EQUIPMENT

M. B. RIORDAN, BYRON-JACKSON CO., LOS ANGELES, CALIF., MEMBER AIME

ABSTRACT

A surface indicating pressure, temperature and flow instrument that employs variable frequency sensing elements has proved useful in evaluating flow characteristics of wells. Relative productivity of individual oil and gas sands in a given well can be analyzed at several back pressures.

The variable frequency sensing elements are an improvement in sensitivity and accuracy and make possible observation of temperature and pressure variations that have not been possible heretofore. The surface indicating feature results in a more direct approach to solving problems and eliminates many assumptions.

All three subsurface factors are evaluated, and correlation between them results in a direct means of analyzing reservoir and well conditions.

Surveys have been used to evaluate well performance, locate gas entry in high ratio wells and to investigate gas injection and water flooding conditions.

INTRODUCTION

In a flowing well that is open to a multiple number of producing sands with varying characteristics, it is valuable to know which sands are producing fluid at a given back pressure and in what relative quantity. Core studies could qualify an interval as productive, and reserves would be computed on this basis. Unless the well is produced so that the interval does contribute, irreparable damage to the interval can occur. It is generally accepted that the optimum condition of pro-

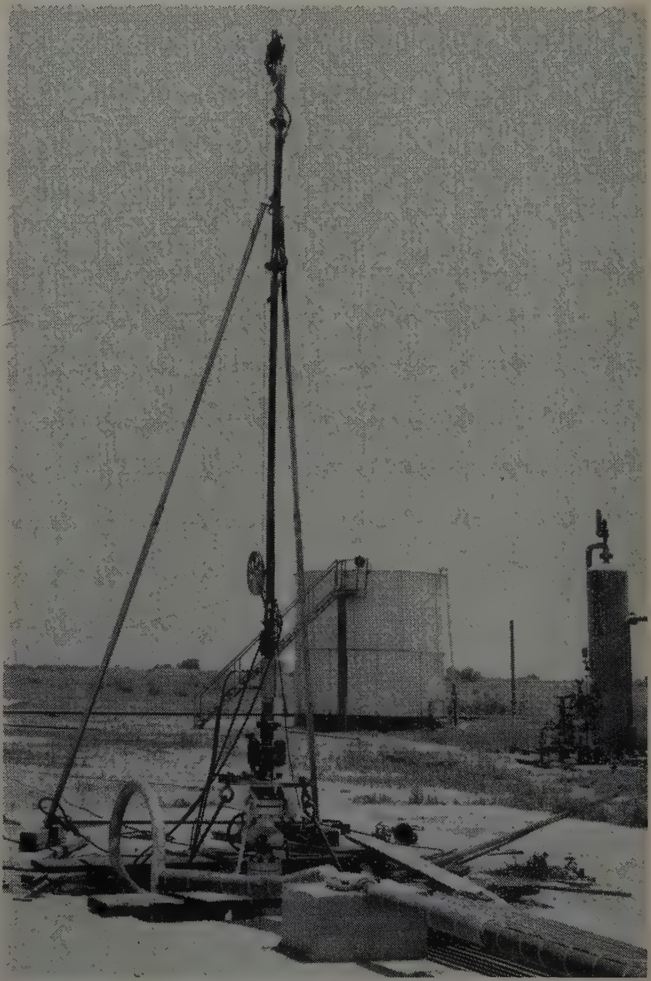

FIG. 1 — VIEW OF PTF EQUIPMENT RIG-UP.

Manuscript received in the office of the Petroleum Branch Oct. 1, 1950. Paper presented at the Petroleum Branch Fall Meeting in Los Angeles, Calif., Oct. 12-13, 1950.

duction of oil in an oil well will be, if the objective is to produce the largest amount of oil at the least cost, to produce oil at such rates of flow that the decline of production and the intrusion of edge water should be uniform as between all portions of the producing horizons producing into the well. An indirect approach to this problem does not always result in a timely practical answer. To insure a correct answer, the condition should be measured as directly as possible, while the well is being produced. The PTF equipment was developed with this objective. Measurements of all variable factors that can be associated with fluid movement, to a high degree of dependability and accuracy, was a design requirement.

Initial field use has indicated that sufficient data can be obtained with the instrument to answer the questioned conditions in a reasonable length of time and at a reasonable cost.

A description of the instrument, the principals of operation, and the field experience are discussed herein.

DESCRIPTION OF THE EQUIPMENT

The equipment consists of:

(1) A special hoist truck designed to handle 15,000 ft of 1-H-0 (.190 OD) Amerigraph single conductor cable. The construction is conventional for wire line trucks except for size and weight. Auxiliary equipment includes a line measuring device, 110 v a-c power generating plant, a sensitive weight indicator and intercommunications system.

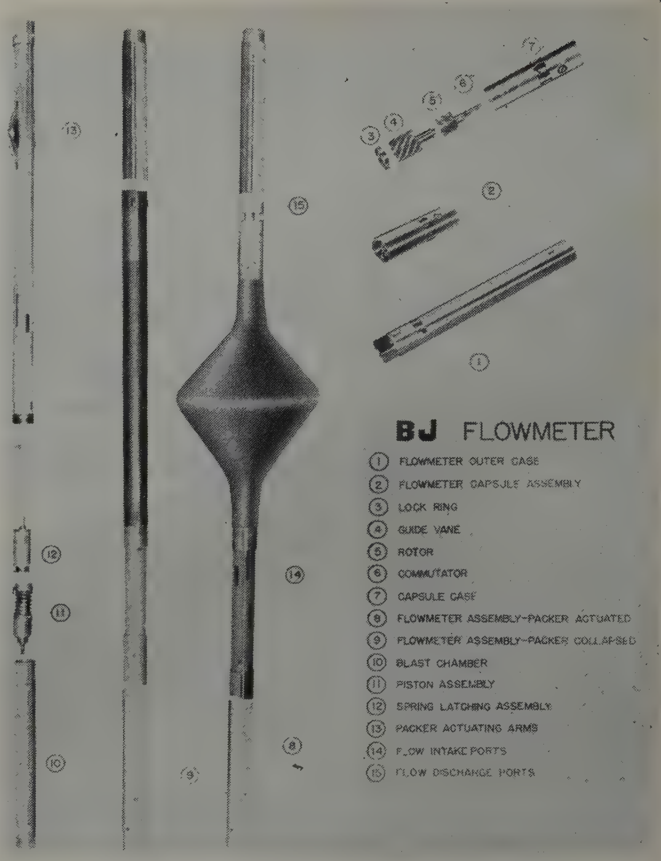

FIG. 3 — EXPLODED AND ASSEMBLED FLOWMETER.

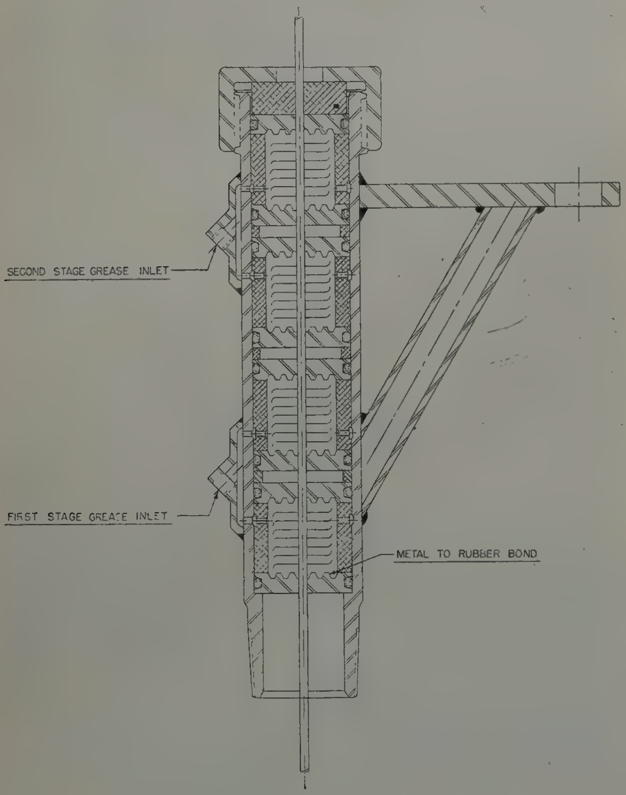

FIG. 2 — LUBRICATOR GLAND.

(2) The lubricator has a unique packing gland system and is designed for pressures up to 3,000 psi. The gland (Fig. 2) is actuated by a hydraulic system that develops the contact pressure between the cable and the rubber cylinder of the gland. This permits gland control from ground level and provides a very flexible and safe system. Maximum pressure drop with minimum line friction is accomplished by staging. The pressure behind each gland stage is independently controlled from ground level. Stage one hydraulic pressure is adjusted to exceed the well head pressure in the lubricator sufficiently to cause the rubber cylinder to contact the cable lightly without supporting the cable weight. The second stage is adjusted to accomplish the same condition on the pressure being passed by stage one. This results in a maximum pressure drop with minimum line friction. When conditions require it, a heavy grease can be injected between glands to increase the pressure drop and lubricate the line. The lubricator structure is capable of supporting the load of the cable and instruments and can be erected over the well by the operating crew. The instruments have been successfully run to depths of 13,000 ft and the cable lubricated in against pressures as high as 2,300 psi. A blow-out ram of similar design and actuated by the same hydraulic system is used below the lubricator trap

assembly as insurance against unexpected conditions. It can be closed around the line or the instrument, or act as a valve for complete closure.

(3) The subsurface flowmeter element is a turbine impeller type that is rotated by the fluid velocity. The impeller drives a commutator through a magnetic coupling which isolates the commutation system from the well fluid and pressure. The commutator interrupts a light beam on a photo cell and a frequency signal is generated. The frequency is a direct function of the volume of fluid passing through the meter. The meter sensitivity is improved by the use of an expansible element that contacts the liner wall and diverts a maximum amount of fluid through the meter. The packer element in the collapsed position (9 in Fig. 3) is run out the bottom of the tubing to the top of the producing interval. A small explosive charge in the blast chamber (part 10) is fired by increasing the voltage on the line at the surface. This releases a spring-actuated mechanism that expands the packer element. When the flow data has been obtained the packer is pulled against the bottom of the tubing to actuate a second trigger. This releases the mechanism and the packer element returns to the original collapsed position.

(4) The subsurface pressure and temperature sensing element are of a novel design that employs the known principle that the natural frequency of transverse vibrations of a stretched wire is proportional to the applied tension on the wire. The element is made up of two parts, the vibrating wire assembly and the subsurface amplifier. It is contained in a tubular envelope, one and three-eighths in. in diameter and 24 in. long (Fig. 4). By arranging the vibrating wire design so that the phenomenon to be measured varies the tension in the wire and the vibrations occur in a magnetic field, a variable frequency signal proportional to the phenomenon is obtained. The

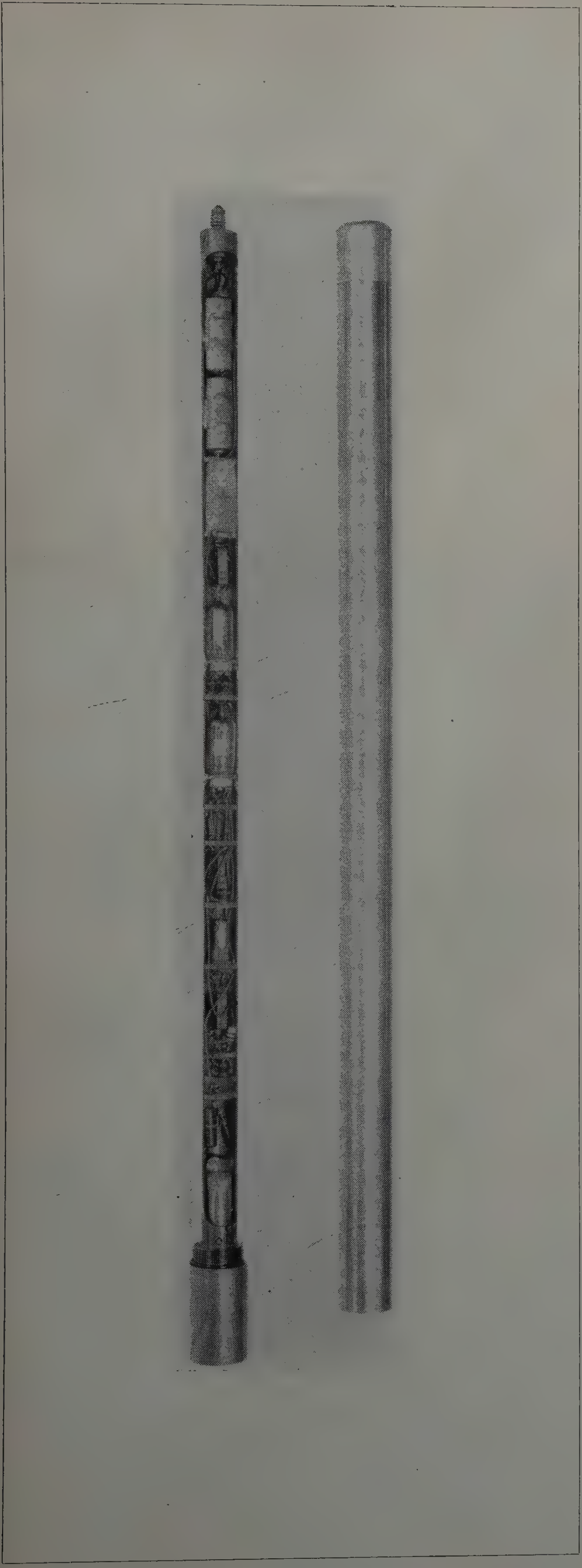

FIG. 4 — SUBSURFACE AMPLIFIER.

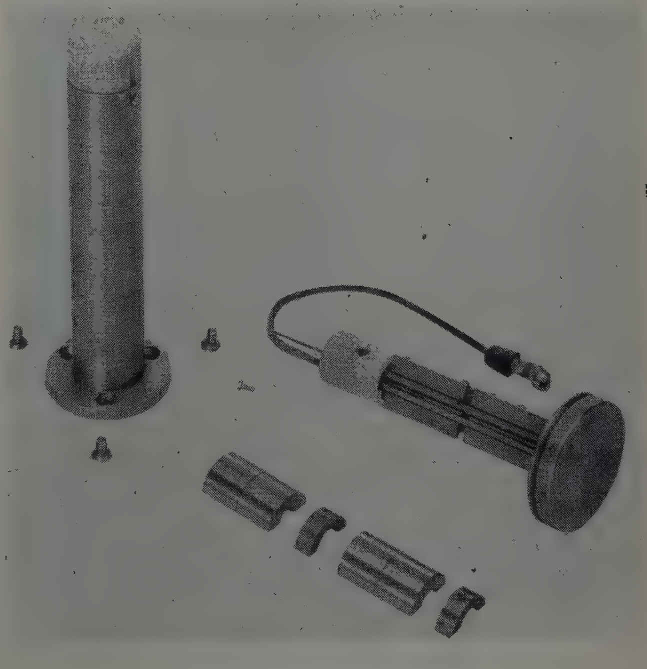

FIG. 5 — PRESSURE ELEMENT.

wire is maintained in vibration by feeding back a portion of the amplified signal to the wire.

This type of sensing element is particularly adapted to subsurface measurements for the following reasons:

(a) It is capable of measuring a wide range of physical properties.

(b) It converts these quantities to a variation in frequency, which can be measured with great accuracy.

(c) The total scale of measurement may be divided into a large number of accurately reproducible units.

(d) The instrument retains its fundamental calibration to a high order of accuracy.

(e) The measurements can be easily transmitted over long lengths of cable without loss of accuracy.

The pressure element (Fig. 5) wire tension is varied by the deflection of a relatively thick-walled diaphragm. Temperature compensation is accomplished by using a wire support frame material of identical expansion coefficient as the vibrating wire.

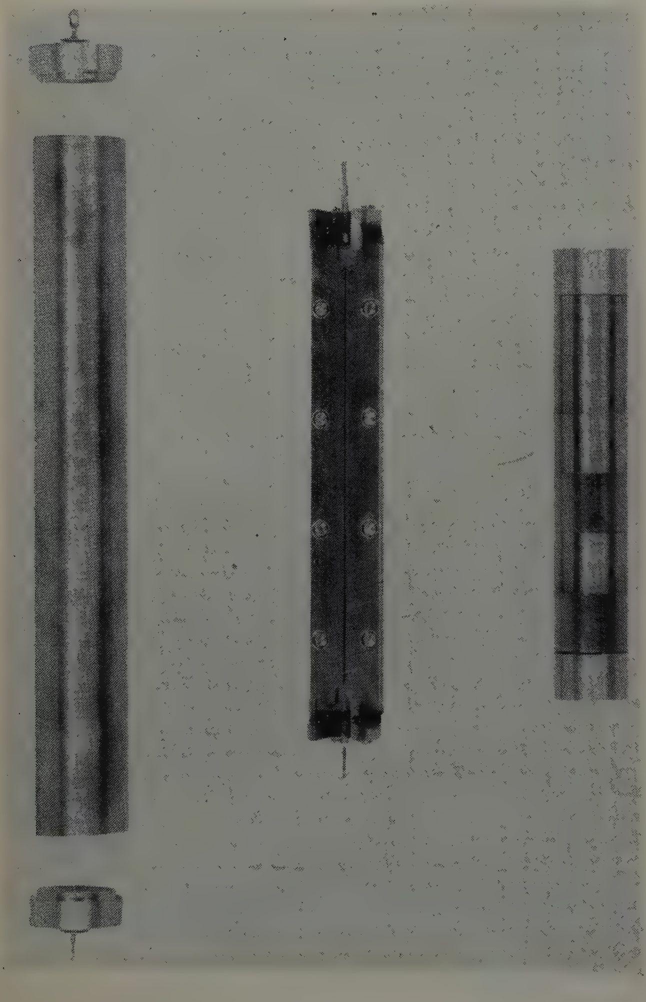

FIG. 6 — TEMPERATURE ELEMENT.

The temperature element (Fig. 6) wire tension is varied by the expansion and contraction of the wire support frame.

The high order of accuracy and ability to reproduce results is accomplished by dealing with the physical constant of the material of construction and eliminating mechanical movement in the elements that are exposed to the varying well conditions.

(5) The surface instrumentation includes a comparator unit, oscilloscope and power supply (Fig. 7).

(a) The comparator unit employs the described vibrating wire element and feed back circuit arranged so that the tension of the wire is varied through a micrometer mechanism to resolve the range of tension readable on a dial in 10,000 divisions. For observation, the calibrated frequency signal from the comparator is fed to the horizontal plates of the oscilloscope, and the subsurface signal is fed to the vertical plates. This null beat system permits visual matching of the surface and subsurface frequency to a fraction of a cycle. The dial reading is convertible from the calibration curve to pressure and temperature values. The sensitivity of the system is apparent when the following facts are considered. The sensing element frequency range from zero to rated load is approximately 3,000 cycles change. The change can be observed and accurately matched to one-fourth of a cycle. A 6,000 psi element has a variable output signal that can be divided into 12,000 detectable units. The frequency of the pressure and temperature sensing elements are adjusted to given band widths, and by using a filter circuit at the surface the two signals transmitted over the single conductor can be separated and observed simultaneously. Switching several vibrating wire assemblies through a subsurface relay to a single amplifier reduces the length of the instrument and makes possible the observation of several factors in a single run. Power for the subsurface amplifier is fed down the cable as direct current. The signal output from the sensing element is alternating current. The d-c power is blocked at the amplifier output by use of a suitable condenser.

FIELD TECHNIQUE

The equipment can be run under the same conditions as pressure bomb surveys. Derricks or "A" frames for sheave support are not necessary.

Time in the well is unlimited because the device is free of clocks or battery power supplies.

The procedure for most problems is to lower the unitized instrument to a position just above the upper perforations and make a temperature traverse, plotting the data as it is taken. Any fluid movement in an oil well has an associated temperature effect. The problem is to locate and interpret these conditions. Any observed anomalies are carefully bracketed by taking sufficient stations to develop a complete picture. The pressure and flow traverses are then made to confirm and expand the detail indicated by the temperature curve.

The value of the data must come from the interpretations of the anomalies. When the three dependent factors, pressure, temperature and flow, are taken at the same time and under the same well conditions with surface indications, the interpretations can be straight forward and conclusive. The data are available as the survey is made and the operator can adjust

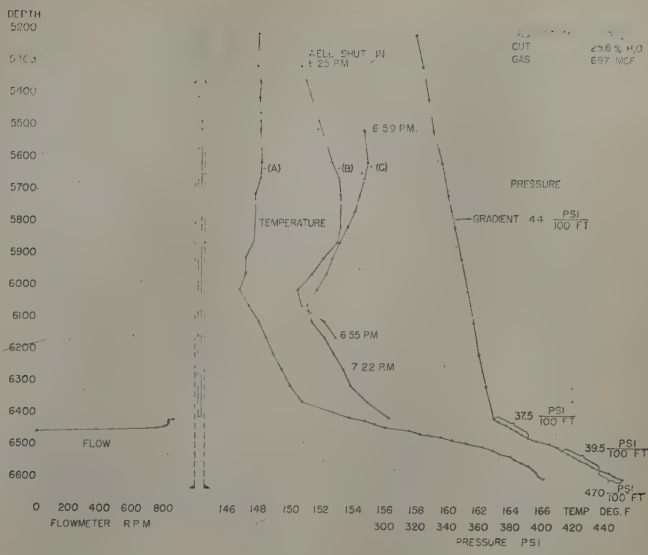

FIG. 8 — DATA CURVE 1, PTF SURVEYS.

the running conditions or well conditions to obtain the maximum detail. Gas entry is indicated by the curve slope changing from the normal geothermal gradient through the vertical to the left. This is a decrease in temperature and is caused by the expanding gas. If a volume of gas is expanding at a given interval in the well, the pressure gradient should be less at this point. It is then always possible to confirm that the temperature curve change to the left is due to gas expansion with the pressure data. The flowmeter traverse will bracket and indicate the relative amount of gas that is physically entering the well. Water entry is indicated by the curve slope changing from the normal geothermal gradient to approach the horizontal to the right. This is an increase in temperature. This condition is developed when a volume of water, which has relatively high specific heat, enters a well bore as the well is made to flow or produce. Again this fluid movement can be confirmed by correlation with the pressure flow equipment. Oil flow, because of its intermediate specific heat value, has an intermediate effect and the temperature anomalies fall between the gas and water extremes. In all cases clearly defined anomalies are assured if the well is shut in or conditioned just prior to making the survey. The surface indication and recording equipment make it possible to follow the complete thermal change to producing equilibrium.

Fig. 8 is a plot of data taken to evaluate the producing conditions of an unsatisfactory completion. The temperature curve (A) was made while the well was flowing. The anomaly from 5,900 to 6,000 ft indicates a principal gas entry centering at 6,000 ft. Note that the temperature values were taken in the tubing. Temperature curves (B) and (C) were taken at one-half hour and one hour after shut-in and the principal deflection is centered at the 6,000-ft interval. The well is shut in with the instrument in the well, and the transition to equilibrium can be followed as it occurs. This practice provides greater differences at anomaly points and confirms conditions that could be questionable under flowing conditions. The temperature, pressure and flow curves indicate that the lowest point of any fluid movement is 6,440 ft. It was interpreted that the indicated fluid movement below the bottom of the tubing had its source from the 6,000-ft interval. The turbulence created by the change of direction of flow and increased velocity extended the movement below the bottom of the tubing. Pressure and flow readings in the interval 6,400 to 6,450 showed considerable fluctuations, indicating that the gas was being produced intermittently. The plotted curves are the average of these observed values.

This example indicates that high ratio wells tubed to bottom can be surveyed conclusively to determine points of principal gas entry. The sensitivity of the temperature instrument and the flexibility added by the surface indication and the surface power supply make this possible.

Fig. 9 is a plot of data taken to evaluate a completed well to determine what portion of the open interval was contrib-

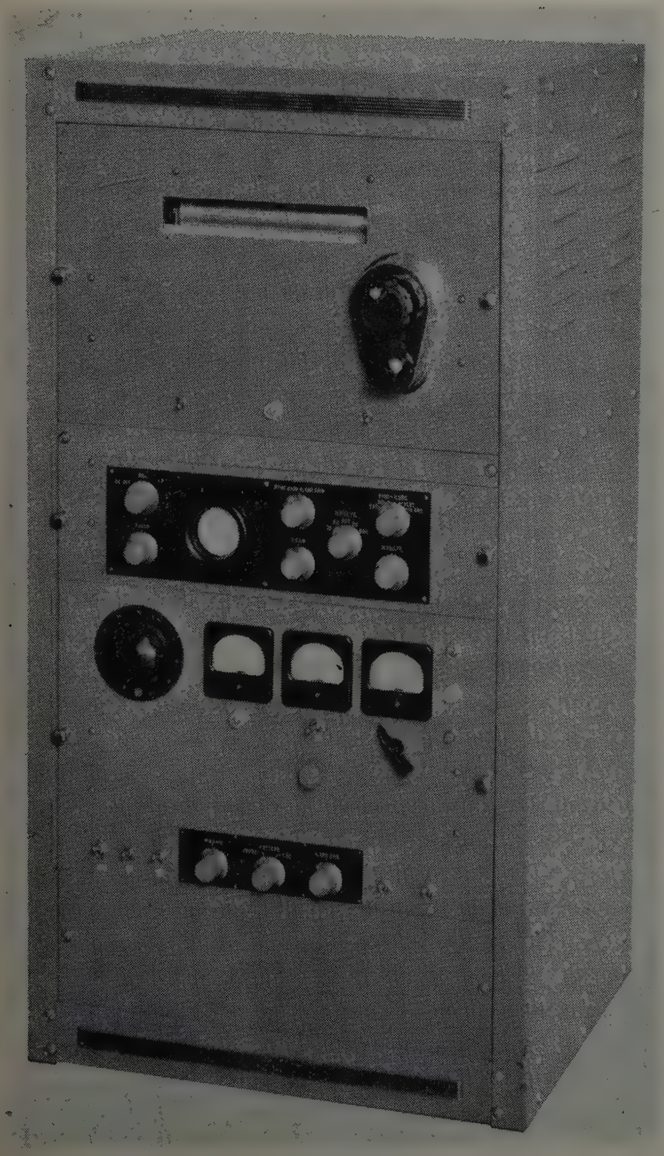

FIG. 7 — COMPARATOR.

uting, and to determine what occurs when the well back pressure is varied. The core permeability is correlated with the PTF data. At the 260 B/D rate the wellhead pressure was 325 psi. Note that the temperature curve indicates the lowest point of fluid movement to be 10,080 ft. The flow curve for the same well condition confirms that the lowest point of fluid movement is 10,080 ft. The bean was changed and time permitted for the well to come to equilibrium. This reduced the production to 125 B/D and the wellhead pressure increased to 975 psi. The temperature curve now indicates the lowest point of fluid movement to be 9,990 ft which is 90 ft above the lowest point indicated at the 260 B/D rate. The flowmeter curve confirms this condition. It is interesting to note that the numerical temperature differences of the interval 9,970 to 10,000 varies as a direct function of the production rate. Two months later the well was rerun to determine if any changes had occurred. The production was 160 B/D and the wellhead pressure was 750 psi. The subsurface producing conditions were found to be very nearly the same as the 125 B/D rate except for the temperature difference at the 9,970 to 10,000-ft interval.

CONCLUSION

It can be concluded from the initial field tests that the described instruments offer the following advantages and possibilities:

(1) The surface recording feature increases the flexibility of taking subsurface data and assures more conclusive results.

(2) The accuracy and sensitivity make possible more detailed data that results in better interpretation.

(3) The availability of all three factors — pressure, temperature and flow — make it possible to evaluate the characteristics of a flowing well. The pressure at which a given sand will produce can be determined.

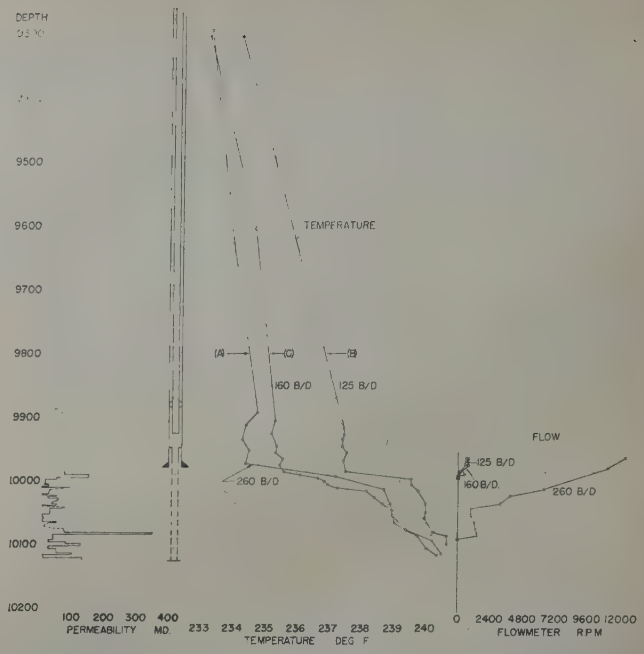

FIG. 9 — DATA CURVE 2, PTF SURVEYS.

(4) Temperature surveys in high ratio flowing wells tubed to bottom can determine points of principal gas entry.

REFERENCES

1. Halbouty: *Temperature,* Amer. Inst. of Phys., 1045.
2. Millikan, C. V.: *Trans.* AIME, **142,** 15.
3. Stormont, D. H.: *Oil and Gas Jour.* (April 13, 1950) 80-81.
4. "Well-Head Stuffing Box for Armored Electric Cable," *Oil and Gas Jour.* (Dec. 9, 1948) 105.

★ ★ ★

T.P. 3192

REPORT ON THE MAMOU FIELD PRESSURE MAINTENANCE PROJECT

WILLIAM O. CREGO,* MAGNOLIA PETROLEUM CO., HOUSTON, TEX., AND **JAMES M. HENAGAN,** MAGNOLIA PETROLEUM CO., MAMOU, LA., MEMBERS AIME

ABSTRACT

The Mamou Field, located in Evangeline Parish, La., is an elongated anticlinal structure on the downthrown side of a major east-west fault with oil and gas production from the upper part of the Wilcox formation. Two main producing horizons occur at an approximate depth of 11,500 ft and have been designated the Morein sand and the Deshotels sand.

The upper sand (Morein) had an original bottom-hole pressure of 6,788 psig, which is some 1,500 psi above the normal pressure for that depth. Oil production with high gas/oil ratios and fluid analyses giving high shrinkage factors prompted a study of the reservoir in its early stages. The results indicated a closed reservoir producing under solution gas drive with low expected ultimate oil recovery.

The early study of the Wilcox formation and its contained hydrocarbons resulted in the presentation of the data to the Department of Conservation of the State of Louisiana, with suggestions for field rules and a request for permission to inject extraneous water into the Morein sand. The water injection plans eventually led to complete unitization of working and royalty interests, to the construction of a gasoline plant, and to a central tank battery installation for the field. Deshotels sand wells were reworked to the Morein sand, and the water injection system was installed and ready for continuous operation in the early part of 1949. The injection of water was started in time to arrest the bottom-hole pressure decline at or near the bubble-point pressure. This injection was calculated to increase the ultimate recovery and to conserve natural resources. Pressure maintenance, the extraction of LPG products, and the sale of residue gas (early 1950) represent an attempt to produce an oil field with utmost efficiency.

INTRODUCTION

The two principal Wilcox oil horizons in the Mamou Field are the Morein sand and the Deshotels sand, occurring at 11,500 ft and 11,700 ft subsea, respectively. Minor oil production has been encountered in Morein stringer sands. (Fig. 1.)

This paper deals only with the Morein sand, which is blanket over the Mamou Field. It is, however, segmented by the northwest-southeast "E" fault as shown in Fig. 2. The west segment is the area involved in the water injection pressure maintenance program. To date the east segment has operated largely under the influence of a strong water drive.

The paper presents (1) a brief history of field development, (2) a resumé of reservoir conditions which led to the decision to inject extraneous salt water into the principal producing horizon, and (3) a summary of reservoir analysis and performance.

FIELD DEVELOPMENT

The Mamou Field is located in Evangeline Parish, La. The discovery well (J. B. Morein No. 1, now Unit No. 5) was completed in December, 1945, after penetrating 200 ft into the Wilcox formation. Initial production from the Morein

---

*Now with the Tennessee Gas and Transmission Co., Houston, Tex.

Manuscript received in the Petroleum Branch office May 26, 1950. Paper presented at the meeting of the Delta Section, AIME, in New Orleans, La., Jan. 9, 1950.

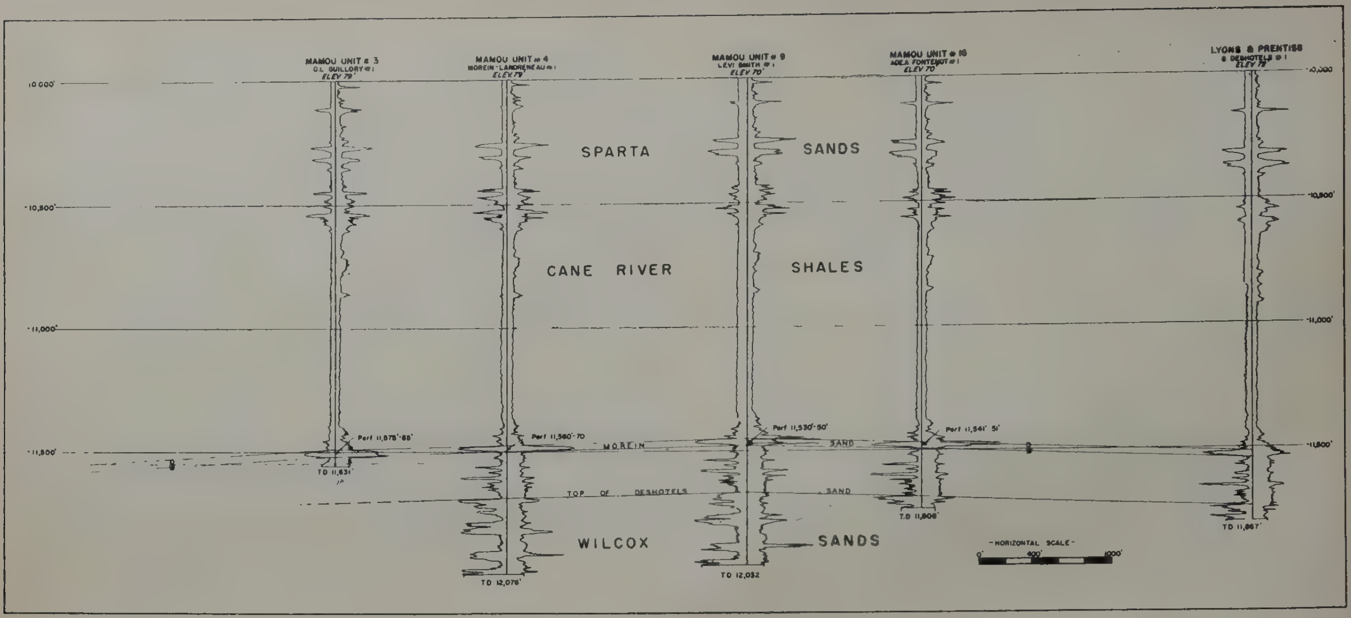

FIG. 1 — NORTH-SOUTH ELECTRIC LOG CROSS-SECTION, MAMOU FIELD.

sand was 208 B/D of pipe line oil through an 8/64-in choke with a tubing pressure of 3,950 psig.

Following the successful completion of the discovery well, preliminary tests were made to evaluate the productivity of the reservoir. Evidence on the character of the reservoir which had to be considered to protect development costs was: (1) a 21-ft sand at 11,500 ft with an average permeability of about 51 md, (2) the possibility of a saturated fluid in a reservoir operating under volumetric depletion, (3) a fluid at or near the critical state, and (4) a solution gas/oil ratio of approximately 4,000 cu ft per bbl of stock tank oil. Expected recovery under these conditions would be very low.

The production rate of 260 B/D of oil was reduced to 150 bbl to conserve reservoir energy while a more thorough investigation was begun in order to predict profitable development of the Morein sand.

By August, 1946, a total of eight wells had penetrated the Morein sand within one mile of the discovery well. Three of these wells were completed in the Morein sand; two were producing from the Deshotels sand; and the remaining three wells were in the process of testing. At the end of 1946 the reservoir pressure was declining at the rate of one lb for each 350 bbl of stock tank oil produced. All available data indicated that the recoverable oil would not warrant continuation of the 40-acre development pattern under which the field was being drilled.

The most efficient recovery mechanism was assumed to be displacement by water while maintaining the reservoir pressure above the saturation point. Eighty-acre drilling units were considered to be an efficient as well as economical pattern if the reservoir could be properly controlled. Field development continued with 80-acre spacing while complete reservoir data were presented to the Department of Conservation of Louisiana requesting field rules. A voluntary unitization agreement between the principal operator and a majority of the royalty owners was presented with a request for the formation of the Mamou Unit, equities to be distributed on the basis of acre-feet of oil productive sand underlying individual leases. Wells in the Deshotels sand were to be recompleted in the Morein sand to complete the spacing pattern; the operator was to construct a natural gasoline plant with the royalty owners sharing in 100 per cent of plant products; and a pilot water injection system was to be initiated to determine the feasibility of pressure maintenance. The field rules with 80-acre spacing and the establishment of the Mamou unit were approved. Permission was granted to inject extraneous water into the Morein reservoir experimentally.

In 1947, the four Deshotels sand wells were reworked to the Morein sand to complete the drainage pattern for the pressure maintenance program in that reservoir. A total of 25 wells was drilled in the Mamou Field; 19 were oil producers and six were dry holes. Following the State order to form the Mamou Unit, work was commenced on a central tank battery, a natural gasoline plant, and a pilot water injection system.

WATER INJECTION SYSTEM

After laboratory tests indicated a reduction in permeability in the Morein sand by use of fresh water, a high pressure, salt water injection system was designed. A dry hole on the north side of the field was selected for injection, and continuous water injection was begun in February, 1949.

Extraneous salt water is supplied by another dry hole perforated in a sand at a depth of 2,300 ft. A deep-well centrifugal pump at a depth of 600 ft lifts the water and delivers it about three-fourths of a mile to the injection well. At the injection station the mixed salt water from the supply well and the salt water produced from the Morein sand is filtered. After passing through a two-element, sand-packed filter, the water goes into a volume tank before it is metered into the suction line of the injection pump. The system is kept under low gas pressure to keep air excluded. This closed system has eliminated the need for chemical treatment.

An inverted, quintuplex pump forces the water into the injection well. In the solid-steel fluid end the water pressure is raised to 3,200 psig. The first plungers used in the pump were plated with porous-chrome steel. During operation, the packing glands are lubricated by castor oil. The porous-chrome plungers were satisfactory but were abrasive to the packing at the high pressure. By substituting solid-ring for the split-ring V-type packing much of the wear was eliminated. Porcelain plungers were tried, but some failures of the plungers have occurred. Power for the injection pump is furnished by two 300 hp engines which are connected to the pump by a 3.2 reduction gear.

At the sand face, 11,631 ft deep, there is 3,600 psi differential between the well bore and the average reservoir pressure while the water is being injected at a rate of 2,000 B/D.

RESERVOIR ANALYSIS AND PERFORMANCE

Reservoir Characteristics — Morein Sand

The results of porosity determinations show a weighted average porosity of 19.7 per cent for 197 ft of cores in the Morein sand and a weighted average permeability of 51 md.

The interstitial water saturation of 34.7 per cent was obtained from cores taken with a water base mud and corrected for infiltration of water from the drilling fluid for 104 ft cored west of the "E" fault. Again the interstitial water was checked by the capillary-pressure method using 11 cores that varied in permeability from 3.4 to 149 md. The resulting curves of interstital water *vs* height above the water table were used with available permeability data to obtain an average interstitial water saturation for the oil zone of 35 per cent.

Placing of Water-Oil Contacts

Data were assembled to determine the boundaries of the oil zone in the Morein sand. The water-oil contact for the south and west flanks was placed mainly from data obtained on the Unit No. 12 well. The sand was perforated in the top two ft of permeable section from 11,487 to 11,489 ft subsea to make a water-free producer. Early appearance of water production from the well placed the perforations near the water-oil contact. Completion of Unit No. 15 through perforations from 11,484 to 11,494 ft subsea tested no water, but the well started making water during the first month of production. From Wells No. 14 and 16, the water-oil contact was placed at 11,500 ft subsea for the west and south flanks of the west segment (See Fig. 2).

The La Haye Brothers No. 1 well cut the water-oil contact as shown by core analysis report and by a slight show of oil on a drill stem test from 11,550 to 11,555 ft subsea. Unit No. 3 with perforations from 11,496 to 11,506 ft subsea, 13 ft lower than Unit No. 13 on the south flank, has produced over

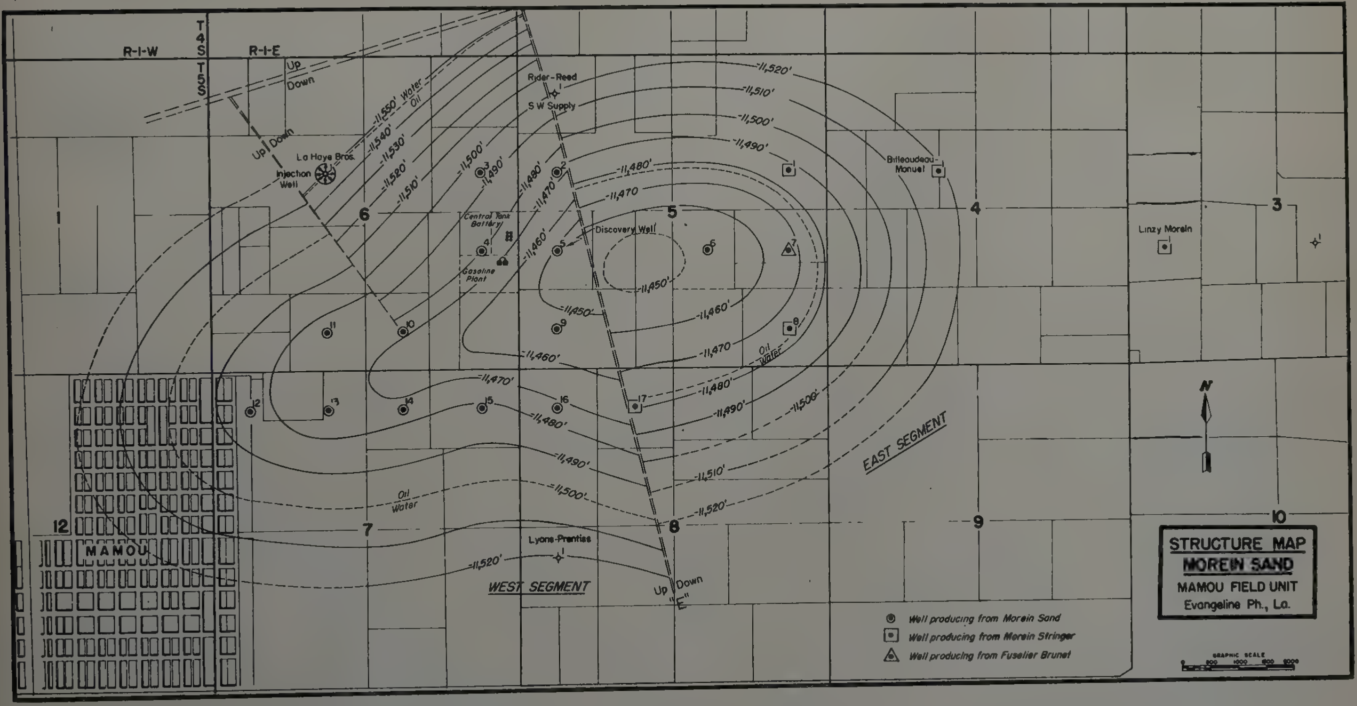

FIG. 2 — STRUCTURE MAP, MOREIN SAND, MAMOU FIELD UNIT.

130,000 bbl of oil with no water. The water-oil contact was placed at 11,549 ft subsea in an area that is shut off by effective barriers to the north, east, and west.

Reservoir Volume, Temperatures and Pressures

The estimated reservoir volume for the pressure maintenance area is 14,917 oil acre-ft, based on 963 surface acres and an average sand thickness of 15.5 ft.

All bottom-hole pressure tests in the Morein reservoir have been corrected to 230°F and to the datum of 11,428 ft subsea. A study of the early bottom-hole pressure tests and calibrations indicated the initial bottom-hole pressure for the Morein sand of 6,788 psig measured on Jan. 2, 1946, to be correct. Sufficient pressures were available to form and follow the pressure trends in the early life of the field. Since June, 1947, there have been pressure surveys every three months to give excellent reservoir pressure information. The bottom-hole pressures were adjusted to survey dates and arithmetically averaged, since the well spacing allowed each well approximately the same area.

From prepared isobaric maps, the changes in the pressure pattern were followed as conditions in the reservoir changed. As would be expected, the greatest pressure decline occurred in the area where the first wells were completed on the highest part of the structure. The maps showed a continual movement of the low pressure area from the original area toward the north. Although a greater number of wells were drilled on the south flank, the low pressure area moved to the most northerly producing part of the field.

Following the injection of water, the pressure pattern shifted as shown in Fig. 3, indicating an exertion of pressure inward from all directions except along the "E" fault. The isobaric pattern rapidly improved and began to conform to the structural contours.

On December 22, 1948, the reservoir pressure in the Morein sand west of the "E" fault had declined 1,705 psi to 5,083 psig while 801,312 bbl of stock tank oil had been produced. This is a production of 471 bbl per psi pressure decline (Fig. 4).

Although data acquired indicated some water drive in the southern flank, continuous water injection was commenced on Feb. 16, 1949, to arrest the pressure decline. The decline continued but was gradually reduced until June, 1949, when a pressure of 4,967 psig was noted; thereafter, the water injection has shown the desired effect on the pressure.

Reservoir Production Data

Through September, 1948, all production went into separate tankage for each well. Since the installation of a central tank battery in October and November, 1948, production of oil, gas and water has been broken down on the basis of monthly tests.

The cumulative water production for the Morein sand west of the "E" fault through Aug. 18, 1949, was approximately 51,000 bbl or an average water production of 4.94 per cent. At that time, Units No. 12, 14, 15 and 16 in the pressure maintenance area were producing over 50 per cent water. Cumulative production of oil, gas, and water to January 1, 1951, is shown in Fig. 4.

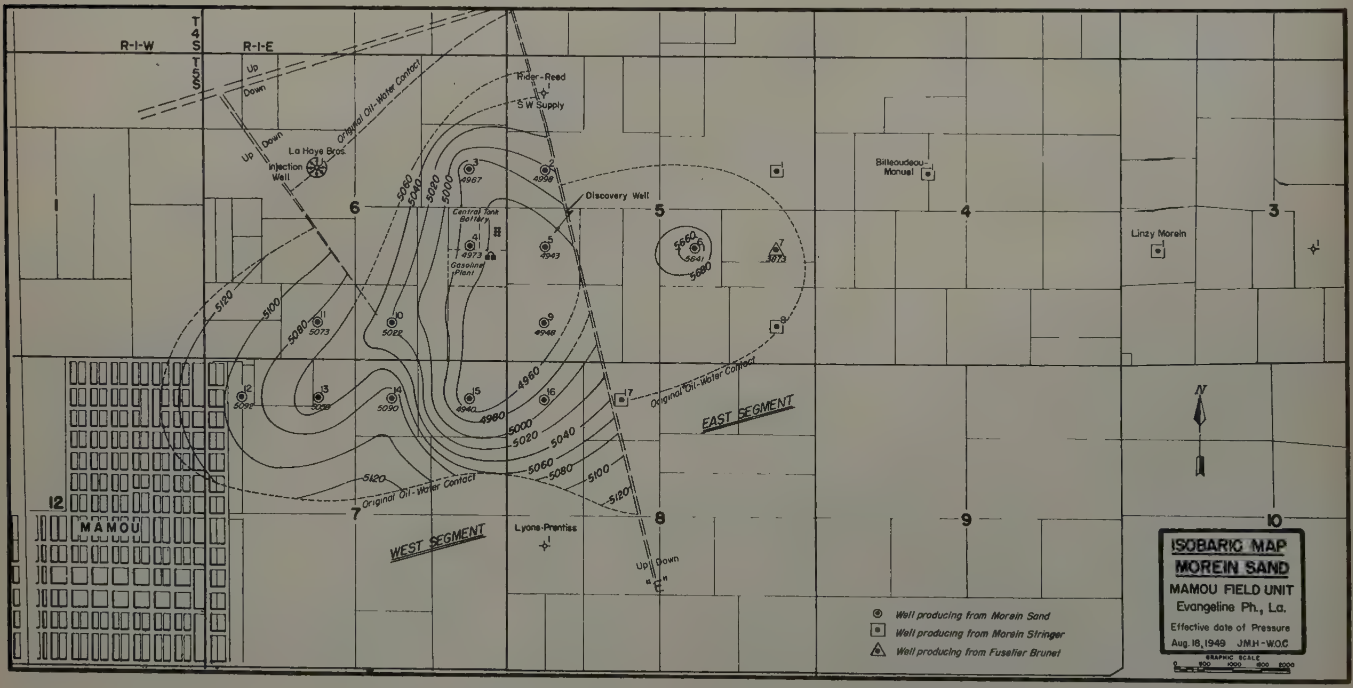

FIG. 3 — ISOBARIC MAP, MOREIN SAND, MAMOU FIELD UNIT.

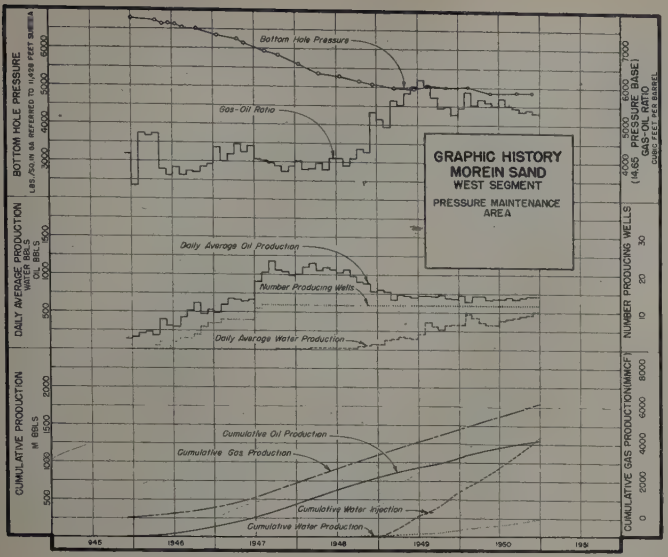

FIG. 4 — GRAPHIC HISTORY, MOREIN SAND, WEST SEGMENT, PRESSURE MAINTENANCE AREA.

Reservoir Fluid Analyses

Summaries of the results of the fluid analyses of two subsurface samples and two surface recombination samples made on the Morein reservoir are shown in Table I. The fluid behavior of two samples from the Unit No. 3 well (O. L. Guillory No. 1, lowest structural position) producing from the Morein sand has been determined. One was a subsurface sample and the other was a recombination sample. The two analyses were performed independently by different laboratories. The bubble points of 4,527 psig and 4,540 psig checked very closely, indicating the reservoir fluid to be undersaturated at reservoir conditions. As the gas/oil ratio by flash liberation checked closely with the producing gas/oil ratio for this well (3,000 cu ft per bbl of stock tank oil), it is believed that these two analyses are fairly representative of the shrinkage and gas/oil ratio behavior of the fluids being produced from this well and wells on a similar structural position.

The fluid behavior of two samples from the discovery well (Unit No. 5), which is producing from the highest structural position, was determined. One was a subsurface sample and the other was a recombination sample. These samples were also analyzed independently by different laboratories. The difference in producing gas/oil ratio flashed to approximately 300 psig was only 40 cu ft per bbl of stock tank oil (3,950 cu ft per bbl of stock tank oil for the bottom-hole sample compared to 3,990 cu ft per bbl of stock tank oil for the recombination sample), which indicated representative samples of fluids from the well. These analyses are fairly representative of the shrinkage and gas/oil ratio behavior of the fluid in the reservoir on the higher part of the structure (Fig. 5).

Water Influx

In October, 1949, the water influx into the reservoir through each of the nine pressure survey periods (through Aug. 18, 1949) was calculated by material balance equations.

The volumetric balance calculations indicated that the reservoir had been produced through a combination of water drive by edge-water encroachment and expansion of reservoir fluid supplemented by water injection. Through the last survey date, Aug. 18, 1949, the energy for the production of oil and maintenance of the reservoir pressure was derived 55 per cent from water influx into the reservoir, 36 per cent from the expansion of the reservoir fluid, and 9 per cent from the injection of water.

The cumulative water production of approximately 51,000 bbl (1.39 per cent of the total reservoir voidage by oil, gas and water production) and wells producing water were consistent with the calculated influx and reservoir volume data. The calculated water influx of 2,009,000 bbl, which has been primarily on the south and southwest flanks, would cause a rise of about 8.6 ft in the water-oil contact if the water advanced uniformly and if the resulting residual oil saturation were 20 per cent of the total pore space. This rise from the original water-oil contact of 11,500 ft subsea would place the contact near the top of the perforations in Unit No. 12, and in August, 1949, this well was producing over 70 per cent water. This rise would also place the contact above the bottom perforations in Unit No. 13 and a rise to nearly the center of the perforated interval in Unit No. 15 with the two wells producing 16 and 57 per cent water, respectively. Considering the accuracy of the depth measurements below 11,000 ft, the aforesaid production of water checks the rise in the water-oil contact rather closely.

Pressure Maintenance

The average rate of pressure decline was approximately 47 psi per month from the original pressure to the time of injection. Three months after injection was initiated, the pressure decline was nearly arrested with the pressure rising slightly after that time.

Although on Aug. 18, 1949, the injection of water had accounted for only nine per cent of the energy for the cumu-

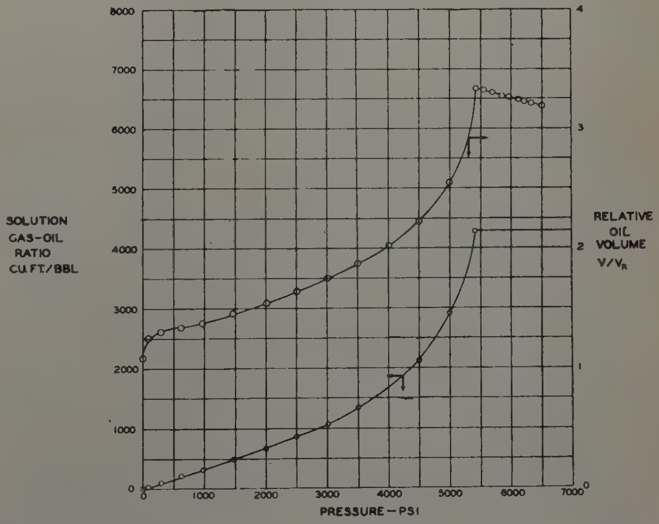

FIG. 5 — SOLUTION GAS DURING DIFFERENTIAL LIBERATION AND RELATIVE OIL VOLUME VS. PRESSURE, J. B. MOREIN NO. 1 — MOREIN SAND, MAMOU FIELD, JULY 26, 1946.

Table I — Fluid Behavior Analysis Summary — J. B. Morein-Wilcox Reservoir

Mamou Field — Evangeline Parish, La.

	O. L. Guillory No. 1 (Surface Recombination)	O. L. Guillory No. 1 (Bottom Hole)	J. B. Morein No. 1 (Surface Recombination)	J. B. Morein No. 1 (Bottom Hole)
Reservoir Temperature, °F	230	230	230	230
Bubble-Point Pressure, psig @ 230°F	4512	4540	5415	6265
Formation Volume Factor, Vr/Vt by diff. lib. @ Res. Temp.	....	3.05	3.14	2.48
Formation Volume Factor, Vr/Vt by flash lib. to 250 psig	2.84*	2.98	2.95	2.42
Formation Volume Factor, Vr/Vt by flash lib. to zero psig	....	3.58	3.80	2.68
Solution Gas/Oil Ratio, CFPB by diff. lib. @ Res. Temp.	....	3734	4296	4160
Solution Gas/Oil Ratio, CFPB by flash lib. to 250 PSIG	2800*	3320	3934	3990*
Gas/Oil Ratio produced by well at time of sampling, CFPB	2794	....	3918	3950
Solution Gas/Oil Ratio, CFPB by flash lib. to zero psig	....	4149	4721	4660
Residual ST Oil gvty. by flash lib. to 250 psig, API at 60°F	49.4**	46.7	44.5	....
Specific gvty. of Sep. Gas flashed to zero psig sep. press.	....	1.027	0.897	0.725
Oil viscosity, cp. at bubble-point press. and Res. Temp.	....	0.177	0.174	0.25
Avg. Compress. at Res. Temp. in the bubble-point region vol/vol psi	70.5x10^{-6}	54.5x10^{-6}	43.8x10^{-6}	22.4x10^{-6}
Thermal expansion of Sat. Oil @ 7,500 psig, % per °F	0.185***	0.0923	0.0968	0.0531
Specific Volume @ Bubble-Point Pressure and Res. Temp.	....	0.03285	0.03494	0.0265

* Based on preliminary report and separator pressure between 280 and 300 psig.
** Gravity of stock tank oil produced when flashed to 282 psig separator pressure.
*** At 6,800 psig.

NOTE: Vr/Vt refers to the number of barrels of fluid at original reservoir conditions required to produce one barrel of stock tank liquid. CFPB refers to cu ft of separator gas at 15.025 psia and 60°F per bbl of stock tank liquid at 60°F.

lative expulsion of reservoir fluids; the last survey period from June 8, 1949, to Aug. 18, 1949, shows that 46 per cent of the energy was furnished by water injection. As the pressure was held nearly constant, the water injection and edgewater encroachment were the only factors that were considered to furnish energy to produce the reservoir fluids. Thus, with an injection slightly in excess of 2,000 B/D, a balance between water encroachment and water injection was established. This balance should keep the reservoir fluids from any shifting which could have resulted by encroachment of water from the south and west only.

Predictions

It was assumed in making the predictions (1) that the vertical rise in the water-oil contact was equal throughout the areal extent of each section, (2) that the efficiency factor for the area west of the "E" fault would be 65 per cent, (3) that the wells will be shut-in when the water-oil contact reaches the top perforations for the well, (4) that the pressure of 5,000 psig will be maintained, and (5) that energy for expulsion of reservoir fluids would be furnished approximately 50 per cent by water injection (north side) and 50 per cent by water encroachment (south and west flanks).

An injection rate of 2,000 B/D at the present time should maintain the reservoir pressure at or near 5,000 psig. As the water-oil contact rises and the wells go to water, the rate of water injection will be decreased proportionally to balance the decrease in the rate of reservoir voidage to maintain a balance between injected water and natural edge-water encroachment.

The reservoir producing rate for the Morein sand in the pressure maintenance area (west segment) will decrease as individual wells are shut in due to water production. The wells along the southern flank of the field are steadily going to higher percentages of water production; however, the rates for each of the other wells should remain near the present level until such time as they are curtailed by encroaching water.

Without water injection the ultimate recovery from the west segment of the Morein sand could be increased approximately 30 per cent by a decrease in reservoir withdrawal rates. This would take full advantage of the natural water drive on the south but would increase the time needed for ultimate recovery by approximately 100 per cent. When consideration is given to reservoir withdrawal reductions, it must be pointed out that an absence of a natural water drive from the north would not allow the area on the north to be swept by water.

The ultimate recovery from the west segment with high pressure salt water injection will be increased approximately 66 per cent over the recovery possible without pressure maintenance and without reservoir withdrawal reduction. Likewise, the ultimate recovery with pressure maintenance will be increased by 28 per cent over recovery by primary production with a reservoir withdrawal decrease, and the time needed for the recovery will be reduced by nearly 50 per cent.

ACKNOWLEDGMENTS

We wish to acknowledge the help and cooperation received from the Producing, Land, Natural Gas, Geological and Petroleum Engineering Departments of the Magnolia Petroleum Co. in obtaining data incorporated in this paper. Appreciation is expressed to the management of the Magnolia Petroleum Co. for permission to publish this paper.

REFERENCE

"A Study of the Mamou Field," Petroleum Engineering Dept., Magnolia Petroleum Co., Dec. 1, 1949 (unpublished).

★ ★ ★

T.P. 3076

INTERSTITIAL WATER DETERMINATION BY AN EVAPORATION METHOD

E. S. MESSER, CONTINENTAL OIL CO., PONCA CITY, OKLA., MEMBER AIME

ABSTRACT

A knowledge of the magnitude of the irreducible interstitial water in a porous medium is so important to petroleum engineering that its determination has become routine in core analyses.

The method of determination, being a production problem, should encompass the basic requirements of simplicity in technique and calculations, with reproducible results obtainable in a short interval of time. The results of the evaluation tests outlined in this report indicate that the evaporation method for determining the irreducible water is a technique which meets the requirements.

The procedure consists, as the name implies, of permitting the saturant in the pore spaces to evaporate until only an irreducible volume remains. The determination of this volume can be made either graphically or by a mathematical comparison of fluid flows; the time required for each determination being dependent on the fluid used.

When fluids other than those having reservoir characteristics were used, a volume factor had to be calculated which was based on the relative volume of various liquids adsorbed on grain surfaces and retained in pores. This factor made possible the calculation of an irreducible water volume when more volatile fluids such as toluene and benzene were used as the saturants.

Also presented is the theoretical discussion necessary for the calculation of the capillary pressure as determined from the evaporation curve. A comparison is made between the calculated values and those obtained by experimental means.

INTRODUCTION

In all geological formations there exists, in the pore spaces of the rock structure, water that is held in a state of equilibrium between capillary and hydrostatic forces. "Interstitial water" is the term given to this water and is defined as that water coexisting in the pore space with the oil prior to exploitation. The term "connate water" has often been used synonymously with this term; however, this can be true only by a specific definition since, geologically, it means the water in place at the time the rock structure was formed.

The quantity of the interstitial water is a variable factor in any formation, since it depends on the hydrostatic forces present in any multiple-phase system. These forces may become unbalanced by the introduction of an extraneous force such as the raising or lowering of the "water table" or the migration of oil into a water-filled formation. Any unbalanced force results in a change in the interstitial water.

There exists, however, an irreducible interstitial water, for a particular sand, that is the fraction of the pore space occupied by water when the capillary pressure at the particular point in question is at an equilibrium with the hydrostatic head of the oil sand in the reservoir. For this discussion the term "irreducible water saturation" will be used in place of "irreducible interstitial water saturation" for the sake of brevity; however, they are understood to be identical.

A great amount of work has been devoted to the theory and methods for studying the irreducible water saturation and its related capillary pressure. As a result of the publications of Leverett;[1] Hassler, Brunner and Deahl;[2] Calhoun and Lewis;[3] and others, the role of capillary pressure studies is being accepted by the industry as a tool for studying subsurface phenomena. Many techniques have been developed and published for determining the capillary pressure and irreducible water. In general, these techniques may be grouped into three classifications. One of the first was the capillary pressure method described by Leverett[1] and expanded by Bruce and Welge.[4] The experimental results were compared with water saturation of cores obtained using oil-base mud. Thornton and Marshall[5] compared the irreducible water saturation of core samples determined by the capillary pressure method and by salinity and reported good agreement between the two methods.

The second classification for determining the irreducible water and capillary pressure may be referred to as the "centrifugal force method." The general technique is similar to the capillary pressure method except that the force driving the reservoir fluid from the sample is of a centrifugal nature. A complete description of this method was presented by J. J. McCullough and F. W. Albaugh.[6]

A process, the reverse of the capillary pressure method, was presented by W. R. Purcell.[7] Mercury under pressure is driven into the pores of the rock and the saturation of the core determined at each applied pressure. The resulting capillary pressure curve is used to evaluate the irreducible water saturation.

The techniques mentioned are singular in their approach to the irreducible water saturation. In all cases, an external force was applied to the core. The forces employed in the evaporation method are the vapor pressure of the liquid causing evaporation, the kinetic diffusion forces, adsorptive forces and, to a lesser degree, the viscous forces resisting flow to the surface.

The basic definition of irreducible water is that water held in a state of equilibrium between capillary and hydrostatic forces. This water has been described by previous investigators as being held in the microcapillaries too small to support fluid flow. Actually, this fluid volume is made up of the water in the microcapillaries and as a film adhering to the surface of the crystals. All capillaries, therefore, possess some liquid as a film, the thickness of the film being dependent on the properties of the fluid and solid. A discussion of experiments with references pertaining to the measurement of this immobile layer next to the solid surface can be found in the text by J. J. Bikerman.[8] Eversole and Lahr calculated the thickness of this layer to be in the order of 10^{-7} to 10^{-6} cm for aqueous solutions and glass. Between two quartz surfaces they found the thickness to be 2×10^{-6} cm. The work of Volkova, on the capillary movement of water and toluene in quartz grains, indicated the thickness of the immobile layers to be near 10^{-5} cm. Since any measurement is an average value, it is easy to understand that an absolute value would depend on the roughness of the surfaces involved and the complexity of the system. A calculated effective pore radius of 2×10^{-5} cm is obtained at the irreducible saturation of a porous media in a water-air system when a capillary pressure of 100 psi is applied. Since the separation of the sand grains is of the same approximate magnitude as the immobile layer,

---

[1] References given at end of paper.

Manuscript received in the office of the Petroleum Branch Aug. 17, 1950. Paper presented at the Fall Meeting of the Petroleum Branch in New Orleans, La., Oct. 4-6, 1950.

it may be probable that the major portion of the irreducible volume can be classified as this multilayer film.

Consider then a core sample that has been saturated with a liquid which wets the solid surfaces and exhibits an approximate zero angle of contact. At the beginning of the evaporation process the fluid surface in the 100 per cent saturated core may be considered nearly flat, and the rate of evaporation is a function of the exposed area of the core surface, the velocity and humidity of the drying media. As evaporation of the fluid proceeds, there will be a migration of the fluid front to the interior section of the core and capillaries of smaller radii, resulting in a reduction in the saturated vapor pressure. Due to the gradual decrease of the vapor pressure, and increase in complex flow path, the rate will decrease as the concentration decreases. The larger pores will be the first to be emptied, and if the process could be brought to an equilibrium at a particular saturation, capillaries of higher meniscus curvature by virtue of the smaller pore diameter than the equilibrium vapor pressure indicated would be completely saturated with the liquid and the larger pores would be lined with a continuous multilayer film. This film would be thick at the concave meniscus and would make a zero angle of contact with the fluid surface. The thickness of the multilayer would decrease as the distance to the outer core surface increased.

The actual mechanism of flow during desaturation is complex; however, it may be considered mainly as vapor migration by evaporation and recondensation on the multilayer film, resulting in a net loss by vapor diffusion to the drying air stream at the exterior of the sample. At the point of irreducible saturation, when the microcapillaries remain completely saturated, further migration of the meniscus results in only a small change in the adsorbed volume and the net loss in weight would be due to the evaporation of the multilayer film lining the larger capillaries. This rate of desaturation would be uniform for a short interval of time due to the approximate constant area and diffusion path.

As the evaporation proceeds, the constant rate of desaturation will decrease as the film lining the pores becomes less thick and the forces associated with the liquid-solid interface become more pronounced. The change in the rate of desaturation after the irreducible saturation has been reached will depend on the liquid and solid surface characteristics.

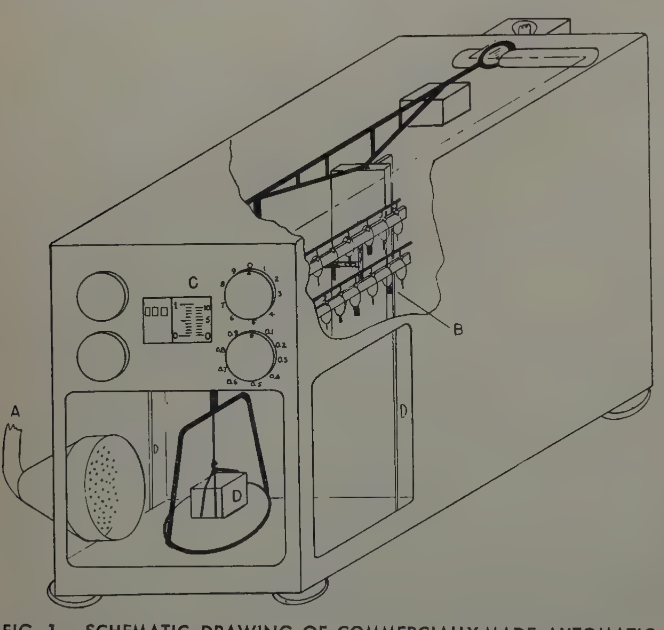

FIG. 1 — SCHEMATIC DRAWING OF COMMERCIALLY-MADE AUTOMATIC BALANCE.

After the initial saturation and the meniscus has receded to the internal section of the core, vapors must diffuse through the pore space of the substance before entering the atmosphere for a second diffusion action. Edward Ledoux,[9] in his text on vapor adsorption, describes the desorption efficiency in the case of an adsorbed liquid inside the adsorbent. For low rates of evaporation, the coefficient of diffusion friction or the change in vapor pressure with distance of diffusion inside the adsorbent is proportional to the mass of flow of vapor and a constant which is characteristic of the structure of the adsorbent. When this diffusing amount reaches the outer surfaces of the adsorbent it will be transferred to the air where the vapor pressure is P^1. The general equation combining the two diffusion processes, inside the adsorbent and from the surface to the air, is then:

$$Qm = K(P_v - P^1) \quad . \; . \; . \; . \; . \; . \; . \; . \; . \; . \quad (1)$$

For practical purposes, with dry air blowing across the face of the sample, its vapor pressure P^1, in the atmosphere at a unit distance above the sample, will be small and may be neglected.

In Equation (1), K is the overall coefficient of vapor transfer for desorption and is essentially a combination of the coefficient of diffusion per unit distance inside the adsorbent and the coefficient of vapor transfer outside the adsorbent. By definition, K is the amount of vapor transferred per unit time, per unit area by a unit vapor pressure difference. The units are therefore $gm\ sec^{-1}\ cm^{-2}\ \triangle P^{-1}$ and the absolute value for a core can be determined only through experimental means.

Before proceeding further with a study of Qm and K, it is necessary to determine the variation of P_v in the porous media during desaturation. If the pressure on the liquid in the pores is exerted by virtue of the curvature of the meniscus, the relationship between the equilibrium vapor pressure P_v over the concave meniscus of a wetting liquid to the vapor pressure P_o over the plane surface may be represented as a function of the radii of curvature by:

$$Ln\frac{P_o}{P_v} = \frac{2\delta M}{\rho R T r} \quad . \; . \; . \; . \; . \; . \; . \; . \; . \; . \quad (2)$$

where δ is the surface tension of the liquid, M the molecular weight of the vapor, R the gas constant, T the absolute temperature, and r the radius of curvature of the meniscus. If the pores are assumed circular, with a zero contact angle between liquid and solid and the adsorbed film negligibly thick, then r is the equivalent pore radius. For water at 20°C, the right-hand side of Equation (2) is $1.07 \times 10^{-7}/r$ and it can be seen that the reduction in vapor pressure due to the capillary curvature is small for pores whose radii are of the order of a few microns. For an average core sample above the irreducible volume, the vapor pressure may be considered constant and the vapor flow varies as the coefficient of vapor transfer.

According to Equation (1) for a particular adsorbent, the mass flow of vapor will remain constant if vapor pressure difference, diffusion area, and liquid characteristics remain constant. A core sample at any saturation below 100 per cent may be considered as consisting of n uniform capillaries of cross sectional area a and volume V_1, completely filled with vapors at an equilibrium vapor pressure. The total volume of vapors V is then $n\ V_1$ which is numerically equal to the pore volume less the liquid volume at saturation S_1. A representative area for diffusion at S_1 is V/L_1, where L_1 is the effective length of the capillary. The total mass vapor flow from the adsorbent is then:

$$Qm = \frac{KV}{L_1}P_v \quad . \; . \; . \; . \; . \; . \; . \; . \; . \; . \quad (3)$$

Table I — Physical Properties of Test Samples

Core No.	Formation	Pore Volume (cc)	Rock Volume (cc)	Porosity %	Air Permeability (md)
DG18	Sandstone	1.53	3.84	28.5	5085
P57	S. Dolomite	1.36	3.94	25.7	2648
CS3	Dolomite	1.76	4.26	29.2	1099
DG1	Sandstone	1.58	4.15	27.6	814
OG9	Sandstone	1.04	4.82	17.8	539
84Z	Sandstone	1.00	4.59	17.9	295
DG8	Sandstone	1.53	4.39	25.8	204
79C	Sandstone	1.37	5.38	20.2	115
02C	Sandstone	1.08	4.56	19.2	78
31C	Sandstone	1.03	4.57	18.4	55
AS1	Sandstone	1.24	4.44	21.8	37
AV20	Sandstone	.80	4.33	15.6	34
87B	Limestone	1.53	7.24	17.5	19
18C	Limestone	1.03	5.06	16.9	16
AD30	Sandstone	1.05	5.11	14.8	14
88E	Limestone	1.37	5.66	19.5	6.5
CS13	Dolomite	.74	5.45	12.0	6
21C	Limestone	1.10	4.94	18.2	2.3
88T	Sandstone	.96	4.68	17.0	1.9
AV7	S. Dolomite	.51	5.85	8.0	.8

If it is assumed that during desaturation equilibrium conditions are approximately maintained, then the combination of Equations (2) and (3) leads to a general relationship for mass vapor flow in terms of liquid and core characteristics:

$$Qm = \frac{K}{L_1} V P_o \exp. -\frac{2\delta M}{\rho R T r} \quad . \ . \ . \ . \ . \ (4)$$

At the saturation representing irreducible volume, the change in V and r is small; K and L_1 remain constant for a short interval of time such that the resulting rate of desaturation remains constant.

As previously stated, desaturation of a core is due to vapor migration by the process of evaporation and recondensation and a film remains on the outer crystals of the core prior to the irreducible volume. The presence of this film was observed by placing a saturated core under a microscope with a stream of dry air passing over the film. In tight formations, there seemed to be periodic drying of the surface; however, it was not continuous as liquid resaturated the crystals. The film existed until irreducible volume was reached; after that, drying occurred.

EXPERIMENTAL PROCEDURE

The evaporation method for determining irreducible water saturation is rapid and, in general, the experimental procedure consists as the name implies of evaporating the fluid from a saturated core until the rate of desaturation first becomes constant for a period of time. The fluid remaining in the core at the beginning of this constant rate represents the irreducible fluid volume.

More specifically, the experimental procedure consists, first, of saturating a clean core with a liquid that forms a zero contact angle with the solid and does not leave a residue when evaporated or cause any chemical reaction with the sample itself. Liquids such as a metal-containing organic compound or its chemical derivative should not be used as they remain deposited in the core sample after the test has been completed. If such a liquid is used, corrections which will be discussed later must be applied to compensate for the deposited weight. Examples of some of the liquids used and found satisfactory are water, toluene, tetrachlorethane, benzene, and n-propyl alcohol.

The liquid-saturated core sample is then placed on the platform of a balance capable of indicating continuous weight change as the fluid evaporates from the pores. A schematic drawing of a commercially-made automatic balance that was used and found satisfactory is shown in Fig. 1. The system is initially in equilibrium, the weight of the saturated core *(D)* being compensated by the removal of weights *(B)* from a suspended bridge fixed to the pan lever system. When the sample changes in weight, as that associated with the evaporation of liquid from the pore spaces, the motion of the balance arm can be observed by a beam of light traveling across a vernier scale *(C)*. By this means the continuous change in sample weight can be observed.

A stream of gas or air from *A*, passing over the sample, speeds the rate of evaporation and reduces the time interval for each test. An air flow of approximately 20 cfm was found satisfactory as it was not sufficient to agitate the balance and cause erroneous readings. During the experiment, weight readings were taken at equal intervals. These, transformed to fluid volume measurements, were plotted as a function of time.

In the first group of tests to evaluate this method, 20 samples from different formations and having different characteristics, shown in Table I, were selected. These samples were saturated with various liquids mentioned and an irreducible liquid volume determined for each sample and liquid according to the theory previously described. Typical desaturation curves for core samples of high and low permeability are shown in Fig. 2 for water, toluene and tetrachlorethane. These curves are characteristic of the solid-liquid system, the irreducible volume being represented by the point where the rate of desaturation becomes approximately constant. In actual laboratory practice, it was not necessary to plot the curves as the irreducible volume could be more accurately determined by a study of the loss in weight per unit time during the test.

Experimental data for the desaturation curve of Core Sample No. 79C is shown in Table II together with the change in volume of the saturant with time. The fluid volume in the core at the point when the rate becomes approximately constant represents the irreducible liquid volume. In the case of Sample No. 79C, for water it would be .221 cc, for tetrachlorethane .251 cc, and for toluene .266 cc. The approximate constant rates are .020 cc per five minutes, .013 cc per five minutes, and .013 cc per minute respectively.

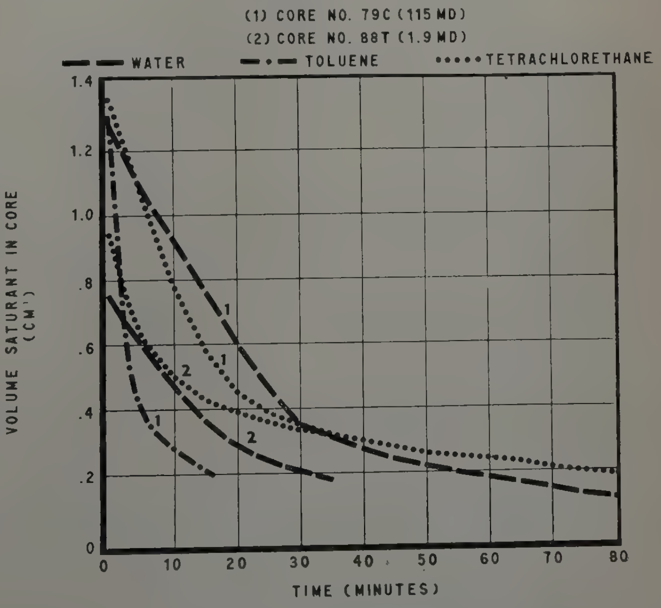

FIG. 2 — PORE FLUID RETENTION.

It can be seen from Table II that the irreducible liquid volumes are different and depend on the liquid used. To calculate the irreducible water saturation, formation water would be the most appropriate to use; however, the depositing of salt in the pores presents another correction to be applied. Distilled water would be the best substitute as it has the same surface tension characteristics. In J. J. Bikerman's text, *Surface Chemistry,*[8] a table is presented from the work of Grinnell Jones on the variation of surface tension of brine with water. For a solution of 25,000 ppm *NaCl*, the ratio of surface tension of the solution to water is 1.00153. The correctness of using water in place of reservoir fluids is further emphasized by the fact that, as a result of the tendency toward free energy of a surface to decrease, the concentration of a solute on the interface may differ from the bulk. If the solute brings about an increase of surface tension as in the case of *NaCl*, its concentration will be less in the surface than in the remainder.

Many investigators in the field of capillary pressure studies have found that distilled water causes swelling and, therefore, a change in core characteristics. Also, the routine core cleaning process with any organic liquid often leaves the solid surfaces preferentially oil-wet and interstitial water determinations involving water or brine would be in error. Organic liquids such as toluene, tetrachlorethane or benzene as saturants insures the wetting of rock surfaces with a zero contact angle. From the experimental data, the irreducible fluid volume for organic liquids was greater than that for water and, therefore, a volume factor had to be applied to change irreducible liquid to irreducible water volume.

A limited search of available literature failed to reveal experimental data for adsorbed volumes with consolidated silica grains and the organic liquids used. A theoretical approach to this problem would be too involved for this paper as it would probably entail functions of free energy of wetting, the mole volumes of liquid involved, free energies of vapor adsorption on the solids, and surface tension of the liquids. In view of the lack of published data, a factor was sought that could be used to change irreducible liquid to irreducible water when the sample was clean and water-wet.

An approximate magnitude of this volume factor can be obtained from the work on liquid adsorption by unconsolidated material. It is realized that a volume factor thus determined may differ for consolidated material because of the added functions involved; however, the agreement in the experimental data indicated that either the added factors were negligible or compensating by their complexity.

Table II — Pore Fluid Retention Data

Pore Vol. 1.37 Core No. 79C

Time (min)	Water Fluid Vol. (cc)	Water ΔV (cc)	Tetrachlorethane Fluid Vol. (cc)	Tetrachlorethane ΔV (cc)	Time (min)	Toluene Fluid Vol. (cc)	Toluene ΔV (cc)
0	1.285		1.361		0	1.300	
5	1.083	.202	1.059	.302	1	.949	.351
10	.922	.161	.790	.269	2	.704	.245
15	.762	.160	.582	.208	3	.540	.164
20	.599	.163	.452	.130	4	.450	.090
25	.458	.141	.385	.067	5	.399	.051
30	.353	.105	.346	.039	6	.365	.034
35	.305	.048	.319	.027	7	.334	.031
40	.267	.038	.298	.021	8	.314	.020
45	.240	.026	.279	.019	9	.296	.018
50	.221	.020	.264	.015	10	.279	.017
55	.202	.019	.251	.013	11	.266	.013
60	.184	.018	.238	.013	12	.252	.014
65	.167	.017	.226	.012	13	.239	.013
70	.150	.017	.214	.012	14	.227	.012
75	.134	.016	.202	.012	15	.215	.012
80	.119	.015	.191	.011	16	.204	.011

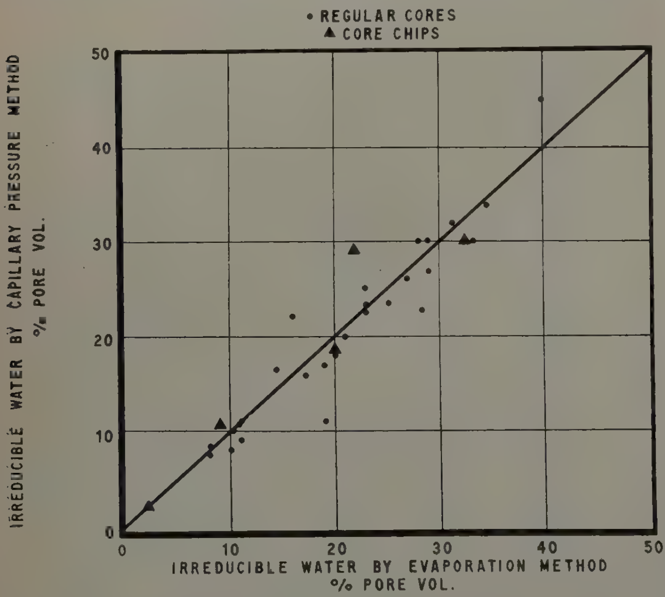

FIG. 3 — IRREDUCIBLE WATER PER CENT PORE VOLUME. EVAPORATION AND CAPILLARY PRESSURE METHODS.

Bartell and Greager,[10] in their work with powdered silica and calcium fluoride, found the adsorbed volume to be a function of the solid surface and the degree of wetting or adhesion tension. It has been shown by Harkins and Livingston[11] and A. D. Garrison[12] that the degree of wetting of a solid by a liquid is a measure of the adhesion tension. There exists, therefore, a definite relationship between fluid adsorption and adhesion tension. Bartell and Greager used the method of Gardner and Coleman to determine the adsorption factor of various fluids with calcium fluoride and silica. They found that silica would adsorb approximately 1.13 cc of toluene or benzene to 1 cc of water. The ratio was 1.40:1 for the two liquids with calcium flouride. If a direct relationship exists between adsorption and adhesion tension, the volume factor would be 1.16:1 and 1.33:1 for tetrachlorethane on the two solid surfaces. A simplified Gardner and Coleman method was tried for limestone and dolomite and volume factors of 1.24:1 for toluene and benzene, and 1.16 for tetrachlorethane, were obtained.

Harkins and Ewing[13] found the volume of liquids adsorbed by the same charcoal increased in the same order as the percentage compression for a definite high pressure. They classified macropores as being 12×10^{-4} cm in diameter and micropores less than 10^{-5} cm. Liquid in the micropores is very highly compressed by adsorption and this compression is greater the greater the compressibility of the liquid in bulk. The relationship between compressibility in bulk and in the pores is not a direct relation since the liquid is not compressed iso-tropically. Their experiments with charcoal show an adsorption of .39 cc benzene, .35 cc water, and .41 cc of ether or a ratio of 1.11:1 and 1.17:1.

To establish a suitable volume factor that could be used in the evaporation method, a number of clean sandstone and limestone samples were selected and saturated with various fluids after the wettability of the sample to that fluid had been determined. The factor necessary to change the irreducible liquid to water volumes within the range of experimental error was found to be 1.10 for toluene and benzene and 1.13 for tetrachlorethane with limestone and dolomite.

These factors were used in all tests when liquids other than water was used.

Experimental results obtained by the evaporation method were compared with measurements on the same sample by the capillary pressure method. Since this latter method has been evaluated by previous investigators, the comparison indicates that the evaporation method is a rapid means of determining irreducible water. A total of 110 tests have been made using both methods and the general trend is shown in Fig. 3. Only the experimental results for toluene as the saturant in the evaporation method are shown since excellent agreement was obtained between the various liquids using the volume factors; each point on the curve therefore represents several tests. The method was carried out using core chips of approximately 1/10 the bulk volume of a regular core and the results are indicated in Fig. 3. The general distribution of differences between the evaporation and capillary pressure methods is shown in Fig. 4. For 54 out of 110 tests, the difference was only ±1 per cent.

In the routine determination of irreducible water saturation for core analysis, it is often advisable to study the trend of the saturation with permeability. Since permeability alone will not establish the irreducible water for a fixed type of formation such relationships have statistical significance. When a curve is determined for a particular zone of interest, it may be used to estimate the gross irreducible content of the formation and also the local values of the irreducible water saturation from the permeabilities of the individual samples. A permeability relationship for a single formation is shown in Fig. 5.

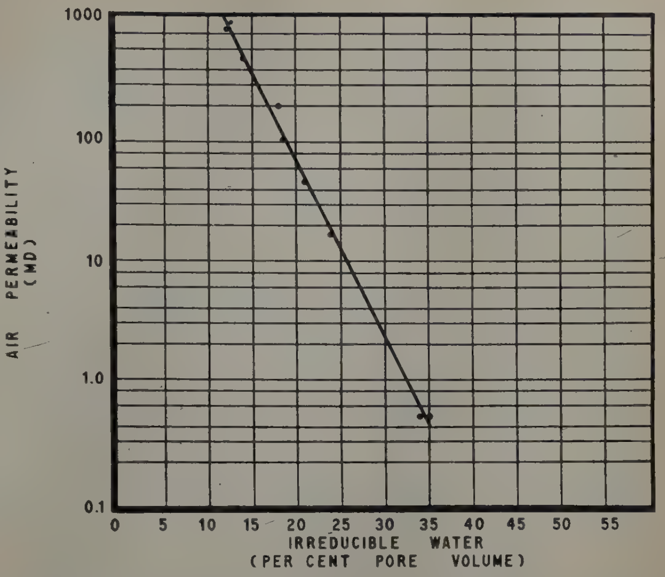

FIG. 5 — IRREDUCIBLE WATER AND AIR PERMEABILITY, CAT CREEK FIELD, SECOND KOOTENAI FORMATION.

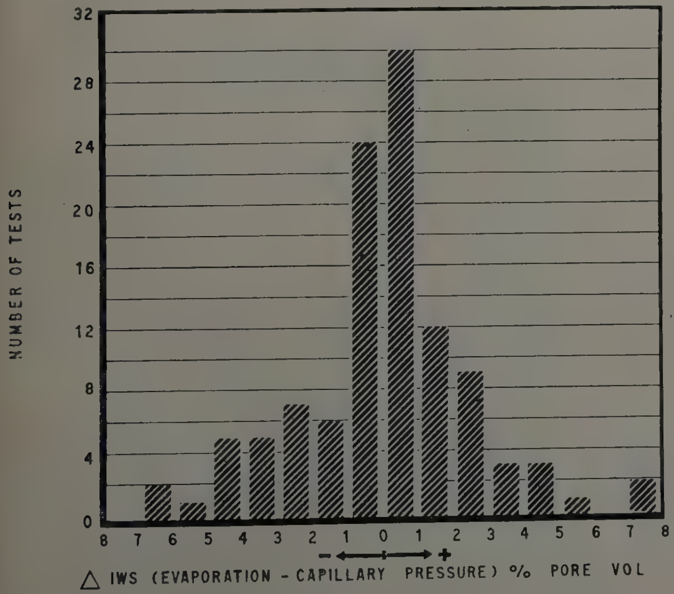

FIG. 4—DISTRIBUTION OF DIFFERENCES BETWEEN IRREDUCIBLE WATER SATURATIONS BY EVAPORATION AND CAPILLARY PRESSURE METHODS. 110 TESTS.

CAPILLARY PRESSURE AND PORE RADII

The role of capillary pressure has become important in the investigation of core characteristics and the values have been used by many authors[7,14] to calculate pore size distribution and permeability. In the evaporation method previously described capillary pressures and pore radii are not a part of the data but a calculation of the trend in capillary pressures can be obtained by considering the vapor diffusion as represented by Equation (1). Capillary pressure and vapor pressure lowering are a function of the liquid saturation of porous media. A qualitative relationship between these functions can be obtained by considering the water and vapor as continuous phases in the system. If at any time the two phases are in equilibrium, the equation relating the vapor pressure above a curved surface with the capillary pressure is equivalent to Equation (2) and has been reported by Freundlich,[15] Calhoun and Lewis,[3] Ledoux,[9] and others as:

$$\frac{2\delta}{r} = P_c = \frac{RT\rho_L}{M} Ln \frac{P_o}{P_v} \quad . \ . \ . \ . \ . \ . \ . \quad (5)$$

where ρ_L is the density of the liquid.

Since P_v is approximately equal to P_o in core samples whose capillaries are of the order of 10^{-4} cm, $Ln\ P_o/P_v$ can be written as $\frac{P_o}{P_v} - 1$ and Equation (5) can be simplified after substitution of P_v from Equation (3) to:

$$P_c = \frac{RT\rho_L}{M}\left(\frac{P_o}{QL_1/VK} - 1\right) \quad . \ . \ . \ . \quad (6)$$

Equation (6) represents a general expression for capillary pressure in terms of vapor flow from the sample during an evaporation experiment. In experimental tests, due to the air stream across the face of the core, variation in sample size and operating temperature. the values of P_o, L_1, K, ρ_L are unknown but can be evaluated as constants if the capillary pressure and Q/V values are known for any saturation. The validity of the assumption that P_o K/L and $T\rho_L$ remained constant or compensating after the liquid meniscus had migrated into the core can be based on the excellent agreement that was obtained between calculated and observed capillary pressure values.

The constants and capillary pressure curves were calculated for 15 samples saturated with water and the typical data are shown in Table III for Core Sample 79C. In this case, P_o K/L was 14.1×10^{-4} gm/cm³ sec and $RT\rho_L/M$ was 7.6×10^4 dynes/cm². Using these constants, the remaining capillary pressure values were calculated. Additional calculated and observed capillary pressure values are shown in Fig. 6 for Samples 09G and 84Z.

Examination of the calculated capillary pressure curves for the 15 samples and the necessary constants indicated that, for samples of very high permeability where the experimental capillary pressure curve was nearly horizontal to the point of irreducible saturation, two equations were necessary to represent the complete curve, one for the horizontal portion

Table III — Calculated Capillary Pressure
Sample LW 20 — Water

Time (min)	Vol. (cc)^3	Sat. %	Q/V 10^4	Cap. Pressure psi Cal.	Obser.
0	2.26	100			
5	2.18	96			.2
10	2.04	90	19.7	.1	.4
15	1.91	86	12.2	.5	.8
20	1.79	79	9.1	1.0	1.0
25	1.67	74	7.2	1.4	1.4
30	1.55	67	5.8	2.0	1.8
35	1.42	63	4.9	2.4	2.2
40	1.29	57	4.3	2.9	2.6
45	1.18	52	3.8	3.3	3.0
50	1.05	46	3.4	3.8	3.6
55	.93	41	3.0	4.3	4.0
60	.80	36	2.8	4.8	4.8
65	.68	28	2.5	5.3	5.4
70	.56	25	2.2	6.1	6.0
75	.45	20	1.9	7.1	8.0
80	.35	16	1.4	10.0	10.0
85	.29	13	1.0	14.3	17.0
90	.24	11	.8	19.4	22.0
95	.20	9	.5	29.4	26.0

and another for the vertical section. For samples whose permeability was between 100 and 600 md, one equation was sufficient to calculate the capillary pressure curve from approximately 50 per cent saturation to the irreducible value. For cores of permeability less than 100 md, one set of constants permitted the determination of a curve from 90 per cent saturation to the end point.

Because of the limited number of samples from any one formation, it was impossible to note a definite relationship between the constants and some other physical property of the core. For sandstone there was an apparent relationship between $P_o K/L$ and permeability; however, because of insufficient evidence, the dependency on permeability alone could not be established.

CONCLUSIONS

Investigation of the data obtained by the evaporation method, and comparison of the resultant irreducible water saturation with that obtained by capillary pressure, indicates this method fulfills the requirements for production laboratory use. Several distinct advantages of the method are:

1. The time required to determine the irreducible saturation depends on the saturant. For water, the average time was one hour.
2. Use of more volatile fluids as toluene and benzene reduces the time to approximately 20 minutes and the volume factor permits the calculation of an equivalent irreducible water saturation.
3. Since the sample tends to be oil-wet after cleaning, the solid surfaces need not be changed inasmuch as such organic liquids as toluene will wet the solid with an approximate zero contact angle.
4. The characteristics of the sample are not altered by the test and they can therefore be used for other analyses.
5. The irreducible saturation can be obtained for samples of varying size without a uniform or flat external surface.
6. The method can be used on small core chips.

If two capillary pressure values are known, the complete curve can be determined. This reduces the time element for the determination of a capillary pressure curve. Further experimental determination may indicate a relationship between the constants of Equation (6) and some other physical property such that a capillary pressure curve can be determined on the basis of the evaporation data.

ACKNOWLEDGMENTS

The author wishes to express his appreciation to the management of the Continental Oil Co. for permission to publish this paper and to J. J. Reynolds, Director, Production Research Division, for his helpful criticism and encouragement during its preparation. Acknowledgment is also made to the personnel of Continental's production laboratory for their assistance in taking data and making calculations.

REFERENCES

1. Leverett, M. C.: *Trans.* AIME (1941) **142,** 152.
2. Hassler, G. L., Brunner, E., and Deahl, T. J.: *Trans.* AIME (1944) **155,** 155.
3. Calhoun, J. C., Lewis, M., and Newman, R. C.: *Trans.* AIME (1949) **186,** 189.
4. Bruce, W. A., and Welge, H. J.: "Restored State Method for Determination of Oil in Place and Connate Water," *Oil and Gas Jour.* (July, 1947) **156,** 21.
5. Thornton, O. F. and Marshall, D. L.: *Trans.* AIME (1947) **170.**
6. McCullough, J. J., and Albaugh, F. W.: "Determination of Interstitial Water Content of Oil and Gas Sand by Laboratory Tests of Core Samples," API *Drill. and Prod. Prac.* (1944) **180.**
7. Purcell, W. R.: *Trans.* AIME (1949) **186,** 39.
8. Bikerman, J. J.: *Surface Chemistry,* Academic Press.
9. Ledoux, Edward: *Vapor Adsorption,* Chemical Publishing Co.
10. Bartell, F. E., and Greager, O. H.: "Relation of Adhesion Tension to Liquid Absorption," *Industrial and Eng. Chem.* (1929) **21.**
11. Harkins, W. D., and Livingston, H. K.: "Energy Relation of the Surface of Solids," *Jour. of Chem. Physics* (1942) **10.**
12. Garrison, A. D.: "Selective Wetting of Reservoir Rocks and Its Relation to Oil Production, API (1935) 130.
13. Harkins, W. D., and Ewing, D. T.: "High Pressure Due to Adsorption and Density and Volume Relation of Charcoal," *J. Am. Chem. Soc.* (1921) **43,** 1787.
14. Burdine, N. T., Gournay, L. S., and Riechertz, P. P.: *Trans.* AIME (1950) **189,** 195.
15. Freundlich, H.: *Colloidal and Capillary Chemistry,* Dutton and Co.

★ ★ ★

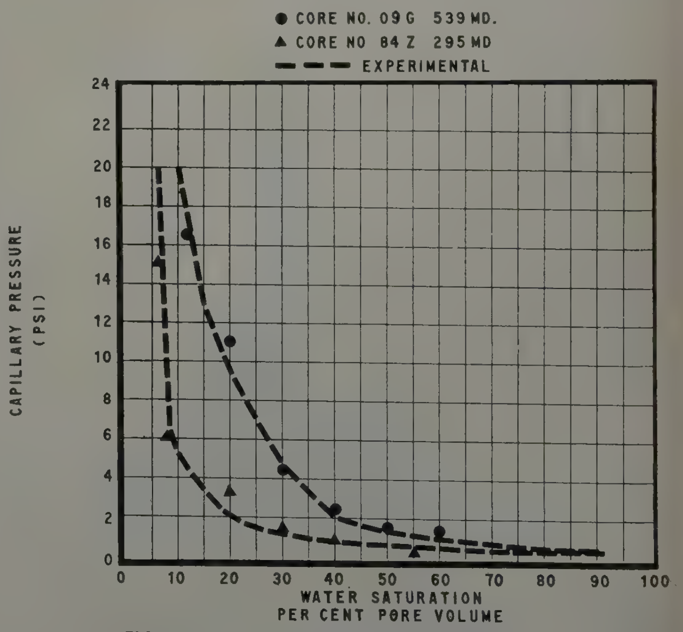

FIG. 6 — CALCULATED CAPILLARY PRESSURES.

T.P. 3169

FLUID SATURATION IN POROUS MEDIA BY X-RAY TECHNIQUE

A. D. K. LAIRD AND **J. A. PUTNAM**, MEMBER AIME, UNIVERSITY OF CALIFORNIA, BERKELEY, CALIF.

ABSTRACT

This paper describes the application of x-ray theory to design procedures in connection with fluid saturation determinations during fluid flow experiments with porous media. A reliable and rapid method for calibrating the x-ray apparatus is described. Extension of the method to fluid saturation determinations in three-fluid systems is described.

INTRODUCTION

In research on oil production problems a method is required which will give quickly the quantity of each component of a fluid flow system present at any cross-section of a porous medium.

The sample of porous medium under investigation is usually referred to as a core. The ratio of the volume of one component to the total fluid volume is defined as the saturation of the porous medium by that component. This ratio is generally given as per cent saturation.

Some means of measuring saturation which have received consideration include: electrical conductivity of the fluids;[1,2] emissions from radioactive tracers dissolved in the fluids; the radioactivity of silver caused by reflection of neutrons from hydrogen atoms in the fluids;[3] the attenuation of a microwave beam, the diminution and phase shift of ultrasonic wave trains,[4,5] and the reduction in intensity of x-ray beams in passing through the fluids.

X-rays have already been used with some success. Since every material has a different power to absorb x-rays, the reduction in intensity of an x-ray beam as it passes through a core depends on the fluids present. The strength of the emergent beam can be found by converting its energy into a measurable form such as heat or ionic current, or by its effect on a photographic plate or fluorescent screen. The beam strengths could be interpreted as quantities of known fluids in the core if, previously, these beam strengths had been identified with a known combination of the same fluids. With some fluid combinations it might be desirable to dissolve powerful x-ray absorbing materials in one or more of the fluids, to increase the differences in the beam strengths for various fluid saturations.

Boyer, Morgan and Muskat[6] have described a method of measuring two component fluid saturation. One component was air or water; the other, mineral seal oil in which was dissolved 25 per cent by weight of iodobenzene to increase its absorbing power. The x-ray source was a tungsten target tube operated at 43 kv potential. The beam emerging from the core was measured as ionic current flowing across an air-filled ionization chamber by means of an amplifying circuit and galvanometer. Another portion of the beam from the x-ray tube was passed through a metal plate and measured in another ionization chamber. This portion, called the monitor beam, was used as an indication of the performance of the x-ray tube. The galvanometer readings were calibrated against air-oil core saturations, gravimetrically determined. The method was apparently established by experimental means.

In the present investigation the available theory of x-radiation was surveyed with a view to extending the usefulness of the method and to developing design procedures for its application to measurement of fluid saturation in porous media. Application of the theory permits prediction of relative meter readings to be expected for any combination of porous matrix, various saturating fluids and auxiliary filtering media. It is thus possible to calibrate the equipment in terms of fluid saturation by an indirect but rapid technique. The results of calculations based on x-ray theory indicate, and results of the saturation calibration technique confirm, that a valid measurement of the saturation of the core can be made for any two components and in some cases for three components.

THEORY

The strength of an x-ray beam, after it has passed through a distance, l, of matter of density, ρ, and mass absorption coefficient, μ, at a given wavelength, λ, may be expressed by the absorption formula

$$I = I_o \, e^{-\mu\rho l} \quad . \; . \; . \; . \; . \; . \; . \; . \; . \; . \; . \quad (1)$$

where I_o represents the intensity of the incident x-ray beam and I is the intensity of the emergent beam. The expression $e^{-\mu\rho l}$ is called the transmission factor of the material.

The variation of I_o with wavelength depends upon the materials through which the x-ray beam has previously passed and upon the spectral distribution of energy at the source of the x-radiation. A group of curves, called spectra, which show the variation of intensity with wavelength and x-ray tube voltage are given in Fig. 1. These curves represent the general radiation from a tungsten target tube. When the tube voltage is greater than 69.3 kv, the characteristic radiation of the tungsten is emitted and is superposed on the general radiation. At a given voltage the minimum wavelength λ_{min} at which energy can be emitted by an x-ray tube is given by the formula

$$\lambda_{min} = \frac{12{,}340}{\text{volts}} \quad . \; . \; . \; . \; . \; . \; . \; . \; . \; . \; . \quad (2)$$

where λ_{min} is in Angstrom units. The wavelength at which the spectra have maximum intensity also decreases with increasing x-ray tube voltage. The area under each curve represents to an arbitrary scale the total energy emerging from the x-ray tube for that voltage.

The variation of μ with wavelength has been determined for many substances and may be found in such references as those by Compton and Allison[7] and by Hodgman.[8] The phenomenon of absorption is composed chiefly of the capture of photons by the atoms of the absorbing material with associated displacement of electrons, and of the scattering, or the deflection, of the photons by the atoms. Curves of these mass absorption coefficients show jump discontinuities, or absorption edges, at wavelengths which are short enough for the photons,

---

[1] References given at end of paper.

Manuscript received in the office of the Petroleum Branch Oct. 30, 1950. Paper presented at the Fall Meeting of the Petroleum Branch in Los Angeles, Calif., Oct. 20-21, 1949.

or bundles of x-ray energy, to be at a high enough energy level to eject electrons from the successive shells of the atoms (c.f. pp 526-531 of Compton and Allison).[7] These edges are given the designations *K*, *L*, *M*, etc., of the corresponding atomic electron shells from which the electrons are ejected. This added means of capturing photons causes the material to be a much more effective absorber on the shorter wavelength side of each discontinuity. The absorption edges of the elements occur at decreasing wavelengths as the atomic numbers increase.

The curves of ionization chamber efficiency as a function of wavelength shown in Fig. 2 were calculated by means of the approximate theory given on pp 484-496 of Compton and Allison.[7] The chamber gases with the higher product $\mu\rho$ produce the higher ionization chamber efficiencies, except possibly on the shorter wavelength side of an absorption edge. In calculating these curves, the effect of scattering on the chamber efficiency has been neglected without impairing their usefulness.

When x-radiation is absorbed in a gas, ions are produced in proportion to the energy of the x-ray beam. In the ionization chamber, the electrical potential between the collecting plates should be kept high enough to sweep practically all the ions formed to the plates. If the ionic current so produced is strong enough it may be measured and thus indicate the strength of the x-ray beam entering the ionization chamber.

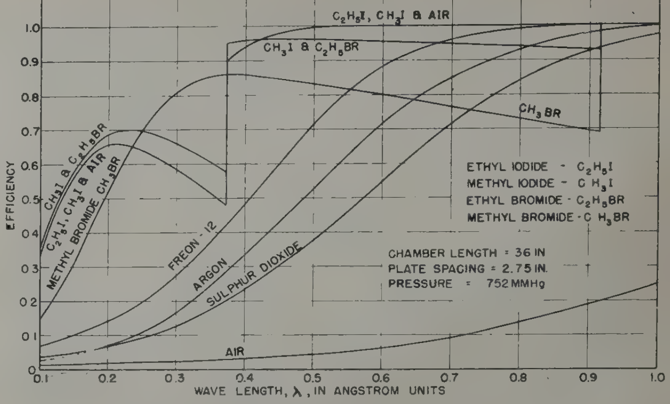

FIG. 2—IONIZATION CHAMBER EFFICIENCY FOR DIFFERENT GASES.

Since each fluid has a different absorption characteristic, it should be possible to determine an unknown core fluid saturation from the ionization current meter readings, by referring to a previous calibration in which the meter readings had been identified with known core saturations with the same fluid.

The relative meter readings to be expected from combinations of core saturations by different fluids may be calculated in the following manner. The spectral intensity at each wavelength for a given x-ray tube voltage may be multiplied by the ionization chamber efficiency and by the fraction of the beam transmitted by each material in its path. The values so calculated may then be plotted as a function of wavelength. The area under the resulting curve represents the meter reading to an arbitrary scale. These operations are illustrated in Fig. 3.

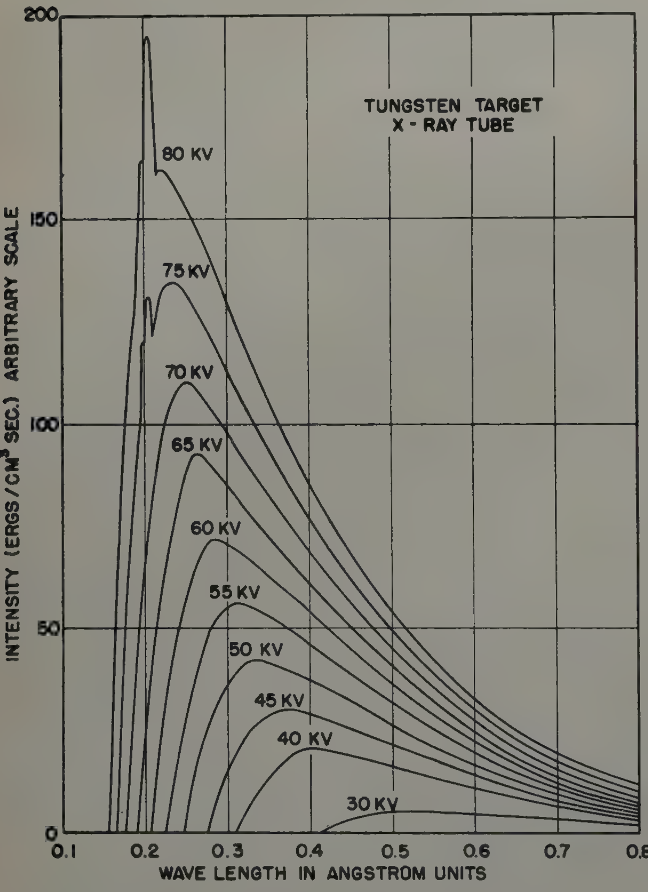

FIG. 1—X-RAY SPECTRA AT DIFFERENT VOLTAGES.

APPARATUS

X-Ray Equipment

The source of x-radiation was a thermax, 140 KVP, water-cooled, tungsten target tube, manufactured by Machlett Laboratories. The continuous rating of the tube was 11 milliamperes at 100 kv peak. The tube was mounted in a shockproof, rayproof head, connected by eight feet of shielded cable to a Westinghouse, 100 KVC, industrial type, x-ray transformer and control panel.

A General Electric automatic voltage stabilizer, rated at 2 KVA on 230 v service, was used to reduce fluctuations in the x-ray power supply voltage. A Type 1226, 2.4 KVA Powerstat, variable voltage transformer in parallel with the x-ray control panel, supplied a non-reactive load and was adjusted manually to keep a constant load on the stabilizer. This arrangement was used to avoid the change of effective x-ray tube voltage at a given peak voltage, caused by the variation of stabilizer output wave form with load.

The x-ray tube current was indicated by a milliammeter with a 0.2 ma least count. The high potential transformer primary voltage and the x-ray tube potential were indicated by a voltmeter with a least count of 1 v on its 0-150 v scale, and of 2 v on the 0-300 v scale. The relation between the readings of this meter and the x-ray tube peak voltage was established by means of a standard sphere-gap. The voltage output of the stabilizer was indicated by a push-button meter on the control panel. Ammeters were provided for the stabilizer output and the high potential transformer currents.

Changes in temperature of the high potential transformer of as little as 2°F caused noticeable differences in electrometer readings. Consequently, a small heat exchanger was installed to transfer heat from the transformer oil to cooling water. Circulation was effected by means of a small reciprocating pump. This arrangement held the transformer temperature within satisfactory limits.

Ionization Chambers and Electrometers

A 110 v Sola, constant voltage transformer was used on the supply to the electrometer rectifier circuit. This common rectifying circuit supplied two direct current amplifiers, each connected to an electrometer circuit mounted on an ionization chamber. The circuits used were of the same type as those described by G. L. Mellen.[9] These electrometers could be attached to either ionization chamber and to either amplifying circuit. All exposed electrical wiring was shielded. The reading of the electrometer attached to the monitor ionization chamber was recorded with each reading of the core ionization chamber electrometer, so that no momentary fluctuation in x-ray output would go undetected during a set of readings.

Both ionization chambers were made of 5 in. diameter, ⅛ in. thick brass tubing. The core chamber was 36 in. long, and the monitor 24 in. long. The parallel brass collecting plates, 2¾ in. wide and 1/16 in. thick were symmetrically placed 2¾ in. apart with at least ⅛ in. air gap all around. Polysterene was used to support and insulate the plates from the grounded shell. "Kovar" seals were used to insulate the plate connections from the shell. The entrance and exit windows of the chambers were of AM 3-SH, magnesium alloy, 1/32 and 3/32 in. thick, respectively. A capped tube was sealed into each shell and through the lead shielding to simplify filling the chambers.

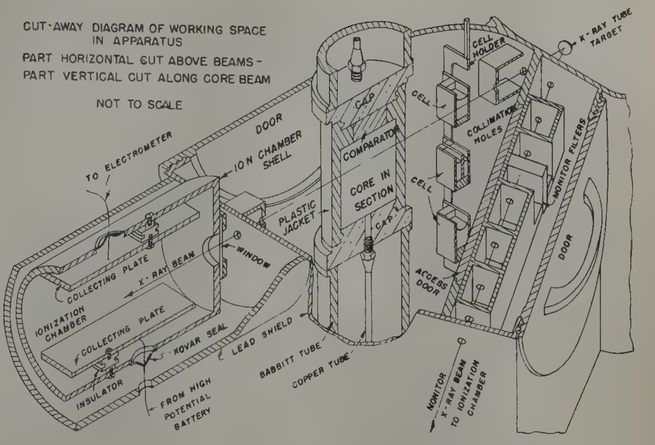

FIG. 4 — CUT-AWAY VIEW OF X-RAY APPARATUS.

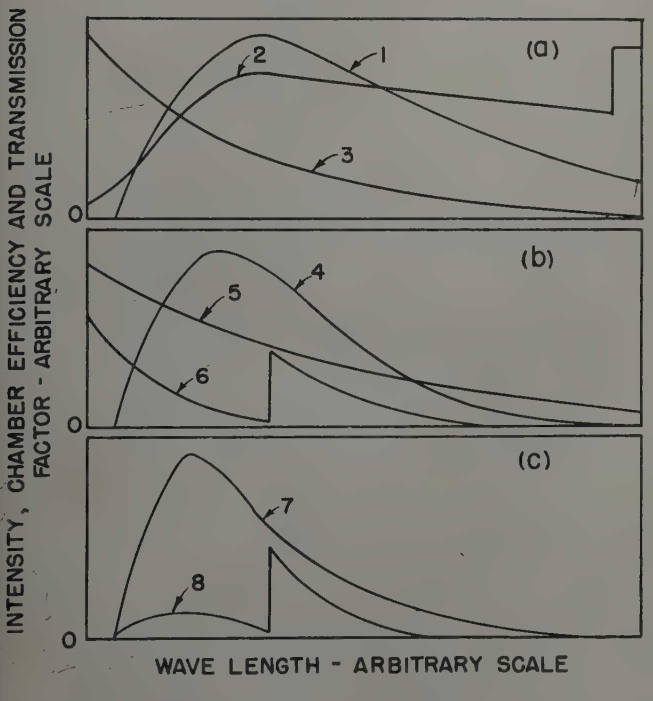

CURVE 1 SPECTRAL CURVE AT A GIVEN X-RAY TUBE POTENTIAL
2 IONIZATION CHAMBER EFFICIENCY
3 TRANSMISSION FACTOR FOR THE SOLIDS AND AIR IN THE X-RAY BEAM PATH.
4 PRODUCT OF ORDINATES OF CURVES 1, 2 & 3.
5 TRANSMISSION FACTOR FOR THE FLUID IN THE CORE.
6 SAME AS 5 BUT FLUID HAS AN ABSORPTION EDGE.
7 PRODUCT OF THE ORDINATES OF CURVES 4 & 5.
8 SAME AS 7 FOR CURVES 4 & 6.

THE RATIO OF THE AREAS UNDER CURVES 7 & 8 GIVES THE RATIO OF THE METER READINGS TO BE EXPECTED.

FIG. 3 — DIAGRAM SHOWING A TYPICAL EXAMPLE OF CALCULATIONS TO PREDICT RELATIVE METER READINGS.

The ionization chamber plate potential of approximately 900 v was taken from a group of 150 v dry cell batteries.

Porous Media

The porous media tested were Norton cylindrical consolidated alundum cores, 1 in. in diameter and 5 in. long. They had a porosity of about 26 per cent.

A 1 in. diameter piece of Alcoa 24 ST aluminum alloy about ½ in. long was cut on two parallel chords to a thickness of about 0.8 in. This piece, called the comparator, was placed on one end surface of the core. With each set of core electrometer readings a reading was taken with the x-ray beam passing through the flattened part of the comparator to show that the x-ray producing and indicating circuits were performing satisfactorily. The comparator also gave a datum for resetting circuit constants when desired. The comparator need not be mounted integrally with the core but it should be so located that it can be scanned by the x-ray beam independently of the core.

A brass cap with threaded tubing connections was provided for each end. The cap next to the aluminum had two holes communicating with the core through the aluminum. The cap at the other end had one hole to the core. The annular space around the core and aluminum, between the two caps, was filled with thermosetting plastic, Paraplex P-43. This jacket was machined to approximately 1.5 in. diameter.

General Arrangement

The x-ray head, ionization chambers and the working space between them were enclosed in lead. Tubing connections were made to the core caps through 2 in. diameter babbit tubes running in packing glands on the lead shield of the working space. The core was held at a constant elevation by the babbit tubes. The fluid piping and the babbit tubes were attached to a frame which permitted the core to be rotated about its axis through an angle of 76°. Fig. 4 illustrates the arrangement.

EXPERIMENTAL TECHNIQUES

X-rays are affected by the elements through which they pass, without regard to their chemical or physical arrangement. Advantage was taken of this fact to develop a method of identifying the electrometer readings with fluid saturation. The fluids were put in a box, or cell, shown in Fig. 4, which presented a fluid path length to the incident x-ray beam equal to that in the core. A number of these cells was mounted on a rack-and-pinion which permitted insertion of the cells into the x-ray beam. By this arrangement, the amount of the materials in the path of the x-rays remained the same; merely the order was changed. The length of the fluid path in the core was approximately equal to the product of the core diameter and porosity. The effective path is slightly less than the diameter because of the core curvature, but approaches the core diameter as the x-ray beam diameter decreases. The core and beam diameters were known and the effective path length was calculated. The thin-sided cells were made up of Paraplex P-43, of breadth inside equal to the effective path length of the core. Partitians were built into some cells to allow the simulation of various fluid saturation combinations in increments of 25 per cent.

To prepare a core for fluid calibration, its dimensions were taken and it was then encased in plastic and mounted in the apparatus as previously described. The core was scanned with the x-ray beam on three diameters, spaced 38° apart, over the full length, to test for uniformity of porosity. The calibration required was then carried out at several voltages close to the one chosen for the particular system of materials.

During a calibration, each well was positioned in the x-ray beam by reference marks attached to the rack. In this way, readings could be taken corresponding to several percentages of fluid saturation without opening the door of the core compartment.

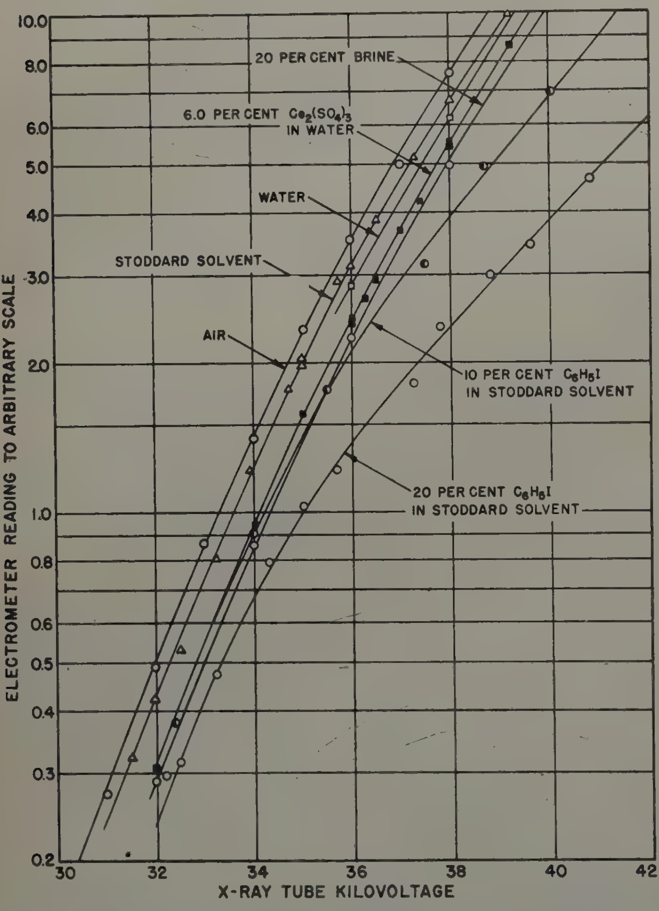

FIG. 5 — EXPERIMENTALLY DETERMINED ELECTROMETER READINGS AS A FUNCTION OF X-RAY TUBE POTENTIAL USING CELLS FILLED WITH FLUIDS INDICATED, PLACED IN FRONT OF AN AIR FILLED ONE-IN. DIAMETER ALUNDUM CORE. LOW VOLTAGE RANGE.

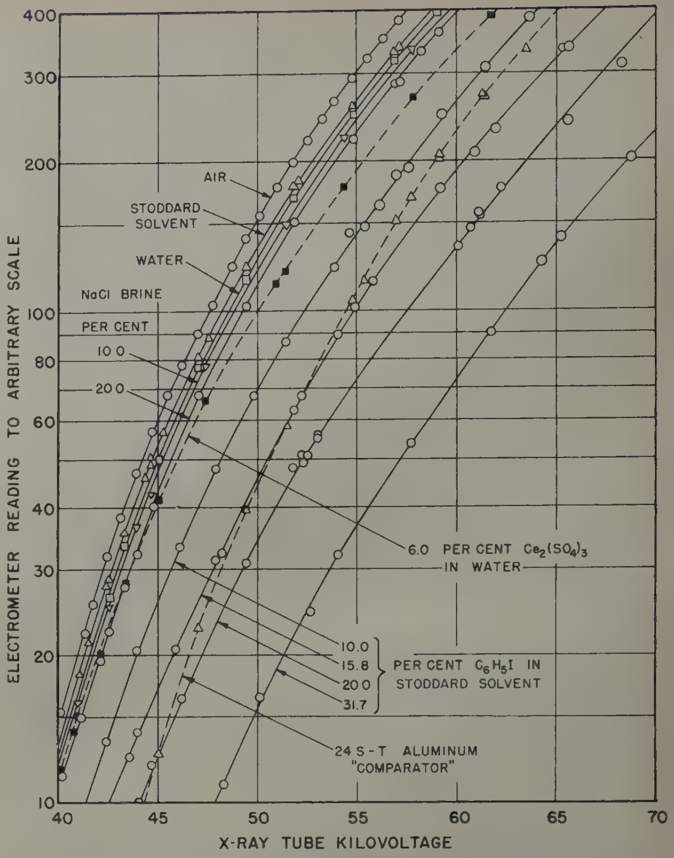

FIG. 6 — EXPERIMENTALLY DETERMINED ELECTROMETER READINGS AS A FUNCTION OF X-RAY TUBE POTENTIAL USING CELLS FILLED WITH FLUIDS INDICATED, PLACED IN FRONT OF AN AIR-FILLED ONE-INCH DIAMETER ALUNDUM CORE, HIGH VOLTAGE RANGE.

In calibrating a core and fluid system to be used in flow experiments, to be sure of getting a good calibration, one should make up cells in sets based on cell breadths corresponding to several percentages of porosity on both sides of the given percentage. In this investigation, it was sufficient to make up one set of cells corresponding to the known per cent porosity, and four other cells representing complete saturation by one fluid for two porosity percentages above and two below. After the core had been filled with liquid, the meter reading, corresponding to 100 per cent saturation of the filling fluid, was compared with the readings obtained with the cells of assorted sizes, to determine the effective porosity of the core.

Systems of Fluids and Filters

The fluids used in the saturation calibration tests were air, boiled tap water, aqueous solutions of sodium chloride and cerium sulphate, a mixture of light hydrocarbons known as Stoddard solvent, and mixtures of Stoddard solvent and iodobenezene.

Filters of barium dioxide, of various thicknesses, as indicated by the theory, were made up by tamping powdered barium dioxide into Paraplex cells. These filters, inserted between the x-ray tube and the core, were used to change the relative magnitude of the meter readings. Although the use of filters with monochromatic radiation may be advantageous, no improvement in the present system was obtained.

The above fluids were combined into systems that might coexist in a core as two or three components. The effect of

Table I — Meter Readings as a Function of Voltage and Core Porosity

Voltage	Per cent Porosity					
kv	21	23	25	Filled Core	27	29
59	172.5	167.5	164.5	163.0	163.0	161.5
60	185.0	182.5	179.0	178.8	179.0	177.0
61	198.0	195.5	192.0	191.0	190.0	188.0

Average porosity = 26.0 ± 0.5 per cent

these systems was determined by performing a calibration test on each, over the range of voltages from 30 to 90 kv, both with the barium dioxide filter and without it.

An interesting use of the comparator was in the magnification of the difference between meter readings for two different fluids. For example, water and Stoddard solvent gave comparatively small differences of meter readings during fluid saturation calibration, as indicated by Figs. 5 and 6. With ordinary use of the electrometer, this difference was too small to give satisfactory precision, because of the errors in reading the meter. This small difference was magnified by manipulating the electrometer. The meter was operated at low sensitivity at a voltage such that the comparator and the smaller of the two fluid readings coincided. This is always possible at a voltage high enough for readings to be made on a low sensitivity scale by using a thinner comparator and adding extra metal in the beam path externally as required. The x-ray tube was left operating and the electrometer zero adjuster was turned to zero the meter with the x-ray beam passing through the comparator. The meter was then switched to a higher sensitivity scale and the two fluid readings were taken. Proper choice of sensitivity gave nearly full scale differences in readings, with corresponding increase in the precision of the fluid saturation determinations. Upon completion of the reading, the meter was switched back to the low sensitivity scale and the zero adjustment was turned to give the original comparator reading. The return of the meter to its customary zero upon shutting off the x-ray tube circuit was considered as evidence that the settings had been made accurately.

RESULTS

The experimentally determined electrometer readings as a function of x-ray tube potential, using cells filled with the various fluids mentioned above and placed in front of an air-filled alundum core, are shown in Figs. 5 and 6. The curves drawn on these figures were faired in so as to best represent the experimental data. A table of the coordinates of these curves is available.[10] Similar data and curves are available in the tube potential range 70 kv to 90 kv but are not included here as still another logarithmic cycle would be required and the experimental points all fell on the monotonic curves representing the data. It is to be noted that the greatest scatter of the data occurs in the tube potenial range below 40 kv. In this region the experimental error is not better than five per cent. In the neighborhood of 40 kv the error is about two per cent and decreases to considerably less than one per cent at the higher voltages.

The dashed curves shown in Fig. 7 were obtained by taking direct ratios of the electrometer readings for any given fluid to the readings for air at corresponding tube potentials and utilizing the faired curves shown in Figs. 5 and 6. The solid curves of Fig. 7 represent the corresponding ratios calculated from theory. The reasonably close agreement between the two sets of curves demonstrates that the method of predicting meter readings is satisfactory.

Some data taken during tests of the validity of the cell method of establishing a core saturation calibration are shown in Table I. The meter readings were taken at three neighboring x-ray tube voltages with five cells representing 100 per cent liquid saturation of cores with porosities ranging from 21 to 29 per cent. The core was then filled and readings were taken at the same voltages. Analysis of the data shows that the reading at 60 kv for the 27 per cent porosity cell was in error. The average porosity indicated was 26 per cent, which is the value found for similar cores by other methods. Any discrepancies that might have appeared in this check could have been due to incomplete filling of the core, to faulty porosity data for the core or to the inaccuracy of the cell calibration data or method.

The approximate core porosity and its variation on different diameters are shown in Table II for two cores. In this method, variations of porosity resulted in approximately twice the percentage variation in meter readings.

DISCUSSION

The spectra shown in Fig. 1 were developed from average values of published spectra for tungsten target x-ray tubes. The wavelengths of the maximum intensities of the curves shown were determined by experiments designed to establish

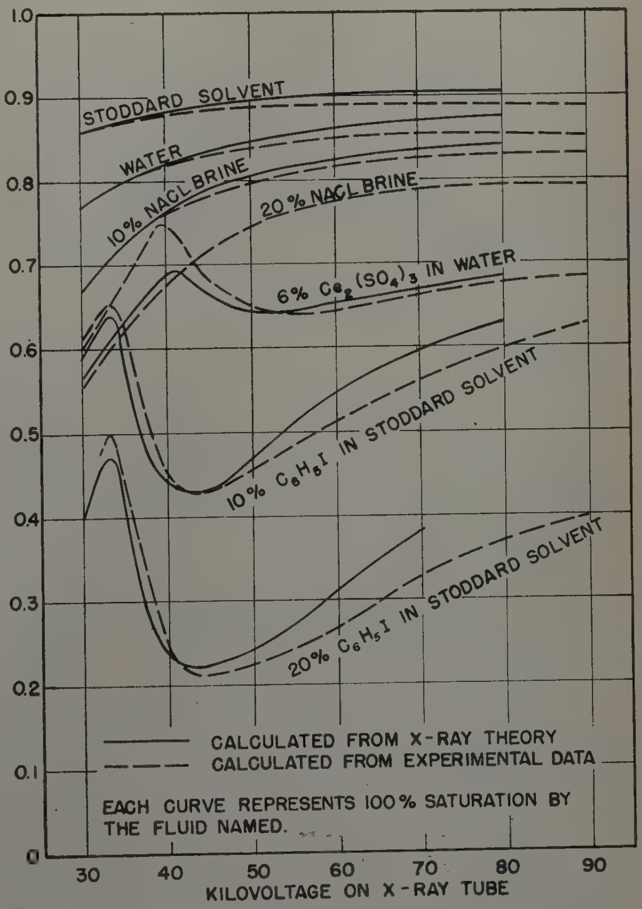

FIG. 7 — RATIOS OF STRENGTHS OF X-RAY BEAMS EMERGING FROM CORE CONTAINING DIFFERENT FLUIDS AT VARIOUS VOLTAGES, TO THOSE FROM CORE CONTAINING AIR. NO FILTER.

Table II — Uniformity of Core Porosity

Distance from end of core in in.	Per cent Porosity of Core				
	Core 1		Core 2		
	Diam. 1	Diam. 3	Diam. 1	Diam. 2	Diam. 3
1/8	26.6	26.0	----	----	---
3/8	25.7	25.4	26.0	26.0	26.4
5/8	26.0	27.4	26.0	26.0	26.4
7/8	25.7	26.0	26.2	26.0	26.4
1 1/8	25.7	26.0	26.4	26.7	26.7
1 3/8	25.4	26.0	26.6	26.8	26.6
1 5/8	26.0	26.0	26.6	26.7	26.5
1 7/8	26.0	26.3	26.6	26.5	26.3
2 1/8	26.0	26.0	26.7	26.7	26.4
2 3/8	26.0	26.0	26.5	26.8	26.9
2 5/8	26.0	26.0	26.7	27.4	27.4
2 7/8	26.0	26.0	27.2	27.5	27.6
3 1/8	26.0	26.0	27.2	27.5	27.6
3 3/8	26.1	26.0	27.1	27.4	27.3
3 5/8	25.9	26.0	27.2	27.5	27.0
3 7/8	25.9	26.0	27.1	27.4	27.3
4 1/8	25.9	26.0	27.4	27.4	27.4
4 3/8	25.7	26.0	27.3	27.4	27.4
4 5/8	26.0	26.0	27.8	28.0	28.0
4 7/8	26.0	26.0	27.8	27.7	27.6

Diameters 1 and 3 were 76° apart and Diameter 2 was 38° from both.

the relation between tube voltages and the effect of the absorption edges upon the meter readings. These spectra make useful analytical predictions of experimental results possible.

General x-radiation was used in this exploratory investigation because it was believed that with it results could be obtained more certainly and economically than with the very much weaker narrow wavelength band, or monochromatic x-radiation. A small amount of work done with selected wavelength bands gave results similar to those using general radiation. There may, however, be some cases where monochromatic radiation would be advantageous.

Equipment

Commercial equipment was used as the source of x-radiation because of its simplicity and relatively low cost. Similarly, ionization chambers and direct current amplifiers provided an economical means of indicating the strength of x-ray beams. Atmospheric pressure was used in the ionization chambers to avoid any change of efficiency characteristics due to gas leakage. Under this condition methyl bromide was used because of the resultant high ionization chamber efficiency. In the wavelength range between 0.3 and 0.6. A, the efficiency is approximately 80 times greater than with air. This compound also has the advantage of being a vapor at room conditions so that the density in the chamber was independent of changes in room temperature. If the chamber were kept at constant temperature, mixtures of some other compounds might be used which would give even better efficiencies.

For high absorption of x-rays from the primary beam the ionization chambers were made as long as practical. Similarly, to reduce the losses to the shell and plates from fluorescence of the gas, the chambers were made wide. The dimensions were limited by space, cost and the potential necessary between the collecting plates to ensure a high yield of current from the ions produced. To prevent the build up of static charges under x-ray bombardment, all parts of the chambers except the insulators were made of metal.

Choice of Fluids

The fluids used in the saturation calibration were selected for their chemical stability and mutual insolubility. The powerful absorbers used to accentuate the effect of one component had to be soluble in that component alone. Cerium sulphate and cerium chloride made it possible to use the absorber in water. Cerium was the only heavy element found which had compounds suitable for use in aqueous solution, that is, they would not decompose nor precipitate. Sodium chloride brine was satisfactory, and also represented common saline solutions occurring in many oil fields. Stoddard solvent was a satisfactory liquid hydrocarbon component, but many other oils might have been used as well or better. Iodobenzene was used in the oil and appeared to be satisfactory for tests of a month's duration.

Tests were made on the decomposition of cerium sulphate and iodobenzene under the influence of x-radiation. Tests were continued for four hours continuous irradiation without any change being noted. The sensitivity of the measurement was about one per cent.

A comparison of the absorption power of solutions of cerium sulphate in water and of iodobenzene in oil was made on old and new samples of these materials. After three months standing, the cerium sulphate solution had not changed. The iodobenzene solution, however, had decreased approximately six

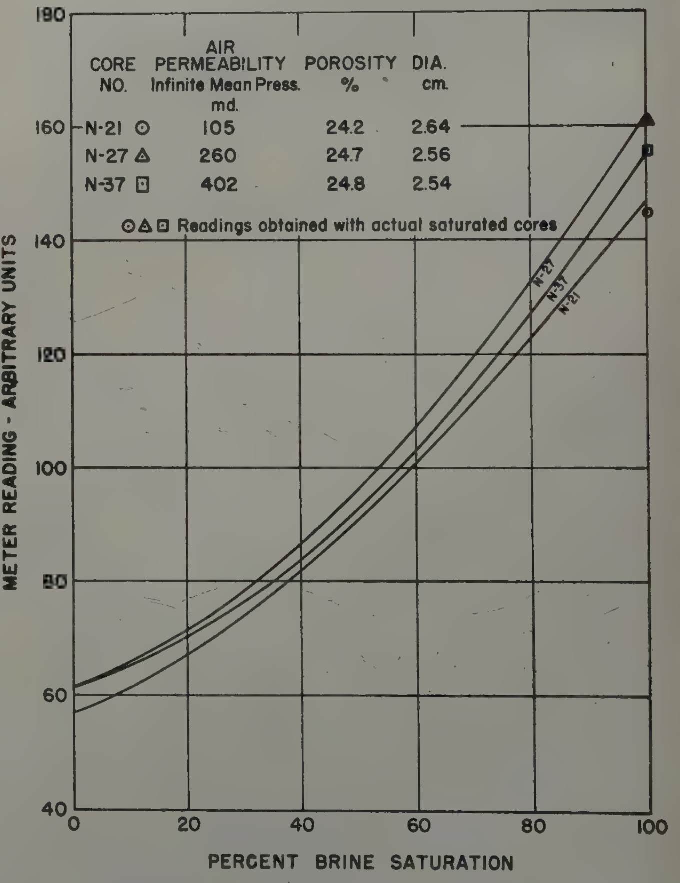

FIG. 8 — CALIBRATION CURVES ESTABLISHED BY CELL METHOD FOR THREE ALUNDUM CORES AND FLUID SYSTEM OF BRINE (0.5N NaCl IN DISTILLED WATER) AND OIL (20 WT. % C_6H_5I IN ISO-OCTANE).

per cent in absorbing power, although it had been shielded from light and tightly stoppered.

Small samples of Paraplex were tested for absorption of fluids and consequent effect on x-ray measurements. Samples were soaked in air, water, a six per cent cerium sulphate solution, and a 16 per cent mixture of iodobenzene with Stoddard solvent. Frequent tests made over a period of four weeks showed no detectable changes.

Two-Component Saturation Measurement

In Fig. 8 are shown calibration curves for three different alundum cores. These curves were established by use of the cell technique for 61 kv x-ray tube voltage. At the time of writing this report cores of known two-fluid saturation had not yet been compared with the calibration curves except at 100 per cent brine saturation as shown in Fig. 8. At least at this saturation the deviation of the plotted points is within the accuracy of the method.

Maximum accuracy of the present apparatus may be estimated as follows: by using an absorber in one component, the electrometer could be made to show a difference in direct reading of 150 units between 100 per cent saturation by one component and 100 per cent saturation by the other component. When the meter was used this way the reproducibility of a single reading was within two units, and for many readings the mean was probably within one-half unit of the calibrated value. This indicates an error of less than 0.5 per cent. If by means of the comparator the magnification of the meter reading differences were carried out carefully, an error of less than one per cent might be expected without any absorbers having been added to the fluids. Other errors due to changes of the fluid properties and of the equipment characteristics might increase the error by a small amount. The use of the comparator, however, assures that the total errors will be of the same size as the errors in setting the electrometer circuit constants, which are less than one per cent. Consequently, it is reasonable to suppose that the total error in fluid saturation measurement would be less than twice the estimated error. that is, less than two per cent.

Three-Component Saturation Measurement

According to the theory it should be possible to extend the x-ray technique to saturation determinations for three-fluid components. In order to determine the saturation of n components, n-1 readings, each at a different voltage, would be necessary. The nth component can then be found by difference. Further, the rate of change of readings with saturation would have to be different for the various voltages employed. This requirement is equivalent to the conditions of the linear independence of n simultaneous equations.

The following describes a calculated calibration for a three-component system utilizing air, a brine composed of 20 weight per cent sodium chloride and a light hydrocarbon oil known as Stoddard's Solution.

Since Equation (1) applies to a single wavelength it was put in the following form:

$$\frac{I}{I_g} = \frac{\int_{\lambda_{\min}}^{\infty} (I\eta'F')\, e^{-l\,[(S\rho\mu')_o + (S\rho\mu')_w + (S\rho\mu')_g]}\, d\lambda}{\int_{\lambda_{\min}}^{\infty} (I\eta'F')\, e^{-l\,(S\rho\mu')_g}\, d\lambda} \qquad (3)$$

where I is proportional to the meter reading with three fluids in the core.

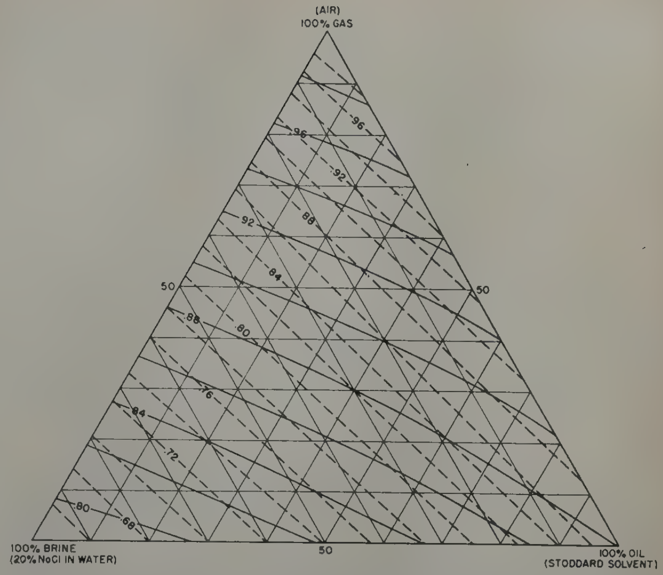

FIG. 9 — CALCULATED LINES OF CONSTANT METER READING REFERRED TO METER READING WITH AIR-FILLED CORE. SOLID LINES AT 70 KV AND DASHED LINES AT 34 KV.

I_g is proportional to the meter reading with only air in the core.

I', η', F' represent target radiation intensity, ionization chamber efficiency and transmission factor for the solids and air in the x-ray beam path. Evaluation of these factors is described by Laird.[10]

l = effective path length of x-rays through the fluid in the core and is approximately equal to the product of the core diameter and porosity.

S = saturation of fluid in the core.

ρ = fluid density.

μ' = mass absorption coefficient of the fluid.

Subscripts (o), (w) and (g) refer to oil, brine, and air respectively.

All terms with superscript (′) are dependent upon the wavelength.

In equation (3) the term $e^{-l\,(S\rho\mu')_g}$ equals unity because the product $\rho\mu'$ is negligible compared to the corresponding values for the liquids.

Equation (3) was then evaluated by means of a rather lengthy tabular calculation procedure and graphical integration of curves similar to curve 7 of Fig. 3 in order to cover the appropriate wavelength ranges corresponding to 70 kv and 34 kv. The results are plotted in Fig. 9, which shows the fluid saturations in conventional manner on a triangular coordinate scheme. The solid lines represent constant values of the ratio of meter reading with three fluids present to meter readings with only air in the core at 70 kv. The dashed lines represent the same ratio of readings for 34 kv.

In application, suppose that a core has these three fluids present but in unknown amounts and that at 70 kv and at 34 kv reading ratios of 0.88 and 0.82, respectively, are obtained. The point of intersection of these two curves on Fig. 7 shows that the core contains, at the point of measurement, 30 per cent brine, 40 per cent oil, and 30 per cent air.

Although the calibration procedure described here for three components has not yet been verified by direct comparison with a core of known three-phase saturation, the procedure is theoretically possible. However, assuming that the electrometer reading ratios can be obtained to an accuracy of 0.5 per cent the three-fluid saturations, according to Fig. 9, could have maximum theoretical errors as follows: oil, ±10 per cent; gas, ±5 per cent, and brine, ±4 per cent. These errors could be considerably reduced by utilizing fluid combinations that would give larger intercept angles on Fig. 9. In any event, the practical use of the three-component method leaves much to be desired and it certainly requires further development.

CONCLUSION

The present investigation indicates that the approximate theory of x-radiation may be used satisfactorily to predict the strength of x-ray beams emerging from cores of porous materials containing various combinations of fluids. The theory thus permits a survey to be made of a wide variety of materials with a view to selecting suitable combinations for application to a particular problem.

Making use of the fact that absorption of x-radiation is independent of the order in which various materials are traversed, a method has been developed for calibrating the x-ray emergent beam strengths in terms of fluid saturation of the core. This method employs equivalent absorbing media thereby avoiding the difficulties associated with changing the saturation of a core which would be employed in a direct calibration procedure.

A method for determining the saturations in a three-fluid system has been shown to be theoretically feasible, but requires additional development to place it on a practical basis.

ACKNOWLEDGMENTS

This investigation was carried out as a part of the activities of Research Project 47A of the American Petroleum Institute. The cooperation and financial support of that organization is gratefully acknowledged. Special thanks are due to R. W. Ravenscroft, A. E. Peck, F. E. Snodgrass and R. E. Buckland for assistance with the experiments. For assistance in the design of the ionization chambers, special thanks are due to B. J. Moyer of the Radiation Laboratory.

REFERENCES

1. Leverett, M. C.: *Trans.* AIME (1939) **132,** 149.
2. Wyckoff, R. D., and Botset, H. G.: *Physics* (1936), **7,** 325.
3. Brunner, E., and Mardock, E. S.: *Trans.* AIME (1946) **165,** 133.
4. Keller, E. G.: Tech. Report No. 2, API Project 47A (Oct., 1948).
5. Keller, E. G., Smith, O. J. M., and Putnam, J. A.: Tech. Report No. 3, API Project 47A (July, 1949).
6. Boyer, R. L., Morgan, F., and Muskat, M.: *Trans.* AIME (1947) **170,** 15.
7. Compton, A. H., and Allison, S. K.: *X-Rays in Theory and Experiment, 2nd Ed.,* D. Van Nostrand, New York (1935).
8. Hodgman, C. D.: *Handbook of Chemistry and Physics, 30th Ed.,* Chemical Rubber Pub. Co., Cleveland (1947).
9. Mellen, G. L.: *Electronics* (April, 1946) **19,** 1-6, 142.
10. Laird, A. D. K.: MS Thesis, University of California (1949).

DISCUSSION

By W. J. West, California Research Corp., La Habra, Calif.

The authors have essentially followed the method of Boyer, Morgan, and Muskat in measuring fluid saturations of cores. It might be worthwhile to point out the similarities and the distinguishing features of the two methods. The authors of the present paper have used a strong absorber in the oil component as was done earlier by Boyer, Morgan and Muskat. The experimental apparatus and method of calibration are essentially the same. The difference is that Laird and Putnam have analyzed the theory of absorption of the entire spectrum of an x-ray tube and have shown that there are optimum voltages across the x-ray tube that will give maximum accuracy. These optimum voltages are shown to be related to the critical absorption wavelength of the absorbing element.

The theory was extended to show the possibility of using three fluid components, but no experimental work was done to confirm the theory. The authors have shown that the accuracy to be expected for a three-component system is rather poor. This inaccuracy is largely a result of the small angle of intersection of the dashed and solid curves of Fig. 9. The requirement of the use of two liquids that give slopes of meter readings *vs* saturation of opposite sign, plus the requirement that the angle of intersection be large as possible, greatly limits the fluids that could be used in the proposed method of measuring saturation in a three-component system.

The experimental apparatus appears quite satisfactory. A good job seems to have been done in stabilizing the output of the x-ray tube. The troubles involved with ion chambers due to their bulkiness, their high background readings, and zero drift are conveniently and simply eliminated by the use of Geiger counters.

The question arises as to what is to be done for core materials that are non-uniform in porosity or chemical composition, or both. Apparently a fluid calibration using the liquid cells must be made for each point along the sample and means provided whereby the core sample is returned to those exact positions during the test run.

The x-ray absorption edges of the elements can be used in a somewhat different manner for determining the amount of a given element that is present in the core. They have been so used by Arne Engstrom[1] to analyze biological materials. His method is essentially independent of core materials and other liquids present.

The method is described briefly as follows: Referring to Fig. 1-A, let the wavelength λ_c be the critical absorption wavelength of one of the elements in the test sample. Let the wavelength of a monochromatic beam of x-rays be changed from λ_1 to λ_2, λ_1 and λ_2 being on opposite sides of the critical absorption wavelength at which the transmitted intensity changes

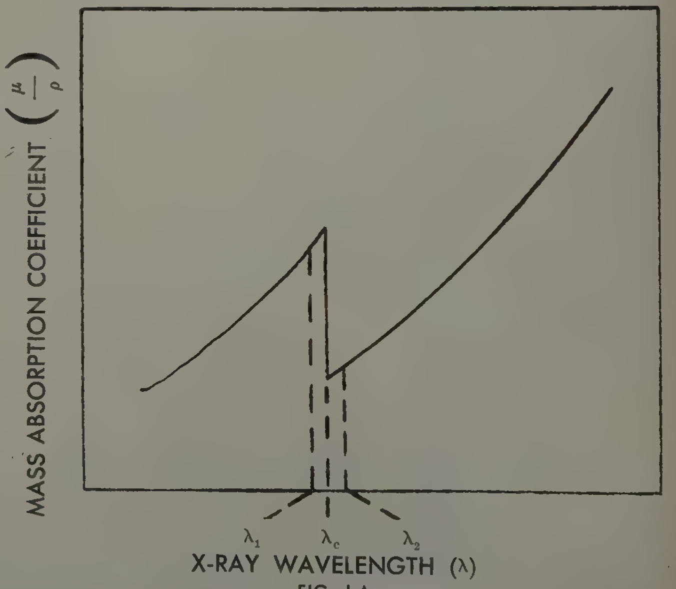

FIG. 1-A

abruptly. When λ_1 and λ_2 are close to λ_c, the ratio of the intensities at λ_1 to those at λ_2 is

$$\frac{I'_1/I_1}{I'_2/I_2} = e^{-\left[\frac{\mu_1}{\rho}-\frac{\mu_2}{\rho}\right]\rho x} \quad . \quad . \quad . \quad . \quad . \quad (1)$$

provided no other elements in the path of the x-ray beam have absorption edges in the wavelength range λ_1 to λ_2. I'_1 and I'_2 are the transmitted, and I_1 and I_2 are the incident intensities of the x-ray beam at wavelengths λ_1 and λ_2. The change in the mass absorption coefficient $\left[\frac{\mu_1}{\rho}-\frac{\mu_2}{\rho}\right]$ at the absorption edge is known for nearly all the elements. The mass in grams of core material per square centimeter of the x-ray beam is just ρx and can be calculated from Equation (1).

This method is somewhat more elaborate than the usual absorption type method because it utilizes monochromatic radiation. A curved crystal type monochrometer could be used or a system of Ross balanced filters. The Ross filters would be simpler and more economical, but would restrict the number of elements that could be used for indicators.

The Engstrom method would be unaffected by non-uniformity in porosity and independent of the chemical composition of the core, provided that the elements used for indicators were not present in the core material.

REFERENCE

1. Engström, Arne: *Quantitative Micro- and Histochemical Elementary Analysis by Roentgen Absorption Spectrography, Acta Radiologica Supplementum LXIII*, P. A. Mosstedt and Soner, Stockholm (1946).

DISCUSSION

By Alexander Grenall, Union Oil Co. of California, Wilmington, Calif.

At the time that Boyer, Morgan and Muskat[1] presented their paper describing application of the x-ray absorption technique to studies of core saturation, there was considerable discussion of the method. Among those offering criticisms was Frevel, a well-known investigator in the field of x-ray techniques, who pointed out that the accuracy and sensitivity of the method suffered materially from the use of white x-rays, and that the selection of an ionization chamber as x-ray detector in preference to a sensitive Geiger-Muller counter was not explained in the text.

The present work is subject to the same analysis. There are a number of points which I am interested in commenting on but perhaps the discussion regarding use of white x-rays could bear amplification from the point of view of x-ray theory.

It is known that the quality of a white x-ray beam changes with the type and thickness of material penetrated. Fig. 1-B illustrates the effect of thickness.[2] The first layers of the absorbing material remove a large fraction of the "soft" radiation and only the "hard" portions reach the final layers. Thus the mass absorption coefficient, μ/ρ, is effectively greater in value for rays entering an absorber than for those that leave.

The fundamental absorption equation,

$$I = I_o e^{-\mu/\rho\,\rho\, l} \quad . \quad . \quad . \quad . \quad . \quad . \quad . \quad . \quad . \quad . \quad (1)$$

is derived on the assumption that μ/ρ is constant over all values of the path length, l. This has been shown experimentally to hold only for monochromatic radiation. Thus Equation (1) cannot be applied directly to the case of white x-rays.

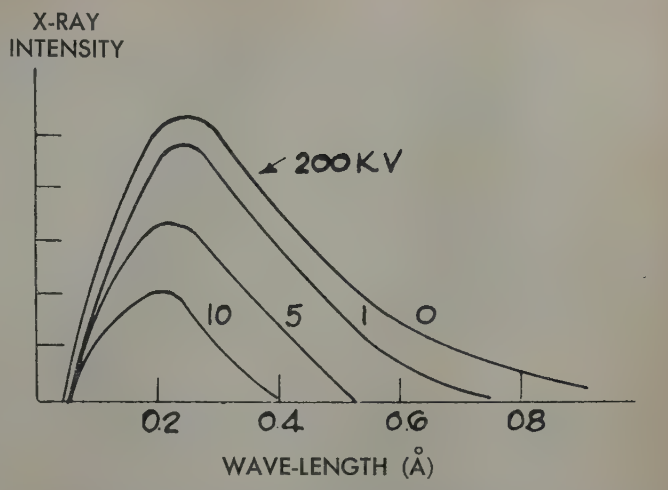

FIG. 1-B — CURVES SHOWING THE EFFECT PRODUCED ON X-RAY INTENSITY AND WAVE-LENGTH WHEN A HETEROGENEOUS X-RAY BEAM IS PASSED THROUGH 1, 5 AND 10 MM OF ALUMINUM.

If we force the use of Equation (1) it becomes necessary to account for the variation of μ/ρ with wavelength. This may be attempted as follows. It has been shown empirically[3] that, for certain wavelength ranges the relationship is,

$$\mu/\rho = \frac{1.60 \times 10^{-2} \ \Sigma^{3.94} \ \lambda^3}{A} + \frac{\sigma}{\rho} \quad . \quad . \quad . \quad (2)$$

where Σ = atomic number, λ = wavelength, A = atomic weight and σ/ρ = scattering coefficient, given as 0.2 for $\Sigma > 6$ and 0.15 for $\Sigma < 6$. The use of Equation (2) is open to the objection, however, that it does not hold adequately when it becomes necessary to express absorptions over a wide range of wavelengths and materials, as in the present case. A more complex relationship must be developed.

Further complications are added when various kilovoltages are employed in generating white x-rays. Different wavelength ranges are produced with different intensity distributions in each case. It then becomes necessary to evaluate each kilovoltage setting in terms of the expressions discussed previously.

Still another uncertainty in measurement is introduced when fluctuation of voltage applied to the x-ray tube occurs. Change in voltage alters intensity distribution and wavelength range; in turn affecting penetrative ability and integrated intensity of the x-ray beam. These fluctuations are not necessarily compensated for by a monitor beam-absorber combination, because while the monitor apparently compensates for intensity changes, there is no compensation for the change produced in effective wavelengths, unless the monitor absorber has identical paths of the same materials contained in the working core.

These remarks are not to be taken as implying that empirically the method may not be made to work by careful standardization of procedure and calibration. But, from the theoretical viewpoint, it would seem that there are a number of pitfalls introduced by employing white x-radiation. On the other hand, the use of monochromatic radiation will unquestionably eliminate or minimize the complications and uncertainties, and lead to improvement in accuracy of measurement. For example, the use of Equation (1) becomes theoretically sound. For another, simplification is achieved because the values of μ/ρ are readily obtainable from standard tables. Finally, a monitor beam becomes an effective compensator for intensity variation with fluctuation in applied voltage.

There are still other advantages to be gained by eliminating the highly penetrative tungsten rays and substituting instead relatively "soft" monochromatic x-rays. Because the absorption coefficients are so much greater in relative value for long wavelengths, increased sensitivity in detecting small saturation changes should be obtained. It would no longer be necessary to load fluids with highly absorptive materials, foreign to oil well formations, in order to produce detectable intensity changes. The differences in mass absorption coefficients and fluid densities will lead to appreciable differences in transmitted intensities. It will then be possible to make saturation measurements with materials analogous to those found in natural formations. To illustrate this point, approximate values of copper radiation absorption per unit path length of air, oil and water at 20°C have been calculated and are given in the following table.

	$-\ln I/I_o$	Ratio to Air
Air	0.0144	1
Oil[a]	5	350
Water	13	900[b]

[a] Density of 0.8.

[b] The addition of, say, 2 per cent *NaCl* to the water would increase this ratio still more.

It is true that the use of monochromatic radiation "softer" than tungsten will entail a loss in penetrative power and overall x-ray transmission, but this can readily be offset by employing the extremely sensitive Geiger-Muller counter as the detection device. An added advantage given by the Geiger counter is the ability to achieve a predetermined precision measure by prolonging counting time until sufficient x-ray quanta have been tallied.

The ingenious cell calibration method devised by the authors should prove to be a time-saver and of great usefulness to those who choose to employ x-ray absorption techniques in studying fluid saturations.

The proposed procedure for determining three component saturation values appears to be a valuable contribution and promises that this difficult problem will yield to experimental attack. The hope is expressed that experiments to evaluate its practicability will not be delayed.

R. H. Zinszer should like to join me in congratulating the authors for the interesting contribution made by their work. He suggested that, in following up these studies, data collected on a 2 per cent brine solution would be of far greater usefulness than for the 20 per cent solution used in the present work.

REFERENCES

1. Boyer, R. L., Morgan, F., and Muskat, M.: *Trans.* AIME (1947) **170,** 15.
2. Clark, G. L.: *Applied X-Rays,* McGraw-Hill Book Co. (1940) 145.
3. *International Tables for the Determination of Crystal Structure* (1944) **II,** Borntraeger.

AUTHORS' REPLY TO MESSRS. WEST AND GRENALL

In view of the discussions it seems pertinent to reiterate some statements made in the paper and to clarify others.

The purpose of this paper was to outline the method of predicting results and to show experimental confirmation of this method. The theory of x-radiation will allow the calculation of the range and sensitivity of the instruments required to measure an arbitrary effect to a desired degree of accuracy. No matter what combination of fluids, solids and dimensions; x-ray tube voltage, target, current and wavelength band; recording device such as ionization chambers, Geiger counters, electroscopes, fluorescent screens, photographic plates or whatever, any idea based on x-ray absorption may quickly be put to test without recourse to costly experiments.

To allay possible misunderstanding arising from misreading this paper it seems appropriate to reply to the discussions in detail.

Grenall's discussion offers excellent opportunity for clarification of the method of calculation and of some of the theory. The use of white x-ray was dictated by the flexibility required in an exploratory investigation. Consequently an ionization chamber was used because the white beams were too strong to be measured by a Geiger counter and a range of over eight orders of magnitude was used in testing the applicability of the theory. The remarks on Equation (1) are unnecessary since it is stated clearly in the paper that this equation is to be used at one wavelength at a time and that the total effect is to be found by integration. The mass absorption coefficient is constant for each wavelength. However, this points up the confusion that can result from not realizing that the method outlined in Fig. 3 is theoretically correct for all thicknesses of material and for each wavelength emitted by the tube, and there certainly are no pitfalls introduced by white radiation when the method of Fig. 3 is used. For confirmation and details reference should be made to p 512 of Compton and Allison.[7]

The ranges of wavelength and the intensities are given in Fig. 1 for use in computation.

It is true that the voltage and current regulation of the equipment used was not precise. For this reason, as stated in the paper, the monitor tube was used to detect momentary departures of the x-ray output from its average value. Later stabilization of the x-ray output was effective in reducing the aberrations. The polysterene ion chamber insulators were replaced with quartz. Care should be taken in selecting the wavelength of monochromatic x-rays in such a system as outlined in Grenall's table. The values in the table indicate that if 1,000 counts per minute were recorded for an air-filled core, then if the core were oil-filled 6.8 counts per minute would be recorded while, if water-filled, only 0.0023 counts per minute would result. Or, if an oil-filled core gave 1,000 counts per minute a water-filled core would give 0.34 per minute. Consequently, to obtain the advantage of the increase of accuracy with time when using the Geiger counter, one could be obliged to maintain rigid control of his fluid variables for a very long period of time. There are, however, harder monochromatic emanations that would give more reasonable times, but the effects would be similar to those mentioned in the body of this paper.

As pointed out by West, no experimental results were included to support Fig. 9. However, data were taken which qualitatively confirmed the theory, but the accuracy was poor due to erratic operation of a circuit and consequently they were not mentioned. The background and zero drift of the ionization chambers were shown to be at least two orders of magnitude smaller than the intensities which were used for the data presented. On the other hand it is usual to have a background count in a Geiger counter at counting rates slow enough to be accurate.

Engstrom's absorption jump method is an interesting application of the Fig. 3 method of predicting results but should be modified in some details. Although the differences in absorption are known the accuracy is poor (p. 527 of Compton and Allison).[7] Moreover, the path length is a linear function of the porosity so non-uniform porosity would have to be handled as described in the body of this paper. Inherent inaccuracies due to the finite size of the wavelength increment $(\lambda_2 - \lambda_1)$, which is not constant (p. 664)[7] should yield to calibration. It is, however, difficult to pick filters and x-ray beams with narrow wavelength bands that coincide with absorption edges. Nevertheless the jump method may have some valuable applications.

★ ★ ★

T.P. 3201

PHASE EQUILIBRIA IN HYDROCARBON-WATER SYSTEMS

IV- Vapor-Liquid Equilibrium Constants in the Methane-Water and Ethane-Water Systems

O. L. CULBERSON, GULF RESEARCH AND DEVELOPMENT CO., HARMARVILLE, PA., AND **J. J. McKETTA, JR.**,
MEMBER AIME, DEPARTMENT OF CHEMICAL ENGINEERING, THE UNIVERSITY OF TEXAS, AUSTIN, TEX.

INTRODUCTION

The equilibrium constants for methane and for water, and for ethane and water have been calculated from experimental data for the two binary systems.[2,3,11,12] These constants are for the two-phase systems for the temperature range of 100° to 340°F and the pressure range of 200 to 10,000 psia.

The constants for ethane are greater than those for methane. Equilibrium constants for a natural gas from a natural gas-water system[6] are about the same as those for methane. Equilibrium constants for water in all three systems are very nearly the same over the greater part of the range of temperatures and pressures studied.

In ideal solutions, the vapor-liquid equilibrium constants for a component should be the same in all such solutions at a given temperature and pressure.[5] Few solutions are ideal, and consequently the use of generalized constants often leads to error in situations where they do not actually apply. In decidedly non-ideal systems, it is desirable to have equilibrium constant data for the specific system.

Vaporization equilibrium constants may be calculated either by thermodynamic methods or from experimental vapor-liquid equilibrium data. In the thermodynamic calculation, the equilibrium constant K may be shown to be[10]

$$K = f_{pi}/f_p \quad \ldots\ldots\ldots\ldots \quad (1)$$

where f_{pi} is the fugacity of the pure component i at the given temperature and at the vapor pressure of the pure component, and f_p is the fugacity of pure i in the gaseous state at the temperature and total pressure of the system. At best the thermodynamic calculation results in a K applicable to ideal solutions. Equilibrium constants calculated from Equation (1) have been found to have only limited agreement with experimental values, even though the solutions for which they were calculated approached ideality.[8,9] If the more volatile component is at a temperature above its critical, the accuracy of the equilibrium constant for the component is made more doubtful by the use of the vapor pressure term under such conditions. In order to make the thermodynamic calculation on a component above its critical temperature, one must resort to one of the empirical methods of extrapolation of the vapor pressure to conditions above its critical point.[13] Application of the thermodynamic equilibrium constant then to the methane-water or the ethane-water systems would be risky since the systems are non-ideal, and the methane and ethane are above their critical in most petroleum operations.

ETHANE-WATER SYSTEM

In the temperature range of from 100° to 340°F and for pressures up to 10,000 psia, the vapor-liquid equilibrium data

Table I — Vaporization Equilibrium Constants for Ethane in the Ethane-Water System

Pressure psia	100°F	160°F	220°F	280°F	340°F
200	3,034	5,639	6,335	4,962	3,678
400	1,868	2,837	3,194	2,557	1,882
600	1,496	2,074	2,159	1,729	1,280
800	1,333	1,746	1,747	1,339	1,001
1,000	1,260	1,583	1,515	1,146	838
1,250	1,215	1,457	1,326	993	723
1,500	1,177	1,366	1,198	898	652
2,000	1,125	1,265	1,035	789	554
2,500	1,092	1,200	971	726	489
3,000	1,071	1,142	924	679	445
3,500	1,042	1,093	885	645	416
4,000	1,018	1,049	854	620	396
4,500	990	1,012	833	599	384
5,000	968	984	813	579	374
6,000	925	941	772	550	354
7,000	899	909	736	528	337
8,000	888	874	704	511	322
9,000	885	841	679	494	308
10,000	882	813	663	479	295

Table II — Vaporization Equilibrium Constants for Water in the Ethane-Water System

	K x 10^3				
Pressure psia	100°F	160°F	220°F	280°F	340°F
200	5.009	24.49	87.83	250.7	595.5
400	2.642	12.69	45.08	127.9	303.7
600	1.860	8.783	30.80	86.98	206.6
800	1.475	6.837	23.73	66.66	158.2
1,000	1.245	5.679	19.52	54.51	129.2
1,250	1.066	4.755	16.17	44.91	106.3
1,500	0.950	4.150	13.97	38.45	90.60
2,000	0.813	3.412	11.22	30.55	71.81
2,500	0.735	2,981	9.620	25.81	60.54
3,000	0.689	2.711	8.562	22.75	53.33
3,500	0.659	2.523	7.836	20.56	48.16
4,000	0.641	2.392	7.308	19.08	44.36
4,500	0.627	2,294	6.913	17.94	41.48
5,000	0.621	2.220	6.611	17.04	39.16
6,000	0.618	2.120	6.181	15.73	35.70
7,000	0.620	2.070	5.898	14.78	33.28
8,000	0.624	2.032	5.658	13.99	31.26
9,000	0.627	1.995	5.439	13.35	29.53
10,000	0.630	1.954	5.215	12.77	28.04

---

[2] References given at end of paper.

Manuscript received in the office of the Petroleum Branch March 16, 1951.

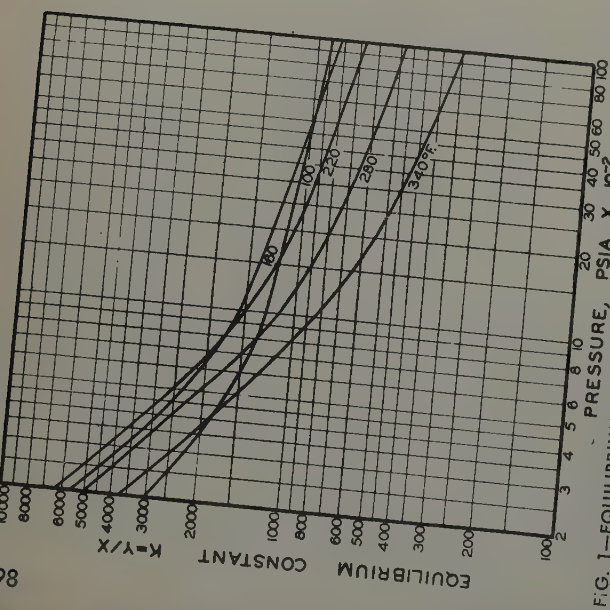

FIG. 1—EQUILIBRIUM CONSTANTS FOR ETHANE IN ETHANE-WATER SYSTEM (K-P).

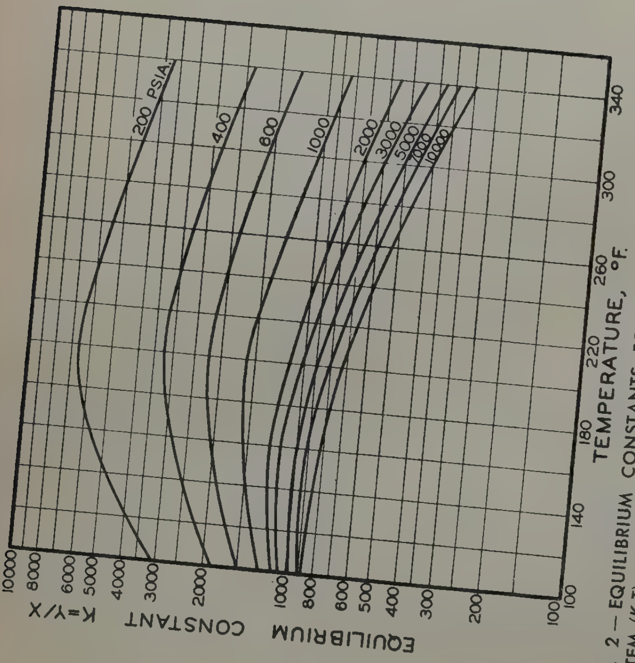

FIG. 2 — EQUILIBRIUM CONSTANTS FOR ETHANE IN ETHANE-WATER SYSTEM (K-T).

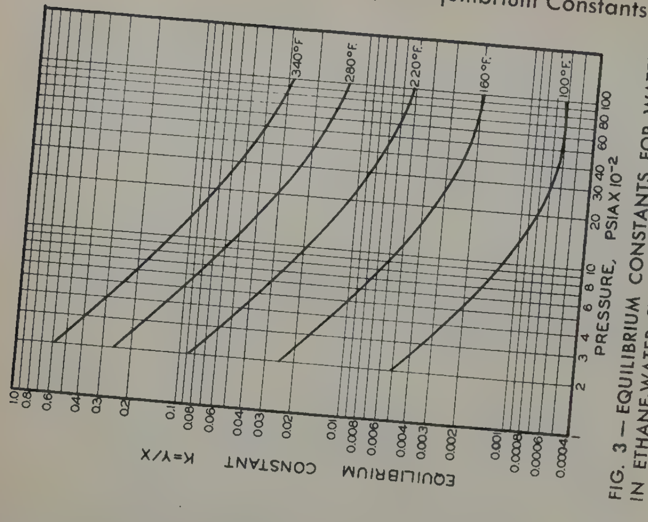

FIG. 3 — EQUILIBRIUM CONSTANTS FOR WATER IN ETHANE-WATER SYSTEM (K-P).

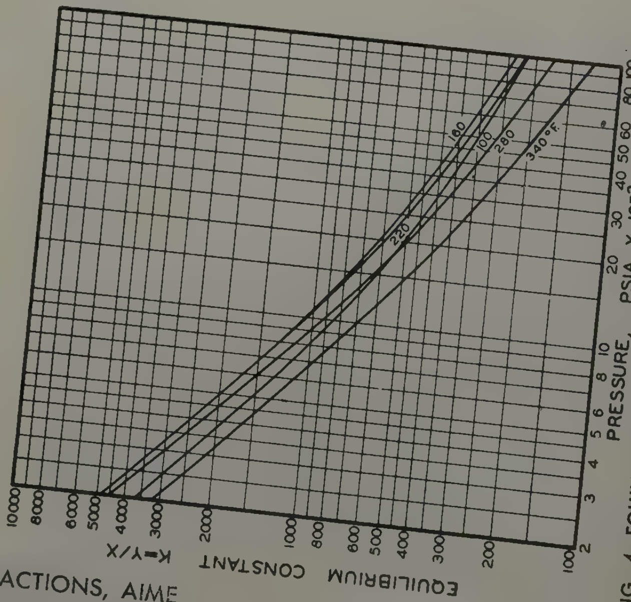

FIG. 4—EQUILIBRIUM CONSTANTS FOR METHANE IN METHANE-WATER SYSTEM (K-P).

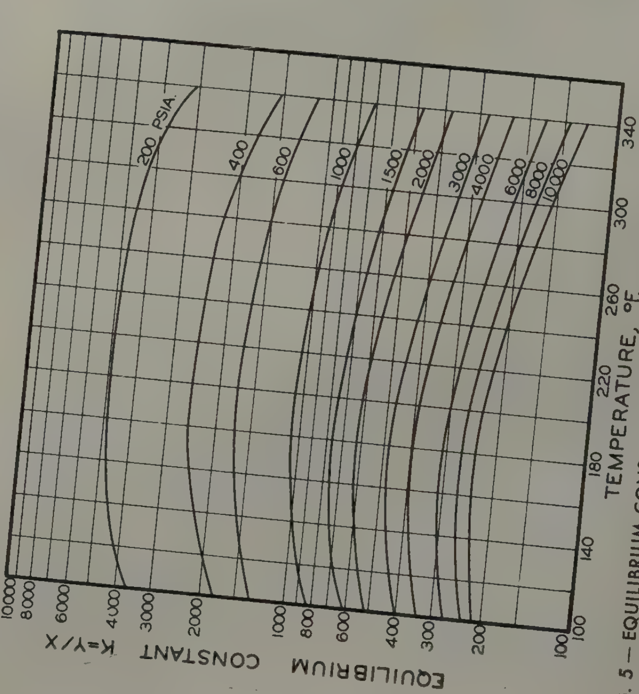

FIG. 5 — EQUILIBRIUM CONSTANTS FOR METHANE IN METHANE-WATER SYSTEM (K-T).

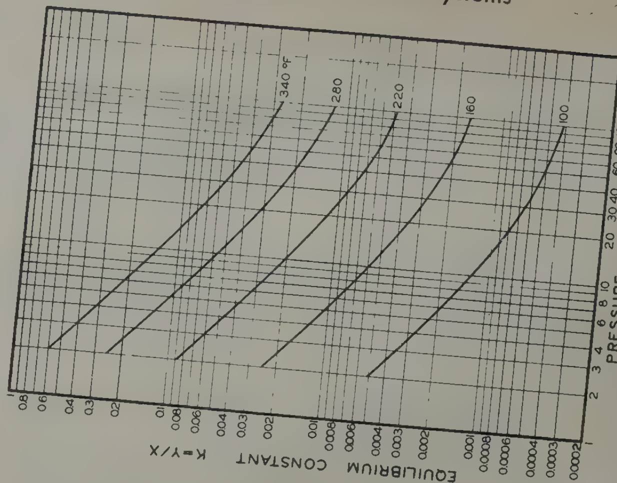

FIG. 6 — EQUILIBRIUM CONSTANTS FOR
IN METHANE

Table III — Experimental Determinations of Vapor Phase Composition in the Ethane-Water System at 100°F

Pressure psia	Mole Fraction H_2O x 10^3 Experimental	Literature Smoothed[12]	Experimental % Deviation
608	2.090	1.830	+ 14.2
629	1.836	1.790	+ 2.57
655	1.638	1.733	– 5.48
718	1.726	1.605	+ 7.54
728	1.195	1.570	– 23.9
1,745	0.919	0.910	+ 1.00
		Average Deviation	9.11%

Table IV — Vaporization Equilibrium Constants for Methane in Methane-Water System

Pressure psia	100°F	160°F	220°F	280°F	340°F
200	3,644	4,804	4,847	4,537	3,080
400	1,889	2,425	2,491	2,244	1,620
600	1,313	1,654	1,693	1,501	1,130
800	1,013	1,273	1,297	1,149	873
1,000	833	1,052	1,054	929	705
1,250	701	878	856	750	568
1,500	617	761	736	631	478
2,000	512	620	595	489	377
2,500	445	536	505	413	318
3,000	399	476	444	365	280
3,500	365	432	400	328	252
4,000	337	397	368	299	230
5,000	297	346	321	258	198
6,000	270	310	288	231	176
7,000	251	284	265	210	159
8,000	236	264	247	195	145
9,000	224	249	232	181	134
10,000	214	237	219	171	126

Table V — Vaporization Equilibrium Constants for Water in Methane-Water System

Pressure psia	K x 10^3 100°F	160°F	220°F	280°F	340°F
200	5.089	24.85	88.79	251.47	596.61
400	2.709	13.02	45.95	129.33	306.96
600	1.914	9.010	31.64	88.70	210.39
800	1.515	7.082	24.49	68.33	161.68
1,000	1.277	5.894	20.20	56.25	132.57
1,250	7.086	4.948	16.78	46.43	109.40
1,500	0.956	4.308	14.47	39.82	93.72
2,000	0.796	3.510	11.60	31.58	74.05
2,500	0.700	3.038	9.891	26.65	62.25
3,000	0.637	2.719	8.739	23.38	54.47
3,500	0.592	2.494	7.926	21.04	48.87
4,000	0.558	2.324	7.303	19.29	44.77
5,000	0.512	2.088	6.444	16.90	38.87
6,000	0.481	1.933	5.880	15.32	34.89
7,000	0.457	1.823	5.491	14.17	31.96
8,000	0.439	1.748	5.211	13.29	29.76
9,000	0.424	1.689	5.003	12.61	28.00
10,000	0.414	1.648	4.834	12.07	26.61

have been determined by Reamer, Olds, Sage, and Lacey[12] for the vapor phase, and by Culberson, Horn, and McKetta[4] and Culberson and McKetta[2] for the liquid phase. Throughout this region of pressures and temperatures, only two phases were present at any time. The critical temperature of ethane is 90°F; therefore, an ethane-rich liquid phase was not present. Likewise, the conditions of temperature and pressure in the hydrate region[7] are not considered here.

With the vapor-liquid equilibrium data available, it was possible to calculate the equilibrium constants since by definition

$$K = y_i/x_i \quad . \quad . \quad . \quad . \quad . \quad . \quad . \quad . \quad . \quad . \quad . \quad (2)$$

In Equation (2), y_i is the mole fraction of component i in the vapor phase, and x_i is the mole fraction of the same component in the liquid phase.

Vaporization constants calculated by Equation (2) have been tabulated for ethane in Table I and plotted in Figs. 1 and 2. In Table II are tabulated the vaporization equilibrium constants for water in the ethane-water system. These constants for water are plotted in Fig. 3. In Fig. 3, it may be noted that at 100°F the equilibrium constant passes through a minimum and would probably continue to increase as the pressure increased to the convergence pressure.

METHANE-WATER SYSTEM

In the temperature range of 100° to 340°F and for pressures up to 10,000 psia, the vapor phase data were determined by Olds, Sage, and Lacey[11] and the liquid phase data by Culberson and McKetta.[3] As was the case in the ethane-water system, only the hydrocarbon-rich vapor phase and the water-rich liquid phase were present. The hydrate region is not covered, and the methane was above its critical temperature.

Equilibrium constants were calculated by Equation (2) and these values are tabulated in Table IV for methane and in Table V for water. Figs. 4 and 5 are plots of the equilibrium constants for methane. Equilibrium constants for water are shown in Figs. 6 and 7.

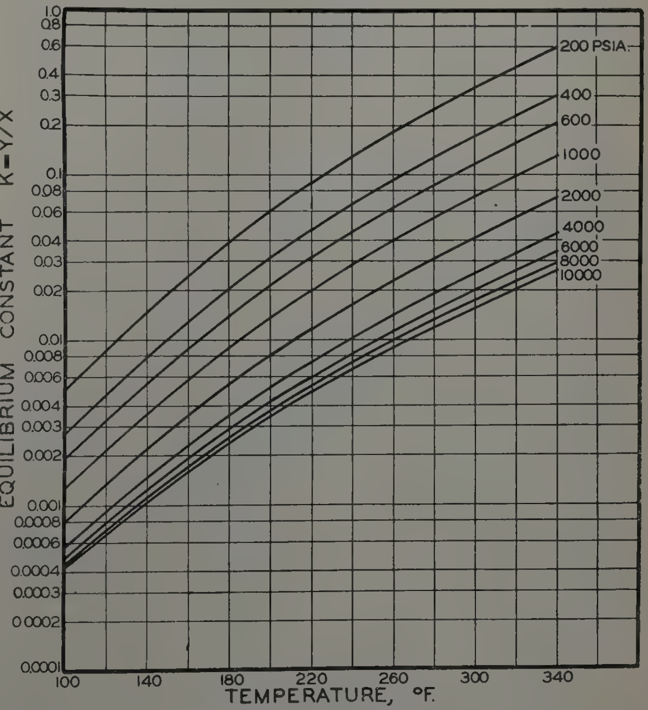

FIG. 7 — EQUILIBRIUM CONSTANTS FOR WATER IN METHANE-WATER SYSTEM (*K-T*).

DETERMINATIONS OF VAPOR-PHASE COMPOSITIONS

The apparatus which was used to obtain the liquid phase data had never been used to determine the composition of a vapor phase. For that reason it was decided to make vapor phase determinations in the ethane-water and methane-water systems to study the applicability of the apparatus to such work. Only qualitative results were sought, and an elaborate analytical train was not set up. The train used consisted of drying tubes containing magnesium perchlorate, a saturator where the dehydrated hydrocarbon was resaturated with water, and a receiving flask where the resaturated hydrocarbon was collected over water which had in turn been previously saturated with the hydrocarbon. The amount of water in the sample was taken to be the gain in weight of the drying tubes. The amount of hydrocarbon was calculated from PVT conditions in the receiving flask where the hydrocarbon pressure was taken to be the total pressure less the vapor pressure of water at the temperature within the flask.

The results of such determinations are given in Table III for the ethane-water system and in Table VI for the methane-water system. In the ethane-water system, the average deviation of the experimental values from the smoothed curve is probably slightly greater than the average deviation of the data of Reamer, Olds, Sage, and Lacey.[12] The average deviation for the methane-water system shown in Table VI compares with that of Olds, Sage, and Lacey.[11]

DISCUSSION

The equilibrium constants for methane and for ethane are compared with those for a natural gas in a natural gas-water system[6] in Fig. 8. It is shown that the constant for the ethane is greater than those of the methane and natural gas. The natural gas was 88.51 per cent methane; therefore, it is not surprising that its equilibrium constants were approximately the same as those of pure methane. The water solvent evidences two major effects which are not indicated in the equilibrium constants normally accepted in hydrocarbon-solvent systems.[1] The equilibrium constants for the hydrocarbons in the hydrocarbon-water systems are much greater than for the hydrocarbons in water-free hydrocarbon systems. Also, in the water-solvent systems, the equilibrium constants for the hydrocarbons pass through a maximum not common to the hydrocarbon-solvent systems.

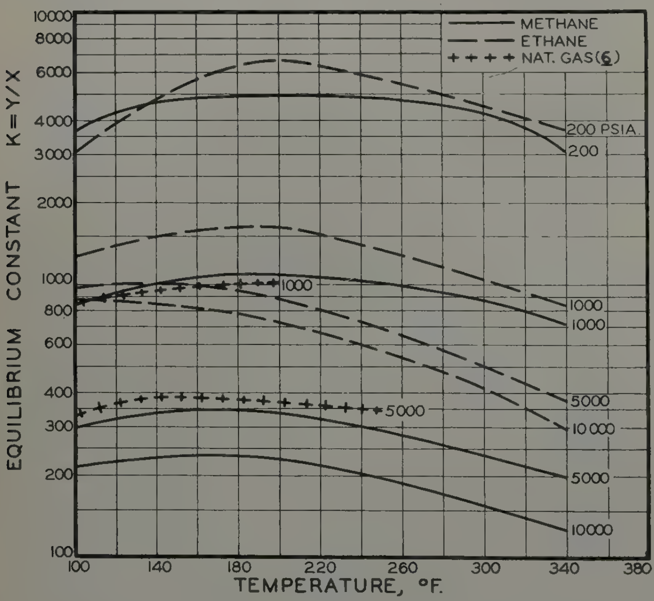

FIG. 8 — COMPARISON OF EQUILIBRIUM CONSTANTS FOR LIGHT HYDROCARBONS IN WATER.

Table VI — Experimental Determinations of Vapor Phase Composition in the Methane-Water System at 100°F

Pressure psia	Mole Fraction H_2O x 10^3 Experimental	Mole Fraction H_2O x 10^3 Literature Smoothed[11]	Experimental % Deviation
758	1.770	1.580	+ 12.0
1,600	0.762	0.900	− 15.3
2,375	0.745	0.730	+ 2.06
3,615	0.483	0.580	− 16.7
5,185	0.502	0.515	− 2.52
		Average Deviation	9.72%

No graphical comparison was made of the equilibrium constants for water in the systems. In the methane-water and ethane-water systems, the constants for water are almost identical under all the conditions studied except for conditions of high pressure and low temperature. The greatest difference occurred at 100°F and 10,000 psi where the constants differed by about 50 per cent (based upon the methane).

In systems such as these where the composition of the liquid phase is of the order of 99+ mole per cent water, the equilibrium constants for the hydrocarbon will be controlled by the liquid phase. When the very small mole per cent of hydrocarbon is used in the denominator of Equation (2), it affects the value of K for the hydrocarbon tremendously. In the same manner, the composition of the vapor phase controls the value of the equilibrium constant for water since the denominator of Equation (2) is always approximately unity.

REFERENCES

1. Brown: *N.G.A.A. Tech. Manual*, 5th Ed. (April, 1946) 64.
2. Culberson, O. L., and McKetta, J. J.: *Trans.* AIME (1950) **189,** 319.
3. Culberson, O. L., and McKetta, J. J.: *Trans.* AIME (1951) **192,** 223. (*Jour. Petr. Tech.*, Aug., 1951.)
4. Culberson, O. L., Horn, A. B., and McKetta, J. J.: *Trans.* AIME (1950) **189,** 1.
5. Dodge: *Chemical Engineering Thermodynamics*, McGraw-Hill Book Co., New York (1944) 579.
6. Dodson and Standing: *API Drill. and Prod. Prac.* (1944) 173.
7. Katz: "Phase Relationships in Oil and Gas Reservoirs," *Tex. A.&M. Eng. Exp. Sta. Bull.* (1948) **114,** 30.
8. Kay: "Liquid-Vapor Phase Equilibrium Relations in the Ethane – *n*-Heptane Systems," *Ind. Eng. Chem.* (1938) **30,** 459.
9. Kay: "Liquid-Vapor Equilibrium Relations in Binary Systems: The Ethane – *n*-Butane System," *Ind. Eng. Chem.* (1940) **32,** 353.
10. Lewis and Luke: "Vapor-Liquid Equilibria of Hydrocarbons at High Pressure," *Ind. Eng. Chem.* (1933) **25,** 103.
11. Olds, Sage and Lacey: "Composition of the Dew Point Gas of the Methane-Water System," *Ind. Eng. Chem.* (1942) **34,** 1223.
12. Reamer, Olds, Sage and Lacey: "Composition of the Dew Point Gas of the Ethane-WaterSystem," *Ind. Eng. Chem.* (1943) **35,** 790.
13. Sherwood: *Absorption and Extraction*, McGraw-Hill Book Co., New York (1937) 102.

* * *

T.P. 3200

MEASURING THE WATER VAPOR CONTENT OF GASES DEHYDRATED BY TRIETHYLENE GLYCOL

IRWIN POLITZINER,* F. M. TOWNSEND, BLACK, SIVALLS AND BRYSON RESEARCH FELLOW, AND **L. S. REID,**
MEMBER AIME, SCHOOL OF CHEMICAL ENGINEERING, UNIVERSITY OF OKLAHOMA, NORMAN, OKLA.

ABSTRACT

Recently published data indicate that the water vapor content of a gas, as determined by dew point measurement, is inaccurate when the gas has been dehydrated with diethylene glycol. Water vapor contents and dew point measurements of gases dehydrated with triethylene glycol have been obtained in this investigation in order to determine the magnitude of a similar error, if one exists.

Experimental data show a very low concentration of triethylene glycol vapor in gases dehydrated at atmospheric temperatures and pressures ranging from 500 to 2,500 psia, and that the accuracy of dew point measurements is not impaired by the presence of triethylene glycol vapor.

INTRODUCTION

Nearly all natural gas transported by pipe line to northern and eastern markets must be dehydrated to a low residual moisture content in order to assure maximum transmission efficiency and continuous delivery under peak load conditions. Without dehydration, water vapor often condenses in pipe lines in quantities sufficient to restrict the flow[3] and, under low atmospheric temperature conditions, gas hydrates may form and plug gathering, transmission and distribution facilities.

Gas may be dehydrated to pipe line specifications by a number of methods. The most widely used methods are (1) adsorption of water vapor on a solid dessicant such as activated bauxite, alumina or silica gel,[1] (2) by absorption of water vapor by either diethylene or triethylene glycol-water solutions of high glycol concentration,[11,13] and (3) by simultaneous expansion-refrigeration of very high pressure gas in which gas hydrates are purposely formed and then quickly decomposed.[10,11] Of these three fundamental methods, the adsorption and absorption processes provide the bulk of the dehydrated gas moving to market at the present time. The expansion-refrigeration process, a relatively new development, is gaining in favor because of its simplicity but is sharply limited in its application by available differentials between source and gathering system pressures.

Where gas sale or purchase contracts contain a maximum water vapor content specification, the water vapor content is usually determined by measuring the dew point of the gas at system pressure. Knowing the dew point temperature and the system pressure, the water vapor content of the gas is determined from a graphical correlation of saturation, or dew point, temperature *vs* the water vapor content of the gas which is customarily expressed as pounds of water vapor per million cubic feet of gas measured at 14.7 psia and 60°F. Dew points are usually measured with the U. S. Bureau of Mines Dew Point Tester, shown in Fig. 1, which is well suited for use at temperatures lower than 120°F and at pressures ranging from atmospheric to 3,000 psi. A number of correlations of dew point temperatures *vs* water vapor content are available,[3,5,15] the most recent of which is that by McCarthy *et al.*[4]

Where natural gas is dehydrated by absorbing contact with concentrated diethylene glycol-water solutions, considerable difficulty is experienced in observing water dew points due to condensation of liquid hydrocarbon and glycol films on the mirrored surface of the dew point tester. Riesenfeld and Frazier[12] report that the dew point method for determining the water vapor content of a diethylene glycol-treated natural gas is in error due to the glycol content of the condensate formed on the tester mirror, and that the water vapor content of the gas tested is actually lower than that indicated by the standard dew point-water vapor content correlation.

Extensive experience in testing gases dehydrated by concentrated triethylene glycol-water solutions has not revealed difficulties of the nature cited above for diethylene glycol. Water dew points are clear and sharp and condensation of

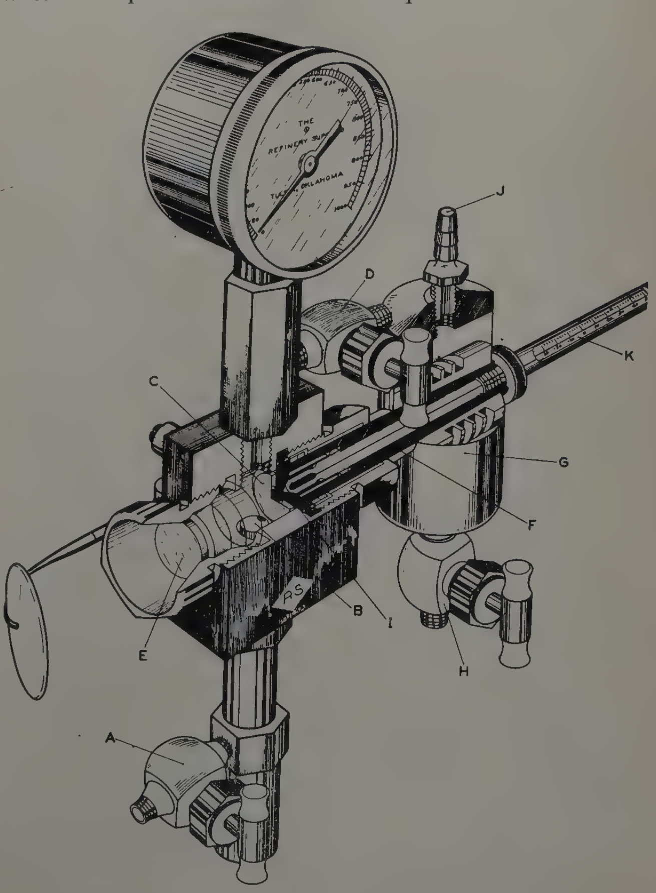

FIG. 1 — DEW POINT TESTER, U. S. BUREAU OF MINES TYPE.

---

[1] References given at end of paper.

Manuscript received in the office of the Petroleum Branch January 25, 1951. Paper presented at the Annual Meeting of the AIME in St. Louis, Mo., February 17-22, 1951.

*This paper is a condensation of a thesis submitted by Irwin Politziner in partial fulfillment of the requirements for the MChE degree conferred by the University of Oklahoma in June, 1951.

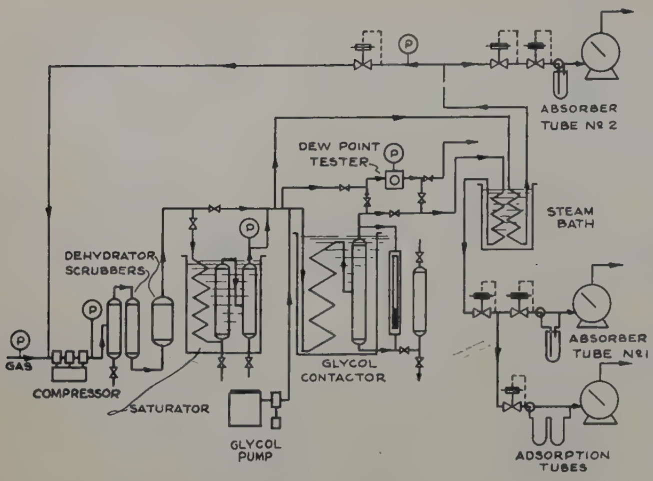

FIG. 2 — FLOW DIAGRAM.

glycol has not been observed except in those instances when the absorber has been substantially overloaded. Triethylene glycol has a vapor pressure substantially lower than that of diethylene glycol[14] and it is known that the vaporization losses of triethylene glycol[6] are considerably smaller than losses sustained when using diethylene glycol.[13] Preliminary investigations conducted by Porter *et al.*[8] failed to reveal any unusual discrepancy between water vapor contents determined by the dew point method and those determined by gravimetric analysis.

However, it has been assumed by many that the error reported in the water vapor content measurement of diethylene glycol-treated gases is also inherent in similar measurements where triethylene glycol is employed. The purpose of this investigation was to determine whether or not such an error exists and, if so, the magnitude of this error.

EXPERIMENTAL MATERIALS

The natural gas employed in this investigation was taken from the mains of the Oklahoma Natural Gas Co. at Norman, Okla. A representative analysis of this gas is shown in Table I. In view of the fact that this gas contains approximately 12 per cent air, several experimental determinations were made using oil-pumped nitrogen gas as the gas phase. This compressed nitrogen gas was obtained from the Air Reduction Magnolia Co. at Oklahoma City, Okla.

The triethylene glycol used was an air-treatment grade supplied by the Carbide and Carbon Chemicals Division, Union Carbide and Carbon Corporation.

EXPERIMENTAL EQUIPMENT

The dynamic equilibrium absorption apparatus described by Porter *et al.*[8] was employed in this investigation with only slight modifications, as shown in Fig. 2. The general plan of attack employed direct observation of the dew point of the dehydrated gas, using the U. S. Bureau of Mines Dew Point Tester and, simultaneously, determining the water vapor content of the gas by gravimetric analysis. The apparatus was modified to pass all glycol-treated gas through the dew point tester and, after heating in a hot water bath, the pressure was reduced to 60 psig by means of a pressure reducing regulator. Downstream from this regulator, the gas stream was split in two streams. One passed through a second regulator, where the gas pressure was reduced to near atmospheric, thence to two Pyrex adsorption tubes, filled with anhydrous magnesium perchlorate, thence to a wet test meter for measurement. The second stream was also passed through a pressure reducing regulator to expand the gas to near atmospheric pressure and passed into the bottom of Absorber Tube No. 1, consisting of a standard 10-in. test tube filled with glass Raschig rings and closed with a neoprene stopper. Glycol vapors were absorbed in distilled water in this device. Effluent gas passed to a second wet test meter for measurement.

A third sample stream of gas was taken from the apparatus upstream from the glycol contacting section, heated and expanded to near atmospheric pressure and passed in absorbing contact with fresh distilled water in a second absorption tube, designated as Absorber Tube No. 2 in Fig. 2. This glycol-free gas was used to determine the solubility of the natural gas in water, and employed in correcting the total glycol vapor and paraffin hydrocarbons absorbed in Absorber Tube No. 1. Effluent gas from this tube was passed to a wet test meter for measurement. Gas from all meters was vented to atmosphere.

EXPERIMENTAL TECHNIQUES

The experimental techniques employed in this investigation were essentially the same as those reported by Porter *et al.*[8] except for certain modifications outlined below.

All gas delivered to the apparatus by the compressor was dehydrated by adsorbing the moisture on a freshly reactivated charge of dessicant, and then re-saturated at the desired system temperature and pressure once those conditions had been established. It was found that this procedure would avoid condensation of water in the experimental apparatus.

Only that portion of the gas stream discharged by the compressor which was necessary for dew point and gravimetric analysis was passed through the glycol contactor. Most of the compressed gas was heated and then expanded to compressor suction pressure so that only the gas comprising the three sample streams was vented. All glycol-treated gas was passed through the dew point tester at all times to assure continuous flow at a steady rate and to eliminate any possibility of trapping gas with a variable glycol-water vapor content.

Triethylene glycol solution rates were established at 35 gal per standard Mcf of gas entering the absorber and this ratio was held constant during all experimental runs, regardless of pressure. Glycol solution concentrations were determined by the relative viscosity method described by Porter and Reid.[9]

The total quantity of gas passed through the adsorption train varied but the minimum quantity approximated 12 stand-

Table I — Analysis of Natural Gas

Component	Volume or Mol %
Carbon Dioxide	0.50
Oxygen	2.60
Nitrogen	14.05
Methane	67.29
Ethane	9.50
Propane	4.27
Butanes	1.36
Pentanes	0.31
Hexane and Heavier	0.12
	100.00
Specific Gravity	0.7470

ard cu ft. Magnesium perchlorate was chosen as the adsorbent because it extracts virtually all vapors from a gas stream. A final concentration of 0.002 mg of water vapor per liter of gas is reported for this desiccant.[2] A 40 mg increase in weight of the drying tubes was desired in order to minimize weighing errors.

The adsorption tubes were weighed on an analytical balance before and after each run and care was taken to replace the tubes in the train in the same order after each weighing. When the weight gained by the second tube exceeded five per cent of that gained by the first, the desiccant in the first tube was replaced. Prior to use, dehydrated gas was always passed through a freshly charged tube to displace the air and to saturate the desiccant with any adsorbable components of the gas.

Eight standard cu ft of gas was passed through Absorption Tube No. 1, and an identical quantity was passed through Absorption Tube No. 2. Residue gas streams from the adsorption train and the two absorption tubes were measured to 1/1000 cu ft and then corrected to standard conditions of 29.92 in. of mercury and 60°F.

The quantity of triethylene glycol vapor in the gas stream was determined by reacting the liquid contents of Absorption Tube No. 1 with potassium dichromate and concentrated sulfuric acid and, after the oxidation-reduction reaction was complete, titrating the excess potassium dichromate with ferrous-ammonium sulfate. A correction for hydrocarbons dissolved in water was determined by subjecting the liquid contents of Absorption Tube No. 2 to the same procedure. Complete details of this analytical procedure are reported by Politziner.[7]

Results of these analyses were computed in terms of grams of triethylene glycol vapor per standard cubic feet of gas and this quantity was subtracted from the grams of water and glycol vapor adsorbed per standard cubic foot of gas. The remainder was the grams of water vapor per standard cubic foot which was then converted to pounds of water vapor per standard million cubic feet of gas. This result was used to predict the dew point of the gas from the correlation of McCarthy *et al.*[4]

Although the water vapor content was obtained by difference, the results are quite accurate because the quantity of triethylene glycol vapor present in the gas was found to range from one to three per cent by weight of the total glycol and water vapor content. See Table II.

Since McCarthy's correlation pertains to essentially nitrogen-free gas, several experimental runs were made employing oil-pumped nitrogen as the gas phase, replacing the air-diluted natural gas used in the major portion of this research. It was felt that this series of special runs might throw some light on the effect of nitrogen on the water vapor content of nitrogen-bearing natural gas mixtures.

Table II — Triethylene Glycol in the Gas Stream — Weight Per Cent of Total Glycol and Water Vapor Content

System Temperature: 80°F

Run No.	TEG Concentration Weight Per Cent	System Pressure psia	Lbs. TEG Vapor Per 100 lbs. TEG and Water Vapor in Effluent Gas
15	99.5	500	1.28
29	95	1,000	1.29
16	99.5	1,000	1.33
27	95	1,500	2.13
17	99.5	1,500	4.84
28	95	2,000	2.12
9	99.5	2,000	2.32
26	95	2,500	3.37
19	99.5	2,500	3.44

Table III — Comparison of Observed and Calculated* Water Dew Points of Natural Gas Dehydrated By Triethylene Glycol

Run No.	TEG Concentration % by Wt.	System Temp. °F	System Press. psia	Water Content per std. MMcf	Calculated dew point °F	Observed dew point °F	Difference between calculated and observed dew points °F
30	95	80	500	17.10	43	43.5	+ 0.5
29	95	80	1,000	10.30	43	39	− 4
20	99.5	70	1,000	2.92	11	12.5	+ 1.5
16	99.5	80	1,000	4.78	22.5	19	− 3.5
37	99.5	90	1,000	6.37	30	30	0
27	95	80	1,500	7.19	42	40.5	− 1.5
28	95	80	2,000	7.85	49	47	− 2
9	99.5	80	2,000	3.41	26	25	− 1
23	99.5	90	2,000	2.40	17.5	20	+ 2.5
35	95	90	2,000	9.71	55	56.7	+ 1.7
36	99.5	90	2,000	6.02	41	43.3	+ 2.3
26	95	80	2,500	7.22	50	49.5	− 0.5

*Based on correlation by McCarthy, Boyd and Reid[4]

DISCUSSION OF RESULTS

Experimental determinations of water vapor content of glycol-dehydrated natural gas were made at pressures ranging from 500 to 2,500 psia and at system temperatures of 80 and 90°F, employing solutions of 95 and 99.5 per cent by weight triethylene glycol, the remainder being water. Six additional determinations were made in which oil-pumped nitrogen gas replaced the natural gas. All nitrogen runs were conducted at 80°F with pressures ranging from 500 to 2,000 psia, employing glycol solutions of the concentrations noted above.

The results obtained from this investigation are shown in Table III, where observed dew points are compared to dew points calculated from the gravimetric analyses by means of McCarthy's correlation. Inspection of these data show that, in general, the discrepancy between observed and calculated dew points is approximately two degrees F; also that these discrepancies are quite evenly distributed, plus and minus, indicating a small experimental error in manipulating the dew point tester at the low flow rate imposed by gravimetric sampling limitations. It is also significant to note that lower dew points were obtained when the gas was dehydrated by the 99.5 per cent glycol solution. The relatively low residual water vapor content of gas dehydrated in this manner tended to magnify the discrepancy between observed and calculated dew points. With but one exception, the greatest discrepancies are associated with determinations in which this highly concentrated solution was employed. A similar distribution was noted in the nitrogen runs, as shown in Table IV.

Three separate and distinct dew points were observed during this investigation. Fortunately, they are not similar in appearance and distinctions are readily drawn. The first of these is a hydrocarbon dew point which appears as a bright, highly mobile liquid film cascading across the mirror. This cannot be confused with a water dew point because of its distinctive appearance and because it appears almost immediately after cooling is begun. Where hydrocarbon condensation is severe and liquid accumulates in the dew point tester to the extent that it is cycled against the mirror by the gas jet, the entire body of the tester should be inverted. This will permit the liquid to drain off as fast as it is formed.

The second dew point appears to be a thin film of glycol which accumulates gradually on a clean mirror and forms a haze. This film does not disappear when the tester tempera-

Table IV — Comparison of Observed and Calculated* Water Dew Points of Nitrogen Dehydrated By Triethylene Glycol

Run No.	TEG Concentration % by Wt.	System Temp. °F	System Press. psia	Water Content lbs. per std. MMcf	Calculated dew point °F	Observed dew point °F	Difference between calculated and observed dew points °F
32	95	80	524	21.55	51	49.5	− 1.5
40	99.5	80	524	6.17	17.5	21	+ 3.5
41	99.5	80	1,000	3.35	14	18.7	+ 4.7
31	95	80	1,500	9.35	48	45.5	− 2.5
42	99.5	80	1,500	2.62	15	19	+ 4
33	95	80	2,000	8.15	50	49.5	− 0.5

*Based on correlation by McCarthy, Boyd and Reid[4]

ture is raised or when its pressure is released. It has not been observed during tests on commercial dehydration units using triethylene glycol, so the formation of this film is believed to be an inherent characteristic of the experimental apparatus.

As cooling is continued, a third dew point is observed. It appears as a dark spot in the center of the mirror and, if temperature and pressure conditions are conducive to hydrate formation, gas hydrate crystals will be observed forming in this spot immediately after it appears. The temperature at the instant the spot first appears is the water dew point.

True equilibrium distribution of water between the vapor and liquid phases was not obtained in the absorber during this investigation because of absorber velocity restrictions imposed by the gravimetric sampling rates. However, the degree of dehydration accomplished here was of the same order of magnitude as that of most commercial dehydration units. In view of this similarity in performance, Fig. 3 has been prepared as a smoothed plot of a portion of the data of Table II, showing the magnitude of triethylene glycol vapor losses as a function of absorber pressure when operated at 80°F. The glycol concentration of the solution is the parameter. It is significant to note that the triethylene glycol concentration in the effluent gas from the absorber is very low and that this concentration reaches a minimum value in the vicinity of 1,000 psia. The low loss incurred by use of 95 per cent triethylene glycol solution may be even further reduced by increasing the glycol concentration. Glycol vapor losses are well within the limits of sound operating practice when the absorber pressure is as high as 2,500 psia.

The data of Table II indicate that the triethylene glycol vapor concentration in dehydrated gas is unusually small, ranging from one to three per cent by weight of the total water vapor plus glycol vapor content of the gas. Since but a small fraction of this glycol vapor would be condensed when the water dew point was formed, its presence would have a negligible effect. These data lend strong support to the comparisons drawn in Tables III and IV.

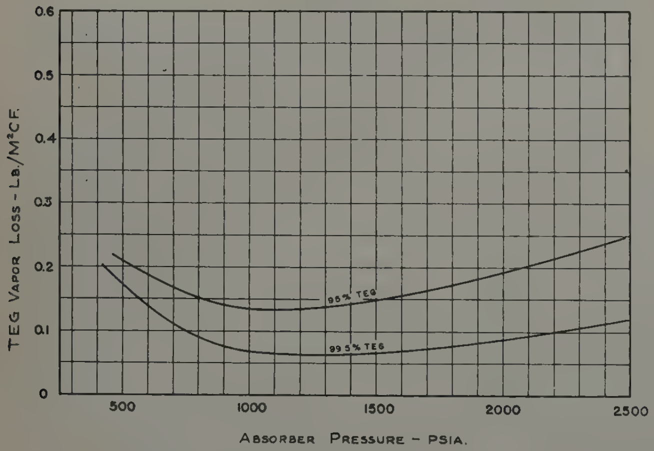

FIG. 3 — TRIETHYLENE GLYCOL VAPOR LOSSES AS A FUNCTION OF PRESSURE AND SOLUTION CONCENTRATION AT 80°F.

CONCLUSIONS

In conclusion, it is evident that:

1. The water vapor content of triethylene glycol-dehydrated gases may be determined accurately by dew point measurement.
2. The quantity of triethylene glycol vapor present in a stream of dehydrated gas is very small, ranging from one to three per cent of the total glycol-water vapor content of that gas.
3. Triethylene glycol vapor losses are, in general, less than 0.2 lb of glycol per standard MMcf of gas processed, over the ranges of temperature, pressure and solution concentration reported here.
4. Triethylene glycol vapor losses may be reduced to a substantial degree by maintaining the glycol concentration of the solution greater than 95 per cent by weight.
5. The water vapor content-saturation temperature correlation by McCarthy *et al.* is accurate for triethylene glycol-dehydrated gases whose specific gravities range as high as 0.75.
6. The variable nitrogen content of a natural gas mixture apparently has scant effect upon its water vapor content.

ACKNOWLEDGMENTS

The air-treatment grade triethylene glycol used in this investigation was furnished by the Carbide and Carbon Chemicals Division of Union Carbide and Carbon Corp.

The oil-pumped nitrogen and the nitrogen storage facilities were furnished by Black, Sivalls and Bryson, Inc.

REFERENCES

1. Amero, R. C., Moore, J. W., and Capell, R. G.: *Chem. Engr. Prog.* (1947) **43,** No. 7, 349.
2. Bower, J. H.: *J. Res. Nat'l Bur. Stds.* (1944) **33,** 199-200.
3. Deaton, W. M., and Frost, E. M., Jr.: *Monograph 8* (1948) U. S. Bureau of Mines.
4. McCarthy, E. L., Boyd, W. L., and Reid, L. S.: *Trans.* AIME (1950) **189,** 241.
5. McKetta, J. J., Jr., and Katz, D. L.: *Trans.* AIME (1947) **170,** 34.
6. Peahl, L. H.: *Oil and Gas Jour.* (1950) **49,** No. 10, 92-96.
7. Politziner, I.: M.Ch.E. Thesis (1951) University of Oklahoma Library.
8. Porter, J. A., and Reid, L. S.: *Trans.* AIME (1950) **189,** 235.
9. Porter, J. A., and Reid, L. S.: *Petr. Engr.* (1950) **22,** No. 5, D-9.
10. Records, L. R., and Seely, D. H., Jr.: *Trans.* AIME (1951) **192,** 61. *(Jour. Pet. Tech.)* Feb. 1951).
11. Reid, L. S.: *Trans. Southwestern Gas Measurement Short Course* (1950) 460, University of Oklahoma.
12. Reisenfeld, F. C., and Frazier, H. D.: *Oil and Gas Jour.* (1949) 48, No. 12, 238.
13. Russell, G. F.: M.Ch.E. Thesis (1944) University of Oklahoma Library.
14. Tech. Bull.: *Glycols,* Carbide and Carbon Chemicals Division, Union Carbide and Carbon Corp., New York (1948).
15. Wade, H. N.: *Petr. Engr.* (1943) **14,** No. 7, 100-104. ★ ★

T.P. 3198

THE LATEROLOG: A NEW RESISTIVITY LOGGING METHOD WITH ELECTRODES USING AN AUTOMATIC FOCUSING SYSTEM

H. G. DOLL, SCHLUMBERGER WELL SURVEYING CORP., RIDGEFIELD, CONN.

ABSTRACT

A ~~new~~ electrical logging method called Laterolog is described which provides for better recording of formation resistivity. In this method a current, preferably of constant intensity, is forced into the formation perpendicularly to the wall of the hole as a sheet of predetermined thickness by means of a special electrode arrangement and of an automatic control system.

The essential advantages of the Laterolog over the regular resistivity logs are explained. With the Laterolog, the mud column has much less influence than with conventional methods. The Laterolog is, therefore, particularly useful in wells drilled with highly conductive mud. Moreover, when the electrode system is located opposite a bed of moderate or small thickness, the disturbing effect of the adjacent formations becomes practically eliminated, provided the bed is thicker than the sheet of current, which itself is usually a few inches to a few feet thick. The sequences of beds are, therefore, much more sharply differentiated, and, in many cases, it is possible to read directly from the logs values close to the true resistivities of the formations without further corrections.

Field examples are shown to illustrate the results of the method in various types of formations.

INTRODUCTION

As soon as it was introduced into the petroleum industry, electrical logging proved to be a powerful instrument for the delineation of the strata traversed by bore holes and for correlation of such strata.[1,2] Research and engineering efforts were mostly devoted at this early time to the design of the techniques which could provide the best data for these purposes.

Later, attention was directed toward the quantitative analysis of electrical logs, in order to obtain information on reservoir characteristics, and, in particular, on oil and water saturation.[3,4] Efforts have been made, accordingly, with a view to improving the already existing methods, or to finding new methods which could satisfy these new requirements.[5]

Quantitative analysis implies a determination as accurate as possible of the true resistivity of the formations. In fact, however, the "apparent resistivity" recorded in front of a given bed by a conventional electrical logging method is frequently quite different from the true resistivity of this bed. This is due to the combined influence of the mud column, of the adjacent formations both above and below the bed, and of the invaded zone, in which the original fluid has been more or less replaced by mud filtrate.

When the beds are thick enough, and, as is frequently the case in sand and shale formations, when their resistivity is not much greater than that of the mud, it is generally possible to obtain their true resistivity directly on the electric log, or at least to obtain an approximate value which can be corrected without undue difficulty by means of recently published charts known as "departure curves."[6]

When the beds are thin, and particularly when, in addition, their resistivity is substantially greater than that of the mud column, the apparent resistivities recorded on conventional logs are seriously affected, and it is generally very difficult, if at all possible, to estimate their true resistivity with a good enough accuracy. In the most severe cases, such as are encountered in holes drilled through hard formations with muds of high salinity, the conventional logs are so distorted and rounded that they do not even show clearly the boundaries of the different beds.

In order to overcome the effect of the mud column and of the adjacent formations, it is possible to make use of appropriate systems whereby the measurements involve a comparatively thin slice of space at the level of the measuring device.

A mention is due, in this respect, to a measuring system, called the "guarded electrode," invented by C. Schlumberger over 20 years ago. The system, schematically represented in

---

[1] References given at end of paper.

Manuscript received in the office of the Petroleum Branch February 7, 1951. Paper presented at the AIME Annual Meeting in St. Louis, Mo., Feb. 17-22, 1951.

Fig. 1, comprises one short central electrode M and two elongated short-circuited electrodes, G and G' symmetrically placed above and below M, and connected to M by a low resistance shunt S. A current is fed to the electrodes, and that part i of the current which flows through the central electrodes forms a sheet which is confined between two approximately horizontal surfaces. The current i is measured by means of a meter located at the surface and connected to both ends of the shunt. The potential $\triangle V$ of electrode M is also measured by means of another meter at the surface, and the ratio $\frac{\triangle V}{i}$ gives the value of the resistance offered to the current, which resistance is proportional to the resistivity of the formation situated within the current sheet. The guarded electrode makes possible a detailed investigation of thin beds; however, the presence of a long metallic body in the bore hole amounts to short-circuiting the spontaneous current, and may deteriorate the SP log, and furthermore measurements of resistivities with other electrical devices recording at the same level are made practically impossible. Moreover, because of the presence of the shunt, the potential of the guard electrodes is not rigorously equal to the potential of the central electrode, but is greater by an amount which depends on the resistance of the shunt and on the resistivity of the surrounding media. The shape of the beam of current emitted by electrode M is, therefore, affected to an extent which cannot easily be ascertained, and, consequently, the response of the system is not quite defined, particularly when the bore hole is filled with low resistivity mud.

Along the same line, mention is also made of the interesting work done by the Pennsylvania State College.[7,8]

Mention must be made also of the Induction Logging method, which was the subject of an earlier paper,[9] and in which a focusing effect is obtained by an appropriate combination of coils.

The Laterolog system, which is described in this paper, is a new electrical logging method which makes use of a sheet of current of constant intensity and of well calibrated thickness, focused by means of an automatic control. This system furthermore can be used with point electrodes, which, among other advantages, make possible the simultaneous recording of the SP curve, or other electric logs.

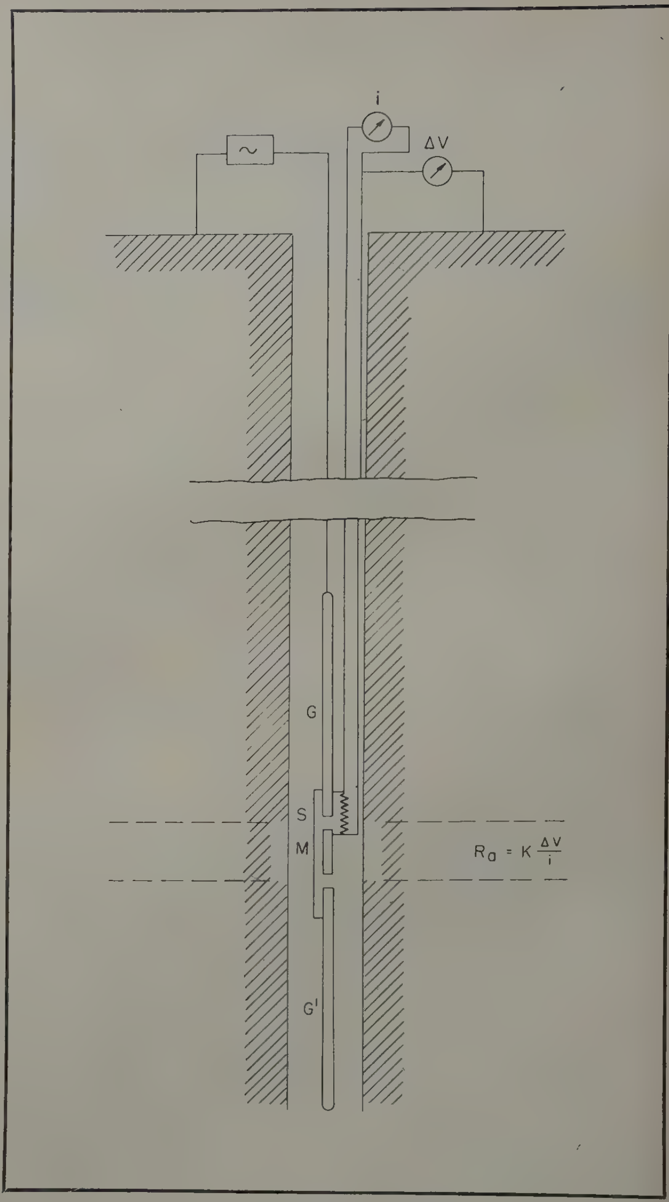

FIG. 1 — GUARDED ELECTRODE

With the Laterolog device, the effect of the mud column can always be neglected, and the effect of the adjacent formations is practically eliminated in all beds whose thickness is greater than that of the focused sheet of current; *i.e.*, from a few inches to a few feet, depending on the electrode combination being used.

Were it not for the invaded zone, a Laterolog would show directly the true resistivity of all beds whose thickness is greater than the limit mentioned above. In practice, the resistivity, as recorded, is quite close to the true value when the diameter of the zone invaded by the mud filtrate does not exceed about two to three times the diameter of the hole, and provided that the resistivity of the invaded zone is not greater than the true resistivity of the bed under investigation. This condition is frequently satisfied for oil-bearing formations, especially when the salinity of the mud is not much lower than that of the connate water.

Because of the comparatively small thickness of the focused sheet of current, the Laterolog gives a very detailed curve, and puts clearly in evidence the sharp contrasts between successive beds, however conductive the mud may be.

The first applications of the Laterolog method have been in holes drilled with high salinity mud. In that case, logs showing sharp contrasts and great details are obtained, where conventional methods would have given quite distorted and rounded curves. Furthermore, and because of the low resistivity of the mud filtrate in that case, the resistivities as recorded on the log are close enough to the true values. Typical examples of Laterologs run under such conditions are shown in Figs. 12, 13 and 14.

More generally, the Laterolog is quite useful in all hard formations because it eliminates the effect of the mud column and of the adjacent formations, which are generally quite large in that case for the conventional methods. It will always give a detailed picture of the formations, and a sharp definition of the boundaries. Whenever the resistivity of the mud filtrate is too great for the effect of the invaded zone to be neglected, the true resistivity will not be read directly from the Laterolog, but corrections could be introduced if the depth of penetration of the mud filtrate, and the resistivity of the invaded zone can be estimated or determined with the help of some other electrical log, which could be, for example, a Laterolog with a smaller depth of investigation.

Qualitatively, in sand and shale formations, the advantage of the Laterolog is not so pronounced since there the conventional logs give a satisfactory answer. The usefulness of the Laterolog in that case will, therefore, depend on its ability to contribute to the determination of the true resistivity of the sands. Unfortunately, the muds that are generally used, in the Gulf Coast and Louisiana, for example, have a salinity which is much lower than that of the connate water, so that many sands, even good oil producers, are less resistive than the invaded zone. Here again, the determination of true resistivity from the Laterolog alone will be generally possible only when the effect of the invaded zone can be estimated by other means.

It is reasonable to envisage that for most formations the best way to accomplish the determination of true resistivity, both in the case of thick and of thin beds, will consist in simultaneously recording a Laterolog and an Induction Log, when the complete development of this last method is achieved.

PRINCIPLE OF THE LATEROLOG

The Laterolog device (Fig. 2) comprises one electrode A_o, and three pairs of electrodes, M_1M_2, $M'_1M'_2$, A_1A_2, positioned symmetrically with respect to A_o, with the pairs being respectively short-circuited. A current of constant and calibrated intensity is fed through electrode A_o. Additional currents of same polarity as the current flowing through A_o are fed through the auxiliary power electrodes A_1 and A_2. The intensity of these currents is automatically and continuously adjusted in such a way that the difference of potential between M_1M_2 and $M'_1M'_2$ is maintained substantially equal to zero. The potential prevailing at any one of these latter four electrodes is recorded. The apparent resistivity measured with the device is proportional to the value of this potential and to a certain geometrical factor which depends on the distances between the various electrodes.

According to this system, the current emitted from A_o is prevented from flowing upward and downward past the meas-

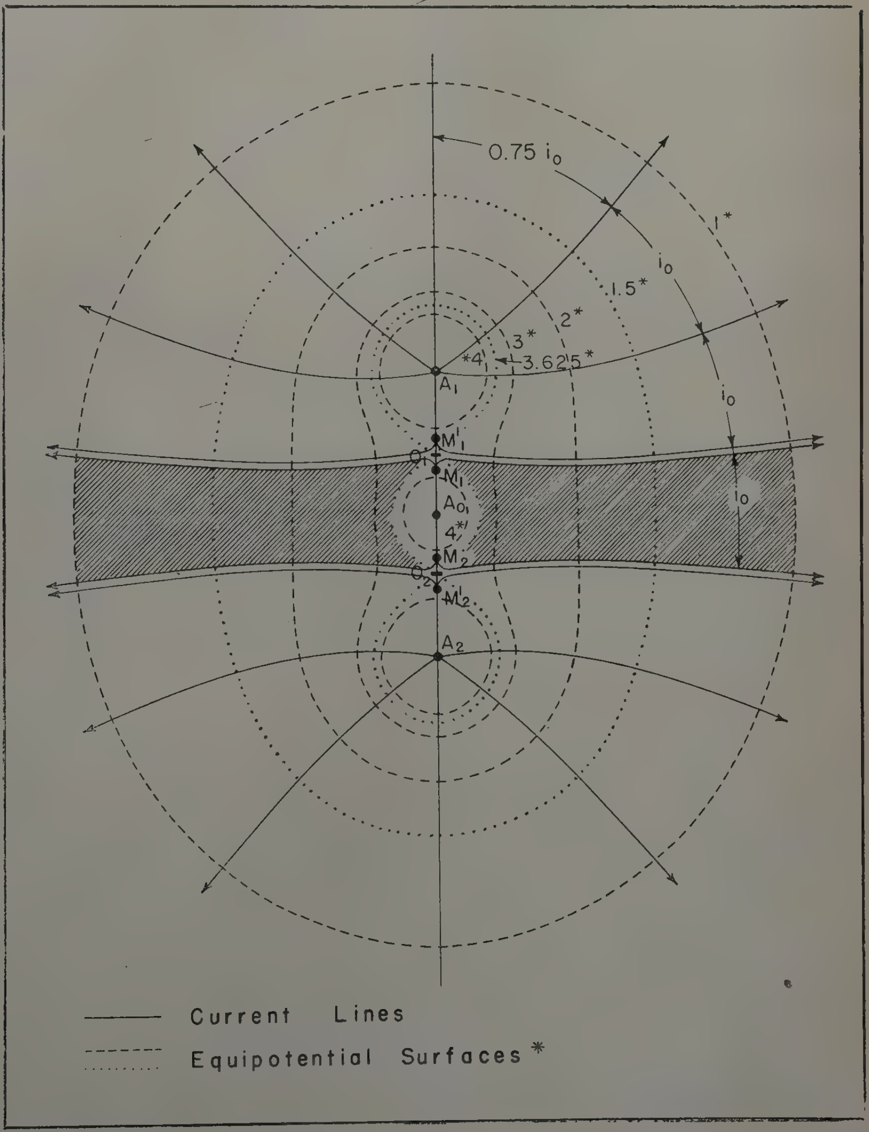

FIG. 2 — LATEROLOG: EQUIPOTENTIAL LINES AND LINES OF CURRENT FLOW IN HOMOGENEOUS MEDIUM (COMPUTED). *TO OBTAIN THE POTENTIALS IN MV MULTIPLY THE FIGURES BY $\frac{Ri_o}{4\pi a}$ WITH a IN METERS, R IN OHM-METERS, AND i_o IN MILLIAMPERES.

uring electrodes $M_1M'_1$ and $M_2M'_2$, as if insulated plugs were placed in the hole at the level of these electrodes. Accordingly, the mud column, which handicaps seriously the conventional logs when the formations are much more resistive than the mud, has very little influence on the measurements made with the Laterolog. Moreover, the electrical conditions created by the controlling system are such that the current emitted by A_0 behaves as if the insulated plugs were extended horizontally far away from the bore hole. The current is therefore obliged to flow within an approximately horizontal slice of space, whose thickness is about equal to the distance separating the middle points O_1 and O_2 of $M_1M'_1$ and $M_2M'_2$.

Fig. 2 shows the distribution of the current lines and of the equipotential surfaces for a Laterolog device placed in a homogeneous medium. The sheet of current issued from A_0, represented by a shaded area, is bounded by two surfaces, which up to a considerable radial distance from the drill hole are close to the two horizontal planes passing through O_1 and O_2. The potential of any of the electrodes M_1, M'_1, M_2, M'_2 represents the drop of potential produced by ohmic effect in the sheet of current, from its origin in the bore hole to a large distance from the hole; and is therefore proportional to the resistivity of the medium. The volume of ground where the resistivity is measured is essentially a horizontal slice, having the same thickness and the same position as the sheet of current.

To explain the operation of the system in the case of thin beds, it is convenient to consider that it is placed in front of a homogeneous bed — referred to as "the bed" — having the same thickness as the current sheet, and bounded above and below by thick homogeneous formations — respectively referred to as upper and lower formations, and to neglect the effect of the mud column.

If the resistivities of the upper and lower formations are equal to that of the bed, the situation is substantially that of an infinite homogeneous medium, and the distribution of current and potentials is as represented in Fig. 2. If it is now assumed that the upper and lower formations are, for example, ten times more conductive than the bed, the auxiliary currents flowing through A_1 and A_2 are automatically increased to about ten times what their value would be in a homogeneous medium — otherwise the potential differences at $M_1M'_1$ and $M_2M'_2$ would not be nil — so that the distribution of potential above and below the bed is automatically brought back to what it would have been in the homogeneous medium. There is, therefore, no tendency for the current of the sheet to be attracted by the upper and lower conductive beds. The sheet of current keeps nearly its normal shape, and produces in the bed a drop of potential which is practically the same as if the bed had been considerably thicker. The apparent resistivity observed opposite the center of the bed is therefore very little different from the true resistivity of the bed.

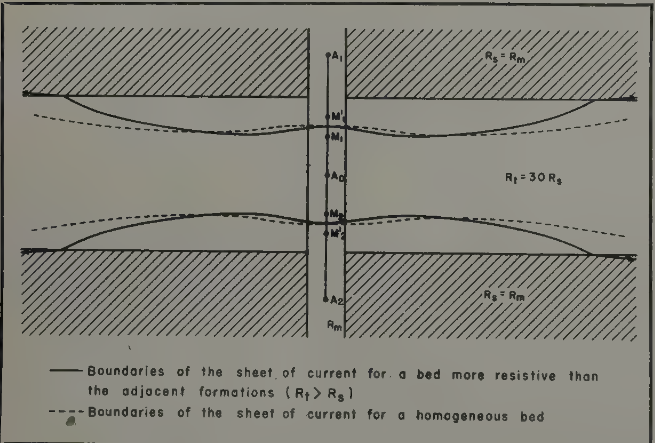
A1
M'1
M1
A0
M2
M'2
A2
Rm
Rs = Rm
Rt = 30 Rs
Rs = Rm
Boundaries of the sheet of current for a bed more resistive than the adjacent formations (Rt > Rs)
Boundaries of the sheet of current for a homogeneous bed

FIG. 3 — LATEROLOG — SHAPE OF THE SHEET OF CURRENT (LABORATORY DETERMINATION). R_t: RESISTIVITY OF BED. R_s: RESISTIVITY OF ADJACENT FORMATIONS. R_m: RESISTIVITY OF MUD.

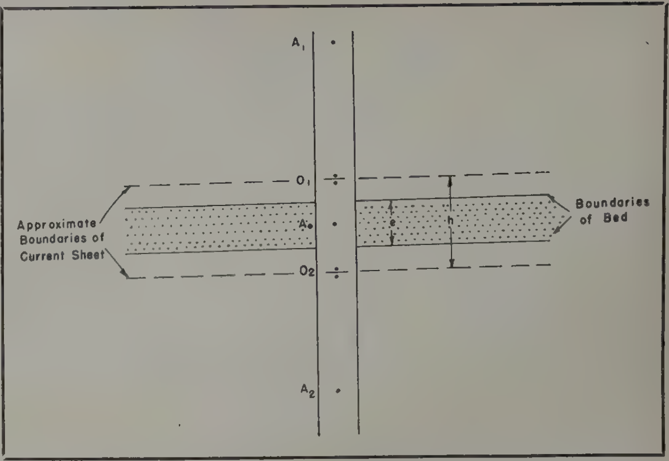

FIG. 4 — LATEROLOG DEVICE OPPOSITE A BED WHOSE THICKNESS IS LESS THAN THE THICKNESS OF THE SHEET OF CURRENT.

When the upper and lower formations are more resistive than the bed, the auxiliary currents are automatically decreased, and an equivalent result is obtained.

The result is practically the same when the sheet of current penetrates a homogeneous bed that is thicker than the current sheet, and the apparent resistivity is again substantially equal to the true resistivity of the bed. As an illustration, Fig. 3 shows the shape of the sheet of current, determined by laboratory experiments, for the case of a bed more resistive than the adjacent formations, and slightly thicker than the sheet of current. For comparison, the shape of the sheet of current, for the same pattern of electrodes, but in the case of a homogeneous medium, is shown in the figure.

In the converse case of a bed whose thickness is smaller than that of the sheet of current, the constant current from A_0 divides itself, according to conductivities and respective thicknesses of the bed and that part of the surrounding formations which is within the lower and upper limits of the sheet of current. The apparent resistivity, as recorded, is in that case an average between the resistivity of the bed and that of the surrounding formations, and depends, of course, on the thickness of the bed. Furthermore, the presence of the more conductive formation within the sheet has a predominant effect on the apparent resistivity.*

---

*It is supposed (Fig. 4) that e is the thickness of the bed and h the thickness of the sheet of current, R_t the resistivity of the bed and R_s the resistivity of the adjacent formations. Since the current lines from A_0 are all practically horizontal starting at a certain distance from the bore hole, the average, or apparent resistivity R_a measured with the device may be computed approximately through the equation:

$$\frac{h}{R_a} = \frac{e}{R_t} + \frac{h-e}{R_s}$$

If, for example, R_t is taken equal to 10, R_s to 1, h to 2 and e to 1, then:

$$\frac{2}{R_a} = \frac{1}{10} + \frac{1}{1} = 1.1$$

hence

$$R_a = \frac{2}{1.1} = 1.8 \text{ so that } R_a = 0.18\ R_t$$

If, converselv, $R_t = 1$ and $R_s = 10$ with the same values for h and e, R_a is again found equal to 1.8, so that $R_a = 1.8\ R_t$.

In order to explain why the Laterolog is better adapted for the investigation of thin beds, it will be compared to a normal device, in the following schematical example of a thin bed of high resistivity R_t, non-invaded and bounded by thick formations of low resistivity R_s, with the thickness of the bed being slightly greater than that of the sheet of current (Fig. 5).

Fig. 5 is divided into two parts by a vertical dash-dot line which coincides with the axis of the bore hole. A power electrode *A* is shown on the axis mid-way between the boundaries of the bed. The distribution of the current emitted from electrode *A*, without any focusing system — case of normal device — is represented qualitatively on the left-hand part of the figure. The distribution corresponding to the use of a focusing system — case of the Laterolog — is shown in the right-hand part.

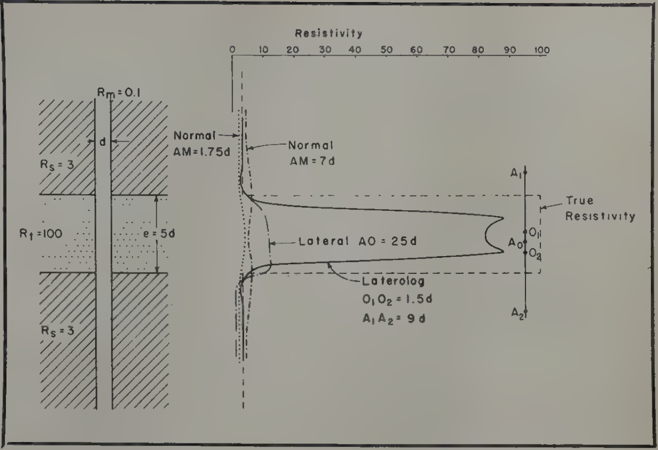

FIG. 6 — RESPONSE OF LATEROLOG AND CONVENTIONAL DEVICES OPPOSITE A THIN RESISTIVE BED, NON-INVADED, WITH LOW RESISTIVITY MUD (LABORATORY DETERMINATION). *d*: DIAMETER OF HOLE. e: THICKNESS OF BED = 5*d*. R_t: RESISTIVITY OF BED = 100. R_s: RESISTIVITY OF ADJACENT FORMATION=3. R_m: RESISTIVITY OF MUD=0.1.

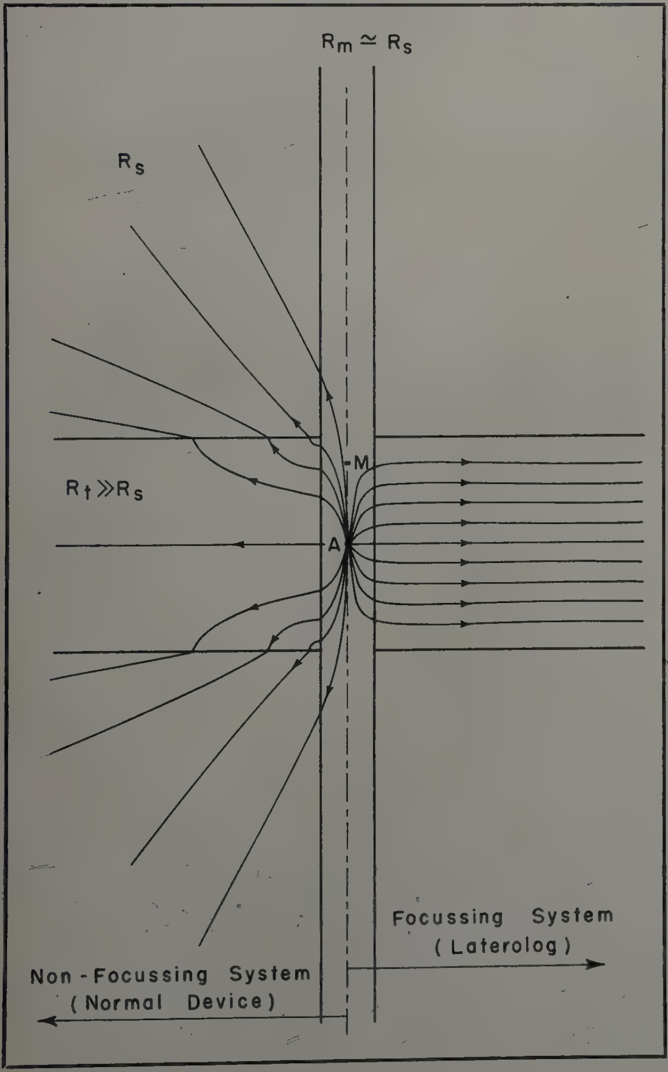
$R_m \simeq R_s$
R_s
$R_t \gg R_s$
M
A
Focussing System (Laterolog)
Non-Focussing System (Normal Device)

FIG. 5 — COMPARISON OF THE DISTRIBUTIONS OF THE CURRENT LINES IN THE CASE OF A NORMAL DEVICE, AND OF THE LATEROLOG, THIN BED MORE RESISTIVE THAN ADJACENT FORMATIONS. (SCHEMATIC DRAWING.) R_t: RESISTIVITY OF BED. R_s: RESISTIVITY OF ADJACENT FORMATIONS. R_m: RESISTIVITY OF MUD.

The apparent resistivity is proportional to the potential prevailing at an electrode *M*, close to the power electrode *A*, and consequently to the resistance between the equipotential surface passing through *M*, and infinity. In the case of the device without focusing system (left-hand side of Fig. 5), the current lines diverge from *A* in all directions and are definitely attracted upward and downward by the adjacent formations, more conductive than the bed, so that the resistance offered by the bed to the current is, to a great extent, by-passed. The apparent resistivity read opposite the bed is therefore much lower than the true resistivity of the bed. With the Laterolog, on the contrary (right-hand side of Fig. 5), all the current lines flow within the boundaries of the bed, at least for a large distance from the bore hole, so that the resistance between the equipotential passing through *M*, and infinity, and accordingly the potential at *M*, is directly controlled by the resistivity of the bed. The apparent resistivity then is very close to the true resistivity of the bed.

This simple example was given to illustrate schematically the comparative behavior of the normal and the Laterolog devices. Similar comparisons could be made for other cases, but a complete review would be too long to be contained within the scope of this paper.

These general indications on the characteristics of the Laterolog will be made more precise by the results of a laboratory experiment given as example, and of theoretical studies, relative to the determination of true resistivity.

LABORATORY EXAMPLE OF LOGGING IN THIN BED

Fig. 6 shows a typical example of a curve recorded in the laboratory with a Laterolog device opposite a thin bed, more resistive than the adjacent formations, and traversed by a bore hole filled with mud of low resistivity.

In Fig. 6 the thickness of the bed *e* is equal to five times the hole diameter *d*. The spacing of the Laterolog device is $O_1O_2 = 1.5d$, with A_1A_2 being equal to six times O_1O_2. For a usual value of hole diameter, say about 9 in., these values correspond respectively to a bed thickness slightly less than 4 ft, and to a thickness of the current sheet slightly greater than one ft. The resistivity of the bed R_t is equal to 100, the resistivity of the mud R_m to 0.1, and the resistivity of the adjacent formations R_s to 3.

The curves recorded with a short normal $AM = 1.75d$ (16 in.), a long normal $AM = 7d$ (64 in.) and a lateral device $AO = 25d$ (18 ft 8 in.) are also shown on the figure, for comparison.*

It is seen in the figure that the Laterolog device gives a much sharper and more accurate indication of the boundaries of the bed than the conventional deviecs. Moreover, the value of the apparent resistivity read with the Laterolog on the center plane of the bed is equal to 80, *i.e.*, only 20 per cent less than the true resistivity, whereas the normal devices and the lateral device show respectively 4, 5 and 12 instead of 100.

DETERMINATION OF THE TRUE RESISTIVITIES

The purpose of the Laterolog is not only to give a detailed qualitative delineation of the beds but also to provide directly on the log values close to the true resistivity of the beds, whatever their thickness, provided, of course, this thickness is not exceedingly small.

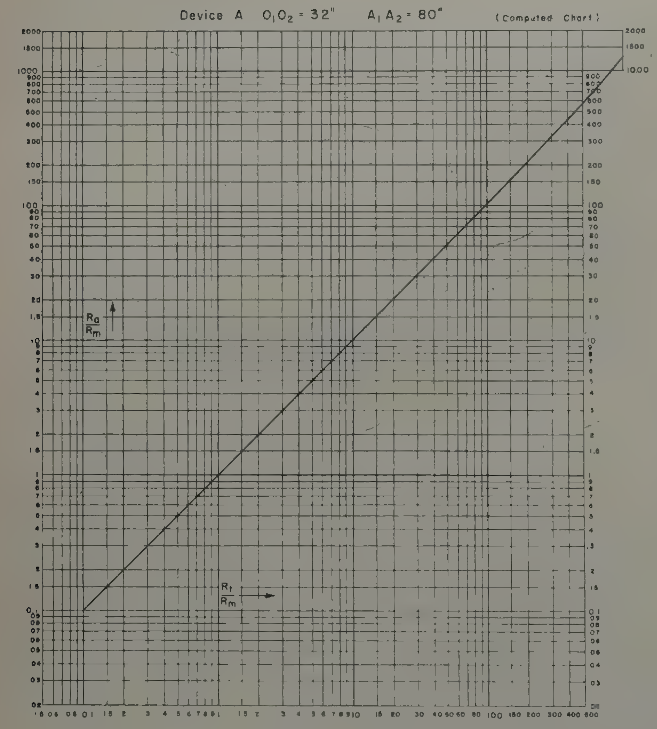

FIG. 7 — RESPONSE OF LATEROLOG DEVICE, HOMOGENEOUS BED OF INFINITE THICKNESS, NO INVASION.

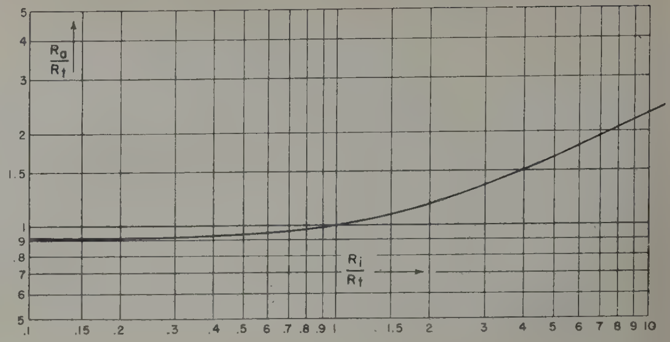

FIG. 8 — RESPONSE OF THE LATEROLOG DEVICE A, BED OF INFINITE THICKNESS, DIAMETER OF INVADED ZONE $D_i = 2d$ (APPROXIMATE COMPUTATION). R_t: RESISTIVITY OF BED. R_s: RESISTIVITY OF ADJACENT FORMATIONS. R_i: RESISTIVITY OF INVADED ZONE. R_a: APPARENT RESISTIVITY.

In order to realize what is the capability of the Laterolog in this respect, it is convenient to examine first its response with reference to true resistivity determination in the simple case of very thick beds — then how its response is affected by the presence of adjacent formations in the case of thin beds. These two cases will be considered hereafter.

Case of Thick Beds

The value of the apparent resistivity measured with a Laterolog device can be computed exactly in this case in terms of the various factors involved: true resistivity of the bed, mud column, and invaded zone, if any. It is thus possible to determine what distances should be selected between the electrodes to give the best possible response. The criterion, in this respect, is to obtain values of apparent resistivities R_a as close as possible to the values of true resistivity R_t, in a non-invaded formation for any ratio of the resistivity R_t of the bed to the resistivity R_m of the mud.

The chart of Fig. 7 is related to the following combination, called "device *A*":

$$O_1O_2 = 32 \text{ in. and } A_1A_2 = 80 \text{ in.}$$

In this chart, the values of $\frac{R_a}{R_m}$ recorded with device *A* are plotted in terms of the values of $\frac{R_t}{R_m}$.

The computations have been made for two widely different values of the hole diameter (namely 8 in. and 13 in.) — but the results have been found practically identical — so that the curve represented on the figure may be considered as being valid for all usual hole diameters.

The curve is traced for a very wide range of values of $\frac{R_t}{R_m}$, namely between 0.1 and 1,000. It is seen that when $\frac{R_t}{R_m}$ is less than about 300, the values of $\frac{R_a}{R_m}$ are equal to the corresponding values of $\frac{R_t}{R_m}$. When $\frac{R_t}{R_m}$ is greater than 300, the values of $\frac{R_a}{R_m}$ are slightly higher, and the difference attains 20 per cent for $\frac{R_t}{R_m} = 1{,}000$.

---

*The lateral curve, traced on the figure, has not been determined in the laboratory because of the insufficient size of the experimental tank. This curve is derived from the computation made, supposing the bore hole effect negligible. The maximum apparent resistivity thus computed is likely to be somewhat higher than the value which would be observed if the bore hole effect were taken into account.

The behavior of device *A* will now be examined for the case of an invaded bed. Fig. 8 relates to a bed of infinite thickness, traversed by a bore hole of diameter *d*, the diameter *Di*[*] of the invaded zone being equal to 2*d*. The chart is intended to show how the response of the Laterolog varies according to whether the invaded zone is more or less resistive than the uncontaminated part of the bed. To this end, the ratio of the resistivity of the invaded zone R_i to the true resistivity of the bed R_t is born in abscissae, and the ratio of the apparent resistivity R_a to the true resistivity R_t is born in ordinates. The points plotted on this chart were also determined by computations.

For $\frac{R_i}{R_t}$ less than 1 (conductive muds, and, consequently, conductive mud filtrate), the average curve is very close to the horizontal line of ordinate 1; and for values of $\frac{R_i}{R_t}$ greater than 1 (fresh mud, and, consequently, fresh mud filtrate), the curve rises progressively. In other words, as long as R_i is less than R_t, the apparent resistivity is about equal to the true resistivity; when R_i is slightly greater than R_t, say less than twice as great as R_t, R_a is still close to R_t, but a little higher — the difference not exceeding 30 per cent; for greater values of $\frac{R_i}{R_t}$, R_a becomes much greater than R_t and attains a value of about 2 to 2.5 R_t when $\frac{R_i}{R_t}$ is equal to 10.

The conclusion of this analysis is that the Laterolog device gives values of resistivity which are practically not affected by the invaded zone, provided the resistivity of the invaded zone is not appreciably greater than the resistivity of the uncontaminated part of the bed. In the case of a formation of comparatively low porosity, the depth of invasion may be greater than 2*d*, and the influence of the invaded zone may be somewhat more important than is shown on the chart. The values of apparent resistivity are, nevertheless, still reasonably close to the true resistivity when R_t is greater than R_i.

It is clear that conditions favorable to the use of the Laterolog are obtained when the resistivity of the invaded zone and, accordingly, the resistivity of the mud, is low. Of course, it would not be advisable to decrease purposely the resistivity of the mud too much in order to improve the response of the Laterolog, because, for too low a mud resistivity, the SP curve is reduced to an almost flat line. But, in those regions where the mud is of high salinity anyway, because of the presence of a salt rock bed above the formations to be surveyed, the Laterolog finds automatically an excellent field of application, and more so because in that case all the conventional electric logs are either featureless or very much distorted.

Other combinations of electrodes are possible wherein the thickness of the sheet of current is taken smaller than with device A. One of these combinations corresponds to $O_1O_2 =$ 12 in. and $A_1A_2 = 72$ in. (device B). The response of this device, as calibrated for practical use, is shown on the computed chart of Fig. 9.

It is seen that with device B, when $\frac{R_t}{R_m}$ is greater than about 20, the values of $\frac{R_a}{R_m}$ are very close to the corresponding values of $\frac{R_t}{R_m}$, namely within a few per cent. When $\frac{R_t}{R_m}$ is less than 20, the values of $\frac{R_a}{R_m}$ are greater than $\frac{R_t}{R_m}$, and the less $\frac{R_t}{R_m}$, the greater the difference.

In the case of bore holes drilled with high salinity mud, and more generally, for holes drilled through hard formations, the ratio of formation resistivity to mud resistivity is almost always greater than 20, or at least greater than 10, so that the values of $\frac{R_a}{R_m}$ recorded opposite any non-invaded formation will fall in that part of the curve where $\frac{R_a}{R_m}$ is substantially equal to $\frac{R_t}{R_m}$.

Device B is therefore well adapted to the determination of true resistivities in wells drilled with high salinity mud, or in hard formations, and it has, furthermore, the advantage over

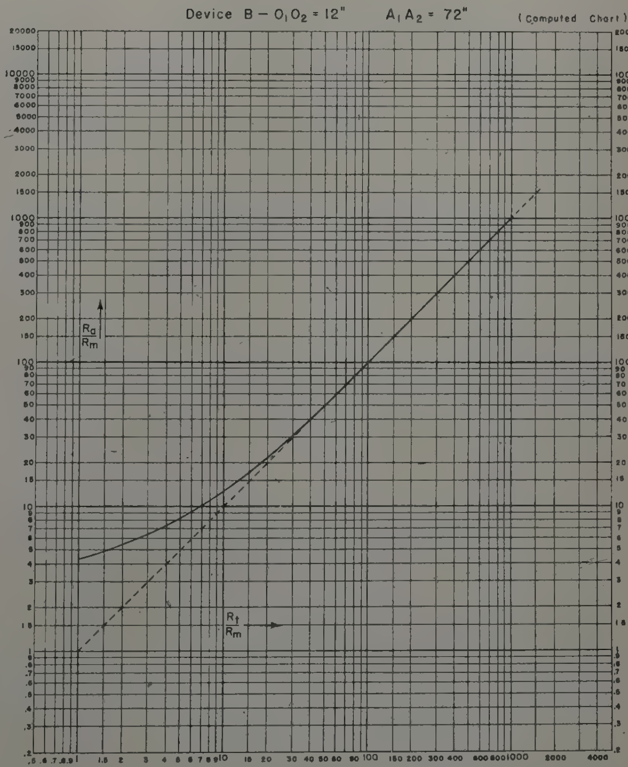

FIG. 9 — RESPONSE OF LATEROLOG DEVICE, HOMOGENEOUS BED OF INFINITE THICKNESS, NO INVASION.

---

[*] It is supposed, for the convenience of the discussion, that the invaded zone is equivalent to a homogeneous medium, bounded by two co-axial cylindrical surfaces of diameters *d* and *Di*. In fact, this representation is not entirely exact, and there is more likely a progressive change of resistivity between the invaded zone and the uncontaminated part of the bed.

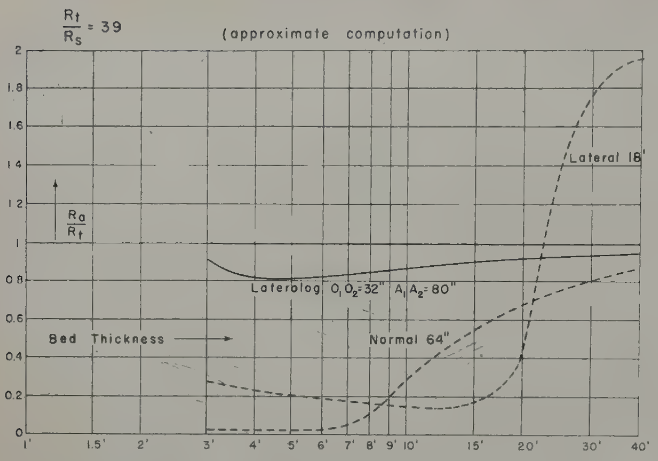

FIG. 10 — EFFECT OF BED THICKNESS ON THE RESPONSE OF THE LATEROLOG DEVICE AND THE CONVENTIONAL DEVICES, NO INVASION, HOLE NEGLECTED. R_t: RESISTIVITY OF BED. R_s: RESISTIVITY OF ADJACENT FORMATIONS. R_a: APPARENT RESISTIVITY.

device A that it makes possible the investigation of thinner beds, since the thickness of the current sheet is only equal to about 1 ft instead of about 3 ft.

Influence of Bed Thickness

The exact computation of the true resistivities recorded with a Laterolog device opposite a bed of finite thickness traversed by a bore hole does not seem to be possible in the present stage of our knowledge. The problem, therefore, has been, and is still being investigated by means of laboratory tests on models. Some of the results obtained thus far have been reproduced in Fig. 6, which illustrates the preceding section of this paper. Although quite a few laboratory determinations have already been made, the results are not yet numerous enough at present to provide a complete information on the effect of the bed thickness, but they show that this effect is small, provided the bed thickness is greater than the thickness of the sheet of current.

Approximate indications can furthermore be obtained by means of computations when the effect of the bore hole is neglected. Fig. 10 shows the results of such computations for the case of a bed, whose resistivity R_t has been taken equal to 39 times the resistivity R_s of the surrounding formations. On the figure, bed thicknesses, in feet, are born in abscissae, and the corresponding computed values of $\frac{R_a}{R_t}$ are in ordinates. Three curves are traced which correspond respectively to the Laterolog device ($O_1O_2 = 32$ in. and $A_1A_2 = 80$ in.) to the long normal device ($AM = 64$ in.), and to the lateral device ($AO = 18$ ft.).

If the bore hole were taken into consideration, the departure between the apparent resistivity and the true resistivity for thin beds with the normal and the lateral device would be greater than is shown on the chart, whereas, for the Laterolog device, the departure would be substantially the same.

Quite similar results are obtained for other values of $\frac{R_t}{R_s}$. The relative departure of R_a from R_t is, however, more important for a bed more conductive than the adjacent formations, but, in this case, further laboratory experiments are necessary to determine the exact response of the Laterolog device.

FIELD TECHNIQUE

Fig. 11a shows schematically the circuit generally used for recording the Laterolog curve. An AC current of constant intensity is fed through electrode A_o by means of a generator located at the surface. Electrodes M_1M_2 *and* $M'_1M'_2$ on the one hand, electrodes A_1A_2 and surface electrode B_1 on the other hand, are respectively connected to the input and output terminals of an automatic control apparatus (1). By means of this apparatus, a current is fed through A_1 and A_2 which continuously acts to maintain the difference of potential between M_1M_2 and $M'_1M'_2$ substantially equal to zero. The common potential of electrodes $M_1M_2M'_1M'_2$ is recorded by means of meter (2), with reference to an electrode N placed in the bore hole at a great distance from the measuring device.

The automatic control system used to keep the potential difference between M_1M_2 and $M'_1M'_2$ equal to zero can be applied equally well to another electrode arrangement as shown in Fig. 11b. In this case, instead of the point electrodes of the standard Laterolog, elongated electrodes are used, namely one central electrode A'_o, and two symmetrical and

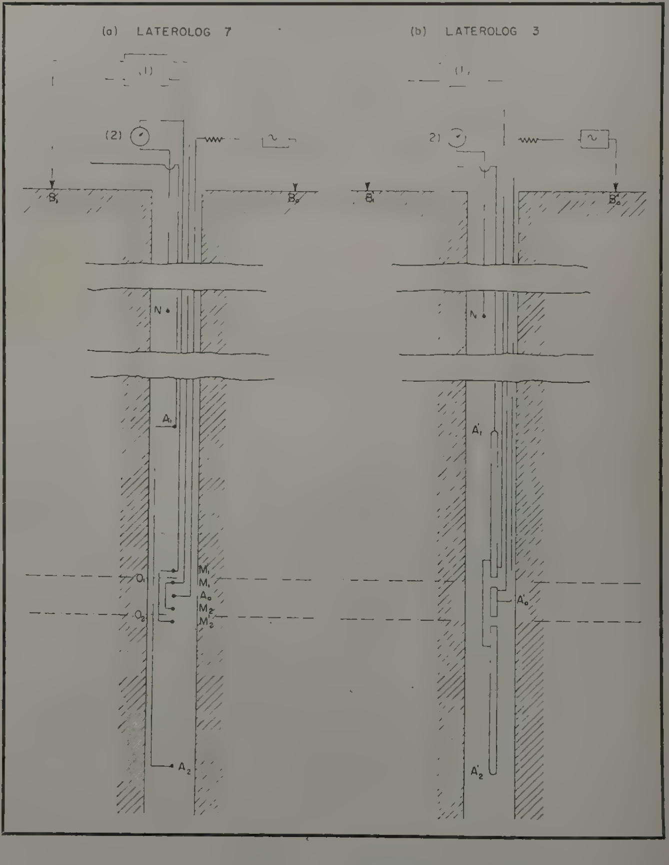

FIG. 11 — LATEROLOG — SCHEMATIC CIRCUITS.

short-circuited electrodes $A'_1A'_2$. The technique of measurement is essentially the same as that just described; a current of constant intensity is fed to electrode A'_0 and the difference of potential between A'_0 *and* $A'_1A'_2$ is maintained substantially nil by means of the same automatic control apparatus (1'). The common potential of $A'_0A'_1A'_2$ is recorded by means of meter (2). For the sake of differentiation, this system can be designated as "Laterolog 3" (3-electrode Laterolog), and the standard system as "Laterolog 7" (7-electrode Laterolog).

It appears that with Laterolog 3, the current is made to flow within a substantially horizontal sheet of space, whose thickness is about equal to the length of electrode A'_0. If the length of electrode A'_0 in Laterolog 3 is taken equal to the distance O_1O_2 in Laterolog 7, the thicknesses of the sheets of current in both cases will be the same, and both devices will have similar abilities for the detection of details.

The response of Laterolog 3 cannot be determined by computations — as is the case for the Laterolog with point electrodes — and must be investigated by laboratory experiments on scale models. Although such experiments are not yet sufficient to provide a complete answer, it seems possible to foresee that Laterolog 3 will give results substantially equivalent to those of Laterolog 7, provided its overall length is appreciably greater.

One important feature is that with Laterolog 3, the presence of a long metallic body in the bore hole affects the SP curve adversely. This fact, however, will present no practical drawback in the case of wells filled with high salinity mud, where the SP curve is reduced to a practically flat line anyway. It is reasonable to think that, in the case where the mud is not very salty, and where, therefore, the SP curve gives valuable indications, the use of Laterolog 7 will be preferable. Laterolog 7 has also the advantage that other resistivity logs with electrodes, or induction logs, can be recorded simultaneously without the fundamental difficulty that would result from the presence of a long metallic body.

FIELD EXAMPLES

Fig. 12 is an example of application of Laterolog 7 in the case of limestones drilled with a mud saturated with salt (West Texas). The figure also includes, for comparison, the resistivity curves recorded with the conventional device, and the SP curve — although this last curve is reduced to a straight line in this case.

One striking feature on the figure is the considerable difference in the amplitudes of the resistivities recorded with the various devices.

The resistivities recorded with the short normal and the limestone sonde are very low, not greater than about ten ohm-m, because the radii of investigation of these devices are small and the by-pass effect of the mud column is particularly important. In comparison, resistivities as high as 250 ohm-m are obtained with the lateral device, whose radius of investigation is very large, and also with the Laterolog device.

The Laterolog furthermore gives a sharp and detailed delineation of the beds. Some of these details correspond to slight excursions on the limestone sonde curve, which is reproduced on the right-hand track with an amplified resistivity scale. Many details clearly indicated on the Laterolog, however, are lacking on the limestone sonde curve, despite the enlarged scale.

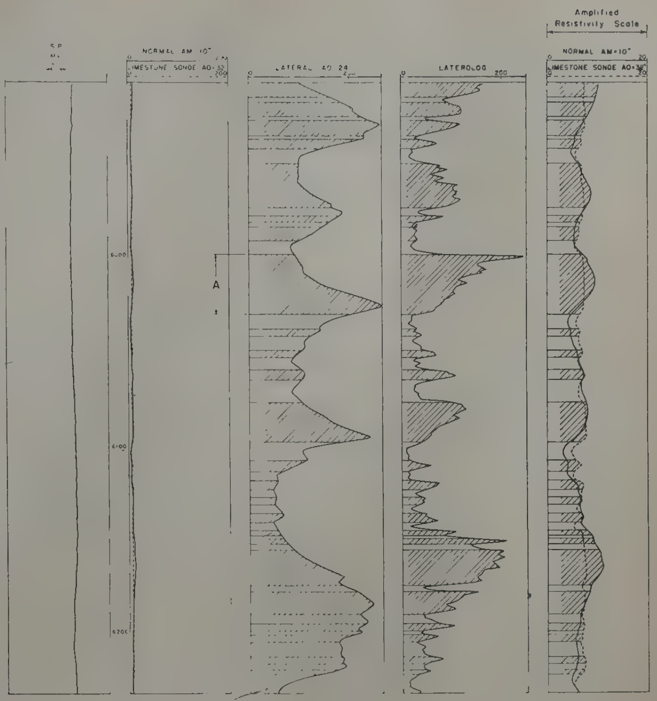

FIG. 12 — EXAMPLE OF LATEROLOG 7, HARD FORMATIONS, HIGH SALINITY MUD (WEST TEXAS). HOLE DIAMETER 7⅞ IN., MUD RESISTIVITY (CORRECTED FOR TEMP.): 0.04 OHM-M. SHADED AREAS ARE TRACED FROM THE LATEROLOG AND CORRESPOND TO THE BEDS WHICH ARE MORE RESISTIVE THAN ADJACENT FORMATIONS.

Although large contrasts of resistivities are observed both on the lateral curve and on the Laterolog, the shapes of the two curves are markedly different. As proven by theoretical and laboratory studies, the Laterolog gives an exact record of the formations, and can be taken as a reference log. The comparison between the lateral curve and the Laterolog curve shows clearly therefore how much the former is distorted by the effect of the mud column, although it gives approximately the value of the average resistivity over large sections of formation. If interval (A) is considered, for example, it appears from the Laterolog curve that the resistivity actually decreases from the top to the bottom. On the lateral curve, a "blind zone" is noticed below the upper boundary, and a maximum is attained near the lower boundary, which gives the erroneous impression that the resistivity increases downward.

Fig. 13 is another example of Laterolog 7 in hard formations drilled with high salinity mud (Kansas). Quite similar remarks can be made regarding this example.

Fig. 14 is a comparative example showing curves recorded with Laterolog 7 and Laterolog 3 in high resistivity formations (Kansas). In this well both Laterologs were recorded in comparatively conductive mud (resistivity, corrected for temperature = 0.2 ohm-m). The conventional logs were recorded after the salt mud had been replaced by fresh mud (resistivity: corrected for temperature, 1.7 ohm-m). In this example, the thicknesses of the beams were respectively 6 in. and 12 in. for the Laterolog 3 and the Laterolog 7, and the overall lengths of both sondes were substantially equal. A few minor details, which are indicated by the Laterolog 3, do not appear as clearly on the curve with the Laterolog 7: these details correspond to thin beds, whose thickness is below 12 in. On the other hand, those thin beds which are more than 12 in. thick give rise to a sharper contrast with the Laterolog 7 than with the Laterolog 3, because in this particular instance the focusing properties of the former system are better than those of the latter one.

CONCLUSION

A new method for the measurement of resistivity in bore holes has been described, which involves a controlled focusing system of electrodes, whereby the current used for the measurement is obliged to flow within a narrow slice of space, the boundaries of which are substantially horizontal up to a great distance from the bore hole. With this method, the effect of the mud column, and of the adjacent formations on the value of the apparent resistivity measured opposite a given bed is practically eliminated, wherever the thickness of the bed is at least equal to the thickness of the sheet of current, *i.e.*, a few inches to a few feet, depending on the distances between the electrodes.

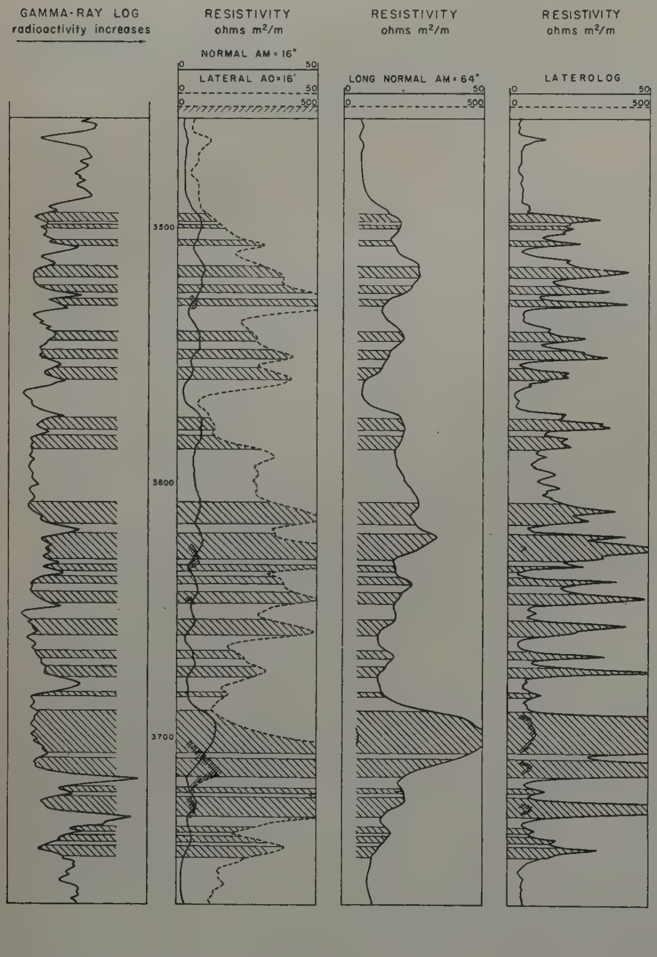

FIG. 13 — EXAMPLE OF LATEROLOG 7, HARD FORMATIONS, HIGH SALINITY MUD (KANSAS). HOLE DIAMETER 7⅞ IN., MUD RESISTIVITY (CORRECTED FOR TEMP.): 0.07 OHM-M. SHADED AREAS ARE TRACED FROM THE LATEROLOG AND CORRESPOND TO THE BEDS WHICH ARE MORE RESISTIVE THAN THE ADJACENT FORMATIONS.

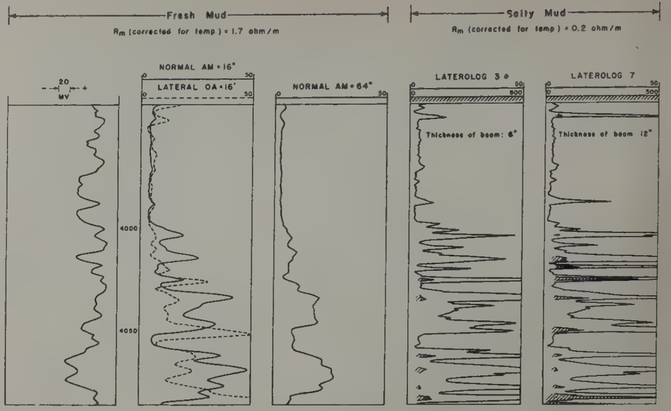

FIG. 14 — COMPARATIVE EXAMPLE OF LATEROLOG 3 AND LATEROLOG 7 IN HARD FORMATIONS (KANSAS).

By means of the Laterolog an accurate and detailed delineation of formations is obtained. The new method furthermore gives values of apparent resistivity which are close to the true values, provided the depth of invasion of mud filtrate is not too deep, and provided the resistivity of the invaded zone is not greater than the resistivity of the uncontaminated part of the bed under survey. This last condition is frequently satisfied in the case of oil-bearing beds, particularly when the salinity of the mud is not much lower than the salinity of the connate water.

Because of its remarkable ability to overcome the by-pass effect of the mud column, the Laterolog has been first introduced in those regions where this effect is particularly detrimental for conventional electrical logs, *i.e.*, where high salinity muds are commonly used. The usefulness of the Laterolog, however, is not limited to this case, but, on the contrary, should extend at least to all hard formation territories.

ACKNOWLEDGMENT

The author wishes to express his appreciation to the numerous engineers of the SWSC who cooperated in the development of the method, both at headquarters and in the field. Special acknowledgment is due to J. Bricaud, who was instrumental in designing the equipment and in conducting the experiments, and to A. Poupon, for his cooperation in the computation of the theoretical charts. The author also wishes to acknowledge the courtesy of the oil companies which provided bore holes for the experiments and which made examples available for the illustrations of this paper.

REFERENCES

1. Schlumberger, C. and M., and Leonardon, E. G.: "Electrical Coring: A Method of Determining Bottom-Hole Data by Electrical Measurements," AIME, Geophysical Prospecting (1934) **110**, 237.

2. Schlumberger, C. and M., and Leonardon, E. G.: "Some Observations Concerning Electrical Measurements in Anisotropic Media and Their Interpretations," *Trans.* AIME (1934) **110,** 159.
3. Martin, M., Murray, G. H., and Gillingham, W. J.: "Determination of the Potential Productivity of Oil-Bearing Formations by Resistivity Measurements," *Geophysics* (July, 1938) **3,** 258.
4. Archie, G. E.: *Trans.* AIME (1942) **146,** 54.
5. Doll, H. G., and Martin, M.: "Recent Developments in Electrical Logging and Auxiliary Methods," *Quarterly of the Colorado School of Mines* (October, 1950) **45,** No. 4A, 48.
6. Doll, H. G., Legrand, J. C., and Stratton, E. F.: "True Resistivity Determination from the Electric Log — Its Application to Log Analysis," *Oil and Gas Jour.* (September 20, 1947) **46,** No. 20.
7. Keller, G. V.: "An Improved Electrode System for Use in Electric Logging," *Producers Monthly* (August, 1949).
8. Keller, G. V.: "Modified Monoelectrodes for Improved Resistivity Logging," *Producers Monthly* (July, 1950).
9. Doll, H. G.: *Trans.* AIME (1949) **186,** 148.

★ ★ ★

DISCUSSION

By B. F. Howell, Jr., Pennsylvania State College, State College, Pa.

The need for a commercially available service offering this logging method has been apparent for some time. It is not a new technique. Similar, though somewhat different, ideas are described in U. S. Patents No. 2,446,303 and No. 2,347,794. The technique described in this paper was developed independently several years ago by the Pennsylvania State College Mineral Industries Experiment Station in cooperation with the Pennsylvania Grade Crude Oil Association, and has been in use by them in making electric logs as a part of their geophysical research program in the Bradford Field of Pennsylvania since 1949. Two preliminary papers by George V. Keller of Pennsylvania State College have been published describing the technique,* and a final report on its theory, applications and limitations will be published soon.

The method is particularly adapted to fields where beds are very thin. In such cases, it appears to give more detailed and more accurate measurements than any other logging system known. It is of particular value where the electric logs are to be used for quantitative calculations of reservoir properties. In the experience of this laboratory it is the only logging method which can be used dependably for this purpose where bed thicknesses are less than one ft.

AUTHOR'S REPLY TO MR. HOWELL

I agree with Howell that the technique of measuring formation resistivities in a bore hole by means of a focused sheet of current is not new. But I wish to remark that the system which constitutes the essential subject of the paper is the Laterolog with point electrodes and automatic control (called Laterolog 7), whereas any previous work, to my knowledge, is related to systems involving elongated electrodes. The use of point electrodes has the advantage of making possible the simultaneous recording of an accurate SP curve — assuming, of course, that there are SP's available, which is not true in high salinity mud — and also of other resistivity curves. Such recording would be particularly difficult to make in the case of a system with elongated electrodes.

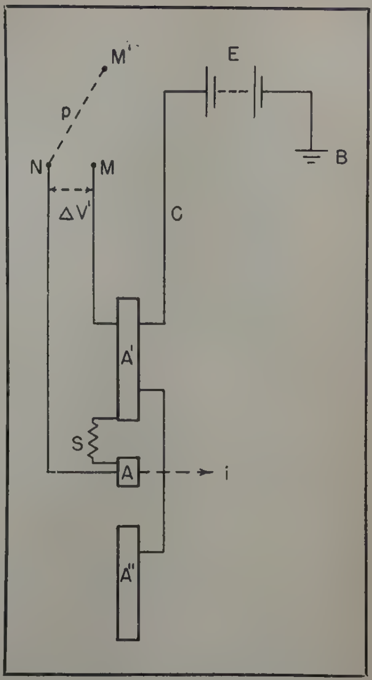

FIG. A — SCHEMATIC CIRCUIT OF GUARDED ELECTRODE AFTER C. SCHLUMBERGER'S DRAWING ON HIS MEMORANDUM OF OCT. 13, 1927.

I would say that I do not know of any reference of other work regarding the Laterolog with point electrodes. As for the use of elongated electrodes, this technique was invented by C. Schlumberger a long time ago, as mentioned in the introduction of my paper, and made public in 1940-41, during a litigation.

At that time, the matter was discussed at length, and, among other documents, the following information was disclosed:

1. A memorandum from C. Schlumberger dated Oct. 13, 1927.* This memorandum first contains a description of a system for measuring the formation resistivity in a bore hole by means of a monoelectrode. Then, the guarded electrode is described, as quoted hereafter:

> "If the formations considered are assumed to be formed of relatively thin horizontal layers, it is necessary to add two end electrodes A' and A'' to the earth connection A, of substantially the same potential as A, and which force the lines of current leaving A to follow a horizontal path, corresponding to a cylindrical distribution of the potentials. The operation will be carried out as shown on the sketch, the current being led by the cable C and the shunt S being placed between A and A'."

Fig. A shows a schematic circuit redrawn from the original drawing made by C. Schlumberger on the hand-written copy of the said memorandum.

2. A log which I recorded in December, 1927, and concerning which I gave some information as follows:**

> ". . . We tried a slight improvement in the method with one electrode in the case of thin layers, by adding to the monoelectrode two guard rings, in accordance with Mr. Schlumberger's memorandum . . . This device was, in par-

---

*Keller, G. V.: "An Improved Electrode System for Use in Electric Logging," *Producers Monthly* (August, 1949); and "Modified Mono-Electrodes for Improved Resistivity Logging," *Producers Monthly* (July, 1950), also published in the proceedings of the Twelfth Technical Conference on Petroleum Production, Pennsylvania State College Mineral Industries Experiment Station Bulletin No. 54.

*U. S. Circuit Court of Appeals — Fifth Circuit — Transcript of Record No. 10063, Halliburton Oil Well Cementing Co. *vs* Schlumberger Well Surveying Corp., 5, 3396.

***Ibid.* 3335.

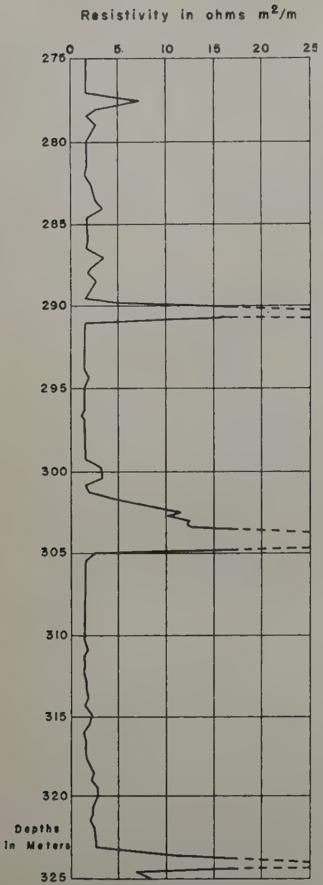

FIG. B—RESISTIVITY LOG WITH GUARDED ELECTRODE IN WELL LOBSANN NO. 47, PECHELBRONN, FRANCE, DEC. 12, 1927.

ticular, tested by me in the Lobsann drill hole, derrick 47, on Dec. 12, 1927, as this drill hole had interesting thin layers (gypsum layers) . . ."

A copy of this log is given in Fig. B.

The device described in the present paper, under the name of Laterolog 3, is an improvement over the guarded electrode, characterized by the fact that it involves the same automatic control system as the Laterolog 7.

Finally, I would add that I am very glad to make references to the interesting articles published by G. V. Keller in the *Producers Monthly* issues of August, 1949, and July, 1950.

DISCUSSION

By Ray L. Braeutigam, Sinclair Oil and Gas Co., Tulsa, Okla., Member AIME

I should like to extend my congratulations to Doll and his associates on their splendid work on this paper — and the Laterolog. Frankly, my curiosity is aroused. From the examples presented in this paper, and from a few actual logs I have observed I think it can be seen that the Laterolog is capable of great detail in recording electrical responses and at the same time considerable depth penetration can be obtained. There is also evidence that bore hole effects can be eliminated to a large extent. Anyone engaged in detail studies of electric logs will welcome this group of desirable characteristics. All in all the prospects seem good for overcoming many of the problems which confront us when analyzing the regular electric logs. It is not too difficult to foresee the possibilities that this Laterolog may become a curve of major importance for both qualitative and quantitative reservoir analysis from the electric log. True, more work remains to be done, but the present outlook gives us good reason to set our expectations rather high.

The apparent resistivities, R_a, which this curve records are primarily R_i plus R_t. It is indicated here that the conversion from R_a to R_t in many cases will be more easily accomplished than is now possible through the standard, or present electric logs. I think it would also be well to emphasize that by varying the $\frac{A_1 \text{ to } A_2}{O_1 \text{ to } O_2}$ spacing ratios, differences in depth penetration can be accomplished. This presents us with another possibility — the recording of two of these curves employing two different spacing ratios to give us R_i to R_t. An accomplishment of this nature could greatly simplify quantitative interpretations from the electric log. After certain recording technique problems are solved, it may even be possible to record these two curves simultaneously.

I feel sure that the oil industry will welcome any further information on the Laterolog, as soon as Doll is prepared to offer it.

DISCUSSION

By M. R. J. Wyllie, Gulf Research and Development Co., Pittsburgh, Pa., Member AIME

Doll is to be congratulated upon the successful development of a logging device which has already done much to dispel the difficulties of logging in highly saline muds and which also contributes so signally to overcoming the thin bed problem. The device is presently not suited to the determination of the true resistivity of permeable conductive beds, but the running of a Laterolog and an induction log should theoretically give rise to sufficient equations to enable even this problem to be overcome. This assumes that some estimate of the depth of mud filtrate invasion can be made.

I should like to ask Doll if he can estimate the extent of the radial investigation of a Laterolog in homogeneous resistant beds. Possibly the radial distance into the formation which contributes 90 per cent of the observed resistivity, as a function of the Laterolog "spacing," might be a suitable way of expressing this result.

AUTHOR'S REPLY TO MESSRS. WYLLIE AND BRAEUTIGAM

I wish to thank Wyllie and Braeutigam for their interesting comments.

I would point out that the extent of the radial investigation of a Laterolog is mostly a function of the overall length of the electrode system. For the Laterolog 7 and in the case of homogeneous formation, the computations show that 90 per cent of the potential drop between the wall of the hole and infinity is obtained within a distance from the axis of the hole which is about three times the length A_1A_2. This result is no longer correct in the case of thin beds, more resistive than the adjacent formations, because, in this case, the sheet of current opens at a shorter distance from the hole than in the case of a very thick formation. This question of the investigation of thin beds with the Laterolog is the subject of intensive laboratory research at the present time.

It is right that the Laterolog is not well suited to the determination of the true resistivity of permeable conductive beds, it being the case, however, only when the resistivity of the bed is appreciably less than the resistivity of the invaded zone. As remarked by both writers, an improvement in the investigation of true resistivity should come from the combination of two resistivity measuring devices with different responses — as for example two Laterologs with different distributions of electrodes, or preferably one Laterolog combined with induction logging.

★ ★ ★

T.P. 3217

THE CALCULATION OF PRESSURE DROP IN THE FLOW OF NATURAL GAS THROUGH PIPE

FRED H. POETTMANN, PHILLIPS PETROLEUM CO., BARTLESVILLE, OKLA., JUNIOR MEMBER AIME

ABSTRACT

An equation has been derived for use in calculating the sandface pressure of flowing gas wells in which the variation of the compressibility factor of the gas with pressure is taken into consideration. This variation due to compressibility has been put into both graphical and tabular form. Comparison of calculated results with field measured results were made on 20 dry gas wells from a given field and 11 distillate wells from different fields. The agreement between calculated and observed results is good.

In addition to their use in the calculation of sandface pressures of flowing wells, the factors can be used in the direct calculation of the static bottom hole pressure of gas wells, the capacity of gas transmission lines, and in the calculation of the theoretical isothermal horsepower necessary to compress a natural gas. Examples demonstrating the use of various equations are given.

INTRODUCTION

Many of the equations used to calculate the sandface pressures of flowing gas wells from well head data do not take into consideration rigorously the deviation of the natural gas from ideal gas behavior. For low pressure wells this error is not serious. For high pressure wells flowing at high rates this error can be serious. Sandface pressures are used to determine the producing capacity of gas wells as shown in the U. S. Bureau of Mines' Monograph 7.[7]

An equation has been derived for use in calculating the sandface pressure of flowing gas wells in which the variation of compressibility of the gas with pressure is taken into consideration. This variation due to compressibility has been put into both graphical and tabular form. In addition to their use in the calculation of sandface pressures, these "factors" can also be used to give a direct solution in the calculation of the static bottom hole pressure of gas wells, the calculation of the capacity of gas transmission lines, and the calculation of the isothermal horsepower necessary to compress a gas.

CALCULATION OF SANDFACE PRESSURE OF FLOWING GAS WELLS

The starting point in the derivation of any specific flow equation is an energy balance on the fluid flowing between any two points in the system. This energy balance based on one pound of flowing fluid is expressed by the well known general flow equation:

$$\int_{P_1}^{P_2} V\,dP + \Delta \mathrm{h} + \frac{\Delta v^2}{2\,g_c} + W_f + W_s = 0 \qquad . \quad . \quad (1)$$

where

V = specific volume of flowing fluid in cu ft/lb
P = pressure in lb per sq ft
Δh = difference in height above datum plane in ft
$\dfrac{\Delta v_2}{2\,g_c}$ = kinetic energy change of one lb of flowing fluid, v equals velocity in ft/sec and $g_c = 32.174$
W_s = Work done by fluid while in flow (similar to shaft work in driving a turbine)
W_f = Energy losses due to the irreversibilities of the flowing fluid

This equation contains no limiting assumptions and can be made the basis of any fluid flow relationship by limitations or substitutions. The energy units are usually expressed in terms of foot-pounds of energy per pound of mass.

Considering the vertical flow of gas through tubing or annulus, the external work W_s done by the gas is zero. Let us also assume that the value of the kinetic energy function is small and can be neglected. Equation (1) is reduced to:

$$\int_{\mathrm{P}_1}^{P_2} V\,dP + \Delta h + W_f = 0 \qquad . \quad . \quad . \quad . \quad . \quad . \quad . \quad (2)$$

The energy losses W_f can be expressed in terms of the well known Fanning equation:

$$W_f = \frac{4\,f\,L\,\bar{v}^2}{2\,g_c D} \qquad . \quad . \quad . \quad . \quad . \quad . \quad . \quad . \quad . \quad . \quad . \quad . \quad . \quad (3)$$

where

L = the integrated average velocity in ft/sec of vertical flow in a uniform flow string $\Delta h = L$
$\bar{v}$ = the integrated average velocity in ft/sec
f = dimensionless correlating function

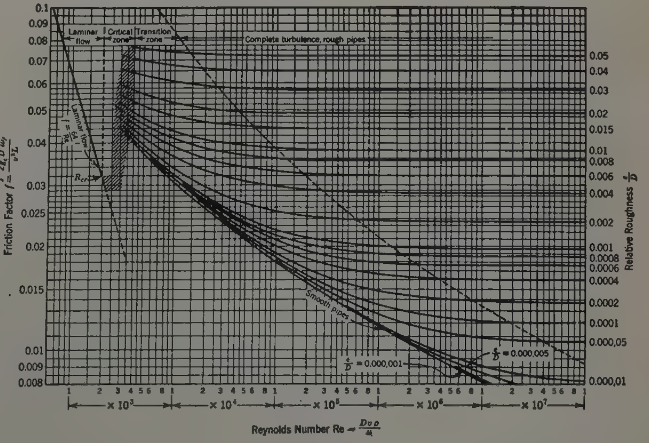

FIG. 1 — FRICTION FACTOR AS A FUNCTION OF REYNOLDS NUMBER WITH RELATIVE ROUGHNESS AS A PARAMETER.[5]

---

[7] References given at end of paper.

Manuscript received in the office of the Petroleum Branch May 23, 1951. Paper presented at the Fall Meeting of the Petroleum Branch in Oklahoma City, Okla., Oct. 3-5, 1951.

Values of f are correlated as functions of the Reynolds number $\frac{D\rho v}{\mu}$ and relative roughness $\frac{\epsilon}{D}$. Care must be taken to avoid confusion as quite often a multiple of four times f is plotted as a function of the Reynolds number and relative roughness ($f' = 4f$).[5]

Substituting Equation (3) in Equation (2) and simplifying gives:

$$L = \frac{\int_{P_2}^{P_1} V dP}{1 + \frac{4 f \bar{v}^2}{2 g_c D}} \quad \ldots\ldots (4)$$

The specific volume V can be expressed in terms of the gas law:

$$V = \frac{ZRT}{MP} \quad \ldots\ldots (5)$$

Where

Z = Compressibility factor
R = Gas constant 1544
T = Temperature °R
M = Molecular weight of gas
P = Pressure, lb/sq ft

Then:

$$\int_{P_2}^{P_1} V dP = \frac{RT}{M} \int_{P_2}^{P_1} \frac{Z}{P} dP \quad \ldots\ldots (6)$$

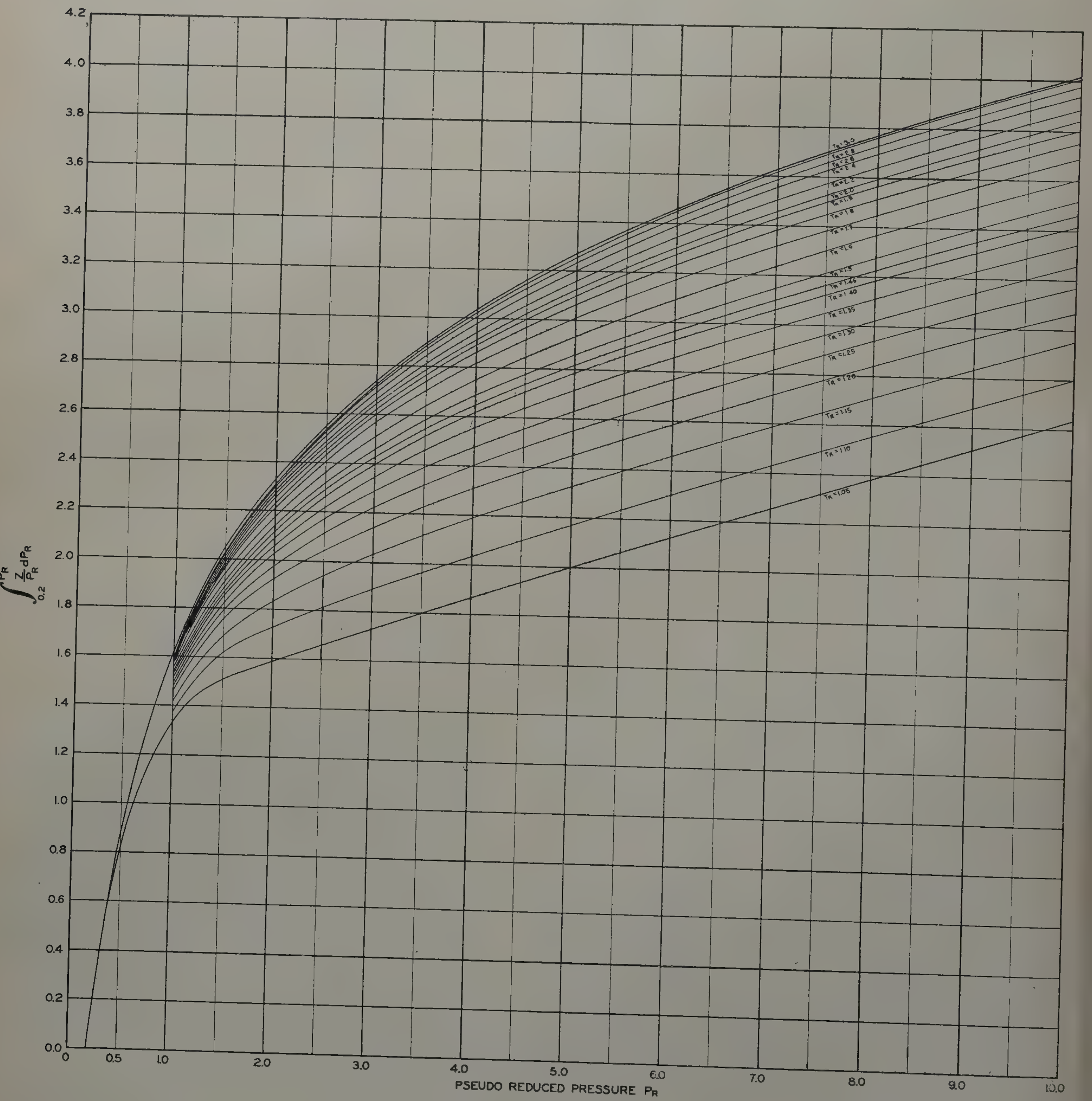

FIG. 2 — VARIATION OF $\int_{0.2}^{P_r} \frac{Z}{P_r} dP_r$ WITH P_r.

Table I

Values of $\int_{0.2}^{P_r} \frac{Z}{P_r}\, dP_r$

Pseudo Reduced Pressure P_r	Pseudo Reduced Temperature T_r 1.05	1.10	1.15	1.20	1.25	1.30	1.35
0.2	0	0	0	0	0	0	0
0.3	0.350	0.350	0.350	0.350	0.350	0.350	0.350
0.4	0.615	0.619	0.623	0.626	0.628	0.630	0.632
0.5	0.805	0.816	0.826	0.834	0.839	0.844	0.848
0.6	0.955	0.971	0.985	0.998	1.011	1.022	1.032
0.7	1.078	1.100	1.124	1.145	1.162	1.178	1.190
0.8	1.175	1.207	1.239	1.264	1.285	1.300	1.313
0.9	1.256	1.300	1.335	1.365	1.386	1.403	1.417
1.0	1.327	1.375	1.420	1.455	1.479	1.500	1.415
1.1	1.380	1.438	1.435	1.528	1.552	1.573	1.591
1.2	1.433	1.500	1.550	1.600	1.625	1.645	1.666
1.3	1.463	1.545	1.602	1.657	1.684	1.709	1.731
1.4	1.492	1.590	1.654	1.713	1.742	1.772	1.795
1.5	1.510	1.620	1.690	1.757	1.791	1.824	1.848
1.6	1.527	1.649	1.726	1.800	1.839	1.875	1.900
1.7	1.544	1.670	1.754	1.834	1.876	1.917	1.943
1.8	1.560	1.690	1.782	1.867	1.913	1.958	1.985
1.9	1.575	1.708	1.808	1.896	1.944	1.993	2.022
2.0	1.590	1.725	1.833	1.924	1.975	2.027	2.059
2.1	1.604	1.743	1.854	1.947	2.003	2.057	2.092
2.2	1.617	1.761	1.876	1.971	2.031	2.086	2.125
2.3	1.631	1.779	1.897	1.994	2.059	2.116	2.157
2.4	1.644	1.797	1.919	2.018	2.087	2.145	2.190
2.5	1.658	1.815	1.940	2.041	2.115	2.175	2.223
2.6	1.672	1.830	1.958	2.061	2.137	2.198	2.249
2.7	1.685	1.845	1.976	2.081	2.159	2.221	2.275
2.8	1.699	1.860	1.994	2.101	2.180	2.245	2.302
2.9	1.712	1.875	2.012	2.121	2.202	2.268	2.328
3.0	1.726	1.890	2.030	2.140	2.224	2.291	2.354
3.1	1.740	1.904	2.046	2.157	2.243	2.311	2.376
3.2	1.754	1.918	2.062	2.175	2.261	2.331	2.397
3.3	1.767	1.932	2.078	2.192	2.280	2.350	2.419
3.4	1.781	1.946	2.094	2.210	2.298	2.370	2.440
3.5	1.795	1.960	2.110	2.227	2.317	2.390	2.462
3.6	1.808	1.974	2.125	2.243	2.333	2.407	2.480
3.7	1.822	1.988	2.140	2.259	2.349	2.424	2.498
3.8	1.835	2.002	2.155	2.275	2.365	2.440	2.517
3.9	1.849	2.016	2.170	2.291	2.381	2.457	2.535
4.0	1.862	2.030	2.186	2.306	2.397	2.474	2.553
4.1	1.875	2.044	2.201	2.321	2.413	2.490	2.569
4.2	1.889	2.058	2.216	2.336	2.429	2.506	2.586
4.3	1.902	2.073	2.230	2.351	2.444	2.523	2.602
4.4	1.916	2.087	2.245	2.366	2.460	2.539	2.619
4.5	1.929	2.101	2.260	2.381	2.476	2.555	2.635
4.6	1.942	2.115	2.274	2.395	2.491	2.570	2.651
4.7	1.955	2.128	2.288	2.409	2.507	2.586	2.666
4.8	1.969	2.142	2.301	2.423	2.522	2.601	2.682
4.9	1.982	2.155	2.315	2.437	2.538	2.617	2.697
5.0	1.995	2.169	2.329	2.451	2.553	2.632	2.713
5.1	2.009	2.183	2.342	2.465	2.567	2.646	2.728
5.2	2.024	2.197	2.355	2.479	2.581	2.661	2.743
5.3	2.038	2.210	2.369	2.492	2.595	2.675	2.758
5.4	2.053	2.224	2.382	2.506	2.609	2.690	2.773
5.5	2.067	2.238	2.395	2.520	2.623	2.704	2.788
5.6	2.079	2.251	2.408	2.533	2.636	2.718	2.801
5.7	2.091	2.264	2.421	2.547	2.650	2.731	2.815
5.8	2.102	2.277	2.435	2.560	2.663	2.745	2.828
5.9	2.114	2.290	2.448	2.574	2.677	2.758	2.842
6.0	2.126	2.303	2.461	2.587	2.690	2.772	2.855
6.1	2.139	2.316	2.474	2.600	2.703	2.785	2.869
6.2	2.152	2.328	2.486	2.612	2.716	2.799	2.882
6.3	2.165	2.341	2.499	2.625	2.729	2.812	2.896
6.4	2.178	2.353	2.511	2.637	2.742	2.826	2.909
6.5	2.191	2.366	2.524	2.650	2.755	2.839	2.923
6.6	2.204	2.379	2.536	2.662	2.768	2.852	2.936
6.7	2.217	2.391	2.548	2.675	2.781	2.864	2.949
6.8	2.229	2.404	2.560	2.687	2.794	2.877	2.963
6.9	2.242	2.416	2.572	2.700	2.807	2.889	2.976
7.0	2.255	2.429	2.584	2.712	2.820	2.902	2.989
7.1	2.268	2.442	2.597	2.724	2.832	2.915	3.002
7.2	2.281	2.454	2.609	2.737	2.844	2.928	3.014
7.3	2.294	2.467	2.622	2.749	2.856	2.941	3.027
7.4	2.307	2.479	2.634	2.762	2.868	2.954	3.039
7.5	2.320	2.492	2.647	2.774	2.880	2.967	3.052
7.6	2.333	2.505	2.660	2.786	2.892	2.979	3.065
7.7	2.346	2.517	2.672	2.799	2.904	2.991	3.077
7.8	2.359	2.530	2.685	2.811	2.916	3.003	3.090
7.9	2.372	2.542	2.697	2.824	2.928	3.015	3.102
8.0	2.385	2.555	2.710	2.836	2.940	3.027	3.115
8.1	2.398	2.568	2.723	2.848	2.952	3.039	3.127
8.2	2.411	2.580	2.736	2.861	2.964	3.051	3.139
8.3	2.424	2.593	2.748	2.873	2.977	3.064	3.151
8.4	2.437	2.605	2.761	2.886	2.989	3.076	3.163
8.5	2.450	2.618	2.774	2.898	3.001	3.088	3.175
8.6	2.462	2.631	2.787	2.910	3.013	3.100	3.187
8.7	2.475	2.643	2.799	2.923	3.025	3.112	3.199
8.8	2.487	2.656	2.812	2.935	3.038	3.124	3.211
8.9	2.500	2.668	2.824	2.948	3.050	3.136	3.223
9.0	2.512	2.681	2.837	2.960	3.062	3.148	3.235
9.1	2.524	2.693	2.849	2.972	3.074	3.159	3.246
9.2	2.536	2.706	2.861	2.985	3.085	3.170	3.257
9.3	2.549	2.718	2.872	2.997	3.097	3.182	3.268
9.4	2.561	2.731	2.884	3.010	3.108	3.193	3.279
9.5	2.573	2.743	2.896	3.022	3.120	3.204	3.290
9.6	2.585	2.755	2.908	3.034	3.131	3.216	3.302
9.7	2.597	2.767	2.919	3.045	3.142	3.228	3.314
9.8	2.610	2.780	2.931	3.057	3.153	3.239	3.326
9.9	2.622	2.792	2.942	3.068	3.164	3.251	3.338
10.0	2.634	2.804	2.954	3.080	3.175	3.263	3.350
10.1	2.646	2.816	2.966	3.092	3.187	3.274	3.361
10.2	2.658	2.828	2.978	3.103	3.199	3.286	3.372
10.3	2.671	2.840	2.989	3.115	3.211	3.297	3.382
10.4	2.683	2.852	3.001	3.126	3.223	3.309	3.393
10.5	2.695	2.864	3.013	3.138	3.235	3.320	3.404
10.6	2.707	2.876	3.025	3.150	3.246	3.332	3.416
10.7	2.719	2.888	3.037	3.161	3.258	3.343	3.428
10.8	2.732	2.900	3.048	3.173	3.269	3.355	3.440
10.9	2.744	2.912	3.060	3.184	3.281	3.366	3.452
11.0	2.756	2.924	3.072	3.196	3.292	3.378	3.464
11.1	2.768	2.936	3.084	3.208	3.304	3.389	3.475
11.2	2.780	2.948	3.096	3.220	3.315	3.401	3.486
11.3	2.793	2.960	3.108	3.231	3.327	3.412	3.497
11.4	2.805	2.972	3.120	3.243	3.338	3.424	3.508
11.5	2.817	2.984	3.132	3.255	3.350	3.435	3.519
11.6	2.829	2.996	3.144	3.267	3.361	3.446	3.529
11.7	2.841	3.008	3.156	3.279	3.373	3.456	3.540
11.8	2.854	3.020	3.168	3.290	3.384	3.467	3.550
11.9	2.866	3.032	3.180	3.302	3.396	3.477	3.561
12.0	2.878	3.044	3.192	3.314	3.407	3.488	3.571

Pseudo Reduced Pressure P_r	Pseudo Reduced Temperature T_r 1.40	1.45	1.50	1.60	1.70	1.80	1.90
0.2	0	0	0	0	0	0	0
0.3	0.350	0.350	0.350	0.350	0.350	0.350	0.350
0.4	0.633	0.634	0.635	0.636	0.637	0.638	0.639
0.5	0.851	0.854	0.856	0.860	0.862	0.864	0.866
0.6	1.040	1.045	1.048	1.049	1.049	1.050	1.050
0.7	1.199	1.203	1.207	1.210	1.211	1.213	1.214
0.8	1.322	1.332	1.340	1.347	1.352	1.357	1.359
0.9	1.429	1.440	1.450	1.462	1.472	1.480	1.485
1.0	1.530	1.541	1.551	1.568	1.580	1.590	1.598
1.1	1.606	1.616	1.631	1.653	1.667	1.676	1.684
1.2	1.682	1.690	1.710	1.737	1.753	1.761	1.770
1.3	1.746	1.758	1.779	1.810	1.828	1.836	1.845
1.4	1.810	1.825	1.847	1.882	1.903	1.911	1.920
1.5	1.867	1.884	1.906	1.938	1.962	1.973	1.984
1.6	1.923	1.943	1.964	1.993	2.021	2.035	2.047
1.7	1.969	1.991	2.012	2.043	2.072	2.089	2.102
1.8	2.014	2.038	2.060	2.093	2.123	2.142	2.157
1.9	2.054	2.079	2.100	2.136	2.165	2.187	2.204
2.0	2.093	2.119	2.140	2.178	2.207	2.231	2.250
2.1	2.126	2.153	2.176	2.215	2.248	2.272	2.292
2.2	2.160	2.187	2.212	2.252	2.288	2.313	2.334
2.3	2.193	2.222	2.249	2.288	2.329	2.354	2.375
2.4	2.227	2.256	2.285	2.325	2.369	2.395	2.417
2.5	2.260	2.290	2.321	2.362	2.410	2.436	2.459
2.6	2.288	2.318	2.350	2.392	2.442	2.469	2.492
2.7	2.316	2.347	2.379	2.423	2.474	2.502	2.525
2.8	2.344	2.375	2.407	2.453	2.506	2.534	2.557
2.9	2.372	2.404	2.436	2.484	2.538	2.567	2.590
3.0	2.400	2.432	2.465	2.514	2.570	2.600	2.623
3.1	2.423	2.455	2.489	2.540	2.597	2.628	2.652
3.2	2.446	2.478	2.512	2.565	2.623	2.657	2.681
3.3	2.469	2.502	2.536	2.591	2.650	2.685	2.709
3.4	2.492	2.525	2.559	2.616	2.676	2.714	2.738
3.5	2.515	2.548	2.583	2.642	2.703	2.742	2.767
3.6	2.535	2.568	2.603	2.664	2.726	2.766	2.792
3.7	2.556	2.588	2.624	2.686	2.748	2.791	2.817
3.8	2.576	2.609	2.644	2.708	2.771	2.815	2.843
3.9	2.597	2.629	2.665	2.730	2.793	2.840	2.868
4.0	2.617	2.649	2.685	2.752	2.816	2.864	2.893
4.1	2.634	2.667	2.703	2.771	2.836	2.885	2.915
4.2	2.651	2.685	2.721	2.789	2.856	2.907	2.937
4.3	2.669	2.702	2.740	2.808	2.875	2.928	2.958
4.4	2.686	2.720	2.758	2.826	2.895	2.950	2.980
4.5	2.703	2.738	2.776	2.845	2.915	2.971	3.002
4.6	2.719	2.754	2.793	2.863	2.933	2.990	3.022
4.7	2.735	2.770	2.810	2.881	2.952	3.009	3.041
4.8	2.752	2.786	2.826	2.899	2.970	3.027	3.061
4.9	2.768	2.802	2.843	2.917	2.989	3.046	3.080
5.0	2.784	2.818	2.860	2.935	3.007	3.065	3.100
5.1	2.799	2.834	2.876	2.952	3.024	3.082	3.118
5.2	2.814	2.850	2.892	2.968	3.042	3.099	3.136
5.3	2.830	2.865	2.908	2.985	3.059	3.117	3.153
5.4	2.845	2.881	2.924	3.001	3.077	3.134	3.171
5.5	2.860	2.897	2.940	3.018	3.094	3.151	3.189

Table I (Continued)

Pseudo Reduced Pressure P_r	Pseudo Reduced Temperature T_r						
	1.40	1.45	1.50	1.60	1.70	1.80	1.90
5.6	2.874	2.912	2.955	3.037	3.110	3.168	3.206
5.7	2.888	2.926	2.970	3.049	3.125	3.185	3.224
5.8	2.902	2.941	2.985	3.065	3.141	3.201	3.241
5.9	2.916	2.955	3.000	3.080	3.156	3.218	3.259
6.0	2.930	2.970	3.015	3.096	3.172	3.235	3.276
6.1	2.943	2.984	3.029	3.111	3.187	3.250	3.292
6.2	2.956	2.997	3.043	3.125	3.202	3.266	3.308
6.3	2.970	3.011	3.056	3.140	3.218	3.281	3.323
6.4	2.983	3.024	3.070	3.154	3.233	3.297	3.339
6.5	2.996	3.038	3.084	3.169	3.248	3.312	3.355
6.6	3.009	3.051	3.098	3.183	3.262	3.327	3.370
6.7	3.022	3.064	3.112	3.197	3.276	3.341	3.385
6.8	3.034	3.077	3.126	3.210	3.291	3.356	3.399
6.9	3.047	3.090	3.140	3.224	3.305	3.370	3.414
7.0	3.060	3.103	3.154	3.238	3.319	3.385	3.429
7.1	3.073	3.116	3.167	3.251	3.332	3.399	3.443
7.2	3.085	3.129	3.180	3.264	3.345	3.413	3.457
7.3	3.098	3.141	3.194	3.278	3.359	3.427	3.472
7.4	3.110	3.154	3.207	3.291	3.372	3.441	3.486
7.5	3.123	3.167	3.220	3.304	3.385	3.455	3.500
7.6	3.135	3.180	3.233	3.317	3.398	3.468	3.514
7.7	3.147	3.192	3.246	3.330	3.411	3.482	3.528
7.8	3.160	3.205	3.260	3.344	3.424	3.495	3.541
7.9	3.172	3.217	3.274	3.357	3.437	3.509	3.555
8.0	3.184	3.230	3.287	3.370	3.450	3.522	3.569
8.1	3.197	3.242	3.299	3.382	3.462	3.534	3.581
8.2	3.209	3.254	3.311	3.394	3.474	3.546	3.594
8.3	3.222	3.266	3.323	3.407	3.486	3.559	3.606
8.4	3.234	3.278	3.335	3.419	3.498	3.571	3.619
8.5	3.247	3.290	3.347	3.431	3.510	3.583	3.631
8.6	3.259	3.302	3.359	3.443	3.523	3.595	3.643
8.7	3.270	3.315	3.370	3.456	3.535	3.607	3.655
8.8	3.283	3.327	3.382	3.468	3.548	3.619	3.666
8.9	3.293	3.340	3.393	3.481	3.560	3.631	3.678
9.0	3.305	3.352	3.405	3.493	3.573	3.643	3.690
9.1	3.317	3.364	3.417	3.505	3.585	3.655	3.702
9.2	3.329	3.376	3.429	3.517	3.597	3.667	3.714
9.3	3.340	3.388	3.440	3.530	3.608	3.678	3.725
9.4	3.352	3.400	3.452	3.542	3.620	3.690	3.737
9.5	3.364	3.412	3.464	3.554	3.632	3.702	3.749
9.6	3.376	3.424	3.475	3.565	3.644	3.713	3.760
9.7	3.388	3.435	3.487	3.576	3.656	3.724	3.772
9.8	3.399	3.447	3.498	3.588	3.667	3.736	3.783
9.9	3.411	3.458	3.510	3.599	3.679	3.747	3.795
10.0	3.423	3.470	3.521	3.610	3.691	3.758	3.806
10.1	3.434	3.482	3.532	3.622	3.702	3.769	3.817
10.2	3.446	3.494	3.544	3.633	3.714	3.780	3.828
10.3	3.457	3.506	3.555	3.645	3.725	3.790	3.840
10.4	3.469	3.518	3.567	3.656	3.737	3.801	3.851
10.5	3.480	3.530	3.578	3.668	3.748	3.812	3.862
10.6	3.492	3.541	3.588	3.679	3.758	3.823	3.873
10.7	3.504	3.552	3.598	3.689	3.769	3.834	3.883
10.8	3.515	3.562	3.609	3.700	3.779	3.844	3.894
10.9	3.527	3.573	3.619	3.710	3.790	3.855	3.904
11.0	3.539	3.584	3.629	3.721	3.800	3.866	3.915
11.1	3.551	3.595	3.639	3.732	3.811	3.877	3.926
11.2	3.562	3.605	3.650	3.743	3.822	3.888	3.937
11.3	3.574	3.616	3.660	3.753	3.832	3.899	3.947
11.4	3.585	3.626	3.671	3.764	3.843	3.910	3.958
11.5	3.597	3.637	3.681	3.775	3.854	3.921	3.969
11.6	3.607	3.648	3.692	3.786	3.865	3.932	3.980
11.7	3.617	3.658	3.702	3.797	3.876	3.943	3.991
11.8	3.628	3.669	3.713	3.808	3.886	3.955	4.003
11.9	3.638	3.679	3.723	3.819	3.897	3.966	4.014
12.0	3.648	3.690	3.734	3.830	3.908	3.977	4.025

Pseudo Reduced Pressure P_r	Pseudo Reduced Temperature T_r					
	2.00	2.20	2.40	2.60	2.80	3.00
0.2	0	0	0	0	0	0
0.3	0.350	0.350	0.350	0.350	0.350	0.350
0.4	0.639	0.640	0.640	0.640	0.640	0.640
0.5	0.867	0.868	0.869	0.869	0.869	0.869
0.6	1.050	1.051	1.051	1.052	1.052	1.052
0.7	1.216	1.218	1.219	1.220	1.220	1.220
0.8	1.360	1.363	1.364	1.364	1.364	1.364
0.9	1.489	1.492	1.494	1.495	1.495	1.495
1.0	1.602	1.607	1.608	1.609	1.610	1.610
1.1	1.691	1.699	1.702	1.706	1.709	1.711
1.2	1.780	1.790	1.795	1.802	1.808	1.812
1.3	1.858	1.868	1.875	1.883	1.890	1.896
1.4	1.935	1.945	1.954	1.964	1.972	1.980
1.5	1.997	2.010	2.019	2.027	2.036	2.045
1.6	2.059	2.074	2.083	2.090	2.100	2.110
1.7	2.116	2.131	2.141	2.148	2.159	2.169
1.8	2.172	2.188	2.198	2.205	2.217	2.227
1.9	2.219	2.237	2.247	2.256	2.267	2.279
2.0	2.265	2.285	2.295	2.307	2.317	2.330
2.1	2.307	2.326	2.337	2.350	2.361	2.375
2.2	2.349	2.366	2.380	2.394	2.404	2.420
2.3	2.391	2.407	2.422	2.437	2.448	2.465
2.4	2.433	2.447	2.465	2.481	2.491	2.510
2.5	2.475	2.488	2.507	2.524	2.535	2.555
2.6	2.508	2.523	2.544	2.562	2.574	2.593
2.7	2.541	2.559	2.581	2.599	2.612	2.630
2.8	2.575	2.594	2.617	2.637	2.651	2.668
2.9	2.608	2.630	2.654	2.674	2.689	2.705
3.0	2.641	2.665	2.691	2.712	2.728	2.743
3.1	2.670	2.694	2.722	2.744	2.759	2.775
3.2	2.700	2.723	2.753	2.775	2.790	2.806
3.3	2.729	2.752	2.783	2.807	2.821	2.838
3.4	2.759	2.781	2.814	2.838	2.852	2.869
3.5	2.788	2.810	2.845	2.870	2.883	2.901
3.6	2.813	2.836	2.872	2.910	2.911	2.929
3.7	2.839	2.862	2.899	2.950	2.938	2.957
3.8	2.864	2.888	2.925	2.990	2.966	2.984
3.9	2.890	2.914	2.952	3.030	2.993	3.012
4.0	2.915	2.940	2.979	3.070	3.021	3.040
4.1	2.938	2.963	3.002	3.081	3.045	3.064
4.2	2.960	2.985	3.025	3.092	3.069	3.088
4.3	2.983	3.008	3.049	3.103	3.094	3.112
4.4	3.005	3.030	3.072	3.114	3.118	3.136
4.5	3.028	3.053	3.095	3.125	3.142	3.160
4.6	3.048	3.074	3.117	3.147	3.164	3.182
4.7	3.068	3.095	3.139	3.168	3.186	3.203
4.8	3.088	3.115	3.161	3.190	3.209	3.225
4.9	3.108	3.136	3.183	3.211	3.231	3.246
5.0	3.128	3.157	3.205	3.233	3.253	3.268
5.1	3.146	3.177	3.225	3.253	3.274	3.288
5.2	3.164	3.196	3.244	3.273	3.295	3.308
5.3	3.182	3.216	3.264	3.294	3.315	3.328
5.4	3.200	3.235	3.283	3.314	3.336	3.348
5.5	3.218	3.255	3.303	3.334	3.357	3.368
5.6	3.235	3.273	3.321	3.352	3.375	3.386
5.7	3.252	3.291	3.339	3.370	3.393	3.405
5.8	3.270	3.309	3.356	3.389	3.412	3.423
5.9	3.287	3.327	3.374	3.407	3.430	3.442
6.0	3.304	3.345	3.392	3.425	3.448	3.460
6.1	3.321	3.362	3.409	3.442	3.466	3.477
6.2	3.337	3.379	3.426	3.459	3.483	3.494
6.3	3.354	3.395	3.443	3.476	3.501	3.511
6.4	3.370	3.412	3.460	3.493	3.518	3.528
6.5	3.387	3.429	3.477	3.510	3.536	3.545
6.6	3.402	3.444	3.493	3.526	3.551	3.561
6.7	3.417	3.459	3.508	3.542	3.567	3.577
6.8	3.432	3.475	3.524	3.557	3.582	3.592
6.9	3.447	3.490	3.539	3.573	3.598	3.608
7.0	3.462	3.505	3.555	3.589	3.613	3.624
7.1	3.477	3.520	3.570	3.604	3.628	3.639
7.2	3.491	3.534	3.584	3.618	3.643	3.654
7.3	3.506	3.549	3.599	3.633	6.659	3.670
7.4	3.520	3.563	3.613	3.647	3.674	3.685
7.5	3.535	3.578	3.628	3.662	3.689	3.700
7.6	3.548	3.591	3.642	3.676	3.703	3.714
7.7	3.562	3.605	3.656	3.690	3.718	3.728
7.8	3.575	3.618	3.670	3.704	3.732	3.742
7.9	3.589	3.632	3.684	3.718	3.747	3.756
8.0	3.602	3.645	3.698	3.732	3.761	3.770
8.1	3.615	3.658	3.711	3.745	3.774	3.783
8.2	3.627	3.671	3.723	3.758	3.788	3.796
8.3	3.640	3.684	3.736	3.771	3.801	3.810
8.4	3.652	3.697	3.748	3.784	3.815	3.823
8.5	3.665	3.710	3.761	3.797	3.828	3.836
8.6	3.677	3.722	3.773	3.810	3.840	3.849
8.7	3.690	3.734	3.786	3.823	3.853	3.862
8.8	3.702	3.746	3.798	3.835	3.865	3.875
8.9	3.715	3.758	3.811	3.848	3.878	3.888
9.0	3.727	3.770	3.823	3.861	3.890	3.901
9.1	3.739	3.782	3.835	3.873	3.902	3.913
9.2	3.750	3.794	3.847	3.885	3.915	3.925
9.3	3.762	3.806	3.859	3.897	3.927	3.938
9.4	3.773	3.818	3.871	3.909	3.940	3.950
9.5	3.785	3.830	3.883	3.921	3.952	3.962
9.6	3.797	3.842	3.895	3.933	3.964	3.974
9.7	3.809	3.854	3.907	3.945	3.976	3.986
9.8	3.820	3.865	3.918	3.957	3.987	3.999
9.9	3.832	3.877	3.930	3.969	3.999	4.011
10.0	3.844	3.889	3.942	3.981	4.011	4.023
10.1	3.855	3.900	3.953	3.992	4.023	4.035
10.2	3.867	3.911	3.965	4.004	4.035	4.046
10.3	3.878	3.923	3.976	4.015	4.046	4.058
10.4	3.890	3.934	3.988	4.027	4.058	4.069
10.5	3.901	3.945	3.999	4.038	4.070	4.081
10.6	3.912	3.956	4.010	4.049	4.081	4.092
10.7	3.923	3.967	4.021	4.060	4.093	4.104
10.8	3.933	3.978	4.031	4.071	4.104	4.115
10.9	3.944	3.989	4.042	4.082	4.116	4.127
11.0	3.955	4.000	4.053	4.093	4.127	4.138
11.1	3.966	4.011	4.064	4.104	4.138	4.149
11.2	3.977	4.022	4.075	4.116	4.150	4.160
11.3	3.988	4.033	4.087	4.127	4.161	4.172
11.4	3.999	4.044	4.098	4.139	4.173	4.183
11.5	4.010	4.055	4.109	4.150	4.184	4.194
11.6	4.022	4.067	4.121	4.161	4.195	4.205
11.7	4.034	4.079	4.132	4.172	4.206	4.216
11.8	4.045	4.090	4.144	4.183	4.217	4.227
11.9	4.057	4.102	4.155	4.194	4.228	4.238
12.0	4.069	4.114	4.167	4.205	4.239	4.249

The absolute temperature T was removed from within the integral sign by assuming a constant average temperature in the flow string. This is not a serious assumption since temperature usually varies as a straight line function of depth.

The compressibility factors for natural gases are correlated as a function of pseudo reduced pressure and temperature.

$$P_r = \frac{P}{P_c} \qquad (7)$$

Table II — Flow String Weights and Sizes

Nominal Size In.	API Rating In.	Weight Per Ft	Outside Diameter In.	Inside Diameter In.
1¼	----	2.3 or 2.4	1.660	1.380
1½	----	2.9 or 2.748	1.900	1.610
2	2⅜	4.00	2.375	2.041
2	2⅜	4.5 or 4.7	2.375	1.995
2½	2⅞	5.897	2.875	2.469
2½	2⅞	6.25 or 6.5	2.875	2.441
3	3½	7.694	3.500	3.068
3	3½	8.50	3.500	3.018
3	3½	9.30	3.500	2.992
3	3½	10.2	3.500	2.922
3½	4	9.26 or 9.50	4.000	3.548
3½	4	11.00	4.000	3.476
4	4½	10.98	4.500	4.026
4	4½	11.75	4.500	3.990
4	4½	12.75	4.500	3.958
4½	4¾	16.00	4.750	4.082
4½	4¾	16.50	4.750	4.070
4¾	5	12.85	5.000	4.500
4¾	5	13.00	5.000	4.494
4¾	5	15.00	5.000	4.408
4¾	5	18.00	5.000	4.276
4¾	5	21.00	5.000	4.154
- ---	5¼	16.00	5.250	4.648
5 3/13	5½	17.00	5.500	4.892
5 3/16	5½	20.00	5.500	4.778
------	5¾	14.00	5.750	5.290
------	5¾	17.00	5.750	5.190
------	5¾	19.50	5.750	5.090
------	5¾	22.50	5.750	4.990
5⅝	6	20.00	6.000	5.350
6¼	6⅝	20.00	6.625	6.049
6¼	6⅝	24.00	6.625	5.921
6¼	6⅝	26.00	6.625	5.855
6¼	6⅝	28.00	6.625	5.791
6¼	6⅝	29.00	6.625	5.761
6⅝	7	20.00	7.000	6.456
6⅝	7	22.00	7.000	6.398
6⅝	7	24.00	7.000	6.336
6⅝	7	26.00	7.000	6.276
6⅝	7	28.00	7.000	6.214
6⅝	7	30.00	7.000	6.154
API	7⅝	34.00	7.625	6.765
7⅝	8	26.00	8.000	7.386
API	8⅛	28.00	8.125	7.485
API	8⅛	32.00	8.125	7.385
API	8⅛	35.50	8.125	7.285
API	8⅛	39.5 or 40.00	8.125	7.185
API	8⅛	42.00	8.125	7.125
8¼	8⅝	24.00	8.625	8.097
8¼	8⅝	28.00	8.625	8.017
8¼	8⅝	32.00	8.625	7.921
8¼	8⅝	32.00	8.625	7.907
8¼	8⅝	36.00	8.625	7.825
8¼	8⅝	38.00	8.625	7.775
8¼	8⅝	43.00	8.625	7.651
8¼	8⅝	44.85	8.625	7.625
8⅝	9	34.00	9.000	8.290
8⅝	9	38.00	9.000	8.196
8⅝	9	40.00	9.000	8.150
8⅝	9	45.00	9.000	8.032
8⅝	9	54.00	9.000	7.812
API	9⅝	43.80	9.625	8.755
API	9⅝	47.20	9.625	8.681
API	9⅝	53.60	9.625	8.535
API	9⅝	57.40	9.625	8.451
9¼	9⅝	36.00	9.625	8.921
9⅝	10	33.00	10.000	9.384
9⅝	10	60.00	10.000	8.780
10	10¾	32.75	10.750	10.192
10	10¾	35.75	10.750	10.136
10	10¾	40.00	10.750	10.054
API	10¾	40.50	10.750	10.050
10	10¾	45.00	10.750	9.960
API	10¾	45.50	10.750	9.950
10	10¾	48.00	10.750	9.902
API	10¾	51.00	10.750	9.850
10	10¾	54.00	10.750	9.784

$$T_r = \frac{T}{T_c} \qquad (8)$$

P_r = Pseudo reduced pressure
T_r = Pseudo reduced temperature
P_c = Pseudo critical pressure
T_c = Pseudo critical temperature in degrees absolute

Differentiating Equation (7)

$$P_c dP_r = dP$$

and substituting Equations (7) and (9) in Equation (6); Equation (6) can be expressed in reduced form.

$$\frac{RT}{M}\int_{P_2}^{P_1}\frac{Z}{P}\,dP = \frac{RT}{M}\int_{P_{r_2}}^{P_{r_1}}\frac{Z}{P_r}\,dP_r \qquad (10)$$

By arbitrarily setting a lower pressure limit of P_r of 0.2 the value of the integral can be evaluated:

$$\int_{P_2}^{P_1}\frac{Z}{P}\,dP = \int_{P_{r_2}}^{P_{r_1}}\frac{Z}{P_r}\,dP_r = \int_{0.2}^{P_{r_1}}\frac{Z}{P_r}\,dP_r - \int_{0.2}^{P_{r_2}}\frac{Z}{P_r}\,dP_r \qquad (11)$$

Values of $\int_{0.2}^{P_r}\frac{Z}{P_r}\,dP_r$ have been determined in both graphical (Fig. 2) and tabular form (Table I) from the compressibility factor chart for natural gases as functions of reduced temperature and pressure.[2] A similar function was used by Fowler[4] in the direct solution for calculating the static bottom hole pressures of gas wells. Fowler's curves were calculated for methane.

The integrated average value of velocity $\bar{v}$ can also be expressed as a function of

$$\int_{P_{r_2}}^{P_{r_1}}\frac{Z}{P_r}\,dP_r$$

$$v = \frac{VW}{A} \qquad (12)$$

where

W = Pounds gas flowing per second
A = Cross sectional area of flow path in sq ft

$$v = \left(\frac{RT}{M}\right)\left(\frac{Z}{P}\right)\left(\frac{W}{A}\right) \qquad (13)$$

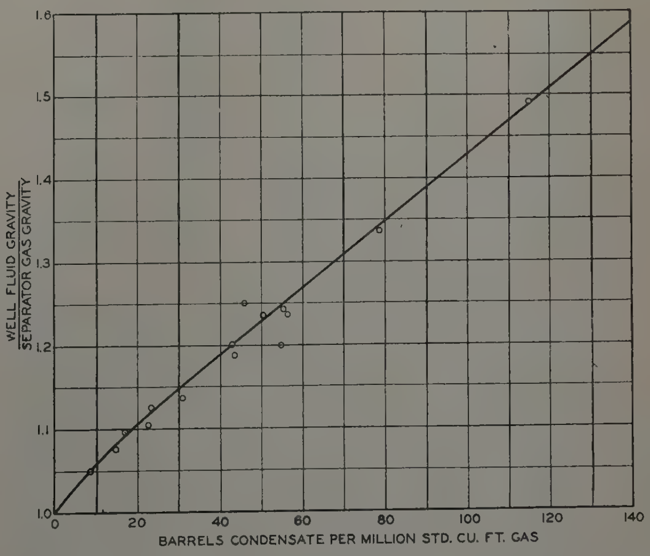

FIG. 3 — GRAVITY RATIO VS STOCK-TANK YIELD OF CONDENSATE.[5]

$$\bar{v} = \frac{\int_{P_2}^{P_1} v\,dP}{P_1 - P_2} = \frac{\left(\frac{W}{A}\right)\left(\frac{RT}{M}\right)\int_{P_{r_2}}^{P_{r_1}} \frac{Z}{P_r}\,dP_r}{\Delta P} \quad . \; . \quad (14)$$

$$\bar{v}^2 = \left(\frac{W}{A}\right)^2 \left(\frac{RT}{M}\right)^2 \frac{1}{(\Delta P)^2} \left[\int_{P_{r_2}}^{P_{r_1}} \frac{Z}{P_r}\,dP_r\right]^2. \quad (15)$$

$$\bar{v}^2 = \left(\frac{W}{A}\right)^2 \left(\frac{RT}{M}\right)^2 \frac{1}{(\Delta P)^2} \left[\int_{0.2}^{P_{r_1}} \frac{Z}{P_r}\,dP_r - \int_{0.2}^{P_{r_2}} \frac{Z}{P_r}\,dP_r\right]^2 \quad . \; . \; . \; . \; . \; . \; . \; . \; . \quad (16)$$

$$\text{Let } L_s = \frac{RT_{\text{avg}}}{M} \left[\int_{0.2}^{P_{r_1}} \frac{Z}{P_r}\,dP_r - \int_{0.2}^{P_{r_2}} \frac{Z}{P_r}\,dP_r\right]. \quad (17)$$

$$L_s = \frac{53.241\,T_{\text{avg}}}{G} \left[\int_{0.2}^{P_{r_1}} \frac{Z}{P_r}\,dP_r - \int_{0.2}^{P_{r_2}} \frac{Z}{P_r}\,dP_r\right]. \quad (18)$$

Where: G equals gas gravity (air = 1)
Then substituting Equations (10), (16) and (18) in Equation (4):

$$L = \frac{L_s}{1 + \frac{4f}{2\,g_c D}\left(\frac{W}{A}\right)^2 \frac{(L_s)^2}{(\Delta P)^2}} \quad . \; . \; . \quad (19)$$

Further simplification results in:

$$L = \frac{L_s}{1 + 3.8085 \times 10^{-6}\,\frac{f\,Q^2\,G^2}{D^5}\,\frac{(L_s)^2}{(\Delta P)^2}} \quad . \; . \; . \quad (20)$$

Where:

L = depth in ft
Q = MMcf/D of gas at 14.65 and 60°F
D = diameter of tubing in ft
$\Delta P = P_1 - P_2 = P_c\ (\Delta P_r)$ in psia
G = gas gravity (air = 1)

Thus an expression relating the difference in elevation L between any two pressure limits P_2 and P_1 as a function of flow rate, gas gravity, tubing diameter, average flowing temperature, and correlating factor f is available.

Values of f can be obtained from Fig. 1, which is a plot of $f' = 4f$, as a function of Reynolds number and relative roughness. Values of $\int_{0.2}^{P_r} \frac{Z}{P_r}\,dP_r$ can be obtained from Fig. 2 or Table I, whichever is most convenient. The increments of pseudo reduced pressure and temperature of Table I are such that linear interpolation may be used. Table II lists the pertinent data on the various flow string sizes.

The literature contains many equations for the determination of the value of f. At present it appears that one of the best ways to determine f is by the relative roughness method.[5] To use the relative roughness method it is necessary to establish a value for the absolute roughness of the pipe wall. This can best be accomplished by an analysis of experimental flow data. Cullender and Binckley[3] have shown from data presented in U. S. Bureau of Mines Monograph 6,[9] that an absolute roughness of 0.0006 in. is satisfactory for clean pipe.

The factor f can be expressed as a power function of the Reynolds number and pipe diameter for a given absolute

Table III — Comparison of Observed Data and Calculated Results, Flow of Gas in Vertical Pipe

Part A — Dry Gas Wells

Test No.	Tubing Size In. Nominal	Tubing Size In. ID	Q MMcf/D	L Ft	T_{avg} °F	Specific Gravity of Flowing Fluid	Tubing Pressure P_w Psia	Sand Face Pressure P_s Observed Psia	Sand Face Pressure P_s Calculated Psia	Deviation Psia	Deviation Per Cent
1	2½	2.441	5.109	5190	92	0.600	1253.0	1495	1490	– 5	–0.334
2	2½	2.441	9.514	5190	94	0.600	1112.4	1478	1483	+ 5	+0.338
3	2½	2.441	14.068	5190	96	0.600	832.0	1475	1500	+25	+1.695
4	2½	2.441	6.299	4922	91	0.605	1297.4	1593	1554	–39	–2.448
5	2½	2.441	5.695	5195	92	0.595	1210.0	1462	1455	– 7	–0.479
6	2½	2.441	9.298	5195	93	0.595	1084.4	1452	1451	– 1	–0.069
7	2½	2.441	13.176	5195	94	0.595	802.4	1438	1412	–26	–1.808
8	2½	2.441	4.827	4750	93	0.602	1188.4	1411	1392	–19	–1.346
9	2½	2.441	8.025	4750	93	0.602	1099.4	1411	1389	–22	–1.559
10	2½	2.441	13.680	4750	95	0.602	764.4	1401	1382	–19	–1.356
11	2½	2.441	2.432	4764	90	0.599	1102.4	1260	1261	+ 1	+0.079
12	2½	2.441	4.127	4764	90	0.599	1043.4	1216	1236	+20	+1.618
13	2½	2.441	6.167	4764	90	0.599	923.4	1156	1148	– 8	–0.692
14	2½	2.441	3.810	5242	93	0.591	1433.4	1690	1654	–36	–2.130
15	2½	2.441	5.379	5242	93	0.591	1302.4	1579	1550	–29	–1.837
16	2½	2.441	7.663	5195	92	0.595	919.4	1257	1220	–37	–2.943
17	2½	2.441	10.598	5195	92	0.595	680.4	1247	1173	–76	–6.308
18	2½	2.441	11.841	5195	92	0.595	650.4	1247	1227	–20	–1.604
19	2½	2.441	4.384	5195	92	0.595	1028.4	1240	1223	–17	–1.371
20	2½	2.441	6.585	5195	92	0.595	966.4	1230	1226	– 4	–0.325

Part B — Distillate Wells

Test No.	Tubing Size In. Nominal	Tubing Size In. ID	Q MMcf/D	L Ft	T_{avg} °F	Gas/Oil Ratio MCF/Bbl	°API Gravity Liquid	Specific Gravity of Flowing Fluid	P_w Psia	P_s Observed Psia	P_s Calculated Psia	Deviation Psia	Deviation Per Cent
21	2.0	1.995	4.461	5529	122.5	341.2	47.7	0.7083	1873	2266	2307	+41	+1.809
22	2.0	1.995	3.765	5529	122.5	341.2	47.7	0.7083	1951(?)	2276	2370	+94	+4.130
23	2.0	1.995	3.055	5529	121.0	341.2	47.7	0.7083	1953	2287	2348	+61	+2.667
24	2.0	1.995	2.675	9110	157.5	40.7	54.0	0.7163	1979	2688	2593	–95	–3.534
25	2½	2.441	4.803	8226	164.0	65.8	51.3	0.761	2272	2893	2944	+51	+1.763
26	2½	2.441	3.207	8226	161.0	65.8	51.3	0.761	2320	2902	2970	+68	+2.343
27	2½	2.441	1.338	8226	160.0	65.8	51.3	0.761	2373	2911	3003	+92	+3.160
28	2.0	1.995	5.153	5790	121.5	787.89	35.3	0.604	2122	2565	2556	– 9	–0.351
29	2.0	1.995	3.522	5790	119.0	787.89	35.3	0.604	2202	2593	2580	–13	–0.501
30	2.0	1.995	2.760	5790	118.5	787.89	35.3	0.604	2232	2601	2593	– 8	–0.308
31	2.0	1.995	2.046	5790	117.5	787.89	35.3	0.604	2260	2605	2610	+ 5	+0.192

roughness.[3] For an absolute roughness of 0.0006 in. and in terms of Q, G, D and viscosity μ:

$$f = \frac{7.7302 \times 10^{-3}\ Q^{-0.065}\ D^{-0.058}\ G^{-0.065}}{\mu^{-0.065}} \quad . \quad . \quad . \quad . \quad (21)$$

Substituting Equation (21) into Equation (20), gives:

$$L = \frac{L_s}{1 + 2.94409 \times 10^{-8}\ \dfrac{Q^{1.935}\ G^{1.935}\ L_s^{2}}{D^{5.058}\ \mu^{-0.065}\ (\triangle P)^{2}}} \quad . \quad . \quad . \quad (22)$$

where μ = viscosity in pounds per foot second.

Comparison with Field Data

In order to present an idea of the deviation of the calculated results from field measurements for a given set of conditions, Table III was prepared. Comparisons were made on 20 flowing conditions in dry gas wells from a given field and 11 flowing conditions in distillate wells from different fields. Equation (22) was used to calculate the pressure traverses. Only sandface pressures were compared. The deviations shown reflect to a considerable degree the accuracy of the data used in making the calculations and the accuracy of the recorded flowing pressures, not the accuracy of the mathematical development. In the cases of the dry gas wells, for example, most of the deviations are negative, indicating that perhaps for the tubing in this field, the absolute roughness and thus the factor f were slightly underestimated. However, the agreement between the calculated and observed results is good.

The application of Equation (20) or (22) to distillate wells may be somewhat limited by the amount of liquid in the flow string. However, it is of interest to note that for a ratio as low as 40,000 cu ft per bbl, reasonable agreement is still obtained. The higher the gas/oil ratio the more accurate one can expect the calculated results to be. It is likely that the procedures can be applied to wells with ratios considerably lower than 40,000 cu ft per bbl without appreciable error in the computed results. Table III also summarizes the data used to calculate the pressure traverses.

The gas gravity G of Equation (20) or (22) can be calculated from the composition of the flow stream or experimentally measured. In the case of distillate wells, if the composition is not available, gas gravity may be calculated from the following equation:[6]

$$G = \frac{G_g + \dfrac{4{,}591\ G_e}{R_a}}{1 + \dfrac{1{,}123}{R_a}} \quad . \quad . \quad . \quad . \quad . \quad . \quad . \quad . \quad . \quad . \quad (23)$$

where:

G_g = Separator gas gravity
G_e = Specific gravity of condensate
R_a = gas/liquid ratio, cu ft/bbl

Rzasa and Katz[8] developed a simple correlation based on field data, Fig. 3, from which can be estimated the well fluid gravity of distillate wells, if Equation (23) is not used.

The pseudo (molal average) critical temperature and pressure of the gas may be calculated from the gas composition. If composition is not available, Fig. 4 may be used to estimate the pseudo critical temperature and pressure.[2]

The viscosity of the natural gas may be obtained from Figs. 5 and 6.[1]

In the case of flow through the annulus, D^5 of Equation (20) must be replaced by[3]

$$D^5 = (D_1 + D_2)^2\ (D_1 - D_2)^3 \quad . \quad . \quad . \quad . \quad . \quad . \quad . \quad . \quad (24)$$

and $D^{5.058}$ of Equation (22) by[3]

$$D^{5.058} = (D_1 + D_2)^{1.935}\ (D_1 - D_2)^{3.123} \quad . \quad . \quad . \quad . \quad . \quad (25)$$

Where D_1 = Internal diameter of casing in ft
D_2 = External diameter of tubing in ft

The use of Equation (22) is perhaps best explained by a numerical example.

Example: Calculate the sandface pressure of gas-distillate well from the following surface measurements:

Q = 5.153 MMcf/D
D = 1.995 in. = 0.1663 ft
Gravity separator gas = 0.600
Gravity distillate = 35.3 °API
Separator gas/liquid ratio = 787.89 Mcf/bbl
Depth of well = 5,790 ft
Bottom hole temperature = 160°F
Well head flow temperature = 83°F
Tubing pressure = 2,122 psia
Viscosity = 0.0185 centipoise (Figs. 5 and 6)
= 1.2432×10^{-5} lb/ft-sec

$$\text{Average flow string temperature} = \frac{160 + 83}{2} = 121.5°\text{F}$$
$$= 581.5°\text{R}$$

Gas gravity of flow stream from Equation (23)

$$G = \frac{G_g + \dfrac{4{,}591\ G_e}{R_a}}{1 + \dfrac{1{,}123}{R_a}}$$

$$G = \frac{0.600 + \dfrac{(4{,}591)\ (0.8483)}{787{,}890}}{1 + \dfrac{1{,}123}{787{,}890}}$$

$$G = 0.604$$

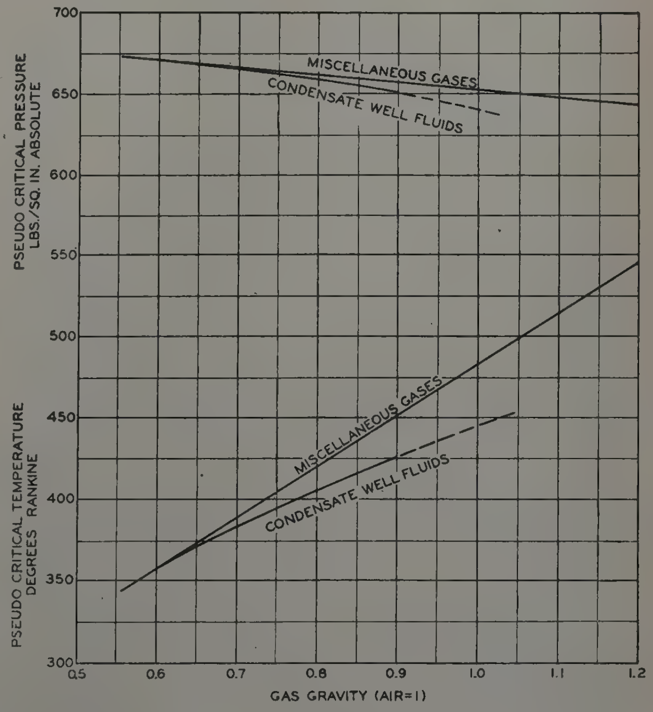

FIG. 4 — PSEUDO CRITICAL PROPERTIES OF CONDENSATE WELL FLUIDS AND MISCELLANEOUS NATURAL GASES.[2]

Pseudo critical temperature and pressure from Fig. 4

$P_c = 671$ psia

$T_c = 360°\text{R}$

Pseudo reduced temperature

$$T_r = \frac{T}{T_c} = \frac{581.5}{360.0} = 1.615$$

Calculate L_s for various downhole pressures

1	2	3	4	5
P	P_r	$\int_{0.2}^{P_r} \frac{Z}{P_r}\,dP_r$	$\int_{.2}^{P_{r_1}} \frac{Z}{P_r}\,dP_r - \int_{.2}^{P_{r_2}} \frac{Z}{P_r}\,dP_r$	L_s (Equation 18)
2122	3.162	2.564	—	—
2300	3.428	2.632	0.068	3483.7
2600	3.875	2.734	0.170	8709.7

Column 1 shows the various downhole pressures for which L_s is to be calculated. Column 2 is the pseudo reduced pressure and is column 1 divided by 671 psia. Column 3 was obtained from Table I by interpolation. Column 4 is the value of $\int_{P_{r_2}}^{P_{r_1}} \frac{Z}{P_r}\,dP_r$ between the downhole pressure and the tubing pressure. Column 5, L_s is calculated from Equation (18).

The various depths L corresponding to the pressures P of column 1 are then calculated from Equation (22).

P	L
2,122	0
2,300	2,445
2,600	6,365

Fig. 7 shows a plot of this pressure traverse. At a depth of 5,790 ft the sandface pressure is 2,556 psia as obtained by plotting the traverse on large scale graph paper.

CALCULATION OF STATIC BOTTOM-HOLE PRESSURES OF GAS WELLS

Fowler[4] suggested the use of factors similar to those listed in Table I or plotted on Fig. 2 in a method involving the direct solution of the static bottom hole pressures of gas wells.

For zero flow rate ($Q = 0$) Equations (20) and (22) reduce to:

$$L = L_s = \frac{53.241\ T_{avg}}{G}\left[\int_{0.2}^{P_{r_1}} \frac{Z}{P_r}\,dP_r - \int_{0.2}^{P_{r_2}} \frac{Z}{P_r}\,dP_r\right] \quad . . . . \quad (26)$$

By rearranging.

$$\int_{0.2}^{P_{r_1}} \frac{Z}{P_r}\,dP_r = \frac{LG}{53.241\ T_{avg}} + \int_{0.2}^{P_{r_2}} \frac{Z}{P_r}\,dP_r \quad . \quad (27)$$

Equation (27) is a direct solution for the static bottom hole pressure.

The factor corresponding to tubing pressure $\int_{0.2}^{P_{r_2}} \frac{Z}{P_r}\,dP_r$ can be obtained directly from Table I or Fig. 2, $\frac{LG}{53.241\ T_{avg}}$ can be evaluated directly, the sum of the two then gives the factor $\int_{0.2}^{P_{r_1}} \frac{Z}{P_r}\,dP_r$ corresponding to the bottom hole pressure. The pseudo reduced bottom hole pressure can be ob-

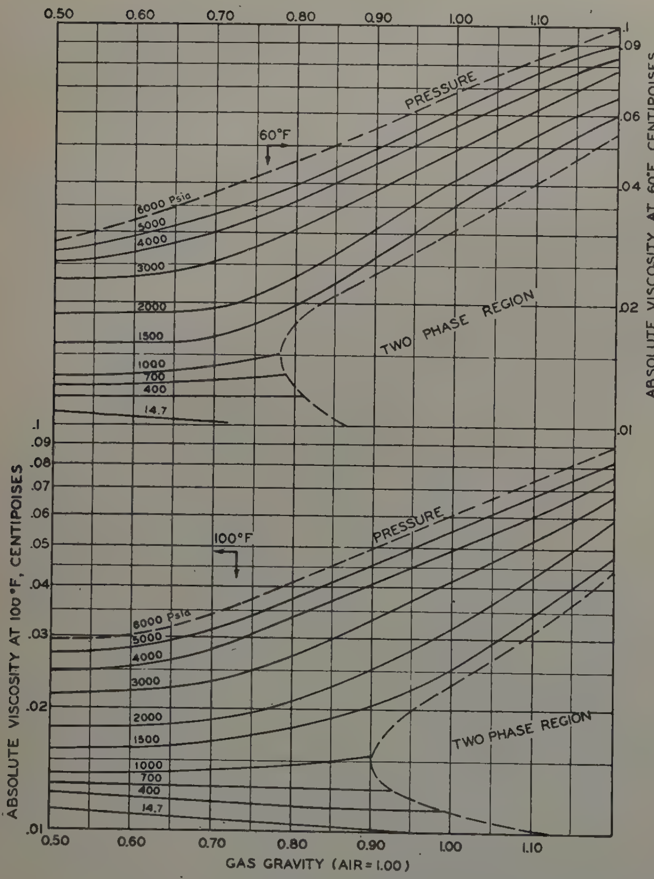

FIG. 5 — VISCOSITY OF NATURAL GAS.[1]

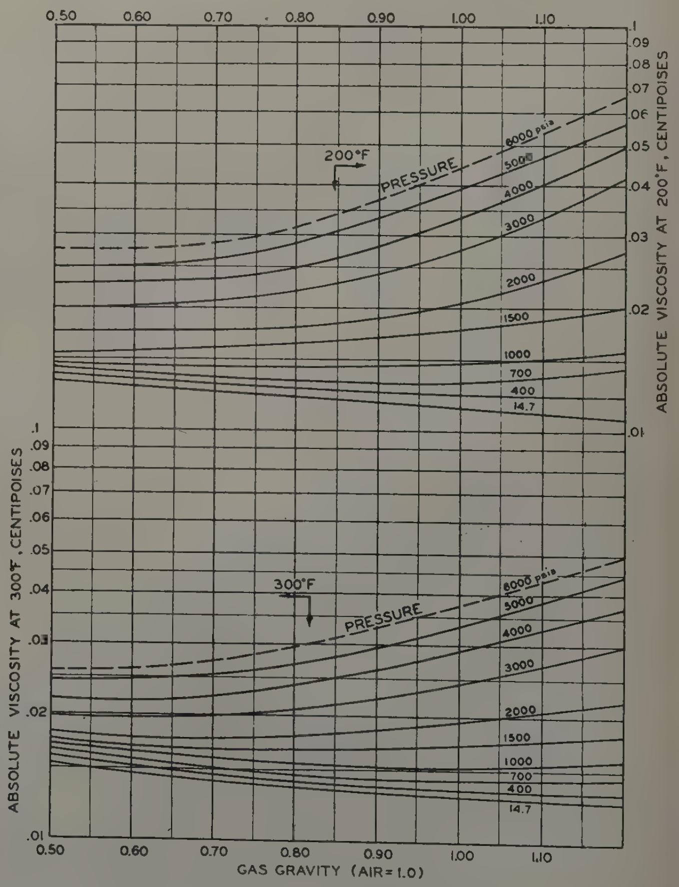

FIG. 6 — VISCOSITY OF NATURAL GAS.[1]

tained from Table I or Fig. 2. Multiplying this pseudo reduced pressure by the pseudo critical pressure gives the static bottom hole pressure.

Example: Calculate the static bottom hole pressure of a gas well having a depth of 5,790 ft. The gas gravity is 0.600 and the pressure at the well head is 2,300 psia. The average temperature of the flow string is 117°F.

From Fig. 4

$$T_c = 358°R$$

$$P_c = 672 \text{ psia}$$

$$T_r = \frac{T}{T_c} = \frac{117 + 460}{358} = 1.612$$

$$P_{r_2} = \frac{2300}{672} = 3.423$$

From Table I

$$\int_{0.2}^{P_{r_2}} \frac{Z}{P_r}\, dP_r = 2.629$$

$$\frac{LG}{53.241\ T_{avg}} = \frac{(5{,}790)\ (.600)}{(53.241)\ (577)} = 0.113$$

Therefore from Equation (27):

$$\int_{0.2}^{P_{r_1}} \frac{Z}{P_r}\, dP_r = 2.629 + 0.113 = 2.742$$

From Table I 2.742 at a T_r of 1.612 corresponds to a P_r of 3.918

$$P = (3.918)\ (672) = 2.633 \text{ psia}$$

HORIZONTAL FLOW OF GAS

Equations for use in estimating the capacity of pipe lines quite often disregard the deviation of the natural gas from ideal gas behavior. For low pressures this error is not serious. For high pressures, this deviation from ideality must be taken into consideration. An equation can be derived which makes use of the factors tabulated in Table I or of Fig. 2.

Starting with the general flow equation and assuming no difference in elevation ($\triangle h = 0$), no external work ($W_s = 0$) and a negligible kinetic energy term, then:

$$\int_{P_1}^{P_2} V dP + W_f = 0 \quad \ldots\ldots\ldots\ldots \quad (28)$$

It has been shown in the foregoing sections that:

$$\int_{P_2}^{P_1} V dP = \frac{53.241\ T_{avg}}{G} \left[\int_{0.2}^{P_{r_1}} \frac{Z}{P_r}\, dP_r - \int_{0.2}^{P_{r_2}} \frac{Z}{P_r}\, dP_r \right] \quad \ldots\ldots\ldots\ldots \quad (29)$$

and

$$W_f = \frac{4fL}{2\ g_c D} \left(\frac{53.241\ T_{avg}}{G} \right)^2 \left[\int_{0.2}^{P_{r_1}} \frac{Z}{P_r}\, dP_r - \int_{0.2}^{P_{r_2}} \frac{Z}{P_r}\, dP_r \right]^2 \left(\frac{W}{A} \right)^2 \frac{1}{(\triangle P)^2} \quad . \quad (30)$$

by substitution of Equations (29) and (30) into Equation (28) and division by Equation (29)

$$1 - \frac{4fL}{2\ g_c D} \left(\frac{53.241\ T_{avg}}{G} \right) \left[\int_{0.2}^{P_{r_1}} \frac{Z}{P_r}\, dP_r - \int_{0.2}^{P_{r_2}} \frac{Z}{P_r}\, dP_r \right] \frac{1}{(\triangle P)^2} \left(\frac{W}{A} \right)^2 = 0 \quad . \quad (31)$$

Simplification of Equation (31) then results in:

$$Q = \left[\frac{4{,}976.18\ D^5\ (\triangle P)^2}{fL\ T_{avg}\ G \left[\int_{0.2}^{P_{r_1}} \frac{Z}{P_r}\, dP_r - \int_{0.2}^{P_{r_2}} \frac{Z}{P_r}\, dP_r \right]} \right]^{0.5} \quad . \quad (32)$$

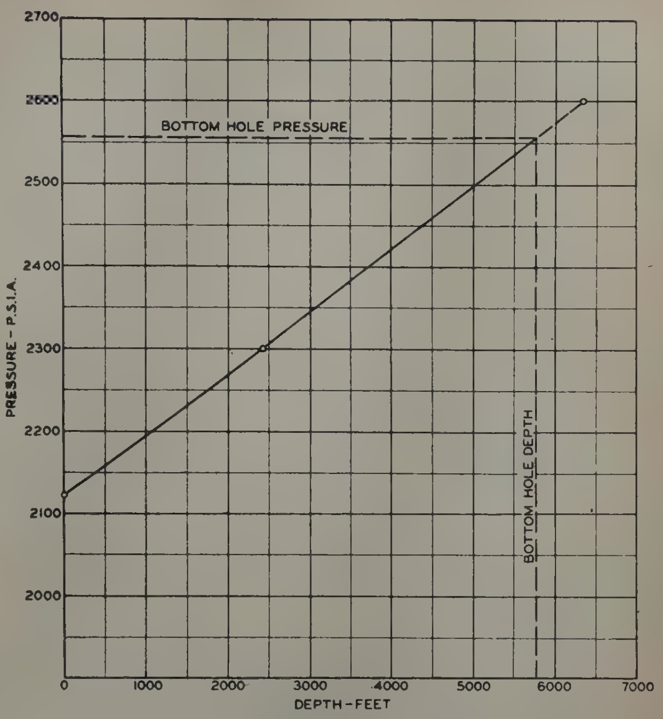

FIG. 7 — PRESSURE TRAVERSE OF FLOWING GAS WELL.

where

Q = MMcf/D of gas at 14.65 and 60°F
D = Diameter of tubing in ft
$\triangle P = P_1 - P_2$ in psia
G = Gas gravity (air = 1)
T_{avg} = Average flowing temperature
L = Length of line in ft

Expression of the f factor in terms of Q, G, D, and μ, Equation (21), and substitution into Equation (32), results in:

$$Q = \left[\frac{6.43732 \text{ x } 10^5\ D^{5.058}\ (\triangle P)^2}{L\ T_{avg}\ G^{+0.935}\ \mu^{+0.065} \left[\int_{0.2}^{P_{r_1}} \frac{Z}{P_r}\, dP_r - \int_{0.2}^{P_{r_2}} \frac{Z}{P_r}\, dP_r \right]} \right]^{0.5168} \quad (33)$$

where μ = viscosity in lb/ft-sec

Example: Calculate the capacity of a pipe line consisting of 50 miles of 26 in. OD pipe having an ID of 25.44 in. The natural gas has a specific gravity of 0.6124. The temperature of the flowing gas is 60°F. The upstream pressure is 825 psia and the downstream pressure 565 psia.

The analysis of the gas is:

Component	Mole Per Cent
CO_2	0.90
N_2	1.38
CH_4	91.75
C_2H_6	4.31
C_3H_8	1.08
iC_4H_{10}	0.17
nC_4H_{10}	0.21
iC_5H_{12}	0.02
nC_5H_{12}	0.02
C_6H_{14}	0.11
C_7H_{16} plus	0.05
	100.00

Pseudo critical temperature, 358.4°R
Pseudo critical pressure, 674.0 psia
Pseudo reduced temperature, 1.45

$$\text{Pseudo reduced pressures, } P_{r_1} = \frac{825}{674} = 1.224$$

$$P_{r_2} = \frac{565}{674} = 0.838$$

From Table I or Fig. 2

$$\int_{0.2}^{P_{r_1}} \frac{Z}{P_r}\, dP_r = 1.706 \text{ at } P_{r_1}$$

$$\int_{0.2}^{P_{r_2}} \frac{Z}{P_r}\, dP_r = 1.373 \text{ at } P_{r_2}$$

From Fig. 5 at average pressure

$\mu = 0.0135$ centipoise

$\mu = 9.072 \times 10^{-6}$ lb/ft sec

From Equation (33)

$$Q = \left[\frac{(6.43732 \times 10^5)\ (2.12)^{5.058}\ (260)^2}{(5280)\ (50)\ (520)\ (0.6124^{+0.935}\ (9.072 \times 10^{-6})^{+0.065}\ (1.706-1.373)}\right]^{0.5168}$$

$$Q = (14.32489 \times 10^4)^{0.5168}$$

$$Q = 462.0 \text{ MMcf/D}$$

CALCULATION OF ISOTHERMAL HORSEPOWER REQUIRED TO COMPRESS A NATURAL GAS

Quite often it is necessary to calculate the isothermal horsepower required to compress a natural gas taking into consideration the deviation from ideal gas behavior. Starting with the general flow equation, for any compression operation, there is no difference in elevation ($\triangle h = 0$), there is a negligible kinetic energy term $\left(\frac{\Delta v^2}{2g_c} = 0\right)$ and no energy loss, ($W_f = 0$), then:

$$\int_{P_1}^{P_2} V dP + W_s = 0$$

$$W_s = \int_{P_2}^{P_1} V dP$$

Since by definition, W_s is work done by the fluid while in flow, work done on the fluid by an external source would then be numerically negative.

From Equation (29)

$$W_s = \int_{P_2}^{P_1} V dP = \frac{53.241\ T}{G}\left[\int_{0.2}^{P_{r_1}} \frac{Z}{P_r}\, dP_r - \int_{0.2}^{P_{r_2}} \frac{Z}{P_r}\, dP_r\right]$$

Expressing the work W_s in terms of theoretical isothermal horsepower required to compress 1,000,000 standard cu ft of gas per day (60°F, 14.65 psia), results in:

$$HP = 0.08531\ T\left[\int_{0.2}^{P_{r_1}} \frac{Z}{P_r}\, dP_r - \int_{0.2}^{P_{r_2}} \frac{Z}{P_r}\, dP_r\right] \quad . \quad . \quad (34)$$

Example: Calculate the theoretical isothermal horsepower necessary to compress 1,000,000 standard cu ft per day of a natural gas of 0.600 gravity (air = 1) from 200 to 1,000 psia at 100°F.

From Fig. 4

$T_c = 358°\text{R}$

$P_c = 671$ psia

$$T_r = \frac{100 + 460}{358} = 1.564$$

$$P_{r_1} = \frac{200}{671} = 0.298$$

$$P_{r_2} = \frac{1000}{671} = 1.490$$

From Table I or Fig. 2

$$\int_{0.2}^{0.298} \frac{Z}{P_r}\, dP_r = 0.343$$

$$\int_{0.2}^{1.490} \frac{Z}{P_r}\, dP_r = 1.920$$

From Equation (34)

$$HP = 0.08531\ T\left[\int_{0.2}^{P_{r_1}} \frac{Z}{P_r}\, dP_r - \int_{0.2}^{P_{r_2}} \frac{Z}{P}\, dP_r\right]$$

$HP = 0.08531\ (560)\ (0.343-1.920)$

$HP = -75.34$ hp per 1,000,000 standard cu ft of gas per day.

In other words, the theoretical isothermal horsepower necessary to compress 1,000,000 standard cu ft of gas per day is 75.34 hp.

CONCLUSION

Equations have been derived for the calculation of the sandface pressure of flowing gas wells, the static bottom hole pressure of gas wells, and the capacity of gas transmission lines, which take into consideration the variation of the compressibility factor of the gas with pressure. This variation with pressure has been put into both graphical and tabular form. These factors can also be used to calculate rigorously the theoretical isothermal horsepower necessary to compress a natural gas. Examples demonstrating the use of the various equations are given. In the case of the sandface pressure of flowing gas wells, comparison of the calculated results with field measured results are made for 31 different flowing conditions, for 11 dry gas and distillate wells. The agreement between observed and calculated results is good.

ACKNOWLEDGMENT

The author wishes to acknowledge his indebtedness to M. H. Cullender and C. W. Binckley of the Natural Gas Department of the Phillips Petroleum Co. for the aid extended him during the development of this paper, to the Railroad Commission of Texas for providing the data on the distillate wells and to the management of the Phillips Petroleum Co. for permission to publish this report.

REFERENCES

1. Beal, C.: *Trans.* AIME (1946) **165,** 94.
2. Brown, G. G., Katz, D. L., Oberfell, G. G., and Alden, R. C.: *Natural Gasoline and the Volatile Hydrocarbons,* N.G.A.A. (1948).
3. Cullender, M. H., and Binckley, C. W.: Phillips Petroleum Co. Report Presented to the Railroad Commission of Texas Hearing, November 9, 1950, Amarillo, Tex.
4. Fowler, F. C.: *The Petr. Engr.* (1947) **19,** No. 3, 88.
5. Moody, L. F.: *Trans.* ASME (1944) **66,** 671.
6. Railroad Commission of Texas: Back Pressure Test for Natural Gas Wells, State of Texas.
7. Rawlins, E. L., and Schellhardt, M. A.: U. S. Bureau of Mines Monograph 7 (1936).
8. Rzasa, M. J., and Katz, D. L.: *Trans.* AIME (1945) **160,** 100.
9. Johnson, T. W., and Berwald, W. B.: U. S. Bureau of Mines Monograph 6 (1935).

★ ★ ★

T.P. 3230

THE EFFECT OF WITHDRAWAL RATE ON THE UNIFORMITY OF EDGEWATER INTRUSION

M. MUSKAT, GULF OIL CORP., PITTSBURGH, PA., MEMBER AIME

ABSTRACT

Calculations are reported on the differential sensitivity of the updip invasion of oil strata of varying permeability to the driving pressure differential. It is assumed that the water-oil interfaces advance with sharp fronts, or that the microscopic displacement efficiency is independent of rate and capillary pressure effects. It is found that, under such conditions, limitations of withdrawal rates will not greatly inhibit the "fingering" and bypassing tendency through high permeability strata unless the differential fluid head across the original oil column is of the order of or exceeds about 80 per cent of the driving pressure differential. In practice, such restrictions will be feasible only for oil reservoirs and aquifers of high permeability and dip, but may develop automatically under combined gas injection and water drive operations.

INTRODUCTION

A commonly expressed view regarding the intrusion of edgewaters into oil producing formations is that the geometry of such advance is rate sensitive. Specifically, it has been suggested that high rates of advance, stimulated by rapid withdrawals, will lead to "fingering" and an irregular type of invasion, whereas at low withdrawal rates the water encroachment will be more uniform. Two factors tend to support this view. One is the resultant effect of capillary pressure and gravity gradients in the displacement processes[1] involved in water intrusion, which are magnified at low rates of flow so as to improve the recovery efficiency. The other is the direct retarding effect of the rising water head as it advances upslope into the producing area.

Capillary pressure forces give rise to a rate sensitivity of the oil recovery by water displacement in uniform strata as well as differential effects in non-uniform formations. These are basically independent of the effect of gravity and would also occur in horizontal beds or when the oil and water have the same density. Unfortunately, however, the fundamental equation describing the displacement process under the action of capillary pressures can be solved only by numerical or graphical procedures, and moreover the solutions are sensitive to the character of the capillary pressure and relative permeability curves.* On the other hand, the direct effect of gravity can be given a formal analytical solution if the simplifying assumption is introduced that the water advances with sharp fronts in the individual uniform strata. It depends on the absolute permeabilities of the water invaded zones and hence results in a rate sensitivity of the differential invasion in stratified media. Although a treatment of this factor alone will not give a complete evaluation of the effect of rate on water intrusion in non-uniform pays, it should provide at least a semiquantitative measure of the sensitivity of "fingering" to withdrawal rate. Such a treatment will be presented in the following sections.

GENERAL THEORY

The basic element of the theory is the history of water advance updip in a uniform stratum (Fig. 1). In contrast to the assumption of constant flow rate, generally made in the analysis of displacement processes, we shall assume here that

---

[1] References given at end of paper.

Manuscript received in the office of the Petroleum Branch May 28, 1951. Paper presented at the Fall Meeting of the Petroleum Branch in Oklahoma City, Okla., Oct. 3-5, 1951.

*The complexity of the quantitative treatment of oil displacement by water when including the capillary pressure terms is well illustrated by the recent work of J. C. Calhoun, Jr. and J. W. LaRue (Producers Monthly, April, 1951, 15, 20-29) in which the numerical analysis had to be limited to approximate evaluations of the *type* of effects to be expected (*cf.* also S. J. Pirson, *Elements of Reservoir Engineering*, Chapter 6).

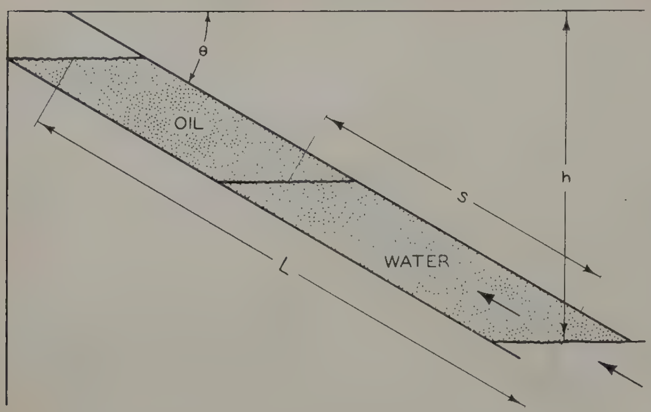

FIG. 1 — DIAGRAMATIC REPRESENTATION OF WATER INVASION UP-DIP INTO AN OIL PRODUCING PAY.

the driving pressure or fluid head differential is constant. Denoting the mobilities (effective permeability to viscosity ratios) behind and ahead of the water-oil interface to have the constant values m_w and m_o, it may be shown by straightforward application of potential flow considerations that the rate of advance of the interface will be given by the differential equation:

$$\frac{G}{1-\bar{m}} \frac{dx}{d\bar{t}} = \frac{1-Gx}{1-(1-\bar{m})\,x} \quad \ldots \ldots \quad (1)$$

where:

$$\bar{m} = \frac{m_o}{m_w};\ g = \bar{g} L \bigtriangleup \gamma \sin \theta;\ \bar{t} = \frac{\bar{g} m_o t}{\bar{f} L^2 (1-\bar{m})};\ G = \frac{\bar{g}}{\Delta p} \quad \ldots \ldots \quad (2)$$

and x is the fraction of the length, L, of the stratum to which the interface has advanced at the time t, g is the acceleration of gravity, $\bigtriangleup \gamma$ is the difference in density between the oil and water, $\bar{f}$ is the displacement porosity, *i.e.*, the porosity times the increase in water saturation in the water invaded pay, and Δp is the driving pressure difference measured at the same datum level, and corrected for an oil gravity gradient. L represents the total distance along the stratum of interest. The integral of Equation (1) is:

$$\bar{t} = x + \left(\frac{1}{G} - \frac{1}{1-\bar{m}} \right) \log (1-Gx) \quad \ldots \quad (3)$$

For the special case $G \sim 0$, where there is no gravity effect, Equation (3) reduces to:

$$\frac{m_o\, t\, \Delta p}{(1-\bar{m}) \bar{f} L^2} = x \left[\frac{1}{1-\bar{m}} - \frac{x}{2} \right] \quad \ldots \quad (4)$$

And when the mobilities ahead and behind the water-oil interface are the same ($\bar{m} = 1$), Equation (3) takes the simple form:

$$\frac{\bar{g} m_o t}{\bar{f} L^2} = -\log (1-Gx) \quad \ldots \ldots \quad (5)$$

Examples of the time histories predicted by Equation (3) are plotted in Fig. 2 for $\bar{m} = 0.2$ and $\bar{m} = 2$ for various values of G. To make the time scales comparable for the two values of $\bar{m}$, the abscissa variable was chosen as $(1-\bar{m})\bar{t}$. The different values of G correspond to differences in the values of the driving head.

As is to be expected, the curves for $\bar{m} = 2$ require longer time periods for completion of the advance of the water through the oil column than those for $\bar{m} = 0.2$. This results from the increasing flow resistance of the column as the oil is replaced by the water when $\bar{m} > 1$. This increase becomes aggravated as the advance continues, leading to the convex upward character of the curves. The converse behavior occurs for $\bar{m} < 1$.

The shift of the curves to the right as G increases simply reflects the corresponding decrease in driving head. In the limit when G approaches unity, the time for complete invasion becomes infinite. In fact, if the driving head is not sufficient to support the total differential head $gL \bigtriangleup \gamma \sin \theta$, the interface will asymptotically come to rest at a value $x = 1/G = \Delta p / gL \bigtriangleup \gamma \sin \theta$, as follows from Equation (3) and as can be derived directly from equilibrium considerations.

EFFECT OF RATE ON INTERFACE HISTORY

Since the individual or absolute mobilities enter the above equations only in the dimensionless time $\bar{t}$, the basic functional history of advance of the water-oil interface, *i.e.*, Equation (3), will be independent of the permeability of the stratum. The latter will control only the time scale. On the other hand

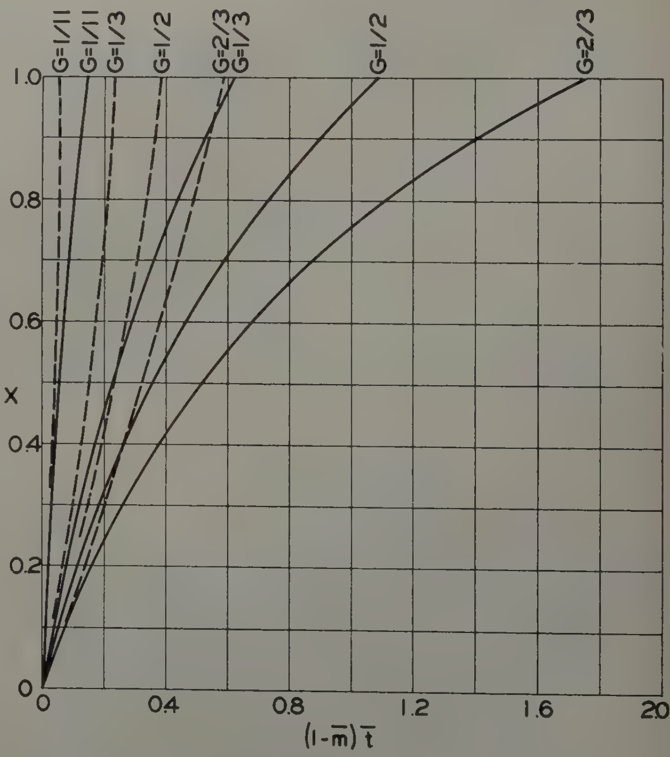

FIG. 2 — HISTORY OF UP-DIP WATER INVASION INTO UNIFORM OIL PRODUCTIVE FORMATIONS.

x = Fraction of total length of oil stratum invaded by water. $\bar{m}$ = (mobility of oil ahead of interface)/(mobility of water behind interface). $\bar{t}$ = Dimensionless time. G = Ratio of total differential fluid head of oil stratum to pressure differential at datum of original water-oil interface. Solid curves, $\bar{m}$ = 2. Dashed curves, $\bar{m}$ = 0.2.

since this functional history involves the rate sensitive term G representing the effect of gravity, the relative advance of the interface in zones of different permeability at any given time will also depend on the term G.

This rate sensitivity of the water invasion process may be evaluated by comparing the relative degrees of advance of the water in strata of different permeability as a function of the gravity parameter G. This could be done by reference to the time history curves such as are plotted in Fig. 2. A more direct procedure, however, is that of determining the extent of the advance of the water-oil interface in a stratum of relatively low permeability at the time when complete invasion has developed in an otherwise identical zone but having a higher absolute permeability. Denoting by R the ratio of the mobility of either fluid in stratum (2) to that in stratum (1), and assuming* all other characteristics to be identical, *i.e.*, on setting:

$$R = \frac{m_{w2}}{m_{w1}} = \frac{m_{o2}}{m_{o1}} \quad . \; . \; . \; . \; . \; . \; . \; . \; . \; . \quad (6)$$

it may be shown by application of Equation (3) that the fractional invasion in stratum (2) at the time stratum (1) has been completely flooded will be:

$$x_2 = R + \left(\frac{1}{1-\overline{m}} - \frac{1}{G}\right)[\log(1-Gx_2) - R\log(1-G)] \quad (7)$$

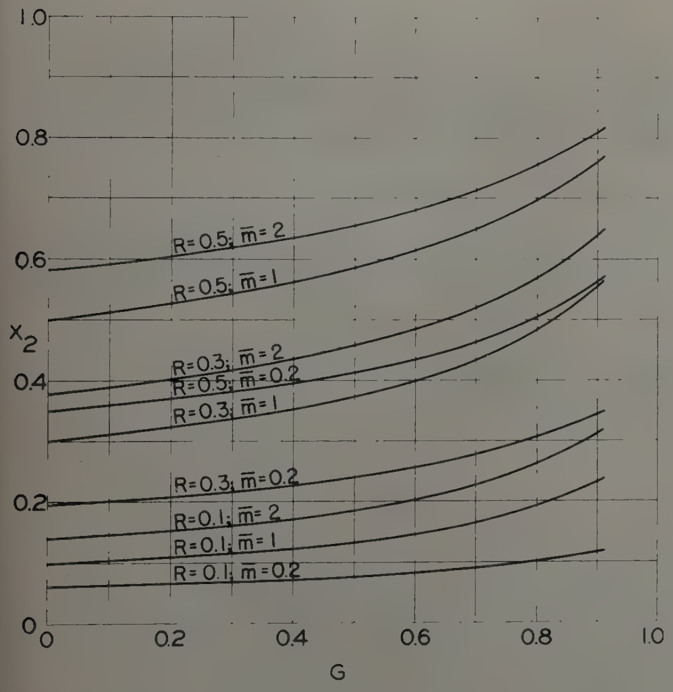

FIG. 3 — THE RELATIVE ADVANCE OF WATER-OIL INTERFACES IN TIGHT STRATA BY THE TIME INVASION HAS BEEN COMPLETED IN PERMEABLE STRATA.

x_2 = Fractional extent of invasion in tight stratum at time permeable zone is completely flooded. R = (Permeability of tight stratum)/(permeability of completely invaded stratum). m = (mobility of oil ahead of interface)/(mobility of water behind interface). G = Ratio of total differential fluid head of oil stratum to pressure differential at datum of original water-oil interface.

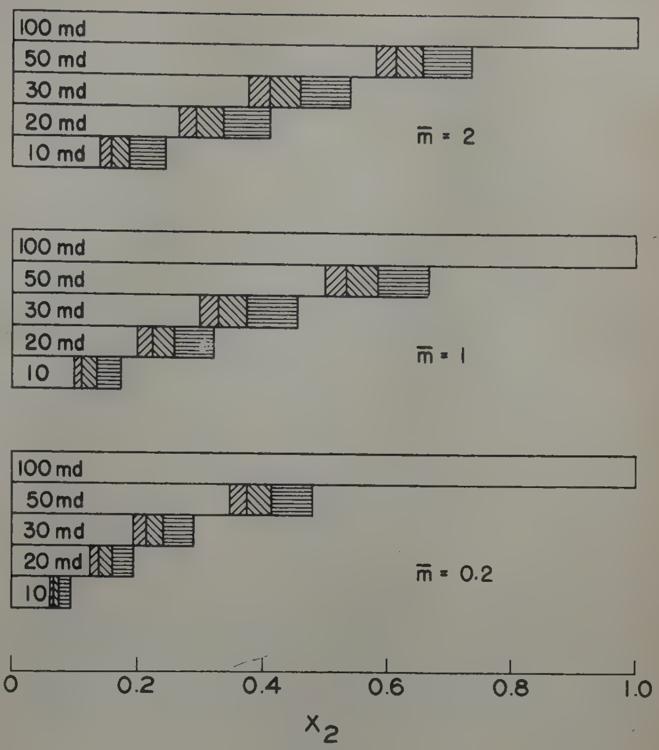

FIG. 4 — DIAGRAMATIC REPRESENTATION OF DEGREES OF ADVANCE OF WATER IN STRATA OF PERMEABILITIES 50, 30, 20, AND 10 MD, AT THE TIME A PARALLEL 100 MD STRATUM IS COMPLETELY FLOODED BY INVADING EDGEWATER.

$\overline{m}$ = (mobility of oil ahead of interface)/(mobility of water behind interface). x_2 = Fractional distance of advance of water-oil interface in tighter strata at the time the 100 md zone is completely flooded. G = Ratio of total differential fluid head of oil pay to driving pressure differential at datum of initial water-oil contact. 1st interface refers to G = 0; 2nd interface refers to G = 0.25; 3rd interface refers to G = 0.50; most advanced interface corresponds to G = 0.75.

For the special case $\overline{m} = 1$, Equation (7) reduces to:

$$x_2 = [1-(1-G)^R]/G \quad . \; . \; . \; . \; . \; . \; . \quad (8)$$

Several illustrative curves of x_2 *vs* G, as computed by Equations (7) and (8), are plotted in Fig. 3. The relative positions of the curves for the different values of R reflect the direct effect of the permeability on the rate of water invasion. In the limit $R = 1$, x_2 would equal 1 for all $\overline{m}$ and G, since the two strata (1) and (2) would then be identical. The ordinate intercepts for $G = 0$ give the advance in the tighter strata when the more permeable zone is completely flooded if gravity had no effect, *i.e.*, for horizontal beds or water and oil of equal density. These intercepts equal R when $\overline{m} = 1$, but differ from R when $\overline{m} \neq 1$, because of the changing fluid conductivity of the system as the water invasion progresses.*

The rising trend of the curves gives a direct measure of the rate sensitivity of the invasion process. This sensitivity does not vary greatly with $\overline{m}$ and R, but it does increase as G increases. And in the limit as $G \rightarrow 1$, x_2 in all cases approaches 1. This means that all zones will be flooded out at the same (infinite) time regardless of their permeability.

A somewhat more graphic representation of the effect of gravity in equalizing the differential water advance in strata of different permeability is shown in Fig. 4. Here are plotted diagramatically the relative degrees of advance in a series of parallel strata of 10, 20, 30, 50 and 100 md permeability.* These correspond respectively to strata for which $R = 0.1$, 0.2, 0.3, 0.5, and 1.0. In this figure are shown the relative positions of the water-oil interface in the tighter strata at the time the 100 md zone is completely flooded out. The first interfaces give the positions if gravity were not acting on the system, or if the latter were horizontal ($G = 0$). The subsequent interfaces, separated by the hatched areas, denote the positions for values of $G = 0.25$, 0.50, and 0.75 respectively. Three such systems are illustrated, *i.e.*, those for which $\overline{m} = 0.2$, 1.0, and 2.0. The comparative features of these diagrams illustrate the same trends plotted in Fig. 3.

---

*It is further assumed that there is no cross flow between the layers of different permeability.

*This factor has been previously analyzed in detail for continuously stratified media (*cf.* M. Muskat, *Trans.* AIME, 1950, 189, 349-358).

Aside from the validity of the simplifications introduced in carrying through the above analyses and calculations, the practical significance of the results depends on the range of values of G which may be expected to occur under actual field conditions. From the definition of G in Equation (2) it follows that its value will depend both on the fixed reservoir-fluid properties, $\triangle \gamma L \sin \theta$, and the pressure drop $\triangle p$ supporting the water invasion, and which can be controlled, in principle, by the withdrawal rates. If we choose for the density difference $\triangle\gamma$, the value 0.3, and a dip angle θ of 10°, the vertical differential head for a surface distance of 1,000 ft will be equivalent to 23 psi. G will then be the ratio of this head to the pressure drop at the same datum over the 1,000 ft distance. From Figs. 3 and 4, it appears that substantial equalization in the water advance will not develop until G is about 0.8 or greater. This would correspond to a pressure drop of only about 30 psi in this particular case.

To see what this would imply in terms of field withdrawals, we may suppose the equivalent gradient of about 0.03 psi/ft is applied along the periphery of a circular field, one mile in radius ($\sim$ 2,000 acres area), the productive section being 25 ft thick and the average effective mobility being 25 md/cp. A corresponding initial and maximum rate of water influx would then be 675 B/D. If the field is operated by complete water drive, and is developed on a 40-acre spacing the withdrawal rate per well would have to be only 13.5 B/D in reservoir volume. Moreover, this will decrease as the water entry continues and the retarding head of the water column reduces the net driving force.

In this particular example an effective control of edgewater "fingering" of the type considered here by limiting the producing rate would hardly be practical. And it appears likely that in most actual producing operations in fields of moderate permeability, where an attempt is made to produce by the water drive mechanism the possibility of controlling the uniformity of advance of the edgewater by varying the withdrawal rates will be rather limited. On the other hand, in steeply dipping and highly permeable formations definite benefits may well result from withdrawal control. Thus, in the above example, if the effective fluid mobility be increased by a factor of 10, the initial rate of water influx could support a withdrawal rate of 135 B/D per well in reservoir volume, and yet have a value of $G = 0.8$.

Another situation where low gradients near the water-oil contact may be effective in equalizing the differential advance of the interface is that where the major producing mechanism is that of gravity drainage, supplemented by gas cap injection and expansion. If water invasion is not the primary agent for the mass oil migration, the low gradients near the interface will tend to make such intrusion as does take place more uniform than would occur under rapid water drive encroachment.

ACKNOWLEDGMENT

The writer is indebted to Miss M. O. Taylor, of the Gulf Research and Development Co., for carrying through the numerical calculations cited in this paper.

REFERENCES

1. Buckley, S. E., and Leverett, M. C.: "Mechanism of Fluid Displacement in Sands," *Trans.* AIME (1942) **146,** 107. ★

---

*This treatment of a discreet layer system can be generalized to continuously stratified media. For the special case of a linear permeability distribution, it is found that the fraction of the total section which would be flooded by the time the water has just broken through the most permeable zone will be:

Fraction flooded $\simeq$

$$\frac{r}{(r-1)\,[1-\alpha \log(1-G)]}\left[\frac{1-x_m^2}{2}-\alpha\,(1-x_m)+\frac{\alpha}{G}\log\frac{1-Gx_m}{1-G}\right]$$

where r is the ratio of maximum to minimum permeability, x_m is the fractional advance in the tightest layer, and $\alpha = \dfrac{1}{1-\overline{m}} - \dfrac{1}{G}$, the rest of the notation being the same as in the text.

T.P. 3219

A RESERVOIR ANALYZER STUDY OF THE WOODBINE BASIN

R. C. RUMBLE, H. H. SPAIN, MEMBERS AIME; AND **H. E. STAMM, III,** JUNIOR MEMBER AIME; HUMBLE OIL AND REFINING CO., HOUSTON, TEXAS

ABSTRACT

This paper presents a reservoir analyzer study of the performance of the Woodbine formation in the East Texas basin. The study was made possible by the compilation of available information on the configuration, thickness and the pressure drawdown of the formation. The investigation was made of the pressure variations in the basin incident to production from the several Woodbine reservoirs. In addition, the apparent compressibility of Woodbine water was evaluated so that the potential water yield of the formation could be determined. The distribution of permeability of the Woodbine sand and the interference between producing areas were also investigated. In conjunction with this basic study of the Woodbine sand, an acceptable match of the production-pressure relationship in the East Texas Field was established on the analyzer.

INTRODUCTION

When production is taken from a reservoir contiguous to an aquifer, the resultant pressure gradient causes a water influx into the reservoir. For some years it has been the practice to predict the performance of water drive reservoirs with mathematical equations that relate the water influx into reservoirs to their pressure behavior. A rigorous solution of these equations is quite complex; hence, the conventional method requires the simplifying assumptions that the formation have constant thickness, permeability and porosity, and that it have a known and regular shape. It is necessary to use performance records of the reservoir in question to determine the equation constants that make the results of the mathematical calculations duplicate the reservoir history. The values of the constants determined in this manner sometimes differ so greatly from theoretical or measured values that the constants appear unreasonable. The equation constants comprise such factors as the thickness, porosity and permeability of the formation, and the viscosity and compressibility of water. Usually the thickness, porosity and viscosity are known within a reasonable degree of certainty, whereas the formation permeability and the water compressibility are known with considerably less certainty. Hence, permeability and compressibility values are arbitrarily selected that will make the mathematical equations duplicate the reservoir behavior. In many reservoir studies the value of the compressibility of water thus selected has exceeded the reported value by a factor of from severalfold to manyfold. Whether this excessive value results from the inadequacy of the mathematical approach to take into account the shape irregularities and the heterogeneities of the aquifer, or is due to some type of formation compaction and decrease of porosity has not been established. Because of the significance of the potential water yield of formations with reference not only to oil reservoirs but to water resources as well, it is very important that a representative value for the effective water compressibility be determined.

One of the best known examples of a field for which it has been possible in the past to predict the future reservoir pressure is the East Texas Field. Until about 1943 it was possible by means of mathematical equations to duplicate past pressure behavior and to predict with a high degree of accuracy the reservoir pressure of the field. Since 1943, however, the calculated pressures have deviated progressively from the observed pressures to such a degree that in recent years, it has

---

[1] References given at end of paper.

Manuscript received in the office of the Petroleum Branch August 28, 1951. Paper presented at the Petroleum Branch Fall Meeting in Oklahoma City, Oct. 3-5, 1951.

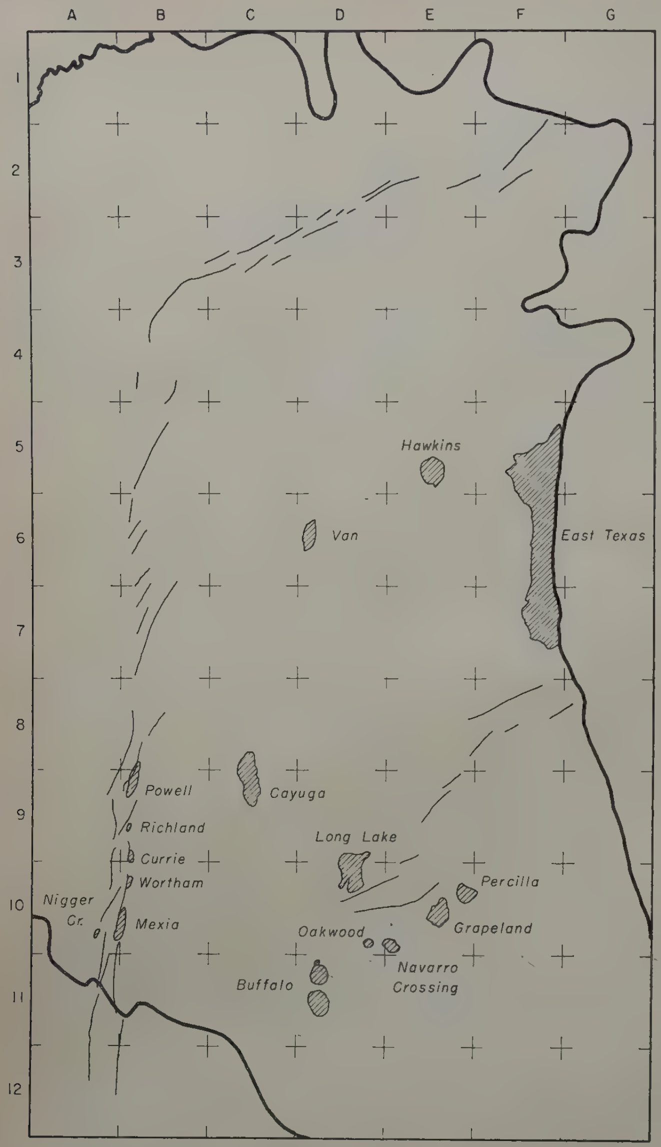

FIG. 1 — SUBDIVISION OF WOODBINE BASIN.

not been possible to predict accurately the future pressure of the field using the equation constants that were employed in the past. The geometric configuration and the permeability variation of the Woodbine aquifer, which is the source of the water drive for the field, and the production from other Woodbine fields were thought to be causing the discrepancy between the observed and calculated pressures.

As an approach to these problems, a detailed study of the Woodbine basin was made with an electric reservoir analyzer to determine the apparent compressibility of the formation water and the permeability variation throughout the basin, and to obtain a reliable means of predicting the pressure of the East Texas Field. In this study the aquifer was represented by an electric analogy in which variations in the geometry and the permeability of the sand were included. The apparent water compressibility and the permeability variations were determined from the analyzer constants and network condenser and resistor values that gave a basin pressure distribution consistent with the observed pressure history of the East Texas Field and the known pressure drawdown in the basin as of Jan. 1, 1947. The pressure pattern throughout the basin during the entire history of production from the Woodbine formation was derived simultaneously with this study.

In addition, the study provided a satisfactory means of determining the pressure history of the East Texas Field. From the electric characteristics of the analog, the influence of production from other fields on the pressure of the East Texas Field was determined, and predictions of the future pressure-production behavior of this field were made.

Insofar as is known by the authors, the Woodbine basin is the only producing formation about which sufficient data have been compiled to permit a quantitative study of an entire aquifer. Basic information available for this study included Woodbine formation pressures derived both from field measurements and from drill stem tests throughout the basin. The configuration of the Woodbine formation and the distribution of the net sand thickness were also known.

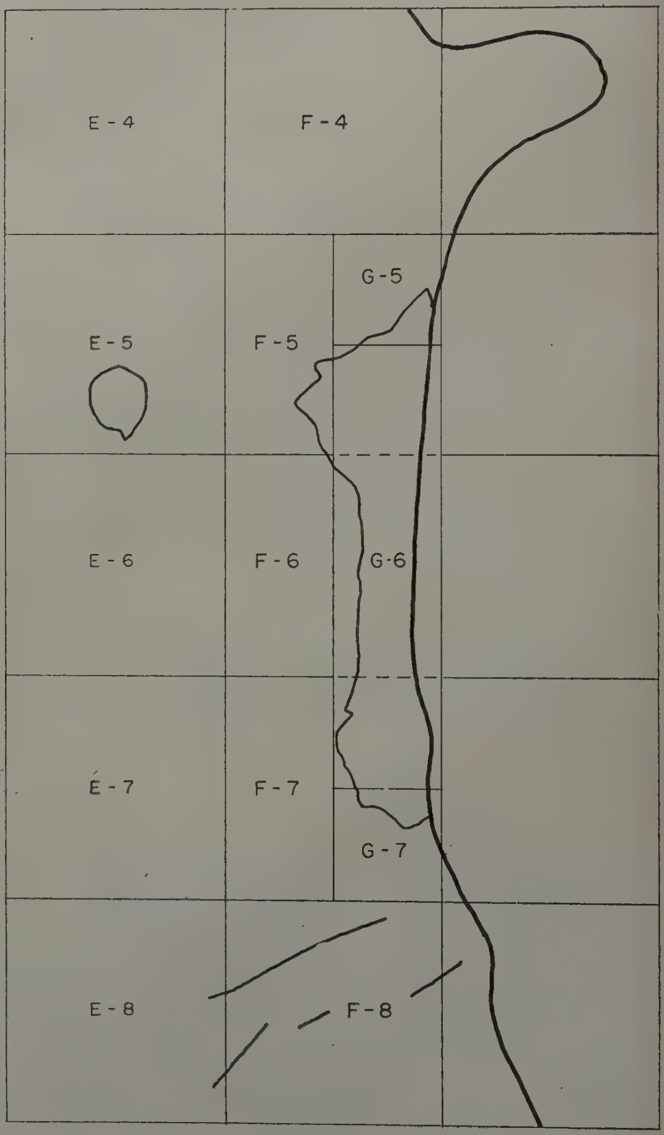

FIG. 2 — SUBDIVISION OF AREA AROUND EAST TEXAS FIELD.

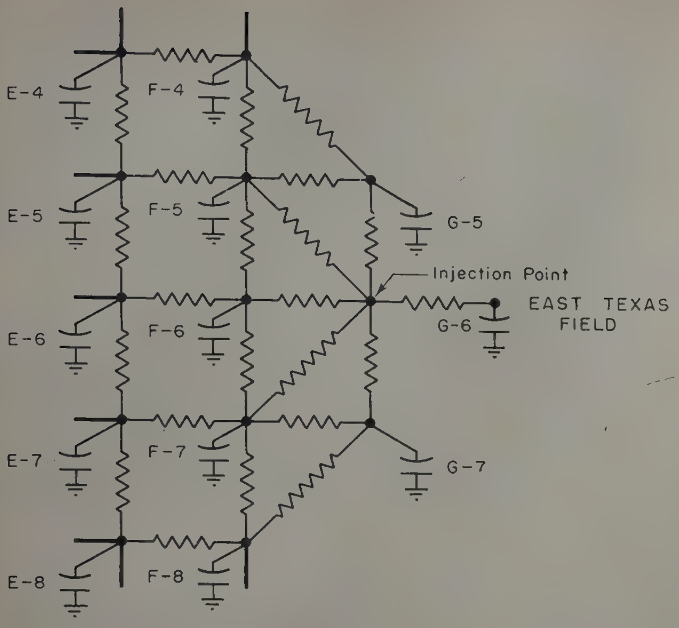

FIG. 3 — RESISTOR NETWORK.

STUDY OF THE BASIN

Electric Representation of the Woodbine Basin

To represent the Woodbine basin electrically on the pool unit of the reservoir analyzer, the area of the basin was divided into a number of squares 15.42 miles on the side as shown by the grid map on Fig. 1. On this map are shown the location of the Woodbine reservoirs that were considered in this study. The three squares enclosing the East Texas Field were subdivided further as shown on Fig. 2 so that the subdivision in which the field lay approximated closely the areal extent of the field. For each of the integral formation volumes corresponding to these area subdivisions, the fluid capacitance, which is defined as the product of the interstitial fluid volume and the appropriate fluid compressibility, was represented by an electric condenser. The equation for arriving at the relative condenser values is shown below:

$$C_E = M\, c\, ab\, \phi \quad . \; . \; . \; . \; . \; . \; . \; . \; . \; . \quad (1)$$

where,

C_E = electric capacity of condenser, microfarads

M = analyzer proportionality constant between fluid and electric units, $\dfrac{\text{microfarads}}{\text{bbl/psi}}$

c = compressibility of interstitial fluid, vol/vol/psi

ab = volume of formation sand within each square, bbl

ϕ = porosity of sand, fraction of total sand volume

The compressibility of the water and the porosity of the sand were assumed to be constant everywhere in the aquifer, whereas the sand volume corresponding to each areal subdivision was determined from the average clean sand thickness for each subdivision as indicated by electric logs of the wells drilled throughout the basin.

The condensers representing the fluid capacitance of the Woodbine formation were arranged in the same pattern as the corresponding areas. The resistance to fluid flow between the centers of adjacent formation subdivisions was represented by a variable resistor, so that for each boundary common to two areal units there was a resistor connecting the corresponding condensers. The resistors representing paths of flow from the aquifer across the East Texas Field boundary were tied together to form a common point to which was attached a single resistor terminated by the condenser representing the East Texas Field. Each resistor bears the inverse relationship to the corresponding formation permeability shown by the following equation:

$$R_E = \frac{N\, \mu}{0.001127\, K\, b} \quad . \; . \; . \; . \; . \; . \; . \; . \; . \; . \quad (2)$$

where,

R_E = electric resistance, megohms

N = analyzer constant, $\dfrac{\text{megohms}}{\dfrac{\text{psi}}{\text{B/D}}}$

μ = viscosity of Woodbine water, centipoises

0.001127 = proportionality constant to change millidarcys to $\dfrac{\text{(bbl) (sq in.) (cps)}}{\text{(lb) (day) (ft)}}$

K = permeability, md

b = clean sand thickness on side of formation subdivision, ft

In order to simulate production from the fields producing from the Woodbine sand, current was withdrawn from the charged resistor-condensor network at the appropriate mesh points. To simulate injection of water along the western edge of the East Texas Field, current proportional to the volume of water injected into the field was introduced at the junction of the resistor leading to the field and the resistors leading to the aquifer as is shown on Fig. 3.

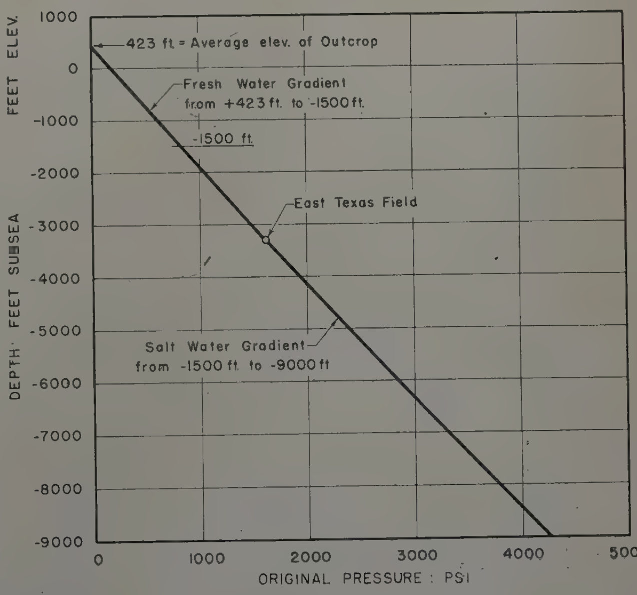

FIG. 4 — WOODBINE BASIN — PRESSURE VS DEPTH.

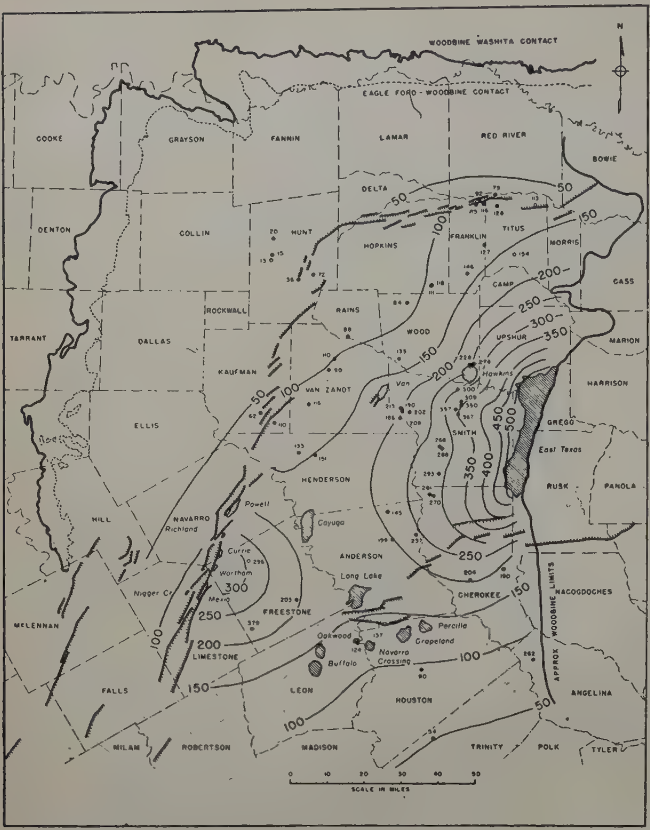

FIG. 5 — PRESSURE LOSS IN WOODBINE BASIN ON JAN. 1, 1947.

Pressure Loss in the Basin

During the last decade, drill stem tests were made on many of the wells drilled into the Woodbine formation. In conjunction with these tests, pressures were measured in the Woodbine formation, and water samples were taken.[1] From the density and chloride content of these samples, and the depths at which they were taken, the relationship between original pressure in the Woodbine sand and subsea depth was established. This relationship is shown on Fig. 4. By means of this relationship and the measured pressures, the change from original pressure was determined for each of the different well locations as of the date on which the pressure measurement was made. A preliminary analyzer study of these pressure changes provided an indication of the approximate rates of change in pressure in the various parts of the basin. These were used to adjust observed pressures to an arbitrary date of Jan. 1, 1947.

In an analyzer study of the performance of a reservoir, a charged condenser of an arbitrary capacity is used to express the product of the volume of a compressed fluid and its compressibility. The original voltage across the condenser is analogous to the original formation pressure. In such an analogy the drop in voltage across the condenser remains proportional to the volume-weighted pressure decline in the formation. Therefore, volume-weighted pressures were used in this study.

The pressure drawdown of the Woodbine basin, contoured at 50 psi intervals by the use of adjusted pressure losses, is shown on Fig. 5. Volume weighted pressure losses for the squares into which the basin had been sub-divided were determined from this map of pressure drawdown in the basin in conjunction with an isopach map of the clean sand thickness in the basin and are presented on Fig. 6.

Match of Pressure Loss in the Basin

The reservoirs that had produced or were producing from the Woodbine formation were surveyed to determine which of them had production of sufficient magnitude to cause water efflux from the basin into the reservoirs in such quantities as to affect appreciably the pressure pattern of the basin. The water efflux from the basin was expressed in terms of the rates of water influx into the various reservoirs considered. The water influx rates of each of these reservoirs were calculated for their producing histories where the necessary data existed and were carefully estimated for the fault line fields where water production data were not available. The effects

Table I — Daily Average Water Influx Rates

Year	Prod. Contr. No. 1 Sq.: F-5a* East Texas B/D	Prod. Contr. No. 2 Sq.: E-5 East and West Hawkins B/D	Prod. Contr. No. 3 Sq.: D-6 Van B/D	Prod. Contr. No. 4 Sq.: C-9 Cayuga B/D	Prod. Contr. No. 5 Sq.: D-10 Long Lake B/D	Production Controller No. 6 Sq.: E-10					Production Controller No. 7 Sq.: B-9				Production Controller No. 8 Sq.: B-10			
						Navarro Crossing B/D	Buffalo B/D	Grapeland B/D	Percilla B/D	Group Total B/D	Powell B/D	Richland B/D	Currie B/D	Group Total B/D	Wortham B/D	Nigger Creek B/D	Mexia B/D	Group Total B/D
1921																	17,000	17,000
1922													7,000	7,000			137,000	137,000
1923											103,000		9,000	112,000			103,000	103,000
1924											189,000	17,000	8,000	214,000			81,000	81,000
1925											142,000	25,000	5,000	172,000	11,000		67,000	78,000
1926											119,000	22,000	4,000	145,000	57,000	8,000	64,000	129,000
1927											112,000	23,000	4,000	139,000	39,000	35,000	64,000	138,000
1928											98,000	25,000	4,000	127,000	31,000	22,000	57,000	110,000
1929											95,000	24,000	5,000	124,000	24,000	15,000	53,000	92,000
1930			13,000								93,000	18,000	4,000	115,000	19,000	10,000	48,000	77,000
1931	379,000		39,000								76,000	7,000	4,000	87,000	9,000	4,000	43,000	56,000
1932	504,000		56,000								63,000	4,000	3,000	70,000	4,000		36,000	40,000
1933	725,000		53,000								77,000	4,000	3,000	84,000	3,000		36,000	39,000
1934	646,000		14,000								71,000	4,000	3,000	78,000	3,000		36,000	39,000
1935	621,000		76,000								72,000	3,000	3,000	78,000	3,000		40,000	43,000
1936	603,000		25,000								75,000	2,000	3,000	80,000	2,000		40,000	42,000
1937	666,000		33,000		12,000			1,000		1,000	82,000	1,000	4,000	87,000	2,000		40,000	42,000
1938	629,000		11,000		34,000		2,000	—		2,000	78,000	2,000	3,000	83,000	2,000		39,000	41,000
1939	637,000		15,000		27,000		2,000	—		2,000	74,000	2,000	4,000	80,000	2,000		38,000	40,000
1940	624,000		12,000		16,000	8,000	1,000	4,000		13,000	71,000	2,000	4,000	77,000	4,000		36,000	40,000
1941	724,000		11,000		11,000	—	—	14,000		14,000	69,000	4,000	4,000	77,000	13,000		38,000	51,000
1942	697,000		2,000	4,000	28,000	6,000	—	14,000		20,000	62,000	3,000	5,000	70,000	13,000		40,000	53,000
1943	609,000		—	42,000	54,000	1,000	3,000	17,000		21,000	54,000	2,000	6,000	62,000	11,000		37,000	48,000
1944	559,000		11,000	70,000	48,000	—	1,000	33,000		34,000	54,000	2,000	5,000	61,000	8,000		37,000	45,000
1945	545,000	7,000	23,000	124,000	61,000	4,000	3,000	22,000		29,000	49,000	2,000	5,000	56,000	7,000		36,000	43,000
1946	489,000	13,000	21,000	134,000	46,000	6,000	2,000	24,000	1,000	33,000	60,000	3,000	5,000	68,000	6,000		36,000	42,000
1947	467,000	12,000	19,000	70,000	60,000	9,000	12,000	21,000	1,000	43,000	60,000	3,000	5,000	68,000	6,000		36,000	42,000
1948	443,000	15,000	32,000	69,000	82,000	7,000	8,000	18,000	3,000	36,000	60,000	3,000	5,000	68,000	6,000		32,000	38,000
1949	368,000	16,000	33,000	55,000	73,000	5,000	2,000	14,000	2,000	23,000	64,000	3,000	4,000	71,000	7,000		28,000	35,000
1950	372,000	14,000	25,000	52,000	63,000	8,000	2,000	3,000	2,000	15,000	63,000	3,000	4,000	70,000	6,000		28,000	34,000

*Note: The squares in which East Texas Field lay were subdivided into smaller divisions so that one condenser represented just the fluid capacitance of East Texas Field.

of production from the various reservoirs were reproduced on the analyzer by the withdrawal of currents proportional to the rates of water influx from the condensers corresponding to the areas in which the reservoirs lay. Since the analyzer used in this study has only eight current controller units, some of the reservoirs were grouped together. The water influx rates, reservoir groups, and squares from which current withdrawals were made are presented in Table I.

By a trial-and-error procedure of adjusting the resistor values representing the resistance to flow and the magnitude of the currents proportional to the water influx rates, the change in voltage across the condenser representing each square was made proportional to the volume-weighted pressure drop calculated for the square as of Jan. 1, 1947. In order to obtain a more nearly unique match of the whole basin, the voltage decline of the condenser representing the East Texas Field was made to simulate the volume weighted pressure decline of the field. The resultant voltage declines of the two condensers representing the Van Field and the Oakwood Field were then found to be reasonably consistent with the observed pressure declines in the two fields. Since these two comparisons appeared reasonable, it was felt that a fairly accurate solution of the pressure distribution had been obtained. Fig. 7 shows the distribution of the pressure drawdown in the basin as of Jan. 1, 1947, obtained with the analyzer. The agreement of these pressure changes with those shown on Fig. 6 is indicative of the accuracy of the analogy used.

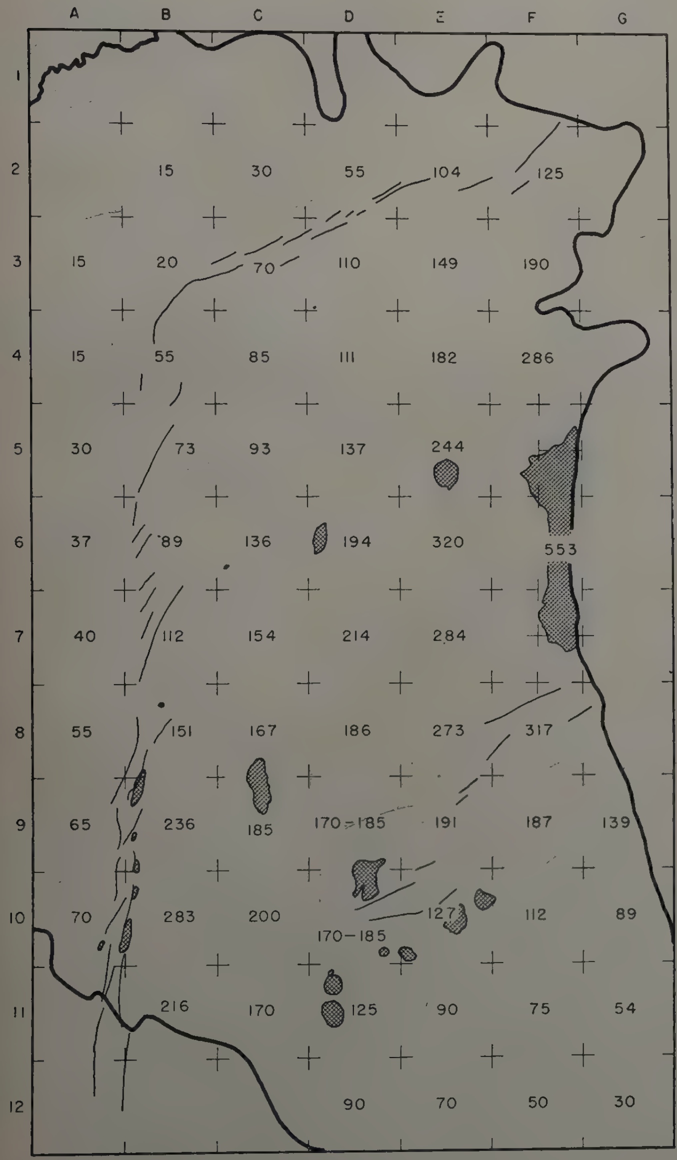

FIG. 6 — VOLUME-WEIGHTED PRESSURE LOSS AS OF JAN. 1, 1947 — OBSERVED.

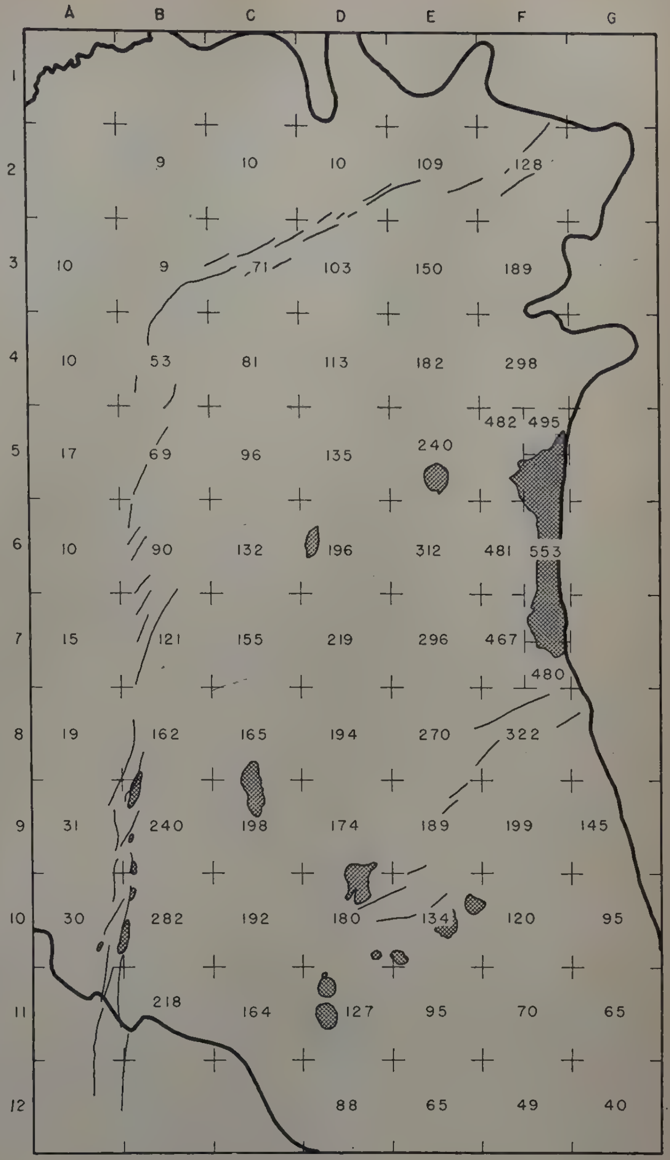

FIG. 7 — PRESSURE LOSS AS OF JAN. 7, 1947 — ANALYZER.

Compressibility of Water

The proportionality constants, or analyzer constants, between fluid units and electrical units determined from the study of the basin distribution of pressure are presented in Table II. One of these constants, "M," which was found to be 3.28×10^{-6} microfarads/bbl/psi, was used in Equation (1) with the values of the condensers representing the basin to compute the apparent compressibility of the water in the Woodbine basin. The porosity of this formation throughout the basin was assumed to be constant at 25 per cent. This computed value for the apparent compressibility, 5.3×10^{-8} vol/vol/lb/sq ft, is somewhat higher than the value of 1.85×10^{-8} vol/vol/lb/sq ft that was measured on samples of Woodbine water taken during drill stem tests. A study of the production-pressure relationship in the East Texas Field reported in the literature in 1938 indicated an apparent compressibility of 1.11×10^{-7} vol/vol/lb/sq ft for Woodbine water.[2] Earlier investigators reported values as high as 12 times the compressibility of pure water.[3,4]

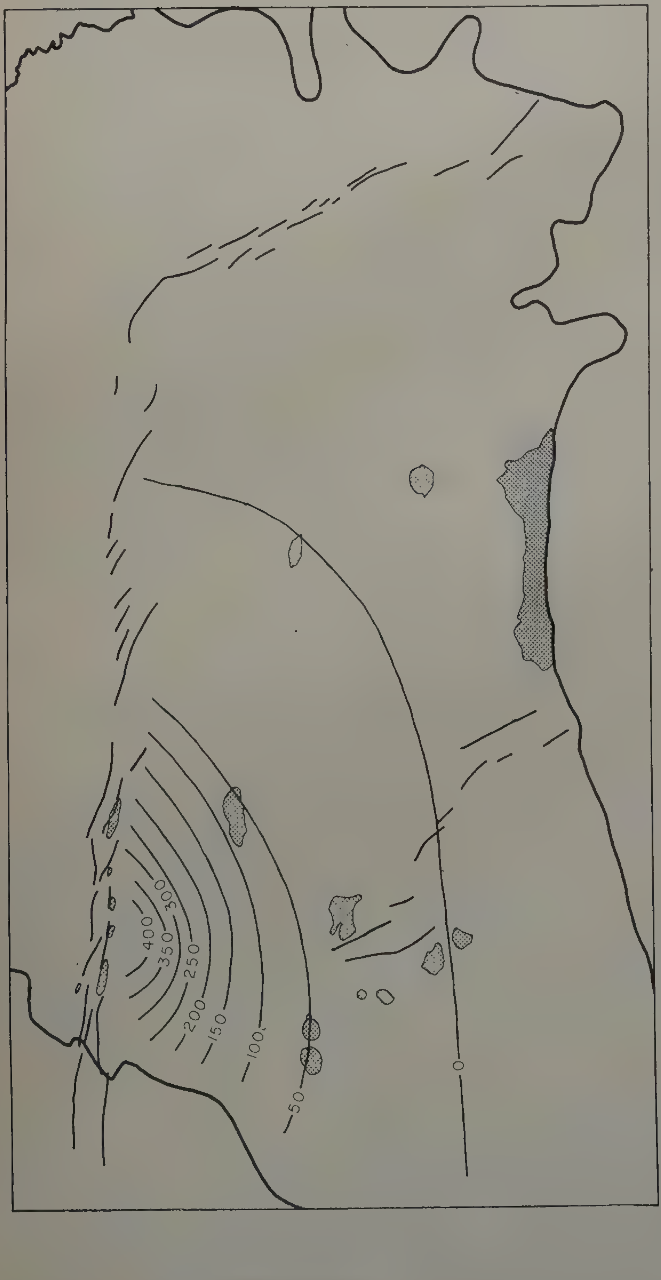

FIG. 8 — PRESSURE LOSS — JAN. 1, 1930.

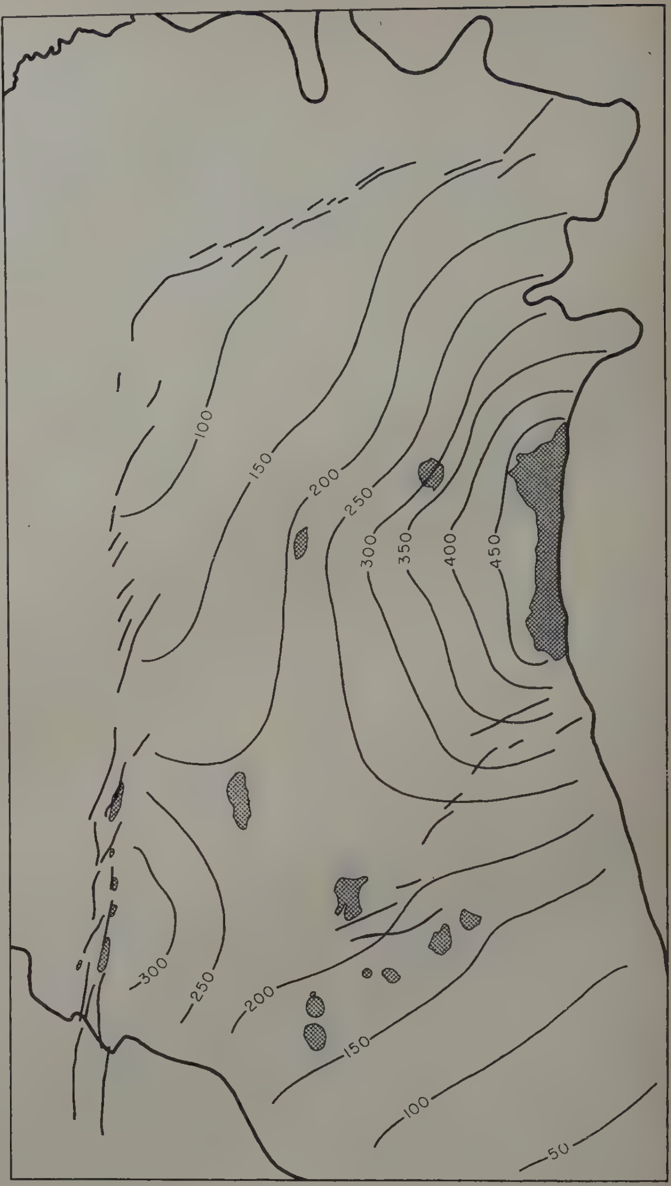

FIG. 9 — PRESSURE LOSS — JAN. 1, 1950.

A Bureau of Mines publication on the compressibility of consolidated sandstones presented information from which the effect of pressure on the pore volume could be computed.[5] The measured effect of pressure loss on Woodbine sand was to reduce the size of the pore volume by an amount equal to 2.85×10^{-8} vol/vol/lb/sq ft. On the assumption that this effect would be additive with the compressibility of the Woodbine water, the effective compressibility in the Woodbine aquifer would be 4.7×10^{-8} vol/vol/lb/sq ft. The agreement between this value and that experimentally determined with the analyzer is rather close and is well within the over-all accuracy of the analyzer study. However, the difference between the two might be accounted for by some other phenomenon which would result in a reduction of the volume of the pore space or by the intrusion of extraneous water into the Woodbine formation.

Table II — Analyzer Constants

Constant	Units	Pool Unit	Water-Drive Unit
L	volts/psi	0.300	0.3261
L/N	$\frac{\text{microamps}}{\text{B/D}}$	1.44×10^{-4}	1.246×10^{-4}
MN	sec/D	6.849×10^{-3}	8.219×10^{-2}
N	$\frac{\text{megohms}}{\text{psi/B/D}}$	2088	2617
M	$\frac{\text{microfarads}}{\text{B/psi}}$	3.28×10^{-6}	3.141×10^{-5}

As in independent approach, the apparent compressibility of Woodbine water was determined from the ratio of cumulative water yielded by the formation to the integrated product of the volume of Woodbine water and its observed loss in pressure to Jan. 1, 1947. For this purpose the water yielded was considered to be the sum of the volume of water influx into all fields producing from the Woodbine formation. This procedure gave a value of 5.6×10^{-8} vol/vol/lb/sq ft. The difference between this value and that obtained with the analyzer indicates the accuracy with which the basin pressure behavior was simulated on the analyzer.

Permeability Distribution

From another analyzer constant, "N," which was found to be 2,088 megohms/psi/B/D, Equation (2), and the values of the various resistors, the effective permeabilities at various locations in the basin were determined. In general, the permeability was found to be in the range of 1,000 to 1,500 md around the East Texas Field and to decrease to values from 100 to 700 md as the Mexia-Talco fault line is approached. Continuity across the fault block appeared to be very limited.

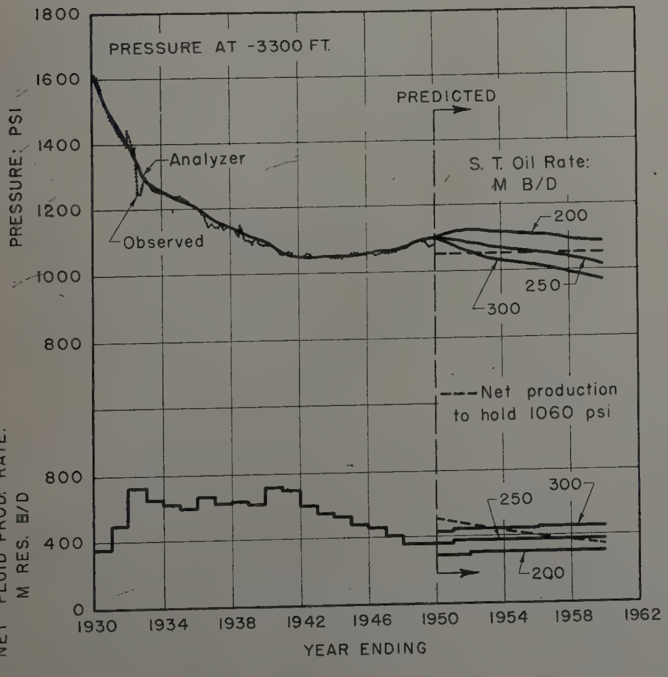

FIG. 10 — POOL UNIT REPRESENTATION, EAST TEXAS FIELD.

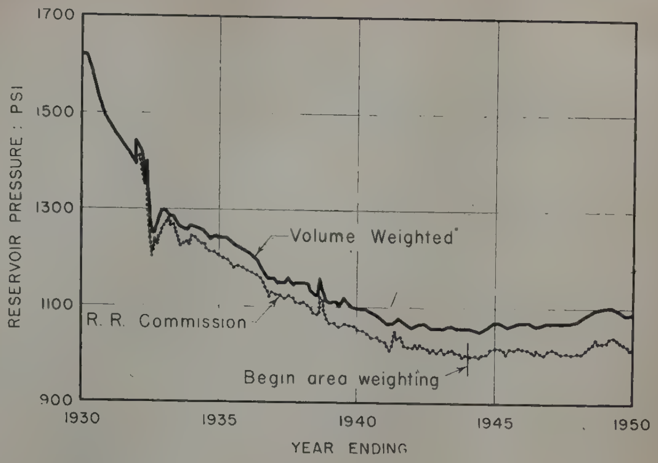

FIG. 11 — COMPARISON OF VOLUME-WEIGHTED AND AREA-WEIGHTED PRESSURES, EAST TEXAS FIELD.

Basin Pressure Behavior

The analyzer study indicated the manner in which the pressure drawdown throughout the basin has developed since production of the Woodbine fields began. Figs. 8 and 9 show the pressure drawdown of the basin in 1930 and 1950. Major production from the basin began in 1921 with production from the Mexia-Powell fault-line fields, and by 1930 a pressure sink of some 400 psi was established around the Mexia-Powell area with a perceptible drawdown occurring as far east and north as 60 to 70 miles. The East Texas Field was discovered and began producing from the east edge of the basin late in 1930. Between this date and 1950 the production from the fault line fields declined, and the production from the East Texas Field became the dominant influence on the pressure of the basin. By 1950 marked interference existed between these two producing areas as is evident by the distortion of the pressure distribution about them, and their effects caused a pressure drawdown in all of the basin east and south of the Mexia-Talco fault.

STUDY OF THE EAST TEXAS FIELD

Pressure Predictions with the Pool Unit

One of the major controls in obtaining a match of the pressure distribution of the Woodbine basin on the reservoir analyzer was the duplication by the analyzer of the pressure history of the East Texas Field. This match of the pressure-production history of East Texas with the pool unit is shown on Fig. 10. The observed pressures in this illustration are the average pressures obtained by volume weighting. This

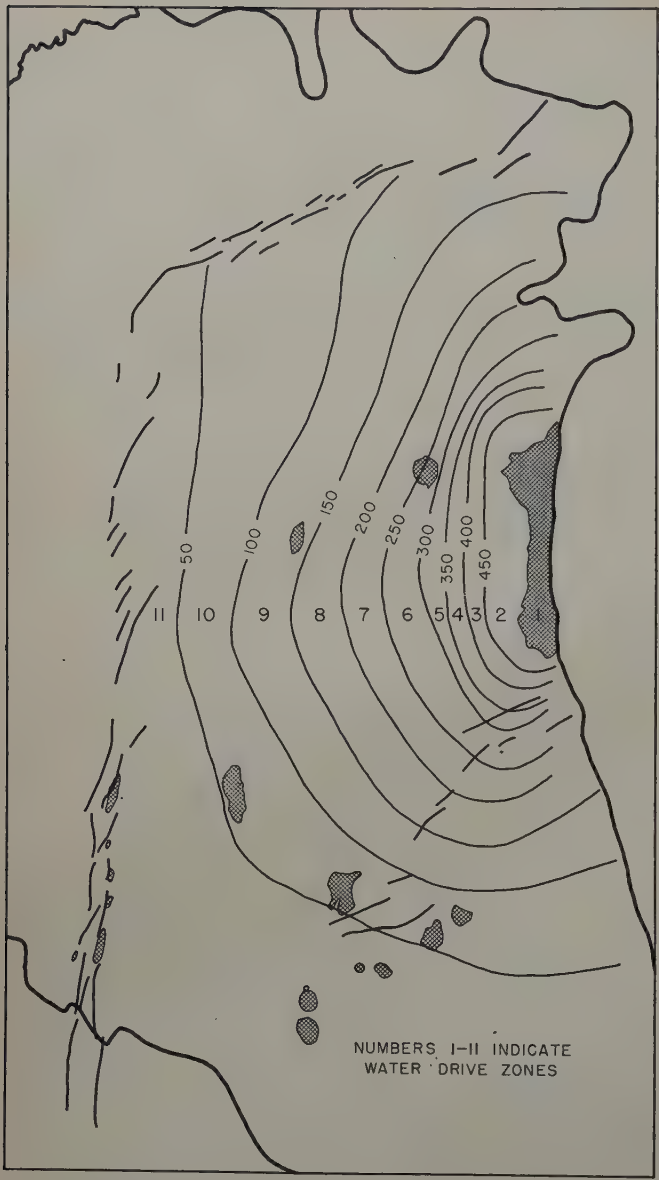

FIG. 12 — PRESSURE DRAWDOWN OF WOODBINE BASIN DUE TO EAST TEXAS FIELD PRODUCTION.

Table III — Estimates of Water Production

Oil Rate S.T. B/D	Date	Water Rates Production B/D	Water Rates Injection B/D
200,000	1-1-51 to 9-1-52	502,200	452,000
	9-1-52 to 9-1-59	637,400	573,700
	9-1-59 to 1-1-61	688,100	619,300
250,000	1-1-51 to 4-1-52	532,300	479,000
	4-1-52 to 10-1-57	707,600	636,800
	10-1-57 to 1-1-61	769,000	692,100
300,000	1-1-51 to 1-1-52	563,100	506,760
	1-1-52 to 7-1-56	777,700	700,000
	7-1-56 to 1-1-61	851,750	766,600

method of obtaining an average pressure for the field was used in place of the customary procedure of area-weighting, since the pressure obtained from the analyzer is a volume-weighted pressure. A comparison of the pressures derived from the two methods of averaging is presented on Fig. 11.

The pool unit representation of the East Texas Field was used to make predictions of the pressure in the field for the period Jan. 1, 1951, to Jan. 1, 1961, using oil production rates of 200,000, 250,000, and 300,000 bbl of stock-tank oil per day. The estimates of water production presented in Table III were based on the following assumptions:

1. The number of marginal wells will remain constant.
2. The rate of oil production from the marginal wells will remain at 20,419 bbl of stock-tank oil per day, the rate existing on Jan. 1, 1950.
3. The other wells will produce at a rate of 20 bbl of stock-tank oil per producing day.
4. Ninety per cent of the produced water will be returned to the Woodbine formation.
5. The rate of fluid production from the other fields producing from the Woodbine will be maintained at their 1950 rates.

Fig. 10 shows the predicted pressure behavior of the East Texas Field for the above rates of oil production. The 200,000 bbl of stock-tank oil per day rate resulted in a pressure rise from 1,100 to 1,130 psi by 1953, followed by a gradual decline to 1.095 psi by Jan. 1, 1961. The 250,000 bbl of stock-tank oil per day and the 300,000 bbl of stock-tank oil per day rates caused the reservoir pressure to decline over the 10-year period to 1,060 and 970 psi, respectively.

In addition to these predictions, the rate of net reservoir withdrawal that would be required to hold the volume-weighted pressure constant at 1,060 psi was determined for the period 1951 to 1961. A volume-weighted pressure of 1,060 psi during this period corresponds to an area-weighted pressure of approximately 990 psi. This rate was found to decrease gradually from the initial net fluid withdrawal rate of 500,000 reservoir B/D to 360,000 reservoir B/D. These rates are equivalent to 320,000 and 230,000 bbl of stock-tank oil per day, respectively. This study indicated that, even though the basin is considerable in expanse, the portion readily available for the water drive under which the East Texas Field is producing is bounded on the north and west by the Mexia-Talco fault, across which there is limited continuity. This should have a significant effect on future field behavior, and should necessitate the return to the formation of nearly all produced water and a gradual decrease in production rate to maintain an area-weighted pressure of 990 psi.

Determination of Available Water

In order to determine whether the water yield will be sufficient from the Woodbine basin to produce by water drive the two and a half billion bbl of recoverable oil remaining in the East Texas field, the effects of maintaining the pressure at two different levels were investigated by means of the pool unit representation of the basin. It was determined that if the volume-weighted pressure in the reservoir is maintained at 1,020 psi, six billion bbl of water will enter the East

Table IV — Average Permeability in the Water-Drive Zones

Zone	Permeability millidarcys	Zone	Permeability millidarcys
1-2	1,644	6-7	723
2-3	1,866	7-8	699
3-4	755	8-9	722
4-5	761	9-10	351
5-6	655	10-11	294

Texas reservoir from the Woodbine basin. Similarly, if the reservoir pressure is maintained at 820 psi, ten billion bbl of Woodbine water will enter the reservoir. Hence, it appears that there will be more than sufficient water yield from the Woodbine aquifer to produce by water drive the remaining two and a half billion bbl of stock-tank oil from the East Texas Field if the present practice of returning 90 per cent or more of the produced water to the Woodbine formation is continued.

Representation on the Water-Drive Unit

The detailed variations in reservoir pressure caused by abrupt changes in the production rate were not duplicated on the pool unit of the analyzer, since the field was assumed to have an average rate of withdrawal for each year. To match the month-to-month fluctuations in pressure, it was desirable that the water-drive unit be employed because the greater number of time periods available on that unit permitted a breakdown of the production history into smaller increments. To transfer the problem from the pool unit to the water-drive unit, it was desirable to determine the pressure distribution in the Woodbine basin due to production from the East Texas Field alone. With the same pool-unit network used to obtain the match of the volume-weighted pressure decline of the East Texas Field, the basin pressure drawdown due solely to the production from the East Texas Field was determined as of Jan. 1, 1947, and is shown on Fig. 12.

In the transfer of the problem from the pool unit to the water-drive unit of the analyzer, the Woodbine aquifer was divided into 11 approximately semi-circular, concentric zones about the East Texas Field with zone boundaries corresponding to the pressure contours shown on Fig. 12. Each of these zones was represented by an electrical capacitance, the value of which was computed from the water compressibility determined on the pool unit to be 5.3×10^{-8} vol/vol/lb/sq ft and from data regarding the size and thickness of the aquifer.

Table V — Water-Drive Resistor and Condenser Values

Zones	Resistor megohms	Condenser microfarads
1	0.280	8
2	.200	10
3	.200	15
4	.300	19
5	.200	15
6	.300	45
7	.300	81
8	.300	103
9	.800	155
10	1.600	250
11	off	310

To arrive at apparent permeabilities for each of the zones, the zone boundaries were superimposed on a map showing the apparent permeabilities that were obtained from the pool unit. An average value was then estimated for the permeability between adjacent concentric zones. These values are presented in Table IV and were used in calculating the values of the water-drive resistors. The representation of the East Texas Field and its aquifer on the water-drive unit, then, was consistent with the pool-unit representation insofar as compressibility of the Woodbine water and the apparent permeability distribution of the aquifer were concerned. The constants for both the pool-unit and water-drive unit studies are presented in Table II. Table V presents the values of the water-drive resistors and condensers.

In an ideal aquifer for any finite time, the pressure drawdown at a point a given distance from a production point is theoretically a linear function of the rate of production. This fact, in conjunction with the principle of superposition, indicates that the pressure drawdown resulting from production a given distance away is always independent of the number of production points. This would indicate that the effect of any basin production on the pressure in the East Texas Field might be closely approximated in the water-drive unit study by the withdrawal of a proportional current from the zone condenser corresponding to the area in which the point of production lay.

A satisfactory match of the volume-weighted pressure behavior of the East Texas Field was obtained on the analyzer by the withdrawal of appropriate production from the zones in which producing fields lay. This match is shown on Fig. 13. As a further check on the validity of this method of representing the problem, predictions of the pressure behavior of the East Texas Field were made at the same rates of produc-

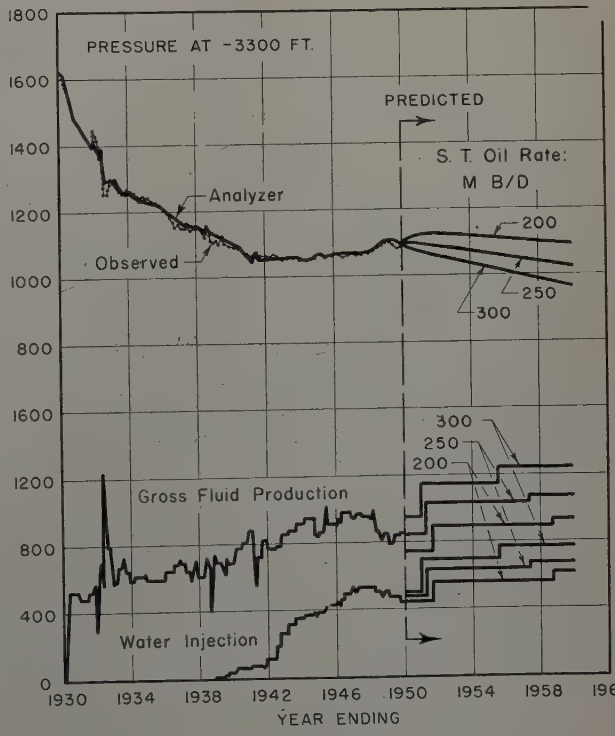

FIG. 13 — WATER DRIVE UNIT REPRESENTATION, EAST TEXAS FIELD.

tion as were used in the pool-unit study. The predictions with the water-drive unit are presented on Fig. 13. These predictions check closely with those obtained in the pool-unit study. The close agreement between the two methods indicates that even though there is interference between fields, reservoir studies can be made of those fields with the water-drive unit.

CONCLUSIONS

The analyzer study of the Woodbine basin indicates that the value of the effective compressibility of water used in conventional mathematical reservoir studies should be higher than that of the water alone. The agreement between the value, 5.3×10^{-8} vol/vol/lb/sq ft, obtained for the apparent compressibility of the Woodbine water and the sum, 4.7×10^{-8} vol/vol/lb/sq ft, of the measured compressibilities of the water and sand indicates that these may be the major components of the apparent compressibility.

The study indicated that the apparent permeability of the Woodbine sand is 1,000 to 1,500 md in the vicinity of the East Texas Field, and decreases to 100 to 700 md near the Mexia-Talco fault line. The data on the pressure drawdown west of the Mexia-Talco fault line were too meager to determine accurately the long range effect of the fault on the pressure distribution in the Woodbine basin; however, there appears to be little effective communication across the fault line.

The presentation of the Woodbine basin on the analyzer provides a satisfactory match of the pressure performance in the East Texas Field, and should therefore furnish a convenient means of predicting future pressures. However, the pressure behavior of the field should still be predictable with the use of the mathematical equations if the proper boundary conditions are applied. The magnitude of the effects of the Mexia-Talco fault line and the production from other fields on the pressure of the East Texas Field are of sufficient magnitude that they must now be accounted for in any computation of the performance of the field. This study of the performance of the East Texas Field and of the associated Woodbine aquifer on the reservoir analyzer indicated that if the present practice of returning 90 per cent or more of the produced water to the Woodbine formation is continued, an area-weighted pressure of 990 psi can be maintained provided there is also a gradual decrease in the rate of production. The study further indicated that with the current practice of return of produced water, there will be sufficient water yield from the aquifer to produce the East Texas Field to depletion under the water-drive mechanism.

REFERENCES

1. Bell, John S., and Shepherd, J. M.: "Pressure Behavior in the Woodbine Sand," *Trans.* AIME (1951) **192,** 19.
2. Buckley, S. E.: "The Pressure-Production Relationship in the East Texas Field," API *Drill. and Prod. Prac.* (1938), 140.
3. Schilthuis, R. J., and Hurst, W.: "Variations in Reservoir Pressure in the East Texas Field," *Trans.* AIME (1935) **114,** 164.
4. Muskat, M.: "Flow of Compressible Fluids Through Porous Media and Some Problems in Heat Conduction," *Physics* (1934) **5,** 71.
5. Carpenter, C. B., and Spencer, G. B.: "Measurements of Compressibility of Consolidated Oil-Bearing Sandstones," *Bureau of Mines RI 3540* (October, 1940).

★ ★ ★

T.P. 3231

POROSITY-MEASUREMENT COMPARISONS BY FIVE LABORATORIES

B. J. DOTSON, MAGNOLIA PETROLEUM CO., DALLAS, TEX., **R. L. SLOBOD**, THE ATLANTIC REFINING CO., DALLAS, TEX., MEMBER AIME, **P. N. McCREERY**, PHILLIPS PETROLEUM CO., BARTLESVILLE, OKLA., AND **JAMES W. SPURLOCK**, STANOLIND OIL AND GAS CO., TULSA, OKLA., MEMBER AIME

ABSTRACT

A core sample porosity-check program is described. A number of laboratories participated in the investigation, which comprised measuring the porosities of ten selected natural and synthetic core samples. Each laboratory employed its own method (or methods) of measurement. These included Boyle's Law, water-saturation, and organic liquid-saturation methods. Brief descriptions of each method employed are given. In general, the measured values of porosity were in reasonably good agreement. The average deviation of porosity from the mean or average values for the group of samples was ±0.5 porosity per cent. The results of these measurements are compiled and presented in graphical form.

INTRODUCTION

The total bulk volume of a porous sample is derived from the sum of two volumes, the void or pore volume and the solid* or grain volume. The porosity fraction of the sample is defined as the ratio of the void volume to the bulk volume. Multiplication of this ratio by 100 converts it to per cent porosity.

Distinction is made here between total porosity and effective porosity. The former includes all void space, both interconnected and isolated, while the latter includes only those voids which are interconnected. This investigation deals only with the effective porosity.*

Numerous cases had been noticed in which there appeared to be appreciable discrepancies in the results of porosity determinations on core samples. Differences of as much as 10 to 15 porosity per cent had been reported from different sources

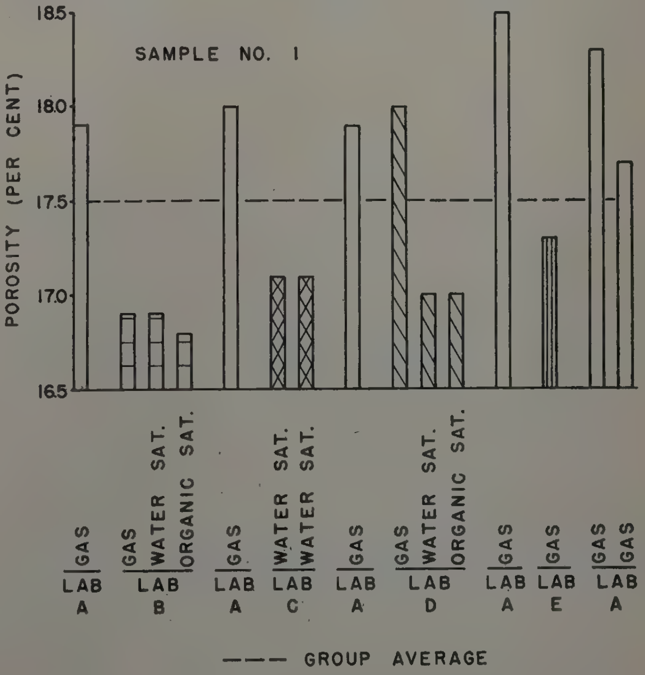

FIG. 1 — CORE SAMPLE POROSITY.

Manuscript received in the office of the Petroleum Branch Aug. 8, 1951.

*In this paper, the term "solid volume" includes all entrapped or non-interconnected void space.

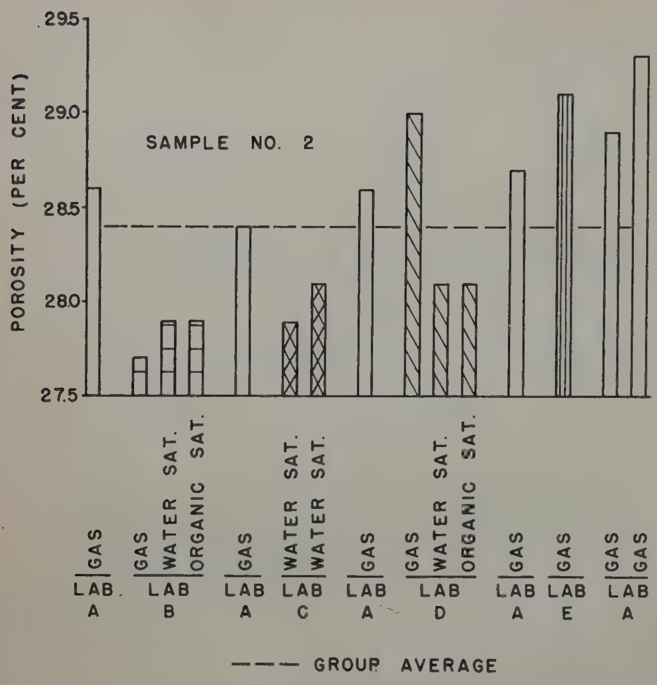

FIG. 2 — CORE SAMPLE POROSITY.

for the same sample. It was believed that the petroleum industry would be desirous of knowing the order of reproducibility of results that would be obtained, under controlled conditions, where different current methods of measurement were employed, or where different operators of the same method were involved.

A number of laboratories* agreed in November, 1949, to lend their efforts to such an investigation and to submit the information obtained for publication. Each laboratory was to employ its own method (or methods) for measurement, and preferably make these measurements under normal routine conditions.

PROCEDURE

Ten core samples which were quite varied in their characteristics were selected for the porosity-check program (See Table I). Both natural and synthetic samples with varying degrees of consolidation were included in this set of core samples.

The size of the samples was limited to three-fourths to seven-eighths inches in diameter by three-fourths to seven-eighths inches in length, to insure that all could easily be accommodated in the various pieces of measuring equipment.

The following procedure was agreed to by all participants in the program. The porosity values were first determined by Magnolia Petroleum Co.'s Field Research Laboratories, after which the samples were shipped to another one of the participating laboratories, together with a printed form data sheet. The samples, as shipped, were ready for porosity determinations, except for any extra drying procedure deemed advisable by each laboratory. Upon completion of the measurements by each recipient, the samples, together with the completed data form, were returned to the Field Research Laboratories for re-measurement. This process was then repeated until measurements had been made by all participants. In this manner, control data were obtained which should indicate any progressive change in the properties of the samples as a result of handling or treatment.

Table I — Characteristics of Samples Used in the Porosity-Check Program

Sample Number	Type	Sample Supplied By	Approximate Gas Permeability (md)	Approximate Porosity (%)
1	Limestone	Atlantic	1	15
2	Fritted Glass	Magnolia	2	35
3	Sandstone	Magnolia	20	15
4	Sandstone	Magnolia	1,000	20
BZE	Semi-quartzitic sandstone	Atlantic	0.2	4
BZG	Semi-quartzitic sandstone	Atlantic	0.8	4
61-A	Alundum	Magnolia	1,000	26
722	Alundum	Atlantic	3	17
1123	Chalk	Magnolia	1.6	33
1141-A	Sandstone	Magnolia	45	20

In addition to porosity values, the bulk, pore, and solid volumes were measured and recorded along with the ambient temperatures at which the data were obtained. From one to three determinations were made on each sample by each of the laboratories. The order of measurement, by participants, followed no particular sequence. The order was arranged,

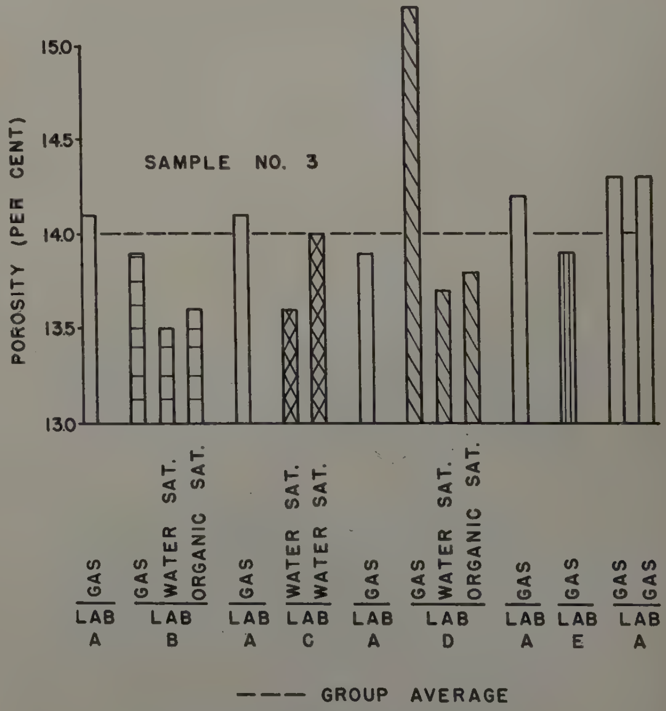

FIG. 3 — CORE SAMPLE POROSITY.

---

*The Atlantic Refining Co., Magnolia Petroleum Co., Phillips Petroleum Co., and Stanolind Oil and Gas Co.; General Petroleum Corp. of California also entered the program at a later date.

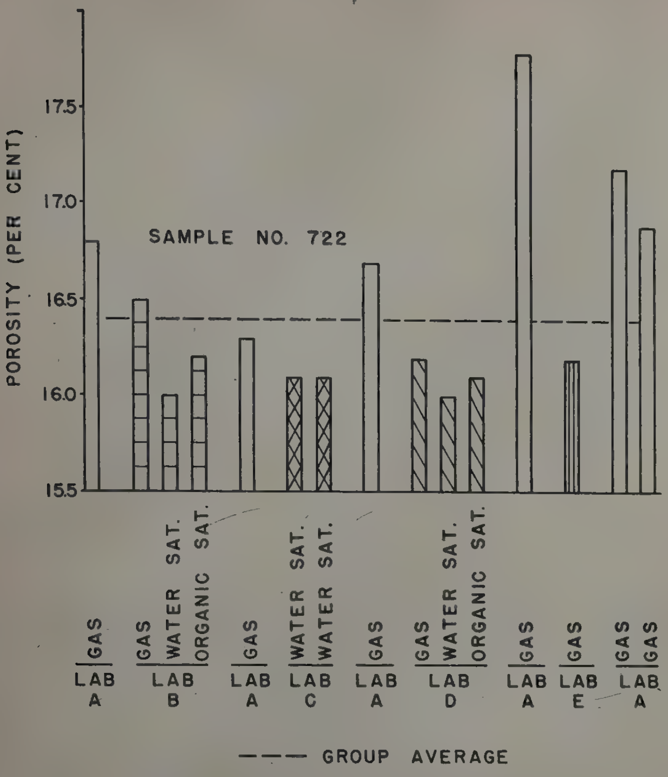

FIG. 4 — CORE SAMPLE POROSITY.

however, to permit the Magnolia Laboratories to make control measurements alternately with the other laboratories, as previously mentioned.

In order to furnish additional control data on the samples, weights of the samples were obtained by each laboratory prior to its porosity determinations and immediately prior to shipment. Weighings were also made at other times. Determinations of the gas permeabilities were made periodically throughout the investigation by the Magnolia Laboratories.

METHODS OF POROSITY MEASUREMENT*

Laboratory A employed the Kobe Porosimeter for porosity measurement. Both the solid and bulk volumes are determined in the instrument, bulk volume by mercury displacement and solid volume by air displacement. The fractional porosity is obtained by dividing the difference between the bulk and solid volumes by the bulk volume.

Laboratory B employed three methods for porosity determination. These are as follows:

1. Gas Method

   The solid volume of the sample is determined directly in a Modified Bureau of Mines Boyles Law Air Porosimeter. The bulk volume is determined by mercury displacement. Subtracting the solid volume from the bulk volume and dividing this result by the bulk volume yields the fractional porosity.

2. Water Saturation

   The pore volume is determined from the difference between the weights of the dry sample and the sample saturated with distilled water, divided by the density of the water. Determination of the bulk volume is made by weighing the water-saturated sample in air and again weighing it submerged in water. The difference between these weights divided by the density of water yields the bulk volume. The ratio of the pore volume to the bulk volume is the fractional porosity.

3. Organic Liquid Saturation

   This method is identical with that of No. 2 except that tetrachlorethane is used in place of water.

Two methods of porosity measurement were employed by Laboratory C.

1. The solid volume is determined by the difference in weights of the dry sample (in air) and the sample saturated with and suspended in water, divided by the density of water. The bulk volume is determined from the mercury displacement produced by the water saturated sample. The fractional porosity is the difference between the bulk and solid volumes divided by the bulk volume.

2. According to the second method, the pore volume is determined by the difference between the weight (in air) of a water-saturated core sample and the weight of the dry sample, divided by the density of water. This result, divided by the bulk volume, as determined by Method No. 1, yields the fractional porosity.

Laboratory D employed three methods of porosity measurement. These are as follows:

1. Gas Method

   The bulk volume is determined by weighing the core saturated and suspended in saturant. The difference in these weights divided by the density of the saturant gives the bulk volume. The solid volume is determined directly by a gas expansion porosimeter. The porosity fraction is given by the bulk volume minus the solid volume divided by the bulk volume.

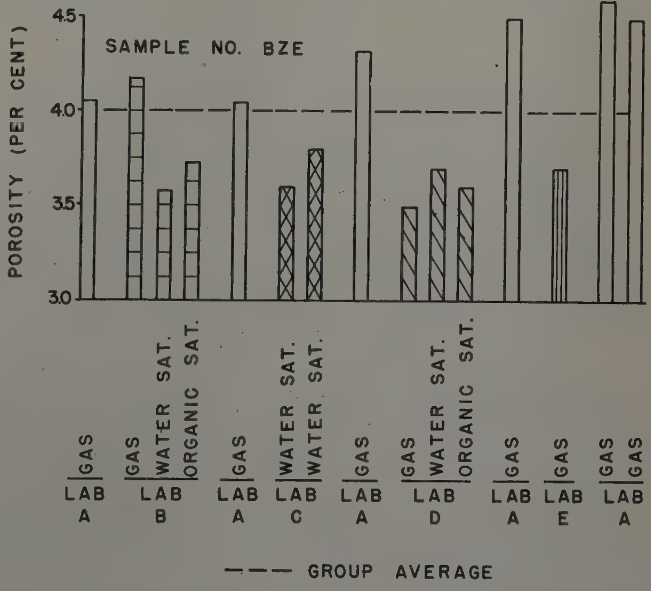

FIG. 5 — CORE SAMPLE POROSITY.

---

*References given at end of paper.

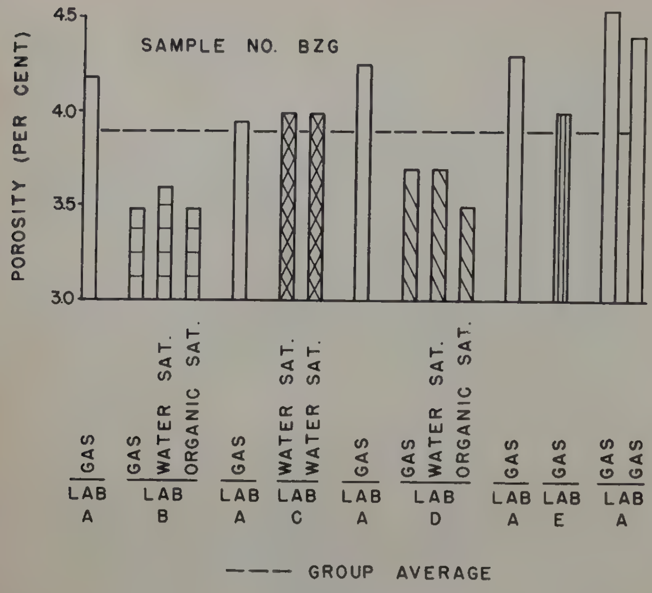

FIG. 6 — CORE SAMPLE POROSITY.

2. Water Saturation

In this method the pore volume was determined from the difference in weights of the water-saturated sample in air and the weight of the dry sample in air. This weight difference (corrected for liquid density) yields the pore volume. This pore volume divided by the bulk volume, determined as described in the gas method procedure above, yields the fractional porosity.

3. Organic Liquid Saturation

This method is identical with that of No. 2 above except that the hydrocarbon, tri-isobutylene, is used in place of distilled water for both the pore- and bulk-volume determinations.

Laboratory E also used the Kobe Porosimeter for porosity measurements. The procedure is the same as that described above for Laboratory A, except that helium was used in place of air.

RESULTS AND CONCLUSIONS

The core sample porosity-check program was completed as planned. Porosity measurements of ten selected, natural and synthetic, core samples were made by five laboratories.

During the course of the investigation, the samples were subjected to a variety of methods of measurement. These included physical measurement, gas, and saturation (with both water and organic liquids) methods.

In general, the measured values were in reasonably good agreement. The results of the porosity measurements are shown graphically in Figs. 1 through 10, inclusive. The measured values, expressed in terms of per cent porosity, are shown along the ordinate and the number of measurements are shown along the abscissa. These are arranged from left to right in chronological order of measurement by the participants. The average, or mean, porosity value and the average deviation from the mean porosity values for the samples are shown in Table II.

Table II — Results of Porosity Measurements

Sample Number	Mean Porosity Value (%)	Average Deviation from Mean Porosity (%)
1	17.5	± 0.5
2	28.4	± 0.4
3	14.0	± 0.3
4	30.3	± 1.0
BZE	4.0	± 0.3
BZG	3.9	± 0.3
61-A	28.4	± 0.5
722	16.4	± 0.4
1123	32.6	± 0.6
1141-A	19.4	± 0.4

The average deviation of porosity from the mean or average values for all samples was ±0.5 porosity per cent. Lack of agreement was the greatest for sample No. 4, which was a friable, high-permeability, sandstone sample. The average deviation from the mean porosity value for this sample was ±1.0 porosity per cent. The largest difference of values for sample No. 4 was 5.6 porosity per cent; *i.e.*, a variation from 26.8 to 32.4 porosity per cent. Exclusive of this sample, the largest variation of individual values occurred for sample No. 1123. The individual measurements of porosity in this case exhibited a total range of 2.1 porosity per cent; *i.e.*, from 31.7 to 33.8 porosity per cent.

The results of the porosity measurements are considered fairly good, and the variations which occurred were not of the order of magnitude that was suspected when this program

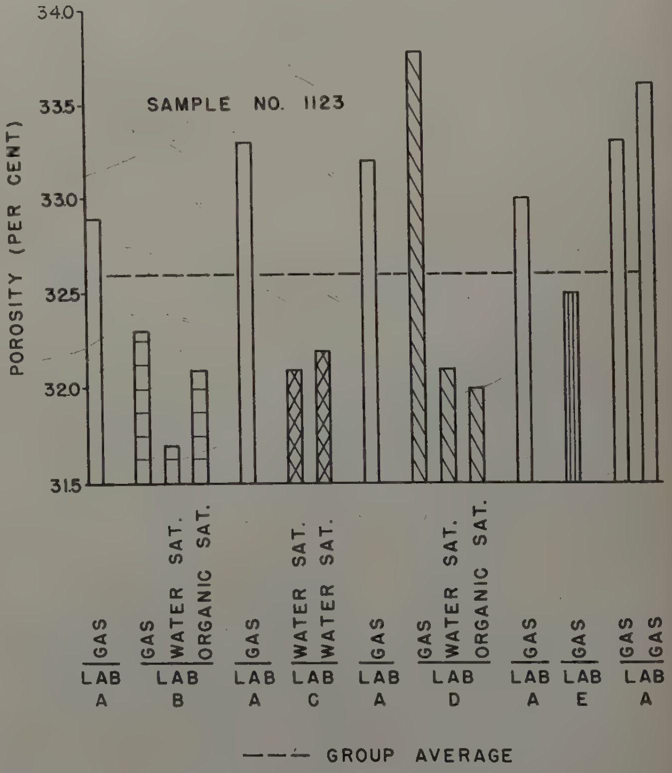

FIG. 7 — CORE SAMPLE POROSITY.

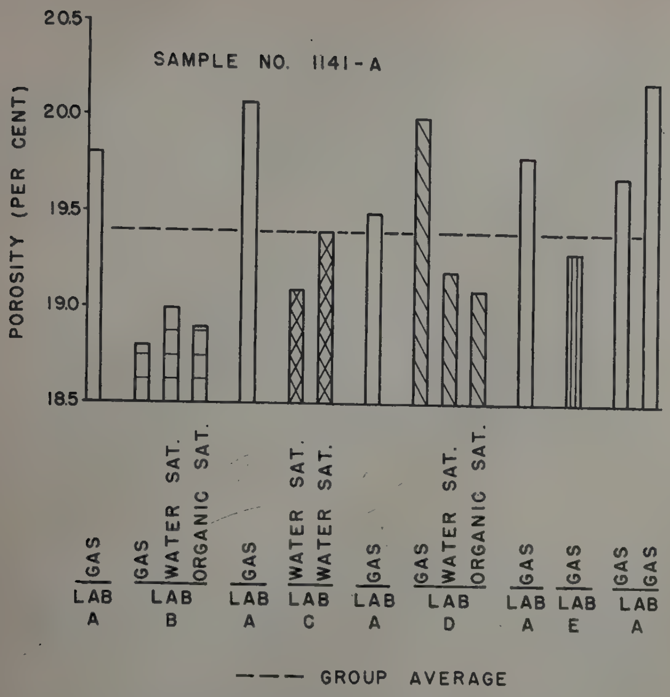

FIG. 8 — CORE SAMPLE POROSITY.

was initiated. However, it is well to emphasize that the samples selected were an idealized group, in that, as far as is known, they were relatively immune to reaction with the materials which made contact with them during the porosity measurements. Thus, the investigation resulted in being, primarily, a check of methods and instruments. The differences actually observed between the various methods, while small, are considerably greater than the individual reproducibility of each method. This paper makes no effort to account for these differences, nor does it present any estimate of the relative reliability of the various methods.

Since the porosity values shown in Figs. 1 through 10, inclusive, are derived from the measured quantities, bulk, solid and pore volumes, it is then evident that the variations experienced in the porosity values are the result of a combination of variations in these quantities. The determinations of bulk volume were the most reproducible of the quantities measured. However, this excludes the method of caliper measurement, since this method inherently yields a value which is too large. The lack of reproducibility of the solid and pore volume measurements was of the same order of magnitude.

In general, the gas methods gave slightly higher values, on the average, than liquid saturation methods. This may be partially due to the presence of adsorbed gases in the Boyle's Law Method or to lack of complete saturation of the samples in the saturation methods, or a combination of both.

It is apparent from this investigation that the problem of reproducibility of porosity measurement is not as serious as was considered possible at first. This is true at least for samples not affected by the materials used in the method of measurement. It is believed that, when made with reasonable care, future porosity measurements by the methods described can be expected to agree within the same order of magnitude as reported herein. This does not include measurements, by water saturation techniques, on samples having high clay contents, or on samples for which complete extraction of the contained crude oil has not been achieved.

A weight check maintained on the samples showed that, with the exception of three samples, the weights remained essentially constant. Samples No. 3, 4, and 1123 showed a progressive decrease in weight which was evidently caused by the loss of solid material from the samples with handling. This loss of material was also readily apparent in the trend of the bulk and solid volume measurements on these samples. The decrease was most pronounced in the case of sample No. 4, a very friable high-permeability sandstone sample. As

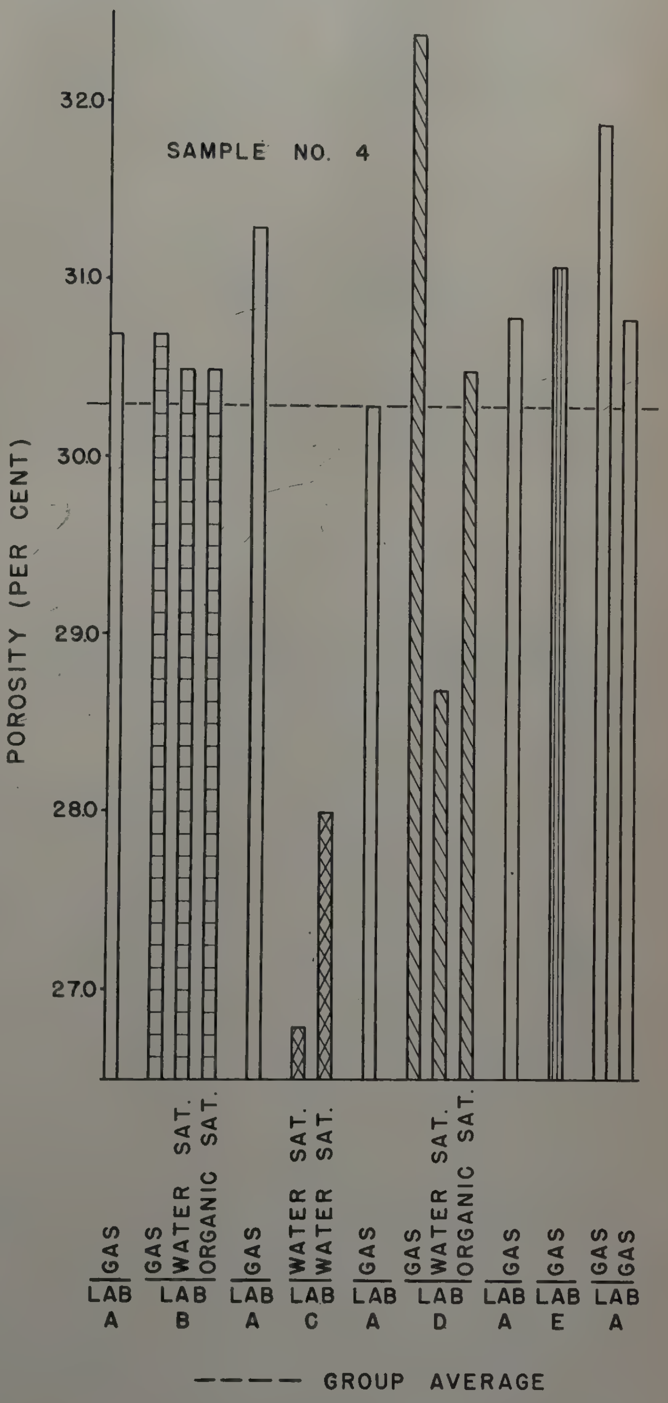

FIG. 9 — CORE SAMPLE POROSITY.

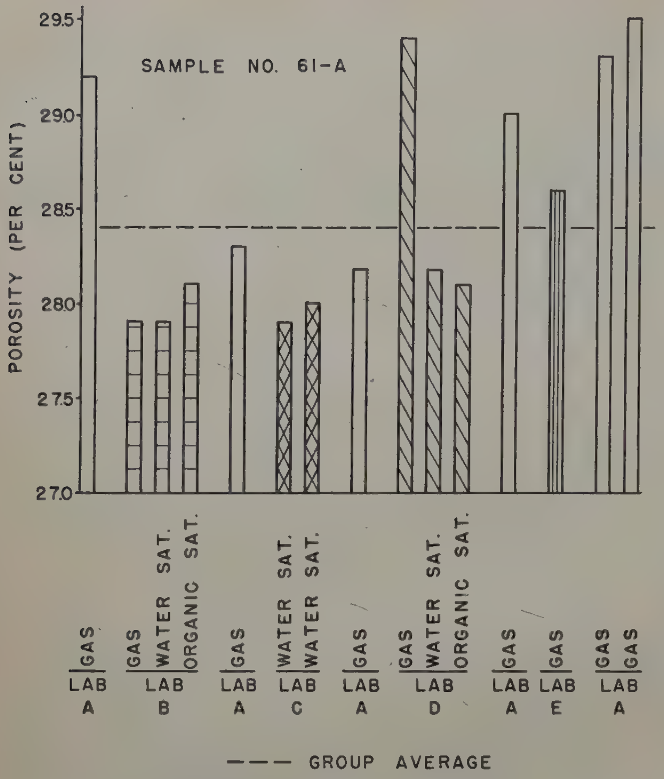

FIG. 10 — CORE SAMPLE POROSITY.

a matter of interest, it might be noted that the weight measurements obtained by the participating laboratories were very consistent.

Gas permeabilities of the samples were measured periodically during the investigation by the Magnolia Laboratories. The permeabilities were fairly constant throughout the investigation. Variations which occurred for two of the samples were probably due to measuring equipment difficulties, and not to an actual change in the samples.

Ambient temperatures occurring at the time of the porosity measurements were recorded; however, since the temperatures were essentially the same for all the measurements, slight variations in temperature were not considered in the compilation of results.

ACKNOWLEDGMENT

The authors are grateful to The Atlantic Refining Co., General Petroleum Corp., Magnolia Petroleum Co., Phillips Petroleum Co., and Stanolind Oil and Gas Co., for permission to publish this paper.

REFERENCES

Although the following list is not intended to be a complete bibliography on the subject, these references are included to furnish the reader with additional sources of information on porosity measurement.

Gas Methods of Porosity Measurement:

1. Beeson, Carrol M.: "The Kobe Porosimeter and the Oilwell Research Porosimeter," *Trans.* AIME (1950) **189**, 313.
2. Taliaferro, D. B., Jr., Johnson, T. W., and Dewees, E. J.: "A Method of Determining Porosity: A List of Porosities of Oil Sands," *U. S. Bureau of Mines R. I. No. 3352* (September, 1937).

Water Saturation Methods of Porosity Measurement:

3. Beecher, M. F.: *Transaction American Ceramic Society Bulletin No. 17* (1915) 102.

Organic Liquid Saturation Methods of Porosity Measurement:

4. Barnes, K. B.: *Pennsylvania State College, Mineral Industries Experiment Station Bulletin No. 10* (1931). ★

T.P. 3222

THE GUARD ELECTRODE LOGGING SYSTEM

JOHN E. OWEN, GEOPHYSICAL RESEARCH CORP., TULSA, OKLA., AND **WALTON J. GREER**, HALLIBURTON OIL WELL CEMENTING CO., HOUSTON, TEX., MEMBER AIME

ABSTRACT

The guard electrode system measures the resistivity of formations by employing a thin disk of current which is caused to flow perpendicular to the bore hole. The control of this current disk is obtained in a brute force manner through the use of relatively long equipotential electrodes above and below the measuring electrode.

The log obtained from the system is free of "lag," "plateau," "shadow," "reflection" and other distortions evident on conventional logs. The proportionate contributions of the hole size and invaded zone resistivity to the apparent resistivity reading are reduced when the mud and filtrate resistivities are lower. Thus, the guard system favors the use of conductive muds.

The mathematical development of the theory is given in an appendix. Equations are derived to evaluate the effects of mud resistivity, hole size, invaded zone resistivity and depth, and the true formation resistivity.

Sample logs from several provinces are reproduced and compared with conventional electric logs to illsutrate the much greater detailed lithology that can be presented by the guard electrode system.

INTRODUCTION

With increased ability of those in the petroleum industry to analyze formation characteristics from electrical resistivity data, there has become apparent the need for more precise measures of that parameter.

The measurement of the resistivity of a homogeneous and isotropic material can be made simply when the body of the material is infinite in all dimensions and the measuring electrodes can be placed within the body. In such a case, the current leaving an electrode follows a spherical distribution and the mathematical expression for the potential level at any distance from that electrode can readily be derived.[1,2]

If it is considered that the active electrodes are within a bore hole filled with mud of a resistivity different from that of the formation, the current does not flow in a spherical pattern near the current source or sink, and the calculations of potential levels become more difficult. The additional consideration of a section of formation invaded by mud filtrates, and thus having resistivity different from either that of the mud, the adjacent formations or of the undisturbed formation, makes the mathematical problem extremely complex. Should the vertical dimensions of the formations be considered as finite, the problem becomes so complex as to preclude reasonable solution. Yet, even these considerations have not described adequately the conditions encountered in a large proportion of the wells to be studied.

In efforts to evaluate the effects of the various conditions, combinations of two, three, and four electrode logging configurations of the conventional types have been used. The resulting logs have left much to be desired in some provinces. It has become apparent that the use of such configurations will not result in adequate measurements being made, particularly in cases where the formation is composed of thin sections.

If all the current of a resistivity measuring circuit is made to flow through the formation opposite the exploring electrode, many of the shortcomings of the conventional measuring system are eliminated. In the guard electrode method of electrical well logging to be discussed in this paper, the current is so controlled by causing it to flow in a thin disk normal to the axis of the logging tool.

EARLY HISTORY

The guard electrode method of electrical well logging in its early years was a joint development by the Geophysical Research Corp. and the Amerada Petroleum Corp. The method was first experimentally investigated by means of model studies. The results of these studies indicated that current focusing systems properly applied to electrical well logging

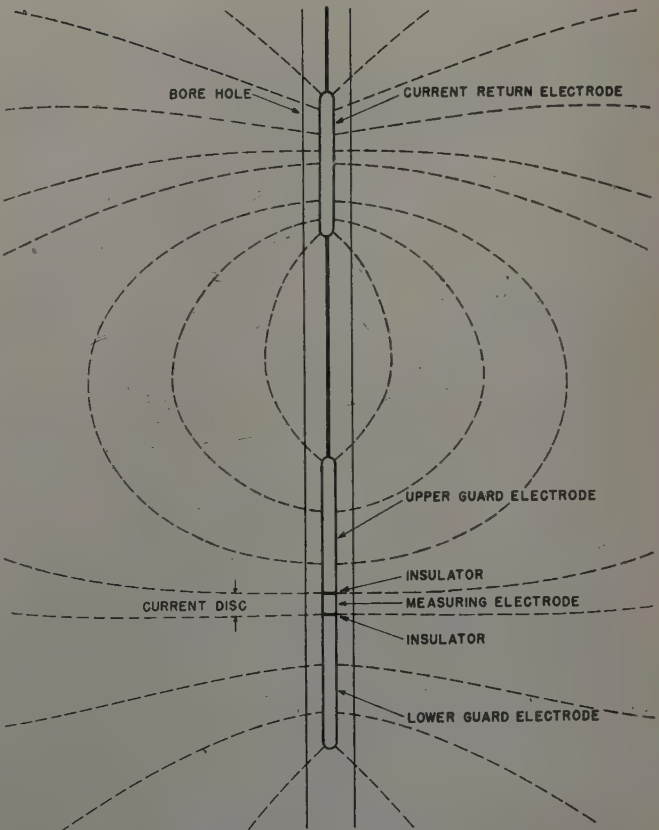

FIG. 1 — CURRENT FLOW PATTERN IN GUARD ELECTRODE SYSTEM.

---

[1] References given at end of paper.

Manuscript received in the office of the Petroleum Branch June 22, 1951. Paper presented at the Petroleum Branch Fall Meeting in Oklahoma City, Okla., Oct. 3-5, 1951.

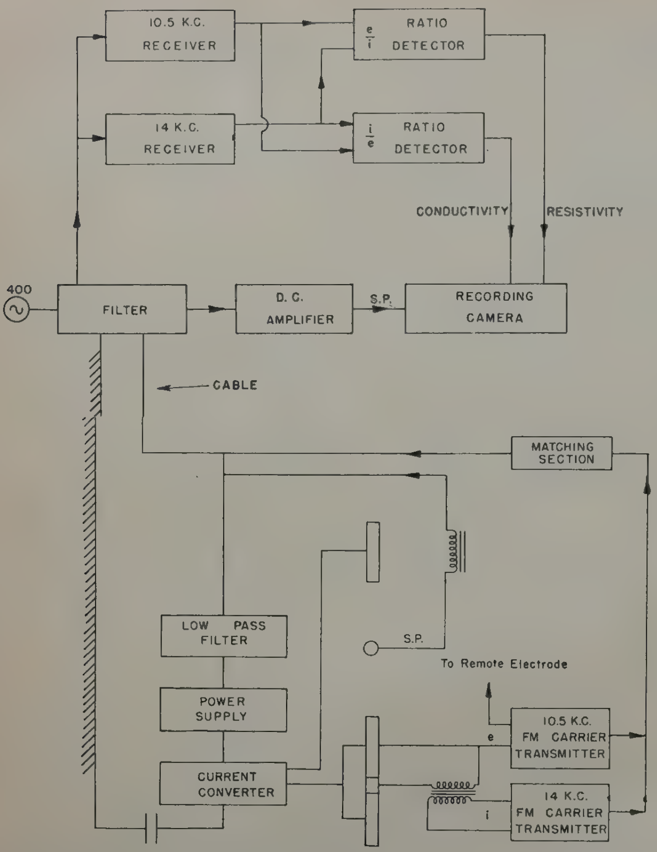

FIG. 2—BLOCK DIAGRAM OF INSTRUMENTATION EMPLOYED IN GUARD ELECTRODE LOGGING.

might have great possibilities in improving existing methods, and the decision was reached to build the necessary logging equipment and to carry the work into the field. This occurred in the period just preceding World War II. Critical shortages of materials during the war made the acquisition of field equipment extremely difficult; and as a result, actual field trials were not made until after the end of the war.

Some advantage was taken of these delays, however. Various current focusing systems were studied and the one that showed the most promise was selected for a field trial. There was developed during this period a wholly electronic system for supplying electrical power to the focusing electrode system and for combining for suitable recording at normal logging speeds the intelligence transmitted to the surface over the logging cable. This last phase of the work included, among other things, the development of an analog type of computer. This computer is an electronic instrument called a ratio detector, a device which permits the simultaneous logging of the resistivities and conductivities of formations traversed by the bore hole.

In the period that guard electrode well logging was carried out as an experimental project by the Geophysical Research Corp. and the Amerada Petroleum Corp., 31 wells were logged for a total of approximately 175,000 ft. Most of these wells were located in Oklahoma, in the West Velma, Sholem-Alechem, and Northwest Knox Fields. Other wells that were logged were in the Bloomington Field in the Gulf Coast of Texas, in the Fargo Field in North Texas, in the Barnhart Field in West Texas, and in three fields in California.

During the year 1950, the Halliburton Oil Well Cementing Co. assumed the development of a commercial logging device based on the principles proposed by Geophysical Research Corp. This involved adapting the instrumentation to a single-conductor transmission system instead of the multiple-conductor system used in the early development.

ELEMENTS OF GUARD ELECTRODE METHOD OF ELECTRICAL WELL LOGGING

The principles of the guard electrode logging device are illustrated in Fig. 1. All surfaces of the bottom electrode assembly are kept at essentially the same potential. This guard electrode assembly is made up of an upper guard electrode, a measuring electrode, and a lower guard electrode. An alternating current is passed between the bottom electrode assembly and the current return electrode. The path the current takes in going from the guard electrode assembly to the current return electrode through the earth is indicated by the dotted lines. The all-important feature of this system is that the current from the measuring electrode flows outwardly in essentially a horizontal direction for a considerable distance, and hence is confined to a disk-shaped space having a thickness approximately the same as the length of the measuring electrode. Variations in earth resistivity within this disk-shaped region control the amount of current flowing from the measuring electrode. It is desirable that variations in earth resistivity in the neighborhood of the current return electrode do not affect the resistivity or conductivity measurements that are obtained. This is accomplished by proper instrumentation, as will be shown.

The electrical measures needed from this system to provide the desired readings of resistivity and conductivity consist of (1) a measurement of the current emitted by the measuring electrode, and (2) a measurement of the voltage between this electrode and a point remote from any area of current concentration. A resistivity value is obtained by recording the ratio of the voltage between the measuring electrode and this distant point to the current passing into the earth from the measuring electrode. A conductivity value is obtained by recording the ratio of the current from the measuring electrode to the voltage between it and the distant point. Because the measured voltage is from the measuring electrode to a remote point which does not change in potential, the resistivity and conductivity values which are determined are not influenced by resistivity changes near the current return electrode in the hole. The reference depth is the depth of the measuring electrode. The geometry of this electrode system thus compares in simplicity with that of the single or point electrode.

INSTRUMENTATION

The instrumentation employed to furnish the necessary current to the electrode system and to measure the voltage and exploring current values and transmit them to the surface over a single-conductor cable is shown in block form in Fig. 2.

Located within the guard electrode assembly are all the electronic circuits required. The power necessary for these circuits is supplied by a gasoline engine driven 400-cycles-per-sec alternator located on the logging truck. The 400-cycles-per-sec current is impressed onto the line in a filter section as shown. In the tool, this current is directed by a low pass filter first through the power supply which provides the necessary heater and plate potentials for the various electronic tubes. From the power supply, the current is directed through a current converter which supplies the guard electrode system with current at 200 cycles per sec. The current then passes through a condenser to the sheath of the cable and returns to the alternator. The condenser blocks the SP signal from the sheath.

The total 200-cycles-per-sec current flows between the guard electrode and a current return electrode located some 60 ft up the cable from the exploring electrode. The exploring current is measured by a vacuum tube circuit which requires an extremely small signal.

The potential of the guard electrode is measured by another vacuum tube circuit connected between the guard electrode and a reference electrode located about 200 ft up the cable.

The measures of the exploring current and the potential modulate in frequency oscillators with center frequencies of 14 kc and 10.5 kc respectively. These carrier frequencies are impressed onto the single-conductor cable by a matching section which raises the power level of the combined signals and matches the impedance of the line.

At the surface, the carrier frequency signals are removed from the cable by the filter section and directed to their respective receivers. From these, current and voltage signals corresponding to those measured in the tool are obtained and directed to the ratio detector. The ratio detector provides a current corresponding to the resistivity or to the conductivity of the formation being logged. The output depends, of course, upon which of the current and potential measures is used as the numerator and which the denominator.

Provision is made for the logging of an SP curve simultaneously with that of the conductivity and resistivity. The signal is picked up by a separate electrode and applied to the conductor of the cable through a high inductance choke. In present tools the SP is located 30 ft above the exploring electrode. This offset is made necessary by the mass of exposed metal of the guard electrode which short circuits the SP in the vicinity of the exploring electrode. On the finished log, the SP curve is shifted the corresponding 30 ft in order to present the log at its proper depth. The location of the electrode prevents the logging of SP over the bottom section of the hole. The distance missed is 30 ft plus half the length of the guard electrode.

Graphs of the resistivity, conductivity, and SP values are recorded in a conventional electric logging camera.

THEORETICAL RESPONSE OF THE GUARD ELECTRODE SYSTEM

The proportionality factors by which the values measured are converted to resistivities and conductivities are, of course, the calibration factors which must be determined for the electrode configuration that is used. In the first well that was logged with guard electrode equipment by Amerada, a thick shale section of uniform resistivity was found. The first calibration of the guard electrode equipment was thus empirically obtained by assigning such a value to the calibration constant for the guard electrode equipment that agreement was reached between the guard electrode recorded apparent resistivity in this shale section and the corresponding apparent resistivity recorded on the conventional electrical log that was taken on the same well.

Computations of this calibration factor were later made, as were also extensions of the theory to include the effects of the resistivity of the fluid in the bore hole and the resistivity of the invaded zone.*

Certain of the formulæ that have been derived are of sufficient interest that they may be called to attention here. It should be understood that the derivation in the appendix is based on the assumption that the electrode has the shape of a prolate spheroid. This is considered to be a sufficiently close approximation to the actual shape of the electrode that formulæ thus developed are applicable. The following notation is used:

$2c$ = overall length of guard electrode assembly
$2b$ = length of measuring electrode
$2a$ = diameter of measuring electrode
$2a_2 = d$ = diameter of bore hole
$2a_3 = d_1$ = diameter of invaded zone
ρ_A = apparent resistivity as recorded on guard electrode log
ρ_m = resistivity of fluid in bore hole
ρ_i = resistivity of invaded zone
ρ_t = resistivity of uninvaded formation
I_a = current from measuring electrode
V_e = voltage between measuring electrode and distant ground reference

One equation of interest relates the resistivity of a formation of large extent in which the guard electrode assembly is buried, the voltage on the electrode, and the current from the measuring electrode. This determines the calibration factor for the electrode. For this case,

$$\rho_t = \rho_A = \frac{4\pi b}{ln\,\dfrac{c+k}{a}} \cdot \left(\frac{V_e}{I_a}\right) \quad . \; . \; . \; (1)$$

Another equation of interest is one expressing, in the case of no invasion, the relationship between the apparent resistivity of a formation, its true resistivity, and the resistivity of the mud in the bore hole. Here,

$$\frac{\rho_A}{\rho_m} = 1 + \left(\frac{\rho_t}{\rho_m} - 1\right) \frac{ln\,\dfrac{2(c_2+k)}{d}}{ln\,\dfrac{c+k}{a}} \quad . \; (2)$$

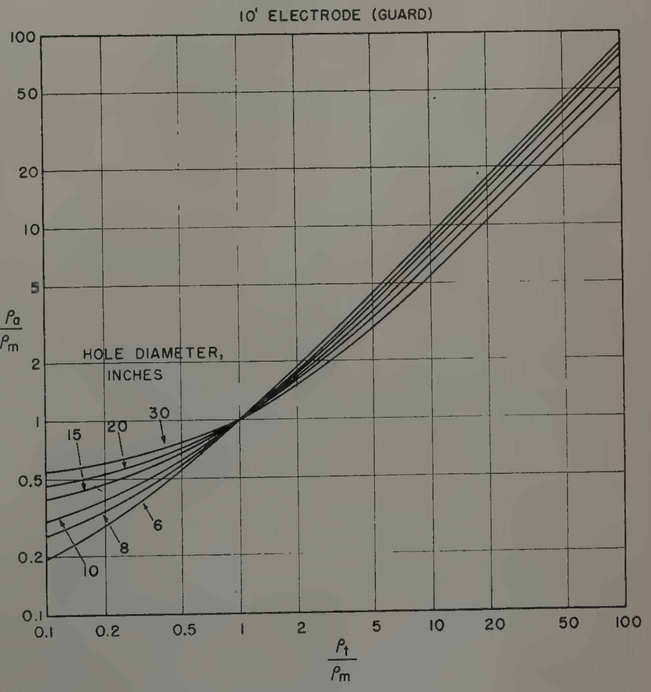

FIG. 3 — EFFECT OF HOLE SIZE AND MUD RESISTIVITY ON VALUES MEASURED BY GUARD ELECTRODE.

---

*This work was first done by A. Wolf and J. E. Owen of the Geophysical Research Corp., and later by Guy O. Buckner, Jr., of the Halliburton Oil Well Cementing Co. The results that were obtained were essentially equivalent. In the appendix of this paper, the derivation by Buckner is given.

The curves of Fig. 3 are calculated from Equation (2) and illustrate the effect of the bore hole diameter and the mud resistivity upon the readings of a system employing a total guard electrode length of ten ft and a measuring electrode of three in.

For the case in which there is invasion:

$$\frac{\rho_A}{\rho_m} = 1 + \left(\frac{\rho_i}{\rho_m} - 1\right)\frac{ln\frac{2(c_2+k)}{d}}{ln\frac{c+k}{a}} + \left(\frac{\rho_t}{\rho_m} - \frac{\rho_i}{\rho_m}\right)\frac{ln\frac{2(c_3+k)}{di}}{ln\frac{c+k}{a}} \quad \ldots\ldots\ldots\ldots \quad (3)$$

c_2, c_3, and k are defined in the appendix.

From Equation (2), it is apparent that the relative contribution of formation resistivity to the reading of apparent resistivity increases as the mud resistivity decreases. Likewise, from Equation (3), the relative contribution of the invaded zone can be made less by reducing its resistivity. This could be realized, of course, by reducing the filtrate resistivity.

Still another equation of interest is the one giving the thickness t of the current measuring disk at a distance r from the axis of the bore hole, and for the case in which the guard electrode assembly is located within a thick bed. Here,

$$t = 2b\sqrt{1 + \frac{r^2}{c^2 - a^2 - b^2}} \quad \ldots\ldots \quad (4)$$

and for the usual case in which $c \gg a$, and $c \gg b$,

$$t = 2b\sqrt{1 + \frac{r^2}{c^2}} \quad \ldots\ldots\ldots\ldots \quad (5)$$

to a sufficiently close approximation.

Fig. 4 illustrates the thickening of the current disk corresponding to equipment in which $c = 10$ ft, $a = 1\frac{1}{2}$ in., and $b = 1\frac{1}{2}$ in. Here it is seen that the current disk doubles in thickness at a distance of 17.3 ft from the axis of the electrode.

The thickening of the measuring current disk for short guard electrodes occurs much faster with radial distance than for long guard electrodes. The use of long and short guard electrodes thus shows promise of being the means for making resistivity measurements at different radial distances from the bore hole. Calculations which must be considered to be only approximate at this stage of the development of the method indicate that the depth of investigation may thus readily be controlled from a few inches to a few feet.

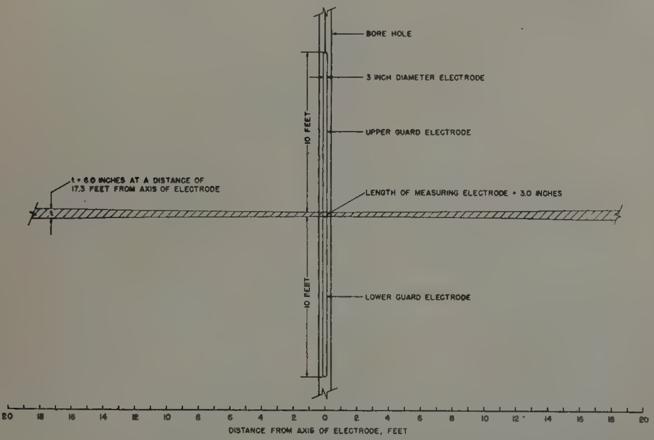
BORE HOLE
3 INCH DIAMETER ELECTRODE
10 FEET
UPPER GUARD ELECTRODE
t = 6.0 INCHES AT A DISTANCE OF 17.3 FEET FROM AXIS OF ELECTRODE
LENGTH OF MEASURING ELECTRODE = 3.0 INCHES
10 FEET
LOWER GUARD ELECTRODE
20 18 16 14 12 10 8 6 4 2 0 2 4 6 8 10 12 14 16 18 20
DISTANCE FROM AXIS OF ELECTRODE, FEET

FIG. 4 — DISTRIBUTION OF CURRENT FROM MEASURING ELECTRODE OF GUARD ELECTRODE SYSTEM IN A HOMOGENEOUS, ISOTROPIC MEDIUM.

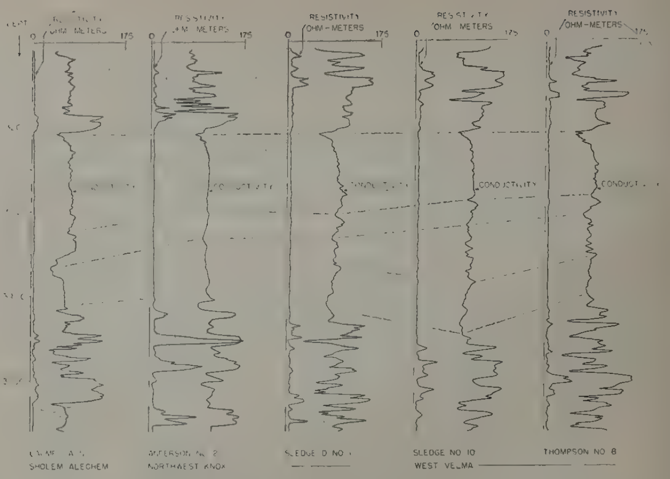

FIG. 5 — CONDUCTIVITY CORRELATIONS BETWEEN WELLS IN THREE OKLAHOMA OIL FIELDS.

The values recorded by the system will be exactly as calculated above so long as the actual conditions do not depart from those assumed. The mathematical equations presented were all derived with the considerations that the guard electrode has the surface of a prolate spheroid and that the entire surface is maintained at the same potential. These conditions are not held precisely.

In practice, the electrode has a cylindrical surface. For the configurations now being used, where the length of the electrode is large compared to the diameter, this difference in surfaces need not be considered. It is probable that logs made with configurations using very short guard lengths will be found valuable for the solutions of some problems. If guard lengths of the order of a few inches should be employed, correction factors would be required. No method has yet been devised to calculate such factors. They will be supplied by controlled model studies if the continued mathematical study fails to produce them.

The potential of the surface of the measuring electrode is always less than that of the guard electrode. This results from the necessity of there being a finite resistance in the current measuring circuit between the guard electrode and the measuring electrode through which the exploring current must flow. The proportional difference in potential between the electrodes in such a system is a function of the resistance of the electrode, which in turn is a function of the mud and formation resistivities. In present tools, the resistance between the surfaces is 0.05 ohms. This results in such small differences of potentials that for all values of mud and formation resistivities of 0.2 ohm-meter, or greater, the resulting errors in recorded values are less than 5 per cent. With lower mud and formation resistivities, the error increases rapidly. If the electrode assembly should be buried in a material of 0.09 ohm-meter resistivity, the recorded value would be 25 per cent greater than true.

Consideration thus far has been given only to the logging of thick beds. The problem of thin beds, however, has proved to be one for which some of the most outstanding results have been obtained with guard electrode equipment. The model work that was first done with the guard electrode indicated, and later field work has verified, that the response of the system to thin beds is greater than for any other logging system known to be in use. Furthermore, there are for the guard electrode no shadow zones of the type associated with the so-called lateral device. The boundaries of thin beds, thick beds, and beds of intermediate thickness are sharply defined without the spurious responses of geometrical origin so common to conventional logs. For reasons such as these, the guard electrode has been found to provide a superior tool for correlation, for the recognition of conditions of inhomogeneity, and for locating accurately the depths of resistivity boundaries.

SAMPLE GUARD ELECTRODE LOGS IN THE MID-CONTINENT AREA

In Fig. 5 are reproduced sections of guard electrode logs made in Southern Oklahoma. In this figure, both the resistivity and conductivity traces of the logs are reproduced. All of these conductivity logs have the same sensitivity. These logs are from three fields, separated by distances of approximately 25 miles. The correlations between fields that are indicated in the figure were made by using the conductivity logs, and without benefit of any geological information on the wells they represent. There are large differences between the recorded resistivity values in corresponding sections in the different wells, and consequently the resistivity logs were of little value in field-to-field correlations. Several other correlations between the wells in the different fields were made by using portions of the conductivity logs not reproduced.

Three logs from the West Velma Field are included in the figure to illustrate the character that the guard electrode conductivity logs usually show in shale sections. The character in the shale section is seen to have significance, for by means of it, correlations within these sections can be established. For purposes of geological correlation, the guard electrode logs were found to be markedly superior to the standard electrical logs of these wells.

Fig. 6 illustrates some features of guard electrode logs that have direct bearing on reservoir studies. No conductivity logs are included in Fig. 6. The guard electrode log on the Calmes No. 2 shows a sand section from approximately 3,670 to 3,720 ft. This section has a definite resistivity gradient. Immediately below this is a shale section approximately 25 ft in thickness. Below this, there is a broken sand section or several sands through which a gradient may be drawn to the water table established for this well by production tests. Logs on other wells in the field indicate that the shale section from 3,720 to 3,745 ft in the Calmes No. 2 extends over the entire field, and hence, the upper sand may be considered to be a separate reservoir.

Of further interest in this connection are the logs in the lower part of Fig. 6. These are the logs of this same upper sand in four wells in Sholem-Alechem. These logs all show gradients, and the gradients are a function of the depth of the sand, or possibly its location with respect to the water table. It is not the purpose of, or within the scope of, this paper to

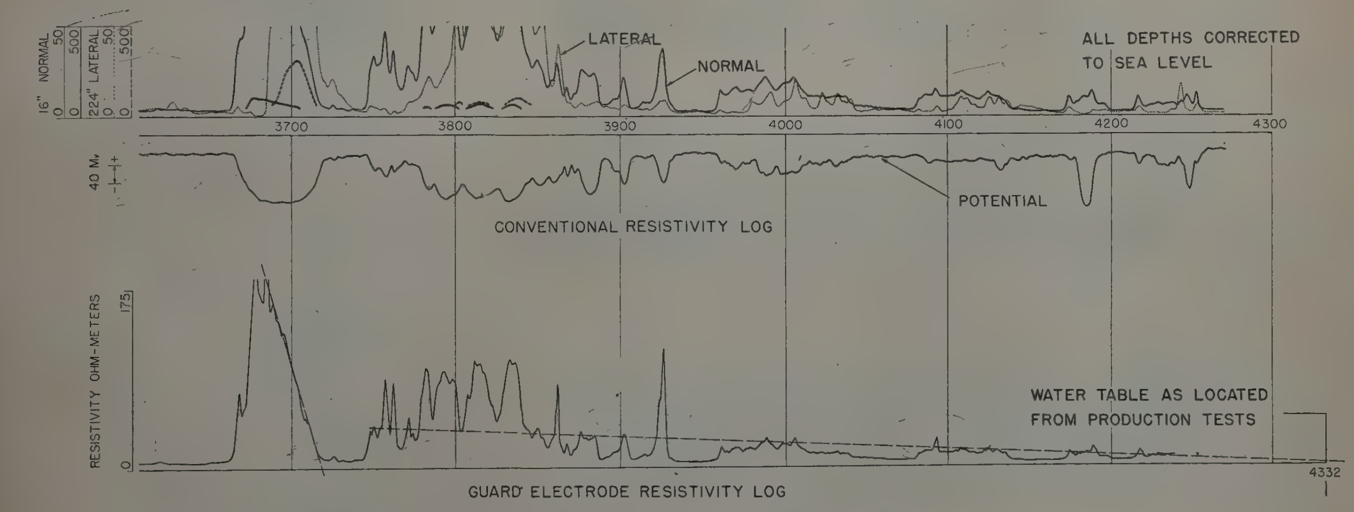

RESISTIVITY LOGS OF CALMES NO. 2, SHOLEM ALECHEM FIELD

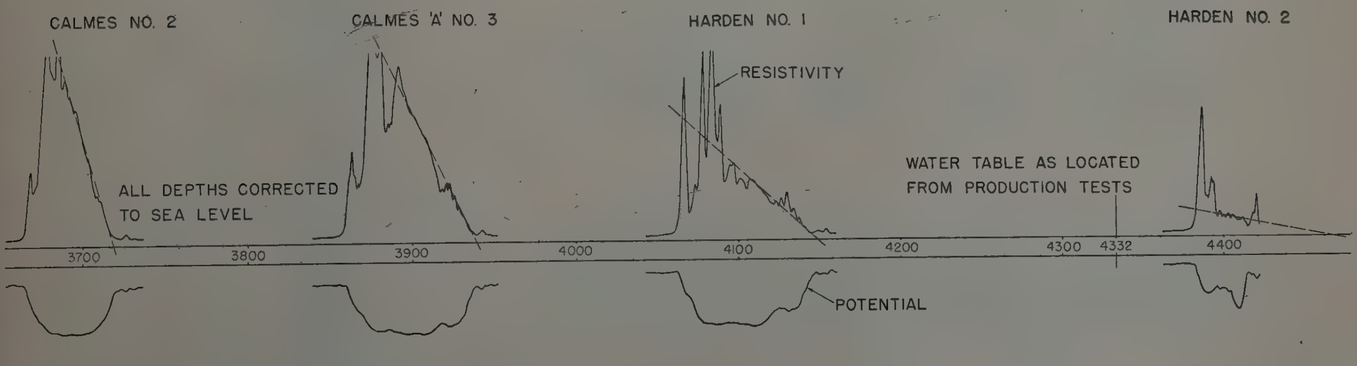

GUARD ELECTRODE RESISTIVITY LOGS OF UPPER SIMS SAND, SHOLEM ALECHEM FIELD

FIG. 6 — LOGS IN SCHOLEM ALECHEM.

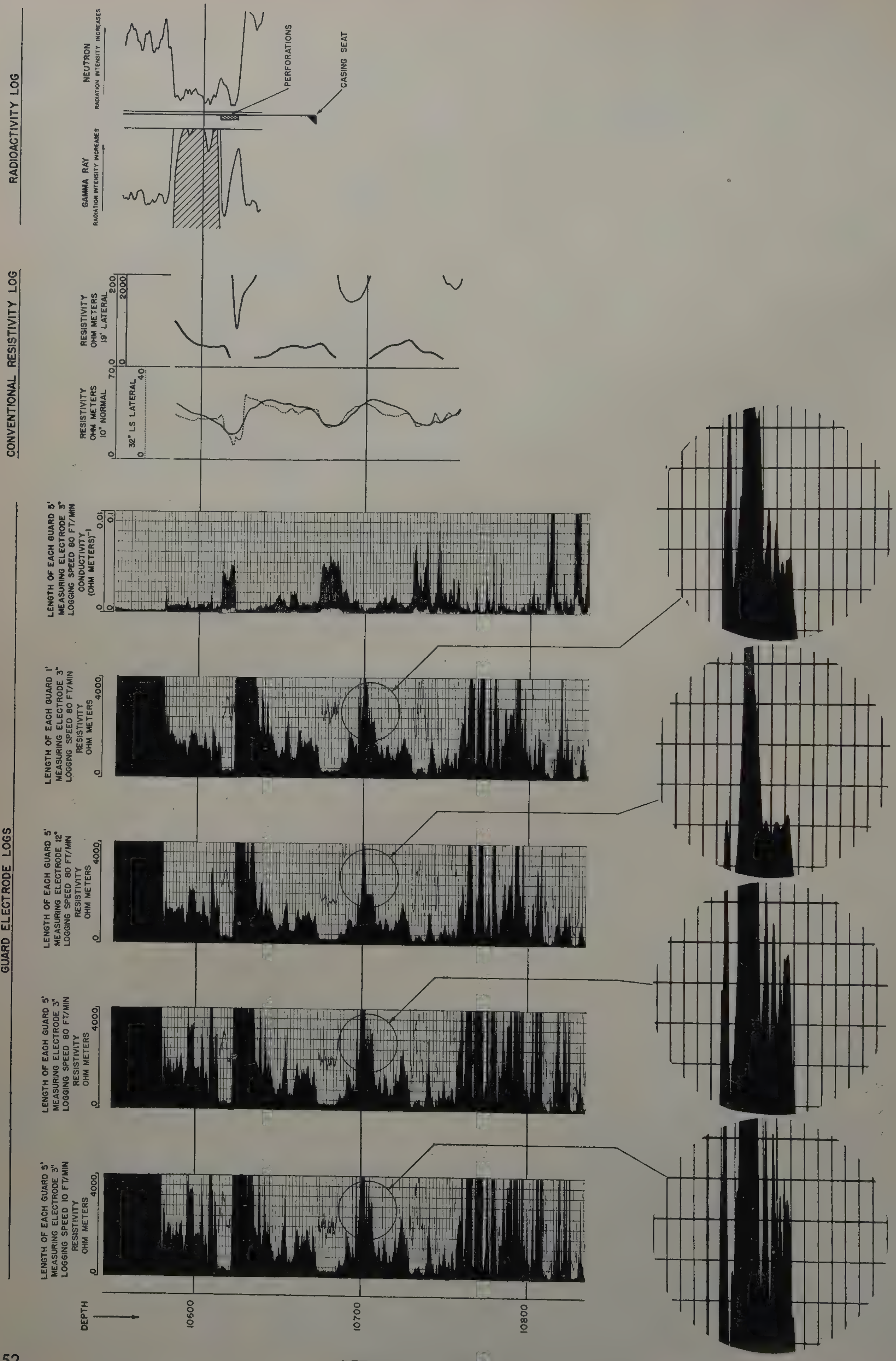

FIG. 7 — GUARD ELECTRODE, CONVENTIONAL RESISTIVITY AND RADIOACTIVITY LOGS, AMERADA D. L. ADCOCK NO. 1, DAWSON COUNTY, TEX.

discuss the significance of these gradients; but, rather to point out that the ability of the guard electrode system to give measurements characteristic of the exact depth at which the measurements are made allows study of reservoir problems within relatively thin sand bodies. The standard electrical logs on these same wells do not show the gradients in the upper sand, although the gradient from 3,750 to 4,332 ft can be determined from the standard log probably as well as from the guard electrode log.

SAMPLE GUARD ELECTRODE LOGS IN THE WEST TEXAS AREA

Guard electrode logs were run in the Amerada No. 1, D. L. Adcock well in Dawson County, Tex. Portions of these logs are reproduced in Fig. 7. Reproduced, also, are the neutron, gamma-ray, and conventional electrical logs for as much of the same section of the hole as these logs are available. The resistivity of the mud was reported as 0.18 ohm-meters at the bottom-hole temperature.

Three combinations of guard and measuring electrode lengths were used for these logs. One log was run with short guards, each guard one ft in length and with a measuring electrode three in. long. A log was run with five-ft guards and a measuring electrode of three in. Another log was run with five-ft guards, but with a 12-in. measuring electrode. Three of the guard electrode logs were run at a logging speed of 80 ft/min. In order to test the possible effect of logging speed on the quality of the log obtained, the log with the five-ft guards and the three-in. measuring electrode was rerun at a logging speed of only 10 ft/min. The two logs of the same type run at the different speeds are quite similar, except for a little additional detail in the log taken at the slower speed. These differences in detail may be seen in the enlarged portions of the logs. A considerable part of the fine detail obtained with the three-in. measuring electrode is missing in the log made with the 12-in. measuring electrode. The detail given by the 12-in. measuring electrode may be sufficient for most purposes, but it is apparent that the logs would lose much of their interpretative value if the thickness of the current measuring disk were made appreciably greater than 12 in.

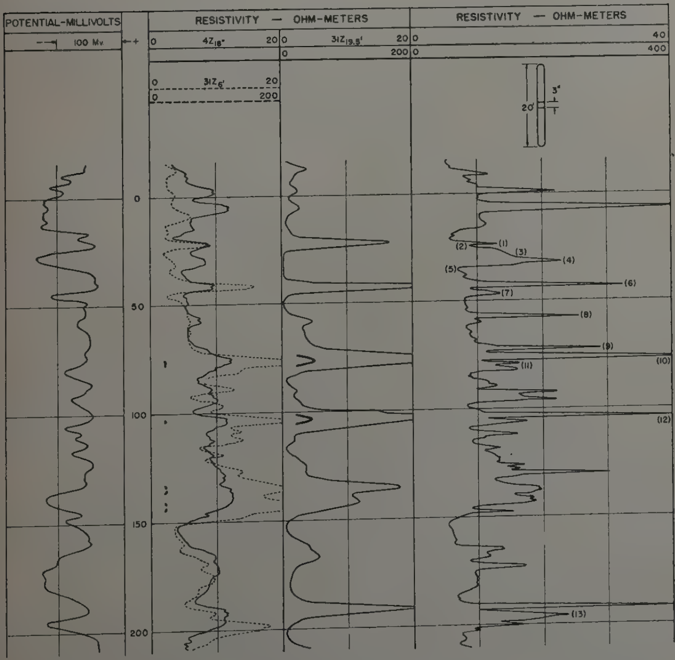

FIG. 8 — COMPARISON OF LOGS FROM GUARD ELECTRODE AND CONVENTIONAL SYSTEMS IN WILCOX SECTION, AUSTIN COUNTY, TEX.

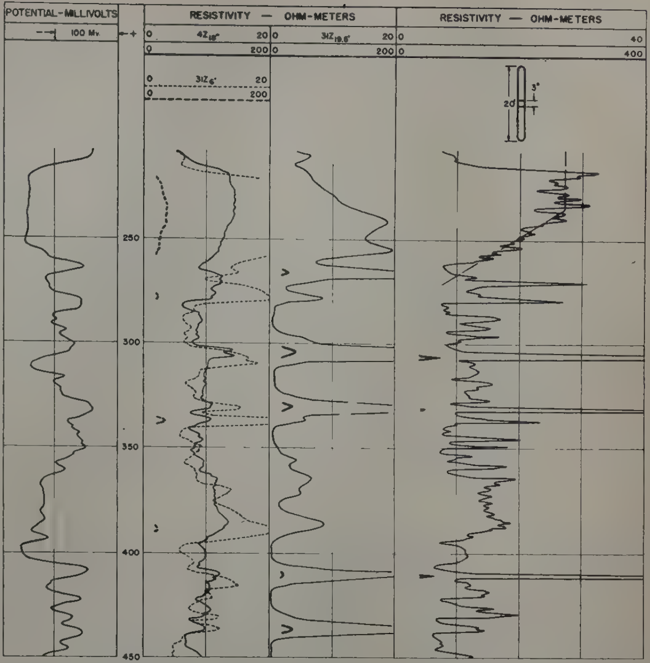

FIG. 9 — COMPARISON OF LOGS FROM GUARD ELECTRODE AND CONVENTIONAL SYSTEMS IN WILCOX SECTION, AUSTIN COUNTY, TEX. (CONTINUED FROM FIG. 8.)

The conductivity log is also reproduced in Fig. 7. Boundaries between shale and lime sections are very sharply defined. Broken, water bearing, permeable zones in the lower portion of the guard electrode logs are clearly shown. The excellent detail of guard electrode logs such as these points to a need for the best possible depth control in taking cores and for all methods of logging and in all steps in well completions in order that full advantage may be taken of the detailed information that the guard electrode gives.

SAMPLE LOGS FROM SOUTH TEXAS

Fig. 8 shows a conventional electric log and a guard log over a Wilcox section in Austin County, Tex. Curves from three resistivity measuring configurations are shown on the conventional log. A four-electrode arrangement with an effective spacing of 18 in. (designated 4Z18") is used for the correlation curve. The other configurations are of the three-electrode type and have spacings of six ft (designated 3IZ6') and 19.5 ft (designated 3IZ19.5'). The guard electrode is 20 ft in length and has a measuring electrode of three in. By a close examination of the logs, the relative presentations can be evaluated.

The SP curve indicates the presence of a sand body between about 0023 and 0033. The long three-electrode curve does not give any indication of resistivity within this section. The entire section appears to be in a shadowed zone insofar as the 19.5′ curve is concerned. There are some indications from the 4Z18″ and 3IZ6′ curves that there may be a resistive streak near the bottom of the sand section. The core for this section was described as six in. of lignite, one ft of shale, four ft of

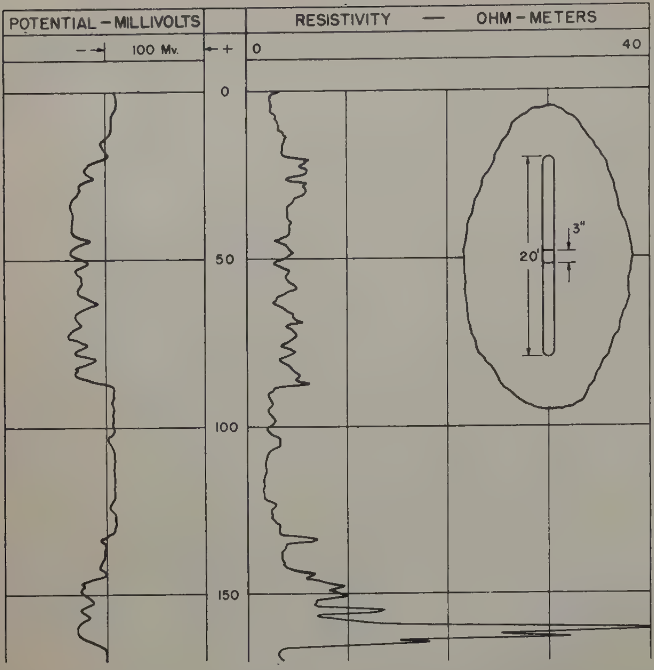

FIG. 10 — EXAMPLE OF GUARD ELECTRODE LOG IN MIOCENE SAND.

sand with oil, and then a mixture of quartzite-like sand, shale and lignite for four ft and then shale. Such detail cannot be read from the conventional log. On the guard record, the area marked (1) is probably the six in. of lignite, (2) is the one ft of shale, (3) is the four ft of oil sand, (4) and (5) are the hard section and the shale, respectively.

At 0042 to 0046, there is a potential anomaly that should indicate a sand body. On the conventional log, the resistivity measures are meaningless because all curves are in a shadowed zone resulting from a highly resistive section at 0042. The reflection on the 3IZ6′ curve is at 0048 and on the 3IZ19.5′ at 0060. The guard log shows the highly resistive sections to be less than two ft in thickness at (6). Immediately below this the resistivity of the sand section is shown at (7). This curve could readily be used to determine the thickness of the sand to be about three ft.

At (8) on the guard log, there is indicated a thin highly resistive streak that is not evident at all on the conventional log. Reading from the guard log, there are defined thin highly resistive sections at (9) and (10) and a sand at (11) with perhaps a total of two ft capable of producing fluid. The conventional log treats this entire section as though there was only one resistive streak at 0075. The interpretation of the section between 0090 to 0108 from the conventional log would be difficult.

There are indications of a sand from the SP curve at 0104. On the conventional log, the resistivity values are extremely high and the resistive section appears to start slightly above the section of possible porosity. Core data show this section to be made up of a lignite streak at the top, a thin streak of hard shale and then a thin section of sand with a show of oil. Such a description can well be correlated with the guard log at (12).

A sand count of the oil-bearing section between 0134 and 0143 can better be made from the guard resistivity log than from any of the curves on the conventional log.

Within the section from 0192 to 0200, there is a section of about four ft of sand containing oil, according to the cores. This section is apparent on the guard log at (13). Such an interpretation would be difficult to make from the conventional log.

The log of this well is continued in Fig. 9. The well is being produced from the sand body shown on the log between 0212 and 0260. The conventional log shows this section to be a uniform sand body with good resistivity values. Due to the nature of three-electrode curves commonly used, it is indicated that the higher resistivity is in the lower part of this body of sand. The guard log indicates an entirely different character. Without too much imagination, it could be claimed that the upper 20 ft of this section has an average apparent resistivity of about 27 ohm-meters and then there is a distinct gradient downward in resistivity through the lower section of the sand body. This character of the resistivity curve from the guard log may well fit into a pattern of theoretical capillary action.

One more sand section shown by cores to be oil bearing that cannot be determined by the conventional log, but is defined by the guard log, is located at 0424 to 0430. The lignite at 0410 blots out all character of the 3IZ19.5′ curve for the next 20 ft.

Fig. 10 shows a section of a guard log made on a well in the Goose Creek Field of Harris County, Tex. The log illustrates the response of the guard system in water and oil-bearing Miocene sands in this area. The upper sand section contains only water; the lower produces oil. Such detail as presented on the log should allow for much more accurate determination of the producing sand count than could be read from the conventional resistivity logs having readings corresponding to averages over larger sections than the thin disk investigated by the guard system.

CONCLUSIONS

The guard records have shown that there rarely exists a formation of uniform characteristics of more than a few feet in thickness. Conventional resistivity logging configurations are not able to indicate apparent resistivities that can be evaluated reasonably except in the most simple cases. Formations located away from the one being investigated up to a distance equal to the spacing of the configuration, or more, will affect the reading. Such terms as shield, shadow, reflection, plateau, and lag are applied to these zones of distortion in the resistivity readings. In the guard system, a brute force method of controlling the investigating current into a thin disk perpendicular to the bore hole is employed. Since the effective measuring current is not allowed to pass through them, the adjacent formations do not affect the reading opposite any given section. Full resistivity value is given to a formation within inches of the boundary with another formation of large contrast in resistivity. Thus, true lithology is recorded provided disk thicknesses of 12 in. or less are used.

Due to the control of the current outward, good resistivity logs can be obtained even when highly conductive muds are used. In fact, when employing long guard lengths, the more conductive the mud, the less will be the proportionate effect of the mud column and the invaded zone on the resistivity reading. It is indicated that by employing several guard lengths, a good evaluation of these zones can be made.

The guard electrode logging system, as illustrated in the examples presented, has already demonstrated its ability to provide superior correlation in shale sections with the conductivity log. The resistivity values recorded are characteristic of the formation directly opposite the measuring electrode and thus facilitate a more exact study of reservoir problems, even within relatively thin bodies.

ACKNOWLEDGMENTS

The authors wish to express their appreciation to the Geophyical Research Corp., the Amerada Petroleum Corp., and the Halliburton Oil Well Cementing Co. for permission to publish this paper.

APPENDIX — POTENTIAL THEORY OF GUARD ELECTRODE

In Fig. 11 is given a prolate spheroid in cylindrical coordinates. This figure closely approximates a cylinder which is used as a resistivity well logging electrode. The entire prolate spheroid is maintained at a potential V_e. The current I_a, flowing from the section between b and $-b$, is metered and the ratio $\frac{V_e}{I_a}$ or $\frac{I_a}{V_e}$ is recorded on a scale reading in resistivity or conductivity.

The equation for the surface of the electrode or the prolate spheroid is:

$$\frac{z^2}{c^2} + \frac{r^2}{a^2} = 1$$

and the equation for the family of equipotential surfaces out from the electrode is:

$$\frac{z^2}{c^2 + \lambda} + \frac{r^2}{a^2 + \lambda} = 1$$

where $\lambda > 0$.

The potential of the equipotential surfaces is given by either Bateman[3] or Smythe[4] as:

$$V = \frac{Q}{2} \int_{\lambda}^{\infty} \frac{du}{(a^2 + u)\ (c^2 + u)^{1/2}}$$

and is integrated by Bateman:

$$V = \frac{Q}{2k}\ ln\ \frac{\sqrt{c^2 + \lambda} + k}{\sqrt{c^2 + \lambda} - k}$$

where $k^2 = c^2 - a^2$, and on substituting $Q = \frac{\rho I}{4\pi}$, we have

$$V = \frac{\rho I}{8\pi k}\ ln\ \frac{\sqrt{c^2 + \lambda} + k}{\sqrt{c^2 + \lambda} - k}$$

With $\lambda = 0$, we have the potential of the electrode:

$$V_e = \frac{\rho I}{8\pi k}\, ln\, \frac{c + k}{c - k}$$

$$V_e = \frac{\rho I}{4\pi k}\, ln\, \frac{c + k}{a}$$

the electrode resistance:

$$R_e = \frac{\rho}{4\pi k}\, ln\, \frac{c + k}{a}$$

and the electrode current:

$$I = \frac{4\,\pi\, k\, V_e}{\rho\, ln\, \frac{c + k}{a}}$$

The surfaces of flow are hyperboloids. The equation is:

$$\frac{z^2}{c^2 + \lambda} + \frac{r^2}{a^2 + \lambda} = 1$$

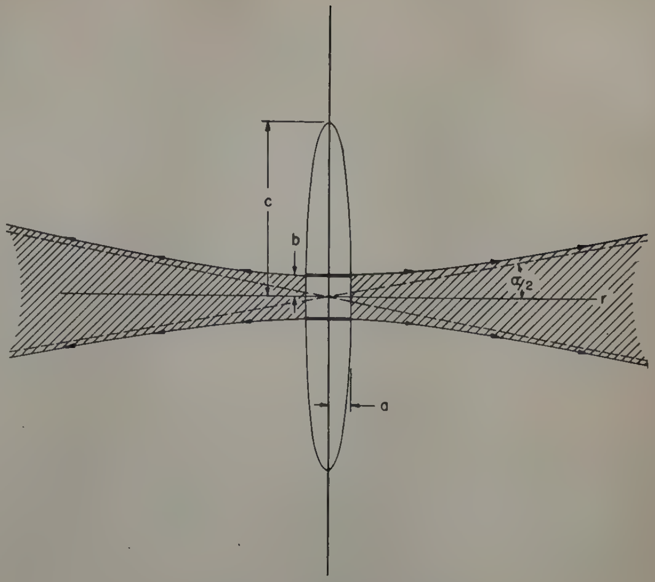

FIG. 11 — GUARD ELECTRODE.

where $-c^2 < \lambda < -a^2$. The equation of the hyperboloid that intercepts the z axis at b, i.e., $r = 0$ and $z = b$, is arrived at:

$$\lambda = b^2 - c^2$$

$$\frac{z^2}{b^2} + \frac{r^2}{a^2 + b^2 - c^2} = 1$$

$$z = b\sqrt{1 + \frac{r^2}{c^2 - a^2 - b^2}}$$

The slope of the flow surface is $\frac{dz}{dr}$. Differentiating, we have:

$$\frac{dz}{dr} = \frac{br}{[(c^2 - a^2 - b^2)^2 + (c^2 - a^2 - b^2)r^2]^{1/2}}$$

The slope that the flow surface approaches as r increases without limit is:

$$\lim_{r \to \infty} \frac{dz}{dr} = \frac{b}{\sqrt{c^2 - a^2 - b^2}}$$

The cone that the hyperboloid approaches as r increases, shown in Fig. 11, makes an angle $\frac{\alpha}{2}$ with the r plane. Angle $\frac{\alpha}{2}$ is:

$$\frac{\alpha}{2} = tan^{-1} \left.\frac{dz}{dr}\right]_{r \to \infty}$$

$$\frac{\alpha}{2} = tan^{-1} \frac{b}{\sqrt{c^2 - a^2 - b^2}}$$

The area of the sphere of infinite radius r_∞ within the angle α is:

$$A_\alpha = 4\,\pi\, r_\infty^2 \int_0^{\frac{\alpha}{2}} \cos\theta\, d\,\theta$$

$$A_\alpha = 4\,\pi\, r_\infty^2\, \sin\frac{\alpha}{2}$$

and the ratio of this area to the total area is:

$$\frac{A_\alpha}{A} = \sin\frac{\alpha}{2}$$

of the ratio of the current within angle α to the total current is:

$$\frac{I_a}{I} = \sin\frac{a}{2}$$

$$\frac{I_a}{I} = \frac{b}{k}$$

Going back to the equation for V_e, and substituting for I, we have:

$$V_e = \frac{\rho I_a}{4\pi b}\, ln\, \frac{c+k}{a}$$

and the resistivity is:

$$\rho = \frac{4\pi b}{ln\,\frac{c+k}{a}} \cdot \frac{V_e}{I_a}$$

In order to evaluate the effect of bore hole or mud invasion on the guard electrode, it is desirable to solve the potential problem of a conductive prolate spheroid within one or more cylindrical interfaces, the first interface being bore hole mud to filter cake, etc. However, if the length of the guard electrode is large compared to the diameter of the tool, the length of the measuring ring, the diameter of the bore hole, or the diameter of the invaded zone, a close approximation may be had by bounding the bore hole mud within a second prolate spheroid of minor diameter equal to the bore hole diameter, the invaded zone within a third prolate spheroid, etc.

Let the surface of the guard electrode be a prolate spheroid surface S_1 of major diameter 2 c_1 and minor diameter of 2 a_1; the next surface S_2 of major and minor diameters of 2 c_2 and 2 a_2, etc. The equation for the family of equipotential prolate spheroid surfaces is:

$$\frac{z^2}{c_1^2+\lambda} + \frac{r^2}{a_1^2+\lambda} = 1$$

where $\lambda > 0$. The equation of the surface S_n of minor diameter 2 a_n follows:

At the point $z = 0$, $r = a_n$

$$a_n^2 = a_1^2 + \lambda$$

$$\lambda = a_n^2 - a_1^2$$

And the equation:

$$\frac{z^2}{c_1^2 + a_n^2 - a_1^2} + \frac{r^2}{a_n^2} = 1$$

$$\frac{z^2}{a_n^2 + k^2} + \frac{r^2}{a_n^2} = 1$$

At the point $z = c_n$, $r = 0$

$$c_n^2 = a_n^2 + k^2$$

$$c_n = \sqrt{a_n^2 + k^2}$$

Consider:

$$\frac{V_e}{I_a} = \frac{\rho}{4\pi b}\, ln\, \frac{c_1+k}{a_1} = R_a \Big]_{S_1}^{\infty}$$

and

$$R_1 = R_a\Big]_{S_1}^{S_2},\quad R_2 = R_a\Big]_{S_2}^{S_3},\ \text{etc.}$$

For a formation of ρ_t, and a bore of ρ_m, we have:

$$R_2 = R_a\Big]_{S_2}^{\infty} = \frac{\rho}{4\pi b}\, ln\, \frac{c_2+k}{a_2}$$

$$R_1 = R_a\Big]_{S_1}^{\infty} - R_a\Big]_{S_2}^{\infty} = \frac{\rho}{4\pi b}\left[ln\,\frac{c_1+k}{a_1} - ln\,\frac{c_2+k}{a_2}\right]$$

and the apparent resistivity is:

$$\rho_A = \frac{4\pi b}{ln\,\frac{c_1+k}{a_1}}\left\{ R_1\Big]_{\rho=\rho_m} + R_2\Big]_{\rho=\rho_t}\right\}$$

$$\rho_A = \rho_m + (\rho_t - \rho_m)\frac{ln\,\frac{c_2+k}{a_2}}{ln\,\frac{c_1+k}{a_1}}$$

or:

$$\frac{\rho_A}{\rho_m} = 1 + \left(\frac{\rho_t}{\rho_m} - 1\right)\frac{ln\,\frac{c_2+k}{a_2}}{ln\,\frac{c_1+k}{a_1}}$$

For a formation of ρ_t, and invaded zone of ρ_i, and a bore hole of ρ_m, we have:

$$R_3 = R_a\Big]_{S_3}^{\infty} = \frac{\rho}{4\pi b}\, ln\, \frac{c_3+k}{a_3}$$

$$R_2 = R_a\Big]_{S_2}^{\infty} - R_a\Big]_{S_3}^{\infty} = \frac{\rho}{4\pi b}\left[ln\,\frac{c_2+k}{a_2} - ln\,\frac{c_3+k}{a_3}\right]$$

$$R_1 = R_a\Big]_{S_1}^{\infty} - R_a\Big]_{S_2}^{\infty} = \frac{\rho}{4\pi b}\left[ln\,\frac{c_1+k}{a_1} - ln\,\frac{c_2+k}{a_2}\right]$$

and the apparent resistivity is:

$$\rho_A = \frac{4\pi b}{ln\,\frac{c_1+k}{a_1}}\left\{ R_1\Big]_{\rho=\rho_m} + R_2\Big]_{\rho=\rho_i} + R_3\Big]_{\rho=\rho_t}\right\}$$

$$\rho_A = \rho_m + (\rho_i - \rho_m)\frac{ln\,\frac{c_2+k}{a_2}}{ln\,\frac{c_1+k}{a_1}} + (\rho_t - \rho_i)\frac{ln\,\frac{c_3+k}{a_3}}{ln\,\frac{c_1+k}{a_1}}$$

or:

$$\frac{\rho_A}{\rho_m} = 1 + \left(\frac{\rho_i}{\rho_m} - 1\right)\frac{ln\,\frac{c_2+k}{a_2}}{ln\,\frac{c_1+k}{a_1}} + \left(\frac{\rho_t}{\rho_m} - \frac{\rho_i}{\rho_m}\right)\frac{ln\,\frac{c_3+k}{a_3}}{ln\,\frac{c_1+k}{a_1}}$$

This procedure can be followed for any number of surfaces provided $a_n << c_1$.

REFERENCES

1. Schlumberger, C. and M., and Leonardon, E. G.: "Electrical Coring: A Method of Determining Bottom-Hole Data by Electrical Measurements," AIME (1934) **110**, 237.
2. Guyod, Hubert C.: Series of 16 articles appearing in various issues of *The Oil Weekly* between Aug. 7 and Dec. 4, 1944.
3. Bateman, H.: *Partial Differential Equations*, Dover Publications (1944).
4. Smythe, William R.: *Static and Dynamic Electricity*, McGraw-Hill Book Co. (1939).

★ ★ ★

T.P. 3218

RESULTS OF GAS INJECTION IN THE CEDAR LAKE FIELD

R. M. LEIBROCK, JUNIOR MEMBER AIME, **R. G. HILTZ**, AND **J. E. HUZAREVICH**, JUNIOR MEMBER AIME,

STANOLIND OIL AND GAS CO., FORT WORTH, TEX.

ABSTRACT

The various factors considered in recommending the initiation of a gas injection project in the southern portion of the Cedar Lake Field are discussed. Performance history under gas injection operations is reviewed and these data are analyzed, utilizing both the material balance method and the fractional flow and frontal advance expressions.

Results of the analysis of the performance data indicate that the injected gas has contacted and affected at least 60 per cent of the reservoir and a substantial increase in ultimate recovery can reasonably be expected. By holding the reservoir pressure appreciably above the bubble point, the well productive capacities have been maintained substantially above the level predicted for primary operations.

The analysis of the Cedar Lake project suggests that in certain limestone reservoirs, at least, the probable success of gas injection cannot be predicted simply from observation of permeability distribution throughout the pay section, as indicated by core analysis data, on either one or a number of wells. Further, the performance of this particular project fails to indicate any basis for classifying carbonate reservoirs in general as being inherently unsuited to a dispersed type gas injection program, thus indicating that each reservoir should be considered on its own merits, regardless of the composition of the reservoir rock.

INTRODUCTION

Early in the life of the Cedar Lake Field, an extensive data gathering program was initiated to provide an accurate record of reservoir performance characteristics. From the study of these data it was apparent that there was a critical need for supplementing the natural reservoir energy in order to maintain well productivities and obtain the maximum ultimate oil recovery. Accordingly, detailed engineering studies were made of the various methods of secondary recovery which might be applicable. As a result of these investigations, the decision was made to initiate a gas injection program of sufficient intensity to maintain reservoir pressure at approximately 600 psia, or some 274 lb above the bubble point pressure of 326 psia.

A full scale dispersed type gas injection program has been in operation on leases of the Stanolind Oil and Gas Co. in the southern portion of the field for nearly five years, and sufficient performance data are now available to evaluate the benefits which have been derived from this project. It is the primary purpose of this paper to analyze the performance data for the Cedar Lake gas injection project and to point out the significance of the observed behavior with respect to certain hypotheses which have been advanced in recent years concerning the probable success of gas injection projects in limestone reservoirs.

This paper properly should be regarded more on the order of a progress report, inasmuch as some revision in interpretation will undoubtedly be required from time to time as additional performance data are obtained, although the satisfactory performance of the project to date leaves little doubt as to the ultimate success of gas injection in the Cedar Lake Field.

As a result of the success of the project to date, a unit was formed in the southern part of the field, effective March 1, 1951, for the purpose of continuation of the gas injection program. Participants in this unit are the Mid-Continent Petroleum Co. and Stanolind Oil and Gas Co.

GEOLOGY AND STRATIGRAPHY

The Cedar Lake Field is located in the northern portion of the Midland Basin area as shown in Fig. 1. The southwest portion of the field lies within a playa, or dry salt lake, which covers an area of approximately eight square miles. As might be expected, it was this lake which furnished the inspiration for the name of the field. Except for its value as a salt water disposal pit, this lake has succeeded only in magnifying the difficulties in developing this portion of the field. Typical of this section of West Texas, the area in general is relatively flat and has a semi-arid climate.

The localized structure which favored the accumulation of oil is an anticline with approximately 100 ft of closure. The major axis of the structure extends in a general southeast-northwest direction. Originally this structure was defined by seismograph data, which have been subsequently confirmed by development.

In general, the geologic column is typical of that found throughout the basin. From the surface to depth of approximately 1,800 ft, surface sands and undifferentiated red beds, probably Triassic, are encountered. Below this point to the producing horizon, all formations are of the Permian age.

Manuscript received in the office of the Petroleum Branch, AIME, Sept. 17, 1951. Paper presented at the Petroleum Branch Fall Meeting in Oklahoma City, Okla., Oct. 3-5, 1951.

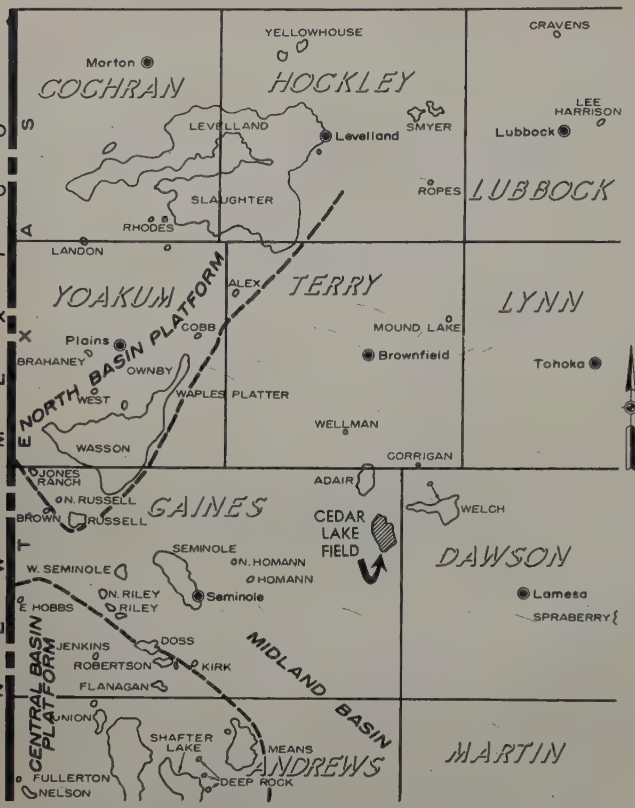

FIG. 1 — MAP SHOWING LOCATION OF CEDAR LAKE FIELD.

Anhydrite and red beds are found at approximately 2,000 ft and continue with varying amounts of salt, principally sodium chloride, to approximately 2,700 ft where the Cloudchief is encountered. This latter point usually represents the base of the salt section and denotes the appearance of the first limestone stringers.

The Yates horizon, consisting of sand, anhydrite, red beds and lime is found at 2,800 ft. The Yates section grades downward into an anhydrite and red bed series at approximately 3,750 ft where an increase in limestone and sand denotes the top of the Brown lime. A second limestone with considerable anhydrite inclusion is found at 4,000 ft.

The San Andres limestone is encountered at approximately 4,350 ft with the producing horizon usually occurring 4,350 ft with the producing horizon usually occurring from 4,600 ft to 4,700 ft. Although this formation is referred to as a limestone, it actually is a light gray crystalline dolomite with relatively minor anhydrite inclusions. The top of the San Andres and the top of the pay interval are separated by a thin chert streak and a thin sand bed. In the Cedar Lake Field this latter sand is generally referred to as an "intra-dolomite sand break" although in the general area it is more commonly referred to as the Lovington Sand.

The top of the pay occurs in a rather erratic fashion and is not considered to be representative for depicting structural conditions. Because of its uniformity throughout the field and because of its proximity to the producing horizon, however, the intra-dolomite sand break is generally accepted as the most suitable basis for structural delineation. Utilizing this sand as a marker, a structure map has been prepared as shown in Fig. 2. These contours on top of the sand break delineate the anticlinal structure quite clearly.

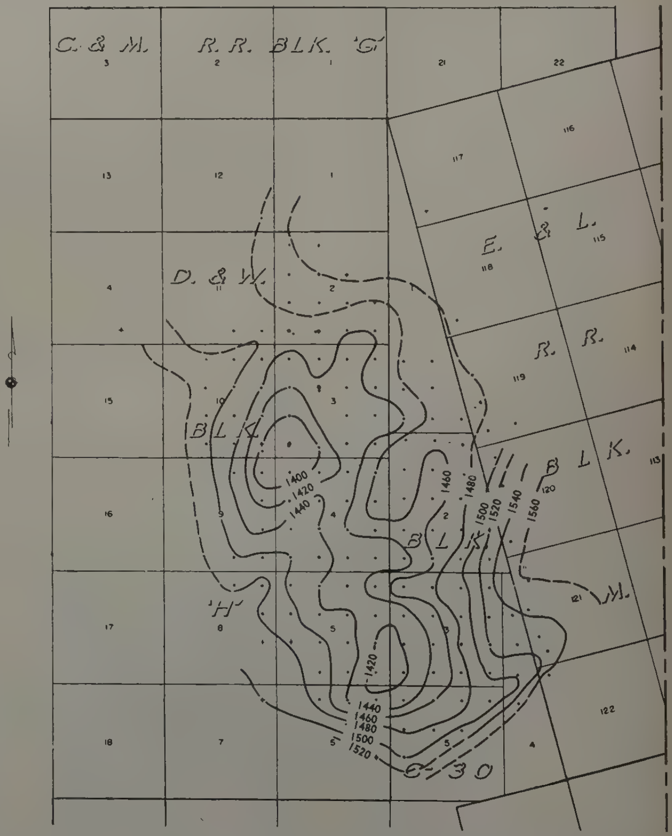

FIG. 2 — STRUCTURE MAP — CONTOURS ON TOP OF INTRA-DOLOMITE SAND BREAK.

CHARACTERISTICS OF PRODUCING FORMATION

As a forerunner to that portion of the paper dealing with the actual analysis of the reservoir behavior under gas injection, a discussion of the characteristics of the producing formation appears to be in order, for without a clear understanding of the petrophysics of the reservoir rock, it is difficult to realize the full significance of the behavior of the gas injection program. While examination of cores, radioactivity and electric logs and various other well completion data cannot be expected to provide a definite answer relative to the degree of success to be expected from conducting a gas injection program, these various sources of information must, nevertheless, be given due consideration if an intelligent interpretation is eventually to be made of the performance data and if experience gained from one project is to be of any value in predicting the susceptibility of other reservoirs to gas injection. Accordingly, certain rock characteristics, as observed from log studies and core analysis data, are discussed herein.

A radioactivity log through the producing section and core analysis data from a typical well in the Cedar Lake Field are shown in Fig. 3. It may be seen that porosity values from the core graph agree reasonably well with the neutron curve of the radioactivity log, a correlation which is demonstrated even more clearly in Fig. 4 where deflections of the neutron curve, measured to the right of the instrument zero line, are plotted against large core analysis porosity values. Such a correlation has proved useful in qualitatively evaluating logs in the gas injection area even though instrument zero values are not available on older logs, the majority of which were obtained

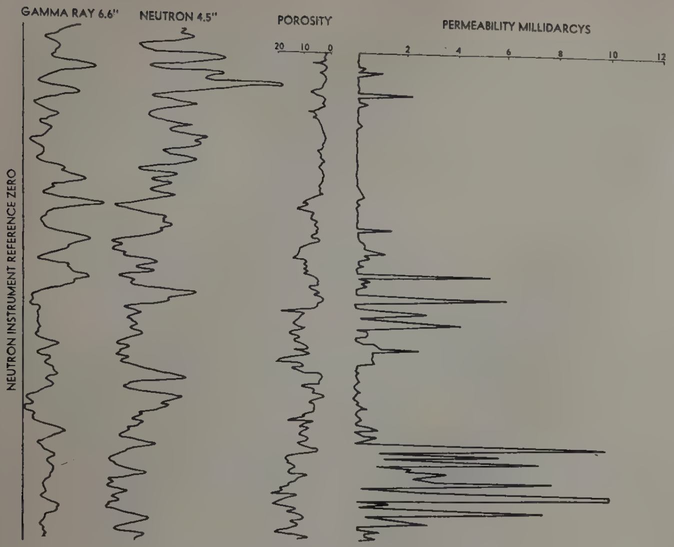

FIG. 3 — TYPICAL CEDAR LAKE WELL LOG.

several years ago. This correlation will prove useful in interpreting pay characteristics in new development areas and in analyzing reservoir behavior, particularly if the injection program is later expanded to include the entire field.

Simply from examination of the permeability profile shown in Fig. 3 and realizing that injection wells were either acidized or shot, it might be concluded that injection into the formation without attempting to control the point of entry would result in the injected gas being confined to an interval of high permeability with the result that a relatively low percentage of the reservoir would be contacted. Elkins and Cook,[1] in observing the behavior of certain pilot gas injection projects, concluded that the part of the reservoir which can be effectively swept by injected gas is a function of permeability profile. While the susceptibility of the reservoir to injected gas must necessarily be dependent on some average condition which exists within the reservoir between the injection and producing wells, it would appear that in limestones and dolomites, at least, this is a condition which cannot be evaluated from observation of core analysis data from one well or several wells, but will necessarily depend on analysis of a well planned and properly controlled injection program.

Referring to Fig. 5, which is a coregraph cross section for four offsetting wells in the Cedar Lake Field, it will be noted that erratic permeability development is encountered in each well; however, closer inspection reveals that intervals of high permeability development cannot be correlated from one well to another. The existence of this condition led to the tentative conclusion by Keller and Morse[2] that vertical variation in permeability, as indicated by core data on individual wells, would be greatly minimized on a reservoir-wide basis to the extent that the flow of injected gas through the formation would be fairly evenly distributed throughout the producing zone. As subsequent discussion will indicate, the validity of this observation seemingly is borne out by the analysis of the performance data.

While most investigators who have studied the physical characteristics of carbonate rocks and sandstones agree that these two types of rock have little in common from the standpoint of pore space geometry, wide differences of opinion apparently exist as to the significance of these lithological dissimilarities. For example, Bulnes and Fitting[3] felt that these observed dissimilarities necessarily would result in reservoir behavior in limestones and dolomites which would differ to a marked extent from the performance observed for sandstones. They believed, for example, that in many limestone fields a large percentage of the oil would be contained in and produced from thick zones having an extremely low order of permeability development and that the rate at which these tight sections produced into more permeable zones would depend in part upon the pressure gradient across the boundary between the two. Since any type of pressure maintenance program would have the effect of minimizing this gradient, it was felt that secondary recovery operations should not be applied indiscriminantly.

Subsequent studies[4,5] of field performance data seemingly have indicated no fundamental differences in the behavior of limestone and sandstone reservoirs, and, as will be shown later in the case of the Cedar Lake reservoir, it has been possible to contact a reasonably large percentage of the reservoir with injected gas. Furthermore it would appear that failure to affect all of the reservoir by injected gas is not attributable to any lithological condition peculiar to carbonate reservoirs but is due simply to formation characteristics which may be found in any reservoir whether it be limestone or sandstone.

In analyzing the behavior of the Cedar Lake injection project, it has been necessary to make use of a relative permeability-liquid saturation relationship derived from the performance of the Slaughter Field[5] where production is also obtained from

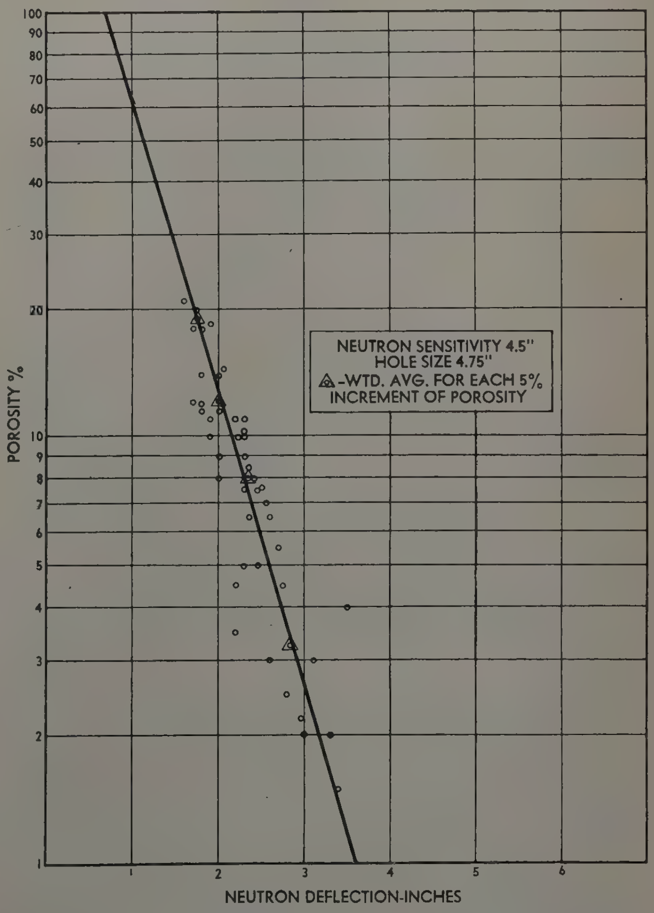

FIG. 4 — NEUTRON DEFLECTION VS LARGE CORE ANALYSIS POROSITY.

---

[1] References given at the end of the paper.

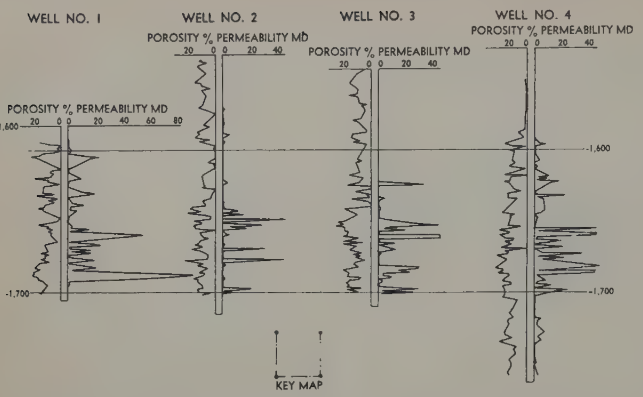

FIG. 5 — CORE GRAPH CROSS-SECTION, CEDAR LAKE FIELD.

the San Andres formation. Use of the Slaughter data is at least partially justified by the fact that a permeability-porosity relationship obtained from a plot of the available core data for the Cedar Lake Field agrees reasonably well with permeability-porosity relationships for San Andres reservoirs located in the North Basin platform area. The relationship for the Cedar Lake Field is shown in Fig. 6. While there is some indication that the San Andres in the Cedar Lake area contains a slightly higher concentration of clayey material than fields in the North Basin area, it nevertheless, occupies roughly the same position on the graph as core data from the Slaughter and Wasson Fields.

CHARACTERISTICS OF RESERVOIR FLUID AND INJECTED GAS

In order to evaluate the reservoir fluid characteristics, a number of representative bottom hole samples have been obtained from various portions of the field. These data indicated close agreement and were combined to provide composite curves as shown in Fig. 7. No significant difference in crude characteristics in different portions of this structure has been detected.

From a review of these composite data, it is readily apparent that the reservoir crude is highly undersaturated, having a bubble point pressure of 326 psia and a solution gas/oil ratio of 156 cu ft/bbl. Original reservoir pressure was indicated to be approximately 1,950 psia. Oil viscosity varies from a value of 2.90 cp at original reservoir conditions to 2.44 cp at the bubble point pressure, at which point the viscosity increases rapidly to 4.5 cp at atmospheric conditions. The relative volume of this crude is 1.0768 at original conditions and increases to 1.0884 at the bubble point.

As pointed out previously, the undersaturated nature and low solution ratio of this crude were important factors in dictating the necessity for the initiation of a pressure maintenance program.

Laboratory fractional analysis of the reservoir oil is given in Table I of the appendix.

Although most of the gas injected to date has been obtained from the nearby Homann Field, attempts are currently being made to develop a source of gas from the Yates Sand horizon within the Cedar Lake Field itself. Fractional analyses of the two gases are given in Table II of the appendix.

Shown in Fig. 8 are compressibility factor curves for the above two gases. As a result of its higher nitrogen content, the Cedar Lake Yates sample is, of course, less compressible and has a higher viscosity. These characteristics have a decided advantage in providing for future make up gas volumes since lower compressibility of this gas would reduce injection requirements by approximately three per cent and the higher viscosity makes it a more efficient displacing fluid.

GAS INJECTION FACILITIES

The Homann Field gas, which is produced from the Yates horizon, is metered and delivered at a maximum pressure of 450 psig to the Stanolind transmission line at its terminus in the Homann Field. Due to resultant lines losses, the gas reaches Stanolind's compressor station at about 325 psig. Being relatively dry and sweet, this gas does not require special treatment prior to entering the compressors.

Compression from an intake pressure of 325 psig to a maximum discharge pressure of 1,600 psig is accomplished in two stages. Following compression, the gas is transmitted to the individual injection wells by injection lines as shown on Fig. 9. Each injection well is equipped with an adjustable choke and adequate valves to permit flexibility in control of the individual wells, and a differential, mercury-type orifice flow meter is provided for measurement of gas injected into each well. The accumulation and freezing of hydrates is minimized through the use of a methanol injector at the plant, and the

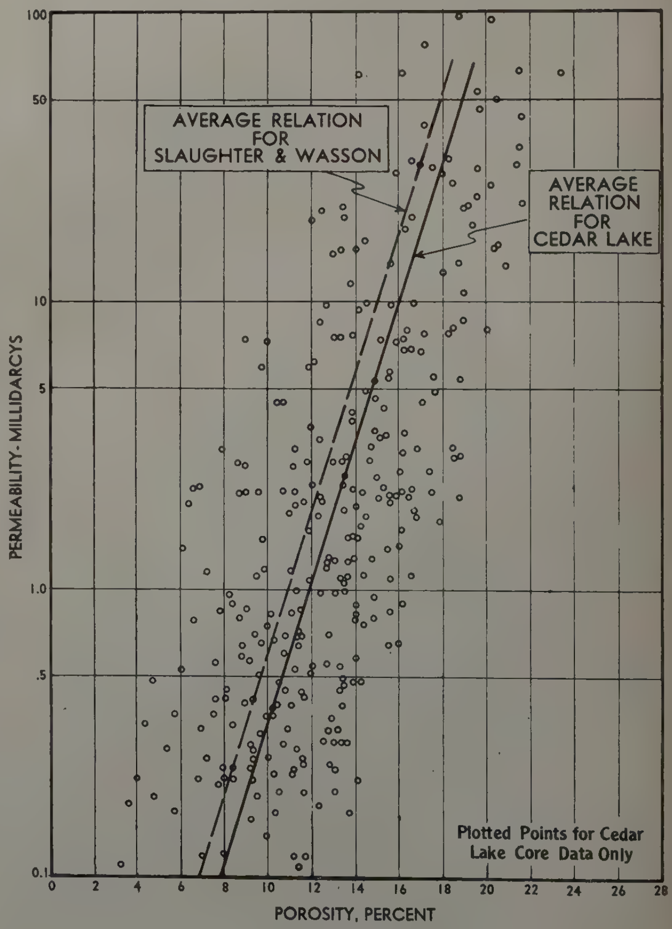

FIG. 6 — POROSITY-PERMEABILITY RELATION.

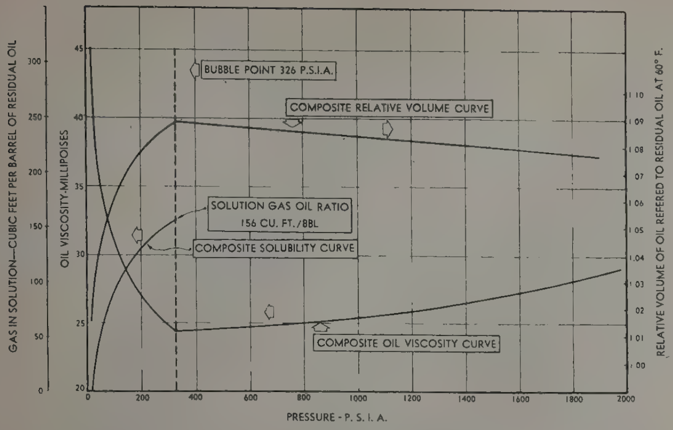

FIG. 7 — CEDAR LAKE FIELD RESERVOIR CRUDE CHARACTERISTICS.

freezing of injection wellhead equipment due to the high degree of expansion across adjustable chokes is controlled by heating the gas in small gas-fired heaters placed a short distance from the individual wellheads.

Gas obtained from the Yates horizon in the Cedar Lake Field is high pressure gas and requires no compression for injection. Connections from the two Yates sand gas wells to the injection system are shown in Fig. 9.

HISTORY AND PAST PERFORMANCE

Following detailed seismic work, Stanolind drilled and completed its J. B. Rayner No. 1, the discovery well for the field, in August, 1939. Development of the field progressed rather slowly during the first few years of the field's history and was essentially halted during the period from 1943 to 1948. An intensified drilling program undertaken since that time, however, has resulted in an extension of field limits a considerable distance to the north and virtually doubled the previously indicated productive acreage. Although the field limits have now been reasonably well defined in the southern half of the field, drilling activity continues at a somewhat lessened pace in the northern portion of the field.

Performance of the injection area prior to initiation of this secondary program is illustrated in Fig. 10. Of particular importance is the rapid decline in bottom hole pressure which occurred during this period when production from the reservoir was attributable only to the energy expended by expansion of the reservoir liquid. In consideration of the relatively low permeability and the attendant high abandonment pressures of the major portion of this reservoir, indications were that under primary operations the field could reasonably be expected to recover not more than 10 to 12 per cent of the oil initially in place. Individual well productivity would, of course, be appreciably reduced when the reservoir pressure declined below the bubble point. During this phase of operations, the presence of liberated solution gas in the reservoir would materially reduce the effective permeability to oil and there would be only a small pressure differential available to move oil to the well bore.

Gas/oil ratio behavior during this period of primary operations was consistent with that expected from bottom hole sample analysis which indicated a solution ratio of 156 cu ft/bbl. Oil production, as shown in Fig. 10 varied over a rather wide range with fluctuations attributable principally to rate of development, early proration practices, and greatly accelerated demand during the war years.

Recognizing the extremely low efficiency of primary operations, gas injection operations were initiated in April, 1946, in one well. Injectivity and fluid depression tests were conducted on the proposed injection wells, and the results indicated that the volumes required to maintain pressure could be achieved at an injection pressure of approximately 1,100 psig. By November of 1946, the number of injection wells had been increased to eight, with a ninth well being added in October, 1948. This amounts to a density of over 250 acres per injection well. At the time the program was initiated the reservoir pressure had declined to approximately 600 psia and original plans were designed to maintain pressure at that level.

A study of Fig. 10 reveals appreciable fluctuation in injection volumes during the early stages of this operation. Since this project essentially represented an experiment as well as a practical application of the principle of gas injection in limestone reservoirs, such variations might be expected during the initial stages. An almost immediate effect on the bottom hole pressure was noted, however, and as injection volumes increased to the point where they exceeded withdrawals, there was a rather significant increase in reservoir pressure. Subsequently, however, injection volumes were readjusted to a value more nearly approaching reservoir withdrawals, and the recorded bottom hole pressure reflected a decline in pressure to the desired value of approximately 600 psia. Continued close supervision of the project is expected to effect a satisfactory balance between withdrawals and injection volumes and to assure maintenance of the reservoir pressure at the desired point. Certainly the program to date has resulted in a very significant alteration of the original trend of pressure observed under primary conditions.

Associated with retardation of pressure decline, we might logically expect a similar arresting of the decline in individual well productivity. Original productivity indices of these wells were in the range of 0.05 to 0.2 B/D per pound drawn down in bottom hole pressure. These PI values, of course, are a further indication of the low order of permeability and furnish additional confirmation of the need for pressure maintenance. Current well productivity is indicated to average ap-

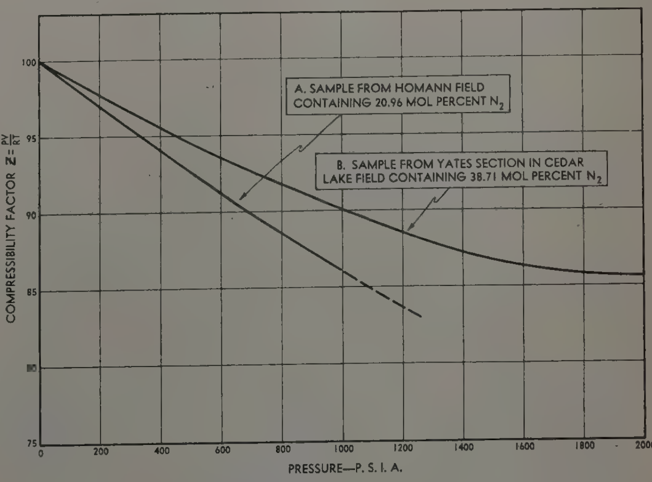

FIG. 8 — COMPRESSIBILITY OF INJECTED GAS, CEDAR LAKE FIELD.

proximately 68 B/D per well, whereas it is estimated that at the present time under primary operation the average well would be capable of producing only 44 B/D.

Since gas injection was initiated at a reservoir pressure well above the bubble point, there was no significant increase in the produced gas/oil ratio during the first 19 to 20 months of the injection program. Gas breakthrough was first detected in the middle of 1948 and a series of produced gas samples were collected and analyzed to confirm the fact that injected gas was being produced.

During this five-year period of injection, actual production has been approximately 400,000 bbl greater than the estimated production under primary operation. This increased production represents the benefits recevied to date from the standpoint of maintaining well productivity.

In general, it is apparent, before even attempting a quantitative evaluation of the performance data, that the behavior of this project to date is indicative of a high degree of success in maintaining reservoir pressure and productive capacity and holds promise of considerable increase in ultimate recovery. In reviewing the various factors affecting the success of this program, we believe that it should be pointed out that one of the most important considerations is the initiation of an adequate data gathering program to permit an intelligent appraisal of the performance of the project and the adoption of a sufficiently flexible plan of operations to permit necessary alterations in the injection program as dictated by the observed performance.

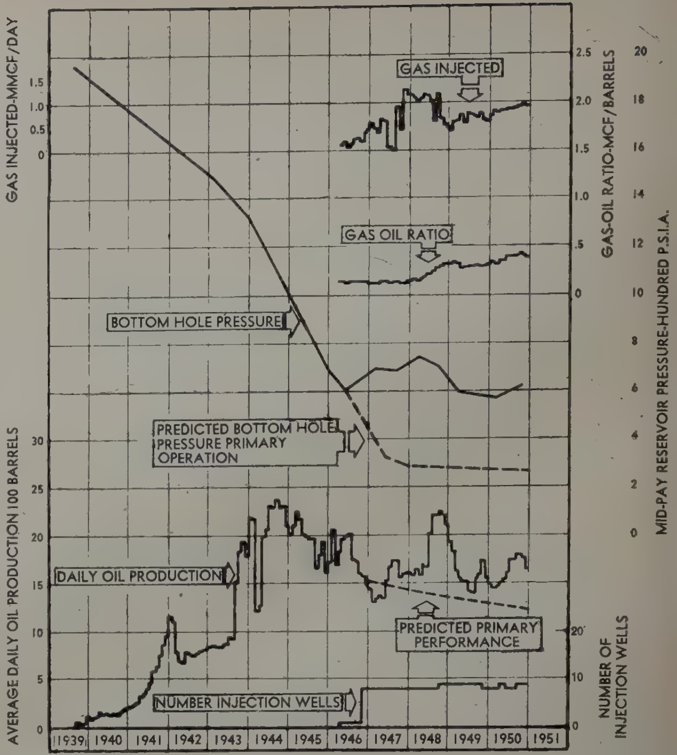

FIG. 10 — PERFORMANCE HISTORY, CEDAR LAKE GAS INJECTION AREA.

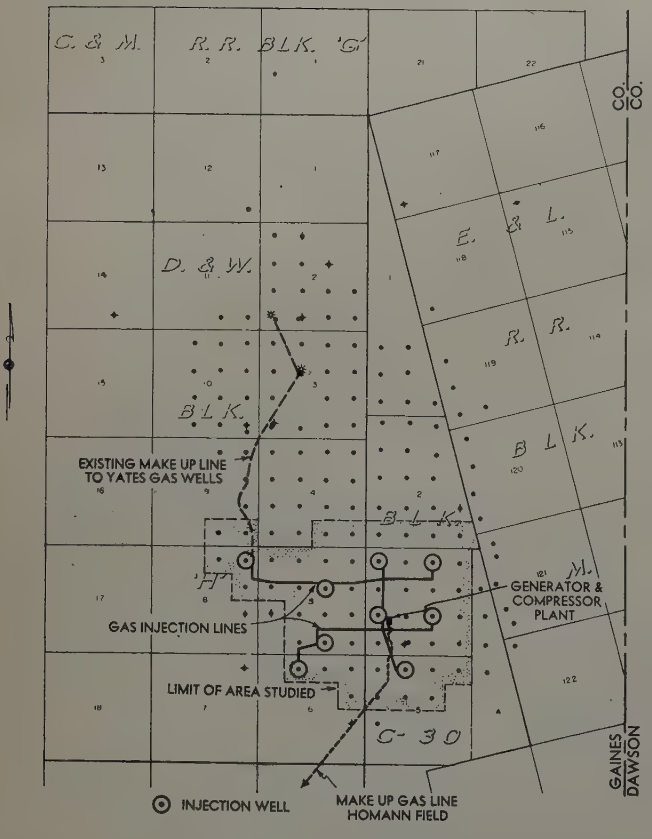

FIG. 9 — INJECTION FACILITIES, CEDAR LAKE FIELD.

ANALYSIS OF RESERVOIR PERFORMANCE

As pointed out previously, full scale gas injection operations had been in progress for a period of approximately 19 to 20 months before any increase in the produced gas/oil ratio was detected. The injection of gas over an extended period of time without any noticeable increase in the ratio was, of course, encouraging in that it provided a qualitative measure of the success of the injection program. At the same time, however, it necessarily delayed any attempt to evaluate quantitatively the performance data.

In analyzing the performance history of a gas injection program in which the pressure is maintained above the bubble point, two avenues of approach are open to the solution of the problem: (1) the material balance method and, (2) the application of the fractional flow and frontal advance expressions. The former, in its conventional form, does not take into consideration the time required for gas breakthrough, whereas the latter method is inherently suited to that particular phase of the gas injection program. It follows then that an attempt to interpret the results of the Cedar Lake injection program properly should utilize both methods of analysis.

Material Balance Method

The material balance method for predicting the behavior of gas drive reservoirs under both primary and gas injection operations has been adequately discussed in the literature[6,7] and will not be repeated at this time. By way of proper introduction to certain material to be presented later, however, it may be well to review briefly the use of the term "conformance factor." This term is generally defined as representing that fractional part of the reservoir contacted and affected by injected gas. This assumes, of course, that the remainder of the formation continues to perform as a simple depletion type reservoir. Modification of the material balance equation to include a conformance factor has been discussed in some detail by Patton[8] and by Pirson.[9]

In predicting the performance of any reservoir under gas injection operation, the most significant unknown is the portion of the total reservoir that will be affected by the injected gas. This factor will, of course, be different for different fields due to the fact that the permeability profile and structural and lithological conditions will vary from one reservoir to another.

The evaluation of the Cedar Lake project makes use of the material balance method to calculate theoretical gas/oil ratio trends assuming various conformance factors. These calculated trends are compared with the gas/oil ratio behavior actually observed in the injection area to determine what fraction of the pay has been affected in this project.

Mention was made previously of the lithological similarities between the Cedar Lake Field of the Midland Basin area and the San Andres reservoirs of the North Basin Platform area. While the order of permeability development is somewhat lower in the Cedar Lake Field than in the Slaughter Reservoir, previously discussed similarities in rock characteristics suggest that a relative permeability-liquid saturation relationship based on performance of certain areas in the Slaughter Field[5] should be applicable to the Cedar Lake reservoir.

Fortunately, considerable core analyses are available in the Cedar Lake Field and these data together with information from radioactivity and electric logs provide a reasonably accurate indication of the volume of oil initially contained in that portion of the reservoir underlying the injection area. This figure together with the Slaughter Field relative permeability relationship provides the basic information required to undertake an analysis of the performance history for the Cedar Lake Injection Project.

Utilizing the Slaughter relative permeability data and Cedar Lake crude characteristics, a number of "apparent" relative permeability-liquid saturation trends have been calculated assuming various conformance factors. These data extend over a conformance factor range of 40 to 100 per cent as shown in Fig. 11. The curve for a conformance factor of 100 per cent, of course, represents the trend actually calculated from Slaughter Field performance data and occupies a position on the graph which might reasonably be expected from analysis of the Cedar Lake Injection project if all of the reservoir underlying the injection area were contacted and affected by injected gas.

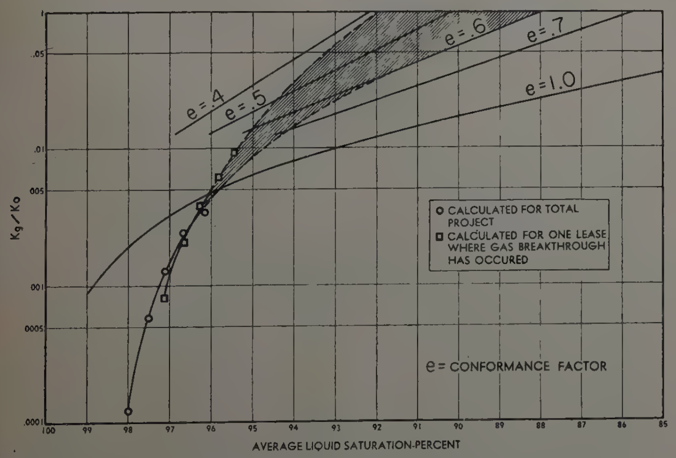

FIG. 11 — RELATIVE PERMEABILITY — LIQUID SATURATION RELATIONS FOR VARIOUS CONFORMANCE FACTORS.

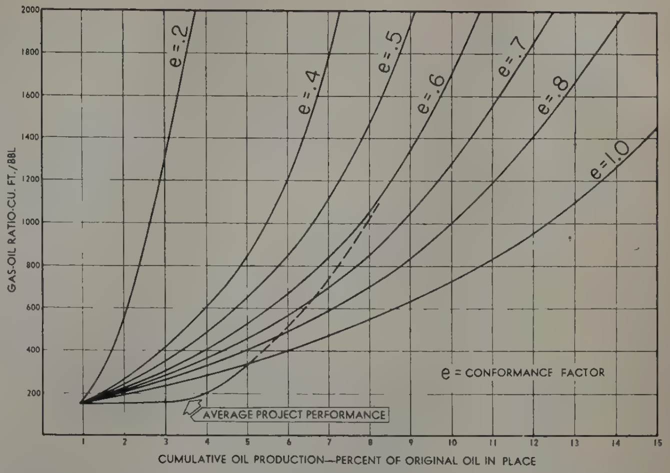

FIG. 12 — GAS/OIL RATIO BEHAVIOR VS CUMULATIVE OIL PRODUCTION FOR VARIOUS CONFORMANCE FACTORS.

Apparent relative permeability trends calculated from the total project performance data and the performance history of a large lease in the area, where gas breakthrough has occurred in the majority of the producing wells, are also shown in Fig. 11. It will be observed that data from the one lease illustrated can reasonably be extrapolated along the trend which would indicate a conformance factor in excess of 40 per cent and the apparent relative permeability trend for the total injection area coincides reasonably well with a conformance factor of 60 per cent.

With regard to the lease performance data shown in Fig. 11, it might be well to mention that the indication of a somewhat less favorable conformance factor is undoubtedly partially attributable to the fact that injection volumes have exceeded withdrawals to a slight degree and that no attempt was made to compensate for this condition in analyzing the performance data. It should be kept in mind that similar situations of an even more extreme nature are frequently observed in pilot projects involving only one or two injection wells, thereby leading to a condition which makes any attempt at a quantitative evaluation extremely difficult. In some instances, failure to recognize the importance of this particular phase of the problem has undoubtedly led to the conclusion that the injected gas had "channeled" and that an injection program on a fieldwide basis would not be economically attractive, whereas proper consideration of all factors involved possibly would not have led to such a conclusion.

Results of the analysis of performance history are shown in a somewhat different manner in Fig. 12, on which is indicated gas/oil ratio trends for conformance factor values ranging from 20 to 100 per cent. As will be noted, the gas/oil ratio behavior for the injection project is practically flat in the early portion of the injection history, occupying a position on the graph well below the theoretical behavior calculated for a reservoir having a conformance factor of 100 per cent. Following gas breakthrough, however, it will be observed that

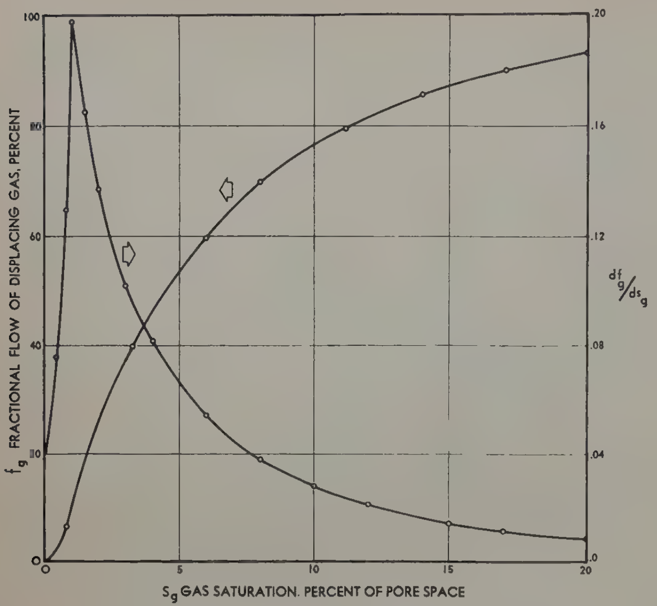

FIG. 13 — f_g AND df_g/ds_g AS FUNCTIONS OF S_g.

the ratio increases along a trend which indicates that a conformance factor of 60 per cent might reasonably be expected.

As mentioned previously, the material balance approach fails to take into account the time required to establish breakthrough of gas where injection is initiated in a reservoir at some pressure above the bubble point and maintained at that level. Utilizing the material balance approach, this results in the calculation of a condition prior to gas breakthrough which is obviously a physical impossibility and which can best be handled through use of the fractional and frontal advance expressions.

Application of Fractional Flow and Frontal Advance Expression

Neglecting the effects of gravity drainage and capillary pressure, the fractional flow formula of Buckley and Leverett may be stated as follows:

$$f_g = \frac{1}{1 + \frac{k_o}{k_g} \cdot \frac{\mu_g}{\mu_o}} \quad \ldots\ldots\ldots\ldots \quad (1)$$

where

f_g = fraction of gas flowing

k_o/k_g = relative permeability ratio of oil to gas

μ_g/μ_o = viscosity ratio of gas to oil

Utilizing the above relation, the fraction of gas flowing (f_g) has been calculated for various values of gas saturation and plotted as shown in Fig. 13. This curve was then differentiated graphically to obtain a plot of df_g/ds_g *vs* gas saturation.

In order to calculate the rate of advance and determine the space position of the front of saturation discontinuity, use has been made of the linear rate of advance equation modified for application to a radial system. This relation is as follows:

$$u = \left(r_w^2 + \frac{2r_w}{\Phi A} Q_t \frac{df_g}{dS_g} \right)^{1/2} - r_w \quad \ldots \quad (2)$$

where:

r_w = radius of well bore

Φ = porosity

A = area of well bore face in net pay interval

Q_t = total volume of displacing fluid in a unit of time

u = distance from well bore face at which the corresponding saturation exists

Utilizing data which are representative of average injection well conditions, Equation (2) has been solved for an injection period of 300 days using a total injection volume of 32,100 Mcf of gas. The results of this calculation, which are shown in Fig. 14, indicate that the injected gas should advance a distance of 398 ft from the well bore in 300 days. A second calculation was made utilizing the average gas volume injected during one day. Since we are concerned with a radial system in which the relationship between injection days and feet of advance of the front is a straight line relationship on logarithmic graph paper provided the injection rate is constant as shown in Fig. 15, additional calculations were unnecessary. Extrapolation of the relationship established by the two calculated points indicates that the gas front should advance 1,320 ft (the average distance between producing and injection wells) in approximately 1,130 days, if all pay were affected. Had these calculations been made on the assumption that only a fraction of the pay were affected by the injected gas, the time required for the front to reach a given distance would be reduced proportionately. Referring to the gas/oil ratio behavior as shown in Fig. 10, it will be observed that an increase in the ratio occurred approximately 19 to 20 months (578 to 608 days) after the project was expanded to include nine injection wells. From the ratio of the observed to calculated time for gas breakthrough, a conformance factor on the order of 50 to 60 per cent appears to be reasonable.

This procedure for analyzing the performance history is subject to at least one rather severe limitation in that it makes use of a portion of a field derived relative permeability relationship over a range of liquid saturations where the calculated relative permeability values are particularly sensitive to variations in stage of depletion of various portions of the reservoir. In other words, it has been commonly assumed that

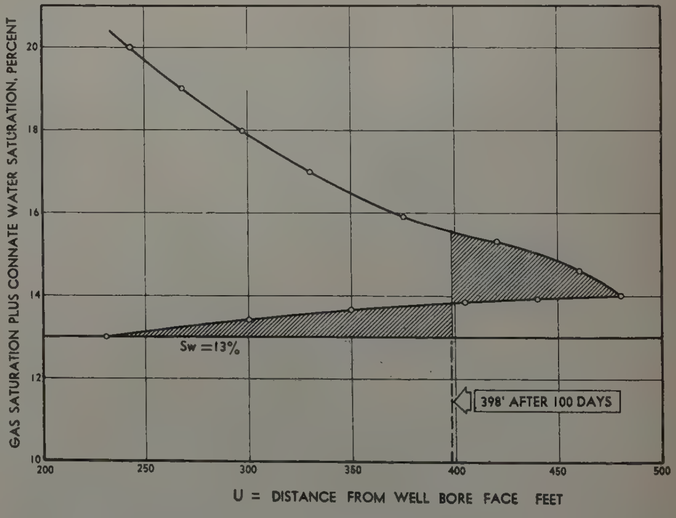

FIG. 14 — CALCULATION OF SATURATION DISTRIBUTION PRIOR TO GAS BREAKTHROUGH.

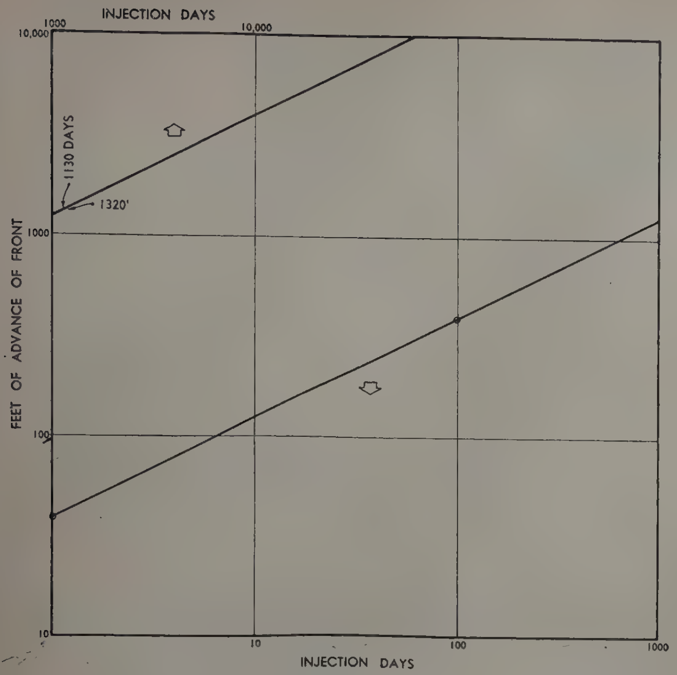

FIG. 15 — INJECTION DAYS VS FEET OF ADVANCE OF FRONT FOR AVERAGE CONDITIONS IN INJECTION AREA, CEDAR LAKE FIELD.

relative permeability trends calculated from field data are pessimistic for high values of liquid saturation due to the increase observed in gas/oil ratio almost immediately in the field's productive history.

In this regard it should be pointed out that the Slaughter Field relative permeability-liquid saturation relationship was calculated from certain selected areas within the field, in which case appreciable spatial variation in liquid saturation appears unlikely. Furthermore, recent laboratory relative permeability work based on internal gas drive experiments has indicated surprisingly good agreement, at high values of liquid saturation, with relationships derived from actual field performance data.[11] For this reason it is felt that there is considerable justification for use of the field derived relative permeability relationship.

FUTURE RESERVOIR BEHAVIOR

As pointed out in the introduction, the primary purpose in presenting this paper was to analyze the available reservoir performance data, however, a statement relative to future behavior of the reservoir would appear to be in order at this time.

Secondary recovery programs are undertaken primarily for the purpose of increasing ultimate recovery and, if the situation demands, maintenance of well productive capacities. In this latter regard, it is apparent from the foregoing discussion that little doubt remains as to ultimate success of the Cedar Lake injection program. Accordingly, it will suffice to say that projection of the observed performance data to depletion, utilizing a conformance factor of 50 per cent, indicates that an appreciable increase over primary recovery can reasonably be expected and; further, that the area under gas injection operation will be depleted in approximately the same length of time as would have been required under primary operation. This is an understandable development when consideration is given to the fact that practically all of the recovery under primary operations would necessarily be obtained after the reservoir pressure had declined to the bubble point of 326 psia, and at this reservoir pressure extremely low pressure differentials would be available for movement of fluid to the well bore.

CONCLUSIONS

In light of the foregoing discussion, the following conclusions appear to be in order:

1. Injection into the oil column in the Cedar Lake Field without attempting to control the point of entry of the gas has resulted in at least 60 per cent of the total reservoir being contacted and affected by the injected gas.
2. Derivation of the "conformance factor" from performance history in the fashion illustrated will permit quantitative evaluation of the ultimate benefits of a dispersed gas injection program, and will permit evaluation of the economics of injection of varying intensity.
3. It would appear that in many limestone reservoirs the probable success of a dispersed type gas injection program cannot be predicted from observation of permeability distribution in either one or a number of wells but necessarily must be determined by conducting a well planned injection program over a sufficiently large area, thereby minimizing the problems frequently associated with the usual pilot type of operation in which only one or two injection wells are involved.
4. The performance of the Cedar Lake gas injection project indicates the absence of any basis for classifying carbonate rocks in general as being inherently unsuited to a dispersed type of gas injection program, thus indicating that each field should be avaluated on its own merits regardless of whether production is obtained from a limestone or a sand.

APPENDIX

The calculation of saturation distribution prior to gas breakthrough, as shown in Fig. 14, makes use of the Buckley and Leverett linear rate of advanced relationship modified for application to a radial system.

For unit volume of a linear system, it has been shown that a material balance expression, relating total influx and efflux of occupying and displacing fluids in the unit volume, may be written as follows:

$$\left(\frac{dS_d}{d\Theta}\right)_u = \frac{q_t}{\Phi A}\left(\frac{df_d}{du}\right)_\Theta \quad . \; . \; . \; . \quad (1)$$

where:

S_d = saturation of displacing fluid
f_d = fractional flow of displacing fluid
q_t = total fluid flow
Φ = porosity
A = area
Θ = time
u = distance

Equation (1) may be reworked mathematically to give:

$$\left(\frac{\partial u}{\partial \Theta}\right)_{S_d} = \frac{q_t}{\Phi A}\left(\frac{\partial f_d}{\partial S_d}\right)_\Theta \quad . \; . \; . \; . \quad (2)$$

which states that the rate of advance of a plane of constant saturation in displacing fluid (S_d) is proportional to the change in composition of the flowing stream caused by a small change in saturation of the displacing fluid. The "rate of advance" equation, (2), was derived for a linear system, but may be adapted to a radial system by multiplying the expression by the ratio $\frac{r_w}{r_w + u}$, where r_w is the well bore radius and u is the radial distance from the bore face. The expression then becomes, for a radial system:

$$\left(\frac{\partial u}{\partial \theta}\right)_{S_d} = \frac{q_t}{\Phi A}\left(\frac{\partial f_d}{\partial S_d}\right)_{\theta}\left(\frac{r_w}{r_w + u}\right) \quad . \quad (3)$$

This differential equation is then rearranged by separation of variables, integrated, and solved for the distance u, which gives:

$$u = \left(r_w^2 + \frac{2r_w}{\Phi A} Q_t \frac{df_d}{dS_d}\right)^{1/2} - r_w \quad . \quad . \quad (4)$$

where:

r_w = radius of well bore

Φ = porosity

A = area of bore face in net pay interval

Q_t = total volume of displacing fluid in a unit of time

u = distance from bore face at which the corresponding saturation exists as a result of injecting Q_t

Actually the values of u obtained for varying values of $\frac{df_d}{dS_1}$ (*i.e.*, gas saturation), when plotted against total saturation, will represent the saturation distribution behind the advancing front. This may then be interpreted to give the actual rate of advance of the front. Hence, we have an expression which relates the rate of advance of a front to the total volume of displacing fluid. In adapting the Equation (4) to our case, the displacing phase becomes injected gas. ($f_d = f_g$ and $S_d = S_g$.)

Table I — Fractional Analysis-Reservoir Oil

Component	Mol. Per Cent
N_2	.39
H_2s	1.05
CO_2	.50
C_1	6.64
C_2	7.78
C_3	9.67
iC_4	1.34
nC_4	5.59
iC_5	2.26
nC_5	2.57
C_6	2.70
C_{7+}	59.51
	100.00

Mol. Wt. (C_{7+}) = 238
API Gravity (C_{7+}) = 29.4°

Table II — Fractional Analysis-Injection Gas

Component	Mol. Per Cent	
	Homann Field	Cedar Lake Field
N_2	20.96	38.71
CO_2		.10
C_1	63.08	49.61
C_2	9.45	6.60
C_3	4.24	3.07
iC_4	.40	.46
nC_4	1.13	.63
iC_5	.20	.25
nC_5	.28	.38
C_6	.19	.14
C_{7+}	.07	.05
	100.00	100.00
Gravity @ 60°F	.767	.8135
Net BTU Cont. cu ft	885	754

ACKNOWLEDGMENT

The authors wish to express their appreciation to the Stanolind Oil and Gas Co. for permission to publish this paper.

REFERENCES

1. Elkins, L. F., and Cooke, J. T.: "Pilot Gas Injection — Its Conduct and Criteria for Evaluation," *Trans.* AIME (1949) **186,** 180.
2. Keller, W. O., and Morse, R. A.: "Some Examples of Fluid Flow Mechanism in Limestone Reservoirs," *Trans.* AIME (1949) **186,** 224.
3. Bulnes, A. C., and Fitting, R. U., Jr.: "An Introductory Discussion of the Reservoir Performance of Limestone Formations," *Trans.* AIME (1945) **160,** 179.
4. Craze, R. C.: "Performance of Limestone Reservoirs," *Trans.* AIME (1950) **189,** 287.
5. Hiltz, R. G., Huzarevich, J. E., and Leibrock, R. M.: "Performance Characteristics of the Slaughter Field Reservoir," *Proceedings for Second Oil Recovery Conference — A Symposium on Carbonate Rocks* (1951) 146.
6. Muskat, M.: "Production Histories of Oil Producing Gas Drive Reservoirs," *Jour. of Applied Physics* (March, 1945) **16,** No. 3.
7. Tarner, J.: "How Different Size Gas Caps and Pressure Maintenance Programs Affect Amount of Recoverable Oil," *Oil Weekly* (June 12, 1944) **114.**
8. Patton, E. C., Jr.: "Evaluation of Pressure Maintenance by Internal Gas Injection in Volumetrically Controlled Reservoirs," *Trans.* AIME (1947) **170,** 113.
9. Pirson, S. J.: *Elements of Oil Reservoir Engineering,* McGraw-Hill Book Co. (1950).
10. Buckley, S. E., and Leverett, M. C.: "Mechanism of Fluid Displacement in Sands," *Trans.* AIME (1942) **146,** 107.
11. Geffen, T. M., Owens, W. W., Parrish, D. R., and Morse, R. A.: "Experimental Investigation of Factors Affecting Laboratory Relative Permeability Measurements," *Trans.* AIME (1951) **192,** 99. (*Jour. Petr. Tech.,* April, 1951.)

FURTHER DISCUSSION OF PAPERS PUBLISHED IN TRANSACTIONS, VOLUME 192 (1951)

RELAXATION METHODS APPLIED TO OIL FIELD RESEARCH

H. DYKSTRA AND R. L. PARSONS, CALIFORNIA RESEARCH CORP., LA HABRA, CALIF., MEMBERS AIME

(Published as T.P. 3145, Page 227)

DISCUSSION

By E. C. Larman, Anglo-Iranian Oil Co., Ltd., Kirklington Hall Research Station, England

It is notable that the authors, in their reply to Nowak, state that the application of the procedure described in their paper is not possible to nonsteady state flow. Since such flow is of great importance in oil field research, and since methods do exist for obtaining a solution by relaxation methods, it is desirable that the false impression should be removed.

Allen and Severn[1] have shown that relaxation methods can be applied to nonsteady state problems. In particular they solve, by way of illustration, an equation of the "heat conduction" type, *viz.*:

$$K\frac{\partial^2 v}{\partial x^2} = \frac{\partial v}{\partial t} \quad . \ . \ . \ . \ . \ . \ . \ . \ . \ . \quad (1)$$

which is of interest in oil field research since, in its general form

$$K\triangle^2 \rho = \frac{\partial \rho}{\partial t}$$

it is the equation governing compressible fluid flow in porous media.[2]

In order to solve a partial differential equation by relaxation it is necessary that the solution satisfies suitable boundary conditions at all points of a closed boundary and we say that such a problem is of a "jury" type.

By way of illustration we may take the case of an ordinary one dimensional differential equation.

The boundary conditions which must be equal in number to the order of the equation may be given in equal numbers at each end or unequally distributed between the ends — perhaps all at one end. The first is a "jury" problem while the others are "marching" problems.[3] We note at once that an odd order equation cannot be a "jury" problem.

Returning to Equation (1) it is apparent that we could lay down a rectangular net of t against x in a similar manner to that for x and y in the article. We extend the t axis up to the value of interest $t = t_1$ and our difficulty is at once apparent. We cannot lay down the conditions for $t = t_1$ because this is just what we are after. The very nature of the problem implies that, at best, we can only know the boundary conditions on three sides, *viz.*, the distribution along x for $t = 0$, the distribution in t for $x = 0$ and the distribution in t for $x = 1$. The answer required is the distribution in x for $t = t_1$ and if we knew it there would be no problem.

Allen and Severn overcame this difficulty in an ingenious way and in a way which would be quite useless by classical methods. They double the order of the equation. Equation (1) is transformed by making the dependent variable a differential function (suitably chosen) of a new dependent variable. The effect of this is to provide the means of having sufficient disposable extra boundary conditions to convert the problem to "jury" type. The substitution chosen results in an equation of the form:

$$\frac{\partial^2 w}{\partial t^2} - K^2\frac{\partial^4 w}{\partial x^4} = 0 \quad . \ . \ . \ . \ . \ . \ . \ . \ . \quad (2)$$

and although this is much more complicated judged by classical standards this is no criterion for a numerical method. The real point at issue is that a nonsteady state problem has been solved by relaxation methods.

It is shown in the paper[1] that the mesh interval in the t direction is not independent of that in the x direction but since we can take the x divisions at will this is no disadvantage. It is also shown that though the finite difference approximation to Equation (2) leads to a more complicated relaxation pattern than for Equation (1) yet for computation that for Equation (2) has a distinct advantage. For a discussion of the necessity for n boundary conditions to deal with a differential of order $2n$ or $2n-1$, consideration of odd order equations, practical points, choice of transformation, added boundary conditions, and a worked example reference should be made to the original paper.[3]

In addition, attention may be drawn to the fact that Allen and Dennis[4] have shown that a three dimensional problem, *e.g.*

$$\frac{\partial^2 w}{\partial x^2} + \frac{\partial^2 w}{\partial y^2} + \frac{\partial^2 w}{\partial z^2} = W\ (x, y, z)$$

can be solved on a sheet of paper (two dimensions) by suitable care in arranging the work.

The writer suggests therefore, that the solution of a "four dimensional" nonsteady state equation, *e.g.*,

$$\frac{\partial^2 w}{\partial x^2} + \frac{\partial^2 w}{\partial y^2} + \frac{\partial^2 w}{\partial z^2} = \frac{1}{K}\frac{\partial w}{\partial t}$$

by relaxation is dependent only on a suitable "storage" mechanism and transformation. In its simplest form the "storage" would consist of many sheets of paper each containing a three dimensional aspect. That this would be a highly involved procedure is obvious but the point to be established is that it is the "storage" problem which is the limiting factor, not the method.

It is not necessarily suggested that relaxation is a good way of solving nonsteady state problems, only that it can, and has been done.

Finally attention may be drawn to a paper by C. J. Tranter,[5] who shows that in some cases a three dimensional problem may be reduced to a set of problems in two dimensions.

REFERENCES

1. Allen, D. N. de G., and Severn, R. T.: *Quart. Jour. Mechs. and Applied Maths.* Oxford (June, 1951) **IV**, 2.
2. Muskat, M.: *Flow of Homogeneous Fluids through Porous Media*, McGraw Hill Book Co. (1937).
3. Richardson, L. F.: *Phil. Trans. R. S.* (A) **226** (1927).
4. Allen, D. N. de G., and Dennis, S. C. R.: *Quart. Jour. Mechs. and Applied Maths.*, Oxford (June, 1951) **IV**, 2.
5. Tranter, C. J.: *Ibid.* (1948) **1**, 281.

AUTHORS' REPLY TO MR. LARMAN

The comments of Larman on our paper "Relaxation Methods Applied to Oil Field Research" are very good. He shows that by suitable transformation a nonsteady state flow problem can be solved by the relaxation principle; we are indebted to Larman for his contribution.

In his concluding comments, Larman suggested that solution by relaxation of nonsteady state problems "would be a highly involved procedure;" and further that even though solution by relaxation be possible, other methods of attack might be better. We agree. In particular, capacitor-resistor network models, such as those developed by V. Paschkis, and later by W. A. Bruce, are designed to handle nonsteady state flow problems. From a practical point of view, anyone attempting to solve a nonsteady state flow problem by relaxation has a job to do; whereas a very similar problem in steady state is simple and quick.

★ ★ ★

THE CALCULATION OF PRESSURE DROP IN THE FLOW OF NATURAL GAS THROUGH PIPE

FRED H. POETTMANN, PHILLIPS PETROLEUM CO., BARTLESVILLE, OKLA., JUNIOR MEMBER AIME

(Published as T.P. 3217, Page 317)

DISCUSSION

By W. C. Mosteller, Southern Counties Gas Co. of California, Los Angeles, Calif.

Poettmann develops by mathematical manipulation of basic equations a means of taking into account the deviation of natural gas from ideal gas behavior. Specific attention is given to:

a. Calculation of pressure loss (or sand surface pressure) of flowing gas wells;
b. Flow of gas in pipe lines;
c. Calculation of isothermal horsepower required to compress natural gas.

I believe the author's flow equation derivation is not mathematically rigorous. This applies to his integration process and treatment of average velocity in Equations (4), (14), (28), (29), (30) and (31). More detailed comment of the author's mathematics is given in Appendix 1 below.

Under some conditions the author's flow equations will give correct results; under others, they will not. For instance, in Poettmann's pipe line example, he computes the flow through a 50-mile 26-in. line with an upstream pressure of 825 psia and a downstream pressure of 565 psia to be 462 MMcf/D. Calculation by a formula derived through rigorous mathematics would, in this case, also give a flow of approximately 462 MMcf/D. If, in this pipe line, however, the upstream pressure had been 825 psia and the downstream pressure 135 psia, the author would have computed a flow rate of 545 MMcf/D; whereas the correctly computed flow rate is 624 MMcf/D (using the author's friction factor in each computation).

W. O. Clinedinst[1] developed a pipe line flow formula along a line of thought similar to that of Poettmann's. Although Clinedinst did not present his material in such a convenient tabular form as Poettmann's Table I, Clinedinst's formula is derived by more exacting mathematics. Later, Joffe[2] extended Clinedinst's work to provide computation charts that are more convenient to read and use. P. MacDonald Biddison[3] developed a simplified procedure for making the deviation correction applicable to pipe lines operating at 2,000 psig or less.

In Poettmann's development of his equation for gas flowing from wells, the kinetic energy factor is eliminated on the assumption that it is negligible. I am of the opinion that the kinetic energy factor would not be negligible in all computations involving flowing gas wells.

In my opinion, Poettmann's Table III, which purports to illustrate the accuracy of his vertical pipe flow equation, is misleading. I believe that the percentage accuracy figures given in the last column of this table are not indicative of the accuracy of his flow formula since these percentages are based upon the total observed pressure and not the relation between the computed pressure drop and the observed pressure drop.

Poettman's formula for isothermal horsepower requirements to compress natural gas is developed in a manner which is mathematically precise. In my opinion, however, actual gas compression is more closely represented by adiabatic conditions instead of isothermal.

REFERENCES

1. Clinedinst, W. O.: "Flow Equations for Gas Considering Deviations from Ideal Gas Laws," *The Oil and Gas Journal* (April 7, 1945).
2. Joffe: "Gas Flow in Long Pipelines," *Chemical Engineering* (August, 1949).
3. Biddison, P. MacDonald: "Gas Flow Computations," 36th Annual Convention Natural Gas Dept., American Gas Association, Dallas, Tex. (1941). Full paper later printed for public distribution by American Gas Association.

APPENDIX 1

Illustration of Non-Rigorous Mathematics

In Paper, "The Calculation of Pressure Drop in the Flow of Natural Gas Through Pipe"

Correct vertical flow equation — neglecting kinetic energy effect:

$$L = \int_{P_2}^{P_1} \frac{V\ (dP)}{1 + \dfrac{4\,f\,u^2}{2\,g\,D}}$$

This cannot be reduced to

$$L = \frac{\int_{P_1}^{P_2} V\ (dP)}{1 + \dfrac{4\,f\,\bar{u}^2}{2\,g\,D}}$$

with the value of $\bar{u}$ determined by separate integration as the author performs in his Equations (14) through (16).

Correct gas flow equation — horizontal flow:

$$L = \int_{P_2}^{P_1} \frac{V\ (dP)}{\dfrac{4\,f\,u^2}{2\,g\,D}}$$

This cannot be reduced to

$$L = \frac{\int_{P_2}^{P_1} V\ (dP)}{\dfrac{4\,f\,\bar{u}^2}{2\,g\,D}}$$

with the value of $\bar{u}$ determined by separate integration as the author performs in his Equations (14) through (16).

AUTHOR'S REPLY TO MR. MOSTELLER

The primary purpose of the paper was to present a procedure for calculating the sandface pressure of flowing gas wells. The other procedures available are those of the Bureau of Mines Monograph 7, and a recent paper by R. V. Smith.[1] In these equations compressibility is either ignored or a constant "effective" compressibility factor was used, the value of "effective" compressibility being left up to the judgment of the user. The calculation of static bottom hole pressure (which was overlooked by Mosteller), the equation for horizontal flow, and the isothermal horsepower equation were added only to illustrate other possible uses of the factors.

I would very much like to see a vertical flow equation mathematically rigorously derived involving the compressibility factor. The use of a constant velocity, whether an integrated average velocity or otherwise, in the energy loss term is not new, and if used as such, Equation (4) is correct as written since the term can then be removed from within the integral sign, for the same reason the so-called constant "effective" compressibility factor in other flow equations[1] was removed from within the integral sign. The use of a constant average velocity in the energy loss term is no more theoretically correct than assuming a constant "effective" compressibility, but if it provides us with a workable equation its assumption is justified. If the calculated results agree with the field measurements the equation is justified. Mosteller's comments concerning Table III are not valid. A gas man is interested in the absolute value of the sandface pressure, not the pressure drop, for purposes of calculating back pressure curves. Therefore, comparisons of the sandface pressures were made. It is the absolute pressure that determines the physical properties of the flowing fluid, not the pressure drop.

I am aware of Clinedinst's development of a horizontal flow equation. It does not assume an average velocity in the energy loss term and as such is more rigorous. It does assume a zero kinetic energy term. Its use is definitely preferred over Equations (32) or (33) of the paper. The Equations (32) and (33) have not been tested against field data. Clinedinst's development cannot be applied to vertical flow and result in a simple workable equation.

The assumption of a negligible kinetic energy term in the vertical flow of gas is valid. We have ample quantitative evidence to support this assumption. If Mosteller has quantitative evidence to the contrary, I would like to see it. Smith[1] has published some specific data, where, for the wells in question, the kinetic energy amounted to only 0.05 per cent of the total available energy.

Mosteller is concerned over the equation for calculating isothermal horsepower. I am familiar with the fact that actual gas compressions are polytropic and tend to approach adiabatic conditions. The equation presented is rigorous and represents the minimum value of the horsepower requirements that we would like to approach, adiabatic compression giving us the maximum horsepower requirements. The adiabatic compression requirements of a real gas can be calculated very simply from an enthalpy-entropy diagram of the gas.[2] From a practical sense, the use of the isothermal horsepower equation may be somewhat limited, but that is no reason for not taking full cognizance of its existence, since it does represent the lower limit of horsepower requirement. Isothermal horsepower is extensively used in gas-lift calculations in calculating lift efficiencies.

$$L = \int_{P_2}^{P_1} \frac{V dP}{1 + \frac{4fv^2}{2g\,D}}$$

If we can assume v constant and equal to $\bar{v}$ by the same logic that Z was assumed to be constant and removed from within the integral sign, in other flow equations,[1] then:

$$L = \frac{\int_{P_2}^{P_1} V dP}{1 + \frac{4f\bar{v}^2}{2g_c D}}$$

REFERENCES

1. Smith, R. V.: "Determining Friction Factors for Measuring Productivity of Oil Wells," *Trans.* AIME (1950) **189,** 73.
2. Brown, G. G.: "A Series of Enthalpy-entropy Charts for Natural Gases," *Trans.* AIME (1944) **160,** 68.

★ ★ ★

Technical Note 65———

A NEW TECHNIQUE FOR THE MEASUREMENT OF THE FORMATION FACTORS AND RESISTIVITY INDICES OF POROUS MEDIA

F. MORGAN, M. R. J. WYLLIE AND **P. F. FULTON,** GULF RESEARCH AND DEVELOPMENT CO., PITTSBURGH, PA., MEMBERS AIME

The importance of formation factor, F, not only in electric logging but as a fundamental rock parameter has recently been stressed.[1,2] The desirability of investigating the range of variation of the resistivity index exponent, n, in the relationship $I = S_w^{-n}$, where I is the resistivity index and S_w the water saturation as a fraction of the void volume of a porous medium, has also been urged.[3] The magnitude and variation of n with saturation and rock texture is a subject not only of theoretical interest but also one of prime importance in the interpretation of electric logs.

A simple technique has recently been developed which enables both F and n to be measured with high accuracy and which may also find acceptance as a convenient method for the determination of irreducible saturation attainment in the restored state method of core analysis.

Experience has taught that reproducible measurements of F are possible only if the resistance measuring electrodes are so arranged with respect to a plane face on a porous medium that they are able to make electrical contact with substantially all entry pores in that plane. In practice this may be achieved by using a platinized-platinum gauze electrode backed by some absorbent material (such as felt) which has been saturated with a fluid identical with that used to saturate the porous medium. Application of pressure to the electrode and absorbent material then forces the gauze against the plane face of the porous medium and simultaneously squeezes saline solution through the meshes of the gauze. By this means the electrode is in continuous aqueous contact with all pores and satisfactory and reproducible low resistance contact with the porous medium is achieved.

Clearly this method, although satisfactory for measurements of F, cannot be applied to the making of continuous resistance measurements on a porous medium while capillary pressure desaturation is being carried out. However, accepting the principle that for satisfactory results electrical contact must be made between a measuring electrode and all pores adjacent to that electrode, methods of bringing electrodes into intimate contact with the surfaces of porous media were investigated. Two methods were ultimately found to be satisfactory: in the one, the metal electrode is formed on the required portion of the porous medium by the use of a metal spray gun, while in the second the electrode is painted on with an ordinary camel's hair brush. The first method has the advantage of permitting the use of any metal which can be sprayed, but has the disadvantage of requiring rather elaborate and expensive equipment. The second method is presently limited to silver electrodes although in principle other metals, *e.g.* platinum or gold, could be used. Moreover, the method is so simple and cheap, and has been found to be so satisfactory that it will be described in some detail.

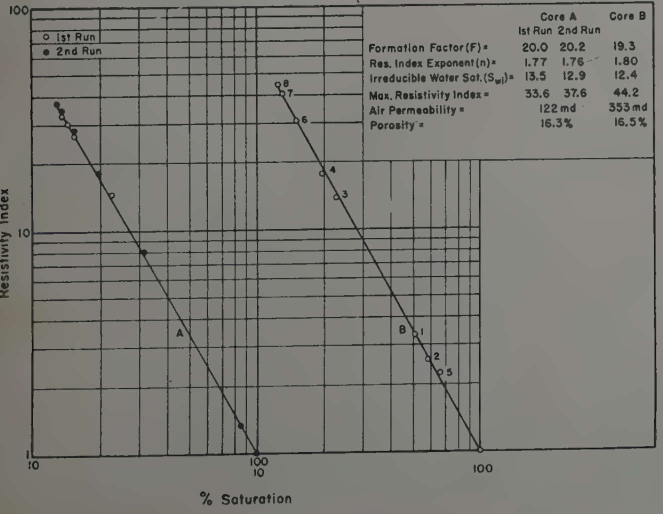

	Core A 1st Run	Core A 2nd Run	Core B
Formation Factor (F) =	20.0	20.2	19.3
Res. Index Exponent (n) =	1.77	1.76	1.80
Irreducible Water Sat. (S_{wi}) =	13.5	12.9	12.4
Max. Resistivity Index =	33.6	37.6	44.2
Air Permeability =	122 md		353 md
Porosity =	16.3%		16.5%

The core being investigated is cut into a right circular cylinder and is extracted and dried in the usual manner. The ends are then lightly painted with silver conducting paint* of the type used in printed electrical circuits. The quantity of paint used is not critical but the minimum compatible with entirely coating the core ends is recommended, particularly on the end that contacts the barrier. The core is then dried at atmospheric temperature for one hour or for shorter periods at any suitable elevated temperature up to about 110°C. It will be found that silver coatings so prepared are not only strongly adherent but also permeable and the core may be desaturated by the ordinary capillary pressure technique through one of the coated faces. The same permeability is characteristic also of thin metal coatings formed using the spray-gun technique.

An ordinary Lucite capillary pressure desaturation cell has been adapted to a form suitable for measuring the resistivity of the saturated silver faced cores both at 100 per cent saturation (*i.e.*, F) and at intermediate saturations down to the irreducible minimum. This has been achieved as follows:

A Coors porcelain barrier, having a displacement pressure of c 30 psi was grooved across a diameter. Dimensions of this groove were c 1 mm deep and 1 mm wide at the top. The groove was then painted thickly with silver conducting paint, the paint in the groove being extended lightly over the edges of the groove for a distance of c 1 mm on each side. A 30 gauge silver wire was then arranged in the groove in a form of a spring bow, each end of the silver being held at diametrically opposite ends of the groove by means of plastic cement. The arc of the bow at its highest point was arranged to be a millimeter or so above the face of the barrier, while one end of the bow wire was led by means of a pressure-tight connection through the wall of the capillary pressure cell. The groove in the barrier was then surrounded by suitably cut portions of Kleenex in the conventional manner so as to ensure capillary continuity from core to barrier, and the core placed on the barrier. The weight of the core distorted the silver spring bow and good electrical contact was thereby made between the outside of the cell and the lower painted silver electrode. Electrical connection to the top painted silver electrode was made in the following manner. On the top electrode was placed a silver plated brass disc of 2 cms diameter and 2 mm thickness. The purpose of this disc was to obviate any corrosion effects resulting either from dissimilar metal contacts or from vapor condensed on the helical spring which was attached to the cap of the capillary pressure cell. This spring served the dual purpose of holding the core in contact with the barrier and silver wire, and making electrical contact with the silver plated disc and thus the top silver painted electrode.

---

*Type S.C. 11 provided by Microcircuits Co., New Buffalo, Mich., has been found to be very satisfactory.

Using this technique with cores 1.91 cm in diameter and approximately 2 cm in height and making use of a conventional 1,000 cycle conductivity bridge to measure resistance, results were reproducible within the accuracy of the resistivity measuring equipment and the saturation determinations. Saturations were determined gravimetrically, no serious difficulties in reproducing the resistance prior to removal being encountered when returning a core to the cell after a weight measurement. The maximum resistance discrepancy thus found has rarely exceeded 3 per cent and it is generally less than 2 per cent.

Two typical results are shown in the figure. In *A* the reproducibility is evident as is the fact that *n* is independent of saturation. In fact no case has been observed where *n* is saturation dependent, except at very low values of saturation where the core matrix resistance itself may be significant.[4] Curve *B* is of interest as a case where, because of barrier breakthrough and other difficulties, the core twice had to be removed from the cell, during which time it was immersed in brine and reimbibed fluid after being partially desaturated. The points are numbered to show the sequence of desaturations and resaturations. It will be observed that no hysteresis effects are apparent.

ACKNOWLEDGMENT

The authors are indebted to B. Greifer for a suggestion which led them to the choice of silver conducting paint. Their thanks are due to Paul D. Foote, executive vice-president, Gulf Research and Development Co., Pittsburgh, Pa., for permission to publish this note.

REFERENCES

1. Wyllie, M. R. J., and Rose, Walter D.: *Trans.* AIME, (1950), 189, 105.
2. Wyllie, M. R. J., and Rose, Walter D.: *Nature* (1950), 165, 972.
3. Dunlap, H. F., Bilhartz, H. L., Bailey, C. R., and Shuler, E.: *Trans.* AIME (1949), 186, 259.
4. Patnode, H. W., and Wyllie, M. R. J.: *Trans.* AIME (1950) 189, 47.

★ ★ ★

Technical Note 66

FLUID DISTRIBUTIONS CHARACTERIZING GAS-LIQUID FLOW

WALTER ROSE, TEXAS PETROLEUM RESEARCH COMMITTEE, AUSTIN., TEX., MEMBER AIME

It is the purpose of this note to call attention to the circumstance complicating the attainment of uniform gas-liquid distributions in multi-phase flow systems, and especially in those of the so-called Hassler type.[1] Although the complication arises directly as a consequence of gas compressibility and the dependence of fluid distributions on interfacial curvature phenomena, little reference to the problem has yet appeared in the literature.[2] In fact, it is only the paper of Geffen et al.[3] which gives any experimental evidence that a problem exists. On the other hand, previous authors[1,4,5] have made the tacit, albeit fallaceous assumption that uniform gas-liquid distributions automatically are established in linear flow systems by the expedient of maintaining the pressure gradients equal in the flowing gas and liquid phases. Such a device, it can be shown, will succeed only if the immiscible fluids are both equally compressible or both essentially non-compressible. Another necessary condition required before uniform fluid-fluid distributions can be achieved is that the porous matrix is isotropic.

Uniform fluid saturation distribution conditions obtain in isotropic media only when the curvature of each interface of contact between wetting and non-wetting fluids is everywhere the same throughout the interspaces. This is a necessary condition which follows from the consideration that variation in interfacial curvature gives rise to finite capillary pressure gradients and therefore to variation in the saturation distribution. That this is not a sufficient condition follows from the consideration that hysteric possibilities allow for different saturations even though the capillary pressure gradient is zero. In any event, it will be recalled that it is the intent in the Hassler scheme of relative permeability determination[1] to obtain initially (by the capillary pressure drainage or imbibition process) uniform conditions of fluid distribution in the core sample, and then to maintain this uniformity during mixture flow so that the resultant fluid mobilities which are calculated will refer to steady-state transfer under fixed conditions of uniform saturation. If the flowing fluids are incompressible, it is recognized that employment of the same value of the pressure gradient in each fluid will result in maintenance of the initially obtained condition of zero capillary pressure gradient. On the other hand, the consequence of gas compressibility is that the gradient in the gas pressure varies from point to point in the flowing stream, and since the pressure gradient in an incompressible liquid is constant it is thus impossible to maintain zero capillary pressure gradient during the simultaneous flow of gas-liquid mixtures. Therefore, one would expect to observe a variation in the gas-liquid saturation in the directions of the capillary pressure gradients, depending in magnitude on the particular way saturation changed with capillary pressure.

In order to formulate the manner gas compressibility effects prevent the attainment of uniform gas-liquid distributions during mixture flow, consider a linear flow system of unit length. As noted, it is necessary to assume an isotropic medium (*viz.* one where permeability is independent of position and direction). One then can arbitrarily set the pressure drops in the gas and liquid phases equal across the linear flow paths. Then the capillary pressure P_c at any point x where $0<x<1$), will be given by:

$$P_{c_{(x)}} = \left[P_{g_{(x=0)}}^{2} - x \left\{ \left(P_{g_{(x=0)}} \right)^{2} - \left(P_{g_{(x=1)}} \right)^{2} \right\} \right]^{1/2} - \left[P_{L_{(x=0)}} - x \left\{ P_{L_{(x=0)}} - P_{L_{(x=1)}} \right\} \right] \quad \ldots\ldots\ldots\ldots \quad (1)$$

where P_g and P_L are the gas and liquid absolute pressures at the point $x=0$ or $x=1$. Implicit in Equation (1) is that the gas is the non-wetting phase and the liquid is the wetting phase. It is instructive to derive from Equation (1), then, an expression for the maximum difference in capillary pressure which will obtain in the given linear gas-liquid flow system. This is:

$$\Delta P_{c_{\max}} = \left[P_{c_{\max}} - P_{c_{\substack{(x=1)\\(x=0)}}} \right] = \frac{\Delta P^{2}}{8\overline{P}} \quad \ldots \quad (2)$$

where ΔP is the arbitrarily fixed pressure drop set equal in the flowing fluids, and $\overline{P}$ is the mean gas pressure. Thus, it is Equation (2) which when used in conjunction with the appropriate capillary pressure data shows the maximum variation in saturation distribution due to the finite capillary pressure gradients obtaining in gas-liquid flow systems of the Hassler type. Equation (2) also explains the statement of Geffen et al.[3] that "using differential pressures small compared to the absolute pressure" minimizes saturation gradients due to gas expansibility. The consequence of Equation (2) is that the effective permeabilities afforded by the uniform medium to the transfer of the non-wetting gas and the wetting liquid will vary with position, such that the laboratory data which are obtained will not measure true steady-state fluid mobilities under conditions of zero saturation gradient.

Equation (2) is an exact formulation, and as such it shows that employing small pressure drops and/or selecting large values of mean gas pressure both contribute to conditions of small capillary pressure gradients, as is desired in the laboratory study of relative permeability phenomena. In fact, these are the conditions which usually characterize reservoir flow processes, especially at points removed from the well face discontinuity. (N.B. Points in the reservoir close to the well face are characterized by the greatest pressure gradients and the smallest values for mean gas pressure.) Obviously, however, it is the variation of saturation with capillary pressure which is the determining factor, together with the maximum variation in capillary pressure along the flow path as expressed by Equation (2). For examples, a given value of $\Delta P_{c_{\max}}$ calculated by Equation (2) can mean only negligible variation in saturation distribution if the wetting liquid is approaching its "irreducible" saturation, whereas it can result in appreciable saturation distribution variation when the gas saturation approaches its "equilibrium" value. This is because of the hyperbolic type variation between saturation and capillary pressure when the capillary pressure approximates the displacement pressure and small changes when maximum values of capillary pressure obtain.

It is concluded, therefore, that Equation (2) should be used in particular instances in conjunction with empirical data showing the variation of saturation with capillary pressure, in order to formulate the necessary conditions of pressure gradient and mean gas pressure which are required to give negligible saturation variations in gas-liquid flow systems. In this connection, it may be surmised from the nature of Equation (2) that previously reported gas-liquid mixture flow data have not been seriously in error except in the range of saturations where the gas relative permeability approaches zero. On the other hand, it will be recalled that the laboratory delineation of gas-oil ratio curves depends much on obtaining accurate relative permeability data in this saturation range.

REFERENCES

1. Hassler, G. L.: U. S. Patent No. 2,345,935, April 4, 1944.
2. Rose, Walter: "Some Problems of Relative Permeability Measurement." Paper to be presented before the Third World Petroleum Congress, The Hague, May 28-June 6, 1951.
3. Geffen, T. M., Owens, W. W., Parish, D. R., and Morse, R. A.: "Experimental Investigation of Factors Affecting Laboratory Relative Permeability Measurements." Paper presented at Fall Meeting, Petroleum Branch, AIME, New Orleans, October 4-6, 1950.
4. Brownscombe, E. R., Slobod, R. L., and Candle, B. H.: "Relative Permeability of Cores Desaturated by Capillary Pressure Method." Paper presented Spring Meeting of the Pacific Coast District, Division of Production, American Petroleum Institute, Los Angeles, May 12, 1949.
5. Brown, Harry W.: "Capillary Pressure Investigations." Paper presented at Fall Meeting, Petroleum Branch, AIME, New Orleans, October 4-6, 1950.

★ ★ ★

Technical Note 67

THE CALCULATION OF WATER RESISTIVITIES FROM CHEMICAL ANALYSES

H. F. DUNLAP, MEMBER AIME, AND **R. R. HAWTHORNE,** JUNIOR MEMBER AIME, ATLANTIC REFINING CO., DALLAS, TEX.

ABSTRACT

A method of calculating formation water resistivities from chemical analyses is presented which is somewhat faster and more accurate than previously described methods. For 26 formation water samples taken from wells in the Texas Gulf Coast, the average deviation of calculated from measured water resistivities was 3.3 per cent, with an average bias of +1.1 per cent in the calculated values. This compares with average deviations of 4.6 per cent and 7.8 per cent, with corresponding average biases of +3.2 per cent and –6.3 per cent, for the two methods previously described in the litera-

ture. All three methods are sufficiently accurate for most purposes; the main advantage of the method presented is its speed and convenience.

DISCUSSION

It is frequently desirable to calculate the formation water resistivity from the chemical analysis of the water, as for example, in electric log interpretation. Two methods have previously been given in the literature[1,2] for accomplishing this. Both methods require that the chemical analysis be given in the Palmer[3] system, as primary and secondary alkalinity and salinity. This conversion of the values of the ppm of the various ions to primary and secondary salinity and alkalinity is time consuming, and many laboratories report only the concentrations of the various ions in parts per million. However, all laboratories report the individual ionic concentrations, whether or not the Palmer system of reporting is also used. Hence it was thought that a method that would permit resistivity calculations directly from these data would be useful.

Table I — Conversion Factors for Calculating Water Resistivity

Na ppm x 1.00 = N_1 Equivalent ppm *NaCl.*
Ca ppm x .95 = N_2 Equivalent ppm *NaCl.*
Mg ppm x 2.00 = N_3 Equivalent ppm *NaCl.*
Cl ppm x 1.00 = N_4 Equivalent ppm *NaCl.*
SO_4 ppm x .50 = N_5 Equivalent ppm *NaCl.*
HCO_3 ppm x .27 = N_6 Equivalent ppm *NaCl.*
CO_3 ppm x 1.26 = N_7 Equivalent ppm *NaCl.*
ΣNi = Total Equivalent ppm *NaCl.*

In the method developed, the various ions reported in the chemical analysis are converted to an equivalent amount of *NaCl*. The sum of the various contributions to the *NaCl* (actual or equivalent) can then be used in conjunction with a plot of *NaCl* concentration versus resistivity to obtain the resistivity of the solution in question. The conversion factors used in this process are shown in Table I and the resistivity vs. *NaCl* saturation plot (I.C.T. data) in Fig. 1. An example of a typical calculation is shown in Table II, together with the measured resistivity.

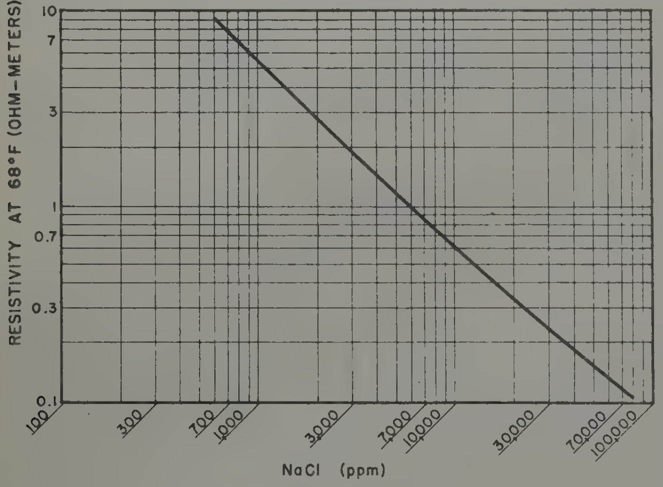

FIG. 1 — *NaCl* CONCENTRATION VS. RESISTIVITY.

These conversion factors for the various ions were obtained by measuring the resistivities of a number of simple solutions containing only two types of ions, one of which was always either Na^+ or Cl^-. Although for dilute solutions of most ions the conversion factors do not depend significantly on the concentration, the 0.5 factor for the $SO_4^=$ is actually the mean determined for three solutions of Na_2SO_4, using $SO_4^=$ concentrations of 676 ppm, 2,030 ppm, and 3,030 ppm. The resistivity conversion factors found for these quantities of $SO_4^=$ were 0.553, 0.532, and 0.412 respectively. It is therefore recommended that a factor of 0.5 for $SO_4^=$ be used for the majority of oil field brine samples, in which the $SO_4^=$ concentration is relatively small compared to the Cl^- concentration. However, in some regions, such as the Rocky Mountains, the $SO_4^=$ concentration is large enough to be relatively important, and in these areas the factor corresponding to the existing $SO_4^=$ concentration should be used.

Table II — Example of Method Applied to a Frio Water from the Aransas Field, San Patricio County, Texas

Ionic Constituent	Concentration PPM	Conversion Factor	Equivalent Concentration of *NaCl* (PPM)
Na (calculated)	21,899	1.00	21,899
Ca	2,449	.95	2,325
Mg	382	2.00	764
Cl	38,292	1.00	38,292
SO_4	381	.50	191
HCO_3	1,098	.27	296
CO_3	0	1.26	0

Total Equivalent *NaCl* concentration =	63,767
Calculated Resistivity (using Fig. 1)	.126ΩM
Measured Resistivity	.131ΩM
Error = –3.8 per cent	

In order to check the accuracy of this method of calculating formation water resistivities, the resistivities of formation waters from 26 wells in the Gulf Coast region were measured in a four pole resistivity cell, using 60 cycle current and a vacuum tube voltmeter of 1 megohm input impedence. The water resistivities ranged from 0.097ΩM at 68°F to 3.52ΩM at 68°F. The chemical analyses of the waters were also available, and the resistivities of these samples were calculated from their analyses according to the methods outlined by Jones and by Tixier, as well as by the method described above, using resistivity vs. concentration data taken from the International Critical Tables.

For the method presented here, the average of the absolute values of the per cent deviation between the measured and calculated resistivities was 3.3 per cent, the calculated resistivity being on the average 1.1 per cent too great. For the Park Jones method, which uses a series of conversion factors to change the primary and secondary salinity and alkalinity to equivalent quantities of *NaCl*, the average of the absolute values of the per cent deviation between the measured and calculated resistivities was 4.6 per cent, with the calculated resistivity being on the average 3.2 per cent too great. For the Tixier method, which adds the reciprocals of the resistivities of the salts formed in the Palmer recombination scheme to obtain the reciprocal of the water resistivity, the average of the absolute value of the per cent deviation was 7.8 per cent with the calculated resistivity being on the average 6.3 per cent too low. Tixier also describes a simplified method of calculation which is identical with that of Park Jones, except that a factor of 0.32 rather than 0.37 is used to convert from secondary salinity to equivalent *NaCl*. Incidentally, in both systems, the 0.4 conversion factor used to go from primary salinity as Na_2SO_4 to equivalent *NaCl* is almost certainly in error. In laboratory prepared solutions of high $SO_4^=$ and low Cl^- content, use of this factor led to resistivity errors as large as 60 per cent. As noted before, high $SO_4^=$ concentrations are encountered mainly in the Rocky Mountain regions.

The principal advantage of the method presented here is its speed and convenience. It is felt that for most purposes, and in particular where the $SO_4^=$ concentration is low, any of the three methods of obtaining water resistivity will give reliable results.

REFERENCES

1. Tixier, M. P.: "Water Analysis vs. Water Resistivity," privately circulated, Oct. 22, 1943.
2. Jones, P. J.: *Oil and Gas Journal,* Nov. 18, 1944, 209.
3. Palmer, Chase: *Geol. Survey Bul.,* No. 479, 1911.

★ ★ ★

Technical Note 83

THEORETICAL NOTE ON LINEAR ABSORPTION METHODS OF DETERMINATION OF FLUID SATURATION IN POROUS MEDIA

LEONARD B. LIPSON, MAGNOLIA PETROLEUM CO., DALLAS, TEX., JUNIOR MEMBER AIME

Boyer, Morgan and Muskat,[1] with improvements by Morgan, McDowell, and Doty,[2] and Laird and Putnam,[3] have described a scheme for the determination of fluid saturation in porous media by measuring the x-ray linear absorbing power of particular fluids in the media. This method is one of several which depend on the linear absorbing power of the fluids in the porous medium. Other examples of linear absorption methods involve measurement of dielectric constant, gamma ray absorption, and ultrasonic attenuation. It is the purpose of this note to demonstrate by theortical considerations that the absorption versus saturation curve for a linear absorption method is not necessarily a single valued function of the saturation. Such non-unique behavior must be considered and evaluated before suitable saturation determinations can be made by a linear absorption method.

To illustrate the discussion, examples will be given only for the simplest cases of combinations of two different dielectrics. The dielectric constant method was chosen for illustration because it was thought to demonstrate most graphically the point in question.

According to Argue and Maass,[4] the resultant dielectric constant of a combination of two different dielectrics depends on the orientation of the dielectrics in the electric field of the test condenser used to measure the dielectric constant. One case involves alternate slabs of dielectrics E_1 and E_2 perpendicular to the electric field of the test condenser, as shown in Fig. 1A. For this case:

$$1/E_m = A/E_1 + B/E_2 \quad . \; . \; . \; . \; . \; . \; . \; . \quad (1)$$

where E_m is the dielectric constant of the combination, A is the ratio of the path length through dielectric E_1 to the distance between the plates of the condenser (assuming the dielectrics have the same cross sectional area as the condenser), and B is the ratio of the path length through dielectric E_2 to the distance between the plates of the condenser.

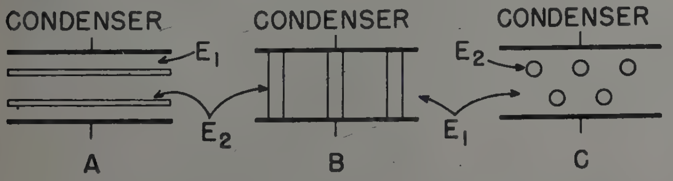

FIG. 1

It will be noted that the constants A and B are numerically equal to the fractional "saturation" of the region between the test plates of the condenser by the two dielectrics E_1 and E_2, respectively.

Another case involves alternate columns of the two dielectrics parallel to the electric field and forming a continuous path between the condenser plates, as shown in Fig. 1B. For this case:

$$E_m = AE_1 + BE_2 \quad . \; . \; . \; . \; . \; . \; . \; . \; . \quad (2)$$

where E_m is the dielectric constant of the combination, A is the ratio of the cross sectional area of dielectric E_1 to the cross sectional area of the condenser plates (assuming the lengths of the dielectrics equal the distance between the condenser plates) and B is the ratio of the cross sectional area of dielectric E_2 to the cross sectional area of the condenser plates. As before the constants A and B are the effective "saturation" of the condenser by the two dielectrics.

Still another case is described by Lichtenecker[5] where dielectric E_2 is shown in the form of small particles distributed at random in dielectric E_1. This is shown in Fig. 1C. For this case:

$$\log E_m = A \log E_1 + B \log E_2 \; . \quad . \; . \; . \; . \quad (3)$$

where E_m is the dielectric constant of the combination, A is the ratio of the volume of dielectric E_1 to the volume of the condenser, *i.e.*, the effective "saturation" of the condenser by dielectric E_1. B is the ratio of the volume of dielectric E_2 to the volume of the condenser, *i.e.*, "saturation" of dielectric E_2.

Equations (1), (2) and (3) are plotted in Fig. 2 for $E_1 = 2.5$ (oil) and $E_2 = 80$ (water).

Equations (1) and (2) may be thought of as representing the limiting cases of the configuration of two fluids which might be expected to exist in a porous medium. Equation (3),

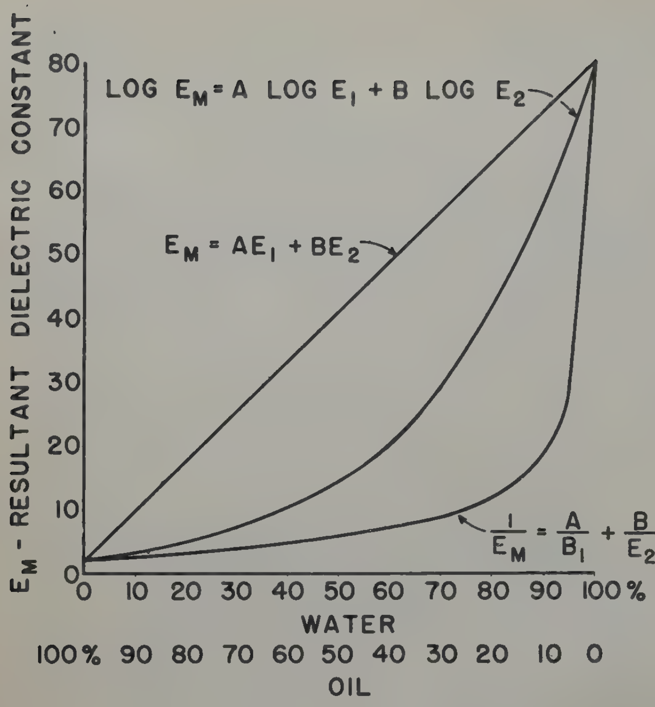

FIG. 2

or one similar in form, may be thought of as describing a fluid distribution more nearly representative of what might be expected actually to exist in a porous medium.

It could be concluded from Fig. 2 that any system of determination of fluid saturation in porous media using linear absorption methods would yield a non-linear calibration curve. This calibration curve would be different for different porous media and for different methods of obtaining a given saturation in the same medium. Therefore, the absorption vs. saturation curve, for a porous medium having both a drainage and an imbibition saturation history, should exhibit the same hysteretic effect[6] shown by the capillary pressure vs. saturation curve for that same medium.

ACKNOWLEDGMENT

Acknowledgment is made to the management of Magnolia Petroleum Co. for permission to publish this note.

REFERENCES

1. Boyer, R. L., Morgan, F., and Muskat, M.: *Trans.* AIME (1947) **170,** 15.
2. Morgan, F., McDowell, J. M., and Doty, E. C.: *Trans.* AIME (1950) **189,** 183.
3. Laird, A. D. K., and Putnam, J. A.: "Fluid Saturation in Porous Media by X-Ray Technique," paper presented before AIME Pet. Branch Fall Meeting, Los Angeles, Calif., Oct. 20-21, 1949. (To be published subsequently in *Trans.* AIME, Vol. **192.**)
4. Argue, G. H., and Maass, O.: *Can. J. Res.* (1935) **13,** 156.
5. Lichtenecker, K.: *Phy. Zeit.* (1926) **27,** 115.
6. Muskat, M.: *Physical Principles of Oil Production,* McGraw-Hill Book Co., Inc., New York (1949) 310. ★ ★ ★

Technical Note 84——

THE INTERPRETATION OF CHEMICAL WATER ANALYSIS BY MEANS OF PATTERNS

HENRY A. STIFF, JR., MEMBER AIME, ATLANTIC REFINING CO., DALLAS, TEX.

ABSTRACT

The classification and correlation of water analysis data presents many problems which can be solved by graphic methods. The pattern system, a new type of graphic procedure described in this communication, is believed to have several advantages over older methods. Examples of the application of the pattern system to the solution of problems encountered in petroleum production are given.

INTRODUCTION

Several graphic methods for presenting analytical water data have been developed and are now in use.[1,2,3,4] It is believed, however, that a recently developed type of graph called the "pattern" offers several advantages over other methods. This system presents a better picture of the total salt concentration than is usual in such graphs. The effect of dilution or concentration has been reduced to a minimum, and at the same time distinction between various types of water has been improved. The system is extremely versatile, yet so simple it can be plotted on ordinary graph paper and adapted to almost any type of filing system.

DISCUSSION

The essential feature of the pattern system is the graph shown in Fig. 1. Horizontal lines extending right and left from a vertical line at zero form the graph. Positive ions are plotted to the left while negative ions are plotted to the right. The figure immediately beneath each ion gives the scale. Most oil field waters can be plotted on a scale where 100 milliequivalents of sodium and chloride and 10 milliequivalents of each of the other ions are represented by one scale unit. For highly concentrated brines, 1,000 milliequivalents of sodium and chloride and 100 milliequivalents of each of the other ions are represented by one unit. For convenience sodium, potassium, lithium, etc., ordinarily determined as the difference between the positive and negative ions, are referred to as sodium.

It will be noted that the chemical unit of "milliequivalents per liter" is employed. If the results of the analysis are in parts per million, they can be readily converted by dividing by the equivalent weight in milligrams or multiplying by its reciprocal. Appropriate conversion factors can be found in standard chemical handbooks.[5]

When the points have been properly placed on the graph, they are connected by lines as shown in Fig. 2, thus forming a closed "pattern." These patterns present a variety of shapes and sizes, each easily recognized and remembered and each characteristic of a certain water.

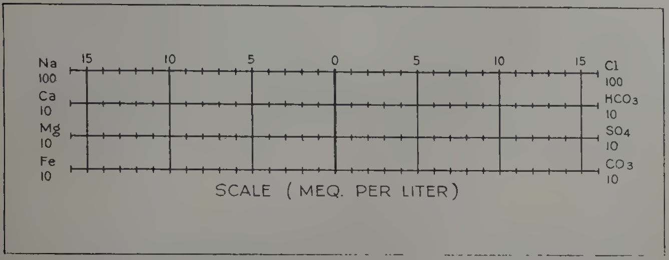

FIG. 1 — ESSENTIAL FEATURE OF THE PATTERN ANALYSIS SYSTEM.

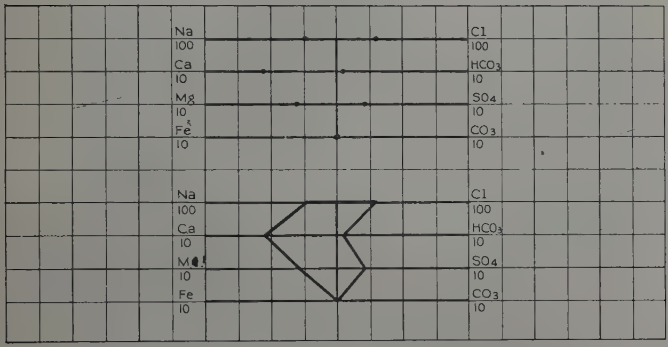

FIG. 2 — METHOD OF CONSTRUCTING A PATTERN.

Fig. 3 shows some common water patterns, including those of fresh water, sea water, chemical solutions and oil field brines. The straight line pattern of fresh water shown in the first diagram results from the use of a scale ordinarily employed for oil field brines. Any system of scales thought suitable to a particular operation may be used. Single scales, in which all ions are represented by an equal number of units, are used in plotting fresh waters, while multiple scales, in which all ions are not represented by the same number of units, find application in work with oil field waters. Various types of multiple scales can be used to advantage in water treatment work, corrosion control, and injection water studies.

One of the distinctive features of the system is the tendency of the pattern to maintain its characteristic shape as the sample becomes dilute. In this way the total salt concentration as well as the chemical composition of the water is shown by the pattern.

The availability of various scales makes it possible to select one which emphasizes the differences and similarities of the waters being studied, thereby making direct comparison and correlation between these waters possible.

Another very valuable feature of this system is its extreme simplicity. The pattern can be constructed by anyone on ordinary graph paper. The use of a printed card containing a graph similar to that shown in Fig. 1, and in addition blank spaces for pertinent well data, is very convenient for this work. By this means a large and very useful library of patterns can be built up in a small space.

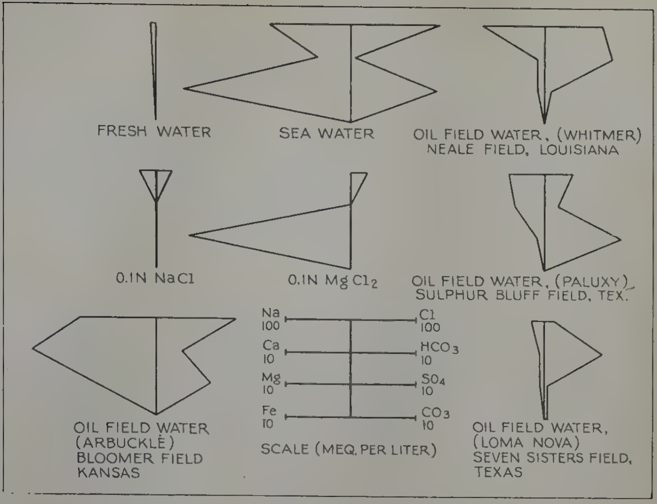

FIG. 3 — COMMON WATER PATTERNS.

APPLICATION

The applications of the pattern system are many and varied. It is believed that this system will facilitate the solution of almost any problem in which water analysis is a factor. The following examples illustrate its application to various problems encountered in petroleum production.

Correlation of Producing Formations

Since the pattern tends to maintain its shape upon concentration or dilution, a formation may be expected to yield water of a characteristic pattern. A study of the water patterns can, in many cases, be utilized to identify different producing strata and correlate them in a given locality. In Kansas, for example, the Arbuckle group of the Ordovician period can be traced from Ellsworth County down through Barton County and into Stafford County by means of water patterns. Fig. 4 shows patterns from Stoltenberg Field (Ellsworth County), Bloomer Field (Barton County), and Drach and St. John's Fields (Stafford County). The characteristic pattern of the Arbuckle formation can be easily followed.

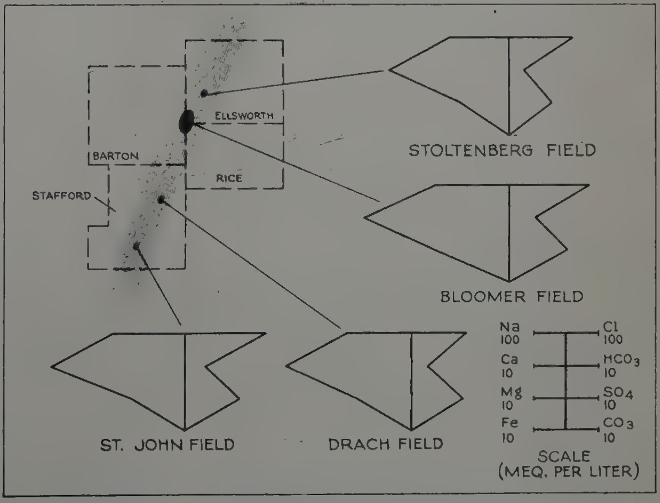

FIG. 4 — COURSE OF ARBUCKLE FORMATION THROUGH KANSAS SHOWN BY WATER PATTERNS.

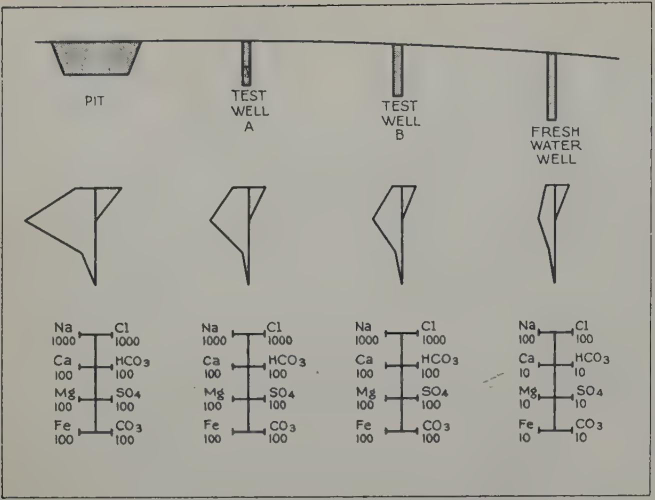

FIG. 5 — PATTERN ANALYSIS USED AS A TRACER.

Tracer Problems

It is often possible to trace the passage of water through a sand by a study of the patterns obtained from properly spaced test holes along its path. In the case presented in Fig. 5, seepage of salt water from a disposal pit into a fresh water well was suspected. Shallow test holes were drilled at *A* and *B* and allowed to fill by seepage. Samples were taken, the water analyzed, and the patterns plotted. The appearance of the disposal pit pattern, somewhat reduced in size, definitely established seepage in the direction of the well. When a sample from the fresh water well plotted on a magnified scale gave the same pattern as the pit, contamination became evident.

Drill Stem Testing

Because of the uncertainty regarding contamination of water samples by drilling mud encountered in drill stem testing; attempts to establish the formation from which such samples originate are often unsuccessful. In some cases, however, this information is extremely helpful. Because of the ease with which one pattern can be compared with another, the pattern system is especially useful for this purpose. Fig. 6 shows the results of a case where pattern analysis was successfully utilized to determine the formation from which a drill stem test sample originated.

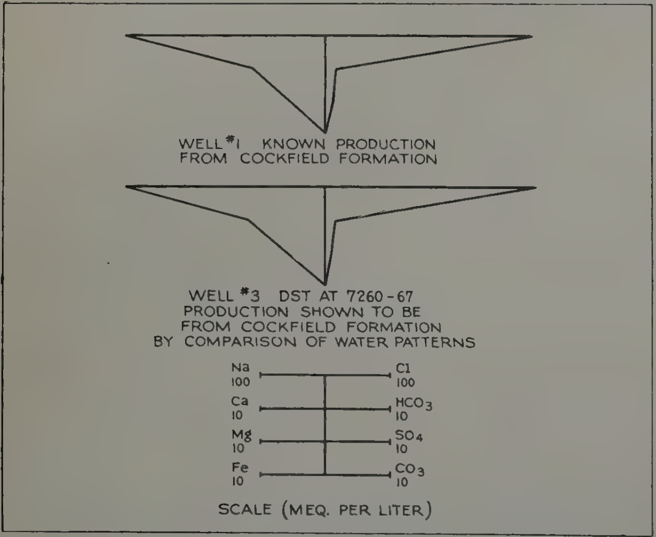
WELL #1 KNOWN PRODUCTION FROM COCKFIELD FORMATION
WELL #3 DST AT 7260-67 PRODUCTION SHOWN TO BE FROM COCKFIELD FORMATION BY COMPARISON OF WATER PATTERNS
Na 100
Cl 100
Ca 10
HCO₃ 10
Mg 10
SO₄ 10
Fe 10
CO₃ 10
SCALE (MEQ. PER LITER)

FIG. 6 — PATTERN ANALYSIS USED IN DRILL STEM TESTING.

Detection of a Foreign Water and the Determination of Its Source

Oil wells are completed so as to yield a minimum of water, but a break in the cement or a leak in the casing may allow extraneous water to enter. Water yielded by a well in the normal course of operation is usually bottom water, that is, water from the producing formation, while water entering through a leak or cement break may come from some other strata. If sufficient information is available on the composition of the waters in the area, the source of a foreign water may be discovered, and its exclusion brought about with a minimum of trouble and expense.

Fig. 7 presents a case in which water patterns were used to determine the source of water entering a well. Well No. 1 had been producing water of a consistent pattern from formation *A* since its completion, when suddenly the water pattern changed. Another well in the field was producing from formation *B* which was located about 150 ft above *A*. This formation had, of course, been cemented off during completion of Well No. 1. The patterns of various mixtures of *A* and *B* were calculated and plotted as shown. It then became evident that the new pattern resulted from a mixture of approximately 25 per cent water from formation *A* and 75 per cent water from formation *B*. It was therefore concluded that foreign water was entering from formation *B* either through a casing leak or through a break in the cement. Accordingly, the casing was pressure tested and since no leak was found, a cement job was undertaken. At the conclusion of this operation the well was again put on production and at the end of several months the pattern was again similar to that of formation *A*.

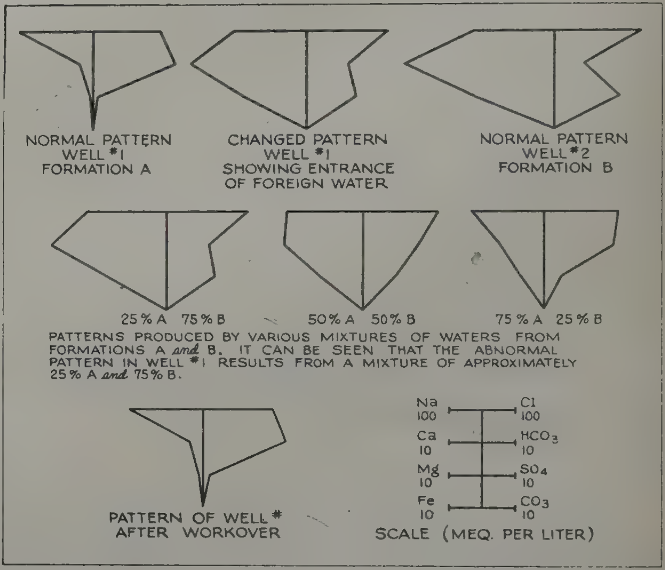
NORMAL PATTERN WELL #1 FORMATION A
CHANGED PATTERN WELL #1 SHOWING ENTRANCE OF FOREIGN WATER
NORMAL PATTERN WELL #2 FORMATION B
25% A 75% B
50% A 50% B
75% A 25% B
PATTERN OF WELL # AFTER WORKOVER
Na 100
Cl 100
Ca 10
HCO₃ 10
Mg 10
SO₄ 10
Fe 10
CO₃ 10
SCALE (MEQ. PER LITER)

PATTERNS PRODUCED BY VARIOUS MIXTURES OF WATERS FROM FORMATIONS A *and* B. IT CAN BE SEEN THAT THE ABNORMAL PATTERN IN WELL #1 RESULTS FROM A MIXTURE OF APPROXIMATELY 25% A *and* 75% B.

FIG. 7 — DETECTION OF FOREIGN WATER AND DETERMINATION OF ITS SOURCE.

CONCLUSIONS

The pattern analysis system presented in this paper offers a simple, practical means of characterizing, comparing, and correlating ground waters. It is particularly useful in facilitating the solution of many petroleum production problems, but can be used to advantage in the study of any question in which water analysis is a factor.

ACKNOWLEDGMENT

The author wishes to thank The Atlantic Refining Co. for permission to publish this paper, and to acknowledge the advice and encouragement given him by J. H. Sullivan and C. M. Pounders.

Credit for the drawings is extended to Gene Nigh.

REFERENCES

1. Tickell, E. G.: *Report of the California State Oil and Gas Supervisor* (1921) **6**, (9), 5.
2. Reistle, C. E.: *U. S. Bureau of Mines Technical Paper 404* (1927).
3. Parker, J. S., and Southwell, C. A. P.: *Journal of Institution of Petroleum Technologists*, London (1929) **15**, 138-182.
4. Corps, E. V.: *Proc. World Petr. Congress 1* (1933) 338.
5. Lange, A. L.: *Handbook of Chemistry*, Handbook Publishers, Inc., Sandusky, O. (1946) 757.

* * *

Technical Note 85———

A HIGH TEMPERATURE GAUGE GLASS FOR THE VISUAL OBSERVATION OF CRITICAL PHENOMENA

JOHN R. SPENCER,* TEXAS PETROLEUM RESEARCH COMMITTEE, AUSTIN, TEX., MEMBER AIME

ABSTRACT

A capillary tube variable volume cell is described, which has operated satisfactorily over a range of 100°F and 3,500 psi to 550°F and 1,500 psi. The cell contents are entirely visible over the length of the capillary with the exception of a space at the top amounting to three per cent of the total volume. Observations on the critical behavior of simple systems have been greatly facilitated by the apparatus, it being possible to establish the critical conditions for a particular mixture in the course of a day's run.

INTRODUCTION

Many types of apparatus have been designed for obtaining data on the phase relationships of hydrocarbon systems. Such apparatus can in general be subdivided into two classifications; (1), indirect measurement of phase volume, and (2), direct visual observation of phase volume, each of which has outstanding advantages and disadvantages.

Indirect measurement of phase volume requires the use of rather elaborate apparatus including internal probes in which are located the device for determining the locus of the interface between phases. Such equipment is by its very nature costly, and is complex from the standpoint of operating technique. Probing techniques can be used, however, over wide ranges of temperature and pressure with a high degree of reproducibility.

Apparatus for visual observation of phase behavior obviously has the advantage of enabling the experimenter to see exactly what takes place, but because the material to be tested is contained in a cell constructed of both metal and glass, is limited severely as to the temperature range of operation. Furthermore, the maximum pressure usually is limited by the choice of material used for sealing the glass to the metal, and by the strength of the glass itself. In the interest of increased efficiency of observation, as much of the cell as possible should be visible to the eye. Glass capillary tubes have been used successfully but have always given difficulty at the metal-to-glass seal. An apparatus has been devised to overcome the problems of sealing and resistance to temperature effects that have heretofore been the limiting factor with glass apparatus in the observation of phase volumes at elevated temperature and pressure.

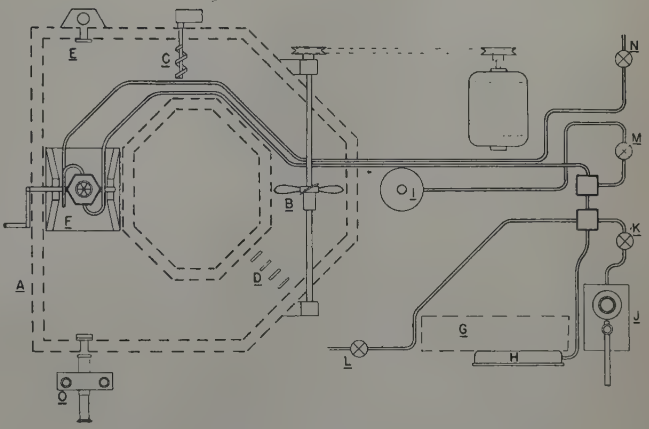

FIG. 1 — GENERAL LAYOUT OF THE APPARATUS.

APPARATUS

The objective which dictated the general arrangement of the apparatus (Figs. 1 and 2) was simplicity of operation. The air bath, *A*, was constructed of an iron framework to which was attached approximately one inch of glass wool bats which were covered on the outside with "Masonite." A roughly octagonal center piece was installed to provide forced circulation of the air by the fan, *B*, past the heaters, *D*, cell, *F*, and thermoregulator, *C*, respectively. The entire top of the box is removable to facilitate charging of the cell and to permit easy maintenance. Two windows are provided before and behind the cell to allow the operator to observe the contents against the background fluorescent light, *E*. The heaters,

---

*Now with the Continental Oil Co., Ponca City, Okla. This Note is Contribution No. 13, Texas Petroleum Research Committee, G. H. Fancher, Director.

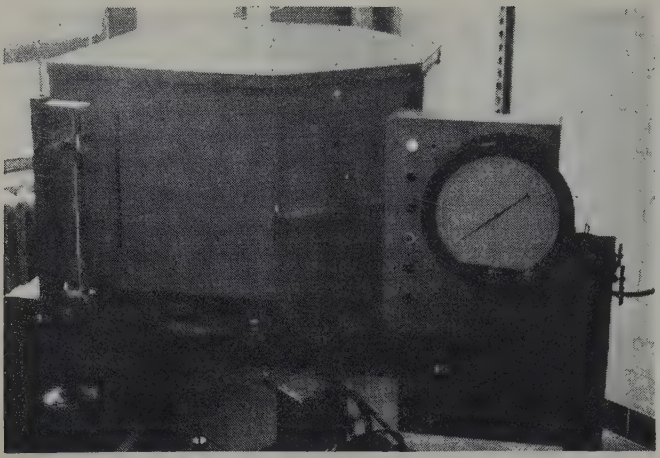

FIG. 2 — PHOTOGRAPH OF THE ASSEMBLED UNIT.

lights, and fan motor are all controlled from the switchboard, *G*.

Mercury is added to the cell from the pump, *J*, and the mercury shut-off valve, *K*, and is removed through the bleeder valve, *L*. Charging is carried out through the valve, *N*, and if the pressure of the gas sample is insufficient the cylinder, *I*, can be connected to allow compression of gas and its subsequent transfer to the cell. The 5,000 psi Heise bourdon tube gauge, *H*, always is connected to the mercury supply during operation. Liquid levels are observed with the screw type microcathetometer, *O*, which can be read consistently to within .002 in.

DETAILS OF CONSTRUCTION

Heat is supplied to the air bath by the four 500-watt heaters, *D*, one of which is connected through a mercury relay to the bimetallic thermoregulator, *C*. Considerable care was taken in designing the heaters to provide for as little restriction to the flow of air as possible. The heaters were constructed of pieces of one-quarter in. transite about two in. wide and 18 in. long, wound with 20-gauge nichrome ribbon. These were mounted in a frame and installed parallel to the air stream directly in front of the fan. The entire heater assembly can be removed as a unit by disconnecting the leads.

Circulation of air is induced by the 10-in. fan, *B*, mounted on a three-quarter in. cold rolled steel shaft which turns between two bearings, both on the outside of the bath. The distance between the bearings, about 30 in., made imperative the use of a heavy shaft to eliminate any tendency of the assembly to "whip." Sleeve bearings were used on both ends of the shaft to keep it in alignment even though the initial assembly of the unit was made somewhat difficult.

Located in the air stream out of direct line of vision from the heaters, the cell receives only that heat supplied by contact with the air, and thus local overheating is prevented that might result from direct radiation from the heaters. The cell is mounted in trunions so that it is free to rotate through an angle of approximately 120° to permit agitation of the cell contents. Connections to the upper and lower ends of the cell are made through coils of one-eighth in. stainless steel tubing.

The appearance of the cell is similar to that of the usual tubular gauge glass used in industrial applications. Certain structural changes have been made, however, that greatly improve the performance characteristics (Fig. 3). The valves on the two ends of the cell are identical and are what is commonly called a "T" type valve, the stem being used to shut off the leg of the "T." These valves were used to allow the seat to be placed near the lower part of the valve, to reduce the volume of that part of the cell which can not be seen. The "T" type valve also facilitates bleeding and cleaning operations. A circular recess is cut in the lower side of the valves to accommodate the flat gaskets which were used. These gaskets are cut from Teflon sheet, 0.035 in. thick, and appear to be stable at temperatures well above those contemplated for the apparatus. The visual portion of the cell is a Pyrex capillary tube about two-and-one-half millimeters ID and about nine millimeters OD. In addition to squaring the ends of the tube by grinding, fire-polishing was found to be necessary if the tube was not to split lengthwise when pressure was applied. In assembly four bolts passing through the outer portion of the valves hold the valves against the ends of the glass tube, the Teflon gaskets providing the seal required.

These bolts must be compensated for thermal expansion because any relative change in length between the bolts and the tube assuredly would cause failure of the seals. An attempt was made to find materials for the bolts that would have the same coefficient of thermal expansion as glass; and none were found. A very simple method was devised whereby any desired coefficient of expansion within limits could be built into the bolts (Fig. 4). This bolt is believed to have many applications other than the one described.

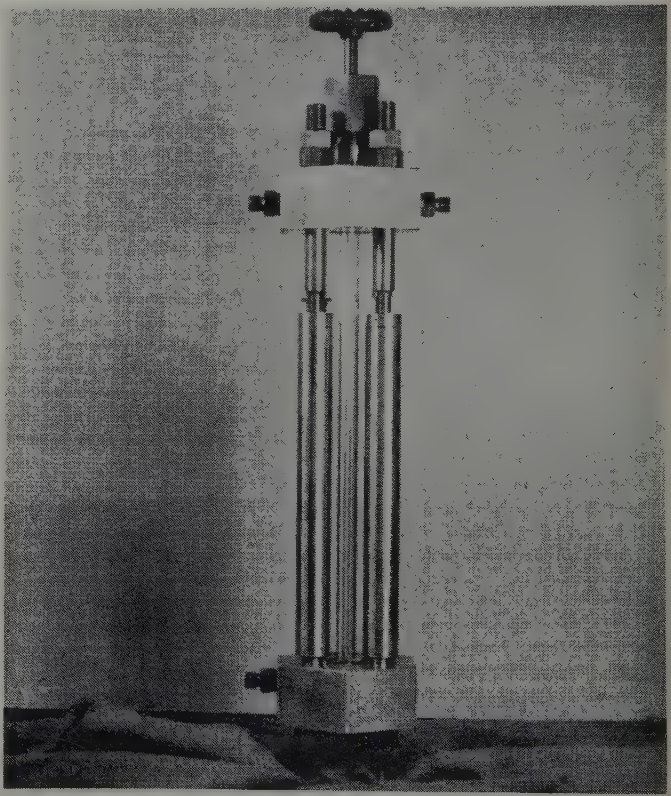

FIG. 3 — PHOTOGRAPH OF THE CAPILLARY CELL ASSEMBLED.

The bolt consists of three distinct parts; (1) the outer barrel, (2) the correcting sleeve, and (3) the inner rod. Any

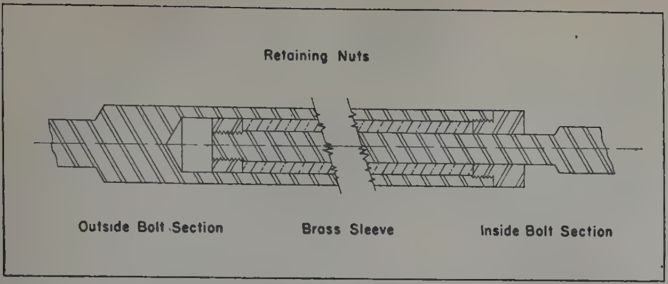

FIG. 4 — CROSS SECTION OF THE THERMALLY COMPENSATED TIE BOLTS.

two metals having different thermal expansion characteristics can be used in its construction. Appropriate materials for the job at hand were cold rolled steel for the portions of the bolt under tension and brass for the correcting sleeve which is under compression when in use.

In order to establish the length of brass sleeve required for the proper thermal compensation, quantities are defined as follows:

l_g = length of the glass tube.
l_h = thickness of one valve between the gasket seat and the tie-bolt nuts.
l_s = length of the bolts as measured between the nuts on the outside of the valves.
l_B = length of brass sleeve required.
$\propto_g$ = average coefficient of linear thermal expansion for glass over the temperature range desired.
$\propto_s$ = average coefficient of linear thermal expansion for steel over the temperature range desired.
$\propto_B$ = average coefficient of linear thermal expansion for brass over the temperature range desired.
Δt = temperature change.

Inasmuch as the relative positions of the parts making up the gauge assembly should remain unchanged, a length of brass sleeve must be used that will allow the bolts to expand by an amount equal to that of the glass plus that of the valve bodies.

The expansion of the bolt will be equal to

$$(\propto_s l_s - \propto_B l_B)\Delta t \quad . \; . \; . \; . \; . \; . \; . \; . \; . \; . \quad (1)$$

that of the end blocks to

$$2\propto_s l_h \Delta t \quad . \; . \; . \; . \; . \; . \; . \; . \; . \; . \; . \; . \quad (2)$$

and that of the glass to

$$\propto_g l_g \Delta t \quad . \; . \; . \; . \; . \; . \; . \; . \; . \; . \; . \; . \; . \quad (3)$$

Consequently,

$$(\propto_s l_s - \propto_B l_B)\Delta t = (\propto_g l_g + 2\propto_s l_h)\Delta t \quad . \quad (4)$$

and

$$\frac{\propto_s (l_s - 2\; l_h) - \propto_g l_g = l_B}{\propto_B} \quad . \; . \; . \; . \; . \; . \; . \quad (5)$$

If the valves and the bolt bodies were constructed from two different materials, Equation (5) could be modified appropriately, the principles employed being the same as those utilized in the derivation of Equation (5).

SUMMARY

This apparatus had been in use for approximately six months at the time this note was prepared (April, 1951), and the data obtained in its use have been satisfactory. One disadvantage is the small amount of sample available for subsequent analysis; however, this difficulty can be overcome by charging mixtures of known composition to the cell or by analyzing the contents of the cell by methods which do not require a large volume of material, as for example, the spectrophotometric method.

ACKNOWLEDGMENT

The author is indebted to W. A. Fickert, of the University of Texas, for the accompanying drawings.

★ ★ ★

Technical Note 93——

A NOTE ON THE INTERRELATIONSHIP BETWEEN WETTING AND NON-WETTING PHASE RELATIVE PERMEABILITY

M. R. J. WYLLIE, MEMBER AIME, GULF RESEARCH AND DEVELOPMENT CO., PITTSBURGH, PA.

In a recent publication[1] wetting phase relative permeability was expressed as:

$$K_{rw} = \frac{1}{I^2 S_w^2} \frac{\int_0^{S_w} dS_w/P_c^2}{\int_0^{1.0} dS_w/P_c^2} \quad . \; . \; . \; . \quad (1)$$

and it was stated that a similar expression applied, *mutatis mutandis*, to non-wetting phase relative permeability; *i.e.*,

$$K_{rnw} = \frac{1}{I_N^2 S_o^2} \frac{\int_{S_w}^{1.0} dS_w/P_c^2}{\int_0^{1.0} dS_w/P_c^2} \quad . \; . \; . \; . \quad (2)$$

In Equations (1) and (2), S_w and S_o are respectively the wetting and non-wetting phase saturations as a fraction of the pore volume; P_c is the capillary pressure; I, the wetting phase electrical resistivity index; I_N, the analogous non-wetting phase electrical resistivity index and K_{rw} and K_{rnw}, the wetting and non-wetting phase relative permeabilities.

$$\text{But,} \int_0^{1.0} dS_w/P_c^2 = \int_0^{S_w} dS_w/P_c^2 + \int_{S_w}^{1.0} dS_w/P_c^2$$

and from this equality it follows that:

$$K_{rnw} = \frac{1}{I_N^2 S_o^2} \left[1 - K_{rw} I^2 S_w^2 \right] \quad . \; . \; . \quad (3)$$

Equation (3) is interesting because it expresses the non-wetting phase relative permeability of a porous medium at any saturation as a function of the wetting phase relative permeability at that saturation, the saturation itself and parameters which bear directly on the distribution within the pores of the non-wetting and wetting phase fluid networks. It is thus inherently plausible.

Equation (3) is not readily checked against experimental data since few reliable relative permeability figures have appeared in the literature; also no published information exists on the probable relationship between I_N and S_o. However, if the K_{rw} and K_{rnw} figures of Leverett[2] for unconsolidated sands are used in conjunction with the relationship $I = S_w^{-2}$ for sands of this type, it is possible for Equation (3) to compute I_N as a function of S_o. The results are shown in the accompanying figure and it will be seen that $I_N = S_o^{-1.72}$. A synthetic sandstone for which Muskat[3] quotes relative permeability data, also gives a straight line plot between I_N and S_o if $I = S_w^{-1.8}$ is assumed. (A resistivity index exponent of 1.8 appears to be the best average for consolidated porous media.) The slope of the $I_N - S_o$ plot is here –1.87, but the non-wetting phase resistivity index is 1.2 at $S_o = 1.0$, and not unity as would be expected. Whether this difference represents experimental error or is of deeper theoretical significance is not yet clear.

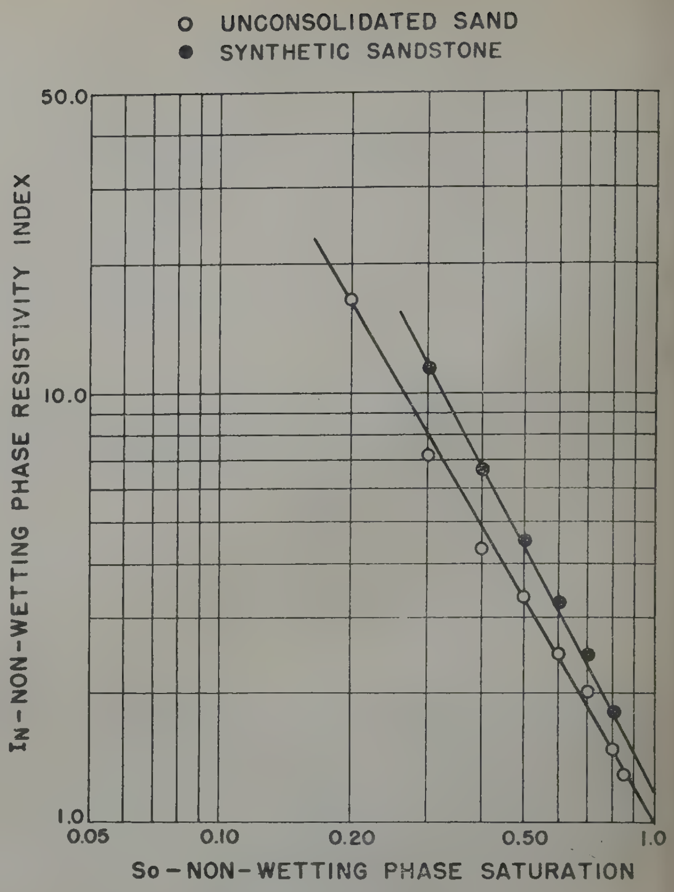

REFERENCES

1. Wyllie, M. R. J., and Spangler, M. B.: "The Application of Electrical Resistivity Measurements to the Problem of Fluid Flow in Porous Media." A.A.P.G., St. Louis (April, 1951).
2. Leverett, M. C.: *Trans.* AIME (1939) 132, 149.
3. Muskat, M.: *Physical Principles of Oil Production.* McGraw-Hill Book Co., New York (1949), 293.

★ ★ ★

INDEX TO TRANSACTIONS, VOLUME 192

(Plus Reference to Articles and Technical Notes Published in *Journal of Petroleum Technology* in 1951)

A

Akins, D. W., Jr.: *Primary High Pressure Water Flooding in the Pettit Lime, Haynesville Field,* 239

B

Bell, John S.:, et al.: *Pressure Behavior in the Woodbine Sand,* 19
Berlin, E. W.: *Manpower — The Most Important Factor in Defense Mobilization,* (Art.), May JPT.
Blair, P. M., et al.: *Laboratory Measurements of Relative Permeability,* 47
Bobrowski, F. P., et al.: *Special Considerations in Predicting Reservoir Performance of Highly Volatile Type Oil Reservoirs,* 37
Bradley, Howard B., et al.: *The Phase Behavior of a Natural Hydrocarbon System,* 233
Bridges, P. M., et al.: *An Experimental and Theoretical Investigation of Gravity Drainage Performance,* 285
Brown, Harry W.: *Capillary Pressure Investigations,* 67
Brownscombe, E. R., et al.: *Further Developments in the Laboratory Determination of Relative Permeability,* 145
Bruce, G. H., et al.: *Carrying Capacity of Drilling Muds,* 111
Bush, Robert E., et al.: *The Quantitative Application of Radioactivity Logs,* 191

C

Cameron, C. V.: *The Benton Water Flood, Franklin County, Illinois,* (Art.), Sept. JPT.
Caudle, B. H., et al.: *Further Developments in the Laboratory Determination of Relative Permeability,* 145
Cement: A modified low-strength cement, 165.
Chambers, Adele, et al.: *Use of Centrifuge for Determining Connate Water, Residual Oil, and Capillary Pressure Curves of Small Core Samples,* 127
Clays: Mineralogical studies of California oilbearing formations, 151.
Cook, Alton B., et al.: *Special Considerations in Predicting Reservoir Performance of Highly Volatile Type Oil Reservoirs,* 37
Cores: Use of centrifuge for determining connate water, residual oil and capillary pressure curves of small core samples, 127.
Crego, William O., et al.: *Report on the Mamou Field Pressure Maintenance Project,* 263
Crog, R. S., et al.: *Mineralogical Studies of California Oilbearing Formations, I — Identification of Clays,* 151
Croxton, Frank C.: *Battelle Memorial Institute and the Petroleum Industry,* (Art.), Jan. JPT.
Culberson, O. L., et al.: *Phase Equilibria in Hydrocarbon-Water Systems. III — The Solubility of Methane in Water at Pressures to 10,000 PSIA,* 223
Culberson, O. L., et al.: *Phase Equilibria in Hydrocarbon-Water Systems. IV — Vapor Liquid Equilibrium Constants in the Methane-Water and Ethane-Water Systems,* 297

D

Davis, Louis F., et al.: *Recent Advances in Gas Lift Equipment and Techniques,* (Art.), Feb. JPT.
Davis, W. B.: *A Study of the Dornick Hills — Springer Sand Reservoir, Velma Pool, Oklahoma,* 29
Doll, H. G.: *The Laterolog: A New Resistivity Logging Method with Electrodes Using an Automatic Focusing System,* 305
Dotson, B. J., et al.: *Porosity-Measurement Comparisons by Five Laboratories,* 341
Drilling: Penetration rates for directional drilling, (Art.), June JPT.
  Plastic flow properties of drilling fluids, 159.
  Modified low-strength cement, 165.
  Drilling problems in the Worland, Wyoming, Field, (Art.), May JPT.
  Advancement in design and technique of rotary fishing tools, (Art.), June JPT.
  Control of lost circulation, 171.
  Gravel pack completion, 183.
  Carrying capacity of muds, 111.
Drilling Fluids: Plastic flow properties, 159.
  Carrying capacity of muds, 111.
Dunlap, H. F., et al.: *The Calculation of Water Resistivities from Chemical Analysis,* (Tech. Note), March JPT.
Dumbauld, G. K., et al.: *A Modified Low-Strength Cement,* 165
Dykstra, Herman, et al.: *Relative Permeability Studies,* 249
Dykstra, Herman, et al.: *Relaxation Methods Applied to Oil Field Research,* 227

E

Electrical logging: The Laterolog, 305.
  Quantitative application of radioactivity logs, 191.
  Electrokinetic component of the self-potential curve, 1.
  Measurement of formation factors and resistivity indices, (Tech. Note), Feb. JPT.
  Guard electrode logging system, 347

- Equipment: Surface indicating pressure, temperature and flow equipment, 257.
  - Advancement in design and technique of rotary fishing tools, (Art.), June JPT.
  - High temperature gauge glass for visual observation, (Tech. Note), Aug. JPT.
- Espach, Ralph H., et al.: *Variable Characteristics of the Oil in the Tensleep Sandstone Reservoir, Elk Basin Field, Wyoming and Montana,* 75
- Evans, W. R., et al.: *The Shuler Jones Sand Pool; Nine Years of Unitized Pressure-Maintenance Operations,* 121

F

- Fatt, Irving, et al.: *Relative Permeability Studies,* 249
- Field studies: Water flooding in the Pettit Lime, Haynesville Field, 239.
  - Dornick Hills-Springer Sand reservoir, Velma Pool, Okla., 29.
  - Elk Basin Field, Wyoming and Montana, 75.
  - Hydrafrac operations in the Spraberry, (Art.), Nov. JPT.
  - Iran and world oil, (Art.), Oct. JPT.
  - Mamou Field pressure maintenance, 263.
  - Progress report on the Scurry Field, (Art.), April JPT.
  - Offshore production in Bay Marchand and Main Pass Fields, (Art.), July JPT.
  - Drilling and production in the Worland, Wyoming, Field, (Art.), May JPT.
  - Southwest Antioch Gibson Sand unit, 199.
  - Pressure behavior in the Woodbine, 19.
  - Shuler Jones Sand Pool, 121.
  - Reservoir analyzer study of Woodbine, 331.
  - Gas injection in Cedar Lake Field, 357.
- Fishing: Advancement in design and technique of rotary fishing tools, (Art.), June JPT.
- Fry, Joseph, et al.: *Variable Characteristics of the Oil in the Tensleep Sandstone Reservoir, Elk Basin Field, Wyoming and Montana,* 75
- Fulton, P. F., et al.: *A New Technique for the Measurement of the Formation Factors and Resistivity Indices of Porous Media,* (Tech. Note), Feb. JPT.

G

- Gas: Today's natural gas industry, (Art.), Aug. JPT.
  - Development and operation of LPG storage cavities in salt strata, (Art.), March JPT.
  - Underwater storage of propane in salt water sand, (Art.), Jan. JPT.
  - Pressure drop in flow of gas through pipe, 317.
  - Vaporization characteristics of carbon dioxide in natural gas-crude oil system, 141.
  - Gas-liquid flow, (Tech. Note), Feb. JPT.
  - Transient flow in gas transmission lines, 217.
  - Low temperature dehydration of natural gas, 61.
  - Measuring water vapor content of gases dehydrated by triethylene glycol, 301.
  - Recent advances in gas lift equipment and techniques, (Art.), Feb. JPT.
  - Gas injection in Cedar Lake Field, 357.
- Geffen, T. M., et al.: *Experimental Investigation of Factors Affecting Laboratory Relative Permeability Measurements,* 99
- Gravel pack: Completion for exclusion of gas and water, 183.
- Gravity drainage: An experimental and theoretical investigation of gravity drainage performance, 285.
- Greer, Walton J., et al.: *The Guard Electrode Logging System,* 347
- Grenall, A., et al.: *Mineralogical Studies of California Oil-bearing Formations. I — Identification of Clays,* 151
- Grossman, Waldo L.: *Hydrafrac Operations in the Spraberry,* (Art.), Nov. JPT.

H

- Hafford, J. A., et al.: *Laboratory Measurements of Relative Permeability,* 47
- Hall, Howard N., et al.: *An Experimental and Theoretical Investigation of Gravity Drainage Performance,* 285
- Hawthorne, R. R., et al.: *The Calculation of Water Resistivities from Chemical Analysis,* (Tech. Note), March JPT.
- Hedlund, Charles J.: *Iran and World Oil,* (Art.), Oct. JPT.
- Henagan, James M., et al.: *Report on the Mamou Field Pressure Maintenance Project,* 263
- Hensley, Harold L.: *Today's Natural Gas Industry,* (Art.), Aug. JPT.
- Hiltz, R. G., et al.: *Results of Gas Injection in the Cedar Lake Field,* 357
- Holmgren, C. R., et al.: *Effect of Free Gas Saturation on Oil Recovery by Water Flooding,* 135
- Horner, William L.: *A Petroleum Engineering Progress Report on the Scurry Field,* (Art.), April JPT.
- Hough, E. W., et al.: *Interfacial Tensions at Reservoir Pressures and Temperatures; Apparatus and the Water-Methane System,* 57
- Howard, George C., et al.: *An Analysis and the Control of Lost Circulation,* 171
- Howard, K. C.: *The Development and Operation of LPG Storage Cavities in Salt Strata,* (Art.), March JPT.
- Huzarevich, J. E., et al.: *Results of Gas Injection in the Cedar Lake Field,* 357
- Hydrafrac: Operations in the Spraberry, (Art.), Nov. JPT.

I

- Interstitial water: Determination by an evaporation method, 269.
  - Use of centrifuge for determining connate water, residual oil and capillary pressure curves of small core samples, 127.
  - Interpretation of chemical water analysis by means of patterns (Tech. Note), Oct. JPT.

J

- Jackson, Gordon: *Penetration Rates for Directional Drilling Operations,* (Art.), June JPT.
- Johnson, Charles B., Jr.: *Underwater Storage of Propane in Salt Water Sand,* (Art.), Jan. JPT.

K

- Kaveler, H. H., et al.: *The Shuler Jones Sand Pool; Nine Years of Unitized Pressure-Maintenance Operations,* 121
- Kerver, J. K., et al.: *Laboratory Measurements of Relative Permeability,* 47

L

- Laird, A. D. K., et al.: *Fluid Saturation in Porous Media by X-ray Technique,* 275
- Laterolog: Logging method using automatic focusing system, 305.
- Leas, W. J., et al.: *Relative Permeability to Liquid in Liquid-Gas Systems,* 83

LeBlanc, J. L.: *Offshore Production and Completion Practices in the Bay Marchand and Main Pass Fields,* (Art.), July JPT.

Leibrock, R. M., et al.: *Results of Gas Injection in the Cedar Lake Field,* 357

Lilienthal, W. B., et al.: *Plastic Flow Properties of Drilling Fluids — Measurement and Application,* 159

Lipson, Leonard B.: *Theoretical Note on Linear Absorption Methods of Determination of Fluid Saturation in Porous Media,* (Tech. Note), Aug. JPT.

LPG: Development and operation of LPG storage cavities in salt strata, (Art.), March JPT.

M

Manpower: An engineering manpower study, (Art.), May JPT.

Mardock, E. S., et al.: *The Quantitative Application of Radioactivity Logs,* 191

McCreery, P. N., et al.: *Porosity-Measurement Comparisons by Five Laboratories,* 341

McDonald, L. L., et al.: *Drilling and Production Problems Relating to the Worland, Wyoming, Field,* (Art.), May JPT.

McKetta, J. J., Jr., et al.: *Phase Equilibria in Hydrocarbon-Water Systems. III — The Solubility of Methane in Water at Pressures to 10,000 PSIA,* 223.

McKetta, J. J., Jr., et al.: *Phase Equilibria in Hydrocarbon-Water Systems. IV — Vapor Liquid Equilibrium Constants in the Methane-Water and Ethane-Water Systems,* 297

Melrose, J. C., et al.: *Plastic Flow Properties of Drilling Fluids — Measurement and Application,* 159

Merrill, W. C., et al.: *Mineralogical Studies of California Oilbearing Formations. I — Identification of Clays,* 151

Messer, E. S.: *Interstitial Water Determination by an Evaporation Method,* 269

Miller, Frank G.: *Steady Flow of Two-Phase Single-Component Fluids Through Porous Media,* 205

Morgan, B. E., et al.: *A Modified Low-Strength Cement,* 165

Morgan, F., et al.: *A New Technique for the Measurement of the Formation Factors and Resistivity Indices of Porous Media,* (Tech. Note), Feb. JPT.

Morris, J. I., et al.: *Drilling and Production Problems Relating to the Worland, Wyoming, Field,* (Art.), May JPT.

Morse, R. A., et al.: *Effect of Free Gas Saturation on Oil Recovery by Water Flooding,* 135

Morse, R. A., et al.: *An Experimental and Theoretical Investigation of Gravity Drainage Performance,* 285

Morse, R. A., et al.: *Experimental Investigation of Factors Affecting Laboratory Relative Permeability Measurements,* 99

Muskat, Morris: *The Effect of Withdrawal Rate on the Uniformity of Edgewater Intrusion,* 327

N

Nahin, P. G., et al.: *Mineralogical Studies of California Oilbearing Formations. I — Identification of Clays,* 151

O

Ockershauser, T. E.: *The Southwest Antioch Gibson Sand Unit,* 199

Offshore operations: Production and completion practices in the Bay Marchand and Main Pass Fields, (Art.), July, JPT.

Olds, R. H., et al.: *Transient Flow in Gas Transmission Lines,* 217

Osoba, J. S., et al.: *Laboratory Measurements of Relative Permeability,* 47

Owen, John E., et al.: *The Guard Electrode Logging System,* 347

Owens, W. W., et al.: *Experimental Investigation of Factors Affecting Laboratory Relative Permeability Measurements,* 99

P

Parrish, D. R., et al.: *Experimental Investigation of Factors Affecting Laboratory Relative Permeability Measurements,* 99

Parsons, R. L., et al.: *Relaxation Methods Applied to Oil Field Research,* 227

Phase equilibria: In hydrocarbon-water systems (solubility of methane in water at pressures to 10,000 psia), 223.
  In hydrocarbon-water systems (vapor liquid equilibrium constants in the methane-water and ethane-water systems), 297.
  Phase behavior of natural hydrocarbon system, 233.
  Interrelationship between wetting and non-wetting phase relative permeability, (Tech. Note), Oct. JPT.

Pipe: Calculation of pressure drop in flow of natural gas through pipe, 317
  Transient flow in gas transmission lines, 217.

Poettmann, Fred H.: *The Calculation of Pressure Drop in the Flow of Natural Gas Through Pipe,* 317

Poettmann, Fred H.: *Vaporization Characteristics of Carbon Dioxide in a Natural Gas-Crude Oil System,* 141

Politziner, Irwin, et al.: *Measuring the Water Vapor Content of Gases Dehydrated by Triethylene Glycol,* 301

Pores: Absorption methods of determination of fluid saturation in porous media, (Tech. Note), Aug. JPT.
  Steady flow of two-phase single-component fluids through porous media, 205
  Fluid saturation in porous media, 275.
  Measurement of formation factors and resistivity indices of porous media, (Tech. Note), Feb. JPT.
  Porosity measurement comparisons, 341.

Prehn, W. L., Jr., et al.: *Use of Centrifuge for Determining Connate Water, Residual Oil, and Capillary Pressure Curves of Small Core Samples,* 127

Pressure: Capillary pressure investigations, 67.
  Pressure maintenance in the Mamou Field, 263.
  Phase equilibria, 223.
  Calculations of pressure drop in flow of gas through pipe, 317.
  Surface indicating pressure equipment, 257.
  Pressure behavior in the Woodbine sand, 19.
  Use of centrifuge for determination of connate water, residual oil and capillary pressure curves of core samples, 127.
  Pressure maintenance in Shuler Jones sand pool, 121
  Interfacial tensions at reservoir pressures and temperatures, 57.

Putnam, John A.: *Education for Research in Petroleum Engineering,* (Art.), Aug. JPT.

Putnam, John A., et al.: *Fluid Saturation in Porous Media by X-ray Technique,* 275

R

Rapoport, L. A., et al.: *Relative Permeability to Liquid in Liquid-Gas Systems,* 83

Records, Louis R., et al.: *Low Temperature Dehydration of Natural Gas,* 61

Reid, L. S., et al.: *Measuring the Water Vapor Content of Gases Dehydrated by Triethylene Glycol,* 301

Relative permeability: Studies, 249
  Factors affecting laboratory relative permeability measurements, 99.
  To liquid in liquid-gas system, 83
  Laboratory measurements, 47.
  Further developments in laboratory determination of relative permeability, 145.
  Interrelationship between wetting and non-wetting phase relative permeability, (Tech. Note), Oct. JPT.
Research: Relaxation methods applied to oil field research, 227.
  Education for research, (Art.), Aug. JPT.
  Utilization of research in production of oil, (Art.), Nov. JPT.
Richardson, J. G., et al.: *Laboratory Measurements of Relative Permeability*, 47
Riordan, M. B.: *Surface Indicating Pressure, Temperature and Flow Equipment*, 257
Rose, Walter: *Fluid Distributions Characterizing Gas—Liquid Flow*, (Tech. Note), Feb. JPT.
Rumble, R. C., et al.: *A Reservoir Analyzer Study of the Woodbine Basin*, 331
Rzasa, M. J., et al.: *Interfacial Tensions at Reservoir Pressures and Temperatures; Apparatus and the Water-Methane System*, 57

S

Sage, B. H., et al.: *Transient Flow in Gas Transmission Lines*, 217
Scott, F. L., Jr.: *Advancement in Design and Technique of Rotary Fishing Tools*, (Art.), June JPT.
Scott, P. P., Jr., et al.: *An Analysis and the Control of Lost Circulation*, 171
Seely, Dwight H., Jr., et al.: *Low Temperature Dehydration of Natural Gas*, 61
SP curve: Investigation of the electro-kinetic component of the self potential curve, 1
Shepherd, J. M., et al.: *Pressure Behavior in the Woodbine Sand*, 19
Sherborne, John E.: *Utilization of Research in Production of Oil*, (Art.), Nov. JPT.
Slobod, R. L., et al.: *Further Developments in the Laboratory Determination of Relative Permeability*, 145
Slobod, R. L., et al.: *Porosity-Measurement Comparisons by Five Laboratories*, 341
Slobod, R. L., et al.: *Use of Centrifuge for Determining Connate Water, Residual Oil, and Capillary Pressure Curves of Small Core Samples*, 127
Spain, H. H., et al.: *A Reservoir Analyzer Study of the Woodbine Basin*, 331
Spencer, G. B., et al.: *Special Considerations in Predicting Reservoir Performance of Highly Volatile Type Oil Reservoirs*, 37
Spencer, John R.: *A High Temperature Gauge Glass for the Visual Observation of Critical Phenomena*, (Tech. Note), Aug. JPT.
Spurlock, James W., et al.: *Porosity-Measurement Comparisons by Five Laboratories*, 341
Stamm, H. E., III, et al.: *A Reservoir Analyzer Study of the Woodbine Basin*, 331
Stiff, Henry A., Jr.: *The Interpretation of Chemical Water Analysis by Means of Patterns*, (Tech. Note), Oct. JPT.

T

Tarner, Jack, et al.: *The Shuler Jones Sand Pool; Nine Years of Unitized Pressure-Maintenance Operations*, 121
Terwilliger, P. L., et al.: *An Experimental and Theoretical Investigation of Gravity Drainage Performance*, 285
Townsend, F. M., et al.: *Measuring the Water Vapor Content of Gases Dehydrated by Triethylene Glycol*, 301

W

Water flood: In the Pettit Lime, Haynesville Field, 239.
  Benton water flood, Franklin County, Illinois, (Art.), Sept. JPT.
  Effect of free gas saturation on oil recovery by water flooding, 135.
Water resistivities: From chemical analysis, (Tech. Note), March JPT.
  New technique for measurement of formation factors and resistivity indices of porous media, (Tech. Note), Feb. JPT.
Weinaug, Charles F., et al.: *The Phase Behavior of a Natural Hydrocarbon System*, 233
West, Thomas S.: *A Gravel Pack Completion for Exclusion of Gas and Water*, 183
Williams, C. E., Jr., et al.: *Carrying Capacity of Drilling Muds*, 111
Willis, Roy M., et al.: *Recent Advances in Gas Lift Equipment and Techniques*, (Art.), Feb. JPT.
Wilsey, L. E., et al.: *An Experimental and Theoretical Investigation of Gravity Drainage Performance*, 285
Wood, B. B., et al.: *Interfacial Tensions at Reservoir Pressures and Temperatures; Apparatus and the Water-Methane System*, 57
Wyllie, M. R. J.: *An Investigation of the Electrokinetic Component of the Self Potential Curve*, 1
Wyllie, M. R. J., et al.: *A New Technique for the Measurement of the Formation Factors and Resistivity Indices of Porous Media*, (Tech. Note), Feb. JPT.
Wyllie, M. R. J.: *A Note on the Interrelationship Between Wetting and Non-Wetting Phase Relative Permeability*, (Tech. Note), Oct. JPT.

★ ★ ★